

Condensed Matter Physics

Condensed Matter Physics

Second Edition

Michael P. Marder

 **WILEY**

A JOHN WILEY & SONS, INC., PUBLICATION

Copyright © 2010 by John Wiley & Sons, Inc. All rights reserved.

Published by John Wiley & Sons, Inc., Hoboken, New Jersey.

Published simultaneously in Canada.

No part of this publication may be reproduced, stored in a retrieval system, or transmitted in any form or by any means, electronic, mechanical, photocopying, recording, scanning, or otherwise, except as permitted under Section 107 or 108 of the 1976 United States Copyright Act, without either the prior written permission of the Publisher, or authorization through payment of the appropriate per-copy fee to the Copyright Clearance Center, Inc., 222 Rosewood Drive, Danvers, MA 01923, (978) 750-8400, fax (978) 750-4470, or on the web at www.copyright.com. Requests to the Publisher for permission should be addressed to the Permissions Department, John Wiley & Sons, Inc., 111 River Street, Hoboken, NJ 07030, (201) 748-6011, fax (201) 748-6008, or online at <http://www.wiley.com/go/permission>.

Limit of Liability/Disclaimer of Warranty: While the publisher and author have used their best efforts in preparing this book, they make no representations or warranties with respect to the accuracy or completeness of the contents of this book and specifically disclaim any implied warranties of merchantability or fitness for a particular purpose. No warranty may be created or extended by sales representatives or written sales materials. The advice and strategies contained herein may not be suitable for your situation. You should consult with a professional where appropriate. Neither the publisher nor author shall be liable for any loss of profit or any other commercial damages, including but not limited to special, incidental, consequential, or other damages.

For general information on our other products and services or for technical support, please contact our Customer Care Department within the United States at (800) 762-2974, outside the United States at (317) 572-3993 or fax (317) 572-4002.

Wiley also publishes its books in a variety of electronic formats. Some content that appears in print may not be available in electronic formats. For more information about Wiley products, visit our web site at www.wiley.com.

Library of Congress Cataloging-in-Publication Data is available.

ISBN 978-0-470-61798-4

Printed in the United States of America.

10 9 8 7 6 5 4 3 2 1

Contents

Preface	xix
References	xxii
I ATOMIC STRUCTURE	1
1 The Idea of Crystals	3
1.1 Introduction	3
1.1.1 Why are Solids Crystalline?	4
1.2 Two-Dimensional Lattices	6
1.2.1 Bravais Lattices	6
1.2.2 Enumeration of Two-Dimensional Bravais Lattices	7
1.2.3 Lattices with Bases	9
1.2.4 Primitive Cells	9
1.2.5 Wigner–Seitz Cells	10
1.3 Symmetries	11
1.3.1 The Space Group	11
1.3.2 Translation and Point Groups	12
1.3.3 Role of Symmetry	14
Problems	14
References	16
2 Three-Dimensional Lattices	17
2.1 Introduction	17
2.2 Monatomic Lattices	20
2.2.1 The Simple Cubic Lattice	20
2.2.2 The Face-Centered Cubic Lattice	20
2.2.3 The Body-Centered Cubic Lattice	22
2.2.4 The Hexagonal Lattice	23
2.2.5 The Hexagonal Close-Packed Lattice	23
2.2.6 The Diamond Lattice	24
2.3 Compounds	24
2.3.1 Rocksalt—Sodium Chloride	25
2.3.2 Cesium Chloride	26
2.3.3 Fluorite—Calcium Fluoride	26

2.3.4	Zincblende—Zinc Sulfide	27
2.3.5	Wurtzite—Zinc Oxide	28
2.3.6	Perovskite—Calcium Titanate	28
2.4	Classification of Lattices by Symmetry	30
2.4.1	Fourteen Bravais Lattices and Seven Crystal Systems	30
2.5	Symmetries of Lattices with Bases	33
2.5.1	Thirty-Two Crystallographic Point Groups	33
2.5.2	Two Hundred Thirty Distinct Lattices	36
2.6	Some Macroscopic Implications of Microscopic Symmetries	37
2.6.1	Pyroelectricity	37
2.6.2	Piezoelectricity	37
2.6.3	Optical Activity	38
	Problems	38
	References	41
3	Scattering and Structures	43
3.1	Introduction	43
3.2	Theory of Scattering from Crystals	44
3.2.1	Special Conditions for Scattering	44
3.2.2	Elastic Scattering from Single Atom	46
3.2.3	Wave Scattering from Many Atoms	47
3.2.4	Lattice Sums	48
3.2.5	Reciprocal Lattice	49
3.2.6	Miller Indices	51
3.2.7	Scattering from a Lattice with a Basis	53
3.3	Experimental Methods	54
3.3.1	Laue Method	56
3.3.2	Rotating Crystal Method	57
3.3.3	Powder Method	59
3.4	Further Features of Scattering Experiments	60
3.4.1	Interaction of X-Rays with Matter	60
3.4.2	Production of X-Rays	61
3.4.3	Neutrons	63
3.4.4	Electrons	63
3.4.5	Deciphering Complex Structures	64
3.4.6	Accuracy of Structure Determinations	65
3.5	Correlation Functions	66
3.5.1	Why Bragg Peaks Survive Atomic Motions	66
3.5.2	Extended X-Ray Absorption Fine Structure (EXAFS)	67
3.5.3	Dynamic Light Scattering	68
3.5.4	Application to Dilute Solutions	70
	Problems	71
	References	73

4	Surfaces and Interfaces	77
4.1	Introduction	77
4.2	Geometry of Interfaces	77
4.2.1	Coherent and Commensurate Interfaces	78
4.2.2	Stacking Period and Interplanar Spacing	79
4.2.3	Other Topics in Surface Structure	81
4.3	Experimental Observation and Creation of Surfaces	82
4.3.1	Low-Energy Electron Diffraction (LEED)	82
4.3.2	Reflection High-Energy Electron Diffraction (RHEED)	84
4.3.3	Molecular Beam Epitaxy (MBE)	84
4.3.4	Field Ion Microscopy (FIM)	85
4.3.5	Scanning Tunneling Microscopy (STM)	86
4.3.6	Atomic Force Microscopy (AFM)	91
4.3.7	High Resolution Electron Microscopy (HREM)	91
	Problems	91
	References	94
5	Beyond Crystals	97
5.1	Introduction	97
5.2	Diffusion and Random Variables	97
5.2.1	Brownian Motion and the Diffusion Equation	97
5.2.2	Diffusion	98
5.2.3	Derivation from Master Equation	99
5.2.4	Connection Between Diffusion and Random Walks	100
5.3	Alloys	101
5.3.1	Equilibrium Structures	101
5.3.2	Phase Diagrams	102
5.3.3	Superlattices	103
5.3.4	Phase Separation	104
5.3.5	Nonequilibrium Structures in Alloys	106
5.3.6	Dynamics of Phase Separation	108
5.4	Simulations	110
5.4.1	Monte Carlo	110
5.4.2	Molecular Dynamics	112
5.5	Liquids	113
5.5.1	Order Parameters and Long- and Short-Range Order	113
5.5.2	Packing Spheres	114
5.6	Glasses	116
5.7	Liquid Crystals	120
5.7.1	Nematics, Cholesterics, and Smectics	120
5.7.2	Liquid Crystal Order Parameter	122
5.8	Polymers	123
5.8.1	Ideal Radius of Gyration	123
5.9	Colloids and Diffusing-Wave Scattering	128

5.9.1	Colloids	128
5.9.2	Diffusing-Wave Spectroscopy	128
5.10	Quasicrystals	133
5.10.1	One-Dimensional Quasicrystal	134
5.10.2	Two-Dimensional Quasicrystals—Penrose Tiles	139
5.10.3	Experimental Observations	141
5.11	Fullerenes and nanotubes	143
	Problems	143
	References	149
II ELECTRONIC STRUCTURE		153
6	The Free Fermi Gas and Single Electron Model	155
6.1	Introduction	155
6.2	Starting Hamiltonian	157
6.3	Densities of States	159
6.3.1	Definition of Density of States D	160
6.3.2	Results for Free Electrons	161
6.4	Statistical Mechanics of Noninteracting Electrons	163
6.5	Sommerfeld Expansion	166
6.5.1	Specific Heat of Noninteracting Electrons at Low Temperatures	169
	Problems	171
	References	173
7	Non-Interacting Electrons in a Periodic Potential	175
7.1	Introduction	175
7.2	Translational Symmetry—Bloch's Theorem	175
7.2.1	One Dimension	176
7.2.2	Bloch's Theorem in Three Dimensions	180
7.2.3	Formal Demonstration of Bloch's Theorem	182
7.2.4	Additional Implications of Bloch's Theorem	183
7.2.5	Van Hove Singularities	186
7.2.6	Kronig–Penney Model	189
7.3	Rotational Symmetry—Group Representations	192
7.3.1	Classes and Characters	198
7.3.2	Consequences of point group symmetries for Schrödinger's equation	201
	Problems	203
	References	206

8	Nearly Free and Tightly Bound Electrons	207
8.1	Introduction	207
8.2	Nearly Free Electrons	208
8.2.1	Degenerate Perturbation Theory	210
8.3	Brillouin Zones	211
8.3.1	Nearly Free Electron Fermi Surfaces	214
8.4	Tightly Bound Electrons	219
8.4.1	Linear Combinations of Atomic Orbitals	219
8.4.2	Wannier Functions	222
8.4.3	Geometric Phases	223
8.4.4	Tight Binding Model	226
	Problems	227
	References	232
9	Electron–Electron Interactions	233
9.1	Introduction	233
9.2	Hartree and Hartree–Fock Equations	234
9.2.1	Variational Principle	235
9.2.2	Hartree–Fock Equations	235
9.2.3	Numerical Implementation	239
9.2.4	Hartree–Fock Equations for Jellium	242
9.3	Density Functional Theory	244
9.3.1	Thomas–Fermi Theory	247
9.3.2	Stability of Matter	249
9.4	Quantum Monte Carlo	252
9.4.1	Integrals by Monte Carlo	252
9.4.2	Quantum Monte Carlo Methods	253
9.4.3	Physical Results	254
9.5	Kohn–Sham Equations	255
	Problems	258
	References	262
10	Realistic Calculations in Solids	265
10.1	Introduction	265
10.2	Numerical Methods	266
10.2.1	Pseudopotentials and Orthogonalized Planes Waves (OPW)	266
10.2.2	Linear Combination of Atomic Orbitals (LCAO)	271
10.2.3	Plane Waves	271
10.2.4	Linear Augmented Plane Waves (LAPW)	274
10.3	Definition of Metals, Insulators, and Semiconductors	277
10.4	Brief Survey of the Periodic Table	279
10.4.1	Nearly Free Electron Metals	280
10.4.2	Noble Gases	282
10.4.3	Semiconductors	283

10.4.4	Transition Metals	284
10.4.5	Rare Earths	286
Problems	286
References	291
III MECHANICAL PROPERTIES		293
11 Cohesion of Solids		295
11.1	Introduction	295
11.1.1	Radii of Atoms	297
11.2	Noble Gases	299
11.3	Ionic Crystals	301
11.3.1	Ewald Sums	302
11.4	Metals	305
11.4.1	Use of Pseudopotentials	307
11.5	Band Structure Energy	308
11.5.1	Peierls Distortion	309
11.5.2	Structural Phase Transitions	311
11.6	Hydrogen-Bonded Solids	312
11.7	Cohesive Energy from Band Calculations	312
11.8	Classical Potentials	313
Problems	315
References	318
12 Elasticity		321
12.1	Introduction	321
12.2	Nonlinear Elasticity	321
12.2.1	Rubber Elasticity	322
12.2.2	Larger Extensions of Rubber	324
12.3	Linear Elasticity	325
12.3.1	Solids of Cubic Symmetry	326
12.3.2	Isotropic Solids	328
12.4	Other Constitutive Laws	332
12.4.1	Liquid Crystals	332
12.4.2	Granular Materials	335
Problems	336
References	339
13 Phonons		341
13.1	Introduction	341
13.2	Vibrations of a Classical Lattice	342
13.2.1	Classical Vibrations in One Dimension	342
13.2.2	Classical Vibrations in Three Dimensions	346
13.2.3	Normal Modes	347

13.2.4	Lattice with a Basis	348
13.3	Vibrations of a Quantum–Mechanical Lattice	351
13.3.1	Phonon Specific Heat	354
13.3.2	Einstein and Debye Models	358
13.3.3	Thermal Expansion	361
13.4	Inelastic Scattering from Phonons	363
13.4.1	Neutron Scattering	364
13.4.2	Formal Theory of Neutron Scattering	366
13.4.3	Averaging Exponentials	370
13.4.4	Evaluation of Structure Factor	372
13.4.5	Kohn Anomalies	373
13.5	The Mössbauer Effect	374
	Problems	376
	References	377
14	Dislocations and Cracks	379
14.1	Introduction	379
14.2	Dislocations	381
14.2.1	Experimental Observations of Dislocations	383
14.2.2	Force to Move a Dislocation	386
14.2.3	One-Dimensional Dislocations: Frenkel–Kontorova Model	386
14.3	Two-Dimensional Dislocations and Hexatic Phases	389
14.3.1	Impossibility of Crystalline Order in Two Dimensions	389
14.3.2	Orientalional Order	391
14.3.3	Kosterlitz–Thouless–Berezinskii Transition	392
14.4	Cracks	399
14.4.1	Fracture of a Strip	399
14.4.2	Stresses Around an Elliptical Hole	402
14.4.3	Stress Intensity Factor	404
14.4.4	Atomic Aspects of Fracture	405
	Problems	406
	References	409
15	Fluid Mechanics	413
15.1	Introduction	413
15.2	Newtonian Fluids	413
15.2.1	Euler’s Equation	413
15.2.2	Navier–Stokes Equation	415
15.3	Polymeric Solutions	416
15.4	Plasticity	423
15.5	Superfluid ⁴ He	427
15.5.1	Two-Fluid Hydrodynamics	430
15.5.2	Second Sound	431
15.5.3	Direct Observation of Two Fluids	433

15.5.4	Origin of Superfluidity	434
15.5.5	Lagrangian Theory of Wave Function	439
15.5.6	Superfluid ^3He	442
	Problems	443
	References	447
IV ELECTRON TRANSPORT		451
16	Dynamics of Bloch Electrons	453
16.1	Introduction	453
16.1.1	Drude Model	453
16.2	Semiclassical Electron Dynamics	455
16.2.1	Bloch Oscillations	456
16.2.2	$\vec{k} \cdot \hat{P}$ Method	457
16.2.3	Effective Mass	459
16.3	Noninteracting Electrons in an Electric Field	459
16.3.1	Zener Tunneling	462
16.4	Semiclassical Equations from Wave Packets	465
16.4.1	Formal Dynamics of Wave Packets	465
16.4.2	Dynamics from Lagrangian	467
16.5	Quantizing Semiclassical Dynamics	470
16.5.1	Wannier–Stark Ladders	472
16.5.2	de Haas–van Alphen Effect	473
16.5.3	Experimental Measurements of Fermi Surfaces	474
	Problems	477
	References	480
17	Transport Phenomena and Fermi Liquid Theory	483
17.1	Introduction	483
17.2	Boltzmann Equation	483
17.2.1	Boltzmann Equation	485
17.2.2	Including Anomalous Velocity	486
17.2.3	Relaxation Time Approximation	487
17.2.4	Relation to Rate of Production of Entropy	489
17.3	Transport Symmetries	490
17.3.1	Onsager Relations	491
17.4	Thermoelectric Phenomena	492
17.4.1	Electrical Current	492
17.4.2	Effective Mass and Holes	494
17.4.3	Mixed Thermal and Electrical Gradients	495
17.4.4	Wiedemann–Franz Law	496
17.4.5	Thermopower—Seebeck Effect	497
17.4.6	Peltier Effect	498

17.4.7 Thomson Effect	498
17.4.8 Hall Effect	500
17.4.9 Magnetoresistance	502
17.4.10 Anomalous Hall Effect	503
17.5 Fermi Liquid Theory	504
17.5.1 Basic Ideas	504
17.5.2 Statistical Mechanics of Quasi-Particles	506
17.5.3 Effective Mass	508
17.5.4 Specific Heat	510
17.5.5 Fermi Liquid Parameters	511
17.5.6 Traveling Waves	512
17.5.7 Comparison with Experiment in ^3He	515
Problems	516
References	520
18 Microscopic Theories of Conduction	523
18.1 Introduction	523
18.2 Weak Scattering Theory of Conductivity	523
18.2.1 General Formula for Relaxation Time	523
18.2.2 Matthiessen's Rule	528
18.2.3 Fluctuations	529
18.3 Metal–Insulator Transitions in Disordered Solids	530
18.3.1 Impurities and Disorder	530
18.3.2 Non-Compensated Impurities and the Mott Transition	531
18.4 Compensated Impurity Scattering and Green's Functions	534
18.4.1 Tight-Binding Models of Disordered Solids	534
18.4.2 Green's Functions	536
18.4.3 Single Impurity	539
18.4.4 Coherent Potential Approximation	541
18.5 Localization	542
18.5.1 Exact Results in One Dimension	544
18.5.2 Scaling Theory of Localization	547
18.5.3 Comparison with Experiment	551
18.6 Luttinger Liquids	553
18.6.1 Density of States	557
Problems	560
References	564
19 Electronics	567
19.1 Introduction	567
19.2 Metal Interfaces	568
19.2.1 Work Functions	569
19.2.2 Schottky Barrier	570
19.2.3 Contact Potentials	572

19.3	Semiconductors	574
19.3.1	Pure Semiconductors	575
19.3.2	Semiconductor in Equilibrium	578
19.3.3	Intrinsic Semiconductor	580
19.3.4	Extrinsic Semiconductor	581
19.4	Diodes and Transistors	583
19.4.1	Surface States	586
19.4.2	Semiconductor Junctions	587
19.4.3	Boltzmann Equation for Semiconductors	590
19.4.4	Detailed Theory of Rectification	592
19.4.5	Transistor	595
19.5	Inversion Layers	598
19.5.1	Heterostructures	598
19.5.2	Quantum Point Contact	600
19.5.3	Quantum Dot	603
	Problems	606
	References	607
V OPTICAL PROPERTIES		609
20	Phenomenological Theory	611
20.1	Introduction	611
20.2	Maxwell's Equations	613
20.2.1	Traveling Waves	615
20.2.2	Mechanical Oscillators as Dielectric Function	616
20.3	Kramers–Kronig Relations	618
20.3.1	Application to Optical Experiments	620
20.4	The Kubo–Greenwood Formula	623
20.4.1	Born Approximation	623
20.4.2	Susceptibility	627
20.4.3	Many-Body Green Functions	628
	Problems	628
	References	631
21	Optical Properties of Semiconductors	633
21.1	Introduction	633
21.2	Cyclotron Resonance	633
21.2.1	Electron Energy Surfaces	636
21.3	Semiconductor Band Gaps	638
21.3.1	Direct Transitions	638
21.3.2	Indirect Transitions	639
21.4	Excitons	641
21.4.1	Mott–Wannier Excitons	641

21.4.2	Frenkel Excitons	644
21.4.3	Electron–Hole Liquid	645
21.5	Optoelectronics	645
21.5.1	Solar Cells	645
21.5.2	Lasers	646
Problems	652
References	656
22	Optical Properties of Insulators	659
22.1	Introduction	659
22.2	Polarization	659
22.2.1	Ferroelectrics	659
22.2.2	Berry phase theory of polarization	661
22.2.3	Clausius–Mossotti Relation	661
22.3	Optical Modes in Ionic Crystals	664
22.3.1	Polaritons	666
22.3.2	Polarons	669
22.3.3	Experimental Observations of Polarons	674
22.4	Point Defects and Color Centers	674
22.4.1	Vacancies	675
22.4.2	F Centers	676
22.4.3	Electron Spin Resonance and Electron Nuclear Double Res- onance	677
22.4.4	Other Centers	679
22.4.5	Franck–Condon Effect	679
22.4.6	Urbach Tails	683
Problems	684
References	686
23	Optical Properties of Metals and Inelastic Scattering	689
23.1	Introduction	689
23.1.1	Plasma Frequency	689
23.2	Metals at Low Frequencies	692
23.2.1	Anomalous Skin Effect	694
23.3	Plasmons	695
23.3.1	Experimental Observation of Plasmons	696
23.4	Interband Transitions	698
23.5	Brillouin and Raman Scattering	701
23.5.1	Brillouin Scattering	702
23.5.2	Raman Scattering	703
23.5.3	Inelastic X-Ray Scattering	703
23.6	Photoemission	703
23.6.1	Measurement of Work Functions	703
23.6.2	Angle-Resolved Photoemission	706

23.6.3	Core-Level Photoemission and Charge-Transfer Insulators	710
Problems	716
References	719
VI	MAGNETISM	721
24	Classical Theories of Magnetism and Ordering	723
24.1	Introduction	723
24.2	Three Views of Magnetism	723
24.2.1	From Magnetic Moments	723
24.2.2	From Conductivity	724
24.2.3	From a Free Energy	725
24.3	Magnetic Dipole Moments	727
24.3.1	Spontaneous Magnetization of Ferromagnets	730
24.3.2	Ferrimagnets	731
24.3.3	Antiferromagnets	733
24.4	Mean Field Theory and the Ising Model	734
24.4.1	Domains	736
24.4.2	Hysteresis	739
24.5	Other Order–Disorder Transitions	740
24.5.1	Alloy Superlattices	740
24.5.2	Spin Glasses	743
24.6	Critical Phenomena	743
24.6.1	Landau Free Energy	744
24.6.2	Scaling Theory	750
Problems	754
References	757
25	Magnetism of Ions and Electrons	759
25.1	Introduction	759
25.2	Atomic Magnetism	761
25.2.1	Hund’s Rules	762
25.2.2	Curie’s Law	766
25.3	Magnetism of the Free-Electron Gas	769
25.3.1	Pauli Paramagnetism	770
25.3.2	Landau Diamagnetism	771
25.3.3	Aharonov–Bohm Effect	774
25.4	Tightly Bound Electrons in Magnetic Fields	777
25.5	Quantum Hall Effect	780
25.5.1	Integer Quantum Hall Effect	780
25.5.2	Fractional Quantum Hall Effect	785
Problems	791
References	794

26 Quantum Mechanics of Interacting Magnetic Moments	797
26.1 Introduction	797
26.2 Origin of Ferromagnetism	797
26.2.1 Heitler–London Calculation	797
26.2.2 Spin Hamiltonian	802
26.3 Heisenberg Model	802
26.3.1 Indirect Exchange and Superexchange	804
26.3.2 Ground State	805
26.3.3 Spin Waves	805
26.3.4 Spin Waves in Antiferromagnets	808
26.3.5 Comparison with Experiment	811
26.4 Ferromagnetism in Transition Metals	811
26.4.1 Stoner Model	811
26.4.2 Calculations Within Band Theory	813
26.5 Spintronics	815
26.5.1 Giant Magnetoresistance	815
26.5.2 Spin Torque	816
26.6 Kondo Effect	819
26.6.1 Scaling Theory	824
26.7 Hubbard Model	828
26.7.1 Mean-Field Solution	829
Problems	832
References	835
27 Superconductivity	839
27.1 Introduction	839
27.2 Phenomenology of Superconductivity	840
27.2.1 Phenomenological Free Energy	841
27.2.2 Thermodynamics of Superconductors	843
27.2.3 Landau–Ginzburg Free Energy	844
27.2.4 Type I and Type II Superconductors	845
27.2.5 Flux Quantization	850
27.2.6 The Josephson Effect	852
27.2.7 Circuits with Josephson Junction Elements	854
27.2.8 SQUIDS	855
27.2.9 Origin of Josephson’s Equations	856
27.3 Microscopic Theory of Superconductivity	858
27.3.1 Electron–Ion Interaction	859
27.3.2 Instability of the Normal State: Cooper Problem	863
27.3.3 Self-Consistent Ground State	865
27.3.4 Thermodynamics of Superconductors	869
27.3.5 Superconductor in External Magnetic Field	873
27.3.6 Derivation of Meissner Effect	876
27.3.7 Comparison with Experiment	879

27.3.8 High-Temperature Superconductors	881
Problems	888
References	890
APPENDICES	895
A Lattice Sums and Fourier Transforms	897
A.1 One-Dimensional Sum	897
A.2 Area Under Peaks	897
A.3 Three-Dimensional Sum	898
A.4 Discrete Case	899
A.5 Convolution	900
A.6 Using the Fast Fourier Transform	900
References	902
B Variational Techniques	903
B.1 Functionals and Functional Derivatives	903
B.2 Time-Independent Schrödinger Equation	904
B.3 Time-Dependent Schrödinger Equation	905
B.4 Method of Steepest Descent	906
References	906
C Second Quantization	907
C.1 Rules	907
C.1.1 States	907
C.1.2 Operators	907
C.1.3 Hamiltonians	908
C.2 Derivations	909
C.2.1 Bosons	909
C.2.2 Fermions	910
Index	913

Preface

Preface to first edition

Using this book.

This textbook provides material for a one-year graduate course on condensed matter physics. It contains introductions to classic subjects, and it also presents topics I believe will continue to occupy the field in the future. The book teaches not only about the effective masses of electrons in semiconductor crystals and band theory, but also about quasicrystals, dynamics of phase separation, why rubber is more floppy than steel, electron interference in nanometer-sized channels, and the quantum Hall effect.

It is arranged in six parts, convenient for dividing into two semesters or three quarters. However, there is more material than can reasonably be covered in one year. My experience suggests that an instructor should aim to cover roughly two-thirds of the material in each part. The remainder is available for reference. Every instructor will find that some of the topics are very elementary and others are quite advanced. However, instructors with different backgrounds will disagree to a surprising extent on which are which. The web site associated with the book, <http://chaos.ph.utexas.edu/~cmp>, contains sample syllabi, as well as corrections, and other information.

Each chapter is followed by a collection of problems. Some are brief derivations, but many introduce new topics and are fairly lengthy. An instructor's manual is available to aid in decisions on what to assign. Whether in academic or industrial posts, experimentalists and theorists must all become fluent in manipulating data and symbols with the computer. Therefore, many of the problems involve numerical work, ranging from no more than plotting graphs to a series of linked exercises that produces a simple band structure code.

The book presumes a working knowledge of quantum mechanics, statistical mechanics, and electricity and magnetism. I decided to exclude many-body Green functions, which become such an absorbing formal world of their own that they too easily drive physical reasoning out of an introductory course. However, as the book proceeds I do begin to employ second quantization, and it becomes quite common by the time of the section on magnetism.

If simple arguments explain a phenomenon, I present them, but I also have paid some attention to the actual historical process by which ideas were accepted, and I try to explain in detail some of the calculations and experimental data that actually convinced the specialists. Not all the subjects discussed in this book are closed; even simple questions do not always have answers; and theory and experiment do not always completely agree. The topics that can today be presented only within a distressing cloud of uncertainty are precisely the ones most likely to remain central to the development of condensed matter physics.

References to original literature. There are two attitudes toward references to original literature. One is that it is ridiculous to “cite the original work of Maxwell, for example, which nobody bothers to look up anyway” [Aharoni (1996), p. vii].

Maxwell himself disagreed. He believed that it “is of great advantage to the student of any subject to read the original memoirs on that subject, for science is always most completely assimilated when it is found in its nascent state” [Maxwell (1904), p. xi]. While it would be impossible to cite all papers responsible for the development of condensed matter physics without having reference lists longer than the remainder of the book, I have cited some of the most influential papers for two reasons. First, anyone who is part of research today knows how strongly all authors feel about having contributions recognized, and it hardly seems fair to have older generations drift entirely out of consciousness simply because they are no longer around to defend themselves. Second, original papers on difficult topics sometimes provide clearer explanations than anything that ever follows. Review articles quickly race over elementary points so as to provide comprehensive coverage of current developments, while textbooks easily make assertions, ignoring the complex web of evidence that eventually produced a consensus.

To try to ensure that major portions of the field were not left unrepresented, I somewhat arbitrarily chose three series of review articles and included a reference to almost every article with a bearing on condensed matter physics in the last 30 years. These are: *Solid State Physics: Advances in Research and Applications*, *Reviews of Modern Physics*, and *Physics Today*. Some of these articles have a very narrow focus, but the degree of difficulty can happily be estimated with little effort by using Ziman’s “coefficient of non-specificity, calculated as follows: transform the title into a succession of A adjectives qualifying S substantives, omitting redundant words like ‘physics’, ‘effects’, ‘properties’, ‘materials’, etc. Then take the ratio A/S . Inspection ... shows quite clearly that if the coefficient is greater than 3 the article is too specialized.... The optimum seems to be in the range $1 \leq A/S \leq 2$ ” [Ziman (1961)].

Origin of the field. The discovery of quantum mechanics raised the hope of explaining the familiar world from equations at the atomic scale. In early stages this enterprise was largely restricted to metals in crystalline form. The field began as “metals physics,” but the term excluded widely studied solids such as ionic crystals. “Solid state physics” was adopted instead, with creation of the Division of Solid State Physics by the American Physical Society in 1947. A decade later even “solid state” was becoming too restrictive for a field tackling liquid metals, liquid helium, liquid crystals, and polymer melts. In 1963, Busch began editing a journal called *Physik der Kondensierten Materie/Physique de la matière condensée/Physics of condensed matter*. The daring term gained usage slowly. The American Physical Society Division of Solid State Physics voted in April 1978 to change its name to the Division of Condensed Matter Physics.

Having set itself the modest goal of explaining the whole material world, including structural and electronic properties of solids and liquids, the field of condensed matter physics has become enormous. It overlaps statistical physics, materials physics, and fluid and solid mechanics. The diversity in topics obscures a unity of approach.

Experiments play a crucial role. The systems studied by condensed matter

physics are far too complicated for anyone to deduce their qualitative behavior from atomic scale considerations. Only once experience has determined the nature of the qualitative problem does theory have a chance of explaining it. On the other hand, most experiments are impossible to interpret quantitatively without theoretical support.

Condensed matter theories search for relations between separate levels of description. The fundamental underlying equations are largely useless, so theories of condensed matter are largely based upon equations whose form is guessed rather than derived, and in which parameters or methods of approximation are constrained by symmetry and determined by experiment. Often there is a friendly competition between simple models, employed for conceptual understanding, and attempts at realistic computation. There is sometimes a tendency to speak a bit contemptuously of the simple models. However, “for many purposes a theory whose consequences are easily followed is preferable to one which is more fundamental but also more unwieldy” [Thomson (1907), p. 2].

Acknowledgements. In the course of preparing this manuscript, I received generous assistance from dozens of people who supplied figures, answered queries, and took the time to debunk anecdotes that not only seemed to good to be true, but were in fact too good to be true. Some who wrote comments include Martin Bazant, Hans Bethe, Danita Boonchaisri, Steve Girvin, Stefan Hüfner, David Lazarus, Neil Mathur, David Mermin, George Sawatzky, and John Ziman. Lynn Boatner, Janie Gardner, and Douglas Corrigan of Oak Ridge National Laboratory contributed the micrograph appearing on the front cover. At The University of Texas at Austin, I was particularly helped by Alex de Lozanne, John Markert, Jim Erskine, Ken Shih, and Hugo Steinfink. Bob Martinez was the first person after me to try teaching from the text. Ted Einstein of the University of Maryland, Sokrates Pantelides of Vanderbilt University, and Rashmi Desai of The University of Toronto have also taught from draft versions, and they found embarrassing errors that I am perfectly glad to see disappear with the drafts. Roberto Diener trapped many additional errors. Caryn Cluiss assisted in the task of organizing permissions from numerous publishers.

As part of writing the book, I wanted to learn about band structure calculations. My colleague Len Kleinman helped with a steady supply of physical insight, provocative commentary, and warnings about the *method of successful approximations*, where twiddling hidden parameters stops as soon as one obtains an expected answer. Hans Skriver kindly supplied me with a copy of the code described in Skriver (1984). Roland Stumpf supplied improved versions of the plane-wave pseudopotential code described in Stumpf and Scheffler (1994), and he also answered interminable series of questions. Most recently, calculations were performed using VASP (Vienna ab-initio simulation program) developed at the Institut für Theoretische Physik of the Technische Universität Wien by Kresse and Hafner (1993), Kresse and Hafner (1994), Kresse and Furthmüller (1996b), and Kresse and Furthmüller (1996a).

I owe special thanks to Qian Niu. On many occasions I found myself baffled

by an apparently simple point, and I asked one expert after another without finding a resolution. When all other avenues failed, I took the stairs one flight down to Qian's office, where after a brief smile he explained matters to me with perfect clarity.

The Exxon Education Foundation and the National Science Foundation gave me the means to buy a laptop computer, which in turn allowed me to continue thinking about condensed metaphysics in unexpected places. My thanks to the citizens of Gavdos for allowing me to use cast-off solar panels, to Elias Kyriakopoulos for repairing a 12-volt power inverter when all seemed hopeless, and to Nikos Papanicolaou for unquestioning hospitality at the University of Crete whenever life without a library became just too difficult. Last thanks of all to my wife Elpida, without whose quiet encouragement and example of determination I would never have had the courage to complete this book.

Austin, Texas
September, 1999

MICHAEL MARDER

References

- A. Aharoni (1996), *Introduction to the Theory of Ferromagnetism*, Clarendon Press, Oxford.
- G. Kresse and J. Furthmüller (1996a), Efficiency of *ab-initio* total energy calculations for metals and semiconductors using a plane-wave basis set, *Computational Materials Science*, **6**, 15–50.
- G. Kresse and J. Furthmüller (1996b), Efficient iterative schemes for *ab initio* total-energy calculations using a plane-wave basis set, *Physical Review B*, **55**, 11 169–11 186.
- G. Kresse and J. Hafner (1993), *Ab initio* molecular dynamics for liquid metals, *Physical Review B*, **47**, 558–561.
- G. Kresse and J. Hafner (1994), *Ab initio* molecular-dynamics simulation of the liquid-metal-amorphous-semiconductor transition in germanium, *Physical Review B*, **49**, 14 251–14 269.
- J. C. Maxwell (1904), *A Treatise on Electricity and Magnetism*, vol. I, 3rd ed., Clarendon Press, Oxford.
- H. Skriver (1984), *The LMTO Method: Muffin-Tin Orbitals and Electronic Structure*, Springer-Verlag, Berlin.
- R. Stumpf and M. Scheffler (1994), Simultaneous calculation of the equilibrium electronic structure and its ground state using density functional theory, *Computer Physics Communications*, **79**, 447–465. The code is available in source from the CPC program library.
- J. J. Thomson (1907), *The Corpuscular Theory of Matter*, Charles Scribner's Sons, New York.
- J. M. Ziman (1961), Book reviews, *Philosophical Magazine*, **6**, 1071.

Preface to second edition

The goal of this second edition is to consolidate thousands of changes suggested by readers since the first was published, to improve presentation of several topics, and to add a small number of new ones.

Minor typographical errors were originally very numerous, and over 40 individuals from all over the world contributed corrections. The top 5 error-finders

found so many that they deserve special recognition: Roberto Diener read the book cover to cover, checked every derivation, and found 244; Dominic Holland found 33; Erkki Thuneberg found 20; Dale Kitchen found 15; Qian Niu found 11. Particularly extensive and detailed comments arrived from Wesley Matthews, Sasha Chernyshev, and Vincenzo Fiorentini.

The primary reason for many students to learn Condensed Matter Physics is for the topics of electron and phonon band structures. The presentation of these topics had been rushed, and the new presentation is slower, working out one-dimensional examples before proceeding to the full three-dimensional and abstract formulations.

The entire discipline of condensed matter is roughly ten percent older than when the first edition was written, so adding some new topics seemed appropriate. For the most part, these new topics were ones whose importance is increasingly appreciated, rather than material first derived in the last few years. They include graphene and nanotubes, Berry phases, Luttinger liquids, diffusion, dynamic light scattering, and spin torques.

The world in which this edition was produced is slightly different from that of the previous one. The first edition required many, many days walking up and down library stacks searching for articles. Now almost all academic publications are available through the internet in the world's most remote corners. Laptop computers were a rare luxury twelve years ago. Now they are a common commodity. The discipline of condensed matter physics itself underlies these technical advances. The benefits of instant connection everywhere to everything are partly offset by the corresponding demand to respond instantly to everyone everywhere about everything. I thank the National Science Foundation for sustained support that allowed me some periods of peace where I could finish this book.

Phalasarna, Crete
June, 2010

MICHAEL MARDER

Permissions

Cover, Upper Image: Zinc oxide (ZnO) is a wide band gap semiconductor with a multitude of applications in the areas of microelectronic devices, catalysis, varistors, light-emitting diodes, gas sensing, and scintillators. ZnO is a hexagonal, wurtzite-structure material that is characterized by polar Zn-terminated and O-terminated surfaces. In the top micrograph, chemical reactions produced by a high-temperature treatment in zinc metal vapor have produced morphological changes on the surface of a ZnO single crystal. Optical interference contrast microscopy reveals the hexagonal-symmetry ZnO surface topology in the form of color variations. Micrograph by: L. A. Boatner and Hu Longmire, Materials Science and Technology Division, Oak Ridge National Laboratory **Bottom Image:** Transition metal carbides are characterized by high melting points, high hardness, high-temperature corrosion resistance, and an ability to maintain their strength at elevated temperatures. The optical interference contrast micrograph shown at the bottom of the cover illustrates the morphological features of a fracture surface on a single crystal of titanium carbide. This material is brittle and is prone to fracture at room temperature, but it can be used as a structural material at high temperatures where the brittleness is reduced. Micrograph by: L. A. Boatner and Hu Longmire, Materials Science and Technology Division, Oak Ridge National Laboratory

Figure 1.1 (B): Reprinted from J. C. Heyraud and J. J. Métois, Establishment of the equilibrium shape of metal crystallites on a foreign substrate: Gold on graphite, 571–574, ©1980, with kind permission from Elsevier Science NL, Sara Burgerhartstraat 25, 1055 KV Amsterdam, The Netherlands. Figure 1.1 (C): Reprinted courtesy of author and with permission of Taylor and Francis from S. Lipson (1987), Helium crystals, *Contemporary Physics*, **28**, pp. 117–142. Figure 1.3: Reprinted from J. C. Meyer, A. K. Geim, M. I. Katsnelson, K. S. Novoselov, T. J. Booth, and S. Roth (2007), The structure of suspended graphene sheets, *Nature*, **446**, 60–63, courtesy of J Meyer and A Geim. Reprinted by permission from Macmillan Publishers Ltd. Figure 3.14: C. G. Shull, W. A. Strauser, and E. O. Wollan, Neutron diffraction by paramagnetic and antiferromagnetic substances, *Physical Review*, **83**, 333–345, ©1951 by the American Physical Society. Figure 3.17: After B. J. Berne and R. Pecora (2000), *Dynamic Light Scattering with Applications to Chemistry, Biology, and Physics*, Figure 5.4.1, Dover, New York. Reprint of 1976 edition. Figure 4.6: C.-L. Cheng, H.-C. Chang, J.-C. Lin, K.-J. Song, and J.-K. Want (1997), Direct observation of hydrogen etching anisotropy on diamond single crystal surfaces, *Physical Review Letters*, **78**, 3713–3716, ©1997 by the American Physical Society. Figure 4.9: W. Braun, L. Däweritz, and K. H. Ploog (1998), Origin of electron diffraction oscillations during crystal growth, *Physical Review Letters*, **80**, 4935–4938, ©1998 by the American Physical Society. Figure 4.13: R. Wolkow and P. Avouris (1988), Atom-resolved surface chemistry using scanning tunneling microscopy, *Physical Review Letters*, **60**, 1049–1052, ©1988 by the American Physical Society. Figure 4.14: Reproduced with permission of M. Tortonese and ThermoMicroscopes. Figure 5.2: Reprinted with permission of Oxford University Press from C. P. Flynn, *Point Defects and Diffusion*, Clarendon Press, Oxford, p. 38, ©1972. Figure 5.3: Reprinted by permission of the McGraw-Hill companies from M. Hansen, *Constitution of Binary Alloys*, McGraw Hill, New York, 2nd ed, ©1958. Figure 5.7: Figure due to B. Hockey, attributed to E. Fuller, and published by R. Thomson (1986), The physics of fracture, *Solid State Physics: Advances in Research and Applications*, **39**, 1–129, reprinted with permission from all parties. Figure 5.8(A): Reprinted from S. M. Allen and J. W. Cahn, A microscopic theory for antiphase boundary motion and its application to antiphase domain coarsening, *Acta Metallurgica*, **27**, 1085–1095, ©1979, with permission from Elsevier Science. Figure 5.8(B): Reprinted courtesy of L. A. Boatner, J. Gardner, and D. Corrigan, Oak Ridge National Laboratory. Figure 5.9(A): After R. Winter, P. A. Egelstaff, W.-C. Pilgrim, and W. S. Howells (1990), The structural properties of liquid, solid and amorphous sulphur, *Journal of Physics: Condensed Matter*, **2**, SA215–SA218. Figure 5.9(B): After C. Vega, C. McBride, E. Sanz, and J. L. F. Abascal (2005), Radial distribution functions and densities for the SPC/E, TIP4P and TIP5P models for liquid water and ices I_h , I_c , II, III, IV, V, VI, VII, VIII, IX, XI and XII, *Physical Chemistry and Chemical Physics*, **7**, 1450–1456, reproduced by permission of PCCP Owner Societies. Figure 5.10: Reprinted by permission of the McGraw-Hill companies from Y. Waseda (1980), *The Structure of Non-Crystalline Materials: Liquids and Amorphous Solids*, McGraw Hill, New York, p. 91. Figure 5.13: N. O. Birge and S. R. Nagel, Specific-heat spectroscopy of the glass transition, *Physical Review Letters*, **54**, 2674–

2677, ©1985 by the American Physical Society. Figure 5.21: After D. A. Weitz and D. J. Pine (1993), Diffusing-wave spectroscopy, in *Dynamic Light Scattering: the Method and Some Applications*, W. Brown, ed., Clarendon, Oxford. Figure 5.22: D. Shechtman, I. Blech, D. Gratias, and J. W. Cahn, Metallic phase with long-range orientational order and no translational symmetry, *Physical Review Letters*, **53**, 1951–1953, ©1984 by the American Physical Society. Figure 5.23: A. R. Kortan, Quasicrystals, in *Encyclopedia of Applied Physics*, G. L. Trigg, ed., vol. 15, ©1996, VCH, New York. Figure 5.31: A. R. Kortan, Quasicrystals, in *Encyclopedia of Applied Physics*, G. L. Trigg, ed., vol. 15, ©1996, VCH, New York. Figure 9.3: After L. Cândido, B. Bernu, and D. M. Ceperley (2004), Magnetic ordering of the three-dimensional Wigner crystal, *Physical Review B*, **70**, 094413/1–6, Figure 1©2005, American Physical Society. Figure 11.2: From J. M. Zuo, M. Kim, M. O’Keeffe, and J. C. H. Spence (1999), Direct observation of *d*-orbital holes and Cu-Cu bonding in Cu₂O, *Nature*, **401**, 49–51. Adapted by permission from Macmillan Publishers Ltd. Figure 12.2: Permission for Figure 5.5 from *The Physics of Rubber Elasticity* by L. R. G. Treloar, third edition, granted by The Royal Society for Chemistry. Figure 13.9: Reprinted from G. Dolling and R. A. Cowley (1966), The thermodynamic and optical properties of germanium, silicon, diamond, and gallium arsenide, *Proceedings of the Physical Society (London)*, **88**, 463–504, with permission of publisher. Figure 13.14: Reprinted from Y. S. Touloukian, R. K. Kirby, R. E. Taylor, and P. D. Desai (1975), *Thermal Expansion: Metallic Elements and Alloys*, vol. 12 of *Thermophysical Properties of Matter*, IFI/Plenum, New York, with permission of publisher. Figure 13.18: S. Wei and M. Y. Chou, Phonon dispersions of silicon and germanium from first-principles calculations, *Physical Review B*, **50**, 2221–2226, ©1994 by the American Physical Society. Figure 13.19: Reprinted with permission from E. G. Brovman and Y. M. Kagan, Phonons in nontransition metals, *Soviet Physics Uspekhi*, **17**, 125–152, ©1974, American Institute of Physics. Figure 13.20 (B): R. S. Preston, S. S. Hanna, and J. Heberle, Mössbauer effect in metallic iron, *Physical Review*, **128**, 2207–2218, ©1962 by the American Physical Society. Figure 14.8: Reprinted from S. Amelinckx, *The Direct Observation of Dislocations*, ©1964, Academic Press. Figure 14.9(A): Reprinted with permission of J. Humphreys, Manchester University. Figure 14.9(B): Reprinted from A. B. Cullis, N. G. Chew, and J. L. Hutchison, Formation and elimination of surface ion milling defects in cadmium telluride, zinc sulphide, and zinc selenide, *Ultramicroscopy*, **17**, 203–212, ©1985 with permission of Elsevier Science. Figure 14.12: Reprinted with permission, from the Annual Review of Physical Chemistry, Volume 47, ©1996, by Annual Reviews Inc. Figure 15.4: From J. D. Ferry, *Viscoelastic Properties of Polymers*, John Wiley and Sons, New York, ©1980. Reprinted by permission of John Wiley & Sons, Inc. Figure 15.7: After M. S. Paoletti, R. B. Fiorito, K. R. Sreenivasan, and D. P. Lathrop (2008), Visualization of superfluid helium flow, *Journal of the Physical Society of Japan*, **77**, 111007/1–7, Figure 5. Figure 15.8: Reprinted with permission from R. J. Donnelly, *Quantized Vortices in Helium II*, Cambridge University Press, Cambridge, ©1991. Figure 15.9: P. W. Karn, D. R. Starks, and W. Zimmerman, Observation of quantization of circulation in rotating superfluid ⁴He, *Physical Review B*, **21**, 1797–1805, ©1980 by the American Physical Society. Figure 15.10: Reprinted with permission from R. J. Donnelly, *Quantized Vortices in Helium II*, Cambridge University Press, Cambridge, ©1991. Figure 16.3: M. ben Dahan, E. Peik, J. Reichel, Y. Castin, and C. Salomon, Bloch oscillations of atoms in an optical potential, *Physical Review Letters*, **76**, 4508–4511, ©1996 by the American Physical Society. Figure 17.5: Reprinted with permission from N. E. Alekseevskii and Y. P. Gaidukhov, The anisotropy of magnetoresistance and the topology of Fermi surfaces of metals, *Soviet Physics JETP*, **10**, 481–484, ©1960, American Institute of Physics. Figure 17.6: After C. Zeng, Y. Yao, Q. Niu, and H. Weitering (2006), Linear magnetization dependence of the intrinsic anomalous Hall effect, *Physical Review Letters*, **96**, 037204/1–4, Figure 4c, ©2006, American Physical Society. Figure 17.8: W. R. Abel, A. C. Anderson, and J. C. Wheatley, Propagation of zero sound in liquid He³ at low temperatures, *Physical Review Letters*, **17**, 74–78, ©1966 by the American Physical Society. Figure 18.2: Reprinted with permission from T. F. Rosenbaum, The disordered insulator: electron glasses and crystals, in *Localization and Metal-Insulator Transitions*, H. Fritzsche and D. Adler, eds., pp. 1–8, Plenum, New York, ©1985. Figure 18.3: Reprinted with permission from P. P. Edwards and M. J. Sienko, The transition to the metallic state, *Accounts of Chemical Research*, **15**, 87–93, ©1982, American Chemical Society. Figure 18.10: M. Ahlskog, R. Menon, A. J. Heeger, T. Noguchi, and T. Ohnishi, Metal-insulator

transition in oriented poly(*p*-phenylenevinylene), *Physical Review B*, **55**, 6777–6787, ©1997 by the American Physical Society. Figure 18.12: From M. Bockrath, D. H. Cobden, J. Lu, A. G. Rinzler, R. E. Smalley, L. Balents, and P. L. McEuen (1999), Luttinger-liquid behaviour in carbon nanotubes, *Nature*, **397**, 598–601. Adapted by permission from Macmillan Publishers Ltd. Figure 19.20 (B): B. J. van Wees, H. van Houten, C. W. J. Beenakker, J. G. Williamson, L. P. Kouwenhoven, D. van der Marel, and C. T. Foxon, Quantized conductance of point contacts in a two-dimensional electron gas, *Physical Review Letters*, **60**, 848–850, ©1988 by the American Physical Society. Figure 19.23: Reprinted with permission from U. Meirav and E. B. Foxman, Single-electron phenomena in semiconductors, *Semiconductor Science and Technology*, **10**, 255–284, ©1996, Institute of Physics Publishing. Figure 21.3: R. N. Dexter, H. J. Zeiger, and B. Lax, Cyclotron resonance experiments in silicon and germanium, *Physical Review*, **104**, 637–44, ©1956 by the American Physical Society. Figure 21.4: Reprinted with permission from E. J. Johnson, Absorption near the fundamental edge, in *Semiconductors and Semimetals*, R. K. Willardson and A. C. Beer, eds., vol. 3, pp. 153–258, Academic Press, New York ©1967 Academic Press. Figure 21.5: M. D. Sturge, Optical absorption of gallium arsenide between 0.6 and 2.75 eV, *Physical Review*, **127**, 768–773, ©1962 by the American Physical Society. Figure 21.6: G. G. Macfarlane, T. P. McLean, J. E. Quarrington, and V. Roberts, Fine structure in the absorption-edge spectrum of Ge, *Physical Review*, **108**, 1377–1383, ©1957 by the American Physical Society. Figure 21.8: P. W. Baumeister, Optical absorption of cuprous oxide, *Physical Review*, **121**, 359–362, ©1961 by the American Physical Society. Figure 22.7: Courtesy of H. Pick, reprinted from Structure of trapped electron and trapped hole centers in alkali halides: “Color centers”, in *Optical Properties of Solids*, F. Abelès, ed., pp. 654–747, North-Holland, Amsterdam, ©1972. Figure 22.8: Reprinted with permission from H. Seidel and H. C. Wolf, ESR and ENDOR spectroscopy of color centers in alkali halide crystals, in *Physics of Color Centers*, W. B. Fowler, ed., pp. 537–624, Academic Press, New York, ©1968. Figure 22.13: Reprinted with permission from U. Haupt, On the temperature dependence and form of the long wavelength excitation band in KI crystals, *Zeitschrift für Physik*, **157**, 232–246, ©1959, Springer-Verlag. Figure 23.4: Reprinted with permission from W. Lang, Velocity loss of medium speed electrons during passage through thin metal foils, *Optik (Stuttgart)*, **3**, 233–246, ©1948. Figure 23.5: Reprinted with permission from C. Kunz, On the angular dependence of characteristic energy loss in Al, Si, Ag, *Zeitschrift für Physik*, **167**, n 53–71, ©1962, Springer-Verlag. Figure 23.7: N. V. Smith, Photoemission studies of the alkali metals. ii: rubidium and cesium, *Physical Review B*, **3**, 3662–3670, ©1970 by the American Physical Society. Figure 23.8: Reprinted with permission of author. Figure 23.9: J. R. Sandercock, Brillouin-scattering measurements on silicon and germanium, *Physical Review Letters*, **28**, 237–240, ©1972 by the American Physical Society. Figure 23.10: C. H. Henry and J. J. Hopfield, Raman scattering by polaritons, *Physical Review Letters*, **15**, 964–966, ©1965 by the American Physical Society. Figure 23.11: Reprinted with permission from B. Dorner, E. Burkel, T. Illini, and J. Peisl, First measurement of a phonon dispersion curve by inelastic X-ray scattering, *Zeitschrift für Physik B: Condensed Matter*, **69**, 179–183, ©1987, Springer-Verlag. Figure 23.12: F. Patthey, J. M. Imer, W. D. Schneider, H. Beck, Y. Baer, and B. Delly (1990), High-resolution photoemission study of the low-energy excitations in 4*f*-electron systems, *Physical Review B*, **42**, 8864–8881, ©1990 by the American Physical Society. Figure 23.14: E. Jensen, R. A. Bartynski, T. Gustafsson, E. W. Plummer, M. Y. Chou, M. L. Cohen, and G. B. Hoflund, Angle-resolved photoemission study of the electronic structure of beryllium: bulk band dispersions and many-electron effects, *Physical Review B*, **30**, 5500–5507, ©1984 by the American Physical Society. Figure 23.15: Reprinted from S. G. Louie Quasiparticle excitations and photoemission, in *Angle-Resolved Photoemission: Theory and Current Practice*, S. D. Kevan, ed., vol. 74 of *Studies in Surface Science and Catalysis*, pp. 33–98, Elsevier, Amsterdam, ©1992 with permission of Elsevier Science. Figure 23.17: R. J. Powell and W. E. Spicer, Optical properties of NiO and CoO, *Physical Review B*, **2**, 2182–93, ©1970 by the American Physical Society. Figure 24.3: R. S. Preston, S. S. Hanna, and J. Heberle, Mössbauer effect in metallic iron, *Physical Review*, **128**, 2207–2218, ©1962, by the American Physical Society. Figure 24.4(A): Reprinted from J. A. Hofmann, A. Paskin, K. J. Tauer, and R. J. Weiss (1956), Analysis of ferromagnetic and antiferromagnetic second-order transitions, *Journal of Physics and Chemistry of Solids*, **1**, 45–60 with permission from Elsevier Science. Figure 24.4(B): B. T. Matthias, R. M. Bozorth, and J. H. van Vleck, Ferromagnetic interactions in

EuO, *Physical Review Letters*, **7**, 160–161, ©1961 by the American Physical Society. Figure 24.5: Reprinted with permission from F. Bertaut and R. Pauthenet (1957), Crystalline structure and magnetic properties of ferrites having the general formula $5\text{Fe}_2\text{O}_3 \cdot 3\text{M}_2\text{O}_3$, *Proceedings of the Institution of Electrical Engineering*, Part B, **104**, Supplement 5, 261–264. Figure 24.13(A): P. Heller and G. B. Benedek, Nuclear magnetic resonance in MnF_2 near the critical point, *Physical Review Letters*, **8**, 428–432, ©1962 by the American Physical Society. Figure 24.13(B): E. A. Guggenheim, The principle of corresponding states, *Journal of Chemical Physics*, **13**, 253–261, ©1945, the American Institute of Physics. Figure 24.14: Reprinted with permission from M. Vicentini-Missoni, Equilibrium scaling in fluids and magnets, in *Phase Transitions and Critical Phenomena*, C. Domb and M. S. Green, eds., vol. 2, pp. 39–77, Academic Press, London, ©1972 Academic Press. Figure 25.5: Reprinted with permission from A. Tonomura, *Electron Holography*, Springer-Verlag, Berlin, ©1993, Springer-Verlag. Figure 25.7: Reprinted with permission from M. E. Cage, Experimental aspects and metrological applications, in *The Quantum Hall Effect*, R. E. Prange and S. M. Girvin, eds., pp. 37–68, Springer-Verlag, New York, ©1987, Springer-Verlag. Figure 25.10: Reprinted with permission from A. M. Chang, Experimental aspects, in *The Quantum Hall Effect*, R. E. Prange and S. M. Girvin, eds., pp. 175–232, Springer-Verlag, New York, ©1987, Springer-Verlag. Figure 25.11: L. Saminadayar, D. C. Glatli, Y. Jin, and B. Etienne, Observation of the $e/3$ fractionally charged Laughlin quasiparticle, *Physical Review Letters*, **79**, 2526–2529, ©1997 by the American Physical Society. Figure 26.4(A): M. Yethiraj, R. A. Robinson, D. S. Sivia, J. W. Lynn, and H. A. Mook, Neutron-scattering study of the magnon energies and intensities in iron, *Physical Review B*, **43**, 2565–2574, ©1991 by the American Physical Society and J. W. Lynn, Temperature dependence of the magnetic excitations in iron, *Physical Review B*, **11**, 2624–2637, ©1975 by the American Physical Society. Figure 26.4(B): Reprinted from M. Ain, W. Reichardt, B. Hennion, G. Pepy, and B. M. Wanklyn (1989), Magnetic excitations in CuO, *Physica C*, **162–164**, 1279–1280, with permission from Elsevier Science. Figure 26.5(A): After G. Binasch, P. Grünberg, F. Saurenbach, and W. Zinn (1989), Enhanced magnetoresistance in layered magnetic structures with antiferromagnetic interlayer exchange, *Physical Review B*, **39**, 4828–4830, Figure 2d, ©1989, American Physical Society. Figure 26.5(B): After M. N. Baibich, J. M. Broto, A. Fert, et al. (1988), Giant magnetoresistance of (001)Fe/(001)Cr magnetic superlattices, *Physical Review Letters*, **61**(21), 2472–2475, Figure 3, ©1988, American Physical Society. Figure 26.7 Adapted from D. Ralph and M. Stiles (2008), Spin transfer torques, *Journal of Magnetism and Magnetic Materials*, **320**(7), 1190–1216 with permission from Elsevier. Figure 26.8: M. Sarachik, E. Corenzwit, and L. D. Longinotti, Resistivity of MoNb and MoRe alloys containing 1% Fe. *Physical Review*, **135**, A1041–A1045, ©1964 by the American Physical Society. Figure 26.11: H. R. Ott, H. Rudigier, Z. Fisk, and J. L. Smith, UBe_{13} : An unconventional actinide superconductor, *Physical Review Letters*, **50**, 1595–98, ©1983 by the American Physical Society. Figure 27.2(A): Reprinted with permission from A. Tonomura, *Electron Holography*, Springer-Verlag, Berlin, ©1993, Springer-Verlag. Figure 27.4: B. S. Deaver and W. M. Fairbank, Experimental evidence for quantized flux in superconducting cylinders, *Physical Review Letters*, **7**, 43–46, ©1961 by the American Physical Society. Figure 27.5: Courtesy of R. C. Jaklevic. Figure 27.8: C. A. Reynolds, B. Serin, W. H. Wright, and L. B. Nesbitt, Superconductivity of isotopes of mercury, *Physical Review*, **78**, 487, ©1950, the American Physical Society. Figure 27.11(A): H. A. Boorse, Superconducting electronic specific heats, the “exponential law,” and the Bardeen, Cooper, Schrieffer theory, *Physical Review Letters*, **2**, 391–393, ©1959, the American Physical Society. Figure 27.11 (B): Y. Masuda and A. G. Redfield, Nuclear spin relaxation in superconducting aluminum, *Physical Review*, **125**, 159–163, ©1962 by the American Physical Society. Figure 27.14: Using several sources, but primarily T. Nakano, N. Momono, M. Oda, and M. Ido (1998), Correlation between the doping dependences of superconducting gap magnitude 2δ and pseudogap temperature t^* in high- t_c cuprates, *Journal of the Physical Society of Japan*, **67**, 2622–2625. Figure 27.15: After H. Ding, M. R. Norman, J. C. Campuzano, et al. (1996), Angle-resolved photoemission spectroscopy study of the superconducting gap anisotropy in $\text{Bi}_2\text{Sr}_2\text{CaCu}_2\text{O}_{8+x}$, *Physical Review B*, **54**(14), R9678–R9681, Figure 2, ©1996, American Physical Society.

Condensed Matter Physics, Second Edition
by Michael P. Marder
Copyright © 2010 John Wiley & Sons, Inc.

Part I

ATOMIC STRUCTURE

1. The Idea of Crystals

1.1 Introduction

From the point of view of the physicist, a theory of matter is a policy rather than a creed; its object is to connect or co-ordinate apparently diverse phenomena, and above all to suggest, stimulate and direct experiment.

—Thomson (1907), p. 1

The goal of condensed matter physics is to understand how underlying laws unfold themselves in objects of the natural world. Because the complexity of condensed matter systems is so enormous, the number of atoms they involve so great, and the possibility of solving all underlying equations in full detail so remote, the laws of greatest importance are principles of symmetry.

A first step is to describe how atoms are arranged. As a mental image of arrangement, the idea of the *crystal* has emerged out of an obscure class of minerals to dominate thought about all solids. Here is symmetry with a vengeance. A small group of atoms repeats a simple pattern endlessly through the stretches of a macroscopic body. The most precise experiments and the most detailed theories of solids are all carried out in perfect crystals. Yet the world is neither a collection of crystals, nor a collection of solids wishing to be crystals but falling short of perfection. Principles of symmetry more general than crystalline order still function in structures bearing no resemblance to the perfect lattice, while a rigid insistence upon considering only solids in crystalline form would force one to abandon most naturally occurring substances and technologically important materials. Nevertheless, the science of condensed matter physics begins with the crystal, its single most important structural idea.

In Greek, the word $\kappa\rho\upsilon\sigma\tau\alpha\lambda\lambda\omicron\varsigma$ originally referred to ice. In the middle ages, the word “crystal” first referred to quartz, and later to any solid whose external form consisted of flat faces intersecting at sharp angles (Figure 1.1). The first law of *crystal habit*, discovered by Steno (1671), and illustrated in Figure 1.2, states that corresponding faces of quartz always meet at the same angle. The second law of crystal habit (see Problem 9 in Chapter 2), discovered by Haüy (1801), states that if one takes three edges of a crystal as coordinate axes and then asks where the planes of other faces intersect these axes, the three intersection points are always rational multiples of one another. Haüy explained this law by assuming, as many other scientists had done since around 1750, that crystals were built of vast numbers of identical units, perhaps small polyhedra, stacked together in a regular fashion.

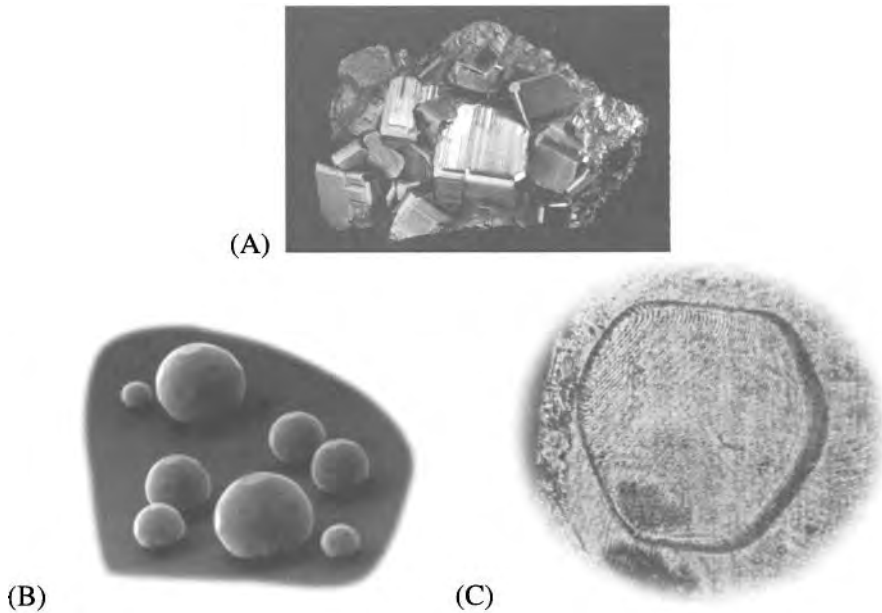


Figure 1.1. (A) Naturally occurring crystals of iron pyrite, showing the intersection of flat faces at definite angles that characterizes the external appearance of all crystals. (Courtesy of J. Sharp, University of Texas.) (B) Small equilibrium crystals of gold at 1000 °C, roughly 5 μm in diameter, showing alternating smooth and faceted surfaces. [Source: Heyraud and Métois (1980), p. 571.] (C) Equilibrium crystal of solid ^4He at 0.8 K. (Courtesy of S. G. Lipson, Technion; see Lipson (1987).)

Figure 1.2(A) shows one of his diagrams, the earliest published image of crystalline arrangement.

As the nineteenth century progressed, an elaborate mathematical theory of symmetry developed, showing that observed symmetries of natural crystals could be identified with the symmetries of regular lattices. The complete enumeration of all possible classes of crystals was completed in 1890, waiting for the discovery of X-ray scattering two decades later that would make it possible to specify crystals down to atomic detail.

1.1.1 Why are Solids Crystalline?

Crystalline order is the simplest way that atoms could possibly be arranged to form a macroscopic solid. Small basic units of atoms repeat endlessly, one placed next to the other, so the whole solid can be described completely by studying a small number of atoms. It is remarkable that this simple structural model can be used to understand so much.

Why are low-energy arrangements of atoms so often periodic? No one really knows. A simple explanation is that if there is some optimal neighborhood for each atom, then the lowest energy state for a large number of atoms gives this same neighborhood to every atom. One might try to check this idea by imagining how

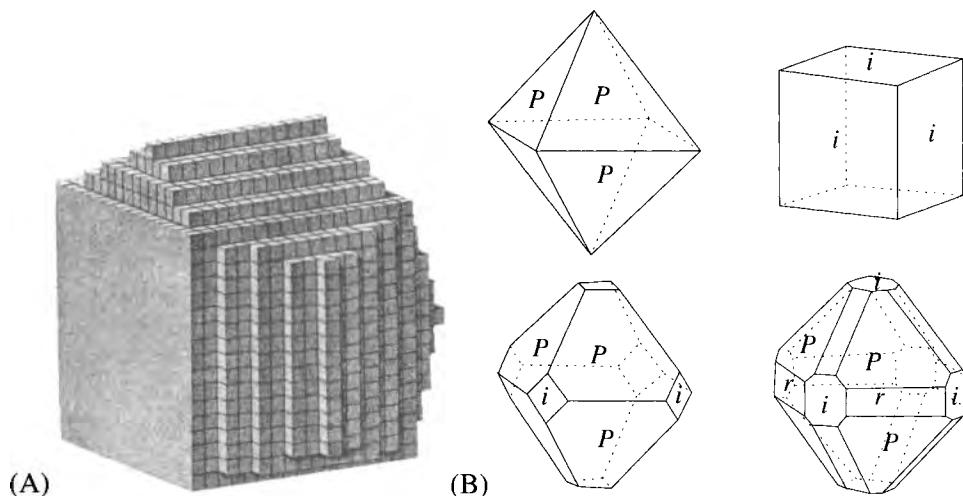


Figure 1.2. (A) The first published picture of the structure of a crystal. [Source: Häüy (1801).] (B) The first law of crystal habit states that when various crystals can be oriented so that their faces can be placed in one-to-one correspondence, with all corresponding faces parallel, then all angles between the faces are the same. The sketches of red copper oxide (Cyprus oxide, Cu_2O) are taken from Häüy (1801), Plate 71. A comprehensive catalog of such diagrams was compiled by Groth (1906–1919).

the energy of a collection of atoms depends upon their relative locations, writing down an energy functional, and then minimizing the functional with respect to all atomic positions (Problem 5). Such a calculation is a serious oversimplification, mainly because it ignores most of the complexities of quantum mechanics, but even in this context there is no theorem to prove that periodic arrays provide ground states. Nevertheless, for almost all the elements and for a vast array of compounds, the lowest energy state is crystalline. The only exception among the elements is helium, which remains liquid at zero temperature and standard pressure.

Equilibrium lattice structure are functions of temperature and pressure. Even at temperatures where vibrations about a particular state are small, the entropy associated with the vibrations may be enough to cause the ions to switch from one configuration to another. This switch is possible because the differences in energy between different crystalline configurations can be very small: according to Table 11.9, as little as one part in 10^4 . Examining a source such as Emsley (1998) shows that most elements change crystal structure several times before they melt. In some cases, more than one crystalline form of an element or compound may be stable at a given temperature and pressure; such compounds are *allotropic*. Carbon at room temperature is stable both as graphite and as diamond, while tin comes as gray tin or white tin, the first of which is a semiconductor and the second of which is a metal. Only one of these states can be a true equilibrium state, yet the time to transform spontaneously from one to the other is so immense that this possibility may safely be neglected.

Even should it eventually be proved that the lowest energy state of assemblages

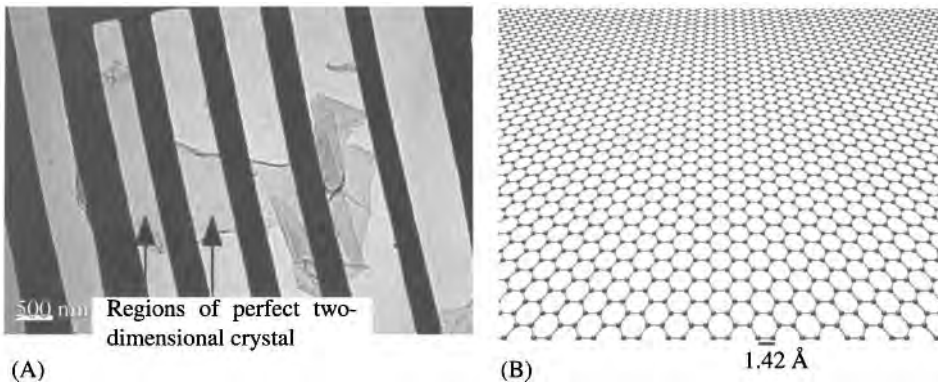


Figure 1.3. (A) Two dimensional crystal of carbon just one atom thick, in the form of *graphene*, hanging freely from a metal scaffold [Source: Meyer et al. (2007), p. 60]. (B) Theoretical image of the honeycomb lattice of graphene at the atomic scale. The spheres represent carbon atoms, and the rods indicate attractive bonds between nearest neighbors.

of atoms really is crystalline, it does not follow that perfect crystalline structures will always appear in nature or provide the greatest interest for study. The world is largely constructed of solids whose crystalline order is defective, or absent altogether.

1.2 Two-Dimensional Lattices

A *crystal* is a solid where the atoms are arranged in the form of a *lattice*. A lattice is an arrangement of points where the same pattern repeats over and over again. If one were to move from place to place over a lattice taking photographs it would be impossible to tell one part of the lattice from another. Two-dimensional lattices are much easier to picture and understand than their three-dimensional counterparts. Therefore, all the central definitions for lattices will first be introduced in a two-dimensional setting. Two-dimensional lattices are not mathematical fictions. They naturally occur as surfaces and interfaces of three-dimensional crystals, and sometimes are created free-standing in their own right (Figure 1.3).

1.2.1 Bravais Lattices

The simplest type of lattice is called a *Bravais lattice*. In a Bravais lattice the neighborhood of each and every point is exactly the same as the neighborhood of every other point. In two dimensions, the location of every point in such a lattice can be described in the form

$$\vec{R} = n_1 \vec{a}_1 + n_2 \vec{a}_2, \quad n_1 \text{ and } n_2 \text{ are integers.} \quad (1.1)$$

where the two-dimensional vectors \vec{a}_i are called *primitive vectors* and must be linearly independent. The choice of primitive vectors is not unique—one makes choices that are as simple as possible or that have some nice symmetry to them.

Example: Hexagonal Lattice. To create a hexagonal lattice, take

$$\vec{a}_1 = a(1 \ 0) \quad a \text{ is the lattice spacing illustrated in Figure 1.4.} \quad (1.2a)$$

$$\vec{a}_2 = a \begin{pmatrix} 1 & \sqrt{3} \\ 2 & 2 \end{pmatrix}. \quad (1.2b)$$

To illustrate that this choice is not unique, one can equally well choose

$$\vec{a}'_1 = a \begin{pmatrix} -1 & \sqrt{3} \\ 2 & 2 \end{pmatrix} \quad (1.3a)$$

$$\vec{a}'_2 = a \begin{pmatrix} 1 & \sqrt{3} \\ 2 & 2 \end{pmatrix}. \quad (1.3b)$$

One way to make a mistake is to choose a set of vectors that is not linearly independent. For example, trying to build the hexagonal lattice out of the three vectors

$$\vec{a}''_1 = a(1, 0) \quad (1.4a)$$

$$\vec{a}''_2 = a \begin{pmatrix} -1 & \sqrt{3} \\ 2 & 2 \end{pmatrix} \quad (1.4b)$$

$$\vec{a}''_3 = a \begin{pmatrix} 1 & \sqrt{3} \\ 2 & 2 \end{pmatrix} \quad (1.4c)$$

would constitute an error since $\vec{a}''_1 = \vec{a}''_3 - \vec{a}''_2$.

1.2.2 Enumeration of Two-Dimensional Bravais Lattices

In two dimensions there are five Bravais lattices, shown in Figure 1.4.

Square Lattice: The *square lattice* is symmetric under reflection about both x and y axes and with respect to 90° rotations.

Rectangular Lattice: When compressed along one axis, the square lattice loses the 90° rotational symmetry and becomes the *rectangular lattice*.

Hexagonal Lattice: The *hexagonal* (or *triangular*) lattice is invariant under reflections about the x and y axes as well as with respect to 60° rotations.

Centered Rectangular: The *centered rectangular lattice* results from a compression of the hexagonal lattice and loses the 60° rotational symmetries.

Oblique Lattice: Finally, an arbitrary choice of \vec{a}_1 and \vec{a}_2 with no special symmetry results in an *oblique lattice*. This lattice still possesses inversion symmetry, $\vec{r} \rightarrow -\vec{r}$.

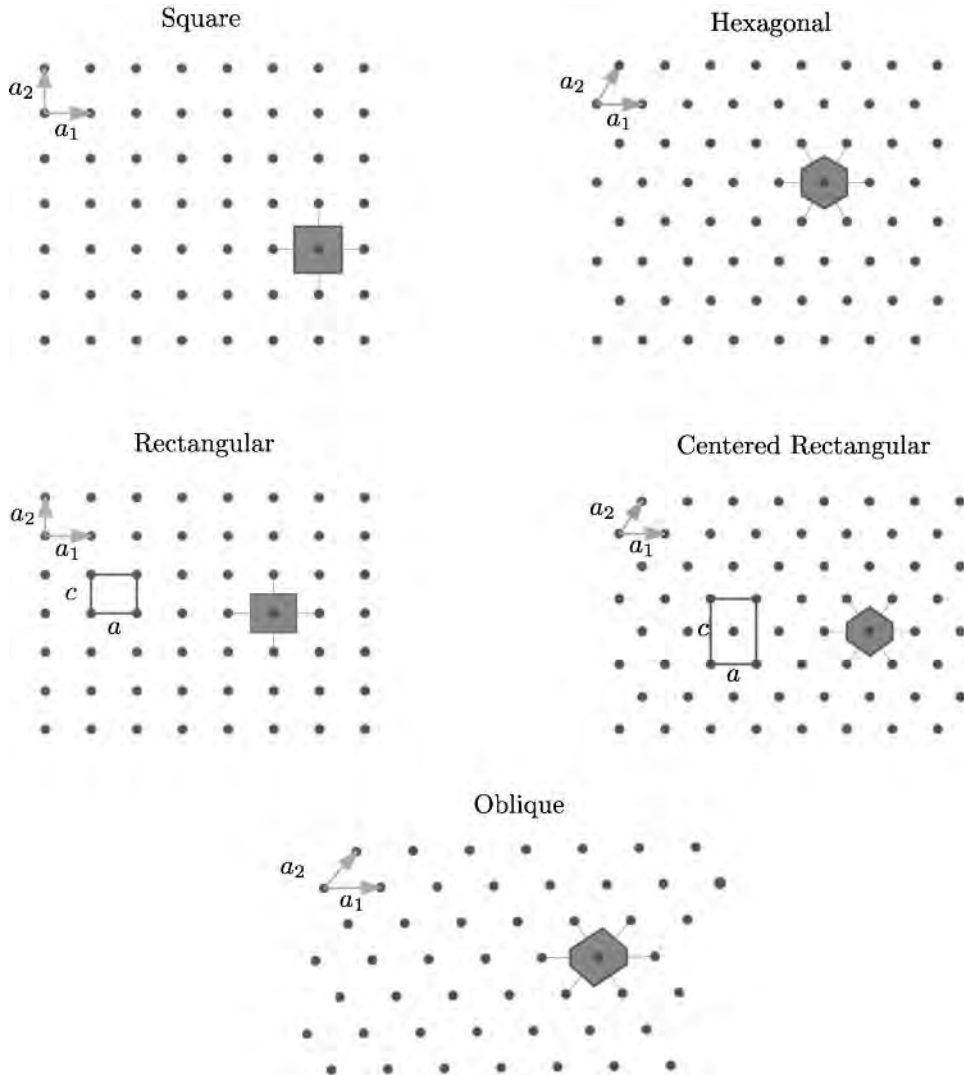


Figure 1.4. The five two-dimensional Bravais lattices. Note that the centered rectangular lattice can be built by repetition of the structure in the hollow box, which shows how it obtains its name. The figure also shows Wigner–Seitz cells for each lattice. One constructs them by choosing some point 0 in the lattice and then drawing the perpendicular bisector of the line between 0 and each of its neighbors. The Wigner–Seitz cell is the region surrounding 0 contained within all these perpendicular bisectors.

1.2.3 Lattices with Bases

It is important to emphasize that the neighborhoods of all particles must be identical under translation in order for a structure to qualify to be a Bravais lattice. Most lattices occurring in nature are not Bravais lattices, but are lattices with a *basis*. Lattices of this type are constructed by beginning with a Bravais lattice, but putting at each lattice site an identical assembly of particles, rather than a single rotationally invariant particle.

Example: Honeycomb Lattice. The *honeycomb lattice*, shown in Figure 1.5, is a lattice with a basis. One can construct it by starting with a hexagonal lattice with primitive vectors of Eq. (1.2) and then decorating every lattice point with basis particles at

$$\vec{v}_1 = a \begin{pmatrix} 0 & \frac{1}{2\sqrt{3}} \end{pmatrix} \quad (1.5a)$$

$$\vec{v}_2 = a \begin{pmatrix} 0 & -\frac{1}{2\sqrt{3}} \end{pmatrix}. \quad \text{The basis vectors are being described in Cartesian coordinates.} \quad (1.5b)$$

Another way to describe basis vectors is in terms of a non-Cartesian coordinate system, where the coordinates refer to multiples of the primitive vectors:

$$\vec{v}_1 = (1/6 \ 1/6) \quad \text{Since } \vec{a}_1/6 + \vec{a}_2/6 = a \begin{pmatrix} \frac{1}{2\sqrt{3}} & 0 \end{pmatrix} = \vec{v}_1. \quad (1.6a)$$

$$\vec{v}_2 = (-1/6 \ -1/6). \quad (1.6b)$$

The left- and right-hand particles in each cell find their neighbors off at different sets of angles. Notice, however, that the neighborhood of every particle is identical if one is allowed to rotate it through $\pi/3$ before making comparisons. While this fact does not make the honeycomb lattice a Bravais lattice, it means that the qualitative arguments explaining why one expects crystalline ground states for interacting particles work just as well for lattices with bases as they do for true Bravais lattices.

Selective Destruction of Symmetry by a Basis. Once one decorates a lattices with a basis, its symmetries change. Adding a basis does not automatically destroy the rotational and reflection symmetries of the original lattice; in general, these symmetries can be destroyed selectively by adding basis elements of various types. For example, if one builds a triangular lattice and then decorates it as shown in Figure 1.6, the rotational symmetries of the original triangular lattice are preserved, but the reflection symmetries are gone.

1.2.4 Primitive Cells

Because lattices are created by repeating small basic units over and over throughout space, the full information of a crystal can be contained in a small region of space. Such a region, chosen to be as small as it can be, is called a *primitive unit cell*. For example, for the square lattice, a square can be used as a primitive cell, as shown in Figure 1.7 (A).

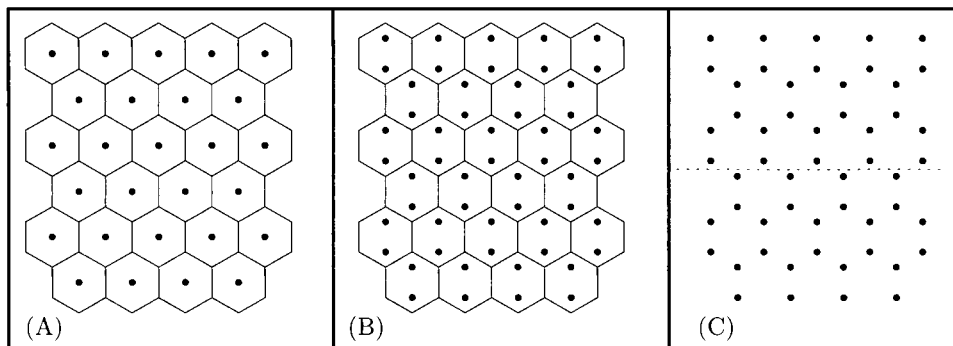


Figure 1.5. One may construct the honeycomb lattice by beginning with a hexagonal lattice (A), and replacing the single point in the center of each cell with a pair of points, as shown in (B). The honeycomb lattice is more obviously visible in (C). Because the top and bottom particles in each cell do not have identical neighborhoods, the honeycomb lattice is a lattice with a basis, and not a Bravais lattice. The dotted line is a glide line; the lattice is invariant when translated horizontally by $a/2$ and reflected about this line, but is not invariant under either operation separately.

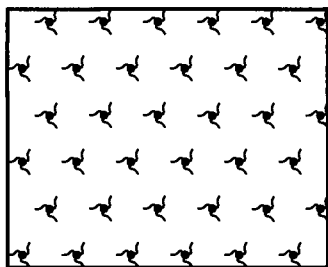
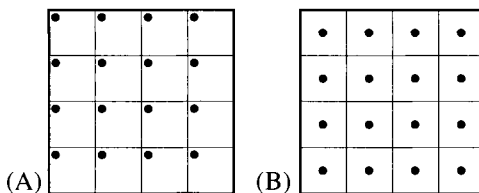


Figure 1.6. A triangular lattice decorated with chiral molecules so as to lose reflection symmetries.

Figure 1.7. Two primitive cells for the square lattice: one cell has a particle at the corner, while the other has a particle at the center.



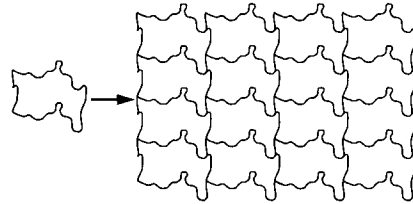
Primitive cells are not unique, as one can see by comparing Figures 1.7(A) and 1.7(B). However all different choices must have exactly the same area. The reason is that in a Bravais lattice the primitive cell contains exactly one particle, while the primitive cells put end to end fill the crystal; therefore the volume of the primitive cell is exactly the inverse of the density of the crystal. Cells are free to have rather peculiar shapes, as in Figure 1.8, just so long as they fit together properly. In two dimensions, one says they form a *tiling* or a *tessellation*.

1.2.5 Wigner–Seitz Cells

It is convenient to have a standard way of constructing the primitive cell, and it is valuable to have a primitive cell invariant under all symmetry operations that

leave the crystal invariant. Such a construction is provided by the *Wigner–Seitz primitive cell*. It is built by associating with each lattice point all of space which is closer to it than to any other lattice point. Because this relation does not change under any operation that leaves the lattice invariant, the Wigner–Seitz cell displays the full symmetry of the lattice. The Wigner–Seitz cells for the symmetrical two-dimensional Bravais lattices are shown in Figure 1.4, where their construction is also described.

Figure 1.8. An unusual tiling of the plane, as discussed by MacGillavry (1976).



Frequently a convenient way to display the full structure of a crystal is by drawing a *nonprimitive unit cell*: one that contains several particles and that produces the full crystal upon repetition. The rectangular box used in Figure 1.4 to illustrate the construction of the centered rectangular lattice provides an example.

1.3 Symmetries

The word symmetry has been used casually in discussing the two-dimensional Bravais lattices, but before continuing to the three-dimensional lattices, it is best to make it a bit more precise.

One motivation for studying crystal structure from the point of view of symmetries is that these are intimately bound up with the experimental observations one is able to make. In the case of scattering, to be studied in Chapter 3, the intensities of peaks result from hosts of details, but the fact of sharp peaks is exclusively the result of lattice symmetries; to understand what a scattering experiment means, one must understand what crystalline symmetries are possible. Equally important is the fact that solutions of Schrödinger's equation in Chapter 7 for electrons in periodic crystals will only be possible when simplifications resulting from symmetry are fully employed.

1.3.1 The Space Group

The general view of symmetries begins from the observation that one is interested in picking the lattice up, moving it rigidly, perhaps rotating or reflecting it, placing it back down, and finding that all the points following this operation overlap the original points. That is, problem is to find the complete set of ways that a given crystal can be transformed so that the distances between all points are preserved, and the crystal perfectly overlap itself after the transformation. Most rigid motions can be composed from simpler ones, so the real goal is to find a minimal set of transformations. Rigid motions include not only translations and rotations, which can be accomplished by twisting a body around in space, but also inversions.

Rigid motions can be described as a translation \vec{a} plus a rotation \mathcal{R} :

$$\mathbf{G} = \vec{a} + \mathcal{R}(\vec{r}, \hat{n}, \theta). \quad (1.7)$$

Explicit expressions for \mathcal{R} in terms of angles and rotation axes appear in books on classical mechanics such as Marion and Thornton (1988) or Goldstein (1980) under the heading of Euler angles.

$\mathcal{R}(\vec{r}, \hat{n}, \theta)$ produces a rotation through θ around axis \hat{n} passing through point \vec{r} . Operators \mathcal{R} that invert or reflect the crystal are also allowed.

The complete set of rigid motions that take a crystal into itself is called the *space group*. It is a group (formally defined in Section 7.3) because it consists of a set of operations (rigid motions) with a natural product (perform a first rigid motion, then another—the combined result is still a rigid motion). The unit element consists of doing nothing.

1.3.2 Translation and Point Groups

Two subgroups of the space group deserve special mention. The *translation group* consists of translations through all lattice vectors of the form $n_1\vec{a}_1 + n_2\vec{a}_2 \dots$, and by definition it leaves the crystal invariant. The *point group* consists of those operations that leave the crystal invariant and which in addition map some particular Bravais lattice point onto itself. It might seem that the space group is simply a product of the point group and the translation group. This is true for Bravais lattices, but not for crystals in general, since there can exist combinations of translation and reflection or rotation that leave a crystal invariant when used together but not separately. The honeycomb lattice (Figure 1.5C) is invariant when translated horizontally by $a/2$ and then reflected about a *glide line*. *Screw axes*, where a lattice is invariant under a combination of translation and proper rotation neither of which is itself a symmetry, first appear in three dimensions. A *nanotube* with symmetry of this type is shown in Figure 1.9.

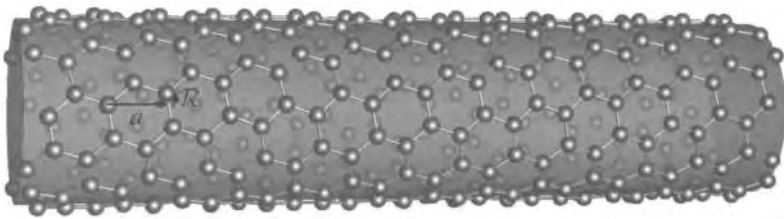


Figure 1.9. The points on this nanotube map back onto themselves after translation through \vec{a} and rotation through \mathcal{R} , but neither of these operations alone is a symmetry of the nanotube.

Does the point group of a lattice define the lattice? The answer is no. Different lattices can be invariant under precisely the same set of point symmetry operations. For example, the rectangular and centered rectangular lattices shown in Figure 1.4 have many symmetries in common:

Translational symmetries: The two crystals can be translated along arbitrary multiples of their two primitive vectors.

Point group symmetries: Choose any lattice point as the origin. Both rectangular and centered rectangular lattices can be reflected about the x or y axes, and each is invariant under a 180° rotation.

Because the rectangular and centered rectangular lattices share the same point group symmetries, they are said to belong to the same *crystal system*, but they are not the same lattice.

One might protest that the rectangular and centered rectangular lattices are obviously different because their primitive vectors are different. However, making this argument would lead one to conclude that two square lattices of different size are different as well. The correct question to ask in determining if two lattices are the same is whether one structure can be deformed continuously into the other without losing symmetries along the way. For example, if one lattice is twice the size of another, but otherwise the same, one would want to call them the same. Although centered rectangular and rectangular lattices share point group symmetries, they are different lattices and have different space groups. They are different because there exists no way to deform the first continuously into the second without temporarily destroying some symmetries, as indicated in Figure 1.10.

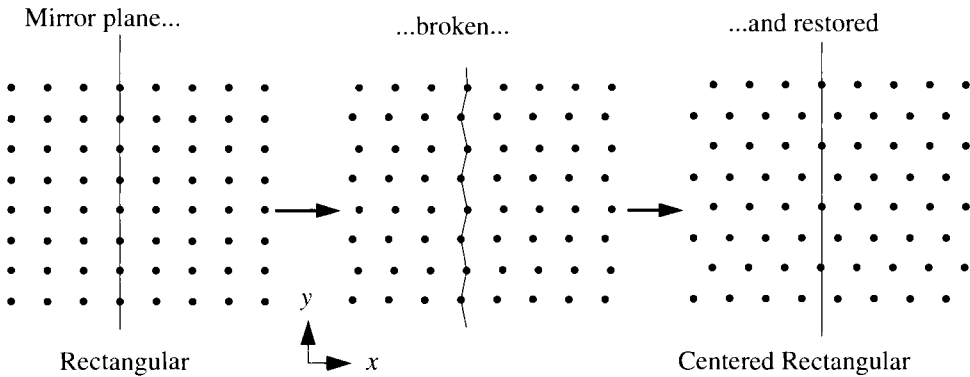


Figure 1.10. In deforming the rectangular lattice into the centered rectangular lattice, reflection symmetry about the y axis is destroyed.

A more formal expression of this same idea uses the idea of a change of coordinates. Suppose one has a first group of symmetry operations, $G = \mathcal{R} + \vec{a}$ and a second group $G' = \mathcal{R}' + \vec{a}'$. Then the two groups are equivalent if there exists a single matrix S (change of coordinates) such that

$$S^{-1}\mathcal{R}S + S^{-1}\vec{a} = \mathcal{R}' + \vec{a}'. \quad (1.8)$$

In other words, G and G' must be the same up to linear changes of coordinate systems. This definition of equivalent lattices is the same as the previous one, because once one has the matrix S , then there is a family of matrices

$$S_t = (1-t)S + tS', \quad (1.9)$$

which varies smoothly between the unit matrix and S as t varies between 0 and 1. It generates explicitly a smooth deformation of one lattice into the other while preserving the group operations.

1.3.3 Role of Symmetry

Perhaps symmetry is more important for physicists to understand the world than it is for the world itself. Most of the exact statements in physics result from symmetry arguments, and often symmetry provides the only path to making any substantive statement about complicated assemblies of matter. Its importance persists in condensed matter physics, although the discipline's domain includes disordered and noisy systems. Helpful books on the formal theory of symmetry in physics include Heine (1960) and Tinkham (1964).

Problems

1. Honeycomb lattice:

- Verify that the honeycomb lattice described by Eq. (1.5) has properly been constructed so that the distance between all neighboring points is identical.
- From Table 2.1, the lattice spacing of graphene is 2.46\AA . Find the distance between nearest neighbors (Figure 1.3).
- Find the density of graphene in gm/cm^2 .

2. Hexagonal lattice:

- The hexagonal lattice may be viewed as a special case of the centered rectangular lattice. Referring to Figure 1.4 and to the conventional unit cell depicted there, find the ratio c/a for which the centered rectangular lattice would become hexagonal.
- Enumerate the symmetries of the hexagonal lattice, and compare them with the symmetries of the centered rectangular lattice.

3. **Nanotube structures:** To form a *single-walled nanotube*, one rolls up a single atomic layer of graphite, graphene, as shown in Figure 1.11. Referring to Figure 1.11 (A) and (B), all nanotubes can be indexed with two integers m and n where $\vec{c} = m\vec{a}_1 + n\vec{a}_2$ and \vec{a}_1 and \vec{a}_2 are primitive vectors; one created in this way is an (m, n) -nanotube.

- Are all structures labeled by distinct pairs of integers $m, n \in (-\infty, \infty)$ different from each other?
- What are the indices for the nanotube appearing in (C)?
- Suppose that the atoms of a two-dimensional crystal lie at locations \vec{R} , and that the crystal is rolled into a cylinder by pulling together two atoms separated by vector \vec{c} as shown in Figure 1.11 (A). Write down an explicit expression for locations of atoms after the sheet has been rolled into a tube.

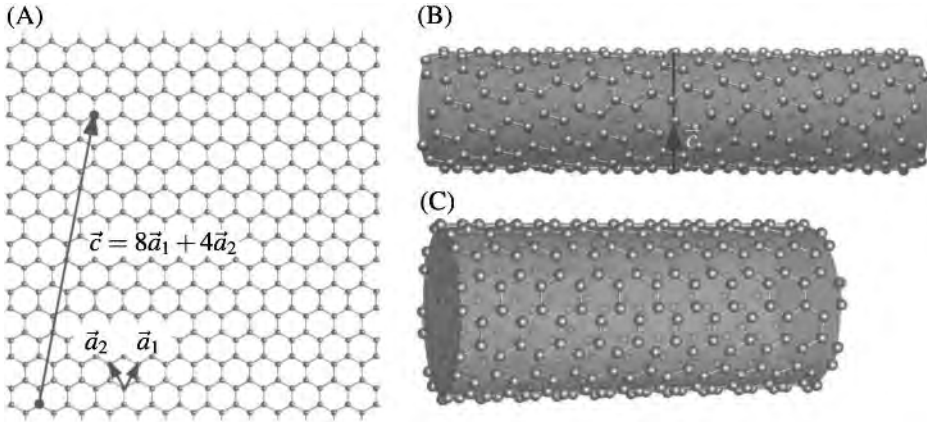


Figure 1.11. How to roll a sheet of graphene into a nanotube.

4. Allowed symmetry axes:

- (a) Consider a two-dimensional Bravais lattice that is left invariant after rotation by angle θ around the origin. Suppose the lattice to have points at $(0, 0)$ and $(a, 0)$. By requiring the image of $(a, 0)$ under rotations through $\pm\theta$ to be in the Bravais lattice, find a simple expression that implicitly specifies all possible rotation axes.
- (b) Prove that the only allowed axes are twofold, threefold, fourfold, and sixfold. In particular, it is impossible for a Bravais lattice to have a fivefold rotation axis.

5. Two-dimensional ground states:

Portions of this problem are most easily carried out with the aid of a computer algebra program or brief compiled programs.

- (a) Consider a collection of particles in two dimensions whose energy is

$$\mathcal{E} = \frac{1}{2} \sum_{i \neq j} \phi(r_{ij}) \quad (1.10)$$

where

$$\phi(r) = \begin{cases} \phi_0 \exp(-r) \left(\frac{1}{r^3} - 1 \right) & \text{if } r < 1.5 \\ 0 & \text{else,} \end{cases} \quad (1.11)$$

and r_{ij} is the distance (measured, say, in Å) between particles i and j . Find the crystal structure in Figure 1.4 which provides a minimum energy state for this potential, and the equilibrium lattice spacing, assuming no particles are at a distance less than 1. The potential has been chosen so that only nearest neighbors interact in the ground state. Do not check all crystal structures explicitly, only the square and hexagonal lattices.

(b) Suppose that ϕ is replaced by

$$\tilde{\phi}(r) = \begin{cases} \phi_0 \exp(-r) \left(\frac{1}{2r} - 1 \right) & \text{if } r < 1.5 \\ 0 & \text{else.} \end{cases} \quad (1.12)$$

Show that particles would collapse into a state of high density. It is not necessary to perform sums numerically: Consider what happens when particles are so closely spaced that they can be thought of as constituting a continuous distribution.

(c) Taking for ϕ

$$\phi(r) = \phi_0 \exp(-r) \left(\frac{1}{r^3} - 1 \right) \quad (1.13)$$

and assuming that the ground state is a lattice of the same symmetry as in part (a), find the equilibrium lattice spacing and energy per particle within 10%. This sum does need to be performed numerically.

References

- J. Emsley (1998), *The Elements*, 3rd ed., Clarendon Press, Oxford.
- H. Goldstein (1980), *Classical Mechanics*, 2nd ed., Addison-Wesley, Reading, MA.
- P. Groth (1906–1919), *Chemische Krystallographie*, W. Engelmann, Leipzig.
- R. J. Haüy (1801), *Treatise on Mineralogy*, Conseil des Mines, Paris. In French.
- V. Heine (1960), *Group Theory in Quantum Mechanics*, Pergamon, New York.
- J. C. Heyraud and J. J. Métois (1980), Establishment of the equilibrium shape of metal crystallites on a foreign substrate: Gold on graphite, *Journal of Crystal Growth*, **50**, 571–574.
- S. G. Lipson (1987), Helium crystals, *Contemporary Physics*, **28**, 117–142.
- C. H. MacGillavry (1976), *Fantasy & Symmetry: The Periodic Drawings of M. C. Escher*, H. N. Abrams, New York.
- J. B. Marion and S. T. Thornton (1988), *Classical Dynamics of Particles and Systems*, 3rd ed., Harcourt Brace Jovanovich, San Diego.
- J. C. Meyer, A. K. Geim, M. I. Katsnelson, K. S. Novoselov, T. J. Booth, and S. Roth (2007), The structure of suspended graphene sheets, *Nature*, **446**, 60–63.
- N. Steno (1671), *The Prodomus to a Dissertation Concerning Solids Naturally Contained Within Solids: Laying a Foundation for the Rendering a Rational Account Both of the Frame and the Several Changes of the Masse of the Earth, as also of the Various Productions in the Same*, London, F. Winter. Translation of: *De solido intra solidum naturaliter*. Readex Microprint, 1973 (Landmarks of Science)
- J. J. Thomson (1907), *The Corpuscular Theory of Matter*, Charles Scribner's Sons, New York.
- M. Tinkham (1964), *Group Theory and Quantum Mechanics*, McGraw-Hill, New York.

2. Three-Dimensional Lattices

2.1 Introduction

In order to classify the crystalline solids found in nature, one must study three-dimensional lattices. While the subject involves few concepts not already present in the two-dimensional case, the number of possible structures is bewilderingly large. Fortunately, a large number of the elements adopts particularly simple structures. On the other hand, alloys and compounds explore countless different forms, of which over 400,000 have now been cataloged; these cannot be summarized in any neat way despite the aid provided by the theory of symmetry.

There are 32 distinct point groups consistent with crystalline symmetry in three dimensions, which were first enumerated by Hessel (1830), spurred on by the desire to classify the shapes of naturally occurring rock crystals. The three-dimensional Bravais lattices were first correctly enumerated by Bravais (1850); solution of this problem may seem easier than that of finding all point groups, but it is more abstract, since crystal surfaces are visible, while lattices are deduced as an economical explanation for their appearance. Listing of lattices with bases was begun by Sohncke (1879), who found 65 lattices. The full number is 230, and these were enumerated by Fedorov (1895) and Schönflies (1891). Fedorov had priority in most respects, but only following correspondence between the two scientists were the final errors corrected; in one of Schönflies' early papers, 227 space groups appear. Many other historical details are related by Ewald (1962), Phillips (1971), and Hoddeson et al. (1992).

This chapter is designed more for reference than for recreational reading. At first the listing of crystal structures may appear more like a dull catalog of animals in some distant land than basic physics. Yet knowledge of crystal structures is the foundation on which much of the rest of condensed matter physics rests. The detailed calculation of electronic and mechanical properties of solids depends on knowing where the atoms lie.

Distribution Among Elements.

A comprehensive account of everything known about crystal structures cannot be confined to one volume, or ten, let alone a chapter. Still, it is worth giving a sense of the types of information available, first the elements and then some of the more common compound structures. The low-temperature crystal structures of the elements are shown in Table 2.1. Room-temperature crystal structures of the elements are shown in the periodic table inside the front cover. Not all structures are known with certainty; boron has a huge unit cell that continues to resist precise determination. The crystal structures mentioned in the chart and in the periodic table are defined in the following sections.

Table 2.1. Low temperature crystal systems and crystal structures of the elements

Element	#	Lattice	a	c or α		
Ac	Actinium	89	CUB	fcc	5.31	
Ag	Silver	47	CUB	fcc	4.09	
Al	Aluminum	13	CUB	fcc	4.05	
Am	Americium	95	CUB	fcc	4.89	
Ar	Argon	18	CUB	fcc	5.26	At 4.2 K.
As	Arsenic	33	RHO		4.13	54° Unit cell has 2 atoms.
Au	Gold	79	CUB	fcc	4.08	
Ba	Barium	56	CUB	bcc	5.02	
Be	Beryllium	4	HEX	hcp	2.29	3.58
Bi	Bismuth	83	RHO		4.75	57°
B	Boron	5	TET		8.74	5.03 Unit cell has at least 50 atoms.
Br ₂	Bromine	35	ORC		6.67	4.48 $b=8.72$. At 123 K. 8 atoms in unit cell.
C	Carbon	6	CUB	dia	3.57	Diamond.
C		6	HEX		2.46	6.70 Graphite, planar structure.
Ca	Calcium	20	CUB	fcc	5.58	
Cd	Cadmium	48	HEX	hcp	2.98	5.62
Ce	Cerium	58	CUB	fcc	5.16	
Ce			HEX	hcp	3.65	5.96
Cl ₂	Chlorine	17	ORC		6.24	4.48 $b=8.26$. At 113 K. 8 atoms in unit cell.
Co	Cobalt	27	CUB	fcc	3.55	
Co			HEX	hcp	2.51	4.07
Cr	Chromium	24	CUB	bcc	2.88	
Cr			CUB	fcc	3.68	
Cr			HEX	hcp	2.72	4.43
Cs	Cesium	55	CUB	bcc	6.05	At 5 K.
Cu	Copper	29	CUB	fcc	3.61	
Dy	Dysprosium	66	HEX	hcp	3.59	5.65 At 49 K.
Er	Erbium	68	HEX	hcp	3.55	5.59
Eu	Europium	63	CUB	bcc	4.61	
F	Fluorine	9				
Fe	Iron	26	CUB	bcc	2.87	
Fe			CUB	fcc	3.59	
Ga	Gallium	31	ORC		4.51	7.86 b axis 1.001 times a axis.
Ge	Germanium	32	CUB	dia	5.66	
Gd	Gadolinium	64	HEX	hcp	3.56	5.80
H ₂	Hydrogen	1	HEX	hcp	3.75	6.49 hcp lattice formed by H ₂ molecules.
He	Helium	2	HEX	hcp	3.57	5.83 At 2 K and 26 atm pressure.
Hf	Hafnium	72	HEX	hcp	3.20	5.06
Hg	Mercury	80	RHO		2.99	71° At 5 K.
Ho	Holmium	67	HEX	hcp	3.58	5.62
I ₂	Iodine	53	ORC		4.79	9.78 $b=7.25$. Unit cell has 8 atoms, set in pairs.
In	Indium	49	TET	bct	3.24	4.94
Ir	Iridium	77	CUB	fcc	3.84	
K	Potassium	19	CUB	bcc	5.23	At 5 K.
Kr	Krypton	36	CUB	fcc	5.72	At 58 K.
La	Lanthanum	57	CUB	fcc	5.30	
La			HEX	hcp	3.75	6.07
Li	Lithium	3	CUB	bcc	3.50	
Lu	Lutetium	71	HEX	hcp	3.50	5.55
Mg	Magnesium	12	HEX	hcp	3.21	5.21
Mn	Manganese	25	CUB		8.89	Unit cell has 58 atoms.
Mn			CUB		6.30	Unit cell has 20 atoms.
Mn			TET	ftc	3.77	3.53

(Continued)

Element	#	Lattice	<i>a</i>	<i>c</i> or α	
Mo	Molybdenum	42 CUB	bcc	3.15	
Mo		CUB	fcc	4.16	
N ₂	Nitrogen	7 CUB		5.64	At 4 K. Unit cell has 8 atoms.
Na	Sodium	11 CUB	bcc	4.29	
Nb	Niobium	41 CUB	bcc	3.30	
Nd	Neodymium	60 HEX	hcp	3.66	5.90
Ne	Neon	10 CUB	fcc	4.43	At 4 K.
Ni	Nickel	28 CUB	fcc	3.52	
Ni		HEX	hcp	2.65	4.33
Np	Neptunium	93 ORC		4.72	6.66
O ₂	Oxygen	8 ORC		5.50	3.82
Os	Osmium	76 HEX	hcp	2.74	4.32
P	Phosphorus	15 ORC		3.31	10.5
P		CUB		7.17	
Pa	Protactinium	91 TET	bct	3.93	3.24
Pb	Lead	82 CUB	fcc	4.95	
Pd	Palladium	46 CUB	fcc	3.89	
Po	Polonium	84 CUB			
Pr	Praseodymium	59 CUB	fcc	5.16	
Pr		HEX	hcp	3.67	5.92
Pt	Platinum	78 CUB	fcc	3.92	
Pu	Plutonium	94 MON		6.18	10.97
Rb	Rubidium	37 CUB	bcc	5.59	
Re	Rhenium	75 HEX	hcp	2.76	4.46
Rh	Rhodium	45 CUB	fcc	3.80	
Ru	Ruthenium	44 HEX	hcp	2.70	4.28
S	Sulfur	16 ORC		10.47	24.5
Sb	Antimony	51 RHO		4.50	58°
Sc	Scandium	21 CUB	fcc	4.54	
Sc		HEX	hcp	3.31	5.27
Se	Selenium	34 HEX		4.36	4.93
Si	Silicon	14 CUB	dia	5.43	
Sm	Samarium	62 RHO		9.00	23°
Sn	Tin	50 CUB	dia	6.49	
Sn		TET		5.82	3.17
Sr	Strontium	38 CUB	fcc	6.08	
Ta	Tantalum	73 CUB	bcc	3.31	
Tb	Terbium	65 HEX	hcp	3.60	5.69
Te	Tellurium	52 HEX		4.45	5.91
Th	Thorium	90 CUB	fcc	5.08	
Ti	Titanium	22 HEX	hcp	2.95	4.69
Tl	Thallium	81 HEX	hcp	3.46	5.53
Tl		CUB	fcc	4.84	
Tl		CUB	bcc	3.88	
Tm	Thulium	69 HEX	hcp	3.54	5.55
U	Uranium	92 CUB	bcc	3.47	
V	Vanadium	23 CUB	bcc	3.02	
W	Tungsten	74 CUB	bcc	3.16	
Xe	Xenon	54 CUB	fcc	6.20	
Y	Yttrium	39 HEX	hcp	3.65	5.73
Yb	Ytterbium	70 CUB	fcc	5.49	
Zn	Zinc	30 HEX	hcp	2.66	4.95
Zr	Zirconium	40 HEX	hcp	3.23	5.15

CUB=cubic, TET=tetragonal, ORC=orthorhombic, MON=Monoclinic, TRI=Triclinic, HEX=hexagonal, RHO=Rhombohedral. Source: Wyckoff (1963–1971), vol. 1.

2.2 Monatomic Lattices

Monatomic lattices are those formed from entirely from atoms of a single element. In the simplest of these, the atoms form a Bravais lattice. This means that atomic positions are given by sums over three primitive vectors, which must be linearly independent:

$$\vec{R} = n_1 \vec{a}_1 + n_2 \vec{a}_2 + n_3 \vec{a}_3. \quad (2.1)$$

$n_1, n_2,$ and n_3 are integers. The subscripts on the vectors a_i do not refer to components of the vectors, but to three separate three-vectors.

2.2.1 The Simple Cubic Lattice

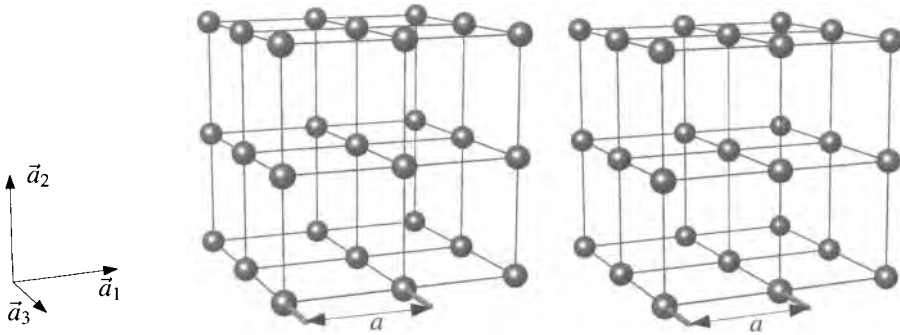


Figure 2.1. The simple cubic lattice, showing the lattice spacing a . To view the stereo pair, hold the image at a distance of around half a meter, cross eyes until left and right images overlap, and focus on the combined image.

The *simple cubic* (sc) lattice is described by primitive vectors

$$\vec{a}_1 = a(1 \ 0 \ 0), \quad \vec{a}_2 = a(0 \ 1 \ 0), \quad \vec{a}_3 = a(0 \ 0 \ 1) \quad (2.2)$$

and pictured in Figure 2.1. The only element ever to choose this structure as its ground state is polonium, partly because the simple cubic lattice has large holes in it, and most elements prefer to take advantage of the fact that other configurations pack space more efficiently. However, the simple cubic lattice does provide a starting point for constructing more common structures.

2.2.2 The Face-Centered Cubic Lattice

The *conventional unit cell* of the *face-centered cubic lattice* (fcc) is constructed by putting atoms on the corners of a cube and then putting an atom on each face, as shown in Figure 2.2. A set of primitive vectors describing an fcc lattice of spacing a is

$$\vec{a}_1 = \frac{a}{2}(1 \ 1 \ 0), \quad \vec{a}_2 = \frac{a}{2}(1 \ 0 \ 1), \quad \vec{a}_3 = \frac{a}{2}(0 \ 1 \ 1). \quad (2.3)$$

Notice that the *lattice spacing*, or *lattice constant* a describes the distance between adjacent corners of the cube. It does not give the distance from an atom to its nearest neighbor. The Wigner–Seitz cell is shown in Figure 2.2 (B).

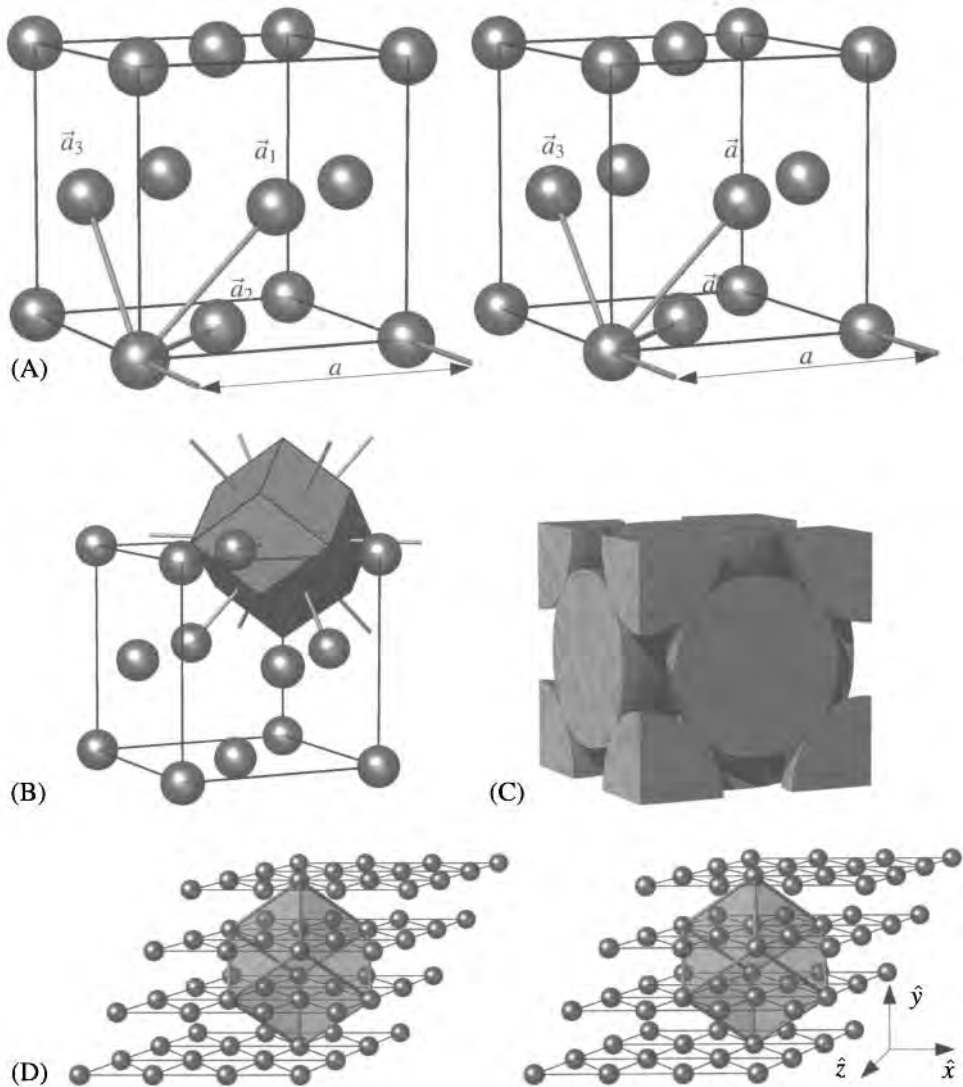


Figure 2.2. (A) The conventional unit cell of the fcc lattice, showing primitive vectors and lattice spacing a (stereo pair). (B) Wigner–Seitz cell of the fcc lattice. (C) If spheres in an fcc lattice are given radii $a/(2\sqrt{2})$, they pack together. (D) The fcc lattice can be constructed by stacking two-dimensional triangular lattices in a regular sequence (stereo pair).

The fcc lattice is sometimes referred to as *cubic close-packed*, because if the fcc lattice is composed of balls with radius $a/(2\sqrt{2})$, they stack neatly together, as shown in Figure 2.2(C). Within the planes normal to the vector $[1,1,1]$, the atoms of an fcc lattice lie in a two-dimensional triangular lattice, and one can view the lattice as being built from layers of triangular lattices stacked one upon the other, as shown in Figure 2.2(D). Primitive vectors to construct the lattice from this point of view are the subject of Problem 2.

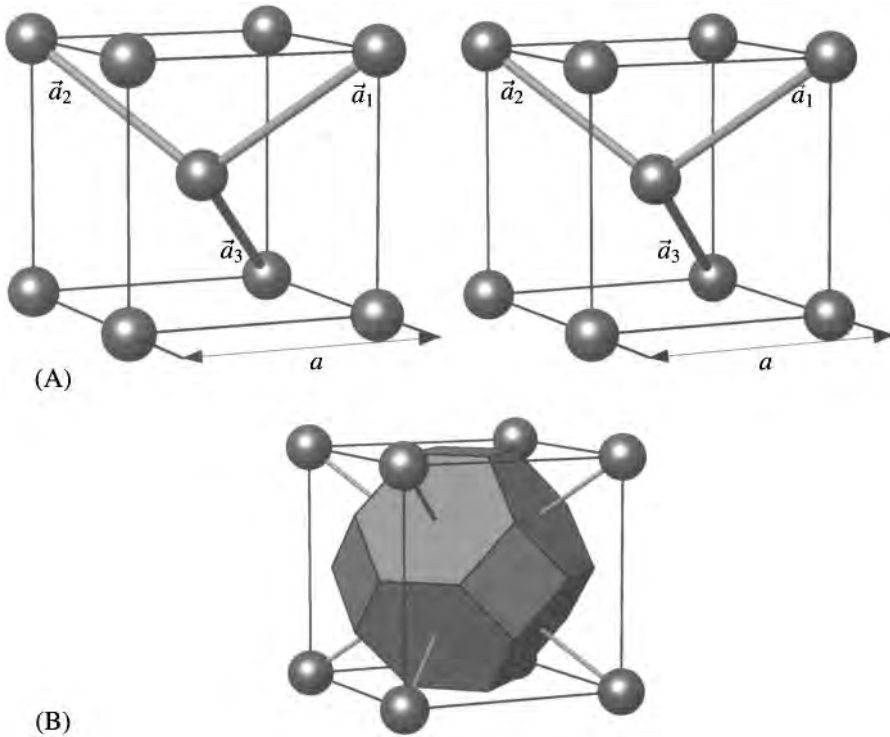


Figure 2.3. (A) The conventional unit cell of the body-centered cubic lattice (stereo pair). (B) Wigner–Seitz cell of the bcc lattice.

The conventional unit cell of the fcc lattice is four times as large as a primitive unit cell, as one may determine by considering the fcc lattice as a cubic lattice with a basis (Problem 1).

More than twenty of the elements adopt the fcc lattice, including copper, silver, gold, and the noble gases at low temperatures.

2.2.3 The Body-Centered Cubic Lattice

The conventional unit cell of the *body-centered cubic* (bcc) lattice is constructed by putting atoms on the corners of a cube and then putting an atom in the middle to fill up the big hole in the center, as shown in Figure 2.3(A). A symmetrical set of primitive vectors for a lattice of spacing a is

$$\vec{a}_1 = \frac{a}{2}(1 \ 1 \ -1), \quad \vec{a}_2 = \frac{a}{2}(-1 \ 1 \ 1), \quad \vec{a}_3 = \frac{a}{2}(1 \ -1 \ 1), \quad (2.4)$$

and the Wigner–Seitz cell appears in Figure 2.3 (B). As in the case of the fcc lattice, the lattice constant a refers to the distance between corners of the cube, not to the distance between nearest neighbors.

The conventional unit cell of the bcc lattice is twice as large as a primitive unit cell (Problem 1). Sixteen elements adopt the bcc structure at low temperature, including iron and uranium.

2.2.4 The Hexagonal Lattice

A hexagonal lattice is pictured in Figure 2.4. This structure does not occur among the elements, except as the starting point for the hexagonal close-packed structure.

Its primitive vectors are

$$\vec{a}_1 = (a\sqrt{3}/2 \ a/2 \ 0), \quad \vec{a}_2 = (a\sqrt{3}/2 \ -a/2 \ 0), \quad \vec{a}_3 = (0 \ 0 \ c), \quad (2.5)$$

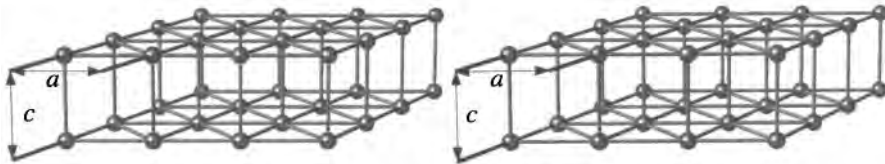


Figure 2.4. Hexagonal lattice described by lattice constants c and a (stereo pair).

2.2.5 The Hexagonal Close-Packed Lattice

The *hexagonal close-packed* (hcp) structure, a common ground state among the elements, is like the honeycomb lattice a lattice with a basis. As shown in Figure 2.5, it is formed by creating a triangular lattice of lattice constant a in two dimensions. Then a copy of this lattice is stacked vertically over the first one, in such a way that particles of the second lattice are directly over centers of triangles of the first one, at height $c/2$. A new copy of the original triangular lattice is now stacked directly over the first one, at height c , and the stacking sequence begins over again. One way to demonstrate that the hcp lattice is not a Bravais lattice is to view it from the top as in Figure 2.16 (Problem 5); from this angle it appears to be a honeycomb lattice, so it must be described as a lattice with a basis.

To construct the hcp lattice, begin with the primitive vectors in Eq. (2.5) and supplement them with basis vectors

$$(0 \ 0 \ 0) \ (a/\sqrt{3} \ 0 \ c/2) \quad \text{In Cartesian coordinates.} \quad (2.6a)$$

$$(0 \ 0 \ 0) \ (1/3 \ 1/3 \ 1/2). \quad \text{In coordinates described by multiples of the primitive vectors, as in Eq. (1.6).} \quad (2.6b)$$

There is no necessary relation between the lattice constants c and a . However, if $c = \sqrt{8/3}a$, the atoms are in just the right location that if expanded to a radius of

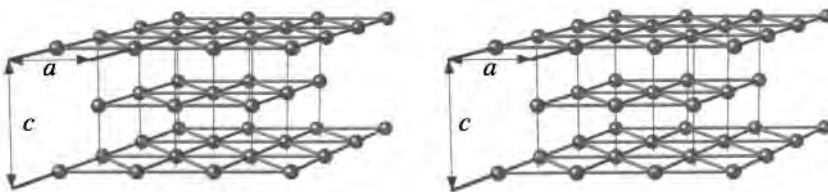


Figure 2.5. Hexagonal close-packed lattice, produced by two interlaced hexagonal lattices (stereo pair).

$a/2$, they form a perfect close-packed structure. The difference between this close-packed structure and the one formed by the face-centered cubic lattice lies in the way that successive triangular layers are stacked upon one another. In Figure 2.5, notice that one has two choices as to where to put the topmost layer of atoms. In the hcp lattice, the layers are stacked so that the structure repeats, after two layers, while to produce the fcc lattice, one stacks them so that they repeat after three, as in Figure 2.2(D). More than 25 elements adopt the hcp lattice, including zinc and titanium.

2.2.6 The Diamond Lattice

The *diamond lattice* is constructed by taking the fcc lattice described by Eq. (2.3) and making a copy of it, displaced relative to the original by $(a/4 \ a/4 \ a/4)$. Every atom in the structure has precisely four nearest neighbors, symmetrically organized around it, as shown in Figure 2.6. Only four elements commonly assume this structure — carbon, silicon, germanium, and tin — but the cultural status of diamond and technological importance of silicon make this a structure of great significance.

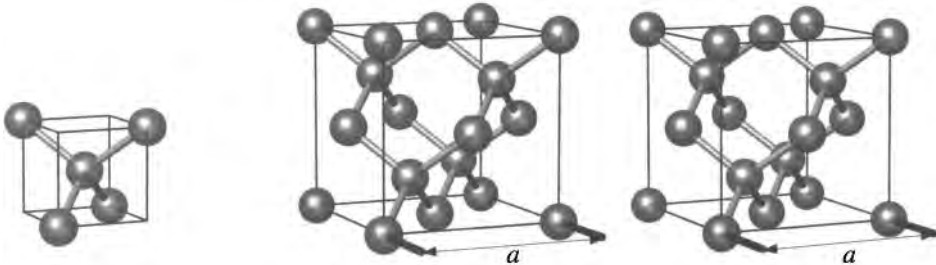


Figure 2.6. Diamond lattice. Each atom has four nearest neighbors, a structure produced by removing four atoms from the bcc structure, as shown in the lower left, and then assembling these tetrahedra as shown in the stereo pair to the right.

2.3 Compounds

Compounds are crystals made of more than one element. Since at least two types of atoms are involved in their construction, they cannot be Bravais lattices, and all must be described as lattices with a basis. Hundreds of thousands of different crystals have been cataloged, and only a few common arrangements are listed below.

2.3.1 Rocksalt—Sodium Chloride

The *sodium chloride* structure (NaCl) alternates sodium and chlorine on points of a simple cubic lattice, as shown in Figure 2.7. This structure can be described as an fcc lattice of lattice constant a , with a basis of a sodium atom at (000) , and a chlorine atom at $a/2(1\ 0\ 0)$ (see Table 2.2).

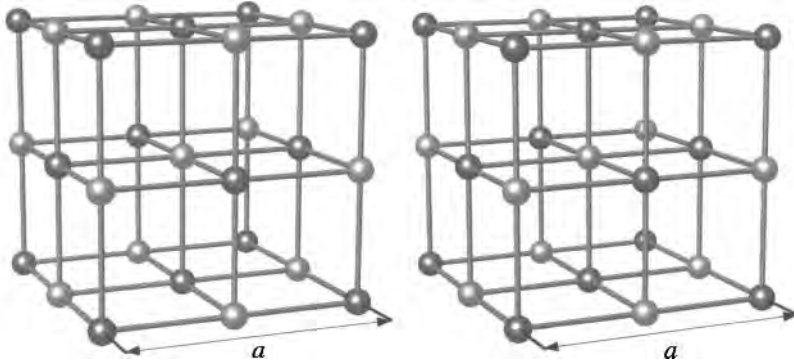


Figure 2.7. The sodium chloride structure can be viewed as a simple cubic lattice in which two different atoms alternate, or as two interpenetrating fcc lattices (stereo pair). Figure 11.3 provides an alternate view of NaCl, showing the sizes conventionally attributed to the two ions.

Table 2.2. Crystals with the sodium chloride structure

Crystal	a	Crystal	a	Crystal	a	Crystal	a	Crystal	a
AgBr	5.77	CrN	4.14	LiI	6.00	NiO	4.17	SrS	6.02
AgCl	5.55	CsF	6.01	MgO	4.21	PbS	5.93	SrSe	6.23
AgF	4.92	FeO	4.31	MgS	5.20	PbSe	6.12	SrTe	6.47
BaO	5.52	KBr	6.60	MgSe	5.45	PbTe	6.45	TiC	4.32
BaS	6.39	KCl	6.30	MnO	4.44	RbBr	6.85	TiN	4.24
BaSe	6.60	KF	5.35	MnS	5.22	RbCl	6.58	TiO	4.24
BaTe	6.99	KI	7.07	MnSe	5.49	RbF	5.64	VC	4.18
CaS	5.69	LiBr	5.50	NaBr	5.97	RbI	7.34	VN	4.13
CaSe	5.91	LiCl	5.13	NaCl	5.64	SnAs	5.68	ZrC	4.68
CaTe	6.35	LiF	4.02	NaF	4.62	SnTe	6.31	ZrN	4.61
CdO	4.70	LiH	4.09	NaI	6.47	SrO	5.16		

Lattice constants a in Å. Source: Wyckoff (1963–1971), vol. 1.

2.3.2 Cesium Chloride

The *cesium chloride* structure (CsCl) alternates cesium and chlorine on the points of a body-centered cubic lattice, as shown in Figure 2.8. This structure can be described as a simple cubic lattice of lattice constant a , with a basis of a cesium atom at (000) , and a chlorine atom at $a/2(1\ 1\ 1)$ (see Table 2.3).

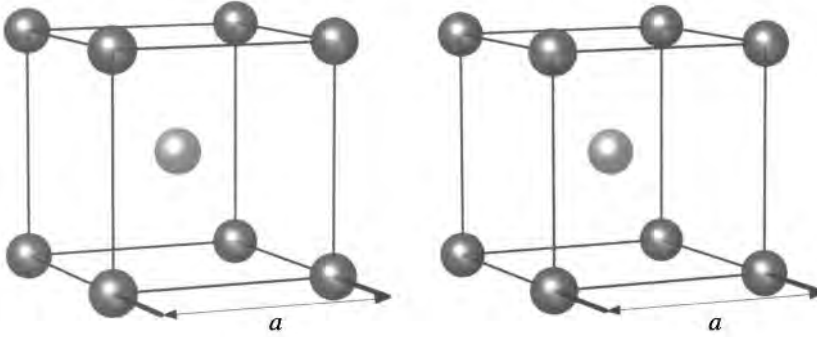


Figure 2.8. The cesium chloride structure can be viewed as a body-centered cubic lattice with an atom of a second type inhabiting the interior of the cube. (stereo pair).

Table 2.3. Crystals with the cesium chloride structure

Crystal	a	Crystal	a	Crystal	a
AgCd	3.33	CsCl	4.12	NiAl	2.88
AgMg	3.28	CuPd	2.99	TiCl	3.83
AgZn	3.16	CuZn	2.95	TlI	4.20
CsBr	4.29	NH ₄ Cl	3.86	TlSb	3.84

Lattice constants a in Å. Source: Wyckoff (1963–1971), vol. 1.

2.3.3 Fluorite—Calcium Fluoride

The *calcium fluoride* structure (CaF₂) may be described as a simple cubic lattice with basis (in units of the lattice spacing a and Cartesian coordinates)

$$(0\ 0\ 0)\ (0\ 1/2\ 1/2)\ (1/2\ 0\ 1/2)\ (1/2\ 1/2\ 0) \quad (2.7)$$

of a first type of atom (calcium) and

$$(1/4\ 1/4\ 1/4)\ (1/4\ 3/4\ 3/4)\ (3/4\ 1/4\ 3/4)\ (3/4\ 3/4\ 1/4) \quad (2.8a)$$

$$(3/4\ 3/4\ 3/4)\ (3/4\ 1/4\ 1/4)\ (1/4\ 3/4\ 1/4)\ (1/4\ 1/4\ 3/4) \quad (2.8b)$$

of a second (fluorine) (see Figure 2.9 and Table 2.4).

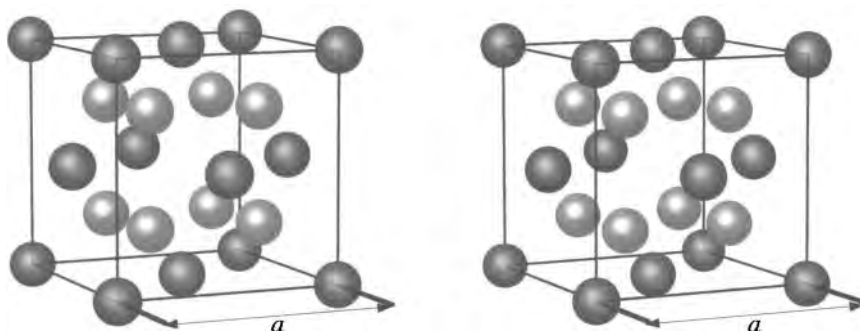


Figure 2.9. The calcium fluoride structure (stereo pair) can be viewed as a face-centered cubic lattice made from a first type of atom (calcium), with the center of the cell inhabited by a cubic arrangement of the second type of atom (fluorine).

Table 2.4. Crystals with the calcium fluoride structure

Crystal	a	Crystal	a	Crystal	a
BaF ₂	6.20	CoSi ₂	5.36	Mg ₂ Si	6.39
CaF ₂	5.46	HfO ₂	5.12	Mg ₂ Sn	6.77
CdF ₂	5.39	Li ₂ O	4.62	Na ₂ S	6.53
CeO ₂	5.41	Li ₂ S	5.71	SrCl ₂	6.98
CmO ₂	5.37	Mg ₂ Pb	6.84	UO ₂	5.47

Lattice constants a in Å. Source: Wyckoff (1963–1971), vol. 1.

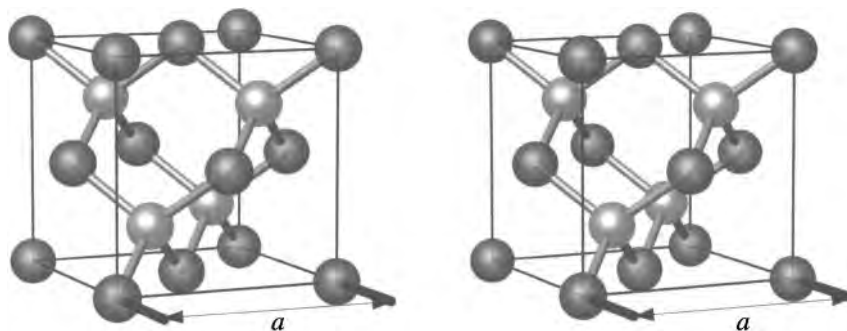


Figure 2.10. The zincblende structure can be viewed as a diamond lattice, in which alternating lattice points are occupied by two alternating elements. (stereo pair).

2.3.4 Zincblende—Zinc Sulfide

The *zincblende* structure (ZnS) is identical to diamond, except that two species of atoms alternate between sites (see Figure 2.10 and Table 2.5) .

Table 2.5. Crystals with the zincblende structure

Crystal	a	Crystal	a	Crystal	a
AgI	6.47	CdTe	6.48	HgSe	6.08
AlAs	5.62	CuBr	5.69	HgTe	6.43
AlP	5.45	CuCl	5.41	InAs	6.04
AlSb	6.13	CuI	6.04	InP	5.87
BeS	4.85	GaAs	5.63	InSb	6.48
BeSe	5.07	GaP	5.45	SiC	4.35
BeTe	5.54	GaSb	6.12	ZnS	5.41
CdS	5.82	HgS	5.85	ZnTe	6.09

Lattice constants a in Å. Source: Wyckoff (1963–1971), vol. 1.

2.3.5 Wurtzite—Zinc Oxide

The *wurtzite* structure (ZnO) is an hexagonal lattice with basis

$$(0 \ 0 \ 0) \ (a/2 \ a/2\sqrt{3} \ c/2) \quad \text{First species; Cartesian coordinates.} \quad (2.9a)$$

$$(0 \ 0 \ cu) \ (a/2 \ a/2\sqrt{3} \ c/2 + cu) \quad \text{Second species; Cartesian coordinates.} \quad (2.9b)$$

or

$$(0 \ 0 \ 0) \ (1/3 \ 1/3 \ 1/2)) \quad \text{First species; primitive vector coordinates: see Eq. (2.5).} \quad (2.9c)$$

$$(0 \ 0 \ u) \ (1/3 \ 1/3 \ u + 1/2)) \quad \text{Second species; primitive vector coordinates.} \quad (2.9d)$$

When $u = 3/8$ and $c/a = \sqrt{8/3}$, every atom is equidistant from four neighbors; although these extra symmetries are not inevitable for the definition of the structure, natural crystals display them (see Figure 2.11 and Table 2.6).

Table 2.6. Crystals with the wurtzite structure

Crystal	a	c	Crystal	a	c
AlN	3.11	4.98	MgTe	4.52	7.33
BeO	2.70	4.38	NH ₄ F	4.39	7.02
CdS	4.13	6.75	SiC	3.08	5.05
CdSe	4.30	7.02	ZnO	3.25	5.23
CuH	2.89	4.61	ZnS	3.81	6.23

Lattice constants a and c in Å. In all cases, $u = 3c/8$. Source: Wyckoff (1963–1971), vol. 1.

2.3.6 Perovskite—Calcium Titanate

The *perovskite* structure (CaTiO₃) is built from three types of atoms. The calcium fill out a simple cubic lattice, the oxygens lie on the face centers, and titanium occupy body centers (see Figure 2.12 and Table 2.7).

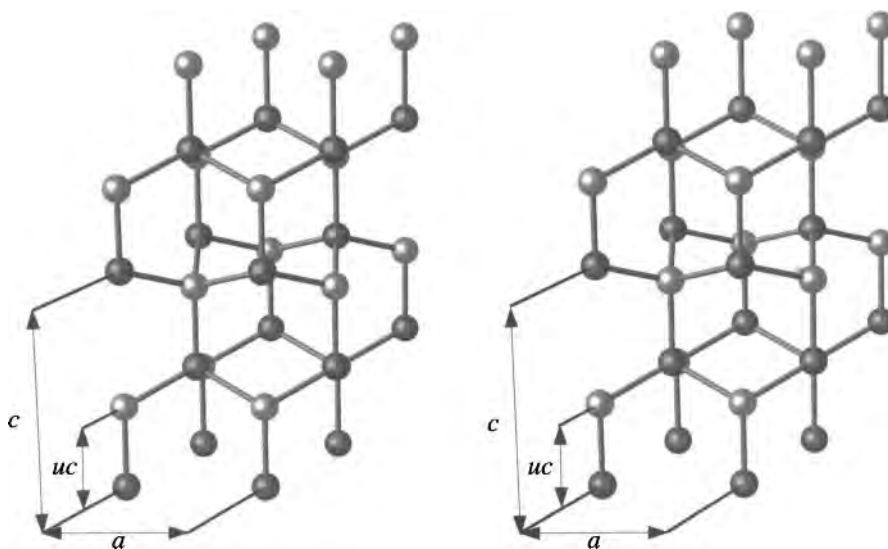


Figure 2.11. The wurtzite (ZnO) structure is an hexagonal structure built with two types of atoms, and it allows each atom to have four nearest neighbors of the opposite type. It can be viewed as two interlaced hcp lattices, just as the diamond and zincblende structures are built as two interlaced fcc lattices (stereo pair).

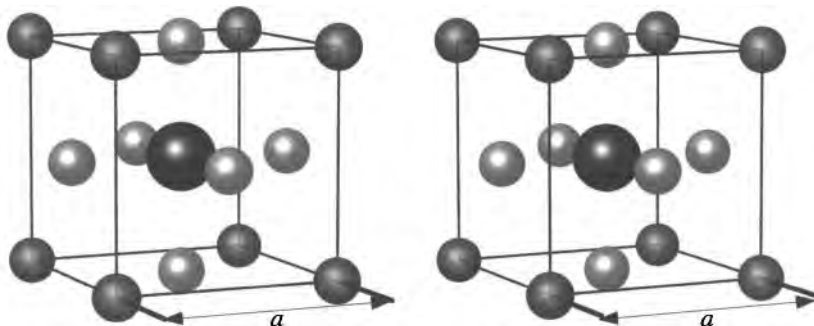


Figure 2.12. The perovskite structure is a simple cubic lattice of calcium, with oxygens occupying face centers, and titanium occupying the body center. (stereo pair).

Table 2.7. Crystals with the perovskite structure

Crystal	a	Crystal	a	Crystal	a
BaTiO ₃	4.01	CsHgCl ₃	5.44	LaAlO ₃	3.78
CaSnO ₃	3.92	CsIO ₃	4.66	LaGaO ₃	3.88
CaTiO ₃	3.84	KIO ₃	4.41	RbIO ₃	4.52
CaZrO ₃	4.02	KMgF ₃	3.97	SrTiO ₃	3.91
CsCdBr ₃	5.33	KNiF ₃	4.01	SrZrO ₃	4.10
CsHgBr ₃	5.77	KZnF ₃	4.05	YAlO ₃	3.68

Lattice constants a in Å. Source: Wyckoff (1963–1971), vol. 2.

2.4 Classification of Lattices by Symmetry

There is a complete classification of lattices by symmetry, which includes no less than 230 distinct types and which will be discussed only briefly.

2.4.1 Fourteen Bravais Lattices and Seven Crystal Systems

There are precisely seven distinct point symmetry groups that arise when one constructs Bravais lattices out of identical point particles. They are called the seven *crystal systems* and are shown in Table 2.8. A related but separate question is how many distinct three-dimensional Bravais lattices can be built out of identical point particles. The answer is 14, and all are listed in Table 2.8.

Cubic system: The first symmetry to strike the eye after inspecting the cube has to do with the square sides. However, the cubic symmetry class derives its name from three threefold axes about lines $[1,1,1]$ between opposite corners of the cube. The cube is also invariant under rotations of 90° about any of three perpendicular axes, and under reflections about the three planes perpendicular to these axes. It has twofold rotation and mirror symmetries about the axis $[1,1,0]$. The three Bravais lattices possessing this set of symmetries are the simple cubic, face-centered cubic, and body-centered cubic lattices.

Tetragonal system: If one stretches the cube to make four of the sides into rectangles, then one has an object with the symmetry of the *tetragonal* group: the threefold symmetry is lost, as well as the 90° rotation symmetry about two of the axes, but the solid is still symmetric under reflections about planes that

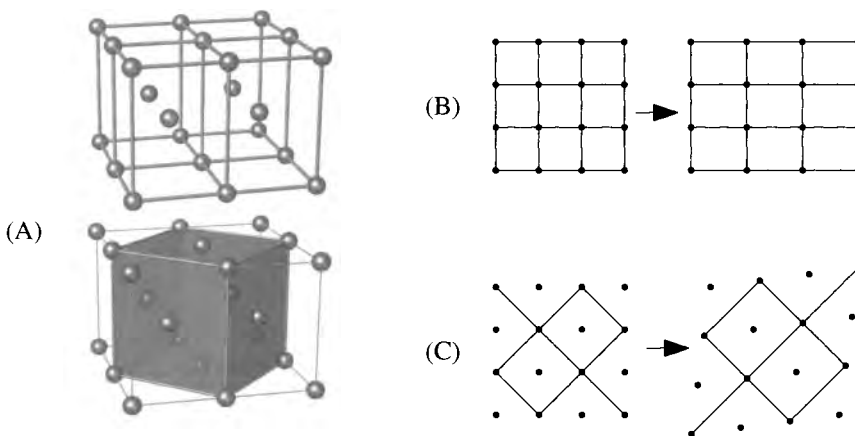


Figure 2.13. (A) If one stretches a bcc lattice by a factor of $\sqrt{2}$ along one of its axes, it becomes an fcc lattice with lattice constant $\sqrt{2}$ times larger, as shown by simply reconnecting the lines between atoms. (B) Deforming tetragonal lattices along their axes produce the simple and centered orthorhombic lattices. (C) Deforming tetragonal lattices along diagonals produces base-centered and face-centered orthorhombic lattices.

Table 2.8. The seven crystal systems and fourteen Bravais lattices in three dimensions

	Simple	Base-Centered	Body-Centered	Face-Centered
Cubic $a=b=c$ $\alpha=\beta=\gamma=90^\circ$				
Tetragonal $a \neq b = c$ $\alpha=\beta=\gamma=90^\circ$				
Orthorhombic $a \neq b \neq c$ $\alpha=\beta=\gamma=90^\circ$				
Monoclinic $a \neq b \neq c$ $\alpha=\gamma=90^\circ$ $\beta \neq 90^\circ$				
Triclinic $a \neq b \neq c$ $\alpha, \beta, \gamma \neq 90^\circ$				
Hexagonal $a = b \neq c$ $\alpha = \beta = 90^\circ$ $\gamma = 120^\circ$				
Rhombohedral $a = b = c$ $\alpha = \beta = \gamma \neq 90^\circ$				

bisect it. Stretching a simple cubic lattice produces a *simple tetragonal* lattice, and stretching either a face-centered cubic or a body-centered cubic lattice produces a *centered tetragonal* lattice. That one can produce only a single structure from deformation of the fcc and bcc lattices follows from the slightly surprising fact that an fcc lattice can be obtained by expanding a bcc lattice along one axis by a factor of $\sqrt{2}$, as illustrated in Figure 2.13(A). Therefore, any distortion of the bcc lattice could have equally well been produced by a distortion of the fcc lattice.

Orthorhombic system: Next, one can deform the top and bottom squares of the tetragonal solid into rectangles, eliminating the last of the 90° rotation symmetries. This solid has *orthorhombic* symmetry. Deforming the simple tetragonal lattice along one of its axes produces a *simple orthorhombic* lattice, and deforming the centered tetragonal lattice produces a *body-centered orthorhombic* lattice, as in Figure 2.13(B). There are two additional orthorhombic lattices, however, which can be produced by stretching the two tetragonal solids along face diagonals, as illustrated in Figure 2.13(C). Deforming the simple tetragonal lattice in this way produces the *base-centered orthorhombic* lattice, while deforming the centered tetragonal in this way produces a *face-centered orthorhombic* lattice .

Monoclinic system: One generates a solid with *monoclinic* symmetry by squeezing a tetragonal solid across a diagonal so as to eliminate the 90° angles on the top and bottom faces, leaving the sides built out of rectangles. There are only two distinct monoclinic lattices. The *simple monoclinic* lattice results from distortion of the simple orthorhombic lattice, while the *centered monoclinic* lattice results from appropriate distortion of the face-centered, base-centered, and body-centered orthorhombic lattices.

Triclinic system: Final in this progression is the *triclinic symmetry* which is produced by pulling the top of a monoclinic solid sideways relative to the bottom so that all faces become diamonds. The only symmetry now remaining is inversion symmetry, and there is only one lattice of this type, the *triclinic lattice*.

Rhombohedral or trigonal system: There are two crystal classes still missing from the list. If one starts with a cube and stretches it across a body diagonal, one gets a solid with *rhombohedral* or *trigonal* symmetry. Stretching any of the three cubic Bravais lattices in this way produces the same Bravais lattice, called the *rhombohedral lattice* or the *trigonal lattice*.

Hexagonal system: Finally, one can form a solid with a hexagon at the base and perpendicular walls to illustrate the *hexagonal* symmetry. There is only one Bravais lattice of this type, the *hexagonal lattice* .

In this way, one has 14 point groups for lattices built out of points with spherical symmetry.

2.5 Symmetries of Lattices with Bases

2.5.1 Thirty-Two Crystallographic Point Groups

The general task of finding all possible symmetries of lattices is far from finished because one must continue to discuss the symmetries of lattices with bases.

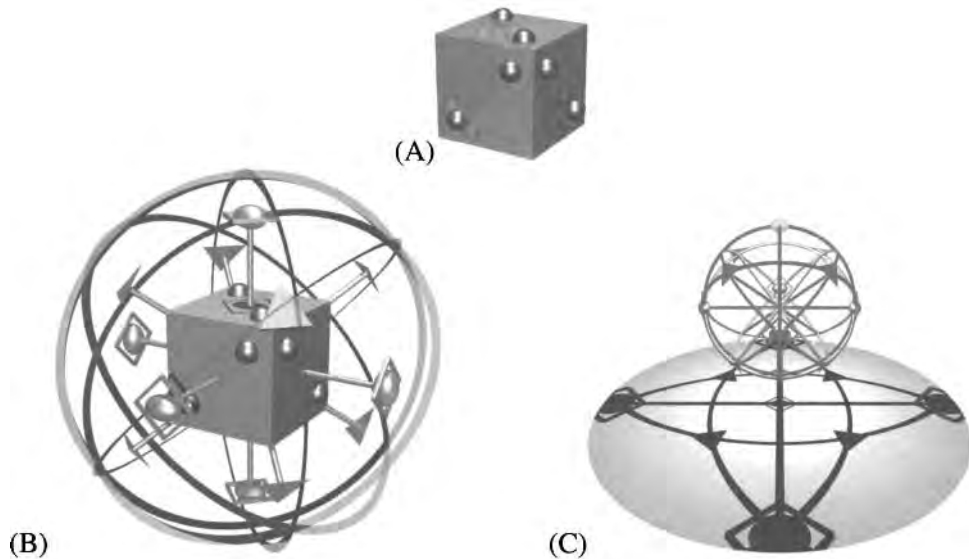


Figure 2.14. A stereogram is a compact two-dimensional representation of the symmetries of a three-dimensional object, shown in (A). Identify all the symmetry planes and axes of the object and inscribe them upon a sphere, as shown in (B). Next, find the shadow of the symmetry planes and axes as shown in (C). This projection is the stereogram, shown in Table 2.9 as T_d .

First, one has to construct all the relevant point groups. There is a grand total of 32 crystallographic point groups, which are illustrated in Table 2.9. The conventional way to describe these groups among crystallographers is through the use of a *stereogram*, whose construction is illustrated in Figure 2.14. Conventionally, stereograms are decorated with symbols, shown in Table 2.10, that describe all possible symmetry axes. A dashed line in a stereogram denotes a plane that is *not* a mirror plane of the object.

There are two sets of notation for the crystallographic point groups. The *Schönflies notation* appears in the upper part of each cell in Table 2.9. In some cases there are two versions of the Schönflies notation, and both are listed.

C = Cyclic; allows successive rotation about main axis.

D = Dihedral; contains two-fold axes perpendicular to main axis.

S = Spiegel; unchanged after combination of reflection and rotation.

T = Tetragonal.

O = Octahedral.

Table 2.9. The 32 crystallographic point groups

Triclinic	Monoclinic	Ortho- rhom- bic	Trigonal	Tetragonal	Hexagonal	Cubic
C_1 1 	C_2 2 		C_3 3 	C_4 4 	C_6 6 	T 23
	C_{1h} C_s $\bar{2}$ m 				C_{3h} $\bar{6}$ 	
	C_{2h} $\frac{2}{m}$ $2/m$ 			C_{4h} $\frac{4}{m}$ $4/m$ 	C_{6h} $\frac{6}{m}$ $6/m$ 	T_h $\frac{2}{m}\bar{3}$ $m\bar{3}$
		C_{2v} $2mm$ $mm2$ 	C_{3v} $3m$ 	C_{4v} $4mm$ 	C_{6v} $6mm$ 	
S_2 C_i $\bar{1}$ 			S_6 C_{3i} $\bar{3}$ 	S_4 $\bar{4}$ 		T_d $\bar{4}3$
		D_2 V 222 	D_3 32 	D_4 422 	D_6 622 	O 432
			D_{3d} $\bar{3}\frac{2}{m}$ $\bar{3}m$ 	D_{2d} V_h $\bar{4}2m$ 		
					D_{3h} $\bar{6}m2$ 	
		D_{2h} V_h $\frac{2}{m}\frac{2}{m}\frac{2}{m}$ mmm 		D_{4h} $\frac{4}{m}\frac{2}{m}\frac{2}{m}$ $4/mmm$ 	D_{6h} $\frac{6}{m}\frac{2}{m}\frac{2}{m}$ $6/mmm$ 	O_h $\frac{4}{m}\bar{3}\frac{2}{m}$ $m\bar{3}m$

Point groups are illustrated by stereograms that display the symmetry axes of each group. The symmetry axes are described by the symbols defined in Table 2.10. A solid line always describes a mirror plane, while a dashed line refers to a plane about which mirror symmetry is *not* present.

Table 2.10. Symmetry axes, together with their conventional symbols

Axis type	Schönflies Notation	International Notation	Symbol	Operation
Inversion	$i = S_2$	$\bar{1}$		$\vec{r} \rightarrow -\vec{r}$
Twofold	C_2	2		
Threefold	C_3	3		
Fourfold	C_4	4		
Sixfold	C_6	6		
Twofold Rotoinversion or Mirror	σ_h, \perp to axis σ_v , plane contains axis σ_d , bisects twofold axes	$\bar{2} \equiv m$		
Threefold Rotoinversion	S_6^{-1}	$\bar{3}$		
Fourfold Rotoinversion	S_4^{-1}	$\bar{4}$		
Sixfold Rotoinversion	S_3^{-1}	$\bar{6}$		

The proper rotations are identical in the Schönflies and International systems. However, the improper rotations are conceived differently. For example, S_3 directs one to rotate counterclockwise by 120° , and then reflect across the mirror plane perpendicular to the rotation axis. This operation is the inverse of $\bar{6}$, which rotates by 60° and then applies an inversion. The two- to sixfold axes do not necessarily have perpendicular mirror planes. However, a twofold rotoinversion axis is identical to a mirror plane perpendicular to the axis, a threefold rotoinversion axis always includes an inversion center, and sixfold rotoinversion axes always have mirror planes perpendicular to the axis.

A subscript $n = 1 \dots 6$ denotes the order of a rotation axis, and subscripts h , v , and d denote the three types of mirror plane described in Table 2.10.

International notation appears in the lower part of each cell in Table 2.9, with complete designations on the left, and conventional abbreviations to the right. The notation associates each group with a list of its symmetry axes, in accord with Table 2.10. Notation such as $6m$ refers to a mirror plane containing a sixfold axis, while $\frac{6}{m}$ refers to a mirror plane perpendicular to a sixfold axis.



Figure 2.15. A solid may have pentagonal symmetry, but one cannot tile the plane with it, so one cannot build a lattice with this symmetry.

Table 2.9 is not a complete list of all possible point groups. Rather, it is a list of point group symmetries that can be exhibited by a lattice. Of course, one can build an object with a fivefold axis, as shown in Figure 2.15. But there is no way to build any sort of completely regular lattice that shares this symmetry, as shown in Problem 1.4. A lattice with a fivefold axis is crystallographically forbidden. See, however, Section 5.10.

2.5.2 Two Hundred Thirty Distinct Lattices

The grand total of distinct lattices with bases is 230, exhaustively discussed by Hahn and Cochran (1992) and Bradley and Cracknell (1972) or in a more pedagogical manner by Borchardt-Ott (1993). A first group of lattices, the *symmorphic* lattices, can be constructed by taking objects of the symmetries described in Table 2.9 and placing them with various orientations at the lattice sites of the 14 Bravais lattices. There are 73 lattices of this type. The remaining lattices are *nonsymmorphic*, which means that they contain symmetry operations in which a translation and rotation or reflection applied simultaneously leave a lattice invariant, although neither the translation nor the rotation applied independently would do so. A structure containing a symmetry of this type was pictured in Figure 1.9. When a translation followed by rotation leaves the lattice invariant, one has a *screw axis*, while when a translation followed by reflection leaves it unchanged, one has a *glide plane*. Problem 5 shows that the hcp lattice contains both glide planes and screw axes.

Decorating lattice points with quantum-mechanical spins creates even more elaborate possibilities for symmetry groups, because a spin $1/2$ particle acquires a phase of -1 after rotation through 2π radians. The symmetry groups obtained in this way are called the *Shubnikov*, *color*, or *magnetic* groups; there are 1651 of them, and they are discussed by Vainshtein (1994) and Lifshitz (1997).

Large though the number of crystal space groups may be, it is small compared to the number of distinct crystals realizing these symmetries, which is without limit. Compilations of crystal structures may be found in Wyckoff (1963–1971), Landolt and Börnstein (New Series), vols. 5–7, 10, and 14, and Pearson (1985). Computer automated hardware and software are making it progressively easier to analyze new and complicated crystal structures. The *Cambridge Structural Database* contains a listing of over 400,000 organic and metal organic compounds. The *NIST Crystal Data Base* contains data for over 230,000 materials. These sources require a paid subscription. For the purposes of most physicists, the 3500 minerals catalogued in the freely available *American Mineralogist Crystal Structure Database* will be sufficient.

2.6 Some Macroscopic Implications of Microscopic Symmetries

Sometimes symmetries of an object that are evident on a macroscopic scale can be used to restrict the possible lattices from which it could possibly be constructed. Here are a few examples.

2.6.1 Pyroelectricity

Pyroelectric crystals, such as tourmaline, have a bulk dipole moment as a result of having a dipole moment in each unit cell. The rather problematic nature of these dipole moments will be discussed in Section 22.2. Under normal conditions, stray electrons in the environment shield this dipole, making it invisible, but upon heating or cooling, the ends of the crystal develop momentarily a measurable charge. Taking the dipole moment to point along the axis of maximum symmetry, one must rule out all point groups that contain a perpendicular mirror plane, or any sort of rotoinversion axis, because the dipole changes sign under any of these symmetry operations, or any rotation axis perpendicular to the main one. The cubic groups can also be ruled out because they all contain threefold axes that are incompatible with a dipole moment. Consulting Table 2.9, one sees that the only point groups remaining are C_n ($n = 1 \dots 6$), C_{nv} ($n = 2 \dots 6$), and C_{1h} .

2.6.2 Piezoelectricity

The *piezoelectric* crystals have no dipole moment in their ground state, but acquire one upon application of a mechanical deformation in some direction. Quartz is the most common example displaying such behavior. Suppose that one deforms the crystal by moving each lattice point a small distance $\vec{u}(\vec{r})$, which varies smoothly as one travels through the crystal. The *strain tensor* is a matrix of deformations of the crystal defined by

$$e_{\alpha\beta} = \frac{1}{2} \left(\frac{\partial u_\alpha}{\partial r_\beta} + \frac{\partial u_\beta}{\partial r_\alpha} \right); \quad \text{If } e_{xx} \text{ is nonzero, the crystal has been stretched in the } x \text{ direction, while if } e_{xy} \text{ is nonzero, the crystal has been sheared in the } x-y \text{ plane.} \quad (2.10)$$

it will be discussed at length in section 12.3. Assuming that the polarization \vec{P} arises as a linear function of the applied strains, it must take the form

$$P_\gamma = \sum_{\alpha\beta} \mathcal{B}_{\alpha\beta\gamma} e_{\alpha\beta}, \quad (2.11)$$

where \mathcal{B} is some tensor describing a general linear relationship between dipole moment and the strain. Now if one performs an inversion on the crystal, sending $\vec{r} \rightarrow -\vec{r}$, the strain tensor is invariant, but the polarization must change sign, and so therefore must \mathcal{B} . This means that if the crystal is invariant under inversion, \mathcal{B} must vanish. All piezoelectric crystals must therefore be *noncentrosymmetric*, and their point groups exclude D_{nh} and S_2 .

2.6.3 Optical Activity

Certain crystals, such as SiO_2 (low quartz) are able to rotate the plane of incoming polarized light. Such behavior is only possible if the unit cells are *chiral*, meaning that there is a mirror image of the cell which cannot be related to it by any translation or rotation. Finding the point groups that have chiral unit cells is the subject of Problem 8.

Problems

- 1. Face-centered and body-centered cubic lattices:** Consider the face-centered and body-centered cubic lattices to be simple cubic lattices decorated with a basis.
 - (a) Determine the number of basis vectors that is necessary, and write down the basis vectors for each of these lattices.
 - (b) Determine in each case the ratio of the volume of the conventional unit cell to the primitive unit cell.
- 2. Face-centered cubic lattice as stacked triangles:**
 - (a) Let \vec{a}_1 and \vec{a}_2 be primitive vectors for a triangular lattice. Referring to Figure 2.2 (C), find a third primitive vector that stacks two-dimensional triangular lattices so as to produce an fcc lattice.
 - (b) The cube shown in Figure 2.2(D) can be brought into the orientation depicted there by a first rotation around the \hat{y} axis, followed by a rotation around the \hat{x} axis. Find the two rotation angles.
- 3. Fourfold coordination:** What is the angle between neighboring bonds in the fourfold coordinated diamond and wurtzite lattices?
- 4. Hexagonal close-packed lattice:**
 - (a) Verify that the basis vectors given by Eq. (2.6) result in placing atoms directly over the centers of triangles along the c axis.

(b) Verify that the hcp lattice forms a close-packed structure when $c/a = \sqrt{8/3}$.

5. **Glide and screw axes:** Let the lower left point in Figure 2.16 be the origin.

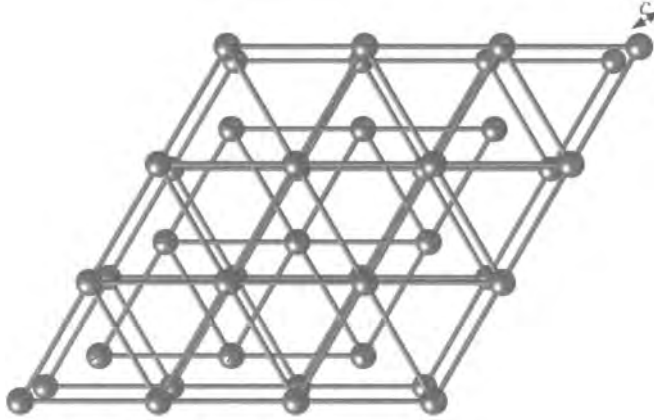


Figure 2.16. Top view of an hcp lattice.

(a) The hcp lattice contains a screw axis in the c direction. Referring to Figure 2.16, describe the Cartesian coordinates of a point through which this axis can pass, so that the lattice remains invariant under translation along \vec{c} by $c/2$ followed by rotation through 60° .

(b) The hcp also has a glide plane, which is parallel to a plane containing both the \vec{a} and \vec{c} axes. Describe where this plane may be located, so that translation along $\vec{c}/2$ followed by reflection about the plane leaves the lattice invariant.

6. **Packing fractions:** It is difficult to avoid asking why elements choose the crystal structure they do. Without a quantitative theory of cohesion, developed in Chapter 11, this question cannot be answered in detail. However, simple arguments can explain a great deal. Many atoms are held together by isotropic attraction that favors packing them as closely as possible. The concept of packing can be addressed by setting the distance between nearest neighbors in a given lattice to 2, putting unit spheres on each lattice site, and asking what portion of space is occupied by the spheres. This number is the *packing fraction* and is displayed in Table 2.11.

Verify the packing fractions listed in Table 2.11. The packing argument explains the great frequency of the hcp and fcc structures, although it cannot explain how crystals would choose between them.

7. **Three-dimensional ground states:** Consider a collection of particles in three dimensions whose energy is

$$\mathcal{E} = \frac{1}{2} \sum_{i \neq j} \phi(r_{ij}) \quad \text{with} \quad (2.12)$$

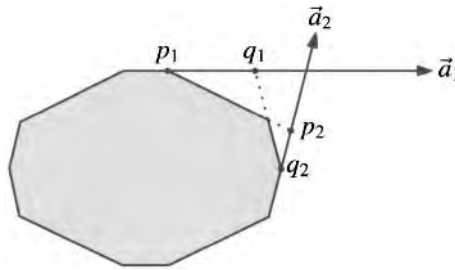
Table 2.11. Packing fractions for various crystal structures

Structure	Packing Fraction
hcp	0.74
fcc	0.74
bcc	0.68
sc	0.52
diamond	0.34

$$\phi(r) = \begin{cases} \phi_0 \exp(-r) \left(\frac{1}{r^3} - 1 \right) & \text{if } r < 1.5 \\ 0 & \text{else,} \end{cases} \quad (2.13)$$

where r_{ij} is the distance (measured, say, in Å) between particles i and j . Compare the energies of the bcc, fcc, and hcp lattices. Find the lattice spacing leading to the minimum energy for each of these three lattices, and find the state of lowest overall energy.

8. **Optical activity:** Find all the crystallographic point groups allowed for crystals which rotate the plane of incoming polarized light. The group C_1 is one of them; it is called asymmetric, and all the others are called chiral.
9. **Second law of crystal habit:**

**Figure 2.17.** Setting for the second law of crystal habit in two dimensions.

The second law of crystal habit, or Haüy's law of rational parameters, relates the possible faces of a crystal to a set of integers. The prescription, found empirically for real crystals follows:

Pick any three linearly independent edges of a crystal (they will not generally be orthogonal) and use them as reference axes, \vec{a}_1 , \vec{a}_2 , and \vec{a}_3 (see Figure 2.17). Take any face of the crystal and find the three points where it cuts the reference axes; call these points (p_1, p_2, p_3) . Next, take any other face of the crystal, and find again the three points (q_1, q_2, q_3) where this second plane cuts the axes. Then $p_1/q_1 = r_1$, $p_2/q_2 = r_2$, and $p_3/q_3 = r_3$ are rational numbers, and the ratios between r_1 , r_2 , and r_3 can be written as the ratios of integers.

- (a) Prove that the law of rational parameters holds for any two-dimensional crystal that is created by drawing straight lines between points of a Bravais lattice.
- (b) Generalize the result to a three-dimensional lattice.

References

- W. Borchardt-Ott (1993), *Crystallography*, Springer-Verlag, Berlin.
- C. J. Bradley and A. P. Cracknell (1972), *The Mathematical Theory of Symmetry in Solids; Representation Theory for Point Groups and Space Groups*, Clarendon Press, Oxford.
- A. Bravais (1850), Memoire on systems formed by points distributed regularly on a plane or in space, *Journal de l'Ecole Polytechnique*, **XIX**(33), 1–128. In French.
- P. P. Ewald, ed. (1962), *Fifty Years of X-Ray Diffraction*, International Union of Crystallography.
- E. Fedorov (1895), Theory of crystal structure, *Zeitschrift für Krystallographie und Mineralogie*, **24**, 209–252. In German.
- T. Hahn and A. J. Cochran, eds. (1992), *International Tables for Crystallography*, vol. A: Space Group Symmetry, 3rd ed., Kluwer Academic Publishers, Dordrecht.
- J. F. C. Hessel (1830), *Crystallonomy: or Crystallonomy and Crystallography*, vol. 5 of *Gehler's physikalisches Wörterbuch*, Schwichert, Leipzig. In German.
- L. Hoddeson, E. Braun, J. Teichmann, and S. Weart, eds. (1992), *Out of the Crystal Maze*, Oxford University Press, Oxford.
- H. Landolt and R. Börnstein (New Series), *Numerical Data and Functional Relationships in Science and Technology*, New Series, Group III, Springer-Verlag, Berlin.
- R. Lifshitz (1997), Theory of color symmetry for periodic and quasiperiodic crystals, *Reviews of Modern Physics*, **69**(4), 1181–1218.
- W. B. Pearson (1985), *Handbook of Crystallographic Data for Intermetallic Phases*, American Society for Metals, Metals Park, OH.
- F. C. Phillips (1971), *An Introduction to Crystallography*, 4th ed., Oliver and Boyd, Edinburgh.
- A. Schönflies (1891), *Krystalssysteme und Krystalstruktur*, Leipzig. In German.
- L. Sohncke (1879), *Development of a Theory of Crystal Structure*, B G Teubner, Leipzig. In German. Readex Microprint, 1972 (Landmarks of Science).
- B. K. Vainshtein (1994), *Fundamentals of Crystals: Symmetry and Methods of Structural Crystallography*, vol. 1 of *Modern Crystallography*, 2nd ed., Springer-Verlag, Berlin.
- R. W. G. Wyckoff (1963–1971), *Crystal Structures*, 2nd ed., John Wiley and Sons, New York.

3. Scattering and Structures

3.1 Introduction

The scattering of X-rays from crystals provided information on the locations of atoms within solids that had been the object of speculation for centuries, and it rapidly led to a huge scientific enterprise of structure determination, but before the first careful experiments of 1912 it was far from obvious that anything could come of it at all.

M. von Laue was struck in 1912 by the intuition that X-rays might scatter off crystals in the way that ordinary light scatters off a diffraction grating. This hunch preceded any mathematical attempt to quantify the size and character of the effect, and if it seems obvious in retrospect, one might keep in mind that neither the periodic character of crystals nor the wave nature of X-rays was known with certainty at the time. Laue discussed

his idea with colleagues Sommerfeld, Wien and others with the result of encountering a strong disbelief in a significant outcome of any diffraction experiment based upon the regularity of the internal structure of crystals. It was argued that the inevitable temperature motion of the atoms would impair the regularity of the grating to such an extent that no pronounced diffraction maxima could be expected. —Ewald (1962), p. 42

This argument against diffraction effects was in fact quite reasonable. Consider, for example, the prospect of scattering off NaCl. The study of elastic deformations was well developed in 1912, and salt crystals were known to be anisotropic, but characterized approximately by Young's modulus Y (defined in Section 12.3.2) of $5 \cdot 10^{11}$ ergs cm^{-3} . The chlorine atom was known to have a mass of 35 g mole^{-1} , and sodium 23 g mole^{-1} ; from salt's known density of 4.29 g cm^{-3} , a characteristic spacing of $d = 2.5 \cdot 10^{-8}$ cm between sodium and chlorine could be determined. To account for the observed Young modulus, one would need a spring constant between atoms on the order of $\mathcal{K} = Yd = 10^4$ dyne cm^{-1} . Making use of the equipartition theorem, the characteristic excursion of atoms due to thermal fluctuations should therefore be expected to be $x = \sqrt{2k_B T / \mathcal{K}} \approx 2 \cdot 10^{-9}$ cm. This distance is fortunately smaller than the interatomic spacing; it has to be, otherwise the crystals would melt. However, the best estimate for the wavelength of X-rays based upon diffraction around small slits was also of order 10^{-9} cm. A diffraction grating whose vibrations are the same size as the incoming waves hardly seemed to pose a promising experiment, and Sommerfeld was reluctant to devote resources or personnel. The work was carried out by Friedrich et al. (1912) with equipment

pirated from elsewhere; it successfully produced diffraction spots from copper sulfate on only the second attempt, the first having failed when photographic plates were placed in front of the crystal in the mistaken expectation that reflected X-rays would produce the largest effect. Laue's mathematical theory for the directions of X-ray maxima followed only a few hours later. At first the theory did not encompass the possibility of a lattice with a basis, with the result that some predicted spots were mysteriously absent from the experiment.

There was some question, at first, about whether the spots observed on the photographic plate were truly due to diffraction from the crystal. The doubts were largely dispelled by a series of experiments which seemed to rule out any other possibility. First the crystalline sample was removed, and it was checked that the diffraction pattern disappeared. Second, the crystal was replaced by a powdered sample of the same material, and again distinct spots disappeared. Finally, the orientation of the crystal was altered slightly, and the spots were observed slightly displaced on the photographic plate. Several years were to pass before it could correctly be explained why thermal agitation did not obliterate the X-ray interference, but by summer of 1912 the phenomenon was well on its way to wide acceptance throughout Germany.

The discovery of X-ray diffraction contains many elements that have been absolutely characteristic of important developments in condensed matter physics. The enterprise began with a theoretical notion to which, however, there were compelling theoretical objections. The experiment rapidly encountered a highly regular set of phenomena with which theory agreed only uneasily in its first incarnation. A rapid simultaneous development of theory and experiment in concert then produced a new set of concepts and a powerful new experimental tool.

3.2 Theory of Scattering from Crystals

3.2.1 Special Conditions for Scattering

X-rays created a world-wide sensation at the end of the nineteenth century because they could produce images of the interior of the human body. This means that they can travel through several centimeters of solid matter, attenuating weakly, and come out the other side. When X-rays travel through crystals this is usually what happens.

However, there is an important exception. When the wavelength of the X-rays is chosen precisely right, and simultaneously the orientation of the crystal is precisely right, there is constructive interference between the waves scattered by successive atoms. Intense narrow beams of X-rays emerge from the crystal in a finite number of special directions. Friedrich, Knipping, and von Laue were not so lucky as to stumble exactly upon the frequency of radiation needed to create the effect. Their X-rays contained a broad spectrum of radiation, and happened to contain the special waves (Section 3.3.1). The same considerations apply to neutrons and electrons, two other types of waves that can reveal atomic positions in condensed matter. Their interaction with matter is mainly linear, so it is enough

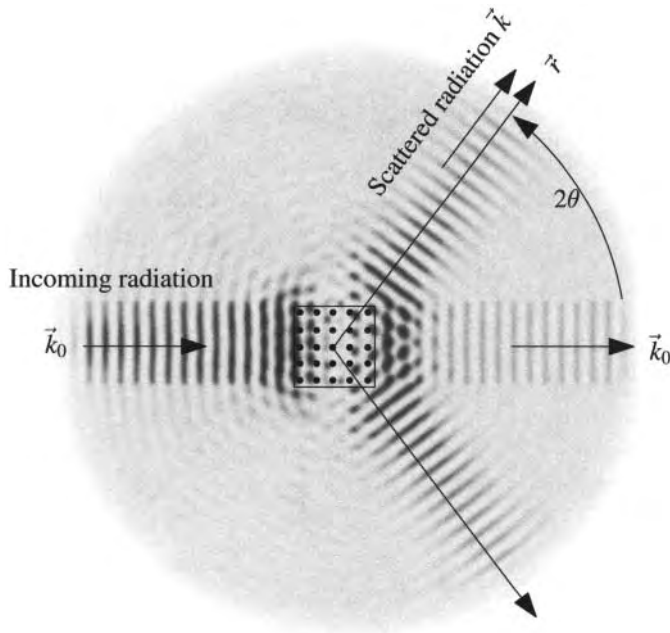


Figure 3.1. Geometry of a scattering experiment. Radiation of wave vector \vec{k}_0 arrives at a sample, inducing a circular ring of radiation to depart from each atom. If \vec{k}_0 is chosen just right, the scattered radiation from the atoms adds constructively in certain directions. It is detected at position \vec{r} , which points in the same direction as the scattered radiation \vec{k} . The Bragg angle θ characterizing the scattering is half the scattering angle at which the radiation is observed. This figure shows the amplitude of the radiation field due to a square crystal composed of 25 atoms; the angular range of constructive interference becomes much narrower for larger crystals. Figure 3.2 contains a more precise characterization of the waves involved in this figure.

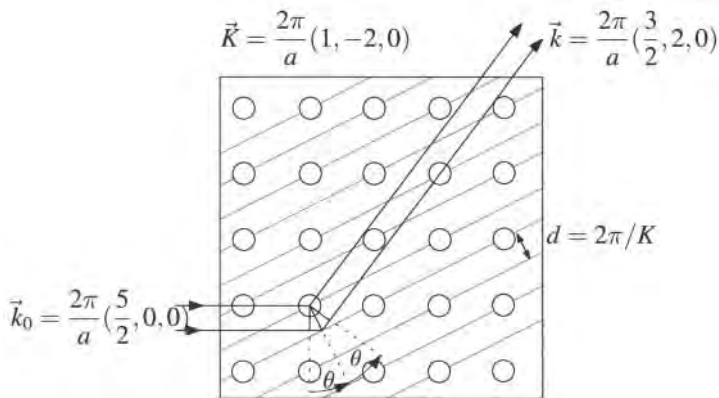


Figure 3.2. Illustration of Bragg scattering at angle $\theta = 26.56^\circ$ from the (21) planes of a square lattice. The magnitudes of \vec{k}_0 , \vec{k} , and \vec{K} are determined using Eqs. (3.38) and (3.39).

to pick a single incoming plane wave, study what happens, and build a theory of more elaborate scattering experiments by superposition.

3.2.2 Elastic Scattering from Single Atom

In a scattering experiment, a plane wave moves into a sample of condensed matter, travels through it, interacts, comes out, and is measured by detectors far away. In the simplest class of scattering experiments, the frequency of the outgoing radiation is the same as that of the radiation sent in, and the scattering is called *elastic*. This phenomenon is most easily explained by invoking wave-particle duality to view the incoming radiation as photons, neutrons, or electrons that bounce without any change of energy off atoms in the sample.

Begin by considering a plane wave that collides with a single atom sitting at the origin and scatters off it. Whether the incoming wave is a neutron or an electron described by quantum mechanics, or an X-ray described by classical electromagnetism, the scattered wave ψ takes a particularly simple form far from the atom:

$$\psi \approx Ae^{-i\omega t} \left[e^{i\vec{k}_0 \cdot \vec{r}} + f(\hat{r}) \frac{e^{ik_0 r}}{r} \right], \quad \text{See, for example, Schiff (1968) p. 115 for the quantum mechanical version, or Jackson (1999) Eq. (9.8) for the electromagnetic version.} \quad (3.1)$$

where the particle enters as a plane wave along \vec{k}_0 , the scattering is measured at a distance r that is much larger than the range of interaction with the atom, at angle 2θ relative to the \vec{k}_0 axis, and f is a form factor containing details about the interaction between the scattering potential and the scattered wave. It is related to the differential scattering cross-section of the atom by

$$I_{\text{atom}} \equiv \frac{d\sigma}{d\Omega}_{\text{atom}} = |f(\hat{r})|^2 \quad \text{The intensity of scattered radiation into solid angle } d\Omega \text{ at distance } r \text{ relative to the incoming beam is } d\Omega \times d\sigma/d\Omega/r^2. \quad (3.2)$$

Forms for f will be given in Section 3.4, but for the moment assume f to be known.

Next ask how Eq. (3.1) changes when the same incoming plane wave scatters off a particle located at \vec{R} rather than at the origin. In this case, when the radiation arrives at point \vec{R} , it has phase $\exp(i\vec{k}_0 \cdot \vec{R})$ relative to what it would have had at the origin. On the other hand, to reach the observation point, it then has only to travel a distance $|\vec{r} - \vec{R}|$ rather than r as previously. Therefore

$$\psi \sim Ae^{-i\omega t} e^{i\vec{k}_0 \cdot \vec{R}} \left[e^{i\vec{k}_0 \cdot (\vec{r} - \vec{R})} + f(\hat{r}) \frac{e^{ik_0 |\vec{r} - \vec{R}|}}{|\vec{r} - \vec{R}|} \right]. \quad \text{The leading exponential is unchanged from Eq. (3.1).} \quad (3.3)$$

For sufficiently large r , one may use the approximation

$$k_0 |\vec{r} - \vec{R}| \approx k_0 r - k_0 \frac{\vec{r}}{r} \cdot \vec{R}. \quad (3.4)$$

Using Eq. (3.4) and defining

$$\vec{k} = k_0 \frac{\vec{r}}{r}, \quad \vec{k} \text{ points in the observation direction} \quad (3.5)$$

\vec{r} and has the same magnitude as k_0 .

$$\text{and } \vec{q} = \vec{k}_0 - \vec{k} \quad (3.6)$$

gives

$$\psi \sim A e^{-i\omega t} \left[e^{i\vec{k}_0 \cdot \vec{r}} + f(\hat{r}) \frac{e^{ik_0 r + i\vec{q} \cdot \vec{R}}}{r} \right]. \quad (3.7)$$

In the denominator of Eq. (3.3) one needs only the first term on the right side of Eq. (3.4). However, within the exponential function, one has to keep all terms that are large compared to 2π , and requires both terms on the right side of Eq. (3.4).

Note that

$$q = 2k_0 \sin \theta. \quad (3.8)$$

Square both sides of Eq. (3.6) and use the fact that $\vec{k}_0 \cdot \vec{k} = k_0^2 \cos 2\theta$.

The quantity $\hbar\vec{q}$ describes the *momentum transfer* between the incoming and outgoing waves, and the angle θ is called the *Bragg angle*.

3.2.3 Wave Scattering from Many Atoms

When one has a large assembly of scatterers, shown in Figures 3.1 and 3.2, the angular dependence of the scattered radiation is the product of two pieces. The first results from the fact that each individual scatterer emits radiation with different intensities in different directions, described by the *form factor* f . The second, which modulates the first, results from interference between the radiation coming from the various objects and therefore contains information about their spatial correlation.

So consider a large collection of scatterers, placing the origin somewhere in the middle of them, and observe the scattering from far away. If the scatterers are dilute, then the total scattered radiation due to the collection will simply be a sum of the radiation due to each one. Ignoring the contributions that arise when the light which has scattered off one atom then scatters off of another one before being observed (*multiple scattering*), as well as ignoring contributions arising from changes in the state of the scatterer (*inelastic scattering*), one has

$$\psi \sim A e^{-i\omega t} \left[e^{i\vec{k}_0 \cdot \vec{r}} + \sum_l f_l(\hat{r}) \frac{e^{ik_0 r + i\vec{q} \cdot \vec{R}_l}}{r} \right]. \quad (3.9)$$

Summing many terms of the sort that arise in Eq. (3.7).

The largest contribution to ψ comes from the incoming beam $\exp[i\vec{k}_0 \cdot \vec{r}]$, which also exits the sample as shown in Figure 3.1. However this bright spot is restricted to an outgoing angle of $\theta = 0$, so with the understanding that one will restrict attention to nonzero scattering angles it is possible to drop the first term on the right-hand side of Eq. (3.9). The intensity per unit solid angle divided by the intensity $|A|^2$ of the incoming beam, $I \equiv |\psi|^2 r^2 / A^2$ is then

$$I = \sum_{l,l'} f_l f_{l'}^* e^{i\vec{q} \cdot (\vec{R}_l - \vec{R}_{l'})}. \quad (3.10)$$

Recall that $|\sum_l C_l|^2 = \sum_{l,l'} C_l C_{l'}^*$. The functions f_l still depend upon the scattering direction \hat{r} , but the dependence is not made explicit.

This basic equation for weak elastic scattering applies to scattering off matter in all forms. The equation is posed in terms of intensity rather than amplitude because intensity is the quantity measured by experimental instruments.

3.2.4 Lattice Sums

Now ask what happens when all of the scatterers in the sum (3.10) are identical and arranged in a Bravais lattice. In this case, the scattering intensity is equal to

$$I = I_{\text{atom}} \sum_{l'l'} e^{i\vec{q} \cdot (\vec{R}_l - \vec{R}_{l'})}. \quad I_{\text{atom}} \text{ is the scattering from a single atom, defined in Eq. (3.2).} \quad (3.11)$$

Inspection of Eq. (3.11) leads to a plausible guess for the wave vectors \vec{q} that will produce strong scattering. If one could choose \vec{q} so that $\exp(i\vec{q} \cdot \vec{R}) = 1$ for all \vec{R} , then all terms in Eq. (3.11) would be one, and summing them would produce a large final result. Otherwise, one might expect terms in Eq. (3.11) to alternate in sign and to cancel out on average.

This guess is correct, but to justify it one must understand sums of the type appearing in Eq. (3.11). Such sums determine the behavior of any waves interacting with a periodic lattice; they are important not only for X-ray scattering, but also for conduction electrons in lattices (Chapter 7). The mathematics of the sum is best explained in one dimension, and then generalized.

One-Dimensional Sum. In one dimension, lattice points must be of the form la , where l is an integer and a is the interparticle spacing. So the relevant sum in Eq. (3.11) becomes

$$\Sigma_q = \sum_{l=0}^{N-1} e^{ilaq}. \quad (3.12)$$

This sum is calculated in Appendix A, which yields the results

$$\Sigma_q = \frac{e^{iNaq} - 1}{e^{iaq} - 1} \quad (3.13)$$

$$|\Sigma_q|^2 = \frac{\sin^2 Naq/2}{\sin^2 aq/2}. \quad (3.14)$$

A plot of Eq. (3.14) appears in Figure 3.3. The graph contains a number of very sharp identical peaks, separated by regions where the scattering intensity is nearly zero. The locations of the peaks are determined by searching for the points at which the denominator of Eq. (3.14) vanishes. They occur whenever

$$aq/2 = l\pi \Rightarrow q = 2\pi l/a. \quad l \text{ is an integer.} \quad (3.15)$$

Glancing back at Eq. (3.12), one sees that peaks in the sum Σ_q correspond exactly to the choices for q such that all terms in the sum (3.12) equal 1 and thus add coherently. For any other choice of q , the terms in the sum add with different phases and signs, giving a much smaller result.

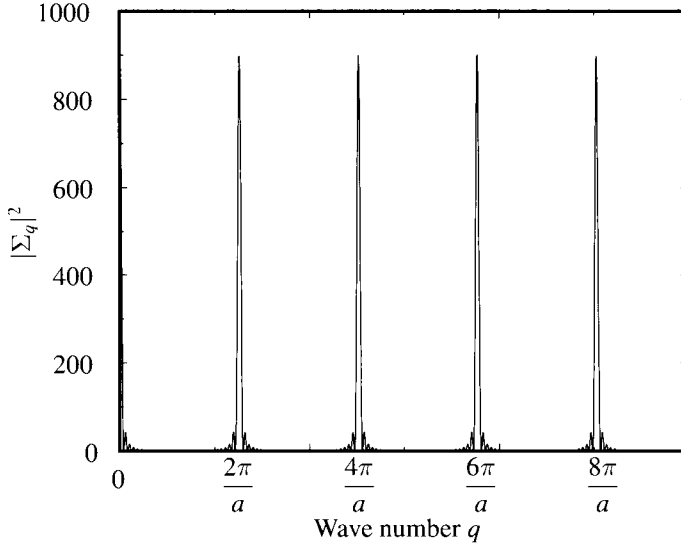


Figure 3.3. Plot of $|\Sigma_q|^2$ from Eq. (3.14), for $N = 30$. Note the sharp peaks centered around points where $q = 2\pi l/a$.

Because the peaks in Figure 3.3 are so sharp, it is natural to view Σ_q as a sum of delta functions. However, because the delta function is defined to have unit area lying beneath it, one must find the area under each peak. It is calculated in Appendix A and is $2\pi N/L$. Thus one has the identity

$$\sum_{l=0}^{N-1} e^{ilaq} = \sum_{l'=-\infty}^{\infty} N \frac{2\pi}{L} \delta(q - 2\pi l'/a). \quad (3.16)$$

3.2.5 Reciprocal Lattice

Returning now to Eq. (3.11), one can state that the requirement for the sum to yield a sharp peak is that \vec{q} be chosen such that

$$\vec{q} \cdot \vec{R} = 2\pi l \quad (3.17)$$

for all \vec{R} in the Bravais lattice, and with l some integer depending upon \vec{R} . Once \vec{q} has been chosen in this fashion, all the terms in the sum (3.11) equal one and add together, producing a *Bragg peak*. Any scattering vector \vec{q} with this property will be denoted by the symbol \vec{K} , and the collection of scattering vectors \vec{K} satisfying

$$\exp[i\vec{K} \cdot \vec{R}] = 1 \text{ or } \vec{K} \cdot \vec{R} = 2\pi l \quad \begin{array}{l} \text{The value of the integer } l \text{ will depend upon} \\ \text{the choice of } \vec{R} \text{ and } \vec{K}. \text{ This equation demands} \\ \text{only that the dot product produce } 2\pi \\ \text{times some integer.} \end{array} \quad (3.18)$$

is called the *reciprocal lattice*. The importance of the reciprocal lattice is that it identifies the collection of wave vectors \vec{K} for which coherent scattering can occur off a Bravais lattice. The strength of the scattering is given by the analog of

Eq. (3.16), which according to Eq. (A.25) is

$$\sum_{\vec{R}} e^{i\vec{R}\cdot\vec{q}} = \sum_{\vec{K}} N \frac{(2\pi)^3}{\mathcal{V}} \delta(\vec{q} - \vec{K}), \quad (3.19)$$

where \mathcal{V} is the volume of the system.

Bragg Planes. Why should there be any \vec{K} that have property (3.18), and why do they form a lattice? First of all, notice that if one finds any two \vec{K} that have this property, then their sum has it. Second of all, suppose that one has found a vector \vec{K} so that

$$\vec{K} \cdot \vec{R} = 0 \quad (3.20)$$

for at least three noncollinear Bravais lattice points \vec{R} . The set of all \vec{r} that satisfy $\vec{K} \cdot \vec{r} = 0$ is a plane passing through the origin, so the \vec{R} that satisfy Eq. (3.20) must lie in such a plane \mathcal{P}_0 (Figure 3.4), and \vec{K} must be the normal to that plane. Thus the direction of every \vec{K} corresponds to a plane containing points in the Bravais lattice. However, it is not enough to guarantee that $\vec{K} \cdot \vec{R} = 0$ for \vec{R} lying on the plane \mathcal{P}_0 ; one needs Eq. (3.18) to hold for all \vec{R} . To achieve this goal, it is essential to note that the whole Bravais lattice can always be constructed by taking the points that lie in the plane \mathcal{P}_0 , all of which are of the form

$$l_1 \vec{a}_1 + l_2 \vec{a}_2, \quad \text{Having chosen a plane, one can then find two primitive vectors that span it.} \quad (3.21)$$

and stacking multiple copies of this plane next to one other, separated by a third primitive vector \vec{a}_3 , as shown in Figure 3.4. There is an infinite number of ways to decompose a crystal in this fashion into *Bragg planes*.

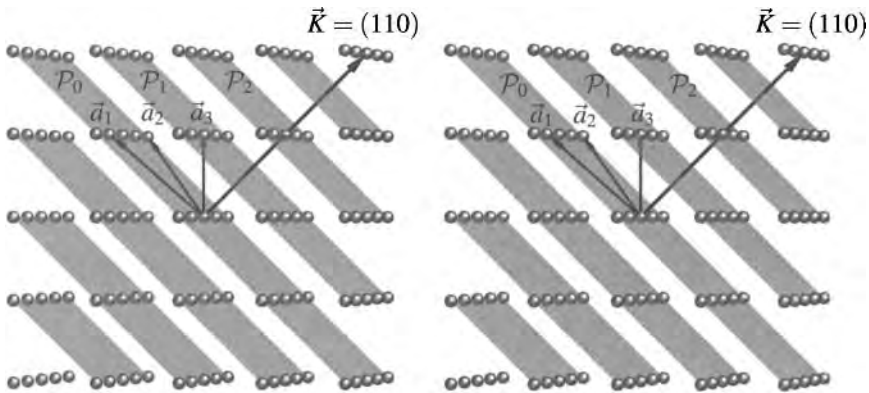


Figure 3.4. Any Bravais lattice can be regarded as composed of parallel planes of points, the Bragg planes. In this case, a simple cubic lattice is built out of parallel planes normal to (110) (stereo pair).

Choose the magnitude of \vec{K} so that

$$\vec{a}_3 \cdot \vec{K} = 2\pi. \quad (3.22)$$

Once Eq. (3.22) is satisfied, one has for any point in the Bravais lattice

$$\vec{K} \cdot \vec{R} = \vec{K} \cdot (l_1 \vec{a}_1 + l_2 \vec{a}_2 + l_3 \vec{a}_3) = 2\pi l_3. \quad (3.23)$$

The integer l_3 simply counts by how many lattice planes the one containing \vec{R} is distant from the origin.

Because the magnitudes of the vectors \vec{K} are not arbitrarily small according to Eq. (3.22) and because the sum of any two is another such vector, the set of \vec{K} 's must themselves form a lattice. One can find primitive vectors for the reciprocal lattice, by choosing any three primitive vectors \vec{a}_1 , \vec{a}_2 , and \vec{a}_3 for the Bravais lattice and then building three primitive vectors \vec{b}_1 , \vec{b}_2 , and \vec{b}_3 for the reciprocal lattice from

$$\vec{b}_1 = 2\pi \frac{\vec{a}_2 \times \vec{a}_3}{\vec{a}_1 \cdot \vec{a}_2 \times \vec{a}_3} \quad (3.24a)$$

$$\vec{b}_2 = 2\pi \frac{\vec{a}_3 \times \vec{a}_1}{\vec{a}_2 \cdot \vec{a}_3 \times \vec{a}_1} \quad (3.24b)$$

$$\vec{b}_3 = 2\pi \frac{\vec{a}_1 \times \vec{a}_2}{\vec{a}_3 \cdot \vec{a}_1 \times \vec{a}_2} \quad (3.24c)$$

$$\text{and in general } \vec{K} = \sum_{l=1}^3 m_l \vec{b}_l. \quad \text{The } m_l \text{ are arbitrary integers.} \quad (3.24d)$$

This construction works because if one takes the dot product of \vec{b}_l with any primitive vector $\vec{a}_{l'}$, the result is either zero or 2π . Therefore, any vector in the direct lattice dotted into linear combinations of the \vec{b}_l 's gives an integer times 2π as required.

Table 3.1 records the reciprocal lattices of four common Bravais lattices. The reciprocal lattice of a fcc lattice of spacing a is, a bcc lattice of spacing $4\pi/a$, the reciprocal lattice of a bcc lattice of spacing a is an fcc lattice of spacing $4\pi/a$, and the reciprocal lattice of an hexagonal lattice is another hexagonal lattice twisted by 30° .

3.2.6 Miller Indices

A traditional notation describing reciprocal lattice vectors, lattice planes, and lattice points is the *Miller index*. The notation is most commonly used for lattices of cubic and hexagonal symmetry.

In cubic crystals, one begins by defining three perpendicular coordinate axes \hat{x} , \hat{y} , and \hat{z} pointing along the edges of the conventional unit cell.

- $[ijk]$ refers to a *direction*

$$i\hat{x} + j\hat{y} + k\hat{z} \quad (3.25)$$

in the lattice specified by the three integers i , j , and k .

Table 3.1. Conventional primitive vectors of four common Bravais lattices and their reciprocal lattices.

Lattice	Lattice Spacing	Primitive Vectors	Reciprocal Lattice Spacing	Reciprocal Lattice Primitive Vectors
sc	a	$(1\ 0\ 0)$ $(0\ 1\ 0)$ $(0\ 0\ 1)$	$\frac{2\pi}{a}$	$(1\ 0\ 0)$ $(0\ 1\ 0)$ $(0\ 0\ 1)$
fcc	a	$(\frac{1}{2}\ \frac{1}{2}\ 0)$ $(\frac{1}{2}\ 0\ \frac{1}{2})$ $(0\ \frac{1}{2}\ \frac{1}{2})$	$\frac{4\pi}{a}$	$(\frac{1}{2}\ \frac{1}{2}\ -\frac{1}{2})$ $(-\frac{1}{2}\ \frac{1}{2}\ \frac{1}{2})$ $(\frac{1}{2}\ -\frac{1}{2}\ \frac{1}{2})$
bcc	a	$(\frac{1}{2}\ \frac{1}{2}\ -\frac{1}{2})$ $(-\frac{1}{2}\ \frac{1}{2}\ \frac{1}{2})$ $(\frac{1}{2}\ -\frac{1}{2}\ \frac{1}{2})$	$\frac{4\pi}{a}$	$(\frac{1}{2}\ \frac{1}{2}\ 0)$ $(\frac{1}{2}\ 0\ \frac{1}{2})$ $(0\ \frac{1}{2}\ \frac{1}{2})$
hex	a, c	$(\frac{1}{2}\ \frac{\sqrt{3}}{2}\ 0)$ $(-\frac{1}{2}\ \frac{\sqrt{3}}{2}\ 0)$ $(0\ 0\ 1)$	$\frac{4\pi}{\sqrt{3}a}, \frac{2\pi}{c}$	$(\frac{\sqrt{3}}{2}\ \frac{1}{2}\ 0)$ $(\frac{\sqrt{3}}{2}\ -\frac{1}{2}\ 0)$ $(0\ 0\ 1)$

- (ijk) refers to a *lattice plane* perpendicular to the normal vector $[ijk]$. (ijk) may also refer to the reciprocal lattice vector of smallest magnitude perpendicular to the plane (ijk) .
- $\{ijk\}$ refers to the complete collection of lattice planes perpendicular to $[ijk]$.
- ijk refers to the X-ray diffraction peak resulting from scattering off the lattice planes $\{ijk\}$.
- Negative integers are denoted by \bar{i} rather than $-i$.
- $\langle ijk \rangle$ refers to the set of all lattice planes or reciprocal lattice vectors related to (ijk) by rotational symmetry.

Examples. For a simple cubic lattice, the reciprocal lattice vector pointing along $(2\pi/a, 0, 0)$ is called (100) , while the one along $(2\pi/a, 2\pi/a, 2\pi/a)$ is called (111) and the one along $(2\pi/a, -2\pi/a, 2\pi/a)$ is called $(1\bar{1}1)$, and so forth. For an fcc lattice, the smallest reciprocal lattice vector is (111) , and it has magnitude $2\sqrt{3}\pi/a$. The collection of reciprocal lattice points referred to by $\langle 100 \rangle$ is (100) , (010) , (001) , $(\bar{1}00)$, $(0\bar{1}0)$, and $(00\bar{1})$.

Alternate Definition. An alternate prescription used by crystallographers to find the Miller index of a plane is to find a lattice point as near as possible to the plane

but not lying within it. Placing the origin at this lattice site, find the three points u , v , and w where the plane intersects the coordinate axes, measured in units of the lattice spacing a . The inverses $i = 1/u$, $j = 1/v$ and $k = 1/w$ of these intercepts are integers equal to Miller indices. This point of view is closely allied with the second law of crystal habit, and therefore rooted in the origins of crystallography (Problem 9 in Chapter 2). If the plane is parallel to one of the coordinate axes, one might for example get $u = \infty$, leading to $i = 0$.

Miller Indices for Hexagonal Lattices. In hexagonal lattices, Miller indices make use of four numbers $(ijkl)$. The last integer, l , points along the \hat{z} axis (the axis of three- or sixfold symmetry), while i , j , and k refer to three axes at 120° to one another, and conventionally

$$k = -(i + j). \quad (3.26)$$

The precise meaning of i , j , and k is most clear if one uses the crystallographer's definition of the Miller indices as inverse distances along crystal axes, as illustrated in Figure 3.5.

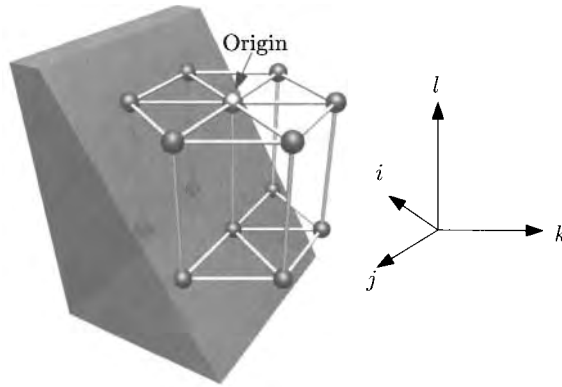


Figure 3.5. The $(1\ 0\ \bar{1}\ \bar{1})$ lattice plane illustrated for an hexagonal lattice. The distances to the plane along the coordinate axes are a , ∞ , $-a$, and $-c$, and the inverses of these distances, in units of the lattice parameters a and c , lead to the Miller indices.

3.2.7 Scattering from a Lattice with a Basis

The precise conditions for sharp scattering peaks are modified if the crystal is not a Bravais lattice, but is instead a lattice with a basis. In this case, every vector in the crystal can be written in the form

$$\vec{R} = \vec{u}_l + \vec{v}_{l'} \quad (3.27)$$

for some l and l' , where \vec{u}_l is a vector in a Bravais lattice and $\vec{v}_{l'}$ is an element in the basis. Assuming all atoms to be identical, as in the diamond or hcp lattices, scattering from such a lattice can be calculated by regrouping the basic sum.

$$\sum_{\vec{R}} e^{i\vec{q}\cdot\vec{R}} = \sum_{l'} e^{i\vec{q}\cdot(\vec{u}_l + \vec{v}_{l'})} \quad (3.28)$$

$$= \left(\sum_l e^{i\vec{q}\cdot\vec{u}_l} \right) \left(\sum_{l'} e^{i\vec{q}\cdot\vec{v}_{l'}} \right) \quad \text{Recall } \sum_{ll'} C_l D_{l'} = \left(\sum_l C_l \right) \left(\sum_{l'} D_{l'} \right). \quad (3.29)$$

$$\Rightarrow I \propto \left(\sum_{jj'} e^{-i\vec{q}\cdot(\vec{u}_j - \vec{u}_{j'})} \right) \left(\sum_{ll'} e^{i\vec{q}\cdot(\vec{v}_l - \vec{v}_{l'})} \right). \quad (3.30)$$

The Bravais lattice vectors and basis vectors appear in a completely symmetrical way. However, the sum over Bravais lattice vectors might have 10^{23} elements while the sum on the basis might have 8, so the sums have qualitatively different character.

The first term in Eq. (3.30) is precisely the sum over Bravais lattice vectors that appeared previously in Eq. (3.10), and it therefore is nonzero only for vectors \vec{q} that lie in the reciprocal lattice \vec{K} given by Eq. (3.18). However, the strength of the peaks is modulated by the function

$$F_{\vec{q}} \equiv \left| \sum_l e^{i\vec{q}\cdot\vec{v}_l} \right|^2. \quad \text{Sum } l \text{ over all vectors in the basis.} \quad (3.31)$$

In some cases, the result may be that $F_{\vec{q}}$ vanishes, and certain peaks disappear altogether. These cases are called *extinctions*.

Example: Diamond Lattice. The diamond lattice, described in Section 2.2.6, is built from the fcc lattice with the basis

$$\vec{v}_1 = (0 \ 0 \ 0), \quad \vec{v}_2 = \frac{a}{4}(1 \ 1 \ 1). \quad (3.32)$$

Because the reciprocal lattice of an fcc lattice is bcc with lattice spacing $4\pi/a$, the reciprocal lattice vectors are

$$\vec{K} = l_1 \frac{4\pi}{2a}(1 \ 1 \ -1) + l_2 \frac{4\pi}{2a}(-1 \ 1 \ 1) + l_3 \frac{4\pi}{2a}(1 \ -1 \ 1). \quad \text{See Eq. (2.4).} \quad (3.33)$$

Therefore,

$$\vec{v}_2 \cdot \vec{K} = \frac{\pi}{2}(l_1 + l_2 + l_3), \quad (3.34)$$

and the modulation factor $F_{\vec{K}}$ is

$$F_{\vec{K}} = |1 + e^{i\pi(l_1 + l_2 + l_3)/2}|^2 \quad (3.35)$$

$$= \begin{cases} 4 & \text{if } l_1 + l_2 + l_3 = 4, 8, 12, \dots \\ 2 & \text{if } l_1 + l_2 + l_3 \text{ is odd} \\ 0 & \text{if } l_1 + l_2 + l_3 = 2, 6, 10, \dots \end{cases} \quad (3.36)$$

So some of the peaks are four times as bright as they were before the basis, some are twice as bright, and some have disappeared. The latter are examples of extinctions.

3.3 Experimental Methods

It remains to determine the implications of these calculations for scattering experiments, and it is probably best to begin by summarizing the mathematical results so

far. Radiation with wave vector \vec{k}_0 impacting a crystal produces a scattered wave along direction \vec{k} , where the magnitudes of \vec{k} and \vec{k}_0 are the same, but only if the wave vector $\vec{q} = \vec{k}_0 - \vec{k}$ equals one of the reciprocal lattice vectors \vec{K} of the crystal. The reciprocal lattice vectors are completely determined by the underlying Bravais lattice of the crystal, and any decoration of the Bravais lattice with a basis serves only to modify the strengths of the scattering peaks, not their positions.

The prescription for a successful experiment at first seems clear. Shine a monochromatic X-ray source at a crystalline sample, put a camera behind it, and start clicking the shutter. But a moment's reflection shows that this brilliant idea will not work. Each point on the photographic paper catching a scattered X-ray corresponds to a single scattering direction \vec{k} , so the experiment scans through a two-dimensional space of scattering vectors. However, the reciprocal lattice is a discrete set of points in three dimensions, and it is therefore exceptionally unlikely that any given two-dimensional surface will cut through any of them. In order to visualize this point, it is convenient to look at the *Ewald construction*, shown in Figure 3.6.

The Ewald construction has the first advantage of showing the necessary scale for the wavelength of incident radiation. In order to resolve atomic structure, its k vector should be comparable to the spacing of reciprocal lattice points, although somewhat larger. One therefore needs wavelengths on the order of an angstrom, which for electromagnetic waves requires the X-ray portion of the spectrum. It also permits one to imagine strategies by which to carry out scattering experiments;

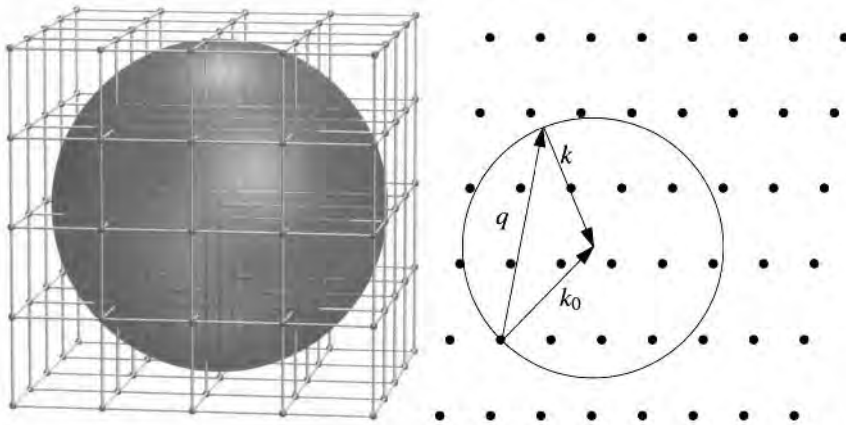


Figure 3.6. For incoming radiation \vec{k}_0 there will be outgoing radiation along direction \vec{k} only if $\vec{q} = \vec{k} - \vec{k}_0 = k_0\hat{r} - \vec{k}_0$ lies in the reciprocal lattice. For a fixed orientation of a crystal and wave number k_0 , all an experiment can do is scan over observation directions \hat{r} . This produces candidate \vec{q} 's in a spherical shell shown at the left (called the *Ewald sphere*; a two-dimensional cross-section appears on the right), and all the reciprocal lattice vectors \vec{K} are shown as dots. For the direction and magnitude of incoming radiation displayed here, an attempted scattering experiment would end with an unexposed piece of film, because there are no intersections of the spherical shell with the reciprocal lattice vectors. This graphical representation of Eq. (3.18) is called the Ewald construction.

there are three traditional solutions to the problem that monochromatic radiation generally does not produce sharp scattering peaks after contact with a fixed crystal: the Laue method, the rotating crystal method, and the powder method.

3.3.1 Laue Method

The first solution is the *Laue method*, found as an accidental offshoot of the manner in which the first X-rays were generated. X-rays were produced by bombarding a tungsten anode with electrons accelerated through about $5 \cdot 10^4$ eV. A slightly higher voltage would excite sharp lines in the tungsten spectrum, corresponding to ionization energies of inner core electrons, but at this voltage the X-ray spectrum is continuous, resulting from multiple collisions, and looks as in Figure 3.7(A). X-rays generated in this fashion are called *Bremsstrahlung* (“braking radiation”).

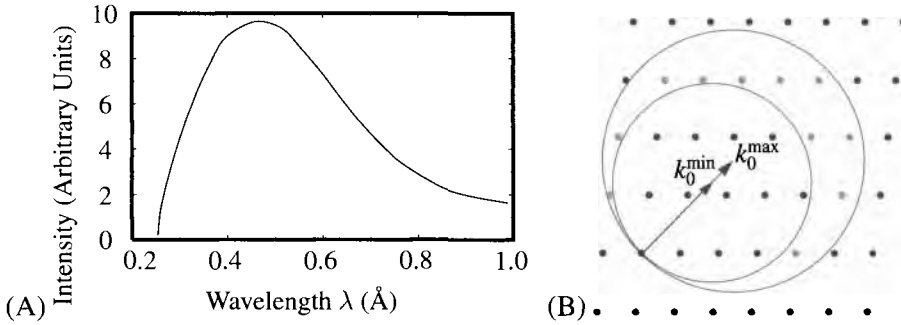


Figure 3.7. (A) Schematic indication of the continuous spectrum resulting from electron collisions upon tungsten at around 50 keV. (B) Ewald construction. The gray points are the scattering peaks that would be visible when incoming radiation has a wave vector between k_0^{\min} and k_0^{\max} .

The continuous component of the radiation was essential to the success of the experiment. As shown in Figure 3.7, if the incident radiation spans a range of wave vectors, the chance that some intermediate wave vector will actually satisfy condition (3.18) becomes considerable. The particular frequency of incoming radiation needed to cause scattering can be obtained from Eq. (3.6) by setting $\vec{q} = \vec{K}$ and writing

$$k_0^2 = k_0^2 - 2\vec{k}_0 \cdot \vec{K} + K^2 \quad (3.37)$$

$$\Rightarrow k_0 = \frac{K^2}{2\hat{k}_0 \cdot \vec{K}}, \quad \text{Because } \vec{K} = \vec{q} \text{ when scattering occurs.} \quad (3.38)$$

while the relation between the Bragg angle θ and the reciprocal lattice vector \vec{K} is

$$\frac{\vec{K} \cdot \vec{k}_0}{Kk_0} = \sin \theta \quad \text{Using Eq. (3.6)} \quad (3.39)$$

The Laue method is not a good method for precise structure identification, because the intensities of spots depend upon both the intensity of incoming X-

rays at varying frequency and properties of the scattering sample. However, for a substance whose lattice parameters are known, it provides an excellent means of orienting the sample. For this purpose, one needs to be able to identify the reciprocal lattice vectors corresponding to spots observed on a photographic image. One way to simplify the task is with the *Mauguin abacus*, which is a ruler whose marks are graduated to indicate $D \tan \theta$ to the left of the origin and $D(\tan 2\theta - \tan \theta)$ to the right of the origin, where D is the distance between sample and film. The reason for this choice is illustrated in Figure 3.8.

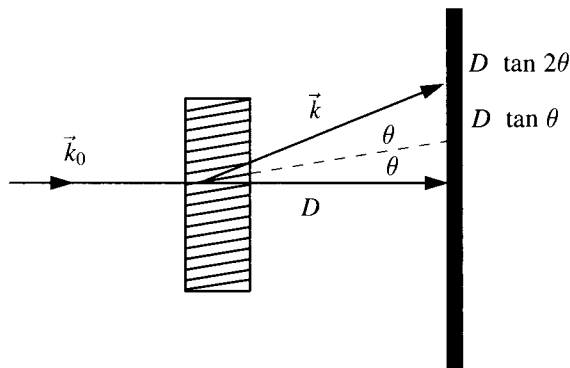


Figure 3.8. The parallel lines within the crystalline sample indicate a set of Bragg planes. If they were extended, they would contact a backing piece of film at height $D \tan \theta$, but the radiation bouncing off the planes hits at height $D \tan 2\theta$ instead. This observation provides a simple geometrical way to deduce Bragg angles θ from Laue photographs.

3.3.2 Rotating Crystal Method

A second method is the rotating crystal method. In contrast to the continuous radiation used for a Laue pattern, this method relies upon an intense monochromatic beam. A crystal is rotated about one or more axes, and in the course of rotation a variety of scattering peaks is recorded on a cylindrical film, as shown in Figure 3.9. Because all the scattering spots on the film result from one frequency of incoming radiation, the intensity of the scattering is meaningful, and the size of the spots recorded on the film can be used for quantitative analysis.

The scattering geometry shown in Figure 3.9 is not employed in practice, in part because reciprocal lattice vectors parallel to the rotation axes cannot be imaged, and in part because scattering spots all cluster tightly on parallel lines on the film, and the results are difficult to decipher accurately. Instead, there is a variety of experimental arrangements where the sample and flat plates of film rotate simultaneously. The operation of one of these, the *precession* camera, is indicated schematically in Figure 3.10(A). Spots appear on the film whenever film and sample are rotated through a Bragg angle θ , and the image of the spots on the film provides an undistorted projection of the reciprocal lattice.

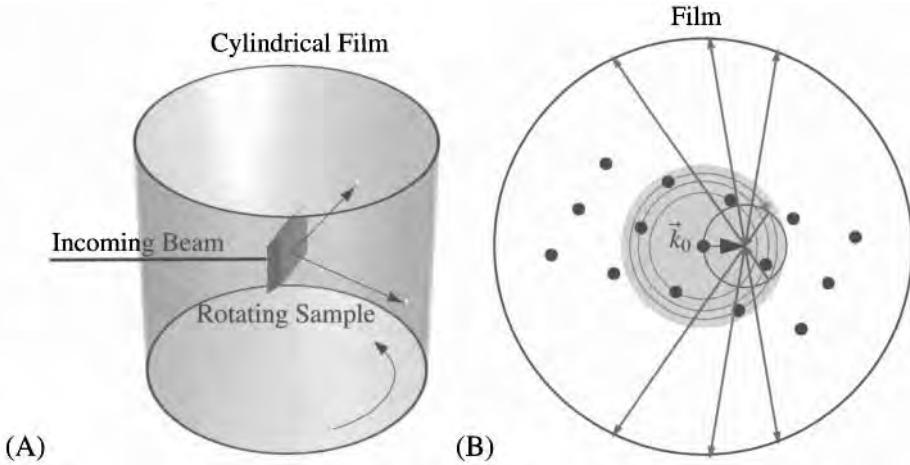


Figure 3.9. When a crystal is rotated about a fixed axis, numerous reciprocal lattice vectors generate scattering peaks when they intersect the Ewald sphere. (A) The geometry of the experiment. (B) The rotation axis comes out of the page, and scattering occurs whenever a reciprocal lattice point intersects the Ewald sphere.

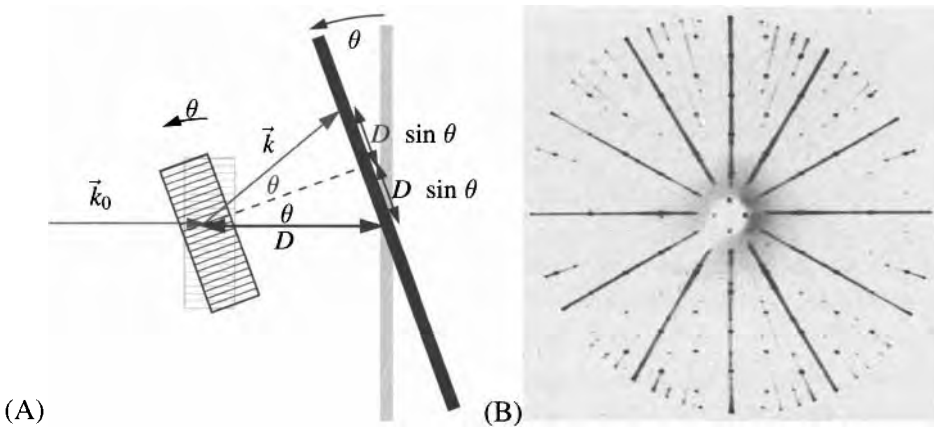


Figure 3.10. (A) Schematic description of a precession camera. The lines in the sample indicate Bragg planes, from which incoming radiation reflects to hit the film in a specular fashion. Whenever both film and sample are rotated through the Bragg angle θ , a spot hits the film at distance $2D \sin \theta$ from the origin, a distance that according to Eq. (3.8) is proportional to the magnitude of the relevant reciprocal lattice vector. By rotating sample and film about multiple axes one obtains an undistorted projection of the reciprocal lattice. (B) Precession image of K_2CrO_4 . (Courtesy of H. Steinfink, University of Texas.)

3.3.3 Powder Method

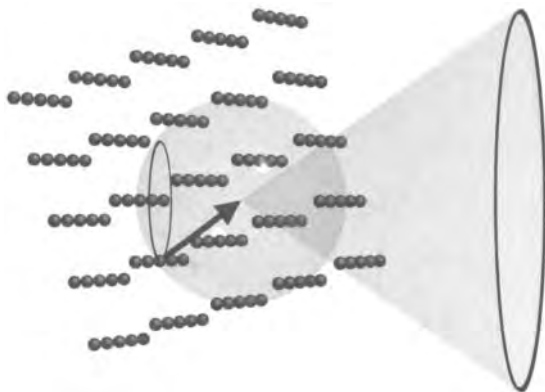


Figure 3.11. The powder method generates every scattering peak from a monochromatic beam that could be produced by a crystal at any imaginable angle. Whenever a reciprocal lattice point contacts the Ewald sphere, rotating the crystal about the direction of the incoming wave continues to produce a scattering peak. Therefore scattering from powdered samples is in the form of rings.

The third general technique for structure determination is the *powder method*, also called the *Debye–Scherrer method*; this method is suitable for materials when a perfect single crystal is not available. The incoming beam needs again to be monochromatic, but now the scattering sample is either polycrystalline, with individual crystallites on the order of a micron, or else a powder made of particles roughly that size. Because small crystals are present in all orientations in the sample, the net effect is the same as a rotating crystal experiment that turns the crystal through all possible directions, and there is a ring of scattering peaks, as shown in Figure 3.11, corresponding to every reciprocal lattice vector of magnitude less than twice that of the incoming beam; the Bragg angles corresponding to the scattering are

$$\theta = \sin^{-1}(K/2k_0) \quad \text{From Eq. (3.8). } K_i \text{ is the magnitude of a reciprocal lattice vector.} \quad (3.40)$$

and the radius r on film of the scattering ring due to reciprocal lattice vector \vec{K} is

$$r = D \tan(2\theta). \quad D \text{ is the distance from sample to film.} \quad (3.41)$$

From the series of rings recorded on film, complicated crystals can be worked out. The process proceeds in stages. The first step is to compare the locations of the rings with those produced by various known crystal structures and to pick out reasonable candidates, trying to identify the Bravais lattice first, and then working out decorations and extinctions next. The second step settles on a set of candidates and carries out a refinement process, varying precise locations of the atoms, varying scattering intensities of the species, and allowing for thermal motion, in order to produce a best fit to the data. In practice, this procedure is usually computerized,

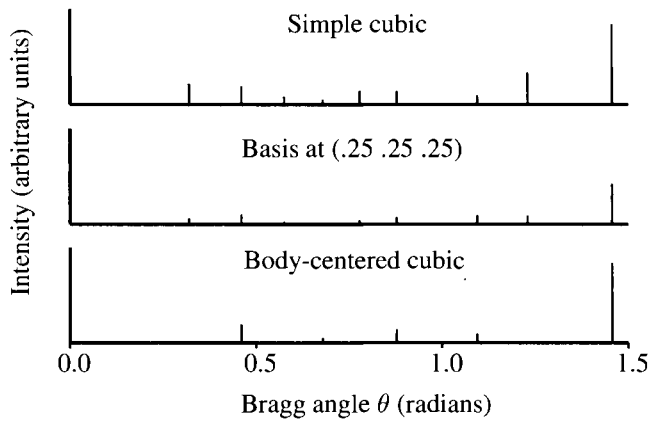


Figure 3.12. Scattering intensity as a function of Bragg angle θ for three monatomic lattices. At the top is a simple cubic lattice with lattice constant a and incoming radiation of wavenumber $k_0 = 10/a$. Each lattice site contains two atoms, to ease comparison with the remaining cases. In the middle is the same lattice, but decorated with basis atoms at the origin and at $(.25, .25, .25)$. Finally, at the bottom the basis moves to $(.5, .5, .5)$, so that the lattice is now body-centered cubic. Notice the increase in scale of the scattering pattern as the physical lattice develops structure on smaller scales.

with locations and intensities of rings being compared automatically with databases of known structures.

A simple example of the results to be expected from powder diffraction appears in Figure 3.12. The intensities of lines in this figure are calculated according to the results obtained in Problem 7.

3.4 Further Features of Scattering Experiments

The discussion so far has presumed that X-rays lie behind all scattering experiments, and that the scattering form factors $f(\vec{r})$ contain no useful information. Neither of these points is correct, and the corrections deserve some discussion although there is no possibility of describing all the refinements and elaborations of structure determination since 1912.

There are three types of particles widely used in scattering experiments: photons, neutrons, and electrons. They differ in the relations between energy and momentum, in the strength and nature of their interaction with condensed matter, and in cost and ease of generation. Some characteristics are displayed in Table 3.2.

3.4.1 Interaction of X-Rays with Matter

The interaction of X-rays with condensed matter is actually quite complicated. The easiest way to get an idea of what it should be is to recall the expressions in classical electromagnetism for the interaction of an electromagnetic wave with an isolated charged particle. The charged particle vibrates at the frequency of the incoming

Table 3.2. Characteristic values associated with different types of radiation

	X-rays	Neutrons	Electrons
Charge	0	0	$-e$
Mass	0	$1.67 \cdot 10^{-27}$ kg	$9.11 \cdot 10^{-31}$ kg
Typical energy	12 keV	0.02 eV	60 keV
Typical wavelength	1 \AA	2 \AA	0.05 \AA
Typical attenuation length	100 \mu m	5 cm	1 \mu m
Typical atomic form factor, f	10^{-3} \AA	10^{-4} \AA	10 \AA

Source: Eberhart (1991).

radiation, and it reradiates a spherical wave. The scattering cross-section for this process is

$$I_{\text{atom}}(\hat{r}) = \frac{e^4}{m^2 c^4} \frac{(1 + \cos^2 2\theta)}{2} \equiv \frac{e^4}{m^2 c^4} P(\hat{r}) \quad \text{See Jackson (1999), Eq. (14.124); } P \text{ is a polarization factor.} \quad (3.42)$$

$$\Rightarrow f(\hat{r}) = \frac{e^2}{m c^2} \sqrt{P(\hat{r})} = 2.82 \cdot 10^{-15} \sqrt{P(\hat{r})} \text{ m} \quad \text{Putting in values for the electron and expressing the answer in meters.} \quad (3.43)$$

Because the nuclei of atoms are so much heavier than the electrons, only the electrons contribute to X-ray scattering. However, the electrons are not tightly localized in space, but instead are characterized by a number density $n(\vec{r})$, which peaks up in the vicinity of ion cores, but does not completely vanish between them, particularly in metals. An expression for X-ray scattering which takes this fact properly into account is

$$f(\hat{r}) = \frac{e^2}{m c^2} \sqrt{P(\hat{r})} \int d\vec{r} n(\vec{r}) e^{i\vec{q} \cdot \vec{r}} = \frac{e^2}{m c^2} \sqrt{P(\hat{r})} n(\vec{q}) \quad (3.44)$$

$$\Rightarrow I_{\text{atom}}(\vec{q}) = \frac{e^4}{m^2 c^4} P(\hat{r}) |n(\vec{q})|^2. \quad n(\vec{q}) \text{ is the Fourier transform of the electron density.} \quad (3.45)$$

Hahn and Cochran (1992) have tabulated $f(\hat{r})$ for all the elements.

3.4.2 Production of X-Rays

The oldest way to generate the monochromatic X-rays needed for rotating crystal and powder methods is to collide electrons upon a metal anode at energies great enough to ionize core electrons, and thereby create a bright resonance at a precise frequency, such as the $K\alpha$ line of copper at 8.98 keV. Although a good fraction of the emitted X-ray power is contained in the desired line, a continuous component to the radiation is unavoidable. One way to omit the continuous component is to obtain a crystal arranged to have a scattering peak at precisely 8.98 keV, and then use the scattered beam from the reference crystal as the incoming radiation for

further experiments. The highly monochromatic beam produced in this way has unfortunately low amplitude, and a brighter but less narrow beam can be chosen by filtering the X-rays through an element that absorbs most of the continuous radiation while leaving the sharp line alone; a good candidate for such a filter is the element one atomic number down in the periodic table, which in the case of copper is nickel. Electron collisions with a metal do not provide an efficient way to generate X-rays; 99% of incoming energy is converted to heat. Even employing tricks such as rapidly rotating the target anode to keep it cool, the maximum X-ray power that can practically be extracted from conventional tubes is around 100 W, and by the time the X-ray has been filtered, fewer than 10 W may be left. The situation is very different at a *synchrotron*, where radiation is generated by rapidly accelerating electrons in huge rings. The total power emitted as X-rays in a broad band up to 200 keV is on the order of 10^6 W, so even after filtering to 0.1% of the 200 keV bandwidth to get a monochromatic beam, 1000 W of power is left. The relative intensities of radiation at various frequencies available from the different types of X-ray sources are compared in Figure 3.13.

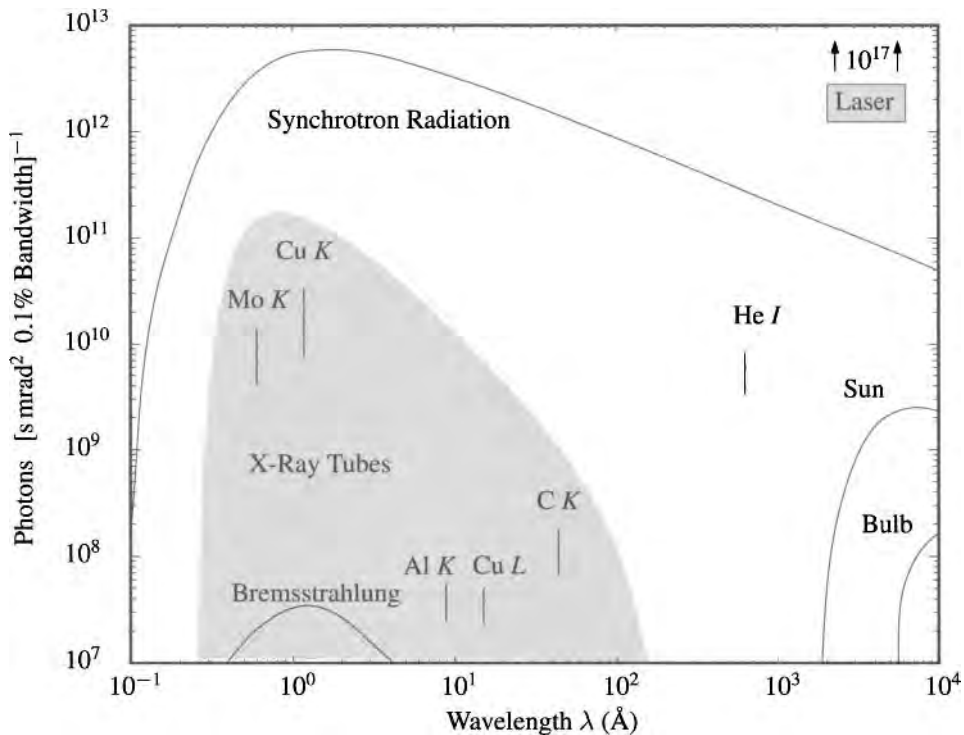


Figure 3.13. Overview of various means of producing radiation, relative to the intensity available from a synchrotron. Intensity for sources spanning a range of wavelengths is measured by finding the number of photons in a frequency interval that is 0.1% of the total wavelength range. Synchrotron radiation is orders of magnitude more intense than any source apart from lasers, and spans a broad range of wavelengths. [After Brefeld and Guertler (1990), p. 285.]

3.4.3 Neutrons

Neutrons scatter only off nuclei, and apart from interesting corrections due to relative spins of incoming neutron and nucleus that make it possible to probe magnetic structures, the interaction is completely isotropic. The scattering form factor $f(\hat{r})$ for neutrons is a constant a for any given element called the *scattering length*. This simplifying fact is the great advantage of neutrons. Their main disadvantage is simply the great expense required to generate beams of useful intensities. A neutron wavelength of 2 \AA corresponds to an energy of 0.02 eV , which corresponds approximately to room temperature, giving neutrons of this energy the name *thermal neutrons*. Figure 3.14 shows neutron powder data used to uncover antiferromagnetic ordering in MnO; the structure is depicted in Figure 24.6.

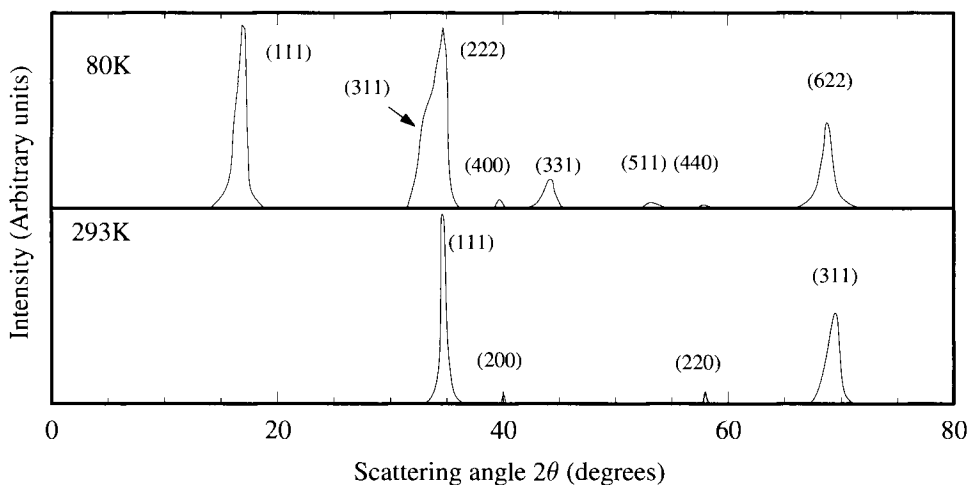


Figure 3.14. Powder pattern for neutron scattering from MnO. Above an antiferromagnetic transition temperature, the scattering pattern is that of a crystal in the NaCl structure, with a lattice parameter of 4.42 \AA . Below the transition temperature, an entirely new set of scattering peaks appears, indicating the antiferromagnetic ordering depicted in Figure 24.6. [Source: Shull et al. (1951), p. 337.]

Elastic scattering, in which the outgoing neutron has the same energy as the incoming neutron, is important for deciphering complicated structures, but *inelastic scattering*, where the neutron loses or gains energy during its passage through the material, is equally important and will be discussed in Section 13.4, as a means of studying excited states of lattices.

3.4.4 Electrons

Electrons interact more strongly with matter than either X-rays or neutrons. This fact might at first seem to present an advantage, but the scattering is so strong that electrons cannot escape through samples without suffering multiple collisions unless the samples are less than approximately 100 \AA thick and unless the electrons travel at fairly high energies, on the order of 100 keV . Electrons therefore are not

employed to deduce the structures of bulk crystals, but they do find use in the study of solid surfaces (Section 4.3), and microscopically thin samples.

Incoming electrons interact with the complete electrostatic potential of the matter into which they travel, including both electrons and nuclei, and in the Born approximation this leads to a scattering amplitude f_{el}

$$f_{el}(\vec{q}) = \frac{2\pi me}{\hbar^2} \int d\vec{r} V(\vec{r}) e^{i\vec{r}\cdot\vec{q}} \quad \text{See Landau and Lifshitz (1977) p. 513, or Schiff (1968), p. 324.} \quad (3.46)$$

which is related to the scattering function for X-rays by

$$f_{el}(\vec{q}) = \frac{me^2}{2\hbar^2 k_0^2 \sin^2 \theta} [Z - n(\vec{q})] \quad \text{Z is the atomic number; } n \text{ is the electron density and is related to the X-ray scattering form factor by Eq. (3.44).} \quad (3.47)$$

as shown in Problem 6.

3.4.5 Deciphering Complex Structures

Teasing crystalline structures out of arrays of spots on film is relatively easy when the structure in question is composed of only a few elements and the unit cell is small. Faced, however, with a protein crystal, with a unit cell containing tens or hundreds of thousands of atoms, the problem of reconstructing atomic positions becomes a daunting one. Ideally, there would be some purely automatic procedure that operates upon the scattering data and reconstructs the scattering potential. In the fields of light and electron microscopy this procedure exists; it is known as a *lens*, which should be understood as a device for recombining scattered waves in a fashion so as to reveal the structure from which they came. An important feature of recombining waves by focusing them is that all information about the relative phase of waves scattered from different parts of the structure is preserved. Mathematically, this information is needed for structure to be deduced from scattering data, and in X-ray and neutron experiments it is almost always lost (see Hauptman (1989)).

Automated procedures for analyzing X-ray data are nevertheless possible, to a point. Suppose one carries out a rotating crystal experiment and measures $I(\vec{q})$, as in Eq. (3.45). Performing an inverse Fourier transform in \vec{q} on these data gives immediately the *Patterson function*, after Patterson (1934), depicted in Figure 3.15, which is proportional to

$$\int d\vec{r}' n(\vec{r}') n(\vec{r} - \vec{r}') \quad \text{\small } n \text{ is the number density per volume of electrons. Constant multipliers such as factors of } 2\pi \text{ are irrelevant for the ensuing arguments, and are being dropped.} \quad (3.48)$$

How much of the information originally present in phases has irredeemably been lost? As Figure 3.15 makes clear, not so much. There is a peak in the Patterson function at all locations $\vec{R}_1 - \vec{R}_2$, where \vec{R}_1 and \vec{R}_2 are peaks of the true density, and the height of each peak is given by the product of the amplitudes of the two original density peaks that produce it. So, while one does not know where all the atoms are from Figure 3.15(B), one can read off a net of vector distances between them. Matters are simplified further if the structure contains a *heavy atom*: an atom

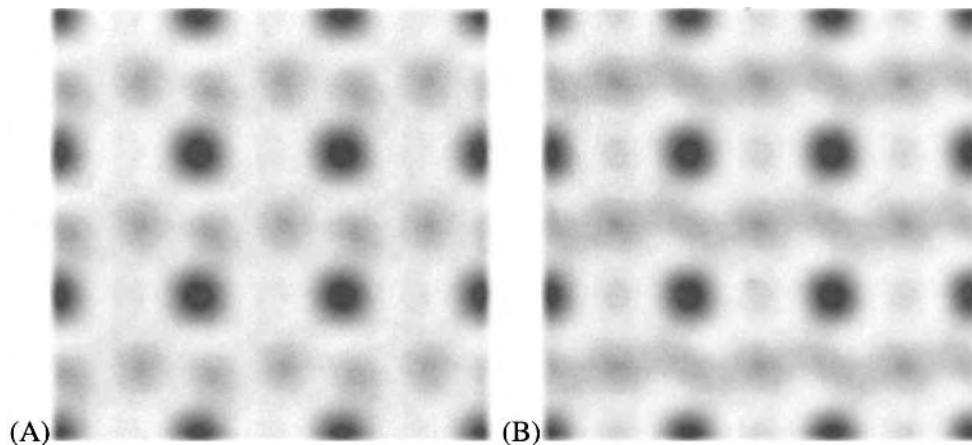


Figure 3.15. (A) A contour map of electron density of an imaginary structure with three atoms per unit cell, a large heavy atom at the origin, and two lighter atoms displaced from it. (B) The Patterson function resulting from this density. Notice that the Patterson function is centrosymmetric and that there is a peak in the density at a distance from the origin corresponding to the distance between the two light atoms.

whose scattering is stronger than any other. Say this atom is at the origin. Then the largest peaks of the Patterson function will be at the origin and at $\pm\vec{R}_i$, where \vec{R}_i are the locations of all the other atoms. So, if a structure has heavy atoms, the greatest remaining uncertainty is whether peaks of $\pm\vec{R}_i$ correspond to atoms at \vec{R}_i , at $-\vec{R}_i$, or at both locations. One of the techniques essential to unraveling the structures of large proteins has been the artificial chemical insertion of heavy atoms at various points in the proteins as replacement for lighter atoms, to provide guides to the structure.

Even the stubborn tendency of X-ray data to make all structures centrosymmetric can be overcome. When incoming X-rays have an energy near to that at which one of the atoms in the sample has an absorption resonance, a bit more phase information becomes available in the region of *anomalous dispersion*; this fact is the subject of Problem 5.

3.4.6 Accuracy of Structure Determinations

Catalogs of crystal structures must always be employed with the possibility in mind that published results are inaccurate or incorrect. Abrahams et al. (1967) describe an effort to determine how big these errors might be, by taking a carefully prepared crystal to multiple research groups and asking them to measure Bragg peak intensities independently. Although each group claimed accuracy in determining structures of around 1%, discrepancies between different groups were typically on the order of 5%–6%, and measurements of the intensity of the (111) reflection varied by 50%. In revisiting the results of this experiment, Mackenzie and Maslen (1968) call the results “grossly discordant.” An example of an incorrect structure determination is provided by the high-cristobalite structure of SiO_2 , on page 318 of

Wyckoff (1963); the correct structure is discussed in Liu et al. (1993). How many other examples like this latter one may exist is difficult to say.

3.5 Correlation Functions

3.5.1 Why Bragg Peaks Survive Atomic Motions

Sommerfeld objected in 1912 to the search for X-ray scattering on the grounds that atoms constantly move large distances from their ideal positions, and the experiment could not work. The theory presented so far assumes atoms sit perfectly still at ideal locations, yet it compares well with experiments performed at room temperature. How can this be?

This is a special case of an even more primitive question, which concerns the nature of crystals. What really defines them? It is not enough to say that all their atoms sit in a perfect lattice, since thermal motions and occasional impurities do not destroy the crystal's essential nature.

The essential nature of a crystal is that positions of atoms are correlated at long distances. This idea can be made precise in any monatomic system by defining the *two-particle* or Van Hove (1954) correlation function $n_2(\vec{r}_1, \vec{r}_2; t)$. This function gives the probability that if some particle is at position \vec{r}_1 at time t_1 , a particle is to be found at position \vec{r}_2 at time $t_1 + t$. Formally,

$$n_2(\vec{r}_1, \vec{r}_2; t) = \left\langle \sum_{l, l'} \delta(\vec{r}_1 - \vec{R}_l(t_1)) \delta(\vec{r}_2 - \vec{R}_{l'}(t_1 + t)) \right\rangle. \quad \text{In Van Hove's original definition, the condition } l \neq l' \text{ is imposed on the sum.} \quad (3.49)$$

The brackets denote either a thermal average or a time average over t_1 , as according to principles of statistical mechanics the two averages should be the same. Variables $\vec{R}_l(t)$ track the locations of the particles.

From the correlation function, define the *dynamic structure factor*, a dimensionless measure of scattering, by

$$S(\vec{q}, t) \equiv \frac{I}{N I_{\text{atom}}} = \frac{1}{N} \sum_{l, l'} \left\langle e^{i\vec{q} \cdot (\vec{R}_l(t_1) - \vec{R}_{l'}(t_1 + t))} \right\rangle \quad \text{This is proportional to the time average or thermal average of Eq. (3.11).} \quad (3.50)$$

$$= \frac{1}{N} \sum_{l, l'} \int d\vec{r}_1 d\vec{r}_2 e^{i\vec{q} \cdot (\vec{r}_1 - \vec{r}_2)} \left\langle \delta(\vec{r}_1 - \vec{R}_l(t_1)) \delta(\vec{r}_2 - \vec{R}_{l'}(t_1 + t)) \right\rangle \quad (3.51)$$

$$= \frac{1}{N} \int d\vec{r}_1 d\vec{r}_2 n_2(\vec{r}_1, \vec{r}_2; t) e^{i\vec{q} \cdot (\vec{r}_1 - \vec{r}_2)} \quad \text{Just insert the definition (3.49).} \quad (3.52)$$

$$= \frac{\mathcal{V}}{N} n_2(\vec{q}, t) \quad \mathcal{V} \text{ is the system volume. If the condition } l \neq l' \text{ had been added to Eq. (3.49), there would be an additive factor of 1.} \quad (3.53)$$

where

$$n_2(\vec{q}, t) = \frac{1}{\mathcal{V}} \int d\vec{r} d\vec{r}' n_2(\vec{r} + \vec{r}', \vec{r}; t) e^{i\vec{q} \cdot \vec{r}'} \quad (3.54)$$

Return to Eq. (3.11). A traditional scattering experiment requires collecting radiation on a photographic plate over times on the order of seconds. Atomic

oscillations occur on a time scale of picoseconds. Scattering experiments thus measure the long-time average of radiation intensity exiting the sample. That is, these experiments do not really measure the quantity in Eq. (3.11), they measure its time average, which is the *static structure factor*,

$$S(\vec{q}) \equiv S(\vec{q}, 0). \quad (3.55)$$

The necessary condition for scattering peaks can now be expressed in a more general way. As \vec{r}' in Eq. (3.54) becomes larger and larger, the static correlation function must continue to exhibit periodic maxima centered on lattice sites, and the amplitudes of these maxima should not diminish when the \vec{r}' becomes large compared to atomic spacings. A specific example comparing solids and liquids appears in Figure 5.9. This is the type of correlation called long-range positional order. Putting matters another way, it does not matter if atoms are in thermal motion, just so long as every atom vibrates around a set of mean locations that constitute a perfect crystal. The effect of vibrations is to decrease the amplitude of Bragg peaks, not their existence or location in frequency space. Explicit expressions for the way that quantum mechanical and thermal fluctuations reduce Bragg peak amplitude appear in Eqs. (13.124) and (13.129).

Placing atoms in lattices is a special case of the more general idea of *long-range order* or *long-range correlations*. Long-range order concerns the average behavior of pairs of particles over time, not their location at any one instant. Long-range order is the fundamental property that separates solids from liquids. More generally, the ideas of correlation and ordering explain qualitative phases of matter including superconducting and superfluid states.

3.5.2 Extended X-Ray Absorption Fine Structure (EXAFS)

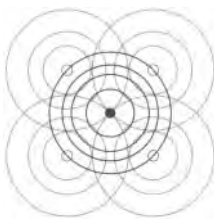


Figure 3.16. Extended X-ray absorption fine structure is observed when a scattered wave impinges on near neighbors, and returns to interfere with the first scattering source.

Extended X-ray absorption fine structure (EXAFS) is an X-ray scattering technique that homes in on small-scale details of the correlation function n_2 in the neighborhood of specifically chosen target atoms. To employ the technique, one illuminates a sample with X-rays whose frequency is chosen to lie near the absorption resonance of some particular atom. For incoming radiation whose energy \mathcal{E} lies above the onset of absorption at \mathcal{E}_a , the receiving atom emits an electron of energy $\mathcal{E} - \mathcal{E}_a$ and wave vector $\hbar k = \sqrt{2m(\mathcal{E} - \mathcal{E}_a)}$, which has been excited out of a core state. Traveling out of the atom that produced it, this electron immediately

begins to scatter off neighboring atoms; the scattered wave returns to the original atom and interferes with the electron emission process, as in Figure 3.16. If this returning wave reduces the electron amplitude at the original atom, X-rays will have increased difficulty ejecting electrons to begin with, and there should be a dip in the X-ray absorption coefficient $\alpha(\mathcal{E})$. Without developing a detailed theory of this rather complicated interference process, it is possible to guess the form the result must have. If X-rays eject electrons from atoms at the origin, and a neighboring atom at location \vec{R}_j scatters them back, then because the total path length from atom to scatterer and back is $2R_j$, interference between the original and scattered wave leads to absorption in the form

$$\alpha(\mathcal{E}) \propto \left\langle \sum_j |1 + [e^{-R_j/l_T} e^{ikR_j} f/R_j]^2|^2 \right\rangle \quad \begin{array}{l} \text{Sum over all neighboring atoms. The} \\ \text{square comes from the fact that the} \\ \text{wave is scattered twice. } f \text{ is a} \\ \text{scattering form factor.} \end{array} \quad (3.56)$$

$$\sim \int d\vec{r} n_2(0, \vec{r}, 0) e^{-2r/l_T} \cos(2kr), \quad \begin{array}{l} \text{Keeping only the leading term} \\ \text{depending on } k. \end{array} \quad (3.57)$$

where l_T is the mean free path of electrons in the solid. In fact the absorption coefficient is observed experimentally to have small oscillations for energies as much as 1000 eV above the absorption edge. According to Eq. (3.57), the Fourier transform of these oscillations is proportional to the correlation function of neighboring atoms times the decay factor $\exp[-2r/l_T]$. Thus EXAFS gives quantitative descriptions of the neighborhoods of atoms of specific types, even in liquid or amorphous environments.

3.5.3 Dynamic Light Scattering

Under the general heading of scattering experiments, there is a wide variety of possibilities. *Dynamic light scattering* presents an interesting contrast with the X-ray, electron, neutron scattering experiments discussed so far. Like these techniques, dynamic light scattering involves sending a beam of radiation into a sample and measuring the outgoing radiation in order to draw conclusions about particle locations. However, almost everything else is different. Dynamic light scattering uses visible light, so it is most suitable for studying particles or structures whose size is comparable to visible wavelengths, on the order of μm . Instead of Bragg peaks, the focus of attention moves to speckles of light emerging from the sample, and their fluctuations in time. The fluctuations in light intensity provide information about the motions of particles in the path of the light beam. Instead of resulting from coherent scattering from many different particles at the same time, dynamic light scattering results from the changes of intensity due to changes in particle locations over time. In terms of correlation functions, conventional X-ray scattering probes the correlations of many particle locations with one another at one time, while dynamic light scattering probes the correlations of particle locations with their own histories.

The study of dynamic light scattering begins with the observation that when electric fields scatter weakly off particles located at $\vec{R}_1 \dots \vec{R}_N$, then the the result-

ing field is

$$E_\alpha(t) = \sum_{l=1}^N E_\alpha^0 e^{i\vec{q}\cdot\vec{R}_l(t)} \quad \text{Taking the form factor } f = 1. \text{ The index } \alpha \text{ is for polarization.} \quad (3.58)$$

$$\begin{aligned} \text{Thus } & \frac{1}{E_0^2} \sum_{\alpha} \langle E_\alpha^*(0) E_\alpha(t) \rangle & E_0^2 &= \sum_{\alpha} |E_\alpha^0|^2 \\ &= \frac{1}{E_0^2} \sum_{\alpha} \sum_{l,l'} E_\alpha^{*0} E_\alpha^0 \langle e^{-i\vec{q}\cdot(\vec{R}_l(0) - \vec{R}_{l'}(t))} \rangle \\ &= \int d\vec{r} d\vec{r}' e^{-i\vec{q}\cdot(\vec{r} - \vec{r}')} n_2(\vec{r}, \vec{r}'; t) \\ &= n_2(\vec{q}, t). & \text{Exactly as in Eq. (3.54).} & \end{aligned} \quad (3.59)$$

Unfortunately, despite this pleasing definition, $n_2(\vec{q}, t)$ cannot be measured directly, because experiments measure intensities at a given time, not electric fields. However, by taking a chance on one new assumption, temporal fluctuations in fields can be related to temporal fluctuations of intensity. The assumption is the *Siebert relation*. Consider

$$\frac{1}{|E_0|^4} \sum_{\alpha\gamma} \langle E_\alpha^*(0) E_\alpha(0) E_\gamma^*(t) E_\gamma(t) \rangle = \frac{1}{I_0^2} \langle I(t) I(0) \rangle. \quad (3.60)$$

This quantity can be measured directly in experiment by keeping a record over time of intensity. Its can be related to Eq. (3.59) if one assumes that the electric field components $E_\alpha(0)$ and $E_\gamma(t)$ are random variables, normally distributed about their mean values, and the deviations from the mean independent of one another. If this assumption holds then one can employ a theorem from statistics discussed by Triantafyllopoulos (2003), analogous to Wick's theorem (Section 13.4.3 or Doniach and Sondheimer (1974), pp. 52–62) saying that the expectation value of products of random variables is given by summing up all possible products of expectation values of pairs of the operators.

In the case of Eq. (3.60), this means that

$$\langle I(t) I(0) \rangle / I_0^2 \quad (3.61)$$

$$= \frac{1}{|E_0|^4} \sum_{\alpha\gamma} \langle E_\alpha^*(0) E_\alpha(0) E_\gamma^*(t) E_\gamma(t) \rangle \quad (3.62)$$

$$= \frac{1}{|E_0|^4} \sum_{\alpha\gamma} \left[\langle E_\alpha^*(0) E_\alpha(0) \rangle \langle E_\gamma^*(t) E_\gamma(t) \rangle + \langle E_\alpha^*(0) E_\gamma(t) \rangle \langle E_\gamma^*(t) E_\alpha(0) \rangle \right] \quad \begin{array}{l} \text{Terms such as } E_{*\alpha}^*(0) E_\gamma^*(t) \\ \text{vanish after averaging over} \\ \text{factors of } e^{2i\omega t}. \end{array} \quad (3.63)$$

$$= 1 + \sum_{\alpha\gamma} \left(\frac{|\langle E_\alpha^*(0) E_\gamma(t) \rangle|}{|E_0|^2} \right)^2 \quad (3.64)$$

$$= 1 + \beta |n_2(\vec{q}, t)|^2. \quad \text{See Gittings and Durian (2006) for an investigation of this approximation.} \quad (3.65)$$

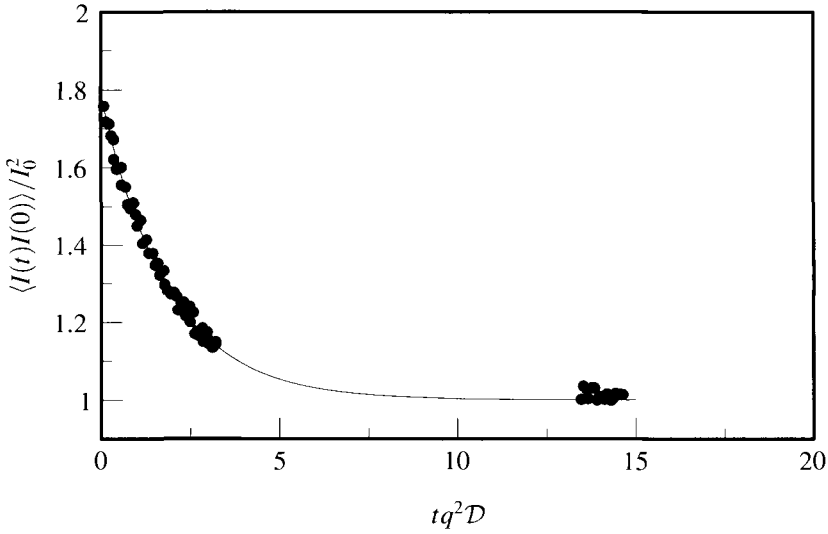


Figure 3.17. Measurement of $\langle I(t)I(0) \rangle$ for a dilute solution of coiled DNA. The scattering angle is 60° so q can be determined from Eq. (3.8). The solid line is an exponential function; it fits the data with a correlation coefficient of 0.996. Thus the data have the form predicted by Eqs. (3.67) and (3.65) with $\beta \approx 0.8$. [Data of H.L. Swinney and J. Newman from Berne and Pecora (2000), p. 61.]

Here β is a constant that depends first of all upon the polarization state of the light. For linearly polarized light, one expects $\beta = 1$ and for circularly polarized light $\beta = 1/2$. In addition, depending upon the size of the photo-detector, the light speckles being measured may be more or less completely spatially correlated, and the degree of correlation affects the success of the approximation leading to Eq. (3.65). The constant β is in practice used during experiments as an adjustable constant to compensate for the approximation.

3.5.4 Application to Dilute Solutions

For a dilute solution of micron-scale particles in liquid, what should the correlation function of Eq. (3.49) look like as a function of time? Small particles undergo Brownian motion which means that they diffuse about, and obey the diffusion equation (5.2), to be derived in Section 5.2.

Exactly the same equation must apply to the the probability $n_2(0, \vec{r}; t)$ that a particle at the origin at time $t = 0$ has moved to \vec{r} in time t :

$$\frac{\partial n_2(0, \vec{r}; t)}{\partial t} = \mathcal{D}\nabla^2 n_2(0, \vec{r}; t), \quad (3.66)$$

Because the particle is originally at the origin, $n_2(0, \vec{r}; 0) = \delta(\vec{r})$. Applying the Fourier transform $\int d\vec{r} \exp[-\vec{q} \cdot \vec{r}]$ to both sides of Eq. (3.66) gives

$$\frac{\partial n_2(\vec{q}, t)}{\partial t} = -\mathcal{D}q^2 n_2(\vec{q}, t) \quad \text{The boundary condition is that } n_2(\vec{q} = 0, 0) = 1.$$

$$\Rightarrow n_2(\vec{q}, t) = e^{-q^2 \mathcal{D}t} \quad (3.67)$$

Figure 3.17 shows an example of intensity correlation data for a dilute solution of coiled DNA. Note that by varying the scattering wave vector $q = k_0 \sin \theta$ of Eq. (3.8) it is possible to obtain many independent measurements of the diffusion constant \mathcal{D} .

Problems

1. Reciprocal lattice vectors:

- (a) Use Eq. (3.24) to verify that the reciprocal lattices of the fcc and bcc lattices are as claimed in Table 3.1.
- (b) Find reciprocal lattice vectors of smallest magnitude for aluminum, beryllium, and bcc iron, and write down their Miller indices.

2. Hcp extinctions:

- (a) Show as claimed in Table 3.1 that the reciprocal lattice of a hexagonal lattice given by Eq. (2.5) is another hexagonal lattice rotated at 30° with respect to the original one, and find primitive vectors for the reciprocal lattice.
- (b) The hcp lattice is built upon the hexagonal, with basis given by Eq. (2.6). Show that the modulation factor induced by the basis is

$$F_{\vec{q}} = |1 + e^{i\frac{\pi}{3}[2(n_1+n_2)+3n_3]}|^2. \quad (3.68)$$

- (c) Describe all the cases in which scattering from the hcp lattice vanishes because of an extinction.

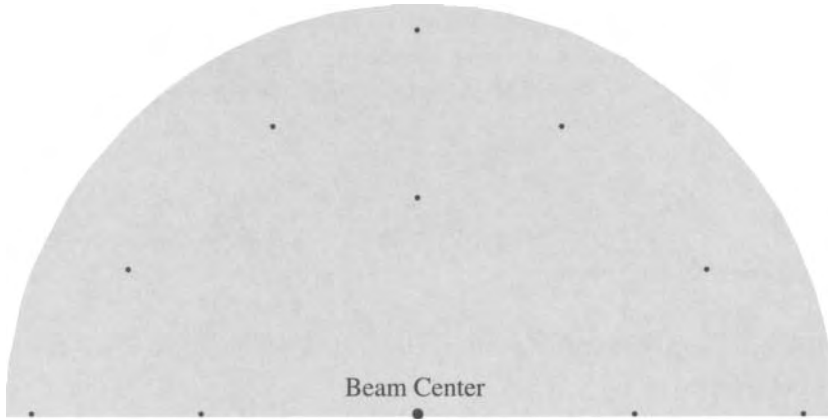
3. Bragg peaks: Bragg's model for reflection of X-rays from a solid was based on the view that the solid was constructed out of a series of parallel planes. X-rays bounced off these planes in such a way that angle of incidence θ equaled the angle of reflection, and diffraction peaks occurred when radiation from successive planes added constructively.

- (a) Verify that the values of \vec{k}_0 , \vec{k} , and \vec{K} given in Figure 3.2 are chosen correctly to produce scattering.
- (b) Show that in general the condition for a scattering peak can be written as

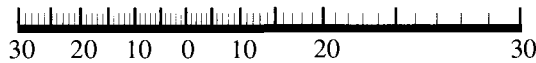
$$2d \sin \theta = l\lambda, \quad (3.69)$$

where d is the distance between lattice planes, θ is the Bragg scattering angle, λ is the wavelength of incoming light, and l is an integer.

4. **Laue pattern:** Suppose that broad-band X-rays are scattered from a crystal onto a photographic plate 1.5 inches away, giving the following pattern:



Only the upper half of the four-fold symmetric scattering pattern is shown. Any scattering peaks at radii falling outside the gray shaded area are not recorded on the photographic plate.



- (a) Use this Mauguin abacus to identify the Bragg angles of each spot. The way to use the abacus is to copy it (preferably onto transparent paper) and lay it down so that a tickmark on the left lies on some scattering spot, while the corresponding tickmark on the right lies on the origin. The Bragg angle is given by the common value of the two tickmarks.
- (b) The lattice has spacing a and is either sc, fcc, or bcc. Which one? Assume the incoming X-rays to have uniform intensity at all wave vectors up to a cutoff of $32/a$. It should be emphasized that the spots are cut off both in real space by the boundaries of the circle and in reciprocal space by $32/a$.

5. **Centrosymmetry:**

- (a) Suppose that all the ionic form factors f_i in Eq. (3.10) are real. Show that the X-ray scattering data will make all crystals appear to be centrosymmetric whether they are so or not (*Friedel's law*).
- (b) Consider next a crystal that is not centrosymmetric, and with two different atoms per unit cell. Suppose that the X-ray frequency is chosen near to a value ω_0 at which one of the atoms has an absorption resonance. Assume that the frequency dependence of the absorption can be modeled by pretending that the atom behaves like a mass on a spring with damping. Show that the amplitude and phase of scattered radiation vary just like the amplitude and phase of a mass on a spring with damping driven by a periodic force. Show that the phases of the two form factors f for the two atoms should be different, and that the scattering intensity now contains information from which can be deduced the fact that the crystal is not centrosymmetric.

6. **Mott–Bethe relation:** Demonstrate Eq. (3.47). Use the fact that the electron density satisfies Poisson's equation, $\nabla^2 V = 4\pi ne$, where V is the electrostatic potential.
7. **Powder pattern intensities :** Consider an array of identical scatterers from which is made a powdered crystal suitable for the Debye scattering method. The intensity of a measured line appearing at Bragg angle θ is

$$|f(\theta)|^2 F_{\vec{q}} \mathcal{M}_q N \frac{N}{V} \frac{\pi^2}{k_0^3 \sin \theta \sin 2\theta} \quad (3.70)$$

Here \mathcal{M}_q is the multiplicity of the relevant k -space point. Sketch the derivation of Eq. 3.70 by showing that the θ -dependent part is the product of two types of terms:

- Form factors f and F such as those in Eqs. (3.47) and (3.31).
- Geometrical factors resulting from averaging over crystallite directions.

Formally, the geometrical factors are obtained by observing that the Bragg reflection due to a reciprocal lattice point \vec{K} is

$$\delta(q_x - K_x) \delta(q_y - K_y) \delta(q_z - K_z). \quad (3.71)$$

In a powder diffraction experiment, the probability that a reciprocal lattice vector of magnitude K should point along angles Θ and Φ is $\sin(\Theta)/4\pi$. Averaging over Θ and Φ , and writing the resulting single delta function as a function of the Bragg angle θ will give the desired result. Use the mathematical result that $\delta(f(x) - y) = \sum_i \delta(x - x_i)/|f'(x_i)|$, where x_i are the roots of $y - f(x)$.

8. **Zinc powder pattern:** Consider the hcp metal zinc in polycrystalline or powdered form, and consider conducting an X-ray scattering experiment in which radiation of 1 Å wavelength is scattered off the sample. Write a computer program calculating the scattering intensity as a function of Bragg angle that should be observed, treating zinc atoms as point scatterers. Use experimental numbers for the lattice constants of zinc, and use Eq. (3.70) for the intensities of the lines.

References

- S. C. Abrahams, L. E. Alexander, T. C. Furnas, W. C. Hamilton, J. Ladell, Y. Okaya, R. A. Young, and A. Zalkin (1967), American Crystallographic Association single-crystal intensity project report, *Acta Crystallographica*, **22**, 1–6.
- J. D. Axe and R. M. Nicklow (1985), Neutron scattering in condensed-matter physics, *Physics Today*, **38**(1), 26–35.
- C. S. Barrett and T. B. Massalski (1980), *Structure of Metals: Crystallographic Methods, Principles and Data*, third, revised ed., Oxford, New York.

- B. J. Berne and R. Pecora (2000), *Dynamic Light Scattering with Applications to Chemistry, Biology, and Physics*, Dover, New York.
- W. Brefeld and P. Guertler (1990), Synchrotron radiation sources, in *Handbook on Synchrotron Radiation*, S. Ebashi, M. Koch, and E. Rubinstein, eds., vol. 4, pp. 269–296, North Holland, Amsterdam.
- P. Carra and B. T. Thole (1994), Anisotropic X-ray anomalous diffraction and forbidden reflections, *Reviews of Modern Physics*, **66**, 1509–1515.
- S. Doniach and E. H. Sondheimer (1974), *Green's Functions for Solid State Physicists*, Benjamin/Cummings, Reading, MA
- J. P. Eberhart (1991), *Structural and Chemical Analysis of Materials: X-Ray, Electron and Neutron Diffraction; X-Ray, Electron and Ion Spectrometry; Electron Microscopy*, John Wiley and Sons, Chichester.
- P. P. Ewald, ed. (1962), *Fifty Years of X-Ray Diffraction*, International Union of Crystallography.
- W. Friedrich, P. Knipping, and M. von Laue (1912), Interference phenomena for X-rays, *Sitzungsberichte. Bayerische Akademie der Wissenschaften*, pp. 303–322. Translated in Glusker (1981), pp. 23–39
- E. A. Galbur and B. L. Stoddard (2001), Time-resolved macromolecular crystallography, *Physics Today*, **54**(7), 33–39
- R. K. Gehrenbeck (1978), Electron diffraction: fifty years ago, *Physics Today*, **31**(1), 34–41.
- A. S. Gittings and D. J. Durian (2006), Gaussian and non-Gaussian speckle fluctuations in the diffusing-wave spectroscopy signal of a coarsening foam, *Applied Optics*, **45**, 2199–2204.
- J. P. Glusker, ed. (1981), *Structural Crystallography in Chemistry and Biology*, Hutchinson Ross, Stroudsburg, PA. Collection of historical papers.
- T. Hahn and A. J. Cochran, eds. (1992), *International Tables for Crystallography*, vol. C: Mathematical, physical, and chemical tables, 3rd ed., Kluwer Academic Publishers, Dordrecht.
- H. A. Hauptman (1989), The phase problem of X-ray crystallography, *Physics Today*, **42**(11), 24–29.
- T. M. Hayes and J. B. Boyce (1982), Extended X-ray absorption fine structure spectroscopy, *Solid State Physics: Advances in Research and Applications*, **37**, 173–351.
- J. D. Jackson (1999), *Classical Electrodynamics*, 3rd ed., John Wiley and Sons, New York.
- L. D. Landau and E. M. Lifshitz (1977), *Quantum Mechanics (Non-relativistic Theory)*, 3rd ed., Pergamon Press, Oxford.
- P. A. Lee, P. H. Citrin, P. Eisenberger, and B. M. Kincaid (1981), Extended X-ray absorption fine structure—its strengths and limitations as a structural tool, *Reviews of Modern Physics*, **53**, 769–806.
- F. Liu, S. H. Garofalini, R. D. King-Smith, and D. Vanderbilt (1993), First-principles studies on structural properties of β -cristobalite, *Physical Review Letters*, **70**, 2750–2753.
- J. K. Mackenzie and V. W. Maslen (1968), Reproducibility of intensity measurements by X-ray diffractometers. A new assessment of data from the single-crystal intensity project of the American Crystallographic Association, *Acta Crystallographica*, **A26**, 628–639.
- E. M. McMillan (1984), A history of the synchrotron, *Physics Today*, **37**(2), 31–37.
- A. L. Patterson (1934), A Fourier series method for the determination of the components of interatomic distances in crystals, *Physical Review*, **46**, 372–376.
- A. Rousse, C. Rischel, and J. C. Gauthier (2001), Colloquium: Femtosecond x-ray crystallography, *Reviews of Modern Physics*, **73**(1), 17–31
- L. Schiff (1968), *Quantum Mechanics*, 3rd ed., McGraw-Hill, New York.
- C. G. Shull, W. A. Strauser, and E. O. Wollan (1951), Neutron diffraction by paramagnetic and antiferromagnetic substances, *Physical Review*, **83**, 333–345.
- K. Siegbahn (1982), Electron spectroscopy for atoms, molecules and condensed matter, *Reviews of Modern Physics*, **54**, 709–728.
- G. H. Stout and L. H. Jensen (1989), *X-Ray Structure Determination: A Practical Guide*, 2nd ed.,

- John Wiley and Sons, New York.
- K. Triantafyllopoulos (2003), On the central moments of the multidimensional Gaussian distribution, *The Mathematical Scientist*, **28**, 125–128.
- B. K. Vainshtein (1994), *Fundamentals of Crystals: Symmetry and Methods of Structural Crystallography*, vol. 1 of *Modern Crystallography*, 2nd ed., Springer-Verlag, Berlin.
- L. Van Hove (1954), Correlations in space and time and born approximation scattering in systems of interacting particles, *Physical Review*, **95**(1), 249–262.
- R. W. G. Wyckoff (1963), *Crystal Structures*, vol. 1, 2nd ed., John Wiley and Sons, New York.

4. Surfaces and Interfaces

4.1 Introduction

Surface physics might seem to be unimportant because the number of atoms sitting at a surface relative to those lying within the bulk is negligible for macroscopic bodies. However, this judgment is incorrect. Surfaces provide the doorways through which material inevitably passes when entering or leaving a solid. The state of a material's surface determines both its strength and its resistance to chemical attack. The manufacture of integrated circuits consists in the deposition of complex sequences of surface layers to build up the desired pathways for electrons. Partly for this last reason there is a continual rapid development of experimental methods for describing and characterizing surfaces. Characterization has in fact outrun the immediate needs of technology, and it allows even surfaces without crystalline order to be pictured in atomic detail.

4.2 Geometry of Interfaces

The simplest deviation from perfect crystalline behavior occurs when a crystal comes to an end, abutting either another crystal or empty space. The first case is a *grain boundary*, and the second one is a *surface*. As discussed by Wolf (1992), these two types of interface can be described in a common way from the geometrical point of view.

One can initially simplify the problem of interfaces by assuming that when a perfect crystal is sliced along a plane, none of the remaining atoms moves from its original location. This assumption is not generally true, but is often a reasonable first approximation. The way in which it fails has to do with the fact that the crystal deforms as it approaches a boundary. The deformation may take a mild form, such as a slight increase or decrease of the volume per atom. It may involve the formation of an entirely new crystal structure right at the interface, called *surface reconstruction*. Or it may involve the formation of an entirely new phase; for example, a thin liquid layer on an otherwise solid body. The region of deformation relative to the perfect crystal is called the *selvage*.

Ignoring surface reconstructions and other deformations, a plane interface between two crystals may be described by ten variables, describing the ways that two perfect planar interfaces can be brought together. Three of the variables describe the precise microscopic three-dimensional positioning of one crystal with respect to another, as shown in Figure 4.1(A): exactly how far the two crystals are from one another, and how far each has been slid along the other in the two in-plane

directions. The seven remaining variables have macroscopic significance. Each of the two crystals has been sliced along a plane. The conventional way to describe planes is with Miller indices, using three numbers, but of course to describe a plane in three dimensions needs only two numbers, the angles along which its unit normal points. However, one needs to describe the precise point along the unit normal where the cut is made. So specifying the two crystal planes takes a total of six numbers. A tenth and final variable θ is needed to specify the relative orientations of the two crystals as they rotate about in the plane where they meet, shown in Figure 4.1(B).

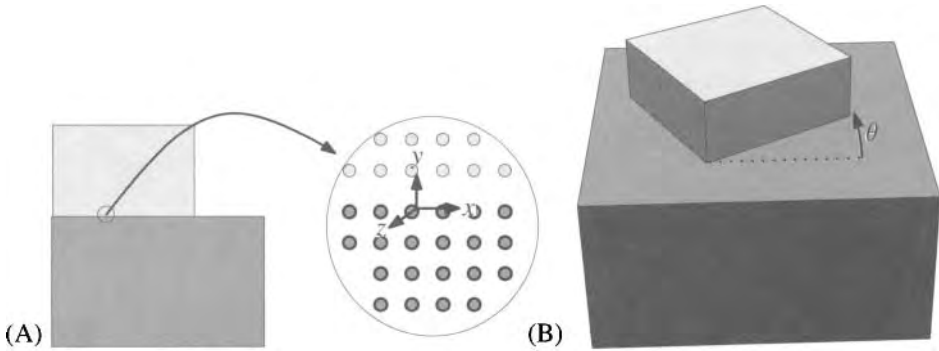


Figure 4.1. (A) Three microscopic variables describe the precise positioning of two ideal interfaces with respect to one another. (B) Angle specifying the relative rotations of two crystal interfaces.

For a free surface, only two variables need to be described; those giving the plane along which it cuts the crystal.

4.2.1 Coherent and Commensurate Interfaces

When two crystal surfaces meet, it is valuable to know if they will mesh well with one another. This question is particularly interesting if one is building a layered structure consisting of alternating crystal types and wants to know if they will bind together. If two crystal surfaces are placed together and the atoms are in perfect registry with one another, then one has a *coherent interface*, and the process of growing such an interface is called *epitaxy*. There is a related concept, that of a *commensurate interface* which is slightly more general. Two interfaces are commensurate if there is some larger two-dimensional lattice on which their atoms coincide, as shown in Figure 4.2. The general condition for two lattices to be commensurate is slightly complicated because one must include the possibility of rotating them at some peculiar angle, as in Figure 4.2. Let \vec{a}_1 , \vec{a}_2 and \vec{b}_1 , \vec{b}_2 be two sets of primitive vectors for the atoms on the two interfaces. Then the two are commensurate if there is an infinite set of integers n_1 , n_2 and m_1 , m_2 , together with

an angle θ such that

$$n_1\vec{a}_1 + n_2\vec{a}_2 = \begin{pmatrix} \cos \theta & \sin \theta \\ -\sin \theta & \cos \theta \end{pmatrix} (m_1\vec{b}_1 + m_2\vec{b}_2). \quad (4.1)$$

The set of points on which the two lattices agree is called the *superlattice*. One can always define \vec{b}_1 and \vec{b}_2 so that the rotation angle in Eq. (4.1) is zero, although it is included for generality.

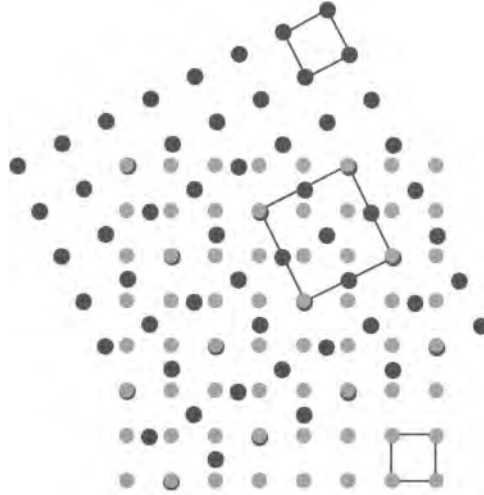


Figure 4.2. Two square lattices whose lattice constants differ by $\sqrt{5}/2$ are commensurate but incoherent, because not all the atoms lie on top of one another.

4.2.2 Stacking Period and Interplanar Spacing

Another interesting geometrical quantity is the *stacking period*, which is defined by counting the number of lattice planes one encounters, while heading directly away from the interface, before hitting a new lattice plane that has all its atoms sitting directly above those on the interface, along the normal. There are some fairly general results for crystals of cubic symmetry. If the Miller index of a surface is (ijk) , then the stacking period in a cubic crystal is

$$P = \delta(i^2 + j^2 + k^2), \quad (4.2)$$

where δ equals 1 or 2, depending on the particular lattice being considered and whether i , j , and k are odd or even, as shown in Figure 4.3.

Probably more important is the interplanar spacing

$$d = \epsilon a / \sqrt{i^2 + j^2 + k^2}, \quad (4.3)$$

where ϵ equals 1/2 or 1 depending upon circumstances. In fcc crystals, for example, ϵ is 1 if i , j , and k are all odd, but otherwise it equals 1/2. Because the

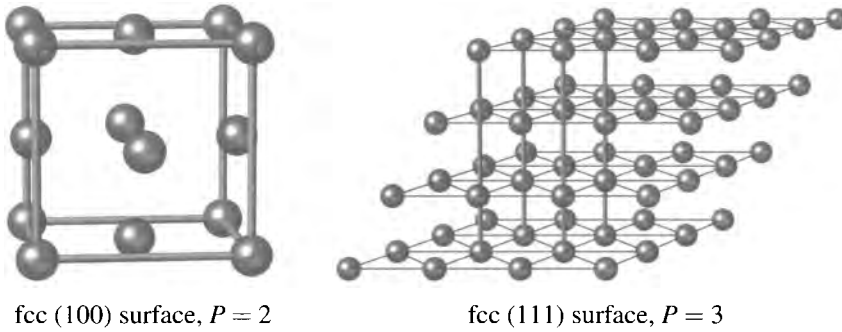


Figure 4.3. The stacking periods of the (100) and (111) planes for the fcc lattice. In the first case, δ of Eq. (4.2) is 2 and ϵ of Eq. (4.3) is $1/2$; in the second case, $\delta = 1$ and $\epsilon = 1$.

product of the interplanar spacing and the area per atom on the interface must be constant, interfaces with large interplanar spacings have the highest density of points on the surface. This situation is energetically favorable if two crystals are brought together, because it gives them opportunities to bond that resemble those of the unbroken crystal. For this reason, interfaces with small Miller indices, (110), (100), and (112), occur frequently in practical situations.

Yet another concept, not so easy to define precisely, is the number of nearest-neighbor bonds one must snap in order to build a given interface. This idea is connected approximately with surface energy, although the energy needed to form a surface cannot usually be encompassed completely by so simple a calculation as the snapping of nearest-neighbor bonds. The process of snapping bonds is relatively easy to visualize in simple cases, such as the (100) surface of an fcc lattice, shown in Figure 4.4.

There is a large vocabulary that has developed to describe the geometries of

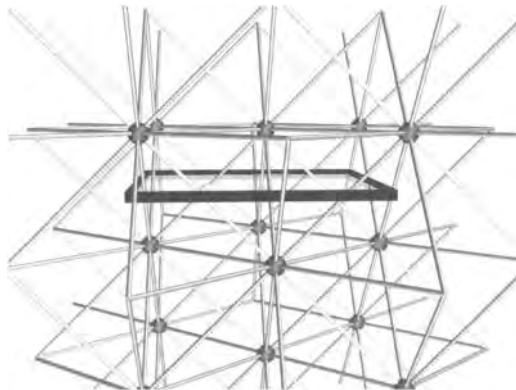


Figure 4.4. Diagram showing the bonds broken in cutting along the (001) plane in an fcc crystal. For planes at oblique angles, determination of the analogous quantity is more difficult, particularly because it may be advantageous for the surface of separation to rise and fall slightly on the atomic scale to cut the smallest number of bonds.

interfaces. If a single crystal is sliced along some plane, and the top half turned upside-down and replaced, the result is called a *twin boundary*, shown in Figure 4.5. The grain boundary in this case is a mirror plane; the high degree of symmetry makes such boundaries energetically favorable and quite common. If instead one rotates the top half of the crystal through some angle around a normal to the interface, one produces a *twist* boundary. If a single crystal has a wedge cut out of it and is then glued back together, the result is a *tilt* boundary; if the wedge is small, the result may be called a *low-angle* grain boundary. Finally, if the two halves of the crystal are brought back together without any tilting or rotation, but out of registry, the interface is a *stacking fault*.

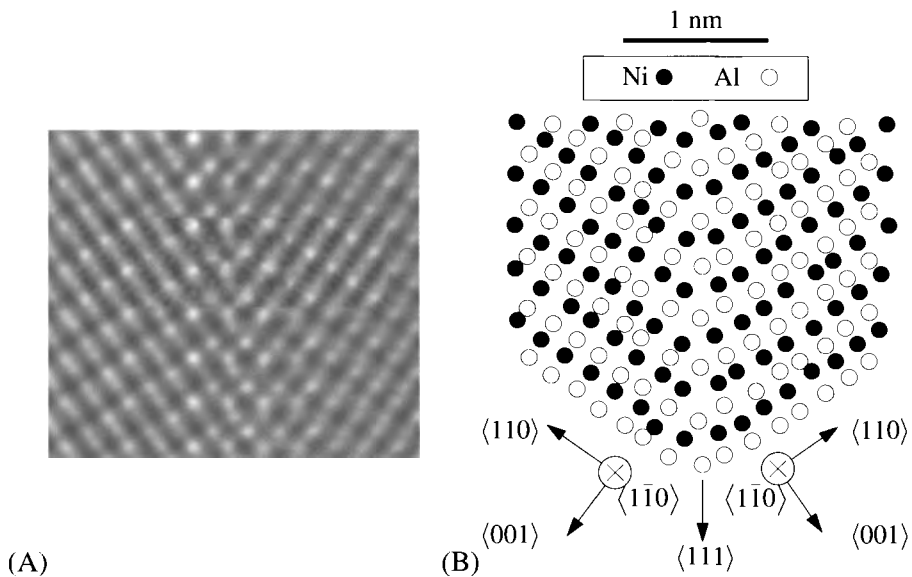


Figure 4.5. (A) (111) twin boundary in NiAl visualized with atomic resolution in a high-resolution electron micrograph. (B) Sketch clarifying locations of atoms. The mirror symmetry between right- and left-hand sides virtually eliminates defects along the interface. [Source: Nadarzynski and Ernst (1996), p. 651.]

4.2.3 Other Topics in Surface Structure

Because surfaces are open to the environment, they easily form thin layers of new structures, generically referred to as *adsorption*. If the attraction of the foreign material is weak, it is called *physisorption*. De Gennes (1985) reviews the phenomenon of *wetting* in which a thin fluid layer covers a solid. Gomer (1975) reviews *chemisorption*, where a chemical species forms a strong chemically bonded layer. All these topics are discussed in more detail by Zangwill (1988).

4.3 Experimental Observation and Creation of Surfaces

Many of the most dramatic recent advances in experimental physics have concerned studies of surfaces. There is an unpleasant tradition of giving each new technique an acronym, which tends to acquire new letters as the technique is refined.

4.3.1 Low-Energy Electron Diffraction (LEED)

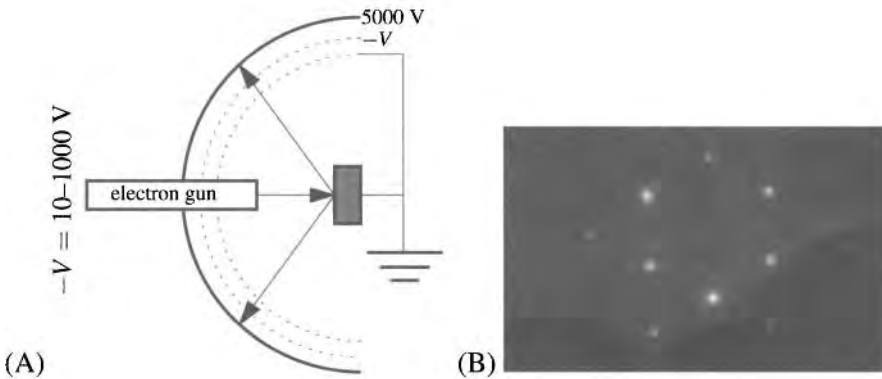


Figure 4.6. (A) Sketch of a LEED experiment. Electrons accelerate from a region with voltage V toward a sample surface. Reflected electrons pass through two grids whose voltage is arranged to allow past only those electrons that lost minimal energy during contact with the sample, and finally are attracted to a screen where they are imaged. (B) Low-energy electron diffraction from a diamond (111) surface with a single hydrogen terminating each dangling carbon bond. [Source: Cheng et al. (1997), p. 3714.]

Low-energy electron diffraction (LEED) is the method used by Davisson and Germer (1927) to establish the wave nature of the electron. The technique uses the fact that electrons of energy less than 10^3 eV have huge scattering cross sections in many materials, due to the intense interaction of electrons with any charged object, and is reviewed by Webb and Lagally (1973).

In the LEED configuration, electrons are directed toward a sample, shown in Figure 4.6. They collide with the surface, penetrating at most a few atomic layers, and some are scattered backwards. These reflected electrons are filtered, and only those suffering minimal energy loss in the scattering process are retained. Effectively, these electrons diffract only off the first layer or two of atoms with which they collide. The wavelength of electrons is given by

$$\lambda = 12.2 [\text{energy/eV}]^{-1/2} \text{ \AA} \quad (4.4)$$

so for typical energies of a few hundred electron volts, wavelengths are on the order of angstroms.

The basic equation for scattering from a surface is still given by Eq. (3.11), but the sum over l is taken only over a two-dimensional collection of atoms lying at the

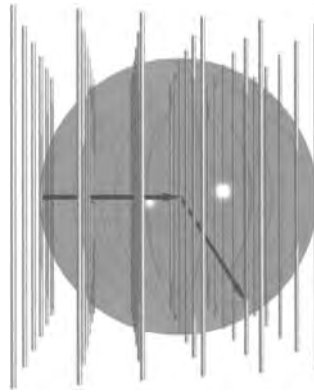


Figure 4.7. The Ewald construction for surfaces is shown, emphasizing that points in the reciprocal lattice become rods, and that the condition for scattering is that these rods be intersected by a spherical shell.

solid surface. Call the scattering surface the x - y plane. The condition for obtaining a strong scattering peak therefore is given by Eq. (3.17) in the form

$$\vec{q} \cdot (R_x, R_y, 0) = 2\pi l. \quad l \text{ must be an integer, but will vary depending on the choice of } \vec{R}. \quad (4.5)$$

The difference between scattering from a bulk solid and scattering from a solid surface results from the fact that while the lattice vectors \vec{R} in Eq. (4.5) lie in a plane, the experiment takes place in a three-dimensional world, where radiation is free to exit in a set of directions indexed by angles θ and ϕ . Then Eq. (4.5) is satisfied by any \vec{q} of the form

$$\vec{q} = (K_x, K_y, q_z). \quad \begin{array}{l} K_x \text{ and } K_y \text{ are components of a reciprocal lattice} \\ \text{vector } \vec{K} \text{ chosen so that } K_x R_x + K_y R_y = 2\pi l. \text{ One} \\ \text{can take } q_z \text{ to be anything at all, because the } z \\ \text{component of } \vec{R} \text{ is zero.} \end{array} \quad (4.6)$$

Constructing the Ewald sphere corresponding to Eq. (4.6), one sees that the geometrical condition to be satisfied is that the surface of a sphere intersect a collection of rods, as in Figure 4.7. This condition is guaranteed to be satisfied at some scattering angles for any choice of incoming wave vector \vec{k}_0 and for any orientation of the sample, in contrast with the bulk case described in Section 3.3. There is no need to rotate the sample, scan through incoming wave vectors, or use powdered samples in order to obtain scattering peaks.

Despite LEED's crucial historical role in demonstrating the wave nature of the electron, it is not easy to determine detailed features of surfaces based upon LEED measurements. Because electrons interact very strongly with solids, multiple scattering is impossible to avoid. Quantitative comparison of theory and experiment requires one to make detailed guesses about surface structure and then carry out lengthy quantum-mechanical calculations for the scattering of electrons from the surfaces, based upon the guesses.

4.3.2 Reflection High-Energy Electron Diffraction (RHEED)

In this technique, electrons of energy on the order of 100 keV are reflected off a surface at a grazing angle. The wave vectors associated with such energies are on the order of 200 \AA^{-1} and are much larger than the spacing between reciprocal lattice vectors, leading to streaky scattering patterns where the Ewald sphere intersects reciprocal lattice rods. Slight rotations of the sample are needed to obtain strong signals in desired directions.

4.3.3 Molecular Beam Epitaxy (MBE)

With the ability to measure the properties of surfaces with precision has come the ability to control their composition with comparable precision. The technique of *molecular beam epitaxy* (MBE) allows building up a solid one atomic layer at a time with precise control over the composition of each layer and the ability to alter composition at will.

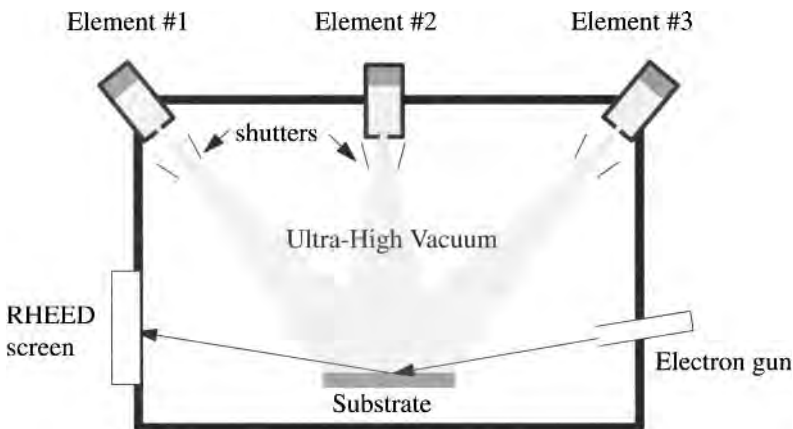


Figure 4.8. Schematic view of MBE. Ballistic beams of atoms escaping from heated chambers impinge upon a substrate and form atomically perfect layers, monitored by RHEED.

A caricature of a molecular beam epitaxy facility appears in Figure 4.8. An atomically flat crystalline surface is placed within an ultra-high vacuum chamber, meaning it is at a pressure of around 10^{-11} torr. Various *Knudsen cells*, each containing a different element to be added to the surface, are aimed at the substrate. Atoms leave the Knudsen cell simply by being heated until they evaporate, and then flying ballistically to the substrate, if the control shutter is open. To obtain atomic control of the deposition process, reflection high-energy electron diffraction is carried out *in situ*. The strength of the specularly reflected electron beam depends upon the state of the surface, as shown in Figure 4.9. If a new surface layer is only half-formed, the electron beam is scattered diffusely, while if it is nearly perfect and smooth, the specular reflection grows stronger. The result is a periodic oscillation of the strength of the electron beam, in which each period represents the deposition of precisely one atomic layer.

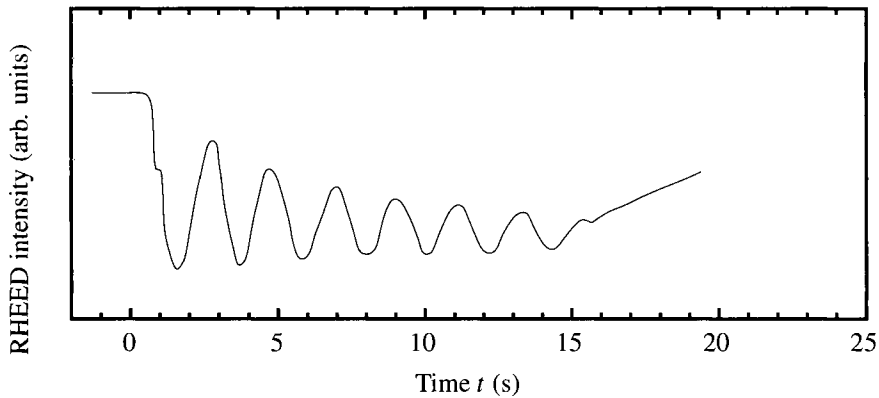


Figure 4.9. The intensity of RHEED scattering from a growing surface depends upon whether the surface is complete, or partially formed. These data show oscillations in RHEED intensity during the growth of a (001) GaAs surface, monitoring the $[\bar{2}10]$ reflection as electrons reflect off the surface at an angle of 0.91° . [Source: Braun et al. (1998), p. 4937.]

To a great extent, layer growth in molecular beam epitaxy is dependent upon the physics by which atoms attach to surfaces, still more of an empirical than a theoretical science. Attempting to deposit silver on GaAs, for example, by this technique produces blobs and islands rather than uniform atomically flat films. Conversely, there are fortunate cases in which deposition layer by layer is possible. One important example is the deposition of GaAlAs on GaAs, where the aluminum may be substituted for the gallium at any desired concentration and where layers of varied composition may be grown with exceptional precision, one upon the other. The interfaces are not absolutely atomically perfect, but errors in which a gallium or aluminum atom finds itself out of place are typically confined to the width of a single atomic spacing.

4.3.4 Field Ion Microscopy (FIM)

A specimen is formed in the shape of a sharp tip. This tip is given a large positive electrical potential, and because sharp tips create singular electrical fields, a field on the order of 10^9 V/cm is generated near the surface. The tip is placed in a neutral gas such as helium or neon at moderately low pressure, and the large fields cause occasional ionization of the gas, thereby capturing an electron and repelling the ion. The ions are captured on a screen. The capture process happens preferentially near protruding atoms on the tip, so that the technique can actually image individual atoms on the tip surface. Disadvantages include the fact that one must be able to build the microscope tip out of the material one wishes to examine, and one can only look at materials that can stand the high fields. This technique has largely been supplanted by tunneling microscopy. It is reviewed by Tsong (1993).

4.3.5 Scanning Tunneling Microscopy (STM)

The idea that quantum mechanics should permit particles to pass through barriers occurred to J. R. Oppenheimer during a drive from the eastern United States to a position as research fellow at Cal. Tech. in 1927. The symbols

$$i \sim \exp \frac{-C}{E} \quad \begin{array}{l} \text{See Davis (1968), p. 23. The tunneling} \\ \text{formula in more familiar notation might} \\ \text{read } \psi \sim \exp[-x\sqrt{2mU/\hbar^2}]. \end{array} \quad (4.7)$$

had just been scrawled on the windshield of his car when he ran off the road into a county courthouse, a rather unsuccessful first attempt to put the formula into practice.

Tunneling spectroscopy became a powerful tool for investigation of metals and superconductors over the next four decades. As discussed by Wolf (1975), it was typically performed between flat millimeter-scale samples with separations between the plates much larger than an angstrom. The macroscopic size of the sample offset the exponentially small current that could flow between the two plates, and the large size also produced an average over the thermal vibrations of the plates.

Gradual improvement of numerous branches of technology made it possible by the 1980s to employ Eq. (4.7) for imaging of surfaces on the atomic scale, in a device invented by Binnig and Rohrer (1987) and called the *scanning tunneling microscope* or STM. The essential idea is to bring an atomically sharp metallic tip near to a conducting surface. Because the current flowing from surface to tip varies exponentially with the distance between them, it can be used as an exceptionally sensitive indicator of surface height, and because the tip is very sharp, it is sensitive to small-scale variations in the horizontal direction as well.

Detailed calculations of the precise rate at which tunneling takes place between surface and tip are not needed to appreciate the device, but it is worth asking how all the quantities appearing in Eq. (4.7) are to be defined in order to apply to the case of the tunneling microscope. A schematic picture of the device appears in Figure 4.10. First, consider the case in which the voltage difference V between tip and sample is zero. The equilibrium chemical potentials of different conductors are not in general the same, which means that in order for tip and sample to be at the same voltage, a small transient current has had to flow between them soon after they were connected together, resulting in a situation where the minimum energy needed to raise an electron from tip or surface to the energy of the vacuum is

$$\phi = \frac{1}{2}(\mu_1 + \mu_2). \quad \begin{array}{l} \text{Thus } \phi \text{ is the average of the work functions} \\ \text{of the tip and surface; work functions are dis-} \\ \text{cussed further in Sections 19.2.1 and 23.6.1.} \end{array} \quad (4.8)$$

The tunneling current Eq. (4.7) follows from the Wentzel–Kramers–Brillouin (WKB) approximation, which gives as an approximate solution of Schrödinger’s equation

$$\psi(x) \sim \exp \left[(i/\hbar) \int^x dx' \sqrt{2m(\mathcal{E} - U(x'))} \right]. \quad \begin{array}{l} \text{See Landau and Lifshitz} \\ \text{(1977), p. 164, or Schiff} \\ \text{(1968), p. 268.} \end{array} \quad (4.9)$$

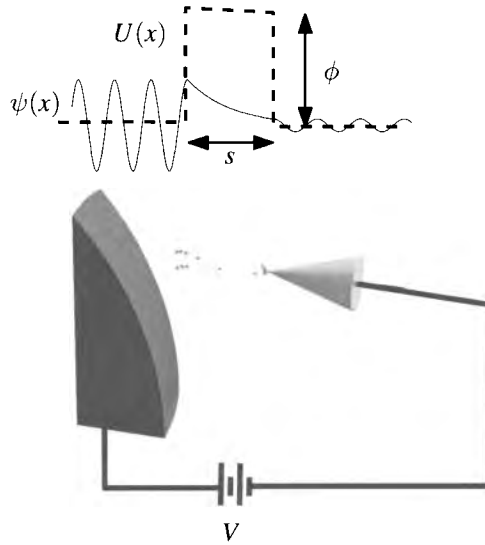


Figure 4.10. Schematic view of scanning tunneling microscope. Electrons tunnel through the vacuum from a metal surface to a metal tip.

An electron wave function which begins on the left side of Figure 4.10 and travels distance s through the vacuum will drop in amplitude by a factor of

$$\exp \left[-s\sqrt{2m\phi/\hbar^2} \right] \quad \begin{array}{l} \text{Because } U - \mathcal{E} = \phi \text{ in the forbidden region.} \\ \text{The calculation is performed in the limit of} \\ \text{vanishing voltage } V, \text{ so one need not consider} \\ \text{the slight drop by amount } V \text{ in the potential} \\ \text{ } U(x). \end{array} \quad (4.10)$$

by the time it reaches the other side. The current must be proportional to the applied voltage V , to the square of the wave function, to the initial density of electrons n_i ready to spring out of the sample, and to the final density of locations in the tip n_f to which they can travel. Thus one estimates the current J to be

$$J \propto n_i n_f V \exp[-2s\sqrt{2m\phi/\hbar^2}] \quad (4.11)$$

$$\propto \exp \left[-1.02[s/\text{\AA}]\sqrt{[\phi/\text{eV}]} \right] . \quad (4.12)$$

Achieving atomic-scale resolution depends upon careful experimental control of a number of different elements. First, external noise and vibrations must be eliminated, because motion of the tip by even 0.5 angstrom relative to the sample is fatal. The seeming impossibility of controlling vibrations is one explanation for why the STM took so long to discover. In the first STM, vibration was controlled by levitating the entire apparatus on permanent magnets over a bowl of superconducting lead. Nested collections of mechanical springs were soon found to be equally effective, but much cheaper. A schematic view of an STM from the point of view of vibration isolation appears in Figure 4.11. The central idea is that large soft springs connect the outside world to the machine through progressively

smaller and stiffer ones, terminating in the tip and sample housing that needs to be as small and stiff as possible.

The next experimental challenge is to bring the tip reliably to within 1 angstrom of the sample and then maintain it either at constant current or constant voltage during scans across the surface. So that the sample can be removed and inserted under the tip, there needs initially to be clearance of around 1 mm. This difficulty also can be surmounted with appropriate use of springs, as indicated in Figure 4.11. Gross vertical motions of the sample are controlled by a large weak spring, which also helps ensure that external vibrations do not reach the sample. The large spring is in series with smaller, much stiffer springs, so pushing up and down upon it results in comparatively small motions of the sample. Fine motions of the tip, which must be controlled well within an angstrom but range over a micron, are controlled by mounting the tip upon a number of piezoelectric elements. The conceptually simplest geometry of the piezoelectric elements controls tip motion with two horizontal elements (whose contraction moves the tip about in the plane) and one vertical element (which controls its height). A widely used piezoelectric material is PbZrTi (PZT), which contracts by around 4 parts in 10^8 per volt applied across it, up to 1000 V. Therefore for 2-cm-long piezoelectric strips sub-angstrom resolution is obtained by controlling voltages to within a percentage of a volt, but at the same time excursions on the order of $1\ \mu\text{m}$ are obtainable. The piezoelectric strips in such a geometry are too long and floppy to provide optimal control, and numerous other designs are employed in practice.

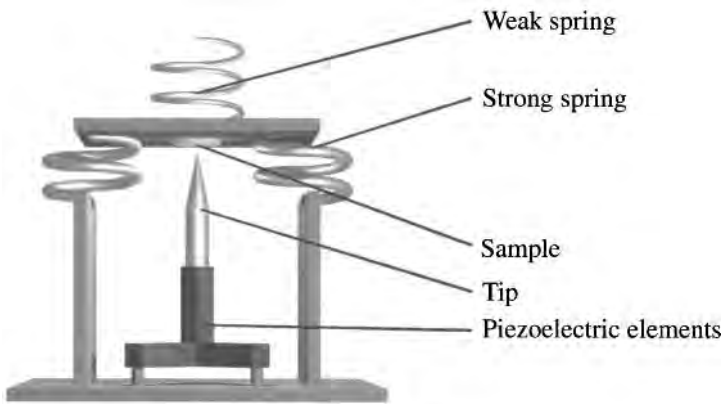


Figure 4.11. Schematic view of mechanical operation of an STM.

Finally, there remains the challenge of creating a tip capable of achieving atomic resolution. Experimental groups have their own secret magical recipes, and no single method dominates because no method has yet been found which is particularly reproducible or reliable. The best tips have literally a single atom protruding from their ends; they are hard to make and last only so long as mechanical stresses during measurement do not make the atom jump about.

It would be difficult to operate a scanning tunneling microscope without modern electronics. On the one hand, the piezoelectric elements must be controlled

continuously and in precise sequence in order to scan the tip across the surface. In addition, all the data for tip height as a function of x, y location have to be recorded and assembled later for interpretation. Computer control and data acquisition are therefore almost indispensable.

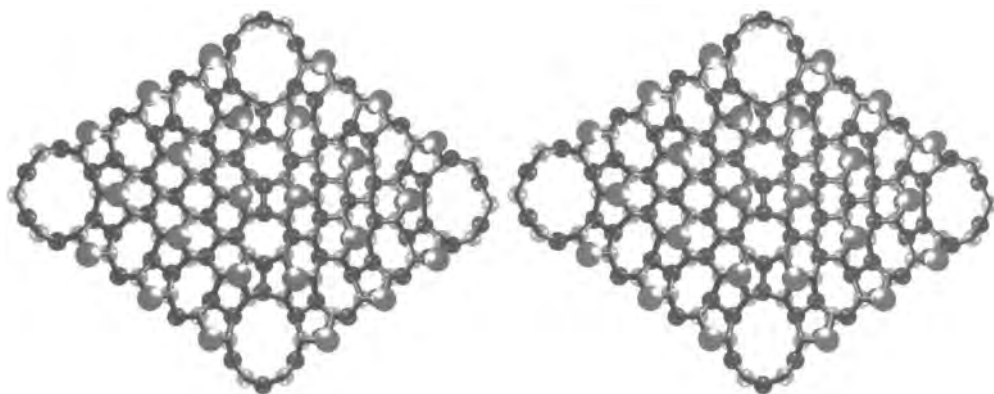

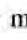
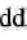


Figure 4.12. Stereo pair showing the locations of atoms in the Si 7×7 reconstruction of the (111) surface. The first three layers of atoms are shown, with different colors assigned to atoms in each layer. Top layer, ; middle layer, ; bottom layer, . The structure occupies 7×7 unit cells, as may be seen by counting the number of cells separating the centers of the large voids at each corner.

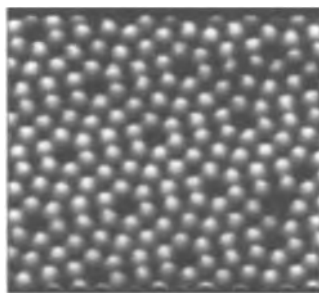


Figure 4.13. Atoms on the (111) surface of silicon form the pattern shown here, which involves a 7×7 atom surface unit cell. The image is produced by scanning tunneling microscopy. [Source: Wolkow and Avouris (1988), p. 1050.]

The STM only became a standard tool in laboratories around the world after proving itself by resolving a long-standing controversy that had resisted all other types of surface analysis, the structure of the Si (111) surface. Although the crystal surface of silicon used in the electronics industry is (100), the (111) surface is easier to prepare for research purposes, because unlike (100) it can be formed by cleavage and made atomically flat with relatively little effort. Prior to the STM, locations of the atoms on the surface were not possible to determine, and the number of different proposals was approximately equal to the number of experimental and theoretical papers published on the subject. The STM resolved the question decisively;

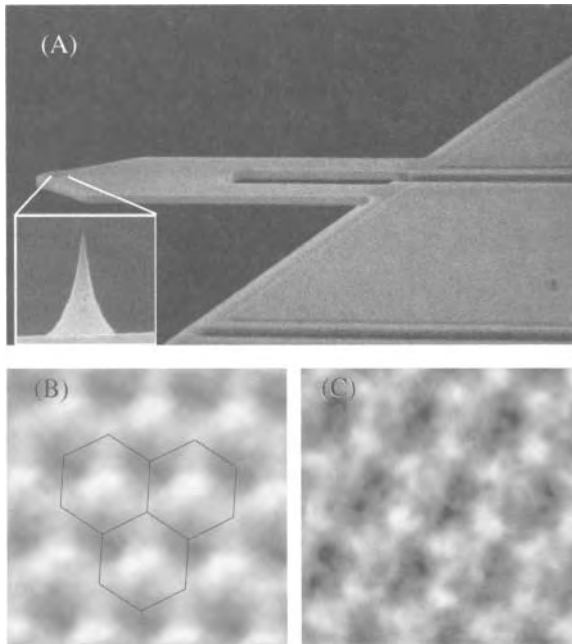


Figure 4.14. (A) Scanning electron micrograph of piezoresistive cantilever and tip used in atomic force microscopy. [Courtesy of M. Tortonese, ThermoMicroscopes and Stanford University.] (B) Atomic-scale image of the surface of graphite. The image is a map of the force between the microscope tip and the sample at a height of 12 pm, with forces ranging from -30 pN (white) to 30 pN (black). Hexagons show crystalline lattice. However, the experimental image has three-fold rather than six-fold symmetry because the AFM tip is not symmetrical and interacts differently with the crystalline lattice in different directions. (C) Map of dissipation per cycle obtained while oscillating the AFM tip at a height of 97 pm over the sample, showing full symmetry of graphite lattice. [(B) and (C) courtesy of U. Schwartz, Yale University. For further details, see Albers et al. (2009).]

the atoms are located in a 7×7 structure illustrated in Figure 4.12. Within a few years, images such as in Figure 4.13 became commonplace. Having shown it could answer questions beyond the capability of any other instrument, very rapid growth both in research use and commercial development began immediately thereafter.

Tempting though it may be to regard the white and black spots of an STM image as atoms, one needs always to think back to Eq. (4.11) in viewing an STM image. What one sees is a contrast between electron densities at various points on the surface. Therefore, an atom on the surface which keeps a close grip on its electrons will be invisible, and some atoms may come in and out of view as one varies the bias voltage between tip and sample. In metals, the electron density is frequently sufficiently uniform that an STM image is featureless; an insulator has no free electrons to donate and is invisible, which leaves semiconductor surface physics as the domain in which the method is most profitable.

4.3.6 Atomic Force Microscopy (AFM)

The *atomic force microscope* (AFM) was developed by Binnig et al. (1986) as a modification of the STM, to permit investigation of insulators. A tip is lowered toward a sample on a lever until it virtually touches, and either the force on the lever is maintained constant as it scans over the sample, or else deflection of the lever is measured by mounting a mirror on it and bouncing a laser beam off the top. The difficulties of controlling motion at the angstrom scale find the same solutions as with STM. An image of the surface of graphite is shown in Figure 4.14. Interpretation of the image requires some caution. It accurately reflects the force between the surface of graphite and the AFM tip, but because the tip is not completely symmetrical, the image has three-fold rather than six-fold symmetry. Bustamante and Keller (1995) show that the AFM technique can be modified to function even in liquids at room temperature, although in such noisy environments atomic-scale resolution is no longer possible.

4.3.7 High Resolution Electron Microscopy (HREM)

High resolution electron microscopy (HREM), described by Spence (1988), allows the study of solids with atomic resolution, and it can only be used on extremely thin sections of samples. An example of the technique has been displayed in Figure 4.5. The image looks like a photograph of atoms, but it must be approached with caution. It actually reflects a complicated smearing out of the actual electron density, and any attempt to extract quantitative density information requires an attempt to deal with the smearing quantitatively.

Problems

1. **Superlattice:** Show that when two crystal surfaces meet in a commensurate fashion, so that there is a superlattice along the interface, the areas of the primitive cells for the two surface lattices must be rational multiples of one another.
2. **Interplanar spacing:** Consider a bcc lattice, and find how ϵ in Eq. (4.3) depends upon i , j , and k for the planes (110), (111), (114), and (137).
3. **Bond breaking:**
 - (a) Consider an fcc lattice in which the energy of a surface is given by the number of broken nearest-neighbor bonds. With reference to Figure 4.4, find the energy needed per area to cut along the (001) plane.
 - (b) Consider the diamond structure, shown in Figure 2.6. How many bonds per area need to be cut to expose the (001) plane?
 - (c) Consider again the diamond structure, but now also consulting Figure 2.2(D). How many bonds per area need to be cut to expose a (111) plane? Which of (001) and (111) should be expected to cleave most easily?

4. Faceting:

- (a) Consider a two-dimensional square crystal. Suppose the energy needed to form a surface of Miller index (ij) is simply the number of nearest-neighbor bonds broken in forming the surface. Show that the surface energy α per unit length is

$$\alpha = \left(\frac{J}{a}\right) \frac{|i| + |j|}{\sqrt{i^2 + j^2}}, \quad (4.13)$$

where J is the energy per bond and a is the lattice spacing.

- (b) Draw a polar plot of Eq. (4.13); that is, draw a curve in polar coordinates where $r(\theta)$ is given by the free energy α appropriate for a surface cut at angle θ .
- (c) Suppose one has a two-dimensional crystal whose surface free energy per unit length is $\alpha(\theta)$ for a surface at orientation θ , or equivalently $\alpha(y')$, where $y(x)$ is a function describing the height of the crystal in Cartesian coordinates, and $y' = dy/dx$. Argue that the equilibrium shape of such a crystal is given by minimizing the functional

$$\int dx \sqrt{1 + y'^2} \alpha(y') - \lambda \int dx y(x), \quad (4.14)$$

where λ is a Lagrange multiplier.

- (d) Define

$$f(y') = \sqrt{1 + y'^2} \alpha(y'). \quad (4.15)$$

Using the calculus of variations, show that

$$\frac{d}{dx} \frac{\partial f}{\partial y'} = \lambda \quad (4.16)$$

and that after obtaining a first integral and then multiplying by y'' , Eq. (4.16) can be integrated to give

$$\sqrt{1 + y'^2} \alpha(y') = \lambda(y'x - y) \quad (4.17)$$

The arbitrary constants obtained during the integrations can be ignored. Why?

- (e) Rewrite Eq. (4.17) in terms of the unit normal \hat{n} to the surface described by $y(x)$. Equation (4.17) describes a geometrical construction in which for every normal direction \hat{n} one draws a line perpendicular to \hat{n} at a distance $r(\hat{n})$ from the origin such that the line hits the polar plot of $\alpha(y')$ from part (b). Then $y(x)$ is the envelope of all these lines. Use this construction to draw a sketch of the equilibrium crystal resulting from the surface energy of Eq. (4.13). For more information on this topic, see Rottman and Wortis (1984) and Tosi (1964) p. 92.

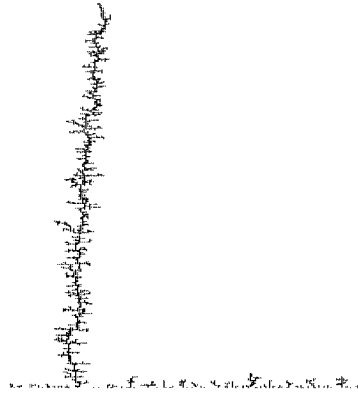


Figure 4.15. A cluster produced by diffusion limited aggregation with 2000 particles.

5. **Diffusion-limited aggregation:** *Diffusion-limited aggregation* or DLA is a simple algorithm for how surfaces might grow in a disordered fashion, first studied by Witten and Sander (1981). The algorithm has the following steps:

- (a) Consider a rectangular grid, periodic in the horizontal direction, with period 200. Particles will be able to visit nodes on the grid, indexed by integers (l_x, l_y) , where $0 \leq l_x < 200$ and $0 \leq l_y$. Create a 200×600 array of integers to represent this grid, and initialize all elements to 0.
- (b) Introduce a particle at site $(100, 0)$, which means setting the array element $(100, 0)$ to 1. The height of the cluster is now 1.
- (c) Now introduce a new particle at height 1, which means randomly choosing an array element on the line $(l_x, 1)$ and setting it to value 1.
- (d) Allow this particle to diffuse. That is, choose randomly from the four direction vectors $(1, 0)$, $(-1, 0)$, $(0, 1)$ and $(0, -1)$, and move the particle as the direction vector indicates by setting the array element where the particle used to be to 0, and also setting the value of the new array element to 1.
- (e) Keep allowing the particle to diffuse until:
 - i. The particle height l_y rises above the maximum height of the cluster (now equal to 1). In this case set its array element to 0, and return to step (c).
 - ii. The particle height hits the floor at $l_y = 0$. In this case, the array element where the particle is located remains at 1, and a new particle is introduced.
 - iii. The particle occupies any lattice site adjacent to the first particle that was introduced, from any side. Again, the second particle is frozen, and a new particle will be introduced. There is now the possibility that the height of the cluster will have risen to 2.
- (f) Introduce more particles in an analogous fashion. Particles are introduced randomly at height $l_{\max} + 1$, where l_{\max} is the highest occupied site on the existing cluster. If they diffuse above the height at which they are introduced,

throw them out, and introduce a new particle. If a particle touches the floor, or any particle already frozen in the cluster, it too freezes, I_{\max} is increased by 1 if necessary, and a new particle is introduced.

- (g) Using this algorithm, produce a cluster with 2000 particles and draw a picture of it (see Figure 4.15).

References

- B. J. Albers, T. C. Schwendemann, M. Z. Baykara, N. Pilet, E. I. A. Marcus Liebmann and, and U. D. Schwarz (2009), Three-dimensional imaging of short-range chemical forces with picometre resolution, *Nature Nanotechnology*, **4**, 307–310.
- G. Binnig, C. F. Quate, and C. Gerber (1986), Atomic force microscope, *Physical Review Letters*, **56**, 930–933.
- G. Binnig and H. Rohrer (1987), Scanning tunneling microscopy—from birth to adolescence, *Reviews of Modern Physics*, **59**, 615–625.
- S. Boseck (1995), Scanning acoustic microscopy and its applications to material characterization, *Reviews of Modern Physics*, **67**, 863–891.
- W. Braun, L. Däweritz, and K. H. Ploog (1998), Origin of electron diffraction oscillations during crystal growth, *Physical Review Letters*, **80**, 4935–4938.
- C. Bustamante and D. Keller (1995), Scanning force microscopy in biology, *Physics Today*, **48**(12), 32–38.
- C.-L. Cheng, H.-C. Chang, J.-C. Lin, K.-J. Song, and J.-K. Want (1997), Direct observation of hydrogen etching anisotropy on diamond single crystal surfaces, *Physical Review Letters*, **78**, 3713–3716.
- N. P. Davis (1968), *Lawrence and Oppenheimer*, Simon and Schuster, New York.
- J. Davisson and L. H. Germer (1927), Diffraction of electrons by a crystal of nickel, *Physical Review*, **30**, 705–740.
- P. G. de Gennes (1985), Wetting: Statistics and dynamics, *Reviews of Modern Physics*, **57**, 827–863.
- A. L. de Lozanne (1993), Scanning tunneling microscopy, in *Investigations of Surfaces and Interfaces—Part A*, B. W. Rossiter and R. C. Baetzold, eds., vol. IXA of *Physical Methods of Chemistry*, pp. 142–207, John Wiley and Sons, New York.
- A. Erzan, L. Pietronero, and A. Vespignani (1995), The fixed-scale transformation approach to fractal growth, *Reviews of Modern Physics*, **67**, 545–604.
- R. Gomer (1975), Chemisorption on metals, *Solid State Physics: Advances in Research and Applications*, **30**, 93–225.
- L. D. Landau and E. M. Lifshitz (1977), *Quantum Mechanics (Non-relativistic Theory)*, 3rd ed., Pergamon Press, Oxford.
- K. Nadarzynski and F. Ernst (1996), The atomistic structure of a $\Sigma = 3$, (111) grain boundary in NiAl, studied by quantitative high-resolution transmission electron microscopy, *Philosophical Magazine A*, **74**, 641–664.
- C. F. Quate (1986), Vacuum tunneling: A new technique for microscopy, *Physics Today*, **39**(8), 26–33.
- C. Rottman and M. Wortis (1984), Statistical mechanics of equilibrium crystal shapes: Interfacial phase diagrams and phase transitions, *Physics Reports*, **103**, 59–79.
- L. Schiff (1968), *Quantum Mechanics*, 3rd ed., McGraw-Hill, New York.
- J. C. H. Spence (1988), *Experimental High-Resolution Electron Microscopy*, 2nd ed., Oxford University Press, New York.

- M. P. Tosi (1964), Cohesion of ionic solids in the Born model, *Solid State Physics: Advances in Research and Applications*, **16**, 1–120.
- T. T. Tsong (1993), Atom-probe field ion microscopy, *Physics Today*, **46**(5), 24–31.
- M. B. Webb and M. G. Lagally (1973), Elastic scattering of low-energy electrons from surfaces, *Solid State Physics: Advances in Research and Applications*, **28**, 301–405.
- T. A. Witten and L. M. Sander (1981), Diffusion-limited aggregation, a kinetic critical phenomenon, *Physical Review Letters*, **47**, 1400–1403.
- D. Wolf (1992), Atomic-level geometry of crystalline interfaces, in *Materials Interfaces: Atomic-level Structure and Properties*, D. Wolf and S. Yip, eds., pp. 1–57, Chapman and Hall, London.
- E. L. Wolf (1975), Nonsuperconducting electron tunneling spectroscopy, *Solid State Physics: Advances in Research and Applications*, **30**, 1–91.
- R. Wolkow and P. Avouris (1988), Atom-resolved surface chemistry using scanning tunneling microscopy, *Physical Review Letters*, **60**, 1049–1052.
- A. Zangwill (1988), *Physics at Surfaces*, Cambridge University Press, Cambridge.

5. Beyond Crystals

5.1 Introduction

The number of possible equilibrium crystal structures is enormous, but these structures represent ideal cases, rarely realized in the natural world. Macroscopic samples of solid matter are rarely close at all to thermal equilibrium, and equilibrium structures are not always crystals. The goal of this chapter is to discuss some of the relations between naturally occurring materials and crystals. The first topic is diffusion, since random displacement of atoms provides one of the primary ways that perfect crystalline order is modified. Metal alloys provide the next topic. Simple statistical arguments show that their crystalline order can be destroyed at a critical temperature well below melting, and that even when one disregards this transition, these alloys are unlikely ever to be in equilibrium. There follows a brief discussion of several other forms condensed matter can take—liquids, glasses, liquid crystals, and polymers—for which the language of crystals is inappropriate. The discussion closes with an introduction to quasicrystals, which provide an example where a structure without true crystalline order can be described with the same precision and completeness that has been found for crystals.

5.2 Diffusion and Random Variables

5.2.1 Brownian Motion and the Diffusion Equation

In 1827, Robert Brown published an account of observations through a microscope, beginning with pollen, and proceeding to a large variety of powders. He concluded

[t]hat extremely minute particles of solid matter, whether obtained from organic or inorganic substances, when suspended in pure water or in some other aqueous fluids, exhibit motions for which I am unable to account and which from their irregularity and seeming independence resemble in a remarkable degree the less rapid motions of some of the simplest animalcules of infusions. —Brown (1827), p. 481

The motions were eventually explained by Einstein (1905) and Perrin (1909) as the result of thermal fluctuations causing fluid molecules to collide with the particles, and exciting them into motion. The microscopic motions became identified with the tendency of small particles to spread apart, as when some ink drops onto a piece of paper or a gel.

5.2.2 Diffusion

Diffusive motion concerns a large population of noninteracting particles kicked about by random forces. Equivalently, it describes the probability distribution of a single particle undergoing random motion.

The mathematical description of diffusion begins with the observation that if $n(\vec{r}, t)$ describes some density distribution of particles then there is a particle current \vec{j} that flows from regions of high density to low. The simplest possible rule for how this happens is that the rate of flow is proportional to the gradient $\vec{\nabla}n(\vec{r}, t)$ (Fick's law) so that

$$\vec{j} = -\mathcal{D}\vec{\nabla}n. \quad (5.1)$$

The constant \mathcal{D} is called the *diffusion constant*. Eq. (5.1) can also be rewritten as

$$\vec{j} = -\vec{v}n \quad \text{where} \quad \vec{v} \equiv -\mathcal{D}\frac{\vec{\nabla}n}{n} \quad (5.2)$$

is the mean velocity of particles.

Continuity Equation. To obtain a closed expression for the particle density n , make use of the fact that particles are conserved. The *continuity equation*, illustrated in Figure 5.1 describes any collection of conserved particles whose coordinates \vec{r} change continuously with velocity \vec{v} . If $n(x, t)$ is the number of particles at position x and they are moving with mean velocity $v(x, t)$, then the number of particles moving into a little region of width dx minus the number moving out is

$$Av(x)n(x) dt - Av(x+dx)n(x+dx) dt \quad (5.3)$$

in time dt . Therefore for variable x one has that

$$\frac{\partial n}{\partial t} = -\frac{\partial}{\partial x}v(x)n(x, t). \quad \text{Divide change in number of particles per time} \quad (5.4)$$

by volume $A dx$ of the box.

If there are many variables, the argument holds for each coordinate in turn and

$$\frac{\partial n}{\partial t} = -\sum_{\alpha} \frac{\partial}{\partial r_{\alpha}}v_{\alpha}(\vec{r})n(\vec{r}, t). \quad (5.5)$$

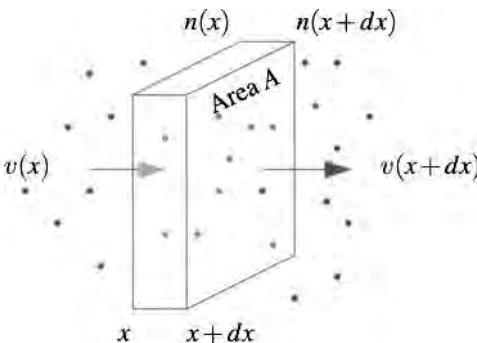


Figure 5.1. The continuity equation applies to any situation in which a conserved collection of particles can be characterized by a mean velocity \vec{v} as a function of coordinate \vec{r} .

Diffusion Equation. Using the velocity \vec{v} for diffusing particles from Eq. (5.2) in the continuity equation (5.5) gives finally the *diffusion equation*

$$\frac{\partial n}{\partial t} = \mathcal{D} \nabla^2 n. \quad \text{Taking Eq. (5.5) to apply to three dimensions.} \quad (5.6)$$

5.2.3 Derivation from Master Equation

The simplest derivations of the diffusion equation do not make it apparent how random motion of particles leads to diffusion. To build this connection, a more sophisticated derivation is required. Again, let $n(\vec{r}, t)$ be the density of particles at location \vec{r} at time t . Assume that at small time dt later the number of particles originally in small volume $\delta\mathcal{V}$ at \vec{r} that end up at $\vec{r} + \vec{s}$ is

$$n(\vec{r}, t) R(\vec{r} \rightarrow \vec{r} + \vec{s}, dt) \delta\mathcal{V}. \quad \begin{array}{l} R \text{ gives the probability that particles start at } \vec{r} \\ \text{and end at } \vec{r} + \vec{s} \text{ after time } t. \end{array} \quad (5.7)$$

Then the change in the number of particles in the volume $\delta\mathcal{V}$ near \vec{r} is the number of particles starting at $\vec{r} + \delta\vec{r}$ and coming to \vec{r} minus the number starting at \vec{r} and leaving, which can be written as

$$n(\vec{r}, t + dt) - n(\vec{r}, t) = \int d\vec{s} \left[\begin{array}{l} R(\vec{r} + \vec{s} \rightarrow \vec{r}, dt) n(\vec{r} + \vec{s}, t) \\ - R(\vec{r} \rightarrow \vec{r} - \vec{s}, dt) n(\vec{r}, t) \end{array} \right] \quad (5.8)$$

Factors of $\delta\mathcal{V}$ have been divided out everywhere. Equation 5.8 is called the *master equation*. It appears very general, but it is based on some strong assumptions that can easily be violated. The most important is that knowing a particle is at \vec{r} is all one needs in order to know the probability it will be at $\vec{r} + \vec{s}$ some time dt later. This need not be true. For example, if the momentum of particles is important, then a collection of particles with momentum \vec{p}_1 will have a different probability distribution for future locations from particles with momentum $\vec{p}_2 \neq \vec{p}_1$. On the other hand, nothing in the derivation requires \vec{r} just to be three position coordinates. The derivation goes through without change when \vec{r} contains many components, including for example momenta as well as positions.

To derive the diffusion equation, observe that $R(\vec{r} + \vec{s} \rightarrow \vec{r}, t)$ should be expected to be a rapidly varying function of s ; the chance of going distance s varies quickly with the distance. However, one should not expect $R(\vec{r} + \vec{s} \rightarrow \vec{r}, t)$ to vary very quickly as a function of \vec{r} : the rate at which particles jump about should not depend very much on where they are. Adopting this assumption, one can insert a Taylor expansion in Eq. (5.8) sending \vec{r} to $\vec{r} - \vec{s}$,

$$\begin{aligned} R(\vec{r} + \delta\vec{r} \rightarrow \vec{r}, dt) n(\vec{r} + \vec{s}, t) &\approx R(\vec{r} \rightarrow \vec{r} - \vec{s}, dt) n(\vec{r}, t) \\ &+ \delta\vec{r} \cdot \frac{\partial}{\partial \vec{r}} R(\vec{r} \rightarrow \vec{r} - \vec{s}, dt) n(\vec{r}, t) \\ &+ \frac{1}{2} \sum_{\alpha\beta} s_\alpha s_\beta \frac{\partial^2}{\partial r_\alpha \partial r_\beta} R(\vec{r} \rightarrow \vec{r} - \vec{s}, dt) n(\vec{r}, t) + \dots \end{aligned} \quad (5.9)$$

Substituting Eq. (5.9) into Eq. (5.8) gives

$$\frac{\partial n}{\partial t} = - \sum_{\alpha} \frac{\partial}{\partial r_{\alpha}} v_{\alpha} n(\vec{r}, t) + \sum_{\alpha\beta} \frac{\partial^2}{\partial r_{\alpha} r_{\beta}} \mathcal{D}_{\alpha\beta} n(\vec{r}, t), \quad (5.10)$$

where, sending $\vec{s} \rightarrow -\vec{s}$ in the integrals,

$$v_{\alpha}(\vec{r}) = \int d\vec{s} s_{\alpha} \frac{R(\vec{r} \rightarrow \vec{r} + \vec{s}, dt)}{dt} \quad (5.11a)$$

$$\mathcal{D}_{\alpha\beta}(\vec{r}) = \int d\vec{s} \frac{1}{2} s_{\alpha} s_{\beta} \frac{R(\vec{r} \rightarrow \vec{r} + \vec{s}, dt)}{dt}. \quad (5.11b)$$

The diffusion equation has now been generalized to include the possibility of a nonzero net flow \vec{v} in a particular direction, and the possibility that the diffusion rate is different in different directions so that \mathcal{D} becomes a tensor.

5.2.4 Connection Between Diffusion and Random Walks

Using Eqs. (5.11), one can connect physical models for how particles move to the diffusion equation. For example, suppose that at time intervals t_0 , particles jump a distance a in a random direction in three dimensions. The mean flow \vec{v} vanishes, because the probabilities of going forward or backward in direction α are equal. Off-diagonal components of \mathcal{D} vanish as well. Since jumping distance a in time t_0 is certain,

$$R(\vec{r} \rightarrow \vec{r} + \vec{s}, t_0) = \frac{\delta(s-a)}{4\pi s^2}. \quad (5.12)$$

The normalization ensures that $\int d\vec{s} R = 1$. Thus

$$\sum_{\alpha} \mathcal{D}_{\alpha\alpha}(\vec{r}) = \int \frac{d\vec{s}}{4\pi s^2} \frac{1}{2} s^2 \frac{\delta(s-a)}{t_0} = \frac{a^2}{2t_0} \quad (5.13)$$

$$\Rightarrow \mathcal{D} = \mathcal{D}_{\alpha\alpha} = \frac{a^2}{6t_0} \quad \text{Since the three components are equal by symmetry} \quad (5.14)$$

Thus a random walk with step length a and time constant t_0 is equivalent to a solution of the diffusion equation with diffusion constant $\mathcal{D} = a^2/6t_0$. This correspondence can be used to find the mean square distance travelled by particles undergoing a random walk. Multiply the diffusion equation (5.6) by r^2 and integrate:

$$\int d\vec{r} r^2 \frac{\partial n}{\partial t} = \mathcal{D} \int d\vec{r} r^2 \frac{1}{r} \frac{\partial^2}{\partial r^2} r n = 6\mathcal{D} \int d\vec{r} r n \quad (5.15)$$

$$\Rightarrow \langle r^2 \rangle = 6\mathcal{D}t = a^2 \frac{t}{t_0} \quad (5.16)$$

Use spherical coordinates for ∂^2/r^2 and assume $n(\vec{r}, t)$ is spherically symmetric. Then integrate twice by parts and use the fact that $\int d\vec{r} n(\vec{r}, t) = 1$.

5.3 Alloys

The importance of metallic alloys is compactly expressed in the fact that eras of human history are named for them. The Bronze Age began around 3000 B.C. in Greece with the discovery that addition of between 10% and 30% of tin to copper produced a metal of greater hardness and lower melting point than either of its components. Bronze was in most respects superior to the alloys of the Iron Age which followed, except that iron was cheaper and easier to mold. The progress of industry in recent centuries has closely been tied to the creation of improved forms of steel, which meant developing ingenious ways to add carbon and other materials in a controlled fashion to iron.

5.3.1 Equilibrium Structures

Consider a pure crystal of some element—say iron—and imagine addition of a very small amount of a second element—say carbon. The second element is always soluble in the first in sufficiently small quantities.

The reason that thermodynamics favors a mixture is a consequence of entropy. Suppose that addition of each atom of the second element to the first incurs an energy penalty $\epsilon > 0$. The number of ways to add M atoms to a lattice of $N \gg M$ sites is

$$\binom{N}{M} = \frac{N!}{M!(N-M)!} \approx \frac{N^M}{M!}, \quad \text{Using the approximation that } N(N-1)\dots(N-M+1) \approx N^M. \quad (5.17)$$

so the entropy associated with the addition of M atoms, in terms of the concentration

$$c = M/N, \quad (5.18)$$

is

$$k_B \ln(N^M/M!) \approx -k_B N(c \ln c - c). \quad \text{The entropy is Boltzmann's constant } k_B \text{ times the log of the number of ways to achieve some macroscopic state; also use } M! \approx M^M e^{-M}. \quad (5.19)$$

Therefore, the free energy \mathcal{F} of the mixture is

$$\mathcal{F} = \mathcal{E} - TS = N[c\epsilon + k_B T c \ln c - k_B T c], \quad (5.20)$$

which has a minimal value for concentration

$$c \sim e^{-\epsilon/k_B T}. \quad \text{Just differentiate Eq. (5.20) by } c, \text{ set to zero, and solve for } c. \quad (5.21)$$

This tendency toward solubility of one element in another that declines exponentially with decreasing temperature is illustrated in Figures 5.2 and 5.3(B).

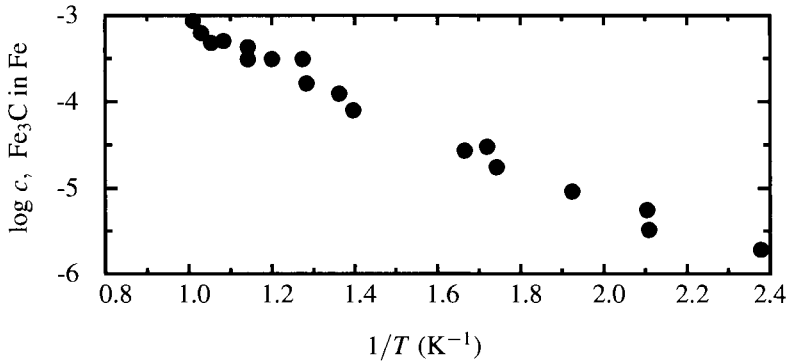


Figure 5.2. The solubility of Fe_3C in Fe drops exponentially, as predicted by Eq. (5.21). [Source: Flynn (1972), p. 38.]

Zone Refining. An immediate consequence of Eq. (5.21) and diagrams such as Figure 5.3 is that the solid elements will not naturally be found in completely pure form, but tend to contain impurities at the level of around 1%. This tendency is particularly unfortunate in the case of the semiconductors intended for use as electronic materials, because certain types of electrically active impurities impair device operation if they are present at levels over one part in 10^{12} . The same physical principle that tends to introduce impurities into solids can also however be used to remove them, motivated by the observation that as temperature increases, the solubility of an impurity in a host increases. *Zone refining* uses this idea by taking an impure crystal and heating it, starting at one end, and slowly moving the front of the heated region toward the other end. Because impurities are much more soluble in the hot material than in the cold, they migrate toward the hotter end. When the process is completed, one end of the crystal has a much higher concentration of impurities than the other. The portion highest in impurities is discarded, and then the process is repeated. With successive passes, the impurities can be filtered away.

5.3.2 Phase Diagrams

The material produced by addition of a slight amount of one substance into another is called a *primary alloy*, since the first material is essentially unchanged by addition of the second. The primary alloys come in two basic types. In a *substitutional alloy*, one atom displaces the other and lives on its lattice sites. Zinc mixed into copper provides an example of an alloy of this type. Alternatively, the additional atoms may choose to sit within empty spaces of the lattice, creating an *interstitial alloy*; the atom sitting within interstices must be small and is usually hydrogen, boron, carbon, or nitrogen.

A *phase diagram* describes the equilibrium state of a mixture of elements, as a function of temperature and relative concentrations. The simplest two-component diagrams belong to a few pairs of elements, including AuAg, AuPd, NiMn, CuPt,

and CuNi. All of these elements share an fcc structure in the ground state, members of the pair have very similar lattice constants (see Table 2.1), and the two metals mix substitutionally into each other in any concentration. The Au–Cu phase diagram provides an example in Figure 5.3(A). Such unlimited solubility is, however, quite rare, and even elements with the same crystal structure and similar lattice constants typically pass through an elaborate sequence of structures. For example, Ag and Al share the fcc structure and have lattice constants differing only by 1%, yet Ag is soluble in Al up to only 0.2% at 200 °C.

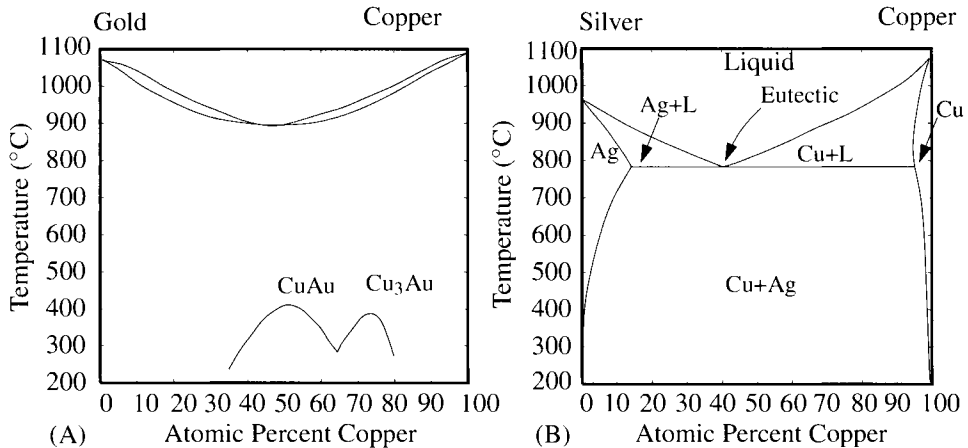


Figure 5.3. (A) Phase diagram of copper and gold, which form a perfect substitutional alloy but have a number of superlattice structures at intermediate temperatures. (B) Phase diagram of copper and silver, which have limited solubility and form a eutectic. [After Hansen (1958).]

In general, beyond a critical concentration that depends upon temperature, the atoms of alloys begin to array themselves into an immense variety of structures. The term *intermetallic compound* applies whenever two metals form a definite crystal structure at some definite concentration. The crystals listed in Tables 2.2, 2.4, 2.5, 2.6, and 2.7 provide many examples. When the concentrations of elements vary continuously between values at which intermetallic compounds form, they form *secondary alloys*, which can be thought of as intermetallic compounds with excess or deficit of some elements. In addition, there are two general types of ordering that can occur. If unlike atoms find it favorable to be near one another, they may choose to form *superlattices*, particularly near favorable concentrations. If, on the other hand, unlike atoms find each others' company energetically unsatisfactory, there will be a tendency toward *phase separation*.

5.3.3 Superlattices

The phase diagram of Figure 5.3(A) shows that gold mixes substitutionally into a primary alloy of copper at all concentrations. The arrangement of the gold with respect to the copper is not, however, always random. At temperatures be-

low 400 °C, X-ray diffraction off copper–gold mixtures, with three parts copper to one part gold, shows a new set of diffraction peaks not present above 400 °C. Furthermore, the strength of these peaks depends upon the way the mixture is prepared. Bragg and Williams (1934) report that lowering of temperature from above 400 °C to 270 °C in a few seconds gives peaks no different from those present above 400 °C—the mixture has been *quenched*. By cooling the solid solution instead over a period of several days—*annealing* it—new peaks form. Following the methods of Chapter 3, the locations of the new peaks can be used to show that the copper and gold have formed a crystalline compound in which gold and copper are arrayed as shown in Figure 5.4, called a *superlattice*. Many other combinations of metals produce similar superlattices, usually when mixed in ratios of 1:1 or 3:1.

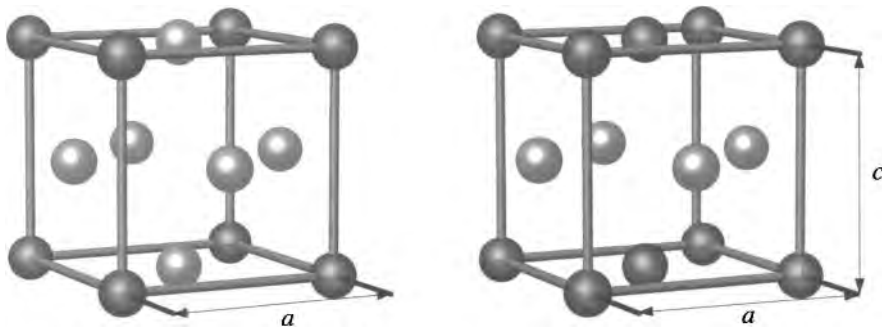


Figure 5.4. (A) A 3:1 mixture of copper and gold has the equilibrium superlattice structure depicted here below a temperature of 400 °C. (B) Superlattice of copper and gold in equal mixtures. The lattice constant c is 7% smaller than a .

The structures of superlattices are no less varied than the structures of intermetallic compounds, and all the crystal structures of Chapter 2 are possible. There is no distinction in principle between intermetallic compounds and superlattices, except that the latter lose their order at a definite transition temperature well below the melting point of the crystal. Among elements mixed in 3:1 ratios, the structure displayed in Figure 5.4(A) is common, while for elements mixed in proportion of 1:1, the CsCl structure (Figure 2.8) frequently occurs, as in the cases of Cu–Zn (β -brass), CuBe, CuPd, AgMg, AgZn, AgCd, AuNi, NiAl, and FeCo. Phase transformations in superlattices are studied in more detail in Section 24.5.1.

Many other structures are, however, possible. Mixed in a ratio of 1:1, copper and gold form a superlattice involving alternating planes of copper and gold atoms, as shown in Figure 5.4(B). When the atoms arrange themselves in this way, the whole lattice contracts by 7% along the c axis, so the symmetry of the crystal changes from cubic to tetragonal. Such macroscopic changes in the shape of the crystal are another frequent feature of superlattices.

5.3.4 Phase Separation

Iron carbide, Fe_3C , is a stable compound. Suppose that only 3 atomic percent of carbon is mixed in with iron. The 3 carbon atoms out of 100 can combine with 9

iron atoms to form 12 atoms' worth of Fe_3C , leaving 88% iron. This process requires the physical separation of the proper mixture of carbon and iron from the rest of the soup, a rearrangement that cannot always occur quickly or spontaneously.

Because phase separation is based upon principles of thermodynamics much more general than their application in alloy systems, a slightly abstract view is appropriate.

Suppose one has any two substances, whose free energy when they are mixed homogeneously among one another has the form shown in Figure 5.5 as a function of their relative concentration. The shape shown in the figure is all the information one needs to conclude that a system prepared with concentration between c_a and c_b will attempt to phase separate in order to minimize its free energy.

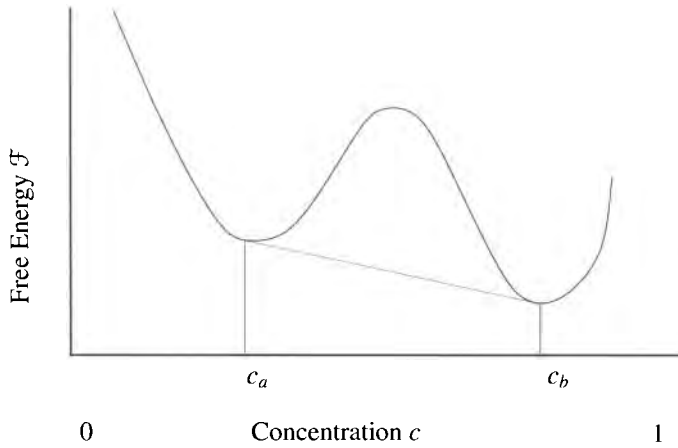


Figure 5.5. When the free energy of a homogeneous mixture of two substances has the form shown in this diagram, whenever the overall concentration lies between c_a and c_b , the system will phase separate into components with those two concentrations.

Phase separation lowers the free energy of a system in the following way. Suppose that the curve displayed in Figure 5.5 is $\mathcal{F}(c)$. If the atoms were to separate into two different domains of concentrations $c_a < c$ and $c_b > c$ (not yet necessarily the concentrations indicated in the figure), the free energy would instead be

$$\mathcal{F}_{\text{ps}} = f\mathcal{F}(c_a) + (1 - f)\mathcal{F}(c_b), \quad (5.22)$$

where f is the fraction of the sample at concentration c_a , and $1 - f$ is the fraction at concentration c_b . The fraction f is not arbitrary, because the overall concentration of the mix must be c , and therefore

$$c = fc_a + (1 - f)c_b \Rightarrow f = \frac{c - c_b}{c_a - c_b} \quad (5.23)$$

$$\Rightarrow \mathcal{F}_{\text{ps}} = \frac{c - c_b}{c_a - c_b} \mathcal{F}(c_a) + \frac{c_a - c}{c_a - c_b} \mathcal{F}(c_b). \quad (5.24)$$

The geometrical interpretation of Eq. (5.24) is that one picks any two points one wishes on the curve $\mathcal{F}(c)$ and draws a straight line connecting them; the straight

line describes free energy of phase separation between those two points. The points c_a and c_b in Figure 5.5 have been chosen so that this construction resulted in the lowest possible free energy.

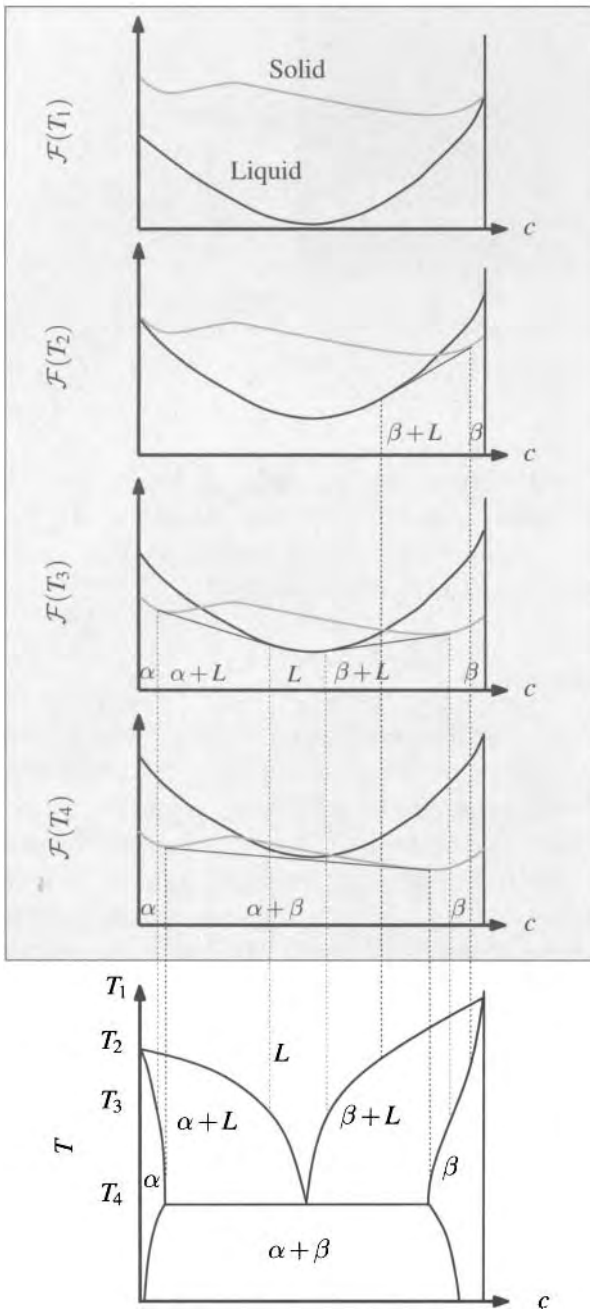
A typical phase diagram is largely occupied with regions of phase separation. Consider the diagram in Figure 5.3(B) for copper and silver. Regions Ag and Cu are primary phases of fcc metal with substitutional impurities. The region marked “Liquid” is also a homogeneous mixture. Everywhere else, the two metals phase separate. The solid lines then indicate the concentrations c_a and c_b as a function of temperature. For example, at 700 °C, separation occurs between the two concentrations that have been marked. In the region denoted “Ag+liquid” a primary alloy of silver coexists with a liquid containing a greater percentage of copper. The line describing the composition of the liquid is called the *liquidus*, while the line determining the composition of the solid is the *solidus*. The point marked “*Eutectic*” has technological significance, since it provides the lowest possible temperature at which the two metals mix in the molten state. As soon as the two metals are cooled below the eutectic temperature, however, they begin to phase separate, so if the goal is a homogeneous material there is a race against time.

Binary phase diagrams have a number of characteristic shapes that appear bizarre at first glance, but which have a rather natural explanation in terms of simple assumptions concerning the free energies of solid and liquid phases. The idea is best illustrated geometrically and is shown in Figure 5.6.

5.3.5 Nonequilibrium Structures in Alloys

A material composed of large numbers of small crystalline regions of different orientations is said to be built out of *grains*, and the interfaces between them are *grain boundaries*. These boundaries may appear on scales ranging from tens of nanometers to meters. When the crystallites are at the small end of the scale, one calls the material *microcrystalline*. Frequently in metals, the crystalline regions are on the micron scale, and the materials are called *polycrystalline*. In sea ice, grains may grow to scales of meters. The orientations of adjoining crystalline regions are fairly random, and if one takes a two-dimensional slice through such a solid, the grain boundaries form a characteristic network, with the grain boundaries meeting in vertices, as shown in Figure 5.7. The manner in which grains grow is the subject of Problem 6.

A type of grain boundary that occurs in substitutional alloys is the *antiphase boundary*, which is a grain boundary where the orientations of the crystals on the two sides are the same, but there is a shift of phase in the lattice as one crosses the boundary. Antiphase boundaries can form snaking labyrinthine structures of great complexity [Figure 5.8(A)]. As the concentration of one element in another increases, one tends to get crystals dominated by one element embedded in crystals dominated by the other element. For example, one can have small crystals of Ni₃Al sitting in a background of nearly pure Al. The forms that these intermixed crystals can take depend upon the dynamical processes by which they form. In the simplest



At sufficiently high temperatures, the liquid phase is of lower free energy at all concentrations c than the solid.

At this temperature, the liquid L is lower in energy to the left, but coexists with solid of type β towards the right, and β is stable for sufficiently high concentrations.

Now solid of type α is stable for low values of c , β is stable for high values, liquid is stable for a small range in the middle, and there are two coexistence regions.

Only solid phases are stable. These can be pure α , pure β , or mixtures $\alpha + \beta$ of the two.

Figure 5.6. Schematic free energies of liquid and solid which would lead to typical binary phase diagram with a eutectic. The upper panels show solid and liquid free energies at various temperatures, while the lowest panel shows the resulting phase diagram. In this schematic view, the effect of temperature is simply a vertical shift in the relative free energies of solid and liquid phases. In reality, the shapes of the free energy curves would change with temperature as well. Unless the solid at temperature T_1 is metastable, there will be no operational way to determine the solid free energy curve at that temperature.

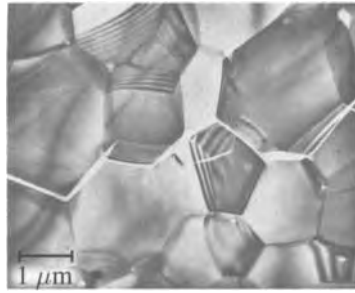


Figure 5.7. Transmission electron micrograph of the grain structure of alumina. Grains are approximately $1\ \mu\text{m}$ across. [Source: B. Hockey, National Institutes of Science and Technology.]

case, one has spheres of one type sitting in a background of the other type. The spheres can be replaced by rods or plates, or can be sufficiently dense that they form an interconnected network. The structures can include treelike *dendritic* shapes [Figure 5.8(B)], arrays of parallel fingers, and bands or stripes.

5.3.6 Dynamics of Phase Separation

Any alloys heated sufficiently form a homogeneous liquid mixture. Upon cooling, the mixture will typically remain homogeneous for a time, even if a phase separated state is ultimately of lower free energy. In some cases, the initial process of breaking apart into spatially separated regions of different phases happens easily, because the homogeneous state is unstable, and the result is called *spinodal decomposition*. It can also happen that the cooled homogeneous state is stable against small fluctuations, and only large rare fluctuations can disturb the situation. The appearance of new domains by such fluctuations is called *nucleation*, and is reviewed by Wu (1997) and Kelton (1991). As shown in Figure 5.8, phase separation during the cooling of solid solutions can produce exceedingly complicated spatial patterns. The patterns have an intrinsic aesthetic appeal, although from a technological point of view they are usually undesirable, and one reason to understand the physics underlying them is to prevent them from occurring.

The basic equation underlying the dynamics of phase separation is simply the law of diffusion, presented in Section 5.2.2. The change in concentration with time following from Eq. (5.1) is

$$\frac{\partial c}{\partial t} = \mathcal{D} \nabla^2 c \quad \begin{array}{l} \text{The concentration } c \text{ is often taken to be a linear func-} \\ \text{tion of actual atomic concentrations; for example, when} \\ \text{phase separating between } c_a \text{ and } c_b, \text{ one might take } c \rightarrow \\ (c - c_a)/(c_b - c_a). \end{array} \quad (5.25)$$

The diffusion equation, (5.25), appears innocent, but, when coupled with appropriate boundary conditions, it is capable of producing the sort of complexity that appears in Figure 5.8. As an illustration of how it functions, consider the problem of a spherical droplet of carbide, carbon concentration c_a , growing in a background

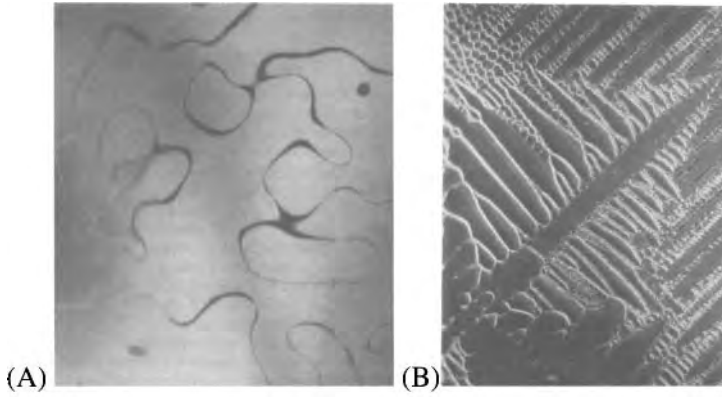


Figure 5.8. (A) Antiphase boundaries in $\text{Fe}_{76}\text{Al}_{23}$. The boundaries mark the dividing line between two chemically identical regions, but where the placement of atoms is out of synchrony. [Source: Allen and Cahn (1979), p. 1093.] (B) Dendrite formed during solidification of stainless steel ($\text{Fe}_{70}\text{Ni}_{15}\text{Cr}_{15}$). (Courtesy of L. A. Boatner, J. Gardner, and D. Corrigan, Oak Ridge National Laboratory.)

mixture of iron and carbon whose overall carbon concentration is $c_\infty > c_a$. Carbon atoms flow toward the droplet, because phase separation is thermodynamically favorable. The simplest calculations employ the *quasi-static approximation*. This approximation requires the time it takes for carbon atoms actually to join the drop and make it grow to be long compared to the time for the concentration of carbon outside the drop to converge to a steady state. In this case, the time variation of $c(r, t)$ can be neglected, and Eq. (5.25) becomes Laplace's equation

$$\nabla^2 c(r) = 0, \quad \text{Place the origin of a system of polar coordinates at the center of the droplet.} \quad (5.26)$$

with boundary conditions

$$c(R) = c_a \text{ and } \lim_{r \rightarrow \infty} c(r) = c_\infty. \quad (5.27)$$

The unique solution of Eq. (5.26) satisfying (5.27) is

$$c(r) = c_\infty + \frac{R}{r}(c_a - c_\infty) \quad (5.28)$$

and from Eq. (5.1) the flux of material into the drop is

$$4\pi R^2 \mathcal{D} \frac{c_\infty - c_a}{R}. \quad \text{Take the gradient of Eq. (5.28) at } R = r, \text{ and multiply by the surface area of the drop.} \quad (5.29)$$

Suppose that for each unit of concentration entering the drop, the volume of the drop changes by v . Then the drop changes in size according to

$$\frac{d}{dt} \frac{4\pi}{3} R^3 = v 4\pi R \mathcal{D} (c_\infty - c_a) \quad (5.30)$$

$$\Rightarrow \dot{R} = \frac{v \mathcal{D}}{R} (c_\infty - c_a) \quad (5.31)$$

$$\Rightarrow R \propto \sqrt{2v \mathcal{D} (c_\infty - c_a) t}. \quad (5.32)$$

The radius of the drop grows as the square root of time. This calculation oversimplifies even the problem of growing drops. It neglects the fact that the surface of each drop exerts a pressure on the material inside, like the skin of a balloon, that causes very small drops to shrink rather than grow. It neglects the fact that after many drops have grown, the background concentration c_∞ of carbon must diminish. Taking these effects into account, Lifshitz and Slyozov (1961) showed that the average size of drops increases as the cube root of time, not the square root.

The reason that Eq. (5.25) is able to exhibit complicated behavior is that the shape of the region where the equation applies is being made to depend upon the concentration field; the coupled motion of the boundaries and concentration field is a complicated nonlinear problem. Further discussion of such pattern-forming problems is provided by Langer (1980).

5.4 Simulations

As the power of computation increases, it is gradually becoming possible to imagine computing the evolution of structures such as shown in Figure 5.8, either from partial differential equations or by starting down at the atomic level. Two important methods for atomic scale calculation are *Monte Carlo* and *molecular dynamics*. They are very similar in conception. Each method treats atoms as classical interacting particles, and each watches them evolve in a fashion meant to mimic the actual evolution they might display in nature. The methods differ only in the detailed manner that they employ to move atoms about.

5.4.1 Monte Carlo

The Monte Carlo method shuffles atoms about randomly, like the cards in the casinos from which it takes its name. The idea behind the method is that if a solid is at some temperature T , then the probability of its atoms adopting a position so that their energy is \mathcal{E} is $\exp[-\beta\mathcal{E}]$, where $\beta = 1/k_B T$. As a corollary, it follows that if one has any two states of the system whose energy differs by $\delta\mathcal{E}$, then the relative probability that these two states be occupied is $\exp[-\beta\delta\mathcal{E}]$.

So suppose one has a collection of N atoms at $\vec{r}_1 \dots \vec{r}_N$, and an energy function $\mathcal{E}(\vec{r}_1 \dots \vec{r}_N)$. What exactly this energy functional might be is discussed further in Section 11.8. In brief, the Monte Carlo method chooses an atom randomly from this collection, and randomly moves it a small distance. If the result of this small move is to lower the energy of the system, the move is always accepted. If the move raises the energy of the system by an amount $\delta\mathcal{E}$, then the move is accepted with probability $\exp[-\beta\delta\mathcal{E}]$.

Suppose one wants to compute the average value in thermal equilibrium of any function $g(\vec{r}_1 \dots \vec{r}_N)$ of particle positions. The function g could be the energy, or anything else. The Monte Carlo method proceeds as follows:

1. Begin with a collection of particles whose locations are known and whose energy $\mathcal{E}(\vec{r}_1 \dots \vec{r}_N) \equiv \mathcal{E}_1$ has been computed. Compute $g(\vec{r}_1 \dots \vec{r}_N)$ and store the result in a variable G .
2. Choose one of these particles at random. Call the particle chosen particle l .
3. Create a random displacement vector. One way to do this is to choose three random numbers $p_1 \dots p_3$ lying in $[0, 1]$ and to form the vector

$$\vec{\Xi} = 2a(p_1 - 1/2, p_2 - 1/2, p_3 - 1/2), \quad (5.33)$$

with a setting the length scale. A natural choice of a is a typical interparticle spacing, although final results should not depend upon the choice of a .

4. Compute the energy difference,

$$\delta\mathcal{E} = \mathcal{E}(\vec{r}_1 \dots \vec{r}_l + \vec{\Xi} \dots \vec{r}_N) - \mathcal{E}_1. \quad (5.34)$$

When particles interact only with near neighbors, it will always be possible to compute this change in energy more efficiently than by computing the energy from scratch for all particles in the system.

5. Check whether $\delta\mathcal{E}$ is positive or negative. If $\delta\mathcal{E}$ is negative, replace \vec{r}_l by $\vec{r}_l + \vec{\Xi}$ and return to step 1. In either case, add the new value of $g(\vec{r}_1 \dots \vec{r}_N)$ to G .
6. However, if $\delta\mathcal{E}$ is positive decide randomly whether to allow particle i to move or not. Pick a new random number $p \in [0, 1]$, and compare p to $\exp[-\beta\delta\mathcal{E}]$. If p is greater than this Boltzmann factor, then leave \vec{r}_l where it is and return to step 1. However, if p is less, set \vec{r}_l to $\vec{r}_l + \vec{\Xi}$ before returning to step 1, despite the fact that this move raises the energy of the system. Once again, add the new value of $g(\vec{r}_1 \dots \vec{r}_N)$ to G .

At the very end, after M steps of the process, an estimate of the thermal average of $g(\vec{r}_1 \dots \vec{r}_N)$ is given by taking the variable G that accumulated the sum of g and computing

$$\bar{g} = \frac{G}{M}. \quad (5.35)$$

At low temperatures, almost the only moves accepted are those which lower the energy of the system. At very high temperatures, almost every move is accepted. The probability of accepting a move with positive $\delta\mathcal{E}$ has been arranged in just such a way that the probability of occupying states differing by $\delta\mathcal{E}$ is $\exp[-\beta\delta\mathcal{E}]$. This fact is easiest to understand by considering a system with just one particle, and which can occupy just two states, but is true generally.

5.4.2 Molecular Dynamics

Molecular dynamics makes use of Newton's laws and random forces, rather than random hops, in order to emulate thermal equilibrium. One form of molecular dynamics operates by computing

$$\vec{F}_l = -\frac{\partial \mathcal{E}}{\partial \vec{r}_l}, \quad (5.36)$$

the force on every particle due to every other particle, and then has the particles move according to

$$m_l \frac{d^2 \vec{r}_l}{dt^2} = \vec{F}_l, \quad m_l \text{ is the mass of particle } l. \quad (5.37)$$

Practitioners usually want to use the largest number of particles that can possibly fit on their computers, and they also want to obtain reasonable accuracy while minimizing intermediate storage. For this reason, an algorithm due to Verlet (1967) is widely employed; a variety of other algorithms is described by Rapaport (1995). Pick a time step dt that is much smaller than any time scale on which forces would cause particles to move appreciably. Let the position of particle l after n steps of the algorithm be \vec{r}_l^n . In order to find positions at the $n+1$ 'st step, compute

$$\vec{r}_l^{n+1} = 2\vec{r}_l^n - \vec{r}_l^{n-1} + \frac{\vec{F}_l^n}{m_l} dt^2 \quad (5.38)$$

with

$$\vec{F}_l^n = \vec{F}_l(\vec{r}_1^n, \vec{r}_2^n, \dots, \vec{r}_N^n) \quad (5.39)$$

This sequence of computations requires only the storage needed to hold \vec{r}_l^n and \vec{r}_l^{n-1} , but makes errors only at order $(dt)^4$ after each time step, as shown in Problem 2.

Nothing more than Newton's laws is required in order to carry out computer simulations of a physical system at temperature T . However, it is not easy to know what the temperature of the system will be before the simulation begins, because while the total energy \mathcal{E} is easily specified in initial conditions, the temperature would have to be found later—for example, from the root mean square velocity of particles. The *fluctuation dissipation theorem* may be used to modify the method so as to specify temperature directly. According to this theorem, interacting particles head toward equilibrium at temperature T when two terms are added to their equation of motion, one a damping term, and the other a random force, giving the *Langevin equation*

$$\ddot{\vec{r}}_l = \frac{\vec{F}_l}{m_l} - b\dot{\vec{r}}_l + \vec{\xi}(t) \quad (5.40)$$

The damping constant b is somewhat arbitrary. The smaller it is, the more closely particles follow Hamiltonian mechanics, while the larger it is, the more quickly they come into thermal equilibrium. Details of a particular physical problem are needed to fix b .

with

$$\langle \xi_\alpha(0) \xi_\beta(t) \rangle = \frac{2bk_B T \delta_{\alpha\beta} \delta(t)}{m_l} \quad \begin{array}{l} \text{The brackets refer either to a time average, or to an} \\ \text{average over statistical realizations of the system.} \\ \text{See Landau and Lifshitz (1980) p. 362 or Problem} \\ \text{10} \end{array} \quad (5.41)$$

A practical implementation of this idea replaces \vec{F}^n in Eq. (5.38) with \vec{G}^n where

$$\vec{G}_l^n = \vec{F}_l^n - bm_l \frac{[\vec{r}_l^n - \vec{r}_l^{n-1}]}{dt} + \vec{\Xi}_l \sqrt{6bm_l k_B T / dt}; \quad (5.42)$$

$\vec{\Xi}_l$ is a vector whose components lie randomly between -1 and 1 , and it can be computed from

$$\vec{\Xi} = 2(p_1 - 1/2, p_2 - 1/2, p_3 - 1/2) \quad \text{Each } p_\alpha \text{ is a random number between 0 and 1.} \quad (5.43)$$

Because molecular dynamics keeps track of both positions and momenta, it is computationally more costly than Monte Carlo, and Monte Carlo is preferable if one only wants to find thermodynamic averages for a system in equilibrium, because it runs faster. However, molecular dynamics paints a more realistic picture of the dynamical fashion in which a system approaches equilibrium. Representative results from molecular dynamics calculations appear in Figures 5.9 and 5.14.

5.5 Liquids

5.5.1 Order Parameters and Long- and Short-Range Order

Every element melts at some temperature, at which point crystalline order disappears. The presence and absence of order is captured by an *order parameter*, which is a function designed to (a) vanish when the desired form of order is absent, and (b) rise up from zero as soon as it is present. Order parameters are often single numbers, although they may also be tensors. The sharp Bragg peaks that characterize scattering from crystalline lattices can be used as crystalline order parameters.

Formally, to create an order parameter $\mathcal{O}_{\vec{K}}$ distinguishing between crystal and liquid, choose any reciprocal lattice vector $\vec{K} \neq 0$ of the crystal, look back to the correlation functions defined in Section 3.5 and define

$$\mathcal{O}_{\vec{K}} = \frac{\mathcal{V}}{N^2} n_2(\vec{q} = \vec{K}, 0). \quad \text{Where } n_2(\vec{q}, t) \text{ was defined in Eq. (3.54).} \quad (5.44)$$

For a crystal where N^2 terms contribute to the sum in Eq. (3.54), this quantity should be of order unity. In a liquid where crystalline order has been lost, it will instead be of order $1/N$.

Radial Correlation Functions.

Comparisons of solids and liquids are often made by additionally averaging the correlation function $n_2(\vec{r}_1, \vec{r}_2; 0)$ defined in Eq. (3.49) over all angular orientations

of the sample and making the result dimensionless by dividing through by the square of the density $n = N/V$. The result is the *radial correlation function*

$$g(r) \equiv \frac{\langle n_2(\vec{r}_1, \vec{r}_2; 0) \rangle_\theta}{n^2} - \frac{\delta(\vec{r}_1 - \vec{r}_2)}{n}. \quad (5.45)$$

Here $r = |\vec{r}_1 - \vec{r}_2|$. The angular braces mean one must average over all angular orientations of the sample. Subtracting off the second term is conventional.

Liquids and glasses are isotropic by nature, while polycrystalline and powdered crystalline samples have been made isotropic as described in Section 3.3.3. For scattering off such materials the structure factor in Eq. (3.52) can be rewritten as

$$S(\vec{q}) = 1 + n \int d\vec{r} g(r) e^{i\vec{q}\cdot\vec{r}} \quad (5.46)$$

Using Eq. (5.45) and the static structure factor of Eqs. (3.55) and (3.54).

$$= 1 + n \int d\vec{r} (g(r) - 1) e^{i\vec{q}\cdot\vec{r}} + n \int d\vec{r} e^{i\vec{q}\cdot\vec{r}} \quad (5.47)$$

Since $g(r) \rightarrow 1$ for large r the integral only converges well after subtracting 1.

$$\approx 1 + n \int d\vec{r} e^{i\vec{q}\cdot\vec{r}} (g(r) - 1). \quad (5.48)$$

The last term on the right hand side of (5.47) is a delta function that only rises above zero when one is staring directly into the scattering beam, and which one therefore can drop.

An integral of the area under the first peak,

$$z = n \int_0^{\text{first peak}} dr 4\pi r^2 g(r), \quad (5.49)$$

gives the average number of nearest neighbors of each atom, known as the *coordination number*. This quantity is slightly ambiguous to the extent that the precise ending point of the first peak is ambiguous.

Figure 5.9 provides typical examples of correlation functions for crystals and liquids taken from experiment and from computer simulation. The defining property of crystals is long-range order (Section 3.5.1), yet the long-range order found for crystals in these examples is not so very long: only around 10 Å. Nevertheless order over these distances is easily sufficient to distinguish the liquids and crystals from each other.

Figure 5.10 displays the static structure factors $S(q)$ for liquid and amorphous nickel. The radial correlation function $g(r)$ can be obtained by inverting the Fourier transform in Eq. (5.48). Differences between static structure functions of liquids and amorphous solids are quite subtle.

5.5.2 Packing Spheres

One of the oldest questions in condensed matter physics goes back to a conjecture of Kepler that the most efficient way to fill space with spheres is to stack them in an fcc or hcp lattice (Figure 2.2 (D)). If one examines any given sphere in the close packed state it has 12 neighbors, but these neighbors are not distributed about it

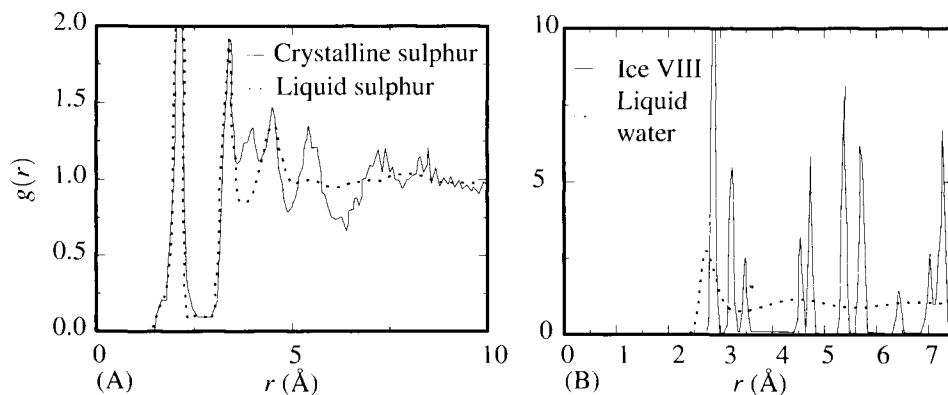


Figure 5.9. (A) Radial correlation function $g(r)$ for liquid and crystalline sulphur obtained from neutron scattering. For nearest neighbors, the correlations in liquid and crystalline sulphur are very similar. [Source: Winter et al. (1990) p. SA218.]. (B) Radial oxygen-oxygen correlation function $g(r)$ for liquid and crystalline water obtained from molecular dynamics simulations. The crystalline water is in the form of Ice VIII at 10 K and pressure of 2.4 GPa. [Source: Vega et al. (2005), pp. 1453 and 1455].

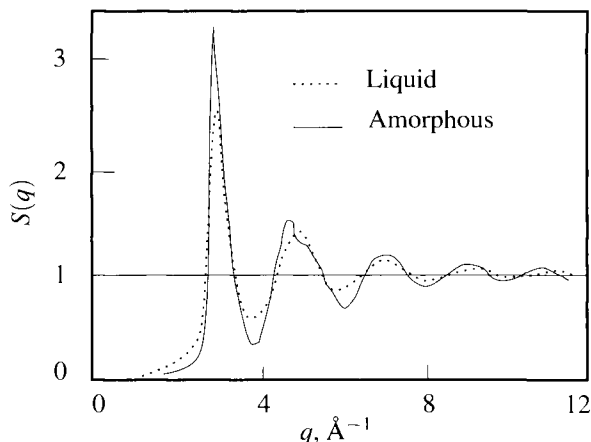


Figure 5.10. Static structure factors $S(q)$ for liquid and amorphous nickel. The difference between the liquid and amorphous states appears in subtle changes in the shape of the second peak. [Source: Waseda (1980), p. 91.]

perfectly symmetrically. Problem 6 in Chapter 2 shows that such collection of hard spheres fills 74% of space. Kepler's conjecture was proved after a slight delay of several centuries by Hales (1997, 2005).

Spheres can also be mixed together randomly, in which case they provide a model of a solid called *dense random packing* or the *Bernal model*. Bernal (1959) carried out experiments with ball bearings and showed that randomly mixed hard spheres fill about 64% of space. They do not instantly and automatically find their way into the closely packed fcc or hcp structures. Furthermore, there seems to be no way to fill space with hard spheres in a uniform way at densities between

74% and 64%. Ensembles of hard spheres provide attractive settings for carrying out computer simulations. The pair distribution function for hard spheres in two dimensions is shown in Figure 5.11. While there is no element that precisely reproduces the three-dimensional hard-sphere distribution function, it is not too far from that for liquid argon. In addition, properties of randomly packed spheres provide a starting point for studies of granular materials like sand [Liu and Nagel (2001); de Gennes (1999); Kadanoff (1999); Jaeger et al. (1996)].

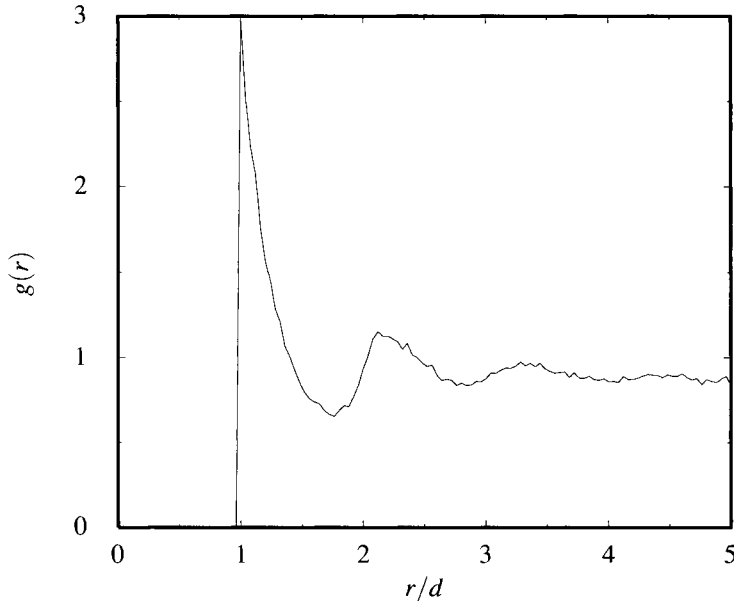


Figure 5.11. The radial distribution function $g(r)$ for hard spheres (disks) of radius d in two dimensions. The energy of a system of hard spheres is defined to be zero if the spheres are not overlapping, and infinite if any two touch. Temperature is therefore irrelevant for this system, and its correlation function depends only upon density, which in this case is chosen to be 0.5.

5.6 Glasses

Just as ball bearings form a static random state when mixed together, so do many collections of atoms. Solids where atomic positions are largely random are called *amorphous materials* or *glasses*. Glasses are distinct from liquids. In liquids, the atoms are constantly moving about and exchanging places, while in glasses they are mainly locked into place. There is not complete agreement on how precisely to define what a glass is, nor which elements are capable of forming glasses. No elements or mixtures are known for which the ground state is glassy; glasses are produced by rapid cooling as indicated in Figure 5.12. On the other hand, with sufficiently rapid cooling, it may be that any collection of atoms forms a glass; a great variety of metals can form glasses, as discussed by Cargill (1975) or Gilman (1975), and so can water, as shown by Debenedetti and Stanley (2003).

To make a glass, start from a liquid and lower the temperature quickly. Below the melting temperature T_M , thermodynamic equilibrium requires atoms to arrange themselves into a crystal. For fast enough cooling rates, which for window glass are around 10 K s^{-1} , and for nickel are 10^7 K s^{-1} , glass forms instead. Density of the liquid increases slowly, but viscosity η increases dramatically, up to a value of around 10^{12} Pa s , obeying the empirical formula, known as the *Vogel–Fulcher law*

$$\eta \propto \exp [C/(T - T_0)] . \quad C \text{ is a constant} \quad (5.50)$$

There is now a variety of theories, discussed by Angell (1988), which can calculate a divergence similar in shape to that of Eq. (5.50). Gradually, the material changes its mechanical nature from a viscous liquid to a (frequently) brittle elastic solid. The first peak in the correlation function $g(r)$ narrows, indicating an increase in short-range order, and the second peak then splits, as shown for amorphous nickel in Figure 5.10.

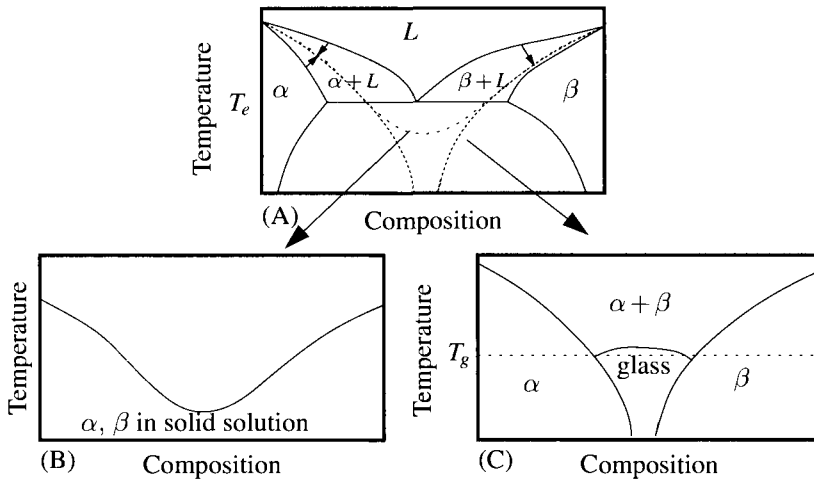


Figure 5.12. (A) Schematic equilibrium phase diagram for a two-phase system with a eutectic. Below the temperature T_e , the alloy phase separates into α - and β -rich regions. If the system is cooled sufficiently rapidly from the liquid phase, then the boundaries of the solid–liquid coexistence region apparently collapse together, and metastable phases appear. In case (B), phases α and β have similar crystal structures, and rapid cooling produces a continuous solid solution. In case (C), the crystal structures of α and β are incompatible, and rapid cooling in the central region produces a glass. Single-component glasses fit roughly within this framework if one component is taken to be vacuum. [After Perepezko and Wilde (1998), p. 1074.]

In addition to these incremental changes, there is a deceptively definite temperature at which the specific heat and thermal expansion coefficient change abruptly, by a factor of around 2, known as the *glass transition temperature* and indicated in Figure 5.12 by T_G . The glass transition is difficult to define precisely, and many features of the problem remain controversial, as discussed by Cusack (1987) or Yonezawa (1991). The precise location of the transition is crucially dependent upon the amount of time one is willing to spend looking for it.

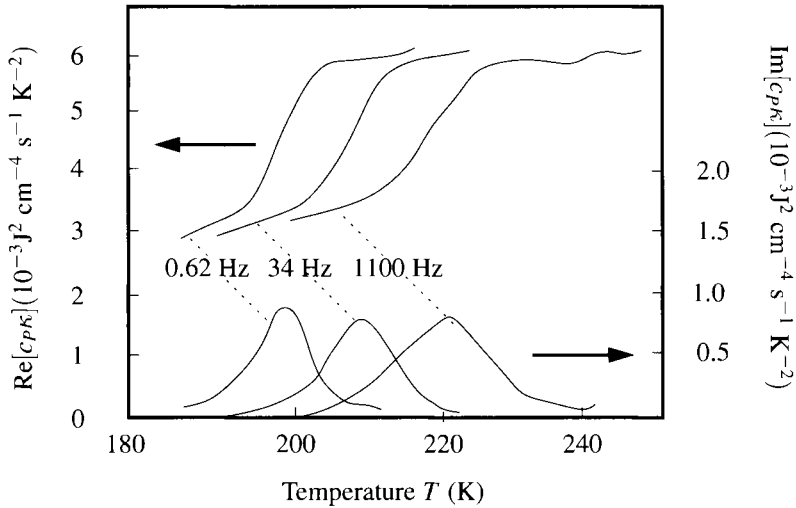


Figure 5.13. Specific heat c_p times thermal conductivity κ for the glassy liquid glycerol as a function of temperature, at three different frequencies. The thermal conductivity does not vary rapidly, so the experiment basically measures c_p . The top portion of the figure shows the real part of $c_p\kappa$, while the bottom portion shows the degree to which the phase of the heat oscillations being injected differs from the phase of the temperature oscillations being measured. Note that there is always a transition in the specific heat, but that the transition temperature increases roughly as the logarithm of the frequency ν , meaning that one can move the transition temperature down by waiting exponentially longer. [Source: Birge and Nagel (1985), p. 2675.]

An experiment demonstrating this effect particularly well has been carried out by Birge and Nagel (1985), illustrated in Figure 5.13. A heat source whose heat output oscillates in time is placed within a glass, and the temperature variation in the glass is measured, as a function of the mean temperature and as a function of the frequency of oscillation ν . For temperature oscillations above a certain frequency, the specific heat is low, because many degrees of freedom are unable to respond quickly enough to contribute to the specific heat. The specific heat rises rapidly as the frequency falls, because more modes are able to follow along. The particular frequency at which the changeover occurs is an exponentially rapidly varying function of temperature. The picture suggested by this and other experiments is that if one observes some dramatic change in the behavior of glass as a function of temperature, it is due to the time scale for some process in the glass passing rapidly across a threshold of patience. Still, there remains the question in principle of whether there really is a transition temperature T_0 , as in Eq. (5.50), at which viscosity diverges, and a glass reaches some type of ideal glassy state. Menon and Nagel (1995) provide tentative experimental evidence of a true divergence.

Rapid cooling permits many metals to be formed in a glassy state, and computer experiments on argon and hard sphere systems indicate that these too would form glasses if only one could cool them fast enough. Materials that form glasses reluctantly, by virtue of very rapid cooling, are called *fragile*. By contrast, there is

a tendency among certain materials to form glasses especially readily. These are *strong* or *network* glasses.

The prototypical network glass is SiO_2 , which is at the heart of most commercial glasses. The basic structure is that of a silicon atom, which wants to bond with four neighbors, surrounded by four oxygens, each of which wants to bond with two neighbors. One model of the glass structure is the *continuous random network*, shown in Figure 5.14. It is crucial that the angles between all the bonds be somewhat variable, or else a crystalline structure must result instead.

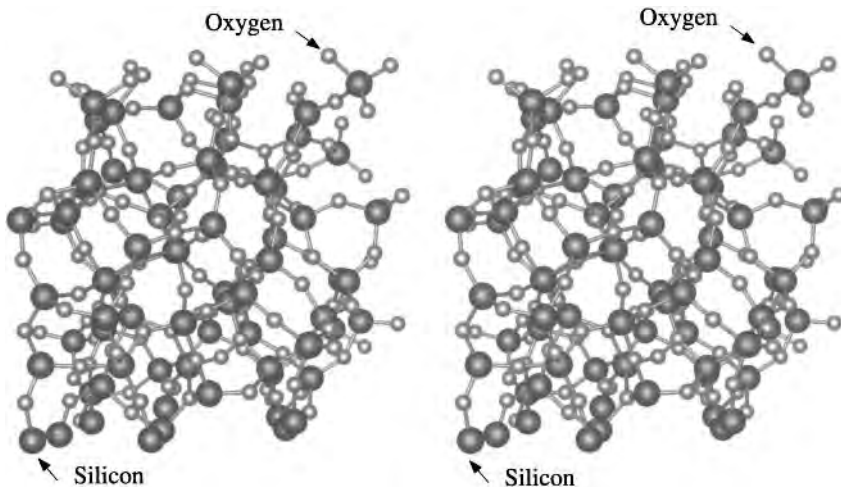


Figure 5.14. The continuous random network was proposed as a model of SiO_2 by Zachariasen (1932). Each silicon tends to have four neighboring oxygens and each oxygen tends to have two neighboring silicons. The picture was produced by a molecular dynamics simulation where silicon and oxygen were raised to a high temperature and then rapidly cooled and allowed to settle (stereo pair).

A rough argument of Phillips (1982b) gives an idea why mixtures where the average coordination number \bar{z} lies between two and three tend to form glasses. If one views the solid as a mechanical system where atoms bond to neighbors, then it tends to form a glass when the number of degrees of freedom in the system just equals the number of mechanical constraints. If there were more degrees of freedom than needed to optimize the constraints, then the network would be mechanically unstable and would flop around, as for polymers (Section 5.8). If there were fewer, the local structure of the network would have a deep energy minimum at some particular configuration, and crystals would be favored. More specifically: When the average coordination number provides z neighbors per atom in a system of N atoms, the system has a total of $N\bar{z}/2$ bonds and must try to choose an optimum length for each of them, providing $N\bar{z}/2$ constraints. Angles between bonds provide more constraints. An atom with two bonds must try to optimize the angle between them. An atom with three bonds must try to optimize the three angles between the three pairs. For these two cases, the number of constraints to try to satisfy is given by $N(2\bar{z} - 3)$. Setting the total number of degrees of freedom, $3N$,

equal to the total number of constraints,

$$3N = N(2\bar{z} - 3) + \frac{N\bar{z}}{2}, \quad (5.51)$$

it follows that

$$\bar{z} = 2.4. \quad (5.52)$$

Thus according to this argument, systems form glasses roughly when the average number of neighbors per atom lies between 2 and 3. This argument is in accord with the picture of the continuous random network in Figure 5.14 and is consistent with observations in silicon oxides, boron oxides (B_2O_3), and the chalcogenide glasses (As_2S_3 and As_3Se , for example). It does not fit amorphous silicon, however, which has fourfold coordination. In attempting more detailed accounts of structure, the most frequently studied case is SiO_2 . While the general picture shown in Figure 5.14 is correct, attempts to calculate the distribution of bond angles and compare predictions with experiment have not yet been conclusive.

5.7 Liquid Crystals

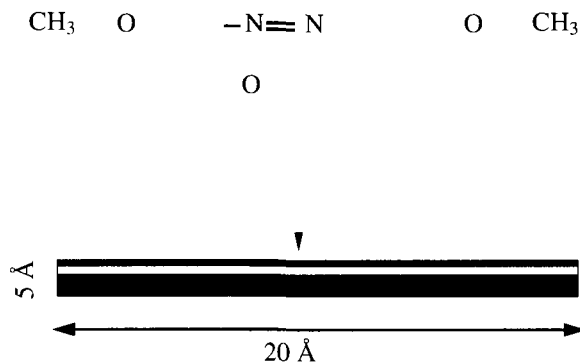


Figure 5.15. Picture of the organic molecule p-azoxyanisole (PAA), which forms a nematic liquid crystal between 116°C and 135°C . It can roughly be regarded as a rigid rod of length 20 \AA and width 5 \AA .

Intermediate in order between liquids and crystals are the *liquid crystals*. Their mechanical properties are those of a liquid, yet certain types of order, particularly in orientation, persist over large distances. The main structural element is a rodlike molecule as shown in Figure 5.15, often made by two linked aromatic rings with various flexible chains hanging off the ends.

5.7.1 Nematics, Cholesterics, and Smectics

Nematics. A *nematic* liquid crystal consists of a series of rods whose centers are arrayed randomly, as are molecules in a liquid. Just as in a liquid, there is no long-range positional order. However, there is *long-range orientational order*, as

shown in Figure 5.16. As a consequence, the refractive index of the liquid varies by around 20% in different directions and must be regarded as a tensor. This tensor has complete rotational symmetry about the axis \hat{n} and has mirror symmetry about the plane normal to \hat{n} as well as the planes containing it; its point group is $D_{\infty h}$ in Schönflies notation, or ∞/mmm in international notation.

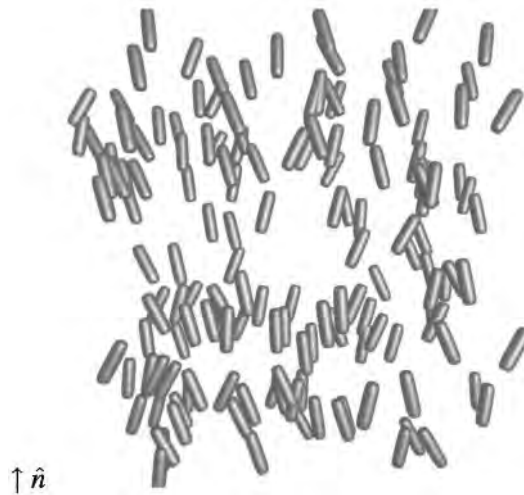


Figure 5.16. The molecules of a nematic liquid crystal have long-range orientational order, but only short-range positional order.

Cholesterics. A variant of the nematic liquid crystal is the *cholesteric* (see Figure 5.17). Now the director \hat{n} rotates slowly along an axis that is perpendicular to it, described by

$$n_x = 0 \quad (5.53a)$$

$$n_y = \cos q_0 x \quad (5.53b)$$

$$n_z = \sin q_0 x. \quad (5.53c)$$

The wavelength of the twist $\lambda = 2\pi/q_0$ is on the order of thousands of angstroms and is therefore much larger than the lengths of the molecules. This length can vary rapidly as a function of temperature. The twist breaks the mirror symmetries about the planes containing the \hat{x} axis, and this loss of symmetry is directly connected to the fact that cholesterics are produced by *chiral* molecules; these molecules are rodlike, but they twist slightly as one moves up the rod.

Smectics. The final major class of liquid crystals is the *smectic*. Now, there is not only long-range orientational order, but long-range positional order in one direction as well. In *smectics A*, the rodlike molecules arrange themselves in layers with a well-defined spacing, although within each layer the structure is liquid-like. The layers are perpendicular to the director \hat{n} . In *smectics C*, the director is no longer perpendicular to the layers, and it may or may not rotate as one moves along the \hat{x} axis, depending upon whether or not the liquid crystal is made of chiral molecules.

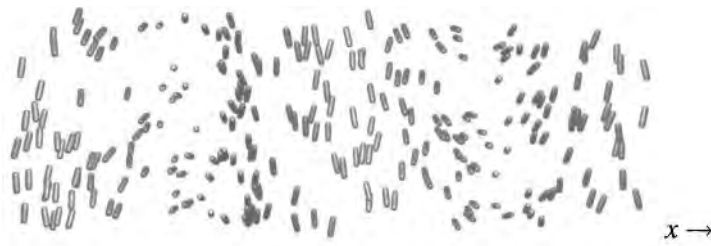


Figure 5.17. The director \hat{n} of a cholesteric liquid crystal rotates as one moves along the \hat{x} axis.

Finally, in *smectics B*, molecules are arranged in a crystalline fashion within the layers, and only the fact that the layers slide about with respect to one another distinguishes the structure from a perfect crystal. These three phases are shown in Figure 5.18.

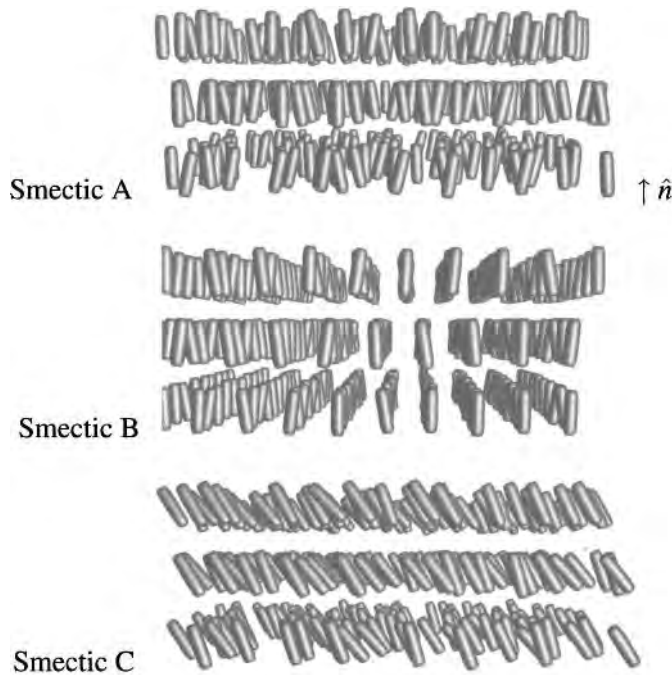


Figure 5.18. The three main smectic phases, A, B, and C display one-dimensional long-range positional order.

5.7.2 Liquid Crystal Order Parameter

One way to define an order parameter that will pick out nematic order is to consider the probability n_1 that a particle is at \vec{r}_1 pointing along θ_1 and define

$$\mathcal{O} = \int d^3r_1 d\theta_1 n_1(\vec{r}_1, \theta_1) \frac{1}{2} (3 \cos^2 \theta_1 - 1). \quad (5.54)$$

The use of the quadrupole moment rather than the dipole moment is dictated by the fact that nematic molecules are unchanged when flipped through 180° , and one does not want to get into the business of deciding which way they are pointing. If they are taken to point up and down with equal frequency, then a dipole moment vanishes. Another possible order parameter is produced by the tensor of dielectric constants, or of magnetic susceptibility, both of which change their symmetries when nematic ordering sets in. So that the result vanishes in an isotropic phase, one might define

$$Q_{\alpha\beta} = \epsilon_{\alpha\beta} - \frac{1}{3} \delta_{\alpha\beta} \sum_{\gamma} \epsilon_{\gamma\gamma}, \quad (5.55)$$

which picks out the anisotropic part of the dielectric tensor. For a computation of the mechanical properties of nematic liquid crystals, see Section 12.4.1, and for more detailed discussions of the topic see Chandrasekhar (1992), de Gennes and Prost (1993), and Chaikin and Lubensky (1995).

5.8 Polymers

Polymers, like liquid crystals, are built from rod-like molecules, but now the rods are floppy and exceptionally long. Polyethylene, for example, consists of thousands of repeating units of CH_2 . One repeating unit is a *homopolymer*, while two or more in alternation form a *copolymer*. The *degree of polymerization* is the number of basic units repeating in a typical chain. In useful materials, this number may be in the tens to hundreds of thousands.

It may seem unlikely that any conceptually simple picture could capture features of polymer behavior. It is from the enormous lengths of the individual polymer chains that simplifications can flow. The molecules are so long that they behave like ideal floppy chains, wiggling randomly in an environment produced self-consistently by all the other polymers. The starting point for study of polymers is therefore a single polymer chain immersed in a solvent liquid.

View the polymer as a collection of identical rigid segments, connected by joints, each of which is completely free to rotate as it wishes, depicted in Figure 5.19. Different segments of the chain are even free to rotate right through each other, an admittedly unrealistic feature of the model that needs to be corrected in a more sophisticated treatment. It may also seem unrealistic to reduce complicated bending energies to rigid rods and joints, but this particular simplification makes little difference.

5.8.1 Ideal Radius of Gyration

One of the most important features of an isolated polymer chain is its characteristic size, called the *radius of gyration* \mathcal{R} , which is the root mean square distance from one end of the polymer to the other. This quantity is the same as the mean square distance traveled by a random walker, Section 5.2.4, but it is interesting to derive it in a different way more directly related to polymer physics. Suppose one end of



Figure 5.19. Illustration of a polymer as a random walk. To prepare this figure, each segment was permitted to turn at an angle up to 26° relative to the previous segment.

the polymer to be sitting at the origin, and suppose that one has already calculated the probability $\mathcal{P}_N(\vec{R}')$ that a polymer of length N has its end at position \vec{R}' . Then the probability $\mathcal{P}_{N+1}(\vec{R})$ that a polymer of length $N + 1$ has its end at position \vec{R} is

$$\mathcal{P}_{N+1}(\vec{R}) = \int d\vec{R}' \mathcal{P}_N(\vec{R}') \mathcal{P}_1(\vec{R} - \vec{R}') \quad \begin{array}{l} \text{The only way for the end of the polymer} \\ \text{to be at } \vec{R} \text{ is for the end of the } N\text{th} \\ \text{segment to have been at } \vec{R}', \text{ and for the} \\ \text{(} N+1\text{)st segment to reach from } \vec{R}' \text{ to } \vec{R}. \end{array} \quad (5.56)$$

$$\Rightarrow \mathcal{P}_{N+1}(\vec{k}) = \mathcal{P}_N(\vec{k}) \mathcal{P}_1(\vec{k}) \quad \begin{array}{l} \text{This is the convolution theorem for the} \\ \text{Fourier transform of } \mathcal{P}; \text{ Section A.5.} \end{array} \quad (5.57)$$

$$\Rightarrow \mathcal{P}_N(\vec{k}) = [\mathcal{P}_1(\vec{k})]^N. \quad \begin{array}{l} \text{By recursion.} \end{array} \quad (5.58)$$

Provided N is large enough, details of $\mathcal{P}_1(\vec{k})$ will not matter; one only needs to know its behavior near $\vec{k} = 0$, where it can be expanded in a Taylor series. Keeping terms up to order k^3 gives (Problem 7)

$$\mathcal{P}_1(\vec{k}) \approx 1 - \frac{C}{2} k^2 \approx e^{-Ck^2/2} \quad (5.59)$$

$$\Rightarrow \mathcal{P}_N(\vec{k}) \approx e^{-NCk^2/2} \quad \begin{array}{l} \text{This approximation is excellent for large } N. \end{array} \quad (5.60)$$

$$\Rightarrow \mathcal{P}_N(\vec{R}) = \frac{1}{\sqrt{2\pi NC}^3} e^{-R^2/2NC}. \quad \begin{array}{l} \text{Inverting the Fourier transform.} \end{array} \quad (5.61)$$

The statement that the probability of a large number of uncorrelated events is described by a Gaussian, as in Eq. (5.61), is known as the *central limit theorem*. One can easily calculate the constant c from

$$C = -\frac{\partial^2}{\partial k^2} \Big|_{\vec{k}=0} \mathcal{P}_1(\vec{k}) \equiv a^2/3 \quad \begin{array}{l} \text{This can be used as a definition of the length} \\ \text{a of an individual polymer segment.} \end{array} \quad (5.62)$$

and can also relate it to the ideal radius of gyration \mathcal{R}_I of the polymer,

$$\mathcal{R}_I^2 = \int d\vec{R} R^2 \mathcal{P}_N(\vec{R}) = 3CN = a^2N \quad \text{Write } R^2 = R_x^2 + R_y^2 + R_z^2, \text{ note that the three terms in the sum must have the same integral, and perform the integral for any one of them.} \quad (5.63)$$

$$\Rightarrow \mathcal{R}_I = a\sqrt{N}. \quad \text{This expression is identical to Eq. (5.16) with } N = t/t_0, \text{ but has been derived in a different way.} \quad (5.64)$$

Polymer Interactions. Two features of this calculation appear questionable. First, the polymer is not actually composed of identical segments that pivot completely independently of one another. In reality, the polymer is rather stiff when viewed at the molecular level. However, two stiff springy units placed end to end have half the spring constant of the original unit, four placed together have one-fourth the spring constant, and by the time one has a chain made up of a million segments, one can safely view it as composed of, say, 20,000 completely floppy sections, each built from 50 of the original springs. Making this idea more precise is the subject of Problem 8. The result is that expressions (5.61) and (5.64) survive, but the constant a must be defined in a more general way.

The more serious defect of the calculation is that it allows different points of the polymer to slide freely through each other. One should recognize that the polymer can never visit the same point twice during its path; the polymer describes a *self-avoiding random walk* (SARW). Such a calculation presents many formal difficulties. A considerably simpler method begins by calculating the forces needed to extend or compress an idealized polymer, and then it determines whether the interactions between polymer segments are powerful enough to cause the overall shape of the polymer to alter noticeably from its idealized shape.

Stretching a Polymer. From Eq. (5.61) one can determine the force needed to stretch a polymer. Fix one end at the origin, grab the far end, and move it to location \vec{R} . This motion costs no energy (because all polymer segments rotate freely) but reduces the entropy. For example, if the end were to be pulled far enough that the whole polymer was made completely straight, it could no longer move, and its entropy would be zero. More generally, the entropy associated with any restricted configuration is just Boltzmann's constant k_B times the log of the probability that the configuration will occur. Because Eq. (5.61) gives the probability that the end of the polymer be found at \vec{R} , one has immediately that

$$S = S_0 - \frac{3}{2}k_B \frac{R^2}{\mathcal{R}_I^2} \quad \text{Use also Eq. (5.64) relating } a \text{ and } \mathcal{R}_I. S_0 \text{ is a constant independent of } R \text{ whose value is unimportant.} \quad (5.65)$$

The free energy resulting from this entropy is

$$\mathcal{F} = \mathcal{F}_0 + \frac{3}{2}k_B T \frac{R^2}{\mathcal{R}_I^2} = \mathcal{F}_0 + \frac{3}{2}k_B T \frac{R^2}{a^2N}, \quad \text{Use Eq. (5.64).} \quad (5.66)$$

and the force \vec{F} needed to pull the end of the polymer away from its preferred location at $\vec{R} = 0$ is

$$\vec{F} = 3k_B T \frac{\vec{R}}{\mathcal{R}_1^2} = \frac{3k_B T}{a^2 N} \vec{R} \equiv \frac{\mathcal{K}}{N} \vec{R}. \quad (5.67)$$

The polymer behaves like an ideal spring of vanishing equilibrium length, with a spring constant that rises in proportion to temperature, and that falls in proportion to the molecular weight $\mathcal{R}_1^2 \propto N$ of the polymer chains.

Compressing a Polymer. While the force needed to stretch a polymer is well indicated by grabbing the far ends and pulling outwards, this calculation says nothing about the forces needed to compress a polymer into a small volume, because not only the far end, but all intermediate points, must now be pressed inwards. A simple estimate of the forces needed for this compression is obtained by imagining a polymer molecule trapped within a sphere of diameter $\mathcal{R} \ll \mathcal{R}_1$. Suppose that wherever the polymer hits the wall of the sphere it sticks permanently, and guess that by finding the free energy of a configuration of this type, one obtains a reasonable estimate of the free energy in the more realistic situation where points of contact between polymer and sphere change with time.

The typical number M of monomers separating points of contact along the polymer should be

$$M \sim \frac{\mathcal{R}^2}{a^2} \quad \text{Since a polymer of length } M \text{ has characteristic size } \sqrt{Ma} \propto \mathcal{R} \quad (5.68)$$

So now one has N/M segments of molecular weight M , each stretched out to distance \mathcal{R} . According to Eq. (5.66), the free energy of such a collection of polymers is

$$\mathcal{F} = \mathcal{F}_0 + k_B T \left(\frac{N}{M} \right) \frac{3}{2} \frac{\mathcal{R}^2}{a^2 M} = \mathcal{F}_0 + k_B T \frac{3N}{2} \frac{a^2}{\mathcal{R}^2} = \mathcal{F}_0 + k_B T \frac{3\mathcal{R}_1^2}{2\mathcal{R}^2}. \quad \text{Use Eq. (5.68)}. \quad (5.69)$$

The pressure the chamber exerts upon the polymer is therefore

$$P = - \frac{\partial}{\partial \mathcal{R}^3} k_B T N \frac{a^2}{\mathcal{R}^2} \propto \frac{k_B T (N/M)}{\mathcal{R}^3}, \quad \text{Drop constants of order unity.} \quad (5.70)$$

which is just the pressure of an ideal gas of N/M particles in volume \mathcal{R}^3 .

Volume Interactions. Although the calculations of the forces needed to extend or compress a polymer will later have direct use in finding the mechanical properties of polymer mixtures, the goal now is to use them in order to determine the importance of interactions between portions of the polymer chain which are not directly adjacent to one another. These interactions are rare when the polymer describes a random walk within a solvent, and therefore their contribution to the free energy should be contained within the virial expansion of statistical mechanics. One need know nothing of the elaborate techniques used to find the coefficients in this expansion; one simply needs to use the fact that the virial expansion is in powers of the density of particles.

Suppose that when the interactions between distant points on the polymer chain, called *volume interactions*, are taken into account, the radius of gyration of the polymer becomes \mathcal{R} , rather than \mathcal{R}_1 . The density of particles available to interact with one another is therefore

$$n = \frac{N}{\mathcal{R}^3} = \frac{\mathcal{R}_1^2}{a^2 \mathcal{R}^3}. \quad \text{Factors such as } 4\pi/3 \text{ are out of place in a qualitative analysis of this type.} \quad (5.71)$$

According to the virial expansion, interactions between particles should produce contributions to the free energy of the form

$$\mathcal{F} \propto k_B T \mathcal{R}^3 [An + Bn^2 + Cn^3 + \dots]. \quad \text{The coefficients } A, B, \text{ and } C \text{ depend upon temperature. The factor of } \mathcal{R}^3 \text{ appears because } \mathcal{F} \text{ is extensive.} \quad (5.72)$$

Adding together Eqs. (5.66), (5.69), and (5.72) therefore gives an estimate of the free energy of a polymer whether it shrinks or expands, and includes the effect of interactions between distant segments. Dropping constants of order unity, one has

$$\mathcal{F} = \mathcal{F}_0 + k_B T \left[\frac{\mathcal{R}^2}{\mathcal{R}_1^2} + \frac{\mathcal{R}_1^2}{\mathcal{R}^2} + \mathcal{R}^3 \left[A \left(\frac{\mathcal{R}_1^2}{a^2 \mathcal{R}^3} \right) + B \left(\frac{\mathcal{R}_1^2}{a^2 \mathcal{R}^3} \right)^2 + C \left(\frac{\mathcal{R}_1^2}{a^2 \mathcal{R}^3} \right)^3 + \dots \right] \right]. \quad (5.73)$$

The condition that \mathcal{F} have a minimum as a function of \mathcal{R} is

$$2 \frac{\mathcal{R}}{\mathcal{R}_1^2} - 2 \frac{\mathcal{R}_1^2}{\mathcal{R}^3} - 3B \frac{\mathcal{R}_1^4}{a^4 \mathcal{R}^4} - 6C \frac{\mathcal{R}_1^6}{a^6 \mathcal{R}^7} = 0. \quad (5.74)$$

If the second virial coefficient, B , is positive, then polymer segments tend to repel one another, and the polymer should swell to a larger size than \mathcal{R}_1 . If $\mathcal{R} \gg \mathcal{R}_1$, then the only two terms that are significant in Eq. (5.74) are

$$2 \frac{\mathcal{R}}{\mathcal{R}_1^2} - 3B \frac{\mathcal{R}_1^4}{a^4 \mathcal{R}^4} = 0 \quad (5.75)$$

$$\Rightarrow \mathcal{R}^5 \propto \frac{B \mathcal{R}_1^6}{a^4} \Rightarrow \mathcal{R} \propto \mathcal{R}_1^{6/5} \propto N^{3/5}. \quad \text{The guess that } \mathcal{R} \gg \mathcal{R}_1 \text{ is confirmed.} \quad (5.76)$$

If on the other hand, the second virial coefficient B is negative, the polymer has a tendency to shrink. The pressure in Eq. (5.70) resists shrinkage, but it is overwhelmed by a negative pressure from the virial expansion. The two most important terms in Eq. (5.74) now give

$$\frac{|B| \mathcal{R}_1^4}{a^4 \mathcal{R}^4} = 2C \frac{\mathcal{R}_1^6}{a^6 \mathcal{R}^7} \Rightarrow \mathcal{R}^3 \sim \frac{C \mathcal{R}_1^2}{|B| a^2} \sim N \Rightarrow \mathcal{R} \sim N^{1/3}. \quad (5.77)$$

Any tendency toward attraction of distant polymer segments leads the whole molecule to collapse into a small ball, whose volume is proportional to the molecular weight.

Finally, if $B = 0$ and C is not too large, \mathcal{F} is minimized for $\mathcal{R} = \mathcal{R}_1$; the polymers behave like an ideal random walk. A solvent tuned so that B vanishes is called a Θ solvent; polymers in Θ solvents execute nearly ideal random walks, as in Figure 5.19.

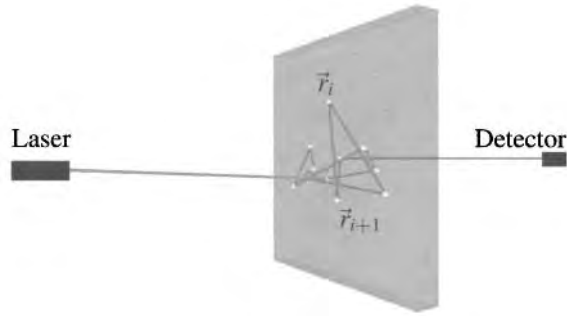


Figure 5.20. Schematic drawing of light path through sample filled with micron-scale particles in diffusing-wave spectroscopy.

5.9 Colloids and Diffusing-Wave Scattering

5.9.1 Colloids

Many familiar liquids including milk, hand creams, and blood are *colloids*, described by Gast and Russel (1998), which means that they are made of particles whose size ranges from nanometer to a micrometer dispersed in a liquid or gas. Electrostatic interactions between the particles can keep them from clumping together, and when their size is comparable to the wavelength of light, even a small fraction of colloidal particles can render a system opaque, as in the case of clouds and fog.

While colloidal particles can form crystals, it is more common for them to be arrayed randomly and move constantly, so that one can only describe their location in a statistical sense. Their strong interaction with light opens up the possibility of studying the spatial arrangement. However, neither the theory of weak scattering from crystals nor dynamic light scattering of Chapter 3 are adequate because light scattering from colloidal particles is dominated by *multiple scattering*. A typical photon travels on a convoluted path through many particles before exiting the liquid.

5.9.2 Diffusing-Wave Spectroscopy

The technique of *diffusing-wave spectroscopy*, developed by Weitz and Pine (1993) exploits the multiple scattering limit in order to measure features of the correlation function Eq. (3.49) that conventional scattering does not. It measures the mean square distance that particles move in time t :

$$\langle \Delta r^2(t) \rangle \equiv \frac{1}{N} \int d\vec{r} d\vec{r}' n_2(\vec{r}, \vec{r}'; t) |\vec{r} - \vec{r}'|^2$$

Look back at the definition in Eq. (3.49). In the present case, the most important correlations will be when $l = l'$ and particle locations are correlated with themselves over time.

(5.78)

How does this correlation function emerge from the process of multiple scattering illustrated in Figure 5.20? The basic idea is that when light scatters from

many particles, its phase when it exits the sample is determined by the total path length through which it has traveled. Even small changes in the locations of particles produce changes in phase. Indeed, multiple scattering increases sensitivity to particle motions. Dynamic light scattering can detect particle motions on the order of a wavelength of light, while diffusing-wave spectroscopy is sensitive to much smaller motions just so long as the cumulative total distance moved by particles in a light path is comparable to a wavelength.

The starting point is the Siegert relation of Eq. (3.64) which shows that the dynamic correlation function $\langle E(t)^* E(0) \rangle$ can be deduced from measurements over time of light intensity exiting a sample at a point.

However, when light scatters many times, the relation between particle locations and $\langle E_\alpha^*(0) E_\gamma(t) \rangle$ is no longer given by Eq. (3.59). Instead, specializing to linear polarization and dropping subscripts on the electric field to simplify matters, let p denote some path that light takes to get from the laser to the detector. Then at the detector

$$\frac{\langle E^*(0) E(t) \rangle}{|E_0|^2} = \frac{1}{I_0} \left\langle \left(\sum_p E_p^* e^{-i\phi_p(0)} \right) \left(\sum_{p'} E_{p'} e^{i\phi_{p'}(t)} \right) \right\rangle \quad (5.79)$$

Here E_p is the amplitude of the electric field along path p and ϕ_p is the phase of the electric field at the end of path p . Assume next that the strongest correlations come from electric fields along the same path at different times, and that the intensity I_p is not correlated with the phase ϕ_p . If this is correct, then only terms where $p = p'$ need be kept in Eq. (5.79), and the average of the product can be replaced by the product of averages giving

$$\frac{\langle E^*(0) E(t) \rangle}{|E_0|^2} = \sum_p \left\langle \frac{I_p}{I_0} \right\rangle \langle e^{-i(\phi_p(t) - \phi_p(0))} \rangle \quad \text{This expression also assumes that the change in amplitude of } E_p \text{ over time } t \text{ is not worth considering, just the change in phase. } I_p \text{ is the intensity } |E_p|^2. \quad (5.80)$$

Phase. What is the change in phase of light that escapes from the sample? For the scattering event that takes light from particle \vec{r}_i to particle \vec{r}_{i+1} , the wave vector of light is

$$\vec{k}_i(t) = k_0 \frac{\vec{r}_{i+1}(t) - \vec{r}_i(t)}{|\vec{r}_{i+1}(t) - \vec{r}_i(t)|} \quad \text{Since for elastic scattering the wavelength of light is fixed at } k_0. \quad (5.81)$$

Thus the phase is

$$\phi_p(t) - \phi_p(0) = \sum_{i=0}^N \vec{k}_i(t) \cdot [\vec{r}_{i+1}(t) - \vec{r}_i(t)] - \vec{k}_i(0) \cdot [\vec{r}_{i+1}(0) - \vec{r}_i(0)]. \quad (5.82)$$

As shown in Problem 9, this phase can be rewritten and approximated as

$$\phi_p(t) - \phi_p(0) \approx - \sum_{i=1}^N \vec{q}_i \cdot \Delta \vec{r}_i(t) \quad (5.83)$$

where $\hbar\vec{q}_i$ is the momentum transfer of the scattering event from particle $i - 1$:

$$\vec{q}_i \equiv \vec{k}_i(0) - \vec{k}_{i-1}(0) \quad \text{and} \quad \Delta\vec{r}_i(t) \equiv \vec{r}_i(t) - \vec{r}_i(0). \quad (5.84)$$

It is now possible to evaluate contributions from the phase in Eq. (5.80). Write

$$\langle e^{-i(\phi_p(t) - \phi_p(0))} \rangle = \langle e^{i \sum_j \vec{q}_j \cdot \Delta r_j(t)} \rangle \quad \text{From Eq. (5.83).} \quad (5.85)$$

$$\approx \langle \prod_j \left(1 + i\vec{q}_j \cdot \Delta r_j(t) - \frac{1}{2} [\vec{q}_j \cdot \Delta r_j(t)]^2 \dots \right) \rangle \quad (5.86)$$

$$\approx \left\langle \prod_j \left(1 - \frac{1}{2} [\vec{q}_j \cdot \Delta r_j(t)]^2 \dots \right) \right\rangle \quad \begin{array}{l} \text{Odd powers of } \vec{q}_j \text{ should vanish since} \\ \text{positive and negative values are equally} \\ \text{likely. Furthermore products such as} \\ \Delta r_1^a \Delta r_2^b \text{ should vanish because} \\ \text{motions of different particles are} \\ \text{uncorrelated.} \end{array} \quad (5.87)$$

$$\approx \prod_j \left(1 - \frac{1}{2} \langle [\vec{q}_j \cdot \Delta r_j(t)]^2 \rangle \right) \quad (5.88)$$

$$\approx \exp \left(\sum_j -\frac{1}{2} \langle [\vec{q}_j \cdot \Delta r_j(t)]^2 \rangle \right) \quad \begin{array}{l} \text{The justification for this move is called} \\ \text{Wick's theorem in field theory (see} \\ \text{Section 13.4.3), and is justified for} \\ \text{normally distributed random variables} \\ \text{in Triantafyllopoulos (2003).} \end{array} \quad (5.89)$$

There is no reason that scattering paths \vec{q}_j and particle displacements $\Delta\vec{r}_j$ should be correlated, so one can write

$$\sum_{j=1}^N \langle (\vec{q}_j \cdot \Delta\vec{r}_j(t))^2 \rangle = \frac{N}{3} \langle q^2 \rangle \langle \Delta r^2(t) \rangle \quad \begin{array}{l} \text{See Problem 9. } \langle q^2 \rangle \text{ means choose any } \vec{q}_j \text{ as} \\ \text{their statistical properties are all the same.} \end{array} \quad (5.90)$$

The average over $\langle q^2 \rangle$ could be a terribly complicated formal problem, since $\vec{q}_j = \vec{k}_j(0) - \vec{k}_{j-1}(0)$ varies from 0 to $2k_0$ depending on the direction light scatters from particle $j - 1$. The standard approach to this problem is to evade it by defining

$$\langle q^2 \rangle \equiv 2k_0^2 \frac{l}{l^*}. \quad (5.91)$$

Here l is the mean distance between scattering sites, and l^* can be interpreted as the mean free path of light in the medium. When l^* is very large, \vec{k}_j is nearly parallel to \vec{k}_{j-1} and $\langle q^2 \rangle$ is small. When light leaves each particle in a nearly random direction, $l^* \approx l$. Using this definition, one has finally

$$\langle e^{-i(\phi_p(t) - \phi_p(0))} \rangle = \left\langle e^{i \sum_j \vec{q}_j \cdot \Delta r_j(t)} \right\rangle = e^{-sk_0^2 \langle \Delta r^2(t) \rangle / (3l^*)} \quad (5.92)$$

where $s = Nl$ is the total path length of light traveling through the sample.

Amplitude. To evaluate Eq. (5.80) still requires dealing with the light intensity I_p of path p . The approach to this problem is to make further use of the idea that light is executing a random walk through the colloidal system. Suppose a flash of light hits the sample at time 0, and exits it at time t . One can immediately deduce that the path length of the light in the sample was $s = ct$. This means one can write Eq. (5.80) as

$$\frac{\langle E^*(0)E(t) \rangle}{|E_0|^2} = \int ds \frac{\langle I(\vec{r}, s/c) \rangle}{l^* I_0} e^{-sk_0^2 \langle \Delta r^2(t) \rangle / (3l^*)} \quad (5.93)$$

The factor of l^* keeps dimensions correct. All the information about the probability of having a path of length s is contained in the solution of the diffusion equation that follows.

Since the probability distribution of particles undergoing random walks obeys the diffusion equation (Section 5.2.4), the intensity of light leaving the sample should be the solution of the diffusion equation, which means a solution of

$$\frac{\partial U_l}{\partial t} = \mathcal{D}_l \nabla^2 U_l, \quad (5.94)$$

where U_l is the energy density of light, and \mathcal{D}_l is a diffusion constant for light. To estimate \mathcal{D}_l , imagine that the light path is a random walk with step length conventionally given as $2l^*$. Then according to Eq. (5.14) the diffusion constant is given by

$$\mathcal{D}_l = cl^*/3. \quad (5.95)$$

Boundary conditions for the diffusion equation are tricky, and there seems some temptation to decide between mathematical boundary conditions on the grounds of agreement between theory and experiment. The problem is that the actual boundary conditions follow from the fact that once the source turns off, all subsequent light waves are outgoing waves at the boundary of the sample. However, approximating light as a diffusing field allows no way to impose this condition exactly. The issue is discussed in most depth in Chapter 9 of Ishimarū (1978). For the purposes of discussion here, a particularly simple boundary condition will be employed, which is that the energy density of diffusing light U_l vanishes at the sample boundaries, because photons that arrive there are immediately whisked away as propagating radiation.

A model calculation that corresponds reasonably well to experiments is to say that at time $t = 0$ a narrow plane wave of light of intensity

$$U_l(x, 0) = I_0 l^* \delta(x - x_0) / 8\pi \quad \begin{array}{l} \text{The multiplicative factors have been chosen} \\ \text{to give correct dimensions.} \end{array} \quad (5.96)$$

is present in a sample at depth $x_0 > 0$. The sample is a slab extending from 0 to L in the x direction, and off to infinity in the other directions. Given this initial condition, the diffusion equation (5.94) can be solved by Laplace transforms. Let

$$\tilde{U}(\vec{r}, \alpha) = \int_0^\infty dt U(\vec{r}, t) e^{-\alpha t}. \quad (5.97)$$

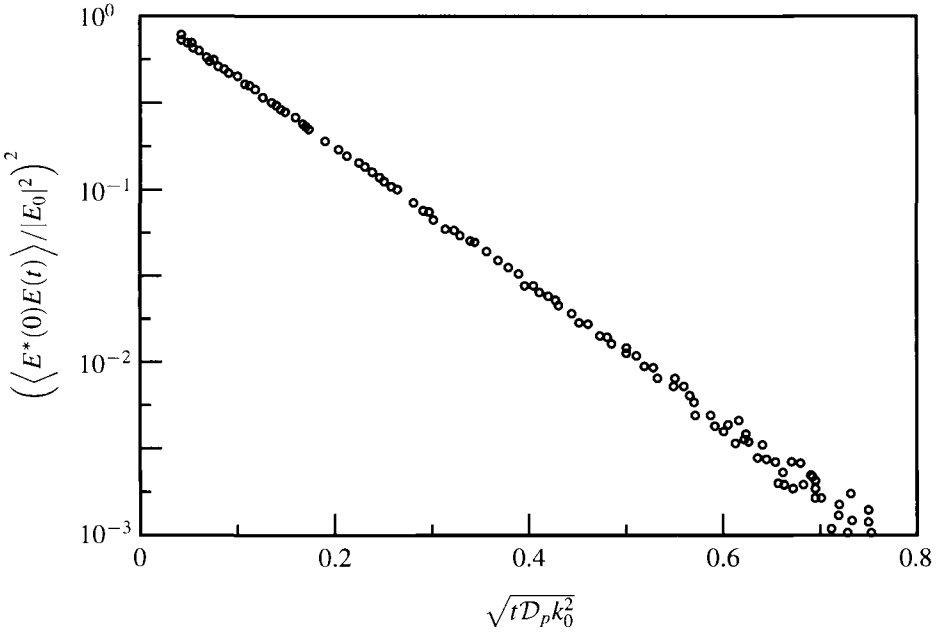


Figure 5.21. Intensity of light scattered back from a suspension of polystyrene spheres in water, volume fraction 5%. The variables displayed in the plot should be linearly related according to Eq. (5.104) and they are. [Source: Weitz and Pine (1993), p. 677].

Then

$$\alpha \tilde{U}(x, \alpha) = I^* I_0 \delta(x - x_0) / (8\pi) + \mathcal{D}_l \frac{\partial^2}{\partial x^2} \tilde{U}(x, \alpha) \quad \text{Only the } x \text{ component of } \vec{r} \text{ matters because this is a plane problem.} \quad (5.98)$$

$$\Rightarrow \tilde{U}(x, \alpha) = A \cosh x\kappa + B \sinh x\kappa + \frac{I^* I_0}{16\pi \mathcal{D}_l \kappa} e^{-|x-x_0|\kappa} \quad (5.99)$$

where

$$\kappa = \sqrt{\alpha / \mathcal{D}_l} \quad (5.100)$$

How can one relate the energy density of diffusing light to the intensity I arriving at a photodetector? The energy current arriving at the edge of the sample is $\mathcal{D}_l \vec{\nabla} U$. Set this equal to the electromagnetic energy current density $cE^2/8\pi = cI/8\pi$, obtaining

$$\frac{\langle E^*(0)E(t) \rangle}{|E_0|^2} = \int ds 8\pi (\mathcal{D}_l / I_0 c I^*) \frac{\partial}{\partial x} U(x, s/c) e^{-sk_0^2 \langle \Delta r^2(t) \rangle / (3I^*)} \quad (5.101)$$

From Eqs. (5.93). Use the energy current $\mathcal{D}_l \vec{\nabla} U$ to find $\langle t \rangle$. Evaluate $\partial U / \partial x$ at the point where light is to be collected.

$$= (8\pi \mathcal{D}_l / I_0 I^*) \frac{\partial}{\partial x} \tilde{U}(x, \alpha), \text{ where } \alpha = ck_0^2 \langle \Delta r^2(t) \rangle / (3I^*) \quad (5.102)$$

In a forward scattering geometry, light is collected at the far end of the sample, $x = L$. Imposing the boundary conditions $\tilde{U}(0, \alpha) = \tilde{U}(L, \alpha) = 0$ and solving for

A and B in Eq. (5.98) gives

$$\frac{\langle E^*(0)E(t) \rangle}{|E_0|^2} = \frac{e^{2\kappa x_0} - 1}{e^{2\kappa L} - 1} e^{\kappa(L-x_0)}, \quad \kappa = \sqrt{ck_0^2 \langle \Delta r^2(t) \rangle / (3Dl^*)}. \quad (5.103)$$

In a backscattering geometry, light is collected instead at $x = 0$ and the opposite sign of the derivative must be used in Eq. (5.102). In the limit $L \rightarrow \infty$ the result is

$$\frac{\langle E^*(0)E(t) \rangle}{|E_0|^2} = e^{-\kappa x_0}, \quad \kappa = \sqrt{ck_0^2 \langle \Delta r^2(t) \rangle / (3Dl^*)}. \quad (5.104)$$

Now suppose that the particles in the fluid are diffusing with particle diffusion constant \mathcal{D}_p , so that according to Eq. (5.16) the square distance a particle moves in time t is $\Delta r^2(t) = 6\mathcal{D}_p t$. Then one has

$$\kappa = \frac{x_0}{l^*} \sqrt{6tk_0^2 \mathcal{D}_p}. \quad (5.105)$$

Weitz and Pine (1993) recommend taking $x_0/l^* \approx 2.1$ in order to compare with experiment. As shown in Figure 5.21, the log of $\langle E^*(0)E(t) \rangle$ is a linear function of $\sqrt{\mathcal{D}_p t}$. The slope of such curves can be used to find \mathcal{D}_p and hence as shown in Problem 10 can be used to estimate particle sizes in suspensions that are not dilute.

5.10 Quasicrystals

First Observation. Shechtman et al. (1984) were not setting out to challenge crystallography, but were preparing melt-spun ribbons of $\text{Al}_{86}\text{Mn}_{14}$. The alloys were made to cool at rates of 10^6 K s^{-1} by pouring molten metal onto a rapidly spinning wheel, cooling rates that could be expected to produce a metallic glass. After examination with an electron microscope, the samples were placed under X-ray diffraction. The startling result was a set of diffraction patterns indicating axes of threefold and fivefold symmetry, shown in Figure 5.22. Fivefold symmetry was completely unexpected, since as proved in Problem 4 of Chapter 1, a fivefold axis is crystallographically impossible. It is impossible to build a lattice with a fivefold axis. Nonetheless, the data unambiguously indicated that the system had this symmetry. In fact, the scattering patterns exhibited the symmetry of an icosahedron, giving tenfold, sixfold, and fivefold symmetric diffraction patterns when tilted at appropriate angles. A picture of a small crystal exhibiting such symmetry appears in Figure 5.23.

The claim that nature had found a way to realize true fivefold symmetries met with some resistance. A collection of five crystals might conceivably bond together at five different orientations to produce an apparent fivefold axis. They would not fit together perfectly, but the scattering pattern would not easily reveal this fact, and such a point of view was vigorously advanced by Pauling (1985). In some materials it turned out to be correct. However, the most interesting proposal, and the one that seems to have carried the day for the original AlMn alloy as well as

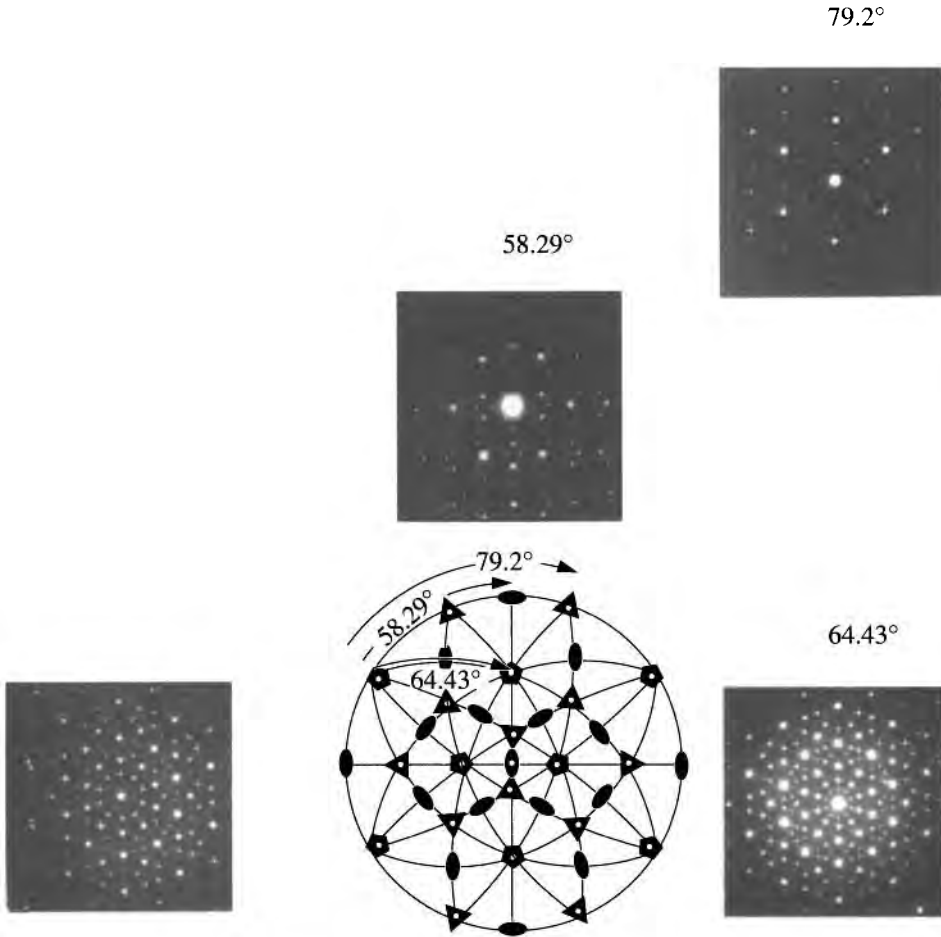


Figure 5.22. X-ray scattering patterns from single grain of Al₈₆Mn₁₄. Angles refer to various orientations of the grain. Note clear fivefold symmetry axis in two of the scattering patterns. [Source: Shechtman et al. (1984), p. 1952.]

many other materials, holds that the explanation of the diffraction pattern lies in a quasi-periodic filling of space which has a true icosahedral symmetry. Levine and Steinhardt (1984) christened this type of lattice a *quasicrystal*. Such ordering generalizes the idea of the crystal, and the simplest explanation of how it works begins in one dimension.

5.10.1 One-Dimensional Quasicrystal

A one-dimensional quasicrystal is a collection of points lying on a line, spaced quasiperiodically. As an example, and to demonstrate the meaning of quasiperiodic, consider the Fibonacci sequence:

$$x_n = n + (\tau - 1)\text{int}(n/\tau). \quad \text{"int}(x)\text{" is the function that finds the largest integer smaller than } x. \quad (5.106)$$

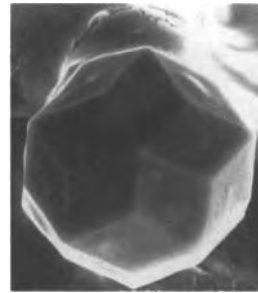


Figure 5.23. Quasicrystal of AlLiCu:
[Source: Kortan (1996).]

This sequence of points is composed of long and short intervals: The distance between successive points is either τ , the golden mean,

$$\tau = 1 + \frac{1}{\tau} = \frac{\sqrt{5} + 1}{2} = 1.618 \dots, \tag{5.107}$$

or 1. The sequence has a *deflation rule*. If one writes out the sequence of differences between successive points (a sequences of 1's and τ 's), then replaces every τ with the little sequence $\tau, 1$, and also replaces every 1 with a τ , the same sequence returns.

Example. Start with the sequence

$$\tau 1 \tau \tau 1 \dots \tag{5.108}$$

Using the deflation rule $\tau \rightarrow \tau 1$ and $1 \rightarrow \tau$ gives

$$\tau 1 \tau \tau 1 \tau 1 \tau \dots \tag{5.109}$$

Another Construction. One can use this procedure to generate longer and longer portions of the Fibonacci sequence, starting from a small subsection. One can also generate the sequence by the construction

$$X_{n+1} = X_n X_{n-1}, \tag{5.110}$$

which means that one builds the sequence in this way:

$$X_{-1} = \tau; X_0 = \tau 1; X_1 = \tau 1 \tau; X_2 = \tau 1 \tau \tau 1 \dots \tag{5.111}$$

$$X_3 = X_2 X_1 = \tau 1 \tau \tau 1 \tau 1 \tau. \tag{5.112}$$

These properties are meant to indicate that the series has many regularities without being periodic. However, it is quasiperiodic, which means that it is periodic in a higher-dimensional space. In this case, the function is periodic in two dimensions, but has been projected into one.

The Fibonacci sequence can be interpreted as a shadow cast in one dimension by a slice through a periodic lattice in two dimensions, as shown in Figure 5.24. To prove this assertion, proceed as follows. Rewrite Eq. (5.106) as

$$x_m = m + \sum_n n \theta(n - m/\tau + 1) \theta(m/\tau - n) / \tau \tag{5.113}$$

Here $\theta(x)$ is the Heaviside step function, which equals one if its argument is larger than 0, and vanishes otherwise. A factor of $(\tau - 1)$ has been replaced by $1/\tau$, using Eq. (5.107).

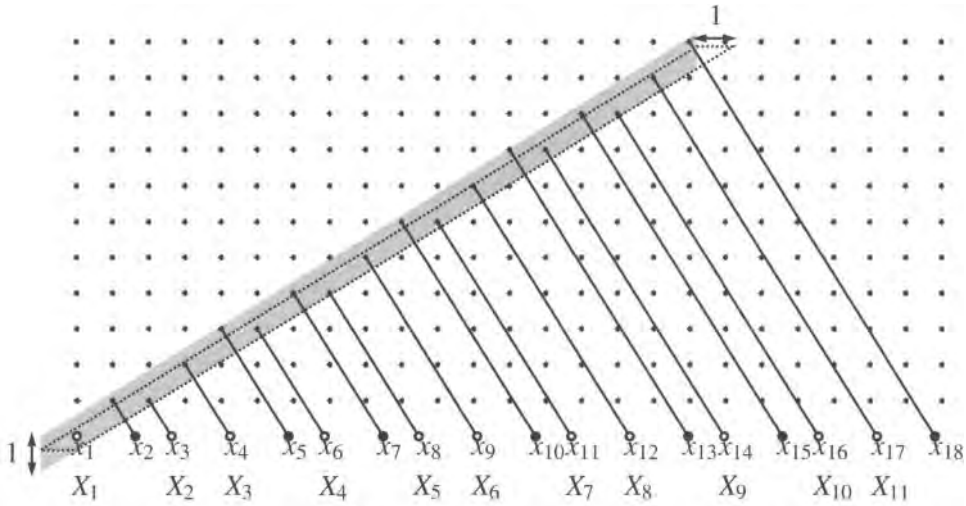


Figure 5.24. Construction showing how the one-dimensional quasicrystal results from a projection down from two dimensions, and how one obtains the deflation rule. The shaded bar has slope $1/\tau$, and vertical height 1. The sequence x_m defined by Eq. (5.106) results from projection of the points lying in this bar onto the x axis. The bar enclosed by the dotted line has slope $1/\tau$ and width 1, and the sequence X_n defined by Eq. (5.118) results from projection of the points inside onto the x axis.

Now consider the points that fall inside the shaded strip in Figure 5.24. The strip has vertical thickness of 1 and has slope $1/\tau$, and points lie inside it if

$$x/\tau > y > x/\tau - 1. \tag{5.114}$$

So for every vertical column of the lattice, indexed by integer m , there is precisely one point inside the strip at location

$$[m, \sum_n n\theta(m/\tau - n)\theta(n - [m/\tau - 1])]. \tag{5.115}$$

This is a Cartesian vector, whose first component is m .

To find where the shadow of this point falls on the x axis along the direction $(1, -\tau)$, one adds an appropriate multiple of $(1, -\tau)$ to (5.115) so that the y coordinate vanishes, and then one checks where one lands along x . The answer is precisely Eq. (5.113). Therefore the geometrical construction of Figure 5.24 is the same as Eq. (5.106).

This geometrical construction can be used in order to prove the deflation rule. Consider the collection of points that fall within the smaller strip of Figure 5.24, which is surrounded by a dotted line and has unit width rather than unit height. Points lie in this smaller strip if

$$(x + 1)/\tau - 1 > y > x/\tau - 1. \tag{5.116}$$

Because this strip has unit width, one lattice point must fall within it from every horizontal row, and one finds the lattice points satisfying Eq. (5.116) to be

$$\left[\sum_m m\theta((m+1)/\tau - 1 - n)\theta(n - [m/\tau - 1]), n \right]. \quad (5.117)$$

Projecting this set of points onto the x axis as before results in the sequence

$$X_{n+1} = \sum_m m\theta((m+1)/\tau - n - 1)\theta(n - m/\tau + 1) + n/\tau. \quad (5.118)$$

This location is defined to be X_{n+1} rather than X_n so that the lower left point in Figure 5.24 will correspond to X_1 as well as to x_1 .

The set of distances X_n is depicted in Figure 5.24 as the hollow circles.

It is not hard to show that the sequence X_m is almost exactly the same as the sequence x_m . After a few simple changes of variables (Problem 11), one finds

$$X_m = -1/\tau + \tau x_m. \quad (5.119)$$

Thus X_m is nothing but the sequence x_m expanded by a factor of τ and slightly displaced; in particular, the sequences of long and short segments of X_m and x_m are exactly the same. It is evident from Figure 5.24 that X_m is obtained from x_m by sliding the upper dotted line up slightly, replacing all long intervals by a long followed by a short, and leaving all short intervals alone. This argument shows the origin of the deflation rule.

Scattering from a One-Dimensional Quasicrystal. The advantage of viewing the quasicrystal as a projection down from higher dimensions is that it makes it possible to compute its Fourier transform and to understand how scattering from such a structure leads to sharp peaks. What will emerge from the analysis is that the mathematical structure of scattering from a quasicrystal differs in some striking ways from that from a crystal. The quasicrystal scattering peaks are countably infinite and dense; any finite strip of q space contains an infinite number of peaks, but most of them have amplitude too small to be seen. This type of scattering spectrum is called *singular continuous*.

The idea behind the calculation is that, as in Figure 5.24, the points contained in a one-dimensional quasicrystal can be expressed as the product of two functions. The first is the two-dimensional square lattice, and the second is a function that equals one within the shaded strip of Figure 5.24 but is zero outside of it. So, roughly speaking, one expects the Fourier transform of the quasicrystal to be a convolution of the Fourier transform of the square lattice with the Fourier transform of the shaded strip.

The sum to be computed is

$$\Sigma_q = \sum_n e^{iqx_n} \quad (5.120)$$

$$= \sum_{n,m} e^{iq(m+n/\tau)} \theta(n - m/\tau + 1)\theta(m/\tau - n) \quad (5.121)$$

The θ functions are only nonzero when m and n have adopted just the right values so as to produce a necessary contribution to the sum.

$$= \int dx dy e^{i\vec{q}\cdot(x,y)} \left[\sum_{m,n} \delta(x-m)\delta(y-n) \right] \theta(y-x/\tau+1)\theta(x/\tau-y) \quad (5.122)$$

$$\text{where } \vec{q} = (q, q/\tau). \quad (5.123)$$

Equation (5.122) is a two dimensional Fourier transform that is to be evaluated along a particular line in q space. To carry out the integral one can use the convolution theorem, Eq. (A.42), to carry out the Fourier transforms of the two halves of the integrand and then integrate them together in the end. The first piece is

$$A(\vec{q}) = \int dx dy \sum_{m,n} \delta(x-m)\delta(y-n) e^{iq_x x} e^{iq_y y} \quad (5.124)$$

$$= N \frac{(2\pi)^2}{V} \sum_{n',m'} \delta(q_x - 2\pi n') \delta(q_y - 2\pi m'). \quad (5.125)$$

Eq. (5.124) describes the scattering from a two-dimensional square lattice, which, according to the two-dimensional analog of Eq. (3.19) produces Bragg peaks at the reciprocal lattice vectors $2\pi(n', m')$.

The second piece is

$$B(\vec{q}) = \int dx \int_{x/\tau-1}^{x/\tau} dy e^{iq_x x + iq_y y} = \int dx e^{iq_x x} \left[\frac{e^{iq_y(x/\tau)} - e^{iq_y(x/\tau-1)}}{iq_y} \right]. \quad (5.126)$$

Convoluting Eqs. (5.125) and (5.126) with \vec{q} given by Eq. (5.123) gives

$$\Sigma_q \propto \int dx dq'_x dq'_y \sum_{n',m'} \left\{ \begin{array}{l} \delta(q - q'_x - 2\pi n') \\ \times \delta(q/\tau - q'_y - 2\pi m') \end{array} \right\} \left[\frac{e^{iq'_y(x/\tau)} - e^{iq'_y(x/\tau-1)}}{iq'_y} \right] e^{iq'_x x} \quad (5.127)$$

$$= \int dx \sum_{n',m'} \left[\frac{e^{i(q/\tau - 2\pi m')(x/\tau)} - e^{i(q/\tau - 2\pi m')(x/\tau-1)}}{iq/\tau - 2\pi i m'} \right] e^{i(q - 2\pi n')x} \quad (5.128)$$

$$= 2\pi \sum_{n',m'} \frac{1 - e^{-i(q/\tau - 2\pi m')}}{iq/\tau - 2\pi i m'} \delta([2\pi m' - \frac{q}{\tau}]/\tau + 2\pi n' - q). \quad (5.129)$$

The peaks of (5.129) are at

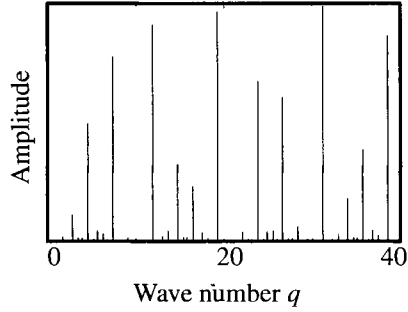
$$\frac{2\pi(m'/\tau + n')}{\tau - 2 + 1} = q \quad \text{All integers } m' \text{ and } n' \text{ are allowed.} \quad (5.130)$$

and their square amplitude is proportional to

$$\sin^2 \left(\pi \left[\frac{m'\tau - n'}{\tau + \tau - 1} \right] \right) / (q/\tau - 2\pi m')^2. \quad (5.131)$$

Therefore, the Fourier spectrum is made up of countably many sharp peaks, as shown in Figure 5.25; in contrast to those produced by a lattice, these are dense and form a singular continuous spectrum. However most of them are sufficiently weak that they are practically invisible. The important ones are those produced by n' and m' whose ratio is near the golden mean—that is, when these integers are neighboring Fibonacci numbers.

Figure 5.25. Plot of the scattering amplitude predicted by Eq. (5.131). This singular continuous scattering spectrum has sharp peaks that fill the k axis in a dense fashion, yet are zero almost everywhere.



5.10.2 Two-Dimensional Quasicrystals—Penrose Tiles

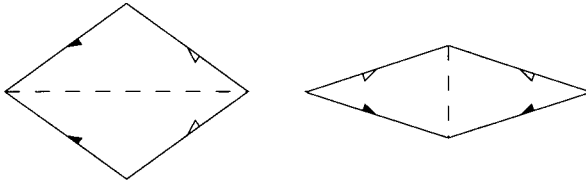


Figure 5.26. Penrose tiles. These are only allowed to join when the arrows match together. The smaller angle of the fat rhombus is $2\pi/5$, and the smaller angle of the skinny rhombus is $2\pi/10$. Taking the lengths of all the sides to be 1, the long diagonal of the fat rhombus (dashed line) has length $\tau = (\sqrt{5} + 1)/2$, and the short diagonal of the skinny rhombus (dashed line) has length $1/\tau$.

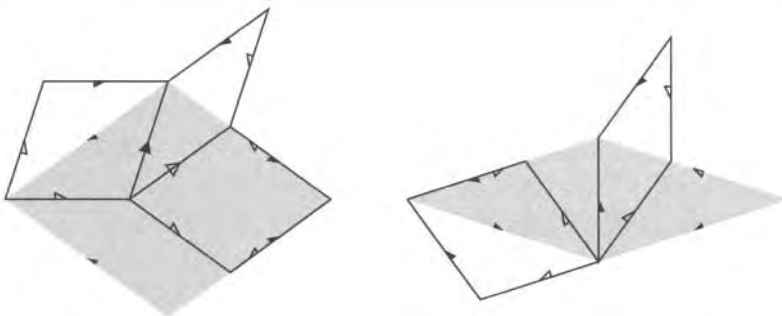


Figure 5.27. If this decoration is engraved on each tile of a Penrose lattice, the result will be a Penrose tiling with more tiles on a smaller scale.

Penrose introduced two-dimensional quasicrystals as a playful mathematical problem in filling the plane nonperiodically; the results were first published for practical purposes by Gardner (1977). The *Penrose lattice* is a tiling of the plane

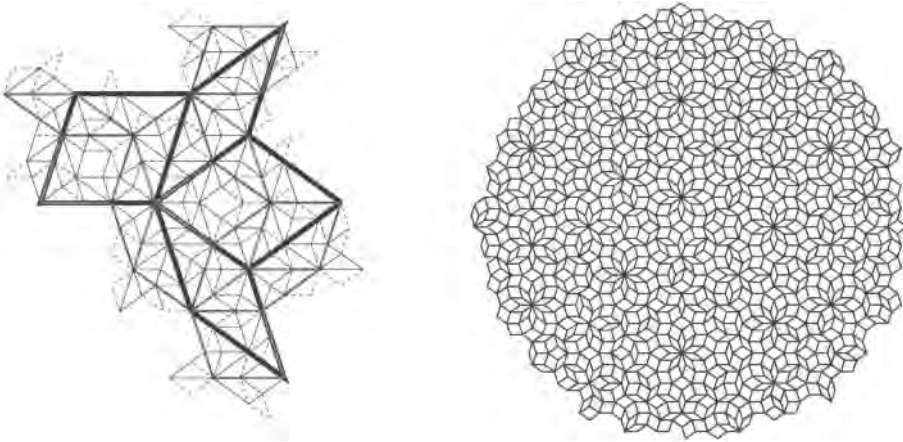


Figure 5.28. The first three applications of the deflation rule to two fat rhombuses and one skinny rhombus are shown here on the left, while on the right is a large circular section of quasicrystal, produced by the method of Problem 13.

by a collection of two tiles, shown in Figure 5.26. These are decorated by arrowheads, and the tiles must be placed together so that matching arrows are always adjacent. It is possible to tile the plane with these objects, and although the result is not periodic, every finite area segment of the lattice repeats infinitely often elsewhere in the lattice. One can partly verify these claims by noticing that the Penrose lattice has a deflation rule. If one decorates each tile as shown in Figure 5.27 with smaller tiles, then a set of big tiles which obeys the matching rules generates a set of many more smaller tiles also obeying the matching rules. Proceeding this way long enough generates a lattice with an arbitrarily large number of tiles in it, shown in Figure 5.28.

An additional curious feature is that one can decorate the tiles with lines as shown in Figure 5.29; then when the tiles are laid on the plane, all the lines drawn on the tiles march across the plane. These lines are called the *Ammann lines*. The spacing between them takes two values, whose ratio is the golden mean. When the deflation rule shown in Figure 5.28 is applied to the Penrose lattice, one can ask what happens to the lattice of Ammann lines. Say the large spacing between lines is τ . After deflation, the new lattice will replace this large spaced pair of lines with three lines, along the same direction; the first is spaced by 1, and the second is spaced by $1/\tau$. All the lines separated by the smaller distance, 1, are not changed.

This deflation rule is precisely the deflation rule for the one-dimensional Fibonacci sequence, showing that the spacings between the Ammann lines are given by Eq. (5.106) Therefore, the Penrose tiling is a two-dimensional generalization of the quasicrystal.

One can build it by choosing five unit vectors, \hat{e}_α , which point at angles of $2\pi/5$ with respect to one another, along the sides of a pentagon. Then the quasicrystal

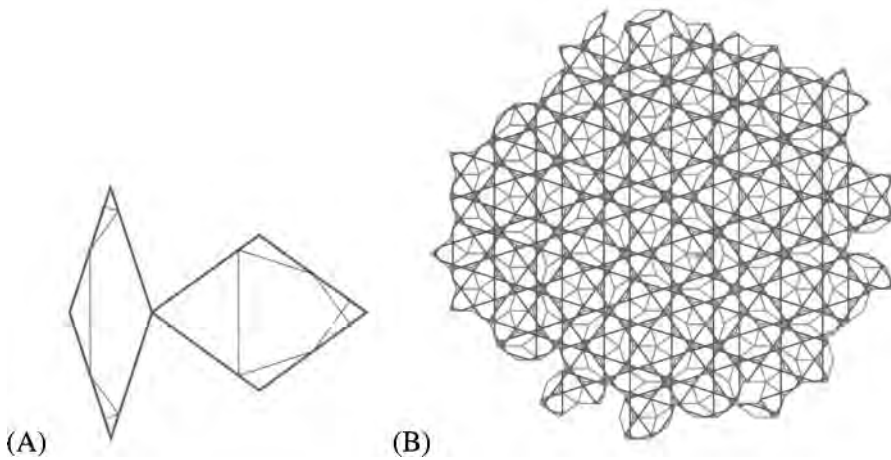


Figure 5.29. In (A) is shown a set of decorative lines drawn upon the fat and skinny tiles. They have the curious property, shown in (B), that when the tiles cover the plane, the lines join up and form five grids of parallel lines, with the spacings of lines in any given direction described by the one-dimensional Fibonacci sequence.

lattice points are the set of points \vec{r} such that

$$\vec{r} \cdot \hat{e}_\alpha = x_{n_\alpha}, \quad \vec{r} \cdot \hat{e}_\beta = x_{n_\beta}, \quad (5.132)$$

where x_n is a member of the Fibonacci sequence. In other words, one places down a set of lines in the plane. The lines travel along the five angles given by the sides of a pentagon. The spacing between groups of parallel lines proceeds as the Fibonacci sequence. The points in the lattice occur at the intersections of two lines. A more general way to create two-dimensional quasicrystals is the subject of Problem 13.

One immediate question is why one has to vary the spacing between the lines in such a complicated way. Because one has created a fivefold axis by brute force, why not choose all the spacings between the lines to be constant? The answer is that if one does this, the vertices where lines cross can come arbitrarily close to one another, and atoms that built such a structure would have to do the same. This difficulty is at the heart of the proof that fivefold symmetry is crystallographically impossible. The Penrose lattice avoids this difficulty, and because it is constructed by assembling together simple geometrical objects, it is possible that molecules might naturally pack together so as to form this particular structure. In fact, dozens of materials are now known where such packing occurs.

5.10.3 Experimental Observations

To understand why naturally forming crystals might have a tendency to create quasicrystals, it is helpful to return to the problem of packing hard spheres. In close-packing arrangements such as fcc or hcp lattices, every sphere has 12 neighbors, but the neighbors are not arrayed about a central sphere with perfect symmetry.

Suppose one takes a sphere and places 12 identical spheres around it in the most symmetrical arrangement. Connecting the centers of the neighbors with lines, one finds that they form an icosahedron, as shown in Figure 5.30. Because of the five-fold symmetry evident in this structure, one knows immediately that it cannot fill space uniformly. Approximate icosahedral symmetry is the basis for a complicated arrangement of atoms first proposed by Frank and Kasper (1958), and reviewed more recently by Nelson and Spaepen (1989). In the *Frank–Kasper phases*, a unit cell is packed with several approximate icosahedra; they must be distorted to fit together, and the unit cell is very complicated. Quasicrystalline phases can be understood as another way for materials to realize icosahedral symmetry.



Figure 5.30. Twelve neighbors symmetrically arranged about a sphere form an icosahedron.

The first quasicrystals were only metastable, and were filled with defects, but alloys such as $\text{Al}_6\text{Li}_3\text{Cu}$ have since been found for which the quasicrystalline phase is truly a free energy minimum. The alloy system shown in Figure 5.31 has the remarkable property of forming a two-dimensional quasicrystal, arranged in layers.

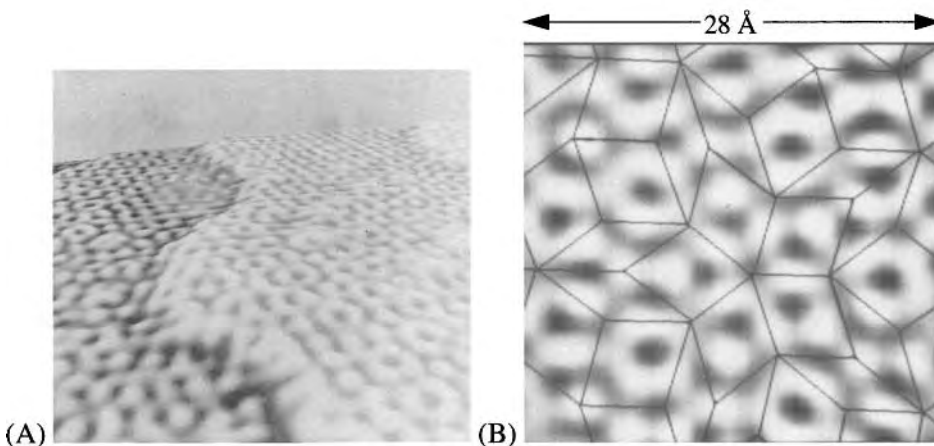


Figure 5.31. (A) Scanning tunneling microscope image of the two-dimensional quasicrystal $\text{Al}_{65}\text{Cu}_{15}\text{Co}_{20}$, viewed from an oblique angle. The three-dimensional crystal consists of stacks of identical two-dimensional quasicrystals. (B) Top view shows how to decorate the atomic locations with Penrose tiles. [Source: Kortan (1996).]

The majority of quasicrystals found to date has the icosahedral symmetry illustrated in Figure 5.22. However, octagonal and decagonal quasicrystals have also

been found.

Three-dimensional quasicrystals can be described using theoretical tools very similar to those employed in two dimensions, and they are discussed by Janot (1992). The essential idea of how fivefold symmetry is realized in nature is explained by the two-dimensional case, but three-dimensional quasicrystallography, discussed by Mermin (1992), is needed to obtain detailed comparison with most experimental systems.

5.11 Fullerenes and nanotubes

A new class of carbon compounds is the *fullerenes*, whose physical properties are reviewed by Smalley (1997) and by Weaver and Poirier (1994). The prototype for these compounds is C_{60} , where 60 carbon atoms are arranged at the vertices of a molecule resembling a soccer ball, or one of the structures designed by the architect Buckminster Fuller.

Ijima (1991) discovered carbon nanotubes in 1991 while examining waste products created during synthesis of fullerenes. Single-walled carbon nanotubes consist in single atomic layers of carbon in a honeycomb structure (graphene) rolled around an axis into a tube (Problem 1.3). When more than a single atomic layer of carbon rolls up into a tube, the result is a *multi-walled carbon nanotube*. Great effort has been spent investigating their properties, as documented by Dresselhaus et al. (2001) and Ebbesen (1996). Nanotubes are extremely stiff and strong, and can grow to lengths of microns.

Novoselov et al. (2004) found that by attaching tape to graphite crystals and pulling it off, it was possible to create micron-sized crystals of graphene that in places were literally one atom thick (Figure 1.3). Thus the study of graphene now encompasses small clusters, tubes, and infinite sheets.

Problems

1. Coordination numbers:

- Find the coordination number z for fcc and bcc lattices
- Find the coordination number z for hcp lattices, depending on c/a .
- Find the average coordination number \bar{z} for sodium chloride and perovskite.
- Find the average coordination number \bar{z} for a continuous random network of SiO_2 .

2. Verlet method:

- Derive Eq. (5.38) and show that errors are only of order dt^4 after each time step by considering the Taylor expansion of the function $\vec{r}(t + dt)$.
- Find an expression for the velocity \vec{v}^n in terms of \vec{r}^{n+1} and \vec{r}^{n-1} that has corrections at order dt^2 .

3. Phase separation:

- (a) Given a specific function $\mathcal{F}(c)$, the endpoints of phase separation in Figure 5.5 can be determined by two algebraic equations. Find these equations.
- (b) Consider the specific case of

$$\mathcal{F}(c) = \frac{1}{2}(c - 0.2)^2(c - 0.8)^2 + c/2. \quad (5.133)$$

Show that the conditions for phases separation are satisfied for $c_a = 0.2$ and $c_b = 0.8$.

- (c) Again considering the free energy (5.133), what is the final equilibrium state of a system that initially is homogeneous and has $c = 0.6$?

4. Peritectic phase diagram:

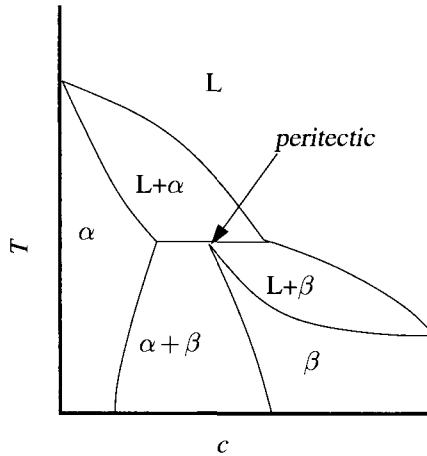


Figure 5.32. Phase diagram with peritectic.

A *peritectic* is a point in a phase diagram above which phase β simultaneously melts and phase separates. Use a series of sketches analogous to Figure 5.6 to show how a such a phase diagram can arise from the competition between liquid and solid free energies.

5. **Monte Carlo:** Consider 20 particles living in one dimension whose potential energy is

$$U = \sum_{l < l'} \phi(x_l - x_{l'}), \quad \phi(x) = \phi_0(x^{-12} - x^{-6}) \quad (5.134)$$

and which are constrained to sit in the interval $[0, L]$, with $L = 30$. Write a Monte Carlo program to calculate $g(x) \equiv n_2(x)/n^2$ at two temperatures, $\beta = 1/k_B T = 10/\phi_0$ and $\beta = 100/\phi_0$.

- (a) Create an array of length 20 to hold particle locations, and also create an array of length NBINS=300 to hold $g(x)$.

- (b) Space the particles evenly initially, at distance 1 from each other.
 (c) Write a subroutine to compute the sum Eq. (5.134). The sum can be limited to near neighbors; five are recommended, as in

```

for i=0 through n
  {
    for j= (maximum of i-5 and 0) through i
      {
        e+=phi(x(i)-x(j));
      }
    }
  }

```

- (d) Wait 100,000 time steps, and then at every 20th time step compute a new contribution to g ; the relevant line might look like

```

for i=0 through n-1
  {
    for j=0 through i-1
      {
        k=(int)(abs(x(i)-x(j))/L*NBINS)
        g(k)=g(k)+1
      }
    }
  }

```

Find the correct normalization of $g(x)$. In a liquid of infinite extent, $g \rightarrow 1$ as $x \rightarrow \infty$. If case of a discrepancy of two, think about the effect of $\text{fabs}(x[i]-x[j])$.

- (e) Carry out a total of 500,000 Monte Carlo time steps for each of the two temperatures. Do not worry about the quality of the random number generator.
 (f) Landau and Lifshitz (1980), p. 537, prove that long-range order is impossible in one dimension at nonzero temperatures for particles with short-range forces. Please comment.

6. **Von Neumann's law:** Consider a two-dimensional array of polycrystalline grains (see Figure 5.33). Assume four facts about the grain boundaries.

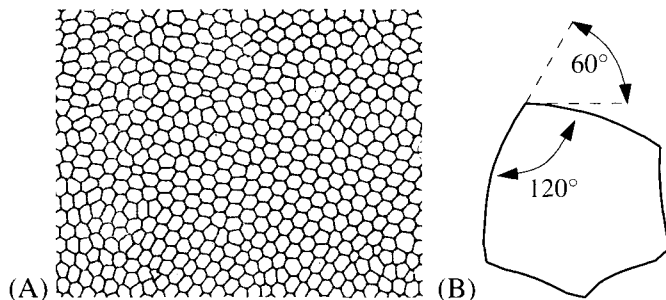


Figure 5.33. (A) An array of two-dimensional soap cells, which obey laws very similar to those of metal grains. (B) Geometry of von Neumann's law.

- (a) When grain boundaries intersect, there are always exactly three arcs departing from the intersection point.
- (b) The sides of the grains are all arcs of circles.
- (c) Where the arcs meet, the angles between them are all exactly 120° . To see why, consider three ropes meeting at a point, all being pulled with the same force. Only with 120° angles can they be in equilibrium.
- (d) For every arc with radius of curvature R and length l , the corresponding grain grows at rate $-kl/R$. Outward-bowing segments cause the grain to shrink; inward bowing segments cause it to grow, because the curved grain boundary exerts pressure like the skin of a balloon. Here k is a constant.

Use these four facts to relate the growth rate of a grain to its number of sides. The result is called von Neumann's law, and it was derived by von Neumann while he sat in a conference listening to a talk on grain growth. A recent review of the topic is by Weaire and McMurry (1997).

7. Polymer integrals:

Consider the probability $\mathcal{P}_1(\vec{R})$ that a single polymer segment reaches from 0 to \vec{R} , and its Fourier transform $\mathcal{P}_1(\vec{k})$ defined in Section 5.8.1. Show that

$$\mathcal{P}_1(\vec{k} = 0) = 1. \quad (5.135)$$

- (a) Show that in a Taylor expansion to cubic order in components of \vec{k} , the only terms allowed are of the form

$$\mathcal{P}_1(\vec{k}) \approx 1 - \frac{c}{2}k^2 \approx e^{-ck^2/2} \quad (5.136)$$

Assume $\mathcal{P}_1(-\vec{R}) = \mathcal{P}_1(\vec{R})$, and that $\mathcal{P}(\vec{R})$ depends upon the magnitude of \vec{R} but not its direction.

8. **Polymer stiffness:** Suppose one has a polymer composed of a sequence of rigid rods, of length a , and suppose that the rods are connected by springs so that if the angle between rod l and rod $l + 1$ is θ_l , the energy of the joint is $\kappa\theta_l^2$ (assume low temperatures so that $\beta\kappa \gg 1$). Show that for long enough polymers the chain executes an ideal random walk.

- (a) Write down the probability $\mathcal{P}(\theta_1 \dots \theta_N)$ of having some set of angles $\theta_1 \dots \theta_N$ for a polymer at temperature T .
- (b) Confine the polymer to two dimensions, and ignore the possibility of self-intersections. Find the x coordinate of the N th bead for some particular set of angles $\theta_1 \dots \theta_N$, given that bead 1 is at the origin.
- (c) Find the expectation value $\langle x_N^2 \rangle$ of the end of the polymer. Take $Nk_B T / \kappa$ to be much greater than 1.
- (d) The result has the same form as expected for an ideal random walk, but the segment length a must be replaced by an effective length \tilde{a} . What is \tilde{a} ?

9. **Diffusing-wave spectroscopy:** Demonstrate Eq. (5.83). In addition to the definitions in Eq. (5.84), also define

$$\Delta \vec{k}_i \equiv \vec{k}_i(t) - \vec{k}_i(0) \quad (5.137)$$

- (a) Show that Eq. (5.82) can be rewritten as the sum of two terms, one of which involves $\Delta \vec{k}_i(t) \cdot [\vec{r}_{i+1}(t) - \vec{r}_i(t)]$ and the other of which appears in Eq. (5.83). Make use of the fact that $\Delta \vec{r}_i$ vanishes when $i = 0$ and $i = N + 1$ because the starting and ending points of the light path are the laser and detector which do not move.
- (b) Argue that the sum involving $\Delta \vec{k}_i$ should be much smaller than the sum involving \vec{q} , so long as particle motions over time t are small compared to the distance between scattering sites, and by discarding the smaller sum, obtain Eq. (5.83).
- (c) Demonstrate Eq. (5.90).
- (d) Complete the calculations to find Eqs. (5.103) and Eq. (5.104).

10. **Diffusion of spheres:** Einstein (1905) first showed that the diffusion of spheres in liquid can be used to deduce their size. To recover this result, start with the Langevin equation, Eq. (5.40), with the external force F set to zero.

- (a) Defining $\vec{v}(t) = \dot{\vec{r}}(t)$, show for a particle starting at rest that

$$v_\alpha(t) = \int_0^t dt' e^{-(t-t')b} \xi_\alpha(t') \quad (5.138)$$

- (b) Consider times t_1 and t_2 that are large compared with $1/b$. Using Eq. (5.41), show that

$$\langle v_\alpha(t_1) v_\beta(t_2) \rangle = \frac{k_B T}{m} \delta_{\alpha\beta} e^{-|t_1 - t_2|b}. \quad (5.139)$$

By setting $t_1 = t_2$ and invoking equipartition of energy, argue that the constants in Eq. (5.41) were chosen correctly to reproduce thermal equilibrium.

- (c) Again considering times t much larger than $1/b$, compute

$$\langle r_\alpha(t) r_\beta(t) \rangle \quad (5.140)$$

and obtain the *Einstein relation*

$$D = \frac{k_B T}{b}. \quad (5.141)$$

- (d) Employing Stokes' relation for the drag resistance of fluid on a slowly moving sphere, Eq. (15.145), relate the diffusion constant D for a sphere in liquid to its radius.

11. **One-dimensional quasicrystal:** Verify that Eq. (5.119) follows from Eq. (5.118). Begin by sending $n \rightarrow m$ and $m \rightarrow n$, and then send $n \rightarrow n + m + 1$.

12. **Quasicrystal scattering:** Consider a two-dimensional quasicrystal that is created in the following way. First take five unit vectors \hat{e}_l , with $l = 1 \dots 5$ pointing along the angles $2\pi l/5$. Construct an array of lines perpendicular to each of these unit vectors, and whose spacing is given by the Fibonacci sequence (5.106), as described by Eq. (5.132).
- Find the two-dimensional Fourier transform of this crystal's density, thus obtaining the diffraction scattering amplitude. Use Eq. (5.129) as a starting point.
 - Prepare a plot in two dimensions of some of the brighter scattering peaks.
13. **The generalized dual method:** A method for generating two-dimensional quasicrystals alternative to the one discussed in the text, and more general, is the generalized dual method. It proceeds in the following steps:

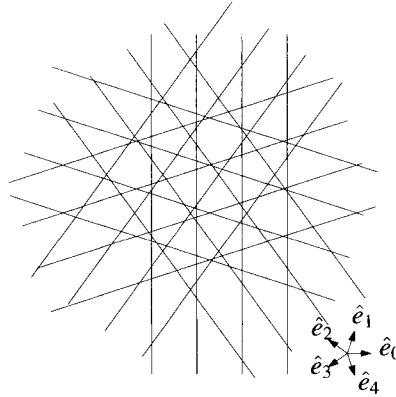


Figure 5.34. Drawing upon which the generalized dual method for constructing quasicrystals is based.

- Write down five unit vectors \hat{e}_j pointing along angles $2\pi j/5$, for $j = 0 \dots 4$.
- For each unit vector, draw a set of parallel *equally spaced* lines perpendicular to the vector. Choose the starting points of the sets of lines so that no more than two meet at an intersection point. Number the lines, and refer with n_j to the n th line along the j th unit vector.
- Every open region between the lines will correspond to a vertex of the quasicrystal. To obtain the location of the vertex, compute $\sum_{j=0}^4 n_j \hat{e}_j$ where the open region is after the n th line in the j direction and before the $(n+1)$ st.
- Choose the intersection point of any two lines in Figure 5.34 and describe what type of shape is generated in the quasicrystal as one travels 360° in a small loop about this intersection point. What are the two basic possibilities for what can happen?
- Write a program to construct the tiling corresponding to Figure 5.34; or, better yet, starting from scratch.

References

- S. M. Allen and J. W. Cahn (1979), A microscopic theory for antiphase boundary motion and its application to antiphase domain coarsening, *Acta Metallurgica*, **27**, 1085–1095.
- C. A. Angell (1988), The glass transition: An assessment of current thinking, *Nuclear Physics B — Proceeding Supplements*, **5A**, 69–80.
- J. A. Barker and D. Henderson (1976), What is ‘liquid’? Understanding the states of matter, *Reviews of Modern Physics*, **48**, 587–671.
- D. Bensimon, L. P. Kadanoff, S. Liang, and B. I. Shraiman (1986), Viscous flows in two dimensions, *Reviews of Modern Physics*, **58**, 977–999.
- J. D. Bernal (1959), A geometrical approach to the structure of liquids, *Nature*, **183**, 141–147.
- N. O. Birge and S. R. Nagel (1985), Specific-heat spectroscopy of the glass transition, *Physical Review Letters*, **54**, 2674–2677.
- W. L. Bragg and E. J. Williams (1934), The effect of thermal agitation on atomic arrangement in alloys, *Proceedings of the Royal Society of London*, **A145**, 699–730.
- W. F. Brinkman and P. E. Cladis (1982), Defects in liquid crystals, *Physics Today*, **35**(5), 48–54.
- J. D. Brock, R. J. Birgeneau, J. D. Litster, and A. Aharony (1989), Liquids, crystals and liquid crystals, *Physics Today*, **42**(7), 52–59.
- R. Brown (1827), *A Brief Account of Microscopical Observations Made in the Monts of June, July, and August 1827 on the Particles Contained in the Pollen of Plants; and On the General Existence of Active Molecules in Organic and Inorganic Bodies*, Not Published.
- G. S. Cargill (1975), Structure of metallic alloy glasses, *Solid State Physics: Advances in Research and Applications*, **30**, 227–320.
- P. M. Chaikin and T. C. Lubensky (1995), *Principles of Condensed Matter Physics*, Cambridge University Press, Cambridge.
- S. Chandrasekhar (1992), *Liquid Crystals*, 2nd ed., Cambridge University Press, Cambridge.
- N. E. Cusack (1987), *The Physics of Structurally Disordered Matter*, Adam Hilger, Bristol.
- S. P. Das (2004), Mode-coupling theory and the glass transition in supercooled liquids, *Reviews of Modern Physics*, **76**(3), 785–851
- P.-G. de Gennes (1979), *Scaling Concepts in Polymer Physics*, Cornell University Press, Ithaca NY.
- P. G. de Gennes (1992), Soft matter, *Reviews of Modern Physics*, **64**, 645–648.
- P.-G. de Gennes (1999), Granular matter: a tentative view, *Reviews of Modern Physics*, **71**(2), S374–S382.
- P.-G. de Gennes and J. Prost (1993), *The Physics of Liquid Crystals*, 2nd ed., Clarendon Press, Oxford.
- P. G. Debenedetti and H. E. Stanley (2003), Supercooled and glassy water, *Physics Today*, **56**(6), 40–46
- M. S. Dresselhaus, G. Dresselhaus, and P. Avouris, eds. (2001), *Carbon Nanotubes*, vol. 80 of *Topics in Applied Physics*, Springer-Verlag, Berlin
- T. W. Ebbesen (1996), Carbon nanotubes, *Physics Today*, **49**(6), 26–32.
- A. Einstein (1905), On the motion of small particles suspended in stationary liquid demanded by the molecular-kinetic theory of heat, *Annalen der Physik (Leipzig)*, **17**, 549–560. In German. Translated in *Investigations on the theory of Brownian movement*, Dover, New York, 1956
- S. R. Elliot (1990), *Physics of Amorphous Materials*, 2nd ed., John Wiley and Sons, New York.
- C. P. Flynn (1972), *Point Defects and Diffusion*, Clarendon Press, Oxford.
- F. C. Frank and J. S. Kasper (1958), Complex alloy structures regarded as sphere packings. I: Definitions and basic principles, *Acta Crystallographica*, **11**, 184–190.
- M. Gardner (1977), Extraordinary nonperiodic tiling that enriches the theory of tiles, *Scientific American*, **236**, 110–121.

- A. P. Gast and W. B. Russel (1998), Simple ordering in complex fluids: colloidal particles suspended in solution provide intriguing models for studying phase transitions, *Physics Today*, **51**(12), 24–30
- J. J. Gilman (1975), Metallic glasses, *Physics Today*, **28**(5), 46–53.
- A. I. Goldman and R. F. Kelton (1993), Quasicrystals and crystalline approximants, *Reviews of Modern Physics*, **65**, 213–230.
- P. Haasen (1996), *Physical Metallurgy*, 3rd ed., Cambridge University Press, Cambridge.
- T. C. Hales (1997), Sphere packings I, *Discrete Computational Geometry*, **17**, 1–51.
- T. C. Hales (2005), A proof of the kepler conjecture, *Annals of Mathematics. Second Series.*, **162**, 1065–1185.
- M. Hansen (1958), *Constitution of Binary Alloys*, 2nd ed., McGraw-Hill, New York.
- D. R. Huffman (1991), Solid C₆₀, *Physics Today*, **44**(11), 22–29.
- S. Ijima (1991), ??, *Nature*, **354**, 56–??
- A. Ishimaru (1978), *Wave Propagation and Scattering in Random Media*, Academic Press, New York.
- H. M. Jaeger, S. R. Nagel, and R. P. Behringer (1996), The physics of granular materials, *Physics Today*, **49**(4), 32–38.
- C. Janot (1992), *Quasicrystals: A Primer*, Clarendon Press, Oxford.
- L. P. Kadanoff (1999), Built upon sand: Theoretical ideas inspired by granular flows, *Reviews of Modern Physics*, **71**(1), 435–444.
- F. J. Kahn (1982), The molecular physics of liquid-crystal devices, *Physics Today*, **35**(5), 66–74.
- K. F. Kelton (1991), Crystal nucleation in liquids and glasses, *Solid State Physics: Advances in Research and Applications*, **45**, 75–177.
- A. J. Koch and H. Meinhardt (1994), Biological pattern formation: From basic mechanisms to complex structures, *Reviews of Modern Physics*, **66**, 1481–1507.
- A. R. Kortan (1996), Quasicrystals, in *Encyclopedia of Applied Physics*, G. L. Trigg, ed., vol. 15, VCH, New York.
- L. D. Landau and E. M. Lifshitz (1980), *Statistical Physics, Part 1*, 3rd ed., Pergamon Press, Oxford.
- J. S. Langer (1980), Instabilities and pattern formation in crystal growth, *Reviews of Modern Physics*, **52**, 1–28.
- J. S. Lannin (1988), Local structural order in amorphous semiconductors, *Physics Today*, **41**(7), 28–35.
- D. Levine and P. J. Steinhardt (1984), Quasicrystals: A new class of ordered structures, *Physical Review Letters*, **53**, 2477–2480.
- I. M. Lifshitz, A. Y. Grosberg, and A. R. Khokhlov (1978), Some problems of the statistical physics of polymer chains with volume interaction, *Reviews of Modern Physics*, **50**, 683–713.
- I. M. Lifshitz and V. V. Slyozov (1961), ??, *Journal of the Physics and Chemistry of Solids*, **19**, 35–??
- A. J. Liu and S. R. Nagel, eds. (2001), *Jamming and Rheology*, Taylor and Francis, London and New York.
- T. B. Massalski (1990), *Binary Alloy Phase Diagrams*, 2nd ed., William W. Scott Jr., Materials Park, Ohio.
- M. Menon and S. R. Nagel (1995), Evidence for a divergent susceptibility at the glass transition, *Physical Review Letters*, **74**, 1230–1233.
- N. D. Mermin (1992), The space groups of icosahedral quasicrystals and cubic, orthorhombic, monoclinic and triclinic crystals, *Reviews of Modern Physics*, **64**, 3–49.
- D. R. Nelson and F. Spaepen (1989), Polytetrahedral order in condensed matter, *Solid State Physics: Advances in Research and Applications*, **42**, 1–90.
- K. S. Novoselov, A. K. Geim, S. V. Morozov, D. Jiang, Y. Zhang, S. V. Dubonos, I. V. Grigorievna, and A. A. Firsov (2004), Electric field effect in atomically thin carbon films, *Science*, **306**, 666–669.

- L. Pauling (1985), Apparent icosahedral symmetry is due to directed multiple twinning of cubic crystals, *Nature*, **317**, 512–514
- J. H. Perepezko and G. Wilde (1998), Alloy metastability during nucleation-controlled reactions, *Berichte der Bunsen Gesellschaft für Physikalische Chemie*, **102**, 1074–1082.
- J. Perrin (1909), Mouvement brownien et réalité moléculaire, *Annales de chimie et de physique*, **8th series**, **18**, 5–114.
- J. C. Phillips (1982a), The physics of glass, *Physics Today*, **35**(2), 27–35.
- J. C. Phillips (1982b), Spectroscopic and morphological structure of tetrahedral oxide glasses, *Solid State Physics: Advances in Research and Applications*, **37**, 93–171.
- D. A. Rabson, N. D. Mermin, D. S. Rokhsar, and D. C. Wright (1991), The space groups of axial crystals and quasicrystals, *Reviews of Modern Physics*, **63**, 699–733.
- D. C. Rapaport (1995), *The Art of Molecular Dynamics Simulation*, Cambridge University Press, Cambridge.
- D. H. Rothman and S. Zaleski (1994), Lattice-gas models of phase separation: Interfaces, phase transitions and multiphase flow, *Reviews of Modern Physics*, **66**, 1417–1479.
- D. Shechtman, I. Blech, D. Gratias, and J. W. Cahn (1984), Metallic phase with long-range orientational order and no translational symmetry, *Physical Review Letters*, **53**, 1951–1953.
- R. E. Smalley (1997), Discovering the fullerenes, *Reviews of Modern Physics*, **69**, 723–730.
- F. Spaepen (1994), Homogeneous nucleation and the temperature dependence of the crystal-melt interfacial tension, *Solid State Physics: Advances in Research and Applications*, **47**, 1–32.
- M. J. Stephen and J. P. Straley (1974), Physics of liquid crystals, *Reviews of Modern Physics*, **46**, 617–704.
- K. Triantafyllopoulos (2003), On the central moments of the multidimensional Gaussian distribution, *The Mathematical Scientist*, **28**, 125–128.
- C. Vega, C. McBride, E. Sanz, and J. L. F. Abascal (2005), Radial distribution functions and densities for the SPC/E, TIP4P and TIP5P models for liquid water and ices I_h, I_c, II, III, IV, V, VI, VII, VIII, IX, XI and XII, *Physical Chemistry and Chemical Physics*, **7**, 1450 – 1456.
- L. Verlet (1967), Computer ‘experiments’ on classical fluids. I. Thermodynamical properties of Lennard-Jones molecules, *Physical Review*, **159**, 98–103.
- Y. Waseda (1980), *The Structure of Non-Crystalline Materials : Liquids and Amorphous Solids*, McGraw-Hill, New York.
- D. Weaire and S. McMurry (1997), Some fundamentals of grain growth, *Solid State Physics: Advances in Research and Applications*, **50**, 1–36.
- J. H. Weaver and D. M. Poirier (1994), Solid state properties of fullerenes and fullerene-based materials, *Solid State Physics: Advances in Research and Applications*, **48**, 1–108.
- D. A. Weitz and D. J. Pine (1993), Diffusing-wave spectroscopy, in *Dynamic Light Scattering: the Method and Some Applications*, W. Brown, ed., Clarendon, Oxford.
- R. Winter, P. A. Egelstaff, W.-C. Pilgrim, and W. S. Howells (1990), The structural properties of liquid, solid and amorphous sulphur, *Journal of Physics: Condensed Matter*, **2**, SA215–SA218.
- T. A. Witten (1990), Structured fluids, *Physics Today*, **43**(7), 21–28.
- F. Wooten and D. Weaire (1987), Modeling tetrahedrally bonded random networks by computer, *Solid State Physics: Advances in Research and Applications*, **40**, 1–42.
- D. C. Wright and N. D. Mermin (1989), Crystalline liquids: The blue phases, *Reviews of Modern Physics*, **61**, 385–432.
- D. T. Wu (1997), Nucleation theory, *Solid State Physics: Advances in Research and Applications*, **50**, 37–187.
- F. Yonezawa (1991), Glass transition and relaxation of disordered structures, *Solid State Physics: Advances in Research and Applications*, **45**, 179–254.
- W. H. Zachariasen (1932), The atomic arrangement in glass, *Journal of the American Chemical Society*, **54**, 3841–3851.

R. Zallen (1983), *Physics of Amorphous Solids*, John Wiley and Sons, New York.

J. M. Ziman (1979), *Models of Disorder : The Theoretical Physics of Homogeneously Disordered Systems*, Cambridge University Press, Cambridge.

Part II

ELECTRONIC STRUCTURE

6. The Free Fermi Gas and Single Electron Model

6.1 Introduction

Much of condensed matter physics lies within a Hamiltonian that one easily can write down in a single line. It is

$$\hat{\mathcal{H}} = \sum_l \frac{\hat{P}_l^2}{2M_l} + \frac{1}{2} \sum_{l \neq l'} \frac{q_l q_{l'}}{|\hat{R}_l - \hat{R}_{l'}|}. \quad (6.1)$$

The sum ranges over all electrons and nuclei in a solid; M_l is the mass of an electron or nucleus, and q_l is its charge. The simplicity is deceptive. Equation (6.1) can be attacked directly by computer for little more than 10 to 20 particles. Dealing with the 10^{23} particles in actual solids requires a series of approximations, few of which are particularly well controlled. One has to replace the original equations with simpler ones, not always possible to justify, but capturing essential features of the system. A number of these approximations is indicated in Figure 6.1. In the study of electronic structure about to begin, the goal will be to start at the lower left hand side of the sketch and work back up toward the top.

Since Eq. (6.1) so completely intractable in its original form as to be almost useless, progress comes about by posing and solving a series of *model problems*. In these model problems, one makes drastic simplifications that make it possible to solve the resulting equations analytically or numerically. The arbiter of success is partly comparison with experiment, and partly the ability to gain qualitative insights. There is now more than 70 years' experience with approximation schemes, and their strengths and weaknesses are fairly well understood.

The simplest model of a metal is the *free Fermi gas*. In this model, the Coulomb interactions between electrons and electrons and electrons and nuclei are all turned off. One considers a collection of electrons moving freely around in a box, and the only nontrivial aspect of reality to be maintained is the Pauli exclusion principle. In applying this model to a metal, one considers just a subset of the material's electrons, the *conduction electrons*. The free Fermi gas model captures the features of some metals remarkably well, particularly the alkali metals such as sodium. It simply cannot be employed for any solid that happens to be an insulator or a magnet.

Some important features of the solution of the free Fermi gas do not depend upon details of the solution. They depend upon the fact that energy of the system of electrons can be written as the sum of energies of individual noninteracting

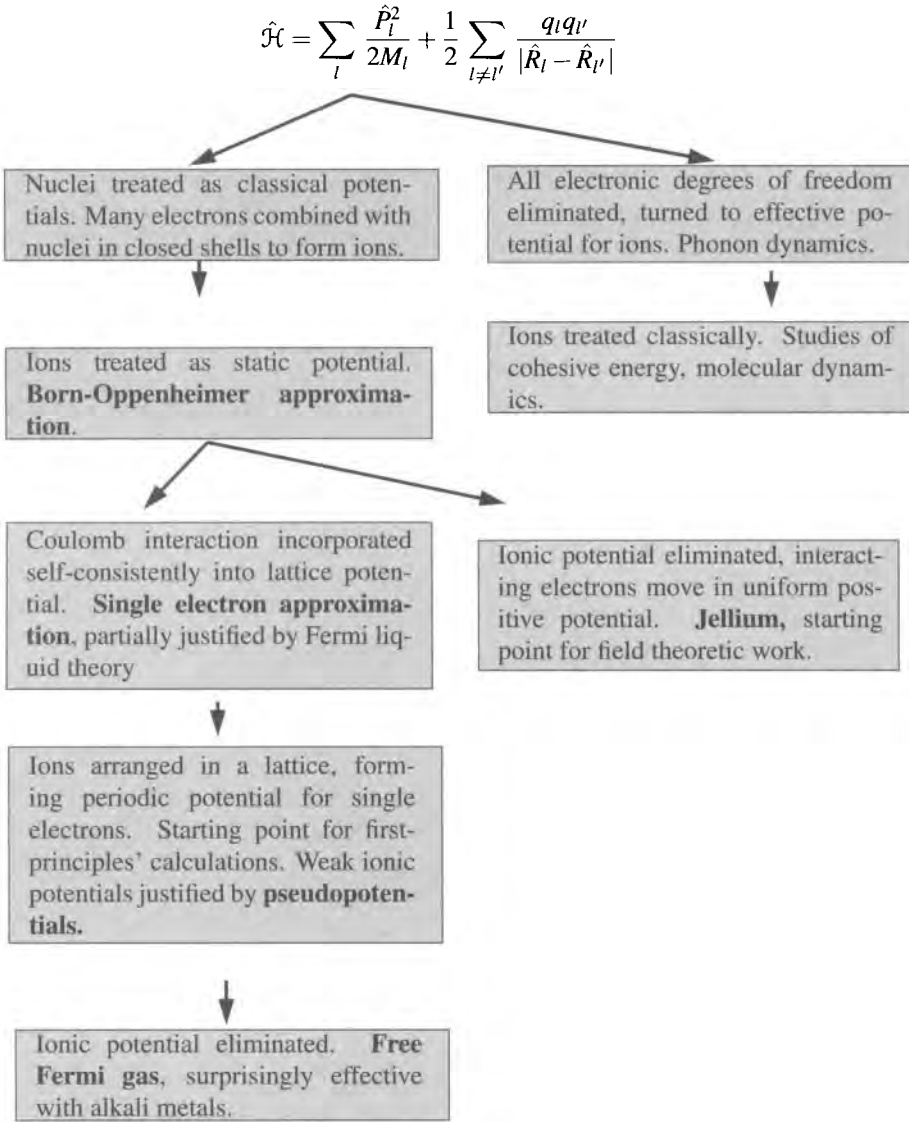


Figure 6.1. Some of the approximations used to make Eq. (6.1) tractable.

electrons. Thus some of the results can quickly be extended to the more general *single electron model*.

The Pauli principle alone is able to resolve the main paradox in the electron theory of solids prior to quantum mechanics. The problem was pointed out by Thomson (1907), and it occurs in trying to account for the specific heat of silver. Silver has one conduction electron per atom, leading to $6 \cdot 10^{22}$ electrons cm^{-3} . Thomson overestimated this number by a factor of 100, partly because his measurements of the charge on the electron were several times greater than the correct values to be obtained by Millikan (1913) several years later, but the conclusions he drew still correctly captured the difficulty. The equipartition of energy should

contribute $k_B T/2$ to the mean energy for each of the three kinetic and potential degrees of freedom for the free electrons plus another $3k_B T$ for the nuclei of the atoms, leading to a specific heat of $c_V = 6nk_B = 1.19 \text{ cal cm}^{-3} \text{ K}^{-1}$. The experimental specific heat is, however, half this value, as if the electrons are somehow immune to the demands of statistical mechanics. Thomson concluded that “ We thus get to a contradiction. The value of the specific heats of the metals shows that the corpuscles [electrons] cannot exceed a certain number, but this number is far too small to produce the observed conductivities...” [Thomson (1907), p. 85] The resolution of the contradiction was not found for 20 years, and lies (as explained below) in the fact that only a tiny fraction of the electrons is permitted by the Pauli principle to participate in the process of absorbing energy.

The free Fermi gas and single electron models are such a crude approximations that it may seem silly to study them at all. Two ideas eventually explained why even the free Fermi gas can have great quantitative success for some metals. Neglect of the periodic potential generated by the lattice of ions is justified by the *pseudopotential* (Section 10.2.1), which shows how a redefinition of the electrons' wave functions turns them into particles interacting with weak potentials. Neglect of the interactions of electrons with one another is justified by the idea of the *Fermi liquid* (Section 17.5), which shows that properly chosen linear combinations of electron states behave like noninteracting particles. But these ideas ultimately provide only partial justification for approximation schemes, so there is no choice but to suspend disbelief and begin to calculate.

6.2 Starting Hamiltonian

The *single-electron model* is defined by the Hamiltonian

$$\hat{\mathcal{H}}\Psi = \sum_{l=1}^N \left(\frac{-\hbar^2 \nabla_l^2}{2m} + U(\vec{r}_l) \right) \Psi(\vec{r}_1 \dots \vec{r}_N) = \mathcal{E} \Psi(\vec{r}_1 \dots \vec{r}_N). \quad (6.2)$$

It describes N conduction electrons, each of which interacts with an external potential U but does not interact with the other conduction electrons. Equation (6.2) is called the single-electron model because if one finds the eigenfunctions $\psi_l(\vec{r}_l)$ for single electrons, obeying

$$\left(\frac{-\hbar^2 \nabla^2}{2m} + U(\vec{r}) \right) \psi_l(\vec{r}) = \mathcal{E}_l \psi_l(\vec{r}), \quad (6.3)$$

then the eigenfunctions describing many particles are simply obtained from products of the one-particle functions. The energy of the many-electron system is just a sum of the energies of the one-electron functions that make it up (Problem 1).

That is, although the equation can be used to study large numbers of electrons, their properties can be obtained one electron at a time.

Writing down Eq. (6.2) requires severe approximations outlined in Figure 6.1. However for a general potential U it is still impossible to solve in general. To start

making progress, throw away the potential U too. The *free Fermi gas*, is described by

$$\frac{-\hbar^2}{2m} \sum_{l=1}^N \nabla_l^2 \Psi(\vec{r}_1 \dots \vec{r}_N) = \mathcal{E} \Psi(\vec{r}_1 \dots \vec{r}_N). \quad (6.4)$$

It describes N conduction electrons, interacting neither with nuclei nor each other. The eigenvalues and eigenfunctions of this Hamiltonian can be found exactly.

No differential equation is completely specified without naming its boundary conditions. A natural choice would be to take Ψ to vanish whenever any of its arguments reaches the boundaries of the system, but this choice is not convenient for calculations. Instead, one conventionally chooses a square box of side length L , $L^3 = \mathcal{V}$ and imposes *periodic boundary conditions*;

$$\begin{aligned} \Psi(x_1 + L, y_1, z_1 \dots, z_N) &= \Psi(x_1, y_1, z_1 \dots z_N) \\ \Psi(x_1, y_1 + L, z_1 \dots, z_N) &= \Psi(x_1, y_1, z_1 \dots z_N) \\ &\cdot \\ &\cdot \\ &\cdot \end{aligned} \quad \begin{array}{l} \text{This boundary condition is what one obtains} \\ \text{by demanding that the system repeat indef-} \\ \text{initely with period } L \text{ along the } x, y, \text{ and } z \\ \text{directions.} \end{array} \quad (6.5)$$

This mathematical condition cannot possibly be realized experimentally. However, almost any physical quantity one might calculate using Eq. (6.5) alters at most by an amount proportional to $1/L$ if one adopts more realistic boundary conditions. So long as L is macroscopic, such corrections are negligible. It is sufficient to impose *some* condition on the wave function at the system boundaries.

One Free Fermion. For the free Fermi gas, obeying Eq. (6.4), one can find the one-electron solutions explicitly. Eigenstates of (6.3) are all of the form

$$\psi_{\vec{k}} = \frac{1}{\sqrt{\mathcal{V}}} e^{i\vec{k} \cdot \vec{r}} \quad \begin{array}{l} \text{Because of the factor of } 1/\sqrt{\mathcal{V}}, \text{ this function} \\ \text{is normalized.} \end{array} \quad (6.6)$$

with \vec{k} of the form

$$\vec{k} = \frac{2\pi}{L} (l_x, l_y, l_z). \quad (6.7)$$

$l_x, l_y,$ and l_z are integers ranging from $-\infty$ to ∞ . Only if \vec{k} is chosen in this way will a function of the form Eq. (6.6) satisfy the boundary condition Eq. (6.5). This enumeration of allowed values of \vec{k} is more general than may now appear and it will survive unchanged when electrons interact with periodic potentials.

The eigenvalue corresponding to the eigenfunction (6.6) is

$$\mathcal{E}_{\vec{k}}^0 = \frac{\hbar^2 k^2}{2m} \quad \begin{array}{l} \text{Simply insert Eq. (6.6) into Eq. (6.4). Setting} \\ \hbar k = p = mv, \text{ the energy is just } \frac{1}{2} mv^2. \end{array} \quad (6.8)$$

Ground States of Many Free Fermions. The ground state of electrons obeying Eq. (6.4) is constructed from products of the one-electron wave functions (6.6). The *Pauli exclusion principle* forbids any given state from being occupied more than once, and therefore any given state indexed by \vec{k} is able to host no more than two electrons, one for each value of spin.

The ground state of N electrons is built by first putting two electrons into the single-particle state of lowest energy, which is $|\vec{k}| = 0$. Next one puts electrons two at a time into all the states with $|\vec{k}| = 2\pi/L$, and so on. The early stages of this process are the subject of Problem 6.2. Because the energy Eq. (6.8) increases with k , as one keeps adding electrons, one always wants to fill states with the lowest available values of \mathcal{E}_k^0 . Since \mathcal{E}_k^0 is proportional to k^2 , this means that successive electrons get added to the ground state in successive spherical shells.

Define the *occupation number* $f_{\vec{k}}$ of a state indexed by \vec{k} to be 1 if this one-electron state is part of the ground state, and 0 otherwise. For a large number N of electrons, the ground state corresponds to setting the occupation number $f_{\vec{k}}$ of all states with k less than a certain wave vector k_F , the *Fermi wave vector*, to 1 and setting all others to 0. That is, the ground state is built out of one-electron wave functions occupying a sphere in k -space, as shown in Figure 6.2. Naturally, one wants to relate the number of electrons within the *Fermi sphere* to the value of k_F , and for this purpose it is necessary to recall Eq. (6.7) and analyze it more closely.

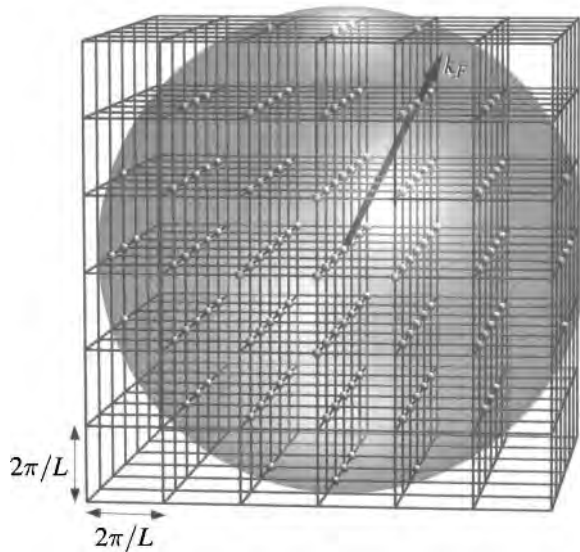


Figure 6.2. The ground state of the free electron gas is constructed by occupying vertices in a cubic grid of states that approximate a sphere of radius k_F in k space. Any other shape would miss opportunities to put electrons as close as possible to the origin in k space, and thus would not minimize the total energy.

6.3 Densities of States

The \vec{k} states described by Eq. (6.7) occupy a cubic lattice in \vec{k} space, also called *reciprocal space*, with neighboring points separated by distances of $2\pi/L$, as shown in Figure 6.2. One can draw a Wigner–Seitz cell around each of these points and can see as a result that the volume of the region of reciprocal space associated with \vec{k} in this way is $(2\pi/L)^3$. Not only is this statement true for the free Fermi

gas, it is also true, as shown in Chapter 7, for electrons moving in general periodic potentials, and as shown in Chapter 13 for phonons. Therefore, all the terminology developed in this section to keep track of k states will recur constantly throughout the remainder of this volume, and the densities of states D defined here will have broad physical significance.

In order to calculate the total number of electrons N , or their energy \mathcal{E} , or any other thermodynamic quantity, one needs to carry out sums of the type

$$\sum_{\vec{k}} F_{\vec{k}}, \quad (6.9)$$

where F is some function of wave vector \vec{k} , with the \vec{k} vectors summed over values allowed by (6.7). Mathematical convenience requests that one convert these sums into integrals over a continuous function $F_{\vec{k}}$. Integration is defined by partitioning space into a large number of volume elements and summing a function over these elements, multiplied by the volume of each one. Because each \vec{k} point is associated with a volume $(2\pi/L)^3$, one obtains

$$\int d\vec{k} F_{\vec{k}} = \sum_{\vec{k}} \left(\frac{2\pi}{L}\right)^3 F_{\vec{k}} \quad \text{This expression constitutes a long wavelength approximation that is only accurate if } F_{\vec{k}} \text{ varies slowly from one } \vec{k} \text{ to its neighbor, a condition that usually obtains in practice.} \quad (6.10)$$

$$\Rightarrow \sum_{\vec{k}} F_{\vec{k}} = \frac{\mathcal{V}}{(2\pi)^3} \int d\vec{k} F_{\vec{k}}. \quad \text{Recall } \mathcal{V} = L^3. \text{ Although this formula has only been derived for large volumes in the shape of a cube, it can be proved to hold for large volumes of arbitrary shape.} \quad (6.11)$$

On some occasions, the function $F_{\vec{k}}$ may involve a delta function, such as $\delta_{\vec{k}\vec{q}}$. Viewed as a function of a continuous variable, this function clearly transforms into some multiple of $\delta(\vec{k} - \vec{q})$. In order to remain consistent with Eq. (6.11), the correspondence must be

$$\delta_{\vec{k}\vec{q}} \rightarrow \frac{(2\pi)^3}{\mathcal{V}} \delta(\vec{k} - \vec{q}). \quad \text{Only in this way do both sides of Eq. (6.11) equal 1 when these delta function are inserted for } F_{\vec{k}}. \quad (6.12)$$

6.3.1 Definition of Density of States D

The sum in Eq. (6.11) is over all wave vectors allowed for free electrons. Because for each wave vector Pauli's exclusion principle allows two electrons, one with spin up and the other with spin down, it is conventional to define the *density of electronic states*, also sometimes called the *density of levels*

$$D_{\vec{k}} = 2 \frac{1}{(2\pi)^3}, \quad \text{The factor of 2 accounts for spin.} \quad (6.13)$$

which is defined to be the quantity allowing one to write

$$\sum_{\vec{k}\sigma} F_{\vec{k}} = \mathcal{V} \int d\vec{k} D_{\vec{k}} F_{\vec{k}}. \quad (6.14)$$

To avoid perpetually writing $D_{\vec{k}}$, which does not even depend upon \vec{k} , the notation

$$\int [d\vec{k}] \equiv \frac{2}{V} \sum_{\vec{k}} = \int d\vec{k} D_{\vec{k}} = \frac{2}{(2\pi)^3} \int d\vec{k} \quad (6.15)$$

will be adopted in the equations that follow.

Energy Density of States. Several separate functions D are all referred to as densities of states. They are distinguished by their arguments. The most important is $D(\mathcal{E})$, the *energy density of states* which is useful in dealing with sums over functions that depend upon \vec{k} only through an energy function $\mathcal{E}_{\vec{k}}$, such as

$$\sum_{\vec{k}\sigma} F(\mathcal{E}_{\vec{k}}) = V \int d\mathcal{E} D(\mathcal{E}) F(\mathcal{E}) . \quad \text{Electrons in periodic potentials will differ from their free-electron counterparts largely because the energy } \mathcal{E}_{\vec{k}} \text{ will differ from the free-electron value given by Eq. (6.8). This definition looks ahead to that possibility.} \quad (6.16)$$

To find $D(\mathcal{E})$, note that

$$\sum_{\vec{k}\sigma} F(\mathcal{E}_{\vec{k}}) = V \int [d\vec{k}] F(\mathcal{E}_{\vec{k}}) \quad \text{First use of Eq. (6.15).} \quad (6.17)$$

$$= V \int d\mathcal{E} \int [d\vec{k}] \delta(\mathcal{E} - \mathcal{E}_{\vec{k}}) F(\mathcal{E}) \quad \text{Integrating the } \delta \text{ function with respect to } \mathcal{E} \text{ just produces 1. However, if one chooses to integrate with respect to } \vec{k} \text{ first, something new comes out.} \quad (6.18)$$

$$\Rightarrow D(\mathcal{E}) = \int [d\vec{k}] \delta(\mathcal{E} - \mathcal{E}_{\vec{k}}) . \quad \text{Obtained by comparing Eq. (6.16) with (6.18).} \quad (6.19)$$

The units of densities of states are able to change without much warning. Often they are expressed in units of $1/[\text{eV atom}]$, which means they are related to the function defined by Eq. (6.19) by a factor of density n .

6.3.2 Results for Free Electrons

For the free Fermi gas, one has that

$$D(\mathcal{E}) = \int [d\vec{k}] \delta(\mathcal{E} - \mathcal{E}_{\vec{k}}^0) \quad \text{Use Eq. (6.15), then switch to polar coordinates in } \vec{k} \text{ space to do the} \quad (6.20)$$

$$= 4\pi \frac{2}{(2\pi)^3} \int_0^\infty dk k^2 \delta(\mathcal{E} - \mathcal{E}_{\vec{k}}^0) \quad \text{integral, because } \mathcal{E}_{\vec{k}}^0 \text{ depends upon the} \quad (6.21)$$

$$= \frac{1}{\pi^2} \int_0^\infty \frac{d\mathcal{E}^0}{|d\mathcal{E}^0/dk|} \frac{2m\mathcal{E}^0}{\hbar^2} \delta(\mathcal{E} - \mathcal{E}^0) \quad \text{Use Eq. (6.8) to express } k \text{ in terms of} \quad (6.22)$$

$$= \frac{m}{\hbar^3 \pi^2} \sqrt{2m\mathcal{E}} \quad (6.23)$$

$$= 6.812 \cdot 10^{21} \sqrt{\mathcal{E}/\text{eV}} \text{ eV}^{-1} \text{ cm}^{-3} . \quad \text{From Eq. (6.8) one has } d\mathcal{E}^0/dk = \hbar^2 k/m; \text{ then use Eq. (6.8) again to write } k \text{ in terms of } \mathcal{E}. \quad (6.24)$$

The number of electrons that can fit into a sphere of radius k_F is

$$N = \sum_{\vec{k}\sigma} f_{\vec{k}} \quad \text{Because } f_{\vec{k}} \text{ is 1 only if the state is occupied.} \quad (6.25)$$

$$= \mathcal{V} \int [d\vec{k}] f_{\vec{k}}, \quad \text{Application of Eq. (6.11)} \quad (6.26)$$

$$= \mathcal{V} \int [d\vec{k}] \theta(k_F - k) \quad \begin{array}{l} \text{Because the occupation number vanishes for} \\ \text{\(k > k_F\). } \theta \text{ is a Heaviside step function that} \\ \text{vanishes when its argument is less than 0 and} \\ \text{is 1 otherwise.} \end{array} \quad (6.27)$$

$$= \frac{\mathcal{V}}{4\pi^3} \frac{4\pi}{3} k_F^3 = \frac{\mathcal{V} k_F^3}{3\pi^2}, \quad \begin{array}{l} \text{Using the formula for the volume of a sphere,} \\ \text{and Eq. (6.15).} \end{array} \quad (6.28)$$

which implies that the Fermi wave vector is related to the density of electrons $n = N/\mathcal{V}$ by

$$k_F = (3\pi^2 n)^{1/3} = 3.09 [n \cdot \text{\AA}^3]^{1/3} \text{\AA}^{-1}. \quad (6.29)$$

The density of electrons is sometimes described by finding the volume per electron \mathcal{V}/N and defining the free-electron sphere to be one with the same volume, so that

$$\frac{4\pi}{3} r_s^3 \equiv \frac{\mathcal{V}}{N} \Rightarrow r_s = \left[\frac{3}{4\pi} \frac{\mathcal{V}}{N} \right]^{1/3}. \quad (6.30)$$

The energy of electrons in the most energetic occupied state is called the *Fermi energy* or *Fermi level* and denoted by

$$\mathcal{E}_F = \frac{\hbar^2 k_F^2}{2m} = 36.46 [n \cdot \text{\AA}^3]^{2/3} \text{eV}. \quad (6.31)$$

The *Fermi surface* is the collection of \vec{k} such that electrons with wave number \vec{k} have energy \mathcal{E}_F . Finally, the *Fermi velocity* is defined to be

$$v_F = \hbar k_F / m = 3.58 [n \cdot \text{\AA}^3]^{1/3} \cdot 10^8 \text{ cm s}^{-1}. \quad (6.32)$$

The density of states $D(\mathcal{E})$ has broad physical significance. Usually, it is not the whole function that is important, but just $D(\mathcal{E}_F)$, the *density of states at the Fermi surface*. Almost every electronic transport property of a solid will be proportional to $D(\mathcal{E}_F)$, whether it be the ability of electrons to absorb heat, or their response to applied electric fields. Electrons lying far in energy below the Fermi surface cannot contribute to transport properties, because all states around them are occupied, and if they cannot change their state, they cannot respond to perturbations. States far above the Fermi surface are not occupied at low temperatures and cannot play any role in responding to external fields. The electron number density right at the Fermi surface is therefore the crucial quantity to determine. For the free Fermi gas, one gets the result

$$D(\mathcal{E}_F) = \frac{3}{2} \frac{n}{\mathcal{E}_F} = 4.11 \cdot 10^{-2} [n \cdot \text{\AA}^3] \text{eV}^{-1} \text{\AA}^{-3}. \quad (6.33)$$

$$\text{Note that } n = \int_0^{\mathcal{E}_F} d\mathcal{E} D(\mathcal{E}) = \int_0^{\mathcal{E}_F} d\mathcal{E} D(\mathcal{E}_F) \sqrt{\mathcal{E}/\mathcal{E}_F}.$$

One- and Two-Dimensional Formulae. Both because certain types of calculations are simpler in one and two dimensions and because techniques associated with microfabrication make it possible to construct experimental systems that are effectively one- and two-dimensional, it is useful to have corresponding formulae for other dimensions. The general expression for density of electron states in d dimensions is

$$D_{\vec{k}} = 2\left(\frac{1}{2\pi}\right)^d. \quad (6.34)$$

In two dimensions, the density of energy states is

$$D(\mathcal{E}) = \frac{m}{\pi\hbar^2}, \quad (6.35)$$

while the density of energy states in one dimension is

$$D(\mathcal{E}) = \sqrt{\frac{2m}{\pi^2\hbar^2\mathcal{E}}}. \quad (6.36)$$

Problems 4 and 7 derive Eqs. (6.35) and (6.36) and extend them to arbitrary dimensions.

General Ground States for Noninteracting Electrons. The ground states of collections of electrons obeying Eq. (6.2) can be constructed in a manner analogous to that used for the free Fermi gas. Order the energies of the one electron states so that

$$\mathcal{E}_0 \leq \mathcal{E}_1 \leq \mathcal{E}_2 \dots \quad \text{These are the energies appearing in Eq. (6.3). For the free Fermi gas,} \quad (6.37)$$

the energies would be $\mathcal{E}_{\vec{k}}^0$, with \vec{k} ranging over all allowed values and each energy appearing twice to account for spin.

The ground state for N electrons is built out of electrons occupying energy levels $\mathcal{E}_0 \dots \mathcal{E}_N$. The most energetic occupied level is still called the Fermi energy. The energy density of states $D(\mathcal{E})$ remains defined as the number of single electron states $D(\mathcal{E})d\mathcal{E}$ to be found per volume in an energy range between \mathcal{E} and $\mathcal{E} + d\mathcal{E}$. When the potential U is periodic, it will be shown possible to index states by a wave vector \vec{k} as well, but for nonperiodic U such a description is usually impossible.

6.4 Statistical Mechanics of Noninteracting Electrons

A first example of the role played by $D(\mathcal{E}_F)$ in determining the response of electrons to outside influence is provided by calculating the specific heat of free electrons. To make this calculation possible, it is necessary to recall the statistical mechanics of noninteracting Fermi particles. This calculation also provides a way to obtain a quantitative criterion for when an ensemble of electrons behaves in a basically classical, as opposed to essentially quantum-mechanical, way. At sufficiently high temperatures or low densities, electrons are classical, but at room temperature and at the densities common in metals, quantum mechanical effects

are of fundamental importance. This calculation will be carried out for the general case of noninteracting electrons, not just the free Fermi gas.

The grand canonical partition function provides the most convenient formal means for studying this problem. Consider a volume \mathcal{V} in contact with a temperature reservoir, and with a reservoir of electrons, which flow in and out. The state of the electrons can completely be described by a collection of integers n_1, n_2, \dots , which equal zero or one and indicate for each of the quantum energy states in Eq. (6.37) whether the state is occupied or not. One can sum over all possible ways that electrons can inhabit the volume by summing over all possible values of all the integers n_l . So the grand partition function Z_{gr} is expressed as

$$Z_{\text{gr}} = \sum_{\text{states}} e^{\beta(\mu N - \mathcal{E})} \quad \text{This is the definition of the grand partition function. The symbol } \beta \text{ is } 1/k_B T, \text{ where } k_B \text{ is Boltzmann's constant and } T \text{ is the temperature.} \quad (6.38)$$

$$= \sum_{n_1=0}^1 \sum_{n_2=0}^1 \sum_{n_3=0}^1 \dots e^{\beta \sum_l n_l (\mu - \mathcal{E}_l)} \quad \text{The total number of particles } N = \sum_l n_l, \text{ and the total energy } \mathcal{E} \text{ is given by } \sum_l n_l \mathcal{E}_l. \quad (6.39)$$

Using the mathematical fact that

$$\sum_{n_1=0}^N \sum_{n_2=0}^N \dots \sum_{n_M=0}^N \prod_{l=1}^M A_{n_l} = \prod_{l=1}^M \left\{ \sum_{n_l=0}^N A_{n_l} \right\}, \quad \text{The identity follows by just asking what happens as one multiplies everything out on the right-hand side.} \quad (6.40)$$

one has that

$$Z_{\text{gr}} = \prod_l \left\{ \sum_{n_l=0}^1 e^{\beta n_l [\mu - \mathcal{E}_l]} \right\} \quad (6.41)$$

$$= \prod_l \left[1 + e^{\beta [\mu - \mathcal{E}_l]} \right]. \quad \text{The sum over each } n_l \text{ has just been carried out explicitly.} \quad (6.42)$$

Therefore the grand potential is given by

$$\Pi \equiv -k_B T \ln Z_{\text{gr}} \quad \text{See Landau and Lifshitz (1980), p. 108.} \quad (6.43)$$

$$= -k_B T \sum_l \ln \left[1 + e^{\beta [\mu - \mathcal{E}_l]} \right]. \quad (6.44)$$

$$= -k_B T \mathcal{V} \int d\mathcal{E} D(\mathcal{E}) \ln \left[1 + e^{\beta [\mu - \mathcal{E}]} \right]. \quad \text{Here is an example showing the utility of defining the density of states } D(\mathcal{E}). \quad (6.45)$$

Fermi Function. From the grand potential all other thermodynamic quantities can be obtained. For example, the average number of electrons N is given by

$$N = - \frac{\partial \Pi}{\partial \mu} \quad (6.46)$$

$$= \mathcal{V} \int d\mathcal{E}' D(\mathcal{E}') \frac{e^{\beta \mu - \beta \mathcal{E}'}}{1 + e^{\beta \mu - \beta \mathcal{E}'}} \quad \text{From Eq. (6.38), } N = k_B T \partial(Z_{\text{gr}}/\partial \mu)/Z_{\text{gr}}. \quad (6.47)$$

$$\Rightarrow n = \frac{N}{\mathcal{V}} = \int d\mathcal{E}' D(\mathcal{E}') f(\mathcal{E}'), \quad n \text{ is the density of conduction electrons.} \quad (6.48)$$

where

$$f(\mathcal{E}) = \frac{1}{e^{\beta(\mathcal{E}-\mu)} + 1} \tag{6.49}$$

is the *Fermi function*, or the *occupation probability*, and is depicted in Figure 6.3.

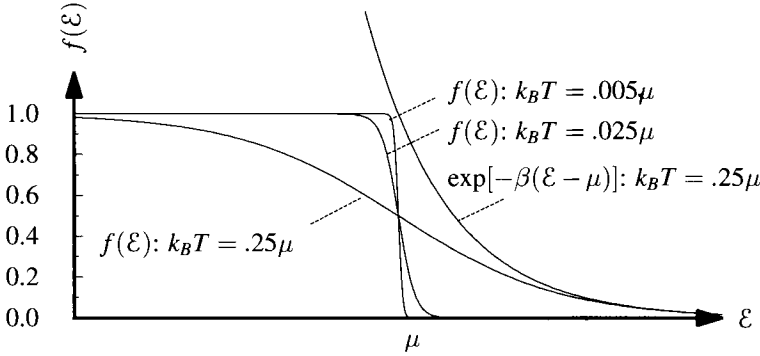


Figure 6.3. Sketch of the Fermi function $f(\mathcal{E})$ for various values of $k_B T$. At low temperatures it differs only slightly from a step function around μ ; the region in which the function differs appreciably from 0 or 1 is of width $k_B T$. For $\mathcal{E} \gg \mu$, the function rapidly becomes indistinguishable from a Boltzmann factor $\exp(-\beta\mathcal{E})$.

The function f gives the probability that the state of energy \mathcal{E} will be occupied in thermal equilibrium at temperature T . In cases where energy is indexed by wave vectors \vec{k} , the Fermi function can be viewed also as a function of \vec{k} :

$$f_{\vec{k}} = \frac{1}{e^{\beta(\mathcal{E}_{\vec{k}}-\mu)} + 1}. \tag{6.50}$$

Furthermore,

$$\frac{\partial \beta \Pi}{\partial \beta} \Big|_{\mu} = \mathcal{E} - \mu N \quad \text{Again, look back at Eq. (6.38). } \mathcal{E} \text{ is the total energy of the system.} \tag{6.51}$$

$$= \mathcal{V} \int d\mathcal{E}' D(\mathcal{E}') (\mathcal{E}' - \mu) f(\mathcal{E}') \tag{6.52}$$

$$\Rightarrow \frac{\mathcal{E}}{\mathcal{V}} = \int d\mathcal{E}' D(\mathcal{E}') \mathcal{E}' f(\mathcal{E}'). \tag{6.53}$$

Thus the total energy of the system is given by an integral over all states of the density of states times the occupation probability, times the energy of each state.

Classical Limit. Electrons are said to be in the classical limit when the probability that an energy state be occupied is given by a Boltzmann factor:

$$f(\mathcal{E}) = C e^{-\beta\mathcal{E}}. \quad \text{Here } C \text{ is some arbitrary constant.} \tag{6.54}$$

This limit obtains whenever

$$f(\mathcal{E}) \ll 1 \Rightarrow e^{\beta(\mathcal{E}-\mu)} \gg 1. \tag{6.55}$$

When conditions (6.55) apply for all conduction electrons up to the Fermi level, one says that *classical* or *Boltzmann statistics* apply and that the electrons are *non-degenerate*, because all the energy states are far from being doubly occupied. Otherwise one says that *Fermi*, or *Fermi–Dirac statistics* apply and that the electrons are *degenerate*. Thus, the larger and more positive μ becomes, the more pronounced are quantum effects; as μ increases, density increases, so the non-classical limit is associated with high densities and low temperatures.

As temperature heads toward zero one sees that

$$f(\mathcal{E}) \rightarrow \theta(\mu - \mathcal{E}). \quad \text{The } \theta \text{ function is zero when its argument is less than zero, and one otherwise.} \quad (6.56)$$

At very low temperatures all states are occupied below the critical energy μ and are unoccupied above it, the same conclusion that was reached in constructing the ground state of the many-electron system. At $T = 0$ the Fermi energy \mathcal{E}_F is equal to the chemical potential μ . This zero temperature limit is intrinsically quantum mechanical, because all states below the Fermi level have occupation number equal to 1, and conditions (6.55) are violated.

It is impossible to determine what “low” and “high” temperatures might correspond to without putting in numbers for real physical systems. One can pretend that metals are nothing but free-electron gases, use a conventional number of conduction electrons per atom and the known density of the various metals to compute k_F and \mathcal{E}_F for the metallic elements. The results appear in Table 6.1. One sees by consulting this table that Fermi energies are on the order of electron volts. In order for electrons to be excited with appreciable probability to such energies in a classical system, they would need to be at a temperature on the order of

$$T_F = \mathcal{E}_F/k_B, \quad (6.57)$$

where T_F is called the *Fermi temperature*. Fermi temperatures are on the order of 10 000 K and higher. Therefore, at room temperature, the electron gas in metals is at very low temperatures and is highly degenerate.

Indeed, the single most important fact about metals is that their conduction electrons form a highly degenerate Fermi gas. No subsequent elaborations of the theory will change this central conclusion.

6.5 Sommerfeld Expansion

The temperatures at which metals remain solid are low in comparison with typical Fermi temperatures, so it makes sense to work out a low temperature expansion for thermodynamic properties. This expansion is due to Sommerfeld (1928), and it makes use of the idea that at low temperatures electrons are only active within a small energy range, $k_B T$ of the Fermi energy. To understand why, consider, for example, the process of adding heat to a metal. As the temperature of a metal rises, the average energy of electrons in it must increase. This increase can only happen if electrons make transitions to higher energy states. Only right in the vicinity

Table 6.1. Properties of free-electron metals

Element	Z	n (10^{22} cm^{-3})	k_F (10^8 cm^{-1})	\mathcal{E}_F (eV)	T_F (10^4 K)	v_F (10^8 cm s^{-1})	r_s/a_0
Li	1	4.60	1.11	4.68	5.43	1.28	3.27
Na	1	2.54	0.91	3.15	3.66	1.05	3.99
K	1	1.32	0.73	2.04	2.37	0.85	4.95
Rb	1	1.08	0.68	1.78	2.06	0.79	5.30
Cs	1	0.85	0.63	1.52	1.76	0.73	5.75
Cu	1	8.49	1.36	7.04	8.17	1.57	2.67
Ag	1	5.86	1.20	5.50	6.38	1.39	3.02
Au	1	5.90	1.20	5.53	6.42	1.39	3.01
Be	2	24.72	1.94	14.36	16.67	2.25	1.87
Mg	2	8.62	1.37	7.11	8.26	1.58	2.65
Ca	2	4.66	1.11	4.72	5.48	1.29	3.26
Sr	2	3.49	1.01	3.89	4.52	1.17	3.59
Ba	2	3.15	0.98	3.64	4.22	1.13	3.71
Zn	2	13.13	1.57	9.42	10.93	1.82	2.31
Cd	2	9.26	1.40	7.47	8.66	1.62	2.59
Hg	2	16.22	1.69	10.84	12.59	1.95	2.15
Al	3	18.07	1.75	11.66	13.53	2.02	2.07
Ga	3	15.31	1.65	10.44	12.11	1.92	2.19
In	3	11.50	1.50	8.62	10.01	1.74	2.41
Sn	4	14.83	1.64	10.22	11.86	1.89	2.22
Pb	4	13.19	1.57	9.45	10.97	1.82	2.30
Sb	5	16.54	1.70	10.99	12.75	1.97	2.14
Bi	5	14.04	1.61	9.85	11.43	1.86	2.26
Mn	4	32.61	2.13	17.28	20.05	2.46	1.70
Fe	2	16.90	1.71	11.15	12.94	1.98	2.12
Co	2	18.18	1.75	11.70	13.58	2.03	2.07
Ni	2	18.26	1.76	11.74	13.62	2.03	2.07

Conduction electron density, Fermi wave vector, energy, temperature, Fermi velocity, and radius parameter r_s [Eq. (6.30)] in units of the Bohr radius, a_0 , for selected metallic elements computed by assigning each element a number of conduction electrons Z , and treating it as a free-electron gas. Densities are obtained from data of periodic table inside front cover, and are measured at 293 K. Assignments of Z to the four transition metals at end of table are conventional but not obvious.

of the Fermi energy are there both (a) an appreciable population of electrons and (b) vacant states of slightly higher energy to which they can move. The number of electron states is proportional to $D(\mathcal{E}_F)$, and the number of states that participate in the specific heat is proportional to T . Fermi statistics predicts that at low temperatures

$$c_V \propto TD(\mathcal{E}_F), \tag{6.58}$$

and in this way resolves the difficulty with specific heats noted by Thomson (1907).

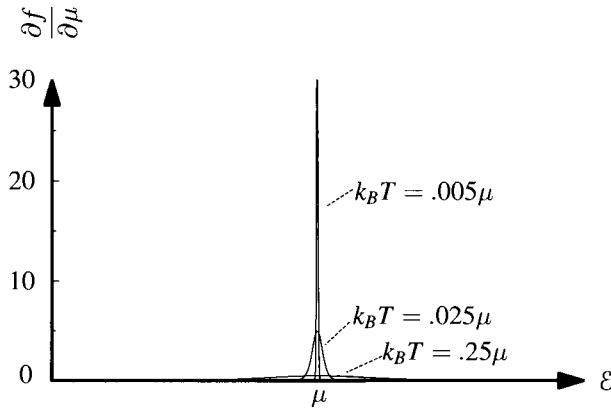


Figure 6.4. Sketch of the derivative of the Fermi function $\partial f(\mathcal{E})/\partial\mu$ for various values of $k_B T$. This function is only nonzero over an energy range of order $k_B T$ around the Fermi energy.

Formal Development. The formal development of this idea begins with a general scheme for calculating averages over Fermi functions. Suppose one has an average of the form

$$\langle H \rangle = \int_{-\infty}^{\infty} d\mathcal{E} H(\mathcal{E})f(\mathcal{E}). \quad \text{Here } f \text{ is the Fermi function, and } H \text{ is an arbitrary function of energy } \mathcal{E}. \tag{6.59}$$

Integrating by parts and assuming the integrand to vanish at the limits $\pm\infty$, one has

$$\langle H \rangle = \int_{-\infty}^{\infty} d\mathcal{E} \left[\int_{-\infty}^{\mathcal{E}} d\mathcal{E}' H(\mathcal{E}') \right] \left[\frac{\partial f}{\partial \mu} \right]. \tag{6.60}$$

Note that $-\partial f/\partial \mathcal{E} = \partial f/\partial \mu$. The crucial step in the formalism is to have $\partial f/\partial \mu$ appear inside the integrand. This function embodies the idea that the only active electrons are those within distance $k_B T$ of the Fermi surface, as shown in Figure 6.4. Now expand the first term in brackets about $\mathcal{E} = \mu$ to obtain the series

$$\langle H \rangle = \int_{-\infty}^{\mu} d\mathcal{E} H(\mathcal{E}) \quad \text{Terms with odd powers of } \mathcal{E} - \mu \text{ vanish by symmetry,} \tag{6.61}$$

since $\partial f/\partial \mu$ is an even function of $\mathcal{E} - \mu$.

$$+ \sum_{n=1}^{\infty} \left[\frac{d^{2n-1}}{d\mu^{2n-1}} H(\mu) \right] \int_{-\infty}^{\infty} d\mathcal{E} \frac{(\mathcal{E} - \mu)^{2n}}{(2n)!} \left[\frac{\partial f}{\partial \mu} \right] \tag{6.62}$$

$$= \int_{-\infty}^{\mu} d\mathcal{E} H(\mathcal{E}) + \sum_{n=1}^{\infty} a_n [k_B T]^{2n} \frac{d^{2n-1}}{d\mu^{2n-1}} H(\mu) \quad (6.63)$$

with

$$a_n = \int_{-\infty}^{\infty} dx \left[-\frac{\partial}{\partial x} \frac{1}{e^x + 1} \right] \frac{x^{2n}}{(2n)!} \quad (6.64)$$

$$= \frac{1}{(2n)!} \left(\frac{d}{db} \right)^{2n} \left[\frac{b\pi}{\sin b\pi} \right] \Big|_{b=0} \quad \text{Proving this relation is the subject of Problem 6.} \quad (6.65)$$

$$\Rightarrow \langle H \rangle = \int_{-\infty}^{\mu} d\mathcal{E} H(\mathcal{E}) \quad \text{One seldom needs any terms beyond } T^2. \text{ This expansion can be viewed as a power series in } k_B T / \mu, \text{ which at room temperature is } 1/40 \text{ or less.} \quad (6.66)$$

$$+ \frac{\pi^2}{6} [k_B T]^2 H'(\mu) + \frac{7\pi^4}{360} [k_B T]^4 H'''(\mu) + \dots \quad (6.67)$$

This formal expression for quantum-mechanical thermal averages at low temperatures is called the *Sommerfeld expansion*.

6.5.1 Specific Heat of Noninteracting Electrons at Low Temperatures

In order to find the specific heat, one can begin by finding the average energy \mathcal{E} of the electrons and then using the relation

$$c_V = \frac{1}{\mathcal{V}} \frac{\partial \mathcal{E}}{\partial T} \Big|_{N\mathcal{V}}. \quad \text{See Landau and Lifshitz (1980), p. 47.} \quad (6.68)$$

Using the energy density of states defined in Eq. (6.16), one has

$$\frac{\mathcal{E}}{\mathcal{V}} = \int d\mathcal{E}' f(\mathcal{E}') \mathcal{E}' D(\mathcal{E}') \quad (6.69)$$

$$= \int_0^{\mu} d\mathcal{E}' \mathcal{E}' D(\mathcal{E}') + \frac{\pi^2}{6} (k_B T)^2 \frac{d(\mu D(\mu))}{d\mu}. \quad \text{This is a straightforward application of Eq. (6.67), with } \mathcal{E}' D(\mathcal{E}') \text{ providing a specific form for } H(\mathcal{E}). \quad (6.70)$$

In order to proceed further one must find how the chemical potential behaves as a function of temperature. To accomplish this task, use the thermodynamic identity

$$\frac{\partial \mu}{\partial T} \Big|_{N\mathcal{V}} = - \frac{\frac{\partial N}{\partial T} \Big|_{\mu\mathcal{V}}}{\frac{\partial N}{\partial \mu} \Big|_{T\mathcal{V}}}. \quad (6.71)$$

One can evaluate the right hand side of Eq. (6.71) because, using Eq. (6.67) with $H(\mathcal{E}) = D(\mathcal{E})$, the number of electrons N is given by

$$N = \mathcal{V} \int d\mathcal{E}' f(\mathcal{E}') D(\mathcal{E}') = \mathcal{V} \int_0^{\mu} d\mathcal{E}' D(\mathcal{E}') + \mathcal{V} \frac{\pi^2}{6} (k_B T)^2 D'(\mu), \quad (6.72)$$

which gives that

$$\frac{\partial \mu}{\partial T} \Big|_{N\mathcal{V}} = - \frac{\pi^2}{3} k_B^2 T \frac{D'(\mu)}{D(\mu)}. \quad \text{There is an additional term that appears in the denominator of this expression, but it is proportional to } T^2 \text{ and therefore very small relative to the term being retained.} \quad (6.73)$$

When the temperature T equals zero, μ equals \mathcal{E}_F , the Fermi energy, so

$$\mu = \mathcal{E}_F - \frac{\pi^2}{6}(k_B T)^2 \frac{D'(\mathcal{E}_F)}{D(\mathcal{E}_F)}. \quad \text{This expression is valid to order } T^2. \quad (6.74)$$

Knowing that $\mu - \mathcal{E}_F$ is of order T^2 , one can now write to order T^2 that

$$\frac{\mathcal{E}}{\mathcal{V}} = \int_0^{\mathcal{E}_F} d\mathcal{E}' \mathcal{E}' D(\mathcal{E}') + \frac{\pi^2}{6}(k_B T)^2 D(\mathcal{E}_F) + \mathcal{E}_F \left\{ (\mu - \mathcal{E}_F) D(\mathcal{E}_F) + \frac{\pi^2}{6}(k_B T)^2 D'(\mathcal{E}_F) \right\} \quad (6.75)$$

One replaces μ in Eq. (6.70) using Eq. (6.74). Notice that μ appears as a limit of integration; here one writes $\mu = \mathcal{E}_F + (\mu - \mathcal{E}_F)$ and expands to first order in $\mu - \mathcal{E}_F$. The term in curly brackets vanishes because of Eq. (6.74).

$$\Rightarrow \frac{\mathcal{E}}{\mathcal{V}} = \int_0^{\mathcal{E}_F} d\mathcal{E} \mathcal{E} D(\mathcal{E}) + \frac{\pi^2}{6}(k_B T)^2 D(\mathcal{E}_F) \quad (6.76)$$

$$\Rightarrow c_V = \frac{\pi^2}{3} k_B^2 T D(\mathcal{E}_F). \quad \text{Using Eq. (6.68).} \quad (6.77)$$

Equation (6.77) shows as predicted by Eq. (6.58) that the specific heat is proportional to $D(\mathcal{E}_F)T$. The linear coefficient of the specific heat $\gamma \equiv c_V/T$ is called the *Sommerfeld parameter*, and it provides a measure of the density of states at the Fermi surface, \mathcal{E}_F .

Free Fermi Gas. It is worthwhile to evaluate the specific heat in the particular case of the free Fermi gas. Using Eq. (6.33) gives

$$\gamma \equiv \frac{c_V}{T} = \frac{\pi^2}{2} \left(\frac{k_B}{\mathcal{E}_F} \right) n k_B. \quad \text{Free Fermi gas only, with } n \text{ the density of conduction electrons from Table 6.1.} \quad (6.78)$$

It requires some foresight to compare Eq. (6.78) with experiment. The specific heat of a metal contains two major components. At room temperature, a solid absorbs heat mainly through the vibrations of ions about their equilibrium positions. However, these contributions vanish as T^3 at low temperatures [see Eq. (13.70)], and at temperatures on the order of 1 K, there is a linear contribution to the specific heat coming from electrons. Experimental data supporting this claim are displayed in Figure 13.11. In addition to predicting the scaling of specific heat with temperature, Eq. (6.78) gets the order of magnitude of the coefficient right for many metals, as shown in Table 6.2.

One way to express measured values of the specific heat is in terms of the *specific heat effective mass* of the electron. The idea behind the definition is that because the Fermi energy is inversely proportional to the mass of the electron, the specific heat shown in Eq. (6.78) is proportional to it. Therefore, one can account for specific heats deviating from (6.78) by pretending that the metals are built from *effective particles* whose mass differs from that of the electron.

This idea is a first example of what will be a common theme: using the conceptual apparatus of a simple model, with modified parameters, to understand more complicated cases.

There are metals in the periodic table for which the free-electron estimate of the specific heat is seriously in error; by a factor of 10 for iron, for example. The *heavy fermion* compounds such as UPt_3 or UPt_3 have low-temperature specific heats that differ by a factor as much as 1000 from the free-electron estimates. The reason for their anomalous behavior will be discussed in Section 26.6.1.

Table 6.2. Comparison of free-electron estimate of Sommerfeld parameter γ with experiment

Metal	Z	γ (mJ mole ⁻¹ K ⁻²)		Metal	Z	γ (mJ mole ⁻¹ K ⁻²)	
		Expt.	Eq. (6.78)			Expt.	Eq. (6.78)
Li	1	1.65	0.74	Al	3	1.35	0.91
Na	1	1.38	1.09	Ga	3	0.60	1.02
K	1	2.08	1.67	In	3	1.66	1.23
Rb	1	2.63	1.90	Sn	4	1.78	1.41
Cs	1	3.97	2.22	Pb	4	2.99	1.50
Cu	1	0.69	0.50	Sb	5	0.12	1.61
Ag	1	0.64	0.64	Bi	5	0.008	1.79
Au	1	0.69	0.64	Mn	2	12.8	1.10
Be	2	0.17	0.5	Fe	2	4.90	1.06
Mg	2	1.6	0.99	UPt_3	450		
Ca	2	2.73	1.51	UPt_3	1100		
Sr	2	3.64	1.79				
Ba	2	2.7	1.92				
Zn	2	0.64	0.75				
Cd	2	0.69	0.95				

Experimental results are obtained from an extrapolation to low temperatures assuming that $c_V/T \sim \gamma + \beta T^2$, as in Figure 13.11. The theoretical estimate uses electron densities n from Table 6.1. Data are presented for metals for which the comparison is fairly successful, for several metals for which it fails noticeably, and for heavy-fermion compounds for which it fails spectacularly. Source: Stewart (1983), and Stewart (1984).

Problems

1. Product wave functions:

(a) Show that a product of wave functions obeying Eq. (6.3),

$$\prod_{l=1}^N \psi_l(\vec{r}_l), \quad (6.79)$$

satisfies Eq. (6.2), and show that the energy \mathcal{E} is given by the sum of energies \mathcal{E}_l .

- (b) The wave function (6.79) is actually not acceptable for many electrons, because the Pauli principle demands that wave functions be antisymmetric under interchange of any two coordinates. The correct form of a wave function is

$$\Psi = \frac{1}{N!} \sum_s (-1)^s \prod_{l=1}^N \psi_{s_l}(\vec{r}_l), \quad (6.80)$$

where the sum over s denotes a sum over all the permutations of N integers, $(-1)^s$ gives the sign of the permutation, and s_l denotes entry l in the permutation. Verify that the energy of Ψ as given in Eq. (6.80) is the same as that found for (6.79).

2. **Ground states:** Consider a free Fermi gas with N electrons. Find the energy of the ground state of the gas as N varies from 1 through 15.
3. **Pressure:** Find the pressure of the ideal Fermi gas in three dimensions at zero temperature.
4. **Densities of states in low dimensions:** Find the density of k and energy states for an ideal noninteracting Fermi gas in one and two dimensions.
5. **Fermi pancakes:** Consider a thin layer of silver, 10^6 \AA wide and 10^6 \AA long along x and y .
 - (a) Take the layer to be 4.1 \AA thick along z . Treat the layer as a free Fermi gas, demanding that the wave function vanish at the boundaries along the z direction. Find the difference between the energies of the lowest- and highest-occupied single-particle states, and compare this difference to the bulk Fermi energy.
 - (b) Repeat the previous problem with a layer 8.2 \AA thick along z .
6. **Sommerfeld's integrals:** Prove Eq. (6.65).

- (a) Show that a_n may be rewritten as

$$a_n = \frac{1}{(2n)!} \left(\frac{d}{db} \right)^{2n} \Big|_{b=0} \int_{-\infty}^{\infty} dx \frac{be^{bx}}{e^x + 1}. \quad (6.81)$$

- (b) Evaluate

$$\int_{-\infty}^{\infty} dx \frac{be^{bx}}{e^x + 1} \quad \text{Assume } 0 < b < 1. \quad (6.82)$$

by performing a contour integral over a rectangle in the complex plane with corners $-R$, R , $R + 2\pi i$, and $-R + 2\pi i$ and letting $R \rightarrow \infty$. There is a single pole within the contour whose residue must be evaluated.

- (c) Obtain Eq. (6.65) and use it to find $a_1 \dots a_4$.

(d) Show by expanding $1/(1 + e^{-x})$ in a Taylor series that

$$a_1 = \sum_{l=1}^{\infty} \frac{1}{l^2} = \frac{\pi^2}{6}. \quad (6.83)$$

7. Densities of states in all dimensions:

(a) Find the volume of a sphere $\mathcal{V}_d(R)$ of radius R in d dimensions. In order to accomplish this task, first find the surface area A_d of a sphere of unit radius in d dimensions by considering the integral

$$I_d \equiv \int dx_1 dx_2 \dots dx_d e^{-(x_1^2 + x_2^2 + \dots + x_d^2)}. \quad (6.84)$$

On the one hand, I_d is easy to evaluate as a product of d separate integrals. On the other hand, it can also be evaluated in polar coordinates, where it equals

$$I_d = \int dr r^{d-1} A_d e^{-r^2}. \quad (6.85)$$

By comparing Eqs. (6.84) and (6.85), find A_d . As a consequence, find

$$\mathcal{V}_d(R) = \int_0^R dr r^{d-1} A_d. \quad (6.86)$$

(b) Find a general expression for the density of k and energy states for an ideal noninteracting Fermi gas in all dimensions.

8. Fermi function:

(a) Consider the electron density appropriate to aluminum. Assuming the conduction electrons to be free noninteracting fermions, find the chemical potential numerically to two place accuracy at 0 K, 300 K, and 10 000 K.

(b) Compare these results with the corresponding results of the Sommerfeld expansion at lowest nontrivial order.

(c) Draw accurate pictures of the Fermi function $f(\mathcal{E})$ for these three values of the chemical potential.

References

- L. D. Landau and E. M. Lifshitz (1980), *Statistical Physics, Part 1*, 3rd ed., Pergamon Press, Oxford.
- R. A. Millikan (1913), On the elementary electrical charge and the Avogadro constant, *Physical Review*, **2**, 109–143.
- A. Sommerfeld (1928), On the electron theory of metals based on Fermi statistics, *Zeitschrift für Physik*, **47**, 1–32; 43–60. In German.
- G. R. Stewart (1983), Measurement of low-temperature specific heat, *Review of Scientific Instruments*, **54**, 1–11.
- G. R. Stewart (1984), Heavy-fermion systems, *Reviews of Modern Physics*, **56**, 755–787.
- J. J. Thomson (1907), *The Corpuscular Theory of Matter*, Charles Scribner's Sons, New York.

7. Non-Interacting Electrons in a Periodic Potential

7.1 Introduction

While Sommerfeld's theory of the free-electron gas provides an excellent starting point for the study of metals, it leads to a new fundamental difficulty. "The main problem was to explain how the electrons could sneak by all the ions in a metal so as to avoid a mean free path of the order of atomic distances. Such a distance was much too short to explain the observed resistances, which even demanded that the mean free path become longer and longer with decreasing temperature" [Bloch (1976), p. 26]. Bloch (1928) had provided the solution of the problem in his thesis. Analyzing a single electron moving in a perfectly periodic potential, he says, "... I found to my delight that the wave differed from the plane wave of free electrons only by a periodic modulation. This was so simple that I didn't think it could be much of a discovery, but when I showed it to Heisenberg he said right away: 'That's it!' " [Bloch (1976), p. 26].

Immediately, the problem was altered from a hard one: "Why is the mean free path so long?" to an easier one: "Why is the mean free path so short?" Scattering of electrons is caused not by the lattice itself but by defects in the lattice, due either to thermal fluctuations or to impurities. At low temperatures, electron mean free paths in metals should increase up to a limit that is set by impurity density (Chapter 18). This behavior is observed experimentally and gives great plausibility to Bloch's great idea to study crystals through single electrons in periodic potentials.

7.2 Translational Symmetry—Bloch's Theorem

The free Fermi gas of Chapter 6 treats solids as if they are empty boxes filled with electrons that interact neither with nuclei nor each other, apart from effects due to the Pauli exclusion principle. Bloch (1928) added back some of the ingredients missing from this simplified view of solids. He first added back the interaction of electrons with the nuclei, treated as a static external potential.

For general potentials $U(\vec{r})$ the problem is still nearly intractable, and Bloch settled on an additional simplification. He posed the problem of electrons moving about in a *periodic potential* $U(\vec{r})$, one which obeys

$$U(\vec{r} + \vec{R}) = U(\vec{r}). \quad \text{For all } \vec{R} \text{ in a Bravais lattice.} \quad (7.1)$$

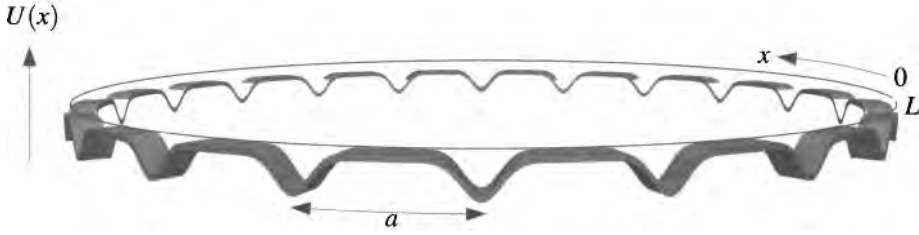


Figure 7.1. The setting for Bloch's theorem in one dimension is a potential $U(x)$ of period a on a periodic domain of length L .

The Hamiltonian is

$$\hat{\mathcal{H}} = \frac{\hat{P}^2}{2m} + U(\hat{R}). \quad (7.2)$$

Now the model contains just the right balance of simplicity and realism. The symmetry (7.1) permits remarkable analytical progress and makes numerical solutions of Eq. (6.3) tractable. The model is realistic enough to predict many physical properties of crystals such as the fact that some are metals and others are electrical insulators.

7.2.1 One Dimension

The basic features of wave functions in periodic potentials are easiest to understand in one dimension. Writing out Schrödinger's equation in the position representation gives

$$-\frac{\hbar^2}{2m} \frac{\partial^2}{\partial x^2} \psi(x) + U(x)\psi(x) = \mathcal{E}\psi(x) \quad (7.3)$$

Take $U(x)$ to be periodic with period a as shown in Figure 7.1.

The one-dimensional space where ψ is defined is of length L . Take ψ to be periodic so that

$$\psi(x+L) = \psi(x). \quad \text{Periodic boundary conditions simplify the calculations considerably without substantially affecting any feature of the solutions. The periodicity of } \psi \text{ over distance } L \text{ should not be confused with the periodicity of } U \text{ over distance } a. \quad (7.4)$$

Suppose that the potential $U(x)$ was just $U(x) = 0$. Then it would be easy to write down all the solutions. They would be

$$\psi_k(x) = \frac{e^{ikx}}{\sqrt{L}} \quad (7.5)$$

When the potential $U(x)$ is not zero, the solutions retain the same basic structure, but change to

$$\psi_k(x) = \frac{e^{ikx}u(x)}{\sqrt{N}}, \quad \text{While } \psi \text{ is normalized over the whole system, } u \text{ is normalized over a single unit cell.} \quad (7.6)$$

where $u(x)$ is a function that like $U(x)$ is periodic with period a , and where $N = L/a$ is the number of cells in the full periodic system. That is, as shown in Figure 7.2, the solutions are plane waves $\exp[ikx]$ modulated by a periodic function $u(x)$.

Periodic function $u(x)$

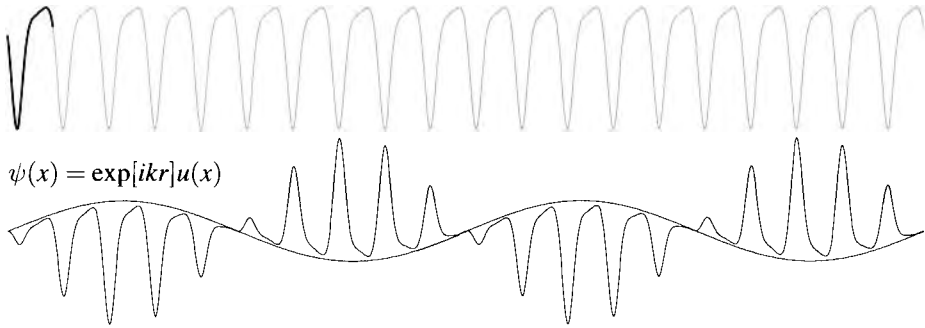


Figure 7.2. Bloch wave functions are periodic functions $u(r)$ modulated by a plane wave of longer period. The lower portion of the figure displays the real part of $\psi(x)$.

The following derivation shows how this form arises, and shows that each and every solution of Schrödinger's equation has the form of Eq. (7.6).

Fourier's theorem [for example, Tolstov (1978)] says that every periodic function can be written as a sum of all the complex exponential functions $\exp[ikx]$ that share the same period. Because ψ is periodic with period L , $\psi(x)$ can be written as a sum of Fourier components $\exp[iq'x]$ where q' is of the form $q' = 2\pi l'/L$ and $l' \in (-\infty \dots -1, 0, 1 \dots \infty)$ is any integer:

$$\psi(x) = \frac{1}{\sqrt{L}} \sum_{q'} \psi(q') e^{iq'x} \quad \begin{array}{l} \text{The sum over } q' \text{ is the same as summing over} \\ l' \text{ with } q' = 2\pi l'/L. \text{ The factor of } \sqrt{L} \text{ fixes} \\ \text{normalization.} \end{array} \quad (7.7)$$

U is periodic with period $a = L/N$, and it can be written as a sum of Fourier components $\exp[iKx]$ where the reciprocal lattice vector K is of the form $K = 2\pi l/a$, and l is an integer:

$$U(x) = \sum_K U_K e^{iKx}. \quad (7.8)$$

Substitute Eqs. (7.7) and (7.8) into Eq. (7.3), finding

$$\sum_{q'} \frac{\hbar^2 q'^2}{2m} e^{iq'x} \psi(q') + \sum_{q'K} e^{i(q'+K)x} \psi(q') U_K = \mathcal{E} \sum_{q'} e^{iq'x} \psi(q'). \quad (7.9)$$

This equation must hold separately for each Fourier component $\exp[iqx]$, a condition imposed formally by choosing $q = 2\pi l/L$, multiplying Eq. (7.9) by $\exp[-iqx]/L$ and integrating from 0 to L . It is easy to verify that

$$\frac{1}{L} \int_0^L dx e^{i(q'-q)x} = \delta_{q,q'}; \quad \frac{1}{L} \int_0^L dx e^{i(q'+K-q)x} = \delta_{q',q-K}. \quad (7.10)$$

Therefore

$$\frac{\hbar^2 q^2}{2m} \psi(q) + \sum_{q'K} \delta_{q',q-K} \psi(q') U_K = \mathcal{E} \psi(q). \quad (7.11)$$

$$\Rightarrow (\mathcal{E}_q^0 - \mathcal{E})\psi(q) + \sum_K \psi(q - K) U_K = 0. \quad \mathcal{E}_q^0 \text{ is defined in Eq. (6.8).} \quad (7.12)$$

Equation (7.12) is a restatement of Schrödinger's equation in Fourier space and it has a remarkable property. Each solution as a function of q is zero except at a discrete and evenly spaced set of q values, like a comb. Here is why.

Suppose one has a solution. There must be at least one $k = 2\pi m/L$ for which $\psi(k)$ is not equal to zero. The equation for $\psi(k)$ involves $\psi(k - K)$ for all K of the form $2\pi l/a$. Pick any of these wave function components, say $\psi(k - K')$, and ask what Eq. (7.12) implies. It says

$$(\mathcal{E}_{k-K'}^0 - \mathcal{E})\psi(k - K') + \sum_K \psi(k - K' - K) U_K = 0 \quad (7.13)$$

$$\Rightarrow (\mathcal{E}_{k-K'}^0 - \mathcal{E})\psi(k - K') + \sum_K \psi(k - K) U_{K-K'} = 0. \quad \text{Send } K \rightarrow K - K' \text{ as the sum index.} \quad (7.14)$$

Equation (7.14) is a different equation from Eq. (7.12) with different coefficients, but it involves exactly the same discrete set of wave function components: components of the form $\psi(k - K)$ where $K = 2\pi l/a$ is in the reciprocal lattice. Therefore, Eq. (7.12) can be viewed as a collection of algebraic equations for this set of wave function components, and all other components can be zero. This structure of the matrix Hamiltonian is illustrated in Table 7.1.

So solutions of Eq. (7.12) have the form

$$\psi(q) = \sum_K \delta_{q, k+K} u_K. \quad \begin{array}{l} \text{The } u_K \text{ are constants. The independent variable is } q, \text{ and} \\ k \text{ is some value of } q \text{ for which } \psi(q) \text{ is not zero. Do not} \\ \text{worry about signs of the index } K, \text{ since both } K \text{ and } -K \\ \text{are in the reciprocal lattice.} \end{array} \quad (7.15)$$

Bloch's Theorem. Transform Eq. (7.15) back into real space by inserting it into Eq. (7.7) to find

$$\psi(x) = \frac{1}{\sqrt{L}} \sum_{q'=K} \delta_{q', k+K} u_K e^{iq'x} = \frac{1}{\sqrt{L}} \sum_K u_K e^{i(k+K)x} \quad (7.16)$$

$$\Rightarrow \psi(x) = \frac{e^{ikx} u(x)}{\sqrt{N}} \quad \text{where} \quad u(x) \equiv \frac{1}{\sqrt{a}} \sum_K u_K e^{iKx}. \quad \begin{array}{l} N = L/a \text{ is the} \\ \text{number of unit cells.} \end{array} \quad (7.17)$$

Equation (7.17) is Bloch's theorem. It says that when a single particle moves in a periodic potential the solutions are products of two pieces (Figure 7.2). The first piece is just the plane wave e^{ikx} the particle would adopt in an empty box (Eq. (6.7)). The second piece is a periodic function $u(x)$ with the same period as the potential $U(x)$. Since $u(x)$ is built entirely from plane waves of the form $\exp[iKx]$, it must be periodic with period a .

To capture all solutions of Eq. (7.12) the notation must be generalized. To index all solutions ψ , one begins by specifying some Fourier component k for which the solution is not zero. It is customary to affix the index both to $\psi(x)$ and $u(x)$, denoting by $\psi_k(x)$ a solution such that

$$\psi_k(x) = \frac{e^{ikx} u_k(x)}{\sqrt{N}} \Rightarrow \psi_k(x+a) = \psi_k(x) e^{ika}. \quad (7.18)$$

Table 7.1. The structure of Bloch’s Hamiltonian in reciprocal space

$$\begin{pmatrix}
 \left(\begin{array}{cccc}
 \mathcal{E}_{K_0}^0 + U_{K_0} & U_{K_{-1}} & \dots & U_{K_{1-M}} \\
 U_{K_1} & \mathcal{E}_{K_1}^0 + U_{K_0} & \dots & U_{K_{2-M}} \\
 U_{K_2} & U_{K_1} & \dots & U_{K_{3-M}} \\
 \vdots & \vdots & \ddots & \vdots \\
 \vdots & \vdots & \vdots & \mathcal{E}_{K_{M-1}}^0 + U_{K_0}
 \end{array} \right) & & & \\
 & 0 \dots & & \\
 & & \left(\begin{array}{ccc}
 \mathcal{E}_{K_1}^0 + U_{K_0} & U_{K_{-1}} & \dots \\
 U_{K_1} & \mathcal{E}_{K_1+K_1}^0 + U_{K_0} & \dots \\
 \vdots & \vdots & \vdots \\
 \vdots & \vdots & \vdots
 \end{array} \right) & \dots & \\
 & & & & \left(\begin{array}{c}
 \psi(K_0) \\
 \psi(K_1) \\
 \psi(K_2) \\
 \vdots \\
 \vdots \\
 \vdots \\
 \psi(K_{M-1}) \\
 \psi(k_1 + K_0) \\
 \psi(k_1 + K_1) \\
 \vdots \\
 \vdots \\
 \vdots
 \end{array} \right)
 \end{pmatrix}$$

This matrix contains blocks that link together wave function components $\psi(k_m + K_l)$ for a given m , where $k_m = 2\pi m/L$ and $K_l = 2\pi l/a$. There are no matrix elements connecting $\psi(q)$ ’s when the q ’s do not differ by reciprocal lattice vectors. The dimension of each block is M , the number of reciprocal lattice vectors retained in the calculation, while the total number of blocks is equal to the total number of unit cells, $N = L/a$.

The Fourier component k is called the *wave number* and $\hbar k$ is called the *crystal momentum*.

Selecting k does not specify a single unique solution $\psi_k(x)$. As shown in Table 7.1, choosing k means selecting one of the blocks that links together wave functions ψ with Fourier components of the form $q = k + K$. The block matrix as shown is of dimension M , and has M eigenvectors. Each of these eigenvectors is a wave function ψ with crystal momentum k . Cataloging these solutions can be done with an additional index n called the *band index*. Actually, M is only finite if the potential $U(x)$ can be constructed from a finite number M of Fourier terms; since in general the number of Fourier terms needed for U is infinite, $M \rightarrow \infty$.

Choosing k specifies a *set* of Fourier components $q = k + K$ from which the wave function ψ_k will be constructed. Choosing $k + K'$ picks out *exactly the same set*. From this point of view, two wave numbers k are physically distinct only if they do not differ by any reciprocal lattice vector K . This means that indices k should be chosen from

$$k = \frac{2\pi m}{L} \text{ where } k \in \left[-\frac{\pi}{2a}, \frac{\pi}{2a}\right] \text{ Taking } k \text{ in the interval } [0, 2\pi/a] \text{ would do just as well.} \tag{7.19}$$

This collection of $k = 2\pi m/L$, $m \in [-N/2, N/2 - 1]$ is called the *first Brillouin zone*, and will be defined in greater generality in Section 7.2.4.

Thus a complete set of solutions to Eq. (7.12) is

$$\psi_{nk}(x) = \frac{e^{ikx} u_{nk}(x)}{\sqrt{N}} \text{ with band energy } \mathcal{E}_{nk}. \tag{7.20}$$

where k lies in the first Brillouin zone, and the band index runs from 0 to ∞ .

The significance of band energies \mathcal{E}_{nk} in explaining the behavior of solids cannot easily be overstated. They contain information on whether a solid is a metal, semiconductor, or insulator. Their slopes give electron velocities, and therefore they predict electrical transport properties. Details of their shapes can be used to calculate minimum energy crystal structures, and even magnetic properties. Several of the following chapters will be devoted to learning how they can be calculated and to examining their consequences.

Since there is still an infinite number of unknown solutions, of what use is Bloch's theorem? Finding that solutions are of the form shown in Eq. (7.20) reduces the computational cost of solving Eq. (7.12) by a factor of N , where N is the number of unit cells in the crystal. In short, the computational time has been reduced by about a factor of 10^{23} . By solving a problem in a single unit cell one obtains a solution that applies to a crystal of arbitrary size. Bloch's theorem provides a *scaling theory* relating microscopic computations to macroscopic phenomena.

7.2.2 Bloch's Theorem in Three Dimensions

Extending Bloch's theorem to three dimensions involves no substantially new ideas, but the notation becomes a little more involved than in one dimension. Generalize to a box of volume $\mathcal{V} = L^3$ in which the wave function $\psi(\vec{r})$ is periodic: $\psi(x+L, y, z) = \psi(x, y, z)$, and the same holds for the y and z components. Thus, choosing \vec{q} as in Eq. (6.7),

$$\psi(\vec{r}) = \frac{1}{\sqrt{\mathcal{V}}} \sum_{\vec{q}} \psi(\vec{q}) e^{i\vec{q}\cdot\vec{r}}. \quad (7.21)$$

The three-dimensional periodic potential $U(\vec{r})$ described in Eq. (7.1) is composed entirely of Fourier components $\exp[i\vec{K}\cdot\vec{R}]$, where \vec{K} are reciprocal lattice vectors (Section 3.2.5) of the Bravais lattice \vec{R} . This claim is easily proved, since if a Fourier component is unchanged after translation by a Bravais lattice vector, then

$$e^{i\vec{k}\cdot(\vec{r}+\vec{R})} = e^{i\vec{k}\cdot\vec{r}}. \quad (7.22)$$

A function can only be periodic over \vec{R} if each of its Fourier coefficients is periodic in the same fashion.

But Eq. (7.22) is nothing other than the condition in Eq. (3.17) for a wave vector $\vec{k} = \vec{K}$ to belong to the reciprocal lattice. So

$$U(\vec{r}) = \sum_{\vec{K}} e^{i\vec{K}\cdot\vec{r}} U_{\vec{K}}. \quad (7.23)$$

A more formal demonstration of the same fact is obtained by taking the Fourier transform of $U(\vec{r})$, explicitly:

$$\int d\vec{r} e^{-i\vec{q}\cdot\vec{r}} U(\vec{r}) = \sum_{\vec{R}} \int_{\text{unit cell}} d\vec{r} e^{-i\vec{q}\cdot\vec{R}} U(\vec{r}+\vec{R}) e^{-i\vec{q}\cdot\vec{r}} \quad \text{Use } U(\vec{r}+\vec{R}) = U(\vec{r}). \quad (7.24)$$

$$= \Omega \sum_{\vec{R}} e^{-i\vec{q}\cdot\vec{R}} U_{\vec{q}}, \quad (7.25)$$

where Ω is the volume of the unit cell, and

$$U_{\vec{q}} \equiv \int_{\Omega} \frac{d\vec{r}}{\Omega} e^{-i\vec{q}\cdot\vec{r}} U(\vec{r}). \quad (7.26)$$

As a subscript on the integral Ω means that the integral is over a unit cell. Substituting \vec{K} for \vec{q} gives a specific prescription for $U_{\vec{K}}$ if $U(\vec{r})$ is known.

The sum over Bravais lattice vectors appearing in Eq. (7.25) obeys the convenient identity, derived as Eq. (A.29) in Appendix A,

$$\sum_{\vec{R}} e^{-i\vec{q}\cdot\vec{R}} = N \sum_{\vec{K}} \delta_{\vec{q}\vec{K}} \Rightarrow \int d\vec{r} e^{-i\vec{q}\cdot\vec{r}} U(\vec{r}) = \mathcal{V} \sum_{\vec{K}} \delta_{\vec{q}\vec{K}} U_{\vec{K}}. \quad \mathcal{V} = N\Omega. \quad (7.27)$$

Therefore, applying an inverse Fourier transformation to Eq. (7.27) gives

$$U(\vec{r}) = \frac{1}{\mathcal{V}} \sum_{\vec{q}} e^{i\vec{q}\cdot\vec{r}} \mathcal{V} \sum_{\vec{K}} \delta_{\vec{q}\vec{K}} U_{\vec{K}} = \sum_{\vec{K}} e^{i\vec{K}\cdot\vec{r}} U_{\vec{K}}. \quad (7.28)$$

Given the forms (7.28) and (7.21) for wave function and potential, one can write Schrödinger's equation in Fourier space. Acting upon ψ with $\hat{\mathcal{H}} - \mathcal{E}$, using the Hamiltonian of Eq. (7.2) gives

$$0 = \frac{1}{\mathcal{V}} \sum_{\vec{q}'} \left[\mathcal{E}_{\vec{q}'}^0 - \mathcal{E} + U(\vec{r}) \right] \psi(\vec{q}') e^{i\vec{q}'\cdot\vec{r}} \quad \text{Recall that } \mathcal{E}_{\vec{q}'}^0 = \hbar^2 q'^2 / 2m. \quad (7.29)$$

$$= \frac{1}{\mathcal{V}} \sum_{\vec{q}'} \left[(\mathcal{E}_{\vec{q}'}^0 - \mathcal{E}) e^{i\vec{q}'\cdot\vec{r}} + \sum_{\vec{K}} e^{i(\vec{K}+\vec{q}')\cdot\vec{r}} U_{\vec{K}} \right] \psi(\vec{q}') \quad (7.30)$$

$$\Rightarrow 0 = \sum_{\vec{q}'} \int \frac{d\vec{r}}{\mathcal{V}} \left[(\mathcal{E}_{\vec{q}'}^0 - \mathcal{E}) e^{i(\vec{q}'-\vec{q})\cdot\vec{r}} + \sum_{\vec{K}} e^{i(\vec{K}+\vec{q}'-\vec{q})\cdot\vec{r}} U_{\vec{K}} \right] \psi(\vec{q}') \quad (7.31)$$

$$= \sum_{\vec{q}'} \left[(\mathcal{E}_{\vec{q}'}^0 - \mathcal{E}) \delta_{\vec{q}\vec{q}'} + \sum_{\vec{K}} \delta_{\vec{q}-\vec{K},\vec{q}'} U_{\vec{K}} \right] \psi(\vec{q}') \quad (7.32)$$

$$\Rightarrow (\mathcal{E}_{\vec{q}}^0 - \mathcal{E}) \psi(\vec{q}) + \sum_{\vec{K}} U_{\vec{K}} \psi(\vec{q} - \vec{K}) = 0. \quad (7.33)$$

Equation (7.33) generalizes Eq. (7.12) to three dimensions. It has similar implications. Suppose that $\psi(\vec{k})$ is nonzero. Then all the components of $\psi(\vec{q})$ involved in Eq. (7.33) are of the form $\psi(\vec{k} + \vec{K})$, where \vec{K} is in the reciprocal lattice, and

$$\psi(\vec{q}) = \sum_{\vec{K}} \delta_{\vec{q},\vec{k}+\vec{K}} u_{\vec{K}}. \quad \text{The coefficients } u_{\vec{K}} \text{ are again constants} \quad (7.34)$$

Thus similar to Eq. (7.17)

$$\psi_{\vec{k}}(\vec{r}) = \frac{e^{i\vec{k}\cdot\vec{r}} u_{\vec{k}}(\vec{r})}{\sqrt{N}} \quad N = \mathcal{V}/\Omega \text{ equals the number of points in the lattice and is convenient to introduce to normalize } u_{\vec{k}}(\vec{r}) \text{ within each unit cell.} \quad (7.35)$$

where $u_{\vec{k}}(\vec{r} + \vec{R}) = u_{\vec{k}}(\vec{r})$ is a periodic function on the Bravais lattice. Mirroring the one-dimensional case, there is an infinite number of solutions $\psi_{\vec{k}}(\vec{r})$ for each

\vec{k} . Now \vec{k} is called the *Bloch wave vector*, and $\hbar\vec{k}$ is again called the crystal momentum. The many solutions for each \vec{k} are again distinguished by the band index n , which also decorates ψ as in

$$\psi_{n\vec{k}}(\vec{r} + \vec{R}) = \psi_{n\vec{k}}(\vec{r})e^{i\vec{k}\cdot\vec{R}} = \frac{u_{n\vec{k}}(\vec{r})e^{i\vec{k}\cdot(\vec{r}+\vec{R})}}{\sqrt{N}}. \quad (7.36)$$

Saying that $\psi_{n\vec{k}}$ solves Schrödinger's equation means that it solves the eigenvalue equation (7.33), and the corresponding band energy is denoted $\mathcal{E}_{n\vec{k}}$.

It is also valuable to restate Eq. (7.33) in terms of Dirac notation; it is

$$\hat{\mathcal{H}} = \sum_{\vec{q}'} |\vec{q}'\rangle \mathcal{E}_{\vec{q}'}^0 \langle \vec{q}'| + \sum_{\vec{q}'\vec{K}'} |\vec{q}'\rangle U_{\vec{K}'} \langle \vec{q}' - \vec{K}'|. \quad \text{Compute } \langle \vec{q} | \hat{\mathcal{H}} - \mathcal{E} | \psi \rangle \text{ to regain Eq. (7.33).} \quad (7.37)$$

7.2.3 Formal Demonstration of Bloch's Theorem

Since Bloch's theorem follows from symmetry of the potential U , there must be some way to derive it that focuses on symmetry and does not require grinding through long computations. Indeed there is, but the derivation is fairly abstract. Recall that the operator generating a translation through a vector \vec{R} is

$$\hat{T}_{\vec{R}} = e^{-i\hat{P}\cdot\vec{R}/\hbar}, \quad \text{See, for example, Landau and Lifshitz (1977), p. 45.} \quad (7.38)$$

where \hat{P} is the momentum operator and \vec{R} a Bravais lattice vector. Since the components of momentum commute, all of these operators, for allowed values of \vec{R} , commute with one another and with the Hamiltonian (7.2) (shown in Problem 2).

Therefore [Landau and Lifshitz (1977), pp. 14 and 34; Schiff (1968), p. 154] all of these operators and the Hamiltonian can be diagonalised simultaneously. Any eigenvector of the Hamiltonian can be taken as an eigenfunction of all the translation operators as well:

$$\hat{T}_{\vec{R}}^\dagger |\psi\rangle = e^{i\hat{P}\cdot\vec{R}/\hbar} |\psi\rangle = C_{\vec{R}} |\psi\rangle. \quad \text{Here } C_{\vec{R}} \text{ is a constant that is yet to be determined.} \quad (7.39)$$

Operating with the bra vector $\langle \vec{r} |$ (eigenfunction of position) on Eq. (7.39) gives

$$\psi(\vec{r} + \vec{R}) = C_{\vec{R}} \psi(\vec{r}). \quad \text{Because } \psi(\vec{r}) \equiv \langle \vec{r} | \psi \rangle \text{ and } \langle \vec{r} | \hat{T}_{\vec{R}}^\dagger = \langle \vec{r} + \vec{R} |. \quad (7.40)$$

On the other hand, operating with the bra vector $\langle \vec{k} |$ (eigenfunction of momentum) on Eq. (7.39) gives

$$e^{i\vec{k}\cdot\vec{R}} \langle \vec{k} | \psi \rangle = C_{\vec{R}} \langle \vec{k} | \psi \rangle \quad (7.41)$$

$$\Rightarrow \text{either } C_{\vec{R}} = e^{i\vec{k}\cdot\vec{R}} \text{ or } \langle \vec{k} | \psi \rangle = 0. \quad (7.42)$$

Therefore, $|\psi\rangle$ can have nonzero overlap with only a single $\langle \vec{k} |$, and that value of \vec{k} is used as an index to label the eigenfunction $\psi_{\vec{k}}$.

Since for a given value of \vec{k} , there is still the possibility of many energy eigenvalues, one must introduce the band index n . The classification of eigenfunctions made possible by periodicity is completed by writing

$$\hat{\mathcal{H}}|\psi_{n\vec{k}}\rangle = \mathcal{E}_{n\vec{k}}|\psi_{n\vec{k}}\rangle \quad (7.43a)$$

$$\hat{T}_{\vec{R}}^\dagger|\psi_{n\vec{k}}\rangle = e^{i\vec{k}\cdot\vec{R}}|\psi_{n\vec{k}}\rangle. \quad \text{Combine Eqs. (7.39) and (7.42). In the position representation, this reproduces Eq. (7.36).} \quad (7.43b)$$

From Eq. (7.43b) the previous forms of Bloch's theorem can be obtained. Acting with $\langle\vec{r}|$ gives

$$\psi_{n\vec{k}}(\vec{r} + \vec{R}) = e^{i\vec{k}\cdot\vec{R}}\psi_{n\vec{k}}(\vec{r}). \quad (7.44)$$

One can also proceed to define

$$u_{n\vec{k}}(\vec{r}) \equiv \sqrt{N} e^{-i\vec{k}\cdot\vec{r}}\psi_{n\vec{k}}(\vec{r}). \quad \text{When } \psi \text{ is normalized over the volume } \mathcal{V}, u \text{ is normalized over the unit cell } \Omega. \quad (7.45)$$

It follows from Eq. (7.44) that u is periodic;

$$u(\vec{r} + \vec{R}) = u(\vec{r}). \quad \text{For all } \vec{R} \text{ in the Bravais lattice.} \quad (7.46)$$

7.2.4 Additional Implications of Bloch's Theorem

Effective Hamiltonian. By virtue of Bloch's theorem, the original Hamiltonian, (7.2), can be transformed into an effective Hamiltonian whose solution no longer needs to be sought over the whole crystal. This Hamiltonian is easily found by searching for the equation to be obeyed by u . Writing ψ in terms of u from Eq. (7.45) and writing out $(\hat{\mathcal{H}} - \mathcal{E})\psi = 0$ yields

$$\hat{\mathcal{H}}_{\vec{k}}u(\vec{r}) = \frac{\hbar^2}{2m}[-\nabla^2 - 2i\vec{k}\cdot\vec{\nabla} + k^2]u(\vec{r}) + U(\vec{r})u(\vec{r}) = \mathcal{E}u(\vec{r}). \quad (7.47)$$

Because u is periodic, this equation can be restricted to a single unit cell, subject to the boundary conditions that whenever \vec{r} lies on one boundary of the unit cell, and $\vec{r} + \vec{R}$ is another boundary point of the cell, then

$$u(\vec{r}) = u(\vec{r} + \vec{R}) \quad \vec{R} \text{ is a Bravais lattice vector.} \quad (7.48a)$$

and

$$\hat{n}(\vec{r})\cdot\vec{\nabla}u(\vec{r}) = -\hat{n}(\vec{r} + \vec{R})\cdot\vec{\nabla}u(\vec{r} + \vec{R}). \quad \hat{n}(\vec{r}) \text{ is a unit normal to the cell boundary at } \vec{r}. \quad (7.48b)$$

Using the relation (7.45) between u and ψ , one can equally well write down Schrödinger's equation, and solve it in a single unit cell, subject to the boundary conditions

$$e^{i\vec{k}\cdot\vec{R}}\psi_{\vec{k}}(\vec{r}) = \psi_{\vec{k}}(\vec{r} + \vec{R}) \quad (7.49a)$$

and

$$e^{i\vec{k}\cdot\vec{R}}\hat{n}(\vec{r})\cdot\vec{\nabla}\psi_{\vec{k}}(\vec{r}) = -\hat{n}(\vec{r} + \vec{R})\cdot\vec{\nabla}\psi_{\vec{k}}(\vec{r} + \vec{R}). \quad (7.49b)$$

In a crystal with 10^{23} atoms, Eq. (7.47) requires 10^{23} times less numerical effort to solve than Eq. (7.2).

Counting \vec{k} . The demonstrations of Bloch's theorem relied on periodic boundary conditions. As a consequence, as discussed in Section 6.3, there are restrictions on the permitted values of the Bloch wave vector \vec{k} . In a cubic crystal of volume $\mathcal{V} = L^3$, \vec{k} takes the form given in (6.7), just as for free electrons. The density of allowed \vec{k} states is therefore still given by Eq. (6.13).

These results can all be generalized to crystals that are not cubic. Consider any lattice described by three primitive vectors \vec{a}_1 , \vec{a}_2 , and \vec{a}_3 as in Eq. (A.17). The vectors \vec{k} consistent with periodic boundary conditions are of the form

$$\vec{k} = \sum_{l=1}^3 \frac{m_l}{M_l} \vec{b}_l, \quad 0 \leq m_l < M_l, \quad \begin{array}{l} M_l \text{ gives the total number of lattice points along} \\ \text{direction } l; \text{ the total number of lattice points is} \\ M_1 M_2 M_3. \end{array} \quad (7.50)$$

where $\vec{b}_1 \dots \vec{b}_3$ are primitive vectors of the reciprocal lattice and are chosen to satisfy

$$\vec{b}_l \cdot \vec{a}_{l'} = 2\pi \delta_{ll'}. \quad (7.51)$$

The primitive vectors $\vec{b}_1 \dots \vec{b}_3$ describe the boundaries of a primitive cell in reciprocal space, and the \vec{k} of (7.50) form a fine network of vectors filling this primitive cell. It is possible to adopt a convention where \vec{k} takes values outside of this cell, allowing the integers m_l to continue on to values greater than M_l . However, the resulting \vec{k} will be redundant, in the sense that they must differ from some \vec{k} within the primitive cell by a reciprocal lattice vector. Any two \vec{k} that differ precisely by a reciprocal lattice vector \vec{K} share the eigenvalue $\exp[i\vec{k} \cdot \vec{R}]$ in Eq. (7.43b), since $\exp[i\vec{K} \cdot \vec{R}] = 1$. Because \vec{k} is nothing but a label for this eigenvalue, two such \vec{k} can be regarded as physically identical.

According to Eq. (7.50), the total number of \vec{k} states in a primitive cell in \vec{k} space is $M_1 M_2 M_3$, which is also the number of lattice points N in the original real space lattice. So one has the convenient and general result that the

$$\begin{array}{l} \text{Number of physically distinct} \\ \text{Bloch wave vectors } \vec{k} \end{array} = \text{Number of lattice sites, } N. \quad (7.52)$$

Brillouin Zone. The primitive cell in \vec{k} space spanned by arbitrary primitive vectors $\vec{b}_1 \dots \vec{b}_3$ is not convenient to use, because it is not uniquely specified, nor does it have the full symmetry of the crystal. A primitive cell that overcomes these defects is the Wigner-Seitz cell of the origin in reciprocal space. As in the one-dimensional case, it is called the *Brillouin zone*, or *first Brillouin zone*. Sums such as in Eq. (7.57) over \vec{k} or \vec{q} are always carried out over the net of vectors in Eq. (7.50) filling the first Brillouin zone. However, any sum over \vec{K} is carried out over a very different set, the reciprocal lattice vectors given by Eq. (3.24d).

Density of States. As in the case of free electrons, it is useful to be able to convert sums over \vec{k} into integrals. To carry out a calculation analogous to Eq. (6.10), one

needs to know the volume of reciprocal space associated with each point \vec{k} . From Eq. (7.50), this volume is

$$\frac{\vec{b}_1 \cdot (\vec{b}_2 \times \vec{b}_3)}{M_1 M_2 M_3} \quad \begin{array}{l} \text{The volume of any parallelepiped whose} \\ \text{edges are given by three vectors } \vec{A}, \vec{B}, \\ \vec{C} \text{ is } \vec{A} \cdot (\vec{B} \times \vec{C}). \end{array} \quad (7.53)$$

$$= \frac{2\pi}{\vec{a}_3 \cdot (\vec{a}_1 \times \vec{a}_2)} \frac{\vec{b}_1 \cdot (\vec{b}_2 \times (\vec{a}_1 \times \vec{a}_2))}{M_1 M_2 M_3} \quad \text{Use Eq. (3.24c).} \quad (7.54)$$

$$= \frac{(2\pi)^3}{M_1 M_2 M_3 \vec{a}_1 \cdot (\vec{a}_2 \times \vec{a}_3)} \quad \begin{array}{l} \text{Using the identity} \\ \vec{A} \times (\vec{B} \times \vec{C}) = \vec{B}(\vec{A} \cdot \vec{C}) - \vec{C}(\vec{A} \cdot \vec{B}). \end{array} \quad (7.55)$$

$$= \frac{(2\pi)^3}{\mathcal{V}} \quad \begin{array}{l} \text{Because the total volume of the crystal} \\ \text{is given by the number of lattice points,} \\ M_1 M_2 M_3, \text{ times the volume of each} \\ \text{primitive cell.} \end{array} \quad (7.56)$$

Therefore any sum that needs to be carried out over the states \vec{k} in the first Brillouin zone can use the relation

$$\sum_{\vec{k}\sigma} F_{\vec{k}} = \mathcal{V} \int [d\vec{k}] F_{\vec{k}}, \quad (7.57)$$

using the density of states in Eq. (6.15) just as for free electrons. The density of energy states in the n th band is similarly given by

$$D_n(\mathcal{E}) = \int [d\vec{k}] \delta(\mathcal{E} - \mathcal{E}_{n\vec{k}}). \quad \text{Compare with Eq. (6.19).} \quad (7.58)$$

Energy Bands and Group Velocity. One of the most important pieces of physical information to be obtained from the energy functions $\mathcal{E}_{n\vec{k}}$ is the velocity $\vec{v}_{n\vec{k}}$ of electrons in the n th band with wave number \vec{k} :

$$\vec{v}_{n\vec{k}} = \frac{1}{\hbar} \vec{\nabla}_{\vec{k}} \mathcal{E}_{n\vec{k}}. \quad \vec{\nabla}_{\vec{k}} \text{ means that one takes derivatives with respect} \quad (7.59)$$

to components of \vec{k} .

Without embarking on the careful but lengthy justification of this relation to be provided in Chapter 16, one can note that Eq. (7.59) is nothing but the statement that solutions of wave equations generally have a *group velocity* $v = \partial\omega/\partial k$. In the context of wave mechanics, a particle is actually a wave packet, which is a sum over wave functions that is contrived so as to have a large peak at position \vec{r} , and simultaneously a dominant wave vector \vec{k} . The flavor of calculations for wave packets is easiest to share if one imagines solutions of Schrödinger's equation with energy $\mathcal{E}_{\vec{k}}$ and for which $u_{\vec{k}}(\vec{r})$ varies only very weakly in space. Then define

$$W(\vec{r}, \vec{k}, t) = \int [d\vec{k}'] w(\vec{k}' - \vec{k}) e^{-i\mathcal{E}_{\vec{k}'}t/\hbar} \psi_{\vec{k}'}(\vec{r}), \quad \begin{array}{l} \text{Here } \psi \text{ is a Bloch wave, and } w \\ \text{is a function sharply peaked} \\ \text{about } \vec{k} - \vec{k}' = 0; \text{ thus } W \text{ is} \\ \text{mainly built out of waves with} \\ \text{wave vector } \vec{k}. \end{array} \quad (7.60)$$

$$\approx e^{i\vec{k}\cdot\vec{r}-i\mathcal{E}_{\vec{k}}t/\hbar} \int [d\vec{k}''] w(\vec{k}'') e^{i\vec{k}''\cdot(\vec{r}-\vec{\nabla}_{\vec{k}}\mathcal{E}_{\vec{k}}t/\hbar)} u_{\vec{k}+\vec{k}''}(\vec{r}), \quad \text{Defining } \vec{k}'' = \vec{k}' - \vec{k} \text{ and} \quad (7.61)$$

expanding the terms in the exponent to first order in \vec{k}'' , because w is peaked about $\vec{k}'' = 0$.

$$\approx e^{i\vec{k}\cdot\vec{r}-i\mathcal{E}_{\vec{k}}t/\hbar} \mathcal{F}(\vec{r} - \vec{\nabla}_{\vec{k}}\mathcal{E}_{\vec{k}}t/\hbar) \quad \text{Assuming the spatial variation of } u_{\vec{k}}(\vec{r}) \text{ can be neglected. The value of the integral } \mathcal{F} \text{ does not matter; just the fact that it is in the form of a traveling wave moving at } \vec{v}_{\vec{k}} = \vec{\nabla}_{\vec{k}}\mathcal{E}_{\vec{k}}/\hbar = \vec{\nabla}_{\vec{k}}\omega_{\vec{k}}. \quad (7.62)$$

7.2.5 Van Hove Singularities

In the course of computing the energy densities of states defined by Eq. (7.58), it is common to encounter divergences called *van Hove singularities*.

In one dimension, suppressing the index n on $\mathcal{E}_{\vec{k}}$ gives

$$D(\mathcal{E}) = \int dk (2/2\pi)\delta(\mathcal{E} - \mathcal{E}_k) \quad (7.63)$$

$$= \frac{2}{\pi} \int \frac{d\mathcal{E}_k}{|d\mathcal{E}_k/dk|} \delta(\mathcal{E} - \mathcal{E}_k) \quad \text{An additional factor of two comes generally from the fact that } \mathcal{E}_k = \mathcal{E}_{-k}. \quad (7.64)$$

$$= \frac{2}{\pi} \frac{1}{|d\mathcal{E}_k/dk|}. \quad (7.65)$$

When explicit solutions of Bloch’s equation are found, as in Figure 7.7, it will emerge that \mathcal{E}_{nk} is a periodic function of k and that $d\mathcal{E}_{nk}/dk$ vanishes at the edge of the Brillouin zone. As a result, the density of states must diverge there. Assuming that $d\mathcal{E}_{nk}/dk$ vanishes linearly as k approaches π/a , the divergence is of the form

$$D(\mathcal{E}) \sim \frac{1}{k - \pi/a} \sim \frac{1}{\sqrt{\mathcal{E}_{\max} - \mathcal{E}}} \quad \text{Taking } \mathcal{E}_k \sim \mathcal{E}_{\max} - C(k - \pi/a)^2, \text{ with } C \text{ some constant near the zone edge.} \quad (7.66)$$

The only way for $d\mathcal{E}/dk$ to vanish in one dimension is at a maximum or a minimum. Therefore, van Hove singularities in one dimension tend to occur only at the beginning or the end of a range of allowed energies. In two and three dimensions, van Hove singularities typically occur in the midst of energy intervals as well—as for example in Figures 13.9 or 18.4. The generalization of Eq. (7.65) is

$$D(\mathcal{E}) = \int d\vec{k} \frac{2}{(2\pi)^d} \delta(\mathcal{E} - \mathcal{E}_{\vec{k}}). \quad \text{The number of dimensions } d \text{ might be 2 or 3.} \quad (7.67)$$

Integrals in the form of Eq. (7.67) can also be expressed as integrals over the energy surface on which $\mathcal{E} = \mathcal{E}_{\vec{k}}$. To obtain the correct expression, begin with the observation that

$$\delta(\mathcal{E} - \mathcal{E}_{n\vec{k}}) = \frac{\theta(\mathcal{E} - \mathcal{E}_{\vec{k}}) - \theta(\mathcal{E} - \mathcal{E}_{\vec{k}} - d\mathcal{E})}{d\mathcal{E}} \quad \text{For } d\mathcal{E} \text{ very small.} \quad (7.68)$$

As shown in Figure 7.3, Eq. (7.67) is therefore given by

- integrating over the energy surface $\mathcal{E} = \mathcal{E}_{n\vec{k}}$ with surface measure $d\Sigma$,

- multiplying by the normal distance to the surface $\mathcal{E} = \mathcal{E}_{\vec{n}\vec{k}} + d\mathcal{E}$, and
- dividing by $d\mathcal{E}$.

What is the normal distance between the two surfaces? First, note (Problem 1) that

$$\hat{n} = \frac{\vec{\nabla}_{\vec{k}} \mathcal{E}_{\vec{k}}}{|\nabla_{\vec{k}} \mathcal{E}_{\vec{k}}|} \tag{7.69}$$

is a unit normal between the two surfaces. Next, let $d\vec{k}$ be any \vec{k} vector such that $\mathcal{E}_{\vec{k}+d\vec{k}} = \mathcal{E}_{\vec{k}} + d\mathcal{E}$. The normal distance between the surfaces is therefore $d\vec{k} \cdot \hat{n}$. But

$$\mathcal{E}_{\vec{k}+d\vec{k}} = \mathcal{E}_{\vec{k}} + d\vec{k} \cdot \nabla_{\vec{k}} \mathcal{E}_{\vec{k}} \quad \text{Taylor expansion.} \tag{7.70}$$

$$\Rightarrow d\vec{k} \cdot \nabla_{\vec{k}} \mathcal{E}_{\vec{k}} = d\mathcal{E}. \tag{7.71}$$

$$\Rightarrow d\vec{k} \cdot \hat{n} = \frac{d\mathcal{E}}{|\nabla_{\vec{k}} \mathcal{E}_{\vec{k}}|}. \tag{7.72}$$

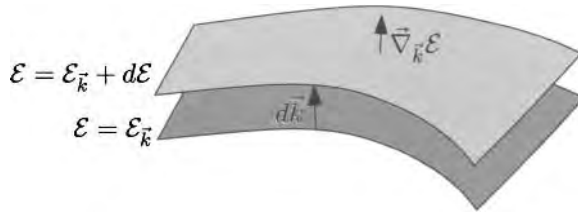


Figure 7.3. Two energy surfaces are separated by distance $d\mathcal{E}$, with a vector $d\vec{k}$ running from one to the other, the normal direction between the surfaces given by $\nabla_{\vec{k}} \mathcal{E}$.

Therefore, denoting by $d\Sigma$ an integral over the energy surface, Eq. (7.67) can be rewritten as

$$D(\mathcal{E}) = \frac{2}{(2\pi)^d} \int \frac{d\Sigma}{|\nabla_{\vec{k}} \mathcal{E}_{\vec{k}}|}. \quad \begin{array}{l} \text{The integral is a } (d-1) \text{ dimensional integral} \\ \text{in } \vec{k}\text{-space carried out over the energy surface} \\ \mathcal{E} = \mathcal{E}_{\vec{k}}. \end{array} \tag{7.73}$$

Comparing with Eq. (7.59), this means that the density of states has a singularity at points in reciprocal space where the electron velocity $\vec{v}_{n\vec{k}}$ vanishes. The origin of this singularity, in a one-dimensional context, is illustrated in Figure 7.4(A). In addition to the maxima and minima of the energy function, there can also be singularities at *saddle points*, [Figure 7.4(B)] which are at a maximum along some direction but a minimum along another.

In two and three dimensions, van Hove singularities behave as

$$D(\mathcal{E}) \sim \ln |\mathcal{E}/\mathcal{E}_0 - 1| \quad \text{or} \quad \theta(\pm \mathcal{E}) \quad \begin{array}{l} \text{In two dimensions; the first expression at sad-} \\ \text{dle, second at maximum or minimum.} \end{array} \tag{7.74}$$

$$D(\mathcal{E}) \sim \begin{cases} \sqrt{\mathcal{E}} & \text{for } \mathcal{E} > 0, \text{ 0 else,} \\ \text{or} \\ \sqrt{-\mathcal{E}} & \text{for } \mathcal{E} < 0, \text{ 0 else,} \end{cases} \quad \begin{array}{l} \text{In three dimensions, at maximum or mini-} \\ \text{mum. At saddle, have square roots meeting} \\ \text{in cusp.} \end{array} \tag{7.75}$$

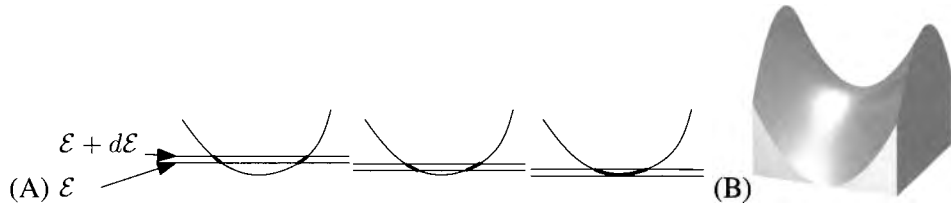


Figure 7.4. (A) If the states that contribute to some process are those that lie between \mathcal{E} and $\mathcal{E} + d\mathcal{E}$, then the number of states becomes singular when \mathcal{E} coincides with an extremal point on the energy surface. Compare with Figure 16.11. (B) A saddle point.

These claims are verified in Problem 3.

The van Hove singularities manifest themselves in a variety of physical contexts. They appear in calculations of electronic densities of states, shown throughout Section 10.4, in calculations of density of vibrational states as shown in Section 13.3.1, and are measured to a limited extent in experiments involving optical absorption, as shown in Section 23.4.

Uniqueness of Label \vec{k} . It may appear that one now has many more \vec{k} wave functions than one had in the case of free electrons. All states of free electrons can be labeled by the index \vec{k} . For electrons in a periodic potential, one has an additional index n as well. In fact, the number of eigenstates has not multiplied; the apparent difficulty is caused by a certain arbitrariness in how to label states.

Given any \vec{k} , one can find a set of wave functions

$$\psi_{1\vec{k}}, \psi_{2\vec{k}}, \psi_{3\vec{k}} \cdots \quad (7.76)$$

with differing energy eigenvalues, but with the same eigenvalues $\exp[i\vec{k} \cdot \vec{R}]$ when acted upon by $\hat{T}_{\vec{R}}^\dagger$. Choosing \vec{K} in the reciprocal lattice, consider now the eigenvalues of $\psi_{n, \vec{k} + \vec{K}}$. Because

$$e^{i(\vec{k} + \vec{K}) \cdot \vec{R}} = e^{i\vec{k} \cdot \vec{R}}, \quad (7.77)$$

it follows that

$$\psi_{n, \vec{k} + \vec{K}} = \psi_{n', \vec{k}}, \quad \text{For some integer } n' \neq n, \text{ since } \psi_{n\vec{k}} \text{ are defined to be all the wave functions with translational eigenvalue } \exp[i\vec{k} \cdot \vec{R}]. \quad (7.78)$$

There now are two possible ways to ensure that the set of all $\psi_{n\vec{k}}$ will be a complete and linearly independent set of wave functions. The first, called the *reduced zone scheme* is to limit the collection of \vec{k} vectors. In this convention, \vec{k} is permitted only if it belongs to the first Brillouin zone. Choosing \vec{k} 's in this way guarantees that no two of them can satisfy $\vec{k} = \vec{k}' + \vec{K}$.

The second way to avoid overcounting states is to drop the index n but allow \vec{k} to range through all of reciprocal space; this is the *extended zone scheme*. A state that was labeled $\psi_{n\vec{k}}$ in the reduced zone scheme will be labeled $\psi_{\vec{k} + \vec{K}_n}$ (for some reciprocal lattice vector \vec{K}_n) in the extended zone scheme.

Example: Free Electron. One can choose to regard a free electron as periodic over any lattice desired. This gives great freedom in indexing the states. Moving to the one-dimensional case for the purpose of illustration, suppose one uses the fact that a free electron Hamiltonian is periodic subject to translations through R . Bloch's theorem says in this case to index the wave function in the form

$$\psi_{nk} = e^{ikr} e^{i n Kr}, \quad \text{One can regard } n \text{ either as the band index,} \quad (7.79)$$

or as describing the multiple of the reciprocal lattice vector K to add to k .

where K is a primitive vector of the reciprocal lattice, and $-K/2 < k < K/2$ is the first Brillouin zone. In the reduced zone scheme, the name of the wave function in Eq. (7.79) is ψ_{nk} , with n a band index. In the extended zone scheme, the wave function is instead named $\psi_{k'}$, with $k' = k + nK$. These two ways of viewing Eq. (7.79) are drawn in in Figure 7.5, together with a third convention, called the *repeated zone scheme*, which shows what would happen if both k and n were allowed to range freely over all possible values.

Summary. To recapitulate, first index solutions of Schrödinger's equation by a vector \vec{k} that lies in the first Brillouin zone. For every value of \vec{k} there is a countably infinite number of energy bands, which can be labeled by band index n (reduced zone scheme) or by adding reciprocal lattice vectors \vec{K}_n to \vec{k} (extended zone scheme). Allowing \vec{k} to range over all reciprocal space and also retaining the band index n duplicates each eigenstate infinitely often (repeated zone scheme).

7.2.6 Kronig–Penney Model

Kronig and Penney (1931) found an exactly soluble model that illustrates the nature of energy bands. Suppose that in each unit cell of a one-dimensional lattice with lattice points $R = na$ and reciprocal lattice vectors K , there is a potential of the form

$$U_0 a \delta(x), \quad a \text{ is the lattice spacing.} \quad (7.80)$$

where U_0 has dimensions of energy. Then U_K as defined in Eq. (7.26) is simply

$$U_K = U_0, \quad (7.81)$$

and Eq. (7.33) becomes

$$0 = (\mathcal{E}_q^0 - \mathcal{E})\psi(q) + \sum_K U_0 \psi(q - K). \quad (7.82)$$

Define

$$Q_q = \sum_K \psi(q - K). \quad (7.83)$$

Then Eq. (7.82) becomes

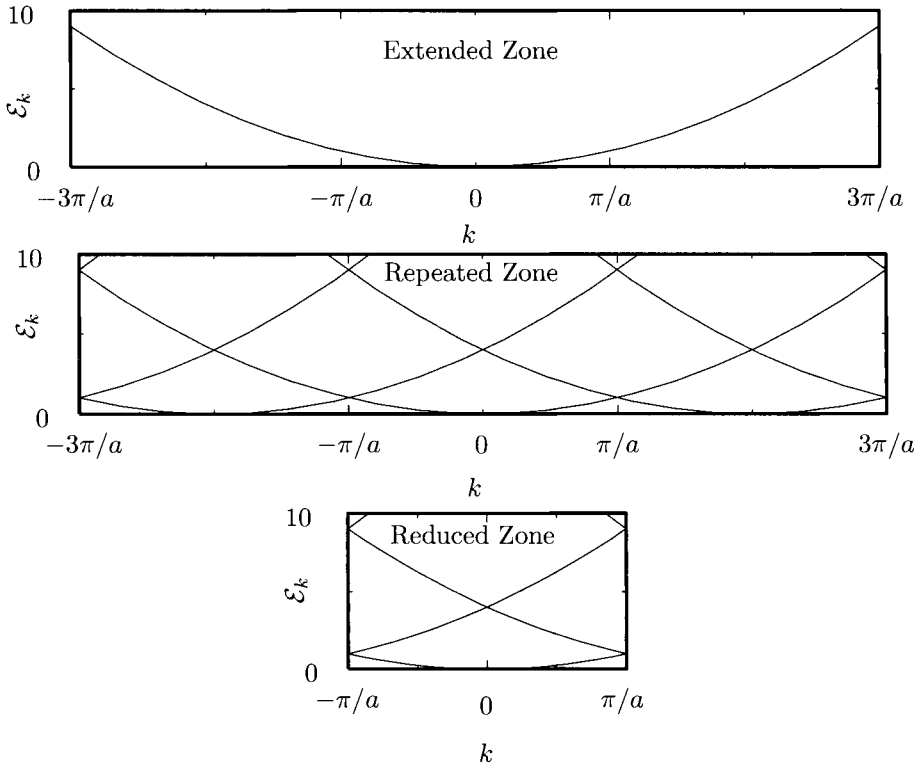


Figure 7.5. Three indexing schemes for labeling \vec{k} states are illustrated by plotting $\mathcal{E}_{\vec{k}}^0$ for the free electron. The first Brillouin zone is taken to extend from $-\pi/a$ to π/a . The extended zone scheme allows k to range throughout all reciprocal space. In the repeated zone scheme, one plots $\mathcal{E}_{\vec{k}}, \mathcal{E}_{\vec{k}+\vec{K}}, \mathcal{E}_{\vec{k}-\vec{K}} \dots$. Finally, in the reduced zone scheme, all wave vectors are mapped into the first Brillouin zone, so that energy levels originating from $k + nK$ are now regarded as belonging to an n th band. The extended zone scheme is the most natural way to plot free electron energy levels; however, in the presence of a periodic potential, $\mathcal{E}_{\vec{k}}$ is discontinuous in the extended zone scheme and is continuous in the reduced zone scheme.

$$\psi(q) + \frac{U_0}{\mathcal{E}_q^0 - \mathcal{E}} Q_q = 0. \tag{7.84}$$

Note from its definition (7.83) that

$$Q_q = Q_{q-K} \tag{7.85}$$

for all reciprocal lattice vectors K . So

$$\psi(k-K) + \frac{U_0}{\mathcal{E}_{k-K}^0 - \mathcal{E}} Q_{k-K} = 0 \quad \text{Just evaluate Eq. (7.84) at } q = k-K. \tag{7.86}$$

$$\Rightarrow \sum_K \left[\psi(k-K) + \frac{U_0}{\mathcal{E}_{k-K}^0 - \mathcal{E}} Q_k \right] = 0 \quad \text{Sum on } K \text{ and use Eq. (7.85).} \tag{7.87}$$

$$\Rightarrow Q_k + \sum_K \frac{U_0}{\mathcal{E}_{k-K}^0 - \mathcal{E}} Q_k = 0. \quad \text{Definition Eq. (7.83).} \tag{7.88}$$

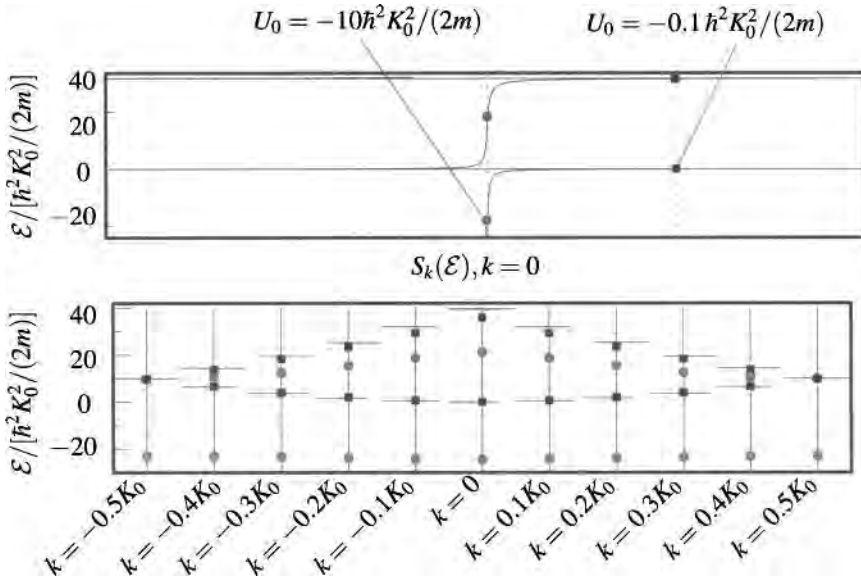


Figure 7.6. In order to solve Eq. (7.89), choose a value of k and then find when the sum $S_k(\mathcal{E}) = \sum_K 1/(\mathcal{E}_{k-K}^0 - \mathcal{E})$ equals $-1/U_0$ by varying \mathcal{E} . The sums are carried out for a chain of spacing a . In the upper portion of the figure, \mathcal{E} lies along the vertical axis, and $S_k(\mathcal{E})$ is plotted on the horizontal axis for $k = 0.2K_0$, where $K_0 = 2\pi/a$. In the lower portion of the figure, this procedure is carried out for 10 consecutive values of k . For each plot of $S_k(\mathcal{E})$, one checks to see where S_k equals $-1/U_0$, shown as a vertical line. The intersection point is a solution of Eq. (7.89), and the collection of intersection points gives \mathcal{E}_k . By varying U_0 , one varies the shapes of the bands \mathcal{E}_k . When U_0 is small, they are free-electron like, while when U_0 is large they are very nearly flat.

Assuming that Q_k does not vanish, one has finally that

$$-\frac{1}{U_0} = \sum_K \frac{1}{\mathcal{E}_{k-K}^0 - \mathcal{E}} \equiv S_k(\mathcal{E}). \tag{7.89}$$

Equation (7.89) is easy to solve numerically. The method is illustrated graphically in Figure 7.6.

Energy levels for the periodic array of delta-function potentials appear in Figure 7.7. This figure should be compared with Figure 7.5. The effects of the potential are especially strong at the edges of the first Brillouin zone. It is crucial to note that \mathcal{E}_k is now discontinuous in the extended zone scheme but continuous in the repeated and reduced zone schemes. The origin of the gaps between the energy levels will be the subject of Section 8.2.

The motivation for creating the repeated and reduced zone schemes should now be evident. These index energy states so that energy levels remain continuous functions of k in the presence of a periodic potential. The band energy \mathcal{E}_{nk} is a continuous, periodic function of k .

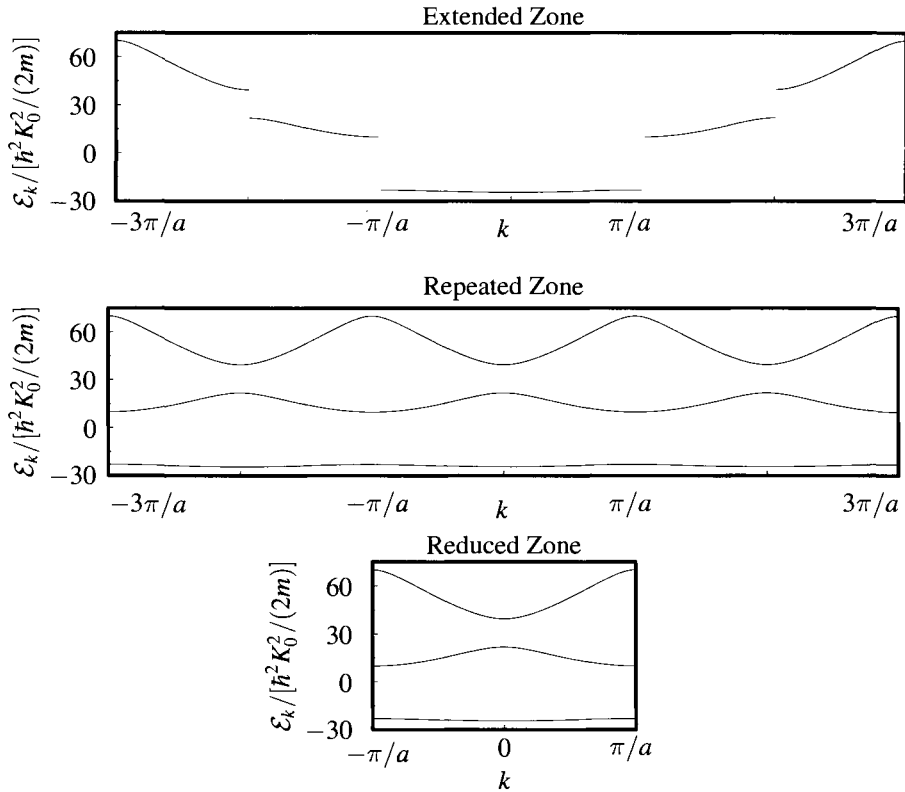


Figure 7.7. Bands resulting from Eq. (7.89) with $U_0 = -10\hbar^2 K_0^2 / (2m)$ and for a one-dimensional lattice of lattice constant a , shown in the reduced, repeated, and extended zone schemes. The calculation sketched in Figure 7.6 produces the bands in the reduced zone scheme directly; by translating these bands through various multiples of the reciprocal lattice vector $K_0 = 2\pi/a$, the upper two plots can be produced.

7.3 Rotational Symmetry—Group Representations

Consider a lattice with a collection of point group operations $\{G\}$ leaving it invariant. All the possible operations are represented by 3×3 unitary matrices and have been listed in Table 2.10; rotations through 60° , 90° , or 120° as well as reflections. The stereograms of Table 2.9 allow one to read off the sets of symmetry operations that correspond to the 32 point groups.

The theory of group representations describes the consequences of these symmetries for solutions of Schrödinger's equation. These consequences are not as dramatic or important as those that follow from translational freedom, as reflected in Bloch's theorem. Bloch's theorem takes a problem involving 10^{23} atoms and reduces it to a problem involving only one or two. By comparison, the simplifications provided by rotational symmetries may only reduce computational effort by a factor of something like 3 or 24. The significance of group representations lies elsewhere. By carefully describing the possible symmetries of electron states, one can obtain *selection rules* that predict when light or other external agents are

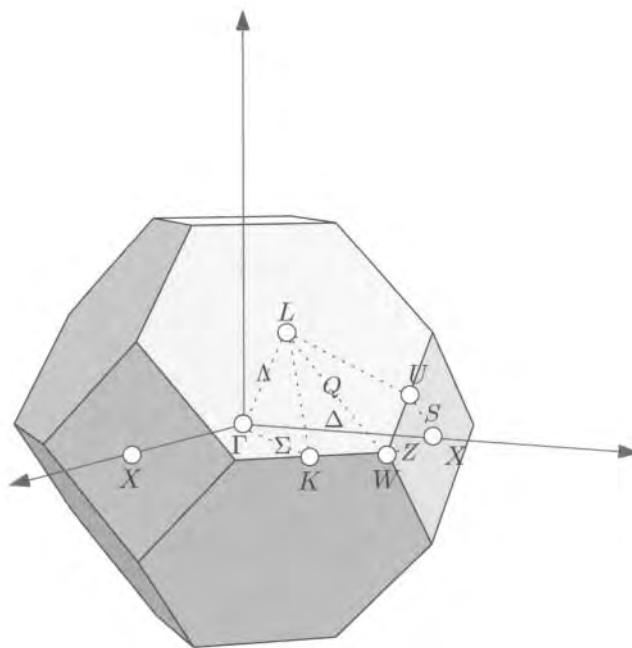


Figure 7.8. First Brillouin zone of the fcc lattice, with conventional notation for points of special symmetry. The reciprocal lattice of fcc is bcc, with lattice spacing of $4\pi/a$, so this polyhedron is the same as in Figure 2.3(B). In units of $2\pi/a$, $\Gamma = (0\ 0\ 0)$, $X = (0\ 1\ 0)$, $L = (1/2\ 1/2\ 1/2)$, $W = (1/2\ 1\ 0)$, $K = (3/4\ 3/4\ 0)$, and $U = (1/4\ 1\ 1/4)$.

capable of inducing transitions from one electron state to another. Predicting the strength of an allowed transition requires lengthy, detailed, and often questionable calculation. By contrast, distinguishing between allowed and forbidden transitions depends upon knowledge of symmetry alone. For this reason, the notation of group representations decorates experimental diagrams in numerous branches of condensed matter physics, particularly those involving optical absorption.

Figures 7.8 to 7.10 show the Brillouin zones of the fcc, bcc, and hexagonal lattices, annotated with points of special symmetry. For many purposes, it is enough to refer back to these figures as a reference for the conventional notation, without knowing the theory of symmetry that accompanies them. The theory is developed at some length, from various points of view, by Bradley and Cracknell (1972), Koster (1957), Lyubarskii (1960), Murnaghan (1938), or Tinkham (1964).

Group Operations. To develop the theory, suppose one has any set of symmetry operations (matrices) $\{G\}$ that form a *group*. The definition of a group demands that the collection $\{G\}$ satisfy three requirements.

1. The group must contain the unit matrix, which in this subject is traditionally denoted by E .
2. The product of any two matrices G_1 and G_2 in the group must be another matrix G_3 in the group.

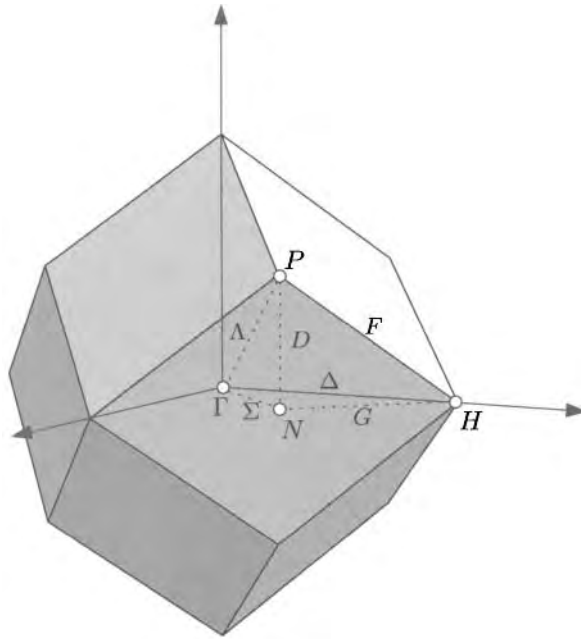


Figure 7.9. First Brillouin zone of the bcc lattice, with conventional notation for points of special symmetry. The reciprocal lattice of bcc is fcc, with lattice spacing of $4\pi/a$, so this polyhedron is the same as in Figure 2.2(B). In units of $2\pi/a$, $\Gamma = (0\ 0\ 0)$, $H = (0\ 1\ 0)$, $N = (1/2\ 1/2\ 0)$, and $P = (1/2\ 1/2\ 1/2)$.

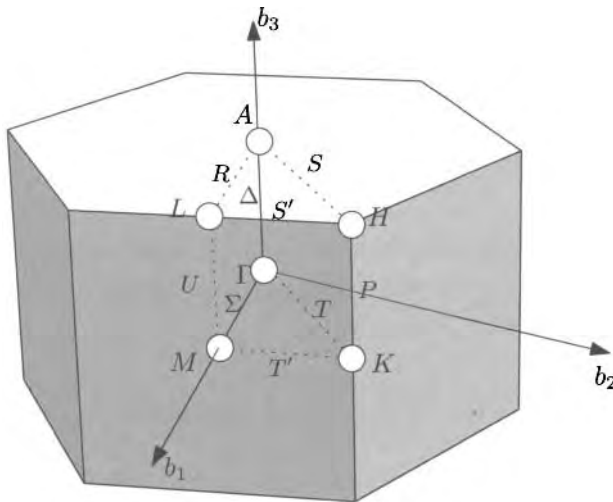


Figure 7.10. First Brillouin zone of the hexagonal lattice, with conventional notation for points of special symmetry. Using coordinates $\vec{b}_1 = 4\pi/a\sqrt{3} (\sqrt{3}/2\ -1/2\ 0)$, $\vec{b}_2 = 4\pi/a\sqrt{3} (\sqrt{3}/2\ 1/2\ 0)$ and $2\pi/c (0\ 0\ 1)$; $\Gamma = (0\ 0\ 0)$, $A = (0\ 0\ 1/2)$, $M = (1/2\ 0\ 0)$, $K = (1/3\ 1/3\ 0)$, $H = (1/3\ 1/3\ 1/2)$, and $L = (1/2\ 0\ 1/2)$.

3. The inverse of every matrix in the group must also belong to the group.

To obtain a *representation* of the group $\{G\}$, pick some function $\psi_j(\vec{r})$, which in practice might be a wave function. Next, create all the functions $\psi_j(G\vec{r})$; that is, take ψ_j , and rotate and reflect it using all the symmetry operations in $\{G\}$. Actually, $\psi_j(G\vec{r})$ rotates ψ_j through G^{-1} , not G , but because G^{-1} is also in the group, it does not matter. Even if the number of matrices in the group, its *order*, is h , the number l of linearly independent functions $\psi(\vec{r})$ generated in this way will generally be less than or equal to h . For each element G in the group, one must have

$$\psi_i(G\vec{r}) = \sum_j A(G)_{ij} \psi_j(\vec{r}). \tag{7.90}$$

In this fashion, one obtains a matrix $A(G)$ corresponding to each symmetry operation G ; the set of matrices $\{A\}$ is called a *representation* of the original group of symmetry operations. The dimensions of the matrices A generally are quite different from the dimensions of the original matrices G , because the dimension of A is determined by the number of linearly independent ψ 's one happens to obtain by applying rotations and reflections G to ψ_j , while all G 's are three-dimensional. Lyubarskii (1960), p. 44, shows that the matrices A can all be taken to be unitary, so one can assume

$$A^* = A^{-1} \text{ as well as } G^* = G^{-1} \text{ This is just the definition of a unitary matrix.} \tag{7.91}$$

in everything that follows.

Two group representations $\{A^{(n)}\}$ and $\{A^{(m)}\}$ are *equivalent* if there exists a single invertible matrix M such that

$$M^{-1}A^{(n)}(G)M = A^{(m)}(G), \text{ This relation has to hold with a single } M \text{ for all the different matrices } A(G) \text{ produced by varying } G. \tag{7.92}$$

which means that one obtains $\{A^{(n)}\}$ from $\{A^{(m)}\}$ just by changing coordinate systems. By making a good choice of M , one will often be able to simplify the matrices $\{A\}$ substantially, by bringing all of them into the form

$$\left(\begin{array}{ccc|ccc} a_{11} & \dots & a_{1l'} & & & \\ \cdot & & \cdot & & & \\ \cdot & & \cdot & & 0 & \\ \cdot & & \cdot & & & \\ a_{l'1} & \dots & a_{l'l'} & & & \\ & & & b_{11} & \dots & b_{1l''} \\ & & & \cdot & & \cdot \\ & 0 & & \cdot & & \cdot \\ & & & \cdot & & \cdot \\ & & & b_{l''1} & \dots & b_{l''l''} \end{array} \right) \tag{7.93}$$

l' and l'' need not be the same, and there could be more than two independent blocks.

The reason that putting all matrices $\{A\}$ into form (7.93) provides such an advantage is that it means that the wave functions ψ_j break into two subsets, one containing l' wave functions, the other containing l'' wave functions, each of which transforms exclusively into itself. The original $l = l' + l''$ -dimensional representation has been simplified into an l' -dimensional representation and an l'' -dimensional representation, and the original representation is called *reducible*. If, on the other hand, no M exists which can put all matrices into the form (7.93) simultaneously, the representation is called *irreducible*.

Faced with 24 ten-dimensional matrices, the task of finding whether there exists some M to bring them into block diagonal form seems rather daunting. The whole question can, however, be settled by diagonalizing a single ten-dimensional matrix. Begin with an absolutely arbitrary matrix X , let $\{A^{(m)}\}$ and $\{A^{(n)}\}$ be any two representations of $\{G\}$ both of dimension l , and form

$$M = \sum_G A^{(m)}(G) X A^{(n)}(G^*). \quad (7.94)$$

Then

$$A^{(m)}(G)M = \sum_{G'} A^{(m)}(G)A^{(m)}(G') X A^{(n)}(G'^*) \quad (7.95)$$

$$= \sum_{G'} A^{(m)}(GG') X A^{(n)}(G'^*) \quad \text{See Problem 6} \quad (7.96)$$

$$= \sum_{G'} A^{(m)}(G') X A^{(n)}(G'^*G) \quad \begin{array}{l} \text{Change order of summation by} \\ \text{sending } G' \rightarrow G^*G' \end{array} \quad (7.97)$$

$$= \sum_{G'} A^{(m)}(G') X A^{(n)}(G'^*)A^{(n)}(G) = MA^{(n)}(G). \quad (7.98)$$

Comparing with Eq. (7.92), at first it appears that all representations have been proved to be equivalent. However, $A^{(m)}$ and $A^{(n)}$ are only equivalent if M has an inverse. One can use M to best advantage by remarking that M^* also obeys Eq. (7.98), and therefore so does $M + M^* = P$, which is Hermitian. So now one has a Hermitian matrix P with

$$A^{(n)}(G)P = PA^{(m)}(G). \quad (7.99)$$

Because P is Hermitian, it can be diagonalized and has an orthonormal basis of real eigenvalues. Express all the matrices $A^{(m)}(G)$, $A^{(n)}(G)$, and P in this basis. One is now in a position to decompose any given representation into irreducible pieces and to show that different irreducible representations are orthogonal.

To accomplish the first task, let $n = m$ be the same, and drop this superscript for the moment. In the basis where P is diagonal, one has for the ij element of Eq. (7.99)

$$A(G)_{ij}P_{jj} = P_{ii}A(G)_{ij} \Rightarrow (P_{ii} - P_{jj})A(G)_{ij} = 0 \quad (7.100)$$

So there are two possibilities. Either $P_{ii} = P_{jj}$, or else $A(G)_{ij} = 0$. However, if even a single off-diagonal element such as $A(G)_{12}$ vanishes for all G , then A is reducible. The reason is this: Saying that $A(G)_{12}$ vanishes means that no group

operation transforms ψ_1 into ψ_2 . This statement means in turn that as one scans over all the wave functions $G\psi_1$, none of them can be transformed into ψ_2 either, for if one could, then the product of the two group operations would take ψ_1 into ψ_2 . Because the sets of wave functions generated by $G\psi_1$ and $G\psi_2$ are disjoint, the representation is reducible.

If there are, say, ten nonzero eigenvalues, of which three have value P_{11} , two have value P_{44} , and the rest are all different from one another, then one has reduced the original ten-dimensional representation into one three-dimensional representation, one two-dimensional representations, and five one-dimensional representations. If, on the other hand, $\{A\}$ is irreducible, then all the P_{ii} are the same, and therefore P and M are simply multiples of the unit matrix.

When the matrix X in Eq. (7.95) is chosen randomly, then the representations uncovered by Eq. (7.100) are almost certainly irreducible. There are definitive tests that allow one to decide this question with certainty, resulting from the fact that either two representations are equivalent or else they are orthogonal to one another, shown as follows:

Suppose the representations $\{A^{(m)}\}$ and $\{A^{(n)}\}$ are both irreducible in Eq. (7.99). Problem 6 shows that from Eq. (7.99) one can also deduce

$$A^{(m)}(G)PP^* = PP^*A^{(m)}(G) \Rightarrow (P_{ii}^2 - P_{jj}^2)A^{(m)}(G)_{ij} = 0. \quad (7.101)$$

Because by assumption $\{A^{(m)}\}$ is irreducible, one cannot allow even a single off-diagonal element of $A^{(m)}(G)$ to vanish for all G , and accordingly all of the diagonal elements P_{ii}^2 are equal. If they are nonzero, then P must be invertible, and accordingly $\{A^{(m)}\}$ and $\{A^{(n)}\}$ are equivalent. If, on the other hand, $\{A^{(m)}\}$ and $\{A^{(n)}\}$ are inequivalent, then all diagonal elements P_{ii} must vanish, for all starting matrices X in Eq. (7.94).

It is interesting to examine the consequences of choosing for X a matrix whose only nonzero element is at position $\beta\gamma$:

$$X_{ij} = \delta_{i\beta}\delta_{j\gamma} \quad (7.102)$$

$$\Rightarrow M_{\alpha\delta} = \sum_{G,i,j} A^{(m)}(G)_{\alpha i} \delta_{i\beta}\delta_{j\gamma} A^{(n)}(G^*)_{j\delta} \quad (7.103)$$

$$= \sum_G A^{(m)}(G)_{\alpha\beta} A^{(n)}(G^*)_{\gamma\delta}. \quad (7.104)$$

Suppose first that $\{A^{(m)}\}$ and $\{A^{(n)}\}$ are not equivalent. Then according to the discussion following Eq. (7.101), P and hence M must vanish. Therefore

$$\sum_G A^{(m)}(G)_{\alpha\beta} A^{(n)}(G^*)_{\gamma\delta} = 0. \quad \text{If } \{A^{(m)}\} \text{ and } \{A^{(n)}\} \text{ are not} \quad (7.105) \\ \text{equivalent representations.}$$

If, on the other hand, $\{A^{(m)}\}$ and $\{A^{(n)}\}$ are the same and irreducible, then M must be a multiple of the unit matrix, and

$$\sum_G A(G)_{\alpha\beta} A(G^*)_{\gamma\delta} = C_{\beta\gamma} \delta_{\alpha\delta} \quad \text{The precise multiple } C_{\beta\gamma} \text{ of (7.106)} \\ \text{the unit matrix depends} \\ \text{upon the choice of } \beta\gamma \text{ in} \\ \text{Eq. (7.102).}$$

$$\Rightarrow \sum_{\alpha} \sum_G A(G)_{\alpha\beta} A(G^*)_{\gamma\alpha} = l C_{\beta\gamma} \quad \text{Evaluate for } \alpha = \delta \text{ and then (7.107) sum on } \alpha.$$

$$= \sum_G A(G^*G)_{\beta\gamma} = h \delta_{\beta\gamma} \Rightarrow C_{\beta\gamma} = \frac{h}{l} \delta_{\beta\gamma} \quad \text{See Problem 6, Eq. (7.133). Recall } l \text{ is the dimension of the representation, } \{A\}. \quad (7.108)$$

$$\Rightarrow \sum_G A(G)_{\alpha\beta} A(G^*)_{\gamma\delta} = \frac{h}{l} \delta_{\beta\gamma} \delta_{\alpha\delta}. \quad h \text{ is the number of elements in the group } \{G\}. \quad (7.109)$$

Finally, Eqs. (7.105) and (7.109) can be combined into the *grand orthogonality theorem*

$$\sum_G A^{(m)}(G)_{\alpha\beta} A^{(n)}(G^*)_{\gamma\delta} = \frac{h}{l} \delta_{nm} \delta_{\beta\gamma} \delta_{\alpha\delta}. \quad \begin{array}{l} l \text{ is the dimension of the} \\ \text{matrices in representation} \\ m = n; h \text{ is the number of} \\ \text{group elements.} \end{array} \quad (7.110)$$

7.3.1 Classes and Characters

In the discussion of Section 2.4, transformations divided naturally into various *classes*, which were all denoted by the same symbol. For example, all rotations by 60° about \hat{z} form one class. The formal definition of a class of operations containing some group element G_1 is that it is the set of all transformation matrices obtained by subjecting G_1 to $G_i^{-1} G_1 G_i$, where i ranges over all elements of the group. The intuitive meaning of this definition is that two transformations belong to the same class if by changing coordinate systems according to symmetries of the group, one transformation turns into the other. In this sense, all the symmetry operations belonging to a class are really the same.

Example: D_{3d} . Consider the point group D_{3d} . Its symmetry elements are given in Table 7.2:

Table 7.2. Symmetry elements in D_{3d}

E	Identity
i	Inversion
$\{2C_3\}$	Rotation about \hat{z} through $\pm 120^\circ$; two elements in class.
$\{2S_3\}$	Rotation-inversion about \hat{z} through $\pm 60^\circ$; two elements in class.
$\{3C_2\}$	Three two-fold rotation axes.
$\{3\sigma\}$	Three mirror planes.

Because the symmetry operations within a class are physically indistinguishable from one another, it is valuable to find mathematical features of group representations that are constant within a class. The most easily calculated quantity of this type is the *character* of a representation,

$$\chi(G) \equiv \sum_{\alpha} A_{\alpha\alpha}(G) = \text{Tr}[A(G)]. \quad \text{The character is the trace of the matrix } A. \quad (7.111)$$

The character of two different members of a class must be the same because for any G_1 and G_2 in the same class, one obtains

$$\chi(G_1) = \text{Tr}[G_1] = \text{Tr}[G_3^* G_2 G_3] \quad \begin{array}{l} G_1 \text{ and } G_2 \text{ are in the same class, by definition,} \\ \text{if there exists } G_3 \text{ so that } G_1 = G_3^* G_2 G_3. \end{array} \quad (7.112)$$

$$= \text{Tr}[G_2 G_3 G_3^*] \quad (7.113)$$

$$= \text{Tr}[G_2] = \chi(G_2) \quad \begin{array}{l} \text{Using the cyclic property of the trace,} \\ \text{Tr}[ABC] = \text{Tr}[BCA], \text{ easily derived by} \\ \text{writing everything out in component} \\ \text{form.} \end{array} \quad (7.114)$$

In terms of the characters χ , the orthogonality theorem, Eq. (7.110) can be recast as

$$\sum_{G\alpha\gamma} A^{(m)}(G)_{\alpha\alpha} A^{(n)}(G^*)_{\gamma\gamma} = \sum_{\alpha\gamma} \frac{h}{l} \delta_{nm} \delta_{\alpha\gamma} \quad (7.115)$$

$$\Rightarrow \sum_G \chi^{(m)}(G) \chi^{(n)}(G^*) = h \delta_{nm} \quad (7.116)$$

$$\Rightarrow \sum_k N_k \chi^{(m)}(C_k) \chi^{(n)*}(C_k) = h \delta_{nm}. \quad \begin{array}{l} \text{The sum on } k \text{ is over the distinct classes } C_k \text{ of (7.117)} \\ G, \text{ each of which has } N_k \text{ elements.} \end{array}$$

One use of Eq. (7.116) is to provide a sure test of whether a representation is irreducible or not. If the representation is irreducible, then taking the traces of all the matrices that compose it, taking their absolute square, and summing over all the matrices, one must get just the order of the group h . If, on the other hand, the representation is reducible, when one forms the sum described by Eq. (7.116) with $n = m$, it must come out to more than h . The reason for this claim is that the character of each matrix equals the sum of the characters of the irreducible representations that compose it. If irreducible representation p occurs s_p times, then the character corresponding to G is $\sum_p s_p \chi^{(p)}(G)$, and instead of getting h upon performing the sum in Eq. (7.116), one gets $h \sum s_p^2$.

A final orthogonality relation can be obtained from Eq. (7.117), if one assumes a theorem whose proof is slightly too lengthy to include here, given by Murnaghan (1938) p. 84, that the number of classes equals the number of irreducible representations. Given this fact, the characters can be used to form square matrices

$$\chi^{(m)}(C_k) \equiv Q_{mk}; \quad \chi^{(m)*}(C_k) N_k \equiv Q'_{km} \quad (7.118)$$

$$\Rightarrow \sum_k Q_{mk} Q'_{kn} = h \delta_{nm} \quad (7.119)$$

$$\Rightarrow \sum_k Q'_{nk} Q_{km} = h \delta_{nm} \quad \begin{array}{l} \text{Using the fact that the matrices} \\ \text{are square, so } Q' = Q^{-1}. \end{array} \quad (7.120)$$

$$\Rightarrow \sum_k N_k \chi^{(k)}(C_n) \chi^{(k)*}(C_m) = h \delta_{nm}. \quad (7.121)$$

The square matrix Q_{mk} is called a *character table*. All the traces $\chi^{(m)}(C_n)$ are integers; using this fact with Eqs. (7.117) and (7.121), it is often possible to work out all the entries of Q without further information.

Table 7.3. Character table for the group D_{3d}

	E	i	$2C_3$	$2iC_3$	$3C_2$	$3iC_2$
L_1	1	1	1	1	1	1
L'_2	1	-1	1	-1	1	-1
L_2	1	1	1	1	-1	-1
L'_1	1	-1	1	-1	-1	1
L_3	2	2	-1	-1	0	0
L'_3	2	-2	-1	1	0	0

Example: D_{3d} .

Consider again the point group D_{3d} . It has six classes, with a total of 12 symmetry elements. One irreducible representation is very easy to find: Map every element of the group to 1. All the characters χ are 1 in this representation, giving the top row of the character table. A column of the character table is easily determined by examining Eq. (7.121) when $n = m$ and choosing for C_n the class of the identity operation E . In an l -dimensional representation, the identity operation is always represented by an l -dimensional unit matrix, and its character is just l ; that is, $\chi^{(m)}(E) = l_m$. Therefore, according to Eq. (7.121), one obtains

$$\sum_m l_m^2 = h. \quad (7.122)$$

When $h = 12$, and there are six integer l 's over which to sum, there is only one way to make things work out, which is to have four representations with $l = 1$ and two representations with $l = 2$. Accordingly, the first column of Table 7.3 is as shown. There is one other class with only one element, inversion i . The column below this class can only contain the same integers that lie under E , because the sum of their squares must still be 12, but negative signs are also allowed. The only way to make this column orthogonal to the preceding one is to distribute minus signs as shown. The minus signs could be ordered a bit differently; for example, the first occurrence of 2 could be negative rather than the second, but this would in the end correspond only to relabeling the rows. Proceed next to the two classes with two elements. The sum of squares of entries in this column must add up to six, a goal that can only be achieved if all entries are ± 1 . There are only two ways to make vectors of ± 1 that are orthogonal to the preceding two columns, and these appear underneath $2C_3$ and $2iC_3$. Finally, one must find two columns of integers where the sum of squares of the entries adds up to four, and which must again be orthogonal to all preceding columns.

Notation for Cubic Group O_h . A companion of the theory of group representations is conventional notation for symmetrical functions. The irreducible representations of O_h are referred to particularly frequently because they describe wave functions and lattice vibrations in cubic crystals, including those with the diamond structure, as in Figures 23.15 and 23.16. Notation for these irreducible representations appears in Table 7.4.

Table 7.4. Irreducible representations of O_h

BSW	K	d	Basis functions
Γ_1	Γ_1^+	1	1
Γ_2	Γ_2^+	1	$x^4(y^2 - z^2) + y^4(z^2 - x^2) + z^4(x^2 - y^2)$
Γ_{12}	Γ_3^+	2	$[z^2 - (x^2 + y^2)/2], [x^2 - y^2]$
$\Gamma_{15'}$	Γ_4^+	3	$[yz(y^2 - z^2)], [zx(z^2 - x^2)], [xy(x^2 - z^2)]$
$\Gamma_{25'}$	Γ_5^+	3	$[xy], [yz], [zx]$
$\Gamma_{1'}$	Γ_1^-	1	$xyz \{x^4(y^2 - z^2) + y^4(z^2 - x^2) + z^4(x^2 - y^2)\}$
$\Gamma_{2'}$	Γ_2^-	1	xyz
$\Gamma_{12'}$	Γ_3^-	2	$[xyz \{z^2 - (x^2 + y^2)/2\}], [xyz \{x^2 - y^2\}]$
Γ_{15}	Γ_4^-	3	$[x], [y], [z]$
Γ_{25}	Γ_5^-	3	$[x(y^2 - z^2)], [y(z^2 - x^2)], [z(x^2 - y^2)]$

Irreducible representations of O_h , using the notation of Bouckaert, Smoluchowski, and Wigner (1936)—BSW—and of Koster (1957)—K; also listed are the dimension d of the representation, along with a set of basis functions that transform into each other in accord with each representation.

7.3.2 Consequences of point group symmetries for Schrödinger’s equation

Point group symmetries and the theory of group representations have two immediate implications for solutions of Schrödinger’s equation in periodic potentials. First, they may be used to reduce the computational effort in calculating energy bands, and second they may be used to identify places in \vec{k} space where energy bands will be degenerate.

The first application is fairly obvious and requires no knowledge of the representations. Suppose one has a point group symmetry G —for example a rotation matrix. No physical measurement can vary if one subjects the crystal to the operation of G . In particular, if one begins with a wave function at wave vector \vec{k} , $\psi_{\vec{k}} = e^{i\vec{k}\cdot\vec{r}} u_{\vec{k}}(\vec{r})$, then another wave function at wave vector $G\vec{k}$ results from constructing

$$\psi_{G\vec{k}} = e^{iG\vec{k}\cdot\vec{r}} u_{\vec{k}}(G^{-1}\vec{r}). \quad \text{Note that } \vec{k}\cdot G\vec{r} = G\vec{k}\cdot\vec{r} \text{ because the dot product is invariant when both vectors in the product are rotated by the same matrix.} \quad (7.123)$$

The two wave functions $\psi_{n\vec{k}}$ and $\psi_{nG\vec{k}}$ can be made orthogonal to one another if need be, and have the same energy eigenvalue. So for all point group symmetries,

$$\mathcal{E}_{n,\vec{k}} = \mathcal{E}_{n,G\vec{k}}. \quad (7.124)$$

Because the first Brillouin zone is invariant under such point group operations, it makes sense to divide the Brillouin zone into regions, called *irreducible zones*, that can be repeated under point group operations to fill out the complete Brillouin

zone. Each irreducible zone is a copy of all the others and has identical energy surfaces, so one can restrict attention to one such zone.

These arguments, however, rely upon the assumption that the symmetry operation G acting upon \vec{k} produced a wave vector physically distinguishable from it, which is not the case if \vec{k} and $G\vec{k}$ differ only by a reciprocal lattice vector. While this assumption is true in general, it fails at special points in the irreducible zone. For these points, a symmetry operation that leaves the wave vector unchanged (up to a reciprocal lattice vector) may or may not produce a new wave function when it acts on the wave function one begins with. If the new wave function produced by the symmetry operation is just a multiple of the old one, there is no particularly interesting conclusion. But if the symmetry operation produces a linearly independent wave function, then more than one wave function corresponds to a single wave vector in the irreducible zone at a given energy; one has a degeneracy.

It is intuitively clear that some points in the Brillouin zone are more symmetrical than others. In Figure 7.11, the point Γ is obviously the most symmetrical of all; points along T are symmetrical, but not as symmetrical as K . The point q is not symmetrical at all. The formal definition of the degree of symmetry for a point in the Brillouin zone is very simple. For a given vector \vec{k} in the Brillouin zone, the group of that vector is the group of point group operations $\{\tilde{G}\}$ such that

$$\tilde{G}\vec{k} = \vec{k} + \vec{K}_i \quad \begin{array}{l} \text{The conventional notation for symmetry point } K \\ \text{and reciprocal lattice vector } \vec{K} \text{ are easily confused.} \end{array} \quad (7.125)$$

for some reciprocal lattice vector \vec{K}_i . For example, the points along T are left invariant when the hexagon is reflected around T ; the point K is left invariant by that reflection, and also can be operated upon by two more reflections and two rotations, which move it to the corners indicated in Figure 7.11. The point Γ is invariant under all point group operations.

Thus, the application of group representations to Schrödinger's equation proceeds by choosing some \vec{k} , such as K in Figure 7.11, and taking the group of operations $\{G\}$ which leaves \vec{k} invariant up to a reciprocal lattice vector. Once $\{G\}$ has been determined, certain consequences follow from its irreducible representations. The only necessary fact is that to the group corresponds a collection of integers, which are the dimensions of its representations. At least one of these integers is 1. If some of these integers are greater than 1, then there must exist some energy levels at this wave vector with the corresponding degeneracy. Unfortunately, the information provided by these dimensions is rather like a political spokesman who raises various possible scenarios, but refuses to confirm or deny any particular one. Any particular energy level could have any degree of degeneracy made possible by any of the dimensions. It could even have greater degeneracy than at first appears possible, if parameters of the Hamiltonian are specially chosen so that two generically different levels coincide, leading to an *accidental degeneracy*.

Example: Symmetry Points in Figure 7.11. The symmetry group of Γ is C_{6v} . Inspection of Table 2.9 shows that this group has six classes: the identity operation,

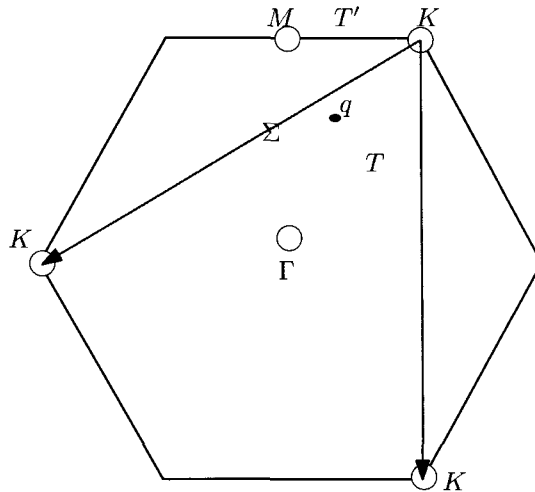


Figure 7.11. Symmetries of a hexagonal unit cell; Γ , M , and K label points, while Σ , T , and T' label lines. All points labeled K are equivalent because they differ only by addition of a reciprocal lattice vector.

one 180° rotation, two 60° rotations, two 120° rotations, and six mirror planes, split into two classes of three each. Referring to Figure 7.11, one class of mirror planes contains those bisecting the faces of the mirror planes, while the other class contains the mirror planes passing through the corners of the hexagon. The number of elements in each class of C_{6v} is exactly the same as the number of elements in each class of D_{3v} , Table 7.3; therefore, as discussed in that case, C_{6v} must have four one-dimensional irreducible representations and two two-dimensional irreducible representations. Therefore, it is possible for an energy level at $\vec{k} = \Gamma$ to be twofold degenerate. The symmetry group at K is obtained by decorating the hexagon of Figure 7.11 with the three circles labeled K . The symmetry classes are the identity, two 120° rotations, and three mirror planes. The sums of the squares of the three irreducible representations must sum to six; there must be two one-dimensional irreducible representations and one two-dimensional irreducible representation. Thus a wave function with Bloch index located at K can also be twofold degenerate. The symmetry groups at all other points allow only one-dimensional irreducible representations. At M , for example, the symmetry classes are the identity, one 180° rotation, and one mirror plane, leading to three one-dimensional irreducible representations. Wave functions therefore have no reason to be degenerate with Bloch index at M .

Problems

1. **Normals to surfaces:** Consider a function $f(\vec{r})$, and consider the surface defined by

$$f(\vec{r}) = \mathcal{E}, \quad (7.126)$$

where \mathcal{E} is a constant. Let $\vec{s}(t)$ be a curve that lies within the surface defined by Eq. (7.126), parametrized by t . Observing that

$$\frac{\partial}{\partial t} f(\vec{s}(t)) = 0, \quad (7.127)$$

show that $\vec{\nabla} f$ is normal to the surface.

2. **Commutation:** Show that the translation operators $\hat{T}_{\vec{R}}$ defined in Eq. (7.38) commute with each other, and with the Hamiltonian (7.2), using the symmetry Eq. (7.1).
3. **Van Hove Singularities:**

- (a) Consider an energy surface defined by $\mathcal{E} = \mathcal{E}_{n\vec{k}}$. Show that $\nabla_{\vec{k}} \mathcal{E}_{\vec{k}}$ is perpendicular to all vectors lying parallel to the energy surface, and therefore points in the normal direction.
- (b) Suppose that one has a two-dimensional crystal and finds a value of \vec{k} near which

$$\mathcal{E}_{n\vec{k}} \approx \mathcal{E}_{\max} - k^2. \quad (7.128)$$

Find the singularity that will be produced in $D(\mathcal{E})$.

- (c) Repeat this problem for a three-dimensional crystal.
4. **Kronig–Penney numerics:** Use a computer to reproduce Figure 7.6 by the methods described in the caption of the figure.
5. **Kronig–Penney model:** Consider an electron in one dimension in the presence of the potential shown in Figure 7.12:

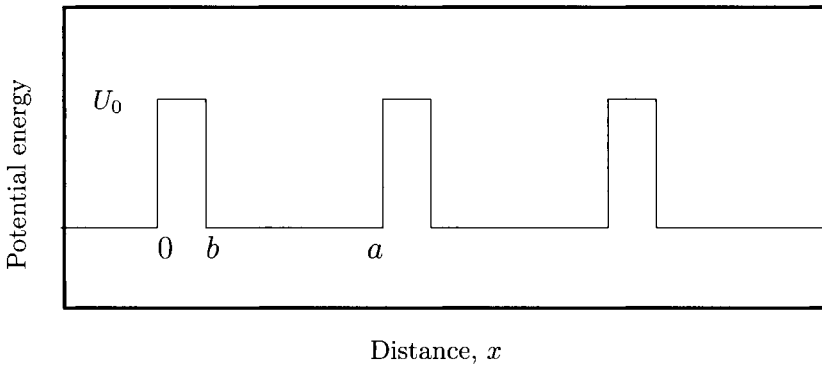


Figure 7.12. Potential energy of Kronig–Penney model.

$$U(x) = \sum_m U_0 \theta(x - ma) \theta(ma + b - x). \quad (7.129)$$

- (a) Restrict attention to a single unit cell, and write down the boundary conditions on Schrödinger's equation that lead to Bloch states in this unit cell.
- (b) Solve Schrödinger's equation in this cell by taking sums of plane waves and imposing suitable boundary conditions at 0, b , and a . The result is a condition on the Bloch index k .
- (c) Take the limit

$$b \rightarrow 0, \quad U_0 \rightarrow \infty, \quad U_0 b \rightarrow W_0 a \frac{\hbar^2 a^{-2}}{m}. \quad (7.130)$$

The condition on the Bloch index should become

$$\cos ka = \frac{W_0}{Ka} \sin Ka + \cos Ka, \quad (7.131)$$

where

$$K = \sqrt{2m\mathcal{E}/\hbar^2}. \quad (7.132)$$

- (d) Produce plots of the two lowest energy bands following from Eq. (7.131) for $a = 1$, $m = 1$, $\hbar = 1$, and $W_0 = 0.5$. Display the bands in the reduced zone scheme and the extended zone scheme.

6. Group Representations:

Consider a group representation $\{A\}$ in which all the matrices are unitary.

- (a) Show that the matrix $A(E)$ representing the identity element of the group $\{G\}$ is always the unit matrix.
- (b) Show that

$$A(G)A(G') = A(GG'). \quad (7.133)$$

- (c) Show that Eq. (7.101) follows from Eq. (7.99), by taking the conjugate of Eq. (7.99).

7. Regular representation: The regular representation provides an automatic procedure that tracks down the irreducible representations of a symmetry group. The procedure can be implemented quite generally in symbolic algebra.

Suppose one has a collection of rotation matrices $G_1 \dots G_h$, that form a group, so $G_i G_j = G_l$ for some l . The *regular representation* is a set of $h \times h$ matrices $A^{(1)} \dots A^{(h)}$,

$$A_{ij}^{(m)} = \begin{cases} 1 & \text{if } G_m G_i = G_j, \\ 0 & \text{otherwise.} \end{cases} \quad (7.134)$$

That is, $A^{(m)}$ is a matrix whose entries encode the rules for multiplying all the matrices in the group by G_m . Each l -dimensional irreducible representation appears within the regular representation l times.

- (a) In a symbolic algebra program, create the six rotation matrices that constitute the group D_3 .
- (b) Form the six matrices $A^{(1)} \dots A^{(6)}$ that constitute the regular representation.
- (c) Form the matrix M defined in Eq. (7.94), and $P = M + M^*$.
- (d) Find the eigenvalues and eigenvectors of P .
- (e) Rewrite each of the matrices $A^{(m)}$ in the basis of these eigenvectors, and verify that it assumes block diagonal form.

8. **Optical transitions:** Optical transitions have an amplitude proportional to matrix elements such as $\langle 1 | \hat{P}_x | 2 \rangle$, where \hat{P}_x is the x component of the momentum operator, and $\langle 1 |$ and $| 2 \rangle$ are two wave functions. Consulting Table 7.4, determine whether symmetry allows or forbids the following transitions, where state $\langle 1 |$ has the first symmetry and state $| 2 \rangle$ has the second. When a representation contains more than one basis function, one has to determine whether any of the functions could make the transition possible.

- (a) $\Gamma_1 \rightarrow \Gamma_{25'}$
- (b) $\Gamma_{25'} \rightarrow \Gamma_{15}$
- (c) $\Gamma_{25'} \rightarrow \Gamma_{2'}$
- (d) $\Gamma_{15} \rightarrow \Gamma_2$

References

- F. Bloch (1928), The quantum mechanics of electrons in crystal lattices, *Zeitschrift für Physik*, **52**, 555–600. In German.
- F. Bloch (1976), Reminiscences of Heisenberg, *Physics Today*, **29**(12), 23–25.
- L. P. Bouckaert, R. Smoluchowski, and E. Wigner (1936), Theory of Brillouin zones and symmetry properties of wave functions in crystals, *Physical Review*, **50**, 58–67.
- C. J. Bradley and A. P. Cracknell (1972), *The Mathematical Theory of Symmetry in Solids; Representation Theory for Point Groups and Space Groups*, Clarendon Press, Oxford.
- G. F. Koster (1957), Space groups and their representations, *Solid State Physics: Advances in Research and Applications*, **5**, 174–256.
- R. Kronig and W. G. Penney (1931), Quantum mechanics of electrons in crystals lattices, *Proceedings of the Royal Society of London*, **A130**, 499–513.
- L. D. Landau and E. M. Lifshitz (1977), *Quantum Mechanics (Non-relativistic Theory)*, 3rd ed., Pergamon Press, Oxford.
- G. Y. Lyubarskii (1960), *The Applications of Group Theory in Physics*, Pergamon Press, New York.
- F. D. Murnaghan (1938), *The Theory of Group Representations*, The Johns Hopkins Press, Baltimore.
- L. Schiff (1968), *Quantum Mechanics*, 3rd ed., McGraw-Hill, New York.
- M. Tinkham (1964), *Group Theory and Quantum Mechanics*, McGraw-Hill, New York.
- G. P. Tolstov (1978), *Fourier Series*, Dover, New York.
- E. Wigner (1959), *Group Theory and its Application to the Quantum Mechanics of Atomic Spectra*, Academic Press, New York.

8. Nearly Free and Tightly Bound Electrons

8.1 Introduction

A rich set of problems becomes available for study when one puts electrons into the periodic potentials proposed by Bloch. However, two cases stand out as conceptually and historically important. These two cases are the *nearly free electron model* and the *tight binding model*. They sit at opposite ends of a conceptual continuum. Nearly free electrons are those that sit in a very weak potential. Their behavior is almost the same as that of electrons in a free Fermi gas. In the opposite limit, ions are treated as very strong attractive forces that bind electrons tightly and keep them nearly immobile.

The nearly free electron model was introduced by Peierls (1930). Placing a single electron in a weak periodic potential results in a solvable problem with a surprise. The potential is never so weak that it can completely be ignored. For those electrons whose Bloch wave vector \vec{k} meets conditions that would lead any wave to scatter strongly from a periodic crystal, the change in electron velocity is large. Only a small subset of electrons have wave vectors meeting these conditions, but they are important for transport properties, and there are easily measurable experimental effects. The response of metals to electric and magnetic fields is almost entirely due to the electrons of maximum energy, those that sit on the Fermi surface. The Fermi surface is a two-dimensional shell sitting in three-dimensional \vec{k} space that can be measured and plotted. When Gold (1958) carried out some of the early experimental measurements, he noticed that to excellent approximation the Fermi surfaces of noble metals consisted in sections of spherical shells, sliced up, slid about, and reassembled in fantastic shapes. The nearly free electron model predicts precisely this behavior; it is a triumph of Peierls' approximation.

Bloch (1928) began in the opposite limit. He modeled electrons as tightly bound to particular atoms, overlapping only weakly with neighbors. The tight-binding model was put on firm formal ground by Wannier (1937), who showed how Bloch eigenfunctions could always be summed together to obtain a complete set of wave functions, centered at single atoms. This approximation turns out to be much richer than the nearly free electron model. It provides the possibility of studying both metals and insulators. It is the beginning of a systematic approach to investigating arbitrary potentials. Tight binding models have long provided the starting point to investigate many of the subtle conceptual questions surrounding

electrons in metals, including the origins of magnetism, superconductivity, and the effects of random disordering of atoms.

8.2 Nearly Free Electrons

Consider an electron traveling in a weak periodic potential. The electron may be viewed as a wave, and from this vantage point it has already been established that for certain rare values of the wave vector, the lattice will cause the electron to scatter into new directions. The criterion, recorded as Eq. (3.38), is that an incoming wave with wave vector \vec{k} scatters strongly off a lattice possessing reciprocal lattice vector \vec{K} only when

$$k = \frac{K}{2\hat{k} \cdot \hat{K}} \Rightarrow \vec{k} \cdot \vec{K} = \frac{1}{2}K^2. \quad (8.1)$$

This equation has two remarkable properties. First, it may be rewritten as

$$\frac{1}{2}k^2 = \frac{1}{2}k^2 - \vec{k} \cdot \vec{K} + \frac{1}{2}K^2 \quad (8.2)$$

$$\Rightarrow \mathcal{E}_{\vec{k}}^0 = \mathcal{E}_{\vec{k}-\vec{K}}^0 \quad \mathcal{E}_{\vec{k}}^0 \text{ is the energy of a free electron, } \hbar^2 k^2 / 2m. \quad (8.3)$$

and in this form it emerges formally from perturbation theory as the condition for strong interaction between electron and lattice. Second, it defines a collection of planes in reciprocal space, which divide the space into a sequence of *Brillouin zones*, equal in volume but of increasingly complex shapes. The intersection of the boundaries of these zones with the Fermi surface plays a crucial role in determining dynamics of electrons.

The first task is to show how Eq. (8.3) emerges from perturbation theory. Consider an electron traveling in a weak periodic potential. It is natural to search for a solution in powers of the strength of the potential. However, perturbation theory must be applied with caution, because, as will be seen, it is possible to have nearly degenerate levels. To begin, return to the Schrödinger equation in form Eq. (7.33):

$$(\mathcal{E}_{\vec{q}}^0 - \mathcal{E})\psi(\vec{q}) + \sum_{\vec{K}} U_{\vec{K}}\psi(\vec{q} - \vec{K}) = 0. \quad (8.4)$$

A formal means to treat the potential U as small is to define

$$U_{\vec{K}} = \Delta w_{\vec{K}} \quad \Delta \text{ is the small parameter in terms of which perturbation theory will expand.} \quad (8.5)$$

and view Δ as a small dimensionless parameter. Perturbation theory requires that one expand all quantities in powers of Δ ; thus

$$\psi(\vec{q}) = \psi^{(0)}(\vec{q}) + \psi^{(1)}(\vec{q})\Delta + \dots; \quad \mathcal{E} = \mathcal{E}^{(0)} + \Delta\mathcal{E}^{(1)} + \dots \quad (8.6)$$

Zeroth Order. Substituting Eqs. (8.6) and (8.5) into Eq. (8.4) and retaining terms that are independent of Δ gives

$$\psi^{(0)}(\vec{q}) \left[\mathcal{E}_{\vec{q}}^0 - \mathcal{E}^{(0)} \right] = 0. \quad (8.7)$$

Compare Eq. (8.7) in the Extended and Reduced Zone Schemes. Solutions of Schrödinger's equation in a periodic potential are labeled with an index \vec{k} that indicates how they transform under translation through arbitrary lattice vectors \vec{R} . In the extended zone scheme, \vec{k} ranges over all of reciprocal space, and there is one energy eigenvalue for each \vec{k} . The requirement that $\psi_{\vec{k}}$ transform according to Eq. (7.43b) is satisfied if one takes

$$\psi_{\vec{k}}^{(0)}(\vec{q}) = \delta_{\vec{k},\vec{q}} \Rightarrow \psi_{\vec{k}}^{(0)}(\vec{r}) = e^{i\vec{k}\cdot\vec{r}} \quad \text{See Eq. (7.21).} \quad (8.8)$$

$$\Rightarrow \mathcal{E}^{(0)} = \mathcal{E}_{\vec{k}}^0 \quad (8.9)$$

In the reduced zone scheme, \vec{k} must remain within the first Brillouin zone, and ψ acquires an additional index n . The transformation requirement (7.43b) is satisfied if one takes

$$\psi_{n\vec{k}}^{(0)}(\vec{q}) = \delta_{\vec{k}_n+\vec{k},\vec{q}} \Rightarrow \psi_{n\vec{k}}^{(0)}(\vec{r}) = e^{i(\vec{k}+\vec{K}_n)\cdot\vec{r}} \quad (8.10)$$

$$\Rightarrow \mathcal{E}_{n\vec{k}}^{(0)} = \mathcal{E}_{\vec{k}+\vec{K}_n}^0. \quad \text{Here } \vec{K}_n \text{ is chosen to be the unique reciprocal lattice vector such that } \vec{q} - \vec{K}_n \text{ lies in the first Brillouin zone.} \quad (8.11)$$

First Order. Again placing Eqs. (8.6) and (8.5) into Eq. (8.4) but now gathering terms linear in Δ gives

$$[\mathcal{E}_{\vec{q}}^0 - \mathcal{E}_{\vec{k}}^0] \psi_{\vec{k}}^{(1)}(\vec{q}) + \sum_{\vec{K}} w_{\vec{K}} \psi_{\vec{k}}^{(0)}(\vec{q} - \vec{K}) - \mathcal{E}^{(1)} \psi_{\vec{k}}^{(0)}(\vec{q}) = 0. \quad (8.12)$$

Taking $\psi_{\vec{k}}^{(0)}$ from Eq. (8.8) and evaluating Eq. (8.12) at $\vec{q} = \vec{k}$ gives immediately

$$\mathcal{E}^{(1)} = w_0. \quad \text{Only } \vec{K} = 0 \text{ survives the sum, because otherwise } \psi_{\vec{k}}^0(\vec{q} - \vec{K}) = 0. \quad (8.13)$$

Next, solving Eq. (8.12) for $\psi^{(1)}$ gives

$$\psi_{\vec{k}}^{(1)}(\vec{q}) = \left\{ \sum_{\vec{K} \neq 0} w_{\vec{K}} \frac{\delta_{\vec{k},\vec{q}-\vec{K}}}{\mathcal{E}_{\vec{k}}^0 - \mathcal{E}_{\vec{K}+\vec{k}}^0} \right\} \quad \text{Using Eq. (8.8) for } \psi_{\vec{k}}^{(0)}(\vec{q}), \text{ and substituting } \vec{K} + \vec{k} \text{ for } \vec{q} \text{ in the denominator. The exclusion of } \vec{K} = 0 \text{ results from Eq. (8.13).} \quad (8.14)$$

$$\Rightarrow \psi_{\vec{k}}^{(1)}(\vec{q}) \approx \delta_{\vec{q},\vec{k}} + \left\{ \sum_{\vec{K} \neq 0} U_{\vec{K}} \frac{\delta_{\vec{k},\vec{q}-\vec{K}}}{\mathcal{E}_{\vec{k}}^0 - \mathcal{E}_{\vec{K}+\vec{k}}^0} \right\}. \quad \text{Assembling } \psi^{(0)} + \Delta\psi^{(1)}. \quad (8.15)$$

Equation (8.15) is of great utility in a wide variety of problems where potentials are effectively weak. However, there is an extremely interesting case where it fails. Whenever

$$\mathcal{E}_{\vec{k}}^0 = \mathcal{E}_{\vec{K}+\vec{k}}^0 \quad \text{This condition is almost exactly what was guessed in Eq. (8.3); replacing } \vec{K} \text{ by } -\vec{K}, \text{ one recovers it exactly.} \quad (8.16)$$

the denominator vanishes, and the perturbation expansion fails to converge. It is precisely at the locations in reciprocal space where Eq. (8.16) holds that effects of the crystalline lattice are strongest and most interesting. One therefore must go back to the beginning of the calculation and proceed more carefully.

8.2.1 Degenerate Perturbation Theory

This difficulty posed by degenerate or nearly degenerate energy levels is resolved by degenerate perturbation theory. Two states whose energies are close mix very strongly when perturbed, and one has to include both of them in the initial state at the beginning of perturbation theory, because even in the limit as U vanishes, the eigenfunctions will involve a sum of the two states.

One way to obtain a resolution of this problem is to recast Schrödinger's equation in variational form, as discussed in Appendix B. According to Eq. (B.10) solving Schrödinger's equation is equivalent to finding extrema of the functional

$$\langle \psi | (\hat{\mathcal{H}} - \mathcal{E}) | \psi \rangle. \quad (8.17)$$

This variational principle is exact, but it also suggests good approximations, because one can find approximate eigenfunctions and eigenvalues by performing the variation with a restricted set of wave functions $|\psi\rangle$. In this approximation scheme, one restricts attention to l wave functions of the form

$$|\psi\rangle = \sum_{i=1}^l C_i |\psi_i\rangle. \quad (8.18)$$

Carrying out the variation of Eq. (8.17) with respect to the l coefficients C_i^* leads to the equation

$$\sum_j \langle \psi_i | (\hat{\mathcal{H}} - \mathcal{E}) | \psi_j \rangle C_j = 0, \quad (8.19)$$

which has solutions only when the $l \times l$ matrix

$$\hat{\mathcal{H}}_{ij}^{\text{eff}} = \langle \psi_i | (\hat{\mathcal{H}} - \mathcal{E}) | \psi_j \rangle \quad (8.20)$$

has vanishing determinant. Degenerate perturbation theory is an approximation of this type. In the present case, the plan is to restrict all attention to wave functions that are linear combinations of the two vectors $|\psi_1\rangle = |\vec{k}\rangle$ and $|\psi_2\rangle = |\vec{k} + \vec{K}\rangle$, but otherwise solve the Hamiltonian exactly. Returning to Eq. (7.37) and forming all the matrix elements needed for (8.20) gives immediately

$$\begin{vmatrix} \mathcal{E}_{\vec{k}}^0 + U_0 - \mathcal{E} & U_{-\vec{K}} \\ U_{\vec{K}} & \mathcal{E}_{\vec{k}+\vec{K}}^0 + U_0 - \mathcal{E} \end{vmatrix}. \quad (8.21)$$

Setting the determinant of (8.21) to zero and solving for \mathcal{E} gives

$$\mathcal{E} = U_0 + \frac{\mathcal{E}_{\vec{k}}^0 + \mathcal{E}_{\vec{k}+\vec{K}}^0}{2} \pm \sqrt{\frac{[\mathcal{E}_{\vec{k}}^0 - \mathcal{E}_{\vec{k}+\vec{K}}^0]^2}{4} + |U_{\vec{K}}|^2}. \quad \text{Because } U(\vec{r}) \text{ is real, } U_{-\vec{K}} = U_{\vec{K}}^*. \quad (8.22)$$

At the point where $\mathcal{E}_{\vec{k}+\vec{K}}^0 = \mathcal{E}_{\vec{k}}^0$ is exactly satisfied, one obtains

$$\mathcal{E} = \mathcal{E}_{\vec{k}}^0 + U_0 \pm |U_{\vec{K}}|. \quad (8.23)$$

Thus the energy gap \mathcal{E}_g between bands is

$$\mathcal{E}_g = 2|U_{\vec{K}}|. \quad (8.24)$$

When \vec{k} and \vec{K} are far from obeying Eq. (8.16), the alteration of the free-electron energy is of order U^2 —much smaller than near the zone boundaries.

Example: Application of Eq. (8.22) to a One-Dimensional Case. Consider an electron in a weak one-dimensional potential, for which the lattice constant is a . Then Eq. (8.16) obtains when k is in the neighborhood of π/a . In the neighborhood of $-\pi/a$, it also obtains, with $K = 2\pi/a$, and generally at $n\pi/a$, substituting $-2n\pi/a$ for K . These points are exactly those where discontinuities in $\mathcal{E}_{\vec{k}}$ are visible in Figure 7.7. The size of the discontinuities in that figure are given by Eq. (8.24), as illustrated in Figure 8.1.

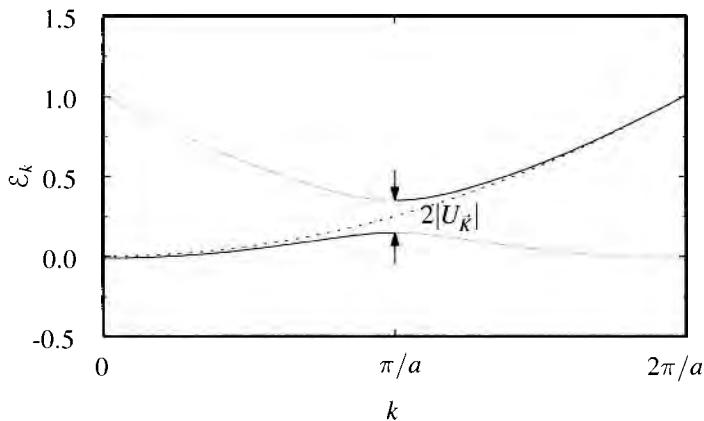


Figure 8.1. Plot of Eq. (8.22), illustrating the gap between energy bands as it appears in the extended zone scheme. The dotted line shows the free-electron parabola for $U_{\vec{K}} = 0$.

As in Figure 7.7, the energy viewed in the extended zone scheme is discontinuous, while energy in the repeated zone scheme is a continuous function of k . The significance of this calculation lies in its implications for electron transport. Electrons travel along continuous portions of the energy surfaces, and a gap as in Figure 8.1 will prevent electrons from traveling between the lower and upper parts of the diagram; it may even be able to turn a metal into an insulator.

8.3 Brillouin Zones

For electrons in very weak potentials, whose energies almost everywhere resemble those of electrons in no potential at all, it is perfectly natural to index states in the extended zone scheme, using just a single wave vector \vec{k} . However, using this indexing convention, the electron energy bands are discontinuous whenever they reach a point in reciprocal space satisfying Eq. (8.1), or equivalently (8.3). To understand the implications of this result, it is helpful to cast it in geometrical

form. Rewrite Eq. (8.1) as

$$\vec{k} \cdot \frac{\vec{K}}{K} = \frac{1}{2}K. \quad (8.25)$$

The set of points satisfying Eq. (8.25) is a plane that is perpendicular to the vector connecting the origin to \vec{K} and lying precisely midway between 0 and \vec{K} . Crossing this plane brings one closer to \vec{K} than to the origin. Constructing many such planes by scanning over all possible \vec{K} encloses the origin within a solid region. This region is nothing but the Wigner–Seitz cell of the origin in reciprocal space, or the first Brillouin zone, as all points inside it are closer to the origin than to any other reciprocal lattice vector.

This construction is illustrated in Figure 8.2, for a two-dimensional centered rectangular lattice. If one travels on any straight line outward from the origin, one will pass one by one lines on which Eq. (8.25) holds. When one passes the n th line, one is closer to precisely n reciprocal lattice points than one is to the origin. Thus the n th Brillouin zone is defined to be the set of points in reciprocal space that is closer to $n - 1$ reciprocal lattice points than it is to the origin. The boundaries of these zones are the points in reciprocal space where nearly free electrons are strongly scattered by weak potentials.

The shape of the n th Brillouin zone becomes rather elaborate as n becomes large; however, the total area of each zone equals the area of the first Brillouin zone. The reason is that the interior of the n th Brillouin zone is the collection of points closer to exactly $n - 1$ reciprocal lattice points than to the origin. If one translates the reciprocal lattice through any reciprocal lattice vector \vec{K} , the interior of the new n th Brillouin zone cannot overlap the old one, because all points inside the old n th Brillouin zone are now n th nearest neighbors of \vec{K} , and not the origin. On the other hand if one continues to translate the lattice through successive reciprocal lattice vectors, all of reciprocal space must eventually be filled with copies of the n th Brillouin zone, because any point one chooses has some n th nearest neighbor in the lattice. Therefore each Brillouin zone has the same volume as the first Brillouin zone and is a primitive cell.

The importance of understanding the structure of energy bands near zone boundaries lies in the way that electrons in a crystal lattice behave under the influence of external fields. A free electron subjected to a small electric field gains energy indefinitely. An electron in a weak periodic potential subjected to a small electric field behaves similarly until its \vec{k} vector approaches a zone boundary plane. At that point, the electron follows the branch of the energy surface which makes energy a continuous function of \vec{k} . The analysis leading to Eq. (8.24) shows that the continuous branch of the energy surface has energy $\mathcal{E}_{\vec{q}-\vec{K}}^0$, not $\mathcal{E}_{\vec{q}}^0$. An electron traveling from the left to π/a along the lower branch in Figure 8.1 continues along the lower dashed line rather than jumping to the upper solid one. The central rule of electron dynamics is that an electron once in the n th Brillouin zone remains in the n th Brillouin zone. This claim will be demonstrated in Chapter 16.

For most purposes, the first Brillouin zone is the most important. Almost all computations involving electrons in crystals are carried out using the reduced zone

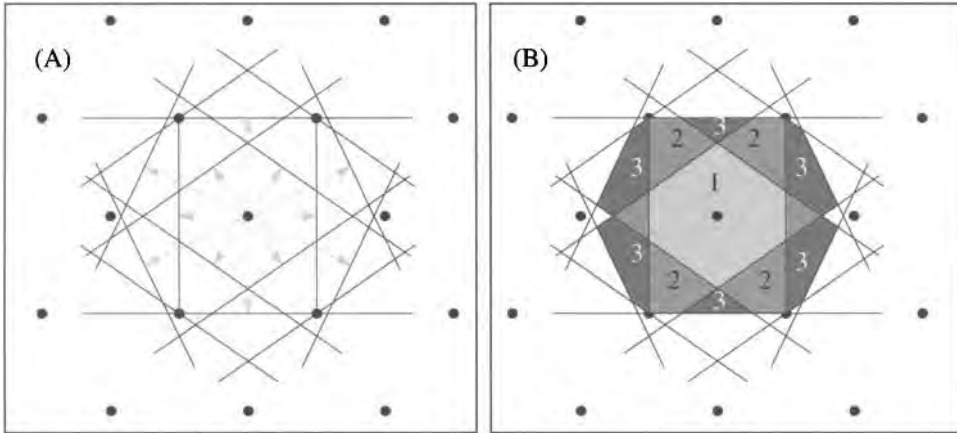


Figure 8.2. Construction of Brillouin zones. (A) Perpendicular bisectors are drawn between the origin and all nearby reciprocal lattice points. These are the zone boundaries. (B) The first, second, and third Brillouin zones are shaded in different colors. The first zone is the set of points closer to the origin than any other reciprocal lattice point, the second zone is the set of points that one reaches by passing a minimum of one zone boundary, and the third zone is the set of points that one reaches by crossing a minimum of two zone boundaries.

scheme for the first Brillouin zone. From this point of view, the only wave vectors \vec{k} that exist are the ones in the first Brillouin zone. Opposite edges of the zone whose wave vector differ by a reciprocal lattice vector are regarded as physically the same. Topologically, the first zone in Figure 8.2(B) is equivalent to the surface of a sphere. A path that appears to exit the zone at some boundary, just re-enters it from the opposite side, as shown in Figure 8.3.

Because the only electrons that are able to contribute to transport phenomena are those that reside at the Fermi surface, the most important task is to understand how the shape of the Fermi surface is affected by the presence of a periodic potential. The answer is that the Fermi surface is almost unchanged in the extended zone scheme, but dramatically altered in the reduced zone scheme, and it is the latter case that matters.

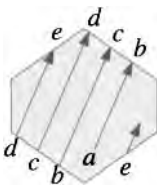
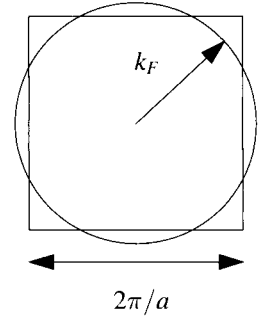


Figure 8.3. The first Brillouin zone can be viewed as a closed surface whose edges are connected to each other. Therefore a path that appears to be leaving from one edge is actually entering from another, as shown in this representation of straight line motion. This view of the first Brillouin zone is motivated by the fact that physical quantities such as $\mathcal{E}_{\vec{k}}$ are periodic functions over the first Brillouin zone.

Example: Brillouin Zone Boundary Intersection for Square Lattice in Two Dimensions.

Suppose the lattice has two conduction electrons per lattice site. As discussed after Eq. (7.50), the number of \vec{k} states in a Brillouin zone equals the number of lattice points, and because each \vec{k} state can accommodate precisely two electrons, the volume that the electrons occupy in \vec{k} space must equal the volume of the Brillouin zone. However, for a weak potential, the shape of the energy surface must be very close to the shape of the energy surface for free electrons—that is, a sphere. For a square lattice with lattice spacing a , the reciprocal lattice is also square, with lattice spacing $2\pi/a$, and the volume of the Brillouin zone is $4\pi^2/a^2$. The Fermi sphere for free electrons must have this same volume, which means $\pi k_F^2 = 4\pi^2/a^2 \Rightarrow k_F = 2\pi/\sqrt{\pi}a = 1.128\pi/a$. Because at its point of closest approach the Brillouin zone boundary is at a distance π/a from the origin of \vec{K} space, the Fermi surface juts slightly out of the first Brillouin zone.



8.3.1 Nearly Free Electron Fermi Surfaces

The consequences of a Fermi surface intersecting a Brillouin zone boundary are depicted in Figure 8.4. This Fermi surface completely contains the first Brillouin zone, and it extends into the second and third zones. Band energies are continuous in the reduced zone scheme, and the Fermi surface should be continuous and differentiable in the reduced zone scheme as well, as shown in Problem 2. The Fermi surface must therefore be modified slightly from its free-electron form near the Brillouin zone boundaries, as shown in Figure 8.4(A). Important as this fact may be for electron dynamics, it is nearly invisible in its effect on the geometry of the Fermi surface, so distortions near the zone edge will not be shown in subsequent figures. Figures 8.4(B) and 8.4(C) show how to displace portions of the free-electron Fermi surface to make them continuous in the reduced zone scheme. In the case of the third Brillouin zone, some trial and error is needed to find ways to displace the disjoint regions through reciprocal lattice vectors so that the energy surface becomes continuous. Figure 8.4(D) illustrates the *Harrison construction*, which provides a systematic procedure by which to obtain pictures of the Fermi surface in the reduced zone scheme. The Harrison construction involves nothing but unions of intersections of spheres with the first Brillouin zone, and therefore it provides a convenient algorithm by which to generate pictures of Fermi surfaces in three dimensions.

Figure 8.5 illustrates the application of this construction to the Fermi sphere of an fcc crystal with three electrons per site. The left side of the figure shows portions of the Fermi sphere lying within the second and third Brillouin zones, while the right hand side of the figure shows how precisely the same sections of

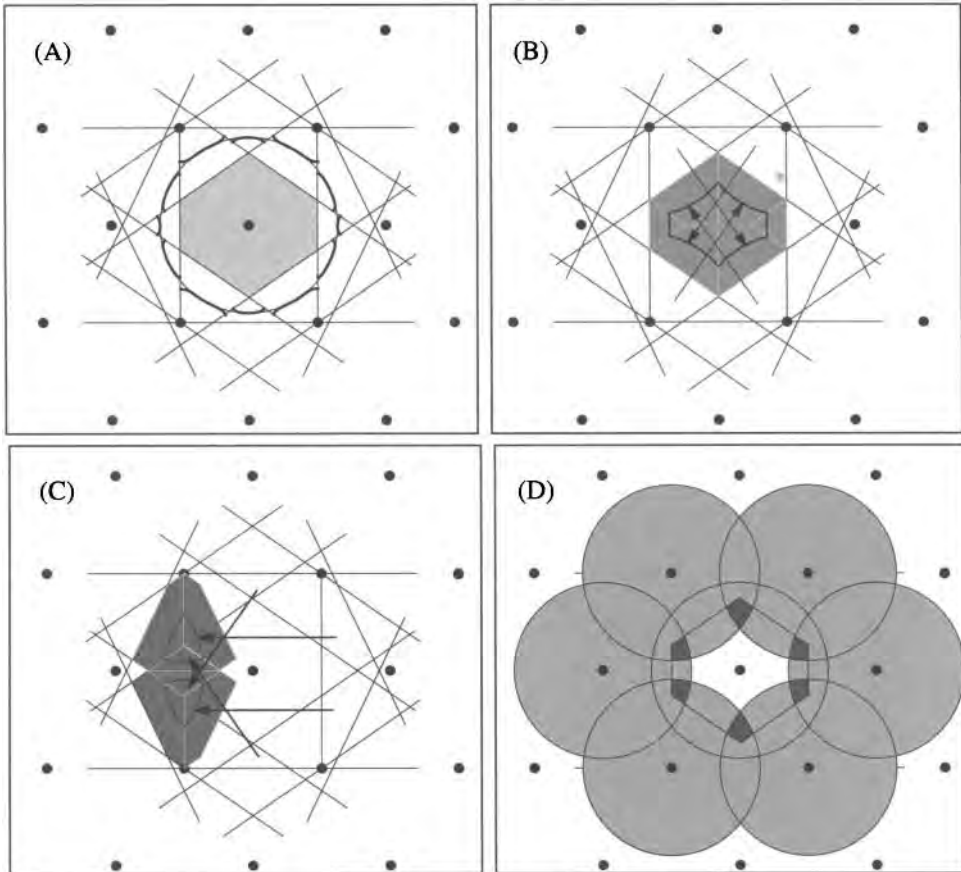


Figure 8.4. (A) A free-electron Fermi surface completely enclosing the first Brillouin zone. The shape of the surface is slightly modified near the zone boundaries, as discussed in Problem 2. (B) The portion of the Fermi surface in the second Brillouin zone mapped back into the first zone so that the energy surface is continuous. (C) The portion of the Fermi surface in the third Brillouin zone made continuous by appropriate translations through reciprocal lattice vectors. Note that the contiguous portions of the third Brillouin zone cannot be mapped into the first Brillouin zone by any single reciprocal lattice vector. (D) The Harrison construction for Fermi surfaces shows how the surface in the n th Brillouin zone looks mapped back into the first Brillouin zone. The image of the interior of the Fermi sphere in the second Brillouin zone is given by all points in the first Brillouin zone that are inside two or more spheres (gray + dark gray regions). The image of the interior of the Fermi sphere in the third Brillouin zone is given by all points in the first Brillouin zone that are inside three or more spheres (dark gray regions). This geometrical construction can be implemented in terms of the operations of constructive solid geometry, and it was used to produce all the images in Figures 8.6, 8.7, and 8.8.





Brillouin zone	Extended zone scheme	Reduced zone scheme
First	Empty	Empty
Second		
Third		

Figure 8.5. Fermi surface for three electrons per site in an fcc crystal. On the left the free-electron Fermi surface is shown in the extended zone scheme, while on the right the same surfaces are projected back into the first Brillouin zone in the reduced zone scheme.

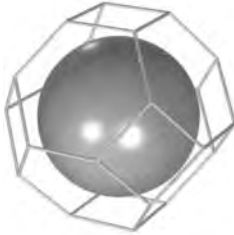




Brillouin zone	1 electron/cell	2 electrons/cell	3 electrons/cell
First			
Second			
Third			

Figure 8.6. Nearly free electron Fermi surfaces for fcc crystals. With three electrons per unit cell the Fermi surface extends slightly into the fourth Brillouin zone, but the pocket is very small and is not shown.

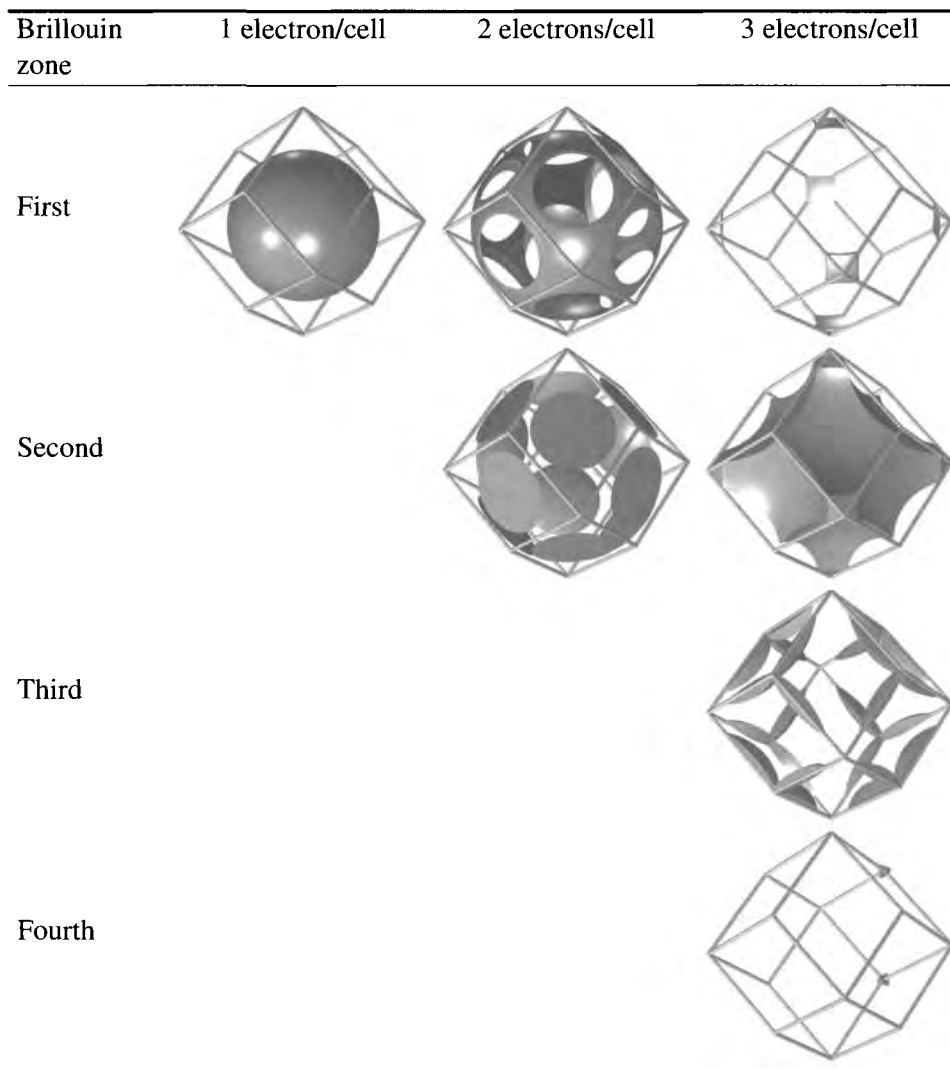


Figure 8.7. Nearly free electron Fermi surfaces for bcc crystals.

the spherical shell appear after translation through reciprocal lattice vectors to form a continuous surface. Figures 8.6, 8.7, and 8.8 provide a summary of the shapes of nearly free-electron Fermi surfaces for the three most common Bravais lattices and for a variety of electron densities. As discussed in Section 16.5.2, shapes similar to these can be measured experimentally, and in some cases such as aluminum the experimentally measured Fermi surface is surprisingly close to the nearly free-electron prediction.

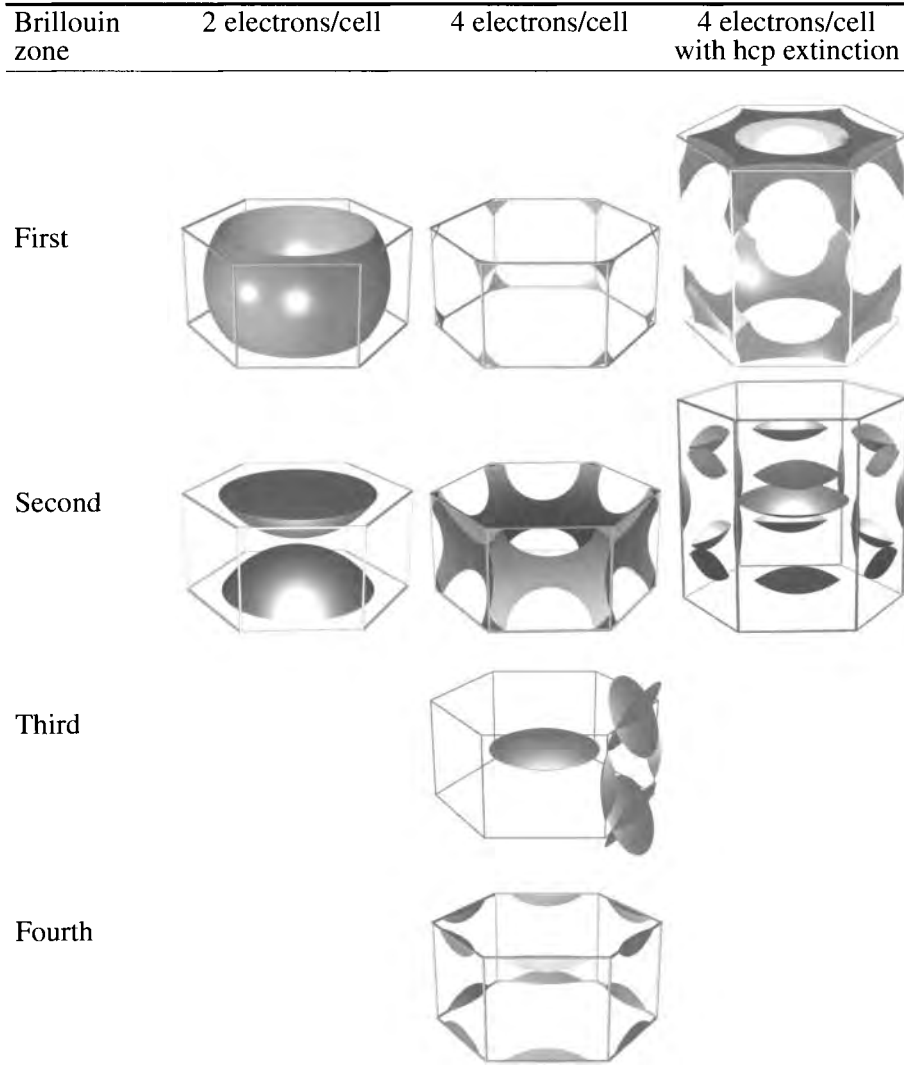


Figure 8.8. Nearly free electron Fermi surfaces for hexagonal crystals. The middle column shows the Fermi surface appropriate for an hexagonal crystal with four electrons per primitive cell. A different surface is sometimes appropriate for divalent hcp crystals, because according to Eq. (3.68) no scattering takes place from the plane at π/c . The third column shows the Fermi surface reconstituted without discontinuities on this plane. Spin-orbit coupling can lead to violations of Eq. (3.68), and it makes the second rather than third column appropriate for heavy divalent hcp metals.

8.4 Tightly Bound Electrons

8.4.1 Linear Combinations of Atomic Orbitals

The free-electron gas has served to this point as the main conceptual model for the study of solids. This choice may seem surprising, for solids are made from atoms, and viewed as a collection of atoms, a solid seems to bear no relation to the free-electron gas. Imagine instead starting with a collection of isolated atoms and slowly bringing them together to form a crystal. Surely in some cases, the most appropriate approximation must begin with atomic wave functions. Such a starting point complements without contradicting the one developed until now, and it is called the *tight-binding model*.

The idea works best for atoms where most of the electrons are closely held in closed shells, and the wave functions of the remaining electrons have an amplitude that decays rapidly away from the nucleus. The following discussion applies to the electrons of the outer shells, neglecting the ones in the inner core. Let $a_{n'}^{\text{at}}$ be the wave function for an electron occupying an isolated atom; the index n' lets one choose more than one electron orbital. The wave function satisfies

$$\hat{\mathcal{H}}^{\text{at}} a_{n'}^{\text{at}}(\vec{r}) = -\frac{\hbar^2}{2m} \nabla^2 a_{n'}^{\text{at}}(\vec{r}) + U^{\text{at}}(\vec{r}) a_{n'}^{\text{at}}(\vec{r}) = \mathcal{E}_{n'}^{\text{at}} a_{n'}^{\text{at}}(\vec{r}), \quad (8.26)$$

where the Hamiltonian and energy $\mathcal{E}_{n'}^{\text{at}}$ refer to an isolated atom. Such atomic wave functions were computed by atomic physicists such as Hartree (1928) starting in the 1920's, but for the present discussion, their most significant feature is that like the wave function of the hydrogen atom, they decrease exponentially as one moves more than a few angstroms from the nucleus.

Now imagine bringing many such atoms together to form a crystal with lattice vectors \vec{R} , obtaining the Hamiltonian

$$\hat{\mathcal{H}} = -\frac{\hbar^2}{2m} \nabla^2 + U(\vec{r}) = -\frac{\hbar^2}{2m} \nabla^2 + \sum_{\vec{R}} U^{\text{at}}(\vec{r} - \vec{R}). \quad (8.27)$$

Using atomic waves functions to solve this Hamiltonian proceeds in two steps. The first is to build some wave functions that automatically satisfy Bloch's theorem, Eq. (7.36). They are

$$\Phi_{n'\vec{k}}(\vec{r}) = \frac{1}{\sqrt{N}} \sum_{\vec{R}} e^{i\vec{k}\cdot\vec{R}} a_{n'}^{\text{at}}(\vec{r} - \vec{R}). \quad (8.28)$$

A quick calculation verifies that

$$\Phi_{n'\vec{k}}(\vec{r} + \vec{R}) = \frac{1}{\sqrt{N}} \sum_{\vec{R}'} e^{i\vec{k}\cdot\vec{R}'} a_{n'}^{\text{at}}(\vec{r} - \vec{R}' + \vec{R}) \quad (8.29)$$

$$= \frac{1}{\sqrt{N}} \sum_{\vec{R}'} e^{i\vec{k}\cdot(\vec{R}'+\vec{R})} a_{n'}^{\text{at}}(\vec{r} - \vec{R}') = \Phi_{n'\vec{k}}(\vec{r}) e^{i\vec{k}\cdot\vec{R}}. \quad (8.30)$$

If it seems too easy to solve the problem with a simple sum, it is. The wave functions Φ are neither normalized, nor eigenfunctions of the Hamiltonian Eq. (8.27). Just because solutions of Schrödinger's equation must have the form of Eq. (7.36) does not mean that all functions of this form solve Schrödinger's equation. They can however be used as *trial wave functions* and summed together so as to get the best solution of Schrödinger's equation possible. This means creating wave functions of the form

$$\psi_{n\vec{k}}(\vec{r}) = \sum_{n'} C_{nn'} \Phi_{n'\vec{k}}(\vec{r}) \quad (8.31)$$

To choose the constants $C_{nn'}$, use the variational principle in Eq. (B.10). Forming $\langle \psi_{n\vec{k}} | \hat{\mathcal{H}} - \mathcal{E} | \psi_{n\vec{k}} \rangle$ and varying with respect to $C_{nn'}$ gives

$$\begin{aligned} 0 &= \sum_{n'} C_{nn'} \langle \Phi_{n'\vec{k}} | \hat{\mathcal{H}} - \mathcal{E} | \Phi_{n'\vec{k}} \rangle \\ \Rightarrow 0 &= \sum_{n'} C_{nn'} (\mathcal{H}_{n'n'} - \mathcal{E}_n \mathcal{S}_{n'n'}) \end{aligned} \quad \begin{array}{l} \text{This is an eigenvalue equation for } \mathcal{E} \text{ and } \vec{C}_n. \\ \text{Adding a subscript on } \mathcal{E} \text{ acknowledges that} \\ \text{the eigenvector } \vec{C}_n \text{ and eigenvalue } \mathcal{E}_n \text{ are linked.} \\ \text{The equation can be put in more familiar form} \\ \text{by multiplying from the left by } \mathcal{S}^{-1}. \end{array} \quad (8.32a)$$

where

$$\mathcal{H}_{nn'} \equiv \langle \Phi_{n\vec{k}} | \hat{\mathcal{H}} | \Phi_{n'\vec{k}} \rangle \quad \text{and the overlap matrix} \quad \mathcal{S}_{nn'} \equiv \langle \Phi_{n\vec{k}} | \Phi_{n'\vec{k}} \rangle. \quad (8.32b)$$

As a first example of how this formalism develops in practice, specialize to the case of a Bravais lattice where the the vectors from any lattice point to the nearest neighbors are denoted by $\vec{\delta}$, and also specialize to the case of a single s orbital, meaning that there is just a single atomic wave function $a^{\text{at}}(\vec{r})$ which is spherically symmetric. Further computation makes use of the localized nature of the atomic wave functions. So, when an integral of the form

$$\int d\vec{r} a^{\text{at}}(\vec{r} + \vec{R}') a^{\text{at}}(\vec{r} + \vec{R}) \quad (8.33)$$

appears, set it to zero unless \vec{R} and \vec{R}' are equal, or are nearest neighbors separated by one of the vectors $\vec{\delta}$. Then there are only three *overlap integrals* that appear in the computation, namely

$$\begin{aligned} \alpha &\equiv \int d\vec{r} a^{\text{at}}(\vec{r}) a^{\text{at}}(\vec{r} + \vec{\delta}) \\ \mathcal{U} &= \int d\vec{r} a^{\text{at}}(\vec{r}) [U(\vec{r}) - U^{\text{at}}(\vec{r})] a^{\text{at}}(\vec{r}). \quad \text{Recall that } U(\vec{r}) = \sum_{\vec{R}} U^{\text{at}}(\vec{r} - \vec{R}) \end{aligned}$$

and

$$\mathcal{t} \equiv \int d\vec{r} a^{\text{at}}(\vec{r}) [U(\vec{r}) - U^{\text{at}}(\vec{r} + \vec{\delta})] a^{\text{at}}(\vec{r} + \vec{\delta}). \quad (8.34)$$

These integrals are independent of the direction of $\vec{\delta}$ because the atomic wave function is spherically symmetric. Note that $U^{\text{at}}(\vec{r} + \vec{\delta})$ is not necessarily very small near the origin where $a^{\text{at}}(\vec{r})$ is large. Thinking of the hydrogen atom, for example, the ground state wave function falls off exponentially, but the potential falls off only as $1/r$.

Now return to Eq. (8.32). Since there is only one orbital, the indices n and n' range over only one value one can call s , and the single constant C_{ss} simply drops out. Thus one can write in the case of a single s orbital that

$$\mathcal{E} = \mathcal{H}_{ss}/\mathcal{S}_{ss}. \quad (8.35)$$

To evaluate \mathcal{S}_{ss} write

$$\begin{aligned} \mathcal{S}_{ss} &= \sum_{\vec{R}\vec{R}'} e^{i\vec{k}\cdot(\vec{R}-\vec{R}')} \frac{1}{N} \int d\vec{r} a^{\text{at}}(\vec{r}-\vec{R}) a^{\text{at}}(\vec{r}-\vec{R}') \quad \text{The atomic wave} \\ &= 1 + \sum_{\vec{\delta}} e^{i\vec{k}\cdot\vec{\delta}} \int d\vec{r} a^{\text{at}}(\vec{r}) a^{\text{at}}(\vec{r}+\vec{\delta}) \quad \text{Whenever } \vec{R} = \vec{R}' \text{ the} \\ &= 1 + \sum_{\vec{\delta}} e^{i\vec{k}\cdot\vec{\delta}} \alpha \quad \text{integral gives 1, and} \\ & \quad \text{there are } N \text{ such} \\ & \quad \text{terms.} \end{aligned} \quad (8.36)$$

Next compute the numerator of Eq. (8.35):

$$\begin{aligned} \langle \Phi_s | \hat{\mathcal{H}} | \Phi_s \rangle &= \sum_{\vec{R}\vec{R}'} \int d\vec{r} a^{\text{at}}(\vec{r}-\vec{R}) \left[-\frac{\hbar^2}{2m} \nabla^2 + U(\vec{r}) \right] a^{\text{at}}(\vec{r}-\vec{R}') \frac{e^{i\vec{k}\cdot(\vec{R}-\vec{R}')}}{N} \\ &= \sum_{\vec{R}\vec{R}'} \int d\vec{r} a^{\text{at}}(\vec{r}-\vec{R}) \left\{ \left[-\frac{\hbar^2}{2m} \nabla^2 + U^{\text{at}}(\vec{r}-\vec{R}') \right] a^{\text{at}}(\vec{r}-\vec{R}') \right\} \frac{e^{i\vec{k}\cdot(\vec{R}-\vec{R}')}}{N} \\ &= \int d\vec{r} \sum_{\vec{R}\vec{R}'} \mathcal{E}^{\text{at}} \frac{a^{\text{at}}(\vec{r}-\vec{R}) a^{\text{at}}(\vec{r}-\vec{R}')}{N} e^{i\vec{k}\cdot(\vec{R}-\vec{R}')} \quad \text{Because } a^{\text{at}} \text{ solves the atomic} \\ & \quad \text{Hamiltonian with eigenvalue } \mathcal{E}^{\text{at}}. \\ & \quad + \int d\vec{r} \sum_{\vec{R}\vec{R}'} a^{\text{at}}(\vec{r}-\vec{R}) [U(\vec{r}) - U^{\text{at}}(\vec{r}-\vec{R}')] a^{\text{at}}(\vec{r}-\vec{R}') \frac{e^{i\vec{k}\cdot(\vec{R}-\vec{R}')}}{N} \\ &= \mathcal{E}^{\text{at}} (1 + \alpha \sum_{\vec{\delta}} e^{i\vec{k}\cdot\vec{\delta}}) + \mathcal{U} + \mathfrak{t} \sum_{\vec{\delta}} e^{i\vec{k}\cdot\vec{\delta}}. \quad \text{Using 8.34.} \end{aligned} \quad (8.37)$$

Thus one obtains the estimate from Eq. (8.35),

$$\mathcal{E}_{\vec{k}} \approx \mathcal{E}^{\text{at}} + \frac{\mathcal{U} + \mathfrak{t} \sum_{\vec{\delta}} e^{i\vec{k}\cdot\vec{\delta}}}{(1 + \alpha \sum_{\vec{\delta}} e^{i\vec{k}\cdot\vec{\delta}})}. \quad (8.38)$$

Discarding terms of order $\alpha\mathcal{U}$ and $\alpha\mathfrak{t}$ on the grounds that α , \mathfrak{t} , and \mathcal{U} are already small, one obtains

$$\mathcal{E}_{\vec{k}} \approx \mathcal{E}^{\text{at}} + \mathcal{U} + \mathfrak{t} \sum_{\vec{\delta}} e^{i\vec{k}\cdot\vec{\delta}}. \quad (8.39)$$

Equation (8.39) shows that the energy of tightly bound electrons is mainly given by the energy of the original atomic orbitals, plus a constant correction due to interactions, plus a *hopping term* proportional to \mathfrak{t} that depends upon \vec{k} , and describes the

interactions of electrons at one atomic site with neighboring sites. The reason to use the word “hopping” is that according to Eq. (7.59), electrons with wave vector \vec{k} move from site to site at speed

$$\vec{v}_{\vec{k}} = \frac{1}{\hbar} \vec{\nabla}_{\vec{k}} \mathcal{E}_{\vec{k}} = i \frac{\mathfrak{t}}{\hbar} \sum_{\vec{\delta}} \vec{\delta} e^{i\vec{k} \cdot \vec{\delta}}. \quad (8.40)$$

Thus the speed at which electrons move is proportional to \mathfrak{t} , and vanishes when \mathfrak{t} vanishes.

Bandwidth. Letting z be the number of nearest neighbors over which the sum on $\vec{\delta}$ is performed, the maximum value of $\mathcal{E}_{\vec{k}}$ is $\mathcal{U} + |\mathfrak{t}|z$, and the minimum possible value is $\mathcal{U} - |\mathfrak{t}|z$. The difference between maximum and minimum energies is defined to be the *bandwidth*; half this value is denoted by \mathcal{W} , so in this case

$$2\mathcal{W} = 2z|\mathfrak{t}|. \quad (8.41)$$

Tight Binding for Lattice with Basis. Using the tight binding method for a single atomic orbital is a bit of a cheat because the method is originally billed as variational, and then it is applied to a single function, leaving nothing to vary. For more complex cases it is necessary to generalize the formalism to accommodate a lattice with a basis $\vec{v}_1 \dots \vec{v}_l$. This can be accomplished by writing

$$\Phi_{n'}(\vec{r}) = \frac{1}{\sqrt{N}} \sum_{\vec{R}} e^{i\vec{k} \cdot \vec{R}} a_{n'}^{\text{at}}(\vec{r} - \vec{R} - \vec{v}_{n'}). \quad (8.42)$$

Now the index n' ranges both over atomic orbitals, and also over basis vectors. The number of values of n' equals the sum over basis vectors of the number of orbitals at each site. With this understanding, the computations leading to Eq. (8.32) are unchanged. Problem 5 shows how to apply the method to obtain an estimate of the band structure of graphene.

8.4.2 Wannier Functions

Calculations employing atomic orbitals can be put on a much more general footing by constructing *Wannier functions*. These are a set of orthonormal wave functions that one can always construct from Bloch functions and which are plausibly localized on atomic sites.

Suppose that one has found all the eigenfunctions of the Hamiltonian and has arranged them as allowed by Bloch’s theorem in the form Eq. (7.44). Then the Wannier function for electrons from band n centered at lattice site R is defined to be

$$\langle \vec{r} | \vec{R} \rangle \equiv w_n(\vec{R}, \vec{r}) = \frac{1}{\sqrt{N}} \sum_{\vec{k}} e^{-i\vec{k} \cdot \vec{R}} \psi_{n\vec{k}}(\vec{r}). \quad (8.43)$$

N is the number of lattice sites, and also the number of \vec{k} in the first Brillouin zone, over which the sum in \vec{k} is performed.

The Wannier functions form an orthonormal set, as may be seen by computing

$$\int d\vec{r} w_n(\vec{R}, \vec{r}) w_m^*(\vec{R}', \vec{r}) = \int d\vec{r} \sum_{\vec{k}} \sum_{\vec{k}'} \frac{1}{N} e^{-i\vec{k}\cdot\vec{R} + i\vec{R}'\cdot\vec{k}'} \psi_{n\vec{k}}^*(\vec{r}) \psi_{m,\vec{k}'}(\vec{r}) \quad (8.44)$$

$$= \frac{1}{N} \sum_{\vec{k}, \vec{k}'} e^{-i\vec{k}\cdot\vec{R} + i\vec{R}'\cdot\vec{k}'} \delta_{m,n} \delta_{\vec{k}, \vec{k}'} \quad (8.45)$$

$$= \delta_{\vec{R}, \vec{R}'} \delta_{n,m}. \quad \text{The sum is normalized because as shown in Section 7.2.4, the number of } \vec{k} \text{ in the first Brillouin zone equals } N. \quad (8.46)$$

If one should happen to know the Wannier functions, the Bloch functions can be recovered from them by computing

$$\frac{1}{\sqrt{N}} \sum_{\vec{R}} w_n(\vec{R}, \vec{r}) e^{i\vec{k}\cdot\vec{R}} = \psi_{n\vec{k}}(\vec{r}). \quad (8.47)$$

Ambiguity in Definition of Wannier Functions. At first it seems that the Wannier functions are completely determined by the prescription given in Eq. (8.43). However, there is a subtle ambiguity. Each Bloch function is determined only within an overall phase factor, so the Wannier functions can be rewritten

$$w_n(\vec{R}, \vec{r}) = \frac{1}{\sqrt{N}} \sum_{\vec{k}} e^{-i\vec{k}\cdot\vec{R} + i\phi(\vec{k})} \psi_{n\vec{k}}(\vec{r}), \quad (8.48)$$

where $\phi(\vec{k})$ is a completely arbitrary real function. Addressing this ambiguity requires an investigation of the phases of wave functions.

8.4.3 Geometric Phases

Geometrical phases have been discovered and rediscovered many times. The earliest paper is probably by Pancharatnam (1956). In the special case of electromagnetic vector potentials, they appeared in Aharonov and Bohm (1959), and then with much greater generality in a paper of Berry (1984) after whom they are widely known as *Berry phases*.

These phases appear very generally in the study of quantum mechanical problems. Suppose one has a Hamiltonian $\mathcal{H}_{\vec{\lambda}}$ that depends upon some collection of parameters $\vec{\lambda} = (\lambda_1(t), \lambda_2(t) \dots \lambda_n(t))$. These parameters change in time, but they change very slowly, meaning one can treat $\dot{\lambda}$ as small. These slow changes are also called *adiabatic*. What are some specific examples? An experimentalist might very slowly lower the temperature of a sample, in which case $\lambda = T$. An electron within a solid might move through electric and magnetic fields that vary weakly in space, in which case the electron's wave vector $\vec{k} = \vec{\lambda}$ can be viewed as slowly changing.

To see how geometric phases arise, let $|\Psi_{\vec{\lambda}}\rangle$ be an eigenstate of the Hamiltonian $\hat{\mathcal{H}}_{\vec{\lambda}}$ with eigenvalue $\mathcal{E}_{\vec{\lambda}}$. According to the *adiabatic theorem* — conventional proof

in Landau and Lifshitz (1977) and later refinements discussed by Zhao (2008) — if $\vec{\lambda}$ changes slowly enough, a particle once placed in state $|\Psi_{\vec{\lambda}}\rangle$ will remain in state $|\Psi_{\vec{\lambda}}\rangle$. Saying that a particle is in an eigenstate, however, says nothing about the phase. Indeed, the collection of wave functions $\langle \vec{r} | \Psi_{\vec{\lambda}} \rangle$ will in general have arbitrary phases, just like the Wannier functions of Eq. (8.48).

One feature of this arbitrary phase is wise to demand at all times; require that the phase be continuous and differentiable. This requirement is not quite as trivial as it sounds, because it extends to cases where the parameter space for $\vec{\lambda}$ is periodic. For example, if the parameter is the wave vector \vec{k} , one should require $\Psi_{\vec{k}}$ to be continuous and differentiable as a function of \vec{k} for \vec{k} lying in the first Brillouin zone, as in Figure 8.3.

Now examine what the time-dependent Schrödinger equation says about phases:

$$-\frac{\hbar}{i} \frac{\partial |\Psi(t)\rangle}{\partial t} = \hat{\mathcal{H}}_{\vec{\lambda}(t)} |\Psi(t)\rangle. \quad (8.49)$$

In the adiabatic limit where $\vec{\lambda}$ changes slowly, guess a solution of the form

$$|\Psi(t)\rangle = e^{-(i/\hbar) \int_0^t dt' \mathcal{E}_{\vec{\lambda}(t')} } e^{i\phi(t)} |\Psi_{\vec{\lambda}(t)}\rangle; \quad (8.50)$$

the wave function equals $\Psi_{\vec{\lambda}}$ up to a phase factor, and the phase factor has two pieces. The first is what one would first guess based upon the time dependence of eigenfunctions, and the second ϕ is a correction.

Inserting Eq. (8.49) into Eq. (8.50) gives

$$\left(\mathcal{E}_{\vec{\lambda}(t)} - \hbar \frac{\partial \phi}{\partial t} - \frac{\hbar}{i} \frac{\partial}{\partial t} \right) |\Psi_{\vec{\lambda}(t)}\rangle = \mathcal{E}_{\vec{\lambda}(t)} |\Psi_{\vec{\lambda}(t)}\rangle \quad (8.51)$$

$$\Rightarrow \frac{\partial \phi}{\partial t} = i \dot{\vec{\lambda}} \cdot \langle \Psi_{\vec{\lambda}} | \frac{\partial}{\partial \vec{\lambda}} | \Psi_{\vec{\lambda}} \rangle \quad (8.52)$$

$$\Rightarrow \phi(t) - \phi(0) = \int_{\vec{\lambda}(0)}^{\vec{\lambda}(t)} d\vec{\lambda} \cdot \vec{\mathcal{R}}_{\vec{\lambda}} \quad \begin{array}{l} \text{The line integral is performed over the circuit} \\ \vec{\lambda} \text{ follows from time 0 to } t; \text{ there is no dependence} \\ \text{on the speed of traversal so long as it is} \\ \text{slow enough.} \end{array} \quad (8.53)$$

$$\text{where } \vec{\mathcal{R}}_{\vec{\lambda}} \equiv i \langle \Psi_{\vec{\lambda}} | \frac{\partial}{\partial \vec{\lambda}} | \Psi_{\vec{\lambda}} \rangle \quad (8.54)$$

The quantity $\vec{\mathcal{R}}_{\vec{\lambda}}$ is called the *Berry connection* because it connects wave functions for slightly differing values of the parameter λ . In many applications $|\Psi_{\vec{\lambda}}\rangle$ is a periodic function of $\vec{\lambda}$. Then in Eq. (8.53), one can choose a circuit such that $\vec{\lambda}$ starts and ends at the same point; the result is in general nonzero, and known as the *geometrical phase* or *Berry phase*

$$\Gamma = \oint d\vec{\lambda} \cdot \vec{\mathcal{R}}_{\vec{\lambda}}. \quad (8.55)$$

Application to Wannier Functions.

For Wannier functions to serve their intended purpose as localized basis functions, they should have as small a spatial spread as possible. This condition can be applied equally well to any of the functions indexed by \vec{R} , and so will be applied to the one centered at the origin $\vec{R} = \vec{0}$. Dropping for the moment reference to $\vec{R} = \vec{0}$ to avoid cluttering the notation, the center of the Wannier function is given by

$$\vec{r}_n = \int d\vec{r} w_n^*(\vec{r}) \vec{r} w_n(\vec{r}) \quad \text{Suppressing notation } \vec{R} = \vec{0}. \quad (8.56)$$

A measure of the spread of the Wannier function is

$$\overline{\delta r_n^2} = \int d\vec{r} w_n^*(\vec{r}) |\vec{r} - \vec{r}_n|^2 w_n(\vec{r}) = \overline{r_n^2} - |\vec{r}_n|^2. \quad \text{The definition of } \overline{r_n^2} \text{ should be clear. Obtain the last identity by multiplying out the square.} \quad (8.57)$$

As shown in Problem 9,

$$\vec{r}_n = \sum_{\vec{k}} \vec{\mathcal{R}}_{n\vec{k}} \quad \text{The sum is over the } N \text{ wave vectors in a single Brillouin zone.} \quad (8.58)$$

where in this case the Berry connection involves the periodic Bloch functions of Eq. (7.45)

$$\vec{\mathcal{R}}_{n\vec{k}} = i \int_{\Omega} d\vec{r} u_{n\vec{k}}^*(\vec{r}) \nabla_{\vec{k}} u_{n\vec{k}}(\vec{r}) \quad \text{The integral is over one unit cell as in Eq. (7.26).} \quad (8.59)$$

Also,

$$\overline{r_n^2} = - \sum_{\vec{k}} \int_{\Omega} d\vec{r} u_{n\vec{k}}^*(\vec{r}) \nabla_{\vec{k}}^2 u_{n\vec{k}}(\vec{r}). \quad (8.60)$$

Take advantage now of the freedom expressed in Eq. (8.47) to modify $u_{n\vec{k}}$ by an arbitrary real function $\phi_n(\vec{k})$ of \vec{k} , periodic over the Brillouin zone. Problem 9 shows that by manipulating ϕ one can minimize the spread $\overline{\delta r_n^2}$ of the Wannier function through the condition

$$\nabla_{\vec{k}}^2 \phi_n(\vec{k}) = \vec{\nabla}_{\vec{k}} \cdot \vec{\mathcal{R}}_{n\vec{k}}. \quad (8.61)$$

In general, this is as far as one can go without proceeding to numerical solutions of the Poisson equation, of which examples can be found in Marzari and Vanderbilt (1997). However, in one dimension, one can write immediately

$$\phi(k) - \phi(0) = \int_0^k dk' \mathcal{R}_{k'}. \quad (8.62)$$

Problem 10 shows that for a one-dimensional lattice of spacing a , Wannier functions defined with this choice of phase are eigenfunctions of the position operator, provided that the positions R are quantized according to

$$R = la + \frac{\Gamma a}{2\pi}; \quad \Gamma = \int_0^{2\pi/a} dk' \mathcal{R}_{k'}. \quad l \text{ is an integer and } \Gamma \text{ is defined also in Eq. (8.55).} \quad (8.63)$$

8.4.4 Tight Binding Model

Thus, by manipulating the phase ϕ , one can optimize the Wannier functions and make them drop off as fast as possible when \vec{r} moves away from \vec{R} . Kohn (1959) first proved that Wannier functions in one dimension decay exponentially away from their centers, and Nenciu (1993) generalized the proof to three dimensions. The precise rate of decay is not easy to determine without detailed computation, but it is related to the size of the energy gap separating different bands of Bloch wave functions from each other. The larger the energy gap separating a band from all other bands, the more completely localized its Wannier functions can be.

Looking forward to the band structures in Section 10.4, this observation implies that electrons in insulators can safely be regarded as sitting in localized orbitals around specific atoms. However, while Wannier functions can be defined for metals, they are not guaranteed to be localized at atomic sites.

If the Wannier function centered at \vec{R} does decay exponentially once it leaves site \vec{R} , then it is very useful to write Schrödinger's equation in terms of a Wannier function basis. This calculation is much more concise than the one with atomic orbitals. Denote the state vector corresponding to $w_n(\vec{R}, \vec{r})$ by $|\vec{R}\rangle$, and write

$$\hat{\mathcal{H}} = \sum_{\vec{R}\vec{R}'} |\vec{R}'\rangle \langle \vec{R}' | \hat{\mathcal{H}} | \vec{R}\rangle \langle \vec{R}|. \quad (8.64)$$

The Hamiltonian in (8.64) is not the full Hamiltonian, but has been restricted to the n th band. It is not difficult to add an extra index and consider many bands, but that is not needed for the following discussion, so the index n will be dropped.

Expression (8.64) is useful if the Wannier function centered at \vec{R} becomes small enough once it is further away from \vec{R} than the nearest neighbors of \vec{R} . In this case, one can neglect the matrix element

$$\mathcal{H}_{\vec{R}\vec{R}'} \equiv \langle \vec{R}' | \hat{\mathcal{H}} | \vec{R}\rangle = \int d\vec{r} w_n^*(\vec{R}', \vec{r}) \left[-\frac{\hbar^2 \nabla^2}{2m} + U(\vec{r}) \right] w_n(\vec{R}, \vec{r}) \quad (8.65)$$

unless \vec{R} and \vec{R}' are nearest neighbors. Problem 6 shows that

$$\mathcal{H}_{\vec{R}\vec{R}'} = \sum_{\vec{k}} \frac{1}{N} \varepsilon_{n\vec{k}} e^{-i\vec{k}\cdot(\vec{R}-\vec{R}')}. \quad \varepsilon_{n\vec{k}} \text{ is the energy of a Bloch state of wave number } \vec{k} \text{ in band } n. \quad (8.66)$$

Therefore, $\mathcal{H}_{\vec{R}\vec{R}'}$ depends only upon the difference between \vec{R} and \vec{R}' . Furthermore, when \vec{R} and \vec{R}' are nearest neighbors, symmetry often dictates that $\mathcal{H}_{\vec{R}\vec{R}'}$ equal a single constant t , while when $\vec{R} = \vec{R}'$, one can denote $\mathcal{H}_{\vec{R}\vec{R}}$ by a constant U . In this case the Hamiltonian (8.64) becomes

$$\hat{\mathcal{H}}_{\text{TB}} = \sum_{\vec{R}\vec{\delta}} |\vec{R}\rangle t \langle \vec{R} + \vec{\delta} | + \sum_{\vec{R}} |\vec{R}\rangle U \langle \vec{R}|. \quad \begin{array}{l} \vec{\delta} \text{ is again a set of vectors pointing from } \vec{R} \\ \text{to its nearest neighbors. This notation helps} \\ \text{suggest the idea of hopping from site } \vec{R} + \vec{\delta} \text{ to} \\ \vec{R}. \end{array} \quad (8.67)$$

The Hamiltonian appearing in Eq. (8.67) is the *tight-binding Hamiltonian*. The first term on the right hand side of (8.67) is the hopping term that allows electrons

to move from one site to another. The second term is an *on-site term* that describes the energy of placing an electron at a lattice site.

The tight-binding Hamiltonian has a simple exact solution. Define

$$|\vec{k}\rangle = \frac{1}{\sqrt{N}} \sum_{\vec{R}} e^{i\vec{k}\cdot\vec{R}} |\vec{R}\rangle, \quad (8.68)$$

for \vec{k} in the first Brillouin zone, so that one has the inversion formula

$$|\vec{R}\rangle = \frac{1}{\sqrt{N}} \sum_{\vec{k}} e^{-i\vec{k}\cdot\vec{R}} |\vec{k}\rangle, \quad \text{Sum only over } \vec{k} \text{ in the first Brillouin zone.} \quad (8.69)$$

Inserting Eq. (8.69) into Eq. (8.67) gives

$$\hat{\mathcal{H}}_{\text{TB}} = \sum_{\vec{R}\vec{\delta}} \frac{1}{N} \sum_{\vec{k}\vec{k}'} |\vec{k}\rangle t e^{-i\vec{k}\cdot\vec{R} + i\vec{k}'\cdot(\vec{R}+\vec{\delta})} \langle \vec{k}' | + \sum_{\vec{R}} \frac{1}{N} \sum_{\vec{k}\vec{k}'} |\vec{k}\rangle U e^{-i\vec{k}\cdot\vec{R} + i\vec{k}'\cdot\vec{R}} \langle \vec{k}' | \quad (8.70)$$

$$= \sum_{\vec{k}} \mathcal{E}_{\vec{k}} |\vec{k}\rangle \langle \vec{k} | \quad (8.71)$$

with

$$\mathcal{E}_{\vec{k}} = U + t \sum_{\vec{\delta}} e^{i\vec{k}\cdot\vec{\delta}}. \quad (8.72)$$

This expression is identical to Eq. (8.39) if one identifies U with $\mathcal{E}^{\text{at}} + \mathcal{U}$.

Although Eqs. (8.72) and (8.39) are identical, they represent a different philosophy. In the first case, there is a series of approximations, and eventually an approximate result is derived in a particular instance. In the second case, generality is maintained whenever possible, and there is only a single approximation, which consists in neglecting interactions except between nearest neighbors. It is easy to pose new questions by modifying the tight-binding Hamiltonian. For example, what happens if the on-site energies U in Eq. (8.67) vary from site to site? This question leads to the theory of localization (Section 18.5). Or what happens if one moves beyond the single-electron approximation, and modifies Eq. (8.72) so that the Hamiltonian has an additional repulsive energy when more than one electron sits on a given site \vec{R} ? This question leads to studies of electron correlation and magnetism in Chapter 26.

Problems

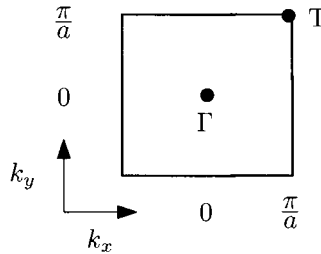
1. Nearly free electrons:

(a) Consider a two-dimensional square lattice of lattice constant a and take

$$U(\vec{r}) = -4U_0 \cos \frac{2\pi x}{a} \cos \frac{2\pi y}{a}. \quad (8.73)$$

Find the Fourier transform $U_{\vec{q}}$ from Eq. (7.26).

- (b) For $\vec{k}_1 = (\pi/a, \pi/a)$, $\psi(\vec{k}_1)$ will couple strongly to three other components of ψ , $\psi(\vec{k}_2) \dots \psi(\vec{k}_4)$. What are $\vec{k}_2 \dots \vec{k}_4$? Identify the values of \vec{K} that one must include when doing perturbation theory to find $\psi(\vec{k}_1) \dots \psi(\vec{k}_4)$ to first order in U_0 .
- (c) Evaluate $U_{\vec{K}}$ for the necessary values of \vec{K} . Show that $U_{\vec{K}} = U_{-\vec{K}}$ is nonzero only for one value of \vec{K} . Therefore perturbation theory can be reduced to the subspace involving only $\psi(\vec{k}_1)$ and, say, $\psi(\vec{k}_2)$.
- (d) Write down Schrödinger's equation in the subspace involving only $\psi(\vec{k}_1)$ and $\psi(\vec{k}_2)$.
- (e) Solve the resulting 2×2 system of equations and find the two allowed energies at Bloch index \vec{k}_1 .



- (f) Sketch $\mathcal{E}_{\vec{k}}$ for the lowest two bands along the line Γ - T , and indicate the size of the energy gap.

2. Smoothness of Fermi surface:

- (a) Show that the unit normal to the Fermi surface must be continuous in the reduced zone scheme, if the energy $\mathcal{E}_{n\vec{k}}$ is continuous and differentiable.
- (b) Show that in the nearly free electron approximation, the Fermi surface is perpendicular to the Brillouin zone boundary.

3. Reciprocal lattice:

- (a) Consider a two-dimensional lattice with primitive vectors

$$a(1, 0), \quad a\left(\frac{1}{2}, 1\right). \quad (8.74)$$

Find primitive vectors for the reciprocal lattice, and draw pictures of the first and second Brillouin zones.

- (b) Find the areas of the first and second Brillouin zones.

4. Two-dimensional Fermi surface: Find the Fermi surface for a triangular lattice in two dimensions, with six noninteracting spin 1/2 electrons per site.

- (a) Calculate the size of the Fermi sphere.
- (b) Draw the reciprocal lattice of the triangular lattice on a piece of tracing paper, and indicate the first three Brillouin zones.

- (c) Draw the Fermi sphere on a separate piece of paper at the same scale used for the Brillouin zones, and by moving the tracing paper over the Fermi sphere, find the Fermi surface.

5. Tight-Binding Band Structure of Graphene: Graphene is a honeycomb lattice (Eq. (1.5)) with lattice spacing $a = 2.46 \text{ \AA}$ (Table 2.1). The electronic band structure of graphene can be computed to reasonable approximation from s and p orbitals. The bands break into two groups. There is a first set of bands that come from the interactions of the s orbital and the p_x and p_y orbital, assuming graphene sits in the x - y plane. These are the σ bands, which require solution of a 6×6 matrix problem, described by Saito et al. (1998). A second set of bands comes from the p_z orbitals, called the π bands. These can be computed completely independently from the σ bands because all integrals of the form $\int d\vec{r} a_{p_z}^{\text{at}}(\vec{r}) a_s^{\text{at}}(\vec{r})$ or $\int d\vec{r} a_{p_z}^{\text{at}}(\vec{r}) a_{p_x}^{\text{at}}(\vec{r})$ vanish by symmetry. Thus for the π bands there is only one orbital $a_{p_z}^{\text{at}}$ to consider, cylindrically symmetrical in the $x - y$ plane, and with symmetry like z in the \hat{z} direction. Because the honeycomb lattice is built from two basis vectors, the matrix in Eq. (8.32) is 2×2 .

- (a) Refer to the two Bravais lattices corresponding to the two basis vectors of the honeycomb lattice as the A and B sublattices. Show that the matrices \mathcal{H} and \mathcal{S} have the form

$$\mathcal{H} = \begin{pmatrix} \mathcal{H}_{AA} & \mathcal{H}_{AB} \\ \mathcal{H}_{AB}^* & \mathcal{H}_{AA} \end{pmatrix} \quad \mathcal{S} = \begin{pmatrix} \mathcal{S}_{AA} & \mathcal{S}_{AB} \\ \mathcal{S}_{AB}^* & \mathcal{S}_{AA} \end{pmatrix} \quad (8.75)$$

Use Eq. (8.42).

- (b) Show more specifically by ignoring overlap integrals between any atoms farther apart than nearest neighbors that

$$\mathcal{H} = \begin{pmatrix} \mathcal{E}_p & t f(\vec{k}) \\ t f^*(\vec{k}) & \mathcal{E}_p \end{pmatrix} \quad \mathcal{S} = \begin{pmatrix} 1 & \alpha f(\vec{k}) \\ \alpha f^*(\vec{k}) & 1 \end{pmatrix} \quad (8.76)$$

where

$$f(\vec{k}) = e^{-ik_y a / \sqrt{3}} + 2e^{ik_y a / (2\sqrt{3})} \cos(k_x a / 2). \quad (8.77)$$

Find the definitions of \mathcal{E}_p , α and t .

- (c) Show that the energies of the two bands that result are

$$\mathcal{E}_{\vec{k}} = \frac{\mathcal{E}_p \pm t w(\vec{k})}{1 \pm \alpha w(\vec{k})} \quad (8.78)$$

where

$$w(\vec{k}) \equiv \sqrt{|f(\vec{k})|^2}. \quad (8.79)$$

- (d) Setting $\mathcal{E}_p = 0$ because it is just a constant, and taking $t = -3.033 \text{ eV}$, $\alpha = 0.129$, plot Eq. (8.78) between Γ and K (Figures 7.10 and 7.11). Show that in the vicinity of K the two bands are degenerate and have the form of $\pm |\vec{k} - \vec{k}_K|$

6. Wannier functions:

- (a) Show that matrix elements of the Hamiltonian between Wannier function coming from different bands must vanish, and that it is therefore legitimate to write down Eq. (8.64).
- (b) Show that the matrix element $\langle \vec{R} | \hat{\mathcal{H}} | \vec{R}' \rangle$ depends only upon $\vec{R} - \vec{R}'$, where $\langle \vec{R} |$ is the Wannier function defined in Eq. (8.43).

7. **Tight-binding model:** Consider a tight-binding Hamiltonian that acts upon a single band of localized states in one dimension,

$$\hat{\mathcal{H}} = 2t \sum_l \left\{ \frac{1}{2} (|l\rangle \langle l+1| + |l\rangle \langle l-1|) + \cos[2\pi l \tau_3] |l\rangle \langle l| \right\} \quad (8.80)$$

with

$$\tau_3 = \frac{5}{3}. \quad (8.81)$$

The integer l should be thought of as indexing sites along a chain of atoms; the state $|l\rangle$ locates an electron on atom l .

- (a) What is the periodicity of the Hamiltonian?
- (b) Use Bloch's theorem to reduce the eigenvalue problem associated with Eq. (8.80) to the solution of a small finite matrix equation.
- (c) Compute and plot the bands for k throughout the Brillouin zone. This task will have to be carried out numerically.

8. **Berry phases:** The definition of the Berry connection of Eq. (8.54) appears to require knowledge of the wave function $\Psi_{\vec{\lambda}}$ for adjacent values of $\vec{\lambda}$ in order to compute the derivative. However, the expression can be recast to involve wave functions at only one point in $\vec{\lambda}$ space.

- (a) Let m and n index separate eigenfunctions and eigenvalues of the Hamiltonian in Eq. (8.49). Show that

$$\langle \Psi_{m\vec{\lambda}} | \vec{\nabla}_{\vec{\lambda}} | \Psi_{n\vec{\lambda}} \rangle = \frac{\langle \Psi_m | (\vec{\nabla}_{\vec{\lambda}} \hat{\mathcal{H}}_{\vec{\lambda}}) | \Psi_n \rangle}{\mathcal{E}_n - \mathcal{E}_m} \quad (8.82)$$

- (b) Specialize to the case where $\vec{\lambda}$ has three components. Return to the definition of the Berry phase Eq. (8.55). Let A be any surface whose boundary is the line around which one integrates $\vec{\lambda}$. Using Stoke's Theorem, show that

$$\Gamma = - \int_A d\vec{n} \cdot \vec{V}_n \quad (8.83)$$

where \hat{n} is a unit normal integrated over surface A and

$$\vec{V}_n \equiv \text{Im} \sum_{m \neq n} \frac{\langle \Psi_{n\vec{\lambda}} | (\vec{\nabla}_{\vec{\lambda}} \hat{\mathcal{H}}_{\vec{\lambda}}) | \Psi_{m\vec{\lambda}} \rangle \times \langle \Psi_{m\vec{\lambda}} | (\vec{\nabla}_{\vec{\lambda}} \hat{\mathcal{H}}_{\vec{\lambda}}) | \Psi_{n\vec{\lambda}} \rangle}{(\mathcal{E}_{m\vec{\lambda}} - \mathcal{E}_{n\vec{\lambda}})^2} \quad (8.84)$$

9. Localization of Wannier functions:

- (a) Verify Eqs. (8.58) and (8.60).
- (b) Replace $u_{n\vec{k}}(\vec{r})$ with $u_{n\vec{k}}(\vec{r})e^{i\phi(\vec{k})}$, where $\phi(\vec{k})$ is periodic over the Brillouin zone. Show that \vec{r}_n is unchanged when the phase $\phi(k)$ changes, and find how $\overline{r_n^2}$ changes as a functional of $\phi(k)$.
- (c) Minimize $\overline{\delta r_n^2}$ with respect to $\phi(\vec{k})$ and show that the condition on $\phi(\vec{k})$ is Eq. (8.61)

10. **Wannier functions in one dimension:** The phases of Wannier functions can be determined in general by the prescription that the spread of the functions be minimized. For one-dimensional systems, there is another way to arrive at the same conclusion, proposed by Kivelson (1982). In one dimension, Wannier functions with phases given by Eq. (8.62) are eigenfunctions of the position operator.

Dropping the band index n and specializing to a one-dimensional crystal with N unit cells of length a , let $w(R, r)$ be Wannier functions, satisfying

$$w(R, r) = \frac{1}{\sqrt{N}} \sum_k e^{-ikR+i\phi(k)} \psi_k(r), \quad (8.85)$$

where $\phi(k)$ satisfies Eq. (8.62), and Eq. (8.59) becomes

$$\mathcal{R}_k = i \int_0^a dr u_k^*(r) \frac{\partial}{\partial k} u_k(r). \quad (8.86)$$

In one slight departure from other calculations, assume that the Bloch functions $\psi_k(r)$ rather than $u_k(r)$ have their phases arranged so as to be periodic functions of k over the Brillouin zone $[0, 2\pi/a]$. Making use of Eq. (8.85) and $\psi_k(r) = \exp[ikr]u_k(r)$ show that

- (a) Show that

$$\begin{aligned} rw(R, r) = & R w(R, r) \\ & + \left(e^{-(2\pi i/a)R+i\phi(2\pi/a)} - e^{i\phi(0)} \right) \frac{\psi_0(r)}{\sqrt{N}} \\ & - \frac{1}{\sqrt{N}} \sum_k \left(\mathcal{R}_k u_k(r) + \frac{\partial}{\partial ik} u_k(r) \right) e^{ik(r-R)+i\phi(k)}. \end{aligned} \quad (8.87)$$

- (b) Multiply the last term of Eq. (8.87) by $w^*(R', r)$ and integrate over r . Show that the result vanishes for all R' and that therefore this last term is zero.
- (c) Show that the condition for the second term of Eq. (8.87) to vanish is the quantization condition on R Eq. (8.63).

References

- Y. Aharonov and D. Bohm (1959), Significance of electromagnetic potentials in quantum theory, *Physical Review*, **115**, 485–491.
- M. V. Berry (1984), Quantal phase factors accompanying adiabatic changes, *Proceedings of the Royal Society of London*, **A392**, 45–57.
- F. Bloch (1928), The quantum mechanics of electrons in crystal lattices, *Zeitschrift für Physik*, **52**, 555–600. In German.
- A. V. Gold (1958), An experimental determination of the Fermi surface in lead, *Philosophical Transactions of the Royal Society of London*, **A251**, 85–112.
- D. R. Hartree (1928), The wave mechanics of an atom with a non-coulomb central field, *Proceedings of the Cambridge Philosophical Society*, **24**, 89–132.
- S. Kivelson (1982), Wannier functions in one-dimensional disordered systems: Application to fractionally charged solitons, *Physical Review B*, **26**, 4269–4277.
- W. Kohn (1959), Analytic properties of Bloch waves and Wannier functions, *Physical Review*, **115**, 809–821.
- L. D. Landau and E. M. Lifshitz (1977), *Quantum Mechanics (Non-relativistic Theory)*, 3rd ed., Pergamon Press, Oxford.
- N. Marzari and D. Vanderbilt (1997), Maximally localized generalized Wannier functions for composite energy bands, *Physical Review B*, **56**, 12 847–12 865.
- G. Nenciu (1993), Existence of the exponentially localised Wannier functions, *Communications in Mathematical Physics*, **91**, 81–85.
- S. Pancharatnam (1956), Generalized theory of interference, and its applications. part i. coherent pencils, *Proceedings of the Indian Academy of Sciences*, **A44**, 247–262.
- R. Peierls (1930), The theory of the electrical and thermal conductivity of metals, *Annalen der Physik (Leipzig)*, **4**, 121. In German.
- R. Saito, G. Dresselhaus, and M. S. Dresselhaus (1998), *Physical Properties of Carbon Nanotubes*, Imperial College Press, Singapore.
- G. H. Wannier (1937), The structure of electronic excitation levels in insulating crystals, *Physical Review*, **52**, 191–197.
- Y. Zhao (2008), Reexamination of the quantum adiabatic theorem, *Physical Review A*, **77**, 032 109/1–8.

9. Electron–Electron Interactions

9.1 Introduction

Bloch's theory for periodic solids brilliantly solves the problem of a single electron in a periodic potential. While engaged in the process of solving this problem, it is easy to forget the severity of the approximations needed to reduce a real periodic solid to a single-electron problem. The problem has two different sides. First, how conceptually can interacting electrons be treated within a one-electron framework at all? An answer to this question will be provided in Section 17.5 by Fermi liquid theory. Yet Fermi liquid theory provides little practical guidance in constructing the effective one-electron potential it shows may exist. The construction is instead provided by a sequence of approximations, whose validity is in principle not quite clear but in practice lies behind all attempts at realistic calculations. There is no internally consistent test for the validity of these calculations, and sometimes they fail rather badly. Even more often, however, they achieve detailed comparison with experiment that is much better than might have been expected. The goal of this chapter is to describe only those treatments of electron–electron interactions leading to practical band structure calculations.

The Hamiltonian that one really should solve is Eq. (6.1), in which electrons and nuclei all appear on an equal quantum-mechanical footing. A first simplification is to remove the nuclei from the quantum mechanics problem. Because nuclei are thousands of times more massive than electrons, they move that much more slowly. Born and Oppenheimer (1927) suggested an approximation scheme that is employed quite universally throughout condensed matter physics. So far as the electrons are concerned, take the nuclei to be static, classical potentials, and solve the electronic problem without worrying about the nuclei further. So far as the nuclei are concerned, the electrons are a rapidly moving shroud of charge that follows them wherever they go. Because the motion of nuclei is accompanied by charge redistribution, the energies involved in moving nuclei about depend upon the solution of the electron problem, and the nuclei interact with complicated effective potentials. All the ideas of different types of interatomic bonding arise from this viewpoint and will be discussed further in Chapter 11.

The *Born–Oppenheimer approximation* may have to be abandoned whenever the electrons and nuclei cannot be disentangled so neatly. The world is full of phenomena where the approximation fails. For example, in striking a flint to create a spark, mechanical motion excites electrons into a plasma that then emits light.

Adopting the Born–Oppenheimer approximation, the electrons in Eq. (6.1) solve

$$\hat{H}\Psi = \frac{-\hbar^2}{2m} \sum_{l=1}^N \nabla_l^2 \Psi + \sum_{l=1}^N U_{\text{ion}}(\vec{r}_l) \Psi + \sum_{l < l'} \frac{e^2}{|\vec{r}_l - \vec{r}_{l'}|} \Psi = \mathcal{E} \Psi, \quad (9.1)$$

where Ψ is an antisymmetric function of the immense number N of electrons in a solid. This problem is still intractable, even on the largest computers, for more than several hundred electrons, a number that makes it impossible to investigate large molecules or solids. The numerical problem grows exponentially with the number of electrons; for macroscopic solids it will never be solved by brute force on a conventional computer. Contemplating this situation in the first days of quantum mechanics, Dirac wrote that “the underlying physical laws necessary for the mathematical theory of a large part of physics and the whole of chemistry are thus completely known, and the difficulty is only that the exact application of these laws leads to equations much too complicated to be soluble” [Dirac (1929), p. 714]. The paradox of condensed matter physics is contained in this simultaneous cry of triumph and despair. The fundamental equations are known, but fundamentally unwilling in their original form to answer most physical questions.

9.2 Hartree and Hartree–Fock Equations

All the computational difficulty arises from the Coulomb interaction. Perhaps this term may somehow be replaced by something more computationally tractable, such as an effective electron–electron potential $U_{ee}(\vec{r})$. A first guess at such an effective potential in which to study the motion of electrons is that each electron moves in a field produced by a sum over all the other electrons. Analogy with classical physics suggests that the potential corresponding to electron–electron interactions could be

$$U_{ee}(\vec{r}) = \int d\vec{r}' \frac{e^2 n(\vec{r}')}{|\vec{r} - \vec{r}'|}, \quad (9.2)$$

where n is the number density of electrons

$$n(\vec{r}) = \sum_j |\psi_j(\vec{r})|^2. \quad (9.3)$$

This guess can immediately be inserted into the Schrödinger equation, giving

$$\frac{-\hbar^2}{2m} \nabla^2 \psi_l + [U_{\text{ion}}(\vec{r}) + U_{ee}(\vec{r})] \psi_l = \mathcal{E}_l \psi_l. \quad (9.4)$$

A derivation follows, but one can simply write this down in the spirit of Eq. (6.3).

Equation (9.4) is the *Hartree equation*, which lay behind the first systematic attempts by Hartree (1928) to deduce atomic spectra from first principles.

9.2.1 Variational Principle

In order to improve upon the Hartree equations, it is desirable to find a formal way to derive them from Eq. (9.1). The best method is the variational principle derived in Appendix B which states that wave functions solving Schrödinger's equation are extrema of the functional

$$F_{\mathcal{H}}\{\Psi\} = \langle \Psi | \hat{\mathcal{H}} | \Psi \rangle, \quad (9.5)$$

subject to the constraint that $\langle \Psi | \Psi \rangle = 1$. As discussed in Section 8.2.1, approximate solutions of Schrödinger's equation are obtained by restricting the search for extrema to a subset of all possible wave functions. The Hartree equations follow from restricting one's search to wave functions Ψ of the form

$$\Psi = \prod_{l=1}^N \psi_l(\vec{r}_l), \quad (9.6)$$

where the ψ_l are orthonormal. If one considers wave functions of this form, uses Lagrange multipliers \mathcal{E}_j to enforce the constraints $\langle \psi_j | \psi_j \rangle = 1$, and demands

$$\frac{\delta F_{\mathcal{H}}}{\delta \psi_l^*(\vec{r})} - \frac{\delta}{\delta \psi_l^*(\vec{r})} \sum_j \mathcal{E}_j \int d\vec{r}' \psi_j^*(\vec{r}') \psi_j(\vec{r}') = 0 \quad (9.7)$$

the Hartree equations (9.4) result almost immediately, apart from one small and slightly annoying discrepancy. The formal calculation indicates that each electron interacts not with the full charge density of the system, but with the charge density minus the density due to the electron itself. The calculations are left as Problem 1, but the more difficult case of Hartree–Fock will now be performed explicitly.

9.2.2 Hartree–Fock Equations

The central failing of the Hartree equation is that it does not recognize the Pauli principle. The true many-body wave function must vanish whenever two electrons occupy the same position, but the Hartree wave function cannot have this property. The Pauli principle forces electrons in metals to occupy single-particle energy states with energies on the order of 10 000 K, even in the ground state—such large energies that this effect must be included in any calculation from the outset to have any hope of realism.

Fock (1930) and Slater (1930) showed that the way to obey the Pauli principle is to work within the space of antisymmetric wave functions. Absolutely the simplest possible type of antisymmetric wave function is obtained by taking a collection of orthonormal one-particle wave functions and antisymmetrizing them:

$$\Psi(\vec{r}_1\sigma_1 \dots \vec{r}_N\sigma_N) = \frac{1}{\sqrt{N!}} \sum_s (-1)^s \psi_{s_1}(\vec{r}_1\sigma_1) \dots \psi_{s_N}(\vec{r}_N\sigma_N) \quad (9.8)$$

The sum is over all permutations s of $1 \dots N$. σ_i is a spin index.

$$= \frac{1}{\sqrt{N!}} \begin{vmatrix} \psi_1(\vec{r}_1\sigma_1) & \psi_1(\vec{r}_2\sigma_2) & \dots & \psi_1(\vec{r}_N\sigma_N) \\ \cdot & \cdot & & \cdot \\ \cdot & \cdot & & \cdot \\ \cdot & \cdot & & \cdot \\ \cdot & \cdot & & \cdot \\ \psi_N(\vec{r}_1\sigma_1) & \psi_N(\vec{r}_2\sigma_2) & \dots & \psi_N(\vec{r}_N\sigma_N) \end{vmatrix} \quad \cdot \quad \begin{array}{l} \text{This type of} \\ \text{wave function is} \\ \text{called a Slater} \\ \text{determinant.} \end{array} \quad (9.9)$$

Because this wave function is not a simple product, but a sum of products, the particles are no longer independent. Varying a single index, \vec{r}_1 for example, causes all the particles to shift around. Thus the Pauli principle induces correlations among the particles. Under these circumstances, it is impossible to be completely casual about spin degrees of freedom, tossing them in at the end of the calculation as a factor of two. Therefore, the spin index σ_i taking values ± 1 is included in every wave function. So long as the Hamiltonian does not involve the spin explicitly, the equations will be solved by giving ψ the simple form

$$\psi_l(\vec{r}_i\sigma_i) = \phi_l(\vec{r}_i)\chi_l(\sigma_i). \quad \begin{array}{l} \text{The spin function } \chi_l \text{ is either the "spin-up" func-} \\ \text{tion, } \delta_{1,\sigma_i}, \text{ or the "spin-down" function } \delta_{-1,\sigma_i}. \end{array} \quad (9.10)$$

It is cumbersome to carry around the arguments of ψ_l , so adopt the shorthand notation

$$\psi_l(\vec{r}_i\sigma_i) \equiv \psi_l(i) \quad (9.11)$$

To obtain the Hartree–Fock equations, one repeats the variational problem that led to the Hartree equations, but now employing the wave function (9.8) rather than (9.6). The calculation is more difficult. The first step is to take the expectation value of the Hamiltonian with the wave function (9.8), and the next step is to require that its functional derivative with respect to each ψ_i vanish. This expectation value can be obtained by working explicitly with the wave function in Eq. (9.8). However, such computations are exactly what second quantization was designed to simplify. Obtaining the Hartree-Fock equations is therefore a sensible starting point to gain practice with second quantization.

As described in Appendix C, given a complete set of states such as ψ_l , the Hamiltonian (9.1) can be rewritten as

$$\hat{\mathcal{H}} = \sum_l \hat{c}_l^\dagger \hat{c}_l \langle \psi_l(1) | \frac{-\hbar^2 k^2}{2m} \nabla_1^2 + \hat{U}_{\text{ion}}(\vec{r}_1) | \psi_l(1) \rangle \quad (9.12)$$

$$+ \frac{1}{2} \sum_{l'l''l'''} \hat{c}_l^\dagger \hat{c}_l \hat{c}_{l''}^\dagger \hat{c}_{l'''} \langle \psi_l(1)\psi_{l'}(2) | \frac{e^2}{|\vec{r}_1 - \vec{r}_2|} | \psi_{l''}(1)\psi_{l'''}(2) \rangle,$$

or, denoting $\langle \psi_l(1) |$ by $\langle l |$ to make the notation even more compact,

$$\hat{\mathcal{H}} = \sum_l \hat{c}_l^\dagger \hat{c}_l \langle l | \frac{-\hbar^2 k^2}{2m} \nabla_1^2 + \hat{U}_{\text{ion}}(\vec{r}_1) | l' \rangle \quad (9.13)$$

$$+ \frac{1}{2} \sum_{l'l''l'''} \hat{c}_l^\dagger \hat{c}_l \hat{c}_{l''}^\dagger \hat{c}_{l'''} \langle ll' | \frac{e^2}{|\vec{r}_1 - \vec{r}_2|} | l''l''' \rangle.$$

The product wave function Ψ takes a very simple form in second quantized notation. One can write it as

$$|\Psi\rangle = |11111 \dots 10000 \dots\rangle \quad (9.14)$$

which means that states $1 \dots N$ are occupied, and all other states are unoccupied. The Hartree-Fock calculation proceeds by computing

$$\langle\Psi|\hat{\mathcal{H}}|\Psi\rangle \quad (9.15)$$

and choosing the functions ψ_l to make the expectation value as small as possible. To compute the expectation value, first consider

$$\langle\Psi|\hat{c}_l^\dagger\hat{c}_{l'}|\Psi\rangle. \quad (9.16)$$

When $\hat{c}_{l'}$ acts upon Ψ it gives 0 unless l' is one of the states obeying $l' < N$ so that it is occupied in Ψ . The annihilation operator $\hat{c}_{l'}$ removes this state from Ψ , which now can be written

$$\hat{c}_{l'}|\Psi\rangle = |\overset{1}{1}\overset{2}{1}\dots\overset{l'}{0}\overset{l'+1}{1}\dots\overset{N}{1}00\dots\rangle \quad (9.17)$$

When the creation operator \hat{c}_l^\dagger acts on (9.17), it had better create an electron in state at l' again, or else when $\langle\Psi|$ acts from the left, the result will be zero. So (9.16) is zero unless $l = l'$, and the first term in Eq. (9.14) becomes

$$\sum_{l \in \text{Occupied States}} \langle l | \frac{-\hbar^2 k^2}{2m} \nabla_1^2 + \hat{U}_{\text{ion}}(\vec{r}_1) | l \rangle \quad (9.18)$$

To compute the expectation value of the Coulomb operator in Eq. (9.13), consider

$$\langle\Psi|\hat{c}_l^\dagger\hat{c}_{l'}^\dagger\hat{c}_{l''}\hat{c}_{l'''}|\Psi\rangle. \quad (9.19)$$

Unless l'' and l''' are among the states occupied in $|\Psi\rangle$, which is to say $l'' < N$ and $l''' < N$ Eq. (9.19) immediately gives zero. Furthermore l and l' must create again the states that l'' and l''' have just destroyed. There are two ways this can happen: $l = l''$ and $l' = l'''$ or $l = l'''$ and $l' = l''$. In the first case, using Eqs. (C.3c) and (C.2b) one obtains from (9.19) the value +1. In the second case, use Eq. (C.3a) to swap \hat{c}_l^\dagger and $\hat{c}_{l'}^\dagger$. Thus one obtains from (9.19) the value -1. The conclusion is

$$\langle\Psi|\hat{c}_l^\dagger\hat{c}_{l'}^\dagger\hat{c}_{l''}\hat{c}_{l'''}|\Psi\rangle = \delta_{l'l''}\delta_{ll'''} - \delta_{l'l'''}\delta_{ll''} \quad \text{And } l \text{ and } l' \text{ must be occupied states} \quad (9.20)$$

which implies

$$\frac{1}{2}\langle\Phi|\sum_{ll''l'''}\hat{c}_l^\dagger\hat{c}_{l'}^\dagger\hat{c}_{l''}\hat{c}_{l'''}\langle ll''|\frac{e^2}{|\vec{r}_1-\vec{r}_2|}|l''l'''\rangle|\Phi\rangle \quad (9.21)$$

$$= \frac{1}{2}\sum_{ll''l'''}[\delta_{ll''}\delta_{l'l'''} - \delta_{l'l''}\delta_{ll'''}]\langle ll''|\frac{e^2}{|\vec{r}_1-\vec{r}_2|}|l''l'''\rangle \quad (9.22)$$

$$= \frac{1}{2}\sum_{ll''}\langle ll''|\frac{e^2}{|\vec{r}_1-\vec{r}_2|}|ll''\rangle - \langle ll''|\frac{e^2}{|\vec{r}_1-\vec{r}_2|}|l'l''\rangle \quad (9.23)$$

Adding together Eqs. (9.23) and (9.18) gives

$$\begin{aligned} \langle \Psi | \hat{\mathcal{H}} | \Psi \rangle = & \sum_i \int d\vec{r}_1 \psi_i^*(1) \left[-\frac{\hbar^2 \nabla^2}{2m} \psi_i(1) + U(\vec{r}_1) |\psi_i(1)|^2 \right] \\ & + \frac{1}{2} \int d\vec{r}_1 d\vec{r}_2 \frac{e^2}{|\vec{r}_1 - \vec{r}_2|} \sum_{\substack{i,j \\ \sigma_1 \sigma_2}} \left[|\psi_i(1)|^2 |\psi_j(2)|^2 - \psi_i^*(1) \psi_j^*(2) \psi_i(2) \psi_j(1) \right] \end{aligned} \quad (9.24)$$

The first of two terms in the double integral in (9.24) is called the *Coulomb integral*. It is precisely the term that appeared in Eq. (9.3). The second is more noteworthy; it is called the *exchange integral* and may be interpreted as saying that particles 1 and 2 flip places in the course of interacting. Because of the antisymmetry of the wave function, such an interaction comes in with a relative minus sign.

Having found this expectation value, the next task is to vary the functional (9.24) with respect to every single-particle function ψ and require each variation to vanish subject to the condition that the ψ 's be orthonormal. The real and imaginary parts of ψ are completely independent functions, so one must vary with respect to them separately. Instead of doing it quite that way, it is legitimate and simpler to treat ψ and ψ^* as independent functions and vary with respect to ψ^* holding ψ constant. In order to restrict the search for wave functions to the space in which all the ψ 's are orthonormal, use the method of Lagrange multipliers to enforce the N^2 constraints $\sum_{\sigma_1} \int d\vec{r}_1 \psi_i^*(1) \psi_j(1) = \delta_{ij}$, and add

$$\sum_{i,j} \mathcal{E}_{ij} \sum_{\sigma_1} \int d\vec{r}_1 \psi_i^*(1) \psi_j(1) \quad (9.25)$$

to the functional before taking the functional derivative.

The result is that

$$\sum_j \mathcal{E}_{ij} \psi_j(1) = \left[\begin{array}{l} -\frac{\hbar^2 \nabla^2}{2m} \psi_i(1) + U(\vec{r}_1) \psi_i(1) \\ + \psi_i(1) \int d\vec{r}_2 \sum_{\sigma_2, j=1}^N \frac{e^2 |\psi_j(2)|^2}{|\vec{r}_1 - \vec{r}_2|} \\ - \sum_{j=1}^N \psi_j(1) \sum_{\sigma_2} \int d\vec{r}_2 \frac{e^2 \psi_j^*(2) \psi_i(2)}{|\vec{r}_1 - \vec{r}_2|} \end{array} \right]. \quad (9.26)$$

Of course, one can vary with respect to $\psi_i(\vec{r})$ instead, and then take the complex conjugate of the ensuing expression. The result is exactly Eq. (9.26), except that \mathcal{E}_{ij} is replaced by \mathcal{E}_{ji}^* . This proves that $\mathcal{E}_{ij} = \mathcal{E}_{ji}^*$ so the matrix \mathcal{E}_{ij} is Hermitian. Therefore the Hartree–Fock equations can be simplified a bit further. Suppose in Eq. (9.9) that the wave functions ψ_i are replaced by

$$\tilde{\psi}_i = \sum_j W_{ij} \psi_j. \quad (9.27)$$

This replacement is equivalent to multiplying the matrix of ψ 's by the matrix W inside the determinant, and therefore it alters the wave function Ψ only by multiplying it by the determinant of W . If one chooses W to be a unitary matrix, its determinant is one, and Ψ takes exactly the same form in terms of the $\tilde{\psi}$'s that it did in terms of the ψ 's. The effect of this transformation upon, for example, the kinetic energy term is

$$\int d\vec{r} \sum_{i\sigma} \tilde{\psi}_i^*(\vec{r}\sigma) \frac{-\hbar^2 \nabla^2}{2m} \tilde{\psi}_i(\vec{r}\sigma) \quad (9.28)$$

$$= \int d\vec{r} \sum_{i\sigma} \sum_{jj'} W_{ij}^* \psi_j^*(\vec{r}\sigma) \frac{-\hbar^2 \nabla^2}{2m} W_{ij'} \psi_{j'}(\vec{r}\sigma) \quad (9.29)$$

$$= \int d\vec{r} \sum_{\sigma jj'} \delta_{jj'} \psi_j^*(\vec{r}\sigma) \frac{-\hbar^2 \nabla^2}{2m} \psi_j(\vec{r}\sigma) \quad (9.30)$$

$$= \int d\vec{r} \sum_{j\sigma} \psi_j^*(\vec{r}\sigma) \frac{-\hbar^2 \nabla^2}{2m} \psi_j(\vec{r}\sigma). \quad (9.31)$$

Similarly, all of the other terms in $\langle \Psi | \mathcal{H} | \Psi \rangle$ are invariant when ψ is turned in for $\tilde{\psi}$. However, the Lagrange multipliers change to

$$\sum_{ij} \sum_{ll'} \psi_i^* W_{li}^* \mathcal{E}_{ij} W_{ll'} \psi_{l'} = \sum_{ll'} \psi_l \tilde{\mathcal{E}}_{ll'} \psi_{l'}, \quad (9.32)$$

where

$$\tilde{\mathcal{E}}_{ll'} = \sum_{ij} W_{li}^* \mathcal{E}_{ij} W_{jl'} \quad (9.33)$$

is the matrix \mathcal{E}_{ij} in the new basis. Because \mathcal{E} is Hermitian, there exists a basis in which $\tilde{\mathcal{E}}$ is diagonal; one may as well therefore just take \mathcal{E} to be diagonal to begin with. Employing this simplification and carrying out the spin sums in Eq. (9.26) gives finally the Hartree–Fock equation

$$\mathcal{E}_i \phi_i(\vec{r}) = \left[\begin{array}{l} \frac{-\hbar^2 \nabla^2}{2m} \phi_i(\vec{r}) + U(\vec{r}) \phi_i(\vec{r}) \\ + \phi_i(\vec{r}) \int d\vec{r}' \sum_{j=1}^N \frac{e^2 |\phi_j(\vec{r}')|^2}{|\vec{r} - \vec{r}'|} \\ - \sum_{j=1}^N \delta_{\chi_i \chi_j} \phi_j(\vec{r}) \int d\vec{r}' \frac{e^2 \phi_j^*(\vec{r}') \phi_i(\vec{r}')}{|\vec{r} - \vec{r}'|} \end{array} \right] \cdot \begin{array}{l} \delta_{\chi_i \chi_j} \text{ is 1 if states } i \text{ and } j \text{ have the same spin} \\ \text{and zero otherwise} \end{array} \quad (9.34)$$

9.2.3 Numerical Implementation

Hartree–Fock calculations divide into two groups, restricted and unrestricted. Restricted Hartree–Fock calculations are ones in which there is an even number of electrons, and one assumes that wave functions divide into two groups: spin-up

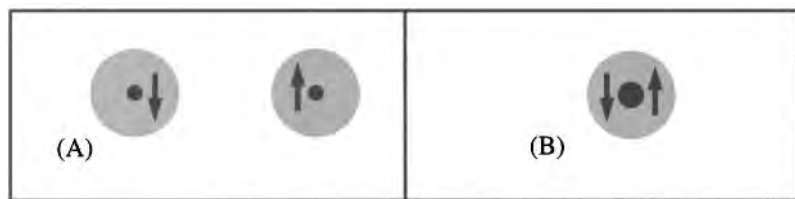


Figure 9.1. (A) For two well-separated H atoms the ground state cannot be described by a single spatial wave function multiplied by two different spin states. (B) But for the same collection of particles assembled as an He atom, it can be.

functions and spin-down functions. The spatial part of a given spin-up electron is exactly the same as the spatial wave function of some corresponding spin-down electron. Unrestricted Hartree–Fock makes no such assumption. Suppose one has two protons, very far separated, as in Figure 9.1. Each has its own private electron, and the ground state places an electron of definite spin on each atom. By contrast, if the same particles are placed in a helium atom, the ground state places both electrons in the same spatial state, differing only in their spin. In the first case, unrestricted Hartree–Fock is necessary, while in the second case, one can cut the size of the computation in half by doing restricted Hartree–Fock.

Whether one attacks a restricted or an unrestricted problem, the Hartree–Fock equations are a complicated set of nonlinear equations that can only be handled numerically. A first instinct would be to describe the various functions on some sort of cubic grid. This approach is used for atoms, but for molecules it is a terribly inefficient idea. A better way to solve the Hartree–Fock equations for molecules is to write each ϕ_i as a linear combination of basis functions that represent informed guesses about the actual shape of the wave functions and that are easy to integrate. The fewer basis functions one needs to represent electronic wave functions, and the easier it is to integrate products of the basis functions, the better off one will be. One set of examples of basis functions is provided by STONG. The STO stands for Slater-type orbitals, while NG stands for N Gaussians. Experience has shown that the electronic wave function at the i 'th nucleus looks roughly like $e^{-\lambda_i|\vec{r}-\vec{r}_i|}$. The problem is that if there is more than one nucleus, one has to do integrals of the form

$$\int d\vec{r} e^{-\lambda_1|\vec{r}-\vec{r}_1|} e^{-\lambda_2|\vec{r}-\vec{r}_2|}, \quad (9.35)$$

and these are numerically expensive integrals. A way to reduce the computational effort is to find a least-square fit to these exponentials using Gaussians,

$$\gamma_l = \sum_{l'} A_{ll'} e^{-a_j(\vec{r}-\vec{R}_{l'})^2}, \quad (9.36)$$

where all the coefficients are chosen to make γ look as much like the desired exponential as possible. One develops a whole family of functions of this form,

$$\gamma_1, \gamma_2 \dots \gamma_K, \quad (9.37)$$

designed to look like best guesses about the actual shapes of the electronic wave functions. The functions $\gamma_1 \dots \gamma_K$ are supposed to provide a basis in which to describe an arbitrary function, so $K \gg N$, but one hopes by choosing the basis functions well to make K as small as possible. The different γ 's are not orthonormal, in general. So one writes

$$\phi_I = \sum_{k=1}^K B_{Ik} \gamma_k, \quad (9.38)$$

and by substituting this form into the Hartree–Fock equations finds a large nonlinear matrix equation for the coefficients B_{Ik} . One also must write $1/|\vec{r}_1 - \vec{r}_2|$ as a sum of products of basis functions, so that inside the Coulomb and exchange integrals one has products of four basis functions to integrate over. The size of the matrix is $K \times K$, which illustrates the importance of choosing as small a basis set as possible. The equations are solved iteratively, starting with a guess for a set of N wave functions. Using these, one calculates all of the Coulomb and exchange integrals. The result is a linear $K \times K$ matrix equation, which is diagonalized using standard numerical routines developed for this purpose. After carrying out the linear algebra, there is a new set of K wave functions. Choosing the N of lowest energy, one again calculates all the Coulomb and exchange integrals, continuing until, if all goes well, the calculation has converged. The most time-consuming part of the process is the calculation of all the Coulomb and exchange integrals, because there are of order K^4 of these (one has to do an integral of the product of any four basis functions). Even if all the necessary integrals are done in advance and stored in memory, just calling up the results to add them together is a K^4 process. These considerations provide a simple explanation for the fact that quantum chemists use a huge portion of the world's supercomputer resources.

What sorts of results may be obtained by carrying out Hartree–Fock calculations? One first of all has an approximation to the ground-state wave function that can be used to calculate such experimentally measurable quantities as the dipole moment. Second of all, one has all of the excited states that were found while diagonalizing the Hartree–Fock Hamiltonian, but not included in the ground state. The lowest lying excited state provides an estimate of the ionization potential of an atom or molecule. Third, one can calculate how the total energy of a molecule varies with the external potential and in this way try to calculate the equilibrium geometry of a molecule. Table 9.1 gives some representative examples of the resulting accuracy compared with experiment.

Hartree–Fock does not do particularly well at computing dipole moments. It is able to calculate only to within about 0.1 in atomic units and may even get the sign wrong, as in the case of CO. Bond lengths come out better than dipole moments, but ionization potentials are again obtained only at about a 10% level. In the case of N_2 , Hartree–Fock incorrectly identifies the first excited state. The molecules in this table have 10 electrons, and therefore they are rather simple test cases. One's conclusion must be that Hartree–Fock provides only a qualitative guide and is not adequate for precise molecular calculations. To obtain better accuracy, chemists

Table 9.1. Theory versus experiment for Hartree–Fock

Molecule	CH ₄	NH ₃	H ₂ O	FH	CO
Bond length (Å): Hartree–Fock	2.048	1.890	1.776	1.696	
Bond length (Å): experiment	2.050	1.912	1.809	1.733	
Ionization potential (eV): Hartree–Fock	0.546	0.428	0.507	0.650	
Ionization potential (eV): experiment	0.529	0.400	0.463	0.581	
Dipole moment (e Å): Hartree–Fock		0.653	0.785	0.764	–0.110
Dipole moment (e Å): experiment		0.579	0.728	0.716	0.044

Bond lengths, ionization potentials, and dipole moments, comparing Hartree–Fock, and experiment. In the delicate case of CO, even the sign of the dipole moment is incorrect. Source: Szabo and Ostlund (1982).

have moved to considerably more elaborate wave functions, including sums of large numbers of determinantal wave functions. The name given to effects that cannot be calculated within Hartree–Fock is *correlation*: the tendency of electrons to respond to the details of each others' presence above and beyond the implications of the Pauli principle and Hartree–Fock theory. Pines posed the problem of correlation this way:

... we have neglected the effect of correlations in the position of the electrons introduced by the Coulomb interactions. The correlations will tend to keep the electrons apart, so that the energy of the system is further reduced This gain in energy will be designated the correlation energy here. Thus, we define the correlation energy as the difference between the energy calculated in the Hartree-Fock approximation and that calculated using any better approximation ... the Coulomb interaction, which on physical grounds makes an independent particle model appear unlikely, on closer mathematical investigation renders it untenable in practice.

—Pines (1955), pp. 373–374

These observations end the brief view of the program of doing chemistry by computer. Chemists have found it crucial to find approximations much better than Hartree–Fock in order to obtain satisfactory accuracy, while the portion of the physics community that carries out calculations of the electronic properties of crystals by necessity contents itself with approximations that are worse. However, the two communities have been converging toward a common approach based upon density functional theory (Section 9.3).

9.2.4 Hartree–Fock Equations for Jellium

The Hartree–Fock equations can be solved exactly for *jellium*, a name that may have come from a comment by Tonks and Langmuir (1929) concerning plasmas

that “when the electrons oscillated, the positive ions behave like a rigid jelly with uniform density of positive charge ne .” Jellium is just a collection of electrons, into which ions are introduced as a spatially uniform background to maintain overall charge neutrality. The Hartree–Fock equations are in this case solved by plane waves. For N electrons in a volume \mathcal{V} they take the form

$$\begin{aligned}
 \mathcal{E}_l \phi_l(\vec{r}) = & \underbrace{\frac{-\hbar^2 \nabla^2}{2m} \phi_l(\vec{r})}_{\text{Kinetic energy}} & & \underbrace{-\phi_l(\vec{r}) \frac{N}{\mathcal{V}} \int d\vec{r}_2 \frac{e^2}{|\vec{r} - \vec{r}_2|}}_{\text{Interaction with ions}} \\
 & + \underbrace{\phi_l(\vec{r}) \int d\vec{r}_2 \sum_{j=1}^N \frac{e^2 |\phi_j(\vec{r}_2)|^2}{|\vec{r} - \vec{r}_2|}}_{\text{Coulomb interaction}} & & - \underbrace{\sum_{j=1}^N \delta_{\chi_l \chi_j} \phi_j(\vec{r}) \int d\vec{r}_2 \frac{e^2 \phi_j^*(\vec{r}_2) \phi_l(\vec{r}_2)}{|\vec{r} - \vec{r}_2|}}_{\text{Exchange interaction}}.
 \end{aligned} \tag{9.39}$$

Insert a plane wave of the form

$$\phi_l(\vec{r}) = \frac{e^{i\vec{k}_l \cdot \vec{r}}}{\sqrt{\mathcal{V}}}. \tag{9.40}$$

The allowable set of \vec{k} 's as in Section 6.3 is given by imposing periodic boundary conditions on the system, producing the usual conclusion that the density of \vec{k} states per volume and per spin is $1/(2\pi)^3$. The kinetic energy term in Eq. (9.39) produces

$$\frac{\hbar^2 k_l^2}{2m} \phi_l(\vec{r}). \tag{9.41}$$

The interaction with the ions and the Coulomb interaction cancel against each other because $|\phi_j(\vec{r}_2)|^2 = 1/\mathcal{V}$. The only calculation remaining is the exchange interaction, which becomes

$$e^2 \sum_{j=1}^N \frac{e^{i\vec{k}_j \cdot \vec{r}}}{\sqrt{\mathcal{V}}} \int \frac{d\vec{r}_2}{\mathcal{V}} \frac{e^{i(\vec{k}_l - \vec{k}_j) \cdot \vec{r}_2}}{|\vec{r} - \vec{r}_2|} \delta_{\chi_l \chi_j} \tag{9.42}$$

$$= e^2 \phi_l \sum_{j=1}^N \int \frac{d\vec{r}'}{\mathcal{V}} \frac{e^{i(\vec{k}_l - \vec{k}_j) \cdot \vec{r}'}}{r'} \delta_{\chi_l \chi_j} \tag{9.43}$$

Changing the variable of integration to $\vec{r}' = \vec{r}_2 - \vec{r}$.

$$= e^2 \phi_l \sum_{j=1}^N \frac{1}{\mathcal{V}} \frac{4\pi}{|\vec{k}_l - \vec{k}_j|^2} \delta_{\chi_l \chi_j} \tag{9.44}$$

The Fourier transform of $1/r$ is $4\pi/k^2$.

$$= e^2 \phi_l \int^{k_F} \frac{d\vec{k}}{(2\pi)^3} \frac{4\pi}{k_l^2 + k^2 - 2\vec{k} \cdot \vec{k}_l} \tag{9.45}$$

Assume that states are occupied up to a Fermi wave vector and turn the sum over j into an integral. However, the restriction that $\chi_l = \chi_j$ cuts in half the density of states in Section 6.3.

$$= e^2 \phi_l(\vec{r}) \frac{1}{2\pi k_l} \left[(k_F^2 - k_l^2) \ln \left\{ \frac{k_F + k_l}{k_F - k_l} \right\} + 2k_l k_F \right]. \tag{9.46}$$

Write $\vec{k} \cdot \vec{k}_l = k k_l \cos \theta$, integrate first $d \cos \theta$, then $k^2 dk$.

So plane waves solve the Hartree–Fock equations, and the energy of state l is

$$\mathcal{E}_l = \frac{\hbar^2 k_l^2}{2m} - \frac{2e^2}{\pi} k_F F(k_l/k_F), \quad (9.47)$$

where the *Lindhard dielectric function* $F(x)$ is

$$F(x) = \frac{1}{4x} \left[(1-x^2) \ln \left\{ \frac{1+x}{1-x} \right\} + 2x \right]. \quad (9.48)$$

This expression has certain peculiarities. In particular, $\partial\mathcal{E}/\partial k$ is infinite at the Fermi surface, which means that the group velocity of electrons at the Fermi surface should be infinite, a conclusion that would have catastrophic consequences for transport properties were it not both unphysical and incorrect. The source of the difficulty is visible in Eq. (9.44); it arises from the divergence when $\vec{k}_l \rightarrow \vec{k}_j$, which in turn arises from the very slow decay at long distances of the Coulomb interaction $1/|\vec{r} - \vec{r}'|$. An effect that the Hartree–Fock approximation has missed is *screening*. The effective interaction of two distant electrons actually falls off much faster than $1/|\vec{r} - \vec{r}_2|$ because the many electrons in between them adjust their positions to hide the distant electrons from one another, but Hartree–Fock misses this fact because the nature of the approximation leads it to treat only two electrons at a time. Screening is the subject of Problem 3 and is reviewed by Echenique et al. (1990).

The energy of a collection of independent electrons is given by a sum of the one-particle energies. This simple relation does not hold for the energies \mathcal{E}_l of Hartree–Fock theory. The sum of all \mathcal{E}_l counts terms resulting from the Coulomb and exchange interactions twice. The correct expression for the total energy is therefore, as shown in Problem 2,

$$\mathcal{E} = \sum_l \left[\frac{\hbar^2 k_l^2}{2m} - \frac{e^2}{\pi} k_F F\left(\frac{k_l}{k_F}\right) \right] \quad F \text{ from Eq. (9.48)}. \quad (9.49)$$

$$= N \left[\frac{3}{5} \mathcal{E}_F - \frac{3}{4} \frac{e^2 k_F}{\pi} \right]. \quad \text{The integration is straightforward, although care needs to be taken as } k \rightarrow k_F. \quad (9.50)$$

9.3 Density Functional Theory

While in the end it will produce formulae that look a great deal like Hartree–Fock, density functional theory has a rather different flavor. In principle, it is an exact account of the many-body wave-function, while in practice it spurs on varied types of daring approximations.

The starting point of the theory is the observation of Hohenberg and Kohn (1964) that electron density contains in principle all the information contained in a many-electron wave function. The electronic density of a many-electron system

at point \vec{r} is defined to be

$$n(\vec{r}) = \langle \Psi | \sum_{l=1}^N \delta(\vec{r} - \vec{R}_l) | \Psi \rangle \quad (9.51)$$

$$= N \int d\vec{r}_1 \dots d\vec{r}_N \Psi^*(\vec{r}_1, \vec{r}_2 \dots \vec{r}_N) \delta(\vec{r} - \vec{r}_1) \Psi(\vec{r}_1 \dots \vec{r}_N). \quad (9.52)$$

Hohenberg and Kohn pointed out that if one knows the density of the ground state of a many-electron system, one can deduce from it the external potential in which the electrons reside, up to an overall constant. It must be kept in mind that the only ways in which two many-electron problems can differ are in the external potentials U and in the number of electrons that reside in the potentials. According to this result, both of these external parameters are determined by the electron density, so one can say that the density completely determines the many-body problem. This statement is surprising, because the density is a real function of a single spatial variable, while the complete quantum mechanical wave function needs N variables for its description.

To prove the claim, suppose that it is false. Suppose that there exist two external potentials $U_1(\vec{r})$ and $U_2(\vec{r})$ that result in the same charge density. Call the Hamiltonians that result from them $\hat{\mathcal{H}}_1$ and $\hat{\mathcal{H}}_2$, and let the ground state wave functions for the two Hamiltonians be Ψ_1 and Ψ_2 . Assume that the ground states of the two Hamiltonians are nondegenerate; this is a technicality that will be avoided completely by an improved version of the argument to be presented shortly. Then the ground-state energy of $\hat{\mathcal{H}}_1$ is realized only by Ψ_1 . So

$$\mathcal{E}_1 = \langle \Psi_1 | \hat{\mathcal{H}}_1 | \Psi_1 \rangle < \langle \Psi_2 | \hat{\mathcal{H}}_1 | \Psi_2 \rangle \quad \text{Because } \Psi_2 \text{ is not the ground state of } \hat{\mathcal{H}}_1. \quad (9.53)$$

$$\Rightarrow \mathcal{E}_1 < \langle \Psi_2 | \hat{\mathcal{H}}_2 | \Psi_2 \rangle + \langle \Psi_2 | (\hat{\mathcal{H}}_1 - \hat{\mathcal{H}}_2) | \Psi_2 \rangle \quad (9.54)$$

$$\Rightarrow \mathcal{E}_1 < \mathcal{E}_2 + \int d\vec{r} n(\vec{r}) [U_1(\vec{r}) - U_2(\vec{r})]. \quad \text{Two Hamiltonians with the same number of electrons can differ only in the potential.} \quad (9.55)$$

However, one can equally well switch indices 1 and 2 to obtain

$$\mathcal{E}_2 < \mathcal{E}_1 + \int d\vec{r} n(\vec{r}) [U_2(\vec{r}) - U_1(\vec{r})]. \quad (9.56)$$

Adding Eqs. (9.55) and (9.56) gives

$$\mathcal{E}_1 + \mathcal{E}_2 < \mathcal{E}_1 + \mathcal{E}_2, \quad (9.57)$$

which is a contradiction. Therefore the potentials U_1 and U_2 must be the same.

As a result of these observations, one can imagine being handed many different solid systems, told that they consist of electrons interacting with one another via Coulomb potentials, moving in potential U , and obeying Schrödinger's equation. If in each case one is given the charge density, as a function of space, then in principle one can deduce U and solve for all properties of the system. Thus one can think of

the ground-state energy \mathcal{E} , kinetic energy T , and so on as being functionals of the density, and can write the following, to indicate this fact:

$$\mathcal{E}[n] = T[n] + U[n] + U_{ee}[n]. \quad (9.58)$$

Here n really means $n(\vec{r})$, a function of space, T is the kinetic energy, U is the potential due to ions, and U_{ee} is the Coulomb interaction between electrons.

Hohenberg and Kohn next observed that if one can find the functional $\mathcal{E}[n]$, then the true ground-state density $n(\vec{r})$ minimizes it, subject only to the constraint that

$$\int d\vec{r} n(\vec{r}) = N. \quad (9.59)$$

This assertion is proved by noting that if one starts with the “wrong” density, n_2 , for Hamiltonian \mathcal{H}_1 , then n_2 should really be associated with a different Hamiltonian $\hat{\mathcal{H}}_2$, which has ground-state wave function Ψ_2 and which does not minimize

$$\langle \Psi_2 | \mathcal{H}_1 | \Psi_2 \rangle = \mathcal{E}_1[n_2]. \quad (9.60)$$

Only n_1 minimizes $\mathcal{E}_1[n_1]$, and this is just what needed to be shown.

The most intriguing feature of this view of the many-body problem is that one can write the energy functional \mathcal{E} as

$$\mathcal{E}[n] = \int d\vec{r} n(\vec{r})U(\vec{r}) + F_{HK}[n], \quad (9.61)$$

where F_{HK} is the sum of kinetic and Coulomb energies:

$$F_{HK}[n] = T[n] + U_{ee}[n]. \quad (9.62)$$

The functional F_{HK} does not depend upon the potential $U(\vec{r})$, and so it constitutes a universal functional for all systems of N particles; if one only could find this functional, it would solve *all* many-body problems for *all* external potentials U .

Second Derivation of Energy Functional. It is desirable to have a second demonstration of the existence of the energy functional \mathcal{E} for two reasons. First, the demonstration given so far relies crucially upon assuming that ground states are nondegenerate. It is worth knowing whether this requirement is a dull technicality or a fatal flaw. Second, it might be possible to find a charge density $n(\vec{r})$ that cannot result from any conceivable potential $U(\vec{r})$. In this case, the functional $\mathcal{E}[n]$ is not yet even properly defined. Both these points are answered by defining a functional $F[n]$ that is the minimum over all wave functions producing density $n(\vec{r})$:

$$F[n] \equiv \min_{\Psi \rightarrow n} \langle \Psi | T + U_{ee} | \Psi \rangle. \quad (9.63)$$

This functional F can be defined even if there does not exist a potential U that would produce density n for some quantum-mechanical ground state. The process

of finding the ground state \mathcal{E}_0 of a many-body system may therefore be carried out in the following way:

$$\mathcal{E}_0 = \min_{\Psi} \langle \Psi | T + U + U_{ee} | \Psi \rangle \quad (9.64)$$

$$= \min_n \left[\min_{\Psi \rightarrow n} \langle \Psi | T + U + U_{ee} | \Psi \rangle \right] \quad \begin{array}{l} \text{Minimize over all wave functions} \\ \Psi \text{ that produce density } n, \text{ and} \\ \text{then minimize over all densities.} \end{array} \quad (9.65)$$

$$= \min_n \left[\min_{\Psi \rightarrow n} \langle \Psi | T + U_{ee} | \Psi \rangle + \int U(\vec{r}) n(\vec{r}) d\vec{r} \right] \quad \begin{array}{l} \text{Because the potential } U \text{ depends} \\ \text{only upon the density.} \end{array} \quad (9.66)$$

$$= \min_n \left[F[n] + \int U(\vec{r}) n(\vec{r}) d\vec{r} \right] \quad (9.67)$$

$$\equiv \min_n \mathcal{E}[n]. \quad (9.68)$$

The problems of defining \mathcal{E} in general and accommodating degenerate ground states are therefore solved simultaneously.

In principle, what has been accomplished here is enormous. In principle, there exists a universal functional $F[n]$ that needs to be found once and for all. One adds to it any particular set of nuclei, in the form of the potential $U(\vec{r})$, and then has only to find the function $n(\vec{r})$ that minimizes it in order to solve the full complexities of Schrödinger's equation. As is often the case, the gap between accomplishments in principle and in practice is also enormous. The functional F is a magical lookup table that is supposed to solve all of quantum mechanics upon request. No one knows the true F , and no one ever will, so it is replaced by various uncontrolled approximations. The decades-long process of discarding approximations that disagree with experiment and improving on the ones that are more successful has encoded a great deal of accumulated physical insight within apparently simple functional forms.

9.3.1 Thomas–Fermi Theory

The simplest approximation providing an explicit form for the functionals $F[n]$ or $\mathcal{E}[n]$ is Thomas–Fermi theory. The basic idea of the theory is to find the energy of electrons in a spatially uniform potential as a function of density. Then one uses this function of the density locally even when the electrons are in the presence of an external potential.

The problem of electrons interacting by a Coulomb interaction in a uniform background (jellium) is unfortunately not possible to solve exactly, except in the limit of high density. It was solved approximately with the Hartree–Fock approximation in Section 9.2.4. The strategy here will be to use the results of the Hartree–Fock approximation to obtain an approximate account of any term in Schrödinger's equation that cannot automatically be expressed in terms of density. The first term of this sort is the kinetic energy; the kinetic energy of a single \vec{k} state is $\hbar^2 k^2 / 2m$, and one must sum over all available \vec{k} , so that the total kinetic energy is

$$T = \mathcal{V} \int [d\vec{k}] \frac{\hbar^2 k^2}{2m} \quad \begin{array}{l} \text{See Eq. (6.15) for the definition of } [d\vec{k}] \end{array} \quad (9.69)$$

$$= \mathcal{V} \frac{\hbar^2 k_F^5}{2m5\pi^2} = \mathcal{V} \frac{\hbar^2}{2m} \frac{3}{5} (3\pi^2)^{2/3} n^{5/3}. \quad \text{Using Eq. (6.29).} \quad (9.70)$$

The electron–electron interaction results within the Hartree–Fock approximation in two terms. The first part, the classical piece, is a functional of electron density automatically, because it equals

$$\frac{1}{2} \int d\vec{r}_2 d\vec{r}_1 \frac{e^2 n(\vec{r}_1) n(\vec{r}_2)}{|\vec{r}_1 - \vec{r}_2|}. \quad (9.71)$$

The second piece, the exchange term, was evaluated in Eq. (9.50) for jellium, where it was shown to be

$$-N \frac{3}{4} \frac{e^2 k_F}{\pi} = -\mathcal{V} \frac{3}{4} \left(\frac{3}{\pi}\right)^{1/3} e^2 n^{4/3}. \quad \text{Just rewrite } N \text{ and } k_F \text{ in terms of density.} \quad (9.72)$$

The idea of Thomas–Fermi theory is to assume that in a system where the charge density is not uniform, but varies slowly, the kinetic energy and exchange term will be given by the same expressions given above, but evaluated locally and integrated over all space. The kinetic energy is

$$T[n] = \int d\vec{r} \frac{\hbar^2}{2m} \frac{3}{5} (3\pi^2)^{2/3} n^{5/3}(\vec{r}), \quad (9.73)$$

and the exchange energy is

$$\mathcal{E}_{xc} = - \int d\vec{r} \frac{3}{4} \left(\frac{3}{\pi}\right)^{1/3} e^2 n^{4/3}(\vec{r}). \quad (9.74)$$

So finally a first explicit density functional is

$$\begin{aligned} \mathcal{E}[n] &= \frac{\hbar^2}{2m} \frac{3}{5} (3\pi^2)^{2/3} \int d\vec{r} n^{5/3}(\vec{r}) + \int d\vec{r} n(\vec{r}) U(\vec{r}) \\ &+ \frac{1}{2} \int d\vec{r}_2 d\vec{r}_1 \frac{e^2 n(\vec{r}_1) n(\vec{r}_2)}{|\vec{r}_1 - \vec{r}_2|} - \int d\vec{r} \frac{3}{4} \left(\frac{3}{\pi}\right)^{1/3} e^2 n^{4/3}(\vec{r}). \end{aligned} \quad (9.75)$$

Actually, this functional constitutes Thomas–Fermi theory only if the last term, due to exchange, is simply omitted; with the exchange term included, the theory is called Thomas–Fermi–Dirac.

The conventional Thomas–Fermi–Dirac equation is obtained by writing down the condition that the functional (9.75) be minimized by n , subject of course to the constraint that the integral of n be N . One has

$$\frac{\delta \mathcal{E}}{\delta n(\vec{r})} = \mu \quad \text{The chemical potential } \mu \text{ arises as the Lagrange multiplier enforcing the constraint that density be conserved.} \quad (9.76)$$

$$\Rightarrow \frac{\hbar^2}{2m} (3\pi^2)^{2/3} n^{2/3}(\vec{r}) + U(\vec{r}) + \int d\vec{r}_2 \frac{e^2 n(\vec{r}_2)}{|\vec{r} - \vec{r}_2|} - \left(\frac{3}{\pi}\right)^{1/3} e^2 n^{1/3}(\vec{r}) = \mu. \quad (9.77)$$

Omitting the last term on the left-hand side of Eq. (9.77) gives the Thomas–Fermi equation.

Thomas–Fermi theory is simple, but not particularly accurate, so its solution is relegated to Problem 4. One result of solving Eq. (9.77) is that the energy of an atom of nuclear charge Z is approximately $-1.5375Z^{7/3}$ Ry. For small atoms, this result is large by a factor of two when compared with Hartree–Fock; even for an atom as large as Xe ($Z = 54$), where one has better hope for an approximation based on slowly varying charge distributions, the equation is still in error by 20%. The Thomas–Fermi–Dirac equation gives energies that deviate even further from reality. Another disturbing feature of the equations is that Thomas–Fermi and Thomas–Fermi–Dirac equations predict that atoms never bind into molecules; the energy of a supposed molecule is always lowered by pushing the nuclei further apart. This subject is discussed by Lieb (1981).

Thomas–Fermi theory smooths out the charge distribution, because it has no way to know that electrons arrange themselves into separate shells. Thomas–Fermi–Dirac is even less physical; it predicts that at some finite radius the charge distribution drops instantaneously to zero. There have been attempts to develop improved theories of this type by bringing in dependence upon gradients of the charge distribution. The original Thomas–Fermi theory is most accurate for nearly uniform charge distributions, so it is natural to work out the corrections that would occur for an electron gas in a linearly varying potential, a quadratically varying potential, and so on, using these results to construct an expansion in terms of gradients of the density. However, none of the theories of this type has gained wide usage.

9.3.2 Stability of Matter

A different type of application of density functional theory is to address the question of the stability of matter. That is, why does the attraction between electrons and nuclei not lead to a collapse in which the electrons crowd in upon the nuclei, producing solids with an atom every 10^{-15} m rather than every 10^{-10} m? On this point there is no need even to turn to experiment; common experience says that elements and compounds are stable. However, it is interesting to find the features of quantum mechanics that make the obvious possible.

To the obvious fact corresponds an obvious answer; the Heisenberg uncertainty principle forbids electrons to come too close to nuclei. The momentum of an electron confined within a box of radius a must scale as \hbar/a , so the kinetic energy must scale as \hbar^2/ma^2 . However, the potential energy to be gained by coming close to the nucleus only scales as $-e^2/a$, so the kinetic energy term seems to win. While this argument is essentially correct, it does not provide the formal tools needed to show that matter is stable. The tools need to provide a good estimate of the kinetic energy of electrons based upon their density, and the Heisenberg uncertainty principle does not do a good job of it. The precise statement of Heisenberg's principle

is that

$$\left[\int d\vec{r} \hbar^2 |\vec{\nabla}\psi|^2 \right] \left[\int d\vec{r} r^2 |\psi|^2 \right] \geq \frac{\hbar^2}{4}; \quad \text{The root mean square momentum times the root mean square fluctuation in position of a wave function must have a product greater than } \hbar/2; \psi \text{ is normalized, and is assumed to be centered at the origin.} \quad (9.78)$$

it can be used to bound electron kinetic energies T through

$$T[n] \geq \frac{\hbar^2}{8m \int d\vec{r} r^2 n(\vec{r})}. \quad (9.79)$$

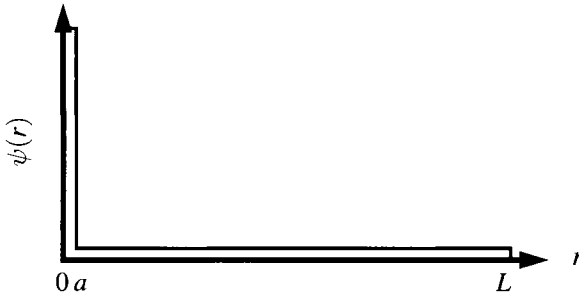


Figure 9.2. Profile of a wave function for which the Heisenberg uncertainty principle provides a particularly poor estimate of kinetic energy.

However, (9.79) can be satisfied by wave functions looking like the one shown in Figure 9.2. The broad base can be chosen to contain, say, half the wave function probability and, by being made of width L , can turn Eq. (9.78) into no more than the weak requirement that kinetic energy be greater than \hbar^2/mL^2 . In the meantime if the central peak in Figure 9.2 is placed over a positive ion, it can lead to huge amounts of potential energy that the weak estimate (9.79) does not counteract.

The vague feeling that a wave function shaped as in Figure 9.2 is cheating does not remove the need to find a way to improve the argument that matter does not collapse. Lieb showed that for a collection of N electrons interacting with each other and with nuclei, the kinetic energy of the electrons is bounded below by

$$T[n] \geq \frac{\hbar^2}{2m} \frac{9.116}{(8\pi)^{2/3}} \int d\vec{r} n^{5/3}. \quad (9.80)$$

Note the very strong resemblance of this exact result to the approximate expression for the kinetic energy of a collection of fermions obtained by using Hartree–Fock theory, as shown in Eq. (9.70). The density n appears raised to the $5/3$ power in both cases.

The arguments leading to Eq. (9.80) are rather elaborate, and those that follow from it to prove the stability of matter are no simpler. Therefore, rather than devote more attention to Eq. (9.80), this section will show how an identical but simpler technique can be used to prove the stability of atoms, and in particular the hydrogen atom.

As shown in Problem 6, the kinetic energy of any wave function

$$T[n] = \frac{\hbar^2}{2m} \int d\vec{r} |\nabla\psi|^2 \quad (9.81)$$

obeys the inequality

$$T[n] \geq \frac{\hbar^2}{2m} K_s \int d\vec{r} n^{5/3}, \quad (9.82)$$

where

$$K_s = 3(\pi/2)^{4/3}, \quad (9.83)$$

and with the density n given by

$$n(\vec{r}) = |\psi(\vec{r})|^2. \quad (9.84)$$

Therefore, for the hydrogen atom, the energy of a wave function ψ is bounded below by

$$\frac{\hbar^2}{2m} K_s \int d\vec{r} n^{5/3} - \int d\vec{r} \frac{e^2 n(\vec{r})}{r}. \quad (9.85)$$

The variational equation that can be used to minimize this functional subject to the constraint

$$\lambda(1 - \int d\vec{r} n) = 0 \quad (9.86)$$

is

$$\frac{5}{3} \frac{\hbar^2}{2m} K_s n^{2/3}(\vec{r}) - e^2/r + \lambda = 0. \quad \text{Here } \lambda \text{ is a Lagrange multiplier enforcing the constraint (9.86).} \quad (9.87)$$

There is also the constraint that n has to be positive. One way to enforce this constraint is to define $n = \sigma^2$ and carry out variations with respect to σ . One formally finds in this way that $n = 0$ is an acceptable local minimum of the functional Eq. (9.87); of course one can't have $n = 0$ everywhere or Eq. (9.86) is violated, but instead

$$n(\vec{r}) = \begin{cases} \left\{ 6m[e^2/r - \lambda]/(5K_s\hbar^2) \right\}^{3/2} & \text{for } r < e^2/\lambda \\ 0 & \text{else} \end{cases}. \quad (9.88)$$

One fixes λ by requiring the integral of n to be 1, and one finds that

$$\lambda = \frac{3me^4}{5\hbar^2 K_s} \left(\frac{\pi^4}{2}\right)^{1/3}; \quad (9.89)$$

inserting this form of n into Eq. (9.85) gives a lower bound to the energy of

$$-\frac{9me^4}{10\hbar^2 K_s} (2\pi^2)^{2/3} = -\frac{6}{5} \frac{me^4}{\hbar^2} = -\frac{12}{5} \text{Ry}. \quad (9.90)$$

The correct answer is of course that the ground-state energy is -1 Ry, so the estimate is not so bad.

In this way, without explicit solutions of Schrödinger’s equation, one can place limits upon the total energy to be gained through compression in the presence of Coulomb forces. Similar arguments prove the stability of matter using Eq. (9.80). What is really crucial is the fact that since one is considering an assembly of electrons, the Pauli exclusion principle forbids them from occupying a single lowest-energy state together. As a result, the kinetic energy penalty for compacting electrons grows as $n^{5/3}$ rather than just as n . The arguments by Lieb (1976) and Lieb et al. (1997) showing that many-electron systems are stable are rather elaborate, but the basic flavor is contained in use of the inequality for the very simple case of the hydrogen atom, and the end result is the same; matter does not implode because it would cost too much in kinetic energy.

9.4 Quantum Monte Carlo

9.4.1 Integrals by Monte Carlo

Despite the intrinsic difficulties of solving Schrödinger’s equation for many particles, there has long been a tenacious effort to solve it with as few approximations as possible. The most impressive progress has come from *quantum Monte Carlo* methods. The starting point is the Monte Carlo method (Section 5.4.1), now applied to the computation of integrals in large-dimensional spaces.

The Monte Carlo idea can be used to compute the average of any function in a probability distribution. Consider a function $g(\vec{x})$ where \vec{x} may be a vector in a n -dimensional space. Suppose that the probability of being at point \vec{x} is $\mathcal{P}(\vec{x})$, where to be a legitimate probability distribution

$$\mathcal{P}(\vec{x}) \geq 0; \quad \int d^n x \mathcal{P}(\vec{x}) = 1. \quad (9.91)$$

The average of g is

$$\bar{g} = \int d^n x g(\vec{x}) \mathcal{P}(\vec{x}). \quad (9.92)$$

To compute this average, follow the same steps as in Section 5.4.1:

1. Pick a starting value, \vec{x}_0 , and compute $g_0 = g(\vec{x}_0)$.
2. Pick a random vector $\Delta\vec{x}$, all of whose components range between $-\epsilon$ and ϵ , where ϵ is some constant.
3. Compute $\mathcal{P}(\vec{x}_0 + \Delta\vec{x})$.
 - (a) If $\mathcal{P}(\vec{x}_0 + \Delta\vec{x})/\mathcal{P}(\vec{x}_0) > 1$ then accept the move: $\vec{x}_1 = \vec{x}_0 + \Delta\vec{x}$.
 - (b) If $\mathcal{P}(\vec{x}_0 + \Delta\vec{x})/\mathcal{P}(\vec{x}_0) < 1$, choose a random number p between 0 and 1.
 - i. If $\mathcal{P}(\vec{x}_0 + \Delta\vec{x})/\mathcal{P}(\vec{x}_0) < p$, then again accept the move so that $\vec{x}_1 = \vec{x}_0 + \Delta\vec{x}$.
 - ii. Otherwise, reject the move and take $\vec{x}_1 = \vec{x}_0$.

In any case, compute $g_1 = g(\vec{x}_1)$, and accumulate the sum of g_0 and g_1 in a variable G .

4. Return to step 1 and repeat M times, continuing to assemble the sum of g in the variable G .

Finally, compute

$$\bar{g} = \frac{G}{M} = \frac{\sum_{i=1}^M g_i}{M}. \tag{9.93}$$

An estimate of the convergence of the integral is provided by the standard error,

$$\Delta g = \frac{1}{\sqrt{M}} \sqrt{\frac{\sum (g_i - \bar{g})^2}{M - 1}}. \tag{9.94}$$

Actually, this expression underestimates the error in the integral because results of successive Monte Carlo steps are not completely uncorrelated.

Not only averages, but any integral can be computed this way. To integrate $f(\vec{x})$, choose any probability distribution obeying Eq. (9.91) and write

$$\int d^n x f(\vec{x}) = \int d^n x \frac{f(\vec{x})}{\mathcal{P}(\vec{x})} \mathcal{P}(\vec{x}) = \overline{f(\vec{x})/\mathcal{P}(\vec{x})}. \tag{9.95}$$

Problem 7 provides a simple example of how to use this method to compute integrals.

9.4.2 Quantum Monte Carlo Methods

Starting with the ability to compute high-dimensional integrals, the quantum Monte Carlo method sets down two paths, *variational Monte Carlo* and *diffusion Monte Carlo*. Diffusion Monte Carlo is the more powerful of the two techniques, but it is quite complicated and will not be described here. Essentially the method involves constructing random walks whose probability is determined by the potential energy terms of the Hamiltonian. However there are complications due to the fact that wave functions change sign under interchange of particles. This *fermion sign problem* means that as the random walkers walk along, the sum one would like to accumulate gets both positive and negative contributions that nearly cancel, leading to a horrible loss of numerical accuracy. See Foulkes et al. (2001) for a description of clever ideas used to evade this problem and details of how to implement diffusion Monte Carlo.

Variational Monte Carlo is more straightforward. Let \vec{y}_1 be shorthand for the space and spin variables $\vec{r}_1 \sigma_1$. Choose a trial wave function $\Psi(\vec{y}_1 \dots \vec{y}_N)$ and compute the ground state energy

$$\mathcal{E} = \frac{\int d^N y \Psi^*(\vec{y}_1 \dots \vec{y}_N) \hat{\mathcal{H}} \Psi(\vec{y}_1 \dots \vec{y}_N)}{\int d^N y \Psi^*(\vec{y}_1 \dots \vec{y}_N) \Psi(\vec{y}_1 \dots \vec{y}_N)}. \tag{9.96}$$

Integrals over y are shorthand for integrating over spatial variables \vec{r} and summing over spin variables σ .

Varying parameters in Ψ , the goal is to find the lowest possible energy, and therefore an estimate of the ground state energy. The Hamiltonian \mathcal{H} might, for example, be the fundamental Hamiltonian Eq. (9.1) for a number of classical nuclei interacting with quantum mechanical electrons. The nuclei and some valence electrons might be replaced by pseudopotentials (Section 10.2.1). The calculations might be carried out in a periodic system where each cell contains N electrons and M nuclei, and the whole many-body system repeats periodically to simulate a solid. In all cases, the basic task is to come up with as good a variational wave function Ψ as possible, and then to compute the integrals in Eq. (9.96).

The first ingredient of conventional trial wave functions is a solution of the Hartree-Fock equations Eq. (9.34) for the Hamiltonian one has decided to solve. This numerical problem is not simple, but techniques to address it are advanced and described in Section 9.2.3. Call this wave function $\Psi_{\text{HF}}(\vec{y}_1 \dots \vec{y}_N)$. There would be no sense using Ψ_{HF} itself as the trial wave function in Eq. (9.96) since the energy that would come out in the end would have to be the energy in the Hartree-Fock equations. The main defect of Hartree-Fock wave functions is that they do not account for correlations between electrons. Correlations can be included by using wave functions of the *Jastrow* form, which means

$$\Psi(\vec{y}_1 \dots \vec{y}_N) = \Psi_{\text{HF}}(\vec{y}_1 \dots \vec{y}_N) e^{\sum_{i=1}^N \chi(\vec{y}_i) - \frac{1}{2} \sum_{i \neq j} u(\vec{y}_i, \vec{y}_j)} \quad (9.97)$$

The functions χ and u are varied to make the energy in Eq. (9.96) as low as possible. A constraint upon u is that it must obey the *cusp conditions*. Assume that u is of the form

$$u(\vec{y}_i, \vec{y}_j) = u_{\sigma_1, \sigma_2}(r_{ij}). \quad \text{Where } r_{ij} = |\vec{r}_i - \vec{r}_j| \quad (9.98)$$

Then if spins are opposite ($\sigma_1 \neq \sigma_2$),

$$\left. \frac{du_{\uparrow\downarrow}}{dr_{ij}} \right|_{r_{ij}=0} = -\frac{1}{a_0} \quad a_0 \text{ is the Bohr radius.} \quad (9.99a)$$

while if they are the same

$$\left. \frac{du_{\uparrow\uparrow}}{dr_{ij}} \right|_{r_{ij}=0} = -\frac{1}{2a_0} \quad (9.99b)$$

These relations are derived in Problem 8.

9.4.3 Physical Results

The most significant result obtained from Quantum Monte Carlo concerns the behavior of jellium, the interacting electron gas described in Section 9.2.4. Calculations concerning this basic system go back to the earliest days of quantum mechanics. The results are usually reported in terms of the electron separation r_s defined in Eq. (6.30) over the Bohr radius a_0 . When r_s/a_0 is large, the electron gas is dilute, while when it is small the gas is dense. Somewhat surprisingly, the problem

is easiest in the limit where the gas is very dense. In this limit, the Hartree-Fock approximation is accurate and from Eq. (9.50) gives an energy per particle of

$$\frac{\mathcal{E}}{N} = \frac{3}{5} \frac{\hbar^2 k_F^2}{2m} - \frac{3}{4\pi} e^2 k_F = \frac{3}{5} \frac{\hbar^2}{2ma_0^2} \left(\frac{9\pi}{4}\right)^{2/3} \frac{a_0^2}{r_s^2} - \frac{3}{4\pi} \frac{e^2}{a_0} \left(\frac{9\pi}{4}\right)^{1/3} \frac{a_0}{r_s}. \quad (9.100)$$

For a high-density gas, the largest energy comes from the kinetic energy of electrons pushed into high-energy states by the Pauli principle. Coulomb interactions of electrons with each other cancel against the interaction with background charge, so the next contribution comes the exchange energy, is negative, and is smaller by a factor of r_s/a_0 . These results were confirmed by Gell-Mann and Brueckner (1957) using methods of quantum field theory, and several additional terms in powers of r_s/a_0 were added to the sum.

However, there had long been indications that an expansion in powers of r_s/a_0 would not fully capture the behavior of jellium. Bloch (1929) performed further calculations using Hartree-Fock theory that predicted that at a certain electron density, the electrons should become completely spin polarized and ferromagnetic. The Hartree-Fock approximation was not thought to be reliable at the electron density at which this prediction was made, so it remained clouded in uncertainty. Soon after, Wigner (1934) examined the problem in the limit where the electron density became very low, r_s/a_0 was large, and concluded that electrons should behave like classical particles and condense into a crystalline lattice, the *Wigner crystal*. Observation of such *Wigner crystals* in semiconductors with low conduction electron densities is discussed by Field et al. (1988).

The electron densities where these transitions occur were first calculated by Ceperley and Alder (1980) using Diffusion Monte Carlo. To find the energy of electron gases, the calculations employed trial wavefunctions with Slater determinants of plane waves times Jastrow functions as in Eq. (9.97). To find the energy of Wigner crystals, the electron wave function was instead taken to be a Slater determinant of Gaussian peaks centered at bcc lattice sites, again multiplied by a Jastrow function. The transition from electron gas to Wigner crystal occurs when the best wave function of the second type has lower energy than the first. The calculations continue to be refined, and a phase diagram of jellium as a function of temperature and electron density appears in Figure 9.3.

9.5 Kohn–Sham Equations

Quantum Monte Carlo calculates properties of solids exactly, but is far too time-consuming to use in all but the simplest cases. Even the Hartree–Fock Eqs. (9.34) are too slow to solve for systems with many atoms. Density functional theories such as the Thomas–Fermi equation are suitably quick, but unacceptably inaccurate. The equation most frequently used in practice for large numerical calculations in solids is a cross between the two and was introduced by Kohn and Sham (1965).

This theory constructs a density functional theory in such a way as to treat electron kinetic energies well, reproduce selected results from Quantum Monte Carlo

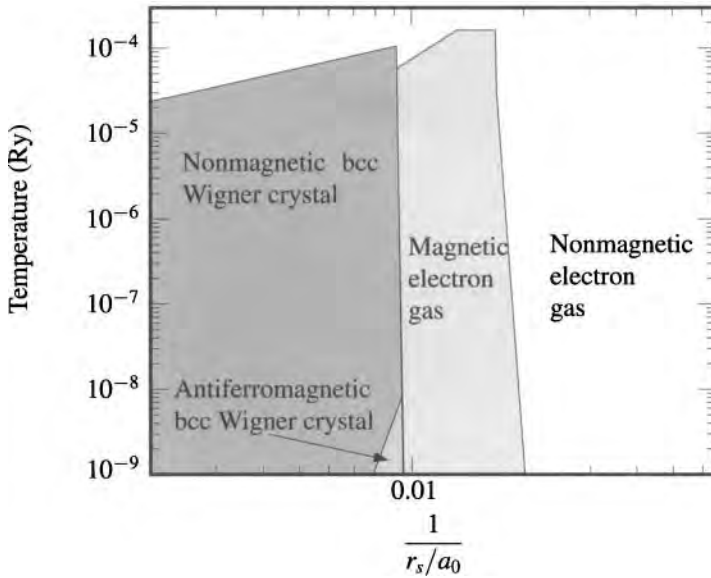


Figure 9.3. Phase diagram for jellium, as deduced by Quantum Monte Carlo methods. The onset of zero-temperature Wigner crystals at $r_s/a_0 = 106 \pm 1$ is the most reliable result; other details of the diagram should probably be viewed as more tentative. [Source: Cândido et al. (2004), p. 2]

exactly, yet retain computational speed. In order to efficiently capture the kinetic energy associated with electronic configurations, Kohn and Sham retreated slightly from the plan of writing all material properties as functions of the electron density, and proposed using instead a set of N single-electron wave functions $\psi_l(\vec{r})$ as the main ingredients, obtaining the density from them by

$$n(\vec{r}) = \sum_{l=1}^N |\psi_l(\vec{r})|^2. \quad (9.101)$$

In Kohn-Sham equations, the kinetic energy term of the energy functional is

$$T[n] = \sum_l \frac{\hbar^2}{2m} \int d\vec{r} |\nabla \psi_l|^2. \quad (9.102)$$

Apart from the kinetic energy, the energy functional has the same basic form as the Thomas–Fermi theory, Eq. (9.77). Instead of varying with respect to charge distribution, one now must vary with respect to the wave function, because one knows the density as a functional of the wave function but does not know the wave function as a functional of the density. Varying with respect to ψ_l^* gives

$$-\frac{\hbar^2}{2m} \nabla^2 \psi_l(\vec{r}) + \left[U(\vec{r}) + \int d\vec{r}' \frac{e^2 n(\vec{r}')}{|\vec{r} - \vec{r}'|} + \frac{\delta \mathcal{E}_{xc}(n)}{\delta n} \right] \psi_l(\vec{r}) = \epsilon_l \psi_l(\vec{r}). \quad (9.103)$$

Table 9.2. Hartree–Fock and LDA compared with experiment

Atom	LDA (KS)	Hartree–Fock	LDA (PZ)	Experiment
He	–2.83	–2.86	–2.92	–2.90
Li	–7.33	–7.43	–7.50	–7.48
Ne	–128.12	–128.55	–129.27	–128.94
Ar	–525.85	–526.82	–528.39	–527.60

Total energies of atoms in Hartrees (27.2107 eV), comparing Hartree–Fock, the local density approximation, LDA (KS) as first described by Kohn and Sham, the local density approximation LDA (PZ) as improved by Perdew and Zunger (1981), and experiment. Source: Tong and Sham (1966) and Perdew and Zunger (1981).

The class of approximations of the form (9.103) is referred to as the *local density approximation* (LDA). If one uses the exchange potential derived in Eq. (9.72), then

$$-\frac{\hbar^2}{2m}\nabla^2\psi_l(\vec{r}) + \left[U(\vec{r}) + \int d\vec{r}' \frac{e^2 n(\vec{r}')}{|\vec{r}-\vec{r}'|} - e^2 \left(\frac{3}{\pi} n(\vec{r}) \right)^{1/3} \right] \psi_l(\vec{r}) = \varepsilon_l(\vec{r}). \quad (9.104)$$

Apart from a much disputed factor of 3/2 in front of the exchange–correlation term, Eq. (9.104) was first written down by Slater (1951).

But the exchange–correlation functional \mathcal{E}_{xc} does not have to be approximated by Eq. (9.72). In principle it could compensate for all approximations and be set up to give exactly the right answer for interacting electron problems. However some approximation must be adopted for practical computation. The main idea in practice is to use the exchange–correlation energy of jellium, whose exact ground-state energy is known as described in Section 9.4.3. That is, the Kohn–Sham equations can be set up to give the exact answer when the external potential U vanishes, and once this is done they have proven wildly successful even after U is turned back on.

The Kohn–Sham equations achieve reasonable correspondence with experiment when applied to single atoms, as shown in Table 9.2. Calculations called *ab initio* or *first principles* are usually based upon Eq. (9.103). The best LDA calculations provide more accurate results than the Hartree–Fock approximation and approach the accuracy demanded by quantum chemists; surveys comparing computations in molecules with experimental results are provided by Curtiss et al. (1998a,b). Many different types of approximations have been tried to bring density functional theory into as close correspondence with experiment as possible. For example, the *generalized gradient approximations* (GGA) add extra derivative terms. See Martin (2004) for detailed descriptions of approximations currently in use.

The pure research problem of painstakingly finding accurate solutions to the electronic energy of jellium thus turned out to have much more practical importance than one might have expected from such a simplified model system. From the quantum Monte Carlo calculations in jellium, it was possible to find the energy

of the electron gas as a function of density. Simple functional fits to these results, for example by Perdew and Zunger (1981), Lee et al. (1988), or Becke (1993), produce the exchange-correlation functionals on which current density functional codes are based. Papers containing these parameterizations win out over all recent Nobel Prize-winning results, and are the most highly-cited papers in all of physics.

Problems

1. Hartree equations:

- (a) Find the expectation value F_H of Eq. (9.1) in a state of form Eq. (9.6).
- (b) Take the variation of F_H , subject to the constraint that each ψ be normalized:

$$\frac{\delta F_H}{\delta \psi_l(\vec{r})} - \frac{\delta}{\delta \psi_l(\vec{r})} \sum_j \mathcal{E}_j \int d\vec{r}' \psi_j^*(\vec{r}') \psi_j(\vec{r}') = 0. \quad (9.105)$$

- (c) Add one extra term (without much justification apart from simplicity) so that the Coulomb interaction term of the Hamiltonian becomes the same for all wave functions. In this way, recover the Hartree equations. Notice that demanding that each ψ be normalized is sufficient to result in an orthonormal set of functions.

2. Koopman's theorem:

- (a) Evaluate the total energy of a collection of N electrons in jellium, obtaining Eq. (9.49). You must add also the energy of the positive ionic background.
- (b) Compare the result with the sum over l of the single particle energies \mathcal{E}_l .
- (c) The ionization potential of an atom is the energy needed to remove the most energetic electron. Consider an atom with N electrons, and suppose it has been solved in the Hartree–Fock approximation, producing wave functions ψ_l and energies \mathcal{E}_l . Suppose that when the electron of highest energy is removed, the remaining $N - 1$ wave functions continue to solve the Hartree–Fock equations, and that the energies \mathcal{E}_l do not change appreciably. Show that in this approximation the ionization potential of the atom is \mathcal{E}_N .

3. **Screening:** The idea of screening comes originally from electrolytic solutions. Imagine placing a charged ion into such a solution. At first the potential due to the added ion extends its influence to the far reaches of the system, dying off slowly as $1/r$. However, mobile ions nearby rapidly react to the intruder, and the motions they make in response have the effect of almost completely canceling out its electric field, except within a characteristic distance called the *screening length*. Because this phenomenon occurs generally for any assembly of charged particles, it can be studied in the context of Thomas–Fermi theory, given by Eq. (9.77).

- (a) Consider Eq. (9.77), omitting for simplicity the last term on the left-hand side resulting from exchange. Suppose that n_0 is the solution of this equation when the potential $U(\vec{r})$ vanishes. If now a small potential $U(\vec{r})$ is added, find the equation governing deviations $\delta n(\vec{r})$ of the density from perfect uniformity to first order in U .
- (b) Consider adding one extra electron to the uniform electron gas, and therefore specialize to the case

$$U(\vec{r}) = \frac{e^2}{r}. \quad \text{Yes, it is dubious to regard such a potential as small, but the basic lesson is still correct.} \quad (9.106)$$

Solve the linearized equation for δn by use of Fourier transforms. The answer should be of the form

$$\delta n \sim \frac{e^{-r/\xi}}{r}. \quad (9.107)$$

Identify the screening length ξ , and express it in terms of the Bohr radius and the average volume per particle of the original uniform electron gas.

- (c) Estimate the screening length for aluminum.
4. **Thomas–Fermi theory:** Use Thomas–Fermi theory to study an atom with nuclear charge Z and Z electrons, so that the potential is

$$U(\vec{r}) = -Ze^2/r. \quad (9.108)$$

- (a) Rewrite Eq. (9.77), omitting the final term and substituting the function $V(\vec{r})$ for $n(\vec{r})$ through

$$n = \frac{[-2mV]^{3/2}}{3\pi^2\hbar^3}. \quad (9.109)$$

- (b) Show that in the vicinity of the origin, $V(\vec{r}) \rightarrow -Ze^2/r$.
- (c) Define

$$V(r) = -\frac{Ze^2}{r}\chi, \quad \vec{r} = b\vec{s}, \quad \text{and } b = \frac{a_0}{2} \left(\frac{3\pi}{4}\right)^{2/3} Z^{-1/3}. \quad a_0 \text{ is the Bohr radius.} \quad (9.110)$$

Show that for spherically symmetric solutions and $s > 0$ one obtains

$$s^{1/2} \frac{d^2\chi}{ds^2} = \chi^{3/2}. \quad (9.111)$$

- (d) Show that the boundary conditions on χ require $\chi(0) = 1$ and $\chi(\infty) = 0$.

5. Thomas–Fermi numerics:

- (a) Solve the two-point boundary problem in Eq. (9.111) numerically, and find the function χ .

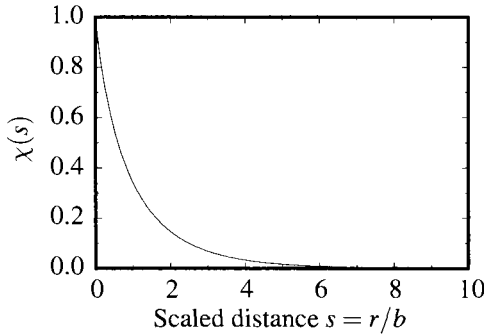


Figure 9.4. Solution of the Thomas–Fermi equation.

- (b) Find in particular the slope of χ at the origin.
 (c) Show that for a neutral atom with $N = Z$ electrons and a nucleus of charge Ze , one obtains

$$\frac{\partial \mathcal{E}}{\partial N} \Big|_{N=Z} = \frac{\partial \mathcal{E}}{\partial Z} \Big|_N. \quad \text{Use the fact that the chemical potential } \mu \text{ vanishes.} \quad (9.112)$$

- (d) Show therefore that

$$\mathcal{E} = - \int_0^Z dZ \int d\vec{r} \frac{e^2 n(\vec{r})}{r}. \quad (9.113)$$

- (e) Express the total energy \mathcal{E} in terms of the slope $\chi'(0)$ of χ at the origin, and verify that the energy of the atom is $-1.5375Z^{7/3}$ Ry.

6. Variational estimates:

- (a) Show that for any square integrable function,

$$T[\psi] = \int d\vec{r} |\nabla \psi(\vec{r})|^2 \geq K_s \left\{ \int d\vec{r} n^3 \right\}^{1/3}, \quad (9.114)$$

where

$$K_s = 3(\pi/2)^{4/3} \quad (9.115)$$

and

$$n(\vec{r}) = |\psi(\vec{r})|^2. \quad (9.116)$$

To carry out the demonstration, consider minimizing

$$K_s = \frac{\int d\vec{r} |\nabla \psi(\vec{r})|^2}{\left\{ \int d\vec{r} |\psi(r)|^6 \right\}^{1/3}}, \quad (9.117)$$

and show that ψ (assumed real) obeys a variational equation of the form

$$-\nabla^2\psi - \alpha\psi^5 = 0. \quad (9.118)$$

Find a formal expression for α . Verify by substitution that

$$\psi(r) = \left(\frac{3a^2}{\alpha}\right)^{1/4}(a^2 + r^2)^{-1/2} \quad a \text{ is an arbitrary length.} \quad (9.119)$$

solves Eq. (9.118) and that K_s is given by Eq. (9.115).

(b) Use the inequality, valid when $1/p + 1/q = 1$,

$$\left| \int g(\vec{r})f(\vec{r})dx \right| \leq \left[\int |f(\vec{r})|^p \right]^{1/p} \left[\int |g(\vec{r})|^q \right]^{1/q} \quad (9.120)$$

to show that

$$T[\psi] \geq K_s \int d\vec{r} n^{5/3}(\vec{r}). \quad (9.121)$$

(c) Verify the result quoted in Eq. (9.90) that as a result one can bound the ground-state energy of the hydrogen atom from below by $-12/5$ Ry.

7. Integrals by Monte Carlo:

Write a routine to compute the volume of a unit sphere in n dimensions. That is, integrate the function

$$f(\vec{x}) = \begin{cases} 1 & \text{if } x^2 < 1 \\ 0 & \text{else.} \end{cases} \quad (9.122)$$

For the probability \mathcal{P} in Eq. (9.95), use

$$\mathcal{P}(\vec{x}) = \frac{1}{\sqrt{\pi^n}} e^{-x^2}. \quad (9.123)$$

Take the constant ϵ governing the size of Monte Carlo steps to be of order 1.

Use this routine to calculate the volume of a sphere within 1% in 1, 2, 3, and 4 dimensions. Monitor convergence of the integral through the standard error, Eq. (9.94), which will however underestimate the error in the integral because successive steps are not completely uncorrelated.

8. **Cusp Conditions in Quantum Monte Carlo:** Consider the *local energy* defined for any wave function $\Psi(\vec{r})$ and the Hamiltonian of Eq. (9.1) by

$$\mathcal{E}_{l0}(\vec{r}) \equiv \frac{1}{\Psi(\vec{r})} \hat{\mathcal{H}}\Psi(\vec{r}) \quad (9.124)$$

(a) Show that if $\Psi(\vec{r})$ is the true ground state wave function, \mathcal{E}_{l0} has no singularities, and in fact is constant.

- (b) Now take a wave function of the form Eq. (9.97) with u given by Eq. (9.98). Assume that the Hartree-Fock wave function is nowhere singular, and that $\chi(\vec{y})$ has no singularities. Focusing on a pair of particles i and j , write

$$\Psi(\vec{r}) = e^{-u(r_{ij})} f(\vec{y}_1 \dots \vec{y}_N), \quad (9.125)$$

where f is defined to be absolutely everything in Ψ except for the one term involving $u(r_{ij})$ that has been singled out. Argue that singularities in the local energy \mathcal{E}_{l0} can be eliminated by ensuring that there are no singularities in

$$\frac{1}{e^{-u(r_{ij})} f} \left(-\frac{\hbar^2}{2m} \nabla_i^2 + \frac{e^2}{r} \right) e^{-u(r_{ij})} f \quad (9.126)$$

$$= \frac{\hbar^2}{2m} \left(u''(r_{ij}) + (u'(r_{ij}))^2 + 2u'(r_{ij}) \hat{r}_{ij} \cdot \frac{\vec{\nabla}_i f}{f} - \frac{\nabla_i^2 f}{f} \right) \quad (9.127)$$

$$+ 2 \frac{\hbar^2}{2m} e^2 \frac{u'(r_{ij})}{r} + \frac{e^2}{r}.$$

- (c) If particles i and j have opposite spin, argue that f remains in general finite as $r_{ij} \rightarrow 0$. Assuming that $\lim_{r \rightarrow 0} u'(r)$ and $\lim_{r \rightarrow 0} u''(r)$ are finite, show that the singularity in Eq. (9.126) can be eliminated by taking

$$\lim_{r \rightarrow 0} u'(r) = -\frac{1}{a_0}. \quad a_0 \text{ is the Bohr radius.} \quad (9.128)$$

- (d) If instead, however, particles i and j have the same spin, then f must be an odd function of \vec{r}_i and \vec{r}_j . As $r_{ij} \rightarrow 0$

$$f \rightarrow \vec{A} \cdot \vec{r}_{ij} + \dots \quad (9.129)$$

Show in this case that

$$\lim_{r \rightarrow 0} u'(r) = -\frac{1}{2a_0}. \quad a_0 \text{ is the Bohr radius.} \quad (9.130)$$

References

- A. D. Becke (1993), Density-functional thermochemistry. III. The role of exact exchange, *Journal of Chemical Physics*, **98**, 5648–5652
- F. Bloch (1929), Note on the electron theory of ferromagnetism and electrical conductivity, *Zeitschrift für Physik*, **57**, 545–555.
- M. Born and J. R. Oppenheimer (1927), On the quantum theory of molecules, *Annalen der Physik*, **84**, 457–484.
- J. Callaway and N. H. March (1984), Density functional methods: theory and applications, *Solid State Physics: Advances in Research and Applications*, **38**, 135–221.
- L. Cândido, B. Bernu, and D. M. Ceperley (2004), Magnetic ordering of the three-dimensional Wigner crystal, *Physical Review B*, **70**, 094413/1–6.

- D. M. Ceperley and B. J. Alder (1980), Ground state of the electron gas by a stochastic method, *Physical Review Letters*, **45**, 566–569.
- L. A. Curtiss, K. Raghavachari, P. C. Redfern, V. Rassolov, and J. A. Pople (1998a), Gaussian-3 (G3) theory for molecules containing first and second-row atoms, *Journal of Chemical Physics*, **109**, 7764–7776.
- L. A. Curtiss, P. C. Redfern, K. Raghavachari, and J. A. Pople (1998b), Assessment of Gaussian-2 and density functional theories for the computation of ionization potentials and electron affinities, *Journal of Chemical Physics*, **109**, 42–45.
- P. A. M. Dirac (1929), Quantum mechanics of many-electron systems, *Proceedings of the Royal Society of London*, pp. 714–733.
- P. M. Echenique, F. Flores, and R. H. Ritchie (1990), Dynamic screening of ions in condensed matter, *Solid State Physics: Advances in Research and Applications*, **43**, 229–308.
- S. B. Field, D. H. Reich, T. F. Rosenbaum, P. B. Littlewood, and D. A. Nelson (1988), Electron correlation and disorder in $\text{Hg}_{1-x}\text{Cd}_x\text{Te}$ in a magnetic field, *Physical Review B*, **38**, 1856–1864.
- V. Fock (1930), A method for the solution of many-body problems in quantum mechanics, *Zeitschrift für Physik*, **61**, 126–148.
- W. M. C. Foulkes, L. Mitas, R. J. Needs, and G. Rajagopal (2001), Quantum monte carlo simulations of solids, *Reviews of Modern Physics*, **73**(1), 33–83
- M. Gell-Mann and K. A. Brueckner (1957), Correlation energy of an electron gas at high density, *Physical Review*, **106**(2), 364–368.
- D. R. Hartree (1928), The wave mechanics of an atom with a non-coulomb central field, *Proceedings of the Cambridge Philosophical Society*, **24**, 89–132.
- P. C. Hohenberg and W. Kohn (1964), Inhomogeneous electron gas, *Physical Review*, **80**, B864–B871.
- R. O. Jones and O. Gunnarsson (1989), The density functional formalism, its applications and prospects, *Reviews of Modern Physics*, **61**, 689–746.
- W. Kohn and L. J. Sham (1965), Self-consistent equations including exchange and correlation effects, *Physical Review*, **140**, A1133–A1138.
- C. Lee, W. T. Yang, and R. G. Parr (1988), Development of the Colle-Salvetti Correlation-Energy Formula Into A Functional of The Electron-Density, *Physical Review B*, **37**(2), 785–789.
- E. H. Lieb (1976), The stability of matter, *Reviews of Modern Physics*, **48**, 553–569.
- E. H. Lieb (1981), Thomas-Fermi and related theories of atoms and molecules, *Reviews of Modern Physics*, **53**, 603–640.
- E. H. Lieb, H. Siedentop, and J. P. Solovij (1997), Stability of relativistic matter with magnetic fields, *Physical Review Letters*, **79**, 1785–1788.
- R. M. Martin (2004), *Electronic structure : basic theory and practical methods*, Cambridge University Press, Cambridge.
- R. G. Parr and W. Yang (1989), *Density Functional Theory of Atoms and Molecules*, Clarendon Press, Oxford.
- J. P. Perdew, K. Burke, and M. Ernzerhof (1996), Generalized gradient approximation made simple, *Physical Review Letters*, **77**, 3865–3868.
- J. P. Perdew and W. Yue (1986), Accurate and simple density functional for the electronic exchange energy: Generalized gradient approximation, *Physical Review B*, **33**, 8800–8802.
- J. P. Perdew and A. Zunger (1981), Self-interaction correction to density-functional approximations for many-electron system, *Physical Review B*, **23**, 5048–5079.
- D. Pines (1955), Electron interactions in metals, *Solid State Physics: Advances in Research and Applications*, **1**, 373–450.
- M. Schluter and L. J. Sham (1982), Density functional theory, *Physics Today*, **35**(2), 36–43.
- G. Senatore and N. H. March (1994), Recent progress in the field of electron correlation, *Reviews of Modern Physics*, **66**, 445–479.

- J. C. Slater (1930), Note on Hartree's method, *Physical Review*, **35**, 210–211
- J. C. Slater (1951), A simplification of the Hartree-Fock method, *Physical Review*, **81**, 385–390.
- A. Szabo and N. S. Ostlund (1982), *Modern Quantum Chemistry: Introduction to Advanced Electronic Structure Theory*, Macmillan, New York.
- B. Y. Tong and L. J. Sham (1966), Application of a self-consistent scheme modeling exchange and correlation effects to atoms, *Physical Review*, **144**, 1–4.
- L. Tonks and I. Langmuir (1929), Oscillations in ionized gases, *Physical Review*, **33**, 195–210.
- E. Wigner (1934), On the interaction of electrons in metals, *Physical Review*, **46**, 1002–1011.

10. Realistic Calculations in Solids

10.1 Introduction

The attempt to construct approximations accurate enough so that properties of solids could be deduced from Schrödinger's equation was initiated seriously by Wigner and Seitz (1933), who computed properties of metallic sodium. They regarded the attempt to proceed much further along these lines with a degree of skepticism, and two decades after their original work they commented that

If one had a great calculating machine, one might apply it to the problem of solving the Schrödinger equation for each metal and obtain thereby the interesting physical quantities, such as the cohesive energy, the lattice constant, and similar parameters. It is not clear, however, that a great deal would be gained by this. Presumably the results would agree with the experimentally determined quantities and nothing vastly new would be learned from the calculation. It would be preferable instead to have a vivid picture of the behavior of the wave functions, a simple description of the essence of the factors which determine cohesion and an understanding of the origins of variation in properties from metal to metal.

—Wigner and Seitz (1955), p. 97

Now that the great calculating machines exist, not all agree that Wigner and Seitz's advice should be adopted. Slater spoke with slight disdain of those "trying to get valid results relating to energy bands from simplified models, rather than through the direct types of calculations which one can make with the methods now in use" [Slater (1975), p. 191]. However, even if the resolution to proceed with large calculations is taken, it is not at all easy to obtain numerical results in agreement with experiment. Many approximations must always be employed, and decades have been devoted to finding the schemes that are most successful and effective. This collection of approximations and numerical techniques is referred to as *band structure calculation*. It has achieved many successes and has reached the stage where many properties of a wide variety of solids can be computed almost automatically, with knowledge of nothing but atomic numbers. The methods can also experience qualitative failures, which only experience and comparison with experiment reveal.

10.2 Numerical Methods

10.2.1 Pseudopotentials and Orthogonalized Plane Waves (OPW)

Band structure calculations all operate within the single-electron framework, meaning that they assume it possible to study the behavior of solids by choosing a potential and studying the behavior of a single electron in that potential. Almost always the potential will be taken to depend self-consistently upon solutions for electron states in the potential, but in the end one solves a problem with only one electron in it. The reason is simply a matter of practicality. The size of the calculation goes up as the power of the number of particles that are treated in it simultaneously. On a lattice of M sites with N particles, the difference between solving the true interacting Schrödinger equation in all its glory and a reduction to one-particle problems is the difference between working with M^N variables as opposed to $M \times N$. The calculations of the previous chapter have shown how to obtain one-particle potentials incorporating information about interactions of electrons with themselves.

Yet even after reduction to a periodic one-electron problem, the task one faces in solving Schrödinger's equation is daunting. Take the case of gold. A variety of experimental probes, such as the low-temperature specific heat in Table 6.2, reveal that gold greatly resembles a nearly empty box containing one electron per atom. Yet gold's atomic number is 79. In some fashion the first 78 electrons per atom simply crowd about the nucleus, screening it from the outside. How then should they be treated? What potential do they leave behind? The answer is provided by *pseudopotentials*, due to Phillips and Kleinman (1959).

In fact, pseudopotentials serve two different purposes simultaneously. On the one hand they provide crucial conceptual justification for the nearly free electron model of solids, showing explicitly how the problem of finding wave functions in the presence of ionic Coulomb potentials can be mapped onto equivalent problems where the potentials are much weaker. Simultaneously, they provide a calculational tool that substantially increases the range of problems in solids that can be brought within computational reach.

The best illustration of the idea is provided by *orthogonalized plane waves*, (OPW) although they have not found much practical use. Suppose one has a periodic solid in which the electrons can safely be divided into two groups, the core states and the conduction states. The core states are localized around particular atomic sites. Denote core states by $|\psi_c\rangle$ and plane waves ($\exp[i\vec{k} \cdot \vec{r}]$) by $|\vec{k}\rangle$. An orthogonalized plane wave indexed by \vec{k} is defined to be

$$|\vec{k}_{ps}\rangle = |\vec{k}\rangle - \sum_c |\psi_c\rangle \langle \psi_c | \vec{k}\rangle, \quad \begin{array}{l} \text{The subscript "ps" indicates that this is a "pseudo"} \\ \vec{k} \text{ state. The following derivation works for any ex-} \\ \text{tended states } |\vec{k}\rangle. \end{array} \quad (10.1)$$

where the sum is over all occupied core levels $|\psi_c\rangle$. Look at the effect on these states of the Coulomb potential for an atom of valence Z , $\hat{U} = Z/\hat{R}$. It is

$$\hat{U}|\vec{k}_{ps}\rangle = \hat{U}|\vec{k}\rangle - \sum_c \hat{U} \langle \psi_c | \vec{k}\rangle |\psi_c\rangle. \quad (10.2)$$

If $|\psi_c\rangle$ were a complete set of states, then $\hat{U}|\vec{k}_{ps}\rangle$ would vanish. As it is, the hope is that all matrix elements of $\hat{U}|\vec{k}_{ps}\rangle$ will be small. Examine the Schrödinger equation in a basis of \vec{k}_{ps} states. It is

$$(\hat{\mathcal{H}} - \mathcal{E})|\vec{k}_{ps}\rangle = \left(\frac{\hat{p}^2}{2m} + \hat{U} - \mathcal{E}\right)|\vec{k}_{ps}\rangle \tag{10.3}$$

$$= \left(\frac{\hat{p}^2}{2m} + \hat{U} - \mathcal{E}\right) \left\{ |\vec{k}\rangle - \sum_c \langle\psi_c|\vec{k}\rangle |\psi_c\rangle \right\} \tag{10.4}$$

$$= \frac{\hbar^2 k^2}{2m} |\vec{k}\rangle + (\hat{U} - \mathcal{E})|\vec{k}\rangle - \sum_c (\mathcal{E}_c - \mathcal{E}) |\psi_c\rangle \langle\psi_c|\vec{k}\rangle \tag{10.5}$$

$$= \left(\frac{\hat{p}^2}{2m} + \hat{U}_{ps} - \mathcal{E}\right)|\vec{k}\rangle = (\hat{\mathcal{H}}_{ps} - \mathcal{E})|\vec{k}\rangle, \tag{10.6}$$

where

$$\hat{U}_{ps} = \hat{U} - \sum_c (\mathcal{E}_c - \mathcal{E}) |\psi_c\rangle \langle\psi_c|. \tag{10.7}$$

\mathcal{E}_c is the eigenvalue of $|\psi_c\rangle$. Note that if $|\psi_c\rangle$ were a complete set of states, U_{ps} would flatten out to the constant \mathcal{E} .

The summary of Eqs. (10.3) through (10.7) is

$$(\hat{\mathcal{H}} - \mathcal{E})|\vec{k}_{ps}\rangle = (\hat{\mathcal{H}}_{ps} - \mathcal{E})|\vec{k}\rangle. \tag{10.8}$$

In particular, if one finds an eigenvector $|\Psi_{ps}\rangle = \sum C_{\vec{k}}|\vec{k}\rangle$ causing the right hand side to vanish, then $|\Psi\rangle = \sum C_{\vec{k}}|\vec{k}_{ps}\rangle$ is an eigenvector for the left hand side.

Thus there is a complete correspondence between the original Schrödinger equation and a new one with a weak pseudopotential \hat{U}_{ps} whose solutions may be close to plane waves, as in Section 8.2. There is some price to be paid for this simplification. The pseudopotential \hat{U}_{ps} is nonlocal; that is, to compute its action upon a general state $\psi(\vec{r})$, one has to perform integrals. In addition, \hat{U}_{ps} depends upon the unknown energy eigenvalue \mathcal{E} , and the eigenvalue problem one needs to solve is more involved than for the usual quantum-mechanical problems.

Empirical and First-Principles Pseudopotentials. Development of the pseudopotential beyond this first suggestive calculation has proceeded along two routes. On the one hand, it could be argued that the most important lesson to take away is that the apparent existence of weak potentials is explained in principle, so one may as well experiment with simple weak potentials, chosen so as to match important features of experiment. One example is the *empty-core potential*, due to Ashcroft (1966), depicted in Figure 10.1. The three free parameters of this potential—its

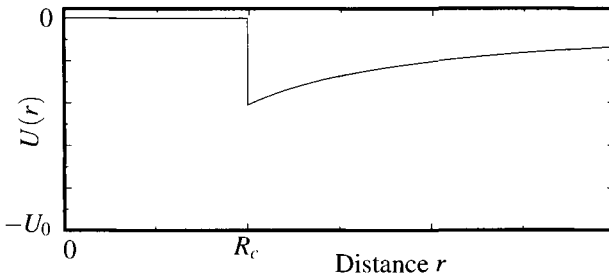


Figure 10.1. The Ashcroft empty core pseudopotential is zero up to a critical radius R_c , and it equals a screened Coulomb potential $-U_0 \exp[-r/d]/r$ thereafter.

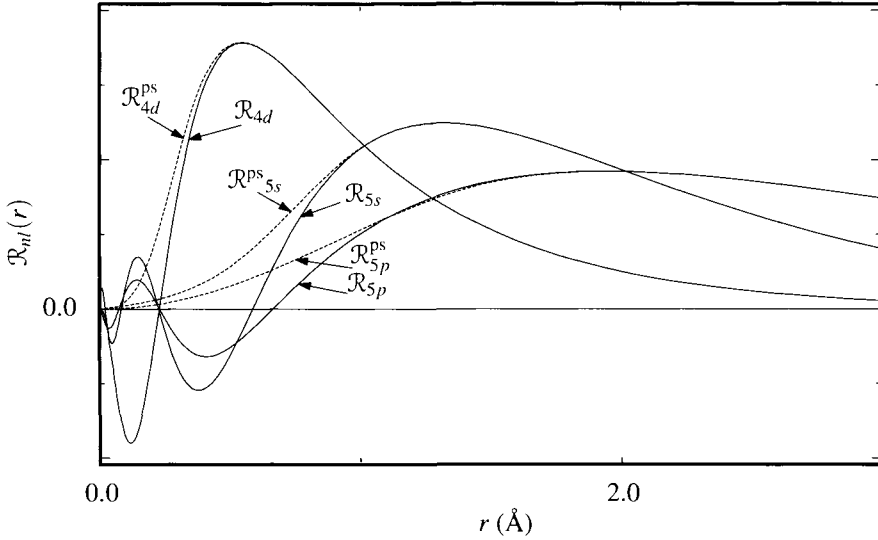


Figure 10.2. Real and pseudo wave functions for the 5s, 5p, and 4d levels of silver. The 5p level is not much occupied in the ground state of silver, but it can be included in the pseudopotential nevertheless.

magnitude U_0 , the cutoff R_c , and the exponential decay length d —can be adjusted to fit measurements taken from optical or magnetic experiments, as shown in Section 23.4. Potentials of this sort are good enough to permit a quantitative comparison with experiment for some of the simpler metals, such as the alkali metals or aluminum. Their use is reviewed by Heine (1970), and the empty core potential will be used for the cohesion of metals in Section 11.4.

On the other hand, it is possible to construct *first-principles pseudopotentials* to encode information about atomic wave functions in a form particularly convenient for transportation into solids. The name given these pseudopotentials promises too much, because numerous approximations are needed to produce them, but the basic idea behind them is worth appreciating. It proceeds in three steps.

1. Choose an atom, and write down the Kohn–Sham equations for it. Employ the approximation that the electron density $n(\vec{r}) = \sum |\psi_i(\vec{r})|^2$ be spherically symmetric about the nucleus, and impose this requirement in replacing n by its spherical average if necessary. Once the equations Eq. (9.104) have been forced to be spherically symmetric, all of their solutions are of the form $\mathcal{R}_{nl}(r)Y_{lm}$, where Y_{lm} is a spherical harmonic and \mathcal{R}_{nl} is a radial wave function. The equation for the radial functions is

$$-\frac{\hbar^2}{2m} \left[\frac{1}{r} \frac{\partial^2}{\partial r^2} r - \frac{l(l+1)}{r^2} \right] \mathcal{R}_{nl} + \left[\int \frac{e^2 n(r')}{|\vec{r} - \vec{r}'|} d\vec{r}' - \frac{e^2 Z}{r} + \frac{\delta \mathcal{E}_{xc}}{\delta n} - \mathcal{E}_{nl} \right] \mathcal{R}_{nl}(r) = 0. \quad (10.9)$$

Solve these equations for all the electrons belonging to the atom. Denote the energies of these states by \mathcal{E}_{nl} .

2. Consider all the outermost s , p , d , and f states lying in partially filled shells. These are the states that contribute to bonding between atoms in molecules and solids, and they will be singled out for special treatment. Drawings of these radial wave functions appropriate to silver appear in Figure 10.2. To form pseudo wave functions $\mathcal{R}_{nl}^{\text{ps}}$ deriving from solutions of Eq. (10.9), simply take each radial function, pick a point beyond its rightmost node, and draw a smooth curve in to the origin. This smooth curve has few constraints to satisfy, and it is easy to construct. It should be without nodes, except at the origin where it should vanish as r^l . It should join on to the original radial function with at least two derivatives continuous. And finally, the wave functions built from these new radial functions should remain correctly normalized. Any function with these properties produces an acceptable pseudo wave function, as illustrated in Figure 10.2.
3. Finally, replace the original Coulomb potential \hat{U} with a pseudopotential \hat{U}^{ps} built so that solving the Kohn–Sham equations gives the functions \mathcal{R}^{ps} rather than \mathcal{R} . This task can be accomplished directly from Eq. (10.9). Just write out the equation for the radial wave functions as

$$U_l^{\text{ps}}(r) = \frac{\hbar^2}{2m} \left[\frac{1}{r\mathcal{R}_{nl}^{\text{ps}}} \frac{\partial^2 r\mathcal{R}_{nl}^{\text{ps}}}{\partial r^2} - \frac{l(l+1)}{r^2} \right] - \left[\int \frac{e^2 n^{\text{ps}}(r')}{|\vec{r} - \vec{r}'|} d\vec{r}' + \frac{\delta\mathcal{E}_{xc}}{\delta n^{\text{ps}}} - \mathcal{E}_{nl} \right]. \quad (10.10)$$

In other words, by brute force, take $U_l^{\text{ps}}(r)$ to be whatever is necessary to have the desired \mathcal{R}_{nl} as the solution. Potentials constructed in this way for silver appear in Figure 10.3. Because there is a different pseudopotential for each angular momentum state, the way the pseudopotential acts upon an arbitrary function $\psi(\vec{r})$ is through first breaking ψ down into its angular momentum components

$$\psi(\vec{r}) = \sum_{lm} Y_{lm}(\theta, \phi) \psi_{lm}(r); \quad \psi_{lm}(r) = \int d\theta d\phi \sin\theta Y_{lm}^*(\theta, \phi) \psi(\vec{r}), \quad (10.11)$$

and then multiplying $\psi_{lm}(r)$ by $U_l^{\text{ps}}(r)$ in forming the Hamiltonian. The need for these integrals means that the pseudopotential is nonlocal.

Analytical results can also be employed to improve the form of the pseudopotential. As remarked in Section 9.2.2, the Hartree-Fock approximation does not properly take into account the many-electron phenomenon of screening, with the consequence of giving incorrect results for electrons near the Fermi surface. The electrons surrounding each nucleus should screen the Coulomb potential, but

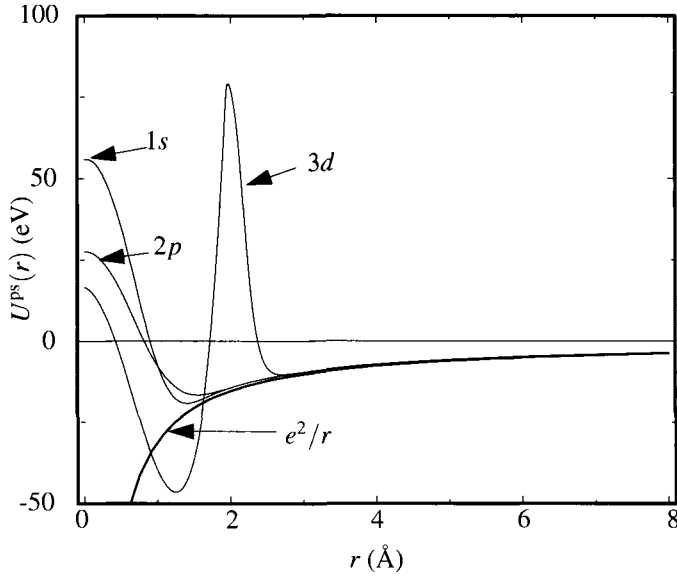


Figure 10.3. Pseudopotentials for the 5s, 5p, and 4d states of silver.

Hartree-Fock and its descendants have no guarantee of handling this phenomenon correctly. An unscreened Coulomb potential Ze^2/r behaves as $4\pi Ze^2/q^2$ once Fourier transformed; the main effect of screening is to eliminate the singularity at $q = 0$, producing a form such as

$$U^{\text{ps}} = \frac{4\pi Ze^2}{q^2 + \kappa^2}, \quad \kappa \text{ is a screening length.} \quad (10.12)$$

Section 20.4.2 presents a general theory of dielectric functions that can be used to address this problem, and according to a model calculation presented as Problem 20.7, an electron cloud will cover each bare nucleus so that

$$\frac{1}{\Omega} U^{\text{ps}}(q=0) = -\frac{2}{3} \mathcal{E}_F. \quad \text{This constraint applies to the Fourier transform of the } l=0 \text{ component of the pseudopotential. } \Omega \text{ is the volume of a unit cell.} \quad (10.13)$$

Relation (10.13) can be used as a constraint on pseudopotentials—for example, to estimate κ in Eq. (10.12).

For heavy atoms, relativistic effects become important because electrons near the nuclei move at speeds that are a significant fraction of the speed of light. The electron wavefunctions near the nuclei must therefore be described by the Dirac equation. However, the pseudopotential method can also be applied here. To determine the radial wavefunctions, one must generalize the Kohn-Sham equations (9.104) so that they correspond to the Dirac equation. Suppose this is done and wave functions and energies have been determined. Then the techniques described above can be employed again; in fact, one can construct a pseudopotential so that

a solution of the ordinary Schrödinger equation gives a wave function that resulted originally from a solution of the Dirac equation. In this way, a code that solves the Schrödinger equation everywhere can secretly account for relativistic effects.

The pseudopotential procedure is not completely without risks. One risk is that it will not work quite as advertised, and the pseudopotential will have in addition to its ground state some low-lying states that enter into later calculations, but bear no resemblance to any state of the original potential. Such states are called *ghosts*, and as discussed by Gonze et al. (1991) they can lead to inaccurate computations.

10.2.2 Linear Combination of Atomic Orbitals (LCAO)

Given a collection of atoms arranged in some fashion on a lattice and their associated pseudopotentials, the next task is to construct corresponding solutions of Schrödinger's equation. One must therefore choose a set of basis functions and devise a procedure that keeps the calculation within reasonable bounds.

One of the first methods employed historically to obtain moderately realistic solutions of Schrödinger's equation is the Linear Combination of Atomic Orbitals introduced in Section 8.4.1.

Application of the method begins with construction of the matrices described by Eqs. (8.32) and (8.42). The minimal number of overlap integrals that needs to be computed, notation to describe them, and detailed calculations for the most common lattices were first outlined by Slater and Koster (1956). These integrals, the *Slater–Koster parameters* can be viewed in two ways. On the one hand they could be the calculational goal of a numerical effort, which finds the atomic wave functions and calculates all the integrals. On the other hand, they can be treated as adjustable parameters that describe the structure of the bands, but whose values are to be determined by any means possible, including a fit to experiment. It was for this latter purpose that Slater and Koster originally developed the formalism.

While methods of this sort were used extensively in early band structure calculations, they have largely been displaced by more general numerical methods described in the following sections. However tight-binding calculations can lead to much more rapid calculations than the more general methods, and therefore may provide the only way to approach quantum-mechanical problems involving large numbers of atoms arranged in a non-crystalline manner. An example of such usage is provided by Bernstein and Hess (2003).

10.2.3 Plane Waves

There is a method for conducting a systematic attack upon Schrödinger's equation that is conceptually even simpler than summing up atomic orbitals. Write down Bloch's theorem in the form Eq. (7.33) and solve it directly. For many years, this strategy was regarded as impractical because computer memories were not large enough and the full benefits of pseudopotentials had not been realized. The situation has changed now that computer memories over 100 MB are no longer exceptional, but it is worth explaining why the problem used to exist.

How many terms does one need in (7.33) to get reasonable accuracy? Suppose that one were not employing a pseudopotential, so that the potential $U(r)$ varied like $1/r$ in each unit cell. Consider the case of silver, whose outermost electron is conventionally assigned to the $5s$ state. In the vicinity of the nucleus, such an electron wave function has four nodes within a distance on the order of an angstrom (see Figure 10.2), so to represent this function accurately in a Fourier basis would require Fourier components with wave vectors up to at least $2\pi \times 4 / (1\text{\AA}) \sim 24\text{\AA}^{-1}$. Because silver has a lattice constant of $a = 4\text{\AA}$, its reciprocal lattice vectors start with a magnitude of around $4\pi/a \sim 3\text{\AA}^{-1}$. Thus in the sum over reciprocal lattice vectors

$$\vec{K} = l_1 \vec{b}_1 + l_2 \vec{b}_2 + l_3 \vec{b}_3 \quad (10.14)$$

one needs to allow l_1 , l_2 , and l_3 to vary from around -8 to around 8 . This simple estimate says that one needs around 5000 plane waves to have any hope of accuracy, and it seems to require trying to diagonalize 5000×5000 nonsparse matrices. This task is by no means impossible, but it is sufficiently time-consuming that plane waves seem at a disadvantage in useful calculations.

Although this argument has been used to justify the need for more sophisticated basis sets, such as augmented plane waves, it is not entirely correct. There are two flaws. The first flaw lies in dealing with real atomic wave functions rather than pseudo wave functions. The pseudo wave functions lack the fine wiggles of their predecessors, and the number of Fourier components needed to describe them diminishes accordingly. For example, in silicon allowing $l_1 \dots l_3$ to vary from -4 to 4 (leading to 800 plane waves) is enough. The second flaw lies in the hasty conclusion that there is a need to diagonalize an 800×800 matrix. In fact, no one is at all interested in finding the energy levels of 800 bands. All one actually needs in order to calculate anything of physical interest is to find the energy levels below, and within a few electron volts above, the Fermi surface; that is, one needs to find the lowest-lying five to ten energy bands.

There are methods of varying degrees of sophistication to extract low-lying eigenvalues and the corresponding eigenvectors from large matrices. One method involves little more than multiplying the matrix repeatedly into a randomly chosen initial vector. This method is rather crude, and it does not converge nearly as well as more sophisticated approaches if the only task at hand is diagonalizing a matrix. However, band structure calculations involve not only diagonalizing a matrix, but also determining the entries in the matrix self-consistently, either because they depend upon charge density through density functional theory or even because ions are being allowed to move in a search for the structural ground state. In the context of such self-consistent problems, Car and Parrinello (1985) found that the crude method of matrix multiplication holds its own rather well, and because this method is so simple it will be described below.

Suppose that one has a Hermitian $N \times N$ matrix \mathbf{M} for which the lowest eigenvalue λ_1 is some large negative number and for which the highest eigenvalue λ_N is zero. Because the matrix is Hermitian, its eigenvectors $\hat{e}_1 \dots \hat{e}_N$ can be chosen orthonormal. Pick a random vector \vec{a}_1 with N components, multiply \mathbf{M} into \vec{a}_1 ,

then multiply the result by \mathbf{M} again, and so on, repeatedly. The effect is to amplify at an exponentially growing rate the component of \vec{a}_1 that is parallel to the lowest eigenvector \hat{e}_1 . After multiplying \vec{a}_1 by \mathbf{M} r times, the result is the vector

$$\sum_{i=1}^N \lambda_i^r \hat{e}_i (\hat{e}_i \cdot \vec{a}_1). \quad \text{Write } \vec{a}_1 \text{ in a basis given by } \hat{e}_i, \text{ and begin multiplying by } \mathbf{M}. \quad (10.15)$$

Because \vec{a}_1 has been chosen randomly, there is no reason for $\hat{a} \cdot \hat{e}_1$ to vanish, and as r grows, the term proportional to this factor must grow to dominate the sum. The rapidity with which this happens depends upon the separation between λ_1 and λ_2 ; if they are degenerate, then the first two terms in the sum grow together. In any event, after sufficient multiplication of \mathbf{M} upon \vec{a}_1 , the result is proportional to \hat{e}_1 , and both the lowest eigenvector and eigenvalue are determined. What of the next-lowest eigenvalue? It may be found by using the knowledge of \hat{e}_1 to eliminate anything proportional to \hat{e}_1 from the sum (10.15). Repeat the multiplication process, but beginning with $\vec{a}_2 = \vec{a}_1 - \hat{e}_1 (\hat{e}_1 \cdot \vec{a}_1)$ rather than \vec{a}_1 . If even a small bit of \hat{e}_1 is left in the result due to numerical error, it will grow exponentially rapidly when \vec{a}_2 is multiplied by \mathbf{M} . After every one or two multiplications one needs to project out the component of \hat{e}_1 again. However, now the part of the sum dominated by the next-lowest eigenvalue will grow exponentially out of all the rest, giving \hat{e}_2 . Given \hat{e}_2 , $\vec{a}_3 = \vec{a}_2 - \hat{e}_2 (\hat{e}_2 \cdot \vec{a}_2)$, provides a starting point for finding \hat{e}_3 , and so on.

The task of multiplying an 800×800 matrix a few times into a vector is a great improvement over the task of finding 800 eigenvalues, but is still burdensome. A great virtue of using plane waves as basis functions lies in the fact that no matrix of such a size needs to be stored at all, and its action upon wave vectors can be computed much more rapidly than might at first seem possible.

Consider, for example, any Hamiltonian of the form

$$\hat{\mathcal{H}} = \frac{\hat{p}^2}{2m} + U(\hat{R}). \quad \text{In order for this method to be effective, } U \text{ should be a pseudopotential, smaller than the true ionic potential and without a singularity near the origin.} \quad (10.16)$$

The goal now is to find the lowest eigenvalues and corresponding eigenvectors of Eq. (10.16), using the form of Schrödinger's equation displayed in Eq. (7.33) and taking the wave function ψ to have the form given in Eq. (7.35). Of course, instead of using an infinite number of reciprocal lattice vectors, one builds ψ out of a finite number of them. If the low-lying eigenvalues are to be deduced by multiplying ψ by $\hat{\mathcal{H}}$ repeatedly, one must begin by ensuring that the large negative eigenvalues of \mathcal{H} are larger in absolute value than the large positive eigenvalues. Suppose K_{\max} to be the magnitude of the largest reciprocal lattice vector appearing in Eq. (7.33). The kinetic energy of the corresponding plane wave would be $\hbar^2 K_{\max}^2 / 2m = \mathcal{E}_{\max}$; the kinetic energy dominates the large positive eigenvalues of \mathcal{H} , because the potential energy of a plane wave with large K_{\max} should be comparatively small. So, taking the operator acting upon ψ to be

$$\hat{\mathcal{H}}\psi = \sum_{\vec{K}'} \left\{ \left[\mathcal{E}_{\vec{k}+\vec{K}'}^0 - \mathcal{E}_{\max} \right] \delta_{\vec{K}\vec{K}'} + U_{\vec{K}-\vec{K}'} \right\} \psi_{n\vec{k}}(\vec{K}'), \quad (10.17)$$

This is a restatement of Eq. (7.33), with $\psi(\vec{q})$ written as $\psi_{n\vec{k}}(\vec{K})$, where \vec{K} is the reciprocal lattice vector so that $\vec{q} - \vec{K} = \vec{k}$ lies in the first Brillouin zone.

one can now begin obtaining eigenvalues. The sum required to evaluate the potential energy seems to be numerically expensive, but in fact costs less than at first appears. The action of the potential energy upon ψ is in the form of a convolution; through use of the *fast Fourier transform* (Appendix A), $\sum_{\vec{K}'} U_{\vec{K}-\vec{K}'} C_{n\vec{K}}(\vec{K}')$ can be evaluated for N_K values of \vec{K} in only approximately $N_K \ln N_K$ operations, rather than N_K^2 as first appears.

Numerous variants of this basic method are possible. For example, instead of multiplying the wave function by \mathcal{H} , one can multiply repeatedly by

$$1 + \hat{\mathcal{H}} dt/\hbar. \quad (10.18)$$

Thus one obtains eigenfunctions recursively from

$$\psi_{n+1} = (1 + \hat{\mathcal{H}} dt/\hbar)\psi_n \Rightarrow \frac{\psi_{n+1} - \psi_n}{dt} = \frac{1}{\hbar} \hat{\mathcal{H}} \psi_n, \quad (10.19)$$

which in the limit $dt \rightarrow 0$ is a version of Schrödinger's equation with the time t replaced by the imaginary quantity it . While electronic eigenfunctions are busy iterating their way toward correct values, one can choose at the same time to allow other features of the problem to vary. Most importantly, as progressively more accurate wave functions are obtained, the charge density following from them must be used to determine the terms dependent upon density in Eq. (9.104). In addition, if the true equilibrium location of all atoms is not known, then at each iterative step the forces on all atoms can be computed and the atoms can be allowed to move in the directions of the forces. In this way, equilibrium atomic positions and electronic wave functions can be computed simultaneously, as opposed to an approach in which certain atomic positions are assumed, wave functions are calculated to high accuracy, forces on atoms determined, the atoms moved, and the process begun again. Car and Parrinello (1985) showed that it is possible to attempt dynamical problems, in which ions move according to Newton's laws, driven by clouds of electrons whose configurations are being calculated self-consistently while the ions move.

10.2.4 Linear Augmented Plane Waves (LAPW)

All methods for solving the Schrödinger equation should in principle be the same. However, numerical calculations for problems with an infinite number of degrees of freedom are always approximate. Many methods aim to choose a set of basis functions that approximate the real solutions as closely as possible, so that the decomposition of true wave functions in terms of the basis with a small number of terms has a hope of being accurate. Some of the most widely used are [linear] augmented plane waves ([L]APW), Korringa–Kohn–Rostoker (KKR), and [linear] muffin tin orbital ([L]MTO). These methods have many features in common with each other, as well as with the plane wave method of the previous section, and emphasize in varying degrees either the free-electron nature of electrons between atoms or else the atomic nature of electrons near the cores. The codes with greatest

claim to accuracy tend to be expensive in terms of computational power and memory usage, while others making more severe approximations run faster on smaller machines.

This section will briefly discuss *augmented plane waves*, which are due to Slater (1937). The starting point is the observation after Eq. (7.47) that Bloch's theorem provides the possibility of finding wave functions for the entire crystal by solving Schrödinger's equation within a single unit cell, subject to the boundary conditions recorded in Eq. (7.49).

In order to make the computation of boundary conditions simple, it is conventional to mangle the periodic potential even beyond the point to which it has been taken so far. The periodic potential U is taken to be of the *muffin-tin form*, which means that within a unit cell the potential is zero except within a sphere in the middle, where it is taken to be spherically symmetric, as shown in Figure 10.4. Because the potential is zero in the region where the boundary conditions are to be applied, wave functions take a simple form that makes the boundary condition easy to handle. In the center, because the potential is chosen to have spherical symmetry, one has a convenient basis of wave functions at his disposal. Lattice symmetries now enter the problem only through the boundary conditions on the cell edge.

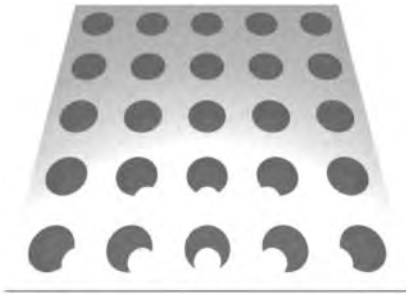


Figure 10.4. The muffin-tin potential is nonzero within a spherical region surrounding each ion and is zero everywhere else.

The augmented plane wave basis set is defined by the following:

1. $\phi_{\epsilon\vec{k}} = e^{i\vec{k}\cdot\vec{r}}$ outside a muffin hole.
2. $-\frac{1}{2m}\hbar^2\nabla^2\phi_{\epsilon\vec{k}} + U(r)\phi_{\epsilon\vec{k}} = \epsilon\phi_{\epsilon\vec{k}}$ within the hole.
3. $\phi_{\epsilon\vec{k}}$ is continuous at the hole boundary.

These conditions specify the basis functions uniquely, but are not very explicit. Within the muffin hole, the potential is some spherically symmetrical function $U(r)$. All solutions can be written in the form

$$\psi_{\epsilon} = Y_{lm}\mathcal{R}_{l\epsilon}(r), \tag{10.20}$$

where $\mathcal{R}_{l\epsilon}$ satisfies the equation

$$\frac{-\hbar^2}{2mr^2} \frac{\partial}{\partial r} r^2 \frac{\partial}{\partial r} \mathcal{R}_{l\epsilon}(r) + [U(r) + \frac{\hbar^2 l(l+1)}{2mr^2}] \mathcal{R}_{l\epsilon}(r) = \epsilon \mathcal{R}_{l\epsilon}(r). \tag{10.21}$$

For an arbitrary \mathcal{E} there are two independent solutions to this equation, one of which diverges at the origin, while the other diverges at infinity. One must discard the solution that diverges at the origin, but divergences at infinity are of no concern, because the solution need remain finite no further than the edge of the unit cell. This second solution is therefore perfectly acceptable, and one can write

$$\phi_{\mathcal{E}\vec{k}} = \sum_{l=0}^{\infty} \sum_{m=-l}^l A_{lm} Y_{lm}(\hat{r}) \mathcal{R}_{l\mathcal{E}}(r), \quad (10.22)$$

where for the moment all of the coefficients A_{lm} are arbitrary. They may be fixed by application of the condition that the wave function be continuous across the muffin hole boundary. Recall that

$$e^{i\vec{k}\cdot\vec{r}} = 4\pi \sum_{l=0}^{\infty} \sum_{m=-l}^l i^l j_l(kr) Y_{lm}^*(\hat{k}) Y_{lm}(\hat{r}). \quad \text{See Landau and Lifshitz (1977), p. 113.} \quad (10.23)$$

Then, taking R_h to be the radius of the muffin hole, one has

$$\phi_{\mathcal{E}\vec{k}} = 4\pi \sum_{l=0}^{\infty} \sum_{m=-l}^l \frac{i^l j_l(kR_h) Y_{lm}^*(\hat{k})}{\mathcal{R}_{l\mathcal{E}}(R_h)} Y_{lm}(\hat{r}) \mathcal{R}_{l\mathcal{E}}(r). \quad (10.24)$$

There is now a function ϕ for every \mathcal{E} and every \vec{k} . The functions have a discontinuity in slope at the muffin boundary, which there is not enough freedom to remove at this stage. Next consider the problem of matching the boundary conditions (7.49) at the edge of the primitive cell. Because the augmented plane waves are no more than plane waves there, one can accomplish this task simply by considering functions built to obey Bloch's theorem in the form

$$\psi_{\vec{k}} = \sum_{\vec{K}} b_{\vec{k}+\vec{K}} \phi_{\mathcal{E},\vec{k}+\vec{K}}. \quad \text{The } \vec{K} \text{ are reciprocal lattice vectors and } b_{\vec{k}+\vec{K}} \text{ are coefficients to be determined. This expression is especially simple because of the decision to set the potential } U \text{ to zero outside the muffin-tin.} \quad (10.25)$$

The parameter \mathcal{E} is still allowed to vary freely. How should one think about it? The augmented plane wave functions form a complete (not orthonormal) set for any \mathcal{E} . But one should only expect them to converge rapidly to a desired eigenfunction by choosing \mathcal{E} to be the eigenvalue corresponding to that eigenfunction. Therefore, during the numerical search for the coefficients $b_{\vec{k}}$, one should vary the parameter \mathcal{E} buried within the augmented plane wave functions so as to correspond to the latest estimate of the eigenvalue and obtain the most rapid convergence of the series. Although one need not set \mathcal{E} equal to the eigenvalue of Schrödinger's equation, they often are the same, and they are denoted by the same symbol for this reason.

The only remaining task is to determine the coefficients $b_{\vec{k}+\vec{K}}$. The best way to do it is to use the variational principle of Eq. (B.11), which directs one to insert Eq. (10.25) into

$$\langle \psi | \hat{\mathcal{H}} - \mathcal{E} | \psi \rangle, \quad (10.26)$$

and then require all variations with respect to each $b_{\vec{k}+\vec{K}}$ to vanish. Let \vec{q} and \vec{q}' be any vectors differing from \vec{k} by a reciprocal lattice vector \vec{K} . The result is then that

$$0 = \sum_{\vec{K}} \langle \phi_{\varepsilon\vec{q}} | \hat{\mathcal{H}} - \varepsilon | \phi_{\varepsilon\vec{q}+\vec{K}} \rangle b_{\vec{q}+\vec{K}}, \quad (10.27)$$

where

$$\langle \phi_{\varepsilon\vec{q}} | \hat{\mathcal{H}} - \varepsilon | \phi_{\varepsilon\vec{q}'} \rangle = \left(\frac{\hbar^2 \vec{q} \cdot \vec{q}'}{2m} - \varepsilon \right) \Omega \delta_{\vec{q},\vec{q}'} + \mathcal{U}_{\vec{q},\vec{q}'}, \quad (10.28)$$

The final answer is given by diagonalizing this matrix. Ω is the volume of the unit cell.

and, with P_l a Legendre polynomial

$$\mathcal{U}_{\vec{q},\vec{q}'} = 4\pi R_h^2 \left\{ \begin{array}{l} - \left(\frac{\hbar^2 \vec{q} \cdot \vec{q}'}{2m} - \varepsilon \right) \frac{j_1(|\vec{q} - \vec{q}'| R_h)}{|\vec{q} - \vec{q}'|} \\ + \sum_{l=0}^{\infty} \frac{\hbar^2}{2m} (2l+1) P_l(\hat{q} \cdot \hat{q}') j_l(q R_h) j_l(q' R_h) \frac{\mathcal{R}'_{l\varepsilon}(R_h)}{\mathcal{R}_{l\varepsilon}(R_h)} \end{array} \right\}. \quad (10.29)$$

These formulae are easily generalized to include more than one hole per unit cell. Relativistic effects are incorporated solving the Dirac rather than the Schrödinger equation. In practice, accuracy on the order of 10^{-3} Ry can be obtained with 20–100 APW basis functions.

10.3 Definition of Metals, Insulators, and Semiconductors

The significance of energy band calculations emerged slowly during the first five years after the discovery of quantum mechanics. Bloch's original understanding of his equations was that all solids were metals, but their degree of conductivity was determined by the degree of wave function overlap between neighboring atoms, such as α in Eq. (8.34). However, Wilson (1931) realized that the real situation was more interesting. In the view of one-electron theory, insulators are solids in which all occupied energy bands are completely filled, while metals are solids in which at least one occupied energy band is only partly filled.

The formal proof of this statement must wait for Chapters 16 and 17. However, it is intuitively plausible. The sketches in Figure 10.5 show characteristic energy bands and sections of Brillouin zones for metals and insulators. In an insulator, all the states of low-lying bands are completely filled. Because the Pauli principle forbids multiple occupation of states, when an electric field is applied, the electrons are locked in place. Their only hope of moving is to travel to an upper band. The energy gap \mathcal{E}_g acts, however, like a physical barrier, and the motion can only occur through quantum-mechanical tunneling, whose rate is roughly $\exp[-k_F \mathcal{E}_g / (eE)]$, where E is the strength of the applied electric field and k_F is the Fermi wave vector; the correct expression will be derived in Eq. (16.64). By contrast, in a metal, at least one band is only partly filled. Therefore electrons at the Fermi surface are free to move into adjoining states. In the presence of an electric field, the electron distribution slides slightly in the direction of the field, in momentum space, giving the electron population a net momentum and leading to current flow. Wilson noted

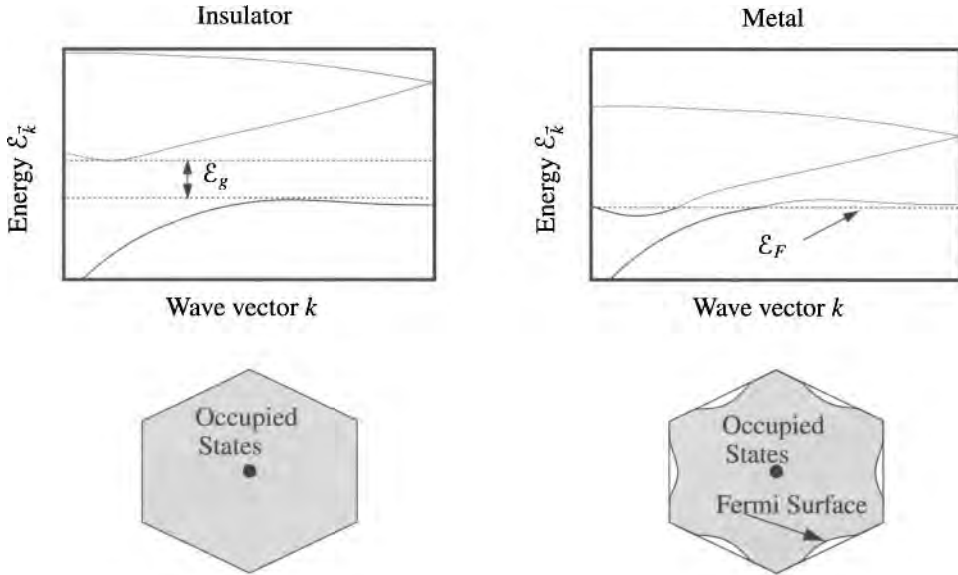


Figure 10.5. Schematic indication of the difference between metal and insulator in the one-electron picture. In an insulator, all occupied bands are completely filled. Because each edge of the Brillouin zone joins periodically and seamlessly onto another portion of the Brillouin zone, there is no boundary to the region of occupied states, and there is no Fermi surface. In a metal, at least one occupied band is only partly filled, and a Fermi surface exists.

an analogy to atomic orbitals. A filled band is like a filled shell; it is stable and rather rigid, while an unfilled band like an unfilled shell is easily polarized. The electronic specific heat, for example, calculated in Eq. (6.77) is proportional to the density of states at the Fermi surface. If there is no Fermi surface, it is as if there are no electrons.

The number of states in a Brillouin zone equals twice the number of primitive cells in the whole lattice, because the state indexed by wave vector k admits two electrons. Therefore, the Brillouin zone of a Bravais lattice can only be completely filled if it has an even number of electrons per site. In Wilson's words, one of the first consequences of this point of view is that "an elemental solid . . . with an odd valency had to be a metal, whereas elements with an even valency might produce either a metal or an insulator" [Wilson (1980), p. 45]. The periodic table bears this observation out completely. There appear at first to be exceptions—for example, in columns 7A and 5A—which are filled with insulators. In none of these cases has the element adopted a Bravais lattice. Instead, it finds a unit cell containing an even number of atoms and an even number of electrons. Equation (11.47) in Chapter 11 will show explicitly how a small distortion of a unit cell can provide a structural energy advantage by turning a metal into an insulator.

Two additional classes of solids can also be defined using the concepts of filled bands. A *semiconductor* is an insulator where the energy gap \mathcal{E}_g is small enough compared to $k_B T$ at room temperature that thermal fluctuations provide a substan-

tial population of conducting electrons. This definition of a semiconductor as an insulator with a gap of 1-2 eV or less, is not precise, and Pauli's kind advice, "One shouldn't work on semiconductors, that is a filthy mess; who knows whether any semiconductors exist" [Pauli (1931)] might be followed if semiconductors were not responsible for such a large portion of the world economy. A *semimetal* is by contrast a metal with such a very small population of conduction electrons at zero temperature that its conducting properties are poor; a semimetal results when only a tiny pocket of electrons escapes the boundaries of the Brillouin zone, leading to conduction electron densities three or four orders of magnitude less than the normal 10^{22} cm^{-3} .

The definition of metals in terms of their band structure is a powerful idea, far from obvious, and extremely productive. Nevertheless, it is neither completely satisfying nor always correct. It has little predictive power regarding the distribution of metals in the periodic table. One might expect all the elements of the second and tenth columns to be insulators, since they have even numbers of electrons per unit cell, and atomic shells have just been filled, but all these elements are metallic. The insulators all appear in a triangle on the right-hand side of the periodic table. A principle other than band structure appears to be deciding whether an element will be insulating or metallic, and the element is then forced to choose a lattice so that its band structure be consistent with this choice. Section 18.3 describes some of the ideas that can be employed to predict whether a compound should be metallic or insulating. There is also a wide range of compounds in which band structure calculations insist that the result should be metallic, yet experimentally the substance is an insulator. These are solids for which electron correlation is very important and calculations based upon single-electron models fail in quantitative ways. Classic examples include NiO and CuO, and they are discussed in Section 23.6.3.

10.4 Brief Survey of the Periodic Table

The technology of band structure calculations opens the possibility of traversing the periodic table and beginning to calculate materials properties. Density functional calculations are not always in a position to operate entirely without assistance from experiment. The difference in energy between competing ground state structures is often so small that calculations cannot objectively choose between them, as indicated for example in Table 11.9. However, given the correct lattice structure, the calculations proceed to make many useful predictions.

For many reasons the process of comparing theory and experiment is not completely straightforward. What the band structure calculations provide is a collection of energy bands \mathcal{E}_{nk} for a large number of wave vectors \vec{k} and for a number of bands. The pictures fill pages with curving lines, but what do they mean?

If the philosophy of density functional theory is followed literally, the one-electron wave functions are simply artifacts that arise in the course of calculating electronic ground state energies of solids and should not be given additional significance. This restrictive view is difficult to maintain, considering that hosts of

physical properties, ranging from electrical conduction to spontaneous magnetization and optical absorption, can be calculated in terms of a single-electron picture. So it is always interesting to examine the bands that arise during density functional calculations and ask if transitions between them correspond to experimental observations. But one cannot be very upset or surprised if predictions obtained in this way lack quantitative accuracy.

For example, optical experiments described in Section 23.6 measure energy bands directly, so it is natural to hope that calculated energy bands correspond directly to these measurable quantities. Seeking predictions about excited electronic states based on a naïve view of band structures is not completely meaningless, but characteristically involves errors on the order of 20–50%. For example, the experimental band gaps of insulators and semiconductors typically differ from band gaps calculated in density functional theory by this amount. Closer correspondence with experiment is only achieved either through the deliberate incorporation of small amounts of experimental information into the density functional formalism, or else through lengthy additional calculations that differ from one element to another and have not yet been formulated as generally applicable procedures.

10.4.1 Nearly Free Electron Metals

Here are samplings of the sorts of information obtained by calculating band structures of the elements.

Several of the elements, particularly those near the top of Table 6.2, are very well described as nearly free electron solids. The description is best for the alkali metals forming the first column of the periodic table, but also works moderately well for the noble metals, copper, silver and gold, forming column 11 (or IB). The closed shells of the valence electrons are nearly inert, and the conduction electrons interact with them rather weakly. Essential to the self-consistency of this picture is the fact that the Fermi surface in these metals is rather far distant from the edge of the Brillouin zone, as shown in Figure 8.7. The only electrons available for transport properties move at energies where the lattice is completely ineffective at scattering them.

The band structure of aluminum appears in Figure 10.6. The calculated bands are compared with free-electron parabolas, whose complicated appearance is purely due to their reduction to the first Brillouin zone. The electrons in aluminum are behaving nearly as if they were noninteracting electrons moving through an empty box.

By contrast, the bands of copper shown in Figure 10.7 contain features both of localized and nearly free electrons. The ten $3d$ electrons lie in a set of narrow bands about 2 eV below the Fermi surface and about 2 eV in width, while the $4s$ electron lies mainly in a band extending from about 10 eV below the Fermi surface to several electron volts above. The density of states looks like the sum of two pieces, the broad band containing the s electron, and the narrow band containing d electrons. The s and d bands hybridize together in the energy range where they

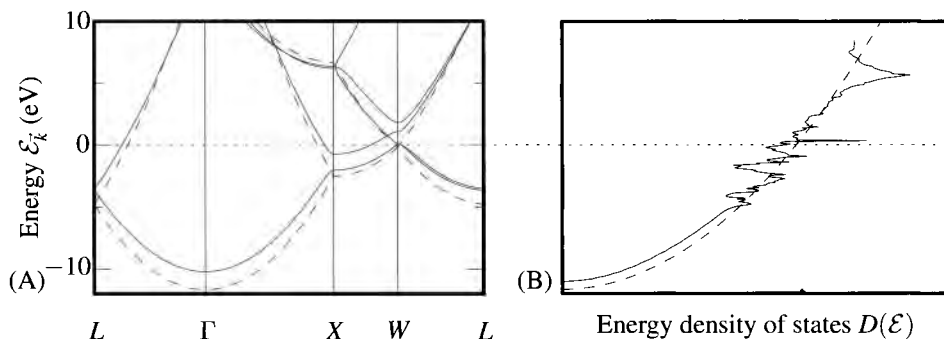


Figure 10.6. (A) Energy bands of aluminum; all energies measured relative to the Fermi energy. Solid lines are calculated with plane-wave pseudopotential code VASP of Kresse and Hafner (1994) and Kresse and Furthmüller (1996). The calculation assumes that aluminum adopts the fcc structure, with a lattice constant of 4.05 Å, and uses several hundred plane waves. Notation for the symmetry points in k space for this figure is given in Figure 7.8. The dashed lines show free-electron parabolas, which are remarkably similar to the calculated bands, indicating that aluminum is described well by the nearly free electron model. (B) Energy density of states of aluminum. The solid line results from calculations from VASP, while the dashed line comes from the free electron model (Eq. (6.24)). Peaks in the density of states are van Hove singularities, as described in Section 7.2.5.

intersect. The energy band calculations indicate the existence of occupied levels sitting 2 eV below vacant levels just above the Fermi surface (gray box in Figure 10.7 (A)). One can expect that the lowest-energy photons copper will absorb should have energy around 2 eV, and experiment bears this out, as shown in Figure 23.8. Making this prediction based upon the one-electron band structure is somewhat risky, for band structure calculations are designed to predict ground-state properties and unoccupied bands that arise in the computations do not necessarily lead to good predictions about excited states.

The elements of the second and twelfth columns of the periodic table could in principle be insulators, because from an atomic perspective, all electrons lie in closed shells, just having filled an s level. However, both band calculations and experiment agree that these elements form metals, in rough accord with the nearly free electron point of view. Instead of contracting to hug the Brillouin zone, the Fermi surface crosses in and out of it, leading in all cases to a metal. The elements of cubic symmetry (Ca, Sr, Ba) have two electrons per unit cell and are described by the second columns of Figures 8.6 and 8.7. The elements with the hcp structure (Be, Mg, Zn, Cd) have four electrons per unit cell, and they roughly correspond to the diagrams in Figure 8.8. For the lighter of these elements, where spin-orbit coupling is small, the middle column is appropriate, while for the heavier elements the rightmost column is the one that applies.

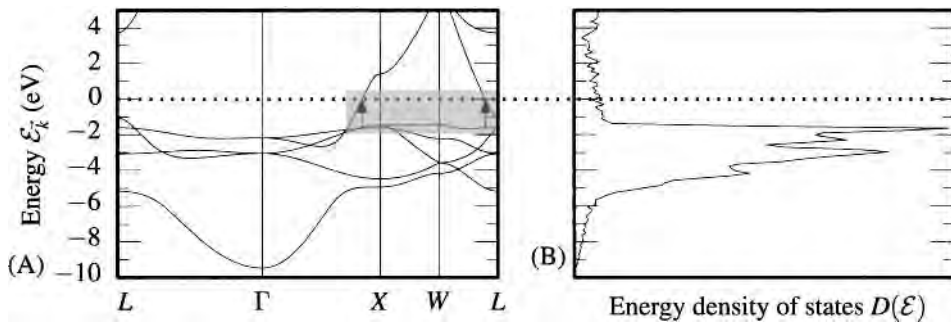


Figure 10.7. (A) Energy bands of copper, as calculated with the plane-wave pseudopotential code VASP of Kresse and Hafner (1994) and Kresse and Furthmüller (1996). All energies are measured relative to the Fermi energy. The calculation assumes that copper adopts the fcc structure, with a lattice constant of 3.61 Å. Not only the outer s electron but also 10 d electrons must be treated by the calculation. The 3d electrons are at a characteristic distance of less than 1 Å from the nucleus, and approximately 1000 plane waves are needed to capture simultaneously the extended s electron and tightly bound d electrons. Light absorption is dominated by the transition indicated by arrows in the gray box; the prediction that absorption sets in at around 2 eV is in reasonable agreement with data in Figure 23.8. (B) Energy density of states of copper. Peaks in the density of states are van Hove singularities, as described in Section 7.2.5.

10.4.2 Noble Gases

Some elements are naturally viewed from the perspective of the tight-binding model (Section 8.4). The noble gases (column 18 of the periodic table) are excellent candidates, since all electrons lie in closed shells that grip them tightly and prevent them from taking part in transport processes. With the exception of helium, all the noble gases form solid crystals at sufficiently low temperature, and the band structures of these gases nicely illustrate the way that bringing atoms together broadens discrete atomic states into bands.

Consider the band structure of krypton, shown in Figure 10.8. The ionization potential of an isolated krypton atom is 14.1 eV, and its first excited state is around 10.5 eV. In solid krypton, the atoms form an fcc lattice with lattice constant $a = 5.72$ Å. Experimentally, the lowest electronic excitation of solid krypton is around 10 eV above the ground state, similar to the value in the isolated atom. The calculation in Figure 10.8 finds instead an energy gap of 6.7 eV, 70% of the experimental value. Such inaccuracy in this quantity is typical of band structure calculations. The calculation does correctly find that the atomic levels have been broadened into energy bands with a width around 2 eV. Atomic levels broaden into bands because in a crystal electrons can hop between atomic sites with a range of kinetic energies. Because the separation between conduction and valence bands is so large, a representation of the valence band in terms of tightly localized Wannier functions should be excellent. Thus the solid has two correct and complementary descriptions: as an assemblage of nearly independent atoms, or in terms of very narrow completely filled bands.

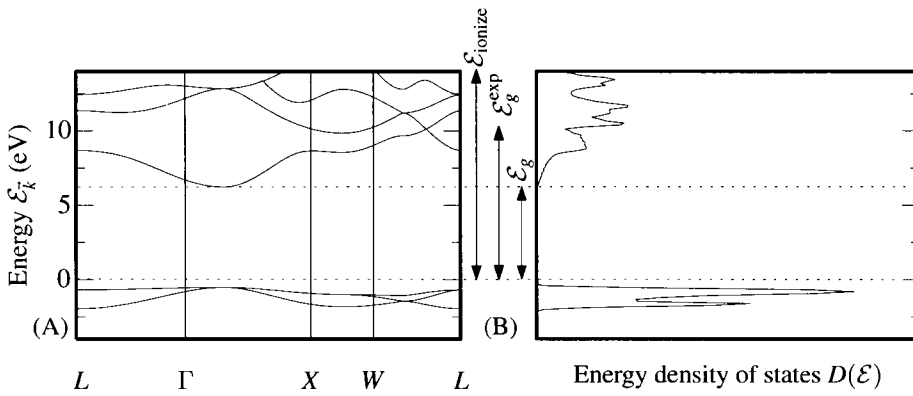


Figure 10.8. (A) Energy bands of krypton, calculated with the plane-wave pseudopotential code VASP of Kresse and Hafner (1994) and Kresse and Furthmüller (1996). All energies are measured relative to the Fermi energy. The calculation uses around 1000 plane waves, and it assumes an fcc structure with lattice parameter $a = 5.72 \text{ \AA}$. The notation for the path traversed in reciprocal space for this figure is given in Figure 7.8. The ionization energy of an isolated krypton atom is $\mathcal{E}_{\text{ionize}}$, the experimental band gap $\mathcal{E}_g^{\text{exp}}$ is 10.5 eV, and the calculated band gap is around 6 eV. (B) Density of states of krypton. The electrons are restricted to three narrow bands, holding six electrons, lying just below the Fermi surface. An additional band at -19 eV , not depicted, holds an additional two electrons. Peaks in the density of states are van Hove singularities, as described in Section 7.2.5

10.4.3 Semiconductors

The fourteenth column of the periodic table separates insulators from conductors, and it is largely populated with semiconductors. Carbon is a semimetal in the form of graphite and is a very wide band semiconductor in the form of diamond; gray tin is semiconducting while white tin is metallic.

The band structure of graphene appears in Figure 10.9 (see also Problem 8.5). Graphene consists in a single atomic layer of carbon atoms in a honeycomb structure. The most notable feature of the band structure is the occurrence of a two-fold degeneracy right at the Fermi surface at symmetry point K . The uppermost degenerate band is unoccupied in the ground state, while the lower one is fully occupied. The density of states at the Fermi surface is extremely small, making graphene, like graphite, a semimetal. When graphene folds around an axis to create a nanotube, the periodic boundary conditions imposed on the wave function make it possible for the tube either to remain a semimetal, or to become a narrow or wide-gap semiconductor. The relation of electrical properties to the geometry of the nanotube is the subject of Problem 3.

The single most important band structure of the elements appears in Figure 10.10: the band structure of silicon. Understanding fine details of electronic excitation and transport and silicon constitutes the foundation of the electronics industry, and will occupy much of Chapter 19. The calculations represented in Figure 10.10 contain valuable information, but also reveal a characteristic weakness of density functional calculations. As with krypton, it is tempting to regard the gap between

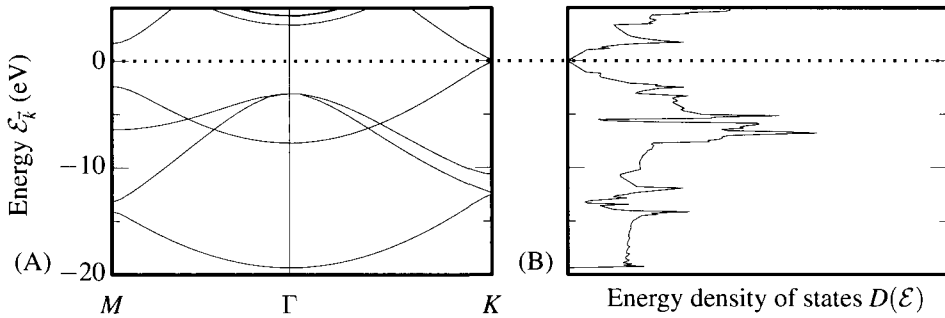


Figure 10.9. (A) Energy bands of graphene, calculated with the plane-wave pseudopotential code VASP of Kresse and Hafner (1994) and Kresse and Furthmüller (1996). All energies are measured relative to the Fermi energy. Notation for the symmetry points in k space in this figure is given by Figure 7.10. Note that at symmetry point K a filled and empty band are degenerate and meet at the Fermi surface. (B) Energy density of states of graphene. At the Fermi level, the density of states falls to zero, reflecting the fact that graphene is a semi-metal. Peaks in the density of states are van Hove singularities, as described in Section 7.2.5

the highest occupied and lowest unoccupied state as the energy that will be characteristic of excitations. The existence of such an energy gap is correct, but the value visible in Figure 10.10 is too small by about a factor of two when compared with experiments, such as optical absorption to be discussed in Section 21. Theoretical curves displayed in Section 23.6.2 cure this problem in two ways—some by deliberately adjusting parameters in the pseudopotentials to improve correspondence with experiment, and others by combining additional information about electron interactions in with ordinary density functional theory.

10.4.4 Transition Metals

The *transition metals* lying in columns 3–8 of the periodic table are not well described by the nearly free electron model. The $3d$, $4d$ and $5d$ shells fill when passing left to right among these elements, but always strongly mixed with the $4s$, $5s$, and $6s$ states, as shown by the calculated band structure of vanadium, in Figure 10.11. The wave functions of silver shown in Figure 10.2 illustrate the fact that the d orbitals are restricted to a radius of about 2 \AA about the atom—in contrast to the s and p orbitals, which extend out many times as far. Therefore, the most appropriate simple starting point for considering the d electrons is a tight-binding model. However, all simple calculations of this type are risky, and only partly because of the need to mix s and p states in with d . Several of the transition metals have magnetic structures in their ground states, a sure sign that the electrons are developing correlations of a sort not readily comprehensible in the one-electron framework.

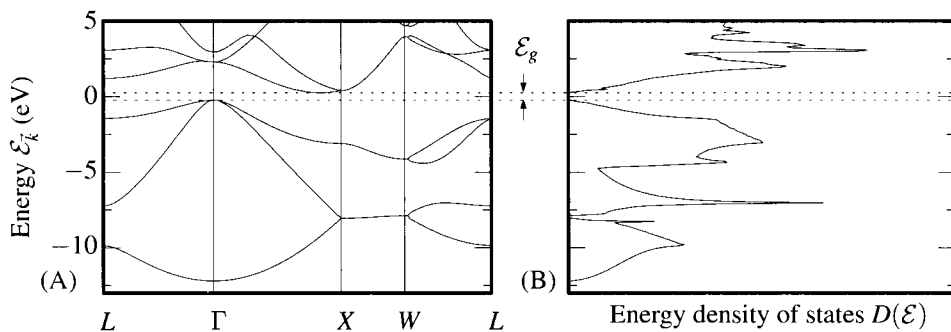


Figure 10.10. (A) Energy bands of silicon, calculated with the plane-wave pseudopotential code VASP of Kresse and Hafner (1994) and Kresse and Furthmüller (1996). All energies are measured relative to the Fermi energy. The calculation assumes that silicon adopts the diamond structure, with a lattice spacing of 5.43 Å, and uses several thousand plane waves. The calculation correctly determines that silicon is a semiconductor, and that the lowest lying spot in the conduction band lies between Γ and X . However the size of the energy gap \mathcal{E}_g is computed to be around 0.5 eV, which is half the value obtained by more sophisticated calculations and experimental measurements shown in Figure 23.16. (B) Energy density of states of silicon. Note that the density of states falls to zero in the gap. Peaks in the density of states are van Hove singularities, as described in Section 7.2.5

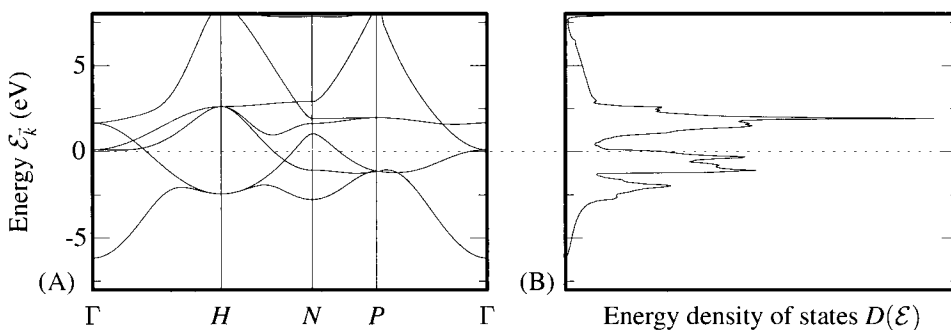


Figure 10.11. (A) Energy bands of vanadium, as calculated with the plane-wave pseudopotential code VASP of Kresse and Hafner (1994) and Kresse and Furthmüller (1996). All energies are measured relative to the Fermi energy. The calculation uses the fact that vanadium adopts the bcc structure, and it requires about 1000 plane waves. Notation for the symmetry points in k space in this figure is given by Figure 7.9. The location of the Fermi level in the midst of the complicated d bands is characteristic of the transition metals. (B) Energy density of states of vanadium, showing the large density of states due to d electrons near the Fermi surface. Peaks in the density of states are van Hove singularities, as described in Section 7.2.5

10.4.5 Rare Earths

The difficulties of applying band theory to the transition metals become even more acute in the case of the lanthanides. In this series of elements, the $4f$ orbitals are incomplete. These orbitals are even more tightly peaked about individual atoms than d orbitals, but nevertheless the solids remain metallic. While the close association of electrons to their respective atoms might seem to make a simple tight-binding model accurate, the actual situation is that the one-electron picture breaks down. For example, it is generally unfavorable for two electrons to occupy the same spatial state with opposite spin, a fact that a one-electron point of view will not be able to comprehend. The origin of these difficulties is Coulomb repulsion between the f electrons. Roughly speaking, Coulomb repulsion for wave functions of radius R will contribute terms to the energy going as $e^2 \exp[-R/\xi]/R$, where ξ is the screening length. Because screening lengths are typically on the order of 0.5 \AA , screening cannot much reduce the interactions of the f electrons, and they are driven to imaginative solutions involving local magnetic moments that band theory does not capture.

Problems

1. **Details of the augmented plane wave:** When there is more than one type of atom per unit cell, one surrounds each atom with a sphere of radius R_n , places the center of each sphere at \vec{r}_n , and proceeds to deduce that for augmented plane waves,

$$\langle \phi_{\varepsilon \vec{q}} | \hat{\mathcal{H}} - \varepsilon | \phi_{\varepsilon \vec{q}'} \rangle = \left(\frac{\hbar^2 \vec{q} \cdot \vec{q}'}{2m} - \varepsilon \right) \Omega \delta_{\vec{q}, \vec{q}'} + \sum_n e^{-i(\vec{q} - \vec{q}') \cdot \vec{r}_n} \mathcal{U}_{n\vec{q}, \vec{q}'}, \quad (10.30)$$

with

$$\mathcal{U}_{n\vec{q}, \vec{q}'} = 4\pi R_n^2 \left\{ - \left(\frac{\hbar^2 \vec{q} \cdot \vec{q}'}{2m} - \varepsilon \right) \frac{j_1(|\vec{q} - \vec{q}'| R_n)}{|\vec{q} - \vec{q}'|} + \sum_{l=0}^{\infty} \frac{\hbar^2}{2m} (2l+1) P_l(\hat{q} \cdot \hat{q}') j_l(q R_n) j_l(q' R_n) \frac{\mathcal{R}'_{nl\varepsilon}(R_n)}{\mathcal{R}_{nl\varepsilon}(R_n)} \right\}. \quad (10.31)$$

Derive Eqs. (10.30) and (10.31).

2. **Pseudopotential for aluminum:** Consider the empty core pseudopotential, shown in Figure 10.1, and normalized for a unit cell of volume Ω as

$$U(r) = U_0 e^{-r/d} \frac{\Omega}{4\pi d^3} \frac{d}{r} \theta(r - R_c). \quad (10.32)$$

Here d is a screening length, and R_c is a parameter describing a length within which the cancellations leading to the pseudopotential are taken to be perfect.

The goal is to determine U_0 , R_c , and d . The experimental data that make it possible come from the de Haas–van Alphen effect (Section 16.5.2) and optical data, as in Problem 2 of Chapter 23. However, all one needs to know is that it has been possible to measure the Fourier transform U_q defined in Eq. (7.26), at two reciprocal lattice vectors, and the results for aluminum are

$$U_{(111)} = 0.245 \text{ eV} \quad (10.33)$$

$$U_{(200)} = 0.762 \text{ eV}. \quad (10.34)$$

The reciprocal lattice vectors are being described by their Miller indices and are measured in units of $2\pi/a$.

In addition, the Fermi energy, measured relative to the lowest-energy \vec{k} state, is

$$\mathcal{E}_F = 11.7 \text{ eV}, \quad (10.35)$$

which can be used in Eq. (10.13).

- (a) Take the Fourier transform of Eq. (10.32).
- (b) Determine U_0 , d , and R_c by finding a reasonable fit of Eq. (10.32) to the measured values Eq. (10.33), (10.34), and (10.13). The agreement cannot be perfect, because one is trying to fit three parameters with two variables. Use any nonlinear fitting routine, or use a process of trial and error as convenient. The final values should be close to those listed after Eq. (10.38).
3. **Nanotube conductivity:** An (m, n) nanotube was defined in Problem 1.3 to be a graphene sheet rolled up so that the atom at $\vec{c} = m\vec{a}_1 + n\vec{a}_2$ finds itself back at the origin, where \vec{a}_1 and \vec{a}_2 are primitive vectors of the graphene sheet.

- (a) Argue that for an (m, n) nanotube, allowed Bloch vectors \vec{k} must satisfy

$$\vec{k} \cdot \vec{c} = 2\pi l. \quad \text{Where } l \text{ is an integer.} \quad (10.36)$$

- (b) Consulting Figures 10.9 and 7.10, note that the nanotube should be expected to be metallic if symmetry point K is an allowed value of \vec{k} , and a semiconductor or insulator otherwise. Show for positive m, n , that the condition for K to be an allowed value of k is

$$m = n \quad \text{or} \quad m - n = 3j. \quad \text{Where } j \text{ is an integer.} \quad (10.37)$$

The nanotubes with $n = m$ are in fact all metallic, while those with $m - n = 3j$ are very narrow-band semi-conductors at very low temperatures, and effectively metallic at room temperature. The remaining nanotubes are semiconductors. See Louie (2001) or Charlier et al. (2007).

4. **Plane wave band structure, part I:** The following five problems outline the construction of a primitive plane wave band structure code. The programming task can be carried out in any language, but the computing environment should be one that

- can carry out complex arithmetic, including multiplication and exponentiation of complex numbers, and
- can take the (discrete) Fourier transform of a three-dimensional array of complex numbers.

The first task is to write a subroutine that takes two arguments. The first is $c(i, j)$, an $N \times M$ -dimensional array of complex numbers. The second is an integer, i_1 . The columns of c are orthonormal up to $i_1 - 1$. The task of the subroutine is to replace the i_1 th column of c with a column that is orthogonal to the preceding $i_1 - 1$ columns and normalized to unity. Test the program on the following numbers:

$c(i,1)$	$c(i,2)$	$c(i,3)$	$c(i,4)$
(0.258198887,0.516397774)	(-0.392356962,-0.249681681)	(0.303851753, 0.138416067)	0
(0.774596632,0.258198887)	(0.321019441,-0.071337625)	(-0.221133977, 0.082717843)	2
(0.,0.)	(0.107006453, 0.749045134)	(0.097649745,-0.087221026)	1
(0.,0.)	(0.321019351, 0.)	(0.889513135, 0.156192154)	0

The first three columns are orthonormal. Find $c(i, 4)$.

5. **Band structure, part II:** Consider the Fourier transform of the pseudopotential in Figure 10.1

$$U_{\vec{K}} = U_0 e^{-R_c/d} \frac{[\sin(R_c K) + Kd \cos(KR_c)]}{dK[d^2 K^2 + 1]} \tag{10.38}$$

Take $d = 0.350$, $R_c = 0.943$, and $U_0 = -31.30$ (the units are angstroms and electron volts). These numbers are appropriate for aluminum and are the subject of Problem 2. The task is to compute

$$U(\vec{r}) = \sum_{\vec{K}} e^{i\vec{K}\cdot\vec{r}} U_{\vec{K}}, \tag{10.39}$$

taking \vec{K} to be the reciprocal lattice vectors of an fcc lattice of spacing $a = 4.05$ (Å).

- Find $U_{\vec{K}=0}$.
- Use Eq. (2.4) to construct the primitive vectors of the reciprocal lattice.
- Consult Appendix A.6 for guidance on the use of the fast Fourier transform. Obtain a routine capable of performing the transform for $N \times N \times N$ arrays of numbers; the problems will use $N = 4, 5, 8,$ and 12 . If such a routine cannot be located, the problems can be performed for $N = 4, 8$ only.
- For a given value of N , for what values of \vec{r} will a fast Fourier transform routine compute $U(\vec{r})$, and how will they be indexed?
- Use the routine to evaluate Eq. (10.39), taking $N = 5$, and printing the 125 values of $U(\vec{r})$ and \vec{r} in the Wigner–Seitz cell. Here are some of the values. The first three numbers are $x, y,$ and z coordinates of \vec{r} in angstroms, and the final number is the value of the potential $U(\vec{r})$ in Rydbergs.

```

0.      0.      0.      ( 0.201763183, 0.)
0.      0.405   0.405   (-0.201839209, 0.)
0.      0.810   0.810   (-0.757843018, 0.)
0.      1.215   1.215   (-0.757843018, 0.)
0.      1.620   1.620   (-0.201839209, 0.)
0.405   0.      0.405   (-0.201839194, 0.)
0.405   0.405   0.810   (-0.658886611, 0.)
0.405   0.810   1.215   (-0.718343496, 0.)
0.405   1.215   1.620   (-0.734894872, 0.)
    
```

If only $N = 4$ is possible, then U does not come out to be real; the first values, in Rydbergs, are

```

0.      0.      0.      ( 0.166458577, 0.      )
0.      0.50625  0.50625  (-0.265354961, 0.240282357)
0.      1.01250  1.01250  (-0.911596537, 0.      )
0.      1.51875  1.51875  (-0.265354961, -0.240282357)
0.50625  0.      0.50625  (-0.265354931, 0.240282387)
0.50625  0.50625  1.01250  (-0.591810703, -0.186816186)
0.50625  1.01250  1.51875  (-0.781587422, 0.103971817)
    
```

6. Plane wave band structure, part III: Consider Schrödinger’s equation in the form of Eq. (7.33).

The task is to find the lowest-lying eigenvalue \mathcal{E} and eigenfunction ψ solving this equation with the potential given by Eq. (10.38). Look for a solution with Bloch index $\vec{k} = 0$; essentially, this means that one sets $\vec{q} = 0$ in Eq. (7.33). Restrict all calculations to the $5 \times 5 \times 5$ set of \vec{K} considered in the previous portion of the problem.

- (a) Define a $5 \times 5 \times 5$ complex array $\psi(\vec{K})$. Let \mathcal{E}_{\max} be $\mathcal{E}_{K_{\max}}^0$, where K_{\max} is the largest value of \vec{K} under consideration. Write a routine to compute

$$\psi'(\vec{K}) \equiv (\mathcal{E}_{\vec{K}}^0 - \mathcal{E}_{\max})\psi(\vec{K}) + \sum_{\vec{K}'} U_{\vec{K}'}\psi(\vec{K} - \vec{K}'). \quad (10.40)$$

The hard part of the computation is the convolution $\sum_{\vec{K}'} U_{\vec{K}'}\psi(\vec{K} - \vec{K}')$. To perform the convolution, use the fact that

$$\sum_{\vec{K}'} U_{\vec{K}'}\psi(\vec{K} - \vec{K}') = \frac{1}{N^3} \mathcal{F}[\mathcal{F}^{-1}[U_{\vec{K}}] \times \mathcal{F}^{-1}[\psi(\vec{K})]]; \quad (10.41)$$

that is, take the inverse Fourier transforms of U and ψ , form a new array by multiplying together each element of U and ψ , take the Fourier transform of the result, and divide by N^3 . This procedure is vastly faster than performing the sums described by the convolution directly.

- (b) To find the ground state of Eq. (7.33),
- i. Choose some random initial normalized $\psi(\vec{K})$, such as $\psi(0) = 1$, with all other components zero.
 - ii. Find ψ' according to Eq. (10.40).
 - iii. Normalize ψ' .
 - iv. Put ψ' back into the right-hand side of Eq. (10.40), and find ψ'' .
 - v. Normalize ψ'' .

- vi. Continue in this fashion until the process converges. One should be left with the lowest-energy eigenstate of Schrödinger's equation.
- vii. What is the eigenvalue \mathcal{E} of this state from Eq. (7.33)?

7. **Plane wave band structure, part IV:** Consider again the potential given in Eq. (10.38). The new task is to compute the lowest-lying six eigenvalues $\mathcal{E}_{n\vec{k}}$ of

$$(\mathcal{E}_{\vec{q}}^0 - \mathcal{E})\psi(\vec{q}) + \sum_{\vec{k}'} U_{\vec{k}'} \psi(\vec{q} - \vec{k}') \quad (10.42)$$

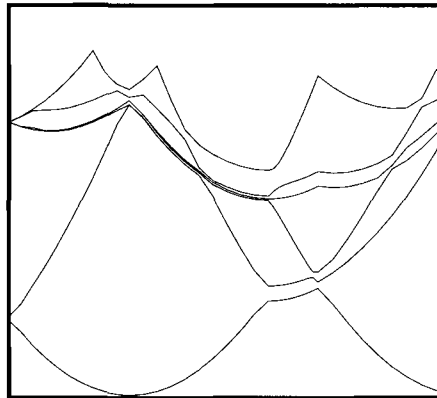
for $\vec{k} = [2\pi/a](.4 \ .4 \ .4)$, and $a = 4.05\text{\AA}$. Combine the routine for computing action of the Hamiltonian on wave functions with the orthogonalization routine Problem 4. Use an $8 \times 8 \times 8$ grid for \vec{K} .

For the first four eigenvalues, on $8 \times 8 \times 8$ and $12 \times 12 \times 12$ grids one has the following in Rydbergs:

$8 \times 8 \times 8$	$12 \times 12 \times 12$
-0.27	-0.27
0.13	0.13
1.17	1.17
1.17	1.17

8. **Plane wave band structure, part V:**

- (a) By adding an outer loop to the program produced in the previous problem, calculate the band structure of aluminum. Use a $4 \times 4 \times 4$ grid. Carry out the calculation along the trajectory L to Γ , Γ to X , X to U , U to Γ . Use about ten k points for each leg of the trajectory. Plot the first six bands. Do not expect the results to be perfect; the energy levels do not always appear in the correct order, and sometimes the convergence is slow. With a cutoff of around 10,000 on iterations for each energy level, one obtains the following figure:



The task is to produce a graph of roughly similar quality, with energies indicated on the y axis in electron volts. Compare with the energy bands of aluminum shown in Figure 10.6.

- (b) Suppose that energies in Figure 10.6 were reported relative to the Fermi level. Outline in words the calculations needed to determine the Fermi level.

References

- N. W. Ashcroft (1966), Electron-ion pseudopotentials in metals, *Physics Letters*, **23**, 48–50.
- N. Bernstein and D. Hess (2003), Lattice trapping barriers to brittle fracture, *Physical Review Letters*, **91**, 025 501/1–4
- D. W. Bullett (1980), The renaissance and quantitative development of the tight-binding method, *Solid State Physics: Advances in Research and Applications*, **35**, 129–214.
- R. Car and M. Parrinello (1985), Unified approach for molecular dynamics and density-functional theory, *Physical Review Letters*, **55**, 2471–2474.
- J.-C. Charlier, X. Blase, and S. Roche (2007), Electronic and transport properties of nanotubes, *Reviews of Modern Physics*, **79**, 677–732.
- M. L. Cohen (1979), The pseudopotential panacea, *Physics Today*, **32**(7), 40–47.
- M. L. Cohen and V. Heine (1970), The fitting of pseudopotentials to experimental data and their subsequent application, *Solid State Physics: Advances in Research and Applications*, **24**, 37–248.
- J. O. Dimmock (1971), Calculation of electronic energy bands by the augmented plane wave method, *Solid State Physics: Advances in Research and Applications*, **26**, 103–274.
- H. Ehrenreich and L. M. Schwartz (1976), The electronic structure of alloys, *Solid State Physics: Advances in Research and Applications*, **31**, 149–286.
- X. Gonze, R. Stumpf, and M. Scheffler (1991), Analysis of separable potentials, *Physical Review B*, **44**, 8503–8513.
- V. Heine (1970), The pseudopotential concept, *Solid State Physics: Advances in Research and Applications*, **24**, 1–36.
- V. Heine and D. Weaire (1970), Pseudopotential theory of cohesion and structure, *Solid State Physics: Advances in Research and Applications*, **24**, 250–463.
- G. Kresse and J. Furthmüller (1996), Efficiency of *ab-initio* total energy calculations for metals and semiconductors using a plane-wave basis set, *Computational Materials Science*, **6**, 15–50.
- G. Kresse and J. Hafner (1994), *Ab initio* molecular-dynamics simulation of the liquid-metal-amorphous-semiconductor transition in germanium, *Physical Review B*, **49**, 14 251–14 269.
- L. D. Landau and E. M. Lifshitz (1977), *Quantum Mechanics (Non-relativistic Theory)*, 3rd ed., Pergamon Press, Oxford.
- H. Landolt and R. Börnstein (New Series), *Numerical Data and Functional Relationships in Science and Technology*, New Series, Group III, Springer-Verlag, Berlin.
- S. G. Louie (2001), *Carbon Nanotubes*, vol. 80 of *Topics in Applied Physics*, chap. Electronic Properties, Junctions, and Defects of Carbon Nanotubes, Springer-Verlag, Berlin.
- W. Pauli (1931), W. Pauli to R. Peierls, 29 September 1931. In von Meyenn et al. (1985), p. 94
- J. C. Phillips and L. Kleinman (1959), New method for calculating wave functions in crystals and molecules, *Physical Review*, **116**, 287–294.
- D. J. Sellmyer (1978), Electronic structure of metallic compounds and alloys: Experimental aspects, *Solid State Physics: Advances in Research and Applications*, **33**, 83–248.
- J. C. Slater (1937), Wave functions in a periodic potential, *Physical Review*, **51**, 846–851.
- J. C. Slater (1975), *Solid-State and Molecular Theory: A Scientific Biography*, John Wiley and Sons, New York.

- J. C. Slater and G. F. Koster (1956), Simplified *LCAO* method for the periodic potential problem, *Physical Review*, **94**, 1498–1524.
- K. von Meyenn, A. Mermann, and V. F. Weisskopf, eds. (1985), *Wolfgang Pauli. Scientific Correspondence with Bohr, Einstein, Heisenberg, a. o., II: 1930–1939*, Springer-Verlag, Berlin.
- E. Wigner and F. Seitz (1933), On the constitution of metallic sodium, *Physical Review*, **43**, 804–810. The first attempt at a realistic band structure calculation.
- E. Wigner and F. Seitz (1955), Qualitative analysis in the cohesion of metals, *Solid State Physics: Advances in Research and Applications*, **1**, 97–126.
- A. H. Wilson (1931), The theory of electronic semiconductors, *Proceedings of the Royal Society of London*, **A133**, 458–491.
- A. H. Wilson (1980), Opportunities lost and opportunities seized, in *The Beginnings of Solid State Physics*, pp. 39–48, Royal Society, London.
- J. M. Ziman (1971), Calculation of Bloch functions, *Solid State Physics: Advances in Research and Applications*, **26**, 1–101.

Part III

MECHANICAL PROPERTIES

11. Cohesion of Solids

11.1 Introduction

The *cohesive energy* of a solid is the energy needed in order to rip a sample apart into a gas of widely separated atoms. By itself, this energy does not have much significance. It is not easy to measure experimentally, and it bears no relation to the practical strengths of solids; practical strength is governed by resistance to flow and fracture, physically quite distinct from cohesive energy.

The question that the cohesive energy makes it possible to address is how crystals choose their equilibrium structure. Electronic structure calculations begin by assuming that atomic positions are known, but in studying cohesive energy, one asks which structure leads to the lowest energy and why. In the course of this study, crystals divide roughly into five classes: *molecular*, *hydrogen bonded*, *ionic*, *covalent*, and *metallic*. These classes blend into each other, but still represent conceptual ideal types. The molecular crystals are composed from atoms whose shells are filled, which hold tightly onto their electrons, and which bind together only because of small induced dipole moments. Hydrogen bonded solids involve hydrogen atoms as part of the bonding process; this might seem too specialized to warrant a separate category except that it includes much of biology. The ionic crystals are composed of pairs of atoms, in which one member of the pair donates an electron to the other, and vast numbers of such pairs are held together by dipole forces. Figure 11.1(A) shows the valence charge density of NaCl; the visible charge sits in a sphere around the chlorine, and charge density drops to very small values between the atoms. The covalent crystals feature even more electrons wandering away from their host atoms, and it is convenient to think of *bonds* between atoms, because charge density is high along lines connecting near neighbors, as shown in Figure 11.1(B). In metals, the conduction electrons are distributed quite uniformly throughout the solid, and the net effect of the interaction between electrons and nuclei is a hydrostatic pressure keeping the solid together. A plot of the conduction electron density in a metal would be flat and almost featureless. As a final illustration of the connection between charge density and cohesion, Figure 11.2 presents experimentally measured charge density for cuprous oxide. This metal oxide does not easily fit classification. The charge density around the copper has the shape of *d* orbitals, and leads to a phenomenon resembling covalent bonding between metal ions.

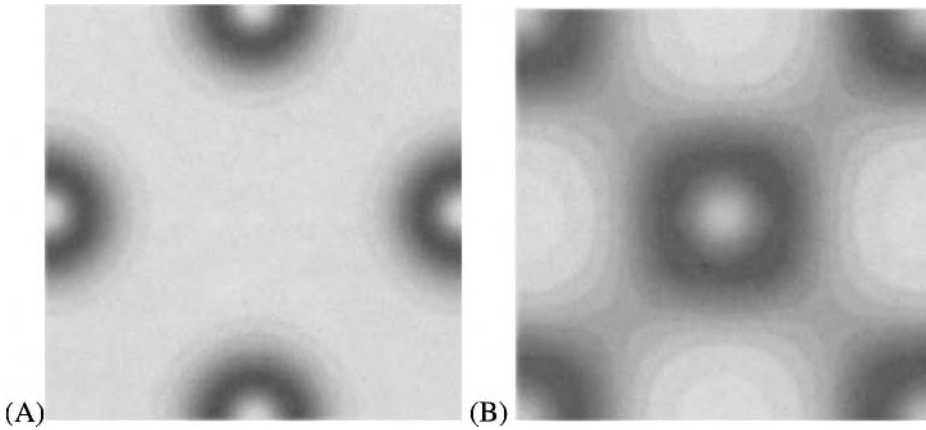


Figure 11.1. (A) Valence charge density of NaCl along a (100) plane, computed by the plane wave pseudopotential code of Stumpf and Scheffler (1994). The seven valence electrons of Cl and one of Na are the only electrons depicted; all electrons sit on the chlorine, in a nearly perfectly spherical configuration, so the sodium is invisible. The valence electrons avoid the core of the atom, which is why their density drops to zero there. (B) Valence charge density of Ge along a (100) plane. The fourfold coordination of the diamond structure is evident, as well as the large charge density lying along the lines between atoms, characteristic of covalent bonding.

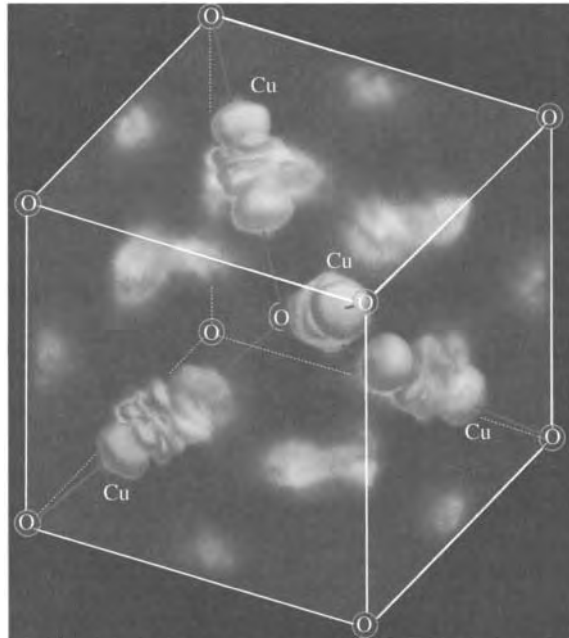


Figure 11.2. Experimentally measured charge density of cuprous oxide Cu_2O . The plot shows the difference between the charge distribution in Cu_2O and the charge distribution in free ions. The charge distribution around the copper atoms looks like d orbitals; the presence of oxygen induces covalent bonding between metal ions. [Source: Zuo et al. (1999), p. 50.]

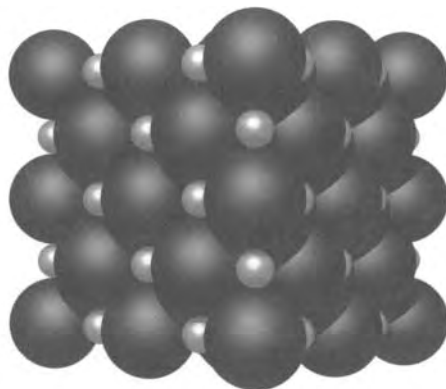


Figure 11.3. Picture of the sodium chloride structure, indicating the sizes of the sodium (small) and chlorine (large) ions. The chlorine ion is large because it has robbed an electron from the sodium.

11.1.1 Radii of Atoms

In searching for ideas by which to explain how atoms assemble themselves, the simplest is to assign each atom a radius, as if it were a hard sphere. An illustration of NaCl, indicating the sizes of the two ions, appears in Figure 11.3. Such an assignment would be without much consequence were it allowed to change every time the atom formed a compound with a new neighbor, but in fact the apparent radii of atoms remain roughly independent of their surroundings. This statement must, unfortunately, be qualified a bit, because the apparent radii do depend upon the class of crystal in which the atom is located.

Table 11.1 contains a summary of phenomenological rules that can be used to estimate lattice constants if crystal structure is known; the origin of these rules is discussed at length by Pearson (1972). Use of these rules should give lattice constants within about 10% of experimental values, and they can serve as a quick check on the results of either experiment, or theoretical calculation.

Example: Cristobalite. According to Wyckoff (1963–1971), quartz in the β -cristobalite form is cubic ($a = 7.12 \text{ \AA}$) and has a basis with eight silicon atoms and sixteen oxygens, which in units of $a/8$ are at

$$\begin{array}{l} \text{Si: } (000) \ (440) \ (404) \ (044) \ (222) \ (266) \ (626) \ (662) \\ \text{O: } (111) \ (551) \ (515) \ (155) \ (177) \ (537) \ (573) \ (133) \\ \quad (717) \ (357) \ (313) \ (753) \ (771) \ (331) \ (375) \ (735) \end{array}$$

The nearest-neighbor distance for this structure is 1.54 \AA . The silicon has four neighboring oxygens, so $Z = z = 4$, while each oxygen has two neighboring silicons, and $Z = 6$, $z = 2$. According to Table 11.1, the covalent radius of silicon is 1.17 \AA , and that of oxygen is $0.74 - 0.14 = 0.60 \text{ \AA}$, which sum to 1.77 \AA . The discrepancy is more than 10%, so there are grounds for concern. Liu et al. (1993) show that Wyckoff's structure is incorrect.

Table 11.1. Effective radii of the elements

El.	Z	M	I	R_1	El.	Z	M	I	R_1	El.	Z	M	I	R_1
Ac	3+	1.88			H	1-	0.78	2.08		Pt	2-	1.39		
Am	3+	1.81			He	0				Pu	3-	1.58		
Ar	0		1.86		Hf	4+	1.58			Rb	1+	2.55	1.48	2.16
Ag	1+	1.45	1.26	1.53	Hg	2+	1.57	1.10	1.49	Re	2-	1.38		
Al	3+	1.43	0.50	1.25	Ho	3+	1.77		1.58	Rh	2-	1.35		
As	3-	1.39	2.22	1.21	I	1-		2.16	1.33	Ru	2-	1.34		
Au	1+	1.44	1.37	1.52	In	3+	1.66	0.81	1.44	S	2-	1.27	1.84	1.04
Ba	2+	2.24	1.35	1.98	Ir	2-	1.36			Sb	3-	1.59	2.45	1.41
Be	2+	1.13	0.35	0.89	K	1+	2.38	1.33	2.03	Sc	3+	1.64	0.81	1.44
Bi	3-	1.70		1.52	Kr	0		2.00		Se	2-	1.40	1.98	1.17
B	3+	0.98	0.20	0.80	La	3+	1.88	1.15	1.69	Si	4+	1.32	0.41	1.17
Br	1-		1.95	1.14	Li	1+	1.56	0.68	1.23	Si	4-		2.71	
C	4+	0.92	0.15	0.77	Lu				1.56	Sm	3+	1.80		1.66
	4-		2.60		Mg	2+	1.60	0.65	1.36	Sn	4+	1.62	0.71	1.40
Ca	2+	1.97	0.99	1.74	Mn	4+	1.30			Sn	4-		2.94	
Cd	2+	1.57	0.97	1.49	Mo	2-	1.40			Sr	2+	2.15	1.13	1.91
Ce	3+	1.83	1.01	1.65	N	3-	0.88	1.71	0.74	Ta	3-	1.47		
Co	2-	1.25			Na	1+	1.91	0.97	1.57	Tb	3+	1.78		1.59
Cl	1-		1.81	0.99	Nb	3-	1.47			Te	2-	1.60	2.21	1.37
Cr	3+	1.36			Nd	3+	1.83		1.64	Th	4+	1.80		
Cs	1+	2.73	1.67	2.35	Ne	0		1.58		Ti	4+	1.46	0.68	
Cu	1+	1.28	0.96	1.35	Ni	2-	1.25			Tl	3+	1.72	0.95	1.46
Dy	3+	1.77		1.59	Np	2-	1.56			Tm	3+	1.75		1.56
Er	3+	1.76		1.57	O	2-	0.89	1.40	0.74	U	2-	1.56		
Eu	2+	2.04		1.85	Os	2-	1.35			V	3-	1.35		
F	1-		1.36	0.72	P	3-	1.28	2.12	1.10	W	2-	1.41		
Fe	2-	1.27			Pa	3-	1.63			Xe	0		2.17	
Ga	3+	1.41	0.62	1.27	Pb	4+	1.75	0.84	1.43	Y	3+	1.80	0.93	1.62
Ge	4+	1.37	0.53	1.22	Pd	2-	1.38			Yb	2+	1.94		1.70
Ge	4-		2.72		Po	2-	1.76		1.53	Zn	2+	1.39	0.74	1.31
Gd	3+	1.80		1.61	Pr	3+	1.83		1.65	Zr	4+	1.60	0.80	

El. = Element; Z = Valency; M = Metallic radius; I = Ionic radius; R_1 = Covalent radius. The metallic radius is intended for use in close-packed structures with coordination number 12. Ionic and covalent radii may need correction by additional factors. The ionic radius is intended for ions with coordination number near 6, and should be multiplied by the factor $[z/6]^{1/(n-1)}$, where z is the number of nearest neighbors, and n is the Born exponent of Table 11.2. The covalent radius gives best results for atoms with coordination number 4, and for an atom with Z valence electrons and z nearest neighbors is given by $R = R_1 - 0.13 \ln[Z/z]$; for $Z < 0$, use $8 - |Z|$. Source: Tosi (1964) and Pearson (1972), pp. 147-153.

Table 11.2. Born exponent n

Ion Type (inert core)	He	Ne	Ar	Kr	Xe
			Cu ⁺	Ag ⁺	Au ⁺
Born exponent n	5	7	9	10	12

Used in correction factor $[z/6]^{1/(n-1)}$ for ionic radii. Source: Pearson (1972).

11.2 Noble Gases

The noble gases are characterized by a very weak attraction between the atoms. The potential energy of a crystal conventionally takes the form of a two-body potential

$$\mathcal{E} = \frac{1}{2} \sum_{ij} \phi(r_{ij}) \quad (11.1)$$

with

$$\phi(r) = -4\epsilon \left[\left(\frac{\sigma}{r} \right)^6 - \left(\frac{\sigma}{r} \right)^{12} \right]. \quad (11.2)$$

Here r_{ij} is the distance between two atoms. The potential in Eq. (11.2) is called the *Lennard-Jones 6-12 potential* and arises partly from basic calculations and partly from phenomenological considerations. The term proportional to r^{-6} accurately represents the interaction at large distances between two molecules without a permanent dipole moment, the *van der Waals* interaction. It arises in the following way.

The interaction between two dipoles is

$$\phi(r) = [\vec{p}_1 \cdot \vec{p}_2 - 3(\vec{p}_1 \cdot \hat{r})(\vec{p}_2 \cdot \hat{r})]/r^3, \quad (11.3)$$

where r is the distance between the atoms, and \hat{r} is a unit vector. Now it will be protested that atoms without dipole moments do not have dipole moments. This is true. However, quantum or thermal fluctuations continually induce tiny dipole moments in each atom. The resulting electric field then polarizes the other atom, producing a small dipole moment in it, of order r^{-3} . The resulting interaction is then of order r^{-6} . The induced dipole moment is always of such a sign as to lower the energy of the system; therefore, the interaction is always attractive. To obtain such a result formally, see Problem 3. One places the quantum operator for Coulomb interactions as a perturbation into the Hamiltonian for two widely separated atoms and then finds a nonzero result in the second order of perturbation theory. The final result is of the form

$$\phi \sim -\frac{\alpha_1 \alpha_2}{r^6}, \quad (11.4)$$

where α_i is the polarizability of atom i . It is only valid when the atoms are well-separated. When they come close together, at distances comparable to the atomic

radii, the force between them becomes repulsive. For this reason, and with no firmer foundation, one adds the term proportional to r^{12} in Eq. (11.2).

In order to provide a firm check on the theory, one can measure the constants ϵ and σ in the gas phase and then use the results to make predictions about the solid phase. The gas phase measurements use the following relation from the virial expansion:

$$b_2 = \frac{1}{2} \int d\vec{r} [1 - e^{-\beta\phi(r)}]. \quad \text{See Landau and Lifshitz (1980), pp. 231-232, who use somewhat different notation.} \quad (11.5)$$

The coefficient b_2 enters the virial expansion for the pressure P in the form

$$P\mathcal{V}/k_B T = 1 - b_2/\mathcal{V} \dots \quad (11.6)$$

so measurements of the equation of state at low densities can be used to find b_2 , and hence fit σ and ϵ (Table 11.3).

Table 11.3. Parameters σ and ϵ for the noble gases

Noble Gas	He	Ne	Ar	Kr	Xe
ϵ (eV)	$8.6 \cdot 10^{-4}$	0.0031	0.0104	0.0104	0.0200
σ (Å)	2.56	2.74	3.40	3.65	3.98

Source: Bernardes (1958) and Hirschfelder et al. (1954), p. 201.

The total energy of a crystal where atoms interact in this way is then

$$\mathcal{E}/N = \frac{1}{2} 4\epsilon \sum_{\vec{R} \neq 0} \left[\left(\frac{\sigma}{R}\right)^{12} - \left(\frac{\sigma}{R}\right)^6 \right]. \quad \text{Taking the crystal to contain } N \text{ atoms, and adopting periodic boundary conditions so that all atoms have identical neighborhoods.} \quad (11.7)$$

Letting d be a nearest neighbor distance, one can rewrite the energy as

$$\mathcal{E}/N = 2\epsilon \sum_{\vec{R}} \left[\left(\frac{\sigma}{d}\right)^{12} \left(\frac{d}{R}\right)^{12} - \left(\frac{\sigma}{d}\right)^6 \left(\frac{d}{R}\right)^6 \right] \quad (11.8)$$

$$\equiv 2\epsilon [A_{12} \left(\frac{\sigma}{d}\right)^{12} - A_6 \left(\frac{\sigma}{d}\right)^6] \quad \text{with } A_l \equiv \sum_{\vec{R} \neq 0} \left(\frac{d}{R}\right)^l. \quad (11.9)$$

Written in this way, one sees that the lattice sums can be carried out once and for all for any particular crystal structure, so that the energy depends only upon the nearest-neighbor separation. The sums converge rapidly because the powers involved are so high. Except for helium, all the noble gases solidify into an fcc structure, and the appropriate lattice sums in this case are shown in Table 11.4.

One can now work out the nearest-neighbor spacing in equilibrium,

$$d_0 = \sigma \left(\frac{2A_{12}}{A_6} \right)^{1/6}, \quad (11.10)$$

Table 11.4. Lattice sums A_6 and A_{12} for various crystal structures

Crystal	fcc	bcc	hcp
A_6	14.4539	12.2537	14.4549
A_{12}	12.1319	9.1142	12.1323
$A_6^2/2A_{12}$	8.6102	8.2373	8.6111

The sums are defined in Eq. (11.9). The final row is proportional to the energy of the crystal. While fcc and hcp have noticeably lower energy than bcc, the energies of the two former structures are too close for these arguments to determine which will appear experimentally; the rare gas solids choose fcc.

Table 11.5. Properties of noble gases compared with predictions of Lennard-Jones potentials

Noble Gas	Ne	Ar	Kr	Xe
Experimental d_0 (Å)	3.13	3.75	3.99	4.33
d_0 from Eq. (11.10) (Å)	2.99	3.71	3.98	4.34
Experimental \mathcal{E}/N (eV/atom)	-0.02	-0.08	-0.11	-0.17
\mathcal{E}/N from Eq. (11.11)	-0.027	-0.089	-0.120	-0.172
Experimental B (dyne/cm ²)	$1.1 \cdot 10^{10}$	$2.7 \cdot 10^{10}$	$3.5 \cdot 10^{10}$	$3.6 \cdot 10^{10}$
B from Eq. (11.13)	$1.81 \cdot 10^{10}$	$3.18 \cdot 10^{10}$	$3.46 \cdot 10^{10}$	$3.81 \cdot 10^{10}$

Results show agreement at roughly the 10% level. Source: Ashcroft and Mermin (1976), p. 401.

the cohesive energy

$$\mathcal{E}/N = -\epsilon \frac{A_6^2}{2A_{12}}, \quad (11.11)$$

and the bulk modulus B which is given by

$$B = \mathcal{V} \frac{\partial^2 \mathcal{E}}{\partial \mathcal{V}^2}. \quad (11.12)$$

For an fcc lattice, the volume per particle \mathcal{V}/N is related to the nearest-neighbor separation d by $\mathcal{V}/N = d^3/\sqrt{2}$. Evaluating Eq. (11.12) gives

$$B = \frac{4\epsilon}{\sigma^3} A_{12} \left(\frac{A_6}{A_{12}} \right)^{5/2}. \quad (11.13)$$

Comparisons of this simple theory with experiment are listed in Table 11.5.

11.3 Ionic Crystals

The simplest ionic crystals are the *alkali halides*, built by combining an element from the first column of the periodic table with an element from the seventh column. The distinctive feature of these crystals is that the alkali metal (Li, Na, K,

Rb, or Cs) gives up an electron relatively easily so as to obtain a closed outer shell, while similarly the halogen (F, Cl, Br, or I) has a strong affinity for acquiring an extra electron to fill its outer shell. In fact, the benefits of closing the electronic shell outweigh Coulomb repulsion, and isolated halogen atoms stably bind extra electrons. Their positive electron affinities are listed in Table 11.6, along with the first ionization potential of the alkalis. The affinity of the halogen is typically less than the ionization potential of the alkali, but bringing the positively and negatively charged ions close together gives enough Coulomb energy to make the resulting structure stable. The Coulomb energy is easily estimated by treating the two ions as possessing a single negative or positive charge and placing them at a distance of about 3 Å apart; this gives a Coulomb energy of around -4 eV, which is enough to overcome the difference between electron affinity and ionization potential. The reason that the I–VII compounds are particularly simple, however, is that the structure stabilizes in such a way that the overlap of electronic charge from neighboring ions is negligible, as shown in Figure 11.1(A).

Four particularly common lattice structures—the sodium chloride structure, the cesium chloride structure, the zincblende structure, and the wurtzite structure—were sketched in Section 2.3.

11.3.1 Ewald Sums

Actually carrying out the sum over positive and negative ions to calculate the energy of the ionic solids is technically tricky. If in the first unit cell the positive ion (*cation*) is at the origin, and the negative one (*anion*) is at \vec{d} , the potential energy associated with a particular cation is

$$\frac{e^2}{d} \sum_{\vec{R} \neq 0} \left[\frac{d}{R} - \frac{d}{|\vec{R} + \vec{d}|} \right] - \frac{e^2}{d} \equiv \frac{e^2}{d} [dS(0) - dS(\vec{d}) - 1], \quad (11.14)$$

and the energy of the crystal as a whole will be $N/2$ times this amount. The difficulty is that the sum (11.14) converges very slowly, and in fact it can be done so as to have any value whatsoever. Physically, different limiting values of the sum correspond to crystals with differing amounts of surface charge, and the Coulomb force is so long range that the surface charges are able to make the crystal energy as

Table 11.6. Electron affinities and ionization potential for the alkalis and the halides

Atom	Electron affinity (eV)	Atom	First ionization potential (eV)
H	0.75	Li	5.32
F	3.40	Na	5.14
Cl	3.61	K	4.34
Br	3.36	Rb	4.18
I	3.06	Cs	3.90

Source: Hotop and Lineberger (1975) and Emsley (1998).

large as one wants. The desired result corresponds to a crystal with no net charge on any surface; thinking of it as a capacitor, one wants it to be discharged. The technique of *Ewald summation* accomplishes this goal and provides an extremely rapid numerical technique for performing the sums as well. The basic idea is that one should treat all the charges far away as a uniform charge distribution, do an integral over all the faraway charges, and not bother with the sums past a certain distance. The trick is to carry this idea out efficiently. Here is how: Write

$$S(\vec{d}) = \sum_{\vec{R} \neq \vec{0}} \frac{1}{|\vec{d} - \vec{R}|} = \int_0^\infty \frac{2 d\rho}{\sqrt{\pi}} \sum_{\vec{R} \neq \vec{0}} e^{-\rho^2 |\vec{d} - \vec{R}|^2} \quad (11.15)$$

$$= \int_0^\infty \frac{2 d\rho}{\sqrt{\pi}} \int \frac{d\vec{k}}{\rho^3 \sqrt{\pi^3}} \sum_{\vec{R} \neq \vec{0}} e^{-k^2/\rho^2 + 2i\vec{k} \cdot (\vec{d} - \vec{R})} \quad (11.16)$$

$$= \int_0^\infty \frac{2 d\rho}{\sqrt{\pi}} \int \frac{d\vec{k}}{\rho^3 \sqrt{\pi^3}} \left[\left\{ \sum_{\vec{K}} \frac{(2\pi)^3}{\Omega} \delta(2\vec{k} - \vec{K}) \right\} - 1 \right] e^{-k^2/\rho^2 + 2i\vec{k} \cdot \vec{d}} \quad (11.17)$$

$$= \int_0^\infty \frac{2 d\rho}{\sqrt{\pi}} \left[\frac{\pi^3}{\rho^3 \sqrt{\pi^3}} \sum_{\vec{K}} \frac{1}{\Omega} e^{-K^2/4\rho^2 + i\vec{K} \cdot \vec{d}} - e^{-d^2 \rho^2} \right] \quad \text{See (A.30).} \quad (11.18)$$

$$= \sum_{\vec{K}} \frac{4\pi}{\Omega K^2} e^{i\vec{K} \cdot \vec{d}} - \frac{1}{d}. \quad \Omega \text{ is the volume of the unit cell surrounding } \vec{R}. \quad (11.19)$$

These mathematical steps seem a bit awkward, because one diverging sum is being reexpressed as another. But one can use the calculation to do much better. First, notice that in the new formulation, Eq. (11.19), all the divergence of $S(\vec{d})$ is concentrated at $\vec{K} = 0$. However, in order to compute the total energy of the crystal, Eq. (11.14), one has to subtract $S(\vec{d})$ from $S(0)$. The divergent term is exactly the same in both cases and cancels exactly, eliminating the problem of the surface charges. Second, notice that the sum (11.15) converges rapidly when ρ is large, while (11.18) converges rapidly when ρ is small. So write

$$\begin{aligned} S(\vec{d}) &= \int_g^\infty \frac{2 d\rho}{\sqrt{\pi}} \sum_{\vec{R} \neq \vec{0}} e^{-\rho^2 (\vec{d} - \vec{R})^2} \\ &\quad + \int_0^g \frac{2 d\rho}{\sqrt{\pi}} \left[\frac{(\pi)^3}{\rho^3 \sqrt{\pi^3}} \sum_{\vec{K} \neq 0} \frac{1}{\Omega} e^{-K^2/4\rho^2 + i\vec{K} \cdot \vec{d}} - e^{-d^2 \rho^2} \right] \quad (11.20) \\ &= \int_g^\infty \frac{2 d\rho}{\sqrt{\pi}} \sum_{\vec{R} \neq 0} e^{-\rho^2 (\vec{d} - \vec{R})^2} + \sum_{\vec{K} \neq 0} \frac{4\pi}{\Omega K^2} e^{-K^2/4g^2 + i\vec{K} \cdot \vec{d}} - \int_0^g \frac{2 d\rho}{\sqrt{\pi}} e^{-\rho^2 d^2}. \end{aligned} \quad (11.21)$$

One chooses the *separation parameter* g to be anything on the order of a reciprocal lattice vector. Then each of the terms in (11.21) converges exponentially fast. The

Table 11.7. Madelung constants α for the most common ionic crystal structures

Structure	Madelung constant α
Cesium chloride	1.76268
Sodium chloride	1.74757
Wurtzite	1.638704
Zincblende	1.63806

In each case, the total energy of the solid is $-N_{\text{ion pairs}}e^2\alpha/d$, where $N_{\text{ion pairs}}$ is the number of ion pairs, and d is the nearest-neighbor separation.

first sum is a sum of Gaussian integrals, and there are good numerical routines for evaluating them. In fact, inspection of Eq. (11.15) shows that $dS(0) - dS(\vec{d})$ is dimensionless and depends only upon the structure of the lattice vectors \vec{R} on which one sums, not upon the scale of the lattice. The quantity

$$dS(\vec{d}) - dS(0) + 1 \equiv \alpha \quad \begin{array}{l} \text{Be aware that while } S(\vec{d}) - S(0) \text{ is indepen-} \\ \text{dent of the separation parameter } g, \text{ the two} \\ \text{terms individually are not.} \end{array} \quad (11.22)$$

is called the *Madelung constant*, in terms of which the electrostatic energy per ion pair is

$$\frac{\mathcal{E}}{N_{\text{ion pairs}}} = -\alpha \frac{e^2}{d} = -\alpha \frac{14.4 \text{ eV}}{[d/\text{\AA}]}, \quad \begin{array}{l} \text{The cohesive energy for the alkali halides is} \\ \text{conventionally taken to be the energy needed} \\ \text{to separate the ions. Energy needed to pro-} \\ \text{duce separated neutral atoms would involve} \\ \text{adding back the ionization energy and elec-} \\ \text{tron affinity.} \end{array} \quad (11.23)$$

and values for the five most common alkali halides are given in Table 11.7. The table indicates why the cesium chloride and sodium chloride structures are common, but concluding that all alkali halides should adopt the cesium chloride structure would be to take this simple theory too seriously.

An energy of the form Eq. (11.23) would of course cause the solid to collapse, and as in the case of the molecular crystals, it is necessary to add some purely phenomenological term—for example, C/d^{12} —that prevents collapse, giving an energy

$$\frac{\mathcal{E}}{N_{\text{ion pairs}}} = -\alpha \frac{e^2}{d} + \frac{C}{d^{12}}. \quad (11.24)$$

One can fix C by matching the minimum of the potential in Eq. (11.24)

$$d_0 = \left[\frac{12C}{e^2\alpha} \right]^{1/11}, \quad (11.25)$$

to the experimentally observed value.

There is no good reason to choose the exponent 12 apart from the analogy with potentials of noble gases. In order to obtain best fits to experimental data, Pearson (1972) recommends using instead of the integer 12 a different exponent n that depends upon the outermost closed shell of the ion, with values given in Table

Table 11.8. Cohesive energies of ionic compounds with the sodium chloride structure, comparing Eq. (11.26) and experiment

Compound	Experimental d_0 (Å)	Experimental $\mathcal{E}/N_{\text{ion pairs}}$ (eV)	Eq. (11.26) $\mathcal{E}/N_{\text{ion pairs}}$ (eV)
LiF	2.01	10.83	11.45
LiCl	2.57	8.85	8.98
LiBr	2.75	8.51	8.39
LiI	3.01	7.92	7.66
NaCl	2.82	8.18	8.18
NaF	2.32	9.62	9.96
NaBr	2.99	7.81	7.72
NaI	3.24	7.32	7.13
KF	2.67	8.55	8.63
KCl	3.15	7.42	7.33
KBr	3.30	7.16	6.99
KI	3.53	6.74	6.53
RbF	2.83	8.18	8.16
RbCl	3.29	7.17	7.01
RbBr	3.44	6.90	6.70
RbI	3.67	6.52	6.28
AgCl	2.77	9.53	8.32
AgBr	2.89	9.40	7.99

Source: Nagasaka and Kojima (1987).

11.2, but the exercise of allowing the exponent to vary so as to fit data is not very illuminating. When evaluated at d_0 , Eq. (11.24) takes the form

$$\frac{\mathcal{E}}{N_{\text{ion pairs}}} = -\frac{11}{12}\alpha\frac{e^2}{d}. \quad (11.26)$$

The results of this expression are compared with experiment in Table 11.8.

11.4 Metals

Cohesion in metals is more difficult to account for by means of simple arguments than cohesion in ionic crystals. The best hope is in the alkali metals, where there is a simple mental picture of well-localized atomic cores contained in a nearly uniform mist consisting of the outermost s electron. This model has already been discussed within the context of Hartree–Fock and density functional theory in Chapter 9; the main results are contained in Eqs. (9.70), (9.72), and (9.75), and they result in three contributions to the cohesive energy:

Kinetic Energy The largest term is the kinetic energy of the electrons, found in Eq. (9.70) to be

$$\frac{\mathcal{E}_{\text{kin}}}{N} = \frac{3}{5} \frac{\hbar^2 k_F^2}{2m} = \frac{3}{5} \frac{\hbar^2}{2m} \left(\frac{9\pi}{4}\right)^{2/3} \frac{1}{r_s^2} \quad (11.27)$$

This term is purely repulsive and by itself predicts that the density of metals would drop to zero. It must be admitted that an inconsistency is being perpetrated here. The electrostatic attraction of the electrons to the ions will be carried out properly using the fact that the ions are distributed in a lattice, while now the kinetic energy is being computed under the assumption that the electron gas lives in a uniform volume populated by a smeared-out background positive charge.

Exchange Next one must include the exchange energy, which was computed for electrons in a uniform positive background in Eq. (9.72) and found to be

$$\frac{\mathcal{E}_{\text{ex}}}{N} = -\frac{3}{4\pi} e^2 k_F = -\frac{3}{4\pi} e^2 \left(\frac{9\pi}{4}\right)^{1/3} \frac{1}{r_s}. \quad (11.28)$$

Electrostatic Interactions Finally, the electron mist interacts with the ion cores and itself according to the classical potential

$$\begin{aligned} \mathcal{E}_{\text{el}} \equiv & - \int d\vec{r} n(\vec{r}) \sum_{\vec{R}} \frac{e^2}{|\vec{r} - \vec{R}|} + \frac{e^2}{2} \sum_{\vec{R} \neq \vec{R}'} \frac{1}{|\vec{R} - \vec{R}'|} \\ & + \frac{1}{2} \int d\vec{r}_2 d\vec{r}_1 \frac{e^2 n(\vec{r}_1) n(\vec{r}_2)}{|\vec{r}_1 - \vec{r}_2|}. \end{aligned} \quad (11.29)$$

The sums and integrals in Eq. (11.29) can be treated by precisely the same techniques that were used for the ionic crystals, if the electron density n is taken to be a constant $n = N/V$. The result (Problem 4) is that

$$\frac{\mathcal{E}_{\text{el}}}{N} = -\frac{\alpha e^2}{2 r_s}, \quad (11.30)$$

where

$$r_s = \left[\frac{3}{4\pi} \frac{\mathcal{V}}{N} \right]^{1/3} \quad (11.31)$$

is the length scale characterizing the distance between electrons tabulated in Table 6.1, and α is a Madelung constant that takes the values shown in Table 11.9. A glance at this table shows that the electrostatic binding energy of metals is almost totally independent of the crystal structure.

The conventional way to discuss these results is by putting all of them in terms of the electron distance r_s/a_0 , where $a_0 = 0.529 \text{ \AA}$ is the Bohr radius, and measuring energies in units of electron volts per atom. Summing Eqs. (11.30), (11.27), and (11.28) in this way gives

$$\frac{\mathcal{E}}{N} = \left[-\frac{24.35}{(r_s/a_0)} + \frac{30.1}{(r_s/a_0)^2} - \frac{12.5}{(r_s/a_0)} \right] \text{ eV/atom}. \quad (11.32)$$

Table 11.9. Values of the Madelung constant α for the uniform electron gas in various lattices

bcc	fcc	hcp	sc	Diamond
1.791 86	1.791 75	1.791 68	1.760 12	1.670 85

The calculation is discussed in Problem 4. Notice that the first three lattices are almost indistinguishable.

Reference to Table 11.9 shows that there is no way to decide at this stage between the fcc, hcp, and bcc lattices, although there is a minute preference for bcc; the energy does depend upon density alone. However, the estimate in Eq. (11.32) is not at all satisfactory. Its minimum occurs at

$$\frac{r_s}{a_0} = 1.6, \quad (11.33)$$

which is quite far from the values 2 to 6 actually observed for the alkali metals in Table 6.1.

The full apparatus of quantum field theory has been brought to bear on this problem, as discussed in Section 9.4.3. Although full treatment of interacting electrons and ions for realistic electron densities is a formidable theoretical problem, it seems in the end possible to deal with it in an extremely simple way, as discussed by Cohen and Heine (1970), Heine and Weaire (1970), Cottrell (1988), or Sutton (1993).

11.4.1 Use of Pseudopotentials

The problem lies not in the inconsistencies regarding the computation of the kinetic and exchange energies, but in the treatment of interactions between conduction electrons and ionic cores. Ionic cores are surrounded by tightly bound electrons. The conduction electrons must avoid them because of the Pauli exclusion principle, which requires the conduction electron wave functions to be orthogonal to those hugging the core. Coulomb repulsion also keeps the two sets of electrons away from each other.

The pseudopotential was introduced previously as a way to organize experimental and computational information about conduction electrons in a compact and physical form. A large number of measurements of different types can be explained to good accuracy by the empty-core pseudopotential, which has the shape depicted in Figure 10.1. The essential point is that with just a few fitting parameters obtained either from experiment or calculations, it is possible to get a good estimate of phenomena ranging from phonon spectra and optical absorption, to superconducting transition temperatures. So it makes sense to try to apply the idea to cohesion. To reduce the number of fitting parameters, take ions to have potentials of the form

$$U(r) = \begin{cases} 0 & \text{for } r < R_c \\ -Ze^2/r & \text{for } r > R_c. \end{cases} \quad \begin{array}{l} \text{The screening length is made infinite, and } U_0 \\ \text{is set to } Ze^2/R_c, \text{ where } Z \text{ is the ionic charge.} \end{array} \quad (11.34)$$

Table 11.10. Pseudopotential radii compared with measured values

Element	R_c (Å)	r_s/a_0 , Eq. (11.38)	r_s/a_0 , measured
Li	0.92	4.09	3.27
Na	0.96	4.23	3.99
K	1.20	5.04	4.95
Rb	1.38	5.65	5.30
Cs	1.55	6.23	5.75

Radii R_c are obtained for example from optical measurements described in Problem 2 and r_s/a_0 is obtained from Eq. (11.38). Source: Cottrell (1988), p. 68.

The main change in cohesive energy produced by use of Eq. (11.34) is that in the Coulomb attraction of the electron cloud to the ions, one must add back the energy

$$\frac{\mathcal{E}_{ps}}{N} = \int_0^{R_c} d\vec{r} \frac{N e^2}{\mathcal{V} r} = \frac{N}{\mathcal{V}} 2\pi e^2 R_c^2 \quad (11.35)$$

$$= \frac{3}{4\pi r_s^3} 2\pi e^2 R_c^2 = 41 \frac{a_0 R_c^2}{r_s^3} \text{ eV/atom} \quad (11.36)$$

$$\Rightarrow \frac{\mathcal{E}}{N} = \left[-\frac{24.35}{(r_s/a_0)} + \frac{30.1}{(r_s/a_0)^2} - \frac{12.5}{(r_s/a_0)} + 41 \frac{a_0 R_c^2}{r_s^3} \right] \text{ eV/atom.} \quad (11.37)$$

Solving Eq. (11.37) to minimize energy as a function of r_s gives

$$r_s/a_0 = \sqrt{11.9[R_c/\text{Å}]^2 + .667} + 0.817. \quad (11.38)$$

Equation (11.38) is compared with experiment in Table 11.10. One can also compare bulk modulus B . For Na, $B = 1.4 \cdot 10^{10} \text{ J m}^3$ versus the experimental value of $B = 0.64 \cdot 10^{10} \text{ J m}^3$, so at least the orders of magnitude are correct. It is not possible to compare Eq. (11.37) directly with the actual cohesive energy of a metal, because as $r_s \rightarrow \infty$ the system goes to a collection of separated ions with a vanishingly thin electron gas between them; in other words, the atoms have been ionized. In reality, if the ions are pulled far enough from one another, the conduction electrons land back on the ions, so the zero of energy one obtains for $r_s \rightarrow \infty$ should be greater by the ionization energy than the actual “zero” energy state of well separated atoms.

11.5 Band Structure Energy

All of the calculated radii in Table 11.10 are about 10% too large. To improve on this result requires that one go about the process of calculating electron kinetic and exchange energy in the presence of the ions more accurately. The whole machinery of band structure calculations, which has been avoided until now, naturally begins to fire up. The basic reason for the inaccuracy and its sign can, however, be obtained without any calculation. The pseudopotential is weak, so the appropriate

calculation to have in mind is the weak perturbation theory of Section 8.2. There it was shown that the effect of a weak potential was to open up gaps in the free electron $\mathcal{E}(\vec{k})$ curves at all \vec{k} that lie at the edge of the Brillouin zone. Let \vec{K} be the reciprocal lattice vector that connects \vec{k} to its counterpart on the other side of the zone. At the inside edge of the zone, the energy levels go down by $U_{\vec{K}}$, on the outside edge of the zone they go up by $U_{\vec{K}}$, where U is the (weak) pseudopotential, and the net effect is that the energy of the electron gas goes down by an amount proportional to $|U_{\vec{K}}|^2$. This contribution to the energy of a system is called the *band structure energy*, and it is the dominant way in which details of the lattice structure make themselves known to the cohesive energy. Without detailed calculation, one can see that the first effect of the band structure energy should be to expand or shrink the lattice in whatever way makes $U_{\vec{K}}$ increase slightly. For all of the metals in Table 11.10, the pseudopotential is positive and of positive slope at the smallest reciprocal lattice vectors, so $U_{\vec{K}}$ increases if \vec{K} increases, and this leads to a tendency for the size of the lattice to shrink. For some other elements—for example Ga and In—estimates such as Eq. (11.38) do in fact give too small an answer, and this result can be traced to the fact that now $|U_{\vec{K}}|^2$ increases if \vec{K} decreases instead.

11.5.1 Peierls Distortion

The principle that lattices rearrange themselves to suit the desires of the conduction electrons moving through them is most easily illustrated by a one-dimensional calculation due to Peierls (1955), pp. 108–112.

Suppose one has a one-dimensional lattice, which when perfectly periodic, has minimum energy for some lattice constant a and for which the elastic energy penalty that must be paid to move atom n a distance Δ_n away from its lattice site is

$$\frac{1}{2}aY\Delta_n^2. \quad \begin{array}{l} Y \text{ has dimensions of energy per volume and} \\ \text{can be understood as Young's modulus for the} \\ \text{one-dimensional chain.} \end{array} \quad (11.39)$$

Suppose that the displacement of atoms takes the form illustrated in Figure 11.4

$$\Delta_n = \Delta_G \cos Gna. \quad \begin{array}{l} G \text{ is a wave vector describing atomic displacements.} \\ 2\pi/G \end{array} \quad (11.40)$$

Figure 11.4. Setting for the calculation of the Peierls distortion. An initially periodic lattice acquires a periodic modulation, which acts as a separate, additive potential for the electrons.

Now, populate this lattice with (noninteracting) conduction electrons. The lattice of period a most affects the energies of electrons whenever the Bloch vector k of an electron is close to $\pm\pi/a$, or other points on the zone boundaries. The electrons also will be affected by the modulation Eq. (11.40), which has period $2\pi/G$,

and which should add to the Hamiltonian for the electrons a term of the form

$$U \cos Gx = (\Delta_G u_0/a) \cos Gx. \quad \text{Thus defining } u_0, \text{ since the interaction energy should be proportional to } \Delta_G. \quad (11.41)$$

To calculate the constant U , one needs a theory for the interaction between electrons and lattice distortions. Such a theory will be needed in later chapters, particularly for the study of superconductivity, but for the moment it is enough to view the lattice distortion as a periodic potential of period $2\pi/G$, and Fourier amplitude U . Assuming that G is far from $2\pi/a$, one can calculate the effect of Eq. (11.41) upon the electrons. According to Eq. (8.22), electrons with indices k in the neighborhood of $G/2$ have energies

$$\mathcal{E} = \frac{1}{2}(\mathcal{E}_k^0 + \mathcal{E}_{k-G}^0) \pm \sqrt{(\mathcal{E}_k^0 - \mathcal{E}_{k-G}^0)^2/4 + |U|^2}. \quad (11.42)$$

The goal is now to see if there is some value of G that is particularly effective in allowing an assembly of conduction electrons to lower its energy; one can guess the correct answer without detailed calculation. If $G > 2k_F$, then an energy gap opens above the Fermi surface, without much changing the energies of any of the electrons below. If $G < 2k_F$, an energy gap opens below the Fermi surface. Electrons below the gap have their energies lowered as indicated by Eq. (11.42), but those above it have their energies raised by nearly an equal amount, and the two effects cancel out. The best arrangement is $G = 2k_F$. With this choice, the gap opens up right at the Fermi surface, and all nearby electrons have their energy lowered by order $|U|$. In particular, the total energy of many electrons obeying Eq. (11.42) minus the energy \mathcal{E}_k^0 they would have if the modulation (11.41) were not present at all is

$$L \int_{-k_F}^{k_F} \frac{dk}{\pi} \left\{ \frac{1}{2}(\mathcal{E}_{k-G}^0 - \mathcal{E}_k^0) - \sqrt{(\mathcal{E}_{k-G}^0 - \mathcal{E}_k^0)^2/4 + |U|^2} \right\} \quad (11.43)$$

\mathcal{E}_k^0 is given by Eq. (6.8). L is the total length of the system, and $1/\pi$ is the density of states.

$$= L \int_{-k_F}^{k_F} \frac{dk}{\pi} \left\{ \frac{\hbar^2}{4m} ([k - 2k_F]^2 - k^2) - \sqrt{\left(\frac{\hbar^2}{4m} ([k - 2k_F]^2 - k^2)\right)^2 + |U|^2} \right\} \quad (11.44)$$

$$= \frac{2L}{\pi} k_F \left\{ 2\mathcal{E}_{k_F}^0 - \sqrt{|U|^2/4 + (2\mathcal{E}_{k_F}^0)^2} - \frac{|U|^2}{8\mathcal{E}_{k_F}^0} \sinh^{-1}(4\mathcal{E}_{k_F}^0/|U|) \right\}. \quad (11.45)$$

Although the conduction electrons lower their energy by distorting the lattice, this distortion costs elastic energy, and it is not immediately clear on balance that it will occur. The cost in elastic energy is

$$\frac{L}{4} \Delta_G^2 Y. \quad \text{A factor of } \frac{1}{2} \text{ comes from the average of the cosine in Eq. (11.41). Another factor of } \frac{1}{2} \text{ was already present in Eq. (11.39).} \quad (11.46)$$

Add together Eqs. (11.45) and (11.46), and substitute $\Delta_G u_0/a$ for U as in Eq. (11.41). Then Taylor expand to leading order in Δ_G , which indeed turns out to be very small, set the result equal to zero and solve for $\Delta_{G=2k_F}$ to find

$$\Delta_{2k_F} = \frac{8a\mathcal{E}_{k_F}^0}{|u_0|} \exp \left\{ \frac{-\pi\mathcal{E}_{k_F}^0 a^2 Y/k_F}{|u_0|^2} \right\}. \quad (11.47)$$

For small u_0 , the amount of distortion Δ_{2k_F} is exponentially small. In two- and three-dimensional crystals, the analog of the argument just given predicts $\Delta = 0$, because the energy cost of elastic distortion outweighs the gains from accommodating the electrons. The basic principle, however, that metals choose lattice structures to bring the Fermi surface as near a Brillouin zone edge as possible is rather general. Furthermore, three-dimensional solids can exhibit a closely related instability called a *charge density wave*, reviewed by Gruner (1988) and Thorne (1996).

Example: Brass. Consider the changes in structure that occur as one adds zinc to copper to form brass. Pure copper is fcc, and its conduction electrons consist of a nearly full d -band that is hybridized with one $4s$ electron. Zinc sits just to the right in the periodic table, with one more s electron. As a simple mental model, treat copper as monovalent, and treat each added zinc atom as the source of one additional conduction electron. In accord with the discussion of the Peierls distortion, zinc–copper solutions stand to gain energy by bringing the Fermi surface close to the Brillouin zone boundary whenever possible. Assuming that the Fermi surface is always essentially spherical, the system accomplishes this task by switching to new lattice structures. As shown in Problem 2, for an fcc crystal, the Fermi surface first contacts the Brillouin zone boundary for a density of 1.36 electrons per lattice site. With 36% atomic percent of zinc in copper, the solid switches from an fcc structure to the bcc structure. For a bcc solid, the Fermi surface first contacts the Brillouin zone for a density of around 1.5 electrons per site. And in fact, at an atomic density of 46% zinc, the solid has another change of lattice constant to a rather complicated unit cell involving 52 atoms.

11.5.2 Structural Phase Transitions

It is a rule rather than an exception that solids change crystal structure as a function of temperature. The consequences of structural change are particularly interesting in cases where the change from one crystal structure to another involves a sudden change in size or shape of the unit cell. A huge single crystal could change its overall macroscopic shape, but the crystallites of a polycrystal cannot do so and remain attached to one another. In a *martensitic transformation*, reviewed by Roitburd (1978), unit cells group themselves in orientations of varying symmetry so as to make the best of the situation, as shown in Figure 11.5.

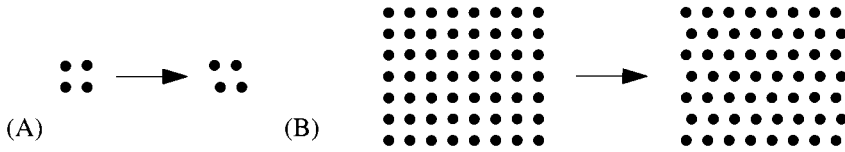


Figure 11.5. When a unit cell makes the transition shown in (A), a crystallite can retain its overall dimensions by ordering as shown in (B); this accommodation by twinning is an example of a martensitic transformation.

11.6 Hydrogen-Bonded Solids

Compounds involving hydrogen are of such variety and importance that they rightly constitute a class of their own. Hydrogen bonds are directional and flexible and can break and reform at energies characteristic of room temperature. Hydrogen-bonded solids, including such primitive examples as H_2O , often have huge numbers of nearly equivalent ground states. Studying the structures of these solids leads into organic chemistry and biology. Viewing biology as a cohesive energy problem is not likely to be profitable, because an organism in its ground state has died. Nevertheless, hydrogen-bonded structures pose fascinating problems in materials science. For introductions, see Desiraju (1989) and *Chemistry of Materials* (1994), vol. 6.

11.7 Cohesive Energy from Band Calculations

Band structure calculations are designed to determine ground state structures, so it is worth asking how well they do. Figure 11.6 shows the result of using plane wave pseudopotential codes to look for the ground-state crystal structure of aluminum. The calculation is carried out by imposing various crystal structures and various lattice constants, and then carrying out a self-consistent energy calculation for each structure. The results are satisfactory. The predicted lattice constant is 4.02 \AA , compared to the experimental value of 4.04 \AA . In addition, both bcc and hcp lattices have higher energy than fcc, in agreement with experiment. This degree of agreement is indicative of the success of density functional theory in predicting ground-state crystal structures.

Scaling Form for Cohesive Energy. Rose et al. (1984) have conducted a systematic survey of the cohesive energies of elemental metals, using band structure codes, and found a surprising regularity in the results. When properly scaled, cohesive energy as a function of lattice constant is a universal function. To describe this function, first define r_W , the radius of the *Wigner–Seitz sphere*, by

$$\frac{4\pi}{3}r_W^3 = \frac{V}{N} \quad \begin{array}{l} r_W \text{ is similar to the parameter } r_s, \text{ but it can} \\ \text{be defined without recourse to the rather ar-} \\ \text{bitrary parameter } Z \text{ describing the number of} \\ \text{conduction electrons per atom.} \end{array} \quad (11.48)$$

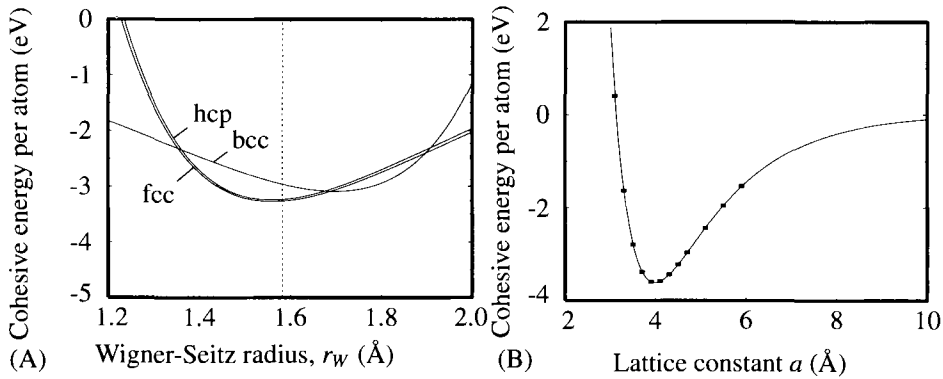


Figure 11.6. (A) Comparison of cohesive energy of fcc, bcc, and hcp structures for aluminum as a function of the Wigner–Seitz radius r_W . The experimental value of $r_W = 1.583$ is indicated by the dotted line. The fcc lattice has the lowest energy, but lies only a minute amount below hcp. The bcc lattice has considerably higher energy. (B) Cohesive energy of fcc aluminum computed as a function of lattice constant a (squares), compared with Eq. (11.50) (solid line). Computations were performed with VASP of Kresse and Hafner (1994) and Kresse and Furthmüller (1996). The computations measure all energies relative to a rather arbitrary zero, so the fit to Eq. (11.50) is needed to determine the cohesive energy, by extrapolating to widely separate atoms and calling the result the zero of energy.

For each element, define a scaled length

$$a_* = \eta \left(\frac{r_W}{r_{W0}} - 1 \right), \quad (11.49)$$

where r_{W0} is the radius of the Wigner–Seitz sphere of the metal in equilibrium, r_W is its radius for expanded or contracted crystals, and η is a dimensionless number that characterizes the anharmonicity of each element. Upon choosing η appropriately and letting \mathcal{E}_0 be the equilibrium cohesive energy of each element, a wide variety of different elements have a cohesive energy described quantitatively by the fitting function

$$\mathcal{E}(r_W) = \mathcal{E}_0 e^{-a_*} \left(-1 - a_* - 0.05a_*^3 \right). \quad (11.50)$$

Table 11.11 records values of r_{W0} and η for a number of metals. These data can be used to determine pressure and bulk modulus over a wide range of lattice parameters, and they are in good accord with experimental measurements of metals under large pressures.

11.8 Classical Potentials

The molecular dynamics and Monte Carlo calculations described in Section 5.4 rely upon a functional giving the energy of a solid as a function of all the nuclear positions. This functional exists; it is just the ground-state energy

$$\mathcal{E} = \langle \Psi | \hat{\mathcal{H}}(\vec{R}_1 \dots \vec{R}_N) | \Psi \rangle \quad (11.51)$$

Table 11.11. Wigner–Seitz radius r_{w0} , scaling parameter η , and cohesive energy \mathcal{E}_0 for selected elements

El.	r_{w0} (Å)	η	\mathcal{E}_0 (eV)	El.	r_{w0} (Å)	η	\mathcal{E}_0 (eV)	El.	r_{w0} (Å)	η	\mathcal{E}_0 (eV)
Ag	1.60	5.94	2.96	Fe	1.41	5.16	4.29	Pt	1.53	6.47	5.85
Al	1.58	4.71	3.34	Gd	1.99	4.27	4.14	Rb	2.75	4.18	0.86
Au	1.59	6.75	3.78	Ge	1.76	5.05	3.87	Re	1.52	6.15	8.10
Ba	2.46	4.41	1.86	Hf	1.74	4.66	6.35	Ru	1.48	6.04	6.62
Be	1.25	4.01	3.33	In	1.84	5.11	2.60	Si	1.68	4.88	4.64
Ca	2.18	4.52	1.83	Ir	1.50	6.52	6.93	Ta	1.62	4.92	8.09
Cd	1.73	8.08	1.16	K	2.57	3.94	0.94	Th	1.99	4.12	5.93
Ce	2.02	3.11	4.77	Li	1.72	3.10	1.65	Ti	1.62	4.76	4.86
Co	1.39	5.31	4.39	Mg	1.77	5.60	1.53	Tl	1.90	5.74	1.87
Cr	1.42	5.59	4.10	Mo	1.55	5.85	6.81	V	1.49	4.81	5.30
Cs	2.98	4.17	0.83	Na	2.08	3.70	1.13	W	1.56	5.69	8.66
Cu	1.41	5.30	3.50	Nb	1.63	4.84	7.47	Y	1.99	4.23	4.39
Dy	1.96	4.85	3.10	Ni	1.38	5.11	4.44	Yb	1.99	3.94	1.60
Er	1.94	4.94	3.30	Pb	1.93	6.37	2.04	Zn	1.54	7.16	1.35
Eu	2.27	4.75	1.80	Pd	1.52	6.41	3.94	Zr	1.77	4.48	6.32

El.= Element. Source: Rose et al. (1984).

of N nuclei, and their accompanying electrons, viewed as a function of ionic positions. Of course, every time a nucleus moves, it is necessary to solve the electron problem over again from scratch. The force on atom l is then

$$\vec{F}_l = -\frac{\partial \mathcal{E}}{\partial \vec{R}_l}. \quad (11.52)$$

When deviations of atoms from equilibrium are small, the subject can be developed systematically and will occupy Chapter 13. For the purposes of molecular dynamics, small deviations are not sufficient, but it is impossible to evaluate Eq. (11.51) exactly. One possibility is to guess that the energy takes the form of Eq. (11.1), and to choose a function for ϕ that reproduces some desired feature of experiment or calculation, such as ground-state crystal structure or melting temperature. Potentials of the two-body form are often clearly inadequate. For example, there does not exist any potential $\phi(r)$ for which the diamond structure is the ground state, which rules out study of silicon and germanium in addition to carbon. The diamond structure can, however, be made the stable ground state of a classical potential if one adds to the energy functional some terms that depend upon angles between bonds. The angle θ in Figure 11.7 is given by $\cos^{-1}[(\vec{R}_1 - \vec{R}_2) \cdot (\vec{R}_3 - \vec{R}_2)]$; terms that are functions of angles depend simultaneously upon locations of three atoms and thus are called *three-body potentials*. Another possibility is suggested by the energy functionals of Section 11.4, which depend upon the overall density

of electrons; if terms of this sort are added to an energy functional, they depend upon the total volume occupied by the atoms, which cannot be expressed in terms either of pair potentials or three-body potentials.

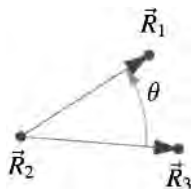


Figure 11.7. Any term depending upon the angle between two bonds must depend simultaneously upon the coordinates of three atoms and therefore introduces triplet or three-body terms into the energy.

By the time that potentials of this type have been employed in enormous computer programs, it is easy to forget that the potentials themselves are not especially well grounded, and represent a mix of functional forms suggested by calculation, constraints provided by experiment, and calculational convenience. Classical potentials often do not give reliable results for physical quantities they were not tuned to get right. For example, a widely used potential for studying silicon was proposed by Stillinger and Weber (1985), involving two- and three-body terms. Its parameters are chosen to give the melting temperature of silicon correctly, but the potential gets the density change at melting wrong by a factor of two and does not correctly predict vibrational spectra or surface reconstructions. A particularly large number of potentials has been proposed for silicon; it is difficult to know how to choose between them. These and other matters related to the construction of classical potentials are discussed by Carlsson (1990).

Problems

1. **Sums for noble gases:** Compute the sums A_6 and A_{12} to five decimal places for an fcc lattice, and verify the results in Table 11.4.
2. **Zinc in copper:** Copper is a monovalent fcc nearly-free electron metal. Zinc is an hcp divalent metal. In small quantities, zinc mixes substitutionally with copper, its main effect being to increase the electron concentration.
 - (a) Find the relationship between electron density n and the Fermi wave vector k_F within the nearly free electron approximation.
 - (b) Still working in the nearly free electron approximation, assume that the zinc-copper mixture will undergo a phase transition to bcc as soon as the Fermi sphere first touches some point on the edge of the Brillouin zone. Show that the transition occurs at 36% zinc. Remember that in an fcc conventional unit cell of lattice constant a there are four ions.
 - (c) As the concentration of zinc further increases, another phase transition next occurs when the Fermi sphere intersects the Brillouin zone of the bcc lattice. What is this second concentration of zinc?

3. Quantum view of van der Waals force:

- (a) Consider two widely separated hydrogen atoms. Let $\hat{\mathcal{H}}_1$ and $\hat{\mathcal{H}}_2$ be the Hamiltonians for the separate, unperturbed atoms, and let \vec{R} be the distance vector between them. Consider now the perturbation

$$\hat{\mathcal{H}}_I = e^2 \left[\frac{1}{R} - \frac{1}{|\hat{R}_1 - \vec{R}|} - \frac{1}{|\hat{R}_2|} + \frac{1}{|\hat{R}_1 - \hat{R}_2|} \right], \quad (11.53)$$

where \hat{R}_1 and \hat{R}_2 are the operators for the positions of the electrons at atoms 1 and 2 (there is no harm done in regarding the electrons as distinguishable, because they are widely separated).

Show that at first order in perturbation theory, the effect of the perturbation is exponentially small, because the ground state of the hydrogen atom is spherically symmetric, and the charge distributions of the two atoms hardly overlap.

- (b) Argue that at second order in perturbation theory, all contributions to the relevant integrals are negligible unless the electrons are very close to their respective atoms:

$$|\hat{R}_1| \ll R \text{ and } |\hat{R}_2 - \vec{R}| \ll R. \quad (11.54)$$

In this case, it is valid to expand Eq. (11.53) to leading (second) order in the two small quantities appearing in Eq. (11.54). Show that as a result the perturbation takes the form

$$-e^2 \left[\frac{3(\hat{R}_1 \cdot \vec{R})([\hat{R}_2 - \vec{R}] \cdot \vec{R})}{R^5} - \frac{\hat{R}_1 \cdot [\hat{R}_2 - \vec{R}]}{R^3} \right]. \quad (11.55)$$

- (c) Show that the leading term in the interaction of the two hydrogen atoms is negative and varies as R^{-6} .

4. Ewald summation for metals:

- (a) Show that when the electron density n is constant, Eq. (11.29) can be rewritten as

$$N \frac{e^2}{2} \left[S(0) - \frac{1}{\Omega} \int_{\text{cell}}^{\text{unit}} d\vec{r} \left[S(\vec{r}) + \frac{1}{r} \right] \right], \quad (11.56)$$

where S is defined by Eq. (11.14).

- (b) Show finally that if $S(0)$ is given by Eq. (11.21) then Eq. (11.56) can be rewritten as

$$N \frac{e^2}{2} \left[S(0) - \frac{\pi}{\Omega g^2} \right]. \quad (11.57)$$

5. **Ewald summation in one dimension:** Suppose that one has a collection of N charged spheres containing charge of magnitude $q_1 \dots q_N$. Overall the spheres are electrically neutral; $\sum_{i=1}^N q_i = 0$. Make many copies of these

spheres, and evenly space them along a line so that the sequence of charges q_l repeats periodically.

The energy per unit cell of such a collection of charges is

$$\frac{1}{2} \sum_{j \neq 0} \sum_{l=1}^N \frac{q_l q_{j+l}}{|j|}. \quad \text{Sum over all positive and negative } j \neq 0. \quad (11.58)$$

The goal of this problem is to use the technique of Ewald summation to rewrite Eq. (11.58) in a form suitable for rapid numerical evaluation. It is useful to define

$$q_k = \sum_l e^{2\pi i k l / N} q_l. \quad \text{Both } l \text{ and } k \text{ are integers.} \quad (11.59)$$

The final answer should have the form

$$\sum_k E_1 \left(\left[\frac{\pi k}{Ng} \right]^2 \right) F_k - \frac{g}{\sqrt{\pi}} \sum_{k=1}^{N-1} \frac{|q_k|^2}{N} + \sum_{j \neq 0} \sum_{l=1}^N \frac{[1 - \text{erf}(gj)]}{|j|} G_{l,j}, \quad (11.60)$$

with

$$E_1(x) \equiv \int_1^\infty \frac{dy}{y} e^{-yx}. \quad (11.61)$$

Find the functions F_k and $G_{l,j}$.

6. Friedel model of d bands:

- Consider the tight-binding model, Eq. (8.67), and specialize to the case of one dimension, with nearest-neighbor interactions. Write down the dispersion relation for energy as a function of wave number, and from it find the density of energy states $D(\mathcal{E})$.
- Friedel's model for electrons in a d band replaces the true three-dimensional density of states $D(\mathcal{E})$ with a function of the form

$$D(\mathcal{E}) \approx \frac{10}{2\mathcal{W}} \theta(\mathcal{E} + \mathcal{W}) \theta(\mathcal{W} - \mathcal{E}). \quad (11.62)$$

Estimate the relation between \mathcal{W} and the coefficient of the hopping coefficient t in Eq. (8.67) appropriate to an fcc metal, assumed to have only nearest-neighbor interactions, in three dimensions; set $2\mathcal{W}$ equal to the bandwidth of the tight-binding model.

- Making use of Eq. (11.62), obtain a simple expression for the cohesive energy of the d band solids as a function of the number Z of electrons per atom in the band.

References

- N. W. Ashcroft and N. D. Mermin (1976), *Solid State Physics*, Saunders, Fort Worth, TX.
- N. Bernardes (1958), Theory of solid Ne, A, Kr, and Xe at 0°K, *Physical Review*, **112**, 1534–1539.
- A. E. Carlsson (1990), Beyond pair potentials in elemental transition metals and semiconductors, *Solid State Physics: Advances in Research and Applications*, **43**, 1–91.
- Chemistry of Materials (1994), volume 6
- M. L. Cohen and V. Heine (1970), The fitting of pseudopotentials to experimental data and their subsequent application, *Solid State Physics: Advances in Research and Applications*, **24**, 37–248.
- A. H. Cottrell (1988), *Introduction to the Modern Theory of Metals*, The Institute of Metals, London.
- G. Desiraju (1989), *Crystal Engineering: The Design of Organic Solids*, Elsevier, Amsterdam.
- J. Emsley (1998), *The Elements*, 3rd ed., Clarendon Press, Oxford.
- G. Gruner (1988), The dynamics of charge-density waves, *Reviews of Modern Physics*, **60**, 1129–1181.
- V. Heine and D. Weaire (1970), Pseudopotential theory of cohesion and structure, *Solid State Physics: Advances in Research and Applications*, **24**, 250–463.
- J. O. Hirschfelder, C. F. Curtiss, and R. B. Bird (1954), *Molecular Theory of Gases and Liquids*, John Wiley and Sons, New York.
- H. Hotop and W. C. Lineberger (1975), Binding energies in the atomic negative ions, *Journal of Physical and Chemical Reference Data*, **4**, 539–576.
- W. Hume-Rothery (1931), *The Metallic State: Electrical Properties and Theories*, Clarendon Press, Oxford.
- J. D. Joannopoulos and M. L. Cohen (1976), Theory of short-range order and disorder in tetrahedrally bonded semiconductors, *Solid State Physics: Advances in Research and Applications*, **31**, 71–148.
- M. Körling and J. Häglund (1992), Cohesive and electronic properties of transition metals: The generalized gradient approximation, *Physical Review B*, **45**, 13 293–13 297.
- G. Kresse and J. Furthmüller (1996), Efficiency of *ab-initio* total energy calculations for metals and semiconductors using a plane-wave basis set, *Computational Materials Science*, **6**, 15–50.
- G. Kresse and J. Hafner (1994), *Ab initio* molecular-dynamics simulation of the liquid-metal-amorphous-semiconductor transition in germanium, *Physical Review B*, **49**, 14 251–14 269.
- L. D. Landau and E. M. Lifshitz (1980), *Statistical Physics, Part 1*, 3rd ed., Pergamon Press, Oxford.
- F. Liu, S. H. Garofalini, R. D. King-Smith, and D. Vanderbilt (1993), First-principles studies on structural properties of β -cristobalite, *Physical Review Letters*, **70**, 2750–2753.
- S. Nagasaka and T. Kojima (1987), Interionic potentials based on the charge-transfer model for ionic and partially ionic substances. I. Alkali halides, *Journal of the Physical Society of Japan*, **56**, 408–414.
- W. B. Pearson (1972), *The Crystal Chemistry and Physics of Metals and Alloys*, Wiley-Interscience, New York.
- R. E. Peierls (1955), *Quantum Theory of Solids*, Clarendon Press, Oxford.
- D. G. Pettifor (1987), A quantum-mechanical critique of the Miedema rules for alloy formation, *Solid State Physics: Advances in Research and Applications*, **40**, 43–92.
- P. H. T. Philipsen and E. J. Baerends (1996), Cohesive energy of 3d transition metals: Density functional theory atomic and bulk calculations, *Physical Review B*, **54**, 5326–5333.
- A. L. Roitburd (1978), Martensitic transformation as a typical phase transformation in solids, *Solid State Physics: Advances in Research and Applications*, **33**, 317–390.
- J. H. Rose, J. R. Smith, R. Guinea, and J. Ferrante (1984), Universal features of the equation of state of metals, *Physical Review B*, **29**, 2963–2969.
- H. Schlosser (1992), Cohesive energy-lattice constant and bulk modulus-lattice constant relationships: Alkali halides, Ag halides, Tl halides, *Journal of Physics and Chemistry of Solids*, **53**, 855–856.

- F. H. Stillinger and T. A. Weber (1985), Computer simulation of local order in condensed phases of silicon, *Physical Review B*, **31**, 5262–5271.
- R. Stumpf and M. Scheffler (1994), Simultaneous calculation of the equilibrium electronic structure and its ground state using density functional theory, *Computer Physics Communications*, **79**, 447–465. The code is available in source from the CPC program library.
- A. P. Sutton (1993), *Electronic Structure of Materials*, Clarendon Press, Oxford.
- R. E. Thorne (1996), Charge-density-wave conductors, *Physics Today*, **49**(5), 42–47.
- M. P. Tosi (1964), Cohesion of ionic solids in the Born model, *Solid State Physics: Advances in Research and Applications*, **16**, 1–120.
- R. W. G. Wyckoff (1963–1971), *Crystal Structures*, 2nd ed., John Wiley and Sons, New York.
- J. M. Zuo, M. Kim, M. O’Keeffe, and J. C. H. Spence (1999), Direct observation of *d*-orbital holes and Cu-Cu bonding in Cu₂O, *Nature*, **401**, 49–51.

12. Elasticity

12.1 Introduction

The theory of elasticity describes the energy needed to deform a solid body, provided that the wavelength of the deformations is large in comparison with any microstructure. The equations are largely derived through considerations of symmetry, depending in the end upon a small number of parameters that can be determined either from experiment or from atomic-level calculation.

12.2 Nonlinear Elasticity

Nonlinear elasticity describes reversible deformation of solid objects without assuming that the deformation is small. In order to describe deformation, one has to decide that in a certain state a piece of material is not deformed. This corresponds to the material sitting quietly without any external forces acting upon it, and in this situation it is in the *reference state*. Describe locations of material points in this reference state with the variable \vec{r} . Now grab the solid, twist it, pull it, bend it. Each material point originally located at \vec{r} is now at a new location $\vec{s}(\vec{r})$.

$$\begin{array}{ccc} \text{Before deformation} & \text{After deformation} & \\ \vec{r} & \vec{s}(\vec{r}) = \vec{r} + \vec{u}(\vec{r}). & (12.1) \end{array}$$

The theory of elasticity assumes that the new energy of the object depends only on the change in distance of material points that were originally close to one another. For example, one can think about point \vec{r} and its nearby neighbor $\vec{r} + d\vec{r}$. The original squared distance between these two points is $d\vec{r} \cdot d\vec{r} = dr_x^2 + dr_y^2 + dr_z^2$. After deformation, the new distance is

$$|\vec{s}(\vec{r} + d\vec{r}) - \vec{s}(\vec{r})|^2 \approx \left| \frac{\partial \vec{s}}{\partial r_x} dr_x + \frac{\partial \vec{s}}{\partial r_y} dr_y + \frac{\partial \vec{s}}{\partial r_z} dr_z \right|^2 \quad (12.2)$$

$$= \sum_{\alpha\beta} g_{\alpha\beta} dr_\alpha dr_\beta \quad \text{where} \quad g_{\alpha\beta} \equiv \frac{\partial \vec{s}}{\partial r_\alpha} \cdot \frac{\partial \vec{s}}{\partial r_\beta}, \quad \alpha \text{ and } \beta \text{ range over } x, y, \text{ and } z. \quad (12.3)$$

The tensor $g_{\alpha\beta}$ is the *metric tensor*. The change in square distance caused by deformation can be found from the *Lagrangian strain tensor* $E_{\alpha\beta}$,

$$\frac{1}{2} \left[|\vec{s}(\vec{r} + d\vec{r}) - \vec{s}(\vec{r})|^2 - |d\vec{r}|^2 \right] \quad \text{The factor of } 1/2 \text{ is conventional.} \quad (12.4)$$

$$= \sum_{\alpha\beta} \frac{1}{2} [g_{\alpha\beta} - \delta_{\alpha\beta}] dr_\alpha dr_\beta \equiv \sum_{\alpha\beta} E_{\alpha\beta} dr_\alpha dr_\beta \quad (12.5)$$

When all distances between nearby points are unchanged, for example by moving a body rigidly from one place to another or rotating it, the Lagrangian strain tensor vanishes. Otherwise it keeps track how much material at each point has been stretched in each direction.

12.2.1 Rubber Elasticity

Most solids are stiff, and deform irreversibly when stretched more than a fraction of a percent, justifying some further simplifications of elastic theory that will occupy succeeding sections. An exception to this general observation is rubber, which can stretch to five or eight times its original length and then snap back to its original form. Thus when using strain tensors to describe rubber, they appear in their full nonlinear glory.

Vulcanized rubber is constituted from a densely intertwined network of polymers that link together at occasional intervals, as shown in Figure 12.1. As described in Section 5.5.8, polymer strands act like springs, and because the polymers making up rubber are typically 350,000 units long and travel a few hundred units between linking points, they can be extended a long way without undergoing permanent damage.

One other experimental observation about rubber is crucial. All the low-energy deformations keep the density of rubber fixed. Rubber can be sheared easily, and it can be stretched, but if stretched in one direction it contracts in other directions so as to keep the volume per molecule fixed. In this respect, rubber resembles an incompressible fluid, such as water. This fact can be accounted for by modifying the free energy of a polymer mixture given by Eq. (5.73), to read

$$\mathcal{F} = \mathcal{F}_0 + k_B T \left[\sum_{j=1}^{N_p} \frac{\mathcal{R}_j^2}{\mathcal{R}_1^2} + \mathcal{V} B n^2 + \mathcal{V} C n^3 + \dots \right]. \quad (12.6)$$

Write the free energy in terms of the density n and volume \mathcal{V} . The sum over j is taken over all the N_p polymers in the rubber. In Eq. (5.73) there is a term involving $1/\mathcal{R}_j^2$ that is omitted here since the monomer density in rubber is so high that the argument producing it is invalid.

The fact that rubber preserves density will follow if Bn and Cn^2 in Eq. (12.6) have magnitude much larger than 1, and B is negative, so that the polymer mixture collapses to a high density given by Eq. (5.77). Any deformations of the rubber that involve changing the density n increase the energy much more than changes that do not.

The basic experimental facts, then, are that the energy of rubber varies as the square of how far it has been stretched. However, the energy is subject to the constraint that the density of the rubber remain constant. In addition, since rubber is isotropic, its energy should be invariant to changes of coordinate axes. Turning now to the Lagrangian strain tensor $E_{\alpha\beta}$ one asks how to construct a theory of this sort. Suppose that the rubber is stretched uniformly by factors λ_x , λ_y , and λ_z along the x , y , and z axes respectively. This stretch can be consistent with the

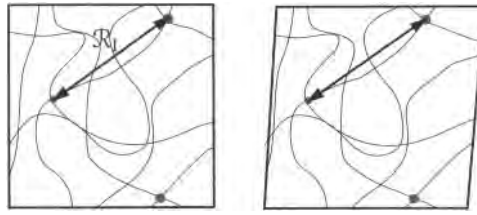


Figure 12.1. Rubber consists of a tangle of polymers, joined occasionally at nodes, but otherwise free to slide about. However, there are forces between all the homopolymers which strongly prefer a certain overall fixed density. The typical distance between nodes where polymers bind together is \mathcal{R}_1 .

conservation of density provided

$$\lambda_x \lambda_y \lambda_z = 1. \tag{12.7}$$

Since $\partial s_x / \partial x = \lambda_x$ describes stretches along x , with similar expressions for y and z , the metric tensor in Eq. (12.3) and strain tensor in Eq. (12.5) become

$$g_{\alpha\beta} = \lambda_\alpha^2 \delta_{\alpha\beta} \tag{12.8}$$

$$\Rightarrow E_{\alpha\beta} = \frac{1}{2}(\lambda_\alpha^2 - 1)\delta_{\alpha\beta} \tag{12.9}$$

The trace of any tensor such as $E_{\alpha\beta}$ is invariant under rotations of coordinate axes. This suggests taking the energy proportional to

$$\text{Tr } E = \frac{1}{2}(\lambda_x^2 + \lambda_y^2 + \lambda_z^2 - 3) \tag{12.10}$$

and imposing incompressibility through Eq. (12.7) to obtain the free energy per volume for rubber due to Mooney (1940),

$$\frac{\mathcal{F}}{\mathcal{V}} = \frac{G}{2} \left(\lambda_x^2 + \lambda_y^2 + \frac{1}{\lambda_x^2 \lambda_y^2} - 3 \right). \quad \begin{array}{l} G \text{ is a constant with dimensions of energy per} \\ \text{volume.} \end{array} \tag{12.11}$$

G is called the elastic modulus of rubber.

Example: Stretching a Circular Sheet. Consider stretching a circular rubber sheet, of initial radius R_0 in the x - y plane and thickness t along z . When the radius increases to $R = R_0 \lambda_x = R_0 \lambda_y$, the thickness must decrease to tR_0^2/R^2 to preserve volume. So Eq. (12.11) becomes

$$\mathcal{F} = \frac{G}{2} \pi R_0^2 t \left[2 \left(\frac{R}{R_0} \right)^2 + \left(\frac{R_0}{R} \right)^4 - 3 \right]. \tag{12.12}$$

The free energy per volume describes the energy attributed to a volume element in the reference frame. So when summing up to get the free energy of the whole object, just multiply by the original volume, not the stretched volume.

A comparison of Eq. (12.12) with experiment appears in Figure 12.2. Notice that G for this sample is on the order of $5 \cdot 10^5 \text{ J m}^{-3} = 0.5 \text{ MPa}$. This is around 10^4 times

smaller than elastic moduli for materials such as glass or metal described in Table 12.2. The reason rubber is so floppy can be understood in part by returning to Eq. (5.73), which describes the free energy of polymers from a microscopic point of view. The overall energy scale is set by $k_B T$ times the number of polymer segments per volume. The number of polymer segments per volume is the density of molecular units per volume (around $10^{22}/\text{cm}^3$) divided by the number of molecular units per polymer chain between linking points (around 100). Assembling these values gives a typical elastic modulus of 0.4 MPa.

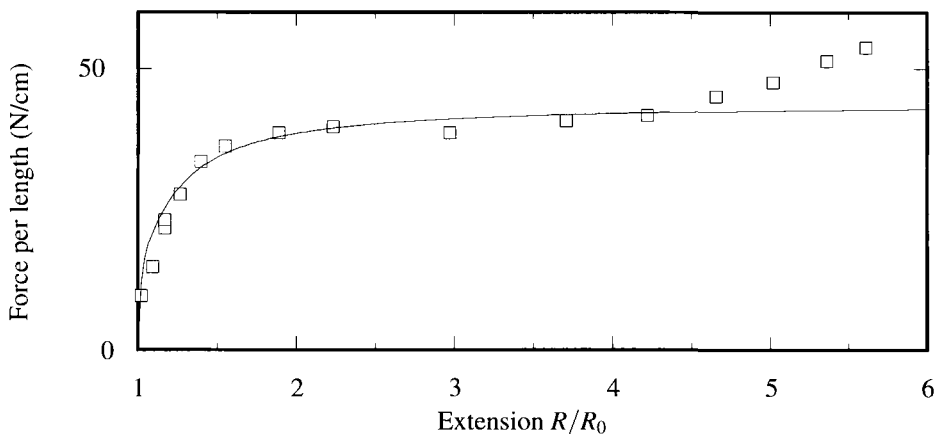


Figure 12.2. Force per length applied to circular rubber sheet, originally 1 cm thick, as it is stretched uniformly beyond original size. Squares are data from Treloar (1975), p. 89, and line is a plot of force per length $(1/R)(d\mathcal{F}/dR)$, using Eq. (12.12), scaled to match data. Deviation of theory from experiment at large values of R is due to the fact that polymer chains stiffen faster than quadratically when stretched too much.

12.2.2 Larger Extensions of Rubber

Figure 12.2 indicates that for large enough extensions, the Mooney theory no longer applies, and rubber stiffens at a higher rate. In searching for a higher-order term to add, symmetry provides a guide. The term should be invariant under rotations of coordinate axes; that is, the energy of rubber should not depend upon an arbitrary decision that some direction is x . To form rotationally invariant quantities from the Lagrangean strain tensor, observe that

$$J(\epsilon) = \det|E - \epsilon I| \quad \text{Here } I \text{ is a } 3 \times 3 \text{ unit tensor and } \epsilon \text{ is a constant.} \quad (12.13)$$

is invariant under coordinate rotations because determinants have this property. The invariance obtains for all values of ϵ , so it must hold for the quantity that multiplies each power of ϵ as well. This observation leads to three *strain invariants*

$$J_1 = \sum_{\alpha} E_{\alpha\alpha} \quad (12.14)$$

$$J_2 = \sum_{\alpha\beta} \{E_{\alpha\beta}E_{\alpha\beta} - E_{\alpha\alpha}E_{\beta\beta}\} \tag{12.15}$$

$$J_3 = \det|E|. \tag{12.16}$$

The first invariant J_1 is just the trace of E , which formed the basis of the Mooney free energy. The third invariant gives the volume of the rubber, which is constant, and so cannot enter into an expression for the energy. That leaves J_2 . The *Mooney-Rivlin* theory of rubber posits that

$$\frac{\mathcal{F}}{\mathcal{V}} = \frac{G}{2}J_1 + BJ_2. \text{ Subject to the constraint that the volume } J_3 \text{ remains constant.} \tag{12.17}$$

A large number of observations can be explained reasonably well by this addition to the energy. A statistical theory that derives an energy of approximately this form from statistical fluctuations of an incompressible solid has been obtained by Xing et al. (2007).

12.3 Linear Elasticity

In the nineteenth century, the theory of linear elasticity was viewed as one of the crowning achievements of physics. For a multitude of purposes, ranging from study of waves motion to the design of buildings and structures, it remains the most useful description of mechanical motion of solids.

To obtain the theory, return to Eq. (12.1) and recall that the displacement of material points is given by $\vec{u}(\vec{r}) = \vec{s}(\vec{r}) - \vec{r}$. The theory of linear elasticity is legitimate when the displacement \vec{u} is small enough that it need be retained in the Lagrangian strain tensor E of Eq. (12.5) only to linear order. To see how this works, write out the metric tensor of Eq. (12.3) in terms of \vec{u} : it becomes

$$g_{\alpha\beta} = \delta_{\alpha\beta} + \frac{\partial u_\beta}{\partial r_\alpha} + \frac{\partial u_\alpha}{\partial r_\beta} + \sum_\gamma \frac{\partial u_\gamma}{\partial r_\alpha} \frac{\partial u_\gamma}{\partial r_\beta}. \tag{12.18}$$

The last term in Eq. (12.18) is what linear elasticity discards. After dispensing with this nonlinear term, the Lagrangian strain tensor is simply called the *strain tensor*, is conventionally denoted by lower case e , and equals

$$e_{\alpha\beta} \equiv \frac{1}{2} \left[\frac{\partial u_\alpha}{\partial r_\beta} + \frac{\partial u_\beta}{\partial r_\alpha} \right]. \tag{12.19}$$

To obtain the theory of linear elasticity, simply assume that the energy of a solid is given by a quadratic functional of the strain tensor. The most general functional of this form is

$$\mathcal{F} = \sum_{\alpha\beta\gamma\delta} \int d\vec{r} \frac{1}{2} e_{\alpha\beta} C_{\alpha\beta\gamma\delta} e_{\gamma\delta}. \tag{12.20}$$

The reason that the free energy is a quadratic functional of the strain tensor is that one wants the undistorted solid with $e_{\alpha\beta} = 0$ to correspond to a state of minimum

energy. If any terms linear in $e_{\alpha\beta}$ were added to the theory, this would not be the case.

Because the strain tensor is symmetric under interchange of its indices, without loss of generality one can take the tensor C to be invariant under the interchanges

$$\alpha \leftrightarrow \beta, \gamma \leftrightarrow \delta \text{ and also } \alpha\beta \leftrightarrow \gamma\delta. \tag{12.21}$$

If C does not have these symmetries, then replace it with $\frac{1}{8}[C_{\alpha\beta\gamma\delta} + C_{\beta\alpha\gamma\delta} + 6 \text{ more terms}]$, which does have them. See Problem 1.

Therefore, C has at most 21 components. Equation (12.20) can also be rewritten as

$$\mathcal{F} = \sum_{\alpha\beta} \int d\vec{r} \frac{1}{2} e_{\alpha\beta} \sigma_{\alpha\beta}, \quad \text{Generalization of "work equals force times distance."} \tag{12.22}$$

with the stress tensor σ given by

$$\sigma_{\alpha\beta} = \sum_{\gamma\delta} C_{\alpha\beta\gamma\delta} e_{\gamma\delta}. \tag{12.23}$$

12.3.1 Solids of Cubic Symmetry

Although 21 independent components of the tensor C are allowed in the most general case, solids with more than triclinic symmetry have simpler tensors. For example, a solid with cubic symmetry can have only three independent elastic constants. Because cubic symmetry implies that the solid must be symmetrical under reflection about the x - y , x - z , and y - z planes, no constant $C_{\alpha\beta\gamma\delta}$ is allowed in which some index assumes a value an odd number of times. For example, C_{xyyy} must be zero because it is the coefficient of $e_{xy}e_{yy}$, and e_{xy} flips sign when $x \rightarrow -x$, but the energy of the crystal must be invariant under this change. Furthermore, a cubic crystal has threefold axes that lead it to be symmetric under $x \rightarrow y \rightarrow z \rightarrow x$. Therefore, any coefficient $C_{\alpha\beta\gamma\delta}$ is equal to all those that can be obtained from it by cyclic permutation of its indices. Three independent parameters survive these considerations; they may be taken to be C_{xxxx} , C_{xyyy} , and C_{xyxy} . The free energy becomes

$$\mathcal{F} = \int d\vec{r} \frac{1}{2} \left\{ \begin{array}{l} C_{xxxx} [e_{xx}^2 + e_{yy}^2 + e_{zz}^2] \\ + 2C_{xyyy} [e_{xx}e_{yy} + e_{yy}e_{zz} + e_{zz}e_{xx}] \\ + 4C_{xyxy} [e_{xy}^2 + e_{yz}^2 + e_{zx}^2] \end{array} \right\}. \tag{12.24}$$

The reason that the last two terms have factors of 2 and 4, respectively, reflects the numbers of times they appear when one sums freely over $\alpha\beta\gamma$ and δ . For example, e_{xy}^2 shows up as the coefficient of C_{xyxy} , C_{xyyx} , C_{yxxy} , and C_{yxyx} .

A conventional notation for elastic constants cuts in half the number of summations that must explicitly be mentioned by defining

$$\begin{array}{cccccc} e_{xx} & e_{yy} & e_{zz} & 2e_{yz} & 2e_{zx} & 2e_{xy} \\ \downarrow & \downarrow & \downarrow & \downarrow & \downarrow & \downarrow \\ e_1 & e_2 & e_3 & e_4 & e_5 & e_6 \end{array} \tag{12.25}$$

Table 12.1. Elastic constants for cubic crystals

Element	C_{11} (GPa)	C_{44} (GPa)	C_{12} (GPa)	Element	C_{11} (GPa)	C_{44} (GPa)	C_{12} (GPa)
Al	108	28.3	62	Li (195K)	13.4	9.6	11.3
Ar (80 K)	2.77	0.98	1.37	Mo	459	111	168
Ag	123	45.3	92	Na	7.59	4.30	6.33
Au	190	42.3	161	Ne (6 K)	1.62	0.93	0.85
Cs (78 K)	2.47	2.06	1.48	Ni	247	122	153
Ca	16	12	8	Nb	245	28.4	132
Cr	346	100	66	O (54.4 K)	2.60	0.275	2.06
Cu	169	75.3	122	Pd	224	71.6	173
C (diamond)	1040	550	170	Pt	347	76.5	251
Fe	230	117	135	Rb	2.96	1.60	2.44
Ge (undoped)	129	67.1	48	Si (undoped)	165	79.2	64
Ge (<i>n</i> -doped, 10^{19} Sb)	128.8	65.5	47.7	Si (<i>n</i> -doped, 10^{19} As)	162.2	78.7	65.4
Ge (<i>p</i> -doped, 10^{20} Ga)	118.0	65.3	39.0	Sr	14.7	5.74	9.9
He ³ (0.4 K, 24 cm ³ /mole)	0.0235	0.01085	0.0197	Ta	262	82.6	156
He ⁴ (1.6 K, 12 cm ³ /mole)	0.0311	0.0217	0.0281	Th	76	46	49
Ir	600	270	260	W	517	157	203
K	3.71	1.88	3.15	V	230	43.2	120
Kr (115 K)	2.85	1.35	1.60	Xe (156 K)	2.98	1.48	1.90
Pb	48.8	14.8	41.4				

Notice that the Cauchy relation $C_{12} = C_{44}$ is badly violated for almost all entries. Source: Landolt and Börnstein (New Series), vol. 11.

$$\begin{array}{cccccc}
 C_{xxxx} & C_{xxyy} & C_{xxzz} & C_{yzxx} & C_{zxxx} & C_{xyxx} \text{ etc.} \\
 \downarrow & \downarrow & \downarrow & \downarrow & \downarrow & \downarrow \\
 C_{11} & C_{12} & C_{13} & C_{41} & C_{51} & C_{61} \text{ etc.}
 \end{array} \tag{12.26}$$

so that the free energy may be rewritten

$$\mathcal{F} = \int d\vec{r} \frac{1}{2} \sum_{\alpha\beta=1}^6 e_{\alpha} C_{\alpha\beta} e_{\beta}. \tag{12.27}$$

The three constants C_{11} , C_{12} , and C_{44} for cubic crystals appear in Table 12.1.

It was shown by Cauchy and Saint Venant that if all the atoms composing a solid interact pairwise through *central forces*—that is, forces that are directed from the center of one ion to another as in Eq. (11.1)—then there is an additional symmetry requiring $C_{44} = C_{12}$ —the *Cauchy relation*. Because many computer simulations of solids assume forces of this form, it is important to observe that for all real cubic solids the relation is badly violated, as shown in Table 12.1. This fact caused considerable controversy in the nineteenth century, because the elastic anisotropy of solids revealed the underlying lattice on a macroscopic scale, but seemed inconsistent with the only imaginable force laws. The paradox was first resolved by Born (1914), who introduced the possibility of angular forces between atoms, such as discussed in Section 11.8.

Bulk modulus. The bulk modulus of any solid is defined as $B = \mathcal{V} \partial^2 \mathcal{F} / \partial \mathcal{V}^2$. Uniform dilation of a solid is obtained by setting $e_{xx} = e_{yy} = e_{zz} = \delta \mathcal{V} / 3 \mathcal{V}$, while the other components of the strain tensor vanish. From Eq. (12.24), for a cubic crystal, the free energy has the form

$$\mathcal{F} = \frac{1}{6} \mathcal{V} [C_{11} + 2C_{12}] [\delta \mathcal{V} / \mathcal{V}]^2, \quad (12.28)$$

and therefore the bulk modulus is given by

$$B = \frac{1}{3} [C_{11} + 2C_{12}]. \quad (12.29)$$

12.3.2 Isotropic Solids

Many solids are effectively isotropic. In some cases, as in glass, it is difficult to find any length scale much above the atomic for which there is any preferred orientation. In other cases, such as commercial cast metals or ceramics, a solid may be composed of so many crystalline grains of varying orientation that for scales much above the grain size, no trace of crystalline anisotropy remains in the elastic response. In this case, the number of elastic constants reduces to two.

To show that one constant disappears relative to the cubic case, it is sufficient to recognize that isotropic solids possess all the symmetries of their cubic counterparts, but with many additional symmetries that may simplify the free energy beyond Eq. (12.24). One could impose, for example, the condition that the free energy remain invariant under infinitesimal variations about the \hat{z} axis. An alternative is to demand the free energy to remain invariant under 45° rotations about the \hat{z} axis. In this case, the strain tensor $e_{\alpha\beta}(\vec{r})$ transforms into $e'_{\alpha\beta}(\vec{r}')$, where

$$e_{\alpha\beta}(\vec{r}) = \sum_{\gamma\delta} R_{\alpha\gamma}^* e'_{\gamma\delta}(\vec{r}') R_{\delta\beta} \quad (12.30a)$$

with

$$\vec{r}' = R\vec{r} \quad \text{and} \quad R = \frac{1}{\sqrt{2}} \begin{pmatrix} 1 & -1 & 0 \\ 1 & 1 & 0 \\ 0 & 0 & \sqrt{2} \end{pmatrix}. \quad (12.30b)$$

Substitute Eq. (12.30) into Eq. (12.24), subtract the free energy of the rotated state from that of the unrotated state, and demand that the result vanish (Problem 3). After carrying out the matrix multiplications and some algebra, the result is

$$0 = (2C_{xyxy} + C_{xxyy} - C_{xxxx})(e_{yy} - 2e_{xy} - e_{xx})(e_{yy} + 2e_{xy} - e_{xx}) \quad (12.31)$$

$$\Rightarrow C_{xxxx} = C_{xxyy} + 2C_{xyxy}. \quad (12.32)$$

Substituting Eq. (12.32) into Eq. (12.24) allows the free energy to be written

$$\mathcal{F} = \frac{1}{2} \int d\vec{r} \lambda \left(\sum_{\alpha} e_{\alpha\alpha} \right)^2 + 2\mu \sum_{\alpha\beta} e_{\alpha\beta}^2. \quad \text{Where } \lambda = C_{xxyy} \text{ and } \mu = C_{xyxy}. \quad (12.33)$$

\mathcal{F} is now rotationally invariant, so there is no point in trying to apply additional rotations to simplify it further. The numbers λ and μ are called the *Lamé constants*; although convenient for analytical work, they are not the conventional constants with which to report experimental properties of isotropic elastic media, so the presentation of typical values is deferred.

Equations of Motion and Equilibrium. Knowing the free energy associated with any possible deformation of the solid and observing that while it is in motion there will also be a kinetic energy

$$T = \int d\vec{r} \frac{1}{2} \rho |\dot{\vec{u}}(\vec{r})|^2, \quad \rho \text{ is the mass density.} \quad (12.34)$$

one can find the equation of motion for \vec{u} , by computing

$$\rho \ddot{u}_\alpha(\vec{r}) = - \frac{\delta \mathcal{F}}{\delta u_\alpha(\vec{r})} = \sum_\beta \frac{\partial}{\partial r_\beta} \sigma_{\alpha\beta}(\vec{r}), \quad (12.35)$$

using Eq. (12.23) for the stress tensor,

$$\sigma_{\alpha\beta} = \sum_{\gamma\delta} C_{\alpha\beta\gamma\delta} e_{\gamma\delta}. \quad (12.36)$$

Because the acceleration of small sections of mass is given by the divergence of the stress tensor, the stress tensor is physically interpreted as giving the forces that each section of the body exerts upon its neighbor. To see why, integrate (12.35) over any small volume \mathcal{V} bounded by closed surface Σ , to get

$$\int_{\mathcal{V}} d\vec{r} \rho \ddot{u}_\alpha = \int d\Sigma \sum n_\beta \sigma_{\beta\alpha} \quad \begin{array}{l} \text{Employ the divergence theorem, with } n_\beta \text{ a} \\ \text{component of the unit normal to surface } \Sigma. \end{array} \quad (12.37)$$

Taking the small volume to be a tiny cube oriented along the coordinate axes, Eq. (12.37) shows that the total force on the material inside the cube is provided by the appropriate components of the stress tensor σ multiplied by the areas of the cube faces.

Specifically, if one imagines taking a knife and using it to sever bonds in a small two-dimensional region, say perpendicular to the x axis, then σ_{xx} gives the force per unit area required to pull the faces of the region together along x , and σ_{xy} and σ_{xz} give the forces per unit area required to stretch the faces in the directions perpendicular to x so that each atom is directly across from the atom that was its neighbor in equilibrium. The directions of the stresses on each face of a small cube within a solid are depicted in Figure 12.3. The first symmetry of Eq. (12.21) implies that $\sigma_{\alpha\beta} = \sigma_{\beta\alpha}$. A glance at Figure 12.3 shows that this requirement is equivalent to demanding that all torques vanish on small volume elements of the solid.

In the special case of an isotropic solid, one obtains

$$\sigma_{\alpha\beta} = \lambda \delta_{\alpha\beta} \sum_\gamma e_{\gamma\gamma} + 2\mu e_{\alpha\beta} \quad (12.38)$$

$$\Rightarrow e_{\alpha\beta} = \frac{-\lambda \delta_{\alpha\beta}}{2\mu(3\lambda + 2\mu)} \sum_\gamma \sigma_{\gamma\gamma} + \frac{1}{2\mu} \sigma_{\alpha\beta}. \quad \text{Just invert the matrix of Eq. (12.38).} \quad (12.39)$$

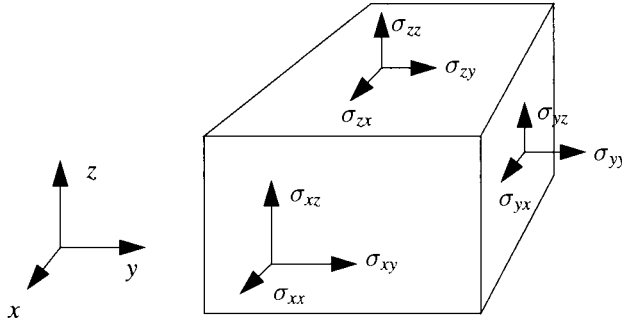


Figure 12.3. Imagine singling out a small cube from within a solid. Every face is potentially under stress in three directions, and the sign conventions for the directions of the stresses are shown here. The total force on each face is given by the stress in each direction times the area of the face.

and the equation of motion Eq. (12.35) becomes

$$\rho \frac{\partial^2 \vec{u}}{\partial t^2} = (\lambda + \mu) \nabla(\nabla \cdot \vec{u}) + \mu \nabla^2 \vec{u}. \quad (12.40)$$

Uniform Stresses. If a body is under uniform stress \mathcal{S} in the \hat{z} direction, as shown in Figure 12.4, then from Eq. (12.39) one has immediately that

$$\mathcal{S} = Y e_{zz} \quad (12.41)$$

with

$$Y = \frac{\mu(3\lambda + 2\mu)}{\lambda + \mu}; \quad (12.42)$$

Y is called the *modulus of elasticity* or *Young's modulus*. Simultaneously, the body contracts in directions perpendicular to the applied stress by an amount

$$e_{xx} = e_{yy} = \frac{-\lambda}{2\mu(3\lambda + 2\mu)} \mathcal{S}, \quad (12.43)$$

and the negative of this perpendicular contraction e_{xx} divided by the extension e_{zz} is *Poisson's ratio*

$$\nu = \frac{\lambda}{2(\lambda + \mu)}. \quad (12.44)$$

Another conventional constant is defined when only $\sigma_{yz} = \mathcal{S}$ is nonzero. Again using Eq. (12.39), one finds that

$$\mathcal{S} = 2G e_{yz} = G \frac{\partial u_y}{\partial z} \quad (12.45)$$

and defines $G = \mu$ to be the *shear modulus*. Typical values of Y and ν appear in Table 12.2.

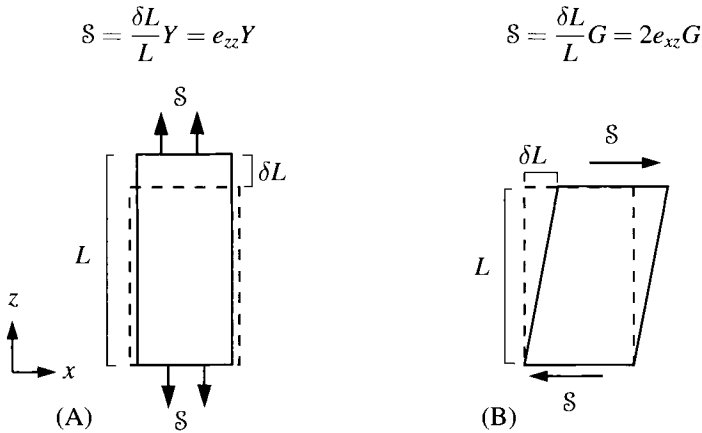


Figure 12.4. Geometries for the definitions of (A) Young’s modulus Y and (B) the shear modulus G .

Table 12.2. Elastic moduli for isotropic materials

Material	Young’s Modulus Y (GPa)	Poisson Ratio ν
Lead (cast)	5	0.5
Tin (cast)	27	0.3
Glass	55	0.16
Aluminum (cast)	68	0.3
Copper (cast)	76	0.4
Zinc (cast)	76	0.3
Copper (soft, wrought)	100	0.4
Iron (cast)	110	0.3
Copper (hard drawn)	120	0.4
Iron (wrought)	200	0.3
Carbon steel	200	0.3
Tungsten	400	0.3

The value of the elastic modulus depends very strongly upon the processing of the material, which means that a hierarchy of structural details starting at the atomic level and proceeding up to the scale of grains all are important. Data are indicative of orders of magnitude. Source: Brady and Clauser (1991) and Grigoriev and Meilkhov (1997).

Traveling Waves. An important feature of the equation of motion (12.40) is that it supports traveling waves of two types, longitudinal and transverse. To study the longitudinal waves, define

$$\Delta(\vec{r}, t) = \vec{\nabla} \cdot \vec{u}(\vec{r}, t) \text{ and } \vec{w}(\vec{r}, t) = \vec{\nabla} \times \vec{u}(\vec{r}, t). \tag{12.46}$$

First take the divergence of Eq. (12.40) to obtain

$$\rho \frac{\partial^2 \Delta}{\partial t^2} = (\lambda + 2\mu) \nabla^2 \Delta, \tag{12.47}$$

and then take the curl to obtain

$$\rho \frac{\partial^2 \vec{w}}{\partial t^2} = \mu \nabla^2 \vec{w}, \quad \text{Because the curl of a gradient vanishes.} \quad (12.48)$$

Supposing \vec{u} to be of the form $\vec{u}_0 e^{i\vec{k}\cdot\vec{r}-i\omega t}$ shows that Eq. (12.47) describes longitudinal waves, where \vec{k} and \vec{u}_0 are parallel, moving with speed

$$c_l = \sqrt{\frac{\lambda + 2\mu}{\rho}}, \quad (12.49)$$

while Eq. (12.48) describes transverse waves, where \vec{k} and \vec{u}_0 are perpendicular, moving with speed

$$c_t = \sqrt{\frac{\mu}{\rho}}. \quad (12.50)$$

12.4 Other Constitutive Laws

12.4.1 Liquid Crystals

Understanding the mechanical forces needed to deform liquid crystals is important for technical applications, because, for example, in liquid crystal displays, electrical fields twist the molecules of the liquid crystal and thereby alter their optical properties. The question naturally arises as to how hard one needs to twist this liquid in order to make it turn. The question will be answered by asking how elasticity is modified while accommodating the symmetries of liquid crystals.

The calculation will be carried out for a nematic liquid crystal and will be restricted to the case where deformations of the material occur over length scales much larger than the molecules of which it is composed. At every point, the liquid crystal is described by a unit vector $\hat{n}(\vec{r})$, whose direction indicates the local axis of the nematic.

The energy needed to deform a nematic is therefore an integral over space of some function involving gradients of the unit vector \hat{n} . Because the gradients are supposed to be small, the theory will stop with the simplest collection of terms that gives a nonzero result. There are two basic symmetries allowing one to reduce the number of terms that must be considered. First, the head and tail of molecules making up a nematic are indistinguishable, so no physical quantity should be able to distinguish between \hat{n} and $-\hat{n}$ or to tell if the system has been reflected about any plane. Second, the free energy of the nematic must be independent of the reference frame in which it is described. In particular, if one picks up a jar containing a nematic and rotates it slightly, the calculation of the free energy cannot change just because the point of view has altered.

Matters would be particularly simple if terms linear in gradients of \hat{n} composed the free energy. Unfortunately, one easily shows that all of them vanish. The only

terms available that are invariant when the sample as a whole is rotated are

$$(\hat{n} \cdot \vec{\nabla})\hat{n} \tag{12.51a}$$

$$\vec{\nabla} \cdot \hat{n} \tag{12.51b}$$

$$\hat{n} \cdot \vec{\nabla} \times \hat{n}. \tag{12.51c}$$

The first of these, Eq. (12.51a) can be rewritten as $\nabla(\hat{n} \cdot \hat{n})/2$, which vanishes because \hat{n} is a unit vector. The second cannot have a nonzero coefficient because it does not respect the symmetry $\hat{n} \rightarrow -\hat{n}$. The third changes sign under reflection about the x , y , or z planes, and it must be discarded on this account. Therefore, one is driven to terms that are quadratic in gradients of \hat{n} .

There is a discouraging number of terms to consider. A general term involving two gradients is of the form

$$\frac{\partial n_\alpha}{\partial r_\beta} \frac{\partial n_\gamma}{\partial r_\delta}, \tag{12.52}$$

and as each index can adopt three values, there is a total of 81 different contributions at the outset. So the free energy is

$$\mathcal{F} = \int d\vec{r} \mathcal{F}(\vec{r}) = \frac{1}{2} \int d\vec{r} \sum_{\alpha\beta\gamma\delta} C_{\alpha\beta\gamma\delta} \frac{\partial n_\alpha}{\partial r_\beta} \frac{\partial n_\gamma}{\partial r_\delta}. \quad \mathcal{F}(\vec{r}) \text{ is the free energy per volume.} \tag{12.53}$$

One can always interchange $\alpha\gamma \leftrightarrow \beta\delta$, because Eq. (12.53) does not change when this switch is performed, but this still leaves 45 independent values of $C_{\alpha\beta\gamma\delta}$. To further reduce this number by application of symmetry, pick a particular point in space, \vec{r} , and choose the \hat{z} axis to coincide with the direction of the director $\hat{n}(\vec{r})$. Most of the calculation will be carried out with this specific choice of coordinate system, until the very end, when the results will be interpreted in a fashion that is independent of it.

A first simplification results immediately from the fact that \hat{n} is a unit vector. All gradients of n_z vanish because

$$0 = \frac{\partial}{\partial r_\alpha} 1 = \frac{\partial}{\partial r_\alpha} (\hat{n} \cdot \hat{n}) \tag{12.54}$$

$$= 2n_z \frac{\partial}{\partial r_\alpha} n_z = 2 \frac{\partial}{\partial r_\alpha} n_z \tag{12.55}$$

Although \hat{n} points along \hat{z} right at \vec{r} , it will not generally point precisely along \hat{z} a small distance away, and therefore gradients of n_z have to be calculated.

There are 21 independent coefficients $C_{\alpha\beta\gamma\delta}$ remaining.

The remaining simplifications are deduced with greater difficulty. Whatever terms enter the free energy must be invariant if one rotates the whole system slightly around the \hat{z} axis. Problem 5 shows that following rotation about the \hat{z} axis through a small angle θ , one obtains

$$\frac{\partial n_\gamma}{\partial r_\delta} \rightarrow \frac{\partial n_\gamma}{\partial r_\delta} + \theta \left[\sum_\beta \frac{\partial n_\gamma}{\partial r_\beta} R_{\beta\delta} - R_{\gamma\beta} \frac{\partial n_\beta}{\partial r_\delta} \right] \tag{12.56}$$

where

$$R = \begin{pmatrix} 0 & -1 & 0 \\ 1 & 0 & 0 \\ 0 & 0 & 0 \end{pmatrix}. \quad (12.57)$$

Placing Eq. (12.56) into the free energy (12.53) and demanding that all terms proportional to θ vanish gives

$$0 = \sum_{\alpha\gamma\delta} \left[\frac{\partial n_\alpha}{\partial y} \frac{\partial n_\gamma}{\partial r_\delta} C_{\alpha\gamma\delta} - \frac{\partial n_\alpha}{\partial x} \frac{\partial n_\gamma}{\partial r_\delta} C_{\alpha\gamma\delta} \right] - \sum_{\beta\gamma\delta} \left[\frac{\partial n_x}{\partial r_\beta} \frac{\partial n_\gamma}{\partial r_\delta} C_{y\beta\gamma\delta} - \frac{\partial n_y}{\partial r_\beta} \frac{\partial n_\gamma}{\partial r_\delta} C_{x\beta\gamma\delta} \right]. \quad (12.58)$$

The coefficient of every term, such as

$$\frac{\partial n_x}{\partial z} \frac{\partial n_y}{\partial y}, \quad (12.59)$$

has to vanish independently. For example, demanding that the coefficient of (12.59) vanish gives

$$0 = -C_{yzyy} + C_{yxxz} + C_{xyxz}. \quad (12.60)$$

The tedious task of constructing all 21 such equations and using them to eliminate as many coefficients as possible is best turned over to any computer algebra system, which within a few minutes will show that only five independent coefficients now survive. These are the coefficients of

$$\left[\frac{\partial n_x}{\partial x} + \frac{\partial n_y}{\partial y} \right]^2 \quad (12.61a)$$

$$\left[\frac{\partial n_x}{\partial z} \right]^2 + \left[\frac{\partial n_y}{\partial z} \right]^2 \quad (12.61b)$$

$$\left[\frac{\partial n_y}{\partial x} - \frac{\partial n_x}{\partial y} \right]^2 \quad (12.61c)$$

$$\left[\frac{\partial n_y}{\partial x} - \frac{\partial n_x}{\partial y} \right] \left[\frac{\partial n_y}{\partial y} + \frac{\partial n_x}{\partial x} \right] \quad (12.61d)$$

$$\frac{\partial n_y}{\partial x} \frac{\partial n_x}{\partial y} - \frac{\partial n_y}{\partial y} \frac{\partial n_x}{\partial x}. \quad (12.61e)$$

The final task is to identify each of these quantities in terms of operators that no longer depend upon the particular choice of \hat{z} as the local axis of the nematic. The quantities appearing in Eq. (12.61) may be rewritten as

$$(\vec{\nabla} \cdot \hat{n})^2 \quad (12.62a)$$

$$|\hat{n} \times (\vec{\nabla} \times \hat{n})|^2 \quad (12.62b)$$

$$(\hat{n} \cdot (\vec{\nabla} \times \hat{n}))^2 \quad (12.62c)$$

$$\hat{n} \cdot (\vec{\nabla} \times \hat{n}) \vec{\nabla} \cdot \hat{n} \quad (12.62d)$$

$$\frac{1}{2} \vec{\nabla} \cdot \left[(\hat{n} \cdot \vec{\nabla}) \hat{n} - \hat{n} (\vec{\nabla} \cdot \hat{n}) \right]. \quad (12.62e)$$

This quantity is difficult to deduce from Eq. (12.61e), although easy to verify once one has made the right guess.

The coefficient of (12.62d) must vanish because this term is odd in \hat{n} . The final term, (12.62e) need not be included in the free energy, because as a divergence it contributes to the surface energy but not to the bulk energy. The free energy density has finally only three terms,

$$\mathcal{F} = \underbrace{\frac{K_1}{2}(\vec{\nabla} \cdot \hat{n})^2}_{\text{splay}} + \underbrace{\frac{K_2}{2}(\hat{n} \cdot (\vec{\nabla} \times \hat{n}))^2}_{\text{twist}} + \underbrace{\frac{K_3}{2}(\hat{n} \times (\vec{\nabla} \times \hat{n}))^2}_{\text{bend}}. \quad (12.63)$$

Problem 10 provides an example of how this free energy can be employed to find the mechanical response of liquid crystals. Many other calculations are found in de Gennes and Prost (1993) Chandrasekhar (1992), and Chaikin and Lubensky (1995).

12.4.2 Granular Materials

Granular materials, such as sand, are peculiar hybrids of solids and liquids. Placed in a pile, they retain their shape like a solid. Poured from glass, they flow like liquids. Their mechanical properties are challenging to describe. An introduction to some of the issues involved is presented by Bergman and Stroud (1992) and Jaeger et al. (1996a,b).

One of the classic ways to examine mechanical properties of a granular solid is in a triaxial test. A tube of sand sustains compressive stress σ_1 from the top, and compressive stress σ_2 from the sides, with $|\sigma_1| > |\sigma_2|$. Using the idea of static friction, one can calculate when grains will begin to slide and the tube of sand fall apart.

The idea of the calculation is to imagine slicing through the tube of sand with imaginary planes pointing in every possible direction. For every plane, calculate the normal force N and the shear force τ . If for any plane $\tau > \mu_s N_i$ where μ_s is the coefficient of static friction, then sand should begin to slip along that plane. So the stability of a granular column comes down to finding normal and shear forces in all possible directions.

Specialize to two dimensions. The stress tensor has the simple form

$$\sigma = \begin{pmatrix} \sigma_1 & 0 \\ 0 & \sigma_2 \end{pmatrix}. \quad (12.64)$$

What is the stress when viewed along some arbitrary direction θ ? In a frame rotated through angle θ , the stress tensor becomes

$$\begin{aligned} & \begin{pmatrix} \cos \theta & \sin \theta \\ -\sin \theta & \cos \theta \end{pmatrix} \begin{pmatrix} \sigma_1 & 0 \\ 0 & \sigma_2 \end{pmatrix} \begin{pmatrix} \cos \theta & -\sin \theta \\ \sin \theta & \cos \theta \end{pmatrix} \\ & = \begin{pmatrix} \cos^2 \theta \sigma_1 + \sin^2 \theta \sigma_2 & (\sigma_1 - \sigma_2) \sin \theta \cos \theta \\ (\sigma_1 - \sigma_2) \sin \theta \cos \theta & \cos^2 \theta \sigma_2 + \sin^2 \theta \sigma_1 \end{pmatrix} \end{aligned} \quad (12.65)$$

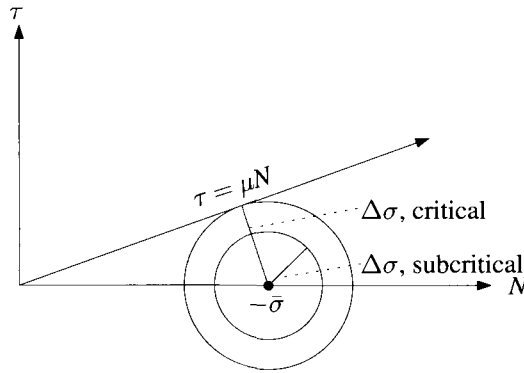


Figure 12.5. Diagram describing the Mohr-Coulomb circle.

The components of the first row give normal N and shear stress τ across the plane at angle θ . They can be rewritten

$$N = -(\bar{\sigma} + \Delta\sigma \cos 2\theta) \quad \text{Introduce the minus sign because the convention with stresses is that they are positive in tension, while in this problem it is natural to take the normal force positive in compression.}$$

$$\tau = -\Delta\sigma \sin 2\theta \quad (12.66)$$

where the average stress $\bar{\sigma}$ and differential stress $\Delta\sigma$ are

$$\bar{\sigma} = \frac{\sigma_1 + \sigma_2}{2}; \quad \Delta\sigma = \frac{\sigma_1 - \sigma_2}{2}. \quad (12.67)$$

Thus a plot of τ versus N describes a circle centered on the point $(|\bar{\sigma}|, 0)$, as shown in Figure 12.5. The figure also shows a line of slope $\tau/N = \mu$, which describes the threshold beyond which the granular tube will be unstable. When stresses are just at the point where instability is about to occur, the circle parametrized by Eq. (12.67) is just tangent to the line. This critical condition occurs when

$$\frac{\Delta\sigma}{\bar{\sigma}} = \mu. \quad (12.68)$$

Problems

1. Symmetries of C :

Complete the comment attached to Eq. (12.21). Write the additional 6 terms needed to symmetrize C , and explain why it is legitimate to replace C by this symmetrized quantity.

2. **Rotations in linear elasticity:** Because the nonlinear term has been discarded from Eq. (12.19), linear elasticity does not treat rotations very well. Suppose that a solid would begin to crumble inside when subjected to a uniform external pressure of $(\lambda + \mu)/5$. Subject this solid to rigid rotations, compute the

(spurious) pressure predicted by linear elasticity, and find the rotation angle at which the solid would begin to come apart.

3. Isotropic solids:

- (a) Derive Eqs. (12.31), (12.32), and (12.33).
- (b) Derive Eq. (12.38).

4. Equation of motion: Derive Eq. (12.35).

5. Rotation of nematics: Derive Eqs. (12.56) and (12.57).

6. Elastic constants:

- (a) Express the bulk modulus B of an isotropic material in terms of the Lamé constants.
- (b) Find Young's modulus Y , as defined in Figure 12.4, along $[100]$ for a crystal of cubic symmetry.

7. Waves in cubic crystals:

- (a) Find the equation of motion Eq. (12.35) in a form appropriate for a cubic crystal. One way to proceed is to begin with Eq. (12.24), evaluate $\delta\mathcal{F}/\delta u_x$, and then generalize the result to the other two components of \vec{u} .
- (b) Assuming that $\vec{u}(\vec{r}, t) = \vec{w} \exp[i\vec{k} \cdot \vec{r} - i\omega t]$, find the matrix equation for \vec{w} .
- (c) Assume that $\vec{k} = k_0[1 \ 0 \ 0]$. Find the two sound speeds in this direction, and evaluate them for undoped silicon.
- (d) Now assume that $\vec{k} = k_0[1 \ 1 \ 1]$. Again find the two sound speeds, and evaluate them for undoped silicon.

8. Surface waves: Consider a two-dimensional isotropic elastic solid stretching from $-\infty$ to ∞ in the x direction, but from $-\infty$ to 0 in the y direction. Surface waves, also called *Rayleigh waves*, can run along the free surface, vanishing exponentially as they reach down into the bulk.

To find the dispersion relation for these surface waves, begin with the observation that any displacement field \vec{u} can be decomposed into longitudinal and transverse parts,

$$\vec{u} = \vec{u}^l + \vec{u}^t. \quad \text{The decomposition can be defined by taking the Fourier transform of } \vec{u}; \text{ the longitudinal part of } \vec{u} \text{ is the part parallel to } \vec{k}, \text{ and the transverse part is whatever is left over.} \quad (12.69)$$

In two dimensions, u^l and u^t derive from potentials ϕ^l and ϕ^t such that

$$\vec{u}^l = \vec{\nabla} \phi^l \text{ and } \vec{u}^t = \left(-\frac{\partial \phi^t}{\partial y}, \frac{\partial \phi^t}{\partial x} \right). \quad (12.70)$$

- (a) Assume that $\phi^l = A \exp[ikx + g_l y - i\omega t]$ and $\phi^t = B \exp[ikx + g_t y - i\omega t]$. Determine g_l and g_t . Use the transverse and longitudinal wave speeds c_l and c_t to carry information about the elastic constants.
- (b) The boundary conditions on the free surface at $y = 0$ are that $\sigma_{yy} = \sigma_{xy} = 0$. Find two homogeneous equations involving A and B by imposing these boundary conditions.
- (c) Find the dispersion relation $\omega = c_R k$, and determine the Rayleigh wave speed c_R in terms of the longitudinal and transverse wave speeds c_l and c_t . Verify that when $c_l = \sqrt{3}c_t$, $c_R = 0.9194c_t$.
9. **Rubber:** Consider a solid cylinder of rubber, of original length L and radius r . What restoring force does it exert as L is stretched beyond its original length?

10. **Friedrichs transition:**

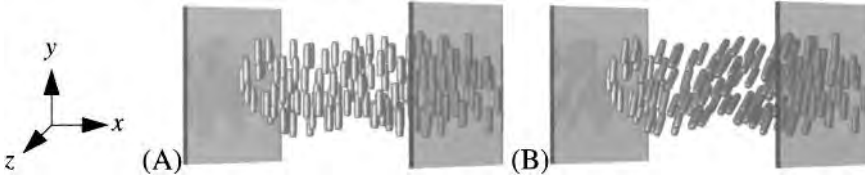


Figure 12.6. A nematic crystal is held between two plates. In (A) the liquid crystal is in equilibrium with no external field, while in (B) it is in equilibrium in the presence of a field along \hat{z} .

Consider a nematic liquid crystal caught between two plates, as shown in Figure 12.6. The director \hat{n} points along \hat{y} at $x = 0$ and $x = L$. Between the plates is applied a uniform magnetic field of strength H , along \hat{z} . When it reaches a critical value H_c , the magnetic field causes the director \hat{n} to begin twisting in the y - z plane, as shown in Figure 12.6(B).

- (a) Assume that the magnetic field enters the free energy of the liquid crystals as

$$-\frac{1}{2}\chi_H \int d\vec{r} (\vec{H} \cdot \hat{n})^2. \quad (12.71)$$

Show that the complete free energy takes the form

$$\mathcal{F} = \frac{1}{2} \int d\vec{r} K_2 \left[n_y \frac{\partial n_z}{\partial x} - n_z \frac{\partial n_y}{\partial x} \right]^2 - \frac{1}{2} \chi_H \int d\vec{r} (\vec{H} \cdot \hat{n})^2. \quad (12.72)$$

- (b) Write $\hat{n} = (0, \cos \theta, \sin \theta)$. Find the Euler–Lagrange equation corresponding to Eq. (12.72).
- (c) Multiplying the Euler-Lagrange equation by $\partial\theta/\partial x$, integrate it and solve for $\partial\theta/\partial x$.

- (d) Assume that for the critical magnetic field H_c , the angle θ is always very close to zero. Making use of this approximation, solve explicitly for θ (up to an overall constant multiplier), and calculate the critical field H_c .

11. **Mohr-Coulomb Failure Criterion** Suppose one has a vacuum-packed bag of coffee. Calculate the heaviest person that can stand on it without it giving way. Neglect the strength of the packaging and treat the coffee as a granular medium under atmospheric pressure. Assume that the top of the coffee bag has an area of 200 cm^2 and that the coefficient of friction of coffee beans is 0.2.

References

- D. J. Bergman and D. Stroud (1992), Physical properties of macroscopically inhomogeneous media, *Solid State Physics: Advances in Research and Applications*, **46**, 147–269.
- M. Born (1914), On the space lattice theory of diamond, *Annalen der Physik*, **44**, 605–642. In German.
- G. S. Brady and H. R. Clauser (1991), *Materials Handbook*, McGraw-Hill, New York.
- P. M. Chaikin and T. C. Lubensky (1995), *Principles of Condensed Matter Physics*, Cambridge University Press, Cambridge.
- S. Chandrasekhar (1992), *Liquid Crystals*, 2nd ed., Cambridge University Press, Cambridge.
- P.-G. de Gennes and J. Prost (1993), *The Physics of Liquid Crystals*, 2nd ed., Clarendon Press, Oxford.
- I. S. Grigoriev and E. Z. Meilkhov, eds. (1997), *Handbook of Physical Quantities*, CRC Press, Boca Raton, FL.
- H. M. Jaeger, S. R. Nagel, and R. P. Behringer (1996a), Granular solids, liquids and gases, *Reviews of Modern Physics*, **68**, 1259–1273.
- H. M. Jaeger, S. R. Nagel, and R. P. Behringer (1996b), The physics of granular materials, *Physics Today*, **49**(4), 32–38.
- L. D. Landau and E. M. Lifshitz (1970), *Theory of Elasticity*, 2nd ed., Pergamon Press, Oxford.
- H. Landolt and R. Börnstein (New Series), *Numerical Data and Functional Relationships in Science and Technology*, New Series, Group III, Springer-Verlag, Berlin.
- M. Mooney (1940), A theory of large elastic deformation, *Journal of Applied Physics*, **11**, 582–92.
- I. S. Sokolnikoff (1956), *Mathematical Theory of Elasticity*, 2nd ed., McGraw-Hill, New York.
- S. Timoshenko and J. N. Goodier (1970), *Theory of Elasticity*, 3rd ed., McGraw-Hill, New York.
- L. R. G. Treloar (1975), *The Physics of Rubber Elasticity*, 3rd ed., Oxford University Press, London.
- X. Xing, P. M. Goldbart, and L. Radzihovsky (2007), Thermal fluctuations and rubber elasticity, *Physical Review Letters*, **98**, 075 502.

13. Phonons

13.1 Introduction

Continuum elasticity is the only theory one needs to find stresses in skyscrapers. However, this description of the motion of solids fails in a qualitative manner as soon as one considers deformations whose wavelength is comparable to interatomic distances. When deformations are small, they must also be fast: taking the speed of sound to be 10^4 m/s, one has vibrations of 10^{-10} m at frequencies of 10^{14} Hz. No ordinary motor can generate vibrations this fast. However, they provide the microscopic underpinning of phenomena ranging from specific heat to electrical resistance.

The quantitative theory of microscopic deformations is by far most advanced in crystalline lattices. The study of *phonons* is the study of how to catalog and name the vibrating modes, how to calculate their frequencies, and of how they interact with mechanical, electromagnetic, and other forces. Phonons are traveling waves in crystals, and many of the techniques used to study electron waves in Chapter 7 carry over immediately to phonons as well.

The first work on lattice dynamics, by Born and van Karman preceded the experimental proof by Laue, Friedrich, and Knipping that solids were crystalline lattices. Born says:

The first paper by Kármán and myself was published before Laue's discovery. We regarded the existence of lattices as evident not only because we knew the group theory of lattices as given by Schoenflies and Fedorov which explained the geometrical features of crystals, but also because a short time before Erwin Madelung in Göttingen had derived the first dynamical inference from lattice theory, a relation between the infra-red vibration frequency of a crystal and its elastic properties.... Von Laue's paper on X-ray diffraction which gave direct evidence of the lattice structure appeared between our first and second paper. Now it is remarkable that in our second paper there is also no reference to von Laue. I can explain this only by assuming that the concept of the lattice seemed to us so well established that we regarded von Laue's work as a welcome confirmation but not as a new and exciting discovery which it really was.

—Born (1965), p. 2

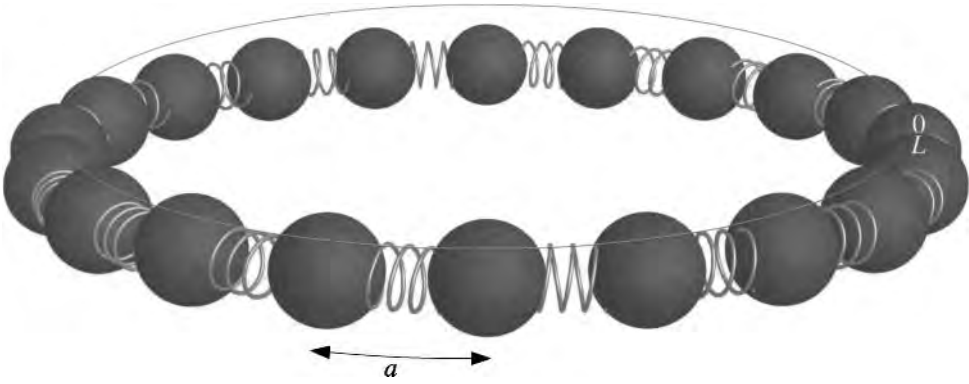


Figure 13.1. A one-dimensional chain of ions connected by springs is the setting for the simplest discussion of phonons.

13.2 Vibrations of a Classical Lattice

13.2.1 Classical Vibrations in One Dimension

Phonons are easiest to understand in one dimension. Consider a one dimensional chain of ions of mass M sitting at equilibrium distance a connected by springs of constant \mathcal{K} , as shown in Figure 13.1. The calculations simplify as much as possible when one adopts periodic boundary conditions, since no ions then need to be treated differently from any others. There are N ions, and the total length of the chain is $L = Na$.

Denote by u^l the deviation of ion $l \in [0 \dots N-1]$ from its equilibrium location, with periodic boundary conditions implying that

$$u^N = u^0. \quad (13.1)$$

Then

$$M\ddot{u}^l = \mathcal{K}(u^{l+1} - u^l) + \mathcal{K}(u^{l-1} - u^l). \quad (13.2)$$

This system of equations is solved by plane waves. Let

$$u^l = \epsilon e^{ikla - i\omega t}. \quad (13.3)$$

It is purely a matter of convention which constants one takes to multiply l in the exponent. One could choose instead $2\pi ikl/N$ or ikl . Different choices would amount to a redefinition of k .

The periodic boundary condition (13.1) requires

$$kNa = 2\pi n \Rightarrow k = 2\pi n/(Na), n \in [0 \dots N-1]. \quad (13.4)$$

Substituting Eq. (13.3) into Eq. (13.2) gives

$$-M\omega^2 \epsilon e^{ikla - i\omega t} = \left[\mathcal{K}(e^{ika} - 1) + \mathcal{K}(e^{-ika} - 1) \right] \epsilon e^{ikla - i\omega t} \quad (13.5)$$

$$\Rightarrow -M\omega^2 = \mathcal{K}(2 \cos(ika) - 2) \Rightarrow \omega = 2\sqrt{\frac{\mathcal{K}}{M} |\sin(ka/2)|}; \quad (13.6)$$

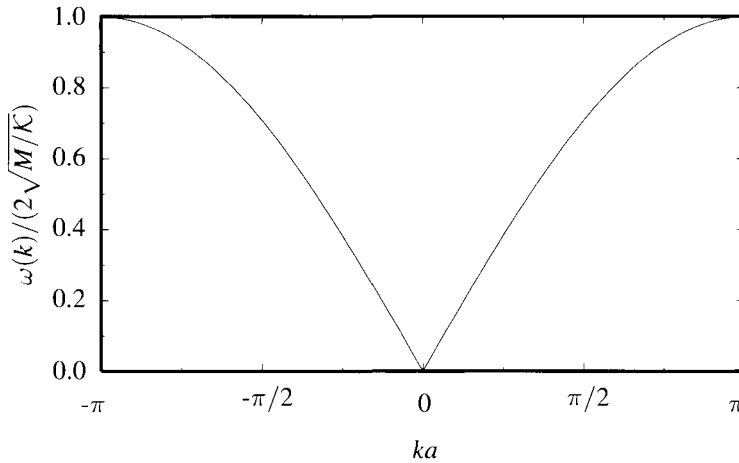


Figure 13.2. The dispersion relation for a one-dimensional lattice with nearest-neighbor interactions calculated in Eq. (13.6).

this *dispersion relation* is plotted in Figure 13.2.

There are two characteristic features of this simple solution that occur quite generally:

1. For small values of k , ω is proportional to the absolute value of k . This is no accident; it is nothing but the recovery of linear elasticity for waves much longer than the interatomic spacing. The slope of the dispersion curve, $d\omega/dk = a\sqrt{\mathcal{K}/M} = c$ near the origin is the sound speed. The branch of solutions whose frequency vanishes as k vanishes results in general from the symmetry requiring the energy of the crystal to remain unchanged when all ions are displaced by an identical amount, as shown in Eq. (13.19). Very long wavelength displacements of the ions are indistinguishable from uniform translation on short length scales, and therefore they have low energy and frequency. Excitations of this type are often referred to as *Goldstone modes*, after Goldstone (1963); see Section 26.3.3.
2. The solution repeats periodically as a function of k , with period $2\pi/a$. This occurs because the phonon problem concerns waves moving in a medium that is periodic with period a , and occurs for exactly the same reason that energies of electrons are periodic functions of wave vector \vec{k} . Just as for electrons, the region $[-\pi/a, \pi/a]$ is called the Brillouin zone. This symmetry will be discussed in greater generality as Eq. (13.21).

One-Dimensional Chain with Basis. Now consider a one-dimensional chain, with lattice parameter a , in which atoms of two different masses, M_1 and M_2 , alternate. Assuming again that each atom interacts only with its nearest neighbors (Figure 13.3), one has

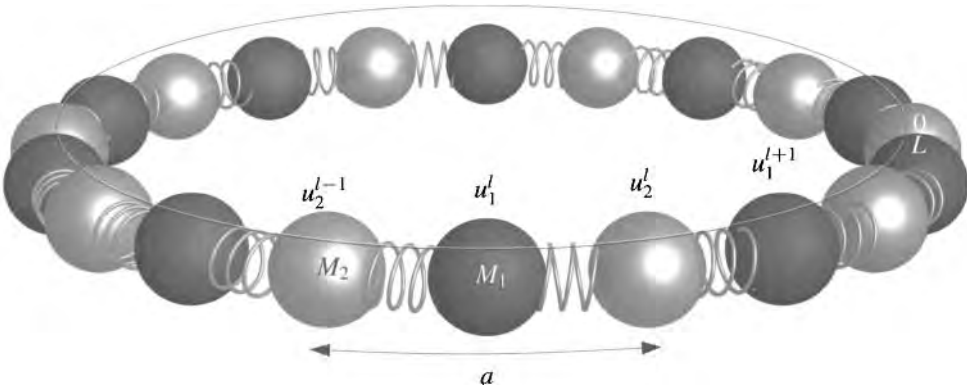


Figure 13.3. Ions of alternating masses M_1 and M_2 interacting with nearest neighbors.

$$M_1 \ddot{u}_1^l = \mathcal{K}(u_2^l - 2u_1^l + u_2^{l-1}) \quad (13.7a)$$

$$M_2 \ddot{u}_2^l = \mathcal{K}(u_1^{l+1} - 2u_2^l + u_1^l) \quad (13.7b)$$

$$\Rightarrow -\omega^2 M_1 \epsilon_1 e^{ikla} = \mathcal{K}(\epsilon_2 - 2\epsilon_1 + \epsilon_2 e^{-ika}) e^{ikla} \quad \text{Assuming a solution of the form } u_j^l = \epsilon_j e^{ikla - \omega t}. \quad (13.8a)$$

$$-\omega^2 M_2 \epsilon_2 e^{ikla} = \mathcal{K}(\epsilon_1 e^{ika} - 2\epsilon_2 + \epsilon_1) e^{ikla} \quad (13.8b)$$

$$\Rightarrow \omega = \sqrt{\mathcal{K}} \sqrt{\frac{M_1 + M_2 \pm \sqrt{M_1^2 + 2M_1 M_2 \cos ka + M_2^2}}{M_1 M_2}}. \quad \text{Set the determinant of the system (13.8) to zero, and solve the resulting polynomial for } \omega. \quad (13.9)$$

The two solutions of Eq. (13.9) are two *branches* of the phonon dispersion relation and are depicted in Figure 13.5. One of the branches vanishes linearly near $k = 0$ and is the *acoustic branch*, as it corresponds to ordinary sound. The second branch is restricted to higher frequencies and is the *optical branch*, since in solids these phonons are characteristically excited by light. For small k , the two branches take the form

$$\omega(k) = \sqrt{\frac{\mathcal{K}}{2(M_1 + M_2)}} ka, \quad \epsilon_1 = 1; \quad \epsilon_2 = 1 + ika/2, \quad (13.10a)$$

$$\omega(k) = \sqrt{\frac{2\mathcal{K}(M_1 + M_2)}{M_1 M_2}}, \quad \epsilon_1 = M_2; \quad \epsilon_2 = -M_1(1 + ika/2). \quad (13.10b)$$

Equation (13.10) shows as illustrated in Figure 13.4, that for the acoustic mode, atoms within the unit cell move essentially in unison, while for the optical mode, atoms within the unit cell vibrate out of phase.

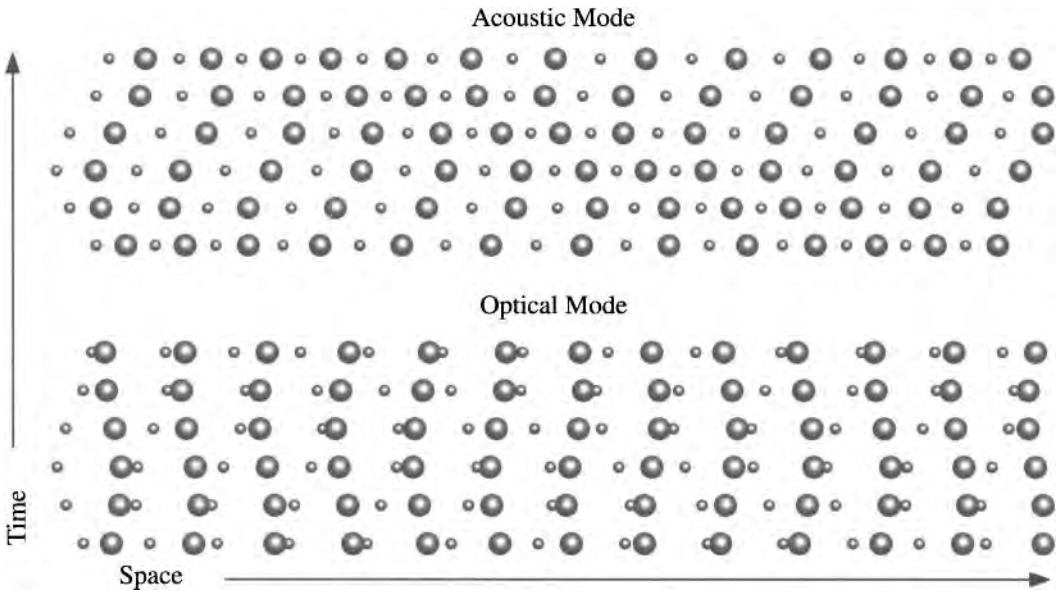


Figure 13.4. Configurations of atoms in optical and acoustic modes. In the acoustic mode, atoms within a unit cell move in concert, while in the optical mode they vibrate against one another in opposite directions.

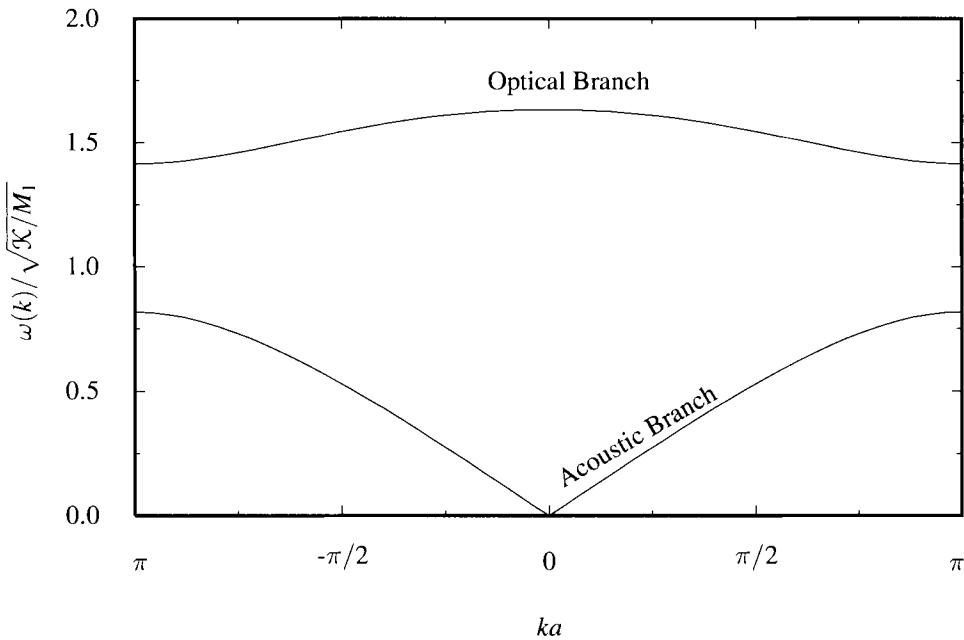


Figure 13.5. Vibrational frequencies of a chain with two alternating masses, as a function of the wave number k of oscillation, calculated in Eq. (13.9). The solution is depicted by measuring ω in units of $\sqrt{K/M_1}$ and setting $M_2 = 3M_1$.

13.2.2 Classical Vibrations in Three Dimensions

Crystalline lattices are not one-dimensional chains of ions connected to nearest neighbors by springs, nor even three-dimensional lattices of masses connected by springs. Nevertheless, viewing them this way is essentially correct when one restricts attention to small deviations of ions from their equilibrium locations. When ions move only a small amount from equilibrium, the restoring forces on them are linear, and the techniques developed for the one-dimensional chain continue to apply.

Here is why linear restoring forces arise so generally. Suppose one knows the location in the ground state of a collection of ions, $1 \dots N$, and let $\vec{u}^1 \dots \vec{u}^N$ describe the vector displacement of these ions from their equilibrium locations $\vec{R}^1 \dots \vec{R}^N$. When ions move, the energy of the crystal goes up; take the energy functional to be

$$\mathcal{E}(\vec{u}^1, \vec{u}^2 \dots \vec{u}^N).. \quad (13.11)$$

Instead of making guesses about the form of the energy functional, as in Section 11.8, assume all the variables \vec{u} are small, and develop Eq. (13.11) in a Taylor expansion in powers of the variables u .

The energy becomes

$$\mathcal{E} = \mathcal{E}_c + \sum_i \frac{\partial \mathcal{E}}{\partial u_\alpha^i} u_\alpha^i + \frac{1}{2} \sum_{\substack{\alpha\beta \\ i'j'}} u_\alpha^i \Phi_{\alpha\beta}^{i'j'} u_{\beta}^{j'} + \dots \quad \begin{array}{l} \alpha \text{ and } \beta \text{ are Cartesian indices running over} \\ \text{basis vectors of three-dimensional space.} \end{array} \quad (13.12)$$

The first term in Eq. (13.12) is the cohesive energy, calculated with such effort in Chapter 11, but which for present purposes is a dull constant and will callously be neglected. Because the lowest energy state is a minimum as a function of ion locations, the linear term in the expansion in \vec{u}^i must vanish, and the first nonzero contribution must be quadratic. That is,

$$\mathcal{E} = \mathcal{E}_c + \frac{1}{2} \sum_{\substack{\alpha\beta \\ i'j'}} u_\alpha^i \Phi_{\alpha\beta}^{i'j'} u_{\beta}^{j'} + \dots \quad (13.13)$$

The 3×3 matrix $\Phi^{i'j'}$ comes immediately from Taylor expansion of the energy and is

$$\Phi_{\alpha\beta}^{i'j'} = \frac{\partial^2 \mathcal{E}}{\partial u_\alpha^i \partial u_\beta^j} \quad \Phi^{i'j'} \text{ is always a symmetric matrix.} \quad (13.14)$$

Periodic Boundary Conditions. The formal study of electron motion employed the simplification of periodic boundary conditions. The same assumption also simplifies calculations concerning lattice vibrations. Proceeding along the direction of any of the three primitive vectors for the Bravais lattice, every physical quantity, including the displacements \vec{u} of the ions, is assumed to repeat after some number of cells is passed. All points in the equilibrium crystal are equivalent; the

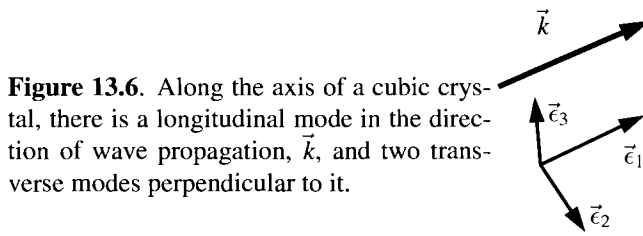


Figure 13.6. Along the axis of a cubic crystal, there is a longitudinal mode in the direction of wave propagation, \vec{k} , and two transverse modes perpendicular to it.

crystal has no surfaces or boundaries. A first consequence of this simplifying assumption is that $\Phi_{\alpha\beta}^{ll'}$ depends only upon $\vec{R}^l - \vec{R}^{l'}$ because if one displaces just two ions \vec{u}^l and $\vec{u}^{l'}$, leaving all others in equilibrium locations, the resulting energy can depend only upon their relative locations.

Equation of Motion. The dynamical equation for phonons follows from Eq. (13.13). The force on ion l is $-\partial\mathcal{E}/\partial u^l$, which leads to

$$M\ddot{\vec{u}}^l = - \sum_{l'} \Phi^{ll'} \vec{u}^{l'}. \quad \text{Subscripts are being suppressed; each } \Phi^{ll'} \text{ is a } 3 \times 3 \text{ matrix.} \quad (13.15)$$

Much of the theory of phonons can be developed without reference to the particular form or value that the matrices $\Phi^{ll'}$ take, so the question of how to calculate them will be left until later. In fact, it would be hard to proceed in any other way, because in order to conceive experimental probes of $\Phi^{ll'}$ one has to know what their consequences will be. One should not be misled by the simplifications in the starting examples; $\Phi^{ll'}$ will usually be nonzero when \vec{R}^l and $\vec{R}^{l'}$ are far from nearest neighbors, particularly in insulators, where the ions carry charges interacting with each other by Coulomb forces.

13.2.3 Normal Modes

Equation (13.15) is solved by plane waves, but as they travel in a three-dimensional crystal, one must keep track of information about their polarization. So take \vec{u} to have the form

$$\vec{u}^l = \vec{\epsilon} e^{i\vec{k}\cdot\vec{R}^l - i\omega t}. \quad \vec{\epsilon} \text{ is a unit vector that will describe the polarization of the vibration.} \quad (13.16)$$

Substituting Eq. (13.16) into Eq. (13.15) gives

$$\begin{aligned} M\omega^2 \vec{\epsilon} &= \sum_{l'} \Phi^{ll'} e^{i\vec{k}\cdot(\vec{R}^l - \vec{R}^{l'})} \vec{\epsilon} \\ &= \Phi(\vec{k}) \vec{\epsilon}, \quad \text{with } \Phi(\vec{k}) = \sum_{l'} e^{i\vec{k}\cdot(\vec{R}^l - \vec{R}^{l'})} \Phi^{ll'}. \end{aligned} \quad (13.17a)$$

$\Phi(\vec{k})$ does not depend upon l because all physical quantities depend only upon $\vec{R}^l - \vec{R}^{l'}$. (13.17b)

If it were not for the three-dimensional nature of the problem, Eq. (13.17) would constitute an explicit solution; as things are, the solution is near at hand. What remains is a matrix equation for the polarization vector $\vec{\epsilon}$. The matrix $\Phi(\vec{k})$ is real and symmetric, and therefore has three orthogonal eigenvectors for every \vec{k} .

Let $\vec{\epsilon}_{\vec{k}\nu}$, $\nu = 1 \dots 3$ be the three unit vectors that diagonalize $\Phi(\vec{k})$, and let Φ_ν be the corresponding eigenvalues. It follows immediately that

$$\omega_{\vec{k}\nu}^2 = \frac{\Phi_\nu(\vec{k})}{M}. \quad (13.18)$$

Roughly speaking, the three polarization vectors $\vec{\epsilon}_{\vec{k}\nu}$ comprise one longitudinal mode for which $\vec{\epsilon}$ points along \vec{k} , and two transverse modes for which $\vec{\epsilon}$ is perpendicular to \vec{k} (see Figure 13.6). This statement is not absolutely correct. It would only be true if one had an isotropic crystal, invariant under all rotations, but no such crystal exists. The closest that one can come is in a cubic crystal. When \vec{k} points along a crystalline axis, then by symmetry one polarization vector points along \vec{k} , and the two remaining polarization vectors correspond to degenerate energies, and point along perpendicular axes.

There are some important symmetries that $\Phi^{ll'}$ must always obey. The energy of the crystal cannot change if all ions are simultaneously displaced by a single vector. Therefore,

$$\sum_{l'} \Phi^{ll'} = 0. \quad (13.19)$$

$$\Rightarrow \Phi(\vec{k} = 0) = 0 \quad (13.20)$$

Because of the assumption of periodic boundary conditions, the allowed values of \vec{k} are given exactly as in Eq. (6.7). Furthermore, notice that

$$\Phi(\vec{k} + \vec{K}) = \Phi(\vec{k}), \quad \text{Look at Eq. (13.17), and notice that addition of any reciprocal lattice vector turns instantly into a multiple of } 2\pi i. \quad (13.21)$$

where \vec{K} is any reciprocal lattice vector. Therefore, one may always take \vec{k} to lie in the first Brillouin zone. Lattice vibrations, just like electrons, are waves that travel in the perfectly periodic potential described by ion locations \vec{R}^l . Exactly the same \vec{k} states can be used to classify the two sets of vibrations.

One difference between the electron problem and the phonon problem has to do with the numbers of modes. There is no upper limit to the number of distinct one-particle electronic states that can inhabit a lattice, and there is no limit to the number of energy bands the states can fill. In contrast, a single Brillouin zone completely exhausts all the phonon states of a Bravais lattice. The reason for the difference is that electron wave functions are defined everywhere in space, and values of the wave function in between lattice sites are physically important. The phonon states are completely described by their values at the lattice sites \vec{R} , and any two functions that are the same on these lattice sites are physically indistinguishable no matter how they may wiggle in between.

13.2.4 Lattice with a Basis

Constructing a lattice with a basis in Section 13.2.1 led to a phonon spectrum with more than one branch, including low-frequency acoustic modes and optical phonons with high frequencies at small wave vector. The same phenomenon

persists in three dimensions. Adding new atoms to a unit cell adds new degrees of freedom to the lattice, and one must consider a correspondingly greater number of normal modes to describe them. For example, in three dimensions with four atoms per unit cell, one has 3×4 normal modes for every value of \vec{k} .

The formal way to calculate these modes is to write

$$M_n \ddot{\vec{u}}^{ln} = - \sum_{l'n'} \Phi^{lnl'n'} \vec{u}^{l'n'}, \tag{13.22}$$

where the superscripts n and n' label the different atoms comprising the basis in each unit cell. Proceeding on the path that led from Eq. (13.15) to Eq. (13.17), one obtains

$$\vec{u}^{ln} = \vec{\epsilon}^n e^{i\vec{k} \cdot \vec{R}^{ln} - i\omega t}, \tag{13.23}$$

$$\Rightarrow M_n \omega^2 \vec{\epsilon}^n = \sum_{n'} \Phi^{nn'}(\vec{k}) \vec{\epsilon}^{n'}. \tag{13.24}$$

In the form Eq. (13.24), the practical mathematical problem that one has to solve is difficult to make out. One way to describe the problem better is to define a new index p that ranges over all degrees of freedom in the unit cell. With four atoms per unit cell, p would range from 1 to 12. The first three values would correspond to the x , y , and z coordinates of the first atom, the next three values would correspond to the coordinates of the next atom, and so on. Using this notation,

$$M_p \omega^2 \epsilon_p = \sum_{p'}^{3N} \Phi_{pp'}(\vec{k}) \epsilon_{p'}. \tag{13.25}$$

For example, Φ_{15} describes the force in the x direction on atom 1 when atom 2 moves in the y direction.

Example: Diamond Lattice. Consider atoms sitting on a diamond lattice (Figure 2.6), interacting through central forces with their four nearest neighbors. The task is to find the phonon dispersion relations. This calculation gives acceptable results despite the fact that the diamond structure is never the ground state of particles interacting with central forces, because only small deviations from equilibrium are permitted.

To begin, it is necessary to record the potentials that result from central forces. Suppose one has a collection of atoms sitting on a Bravais lattice \vec{R}^l with basis \vec{v}^n , take $\vec{R}^{ln} = \vec{R}^l + \vec{v}^n$, and have particles interact with a potential of the form

$$U = \frac{1}{2} \sum_{lnl'n'} \phi_{mm'}(|\vec{u}^{ln} + \vec{R}^{ln} - \vec{u}^{l'n'} - \vec{R}^{l'n'}|). \tag{13.26}$$

The subscript mm' on ϕ allows different breeds of atoms to interact with different force laws.

Expanding to quadratic order in the small deviations \vec{u} and using the fact that terms linear in \vec{u} must vanish, one finds that

$$U \approx \frac{1}{4} \sum_{lnl'n'} [\vec{u}^{ln} - \vec{u}^{l'n'}] \mathbf{f}^{lnl'n'} [\vec{u}^{ln} - \vec{u}^{l'n'}], \tag{13.27}$$

where the components of the 3×3 matrix $\mathbf{f}^{nl'n'}$ are

$$\mathbf{f}_{\alpha\beta}^{nl'n'} = \frac{\partial^2}{\partial r_\alpha \partial r_\beta} \phi_{nn'}(|\vec{r}|) \Big|_{\vec{r}=\vec{R}^{ln}-\vec{R}^{l'n'}} \quad \text{The subscripts on } \mathbf{f} \text{ range over } x, \quad (13.28)$$

y, and z components.

$$= \left\{ \frac{r_\alpha r_\beta}{r^2} [\phi''_{nn'}(r) - \frac{1}{r} \phi'_{nn'}(r)] + \frac{\delta_{\alpha\beta}}{r} \phi'_{nn'}(r) \right\} \Big|_{\vec{r}=\vec{R}^{ln}-\vec{R}^{l'n'}}. \quad (13.29)$$

The condition that the crystal be in equilibrium when all \vec{u} 's vanish is

$$\sum_{l'n'} \frac{\vec{r}}{r} \phi'_{nn'}(r) \Big|_{\vec{r}=\vec{R}^{ln}-\vec{R}^{l'n'}} = 0. \quad \text{This condition does not demand that } \phi' \text{ vanish. Primes on } \phi \text{ mean derivatives.} \quad (13.30)$$

Differentiating Eq. (13.27) to find the force on the atom at ln gives

$$\Phi^{lnl'n'} = \sum_{l''n''} \mathbf{f}^{lnl''n''} (\delta_{ll''} \delta_{nn''} - \delta_{l'l''} \delta_{n'n''}). \quad (13.31)$$

$l''n''$ Deriving this relation is a slightly unpleasant two-line exercise in taking derivatives of sums with large numbers of indices. It is best to write the full sum $\sum_{l''n''} \text{out explicitly and use relations like } \frac{\partial}{\partial u_\alpha^{ln}} u_\alpha^{ln} = \delta_{ll'} \delta_{nn'} \delta_{\alpha\alpha}$

In the present case, where there is only one potential function ϕ , and only the four nearest neighbors at distance d are being considered, Eq. (13.29) really only involves two numbers, which are

$$f_1 - f_2 = \phi''(d) - \frac{1}{d} \phi'(d) \quad (13.32)$$

and

$$f_2 = \frac{1}{d} \phi'(d) \quad (13.33)$$

$$\Rightarrow \mathbf{f}_{\alpha\beta}^{nl'n'} = \frac{r_\alpha r_\beta}{r^2} [f_1 - f_2] + \delta_{\alpha\beta} f_2 \Big|_{\vec{r}=\vec{R}^{ln}-\vec{R}^{l'n'}}. \quad \text{If } \vec{R}^{ln} \text{ and } \vec{R}^{l'n'} \text{ are nearest neighbors, and zero otherwise.} \quad (13.34)$$

So \mathbf{f} depends only a little on details of the potential, and it mainly acquires its structure from the geometry of the lattice. Once the matrix $\mathbf{f}_{\alpha\beta}^{nl'n'}$ has been computed, Φ can be found from Eq. (13.31). Taking \vec{R}^{00} to be the origin, one needs to find Φ only for $l = 0$, for n ranging over the basis (which in this case has two members, the origin and $\frac{a}{4}[111]$) and for $l'n'$ ranging over the nearest neighbors of each of these two sites, a total of eight choices for $nl'n'l'$. Next one computes

$$\Phi^{nn'}(\vec{k}) = \sum_{l'} \Phi^{0nl'n'} e^{i\vec{k} \cdot (\vec{R}^{0n} - \vec{R}^{l'n'})} \quad \text{There are not too many terms in the sum, because only nearest neighbors have nonzero } \Phi^{0nl'n'}. \quad (13.35)$$

and has four 3×3 matrices for the four combinations of n and n' . Finally, one forms the 6×6 matrix Φ according to Eq. (13.25), and from its eigenvalues deduces the vibrational frequencies of the phonons. The construction of the various matrices can be performed relatively painlessly with the use of symbolic algebra, and the final 6×6 matrix quickly diagonalized with any suitable numerical routine. Results of this procedure, roughly appropriate for silicon, appear in Figure 13.7.

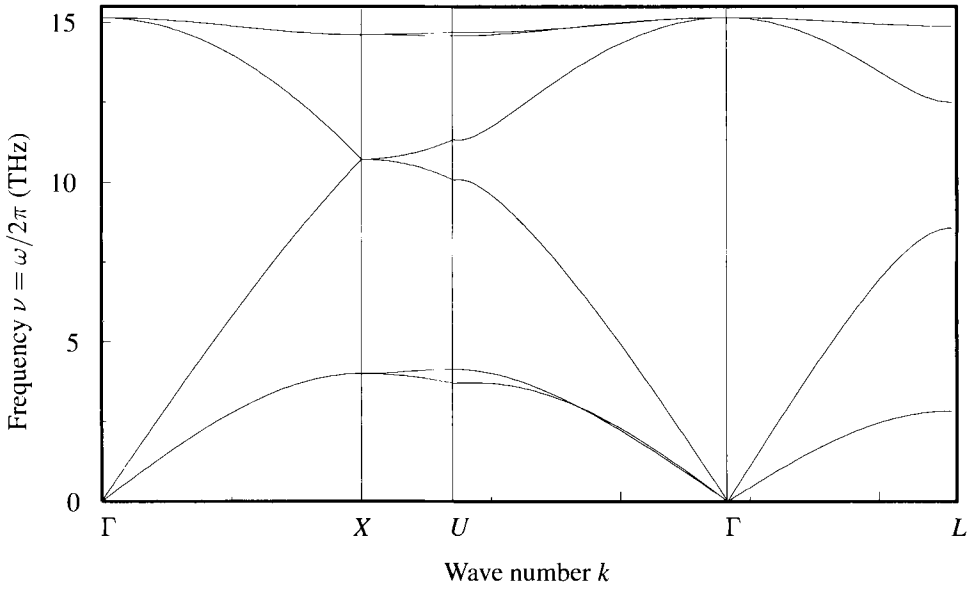


Figure 13.7. Calculation of phonon frequencies from Eq. (13.35). Using $f_1/M = (2\pi)^2 \cdot 78 \text{ THz}^2$ and $f_2/M = (2\pi)^2 \cdot 4 \text{ THz}^2$, the results give a reasonable approximation to the phonon structure of silicon, measured in THz. Results of more accurate computations together with experimental data appear in Figure 13.18. Notation for Brillouin zone locations is given in Figure 7.8.

13.3 Vibrations of a Quantum–Mechanical Lattice

The discussion of lattice vibrations has proceeded until now as if the world obeyed classical mechanics. The reason for this negligence is that classical and quantum mechanics find themselves in nearly complete agreement for harmonic oscillators. The vibrational frequencies of a quantum-mechanical lattice are the same as its classical counterpart. However, whereas in the classical case a mode may have arbitrary amplitude, in the quantum mechanical case the modes are allowed only to have discrete amplitudes. The energy of mode \vec{k} , polarization ν , is permitted only to take values

$$\hbar\omega_{\vec{k}\nu}(n + \frac{1}{2}); \tag{13.36}$$

where $n \geq 0$ is an integer. When $n = 1$, one says that a single phonon of wavenumber \vec{k} has been excited. Because an arbitrary number of phonons n may occupy a given \vec{k} state, one can interpret the excitations of a lattice as particles obeying Bose statistics.

Despite the relatively minor formal differences between the results of the classical and quantum-mechanical analyses, there are several areas in which the physical influence of quantum mechanics is crucial. For example, at low temperatures, the amplitude of lattice vibrations falls below the threshold of possibilities described by Eq. (13.36), and specific heat differs substantially from classical ex-

pectations. For this and other reasons, a brief review of the quantum mechanical theory now becomes necessary.

For a single harmonic oscillator described by the Hamiltonian

$$\hat{\mathcal{H}} = \frac{\hat{P}^2}{2M} + \frac{1}{2}M\omega^2\hat{R}^2 \quad (13.37)$$

one defines raising and lowering operators

$$\hat{a}^\dagger = \sqrt{\frac{M\omega}{2\hbar}}\hat{R} - i\sqrt{\frac{1}{2\hbar M\omega}}\hat{P} \quad \text{This is the "raising" or "creation" operator, which when it acts upon the ground state of the oscillator populates it with one excited state.} \quad (13.38a)$$

$$\hat{a} = \sqrt{\frac{M\omega}{2\hbar}}\hat{R} + i\sqrt{\frac{1}{2\hbar M\omega}}\hat{P}. \quad \text{And this is the "lowering" or "destruction" operator that drags the oscillator down the ladder of excited states each time it acts.} \quad (13.38b)$$

The Hamiltonian expressed in terms of these operators simplifies to

$$\hat{\mathcal{H}} = \hbar\omega\left(\hat{a}^\dagger\hat{a} + \frac{1}{2}\right) = \hbar\omega\left(\hat{n} + \frac{1}{2}\right) \quad \text{The number operator } \hat{n} = \hat{a}^\dagger\hat{a} \text{ measures the degree of excitation of the oscillator, or equivalently the number of phonons occupying it.} \quad (13.39)$$

and the original particle position operator is

$$\hat{R} = \sqrt{\frac{\hbar}{2M\omega}}(\hat{a} + \hat{a}^\dagger). \quad (13.40)$$

Second Quantization of Phonons. To treat motion of the atoms of a solid to quadratic order, write the Hamiltonian

$$\hat{\mathcal{H}} = \sum_l \frac{\hat{P}_l^2}{2M} + \frac{1}{2} \sum_{ll'} \hat{u}^l \Phi^{ll'} \hat{u}^{l'} \dots \quad \text{The operators } \hat{u}^l \text{ describe the deviation of an ion from its equilibrium location } \vec{R}^l, \text{ assumed for the moment to belong to a monatomic Bravais lattice.} \quad (13.41)$$

In order to find all eigenvalues of Eq. (13.41), define the analog of Eq. (13.38),

$$\hat{a}_{\vec{k}\nu} = \frac{1}{\sqrt{N}} \sum_{l=1}^N e^{-i\vec{k}\cdot\vec{R}^l} \vec{\epsilon}_{\vec{k}\nu}^* \cdot \left[\sqrt{\frac{M\omega_{\vec{k}\nu}}{2\hbar}} \hat{u}^l + i\sqrt{\frac{1}{2\hbar M\omega_{\vec{k}\nu}}} \hat{P}^l \right] \quad (13.42a)$$

$$\hat{a}_{\vec{k}\nu}^\dagger = \frac{1}{\sqrt{N}} \sum_{l=1}^N e^{i\vec{k}\cdot\vec{R}^l} \vec{\epsilon}_{\vec{k}\nu} \cdot \left[\sqrt{\frac{M\omega_{\vec{k}\nu}}{2\hbar}} \hat{u}^l - i\sqrt{\frac{1}{2\hbar M\omega_{\vec{k}\nu}}} \hat{P}^l \right]. \quad (13.42b)$$

A brief calculation (Problem 5) inverts these relations and expresses \hat{u}^l in terms of the creation and annihilation operators as

$$\hat{u}^l = \frac{1}{\sqrt{N}} \sum_{\vec{k}\nu} \left[\hat{u}_{\vec{k}\nu} e^{i\vec{k}\cdot\vec{R}^l} + \hat{u}_{\vec{k}\nu}^\dagger e^{-i\vec{k}\cdot\vec{R}^l} \right] \quad \text{with } \hat{u}_{\vec{k}\nu} \equiv \sqrt{\frac{\hbar}{2M\omega_{\vec{k}\nu}}} \vec{\epsilon}_{\vec{k}\nu} \hat{a}_{\vec{k}\nu} \quad (13.43a)$$

and

$$\hat{P}^l = \frac{1}{\sqrt{N}} \sum_{\vec{k}\nu} \left[\hat{P}_{\vec{k}\nu} e^{i\vec{k}\cdot\vec{R}^l} + \hat{P}_{\vec{k}\nu}^\dagger e^{-i\vec{k}\cdot\vec{R}^l} \right] \quad \text{with} \quad \hat{P}_{\vec{k}\nu} = -i\sqrt{\frac{\hbar M \omega_{\vec{k}\nu}}{2}} \vec{\epsilon}_{\vec{k}\nu} \hat{a}_{\vec{k}\nu}. \quad (13.43b)$$

From the commutation relation $[\hat{P}^l, \hat{R}^l] = -i\hbar$, one finds for the creation and annihilation operators the commutation relation

$$[\hat{a}_{\vec{k}\nu}, \hat{a}_{\vec{k}\nu}^\dagger] = 1. \quad (13.44)$$

In moving between Eqs. (13.42) and (13.43), the frequencies $\omega_{\vec{k}\nu}$ and the unit vectors $\vec{\epsilon}_{\vec{k}\nu}$ may in principle be chosen arbitrarily, just so long as the three unit vectors $\vec{\epsilon}_{\vec{k}\nu}$ at every value of \vec{k} are orthonormal. However, the only choice one would sensibly make for these quantities is the one that diagonalizes the Hamiltonian (13.41), which means choosing $\vec{\epsilon}_{\vec{k}\nu}$ to be the eigenvectors of the dynamical matrix Φ and choosing $\omega_{\vec{k}\nu}$ to be related to the eigenvalues by Eq. (13.18). Also notice from Eq. (13.17) that $\Phi(\vec{k}) = \Phi(-\vec{k})$, because one is related to the other just by changing order of summation, and therefore

$$\omega_{\vec{k}\nu} = \omega_{-\vec{k}\nu}. \quad (13.45)$$

Making use of Eq. (13.45) gives

$$\sum_l \frac{\hat{P}^l{}^2}{2M} = \sum_{\vec{k}\nu} \frac{\hbar\omega_{\vec{k}\nu}}{4} \left\{ \begin{aligned} & [\hat{a}_{\vec{k}\nu} \hat{a}_{\vec{k}\nu}^\dagger + \hat{a}_{\vec{k}\nu}^\dagger \hat{a}_{\vec{k}\nu}] \\ & - [\hat{a}_{\vec{k}\nu} \hat{a}_{\vec{k}\nu} \vec{\epsilon}_{\vec{k}\nu} \cdot \vec{\epsilon}_{-\vec{k}\nu} + \hat{a}_{\vec{k}\nu}^\dagger \hat{a}_{\vec{k}\nu}^\dagger \vec{\epsilon}_{\vec{k}\nu}^* \cdot \vec{\epsilon}_{-\vec{k}\nu}^*] \end{aligned} \right\} \quad (13.46a)$$

$$\sum_{l'l'} \frac{1}{2} \hat{u}^l \Phi^{ll'} \hat{u}^{l'} = \sum_{\vec{k}\nu} \frac{\hbar\omega_{\vec{k}\nu}}{4} \left\{ \begin{aligned} & [\hat{a}_{\vec{k}\nu} \hat{a}_{\vec{k}\nu}^\dagger + \hat{a}_{\vec{k}\nu}^\dagger \hat{a}_{\vec{k}\nu}] \\ & + [\hat{a}_{\vec{k}\nu} \hat{a}_{\vec{k}\nu} \vec{\epsilon}_{\vec{k}\nu} \cdot \vec{\epsilon}_{-\vec{k}\nu} + \hat{a}_{\vec{k}\nu}^\dagger \hat{a}_{\vec{k}\nu}^\dagger \vec{\epsilon}_{\vec{k}\nu}^* \cdot \vec{\epsilon}_{-\vec{k}\nu}^*] \end{aligned} \right\}. \quad (13.46b)$$

In order to arrive at Eqs. (13.46), one employs the facts that $\vec{\epsilon}_{\vec{k}\nu}^* \cdot \vec{\epsilon}_{\vec{k}\nu'} = \delta_{\nu\nu'}$ and that $\vec{\epsilon}_{\vec{k}\nu} \cdot \vec{\epsilon}_{-\vec{k}\nu'}$ vanishes unless $\nu = \nu'$. Although one has the freedom in defining $\vec{\epsilon}_{\vec{k}\nu}$ to request that $\vec{\epsilon}_{\vec{k}\nu}^* = \vec{\epsilon}_{-\vec{k}\nu}$ such a choice is very confusing for longitudinal modes, where $\vec{\epsilon}_{\vec{k}\nu}^* = -\vec{\epsilon}_{-\vec{k}\nu}$ is more natural, so no relation between $\vec{\epsilon}_{\vec{k}\nu}^*$ and $\vec{\epsilon}_{-\vec{k}\nu}$ will be assumed.

Summing Eqs. (13.46a) and (13.46b) gives for the Hamiltonian of (13.41) that

$$\hat{\mathcal{H}} = \sum_{\vec{k}\nu} \frac{\hbar\omega_{\vec{k}\nu}}{2} [\hat{a}_{\vec{k}\nu} \hat{a}_{\vec{k}\nu}^\dagger + \hat{a}_{\vec{k}\nu}^\dagger \hat{a}_{\vec{k}\nu}] = \sum_{\vec{k}\nu} \hbar\omega_{\vec{k}\nu} (\hat{a}_{\vec{k}\nu}^\dagger \hat{a}_{\vec{k}\nu} + \frac{1}{2}). \quad \text{Use Eq. (13.44).} \quad (13.47)$$

For a lattice with a basis, Eq. (13.47) still holds true, but the summation acquires an additional index corresponding to the branch of the phonon mode, which ranges over the number of atoms in each unit cell. If the number of indices becomes too cumbersome, one can adopt the abbreviated notation

$$\hat{\mathcal{H}} = \sum_i \hbar\omega_i (\hat{n}_i + \frac{1}{2}). \quad \text{The number operator } \hat{n}_i = \hat{a}_i^\dagger \hat{a}_i. \quad (13.48)$$

where the sum over reciprocal vectors \vec{k} , polarizations ν , and modes is subsumed into the single index i .

Time Evolution. In the study of neutron scattering, it will also be necessary to know how the operators \hat{a} and \hat{u} evolve in time. In the Heisenberg picture, the annihilation operators evolve according to

$$\hat{a}_{\vec{k}\nu}^-(t) = e^{i\hat{\mathcal{H}}t/\hbar} \hat{a}_{\vec{k}\nu}^- e^{-i\hat{\mathcal{H}}t/\hbar} \quad (13.49)$$

so that

$$\frac{\partial \hat{a}_{\vec{k}\nu}^-(t)}{\partial t} = e^{i\hat{\mathcal{H}}t/\hbar} i[\hat{\mathcal{H}}, \hat{a}_{\vec{k}\nu}^-] e^{-i\hat{\mathcal{H}}t/\hbar} / \hbar \quad (13.50)$$

$$= -i\omega_{\vec{k}\nu} \hat{a}_{\vec{k}\nu}^- \quad (13.51)$$

$$\Rightarrow \hat{a}_{\vec{k}\nu}^-(t) = \hat{a}_{\vec{k}\nu}^- e^{-i\omega_{\vec{k}\nu} t}. \quad (13.52)$$

As for the time evolution of \hat{u}^l , Eq. (13.43a) generalizes to

$$\hat{u}^l(t) = \frac{1}{\sqrt{N}} \sum_{\vec{k}\nu} [\hat{u}_{\vec{k}\nu}^- e^{i\vec{k}\cdot\vec{R}^l - i\omega_{\vec{k}\nu} t} + \hat{u}_{\vec{k}\nu}^+ e^{-i\vec{k}\cdot\vec{R}^l + i\omega_{\vec{k}\nu} t}]. \quad (13.53)$$

13.3.1 Phonon Specific Heat

The specific heat of solids was one of the “19th century clouds” over 19th-century physics described by Kelvin (1904). Solid objects were clearly built by connecting small massive objects together with some form of spring. According to the equipartition theorem of statistical mechanics, the specific heat must be $k_B/2$ per degree of freedom. Each mass point must have three kinetic and three potential degrees of freedom, and therefore a specific heat of $C_V = 3Nk_B$, the law of Dulong and Petit. Not many data were available to test this law thoroughly, but by 1907, specific heat had been measured down to around 50 K in diamond. Instead of remaining constant, as shown in Figure 13.8, it declines precipitously at low temperatures. For some reason, oscillators within the solid refused to take in energy at low temperatures.

Einstein conceived the remarkable hypothesis that one might employ Planck’s radiation law, which stated that for black-body radiation the probability of exciting a mode of frequency ω varied as $1/(\exp(\hbar\beta\omega) - 1)$. This formula was still purely empirical, so there was not as yet the possibility of deriving the specific heat of solids from firm underlying principles. However, one could guess that if the solid were built of N oscillators of frequency ω_0 , then the mean energy at temperature T would be given by

$$\mathcal{E} = \frac{3N\hbar\omega_0}{e^{\hbar\beta\omega_0} - 1} \quad (13.54)$$

$$\Rightarrow C_V = \left. \frac{\partial \mathcal{E}}{\partial T} \right|_V = \frac{3N(\hbar\omega_0)^2 e^{\hbar\beta\omega_0} / (k_B T^2)}{[e^{\hbar\beta\omega_0} - 1]^2}. \quad (13.55)$$

A particular strength of this formula was the fact that one was not condemned to fit ω_0 from the specific heat data alone. If the solid were truly built of oscillators concentrated at a certain frequency, then it should absorb radiation at this

frequency. Diamond was known to have a “residual ray,” (Section 22.3.1) at $11 \mu\text{m} \Rightarrow \omega_0 = 1.71 \cdot 10^{14} \text{s}^{-1}$; placing this value into Eq. (13.55) gave the theoretical result shown in Figure 13.8. Despite the promise of this initial comparison, further experimental measurements drew details of the calculation into question. The theory dropped off far too fast at very low temperatures. The resolution of this difficulty was soon found to lie in more accurate computations of vibrational spectra. In order to explain how they entered, one must turn to the formal computation of specific heats.

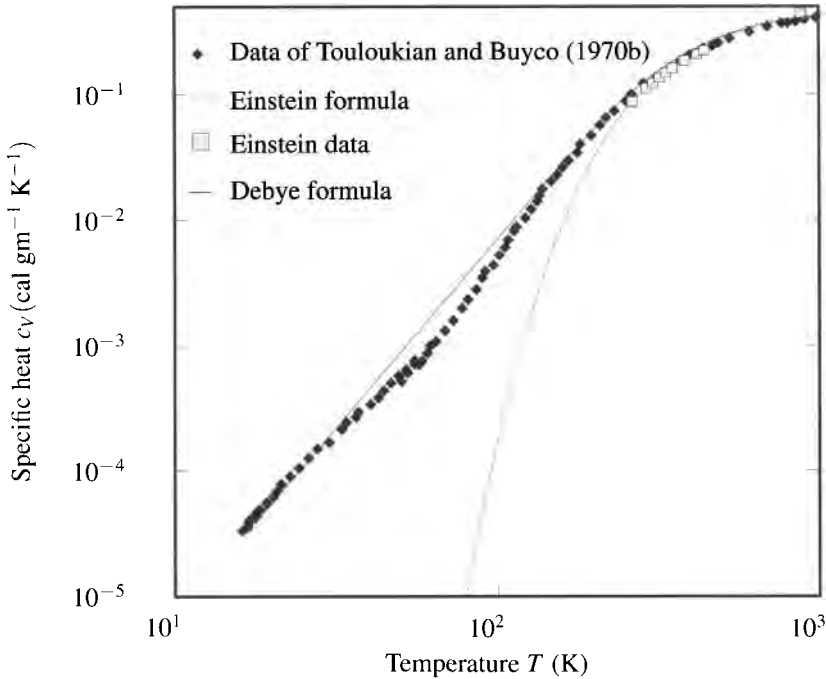


Figure 13.8. Specific heat formula Eq. (13.55) with $\omega_0 = 1.71 \cdot 10^{14} \text{s}^{-1}$ compared with data for diamond available to Einstein (1907) and more recent data of Touloukian and Buyco (1970b). At temperatures below 100 K, the Einstein formula falls below the data. Debye’s formula, Eq. (13.75), is a clear improvement.

In order to calculate the partition function for the Hamiltonian (13.48), one must begin by identifying all its eigenstates. The states of a single harmonic oscillator are indexed by a single integer l ranging from zero to infinity, producing energies $\hbar\omega(l + \frac{1}{2})$, and therefore the states of a large collection of harmonic oscillators are indexed by many integers l_i , each ranging from zero to infinity, and producing energy

$$\mathcal{E} = \sum_i \hbar\omega_i(l_i + \frac{1}{2}). \tag{13.56}$$

The partition function and ensuing thermodynamic quantities are therefore

$$Z = \sum_{l_1=0}^{\infty} \sum_{l_2=0}^{\infty} \dots e^{-\beta \sum_i \hbar\omega_i(l_i+1/2)} \tag{13.57}$$

$$= \prod_{i=1}^{\infty} \left\{ \sum_{l=0}^{\infty} e^{-\beta \hbar \omega_i (l+1/2)} \right\} \quad (13.58)$$

$$= \prod_{i=1}^{\infty} \left\{ \frac{e^{-\beta \hbar \omega_i / 2}}{1 - \exp(-\beta \hbar \omega_i)} \right\} \quad (13.59)$$

$$\Rightarrow \mathcal{F} = -k_B T \ln Z = \sum_i \frac{\hbar \omega_i}{2} + k_B T \ln(1 - e^{-\beta \hbar \omega_i}) \quad (13.60)$$

$$\Rightarrow \mathcal{E} = \frac{\partial \beta \mathcal{F}}{\partial \beta} = \sum_i \frac{\hbar \omega_i}{2} + \frac{\hbar \omega_i}{e^{\beta \hbar \omega_i} - 1} = \sum_i \hbar \omega_i (n_i + \frac{1}{2}) \quad (13.61)$$

with

$$n_i \equiv \frac{1}{e^{\beta \hbar \omega_i} - 1} \quad \text{This expression defines the Bose-Einstein factor } n_i. \quad (13.62)$$

$$\Rightarrow C_V = \frac{\partial \mathcal{E}}{\partial T} \Big|_V = \sum_i C_i = \sum_i \hbar \omega_i \frac{\partial n_i}{\partial T}. \quad (13.63)$$

Phonon Density of States. Just as the density of electronic states plays a crucial role in determining the thermal properties of the electron gas, similarly the *density of phonon states* encodes the information needed to deduce thermal properties of lattices. This density of states is defined by

$$D(\omega) = \frac{1}{\mathcal{V}} \sum_i \delta(\omega - \omega_i) = \frac{1}{\mathcal{V}} \sum_{\vec{k}\nu} \delta(\omega - \omega_{\vec{k}\nu}) = \int \frac{d\vec{k}}{(2\pi)^3} \sum_{\nu} \delta(\omega - \omega_{\vec{k}\nu}), \quad (13.64)$$

and one may use it, for example, to write

$$C_V = \mathcal{V} \int_0^{\infty} d\omega D(\omega) \frac{\partial}{\partial T} \frac{\hbar \omega}{e^{\beta \hbar \omega} - 1}. \quad (13.65)$$

Before presenting the simple models frequently used to represent densities of states and thereby extract thermodynamic quantities, it is best to present some actual data derived from experiment. Figure 13.9 presents representative data for silicon.

Two qualitative lessons are apparent in these data.

1. The characteristic upper frequency at which the phonon modes terminate is 16 terahertz; this is the characteristic frequency of the optical modes and is the upper limit of the acoustic modes.
2. The densities of states are littered with cusps. These cusps are precisely the van Hove singularities discussed in Section 7.2.5. They arise at any point in frequency space where one of the phonon modes passes through an extremal value. In three-dimensional solids the result is a cusp, in two-dimensional solids it is a logarithmic divergence, and for one-dimensional chains it is a square root divergence.

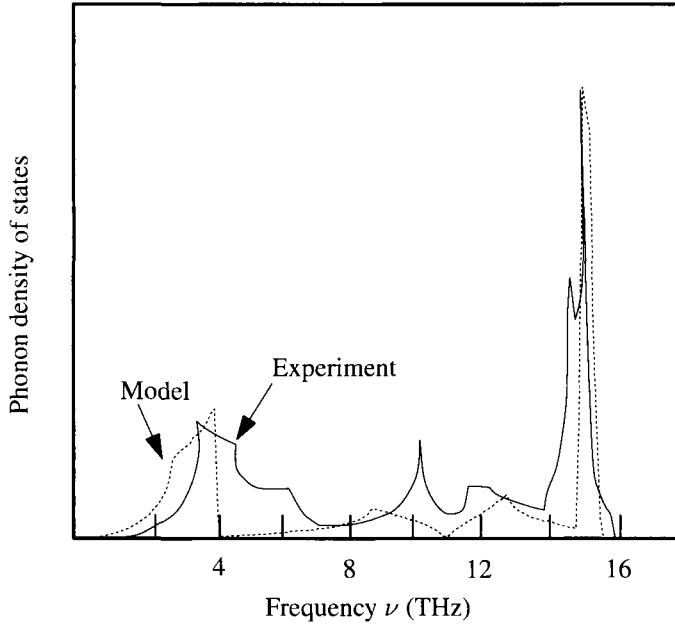


Figure 13.9. Experimental data for the phonon density of states in silicon, compared with results of model calculation that produced Figure 13.7. [Source: Dolling and Cowley (1966), p. 469.]

For temperatures $k_B T$ greater than all the energies $\hbar\omega_i$ of the vibrating lattice, the specific heat takes the form

$$C_V = N_f k_B \quad \text{Take Eq. (13.62) for small } \beta, \text{ and differentiate with respect to } T. \quad N_f \text{ gives} \quad (13.66)$$

number of terms in Eq. (13.63); for monatomic lattice in 3- d , $N_f = 3N$.

This relation is the law of Dulong and Petit, a result of the classical theorem of equipartition of energy. From a classical perspective, it is impossible to understand obtaining any result for specific heat which differs from Eq. (13.66).

The quantum-mechanical expressions for specific heat do however, differ from Eq. (13.66), and at low temperatures they differ substantially. Low temperatures bring several simplifications. Any phonon mode whose energy $\hbar\omega$ is much greater than $k_B T$ contributes nothing of note to the specific heat. At a temperature of 10 K, one needs therefore to focus upon frequencies of order $10 k_B/h \text{ K} = 0.208 \text{ THz}$. Sound speeds in solids are of order 1000 m s^{-1} or more, so such frequencies correspond to wavelengths of 48 \AA , a distance comfortably larger than interatomic spacing. The densities of states in Figure 13.9 are settling into the low-frequency limit for such frequencies. Either argument leads to the conclusion that for temperatures of order 10 K, it should be possible to use the long-wavelength, low-frequency limit $\omega = ck$ for the dispersion relation of the phonons. In this limit, Eq. (13.64) becomes

$$D(\omega) = \int \frac{d\vec{k}}{(2\pi)^3} \sum_{\nu} \delta(\omega - c_{\nu}(\hat{k})k) \tag{13.67}$$

The sum on ν is over the three acoustic modes, approximately one longitudinal and two transverse. However, the sound speed depends generally upon orientation; hence dependence upon \hat{k} .

$$= \frac{3\omega^2}{2\pi^2 c^3} \text{ with } \frac{1}{c^3} = \frac{1}{3} \sum_{\nu} \int \frac{d\Sigma}{4\pi} \frac{1}{c_{\nu}^3(\hat{k})} \tag{13.68}$$

The integral is a surface integral over orientations of \hat{k} .

$$\Rightarrow C_V = \mathcal{V} \frac{\partial}{\partial T} \frac{3(k_B T)^4}{2\pi^2 (c\hbar)^3} \int_0^{\infty} dx \frac{x^3}{e^x - 1} \tag{13.69}$$

$x = \beta\hbar\omega$.

$$= \mathcal{V} \frac{2\pi^2}{5} k_B \left[\frac{k_B T}{\hbar c} \right]^3 \tag{13.70}$$

The integral in Eq. (13.69) was evaluated in Eq. (6.67).

13.3.2 Einstein and Debye Models

Before the theory of lattice vibrations made detailed calculations of the density of states $D(\omega)$ possible, simple guesses for the form of $D(\omega)$ were employed to obtain an estimate for the consequence of quantum mechanics for specific heats. To recover Einstein's theory of specific heats, take the density of states to be

$$D(\omega) = \frac{3N}{\mathcal{V}} \delta(\omega - \omega_0), \tag{13.71}$$

$3N$ gives the total number of oscillatory modes in a solid responsible for the specific heat.

resulting immediately in Eq. (13.55).

The Debye model improves upon the Einstein model. Debye's calculation correctly reproduces Eq. (13.70) at low temperatures and correctly reproduces the law

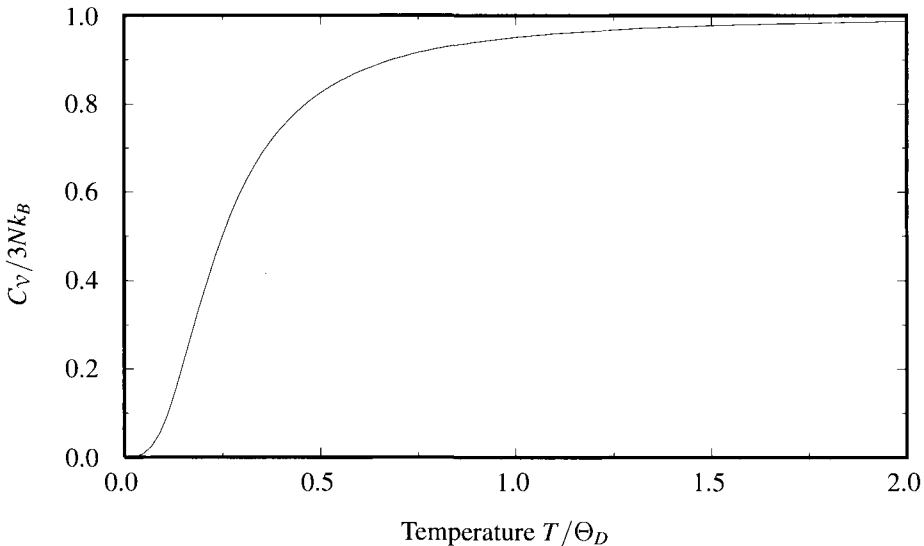


Figure 13.10. Specific heat in the Debye approximation, scaled by the prediction of Du-long and Petit.

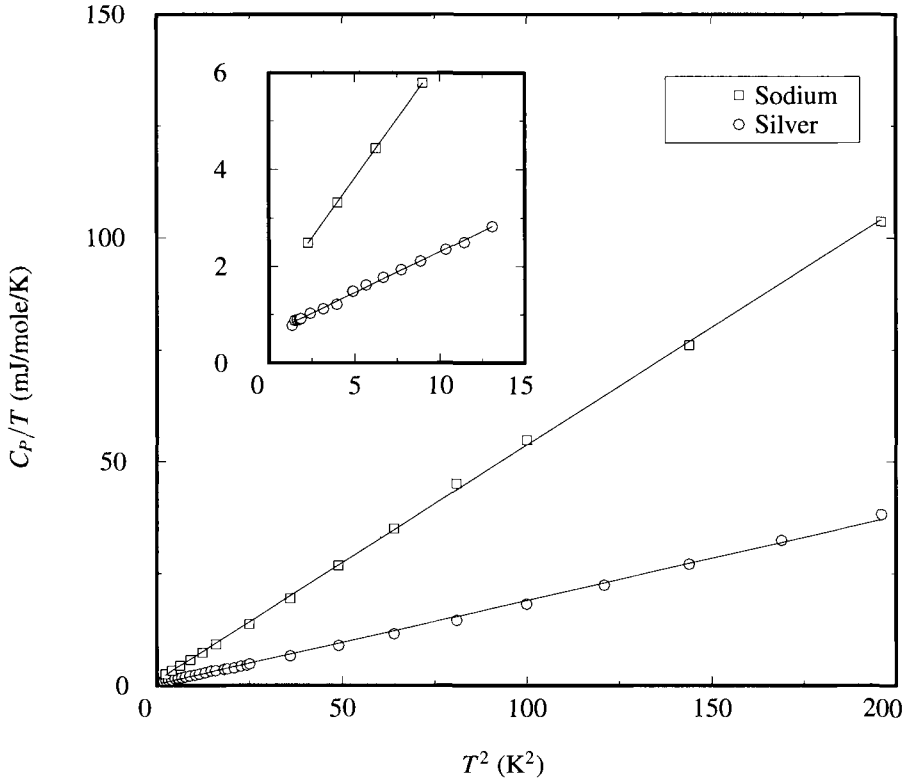


Figure 13.11. The specific heats of sodium and silver are displayed, illustrating the validity of the form (13.76). The intercepts of regression lines accurately reproduce the experimental values given in Table 6.2. [Source: Touloukian et al. (1975).]

of Dulong and Petit at high temperatures. The device to achieve this aim is to approximate the density of states by

$$D(\omega) = \frac{3\omega^2}{2\pi^2c^3}\theta(\omega_D - \omega) \quad \text{See Eq. (13.68). Use the low temperature form for the density of states everywhere, but cut it off to give the right total number of modes.} \quad (13.72)$$

where the sharp cutoff at ω_D , the *Debye frequency*, is chosen so that the total number of modes equals the number of vibrational degrees of freedom:

$$3N = \mathcal{V} \int_0^\infty d\omega D(\omega) \Rightarrow n = \frac{\omega_D^3}{6\pi^2c^3}. \quad n \text{ is the number of ions per volume.} \quad (13.73)$$

The characteristic *Debye temperature* Θ_D at which all phonons become thermally active in this approximation is

$$k_B\Theta_D \equiv \hbar\omega_D \quad (13.74)$$

The specific heat in this approximation is

$$C_V = 9Nk_B \left(\frac{T}{\Theta_D}\right)^3 \int_0^{\Theta_D/T} dx \frac{x^4 e^x}{(e^x - 1)^2} \quad (13.75)$$

Table 13.1. Debye temperatures of elements

El.	Θ_D	El.	Θ_D	El.	Θ_D	El.	Θ_D
Am	121	Eu	118	Na	157	Sm	169
Ar	92	Fe	477	Nb	276	Sn	199
Ag	227	Ga	325	Nd	163	Sr	147
Al	433	Ge	373	Ne	74.6	Ta	245
As	282	Gd	182	Ni	477	Tb	176
Au	162	H	122	Np	259	Te	152
Ba	111	He	34-108	Os	467	Th	160
Be	1481	Hf	252	Pa	185	Ti	420
Bi	120	Hg	72	Pb	105	Tl	78.5
B	1480	Ho	190	Pd	271	Tm	200
C(gr)	412	I	109	Pr	152	U	248
C(dia)	2250	In	112	Pt	237	V	399
Ca	229	Ir	420	Pu	206	W	383
Cd	210	K	91.1	Rb	56.5	Xe	64.0
Ce	179	Kr	71.9	Re	416	Y	248
Co	460	La	150	Rh	512	Yb	118
Cr	606	Li	344	Ru	555	Zn	329
Cs	40.5	Lu	183	Sb	220	Zr	290
Cu	347	Mg	403	Sc	346		
Dy	183	Mn	409	Se	153		
Er	188	Mo	423	Si	645		

Not available for all elements. Source: Stewart (1983).

and is plotted in Figures 13.8 and 13.10.

Because the low-temperature lattice contribution to the specific heat in Eq. (13.70) varies as T^3 , it should disappear in metals beneath the electronic contribution, which is linear in temperature. However, putting in numbers, one finds that very low temperatures, on the order of a few degrees kelvin, are needed before the electronic contribution stands out. The reason is that the natural temperature scale for the electrons is the Fermi temperature, which is on the order of 20 000 K, and the electronic contribution goes as T/T_F . However, the natural temperature scale for the phonons is the Debye temperature, given by $\Theta_D = \hbar\omega_D/k_B$. The contribution of the phonons to the specific heat goes as $(T/\Theta_D)^3$. So the electron and phonon contributions are roughly equal when $T = \Theta_D\sqrt{\Theta_D/T_F}$. Debye temperatures are tabulated in Table 13.1. Because they are typically on the order of a few hundred degrees, the electronic specific heat has barely become visible even at 10 K. Adding together electron and phonon contributions, the low temperature specific heat at constant pressure C_P behaves quite accurately as

$$C_P \approx \gamma T + \beta T^3, \quad \text{The constant } \gamma \text{ is the Sommerfeld parameter.} \quad (13.76)$$

a claim best checked experimentally by plotting C_P/T versus T^2 , as in Figure 13.11.

Debye temperatures are usually 30% to 50% percent of the melting temperature of the element, so that by the time one gets to temperatures high enough to see the fully classical specific heat of $\frac{1}{2}k_B T$ per degree of freedom, the harmonic approximation for phonons is beginning to break down.

13.3.3 Thermal Expansion



Figure 13.12. Thermal expansion of a molecule.

The change of objects’ size and shape as they heat and cool often poses an unpleasant challenge for engineers. Road sections swell and buckle in the summer; engine parts designed to work at high temperatures barely mesh when they are cool. Yet it is a curious fact that the general framework allowing calculation of so many other mechanical properties of condensed matter fails completely to predict the possibility of thermal expansion. A solid whose energy changes only to quadratic order when its atoms move does not change size or shape with temperature at all.

The reason for this somewhat unexpected result is most easily seen in the smallest possible solid, one consisting only of two identical atoms (see Figure 13.12). In a reference frame tied to their center of mass, the energy of the two atoms is

$$\mathcal{E} = \frac{1}{2} \mathcal{K} x^2. \quad \begin{array}{l} x = u_1 - u_2 \text{ is the difference of the deviation} \\ \text{of the two atoms from equilibrium, } \mathcal{K} \text{ some} \\ \text{spring constant.} \end{array} \quad (13.77)$$

In any thermal average over the locations of the atoms, positive and negative values of x occur with equal frequency, and the mean distance between the two atoms does not change no matter how much the molecule may be heated. If there were any solid in which atomic interactions were really only present to quadratic order, it would similarly refuse to change size in response to temperature.

Suppose now that the interaction energy of the molecule is a general function

$$\mathcal{E}(x) = \mathcal{E}_0 + \frac{1}{2} \mathcal{K} x^2 + \dots \quad (13.78)$$

and ask under what conditions the mean size \bar{x} of the molecule changes. The thermal average of x is

$$\bar{x} = \frac{\int dx x e^{-\beta \mathcal{E}(x)}}{\int dx e^{-\beta \mathcal{E}(x)}} = \frac{\partial}{\partial A} \left(\ln \int dx e^{Ax - \beta \mathcal{E}(x)} \right) \Big|_{A=0} \quad \begin{array}{l} A \text{ can be viewed as a purely} \\ \text{formal quantity, but also} \\ \text{can be interpreted as an} \\ \text{external force acting on the} \\ \text{system.} \end{array} \quad (13.79)$$

$$\approx \frac{\partial}{\partial A} \ln \int dx e^{Ax - \beta \mathcal{E}(x_0) - \beta \mathcal{E}'(x_0)(x-x_0) - \beta \mathcal{E}''(x_0)(x-x_0)^2/2} \Big|_{A=0}. \quad (13.80)$$

According to the technique of steepest descents (Appendix B.4), x_0 should be chosen so that the linear term inside the exponential in Eq. (13.80) vanishes; x_0 is determined by

$$A = \beta \mathcal{E}'(x_0) = \beta \mathcal{K} x_0 \quad \begin{array}{l} \text{Maximizing the integrand; } A \text{ can be} \\ \text{taken very small because it is on the} \\ \text{verge of being set to zero, and } x_0 \\ \text{should be viewed as a function of } A. \end{array} \quad (13.81)$$

$$\Rightarrow \bar{x} = \frac{\partial}{\partial A} \left[\ln \sqrt{\frac{2\pi}{\beta \mathcal{E}''(x_0)}} e^{A x_0 - \beta \mathcal{E}(x_0)} \right] \Big|_{A=0} \quad (13.82)$$

$$= \frac{k_B T}{\mathcal{K}} \frac{\partial}{\partial x_0} \left[\ln \sqrt{\frac{2\pi}{\beta \mathcal{E}''(x_0)}} e^{\beta \mathcal{K} x_0^2 / 2 - \beta \mathcal{E}_0} \right] \Big|_{x_0=0} \quad (13.83)$$

$$= -\frac{k_B T}{\mathcal{K} \omega} \frac{\partial \omega}{\partial x} \Big|_{x=0}, \quad \text{with } \mu \omega^2(x) \equiv \mathcal{E}''(x). \quad \begin{array}{l} \mu \text{ is the reduced mass of the} \\ \text{molecule} \end{array} \quad (13.84)$$

The possibility of thermal expansion therefore rests upon a nonzero third derivative of the energy \mathcal{E} about equilibrium, or equivalently upon the change of vibrational frequency ω if the molecule is forced to expand or contract.

General Theory. The general theory of thermal expansion begins with a collection of thermodynamic identities. One wishes to calculate

$$\mathcal{V} \beta_T \equiv \frac{\partial \mathcal{V}}{\partial T} \Big|_P = \frac{\partial P / \partial T \Big|_{\mathcal{V}}}{-\partial P / \partial \mathcal{V} \Big|_T} \quad \begin{array}{l} \text{An identity from thermodynamics concern-} \\ \text{ing partial derivatives; the minus sign is cor-} \\ \text{rect. Do not confuse the coefficient of volume} \\ \text{expansion } \beta_T \text{ with } 1/k_B T. \end{array} \quad (13.85)$$

$$= -\frac{\mathcal{V}}{B} \frac{\partial^2 \mathcal{F}}{\partial \mathcal{V} \partial T}, \quad \text{The bulk modulus } B = -\mathcal{V} \partial P / \partial \mathcal{V}. \quad (13.86)$$

so the formal aim can be achieved by calculating derivatives of the free energy with respect to temperature and volume. Using Eq. (13.60) for the free energy of a collection of interacting ions and using the definition of the Bose–Einstein factor in Eq. (13.62), one has

$$\frac{\partial \mathcal{F}}{\partial \mathcal{V}} \Big|_T = \sum_i (n_i + \frac{1}{2}) \frac{\partial \hbar \omega_i}{\partial \mathcal{V}} \quad (13.87)$$

$$\Rightarrow \frac{\partial^2 \mathcal{F}}{\partial \mathcal{V} \partial T} = \sum_i \frac{\partial n_i}{\partial T} \frac{\partial \hbar \omega_i}{\partial \mathcal{V}}. \quad (13.88)$$

Comparing with Eq. (13.63) for the specific heat, define the *Grüneisen parameter* γ_T

$$\gamma_T = \frac{\sum_i \frac{\partial n_i}{\partial T} (-\mathcal{V} \frac{\partial \hbar \omega_i}{\partial \mathcal{V}})}{\sum_i \hbar \omega_i \frac{\partial n_i}{\partial T}} \quad \begin{array}{l} \text{The Grüneisen constant is an average over the} \\ \text{volume rate of change of the frequencies of} \\ \text{the phonon modes, weighted by the contribu-} \\ \text{tion of each mode to the specific heat.} \end{array} \quad (13.89)$$

$$\Rightarrow -\frac{\partial^2 \mathcal{F}}{\partial \mathcal{V} \partial T} = \frac{\gamma_T C_V}{\mathcal{V}} \quad \begin{array}{l} \text{The denominator of Eq. (13.89) is just the} \\ \text{specific heat; see Eq. (13.63).} \end{array} \quad (13.90)$$

$$\Rightarrow \beta_T = \frac{\gamma_T C_V}{B \mathcal{V}}. \quad \text{Combining Eqs. (13.90) and Eq. (13.86).} \quad (13.91)$$

For an isotropic solid, the coefficient of linear expansion α_T is just one-third of the coefficient of volume expansion β_T . For a crystal, there will generally be different degrees of contraction along different crystalline axes.

Definition of the Grüneisen parameter does not dramatically simplify the task of presenting data on thermal expansion data, but does correctly emphasize the fact that trends in the specific heat, particularly at low temperatures, are likely to be reflected in thermal expansion data. For some materials, the Grüneisen parameter is constant over a wide temperature range, leading the specific heat and thermal expansion coefficient to become indistinguishable when properly scaled, as shown in Figure 13.13. However, even the sign of the Grüneisen parameter can change. Figure 13.14 shows thermal expansion data for Invar, an alloy useful for its extremely small expansion coefficients.

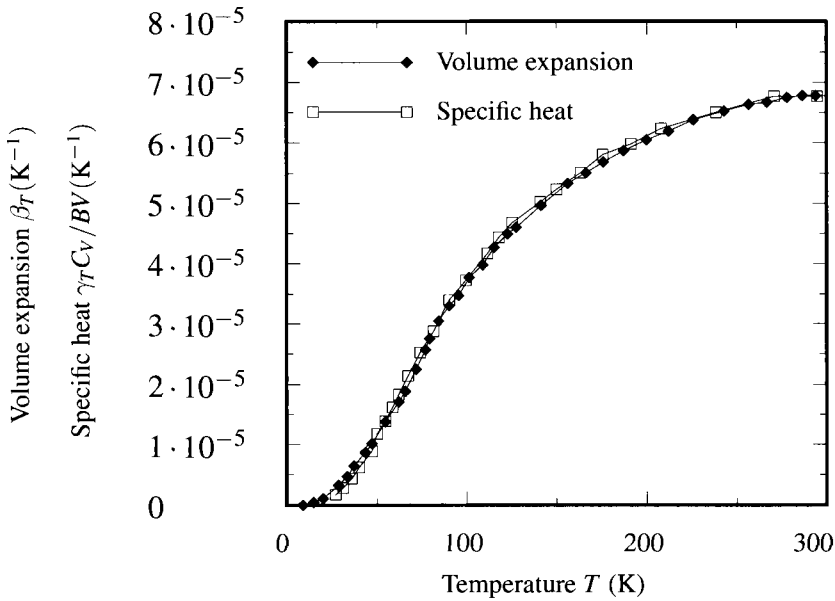


Figure 13.13. Comparison of specific heat C_V and volume expansion coefficient β_T for aluminum using Eq. (13.90). The comparison employs a bulk modulus B of 77 GPa from Eq. (12.29) and Table 12.1, uses a Grüneisen parameter γ_T of 2.2, obtained by matching specific heat and expansion at 300 K, and obtains the coefficient of bulk expansion from linear expansion data through $\beta_T \approx 3\alpha_T$. [Source: Touloukian and Buyco (1970a) and Touloukian et al. (1975).]

Thermal Conductivity. Phonons also participate in thermal conductivity of solids. A review focusing upon insulators is provided by Slack (1979).

13.4 Inelastic Scattering from Phonons

The scattering experiments described in Chapter 3 relied upon elastic scattering; the energy of outgoing particles equals the energy of incoming particles. There is another class of scattering experiments—*inelastic scattering*—where the incoming

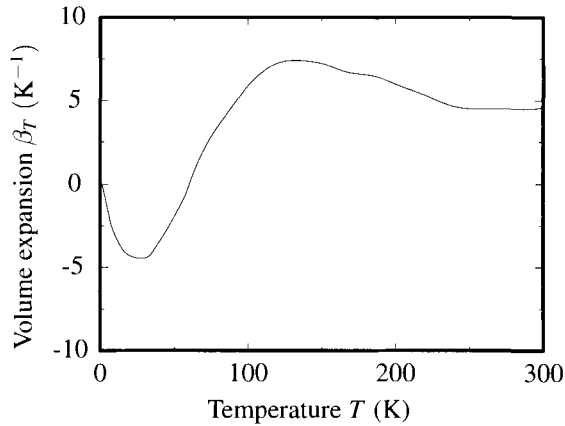


Figure 13.14. Coefficient of volume expansion ($\beta_T \approx 3\alpha_T$) for Invar, a Fe-64% Ni-36% alloy in which reduction of magnetic order with increasing temperature offsets the otherwise natural tendency toward thermal expansion and produces an alloy with minimal tendency to expand. [Source: Touloukian et al. (1975), p. 10a.]

beam gains or loses energy at the expense of the sample. The first type of experiment determines static structures, while the second focuses upon excitations.

The theory needed to explain inelastic scattering experiments is available at two levels. The first level of explanation derives all its conclusions from conservation laws. It is simple and powerful, providing everything needed to deduce phonon dispersion relations from neutron scattering experiments, and is easily generalized. The second level of explanation attacks the problem with a full formal apparatus. It is worth going through the more elaborate analysis because it provides various constants that the simpler theory leaves undetermined, determines the effects of thermal fluctuations, and settles questions about the workings of quantum mechanics.

13.4.1 Neutron Scattering

A particularly important type of inelastic scattering experiment is performed with neutrons, as sketched in Figure 13.15. A beam of neutrons impinges on a sample. Some of the neutrons gain or lose energy by destroying or creating lattice vibrations—phonons—and emerge from the sample scattered in all directions. Almost everything that needs to be known in order to interpret such an experiment can be obtained from two conservation laws.

Energy. Let the wave vector of an incoming neutron of mass m_n be \vec{k} , let its wave vector after scattering be \vec{k}' , and suppose that it creates a phonon with wave vector \vec{q} and energy $\hbar\omega_{\vec{q}\nu}$. Then conservation of energy requires

$$\frac{\hbar^2 k^2}{2m_n} = \frac{\hbar^2 (k')^2}{2m_n} + \hbar\omega_{\vec{q}\nu}. \quad (13.92a)$$

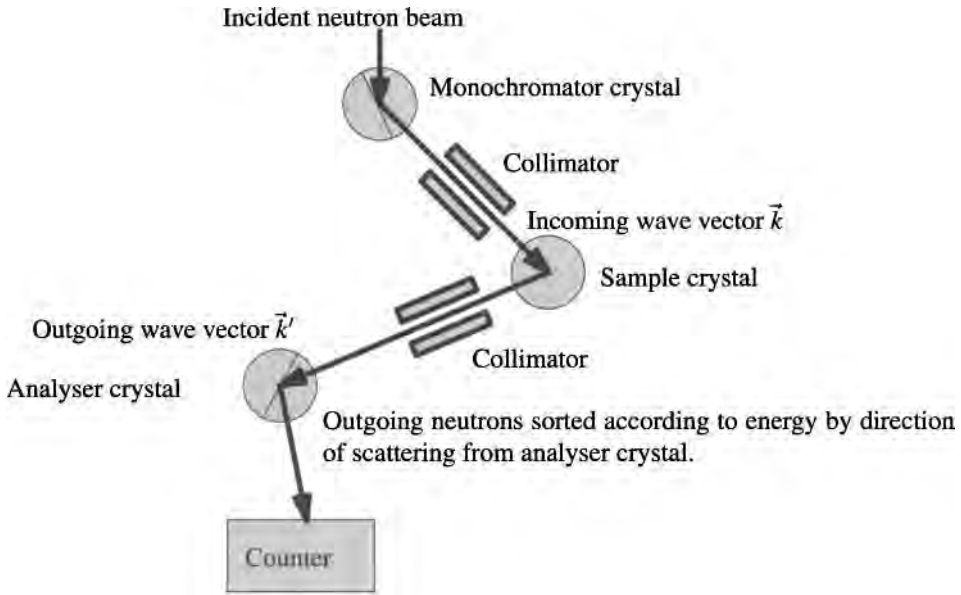


Figure 13.15. Schematic drawing of neutron diffraction experiment. The neutrons pass through a first crystal, undergoing Bragg scattering. By choosing only those traveling in a certain direction, neutrons of a definite energy are selected. These then pass through the sample crystal, and finally through an analyzer crystal, whose purpose, again, is to sort the neutrons of various energies according to their Bragg scattering angles. [After Yarnell et al. (1965) p. 58.]

If, on the other hand, passage of the neutron destroys a phonon and steals its energy, then

$$\frac{\hbar^2 k^2}{2m_n} = \frac{\hbar^2 (k')^2}{2m_n} - \hbar\omega_{\vec{q}\nu}. \quad (13.92b)$$

Crystal momentum. The study of elastic scattering in Chapter 3 shows that momentum is not conserved in scattering from a crystal. A neutron can enter with wave vector \vec{k} and exit with a different one, \vec{k}' . However, \vec{k}' is only permitted if $\vec{k} - \vec{k}' = \vec{K}$, where \vec{K} is a reciprocal lattice vector of the crystal. Crystal momentum $\hbar\vec{k}$ is conserved, where \vec{k} is always retracted into the first Brillouin zone by whatever reciprocal lattice vectors \vec{K} are necessary. Assuming that the same conservation law continues to hold for inelastic scattering events, when a phonon is emitted,

$$\vec{k}' + \vec{q} = \vec{k} + \vec{K} \quad (13.93a)$$

for some reciprocal lattice vector \vec{K} , and when a phonon is absorbed,

$$\vec{k}' - \vec{q} = \vec{k} + \vec{K}. \quad (13.93b)$$

Combining Eqs. (13.92) and (13.93) gives

$$\frac{\hbar^2 k^2}{2m_n} \pm \hbar\omega_{(\vec{k}-\vec{k}'),\nu} = \frac{\hbar^2 (k')^2}{2m_n}, \quad \text{The reciprocal lattice vectors } \vec{K} \text{ disappear from } \omega_{\vec{k}\nu} \text{ because } \omega_{\vec{k}+\vec{K},\nu} = \omega_{\vec{k}\nu}. \text{ Also note } \omega_{-\vec{k},\nu} = \omega_{\vec{k}\nu}. \quad (13.94)$$

where the + sign holds for phonon absorption, and the – sign holds for emission.

What Eq. (13.94) implies is that for any observation direction, \hat{k}' , there should be some neutron scattering. The reason is that although the experiment will gaze at the sample in a fixed direction, the magnitude of k' is arbitrary, and therefore by scanning through k' , there is every reason to hope that one will obtain a discrete number of different k' solutions to Eq. (13.94). If a solution is obtained, the known difference between \vec{k} and \vec{k}' gives the wave vector of the phonon, while the difference in energies between incoming and outgoing neutrons gives the energy of the phonon.

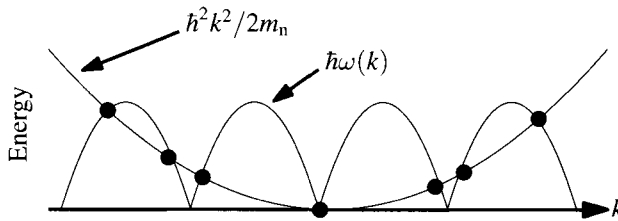


Figure 13.16. Graphical construction illustrating the conditions under which inelastic neutron scattering occurs for $k' = 0$.

Consider first the simplest case, where \vec{k} and \vec{k}' lie along the same line. Then Eq. (13.94) has the graphical interpretation shown in Figure 13.16. Eq. (13.94) is satisfied whenever the neutron parabola crosses the phonon dispersion curve. By measuring the outgoing neutrons as a function of energy, several peaks are located, as shown in Figure 13.17. Each of these peaks constitutes a point on the phonon dispersion curve. By varying the angles both of \vec{k} and \vec{k}' , the phonon dispersion relations can be mapped out completely. Figure 13.18 shows the end result of collecting such data for silicon, and it compares the results with density functional calculations.

13.4.2 Formal Theory of Neutron Scattering

The goal of a formal approach to neutron scattering is to calculate the interaction between phonons and neutrons to first order in perturbation theory. The noninteracting states about which one perturbs are product states, of a free neutron in a plane wave times a lattice state with some number of phonons. The interaction between the ions and the incoming neutrons occurs when the neutrons are within a distance on the order of 10^{-13} cm from the ions. Because this distance is so terribly short compared to a lattice spacing, one may safely represent the interaction as a

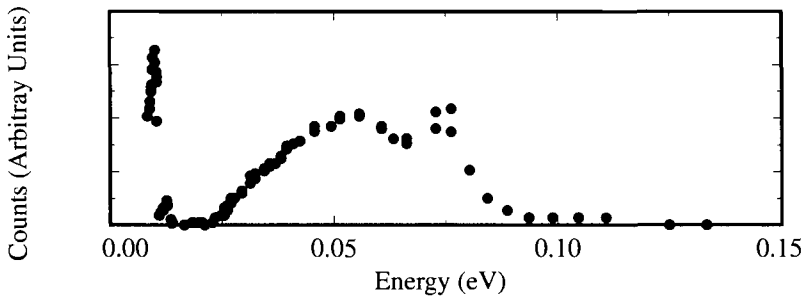


Figure 13.17. Number of neutron counts as a function of energy at 300 K in Ni. Although at nonzero temperatures the neutron peaks are not perfectly sharp, they are certainly visible. [Source: Mozer et al. (1965), p. 68.]

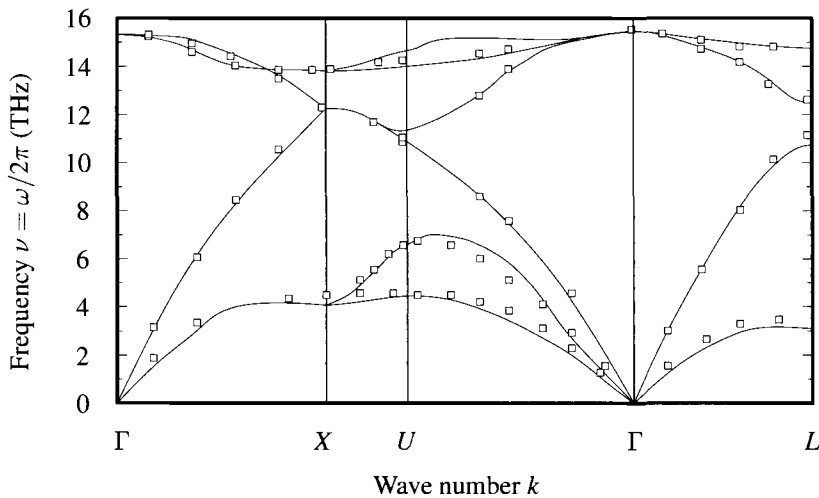


Figure 13.18. The end result of collecting peaks for absorption and emission of single phonons is a phonon dispersion curve. These curves display the phonon dispersion relation of Si, with experimental data from Dolling and Cowley (1966) and Nilsson and Nelin (1972) (boxes) and a detailed theoretical calculation involving pseudopotentials due to Wei and Chou (1994) (solid lines). Compare with the simple estimate in Figure 13.7.

delta function: it is conventionally normalized as

$$\hat{U} = \frac{2\pi\hbar^2 a}{m_n} \sum_l \delta(\hat{R}_n - \vec{R}^l - \hat{u}^l). \tag{13.95}$$

The constant a is the *scattering length* and is chosen so that the total scattering cross section of neutrons off a single ion to first order in perturbation theory is $4\pi a^2$, where m_n is the mass of a neutron, \vec{R}^l is the location of an ion, \hat{R}_n is a position operator for the neutron, and \hat{u}^l is the displacement operator for the ion at \vec{R}^l .

Differential Scattering Cross Section. What an experiment measures is the flux of particles per energy and per solid angle coming out of the sample. Let $\mathcal{P}(\vec{k} \rightarrow \vec{k}')$ give the probability of a transition from state \vec{k} to state \vec{k}' per unit time. Then in a small volume of \vec{k}' space there are

$$\frac{\mathcal{P} \mathcal{V} d\vec{k}'}{(2\pi)^3} \quad \text{Because there are } \mathcal{V} d\vec{k}' / (2\pi)^3 \text{ states in the reciprocal space volume: See Section 6.3.} \quad (13.96)$$

transitions per unit time. Rewriting the small \vec{k}' space volume in terms of neutron energy \mathcal{E}_n and solid angle $d\Omega$, one has

$$\frac{\mathcal{P} \mathcal{V} m_n \hbar k' d\mathcal{E}_n d\Omega}{(2\pi \hbar)^3}. \quad (13.97)$$

However, the number of transitions per time, per energy, per solid angle, and divided by the incident flux, $I = \hbar k / \mathcal{V} m_n$, is just the definition of the differential scattering cross section

$$\frac{d\sigma}{d\Omega d\mathcal{E}_n} = \frac{k'}{k} \frac{(\mathcal{V} m_n)^2}{(2\pi \hbar)^3} \mathcal{P}(\vec{k} \rightarrow \vec{k}'). \quad (13.98)$$

For elastic scattering, as in Eq. (3.2), there is no need to bin the radiation according to its energy, because ingoing and outgoing particles all are the same. For inelastic scattering, it is important to keep track of how many particles have which energy.

Transition Probability \mathcal{P} . The next goal is to find $\mathcal{P}(\vec{k} \rightarrow \vec{k}')$. It can be evaluated with the help of Fermi's Golden Rule [originally derived by Dirac; see Dirac (1958), p. 180]. The formula reads

$$\mathcal{P}(\vec{k} \rightarrow \vec{k}') = \sum_{\text{final states } f} \frac{2\pi}{\hbar} \delta(\mathcal{E}^f - \mathcal{E}^i) |\langle \Psi^f | \hat{U} | \Psi^i \rangle|^2. \quad (13.99)$$

Although the use of this formula should be relatively automatic, it is important to keep in mind the assumptions under which it was derived. The main assumption is that scattering occurs off a structure that is static on time scales needed for a scattering interaction to take place. Because the interaction of a neutron or an X-ray with an ion occurs on times that are very short compared to the time scale on which ions move, the assumption is justified. If an experiment could be conducted on time scales short compared to phonon motion, one could deduce the precise locations of the ions. However, normal experiments just see the time average of this instantaneous scattering, and therefore the appropriate calculation is one that finds the scattering that would result from any given lattice configuration, and then takes the time average over it. Equivalently, one can perform a thermal average instead, and this is in fact what will be done.

The unknown quantity in Eq. (13.99) is the matrix element $\langle \Psi^f | \hat{U} | \Psi^i \rangle$. The wave function $\langle \Psi |$ is a product of $\langle \vec{k} |$ and $\langle \Phi |$, where $\langle \vec{k} |$ describes the neutron, and $\langle \Phi |$ describes all of the phonons. Moving to a representation where \vec{r} is the location

of the neutron, one obtains

$$\langle \Psi^f | \hat{U} | \Psi^i \rangle = \int d\vec{r} \langle \vec{k}' | \vec{r} \rangle \langle \vec{r} | \langle \Phi^f | \sum_l \frac{2\pi\hbar^2 a}{m_n} \delta(\hat{R} - \vec{R}^l - \vec{u}^l) | \vec{k} \rangle | \Phi^i \rangle \quad (13.100)$$

$$= \int \frac{d\vec{r}}{\mathcal{V}} e^{i(\vec{k}-\vec{k}')\cdot\vec{r}} \langle \Phi^f | \frac{2\pi\hbar^2 a}{m_n} \sum_l \delta(\vec{r} - \vec{R}^l - \vec{u}^l) | \Phi^i \rangle \quad (13.101)$$

$$= \frac{1}{\mathcal{V}} \frac{2\pi\hbar^2 a}{m_n} \sum_l \langle \Phi^f | e^{i(\vec{k}-\vec{k}')\cdot(\vec{u}^l + \vec{R}^l)} | \Phi^i \rangle. \quad (13.102)$$

Using Eq. (13.102), with \mathcal{E}_{ph} denoting the energy of a phonon state and with

$$\hbar\omega_n = \frac{\hbar^2 k^2}{2m_n} - \frac{\hbar^2 k'^2}{2m_n} \quad (13.103)$$

denoting the change in energy of a neutron state, one has that

$$\mathcal{P}(\vec{k} \rightarrow \vec{k}') = \frac{(2\pi\hbar)^3}{(m_n \mathcal{V})^2} a^2 \sum_f \delta(\mathcal{E}_f - \mathcal{E}_{\text{ph}}^i + \hbar\omega_n) \left| \sum_l \langle \Phi^f | e^{i(\vec{k}-\vec{k}')\cdot(\vec{u}^l + \vec{R}^l)} | \Phi^i \rangle \right|^2. \quad (13.104)$$

Inserting the transition probability Eq. (13.104) into the differential scattering cross section (13.98) one finds that

$$\frac{d\sigma}{d\Omega d\mathcal{E}_n} = \frac{k'}{k} \frac{Na^2}{\hbar} S^i(\vec{k} - \vec{k}', \omega_n), \quad (13.105)$$

where the *inelastic structure factor* S^i is

$$S^i(\vec{q}, \omega) = \frac{1}{N} \sum_f \delta([\mathcal{E}_{\text{ph}}^f - \mathcal{E}_{\text{ph}}^i]/\hbar + \omega) \left| \sum_l \langle \Phi^f | e^{i\vec{q}\cdot(\vec{u}^l + \vec{R}^l)} | \Phi^i \rangle \right|^2. \quad (13.106)$$

This structure factor still depends upon the initial quantum state “ i ”, which is why it carries the superscript. It serves the same purpose as the structure factor defined in Eq. (3.50), but generalizes it in three ways.

1. S^i is fully quantum mechanical.
2. It describes a dynamical, evolving object, and therefore permits studying inelastic events.
3. After appropriate averaging, it will include the effects of temperature.

To proceed, let $\hat{\mathcal{H}}_{\text{ph}}$ be the phonon Hamiltonian, and write

$$S^i = \frac{1}{N} \sum_f \int \frac{dt}{2\pi} e^{it([\mathcal{E}_{\text{ph}}^f - \mathcal{E}_{\text{ph}}^i]/\hbar + \omega)} \sum_{ll'} e^{i\vec{q}\cdot(\vec{R}^l - \vec{R}^{l'})} [\langle \Phi^i | e^{-i\vec{q}\cdot\vec{u}^l} | \Phi^f \rangle \times \langle \Phi^f | e^{i\vec{q}\cdot\vec{u}^{l'}} | \Phi^i \rangle] \quad (13.107)$$

$$= \frac{1}{N} \sum_f \int \frac{dt}{2\pi} e^{it\omega} \sum_{ll'} e^{i\vec{q}\cdot(\vec{R}^l - \vec{R}^{l'})} [\langle \Phi^i | e^{-i\vec{q}\cdot\vec{u}^l} | \Phi^f \rangle \times \langle \Phi^f | e^{i\hat{\mathcal{H}}_{\text{ph}} t/\hbar} e^{i\vec{q}\cdot\vec{u}^{l'}} e^{-i\hat{\mathcal{H}}_{\text{ph}} t/\hbar} | \Phi^i \rangle] \quad (13.108)$$

$$= \frac{1}{N} \sum_f \int \frac{dt}{2\pi} e^{it\omega} \sum_{ll'} e^{i\vec{q} \cdot (\vec{R}^l - \vec{R}^{l'})} \langle \Phi^i | e^{-i\vec{q} \cdot \hat{u}^{l'}} | \Phi^f \rangle \langle \Phi^f | e^{i\vec{q} \cdot \hat{u}^l(t)} | \Phi^i \rangle \quad (13.109)$$

$$= \frac{1}{N} \int \frac{dt}{2\pi} e^{it\omega} \sum_{ll'} e^{i\vec{q} \cdot (\vec{R}^l - \vec{R}^{l'})} \langle \Phi^i | e^{-i\vec{q} \cdot \hat{u}^{l'}} e^{i\vec{q} \cdot \hat{u}^l(t)} | \Phi^i \rangle. \quad \text{Because } \Phi^f \text{ are a complete set of phonon states.} \quad (13.110)$$

The structure factor still depends upon the initial state of the phonons. The experimental observable is a thermal average over all possible initial states, where the thermal average of an operator \hat{A} is

$$\langle \hat{A} \rangle = \frac{\sum_i \langle \Phi^i | e^{-\beta \hat{H}} \hat{A} | \Phi^i \rangle}{\sum_i \langle \Phi^i | e^{-\beta \hat{H}} | \Phi^i \rangle}. \quad (13.111)$$

After averaging, the structure factor becomes

$$S(\vec{q}, \omega) = \frac{1}{N} \sum_{ll'} e^{i\vec{q} \cdot (\vec{R}^l - \vec{R}^{l'})} \int \frac{dt}{2\pi} e^{i\omega t} \langle e^{-i\vec{q} \cdot \hat{u}^{l'}} e^{i\vec{q} \cdot \hat{u}^l(t)} \rangle \quad (13.112)$$

$$= \frac{1}{N} \int d\vec{r} d\vec{r}' \frac{dt}{2\pi} e^{i\vec{q} \cdot (\vec{r} - \vec{r}')} e^{i\omega t} \sum_{ll'} \langle \delta(\vec{r} - \vec{R}^l - \hat{u}^l) \delta(\vec{r}' - \vec{R}^{l'} - \hat{u}^{l'}(t)) \rangle. \quad (13.113)$$

From (13.113) it is evident that the structure factor is the Fourier transform in space and time of the density-density correlation function.

13.4.3 Averaging Exponentials

Proceeding further with evaluation of Eq. (13.112) requires finding thermal averages of exponentials of operators such as

$$\mathcal{S} \equiv \langle e^{\hat{A}} \rangle \quad (13.114)$$

where \hat{A} is any operator that is linear in harmonic oscillator creation and annihilation operators. For an operator of this form one can write

$$\mathcal{S} = \langle 1 + \hat{A} + \frac{1}{2} \hat{A}^2 + \dots \rangle. \quad (13.115)$$

The second term on the right hand side of (13.115) vanishes because it contains only a single power of a creation or annihilation operator, and so one has

$$\mathcal{S} = 1 + \frac{1}{2} \langle \hat{A} \hat{A} \rangle + \frac{1}{4!} \langle \hat{A} \hat{A} \hat{A} \hat{A} \rangle + \dots \quad (13.116)$$

According to Wick's theorem (Doniach and Sondheimer (1974), pp. 52–62), an expectation value such as $\langle \hat{A}_1 \hat{A}_2 \hat{A}_3 \hat{A}_4 \rangle$ can be replaced by a sum over products of the form $\langle \hat{A}_1 \hat{A}_2 \rangle \langle \hat{A}_3 \hat{A}_4 \rangle$, where the sum is over all unique ways of grouping the operators into pairs. $\langle \hat{A}_1 \hat{A}_2 \rangle$ can be grouped into one unique pair; $\langle \hat{A}_1 \hat{A}_2 \hat{A}_3 \hat{A}_4 \rangle$ can be grouped into the three unique pairs $\langle \hat{A}_1 \hat{A}_2 \rangle \langle \hat{A}_3 \hat{A}_4 \rangle$, $\langle \hat{A}_1 \hat{A}_3 \rangle \langle \hat{A}_2 \hat{A}_4 \rangle$, $\langle \hat{A}_1 \hat{A}_4 \rangle \langle \hat{A}_2 \hat{A}_3 \rangle$;

and a general term with $2l$ operators appearing in it can be grouped into $(2l)!/(l! 2^l)$ unique pairs. Using this result,

$$S = 1 + \frac{1}{2} \langle \hat{A}\hat{A} \rangle + \frac{1}{2!} \frac{1}{2^2} \langle \hat{A}\hat{A} \rangle^2 + \dots + \frac{1}{2^l} \frac{1}{l!} \langle \hat{A}\hat{A} \rangle^l \dots \quad (13.117)$$

$$= \exp\left[\frac{1}{2} \langle \hat{A}^2 \rangle\right]. \quad (13.118)$$

For those who do not want to rely upon Wick's theorem, a straightforward proof of this result is provided by Maradudin et al. (1971), Section VII.2, and a swift and sneaky one by Mermin (1966).

Identical arguments show for operators \hat{A} and \hat{B} linear in creation and annihilation operators that

$$\langle e^{\hat{A}} e^{\hat{B}} \rangle = e^{\frac{1}{2} \langle \hat{A}^2 + 2\hat{A}\hat{B} + \hat{B}^2 \rangle}. \quad (13.119)$$

Because Wick's theorem produces sums over all possible paired groupings of \hat{A} and \hat{B} , this expectation value equals the expectation value $\langle \exp[\hat{A} + \hat{B}] \rangle$.

Equation (13.119) has direct application to the scattering crosssection. One needs to find

$$\mathfrak{M} \equiv \langle e^{-i\vec{q}\cdot\hat{u}^l} e^{i\vec{q}\cdot\hat{u}^l(t)} \rangle. \quad (13.120)$$

Because the mean square displacement of an ion cannot depend upon its location or upon the time, one has

$$\mathfrak{M} = \exp[-\langle (\vec{q}\cdot\hat{u}^l)^2 \rangle] \exp[\langle (\vec{q}\cdot\hat{u}^l)(\vec{q}\cdot\hat{u}^l(t)) \rangle]. \quad (13.121)$$

The first term on the right in Eq. (13.121) is known as the *Debye–Waller factor*. It provides a quantitative description of how quantum and thermal fluctuations limit the size of Bragg scattering peaks. The second term will lead to a physical picture in which incoming neutrons create or destroy zero, one, two, many phonons as they pass through the lattice.

Debye–Waller Factor. For the Debye–Waller factor, one needs to calculate the mean-square ionic displacement

$$2W \equiv \langle (\vec{q}\cdot\hat{u}^l)^2 \rangle = \frac{1}{N} \sum_{\substack{\vec{k}\vec{k}' \\ \nu\nu'}} \langle (\vec{q}\cdot[\hat{u}_{\vec{k}\nu} e^{i\vec{k}\cdot\vec{R}^l} + \hat{u}_{\vec{k}\nu}^\dagger e^{-i\vec{k}\cdot\vec{R}^l}]) (\vec{q}\cdot[\hat{u}_{\vec{k}'\nu'} e^{i\vec{k}'\cdot\vec{R}^l} + \hat{u}_{\vec{k}'\nu'}^\dagger e^{-i\vec{k}'\cdot\vec{R}^l}]) \rangle. \quad (13.122)$$

All the terms in the average (13.111) have the same quantum state on the right and the left; the operators in such an average must therefore leave the quantum state unchanged, which requires $\hat{a}_{\vec{k}\nu}$ and $a_{\vec{k}\nu}^\dagger$ always to multiply each other in pairs.

Therefore, in Eq. (13.122) one has $\vec{k} = \vec{k}'$, $\nu = \nu'$, and

$$2W = \sum_{\vec{k}\nu} \frac{1}{N} \frac{\hbar^2 |\vec{c}_{\vec{k}\nu} \cdot \vec{q}|^2}{2M\hbar\omega_{\vec{k}\nu}} \langle \hat{a}_{\vec{k}\nu}^\dagger \hat{a}_{\vec{k}\nu} + \hat{a}_{\vec{k}\nu} \hat{a}_{\vec{k}\nu}^\dagger \rangle \quad (13.123)$$

$$= \sum_{\vec{k}\nu} \frac{1}{N} \frac{\hbar^2 |\vec{c}_{\vec{k}\nu} \cdot \vec{q}|^2}{2M\hbar\omega_{\vec{k}\nu}} (2n_{\vec{k}\nu} + 1). \quad (13.124)$$

$n_{\vec{k}\nu}$ is the occupation number in thermal equilibrium, and M is the mass of a lattice ion.

At $T = 0$ one can take all the occupation numbers n equal to zero, and thus have

$$2W = \sum_{\vec{k}\nu} \frac{1}{N} \frac{\hbar^2 (\vec{c}_{\vec{k}\nu} \cdot \vec{q})^2}{2M\hbar\omega_{\vec{k}\nu}}. \quad (13.125)$$

Proceeding further requires some particular form for the phonon dispersion relation. Problem 7 evaluates Eq. (13.125) within the Debye model, and it shows that

$$2W = \frac{3}{4} \frac{q^2 \hbar^2}{M\hbar ck_D}. \quad (13.126)$$

Thus the mean-square displacement of ions at zero temperature is given by the ratio of the energy of a free ion with momentum q to a typical phonon energy. Because of the factor $1/\omega$, the sum in (13.124) converges for three dimensions, but not for one or two dimensions. The divergence comes from the Bose occupation factor, which goes as $1/k$ for low enough k at all temperatures. Fluctuations destroy Bragg peaks for one- and two-dimensional crystals. This point will be discussed further in Section 14.3.

13.4.4 Evaluation of Structure Factor

The technique that made it possible to find the Debye–Waller factor makes it possible to complete the evaluation of the structure factor, (13.112), which is

$$S(\vec{q}, \omega) = \sum_{ll'} \frac{1}{N} e^{i\vec{q} \cdot (\vec{R}^l - \vec{R}^{l'})} \int \frac{dt}{2\pi} e^{i\omega t} e^{-2W} e^{i\vec{q} \cdot \vec{u}^l - \vec{q} \cdot \vec{u}^{l'}(t)}. \quad \text{Use Eqs. (13.121) and (13.122).} \quad (13.127)$$

Equation (13.127) cannot be evaluated immediately. One can, however, expand the last exponential and evaluate term by term. This expansion is appropriate so long as ionic displacements u^l are small.

Zeroth Order. The zeroth-order term is

$$S^{(0)}(\vec{q}, \omega) = \sum_l e^{i\vec{q} \cdot \vec{R}^l} \int \frac{dt}{2\pi} e^{i\omega t} e^{-2W} \quad (13.128)$$

$$= \delta(\omega) N e^{-2W} \sum_{\vec{K}} \delta_{\vec{q}\vec{K}}. \quad (13.129)$$

The delta function in ω indicates that the energy transfer from the neutrons is zero; the collisions at this order are completely elastic. The remarkable fact is that despite the possibility of excitations at arbitrarily low energies provided by phonons, neutrons have a nonzero chance to pass through the lattice without exciting a single phonon. The Debye–Waller factor shows that phonons reduce the amplitude of Bragg peaks even at zero temperature; as temperature rises, the amplitude declines further, but does not go to zero so long as the lattice retains its long-range order, as first claimed in Section 3.5.1.

First Order. Now proceed to look at the next order arising from expansion of the exponential in (13.127). One has

$$S^{(1)}(\vec{q}, \omega) = \sum_{l'l''} \frac{1}{N} e^{i\vec{q}\cdot(\vec{R}^l - \vec{R}^{l'})} \int \frac{dt}{2\pi} e^{i\omega t} e^{-2W} \langle (\vec{q} \cdot \hat{u}^{l'}) (\vec{q} \cdot \hat{u}^{l''}(t)) \rangle. \quad (13.130)$$

To evaluate the average, one must once again return to the explicit expression for \hat{u} in terms of creation and annihilation operators. The only difference between the evaluation of Eq. (13.122) and the matrix element appearing in Eq. (13.130) is that now there is dependence upon both \vec{R}^l and t , requiring use of Eq. (13.53). The matrix element in Eq. (13.130) is

$$\begin{aligned} \mathfrak{M}^l &= \langle (\vec{q} \cdot \hat{u}^{l'}) (\vec{q} \cdot \hat{u}^{l''}(t)) \rangle \\ &= \frac{1}{N} \sum_{\substack{\vec{k}\vec{k}' \\ \nu\nu'}} \langle (\vec{q} \cdot [\hat{u}_{\vec{k}\nu} e^{i\vec{k}\cdot\vec{R}^l} + \hat{u}_{\vec{k}\nu}^\dagger e^{-i\vec{k}\cdot\vec{R}^l}]) \\ &\quad \times (\vec{q} \cdot [\hat{u}_{\vec{k}'\nu'} e^{i\vec{k}'\cdot\vec{R}^l - i\omega_{\vec{k}'\nu'} t} + \hat{u}_{\vec{k}'\nu'}^\dagger e^{-i\vec{k}'\cdot\vec{R}^l + i\omega_{\vec{k}'\nu'} t}]) \rangle \end{aligned} \quad (13.131)$$

$$= \sum_{\vec{k}\nu} \frac{1}{N} \frac{\hbar^2 (\vec{\epsilon}_{\vec{k}\nu} \cdot \vec{q})^2}{2M\hbar\omega_{\vec{k}\nu}} \langle \hat{a}_{\vec{k}\nu}^\dagger \hat{a}_{\vec{k}\nu} e^{-i\omega_{\vec{k}\nu} t} + \hat{a}_{\vec{k}\nu} \hat{a}_{\vec{k}\nu}^\dagger e^{i\omega_{\vec{k}\nu} t} \rangle e^{i\vec{k}\cdot(\vec{R}^l - \vec{R}^l)} \quad (13.132)$$

$$= \sum_{\vec{k}\nu} \frac{1}{N} \frac{\hbar^2 (\vec{\epsilon}_{\vec{k}\nu} \cdot \vec{q})^2}{2M\hbar\omega_{\vec{k}\nu}} \left([n_{\vec{k}\nu} + 1] e^{i\omega_{\vec{k}\nu} t} + n_{\vec{k}\nu} e^{-i\omega_{\vec{k}\nu} t} \right) e^{i\vec{k}\cdot(\vec{R}^l - \vec{R}^l)}, \quad (13.133)$$

where $n_{\vec{k}\nu}$ is the occupation number in thermal equilibrium, and M is the mass of a lattice ion. Placing (13.133) into Eq. (13.130) gives finally

$$S^{(1)}(\vec{q}, \omega) = e^{-2W} \sum_{\nu} \frac{\hbar^2 [\vec{q} \cdot \vec{\epsilon}_{\vec{q}\nu}]^2}{2M\hbar\omega_{\vec{q}\nu}} [(1 + n_{\vec{q}\nu}) \delta(\omega + \omega_{\vec{q}\nu}) + n_{\vec{q}\nu} \delta(\omega - \omega_{\vec{q}\nu})]. \quad (13.134)$$

The first term in Eq. (13.134) corresponds to a neutron creating a phonon and giving up energy and momentum to it, while the second corresponds to a neutron destroying a phonon. In this way, the formalism recovers the energy and momentum conservation laws discussed at the beginning of this section, while also giving explicit formulas describing the extent to which thermal and quantum fluctuations destroy the effect.

The probability of creating phonons is proportional to $1 + n_{\vec{q}\nu}$, because they can be created at $T = 0$ when no phonons are initially present. The probability of destroying phonons, however, is proportional to $n_{\vec{q}\nu}$, because it is impossible to destroy what does not exist. These two probability factors were deduced by Einstein (1916) from simple statistical arguments, and they will be discussed again in Section 21.5.2.

13.4.5 Kohn Anomalies

Figure 13.19 provides a final illustration of the power of inelastic neutron scattering. This experiment searches for small discontinuities in the slope of the phonon

dispersion relation predicted by Kohn (1959). Just as the Peierls distortion (Section 11.5.1) tries to create a static lattice distortion with wave number $2k_F$, Kohn argued that phonon dispersion relations should exhibit a singularity whenever $q = 2k_F$. The traces of the singularity are faint but visible in Figure 13.19.

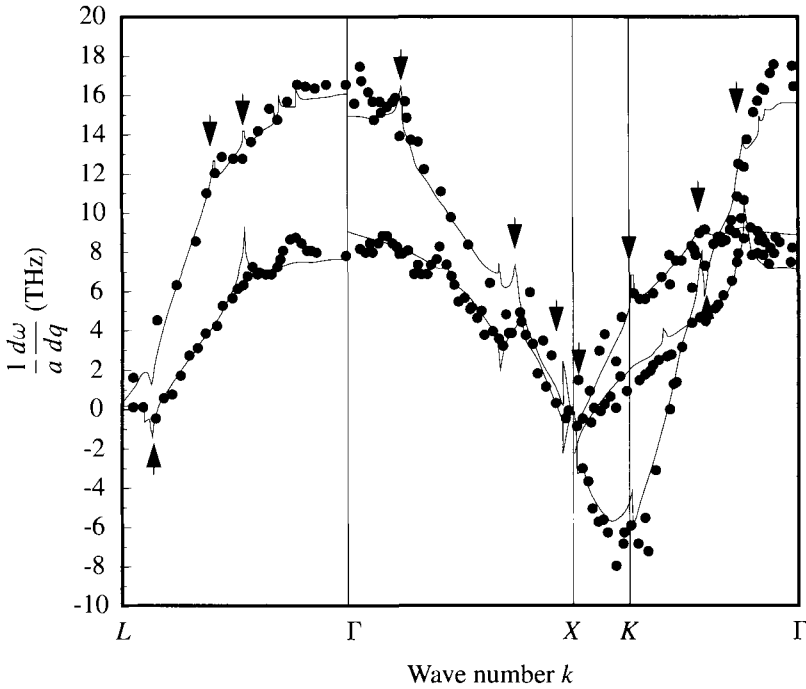


Figure 13.19. Kohn anomalies appear as logarithmic divergences in the first derivative of the phonon dispersion relation. Here neutron scattering data are compared with the theory of Brovman and Kagan (1974) p. 141, showing several Kohn anomalies, marked by arrows, as well as other singularities due to electron-ion coupling. The combined information from theory and experiment allows accurate determination of several points on the Fermi surface.

13.5 The Mössbauer Effect

It is rather remarkable that neutrons are able to scatter elastically from lattices, even at nonzero temperatures. Because the momentum of the neutron changes during the collision, the lattice as a whole must pick up the momentum transferred to the neutron, and it does so as a whole in the zero-phonon case. Although this fact had become commonplace by the 1950's, it was still a surprise when Mössbauer showed that photons impinging upon nuclei of atoms in a lattice could excite nuclear transitions in ways that would be forbidden if the lattice were not present.

Creating nuclear excited states by incoming radiation is impossible for nuclei sitting out in free space. The reason is that when a photon is absorbed by a nucleus, it imparts both energy and momentum. For energy to be conserved, the recoil

energy plus the energy of the excited state at the end of the process must be equal to the initial nuclear energy plus the incoming photon energy. This means that the incoming photon needs to have more energy than just the energy needed for the nuclear excitation. However, if this excess energy is greater than the width of the nuclear excitation (\hbar divided by lifetime), there will be no resonant excitation of the nucleus. In fact, for nuclear transitions, that is the way it works out, and light cannot excite nuclear states of free atoms. However, Mössbauer (1958) discovered that light can excite nuclear states if the nuclei sit in a lattice. The reason is that the lattice binds the nuclei, and the lattice as a whole takes up the momentum of the photon, leaving the energy free to go right to the nuclear excitation.

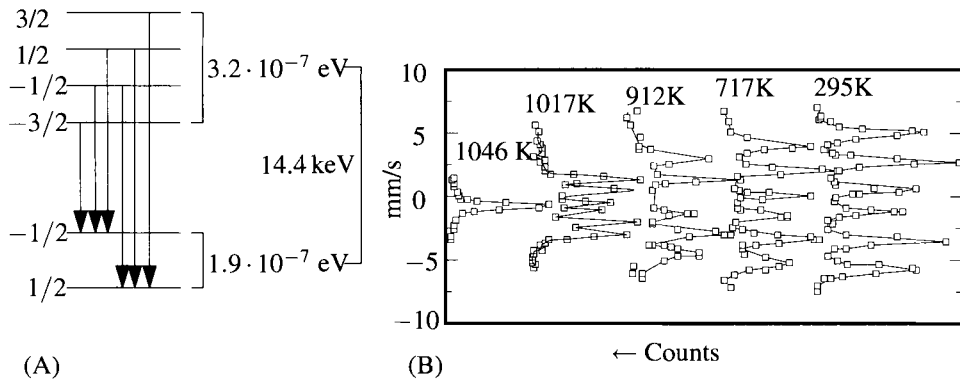


Figure 13.20. (A) Splittings of energy levels of lowest two nuclear states of Fe^{57} in the spontaneous internal magnetic field seen by the nucleus at room temperature. Note that the Zeeman splittings are 10 orders of magnitude smaller than separation between the $I = 1/2$ and $I = 3/2$ states. (B) Absorption of gamma radiation from Co^{57} as a function of temperature. The vertical axis gives the speed v of the Co^{57} source relative to the Fe^{57} sample. The motion produces a Doppler shift $1 + v/c$ in the photon energies, comparable to the splittings produced by internal magnetic fields. [Source: Preston et al. (1962), p. 2212.]

The calculation describing this process is very similar to the one just done for neutron scattering. If \vec{q} is the wave vector of an incoming photon, the nuclear excited state involves an energy $\Delta\mathcal{E}$, and has lifetime Γ , then the probability of exciting the state is

$$S(\vec{q}) = \frac{1}{N} \sum_{ll'} e^{i\vec{q}\cdot(\vec{R}^l - \vec{R}^{l'})} \int_0^\infty \frac{dt}{2\pi} [e^{i(\Delta\mathcal{E}/\hbar + i\Gamma)t} + e^{-i(\Delta\mathcal{E}/\hbar - i\Gamma)t}] \langle e^{-i\vec{q}\cdot\vec{u}^l} e^{i\vec{q}\cdot\vec{u}^{l'}(t)} \rangle. \tag{13.135}$$

The calculation of the matrix element proceeds as before. The main difference between this calculation and the one for neutron scattering is the inclusion of a decay rate Γ . At low temperatures the strength of the resonance absorption is given by a Breit–Wigner form factor

$$\frac{2\Gamma}{(\Delta\mathcal{E}/\hbar)^2 + \Gamma^2} \tag{13.136}$$

This factor appears instead of the $\delta(\omega)$ that appeared for neutron scattering in Eq. (13.129).

multiplied by the analog of the Debye–Waller factor, now called the Lamb–Mössbauer factor,

$$f = \exp \left[-\frac{3}{4} \frac{q^2 \hbar^2}{M \hbar c k_D} \right]. \quad \text{In the Debye approximation.} \quad (13.137)$$

One application of the Mössbauer effect is to take accurate measurements of the internal magnetic fields in iron. Spontaneous magnetization of ferromagnets at zero externally applied field is difficult to measure in bulk samples, because spins arrange themselves into interweaving collections of domains (Section 24.4.1) with spins pointing in differing directions. The internal magnetic fields, however, split the energy levels of nuclei in a way that is independent of the local field directions, shown in Figure 13.20. The strength of the splitting is $2\mu_I \vec{B} \cdot \vec{I}/I$, with $\mu_{1/2} = 4.6 \cdot 10^{-25}$ erg G⁻¹ and $\mu_{3/2} = -8.0 \cdot 10^{-25}$ erg G⁻¹. Radioactive Co⁵⁷ emits 14.4 keV photons, whose energy can be raised and lowered by parts in 10¹⁰ through moving the cobalt at speeds on the order of millimeters per second toward and away from the iron. The Mössbauer line is so sharp that energy shifts of 10⁻⁷ eV can be detected, and resulting measurements of the spontaneous field in iron appear in Figure 24.3. The magnitude of the field at room temperature is 330 kOe, which is comparable to the largest magnetic fields that can be generated in the laboratory.

Problems

- 1. Phonon dispersion with alternating springs:** Consider a one-dimensional array of atoms, in which every mass has mass M , but the springs alternate in strength on every other site between values of \mathcal{K}_1 and \mathcal{K}_2 . Find the vibrational frequencies of this array as a function of wave number k .
- 2. Optic and acoustic modes:** The bulk modulus of (three-dimensional) sodium chloride is $2.4 \cdot 10^{11}$ ergs/cm³, and the lattice parameter a is 5.6 Å. From these facts (at the level of dimensional analysis) estimate the spring constant \mathcal{K} that might describe sodium chloride, modeling it as a one-dimensional chain of atoms of alternating mass. Use the results following Eq. (13.7) to estimate the frequency of the optical mode and the speed of sound.
- 3. Wave Speeds for Two-Dimensional Lattices:** Consider a two-dimensional triangular lattice of particles of mass M and lattice constant a . Let \hat{r}_{ij} be a unit vector pointing from the equilibrium location \vec{R}_i of particle i to the equilibrium location \vec{R}_j of particle j . Let \vec{u}_i give the two-dimensional displacement of particle i from its equilibrium location. Suppose that the force on particle i is

$$\vec{F}_i = M\omega_0^2 \sum_j \hat{r}_{ij} (\hat{r}_{ij} \cdot (\vec{u}_j - \vec{u}_i)). \quad \text{Where } j \text{ indexes nearest neighbors of } i \quad (13.138)$$

- Find a set of two equations in two unknowns whose solution would give the dispersion relation $\omega_{\nu\vec{k}}$ for vibrations of the lattice.

- (b) Take the limit $k \rightarrow 0$ and find the transverse and longitudinal wave speeds of the lattice.
4. **Two-phonon scattering:** Recall that the basic laws governing neutron scattering from phonons could be deduced from conservation of energy and crystal momentum, without detailed quantum-mechanical calculation. Generalize this argument to consider processes in which neutrons incident upon a crystal participate in the creation or destruction of two phonons.
- (a) Enumerate the number of distinct ways in which such a process may occur.
- (b) Show that two-phonon processes do not produce sharp peaks in neutron absorption as a function of incident energy, for fixed observation angle, and may therefore be distinguished from one-phonon processes.
5. **Quantizing vibrations:**
- (a) Verify if creation and annihilation operators are defined by Eq. (13.42) that Eq. (13.43) is then satisfied.
- (b) Verify that the commutation relation Eq. (13.44) is satisfied.
6. **Debye temperature:** Use the data of Figure 13.8 to estimate the Debye temperature of diamond, and compare this estimate with the value tabulated in Table 13.1.
7. **Debye–Waller factor in three dimensions:** Adopt the assumptions of the Debye model, so that polarization vectors $\epsilon_{\vec{k}\nu}$ consist of a longitudinal mode parallel to \vec{k} and two transverse modes perpendicular to it, with the density of states given by Eq. (13.72).
- (a) Show that in three dimensions the Debye–Waller factor is given by Eq. (13.126).
- (b) Show that in one or two dimensions Eq. (13.124) diverges if $T \neq 0$.

References

- M. Born (1965), Reminiscences of my work on the dynamics of crystal lattices, in *Lattice Dynamics*, R. F. Wallis, ed., pp. 1–8, Pergamon, Oxford.
- B. N. Brockhouse (1995), Slow neutron spectroscopy and the grand atlas of the physical world, *Reviews of Modern Physics*, **67**, 735–751.
- E. G. Brovman and Y. M. Kagan (1974), Phonons in nontransition metals, *Soviet Physics Uspekhi*, **17**, 125–152.
- P. Debye (1965), The early days of lattice dynamics, in *Lattice Dynamics*, R. F. Wallis, ed., pp. 9–13, Pergamon, Oxford.
- P. A. M. Dirac (1958), *The Principles of Quantum Mechanics*, 4th ed., Clarendon Press, Oxford.
- G. Dolling and R. A. Cowley (1966), The thermodynamic and optical properties of germanium, silicon, diamond, and gallium arsenide, *Proceedings of the Physical Society (London)*, **88**, 463–504.

- S. Doniach and E. H. Sondheimer (1974), *Green's Functions for Solid State Physicists*, Benjamin/Cummings, Reading, MA
- A. Einstein (1907), Planck's theory of radiation and the theory of specific heat, *Annalen der Physik (Leipzig)*, **22**, 180–190. In German.
- A. Einstein (1916), Quantum theory of radiation, *Mitteilungen der Physikalischen Gesellschaft, Zürich*, **16**, 47–62. In German. Translated in van der Waerden (1967), pp. 63–77.
- J. Goldstone (1963), Field theories with “superconductor” solutions, *Nuovo Cimento*, **19**, 155–164.
- R. Golub (1996), Ultracold neutrons: Their role in studies of condensed matter, *Reviews of Modern Physics*, **68**, 329–347.
- S. K. Joshi and A. K. Rajagopal (1968), Lattice dynamics of metals, *Solid State Physics: Advances in Research and Applications*, **22**, 159–312.
- B. W. T. Kelvin (1904), *19th century clouds over the dynamical theory of heat and light*, Appendix B, Baltimore Lectures on Molecular Dynamics and the Wave Theory of Light, C. J. Clay and Sons, London. Readex Microprint, 1969 (Landmarks of Science)
- W. Kohn (1959), Image of the Fermi surface in the vibration spectrum of a metal, *Physical Review Letters*, **2**, 393–394.
- R. S. Krishnan, R. Srinivasan, and S. Devanarayanan (1979), *Thermal Expansion of Crystals*, Pergamon, Oxford.
- A. A. Maradudin, E. W. Montroll, G. H. Weiss, and I. P. Ipatova (1971), *Theory of Lattice Dynamics in the Harmonic Approximation*, 2nd ed., Academic Press, New York.
- N. D. Mermin (1966), A short simple evaluation of expressions of the Debye-Waller form, *Journal of Mathematical Physics*, **7**, 1038.
- R. Mössbauer (1958), Nuclear resonance fluorescence of gamma rays in Ir¹⁹¹, *Zeitschrift für Physik*, **151**, 124–143. In German.
- B. Mozer, K. Otnes, and H. Palevsky (1965), Measured vibrational frequency distributions of Ni, V, Ti, and Ti₆₇Zr₃₃, in *Lattice Dynamics*, R. F. Wallis, ed., pp. 63–70, Pergamon, Oxford.
- G. Nilsson and G. Nelin (1972), Study of the homology between silicon and germanium by thermal-neutron spectrometry, *Physical Review B*, **6**, 3777–3786.
- R. S. Preston, S. S. Hanna, and J. Heberle (1962), Mössbauer effect in metallic iron, *Physical Review*, **128**, 2207–2218.
- C. G. Shull (1995), Early development of neutron scattering, *Reviews of Modern Physics*, **67**, 753–757.
- G. A. Slack (1979), The thermal conductivity of nonmetallic crystals, *Solid State Physics: Advances in Research and Applications*, **34**, 1–71.
- G. R. Stewart (1983), Measurement of low-temperature specific heat, *Review of Scientific Instruments*, **54**, 1–11.
- Y. S. Touloukian and E. H. Buyco (1970a), *Specific Heat: Metallic Elements and Alloys*, vol. 4 of *Thermophysical Properties of Matter*, IFI/Plenum, New York.
- Y. S. Touloukian and E. H. Buyco (1970b), *Specific Heat: Nonmetallic Solids*, vol. 5 of *Thermophysical Properties of Matter*, IFI/Plenum, New York.
- Y. S. Touloukian, R. K. Kirby, R. E. Taylor, and P. D. Desai (1975), *Thermal Expansion: Metallic Elements and Alloys*, vol. 12 of *Thermophysical Properties of Matter*, IFI/Plenum, New York.
- B. L. van der Waerden (1967), *Sources of Quantum Mechanics*, North-Holland, Amsterdam.
- S. Wei and M. Y. Chou (1994), Phonon dispersions of silicon and germanium from first-principles calculations, *Physical Review B*, **50**, 2221–2226.
- J. L. Yarnell, J. L. Warren, and S. H. Koenig (1965), Experimental dispersion curves for phonons in aluminum, in *Lattice Dynamics*, R. F. Wallis, ed., pp. 57–61, Pergamon, Oxford.

14. Dislocations and Cracks

14.1 Introduction

The perfect crystal presents the perfect starting point for analyzing many features of condensed matter, but some qualitative phenomena it cannot explain at all. Even electrical conductivity technically falls in the latter category; Chapter 16 will show that noninteracting electrons in a perfect crystal oscillate and transport no current. In the case of electrical resistance, the failings of the perfect crystal are somewhat academic. But to understand many mechanical properties of solids, the perfect crystal is tremendously misleading. Wigner said that solid-state physics “deals in a scientific way with those subjects with which we must deal in our everyday experience. For example, we are never afraid when dropping a key that it will fly to pieces, as a glass would.” [Wigner (1936)] The key is *ductile*. It deforms slightly, or bends, but does not break. The glass is *brittle* and shatters. Familiar though these experiences may be, they are not at all easy to explain in a scientific way, for they result from the dynamics of defects. To motivate the study of these defects, it is necessary to point out how far the everyday world is from mechanical equilibrium, how difficult equilibrium is to attain, and how fortunate that the barriers to equilibrium are large.

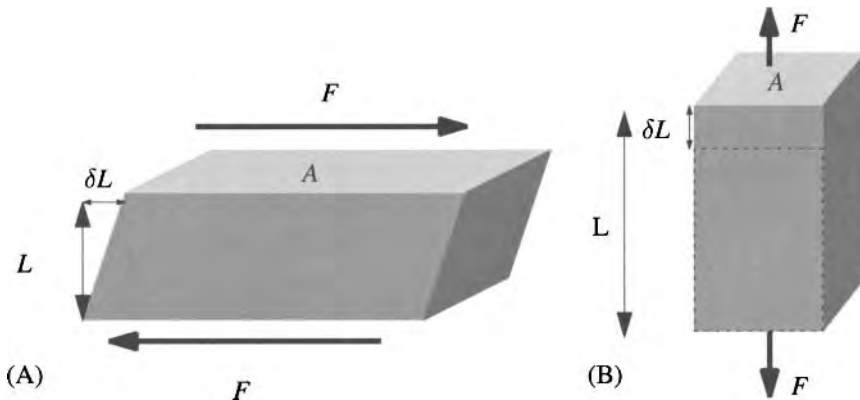


Figure 14.1. Solids of length L are stretched by force F , causing a change of length δL . In (A) the force is a shear, while in (B) it is pure tension.

Consider a piece of rock, of area A and height h . According to equilibrium principles the rock should not be able to sustain its own weight under the force of gravity if it becomes tall enough. To estimate what that critical height should be, note that the gravitational potential energy of the rock is $\rho Ah^2g/2$, where ρ is the

Table 14.1. Shear modulus $G/5$ versus onset of plastic flow for three materials

Material	Shear modulus $G/5$ (10^{11} ergs cm^{-3})	Yield strength (10^{11} ergs cm^{-3})
Iron	1.0–1.6	0.02–1
Copper	1.0	0.005
Titanium	1.0	0.08

Source: Baumeister (1978), pp. 5.2-5.5.

mass density. By cutting the rock into two equal blocks of height $h/2$ and setting them side by side, this energy can be reduced to $\rho Ah^2g/4$, for an energy gain of $\rho Ah^2g/4$. The cost of the cut is the cost of creating new rock surface, which characteristically equals per unit area $\Gamma = 1 \text{ J m}^{-2}$. Estimating $\rho = 2000 \text{ kg m}^{-3}$, the critical height at which it pays to divide the rock in two is

$$h = \sqrt{\frac{4\Gamma}{\rho g}} \approx 1.4 \text{ cm.} \quad (14.1)$$

So every block of stone more than a few centimeters tall is unstable under its own weight; changing the material to steel, concrete, or bone does not dramatically change the estimate.

Obviously rocks can survive to heights of more than 2 cm, so the barriers preventing them from reaching equilibrium must be large. Yet it is not obvious how to compute the barriers correctly. An easy way to obtain an estimate is by imagining what happens to the atoms of a solid as one pulls it uniformly at two ends. At first, the forces between the atoms increase, but eventually they reach a maximum value, and the solid falls into pieces. Interatomic forces vary greatly between different elements and compounds, but the forces typically reach their maximum value when the distance between atoms increases by around 20% of their original separation.

Referring to Figure 14.1(A), the shear force needed to deform a solid by 20% is given by

$$G \frac{\delta L}{L} = \frac{F}{A}, \quad G \text{ is the shear modulus.} \quad (14.2)$$

while as sketched in Figure 14.1(B) the force needed to deform a solid by 20% in tension is given by

$$Y \frac{\delta L}{L} = \frac{F}{A}. \quad (14.3)$$

The force per area, \mathcal{S} , needed to cause deformations of 20% is therefore estimated to be

$$\mathcal{S} = \frac{F}{A} = \begin{cases} \frac{G}{5} & \text{shear} \\ \frac{Y}{5} & \text{tension.} \end{cases} \quad (14.4)$$

Table 14.2. Failure of solids in tension

Material	Young's Modulus $Y/5$ (10^{11} ergs cm^{-3})	Theoretical Strength (10^{11} ergs cm^{-3})	Practical Strength (10^{11} ergs cm^{-3})	Ratio
Iron	4.0	4	0.03	0.008
Titanium	2.2	3.1	0.03	0.009
Silicon	3.2	1.5	0.07	0.05
Glass	1.4	4	0.04	0.01

The stress needed in practice to snap solids in tension is compared with Young's modulus, and with results of detailed calculations that determine the force per area that would be needed to pull a plane's worth of bonds apart at once. The calculations involving realistic accounts of interatomic interactions produce an answer fairly close to the estimate of $Y/5$, but quite far from experimental values. The final column gives the ratio of practical to theoretical strength. Source: Averbach (1968) and Grigoriev and Meilkhov (1997).

As shown in Tables 14.1 and 14.2, these estimates are in error by many orders of magnitude. The problem does not lie in the hasty estimates used to obtain the forces at which bonds separate, but in the whole conception of the calculation. The argument from equilibrium greatly underestimated the practical resistance of solid bodies to separation, and now it has been replaced by an equally incorrect argument that greatly overestimates it. The only way to uncover correct orders of magnitude is to account for the actual dynamical modes by which solids fail. Ductile crystals are those in which line defects called dislocations are mobile, allowing the solid to flow. Brittle materials are those where instead a more severe defect, the crack, is mobile instead.

Theoretical Strength of Silicon. The theoretical tensile strength of silicon can be estimated by using the universal cohesive energy of Eq. (11.50) and the data of Table 11.11. Simply compute the inward pressure that silicon exerts when uniformly expanded,

$$-P = \frac{1}{4\pi r_W^2} \frac{\partial \mathcal{E}(r_W)}{\partial r_W}. \quad (14.5)$$

Equation (14.5) is plotted in Figure 14.2, which gives an estimate for the maximum tensile stress of 1.5×10^{11} erg cm^{-3} .

14.2 Dislocations

Taylor (1934), Orowan (1934), and Polanyi (1934) developed independently the explanation of how crystals flow. The idea of the *dislocation* is that one can obtain a macroscopic rearrangement of a crystal by breaking a very small number of atomic bonds at a time. Figure 14.3 shows how a crystal can be rearranged by the movement of a configuration in which one line of bonds at a time snaps. This type

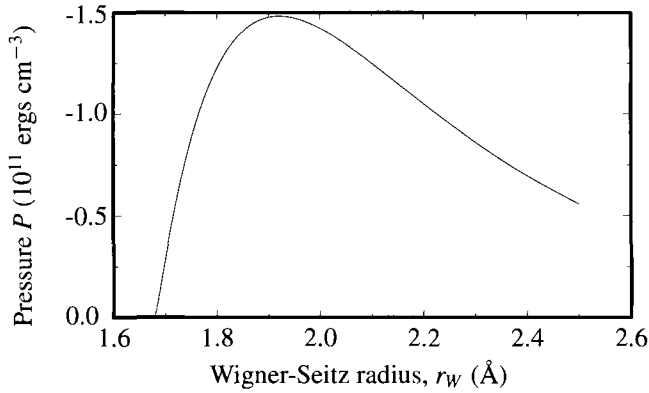


Figure 14.2. Plot of Eq. (14.5), showing that under uniform expansion the maximum cohesive stress of silicon is around 1.5 erg cm^{-3} when silicon has been expanded by about 15%.

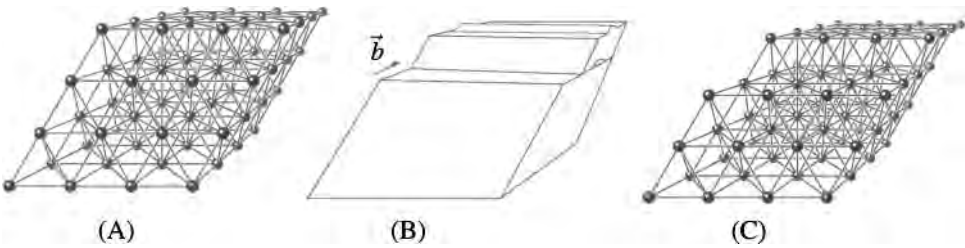


Figure 14.3. A crystal is able to flow in response to external stresses because of dislocations. As this defect moves through the crystal, only one atomic bond is broken at a time, but the net effect is to obtain a macroscopic rearrangement of the crystal. (A) Undeformed crystal. (B) A defect slides backwards, like a bump on a rug being pushed to the back of a room. (C) Top layer of crystal has been displaced by Burgers vector \vec{b} .

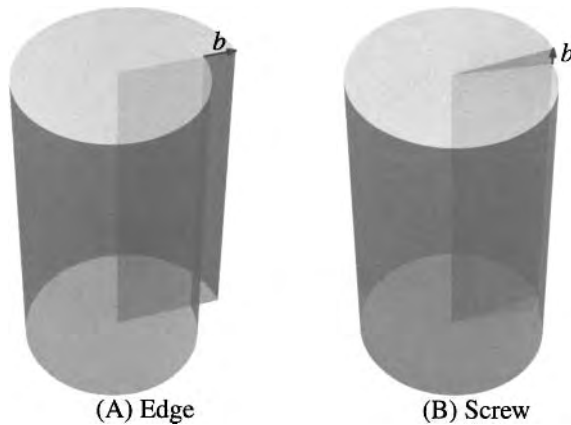


Figure 14.4. The two basic types of dislocations in three dimensions, (A) edge and (B) screw, are pictured from a continuum viewpoint, together with their Burgers vectors \vec{b} .

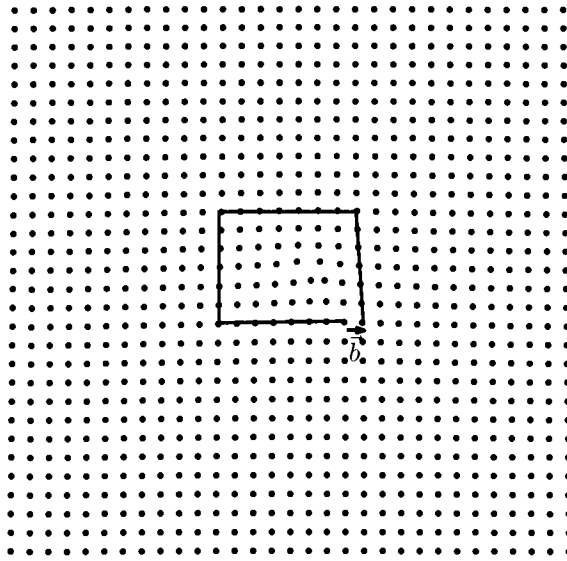


Figure 14.5. The Burgers vector, in this case for an edge dislocation, is constructed by following a counterclockwise path that would close in the perfect crystal. When it surrounds a dislocation, however, the path is open. The Burgers vector is the vector needed to close the path.

of defect costs vastly less energy at any given time than would be needed to pick up a chunk of crystal all at once and place it down at a new location.

There are two basic types of dislocations. The one pictured in Figure 14.3 and in Figure 14.4(A) is an *edge* dislocation. A second type is the *screw* dislocation, shown in Figure 14.4(B).

A basic characterization of a dislocation is its *Burgers vector*. This vector is obtained by going to the vicinity of a dislocation, and then traversing a counterclockwise path around it which would be closed in a perfect crystal—for example, 6 atoms up, 7 to the left, 6 down, and 7 to the right, as in Figure 14.5. When such a path surrounds a dislocation, it does not close, and the Burgers vector is the vector needed to close the path. For an edge dislocation, the Burgers vector is perpendicular to the dislocation line, while for a screw dislocation it is parallel, as shown in Figure 14.4.

From Figure 14.3 it should be clear that there is a unique plane in which it is particularly easy for a given dislocation line to move. This plane is known as the *slip plane* or *glide plane*. Motion perpendicular to that direction, which can only be achieved by difficult rearrangements of atoms, is called *climb*.

14.2.1 Experimental Observations of Dislocations

Theoretical consideration of the sort considered above were far from able to convince practical metallurgists that dislocations were real. Instead, dislocations seemed like elaborate theoretical fictions intended to rescue the improbable theory that

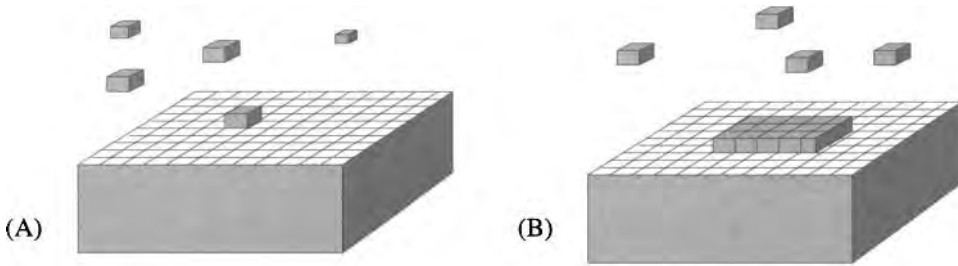


Figure 14.6. In order to add a new layer of atoms to a crystal, it is typically necessary to add a large clump of new atoms simultaneously. (A) A single atom attaching to the surface will be unstable and detach. (B) A large enough clump is stable.

matter was made of atoms from its embarrassing failure to account for the obvious practical properties of solids. Even some physicists felt that “the reality of the ‘dislocations’, which form the basis of [Taylor’s] theory, seems very doubtful.” [Frenkel and Kontorova (1938), p. 2]. Starting in the 1950s new techniques imaged dislocations directly. The first was in response to theories of crystal growth. If one has a flat crystalline surface, it is hard to deposit a new layer of atoms on it. A single atom sitting on a surface is not by and large stable, because only by being surrounded by neighbors on as many sides as possible does the bonding that holds the solid together keep the surface atoms glued on. In Figure 14.6 the atom in (A) is likely to jump off the surface, and a clump as large as the one shown in (B), or even larger, might well be required for stability. However, forming large clumps simultaneously is statistically very unlikely. The calculations of these probabilities were due to Volmer: “Keith Burton showed how you could put numbers into Volmer’s algebraic expressions: and it turned out that while Volmer’s curve for dependence of growth-rate on supersaturation was qualitatively similar to what was observed, there was a quantitative disagreement by a factor of 10^{1000} , which we said was the largest factor of discrepancy we had ever called agreement.” [Frank (1985), p. 9]

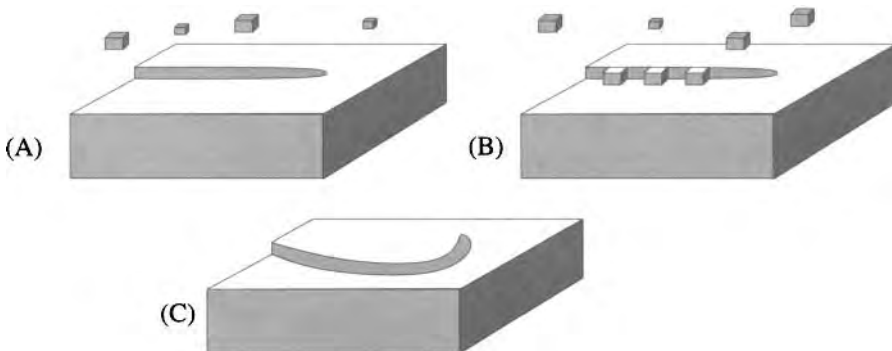


Figure 14.7. Mechanism due to Frank, showing how the presence of a screw dislocation should speed the process of crystal growth, by providing open regions to which atoms can easily attach.

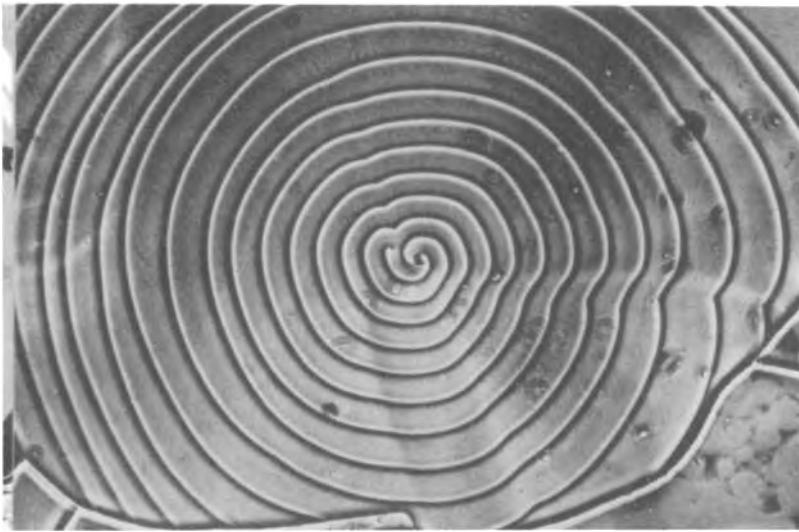


Figure 14.8. Experimental observation of growth spirals on the (0001) plane of silicon carbide. [Source: Amelinckx (1964), p. 5.]

The idea that Frank proposed to rescue the situation was that atoms could easily attach to a screw dislocation at the top of a crystal, as shown in Figure 14.7. Such spiral patterns, greatly magnified in scale by chemical etching, are now routinely observed on crystal surfaces, as shown in Figure 14.8. It is possible, by having impurity atoms diffuse to dislocations, to image them directly with electron, X-ray, and neutron diffraction. A picture showing various dislocations surrounding silica particles in brass appears in Figure 14.9(A). Finally, high-resolution electron microscopy makes it possible to view dislocations at the atomic scale, as shown in Figure 14.9(B).

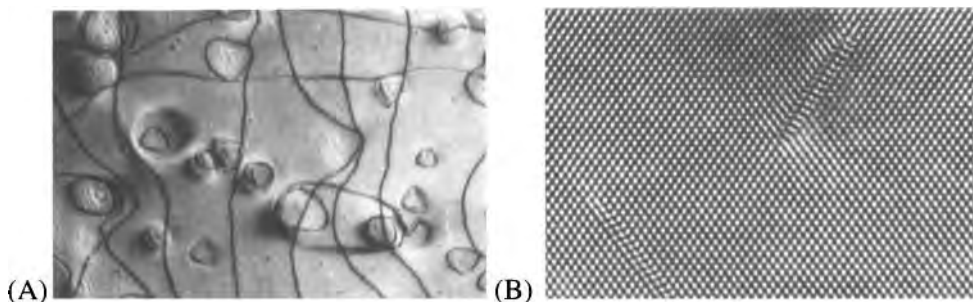


Figure 14.9. (A) Experimental observation of individual dislocation loops surrounding Ni_3Si particles in nickel-silicon alloy. (Courtesy of J. Humphreys, Manchester University.) (B) High-resolution electron micrograph of CdTe, showing dislocation loops imaged at the atomic scale. [Source: Cullis et al. (1985), p. 205.]

14.2.2 Force to Move a Dislocation

A virtual work argument can be used to determine the effectiveness of external stresses in moving a dislocation. Viewing the dislocation as a line being pushed through the crystal, define \vec{f} , the force per length a needed to make the dislocation move. If the dislocation in Figure 14.5 moves from right to left past N atomic sites, then a layer N atoms long moves by the Burgers vector \vec{b} . If an external shearing force F_{ext} has been applied to the top and bottom of the sample, then the total work done in the process is $F_{\text{ext}}b_x$. The work required to move the dislocation over one lattice spacing is then $F_{\text{ext}}b_x/N$, and the force f_x per length a required to move the dislocation must be

$$f_x = \sigma_{xy}b_x, \quad (14.6)$$

where

$$\sigma_{xy} = \frac{F_{\text{ext}}}{Na^2} \quad (14.7)$$

is the external stress applied to the crystal, with a the lattice spacing. Notice that putting the crystal under tension, either with σ_{xx} (pulling along the x axis), or with σ_{yy} (pulling along the y axis) has no power to move the dislocation. If \hat{L} is a unit vector pointing along the dislocation line ($\hat{L} = \hat{z}$ in the case of Figure 14.5), then Eq. (14.6) can be rewritten in coordinate independent form as

$$\vec{f} = (\sigma \cdot \vec{b}) \times \hat{L}. \quad (14.8)$$

The first term on the right-hand side of Eq. (14.8) indicates that one forms the 3×3 tensor σ and takes its dot product with the Burgers vector \vec{b} . The direction of \hat{L} is chosen according to the right-hand rule; the Burgers vector is defined by taking a counterclockwise path around the dislocation, and the direction \hat{L} of the dislocation is the direction the thumb points when the right-hand fingers curl around it. The advantage of describing the force on the dislocation in this form, due to Peach and Kohler (1950), is that it is independent of one's choice of coordinate system, is equally true for edge or screw dislocations, and remains true for a dislocation which curls about or forms a loop.

Equation (14.8) is useful when one supposes that there is a critical force f_c needed per unit length to make the dislocation move. Equation (14.8) then describes the external stress that will be required for a crystal to begin to flow, if it is populated with dislocations. It can also be used, for example, to decide when one dislocation will begin to move because of stresses created by another dislocation.

14.2.3 One-Dimensional Dislocations: Frenkel–Kontorova Model

In order to understand how dislocations allow crystals to flow, it is necessary to determine the critical force f_c . This task is somewhat complicated in two- and three-dimensional settings, so it is helpful to examine a one-dimensional model for dislocations, the model of Frenkel and Kontorova (1938), where the job is easier.

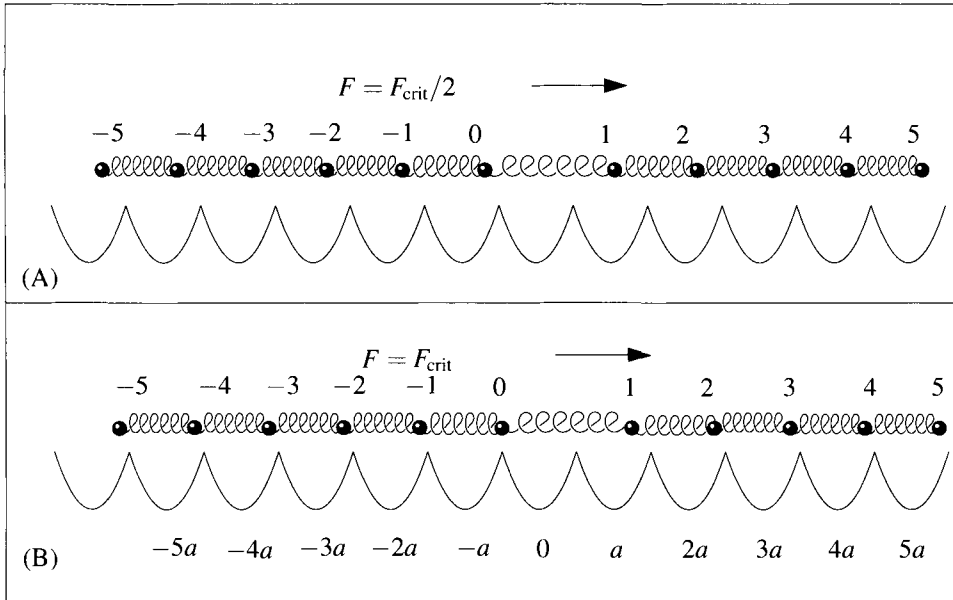


Figure 14.10. The Frenkel–Kontorova model contains a one-dimensional array of parabolic potentials placed side by side, in which are located a collection of masses. The masses are acted upon by a force, which tends to push them over the potential, and are connecting by springs of constant k . (A) Equilibrium dislocation. (B) Dislocation on the verge of beginning to move because the mass at 0 is balanced on the top of the potential.

In this one-dimensional model, pictured in Figure 14.10, one considers a collection of masses connected by springs, and sitting in a periodic potential, described by

$$U(x) = \frac{1}{2}\mathcal{K}[x - a \operatorname{int}(x/a + \frac{1}{2})]^2 - fx, \tag{14.9}$$

where f describes the external forces applied to the particles. The integer part of $x/a + \frac{1}{2}$ gives the integer nearest to x/a . If mass n is located at x_n , then the total force on mass n is

$$f_n = k[x_{n+1} - x_n - a] + k[x_{n-1} - x_n + a] - \frac{\partial U}{\partial x}. \tag{14.10}$$

When a dislocation is present, one of the wells does not have a particle in it. Choose that well to be the one centered at 0, so that particle 0 is now sitting in the well centered at $-a$, and particle 1 is sitting in the well centered at a . This means that Eq. (14.10) can be rewritten

$$f_n = \begin{cases} k[x_{n+1} - x_n - a] + k[x_{n-1} - x_n + a] + f - \mathcal{K}[x_n - (n-1)a] & \text{for } n \leq 0 \\ k[x_{n+1} - x_n - a] + k[x_{n-1} - x_n + a] + f - \mathcal{K}[x_n - na] & \text{for } n > 0. \end{cases} \tag{14.11}$$

In equilibrium, all the forces f_n have to vanish. Guessing the form for $n \leq 0$

$$x_n = f/\mathcal{K} + a(n-1) + A_l e^{qn}, \tag{14.12}$$

one immediately finds that for $n \leq 0$,

$$k(e^q - 2 + e^{-q}) - \mathcal{K} = 0 \quad (14.13)$$

while for $n > 0$ one again has Eq. (14.13) but the solution is of the form

$$x_n = f/\mathcal{K} + an + A_r e^{-qn}. \quad (14.14)$$

The question is, do the two solutions join properly at $n = 0$? They only match if x_0 computed from Eq. (14.14) is the same as x_0 found in Eq. (14.12), and x_1 computed from Eq. (14.12) is the same as x_1 from Eq. (14.14). So one must require

$$-a + A_l = A_r \quad \begin{array}{l} \text{To obtain equivalent results more formally,} \\ \text{carefully write down the two equations } f_0 = 0 \\ \text{and } f_1 = 0, \text{ using Eqs. (14.12) and (14.14).} \end{array} \quad (14.15a)$$

$$A_l e^q = a + A_r e^{-q}, \quad (14.15b)$$

which gives

$$A_l = \frac{a}{e^q + 1} \quad (14.16a)$$

$$A_r = \frac{-a}{e^{-q} + 1}. \quad (14.16b)$$

These are the equilibrium solutions. What should correspond to the motion of a dislocation? The motion should begin as soon as the force on the system is great enough so that mass 0 has reached the peak at $-a/2$ and is about to slide down into well at 0, pulling the mass behind it in its wake. This condition is

$$x_0 = -\frac{a}{2} = \frac{f_c}{\mathcal{K}} - a + A_l \quad (14.17)$$

$$\Rightarrow f_c = \frac{a\mathcal{K}}{2} \tanh \frac{q}{2}. \quad (14.18)$$

The maximum force that the potential U is able to supply is $a\mathcal{K}/2$ —all masses would be able to slide when f reached this value with or without a dislocation—so the hyperbolic tangent in Eq. (14.18) describes the advantage to be gained from having a dislocation. One obtains plasticity with low forces when q is small, which means equivalently that the dislocation is quite extended. This limit is achieved when \mathcal{K}/k is small, in which case one finds

$$q \approx \sqrt{\frac{\mathcal{K}}{k}} \quad (14.19)$$

and

$$f_c \approx \frac{a\mathcal{K}}{4} \sqrt{\frac{\mathcal{K}}{k}}. \quad (14.20)$$

14.3 Two-Dimensional Dislocations and Hexatic Phases

Dislocations play an interesting role in the statistical mechanics of two-dimensional crystals. Two-dimensional crystals do not, in fact, technically exist. Long-range order is almost always destroyed by thermal fluctuations in two dimensions. Another type of order, orientational order, can however exist, and dislocations are central actors in the phase transition that brings orientational order to an end. The mathematics of this phase transition applies almost unchanged to a broad range of other physical systems, ranging from two-dimensional electron gases to thin films of helium, and provides a setting in which to gain an introduction to renormalization group techniques.

14.3.1 Impossibility of Crystalline Order in Two Dimensions

Three dimensions are special in many respects. One surprising property, first realized by Peierls (1934) and Landau (1937), is that three-dimensional space is the lowest dimensionality in which long-range crystalline order is possible. Certainly, one can draw pictures of crystals in two dimensions, but if one built them, they would be destroyed at any nonzero temperature by fluctuations. This fact has already been demonstrated, because Problem 7 in Chapter 13 shows that sharp Bragg peaks cannot survive in one and two dimensions as a result of quantum fluctuations. The same conclusion follows from examining the effect of thermal fluctuations in a purely classical context.

Consider, for simplicity, a two-dimensional elastic medium, where in terms of displacement field u introduced in Section 12.3, the potential energy takes the simple form

$$U = \int d^2r \frac{1}{2} C \sum_{\alpha\beta} \frac{\partial u_\alpha}{\partial r_\beta} \frac{\partial u_\alpha}{\partial r_\beta}. \quad \text{Here } C \text{ is a constant with dimensions of energy per area.} \quad (14.21)$$

In order to study the statistical mechanics of a system whose energy is given by Eq. (14.21), it is best to work with the Fourier transform variable $u_\alpha(\vec{k})$ such that

$$u_\alpha(\vec{r}) = \sum_{\vec{k}} e^{i\vec{r}\cdot\vec{k}} u_\alpha(\vec{k}). \quad (14.22)$$

The idea that u describes only fluctuations on a scale larger than some distance \mathcal{D} that is bigger than an interatomic spacing may be implemented by requiring that

$$\vec{u}(\vec{k}) = 0 \text{ for } k > 1/\mathcal{D}. \quad (14.23)$$

Then Eq. (14.21) can be rewritten as

$$U = \int d^2r \frac{1}{2} C \sum_{\beta\alpha\vec{k}\vec{k}'} k_\beta k'_\beta e^{i(\vec{k}-\vec{k}')\cdot\vec{r}} u_\alpha(\vec{k}) u_\alpha^*(\vec{k}') \quad (14.24)$$

The first time Eq. (14.22) is used, it is substituted directly into Eq. (14.21). To substitute the second time for u_α , however, one uses the fact that u_α is real and substitutes the complex conjugate of Eq. (14.22) instead.

$$= \frac{\mathcal{V}C}{2} \sum_{\alpha\vec{k}} k^2 |u_\alpha(\vec{k})|^2 \quad \text{Use } \mathcal{V}\delta_{\vec{k}\vec{k}'} = \int d^2r e^{i(\vec{k}-\vec{k}')\cdot\vec{r}}, \text{ where } \mathcal{V} \text{ is the two-dimensional volume of the system.} \quad (14.25)$$

With this expression for the energy of a slightly deformed system, one can perform statistical averages. First, examine the expectation value of the average square displacement of particles from their original location, which is

$$\langle u^2 \rangle = \left\langle \int \frac{d^2r}{\mathcal{V}} \sum_{\beta} u_\beta(\vec{r}) u_\beta(\vec{r}) \right\rangle \quad \text{Here } \mathcal{V} \text{ is the two-dimensional volume of the system, and } \langle \rangle \text{ is a thermal average.} \quad (14.26)$$

$$= \sum_{\beta\vec{k}} \langle |u_\beta(\vec{k})|^2 \rangle \quad \text{This calculation is identical to the one that leads to Eq. (14.25), except that the derivatives with respect to } r_\beta \text{ are missing.} \quad (14.27)$$

In order to perform the thermal average, one has to integrate over all allowed values of $\vec{u}_{\vec{k}}$, weighted by the energy of each configuration. Because $\vec{u}(\vec{r})$ is real, one has to restrict this discussion to cases where

$$\vec{u}(\vec{k}) = \vec{u}^*(-\vec{k}) \quad (14.28)$$

and also restrict it to long-wavelength excitations in accord with Eq. (14.23). Otherwise, all possible functional forms of $\vec{u}(\vec{k})$ are permitted. Picking one value from the sum over \vec{k} indicated in Eq. (14.27), one has to compute

$$\begin{aligned} & \langle |u_\beta(\vec{k})|^2 \rangle \\ &= \frac{\int \prod_{\alpha\vec{k}'} du_\alpha(\vec{k}') |u_\beta(\vec{k})|^2 e^{-\beta \frac{\mathcal{V}C}{2} \sum_{\alpha\vec{k}'} k'^2 |u_\alpha(\vec{k}')|^2}}{\int \prod_{\alpha\vec{k}'} du_\alpha(\vec{k}') e^{-\beta \frac{\mathcal{V}C}{2} \sum_{\alpha\vec{k}'} k'^2 |u_\alpha(\vec{k}')|^2}} \end{aligned} \quad \begin{array}{l} \text{Regarding all the } u(\vec{k}') \text{ for} \\ \text{different } \vec{k} \text{ as independent} \\ \text{variables, although subject to} \\ \text{constraint (14.28), and} \\ \text{integrating over them.} \end{array} \quad (14.29)$$

$$= \frac{\int du_\beta(\vec{k}) |u_\beta(\vec{k})|^2 e^{-\beta \mathcal{V}C k^2 |u_\beta(\vec{k})|^2}}{\int du_\beta(\vec{k}) e^{-\beta \mathcal{V}C k^2 |u_\beta(\vec{k})|^2}} \quad \begin{array}{l} \text{Most terms cancel between} \\ \text{numerator and denominator.} \\ \text{The factor of 2 beneath } C \\ \text{disappears because, using} \\ \text{Eq. (14.28), two terms in the} \\ \text{exponential depend on} \\ \text{integration over } u_\beta(\vec{k}). \end{array} \quad (14.30)$$

$$= \frac{\int du^r du^i [(u^r)^2 + (u^i)^2] e^{-\beta \mathcal{V}C k^2 [(u^r)^2 + (u^i)^2]}}{\int du^r du^i e^{-\beta \mathcal{V}C k^2 [(u^r)^2 + (u^i)^2]}} \quad \begin{array}{l} \text{One has to integrate over both} \\ \text{the real and imaginary parts } u_r \\ \text{and } u_i \text{ of } u_\beta(\vec{k}). \end{array} \quad (14.31)$$

$$= \frac{k_B T}{\mathcal{V}C k^2} \quad \text{Use } \int_{-\infty}^{\infty} dx x^2 e^{-x^2} = \sqrt{\pi}/2 \quad (14.32)$$

Returning to Eq. (14.27), one has that

$$\langle u^2 \rangle = \sum_{\alpha\vec{k}} \frac{k_B T}{\mathcal{V}C k^2} \quad (14.33)$$

$$= 2 \int \frac{d^2k}{(2\pi)^2} \frac{k_B T}{C k^2} \quad \text{Using the two-dimensional density of states from Section 6.3.} \quad (14.34)$$

$$= 2 \int_0^{1/D} \frac{dk}{2\pi k} \frac{k_B T}{C} \rightarrow \infty. \quad \text{Recall Eq. (14.23).} \quad (14.35)$$

The integral in Eq. (14.35) diverges logarithmically for small k , just where linear elasticity should be working the best. Assuming that deviations of the crystal from equilibrium are small has led inevitably to the conclusion that they are infinitely large and that long-range translational order is impossible in two dimensions. This result is known as the *Mermin–Wagner theorem*, after Mermin and Wagner (1966). It does not mean that real two-dimensional systems are liquid at any nonzero temperature, nor does it mean that lightning will smite him dead who tries to add the last atom to a two-dimensional array. Rather, as shown in Figure 14.12, it means that Bragg scattering peaks are substantially broadened. In fact, the conclusion is somewhat pedantic. The divergence in Eq. (14.35) is only logarithmic, so in any finite-sized sample the deviations from long-range order may not be overwhelmingly large. Two-dimensional crystals do not melt at all temperatures; they are just somewhat floppy at long distances.

14.3.2 Orientational Order

Although the average fluctuations in positions of atoms are large in a two-dimensional crystal, Mermin (1968) showed that fluctuations in the angles of orientation of atoms with respect to their neighbors are much smaller. This fact may be determined by arguments that closely mirror the previous ones.

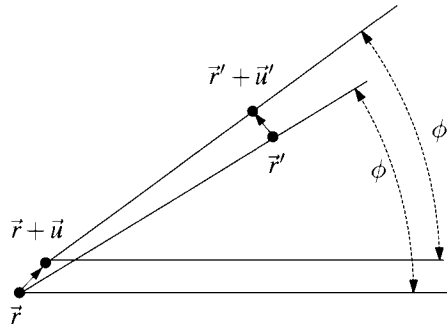


Figure 14.11. Illustration of how a displacement \vec{u} causes the angle ϕ between points \vec{r} and \vec{r}' to shift.

Suppose again that one has a displacement field $\vec{u}(\vec{r})$. How do these displacements cause angles between nearby points to shift? Referring to Figure 14.11, let

$$(dx, dy) = \vec{r}' - \vec{r}. \quad (14.36)$$

The angle ϕ between the two points is

$$\phi = \tan^{-1}(dy/dx). \quad (14.37)$$

When they are displaced by a field $\vec{u}(\vec{r})$, the new locations of \vec{r} and \vec{r}' are

$$\vec{r} + \vec{u}(\vec{r}) \quad \text{and} \quad \vec{r}' + \vec{u}(\vec{r}'). \quad (14.38)$$

Therefore, the new angle between them is

$$\phi' = \tan^{-1} \left(\frac{dy + \partial u_y / \partial x dx + \partial u_y / \partial y dy}{dx + \partial u_x / \partial x dx + \partial u_x / \partial y dy} \right) \quad (14.39)$$

$$\approx \phi + \frac{dx dy}{dx^2 + dy^2} \left[\left(\frac{\partial u_y}{\partial y} - \frac{\partial u_x}{\partial x} \right) + \frac{dx}{dy} \frac{\partial u_y}{\partial x} - \frac{dy}{dx} \frac{\partial u_x}{\partial y} \right] \quad (14.40)$$

$$\Rightarrow \phi' - \phi = \cos \phi \sin \phi \left(\frac{\partial u_y}{\partial y} - \frac{\partial u_x}{\partial x} \right) + \cos^2 \phi \frac{\partial u_y}{\partial x} - \sin^2 \phi \frac{\partial u_x}{\partial y}. \quad (14.41)$$

Averaging over ϕ , one finds that the average change in local orientation $\delta\phi$ at each point \vec{r} is given by

$$\delta\phi(\vec{r}) = \frac{1}{2} \left(\frac{\partial u_y}{\partial x} - \frac{\partial u_x}{\partial y} \right). \quad (14.42)$$

Adopting the Fourier representation Eq. (14.22), one has

$$\delta\phi(\vec{r}) = \frac{1}{2} \sum_{\vec{k}} (ik_x u_y(\vec{k}) - ik_y u_x(\vec{k})) e^{i\vec{k}\cdot\vec{r}}. \quad (14.43)$$

Therefore, the spatial average of orientation fluctuations is

$$\int \frac{d^2 r}{V} \langle \delta\phi(\vec{r}) \delta\phi(\vec{r}') \rangle \quad (14.44)$$

$$= \frac{1}{4} \sum_{\vec{k}} k_x^2 \langle |u_x(\vec{k})|^2 \rangle + k_y^2 \langle |u_y(\vec{k})|^2 \rangle - k_x k_y \langle (u_x(\vec{k}) u_y^*(\vec{k}) + u_y(\vec{k}) u_x^*(\vec{k})) \rangle \quad (14.45)$$

$$= \frac{1}{4} \sum_{\vec{k}} \frac{k_B T}{C \mathcal{V} k^2} (k_x^2 + k_y^2) \quad \text{Using Eq. (14.32), and noticing that } \langle u_x(\vec{k}) u_y^*(\vec{k}) \rangle \text{ must vanish by symmetry.} \quad (14.46)$$

$$= \frac{k_B T}{4C} \int_0^{2\pi} d\theta \int_0^{1/\mathcal{D}} \frac{dk k}{(2\pi)^2} = \frac{k_B T}{16\pi \mathcal{D}^2 C}. \quad (14.47)$$

In contrast to the amplitude fluctuations, orientation fluctuations do not diverge in this analysis. Therefore, it is possible that they will remain finite, although long-range crystalline order has been broken. The crystal has *bond-orientational order*.

14.3.3 Kosterlitz–Thouless–Berezinskii Transition

As the temperature of a two-dimensional crystal increases, there comes a point where temperature fluctuations destroy the long-range orientational order present at low temperatures, just as the long-range positional order of ordinary solids disappears at the melting temperature. The manner in which the transition occurs was first described in detail by Kosterlitz and Thouless (1973) and Berezinskii (1972), with an additional transition at higher temperature found by Nelson and Halperin (1979) and Young (1979).

Experimental Observations. The two-dimensional crystals in which bond-orientational order is observed would be triangular lattices at zero temperature, and therefore they are known as *hexatics*. It is not easy to observe hexatic ordering in atomic scale systems, because free-standing films one atom thick are hard to make. It has been observed in liquid crystal films only a few monolayers high by Pindak et al. (1981). Bond-orientational order has also been observed in *colloidal suspensions*, where latex spheres of about a micron in diameter are placed in a micron-thick bath of water. The spheres interact through electrostatic repulsion.

Figure 14.12 shows experimental scattering data obtained from such a colloidal system. The left panel shows the colloidal system heated above its melting temperature and displaying the correlations typical of a liquid. The center panel shows the system in an intermediate phase, the *hexatic liquid* in which orientational order is still present, but no traces of positional order remain. The right panel shows the *hexatic crystal*, which is the phase described by calculations in the preceding sections. The lack of long-range positional order is indicated by the nonzero widths of the scattering peaks, along with their slow decrease in amplitude away from the upper right-hand corner. Hexatic orientational order, however, is still perfect, so all the peaks are in the location one expects for a perfect crystal. The two-dimensional positional ordering of this structure is called *quasi-long-range order*.

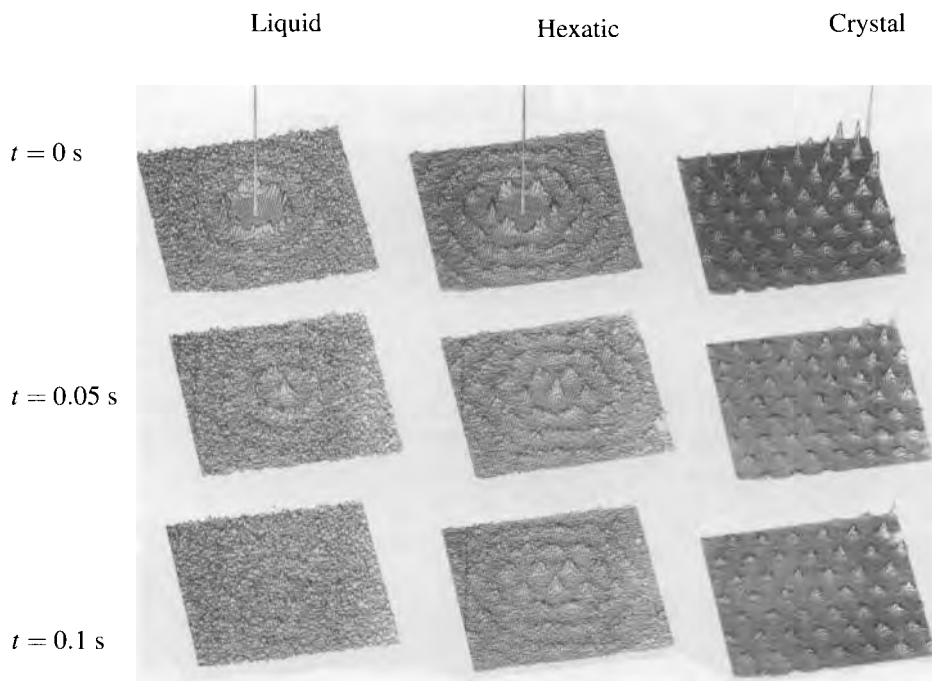


Figure 14.12. Experimental correlation functions $g(\vec{r}, t)$ from a two-dimensional colloidal system. The top panel shows correlation functions at $t = 0$, while the lower panel shows the decay of correlations after 0.05 and 0.1 s. [Source: Murray and Grier (1996).]

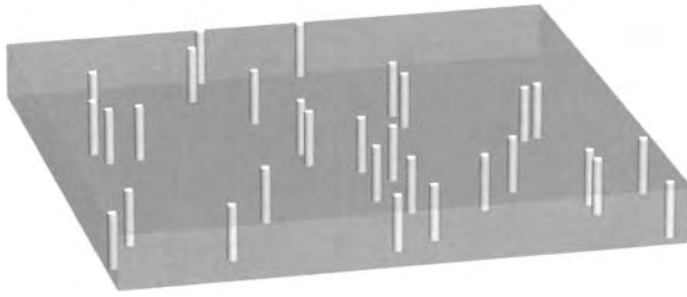


Figure 14.13. A two-dimensional array of parallel screw dislocations.

In the colloidal crystals, particles are confined to a plane, and they move in the x and y directions. The dislocations that arise are edge dislocations, as in Figure 14.5. To study their statistical mechanics, two simplifications will be introduced.

1. The problem will be treated in the framework of linear elasticity. Continuum mechanics only runs into trouble near the core of a dislocation, and it will be sufficient to cut off certain dangerous integrals, as in Eq. (14.47).
2. The vector character of edge dislocations makes them hard to work with, so they will be replaced with screw dislocations, as in Figure 14.13. Thus, instead of permitting points in the plane to have displacements u_x , u_y , for the remainder of the section they will be allowed only displacements u_z , which will be denoted by u . This alteration of the problem simplifies the analysis, but does not change any of the qualitative conclusions.

The displacement fields being considered from now on are of the form

$$u_x = 0, \quad u_y = 0, \quad u(x, y) = u_z(x, y). \quad (14.48)$$

According to Eq. (12.33), the energy of a displacement field obeying Eq. (14.48) is

$$U = \frac{a\mu}{2} \int d^2r (\nabla u)^2 \quad (14.49)$$

The gradient operator is understood to be operating in two dimensions. The factor a out front is needed so that the dimensions of U will turn out correct; think of the solid of having height a in the z direction.

According to Eq. (12.40), such a displacement field in static equilibrium obeys

$$\nabla^2 u = 0. \quad \text{Laplace's equation!} \quad (14.50)$$

Single Dislocation. The simplicity of Eq. (14.50) makes it possible to write down immediately the displacement field of a single dislocation. All analytic functions of a complex variable are solutions of Laplace's equation, so it is sufficient to find within the repertoire of such functions one that has the property of increasing by a Burgers vector when one passes in a complete circuit around the dislocation. The

logarithm is the simplest complex function this property; $\log(x + iy)$ increases by $2\pi i$ for any path that loops once about the origin. A dislocation at the origin with Burgers vector a is described by

$$u(x, y) = \frac{a}{2\pi} \text{Im} \ln[x + iy]. \quad (14.51)$$

What is the potential energy cost of introducing such a dislocation into a solid? Placing Eq. (14.51) into Eq. (14.49) gives

$$U = \frac{a\mu}{2} \left(\frac{a}{2\pi}\right)^2 \int d^2r \left[\frac{-y}{x^2 + y^2} \right]^2 + \left[\frac{x}{x^2 + y^2} \right]^2 \quad (14.52)$$

$$= \frac{a\mu}{2} \left(\frac{a}{2\pi}\right)^2 \int_a^R dr \, 2\pi r \frac{1}{r^2} \quad \begin{array}{l} \text{The limits } a \text{ and } R \text{ are introduced by hand to} \\ \text{keep the integral from diverging, as discussed} \\ \text{below.} \end{array} \quad (14.53)$$

$$\rightarrow \frac{1}{4\pi} (a^3 \mu) \ln \left(\frac{R}{a}\right) + w. \quad \begin{array}{l} w \text{ is added by hand to account for the energy} \\ \text{of the core of the dislocation.} \end{array} \quad (14.54)$$

The passage from Eq. (14.52) to Eq. (14.54) is not completely direct. There is the problem that the integral over r diverges both at large and short lengths. The solution at large lengths is to cut the integral off at a system size R (taking the dislocation to sit at the center of a cylinder). At short lengths, the integral must be cut off at the scale of the lattice spacing a , where continuum mechanics breaks down. To compensate for the very crude treatment of short lengths, it is necessary to add to Eq. (14.55) an additional energy w , which describes the energy needed to form the core of the dislocation, meaning those fine adjustments on the atomic scale that Eq. (14.54) has gotten wrong. This energy w will be added to the energies of all dislocations from now on.

Two Dislocations. The displacement field of two dislocations with equal and opposite Burgers vectors separated by distance x_0 along the x axis is

$$u(x, y) = \frac{a}{2\pi} \text{Im} \{ \ln[x + iy] - \ln[x - x_0 + iy] \}. \quad (14.55)$$

Using the divergence theorem and some properties of complex functions, Problem 2 shows that the energy of such a configuration is

$$2q^2 \ln \left(\frac{x_0}{a}\right) + 2w \quad \text{with } q^2 = \frac{a^3 \mu}{4\pi}. \quad (14.56)$$

The notation of Eq. (14.56) is meant to suggest an analogy with two-dimensional electrostatics. The analogy is almost perfect. The dislocations obey exactly the same equations as lines of charge q : The displacement u serve as the electrostatic potential, and the gradients of u are equivalent to the electrical field. The advantage of employing this analogy is that it permits the use of a subtle quantity, usually taken for granted, the dielectric constant ϵ . There is a slight flaw in the analogy, which emerges as soon as one draws the field lines $\vec{\nabla}u$ that should correspond to

the electric field. As shown in Figure 14.14, the field lines surround the dislocation in an axial fashion. This is the magnetic field configuration surrounding a line of current, not the electrical field around an electric charge. However, because the equations describing the energies of interacting line currents are identical to the energies of interacting charges in two dimensions, the analogy with two-dimensional electrostatics survives and will be employed frequently in what follows.

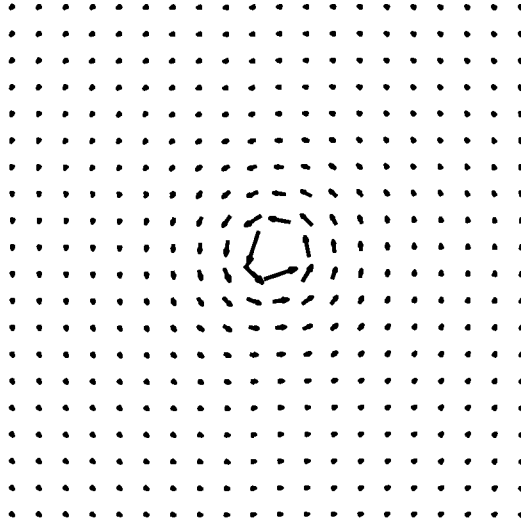


Figure 14.14. Vector field $\vec{\nabla}u$ for a dislocation described by Eq. (14.55). The field is the same as the magnetic field around a line of current.

Statistical Mechanics of Two-Dimensional Dislocations.

According to Eq. (14.54), the energy of an isolated dislocation diverges logarithmically with system size. Despite this divergence, thermodynamic equilibrium may happily permit many such dislocations to form. All depends upon the competition between energy and entropy. The entropy of forming a single dislocation may be estimated by noting that in a square with side length L , there are L^2/a^2 locations at which to put the center of the dislocation, so its entropy is

$$S = 2k_B \ln(L/a), \quad (14.57)$$

while its energy will be

$$\mathcal{E} = q^2 \ln(L/a). \quad (14.58)$$

Picking out the divergent part of the energy, and assuming that the difference between a disk of radius L and a square of side length L is not important.

There should be a critical temperature at which it becomes favorable to flood the system with dislocations. Using the estimates in Eqs. (14.57) and (14.58), the free energy $\mathcal{E} - TS$ becomes negative at a temperature

$$k_B T_c = \frac{q^2}{2}. \quad (14.59)$$

This estimate of the transition is close to the truth, but the numerical value of the transition point will turn out to be slightly different.

Kosterlitz–Thouless Hamiltonian. Motivated by Eq. (14.56), consider a population of screw dislocations interacting with energy

$$\mathcal{H} = \frac{1}{2} \sum_{i \neq j} U(|\vec{r}_i - \vec{r}_j|) + 2w \quad \text{with} \quad U(r) = 2q^2 \ln(r/a) \quad (14.60)$$

At low temperatures, the dislocations group themselves into pairs that form a dilute gas. Proof of this statement comes from comparing the mean square radius of a dislocation pair to the mean square separation between pairs.

At low temperatures, the mean square separation of two dislocations in a pair is

$$\langle r^2 \rangle = \frac{\int_a^\infty dr 2\pi r r^2 e^{-\beta U(r)}}{\int_a^\infty dr 2\pi r e^{-\beta U(r)}} \quad (14.61)$$

$$= a^2 \left[\frac{\beta q^2 - 1}{\beta q^2 - 2} \right]. \quad \text{Insert Eq. (14.60) and perform the integrals.} \quad (14.62)$$

On average, the pairs are situated farther from one another than $\sqrt{\langle r^2 \rangle}$. Consider, for example, the density n of dislocation pairs whose separation lies between r and $r + dr$. The grand partition function for vortex pairs is

$$Z_{\text{gr}} = 1 + \sum_{\vec{r}_1 \vec{r}_2} e^{-\beta U(|\vec{r}_1 - \vec{r}_2|) - 2\beta w} + \dots \quad (14.63)$$

The density $n(r)$ of dislocation pairs with separation lying between r and $r + dr$ in a system of size R^2 is therefore, to leading order in $\exp[-2\beta w]$,

$$n(r)dr = \frac{dr}{aR^2} \langle \delta_{r,|\vec{r}_1 - \vec{r}_2|} \rangle = \frac{dr}{aR^2} \sum_{\vec{r}_1 \vec{r}_2} e^{-\beta U(|\vec{r}_1 - \vec{r}_2|) - 2\beta w} \delta_{r,|\vec{r}_1 - \vec{r}_2|} + \dots \quad (14.64)$$

$$\approx \frac{1}{a^2} \frac{2\pi r dr}{a^2} e^{-\beta U(r) - 2\beta w}. \quad \text{Total sites in system is roughly } R^2/a^2. \quad (14.65)$$

If the core energy w is large enough, $n(r)$ can be made as small as desired for any given r . At low temperatures where large pairs are unlikely, the typical distance between dislocation pairs is therefore much larger than the separation between dislocations in the pair. However, as the temperature rises, the density of pairs rises, and their interaction becomes important.

The essential idea of Kosterlitz, Thouless, and Berezinskii is to treat the interaction of dislocation pairs through a dielectric constant. After all, what one has here is a collection of dipoles of different sizes, which in thermal equilibrium rotate through all angles so there is no spontaneous polarization, but which would orient

and create a polarization P in the presence of any electric field E . This situation is just what the theory of dielectrics was created to handle. In a dielectric medium, the interaction energy of two charges is not $U = 2q^2 \ln(r/a)$, it is $U_{\text{eff}} = 2q^2 \ln(r/a)/\epsilon$, and so interactions between many different dipoles can be accommodated by using U_{eff} instead of U .

However, there is an interesting complication. As the phase transition point is approached, dipoles of larger and larger sizes are created, while simultaneously the number of very small dipoles grows rapidly. The very smallest dipoles do not know they are sitting in a dielectric medium because their charges are much closer together than the distance to any other dipole. The appropriate dielectric constant for them must be 1. Very large dipoles may have large numbers of small dipoles in between them, and therefore they can have a dielectric constant $\epsilon > 1$. So the dielectric constant must be taken to depend upon scale. When the dislocations become numerous, they can be assigned to dipoles by grouping every dislocation with the nearest other dislocation that does not already have a partner, starting with the closest dislocations and moving away in distance. The idea of constructing a *scaling theory* in which the results at one length scale are formulated in terms of the results at a smaller length scale is the basic idea of the *renormalization group*. Similar ideas appear also in the study of metal–insulator transitions (Section 18.5.2), of critical phenomena (Section 24.6), and in the study of the Kondo effect (Section 26.6).

Adopting now completely the language of electrostatics (equivalently, magnetostatics), focus on a dislocation dipole of separation r but arbitrary orientation θ . When placed in an electric field, it will tend to orient itself along the field. The polarizability $\alpha(r)$ of a dipole \vec{p} of size r is given by

$$\vec{p} = \alpha \vec{E} = rq \langle (\cos \theta, \sin \theta) \rangle \quad \text{Taking } \vec{E} \text{ to point along } \theta = 0. \quad (14.66)$$

$$= \int \frac{d\theta}{2\pi} e^{-\beta U(r) - 2\beta w + \beta Eqr \cos \theta} rq \langle (\cos \theta, \sin \theta) \rangle \quad (14.67)$$

$$= \frac{1}{2} \beta q^2 r^2 \vec{E}. \quad \text{Expand the exponential in powers of } E \text{ up to linear order and perform average over } \theta. \quad (14.68)$$

So the contribution to the dielectric susceptibility $d\chi(r)$ from dislocation pairs of size between r and $r + dr$ is, from Eqs. (14.65) and (14.68),

$$d\chi(r) = n(r) dr \alpha(r) = \frac{1}{2} \beta q^2 \left(\frac{r}{a} \right)^2 \frac{2\pi r dr}{a^2} e^{-\beta U/\epsilon(r) - 2\beta w}. \quad (14.69)$$

In order to determine ϵ , make the assumption that all dipoles smaller than r contribute to the dielectric constant screening the interactions at scale r , and all larger ones are irrelevant. This point is the crucial junction where results at one length scale determine an effective theory at larger scales. So, remembering the result from electrostatics that $\epsilon = 1 + 4\pi\chi$, one now has

$$\epsilon(r) = 1 + 4\pi \int_a^r d\chi = 1 + 4\pi \int_a^r dr' n(r') \alpha(r') \quad (14.70)$$

$$\Rightarrow \frac{d\epsilon(r)}{dr} = 4\pi^2 \beta q^2 \frac{r^3}{a^4} e^{-\beta U(r)/\epsilon(r) - 2\beta w} \quad (14.71)$$

$$\Rightarrow \frac{d\epsilon(x)}{dx} = 4\pi^2 \beta q^2 x^{3-2\beta q^2/\epsilon(x)} e^{-2\beta w}. \quad \text{With } x = r/a, \text{ and using Eq. (14.60).} \quad (14.72)$$

Solutions of Eq. (14.72) appear in Figure 14.15. At low temperatures, the dielectric function $\epsilon(x)$ goes to a constant for large x . At a critical temperature, the nature of the solution changes dramatically, and ϵ diverges on large scales. For the electrostatic analog, the transition corresponds to a transition from insulator to metal, because the system becomes infinitely polarizable, while for the original system of dislocations, it corresponds to a melting transition in which the dislocation pairs become unbound. The result is the destruction of quasi-long-range order depicted in Figure 14.12.

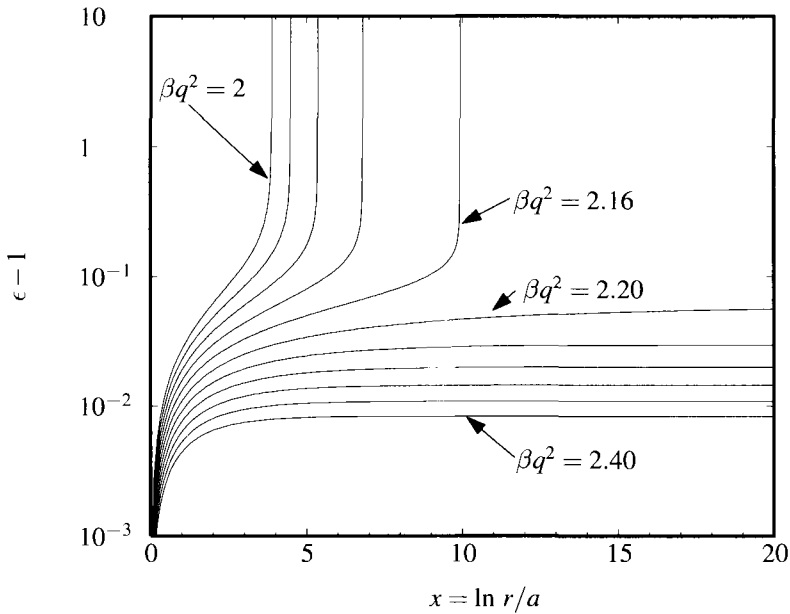


Figure 14.15. Solutions of Eq. (14.70), for $w = 2q^2$ and for βq^2 ranging across the transition point from 2.0 to 2.4. For temperatures below the transition, the dielectric constant flows to a constant value at large distance scales, while above it the dielectric constant diverges, signaling the destruction of quasi-long-range order.

14.4 Cracks

14.4.1 Fracture of a Strip

Ductile materials flow when placed under sufficient stress, but brittle materials break, and the sort of defect that allows them to do so is quite different from the dislocation. Brittle solids fail through propagation of cracks, which are macroscopically long regions of separation, with a microscopically sharp tip. The question

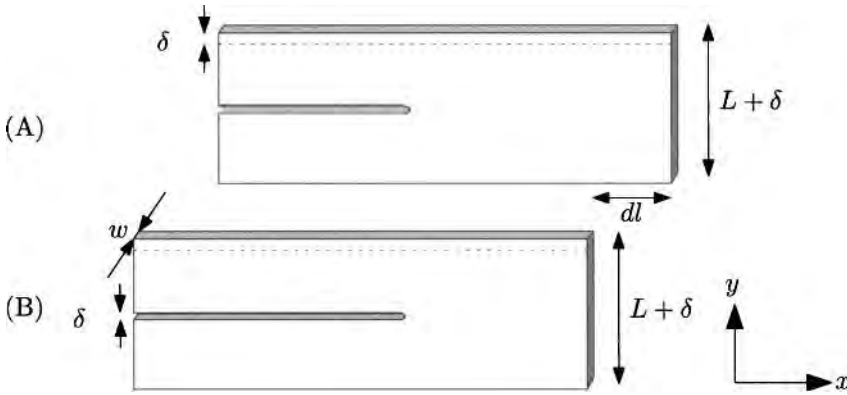


Figure 14.16. The upper surface of a strip of height L and thickness w is rigidly displaced upwards by distance δ . A crack is cut through the center of the strip, and it relieves all stresses in its wake. When the crack moves distance dl from (A) to (B), the net effect is to transfer length dl of strained material into a length dl of unstrained material.

of whether a given solid should be brittle or ductile is not easy to determine theoretically, and it is bound up with the question of whether a sharp crack tip will propagate, or whether it will emit dislocations and become blunt, as reviewed by Carlsson and Thomson (1998). Roughly speaking, when atoms are connected by large numbers of bonds, individual bonds can easily be broken and reformed, dislocations move easily, so fcc and bcc metals such as copper, lead, or iron tend to be ductile. The hexagonal metals, such as beryllium, are more likely to be brittle, and covalent solids such as silicon or carbon tend to be very brittle.

An important feature of cracks is their ability to funnel energy from large expanses of a macroscopic object, and to direct it down to the atomic scale in the service of snapping bonds. The way this process works is quantified by a simple scaling argument.

Consider a long strip with a crack down the middle. The upper and lower boundaries of the strip are rigidly displaced upwards by distance δ , as shown in

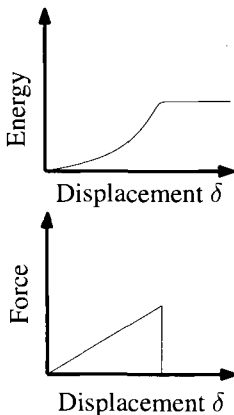


Figure 14.17. For brittle solids under tension, energy and force as a function of displacement take the universal forms shown in these diagrams.

Figure 14.16. Far to the right of the crack, the potential energy U stored per unit length is

$$U = \frac{1}{2} \delta^2 w \frac{Y}{L}, \quad \begin{array}{l} Y \text{ is Young's modulus and } w \text{ is the thickness} \\ \text{of the strip.} \end{array} \quad (14.73)$$

while far to the left there is no stored elastic energy. In Figure 14.16(B) the crack has moved a distance dl . The elastic fields around the crack tip may be complicated, but they are the same in (A) and (B), and the total change dU in the stored elastic energy between the two cases is

$$dU = dl \frac{1}{2} \delta^2 w \frac{Y}{L}. \quad (14.74)$$

The only difference between (A) and (B) is that the crack has moved distance dl . Suppose that it costs fracture energy Γ per unit area to extend the crack, and suppose that all the elastic energy relieved by crack motion goes into creating new crack surface. Then

$$\Gamma w dl = dl \frac{1}{2} \delta^2 w \frac{Y}{L} \quad (14.75)$$

$$\Rightarrow \delta = \sqrt{\frac{2\Gamma L}{Y}} \quad \text{and} \quad \sigma_{yy} = Y \frac{\delta}{L} = \sqrt{\frac{2\Gamma Y}{L}}. \quad (14.76)$$

Therefore the stress needed to make a crack propagate in this geometry is proportional to the square root of Young's modulus and inversely proportional to the height of the strip, meaning that large objects break more easily than small ones.

Consider now a strip without a crack in it at all. Place it under tension. Its energy will rise according to Eq. (14.73) until enough energy is available to allow a crack to run. Once the crack has severed the object, additional tension no longer changes the energy. Note from Eq. (14.76) that the tension at which the crack can initiate becomes smaller and smaller as the height of the system L becomes larger and larger. Therefore, for large enough systems, the energy and force-displacement curves for all solids take a universal form, as shown in Figure 14.17. In principle, these curves represent the thermodynamic minimum energy of solids under tension, with separation occurring when the energy per length equals twice the surface energy γ . In practice, solids only act in this fashion when cracks are initially present and are able to run through them. A brittle solid is by definition one for which the energy-displacement or force-displacement curves resemble Figure 14.17. Equivalently, a brittle solid is one where cracks are able to run consuming a constant amount of energy per unit area.

To understand why cracks are so effective in breaking brittle objects, it is helpful to realize that they concentrate stresses. If one takes a plate, puts an elliptical hole in it, and pulls, then the stresses at the narrow ends of the hole are much larger than those exerted off at infinity, as shown in Figure 14.18.

The ratio of maximum stress at the tip of the hole to the stress applied far away is

$$\frac{\text{Maximum stress}}{\text{applied stress}} \propto \sqrt{\frac{l}{R}}, \quad \begin{array}{l} \text{The coefficient of proportionality is of order} \\ \text{unity.} \end{array} \quad (14.77)$$

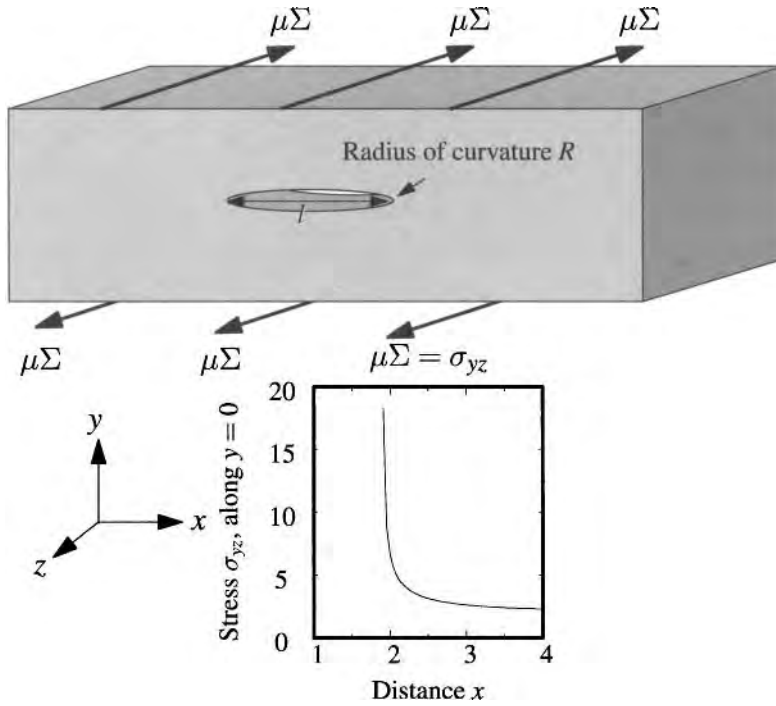


Figure 14.18. The stresses at the tips of an elliptical hole in a solid are much greater than those applied off at infinity. The plot shows a solution of σ_{yz} derived from Eq. (14.99) for $\Sigma = 1$ and $m = 0.9$. Note the 20-fold increase in stress near the crack tip.

where l is the length of the hole and R is the radius of curvature at the tip. Therefore, assuming that typical solids have cracks with tips of radius 10 \AA and of length 10^6 \AA , one can account for the discrepancies in Table 14.2. If thin wires of glass or iron are carefully prepared so as to be absolutely free of surface flaws, then their strength under tension in fact reaches the ideal limits listed in the table.

14.4.2 Stresses Around an Elliptical Hole

It is possible to find the stresses surrounding an elliptical hole sitting within a plate that has been placed under remote tension, as illustrated in Figure 14.18, and to verify Eq. (14.77). To simplify matters as much as possible, assume that the stresses applied to the plate are such as only to create a displacement $u = u_z$ in the z direction, which as in Eq. (14.50) obeys Laplace's equation,

$$\nabla^2 u = 0. \tag{14.78}$$

The theory of complex variables can once again be brought to bear in order to find solutions. For the boundary problem at hand, *conformal mapping* is the appropriate technique. Because u is a solution of Laplace's equation, it can be represented by

$$u = \frac{\phi(\zeta) + \overline{\phi(\zeta)}}{2}, \tag{14.79}$$

where ϕ is analytic, and $\zeta = x + iy$.

The asymptotic behavior of ϕ is easy to determine. Far from the hole, the stress σ_{yz} goes to a constant value $\Sigma\mu$, where Σ is dimensionless. So

$$\sigma_{yz} = \mu \frac{\partial u}{\partial y} = \frac{\mu}{2} [i\phi'(x + iy) - \overline{i\phi'(x + iy)}] \quad (14.80)$$

$$\Rightarrow \phi'(\zeta) \rightarrow -i\Sigma \text{ for } \zeta \rightarrow \infty. \quad (14.81)$$

How does the presence of the hole affect the stress field? Because the edges of the hole are free, all stresses normal to the edge must vanish. Let t be a variable that parametrizes the edge of the hole, so that

$$(x(t), y(t)) \quad (14.82)$$

travels around the boundary of the hole as t moves along the real axis. Then

$$\vec{T} = \left(\frac{\partial x}{\partial t}, \frac{\partial y}{\partial t} \right) \quad \text{and} \quad \vec{N} = \left(-\frac{\partial y}{\partial t}, \frac{\partial x}{\partial t} \right) \quad \begin{array}{l} \text{It is easy to verify that } \vec{N} \cdot \vec{T} = 0, \text{ and because} \\ \vec{T} \text{ is tangent } \vec{N} \text{ must be normal.} \end{array} \quad (14.83)$$

are tangent vector and normal vectors along the edge of the hole, so requiring normal stress to vanish means that

$$(\sigma_{xz}, \sigma_{yz}) \cdot \vec{N} = 0 \quad (14.84)$$

$$\Rightarrow \mu \left(\frac{\partial u}{\partial x}, \frac{\partial u}{\partial y} \right) \cdot \left(-\frac{\partial y}{\partial t}, \frac{\partial x}{\partial t} \right) = 0 \Rightarrow \frac{\partial u}{\partial y} \frac{\partial x}{\partial t} - \frac{\partial u}{\partial x} \frac{\partial y}{\partial t} = 0 \quad (14.85)$$

$$\Rightarrow \left(-\frac{\partial \phi}{\partial ix} + \frac{\partial \bar{\phi}}{\partial ix} \right) \frac{\partial x}{\partial t} = \left(\frac{\partial \phi}{\partial iy} - \frac{\partial \bar{\phi}}{\partial iy} \right) \frac{\partial y}{\partial t} \quad \text{Insert (14.79) for } u. \quad (14.86)$$

$$\Rightarrow \frac{\partial \phi}{\partial t} = \frac{\partial \bar{\phi}}{\partial t} \quad \text{This equality holds only on the boundary.} \quad (14.87)$$

$$\Rightarrow \phi(\zeta) = \overline{\phi(\zeta)} \quad \text{Because } \phi \text{ is arbitrary up to a constant any-} \\ \text{way, there is no worry about dropping a con-} \\ \text{stant of integration.} \quad (14.88)$$

when ζ lies on the boundary.

Equation (14.88) appears innocent, but is in fact a powerful relation that can lead to rapid solution of complicated boundary-value problems. Suppose, to be definite, that the hole is elliptical and thus can be described by

$$\zeta = \omega + \frac{p}{\omega}, \quad p \text{ is a number lying between 0 and 1.} \quad (14.89)$$

with ω lying on the unit circle,

$$\omega = e^{i\theta}, \quad (14.90)$$

and θ real. When $p = 0$, the boundary is circular, and when $p = 1$, the boundary is a cut along the real axis. Considering ϕ as a function of ω , one has

$$\phi(\omega) = \overline{\phi(\omega)} = \bar{\phi}\left(\frac{1}{\omega}\right), \quad \begin{array}{l} \text{The notation } \bar{\phi}(\omega) \text{ means that if } \phi(\omega) \text{ is ex-} \\ \text{panded as a power series in } \omega, \text{ one should} \\ \text{take the complex conjugate of all the coef-} \\ \text{ficients in the expansion.} \end{array} \quad (14.91)$$

because $\bar{\omega} = 1/\omega$ on the unit circle. Equation (14.91) is a relation between two analytic functions that holds over the whole unit circle. The difference between $\phi(\omega)$ and $\bar{\phi}(1/\omega)$ is an analytic function; the Taylor series of the difference vanishes on the unit circle, and by analytic continuation the difference vanishes everywhere, so the two functions must be equal everywhere in the complex plane.

Now $\phi(\omega)$ can be determined completely by analyzing its asymptotic behavior. Outside of the hole ϕ must be completely regular, except for the fact that it diverges as $-i\Sigma\zeta$ for large ζ . The relation between ω and ζ is

$$\omega = \frac{\zeta + \sqrt{\zeta^2 - 4p}}{2}. \quad \text{If the other sign of the square root were chosen here, the argument below would have to be modified in several places, but the final answer would be the same.} \quad (14.92)$$

Therefore, when ζ is large, large, $\omega = \zeta$, and in accord with Eq. (14.81) one obtains

$$\phi(\omega) \rightarrow -i\Sigma\omega \quad \text{for } \omega \rightarrow \infty. \quad (14.93)$$

Consulting Eq. (14.91) one concludes also that

$$\bar{\phi}(1/\omega) \rightarrow -i\Sigma\omega \quad \text{for } \omega \rightarrow \infty, \quad (14.94)$$

which means that

$$\bar{\phi}(\omega) \rightarrow \frac{-i\Sigma}{\omega} \quad \text{for } \omega \rightarrow 0 \quad (14.95)$$

$$\phi(\omega) \rightarrow \frac{i\Sigma}{\omega} \quad \text{for } \omega \rightarrow 0. \quad (14.96)$$

However, $\bar{\phi}(\omega)$ can have no other singularities within the unit circle, or else $\phi(\omega)$ would have corresponding singularities outside the unit circle, which is forbidden if u is to be smooth away from the hole.

Having determined all the possible singularities of ϕ within and without the unit circle, it is determined up to a constant. It must be given by

$$\phi(\omega) = -i\Sigma\omega + i\frac{\Sigma}{\omega} \quad \text{Add Eqs. (14.96) and (14.93).} \quad (14.97)$$

$$\Rightarrow \phi(\zeta) = -i\Sigma\frac{\zeta}{2}\left(1 + \sqrt{1 - 4p/\zeta^2}\right) + i\Sigma\frac{\zeta}{2p}\left(1 - \sqrt{1 - 4p/\zeta^2}\right). \quad (14.98)$$

Use Eq. (14.92) and $1/\omega = \zeta(1 - \sqrt{1 - 4p/\zeta^2})/2p$.

Displacements and stresses can now be determined from Eqs. (14.79) and (14.80). Figure 14.18 shows a plot of σ_{yz} along the line $y = 0$ for a narrow ellipse with $p = 0.9$. Problem 4 uses Eq. (14.98) to verify Eq. (14.77).

14.4.3 Stress Intensity Factor

The limit $p \rightarrow 1$ is particularly interesting. The elliptical hole closes down and becomes a thin crack reaching from $x = -2$ to $x = 2$. The function ϕ acquires a

branch cut over exactly the same region. The displacement u is finite everywhere, but the stress σ_{yz} becomes singular, diverging on the x axis as

$$\sigma_{yz} = \mu \frac{\partial u}{\partial y} = \frac{\mu \Sigma x}{\sqrt{x-2}\sqrt{x+2}} \rightarrow \frac{\mu \Sigma}{\sqrt{x-2}} \quad \text{as } x \rightarrow 2. \quad (14.99)$$

The *stress intensity factor* K is a coefficient of the diverging stress, defined by

$$K = \lim_{r \rightarrow 0} \sqrt{2\pi r} \sigma_{yz}, \quad r = x - 2 \text{ is the distance from the crack tip.} \quad (14.100)$$

In the case of Eq. (14.99), $K = \sqrt{2\pi} \mu \Sigma$.

The stress intensity factor serves for fracture the same purpose as the Peach–Kohler force served for dislocations. A crack is presumed to become mobile when the stress intensity factor reaches a particular critical value that can be tabulated for each material. This criterion is equivalent to assuming, as in the argument accompanying Figure 14.16, that the crack moves when the energy transmitted to its tip reaches a critical value. The relationship between energy flux to crack tips and stress intensity factor is determined in Problem 3.

14.4.4 Atomic Aspects of Fracture

Problem 5 shows that a microscopic theory of crack motion has some features that are difficult to understand from continuum analysis. Cracks can be trapped by a lattice even when continuum calculations predict they should have enough energy to move, as discussed by Thomson (1986).

When a crack begins running in a brittle material, it excites phonons that radiate off behind it, shown in Figure 14.20. The amplitude of these phonons is difficult to calculate, but their frequencies are easily determined by the following argument:

Suppose any object moves at velocity \vec{v} in a medium that supports phonons of frequency $\omega(\vec{k})$. Far from the moving object, radiation must take the form of traveling waves. Take the motion of the object to be along a line of atoms, so that at time intervals a/v the object moves from \vec{r} to $\vec{r} + \vec{R}$, where \vec{R} is a lattice vector of magnitude a . Because the motion of the object is steady, the radiation it emits must be invariant under the replacements

$$\vec{r} \rightarrow \vec{r} + \vec{R} \quad (14.101a)$$

$$t \rightarrow t + a/v. \quad (14.101b)$$

At the same time, because the radiation far away is of the form $\exp[i\vec{k} \cdot \vec{r} - i\omega t]$, the symmetries in Eq. (14.101) require

$$e^{i\vec{k} \cdot (\vec{r} + \vec{R}) - i\omega(t + a/v)} = e^{i\vec{k} \cdot \vec{r} - i\omega t} \quad (14.102)$$

$$\Rightarrow e^{i\vec{k} \cdot \vec{R} - i\omega a/v} = 1 \quad (14.103)$$

$$\Rightarrow (\vec{k} + \vec{K}) \cdot \vec{v} = \omega(\vec{k}) \quad \text{Because } \vec{R}/a = \vec{v}, \text{ with } \vec{K} \text{ a reciprocal lattice vector.} \quad (14.104)$$

$$\Rightarrow \vec{k} \cdot \vec{v} = \omega(\vec{k}). \quad \text{Working now in the extended zone scheme, so } \vec{k} \text{ is not restricted to the first Brillouin zone.} \quad (14.105)$$

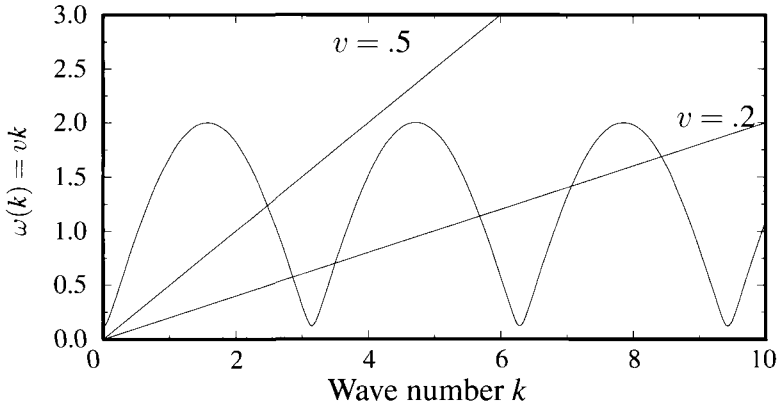


Figure 14.19. Graphical solution of Eq. (14.105), showing the resonances excited by a steadily moving object as it travels through a lattice.

The radiation frequencies emitted by a moving crack are therefore determined by drawing the phonon dispersion relation along the direction of crack motion and then finding where the straight line $\vec{k} \cdot \vec{v}$ crosses the dispersion relation. This graphical construction is illustrated in Figure 14.19.

The condition (14.105) for radiation emitted by moving objects, often ascribed to Cherenkov and Landau, applies to many different situations, including damping in liquid helium (Section 15.5.4) and plasmas (Problem 4 in Chapter 23), and to electrons participating in the anomalous skin effect (Section 23.2.1).

Problems

1. **Tensile stress:** Carry out the computations needed to reproduce Figure 14.2, and estimate the maximum tensile stress of silicon.

2. **Interacting dislocations:**

(a) Show that for the displacement field in Eq. (14.55) it is legitimate to write

$$U = -\frac{a\mu}{2} \int d^2r u \nabla^2 u. \quad (14.106)$$

Why would this equation be incorrect for the displacement field (14.51)?

(b) Show that $\nabla^2 u$ is proportional to a delta function when applied to Eq. (14.51), and find the coefficient of proportionality.

(c) As a consequence, obtain Eq. (14.56). The factor $2w$ is added in by hand, as in Eq. (14.54), and cannot be derived.

3. **Relation between stress singularity and energy flux:** This problem demonstrates that once the strength of the stress singularity around a crack tip is known, the energy flowing to the crack can be determined as well, and the two are simply related.

- (a) Consider a two-dimensional elastic medium subjected to out-of-plane distortions u_z , so that its total energy is

$$\mathcal{E} = \frac{\mu}{2} \int dx dy \left[\frac{1}{c^2} (\dot{u}_z)^2 + (\nabla u_z)^2 \right]. \quad (14.107)$$

By considering $d\mathcal{E}/dt$, show that

$$\vec{J} = \mu \dot{u}_z \vec{\nabla} u_z \quad (14.108)$$

gives the flux of energy at every point in the elastic medium.

- (b) By working with Eqs. (14.98) and (14.100) in the limit $p \rightarrow 1$, show that near a crack tip

$$u = u_z = -i \frac{K}{\mu \sqrt{2\pi}} (\sqrt{\zeta} - \sqrt{-\zeta}). \quad \zeta = x + iy. \quad (14.109)$$

- (c) Consider a crack moving very slowly at velocity $v \ll c$ in the x direction. Thus $\dot{u} = -v \partial u / \partial x$. Suppose that the crack is straight and lies along the negative x axis; also suppose that its tip has just reached the origin. Using Eq. (14.109) in (14.108), find the integrated flux of energy into the crack tip. The most convenient contour for the calculation is one running from $x = -\infty$ to $x = \infty$ while $y = \alpha$, and then from $x = \infty$ back to $x = -\infty$ for $y = -\alpha$; the calculation is carried out in the limit where α is very small. Because the contour is horizontal, only the y component of the energy flux is needed.

4. Stresses at end of an elliptical hole:

- (a) The curvature $\kappa = 1/R$ of a general plane curve is defined by

$$\kappa = \frac{\partial \theta}{\partial s}, \quad (14.110)$$

where θ is the angle of a tangent vector, and s is arc length along the curve. Show that for a general parametrization of the curve one obtains

$$\kappa = \frac{1}{R} = \frac{\frac{\partial x}{\partial t} \frac{\partial^2 y}{\partial t^2} - \frac{\partial y}{\partial t} \frac{\partial^2 x}{\partial t^2}}{\left[\left(\frac{\partial x}{\partial t} \right)^2 + \left(\frac{\partial y}{\partial t} \right)^2 \right]^{3/2}}. \quad (14.111)$$

- (b) Show that the radius of curvature R at the tip of an ellipse described by Eq. (14.89) is

$$R = (p - 1)^2 / (p + 1). \quad (14.112)$$

- (c) Show that the maximum stress at the tip of the ellipse is $2\Sigma\mu/(1 - p)$.
 (d) Verify Eq. (14.77) for ellipses with small radii of curvature R .

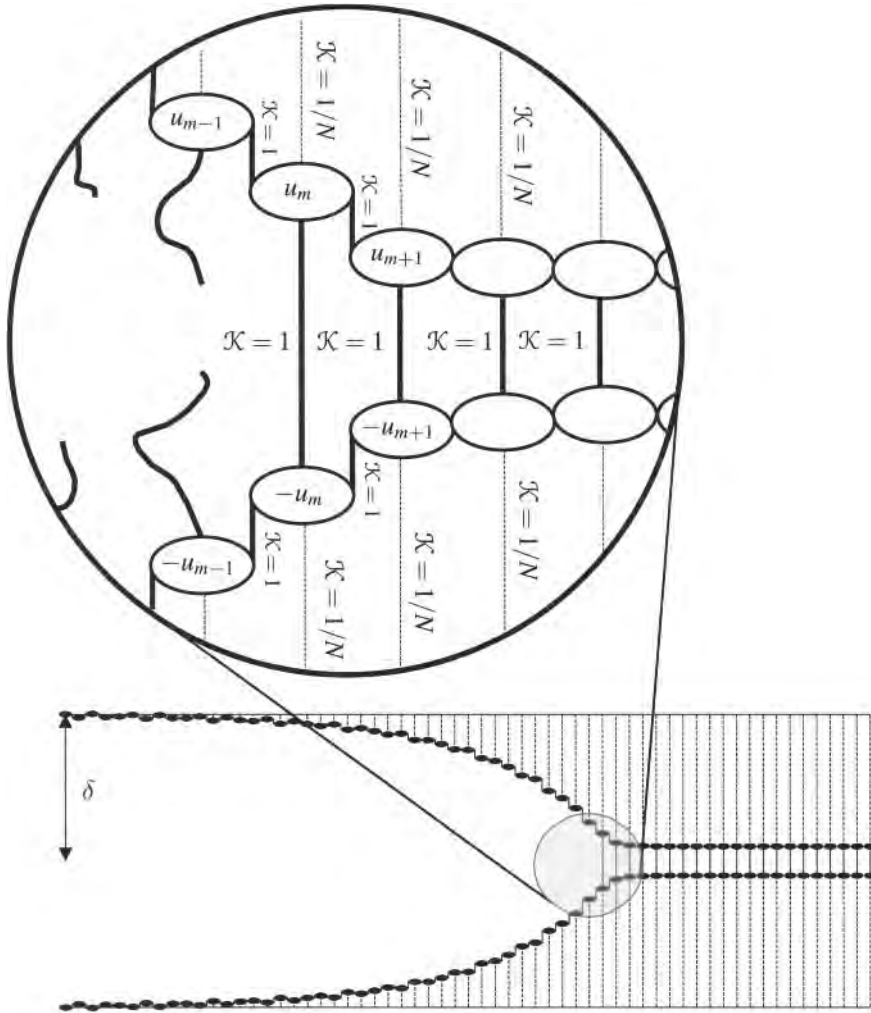


Figure 14.20. This one-dimensional model mimics the motion of a crack in a strip, incorporating effects of discreteness. One can view it as a model for the atoms lying just along the surface of a crack. The mass points are only allowed to move vertically, and they are tied to their neighbors with springs that break when they exceed a certain extension. The lower portion of the figure shows a dynamical solution of the model, where the crack is emitting phonons.

5. **Lattice trapping of cracks:** This problem concerns a one-dimensional model of crack propagation, analogous to the Frenkel–Kontorova model of Section 14.2.3. Consider the model shown in Figure 14.20. One can view it as a model for the atoms lying just along a crack surface. They are tied to nearest neighbors by elastic springs, with spring constant $\mathcal{K} = 1$, and tied to a line of atoms on the other side of the crack line by similar springs, which snap when extended past some breaking point. The lines of atoms are being pulled apart by weak springs of spring constant $\mathcal{K} = 1/N$. These weak springs are

meant schematically to represent N vertical rows of atoms pulling in series. The equation that describes the upper row of mass points is

$$\ddot{u}_m = \begin{cases} u_{m+1} - 2u_m + u_{m-1} & \text{Elastic coupling to neighbors} \\ + \frac{1}{N}(\delta - u_m) & \text{Driven by displacing edges of strip} \\ + (u_{m,-} - u_{m,+})\theta(2 - 2u_m). & \text{Bonds that snap} \end{cases} \quad (14.113)$$

- (a) Consider equilibrium solutions, so that $\ddot{u}_m = 0$. What is the potential energy per bond far to the right of the crack, as a function of the imposed opening extension δ ?
- (b) What is the potential energy per bond far to the left of the crack, including the energy needed to snap the bonds?
- (c) Following the logic of Section 14.4.1, show that the crack should be able to move when $\delta = \sqrt{2N+1}$.
- (d) Following the steps that solve the Frenkel–Kontorova model, find an explicit expression for u_m as a function of δ .
- (e) Show that the bond at 0 reaches height 1 and snaps when

$$\delta = \sqrt{2N+1} \frac{\sqrt{3}+1}{\sqrt{2}}. \quad (14.114)$$

6. **Conformal mapping:** Repeat the calculations leading to Eq. (14.98) but for an elliptical hole of arbitrary length l .
7. **Positional fluctuations in three dimensions:** Return to Eq. (14.26), but consider a three-dimensional crystal rather than a two-dimensional one. Show that the mean square displacement of atoms vanishes at sufficiently low temperature.

References

- H. Alexander and P. Haasen (1968), Dislocations and plastic flow in the diamond structure, *Solid State Physics: Advances in Research and Applications*, **22**, 27–158.
- S. Amelinckx (1964), *The Direct Observation of Dislocations*, Academic Press.
- B. L. Averbach (1968), Some physical aspects of fracture, in *Fracture, an Advanced Treatise*, H. Liebowitz, ed., vol. I, pp. 441–471, Academic Press, New York.
- T. Baumeister, ed. (1978), *Mark's Standard Handbook for Mechanical Engineers*, eighth ed., McGraw-Hill, New York.
- V. L. Berezinskii (1972), Destruction of long-range order in one-dimensional and two-dimensional systems possessing a continuous symmetry group: II Quantum systems, *Soviet Physics JETP*, **34**, 610–616.
- A. E. Carlsson and R. Thomson (1998), Fracture toughness of materials: From atomistics to continuum theory, *Solid State Physics: Advances in Research and Applications*, **51**, 33–280.

- A. B. Cullis, N. G. Chew, and J. L. Hutchison (1985), Formation and elimination of surface ion milling defects in cadmium telluride, zinc sulphide, and zinc selenide, *Ultramicroscopy*, **17**, 203–212.
- A. G. Evans and F. W. Zok (1994), The physics and mechanics of brittle matrix composites, *Solid State Physics: Advances in Research and Applications*, **47**, 177–286.
- C. Frank (1985), Some personal reminiscences of the early days of crystal dislocations, in *Dislocations and Properties of Real Materials*, Institute of Metals, Bristol.
- J. Frenkel and T. Kontorova (1938), On the theory of plastic deformation and twinning, *Physikalische Zeitschrift der Sowjetunion*, **13**, 1–10.
- J. Friedel (1964), *Dislocations*, Addison Wesley, Reading, MA.
- J. E. Gordon (1976), *The New Science of Strong Materials or Why You Don't Fall through the Floor*, 2nd ed., Princeton University Press, Princeton, New Jersey.
- I. S. Grigoriev and E. Z. Meilkhov, eds. (1997), *Handbook of Physical Quantities*, CRC Press, Boca Raton, FL.
- J. P. Hirth and J. Lothe (1982), *Theory of Dislocations*, 2nd ed., John Wiley and Sons, New York.
- J. M. Kosterlitz and D. J. Thouless (1973), Ordering, metastability and phase transitions in two-dimensional systems, *Journal of Physics C*, **6**, 1181–1203.
- L. D. Landau (1937), On the theory of phase transitions, *Physikalische Zeitschrift der Sowjetunion*, **11**, 26 and 545. In German. Translated in Landau (1965), p. 193–216
- L. D. Landau (1965), *Collected Papers of L D Landau*, D. ter Haar, ed., Gordon and Breach, New York.
- R. M. Lynden-Bell and K. H. Michel (1994), Translation-rotation coupling, phase transitions and elastic phenomena in orientationally disordered crystals, *Reviews of Modern Physics*, **66**, 721–762.
- M. Marder and J. Fineberg (1996), How things break, *Physics Today*, **49**(9), 24–29.
- N. D. Mermin (1968), Crystalline order in two dimensions, *Physical Review*, **176**, 250–254.
- N. D. Mermin (1979), The topological theory of defects in ordered media, *Reviews of Modern Physics*, **51**, 591–648.
- N. D. Mermin and H. Wagner (1966), Absence of ferromagnetism or antiferromagnetism in one- or two-dimensional isotropic Heisenberg models, *Physical Review Letters*, **17**, 1133–1136.
- P. Minnhagen (1987), The two-dimensional Coulomb gas, vortex unbinding and superfluid-superconducting films, *Reviews of Modern Physics*, **59**, 1001–1066.
- C. A. Murray and D. G. Grier (1996), Video microscopy of monodisperse colloidal systems, *Annual Reviews of Physical Chemistry*, **47**, 421–452.
- D. R. Nelson and B. I. Halperin (1979), Dislocation-mediated melting in two dimensions, *Physical Review B*, **19**, 2457–2484.
- E. Orowan (1934), On crystal plasticity, *Zeitschrift für Physik*, **89**, 605–659. in German.
- M. Peach and J. S. Kohler (1950), The forces exerted on dislocations and the stress fields produced by them, *Physical Review*, **80**, 436–439.
- R. E. Peierls (1934), Remarks on transformation temperatures, *Helvetica Physica Acta*, **7**, Supplement II, 81–83. In German.
- R. Pindak, D. E. Moncton, S. C. Davey, and J. W. Goodby (1981), X-ray observation of a stacked hexatic liquid-crystal B phase, *Physical Review Letters*, **46**, 1135–1138.
- M. Polanyi (1934), On a type of dislocation that makes metals plastic, *Zeitschrift für Physik*, **89**, 660–666. In German.
- A. K. Sood (1991), Structural ordering in colloidal suspensions, *Solid State Physics: Advances in Research and Applications*, **45**, 1–73.
- K. Strandburg (1992), *Bond-Orientational Order in Condensed Matter Systems*, Springer-Verlag, New York.

- G. I. Taylor (1934), The mechanism of plastic deformation of crystals., *Proceedings of the Royal Society of London*, **A145**, 362–404. Parts I and II
- R. Thomson (1986), The physics of fracture, *Solid State Physics: Advances in Research and Applications*, **39**, 1–129.
- E. Wigner (1936), On the structure of solid bodies, *Scientific Monthly*, **42**, 40–46.
- A. P. Young (1979), Melting and the vector coulomb gas in two dimensions, *Physical Review B*, **19**, 1855–1866.

15. Fluid Mechanics

15.1 Introduction

Raise the temperature of almost any solid sufficiently, and it melts, passing into a liquid state. The transition is dramatic because of the change in mechanical properties. From a structural point of view, the change in the solid at the the transition point is the loss of long-range order, but there is normally no need to set up a neutron scattering experiment in order to detect melting. Liquids flow and solids do not.

15.2 Newtonian Fluids

15.2.1 Euler's Equation

In a hydrodynamic description of a fluid, one specifies a velocity vector at every point in space. To obtain an equation of motion, it is easiest to begin by adopting a reference frame moving with a small volume dV of fluid. If $\vec{f}dV$ is the net force acting upon this section of fluid, and ρ its mass density, then the acceleration of the small volume will be given by \vec{f}/ρ . Now move back to the stationary reference frame. If the velocity of the fluid is described by $\vec{v}(\vec{r}, t)$ at time t , then a short time dt later it will be described by

$$\vec{v}(\vec{r} + \vec{v}dt, t + dt) = \vec{v}(\vec{r}, t) + \vec{f}(\vec{r}, t)dt/\rho \quad \begin{array}{l} \text{The fluid now at } \vec{r} + \vec{v}dt \text{ was at } \vec{r} \\ \text{a time } dt \text{ ago.} \end{array} \quad (15.1)$$

$$\Rightarrow \frac{\partial \vec{v}}{\partial t} + (\vec{v} \cdot \vec{\nabla})\vec{v} = \frac{\vec{f}}{\rho}. \quad \text{Expand to first order in } dt. \quad (15.2)$$

The pressure in a fluid is defined as the force per unit area across any face one imagines inscribing within it. Therefore, the force \vec{f} acting on a small volume of fluid may be identified with $-\vec{\nabla}P$, the gradient of the pressure, and Eq. (15.2) can be rewritten as *Euler's equation*

$$\frac{\partial \vec{v}}{\partial t} + (\vec{v} \cdot \vec{\nabla})\vec{v} + \frac{\vec{\nabla}P}{\rho} = 0. \quad (15.3)$$

The density ρ of a fluid does not have to be constant, but it must obey the equation of continuity

$$\frac{\partial \rho}{\partial t} = -\vec{\nabla} \cdot \rho \vec{v}. \quad \begin{array}{l} \text{This general statement of conservation of mass} \\ \text{first appeared as Eq. (5.25).} \end{array} \quad (15.4)$$

Equation (15.3) can be rewritten in the form of a continuity equation for the conservation of momentum, so that the time rate of change of momentum equals the divergence of a momentum flux. The manipulations are simplest if one moves to a component notation, rewriting Eq. (15.3) as

$$0 = \frac{\partial \rho v_\alpha}{\partial t} - v_\alpha \frac{\partial \rho}{\partial t} + \rho \sum_\beta v_\beta \frac{\partial}{\partial r_\beta} v_\alpha + \frac{\partial}{\partial r_\alpha} P \quad (15.5)$$

$$= \frac{\partial \rho v_\alpha}{\partial t} + v_\alpha \sum_\beta \frac{\partial}{\partial r_\beta} \rho v_\beta + \rho \sum_\beta v_\beta \frac{\partial}{\partial r_\beta} v_\alpha + \frac{\partial}{\partial r_\alpha} P \quad \text{Use Eq. (15.4).} \quad (15.6)$$

$$= \frac{\partial \rho v_\alpha}{\partial t} + \sum_\beta \frac{\partial}{\partial r_\beta} \{ \rho v_\alpha v_\beta + \delta_{\alpha\beta} P \}. \quad (15.7)$$

Momentum in a small region changes because of two additive contributions: One is from forces applied to the region, and the other is from fluxes of neighboring fluid into the region. The fluid stress tensor σ is defined by

$$\sigma_{\alpha\beta} = -\rho v_\alpha v_\beta - \delta_{\alpha\beta} P, \quad (15.8)$$

leading Euler's equation to take the form

$$\frac{\partial \rho v_\alpha}{\partial t} = \sum_\beta \frac{\partial}{\partial r_\beta} \sigma_{\alpha\beta}. \quad \text{Compare with Eq. (12.35).} \quad (15.9)$$

Incompressible Fluids. In many liquids, such as water, the change of pressure needed to produce any appreciable change in density is larger than readily occurs even in turbulent flows. In this case, the fluid is best approximated as *incompressible*, the equation of continuity Eq. (15.4) becomes

$$\vec{\nabla} \cdot \vec{v} = 0, \quad (15.10)$$

and the pressure P must be determined by the condition that the velocity \vec{v} continually obey Eq. (15.10) while evolving according to Eq. (15.7).

The stress tensor in Eq. (15.8) has two physical interpretations. On the one hand, Eq. (15.9) is in the form of a continuity equation, although missing a minus sign that might be expected on the right-hand side, so $\sigma_{\alpha\beta}$ gives the flux of momentum p_α in the direction $-r_\beta$. Sometimes the tensor $\Pi_{\alpha\beta} = -\sigma_{\alpha\beta}$ is defined so as to alter this minus sign convention. The motivation for the sign convention of Eq. (15.9) is to make it identical to the equation of linear elasticity in Eq. (12.35), and corresponding to the sketch in Figure 12.3. Thus $\sigma_{\alpha\beta}$ can also be interpreted as the force along α per area exerted by material outside upon a fluid region of interest.

Apart from the superfluids described in Section 15.5, no real liquid comes terribly close to obeying Euler's equation Eq. (15.7). A fluid obeying Euler's equation conserves energy in the flow, and a swirl of liquid once started never decays. Real fluids have dissipation and behave quite differently. The mathematical properties of

Euler's equation are uncertain. Despite tremendous effort, it is not known whether nonsingular initial conditions remain nonsingular for all times, or whether flow can concentrate into vortices whose rotation rate becomes infinite at some time, after which the equations break down.

15.2.2 Navier–Stokes Equation

The correction of Euler's equation to allow for dissipation can take place in two ways. It can be done by considering the statistical mechanics of fluids and gases, or through phenomenological arguments. In either event, the process is greatly aided by having some idea of the form the theory should take.

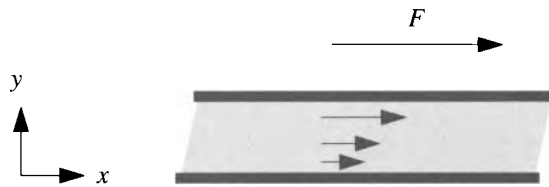


Figure 15.1. When liquid is sheared between two plates, the force is proportional to the shearing speed and is inversely proportional to the separation d .

Newton observed that when water is sheared between two plates (Figure 15.1), if the rate of shearing is not too fast, the force of one plate upon the other is proportional to the shear velocity and is inversely proportional to the distance between the plates. Fluids behaving in this way are *Newtonian*. The force per area applied to the top plate is

$$\frac{F}{A} = \eta \frac{\partial v_x}{\partial y}, \tag{15.11}$$

where η is the *dynamic viscosity* (see Table 15.1). The stress tensor σ of Eq. (15.8) simply does not predict a force of this type. Recall from Eq. (12.37) that the stress tensor component σ_{xy} gives the force in the x direction acting on a surface in the fluid perpendicular to \hat{y} . According to (15.8), this force vanishes, because $v_y = 0$, while Eq. (15.11) says the force is not zero. Therefore the expression for the fluid stress tensor must be modified.

Assume from Eq. (15.11) that the modification of the stress tensor involves first derivatives of the velocity field \vec{v} . Because the fluid is isotropic, the possible ways that these derivatives can enter are limited, and they were given in Eq. (12.38). Additions σ' to the stress tensor can be of the form

$$\sigma'_{\alpha\beta} = \eta \left[\frac{\partial v_\alpha}{\partial r_\beta} + \frac{\partial v_\beta}{\partial r_\alpha} \right] + \left[\zeta - \frac{2}{3}\eta \right] \delta_{\alpha\beta} \sum_\gamma \frac{\partial v_\gamma}{\partial r_\gamma}; \quad \eta \text{ and } \zeta \text{ are two arbitrary positive constants.} \tag{15.12}$$

but for an incompressible fluid obeying (15.10), only the first term of Eq. (15.12) survives, producing

$$\sigma_{\alpha\beta} = -\rho v_\alpha v_\beta - \delta_{\alpha\beta} P + \eta \left[\frac{\partial v_\alpha}{\partial r_\beta} + \frac{\partial v_\beta}{\partial r_\alpha} \right]. \tag{15.13}$$

Table 15.1. Viscosities of various liquids and gases at 300 K

Gas	η (g/[cm·sec])	Liquid	η (g/[cm·sec])
He	$1.99 \cdot 10^{-4}$	NH ₃	$14 \cdot 10^{-4}$
Ne	$3.17 \cdot 10^{-4}$	H ₂ O	$82 \cdot 10^{-4}$
Ar	$2.27 \cdot 10^{-4}$	CO ₂	$6.0 \cdot 10^{-4}$
Kr	$2.55 \cdot 10^{-4}$	Hg	$160 \cdot 10^{-4}$
Xe	$2.33 \cdot 10^{-4}$	Glycerine	$85\,000 \cdot 10^{-4}$
H ₂	$0.89 \cdot 10^{-4}$		
N ₂	$1.79 \cdot 10^{-4}$		
O ₂	$2.07 \cdot 10^{-4}$		
F ₂	$2.36 \cdot 10^{-4}$		
Cl ₂	$1.37 \cdot 10^{-4}$		
CO	$1.78 \cdot 10^{-4}$		
CO ₂	$1.50 \cdot 10^{-4}$		
Air	$1.85 \cdot 10^{-4}$		

Source: Grigoriev and Meilkhov (1997).

Using Eq. (15.13) in (15.9) gives the *Navier–Stokes equation*

$$\rho \frac{\partial \vec{v}}{\partial t} + \rho(\vec{v} \cdot \vec{\nabla})\vec{v} = -\vec{\nabla}P + \eta \nabla^2 \vec{v}. \quad \text{The fluid is assumed incompressible, so } \rho \text{ is constant.} \quad (15.14)$$

Solutions. Solutions of the Navier–Stokes equation constitute a vast subject. One representative and physically important calculation finds the pattern of flow about a slowly moving sphere, and it is treated in Problem 2. Fluid flows range from cases that can be solved in their entirety, through situations profitably studied as stability problems, as in Drazin and Reid (1981), up to turbulent flows best analyzed in statistical fashion, as in Monin and Yaglom (1971–1975). Despite the enormous effort devoted to them, many simple questions in fluid flow are still not solved. It is not known whether the Navier–Stokes equation contains vortex solutions where the speed of fluid flow becomes unbounded in finite time, and the pressure needed to push turbulent fluid through a pipe still cannot be computed from the starting equation.

15.3 Polymeric Solutions

The behavior of simple molecular fluids can be changed in radical ways by the addition of even small quantities of polymers. Any flow pattern will drag the polymers with it, as sketched in Figure 15.2, and stretch them out, while simultaneously they are buffeted by thermal kicks. Because it takes some time, even on the order of seconds, for the polymers to adjust to local flow conditions, the fluid displays complicated time-dependent behavior. Furthermore, the polymers are elastic, and

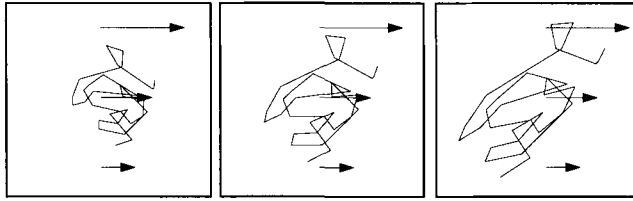


Figure 15.2. A polymer in a shear flow slowly stretches out in response to the fluid motion, exerting forces back on the fluid, but without losing the random twists and turns created by thermal fluctuations.

are constantly tempted to spring back toward unstretched configurations. Accordingly, the fluid responds to rapid changes in stress more like a solid than a liquid. It is easy to construct a fluid with these properties: Put corn starch in a bowl and mix water into it until it just becomes possible to stir slowly with a spoon. A sharp blow shatters the mixture as if it were solid, but if one picks up a lump it soon oozes through the fingers. In its response to time-dependent forces, such a liquid is called *viscoelastic*. It is also called *non-Newtonian*, because the equation for momentum flux is no longer given by the form (15.13).

Dilute polymeric solutions are of particular interest because the theory relating mechanical properties of the polymer chains to the ultimate properties of the flow is quite far advanced. Much more progress has been made along these lines than, for example, in relating the plastic flow of metals to the dynamics of dislocations. The theory in its full glory can be found in Doi and Edwards (1986), Grosberg and Khokhlov (1994), Bird et al. (1987), or de Gennes (1979). The following discussion will simply attempt to give some of the flavor of what can be accomplished.

The theory has two parts. The first part finds the change in the stress tensor $\sigma_{\alpha\beta}$ that should be expected when polymers are present in the flow, if the statistical probability of various polymer configurations is known. The second part obtains an equation of motion for the polymers that depends upon the surrounding fluid flow and upon thermal fluctuations. The probability of polymer configurations can therefore be evaluated, and the theory can be closed.

Stresses Exerted by Polymers. The stress tensor gives the force per unit area across the faces of a small volume in the fluid. In a dilute polymeric solution, the force has two contributions, the first from the fluid acting upon itself, producing the stress tensor of Eq. (15.13). However, if two adjacent beads of the polymer reach across the surface of the small volume, then the force of one bead upon the other also contributes.

Denote the probability that bead l be at \vec{R}^l and that bead $l + 1$ simultaneously be at \vec{R}^{l+1} by

$$g(\vec{R}^l, \vec{R}^{l+1}) = \frac{1}{V^2} g(\vec{R}^{l+1} - \vec{R}^l). \quad (15.15)$$

In a homogeneous system, the probability of finding two beads somewhere depends only upon their relative locations.

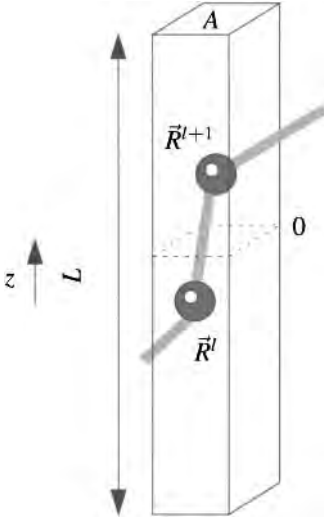


Figure 15.3. When one bead is above the dividing plane at 0 and an adjacent one is below, it exerts a force upon the region below the plane and therefore contributes to the stress tensor.

Let $\vec{F}^{l+1,l}$ be the force that the bead at \vec{R}^{l+1} exerts upon the bead at \vec{R}^l ; more generally, $\vec{F}^{l,l}$ is the force exerted by the bead at \vec{R}^l upon the bead at l . Figure 15.3 depicts a situation in which bead $l + 1$ applies a force upon bead l across the upper x - y plane bounding a small volume, and therefore contributes to the $\sigma_{z\beta}$ component of the stress tensor. This contribution is

$$\sigma_{z\beta} = \frac{1}{A} \int d\vec{R}^l d\vec{R}^{l+1} \frac{1}{\mathcal{V}} g(\vec{R}^{l+1} - \vec{R}^l) \theta(R_z^{l+1}) \theta(-R_z^l) F_\beta^{l+1,l} \quad (15.16)$$

The integrals are over the volume shown in Figure 15.3. Divide by A because stresses are forces per area. The Heaviside θ functions enforce the condition that bead $l + 1$ be above the plane at 0 and that bead l be below it. The subscript β on F indicates a component of the force.

$$= \frac{1}{A\mathcal{V}} \int d\vec{s} d\vec{t} g(\vec{s}) \theta(s_z/2 + t_z) \theta(s_z/2 - t_z) F_\beta^{l+1,l} \quad (15.17)$$

Go over to variables $\vec{s} = \vec{R}^{l+1} - \vec{R}^l$ and $\vec{t} = (\vec{R}^l + \vec{R}^{l+1})/2$.

$$= \frac{1}{\mathcal{V}} \int d\vec{s} g(\vec{s}) s_z \theta(s_z) F_\beta^{l+1,l} \quad (15.18)$$

Integrating \vec{t} along z gives a factor of s_z , and integrating \vec{t} along the other two directions gives a factor of A .

$$= \frac{1}{\mathcal{V}} \left\langle [R_z^{l+1} - R_z^l] \theta(R_z^{l+1} - R_z^l) F_\beta^{l+1,l} \right\rangle \quad (15.19)$$

Moving back to the original spatial variables, and using angular brackets to denote a time or thermodynamic average over relative locations of \vec{R}^l and \vec{R}^{l+1} .

When bead l drifts above the plane at 0 and bead $l + 1$ drifts below it, (15.19) vanishes, but there is an equivalent contribution in which the roles of l and $l + 1$ are interchanged. Because $F_\beta^{l+1,l} = -F_\beta^{l,l+1}$, this contribution to the stress tensor is

$$\frac{1}{\mathcal{V}} \left\langle [R_z^{l+1} - R_z^l] \theta(R_z^l - R_z^{l+1}) F_\beta^{l+1,l} \right\rangle. \quad (15.20)$$

Thus, adding Eqs. (15.19) and (15.20) gives the total contribution $\sigma_{z\beta}^{l,l+1}$ due to

beads l and $l + 1$, which equals

$$\sigma_{z\beta}^{l,l+1} = \frac{1}{\mathcal{V}} \left\langle [R_z^{l+1} - R_z^l] F_\beta^{l+1,l} \right\rangle \quad \begin{array}{l} \text{The reason for the factor } R_z^{l+1} - R_z^l \text{ is that} \\ \text{larger the distance between } R_z^{l+1} \text{ and } R_z^l \text{ in} \\ \text{Figure 15.3, the larger the probability that the} \\ \text{plane at 0 will lie between them.} \end{array} \quad (15.21)$$

$$= \frac{1}{\mathcal{V}} \left\langle [R_z^{l+1} F_\beta^{l+1,l}] \right\rangle + \frac{1}{\mathcal{V}} \left\langle [R_z^l F_\beta^{l,l+1}] \right\rangle \quad (15.22)$$

$$= \frac{1}{\mathcal{V}} \left\langle [R_z^{l+1} F_\beta^{l+1,l}] \right\rangle + \frac{1}{\mathcal{V}} \left\langle [R_z^{l-1} F_\beta^{l-1,l}] \right\rangle. \quad \begin{array}{l} \text{Changing the labeling cannot} \\ \text{affect the results.} \end{array} \quad (15.23)$$

The contribution to the stress tensor obtained by summing over all the beads is

$$\sigma_{\alpha\beta} = \frac{1}{\mathcal{V}} \sum_{l'} \left\langle R_\alpha^{l'} F_\beta^{l',l} \right\rangle. \quad (15.24)$$

The subscript z has been replaced by α , because it does not matter whether x , y , or z was chosen. This expression gives the contribution from the polymer beads, and it must be added to the contribution from the fluid. Equation (15.24) follows from Eq. (15.23) when beads interact with nearest neighbors, but it is true more generally.

Polymer Equation of Motion. In order to evaluate Eq. (15.24) one needs to know the probability that adjacent beads will differ in height by certain amounts, and then to take averages. These probabilities depend upon the flow in which the polymer finds itself, and also upon the magnitude of thermal fluctuations.

There are two common schemes to calculate the motions of polymers. The first is called the *Rouse model*, and it treats the interaction between liquid and polymer in a fairly naïve way. In addition to a shearing force created by the fluid, the polymer beads are subject to random kicks, and they interact with their nearest neighbors. This calculation is oversimplified because of the way it treats the fluid flow around the polymer. In reality, whenever a thermal fluctuation kicks one bead, its motion moves the surrounding fluid and makes other beads move as well. Incorporating the rather long-range effective force between beads due to this effect leads to the *Zimm model*. The word “model” is somewhat misleading because the effective interaction between beads mediated by the fluid is certainly real, and the only question is whether the approximations used by Zimm (1956) are adequate to treat the actual complexity. However, for the sake of simplicity, only the calculation of Rouse (1953) will be presented here.

The motion of bead l is given by

$$\ddot{\mathbf{R}}^l = \frac{1}{m} \sum_{l'} \mathbf{F}^{l',l} - b(\dot{\mathbf{R}}^l - \vec{v}) + \xi^l. \quad \begin{array}{l} \text{As before, } \mathbf{F}^{l',l} \text{ gives the force on bead } l \text{ due} \\ \text{to bead } l'. \text{ } m \text{ is the mass of the bead.} \end{array} \quad (15.25)$$

The form of this equation is in accord with the fluctuation–dissipation theorem mentioned in Eq. (5.41). The constant b describes damping of the bead proportional to the difference between its velocity and the local velocity of the fluid \vec{v} .

The random force $\vec{\xi}^l$ is chosen so that while the time (or thermodynamic) average of any component $\langle \xi_\alpha^l \rangle$ vanishes, the product of two components obeys

$$\langle \xi_\alpha(0) \xi_\beta(t) \rangle = \frac{2b\delta_{\alpha\beta}k_B T \delta(t)}{m}. \quad (15.26)$$

Treating this time correlation function as a delta function means that the thermal kicks are very rapid in comparison with any other dynamical process in the system.

How exactly one should think about the fluid velocity \vec{v} is a matter that at first seems simple, but then becomes complicated after further consideration. In the view of Rouse (1953), \vec{v} is simply the average fluid velocity in the vicinity of the bead at \vec{R}^l , and the drag force on the bead is naturally the Stokes drag $b = 6\pi\eta R$ found in Problem 2. The problem that Zimm (1956) noted with this point of view is that the bead is not a single isolated sphere moving in a flow that arrives asymptotically at a value of \vec{v} . Other beads are nearby, interacting with the flow, pushing at the bead in question whenever they move, and making it difficult to determine how \vec{v} is supposed to be measured.

Neglecting this difficulty, consider the case where particles have sufficiently light mass and sit in a sufficiently viscous and slowly moving fluid that acceleration of particles is negligible. Taking forces between nearest neighbors only, with spring constant \mathcal{K} as given by Eq. (5.67), Eq. (15.25) becomes

$$\dot{\vec{R}}^l = \vec{v} + \frac{\mathcal{K}}{bm} [\vec{R}^{l+1} - 2\vec{R}^l + \vec{R}^{l-1}] + \frac{\vec{\xi}^l}{b}. \quad (15.27)$$

Eq. (5.67) calculated the spring constant \mathcal{K}/N of N monomers in series, while what is needed here is the spring constant \mathcal{K} between two monomers.

Sticking with the simple view in which one pretends that the flow \vec{v} can be set equal to a large smooth macroscopic flow that might be observed externally, note that the flow will vary with the precise location of the bead, but that for small motions and slowly varying flows, only linear spatial variations of \vec{v} should matter. Let W be the tensor giving these variations:

$$v_\alpha = \vec{v}_\alpha^0 + \sum_\beta W_{\alpha\beta} R_\beta^l. \quad (15.28)$$

Assume that the polymer is sufficiently small that W can be considered constant over its full extent. Different polymers at different locations may see different flow features, but each one sees only a uniform shear flow.

Then Eq. (15.27) becomes

$$\dot{\vec{R}}^l = \vec{v}^0 + W\vec{R}^l + \frac{\mathcal{K}}{bm} [\vec{R}^{l+1} - 2\vec{R}^l + \vec{R}^{l-1}] + \frac{\vec{\xi}^l}{b}. \quad (15.29)$$

The resemblance with the tight-binding model of Section 8.4 should suggest the value of moving to Fourier components to solve Eq. (15.29). Denote the Fourier modes by

$$\vec{\psi}^k = \frac{1}{\sqrt{N}} \sum_{l=1}^N e^{2\pi i l k / N} [\vec{R}^l - \vec{v}^0 t]. \quad (15.30)$$

Subtracting $\vec{v}^0 t$ means going to a reference frame that moves with the mean flow, and N is the total number of beads in the polymer.

Substituting Eq. (15.30) into Eq. (15.29) and neglecting the term $W\vec{v}^0t$, which vanishes for pure shear flows, and in any event is quadratic in velocities, gives

$$\dot{\vec{\psi}}^k = \{W - \omega_k\} \vec{\psi}^k + \frac{\xi^k}{b} \quad \bar{\xi}^k = 1/\sqrt{N} \sum \xi^l \exp[2\pi ilk/N]. \quad (15.31)$$

With this normalization, $\bar{\xi}^k$ continues to obey Eq. (15.26).

with

$$\omega_k = \frac{2\mathcal{K}}{mb} (1 - \cos[2\pi k/N]). \quad (15.32)$$

If W is independent of time, one can write

$$\vec{\psi}^k = \int_{-\infty}^t dt' e^{-(t'-t)[W-\omega_k]} \frac{\xi^k(t')}{b}. \quad \text{Remember that } W \text{ is a matrix.} \quad (15.33)$$

In general W depends upon time, as the flow changes, and the polymer is swept into new regions. In this case, it is easiest to solve Eq. (15.31) with perturbation theory, first taking $W = 0$ and then modifying the solution to first order in W . In this perturbative scheme,

$$\psi_\alpha^{(0)k} = \int_{-\infty}^t dt' e^{(t'-t)\omega_k} \frac{\xi^k(t')}{b} \quad \text{Just set } W = 0 \text{ in Eq. (15.33). The superscript } 0 \text{ means zeroth order in perturbation theory.} \quad (15.34)$$

$$\Rightarrow \langle \psi_\alpha^{(0)k}(t) \psi_\beta^{(0)k*}(t') \rangle = e^{-|t-t'|\omega_k} \frac{k_B T}{mb\omega_k} \delta_{\alpha\beta}. \quad (15.35)$$

This result will be useful shortly. It results from a brief calculation employing Eq. (15.26) that is the subject of Problem 5.

$$\psi_\alpha^k \approx \psi_\alpha^{(0)k} + \int_{-\infty}^t dt' \sum_\beta W_\beta(t') \psi_\beta^{(0)k}(t') \quad \text{Keep everything to order } W. \quad (15.36)$$

$$\begin{aligned} \Rightarrow \langle \psi_\alpha^k(t) \psi_\beta^{*k}(t) \rangle &\approx \frac{k_B T}{mb\omega_k} \delta_{\alpha\beta} \\ &+ \int_{-\infty}^t dt' \sum_{\alpha'} \langle \psi_\alpha^{(0)k}(t) W_{\beta\alpha'}(t') \psi_{\alpha'}^{(0)k*}(t') \rangle \\ &+ \int_{-\infty}^t dt' \sum_{\alpha'} \langle \psi_\beta^{(0)k*}(t) W_{\alpha\alpha'}(t') \psi_{\alpha'}^{(0)k}(t') \rangle. \quad \text{Use Eq. (15.35) to calculate the averages.} \end{aligned} \quad (15.37)$$

$$= \frac{k_B T}{mb\omega_k} \left\{ \delta_{\alpha\beta} + \int_{-\infty}^t dt' e^{-(t-t')\omega_k} [W_{\beta\alpha}(t') + W_{\alpha\beta}(t')] \right\}. \quad (15.38)$$

Assembling the Pieces. In Eq. (15.24) the stress tensor is related to an average over bead locations, while Eq. (15.38) evaluates an average of some Fourier transforms of the locations. With a bit of extra manipulation, Eq. (15.38) turns out to be just what is needed to find the stress tensor σ .

Rewrite Eq. (15.24) as

$$\sigma_{\alpha\beta} = \frac{1}{V} \sum_{ll'} \langle F_\beta^{l,l'} R_\alpha^l \rangle = -\frac{\mathcal{K}}{V} \sum_l \langle R_\alpha^l (R_\beta^{l+1} - 2R_\beta^l + R_\beta^{l-1}) \rangle \quad (15.39)$$

$$= \frac{\mathcal{K}}{V} \sum_{k=1}^{N-1} (2 - 2 \cos 2\pi k/N) \langle \psi_\alpha^k \psi_\beta^{k*} \rangle \quad \text{Invert Eq. (15.30) and replace } R_\beta^l \text{ with } \psi^s; \text{ see Problem 5.} \quad (15.40)$$

$$= \frac{mb}{\mathcal{V}} \sum_{k=1}^{N-1} \omega_k \langle \psi_\alpha^k \psi_\beta^{k*} \rangle \quad (15.41)$$

See Eq. (15.32). Why was the term $k = 0$ eliminated? Because $\omega_k = 0$ for $k = 0$. One might worry about factors of ω_k^{-2} arising from Eq. (15.38). However, one can see from Eq. (15.33) that perturbation theory gets the wrong answer when $\omega_k = 0$, that ψ^k is actually finite, and eliminating $k = 0$ from the present sum is correct.

$$= \frac{k_B T}{\mathcal{V}} \sum_{k=1}^{N-1} \left[\delta_{\alpha\beta} + \frac{W_{\alpha\beta} + W_{\beta\alpha}}{\omega_k} \right] \quad \text{Use Eq. (15.38) with } W \text{ assumed constant in time.} \quad (15.42)$$

$$= \frac{k_B T}{\mathcal{V}} \left[N\delta_{\alpha\beta} + 2 \sum_{k=1}^{N/2} \frac{W_{\alpha\beta} + W_{\beta\alpha}}{\omega_k} \right] \quad (15.43)$$

$$\approx \frac{k_B T}{\mathcal{V}} \left[N\delta_{\alpha\beta} + 2 \sum_{k=1}^{\infty} \frac{W_{\alpha\beta} + W_{\beta\alpha}}{\frac{2\mathcal{K}}{mb} \frac{1}{2} \left(\frac{2\pi k}{N} \right)^2} \right] \quad \text{Use (15.32), expand out the cosine to leading order for } k \ll N, \text{ and extend the upper limit of the sum to infinity, because it converges.} \quad (15.44)$$

$$= \frac{k_B T}{\mathcal{V}} \left[N\delta_{\alpha\beta} + (W_{\alpha\beta} + W_{\beta\alpha}) \frac{mbN^2}{12\mathcal{K}} \right] \quad \text{The sum } \sum_{k=1}^{\infty} k^{-2} = \pi^2/6 \text{ was performed in Problem 6, Eq. (6.83) in Chapter 6.} \quad (15.45)$$

The first term of Eq. (15.45) leads to a uniform decrease of fluid pressure; the *osmotic pressure* tries to surround polymers with as much fluid as possible, and will try to suck water away from regions with lower density of polymer to make it happen. The second term corresponds to an increase in viscosity.

Uniform Viscosity. Suppose, for example, that the flow \vec{v} is a uniform shear flow where v_x increases linearly in the y direction, so $W_{xy} = \partial v_x / \partial y$ is nonzero but all other components of W vanish. Then

$$\sigma_{xy} = \frac{k_B T}{\mathcal{V}} mb \frac{N^2}{12\mathcal{K}} \frac{\partial v_x}{\partial y}. \quad (15.46)$$

Compare with Eq. (15.13) and assume that instead of one polymer, there is a concentration c/N of polymers per unit volume, where c is the number of monomers per unit volume, and N is the number of monomers per polymer. Then the viscosity of the fluid is enhanced by an amount

$$\delta\eta = \frac{c}{N} k_B T mb \frac{N^2}{12\mathcal{K}} \quad \text{The increase in the viscosity } \eta. \quad (15.47)$$

$$= \frac{c}{N} mb \frac{N^2 a^2}{12} \quad \text{See Eqs. (5.66) and (5.67), which express the spring constant } \mathcal{K} \text{ as } \mathcal{K} = k_B T / a^2. \quad (15.48)$$

Problem 6 determines the frequency dependence of the viscosity. If a shear velocity field oscillates as $W_{xy}(t) = W_0 \cos \omega t$, then

$$\sigma_{xy} = \sum_{k=1}^{N-1} \frac{W_0 k_B T}{\mathcal{V}(\omega_k^2 + \omega^2)} [\omega_k \cos \omega t + \omega \sin \omega t]. \quad (15.49)$$

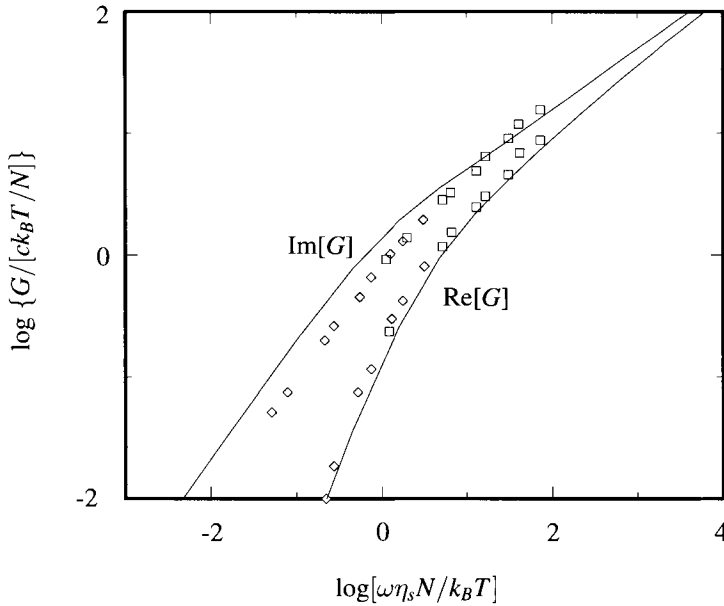


Figure 15.4. Storage ($\text{Re}[G]$) and loss ($\text{Im}[G]$) moduli of polystyrene in Θ solvents compared with the results of the Rouse calculation in Eq. (15.50). A Θ solvent is one specially chosen so that the coefficient B in Eq. (5.74) vanishes. The viscosity η_s is the viscosity of the solvent without any polymer. N is the number of monomers per polymer. The theoretical curves were obtained by evaluating Eq. (15.50) and multiplying G and ω by arbitrary constants to obtain a best fit. Better fits are obtained by including hydrodynamic interactions. [Source: Ferry (1980), p. 197.]

It is possible to use Eq. (15.49) to define a complex viscosity $\eta(\omega)$, but it is more conventional to define the *complex shear modulus* $G^*(\omega) = -i\omega\eta(\omega)$ so that

$$G(\omega) = \frac{k_B T}{\mathcal{V}} \sum_{k=1}^{N-1} \frac{\omega(\omega + i\omega_k)}{\omega_k^2 + \omega^2}. \quad (15.50)$$

The real part of G is called the *storage modulus*, and the imaginary part is called the *loss modulus*. Measurements of dilute mixtures of polystyrene compared with Eq. (15.50) appear in Figure 15.4.

15.4 Plasticity

It is commonplace to think of water flowing, but many metals, however, can also flow. The boundary between those that can and those that cannot is not easy to define precisely. For example, even rocks that ordinarily seem brittle can begin to flow when placed under sufficiently great confining pressure.

The flow of ductile metals resembles in some respects the flow of liquids, but there are also some important differences. A first difference is that metals do not begin to flow noticeably until a critical stress level, the *yield stress* is approached.

The yield stress corresponds to the point where the force per length f on dislocations reaches the critical value needed to make them mobile. Even at very low stresses, flow of metals can be observed, but it is extremely slow and it results from exponentially rare thermal fluctuations that permit rearrangement of small portions of the metal. As a matter of practice, a definite stress at which a metal begins to display irreversible deformation is a useful quantity to define.

The possibility of plastic flow after the yield stress is exceeded is explained in principle by dislocation motion. Knowledge of dislocation mobility has some predictive power for describing flow. Metals in which dislocations are immobile tend to be brittle; those in which dislocations are mobile along one or two directions can be deformed in those directions but still are not fully plastic, while those with five or more independent slip planes will permit flow in any directions, and if assembled into a polycrystalline aggregate will deform in a fully plastic fashion. Dislocations provide only one type of mobile defect permitting flow. Some ceramics can flow at high temperatures through the motion of vacancies, while amorphous materials can flow through rearrangement of local groups of atoms.

The theory of plasticity is a phenomenological account of deformation that does not depend upon the microscopic mechanism that makes it possible. Its construction is an interesting combination of guesswork based upon symmetry principles, a desire for simplicity, and constraints imposed by experimental observations. The most common form of the theory is heavily influenced by the characteristic behavior of structural steels, which provided the greatest impetus for its creation, and the theory might have a different form if aluminum or nickel alloys had an equal practical importance.

Suppose one has an isotropic solid capable of plastic deformation; a practical definition would be that the solid is capable of being drawn into wire. Whether the solid begins to flow at any given location depends upon the state of stress there, described by the stress tensor $\sigma_{\alpha\beta}$. The tensor σ is symmetric, so there is some basis in which it is diagonal, with diagonal elements σ_1 , σ_2 , and σ_3 . The solid is assumed to be isotropic, it cannot matter how these three elements are numbered, and the onset of yield must be determined by some symmetrical function \mathcal{F} of σ_1 , σ_2 , and σ_3 . Demanding that \mathcal{F} be symmetrical is equivalent to requiring it to be a function of symmetrical combinations of $\sigma_1 \dots \sigma_3$. There are three conventional combinations of the elements of the stress tensor, the *stress invariants*, similar to the strain invariants of Eq. (12.16), defined by the eigenvalue equation

$$\det|\sigma - \epsilon I| = -\epsilon^3 + \epsilon^2 I_1 + \epsilon I_2 + I_3 = 0 \quad (15.51a)$$

with

$$I_1 = \sum_{\alpha} \sigma_{\alpha\alpha} \quad (15.51b)$$

$$I_2 = \sum_{\alpha\beta} \{\sigma_{\alpha\beta}\sigma_{\alpha\beta} - \sigma_{\alpha\alpha}\sigma_{\beta\beta}\} \quad (15.51c)$$

$$I_3 = \det|\sigma|. \quad (15.51d)$$

Bridgeman (1949) found that a uniform hydrostatic pressure or tension, so long as it is much less than Young's modulus, does not much affect the yield properties of metals. Letting

$$\sigma = \frac{1}{3} \sum_{\alpha} \sigma_{\alpha\alpha} \quad (15.52)$$

be the hydrostatic component of stress, it follows that yielding depends only upon the *deviatoric stress*

$$s_{\alpha\beta} = \sigma_{\alpha\beta} - \sigma \delta_{\alpha\beta}. \quad (15.53)$$

Three invariants analogous to those defined by Eq. (15.51) can be defined in terms of s . The first of these invariants must vanish, while the others are

$$J_2 = \frac{1}{2} \sum_{\alpha\beta} s_{\alpha\beta} s_{\alpha\beta} \quad (15.54a)$$

$$J_3 = \det|s|. \quad (15.54b)$$

The requirement that yielding of an isotropic material be independent of hydrostatic stress can therefore be expressed by having flow begin when $\mathcal{F}(J_2, J_3)$ reaches a critical value. The *Mises* yielding condition says that flow begins when

$$\sqrt{J_2} = \kappa. \quad \kappa \text{ is some constant that needs to be tabulated for each material. Mises supposed that } J_3 \text{ is irrelevant.} \quad (15.55)$$

The characteristic features of metals that particularly distinguish them from fluids are, first, that flow is negligible below this threshold and, second, that the threshold κ itself evolves as the metal deforms, a bit like egg whites stiffening up as they are beaten, but much more rapid. The tendency for κ to increase is called *work hardening*, and implies that stresses on a metal will continually have to increase if it is to continue to flow.

The theory must now grapple with the question of how precisely a solid deforms once the yield stress has been exceeded. The solid always has both reversible and irreversible components to its deformation, because after removal of stress the solid will snap back to some extent and may continue relaxing into a final configuration over long times. A simplest account of the process keeps only two time scales, an instantaneous elastic relaxation, and a permanent plastic deformation. These are distinguished by stating that the strain tensor $e_{\alpha\beta}$ is the sum of two pieces: $e_{\alpha\beta}^e$, the elastic strain tensor, and $e_{\alpha\beta}^p$, the plastic strain tensor. The elastic part of the strain is defined by Eq. (12.39); when the stress is given, the elastic strain is also instantly known. It would be misleading, however, to say that when stress is relieved the elastic strain instantly vanishes, because after all external stresses on an object have been released, it may have deformed in such a way that internal stresses are still present.

It remains to decide how the plastic strain evolves, in a final flurry of guesses. Guess that flow in any direction is proportional to the deviatoric stress along that

direction;

$$\dot{e}_{\alpha\beta}^p = \begin{cases} w[\sqrt{J_2} - \kappa]s_{\alpha\beta} & \text{if } \sqrt{J_2} - \kappa > 0 \\ 0 & \text{otherwise.} \end{cases} \quad (15.56)$$

w is some unknown constant; the point of this equation is to make an hypothesis about the tensor structure of the flow and to make sure it vanishes when yield conditions are not met.

Not only does Eq. (15.56) have the virtue of simplicity, it also predicts $\sum_{\alpha} e_{\alpha\alpha}^p = 0$, which means that volume is preserved by irreversible flow, in accord with experiment.

It is not easy to decide how precisely the increase in flow stress κ should depend upon the flow history. A common guess makes κ a function of the total plastic work,

$$W = \int dt' \sum_{\alpha\beta} \dot{e}_{\alpha\beta}^p \sigma_{\alpha\beta}. \quad \text{Integral over time. Writing energy as strain times stress comes from Eq. (12.22).} \quad (15.57)$$

Suppose that a plastic body at rest is subject to some small increment in stress $d\sigma_{\alpha\beta}$. According to Eq. (15.56), the body begins to flow. After a time, it hardens up, and flow ceases, resulting in a small increment of plastic strain $de_{\alpha\beta}^p$:

$$de_{\alpha\beta}^p = C ds_{\alpha\beta}. \quad C \text{ is a constant of proportionality.} \quad (15.58)$$

How should the proportionality constant C be chosen so that flow has stopped when just the right amount of hardening has occurred? The plastic work involved in the small amount of flow is

$$dW = C \sum_{\alpha\beta} \sigma_{\alpha\beta} ds_{\alpha\beta} \quad \text{Combine a small change in Eq. (15.57) with Eq. (15.58).} \quad (15.59)$$

$$= C \sum_{\alpha\beta} s_{\alpha\beta} ds_{\alpha\beta} \quad \text{Use Eq. (15.53).} \quad (15.60)$$

$$= C dJ_2, \quad \text{Use Eq. (15.54a).} \quad (15.61)$$

so the change in κ is

$$d\kappa = \kappa' C dJ_2. \quad \text{The prime on } \kappa \text{ means to take a derivative with respect to } W. \quad (15.62)$$

The only way for Eqs. (15.62) and the flow condition (15.55) to be consistent is for the amount of flow C to be

$$C = \frac{1}{2\kappa'\sqrt{J_2}} \quad (15.63)$$

$$\Rightarrow de_{\alpha\beta}^p = \frac{ds_{\alpha\beta}}{2\kappa'\sqrt{J_2}}. \quad \text{Actually, the plastic strain only changes if the change in deviatoric stress is such as to make } J_2 \text{ increase. Otherwise, } de_{\alpha\beta}^p \text{ vanishes.} \quad (15.64)$$

For applications of these equations, and for many solutions in special cases, see Hill (1950) or Lubliner (1990).

15.5 Superfluid ^4He

Failure of Helium to Solidify. Helium stands out among the elements because at atmospheric pressure it remains liquid down to a temperature of absolute zero. A tentative explanation for this perplexing fact, simple but not convincing, follows from data of Table 11.3. Were helium like the other noble gases, then the van der Waals attraction would cause it to crystallize in an fcc structure whose spacing is given by Eq. (11.10) as 2.8 \AA . The zero-point energy of a helium atom confined to a region this size is approximately $\hbar^2/(2md_0^2)$, which, for ^4He , works out to be $2 \cdot 10^{-3} \text{ eV}$. According to Eq. (11.11), the cohesive energy per particle in an fcc structure would be around $7 \cdot 10^{-3} \text{ eV}$. Although from this rough argument crystallizing in fcc appears to be favorable, the substance in actuality finds the penalty of zero-point energy too costly and chooses to remain liquid in the ground state, rather than solid.

The ground-state liquid has, however, bizarre properties matched by no other substance on Earth. Poured into a container, it runs up the sides and flows down over the edges. It flows through tubes as small as 500 \AA in diameter without measurable resistance, while in other respects displaying ordinary liquid viscosity. These facts deserve a more systematic presentation.

Some Experimental Phenomena in ^4He . Liquid ^4He undergoes a phase transition at 2.186 K and atmospheric pressure, called the λ point by Keesom, its discoverer, because of the appearance of the specific heat curve. Below this temperature, helium begins to display the strange phenomena that lead it to be known as a *superfluid*, and thought of as the new phase *He II*. Out of the dozens of ingenious experiments designed to probe properties of helium II, here are two that are particularly revealing.

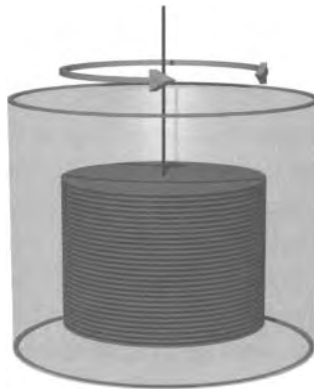


Figure 15.5. Narrowly spaced disks undergo torsional oscillations in a bath of helium II to investigate its viscosity.

The peculiar mechanical properties of superfluid helium are best indicated by an experiment of Andronikashvili (1948), illustrated in Figure 15.5. A collection of 100 mica disks of around 4 cm in diameter and spaced by 0.2 mm is lowered into a bath of superfluid helium, suspended upon a fiber. The experimental quantity

measured is the rotational frequency of the disks, which is given by

$$\omega = \sqrt{\frac{\mathcal{K}}{I_0 + I_F}}. \quad (15.65)$$

Here \mathcal{K} is the spring constant of the fiber in torsion, I_0 is the moment of inertia of the disks, and I_F is the effective moment of inertia of the fluid dragged along with the disks.

Calculating the effective moment of inertia of the fluid I_f is a complicated problem in hydrodynamics, but to first approximation the result is rather simple; a classical fluid should act like a solid mass dragged along in the space between the disks, but not moving outside them. In this approximation, the moment of inertia due to the fluid is simply proportional to its density and independent of its viscosity. When the experiment was performed, the resonant oscillatory frequency of the disks began to rise as the temperature decreased below the λ point, rising to $\sqrt{\mathcal{K}/I_0}$ when the temperature fell to 1 K. It was as if the density of helium began to drop at the λ temperature and fell nearly to zero by 1 K.

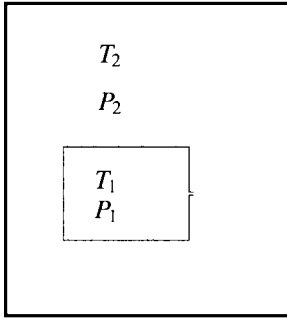


Figure 15.6. A thermally isolated container of helium at temperature T_1 and pressure P_1 is placed inside a second with temperature T_2 and pressure P_2 , the only connection being a micron-scale tube.

A second experiment displays the unusual thermomechanical features of the superfluid and is illustrated in Figure 15.6. Into a bath of helium at temperature T_2 is placed a thermally isolated chamber that communicates with the outside bath only because of a small opening, on the order of a micron in diameter. A resistive coil allows heat to be delivered to the inner chamber, and thermometers measure temperature both inside and outside of it. When heat is supplied to the inner chamber, the pressure P_1 rises in direct proportion to the change in temperature T_1 . This fact is not at first surprising, because fluids typically do expand when heated. However, the phenomenon has nothing to do with ordinary thermal expansion, because it ceases if the microscopic connection between the inner and outer basins is closed. The inner and outer basins are in thermodynamic equilibrium, although they are at different temperatures and pressures. A striking example of this phenomenon is the *fountain effect*. If a thin tube whose base is packed with fine powder is placed into a basin of superfluid helium, then a slight increase in temperature of the helium bath causes superfluid to race up the tube and fly out the top, up to a height of tens of centimeters.

These experimental observations lie behind a phenomenological picture of ^4He called the *two-fluid model*. In this view, He II consists of two intertwined fluids. One of them, the normal fluid, has ordinary fluid properties such as viscosity. The other, the superfluid component, has no viscosity and carries no entropy. There

is no completely accepted microscopic theory to underlie the two-fluid model, but clearly helium does not actually consist of two different fluids. The superfluid component corresponds to a low energy state with quantum-mechanical coherence, while the normal fluid corresponds to thermal excitations traveling about on top of the low energy state.

Andronikashvili's experiment is easy to explain from this point of view. As temperature drops below the λ point, more and more of the fluid converts to the superfluid component. Because this component lacks viscosity, the oscillating mica disks do not perturb it, and only the normal component of the fluid is dragged along with them. In fact, the results of the experiment may be interpreted as a measurement, or even a definition, of the density of the superfluid component.

The thermomechanical experiment shows that two regions of helium may be in contact, particles flowing from one to another, but without the two regions sharing the same temperature or pressure. Let $G_1(T_1, P_1, N_1)$ be the Gibbs free energy of the helium bath, with $G_2(T_2, P_2, N_2)$ the Gibbs free energy of the internal container. Because the two regions of fluid can freely exchange particles, equilibrium demands that

$$0 = \frac{\partial G}{\partial N_1} = \frac{\partial G_1(N_1) + G_2(N - N_1)}{\partial N_1} \Big|_{TP} \quad G = G_1 + G_2 \text{ and } N = N_1 + N_2. \quad (15.66)$$

$$\Rightarrow \frac{\partial G_1}{\partial N_1} = \frac{\partial G_2}{\partial N_2} \Rightarrow \mu_1(T_1, P_1) = \mu_2(T_2, P_2). \quad \mu_1 \text{ and } \mu_2 \text{ are the chemical potentials of the two regions.} \quad (15.67)$$

If entropy could flow between the two fluid regions, then equilibrium would require the condition

$$\frac{\partial \mathcal{E}_1(S_1, V_1)}{\partial S_1} = \frac{\partial \mathcal{E}_2(S_2, V_2)}{\partial S_2} \Rightarrow T_1 = T_2; \quad \text{Not true for superfluid helium!} \quad (15.68)$$

thus the fact that two fluids can be in equilibrium at different temperatures while exchanging particles is a demonstration that the particles moving between them somehow contrive to carry no entropy.

According to Eq. (15.67), equality of chemical potential is the basic requirement for superfluid equilibrium. When temperature and pressure differ only slightly in two regions of superfluid, then μ_2 can be expanded to first order in the small differences $\Delta T = T_2 - T_1$ and $\Delta P = P_2 - P_1$. As a result

$$\frac{\partial \mu_2}{\partial T_2} \Delta T + \frac{\partial \mu_2}{\partial P_2} \Delta P = 0 \quad (15.69)$$

$$\Rightarrow s \Delta T = \frac{1}{\rho} \Delta P \Rightarrow \frac{\Delta P}{\Delta T} = \rho s. \quad \begin{array}{l} s \text{ is the entropy per unit mass, and } \rho \text{ is the} \\ \text{mass density in region 2; obtain these expres-} \\ \text{sions from } \mu = \partial G / \partial N. \end{array} \quad (15.70)$$

The entropy of helium can be measured directly by integrating the specific heat up from zero, so as to verify (15.70).

15.5.1 Two-Fluid Hydrodynamics

The superfluid component of helium differs from an ordinary fluid because of the particular thermodynamic force that makes it move. The thermomechanical effect demonstrates that superfluid flows so as to equalize the chemical potential. Because the chemical potential describes the change in energy of a small portion of fluid due to addition of a single particle, the force per particle acting upon the superfluid is $-\nabla\mu$, and the velocity \vec{v}_s of a region of superfluid is described by

$$\frac{\partial \vec{v}_s}{\partial t} + (\vec{v}_s \cdot \vec{\nabla}) \vec{v}_s = -\frac{\vec{\nabla}\mu}{m}. \quad m \text{ is the mass of a helium atom.} \quad (15.71)$$

As a consequence of the Gibbs–Duhem relation

$$d\mu = \frac{V}{N} dP - \frac{S}{N} dT, \quad \text{See, for example, Landau and Lifshitz (1980) p. 72.} \quad (15.72)$$

one may write alternatively

$$\frac{\partial \vec{v}_s}{\partial t} + (\vec{v}_s \cdot \vec{\nabla}) \vec{v}_s = -\frac{\vec{\nabla}P}{\rho} + s\vec{\nabla}T. \quad \rho = \text{mass density, and } s = S/Nm \text{ is entropy per unit mass.} \quad (15.73)$$

In accord with Eq. (15.70), superfluid can be in equilibrium in the presence of simultaneous pressure and temperature gradients. Equation (15.73) predicts that without pressure gradients, thermal gradients can make a superfluid flow as easily as pressure differences move an ordinary fluid.

The equation describing motion both of superfluid and normal components of helium is

$$\rho_s \left\{ \frac{\partial \vec{v}_s}{\partial t} + (\vec{v}_s \cdot \vec{\nabla}) \vec{v}_s \right\} + \rho_n \left\{ \frac{\partial \vec{v}_n}{\partial t} + (\vec{v}_n \cdot \vec{\nabla}) \vec{v}_n \right\} = -\vec{\nabla}P + \eta \nabla^2 \vec{v}_n. \quad (15.74)$$

At first glance, Eq. (15.74) appears obvious, but it is not. The relation between pressure and acceleration is no longer as clear as for a single-component fluid, because there is no single reference frame in which all the fluid is stationary and in which one can measure the pressure. An alternative to Eq. (15.74) might be an equation in which the left-hand side contains only the total density $\rho = \rho_s + \rho_n$ and the mean velocity $(\rho_n \vec{v}_n + \rho_s \vec{v}_s)/\rho$. A partial justification for Eq. (15.74) is that it produces the correct acceleration of superfluid or normal components if either the normal or superfluid density vanishes, and in addition it is an equation for which the two fluid components are independent; motion of the superfluid does not produce convective transport of the normal fluid, and vice versa. Such arguments cannot, however, rule out the presence of a term such as $\rho_s s \vec{\nabla}T$, because ρ_s vanishes in the normal fluid, while s vanishes in the superfluid. Landau's unambiguous derivation of Eq. (15.74) is described in the final chapter of Landau and Lifshitz (1987).

15.5.2 Second Sound

A remarkable consequence of Eqs. (15.73) and (15.74) is the existence of propagating waves in helium moving at a speed of sound, but involving temperature rather than pressure variations. The origin of these waves can be deduced from Eq. (15.73). Any gradient in temperature spurs a flow of superfluid toward the hot region, trying to cool it down. This motion can occur without noticeable change in the density of the fluid, because an equal amount of normal fluid flows in the opposite direction. The region away from which the superfluid flows heats up, but because the superfluid has already acquired some inertia, it needs some time to reverse course. The consequence is a wavelike oscillation of temperature in which normal fluid and superfluid are out of phase.

Speeds of First and Second Sound in Liquid ^4He . Sound is a disturbance traveling at long wavelengths and small amplitudes. Therefore in analyzing the consequences of Eqs. (15.73) and (15.74) it is enough to retain only first order in all small quantities, and to ignore the dissipative term proportional to ∇^2 , because it is negligible for long-wavelength excitations. In addition to Eqs. (15.73) and (15.74), two conservation laws are needed to describe sound completely. Conservation of mass requires

$$\frac{\partial \rho}{\partial t} + \vec{\nabla} \cdot (\rho_n \vec{v}_n + \rho_s \vec{v}_s) = 0 \quad (15.75)$$

while conservation of entropy requires

$$\frac{\partial \rho s}{\partial t} = -\vec{\nabla} \cdot \rho s \vec{v}_n \quad \begin{array}{l} \text{Because the viscous term in Eq. (15.74) is} \\ \text{neglected, entropy production can be neglected.} \\ \text{Remember that } s \text{ was defined to be entropy} \\ \text{per unit mass and that it is carried only by the} \\ \text{normal fluid.} \end{array} \quad (15.76)$$

Rewriting Eqs. (15.73) and (15.74) to linear order gives

$$\frac{\partial \vec{v}_s}{\partial t} = -\frac{\vec{\nabla} P}{\rho} + s \vec{\nabla} T \quad (15.77)$$

$$\rho_s \frac{\partial \vec{v}_s}{\partial t} + \rho_n \frac{\partial \vec{v}_n}{\partial t} = -\vec{\nabla} P. \quad \text{Dropping the contribution from viscosity.} \quad (15.78)$$

Differentiating Eq. (15.75) with respect to time and using Eq. (15.78) to describe the time evolution of the mass current gives the customary relation between density and pressure

$$\frac{\partial^2 \rho}{\partial t^2} = \nabla^2 P. \quad \begin{array}{l} \text{One is free, for example, to replace } \partial \rho_n \vec{v}_n / \partial t \\ \text{by } \rho_n \partial \vec{v}_n / \partial t \text{ because } \vec{v}_n \text{ is a small quantity,} \\ \text{and multiplying by } \partial \rho_n / \partial t \text{ would produce a} \\ \text{second-order quantity, which may be neglected.} \end{array} \quad (15.79)$$

A second relation, between entropy and temperature, is obtained by writing

$$\frac{\partial s}{\partial t} = \frac{1}{\rho} \frac{\partial s \rho}{\partial t} - \frac{s}{\rho} \frac{\partial \rho}{\partial t} \quad (15.80)$$

$$= \frac{-1}{\rho} \vec{\nabla} \cdot \rho s \vec{v}_n + \frac{s}{\rho} \vec{\nabla} \cdot (\rho_n \vec{v}_n + \rho_s \vec{v}_s) \quad \text{Use Eqs. (15.75) and (15.76).} \quad (15.81)$$

$$= \frac{s \rho_s}{\rho} \vec{\nabla} \cdot (\vec{v}_s - \vec{v}_n). \quad \text{Pulling } \rho_n, \rho_s, \text{ and } s \text{ outside derivatives because they multiply } \vec{v}_n \text{ or } \vec{v}_s, \text{ which are already small, and combining terms.} \quad (15.82)$$

Solving Eqs. (15.77) and (15.78) for $\partial(\vec{v}_s - \vec{v}_n)/\partial t$ gives

$$\frac{\partial}{\partial t} (\vec{v}_s - \vec{v}_n) = s \frac{\rho}{\rho_n} \vec{\nabla} T \quad (15.83)$$

$$\Rightarrow \frac{\partial^2 s}{\partial t^2} = s^2 \frac{\rho_s}{\rho_n} \nabla^2 T. \quad \text{Combining Eqs. (15.82) and (15.83), and bringing zeroth-order quantities outside the derivative.} \quad (15.84)$$

To obtain sound speeds from these relations, one needs to observe that ρ and s are related to P and T by equations of state. The small variations of ρ and s can be rewritten in terms of the deviations $T^{(1)}$ and $P^{(1)}$ of temperature and pressure from equilibrium as

$$\frac{\partial \rho}{\partial P} \Big|_T \frac{\partial^2 P^{(1)}}{\partial t^2} + \frac{\partial \rho}{\partial T} \Big|_P \frac{\partial^2 T^{(1)}}{\partial t^2} = \nabla^2 P^{(1)} \quad \text{Cross terms such as } \partial^2 \rho / \partial P \partial t \text{ are second order and negligible. Comes from Eq. (15.79).} \quad (15.85)$$

$$\frac{\partial s}{\partial P} \Big|_T \frac{\partial^2 P^{(1)}}{\partial t^2} + \frac{\partial s}{\partial T} \Big|_P \frac{\partial^2 T^{(1)}}{\partial t^2} = s^2 \frac{\rho_s}{\rho_n} \nabla^2 T^{(1)}. \quad \text{Comes from Eq. (15.84).} \quad (15.86)$$

Suppose now that both $P^{(1)}$ and $T^{(1)}$ have the form of traveling waves of wave number k and frequency $\omega = ck$. Then

$$\frac{\partial \rho}{\partial P} \Big|_T P^{(1)} + \frac{\partial \rho}{\partial T} \Big|_P T^{(1)} = c^{-2} P^{(1)} \quad (15.87a)$$

$$\frac{\partial s}{\partial P} \Big|_T P^{(1)} + \frac{\partial s}{\partial T} \Big|_P T^{(1)} = c^{-2} s^2 \frac{\rho_s}{\rho_n} T^{(1)}. \quad (15.87b)$$

Because the determinant of Eq. (15.87) vanishes,

$$\left(1 - \frac{c^{-2} s^2 \rho_s / \rho_n}{\frac{\partial s}{\partial T} \Big|_P} \right) \left(1 - \frac{c^{-2}}{\frac{\partial \rho}{\partial P} \Big|_T} \right) = \frac{\frac{\partial s}{\partial P} \Big|_T \frac{\partial \rho}{\partial T} \Big|_P}{\frac{\partial \rho}{\partial P} \Big|_T \frac{\partial s}{\partial T} \Big|_P} \quad (15.88)$$

$$= \frac{C_P - C_V}{C_P} \quad \text{Use } \partial \rho / \partial T \Big|_P / \partial \rho / \partial P \Big|_T = -\partial P / \partial T \Big|_\rho \text{ and the standard relation for the difference between constant volume and constant pressure specific heats } C_P \text{ and } C_V. \quad (15.89)$$

$$\approx 0. \quad \text{The difference between } C_P \text{ and } C_V \text{ is very small for } {}^4\text{He}. \quad (15.90)$$

The two values of c solving Eq. (15.88) are therefore

$$c_1 = \sqrt{\frac{\partial P}{\partial \rho} \Big|_T} \quad (15.91)$$

and

$$c_2 = \sqrt{\frac{T s^2 \rho_s}{C_P \rho_n}} \quad \text{Here } C_P \text{ is the specific heat per unit mass.} \quad (15.92)$$

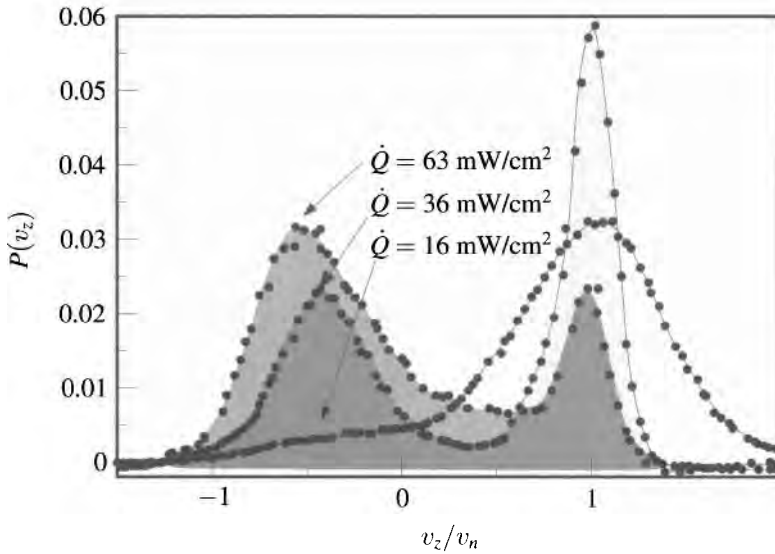


Figure 15.7. Direct observation of two-fluid motion in liquid helium. Hydrogen crystals trapped in vortices move downwards while others move upwards. The figure displays the probability distribution P of different tracer particle velocities for three different flow conditions. The scale is set by v_n in Eq. (15.93a). [Source: Paoletti et al. (2008), p. 5.]

Experimental Observations. These traveling waves were first found experimentally by Peshkov (1946). First sound has a velocity ranging from around 240 m/s at very low temperatures to 220 m/s at the λ point. The second sound velocity vanishes at the λ point, in accord with Eq. (15.92), has a plateau at around 20 m s^{-1} between 1 and 2 K, and then rises to a value greater than 100 m s^{-1} at low temperatures, which approaches $c_1/\sqrt{3}$ as $T \rightarrow 0$.

First sound is generated by inducing periodic variations of pressure in the helium, by tapping it or other mechanical agency. Second sound is induced by temperature variations, such as produced by an oscillating heater. Pressure variations simply will not induce it to any measurable degree, a fact that defeated the earliest experimental attempts to measure it.

15.5.3 Direct Observation of Two Fluids

The two-fluid model of superfluids has often been regarded as a crude representation of a complicated underlying quantum mechanical state, but Paoletti et al. (2008) found an experimental situation in which the two fluids can be observed directly. The experiment is conducted by injecting superfluid helium with micron-sized tracer particles of frozen hydrogen, and then injecting heat into the superfluid from below. The heat is transported upwards by normal fluid, since the superfluid component carries no entropy, while superfluid moves downwards to keep density constant. Specifically, if heat \dot{Q} is injected per time into a system of area A , density

ρ , entropy per unit mass s and temperature T the velocities of the two fluids are

$$v_n = \frac{\dot{Q}}{A\rho s T}, \quad \text{That the full density } \rho \text{ appears here is due to the conventional definition of } s. \quad (15.93a)$$

$$v_s = -v_n \frac{\rho_s}{\rho_n}. \quad \text{To conserve mass density.} \quad (15.93b)$$

Most hydrogen crystals are carried upwards because of drag by the normal fluid. However, some of the crystals become trapped in the cores of vortices, and the vortices move with the superfluid. Thus the experiment produces images where some particles are drifting upwards at a speed centered on the prediction of Eq. (15.93a), while a smaller population drifts downwards, as shown in Figure 15.7.

15.5.4 Origin of Superfluidity

One common explanation for the superfluidity of helium follows from displaying the dispersion relation for propagating modes. These modes, which are the analog of phonons in crystalline solids, can be measured by neutron scattering, using Eq. (13.93), and the results of such investigation are displayed in Figure 15.8. For small values of the wave vector k , neutrons excite long waves capable of traveling long times with little scattering. These are the sound waves described in the previous section. As the wave vector increases, the dispersion curve passes through a maximum, called the *maxon peak*, and then through the *roton minimum* before proceeding to wavelengths too small for measurement. In addition, there is a class of background excitations corresponding roughly to the neutron knocking a single helium atom into motion; this sort of excitation is heavily damped, and therefore

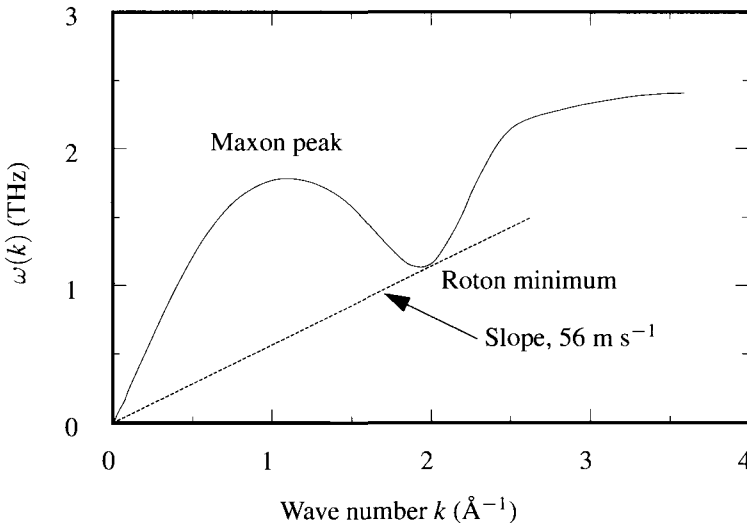


Figure 15.8. Neutron scattering data giving dispersion relation for ${}^4\text{He}$. Dashed line shows Cherenkov–Landau criterion, Eq. (14.105), for exciting an excitation in the helium. [Source: Donnelly (1991), p. 46.]

quite broad, but does not appear to have appreciable amplitude below the solid dispersion curve. According to the Cherenkov–Landau condition Eq. (14.105), illustrated by Figure 14.19, a moving particle in superfluid helium should not be able to transfer any energy until its velocity v_p reaches the smallest value $v_L \approx 56 \text{ m s}^{-1}$ (Landau’s critical velocity) for which the straight line $v_L k$ is able to touch the dispersion curve $\omega(k)$. In fact, negative ions injected into He II at pressures between 21 and 25 atmospheres and below 0.5 K begin to experience drag right around a velocity of 45 m s^{-1} .

However, explanations based upon the dispersion curve in Figure 15.8 do not provide a persuasive account of superfluidity. The velocity v_L is orders of magnitude larger than the characteristic velocities at which flows in narrow capillaries lose their superfluid character. Ions injected by Allum et al. (1976) into helium at atmospheric pressure and velocities on the order of a meter per second display the unexpected property of traveling slower in helium the more energetic they are, behavior that may only be explained quantitatively by supposing that the ions generate a large vortex ring that travels with them. These experimental facts can only be appreciated by making a conceptual shift. An experimental probe such as neutron scattering can confirm the existence of certain sorts of excited states. However, explaining superfluidity requires something different. It requires making plausible the complete absence of any excitation, whether phonon, roton, vortex, or anything else not yet classified, capable of causing a degradation of superfluid flow. For example, the argument needs to provide a way to understand why a superfluid flowing at 1 m s^{-1} through a thin rough-walled vibrating quartz channel is unable to excite any phonons in the quartz, although the quartz dispersion relation, similar to that of Figure 14.19, will permit satisfaction of Eq. (14.105) at all velocities.

The only simple explanation for such phenomena is that helium undergoes a transition to a radically new state below the λ transition. A model for this state is the weakly interacting Bose gas, which is studied as a model for superfluidity in Problem 7. For a highly interacting system such as helium, one cannot hope that the ground state of the ideal Bose gas, in which all particles occupy the same single-particle ground state, provides a quantitative description. However, one can abstract one of the features of this ground state and can guess that the ground-state density of ^4He is almost completely uniform. That is, unlike a crystal in which atoms adopt specific locations relative to one another, the ground state density of ^4He is symmetrical and featureless, except at system boundaries where it rapidly drops to zero. The helium is able to flow through complicated constricted geometries because its wave function is truly smooth, and it does not exert periodic forces upon the containing walls.

This state can be characterized by a wave function $\Psi(\vec{r})$ that gives the quantum mechanical amplitude for finding condensed helium atoms at position \vec{r} . One way to define this wave function is to suppose that one has found the complete wave function $\psi_N(\vec{r}_1 \dots \vec{r}_N)$ for N helium atoms. This wave function might be the ground state eigenfunction or else a low-lying excited state. Suppose that one also knows $\psi_{N+1}(\vec{r}_1 \dots \vec{r}_{N+1})$, which is supposed to be essentially the same as ψ_N , but

with one extra atom added at \vec{r}_{N+1} . Define

$$\Psi(\vec{r}) = \int d^N \vec{r} \psi_N^*(\vec{r}_1 \dots \vec{r}_N) \psi_{N+1}(\vec{r}_1 \dots \vec{r}_N, \vec{r}) \quad (15.94)$$

Far away from \vec{r} , the two wave functions coincide, but in its neighborhood, they differ, because ψ_{N+1} must accommodate the extra particle. The time evolution of Ψ may be determined approximately in closed form. Let

$$\hat{\mathcal{H}}_N = \sum_{l=1}^N \frac{\hat{p}_l^2}{2m} + U(\vec{r}_1 \dots \vec{r}_N) \quad (15.95)$$

be the Hamiltonian for the helium. Applying Schrödinger's equation to Eq. (15.94), almost all kinetic energy terms cancel out and

$$\begin{aligned} \frac{\partial \Psi}{\partial t} &= \int d^N \vec{r} \frac{-i}{\hbar} \left\{ \psi_{N+1} \hat{\mathcal{H}}_N \psi_N^* - \psi_N^* \mathcal{H}_{N+1} \psi_{N+1} \right\} \quad (15.96) \\ &= \int d^N \vec{r} \frac{-i}{\hbar} \psi_N^* \left\{ \frac{-\hbar^2 \nabla_{\vec{r}}^2}{2m} + U_{N+1}(\vec{r}_1 \dots \vec{r}_N, \vec{r}) - U_N(\vec{r}_1 \dots \vec{r}_N) \right\} \psi_{N+1}. \end{aligned} \quad (15.97)$$

Carrying out exactly the integrals associated with the potential energies U is a task lying somewhere between the difficult and the impossible. However, one can make a guess about the nature of the result based upon the picture of low-lying states of helium as corresponding to a featureless liquid. Suppose that the potential energies U_N and U_{N+1} have broad minima of nearly uniform energy corresponding to many equivalent locations of the atoms $\vec{r}_1 \dots \vec{r}_N$. Suppose further that for any atomic configuration not lying within this minimum, the amplitudes ψ_N and ψ_{N+1} drop very rapidly to zero. Thus, the low energy wave functions act like projection operators picking out a large number of atomic configurations of low potential energy, and the functions U_N and U_{N+1} can be replaced by their minimum values. Given this hypothesis and recalling that the chemical potential μ is defined as $\mathcal{E}_{N+1} - \mathcal{E}_N$, one has

$$\frac{-\hbar}{i} \frac{\partial \Psi}{\partial t} = \frac{-\hbar^2 \nabla^2}{2m} \Psi + \mu \Psi. \quad (15.98)$$

The wave function evolves in an effective potential given by the chemical potential for the whole fluid.

The only difference between the wave function for a stationary system and one moving at a uniform velocity \vec{v} is that the latter has a phase of $e^{im\vec{v}\cdot\vec{r}/\hbar}$. Therefore it is valuable to rewrite Ψ in terms of amplitude and phase, as

$$\Psi(\vec{r}) = \sqrt{n} e^{i\phi}. \quad (15.99)$$

Placing Eq. (15.99) into Eq. (15.98) and taking both n and ϕ to be real gives two equations, when (15.98) is separated into real and imaginary parts. The first is

$$\frac{\partial n}{\partial t} = -\vec{\nabla} \cdot \frac{\hbar}{m} \vec{\nabla} \phi n, \quad (15.100)$$

which is an equation of continuity for density n if

$$\vec{v}_s = \frac{\hbar}{m} \vec{\nabla} \phi \tag{15.101}$$

is tentatively identified as the superfluid velocity. The imaginary part of (15.98) is

$$\hbar \frac{\partial \phi}{\partial t} = -(\mu + mv_s^2/2) + \frac{\hbar^2}{2m} \frac{\nabla^2 \sqrt{n}}{\sqrt{n}}. \tag{15.102}$$

The last term of Eq. (15.102) is only appreciable near system boundaries, where the density of helium is dropping to zero, and because helium is a nearly incompressible fluid, this last term is negligible in bulk flow. Once this term is dropped, Eq. (15.102) turns into Euler's equation: Taking its gradient, and using Eq. (15.101) one has

$$m \frac{\partial \vec{v}_s}{\partial t} + m \vec{\nabla} \frac{v_s^2}{2} = -\vec{\nabla} \mu \tag{15.103}$$

$$\Rightarrow \frac{\partial \vec{v}_s}{\partial t} + (\vec{v}_s \cdot \vec{\nabla}) \vec{v}_s = -\frac{\vec{\nabla} \mu}{m} \tag{15.104}$$

Use the identity $(\vec{v}_s \cdot \vec{\nabla}) \vec{v}_s = \vec{\nabla} v_s^2/2 - \vec{v}_s \times \vec{\nabla} \times \vec{v}_s$, and use the fact that because \vec{v}_s is the gradient of a scalar, $\vec{\nabla} \times \vec{v}_s$ vanishes. Thus one obtains Eq. (15.73).

Vortices. In the course of deriving Eq. (15.104), the observation that \vec{v}_s is the gradient of the scalar function ϕ , and that therefore $\vec{\nabla} \times \vec{v}_s = 0$ was crucial. If this description of liquid helium is correct, it should therefore be impossible to set the superfluid into rotational motion. This conclusion is experimentally incorrect. It is true that if a bucket of helium is cooled below the λ point and the bucket then slowly made to rotate, the superfluid component of the helium remains stationary. However, if instead the bucket is set into rotation above the λ point, and then cooled down below the superfluid transition, the fluid continues to rotate, as can be deduced from the bowing of the liquid free surface. Nevertheless, the rotating superfluid continues to exhibit the fountain effect, so superfluidity is not completely destroyed.

The explanation of this apparent paradox is that superfluid is capable of sustaining *vortices*, rotating states at whose cores superfluidity is destroyed and the phase ϕ is not defined. They are perfectly analogous to dislocations in solids. If one assumes that the phase ϕ is destroyed only along isolated lines, but that otherwise the wave function is defined and single-valued, one arrives at the prediction that flow around superfluid vortices must be quantized in units of h/m . To see why, suppose for example that the phase ϕ is not defined along a line passing in the \hat{z} direction through the origin, and integrate the superfluid velocity \vec{v}_s along a closed contour \mathcal{C} in the x - y plane around the vortex core. The condition that the wave function Ψ be single-valued is

$$\int_{\mathcal{C}} d\vec{s} \cdot \vec{v}_s = 2\pi l \hbar / m \tag{15.105}$$

The phase ϕ can change by an integer multiple l of 2π going around a loop and leave the wave function single-valued.

$$\Rightarrow \int_{\mathcal{A}} d^2r \hat{z} \cdot \vec{\nabla} \times \vec{v}_s = \kappa = l \frac{h}{m}. \tag{15.106}$$

Using Stoke's theorem and defining κ to be the total circulation enclosed by the contour \mathcal{C} .

The quantization of vorticity has been observed directly, as shown in Figure 15.9.

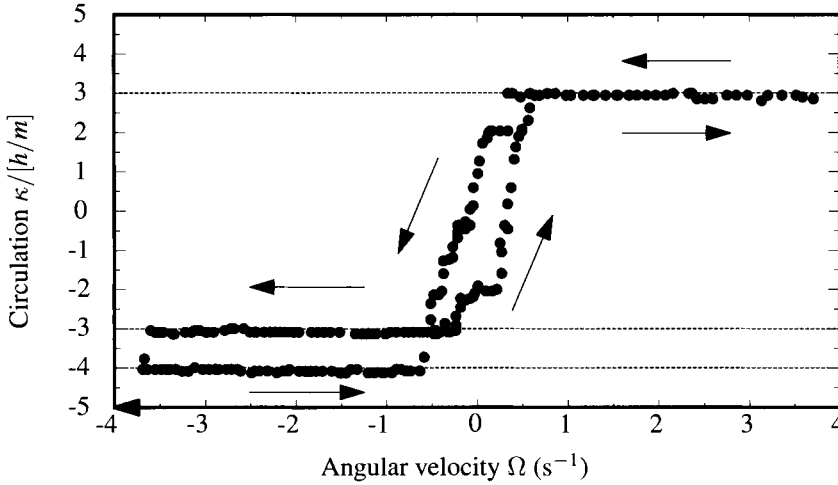


Figure 15.9. Circulation κ of ^4He vortex in units of h/m as a function of the rotation rate Ω of a container. The experiment is conducted by passing a wire of about $25\mu\text{m}$ in diameter through the superfluid and observing its vibrational modes. If a vortex is present, its core can preferentially attach to the wire. The additional angular momentum lying along the wire changes its vibrational frequency and allows a direct measurement of the circulation κ of the vortex. [The method is due to Vinen (1961), while the source of these data is Karn et al. (1980), p. 1799.]

The discussion of vortices in He II also implies a new explanation of the phenomenon of superfluidity. Suppose that superfluid is flowing through a narrow channel from one bath of helium to another. In the two baths the fluid is essentially at rest, so each of them is characterized by a constant phase of the wave function, say ϕ_1 in the first and ϕ_2 in the second. Within the narrow channel, the phase changes linearly (up to multiples of 2π from ϕ_1 to ϕ_2). In order for the flow in the channel to degrade, the gradient of ϕ must decrease. However, it must at all times be compatible with the boundary conditions, which means that the change in ϕ must in some respect be discontinuous and occur in discrete jumps. The superflow can only decay by spawning a vortex, and the difficulty of accomplishing such a transition accounts for the persistence of superfluid flow.

A quantitative theory for the decay of superfluid flow may be obtained by combining a basic fact of statistical mechanics with some results from classical hydrodynamics. The basic fact of statistical mechanics is that the probability of any configuration of energy \mathcal{E} is $\exp[-\mathcal{E}/k_B T]$. The results from hydrodynamics, discussed by Donnelly (1991) p. 23, are that a vortex ring of vorticity κ , radius R , and hollow core at constant pressure of size a in a stationary fluid of density ρ has energy

$$\mathcal{E}_v = \int d\vec{r} \frac{1}{2} \rho v^2(\vec{r}) = \frac{1}{2} \rho \kappa^2 R \left(\eta - \frac{3}{2} \right), \quad \eta = \ln(8R/a) \quad (15.107)$$

and momentum

$$P_v = \left| \int d\vec{r} \rho \vec{v}(\vec{r}) \right| = \rho \kappa \pi R^2 \quad (15.108)$$

and moves at velocity

$$v_v = \frac{\partial \mathcal{E}_v}{\partial P_v} = \frac{\kappa(\eta - \frac{1}{2})}{4\pi R}. \quad \text{This is the rate at which the whole vortex drifts, like a smoke ring.} \quad (15.109)$$

Consider now superfluid flowing at velocity v_s in a pipe. If a vortex forms in this moving superfluid, the change in energy due to the vortex will be

$$\mathcal{E}_{\text{tot}} = \mathcal{E}_v - P_v v_s \quad \text{If the velocity field of the vortex has } \vec{v}_s \text{ subtracted from it and substituted into Eq. (15.107), this form results immediately, using Eq. (15.108) and omitting the constant energy of flow } \vec{v}_s. \quad (15.110)$$

For small radii R , the energy of a system with a vortex increases with R , but eventually the vortex is sufficiently successful in reducing the kinetic energy of fluid motion that it becomes energetically favorable to make it even larger. The saddle point in energy beyond which this change occurs is found from

$$\frac{d\mathcal{E}_{\text{tot}}}{dR} = 0 \Rightarrow \frac{\partial \mathcal{E}_v}{\partial P_v} \frac{\partial P_v}{\partial R} - \frac{\partial P_v}{\partial R} v_s = 0 \Rightarrow v_s = v_v. \quad (15.111)$$

That is, the energy of the vortex reaches the saddle point when it moves against the prevailing flow at just the speed needed to sit stationary in the laboratory frame, as shown by Langer and Fisher (1967).

This theory predicts that superflows will decay through formation of vortices of radius $R_c = \kappa(\eta - \frac{1}{2})/4\pi v_s$, whose energy is $\mathcal{E}_c = \frac{1}{2} \rho \kappa^2 R_c (\eta - \frac{3}{2})$ and whose probability of formation is proportional to $\exp[-\beta \mathcal{E}_c]$. Superflows should last exponentially longer as either the temperature or their velocity decreases. A comparison of these predictions with experiment was carried out by Langer and Reppy (1970).

15.5.5 Lagrangian Theory of Wave Function

Because the the wave function of liquid helium is rather a mysterious object, it is interesting to obtain equations for it in a more systematic way, one that provides a general procedure for finding effective equations of motion in complicated many-body systems. That is, there is a definite set of equations governing the motion of all the helium atoms, but the vast number of atoms and the strength of their interaction makes a direct solution impossible. On the other hand, there is every reason to suspect that most important features of the helium are encoded in a single wave function, a *collective coordinate*, that is much simpler to understand. The question is how to pass from the microscopic laws for the helium atoms to dynamical rules for the wave function in a controlled and consistent way.

Demircan et al. (1996) showed that one way to proceed is to use the formalism of Appendix B.3, which shows that the time-dependent Schrödinger equation derives from a Lagrangian. If one can think of a good approximate wave function for

helium, the formalism describes how it will evolve in time. Feynman (1953) suggested a way of building a wave function. Imagine that the ground-state wave function of helium in some experimental geometry is known, and call it $\phi(\vec{r}_1 \dots \vec{r}_N)$. This ground state wave function may be tremendously complicated, and cannot be found in practice, but in the end one will need to know surprisingly little about it. Only three things need to be assumed. First, it is a true ground state, so

$$i\hbar \frac{\partial}{\partial t} \phi = \left[\sum_l -\frac{\hbar^2 \nabla_l^2}{2m} + \hat{U} \right] \phi. \quad \nabla_l \text{ means } \frac{\partial}{\partial \vec{r}_l}. \quad (15.112)$$

The interactions described by the potential \hat{U} may be quite strong. Second, because ${}^4\text{He}$ is a boson, ϕ is symmetric under interchange of any of its arguments. Third, because ϕ is a ground state, there are no currents flowing anywhere in it, which means that

$$\phi \nabla_l \phi^* - \phi^* \nabla_l \phi = 0. \quad (15.113)$$

Next imagine that all the low-lying excited states of the wave function are of the form

$$\psi(\vec{r}_1 \dots \vec{r}_N) = \exp\left[\sum_l \Psi(\vec{r}_l, t)\right] \phi(\vec{r}_1 \dots \vec{r}_N) = e^{\sum_l \Psi_l} \phi. \quad (15.114)$$

The essential point in this *single-mode approximation* is that there is only a single function $\Psi(\vec{r}, t)$ shared by all the particles; this is the wave function of ${}^4\text{He}$. The wave functions in Eq. (15.114) are not guaranteed to be normalized; one can divide through by a normalization factor at this point, but it is simpler to use a Lagrange multiplier later that ensures $|\psi|^2$ integrates to one.

Adopt abbreviated notation in which Ψ_l is shorthand for $\Psi(\vec{r}_l, t)$, and the arguments of ϕ are not indicated explicitly. The effective Lagrangian defined by Eq. (B.16) corresponding to Eq. (15.114) is

$$\mathcal{L} = \int d^N \vec{r} \phi^* e^{\sum_{l'} \Psi_{l'}} \left[i\hbar \frac{\partial}{\partial t} + \sum_l \frac{\hbar^2 \nabla_l^2}{2m} - \hat{U} \right] e^{\sum_{l''} \Psi_{l''}} \phi. \quad (15.115)$$

In evaluating \mathcal{L} , the only term that is difficult to evaluate is the one involving the spatial gradient:

$$\int e^{\sum_{l'} \Psi_{l'}} \phi^* \nabla_l^2 e^{\sum_{l''} \Psi_{l''}} \phi \quad (15.116)$$

$$= \int e^{\sum_{l'} \Psi_{l'}} \phi^* \left[\phi \nabla_l^2 e^{\sum_{l''} \Psi_{l''}} + 2(\nabla_l e^{\sum_{l''} \Psi_{l''}}) \cdot (\vec{\nabla}_l \phi) + e^{\sum_{l''} \Psi_{l''}} \nabla_l^2 \phi \right] \quad (15.117)$$

Expand derivative.

$$= \int e^{\sum_{l'} \Psi_{l'}} \left[|\phi|^2 \nabla_l^2 e^{\sum_{l''} \Psi_{l''}} + (\vec{\nabla}_l e^{\sum_{l''} \Psi_{l''}}) \cdot (\vec{\nabla}_l |\phi|^2) + e^{\sum_{l''} \Psi_{l''}} \phi^* \nabla_l^2 \phi \right] \quad (15.118)$$

Using Eq. (15.113). Only middle term changes.

$$= \int e^{\sum_{l'} \Psi_{l'}^*} |\phi|^2 \nabla_l^2 e^{\sum_{l'} \Psi_{l'}} - |\phi|^2 \vec{\nabla}_l \cdot e^{\sum_{l'} \Psi_{l'}} (\vec{\nabla}_l e^{\sum_{l'} \Psi_{l'}}) + e^{\sum_{l'} \Psi_{l'} + \Psi_{l'}} \phi^* \nabla_l^2 \phi \quad (15.119)$$

Integrate middle term by parts.

$$= \int e^{\sum_{l'} \Psi_{l'} + \Psi_{l'}} \left[\phi^* \nabla_l^2 \phi - |\phi|^2 |\nabla_l \Psi_l|^2 \right]. \quad \text{Two terms cancel.} \quad (15.120)$$

With the use of Eqs. (15.112) and (15.120) it is simple to evaluate \mathcal{L} from Eq. (15.115) and find

$$\mathcal{L} = \int d^N \vec{r} |\phi|^2 e^{\sum_{l'} \Psi_{l'} + \Psi_{l'}} \sum_l \left[i\hbar \frac{\partial \Psi_l}{\partial t} - \frac{\hbar^2}{2m} |\vec{\nabla}_l \Psi_l|^2 \right]. \quad (15.121)$$

An approximation to Schrödinger's equation is obtained by taking the variation of \mathcal{L} with respect to $\Psi(\vec{r}, t)$. In order to ensure that ψ remain normalized, the variation will be carried out with a constraint enforced by a Lagrange multiplier μ , so the equation of motion for Ψ is

$$\frac{\delta}{\delta \Psi^*} \left[\mathcal{L} - \mu \int d^N \vec{r} |\phi|^2 e^{\sum_{l'} \Psi_{l'} + \Psi_{l'}} \right] = 0. \quad \begin{array}{l} \text{Enforce constraints by taking the thing that is} \\ \text{supposed to remain fixed, multiplying it by a} \\ \text{constant, and adding it to the Lagrangian.} \end{array} \quad (15.122)$$

Before completing the equation of motion for Ψ , it is helpful to define two quantities. The density $n_1(\vec{r})$ is

$$n_1(\vec{r}) = \int d^N \vec{r}' |\phi|^2 e^{\sum_{l'} \Psi_{l'} + \Psi_{l'}} \sum_l \delta(\vec{r} - \vec{r}_l) \quad (15.123)$$

and the structure function $S(\vec{r}, \vec{r}')$ is

$$S(\vec{r}, \vec{r}') = \frac{\mathcal{V}}{N} \int d^N \vec{r} |\phi|^2 e^{\sum_{l'} \Psi_{l'} + \Psi_{l'}} \sum_{ll'} \delta(\vec{r} - \vec{r}_l) \delta(\vec{r}' - \vec{r}_{l'}). \quad (15.124)$$

The functional derivative with respect to Ψ^* in (15.122) has two pieces. First, there is a contribution from $|\vec{\nabla}_l \Psi_l|^2$, and second there is one from the factors of $\exp[\sum_{l'} \Psi_{l'}^*]$. Performing the functional derivative with the methods of Appendix B gives

$$-\frac{\hbar^2}{2m} \vec{\nabla} \cdot n_1 \vec{\nabla} \Psi(\vec{r}) = \sum_{ll'} \int d^N \vec{r}' |\psi|^2 \delta(\vec{r}_{l'} - \vec{r}) \left[i\hbar \frac{\partial \Psi_l}{\partial t} - \frac{\hbar^2}{2m} |\nabla \Psi_l|^2 - \mu \right] \quad (15.125)$$

$$= \frac{N}{\mathcal{V}} \int d^N \vec{r}' \left[i\hbar \frac{\partial \Psi(\vec{r}')}{\partial t} - \frac{\hbar^2}{2m} |\nabla \Psi(\vec{r}')|^2 - \mu \right] S(\vec{r}, \vec{r}'). \quad (15.126)$$

To proceed further, assume that Ψ is small, and that therefore anything involving more than one power of Ψ may be neglected. In particular, any spatial variation of n_1 can be neglected, and the term involving $|\nabla \Psi(\vec{r}')|^2$ can be thrown out. $S(\vec{r}, \vec{r}')$ becomes the static structure factor of the ground-state wave function ϕ , and because

the ground state should be translationally invariant, S should depend only upon $\vec{r} - \vec{r}'$. Taking the Fourier transform of Eq. (15.126) gives

$$\frac{\hbar^2 k^2}{2m} \Psi(\vec{q}, \omega) = [\hbar\omega \Psi(\vec{q}, \omega) - \mu \delta(\vec{q}) \delta(\omega)] S(\vec{q}) \quad (15.127)$$

$$\Rightarrow \hbar\omega(\vec{q}) = \frac{\hbar^2 q^2}{2m S(\vec{q})} = \frac{6.02 k_B [q \cdot \text{\AA}]^2}{S(q)} \text{K}, \quad \text{So long as one stays away from } \omega = 0, \vec{q} = 0. \quad (15.128)$$

where $S(\vec{q})$ is precisely the static structure factor measured in neutron scattering. Equation (15.128) is due to Feynman (1953) and permits comparison of excitation energies (obtained with inelastic neutron scattering) with the static structure factor, as shown in Figure 15.10. The agreement shown in the figure is good only within a factor of two and has been improved substantially through elaboration of the theory, as discussed by Feynman (1972), Chapter 11, and Glyde (1994).

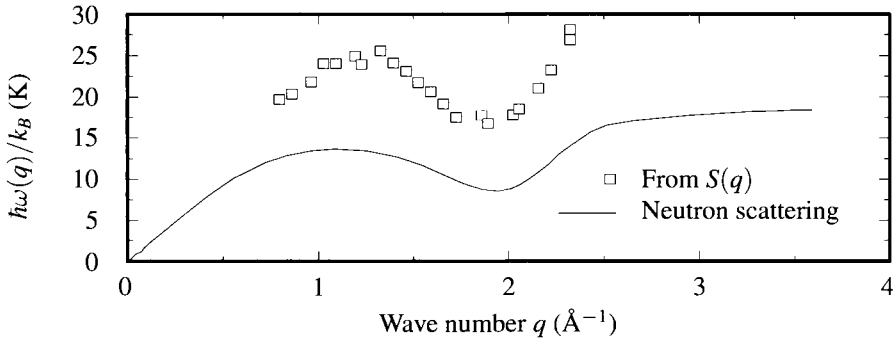


Figure 15.10. Comparison of Feynman's expression (15.128) for excitations in helium with direct measurement using neutron scattering. The neutron scattering data are from Donnelly (1991) p. 46, and data for $S(q)$ are from Svensson et al. (1980).

15.5.6 Superfluid ^3He

Because ^3He particles are fermions, they cannot drop into a Bose condensed state with the same ease as ^4He . They nevertheless form a superfluid. The *Pomeranchuk effect* makes it possible to reach very low temperatures in ^3He . Pomeranchuk observed that at temperatures below 100 mK the entropy of liquid ^3He falls below that of the solid; under pressure, ^3He nucleates solid crystals that cool the cell in which they grow. Building such cells, Osheroff, Richardson, and Lee (1972) observed slight changes in the slope of pressure versus temperature at temperatures around 2.5 mK, and pressures around 30 atmospheres. They first attributed these anomalies to phase changes in the solid, but subsequently determined that the liquid was changing phase and becoming superfluid. Essentially, pairs of ^3He nuclei join together forming effective Bose particles, which can then condense, in a manner reminiscent of superconductivity. Wheatley (1975) and Leggett (1975) reviewed the experimental and theoretical situation not long after the original discovery of

superfluidity, while Osheroff (1997), Richardson (1997), Lee (1997), and Leggett (2006) provide more recent overviews.

Problems

1. **Viscosity obtained from kinetic theory:** Consider a shear flow where $dv_x/dy = v'$. Viscosity may be calculated by drawing a plane at $y = 0$ in Figure 15.1 and finding the rate σ_{xy} at which momentum p_x in the x direction travels across it.

- (a) Argue that

$$\sigma_{xy} = - \langle p_x v_y \delta(\vec{r}) \rangle. \quad (15.129)$$

- (b) The average is not an equilibrium average, because the fluid is flowing, and therefore is not in equilibrium, and Eq. (15.129) would vanish in equilibrium. The *Boltzmann equation*, derived in Section 17.2, deals with this problem by defining $g(\vec{r}, \vec{v}, t)$ to be the normalized probability that a particle has position \vec{r} , and velocity \vec{v} at time t . The time evolution of g is given by

$$\frac{\partial g}{\partial t} = - \frac{\partial}{\partial \vec{r}} \cdot \vec{v} g - \frac{g - g_{\text{eq}}}{\tau}, \quad (15.130)$$

where τ is a characteristic time for a nonequilibrium state to approach equilibrium once driving forces are removed, and g_{eq} is the distribution function

$$g_{\text{eq}}(\vec{r}, \vec{v}) = n \sqrt{\frac{m}{2\pi k_B T}}^3 \exp \left[- \frac{\beta m}{2} ([v_x - v'_y]^2 + v_y^2 + v_z^2) \right]. \quad (15.131)$$

Here n is density, and $v' = dv_x/dy$. At every point in space, this distribution takes the form that equilibrium would demand for the local conditions. So Boltzmann's equation says that the system always tends to drift toward local equilibrium. Show that the solution of Eq. (15.130) is

$$g = \int^y \frac{dy'}{v_y \tau} g_{\text{eq}} e^{-(y-y')/v_y \tau}. \quad (15.132)$$

- (c) Show that

$$\sigma_{xy} = n \tau k_B T v', \quad (15.133)$$

and that the viscosity can therefore be written as

$$\eta = \frac{1}{3} n m l_T \bar{v}, \quad (15.134)$$

where \bar{v} is the root mean square velocity in equilibrium at temperature T , and $l_T = \tau \bar{v}$ is the mean free path.

2. **Flow resistance of a sphere:** Suppose that a sphere of radius R moves at velocity $\vec{u} = u\hat{z}$ in a viscous incompressible liquid. The velocity u is sufficiently slow that the nonlinear term $(\vec{v} \cdot \vec{\nabla})\vec{v}$ is to be neglected everywhere. The goal is to calculate the force that must be applied to the sphere to keep it moving at constant velocity, as originally determined by Stokes (1851).

Move to a reference frame traveling with the sphere; the sphere is stationary, and the fluid moves at velocity $-\vec{u}$ far away. The flow pattern is steady in this reference frame and obeys

$$\eta \nabla^2 \vec{v} = \vec{\nabla} P. \quad (15.135)$$

- (a) Because the liquid is incompressible, $\vec{\nabla} \cdot \vec{v} = 0$. Therefore, \vec{v} results from the curl of a vector potential \vec{A} , $\vec{v} = \vec{\nabla} \times \vec{A}$. Move to spherical polar coordinates. Assume that the solution $\vec{v}(r, \theta, \phi)$ is independent of ϕ and that $v_\phi = 0$. Show that only A_ϕ needs to be considered, and express \vec{v} in terms of A_ϕ .
- (b) From Eq. (15.135) it follows that

$$\vec{\nabla} \times \nabla^2 \vec{v} = 0. \quad (15.136)$$

Show that

$$\left[\frac{1}{r} \frac{\partial^2}{\partial r^2} r + \frac{1}{r^2} \frac{\partial^2}{\partial \theta^2} + \cot \theta \frac{1}{r^2} \frac{\partial}{\partial \theta} - \frac{1}{r^2 \sin^2 \theta} \right]^2 A_\phi = 0. \quad (15.137)$$

- (c) Because far from the sphere, $A_\phi \propto r \sin \theta$, assume that

$$A_\phi = f(r) \sin \theta. \quad (15.138)$$

Show that

$$\left[\frac{1}{r} \frac{\partial^2}{\partial r^2} r - \frac{2}{r^2} \right]^2 f(r) = 0. \quad (15.139)$$

- (d) Show that

$$f(r) = Ar^3 + Br + \frac{C}{r^2} + D, \quad (15.140)$$

with

$$A = 0, \quad B = -u/2, \quad C = -R^3 u/4, \quad \text{and } D = 3Ru/4. \quad (15.141)$$

- (e) Show that the pressure is given by

$$P = P_0 + \frac{3}{2} u \eta \frac{R}{r^2} \cos \theta. \quad P_0 \text{ is a constant background pressure.} \quad (15.142)$$

- (f) The force on the sphere is given by integrating the tangential component of the stress tensor in an appropriate fashion over its surface, including contributions both from pressure and viscosity. Expressing the relevant components of Eq. (15.13) in spherical coordinates as

$$\sigma_{rr} = 2\eta \frac{\partial v_r}{\partial r} - P \quad (15.143)$$

$$\sigma_{r\theta} = \eta \left(\frac{1}{r} \frac{\partial v_r}{\partial \theta} + \frac{\partial v_\theta}{\partial r} - \frac{v_\theta}{r} \right) \quad (15.144)$$

show that the downward force F on the sphere is

$$F = 6\pi\eta Ru \quad (15.145)$$

3. **Vortex I:** The vorticity $\vec{\omega}$ of a flow is defined to be $\vec{\omega} = \vec{\nabla} \times \vec{v}$. A vortex is a swirling flow pattern containing a large amount of vorticity in its core.
- (a) Show that the vorticity of a two-dimensional flow \vec{v} living in the x - y plane points entirely in the z direction.
- (b) Consider the flow \vec{v} that in cylindrical coordinates (r, ϕ) has the form

$$v_r = 0, \quad v_\phi = \frac{\kappa}{r}. \quad (15.146)$$

Show that the vorticity of this flow vanishes.

- (c) Show, however, that the line integral of \vec{v} along any circle surrounding the origin is constant, and find the constant.
- (d) Using Stokes' theorem, relate this integral to an integral over ω , showing that the vorticity has a delta function singularity at the origin.
4. **Vortex II:** It is possible to construct solutions of Euler's equation that behave as a vortex but without any singularities in the flow field. Thus the previous problem provides a rough description of a vortex seen from far away, while this one focuses upon a possible structure for the core.

- (a) By taking the curl of Euler's equation, show that the vorticity obeys

$$\frac{\partial \vec{\omega}}{\partial t} + (\vec{v} \cdot \vec{\nabla}) \vec{\omega} = (\vec{\omega} \cdot \vec{\nabla}) \vec{v}. \quad (15.147)$$

- (b) Consider a time independent, incompressible, two-dimensional flow \vec{v} . Argue that because the flow is incompressible, there exists a stream function ψ with

$$\vec{v} = \left(-\frac{\partial \psi}{\partial y}, \frac{\partial \psi}{\partial x} \right). \quad (15.148)$$

- (c) Rewrite Eq. (15.147) for this steady two-dimensional flow by eliminating \vec{v} in favor of the stream function ψ .

- (d) Show that the preceding equation is satisfied whenever $\omega_z = f(\psi)$, where f is an arbitrary function, and rewrite this condition entirely in terms of ψ .
- (e) Construct a vortex by moving to cylindrical coordinates and by requiring for $r \leq a$:

$$\omega_z = -k^2\psi. \quad k \text{ is a constant.} \quad (15.149)$$

Find a solution of Eq. (15.149) that is proportional to $\sin \phi$ and to a Bessel function of kr .

- (f) For $r \geq a$ require

$$\psi = \left(r - \frac{a^2}{r}\right)U \sin \phi. \quad (15.150)$$

Find the conditions at $r = a$ that make velocity and vorticity continuous, and employ these conditions to complete the solution for the flow field near the center of a vortex.

5. Chain dynamics:

- (a) Using Eq. (15.26), verify Eq. (15.35).
- (b) Verify Eq. (15.40).

6. **Frequency dependence of viscosity:** Assume that W_{xy} in Eq. (15.38) varies as $W_0 \cos \omega t$. Show that the shear stress is given by Eq. (15.49).

7. **Weakly interacting Bose gas:** Bogoliubov (1947) treated the problem of superfluidity in a fashion quite similar to his method for superconductivity, presented in Section 27.3.4. Consider the Hamiltonian for Bose particles

$$\hat{\mathcal{H}} = \sum_{\vec{q}} \epsilon_{\vec{q}} \hat{a}_{\vec{q}}^\dagger \hat{a}_{\vec{q}} + \frac{U}{2\mathcal{V}} \sum_{\vec{k}, \vec{k}', \vec{q}} \hat{a}_{\vec{k}' - \vec{q}}^\dagger \hat{a}_{\vec{k} + \vec{q}}^\dagger \hat{a}_{\vec{k}} \hat{a}_{\vec{q}}. \quad (15.151)$$

$\epsilon_{\vec{q}} = \hbar^2 q^2 / 2m$ is the kinetic energy of a noninteracting Bose particle, and U has dimensions of energy times an interaction volume and will be assumed to be very small. In the ground state, a macroscopic number of particles inhabits the single-particle state $\vec{q} = 0$. The occupation number of $\vec{q} = 0$ should be very high for low-lying excited states as well.

Whenever \hat{a}_0 or \hat{a}_0^\dagger act on a state, they will change the occupation number of the $\vec{q} = 0$ state, it is true, but the change will be negligible compared with the N_0 particles already in this state. Therefore, it should be accurate to replace \hat{a}_0 and \hat{a}_0^\dagger by $\sqrt{N_0}$ whenever they appear. Furthermore make the mean-field approximation of excluding from the interaction term of Eq. (15.151) all terms except those where two or more of the indices equal zero.

- (a) Show that the Hamiltonian becomes

$$\hat{\mathcal{H}} = \sum_{\vec{q}} \epsilon_{\vec{q}} \hat{a}_{\vec{q}}^\dagger \hat{a}_{\vec{q}} + \frac{N_0^2 U}{2\mathcal{V}} + \frac{N_0 U}{2\mathcal{V}} \sum_{\vec{q} \neq 0} [\hat{a}_{-\vec{q}}^\dagger \hat{a}_{\vec{q}}^\dagger + \hat{a}_{-\vec{q}} \hat{a}_{\vec{q}} + 4\hat{a}_{\vec{q}}^\dagger \hat{a}_{\vec{q}}]. \quad (15.152)$$

(b) Using the fact that the total number of particles

$$N = N_0 + \sum_{\vec{q} \neq 0} \hat{a}_{\vec{q}}^\dagger \hat{a}_{\vec{q}} \quad (15.153)$$

is a conserved quantity, rewrite Eq. (15.152), up to a constant, as

$$\hat{\mathcal{H}} = \sum_{\vec{q}} \left[\epsilon_{\vec{q}} + \frac{NU}{\mathcal{V}} \right] \hat{a}_{\vec{q}}^\dagger \hat{a}_{\vec{q}} + \frac{NU}{2\mathcal{V}} \sum_{\vec{q} \neq 0} [\hat{a}_{-\vec{q}}^\dagger \hat{a}_{\vec{q}}^\dagger + \hat{a}_{-\vec{q}} \hat{a}_{\vec{q}}]. \quad (15.154)$$

(c) Introduce the canonical Bogoliubov transformation

$$\hat{a}_{\vec{q}} = u_{\vec{q}} \hat{\gamma}_{\vec{q}} + v_{\vec{q}} \hat{\gamma}_{-\vec{q}}^\dagger \quad (15.155a)$$

$$\hat{a}_{\vec{q}}^\dagger = u_{\vec{q}} \hat{\gamma}_{\vec{q}}^\dagger + v_{\vec{q}} \hat{\gamma}_{-\vec{q}}. \quad (15.155b)$$

Show that for $\hat{\gamma}_{\vec{q}}$ to preserve the Bose commutation relations of Eq. (C.5), one must have $u_{\vec{q}}^2 - v_{\vec{q}}^2 = 1$.

(d) Set out to diagonalize the Hamiltonian. The task can be accomplished if $u_{\vec{q}} = u_{-\vec{q}}$ and $v_{\vec{q}} = v_{-\vec{q}}$, so assume these relations. Putting Eqs. (15.155) into (15.154), find the condition on $u_{\vec{q}}$ and $v_{\vec{q}}$ needed to ensure that the coefficient of $\hat{\gamma}_{\vec{q}}^\dagger \hat{\gamma}_{-\vec{q}}^\dagger$ vanishes. Imposing this condition is enough to diagonalize the Hamiltonian.

(e) Note for later reference that $u_{\vec{q}} v_{\vec{q}}$ must be less than zero. Solve for $v_{\vec{q}}^2$ and $u_{\vec{q}}^2$.

(f) Insert the expressions for $v_{\vec{q}}$ and $u_{\vec{q}}$ into Eq. (15.154), remembering that $u_{\vec{q}} v_{\vec{q}} < 0$, putting the Hamiltonian into the form

$$\sum_{\vec{q}} \mathcal{E}_{\vec{q}} \hat{\gamma}_{\vec{q}}^\dagger \hat{\gamma}_{\vec{q}} + \text{const.} \quad (15.156)$$

(g) In the limit $\vec{q} \rightarrow 0$, $\mathcal{E}_{\vec{q}} = \hbar c q$. Thus even weak interactions are able to change the low-energy excitations from free particle form to sound. Find the sound speed c .

References

- D. R. Allum, P. V. E. McClintock, A. Phillips, and R. M. Bowley (1976), The breakdown of superfluidity in liquid ^4He : An experimental test of Landau's theory, *Philosophical Transactions of the Royal Society of London A*, **284**, 179–224.
- E. L. Andronikashvili (1948), The temperature dependence of the normal density of helium II, *Journal of Experimental and Theoretical Physics (U.S.S.R.)*, **18**, 424.
- G. K. Batchelor (1967), *An Introduction to Fluid Dynamics*, Cambridge University Press, Cambridge.
- R. B. Bird and C. F. Curtiss (1984), Fascinating polymeric liquids, *Physics Today*, **37**(1), 36–43.
- R. B. Bird, C. F. Curtiss, R. C. Armstrong, and O. Hassager (1987), *Dynamics of Polymeric Liquids*, vol. 2: Kinetic Theory, John Wiley and Sons, New York.

- N. N. Bogoliubov (1947), On the theory of superfluidity, *Journal of Physics*, **11**, 23–32. Reprinted in Pines (1961), pp. 292–301.
- P. Bridgeman (1949), *The Physics of High Pressure*, G. Bell and Sons, London. Plasticity of metals under hydrostatic pressure discussed on pp. 408–413.
- D. M. Ceperley (1995), Path integrals in the theory of condensed helium, *Reviews of Modern Physics*, **67**, 279–355.
- E. G. D. Cohen (1984), The kinetic theory of fluids—an introduction, *Physics Today*, **37**(1), 64–73.
- P.-G. de Gennes (1979), *Scaling Concepts in Polymer Physics*, Cornell University Press, Ithaca NY.
- E. Demircan, P. Ao, and Q. Niu (1996), Vortex dynamics in superfluids: Cyclotron-type motion, *PRB*, **54**, 10027–10034.
- M. Doi and S. F. Edwards (1986), *The Theory of Polymer Dynamics*, Clarendon Press, Oxford.
- R. J. Donnelly (1991), *Quantized Vortices in Helium II*, Cambridge University Press, Cambridge.
- R. J. Donnelly (1995), The discovery of superfluidity, *Physics Today*, **48**(7), 30–36.
- P. G. Drazin and W. H. Reid (1981), *Hydrodynamic Stability*, Cambridge University Press, Cambridge.
- T. E. Faber (1995), *Fluid Dynamics for Physicists*, Cambridge University Press, Cambridge.
- J. D. Ferry (1980), *Viscoelastic Properties of Polymers*, John Wiley and Sons, New York.
- R. P. Feynman (1953), Atomic theory of liquid helium near absolute zero, *Physical Review*, **91**, 1301–1308.
- R. P. Feynman (1972), *Statistical Mechanics*, Addison-Wesley, Redwood City, CA.
- W. I. Glaberson and K. W. Schwarz (1987), Quantized vortices in superfluid helium-4, *Physics Today*, **40**(2), 54–60.
- H. H. Glyde (1994), *Excitations in Liquid and Solid Helium*, Clarendon Press, Oxford.
- I. S. Grigoriev and E. Z. Meilkhov, eds. (1997), *Handbook of Physical Quantities*, CRC Press, Boca Raton, FL.
- A. Y. Grosberg and A. R. Khokhlov (1994), *Statistical Physics of Macromolecules*, AIP Press, New York.
- P. Hakonen and O. V. Lounasmaa (1987), Vortices in rotating superfluid ^3He , *Physics Today*, **40**(2), 70–78.
- R. Hill (1950), *The Mathematical Theory of Plasticity*, The Clarendon Press, Oxford.
- P. W. Karn, D. R. Starks, and W. Zimmerman (1980), Observation of quantization of circulation in rotating superfluid ^4He , *Physical Review B*, **21**, 1797–1805.
- I. M. Khalatnikov (1965), *An Introduction to the Theory of Superfluidity*, W A Benjamin Inc., New York.
- S. H. Lamb (1945), *Hydrodynamics*, sixth ed., Dover Publications, New York.
- L. D. Landau and E. M. Lifshitz (1980), *Statistical Physics, Part I*, 3rd ed., Pergamon Press, Oxford.
- L. D. Landau and E. M. Lifshitz (1987), *Fluid Mechanics*, 2nd ed., Butterworth and Heinemann, Oxford.
- C. T. Lane (1962), *Superfluid Physics*, McGraw-Hill, New York.
- J. S. Langer and M. E. Fisher (1967), Intrinsic critical velocity of a superfluid, *Physical Review Letters*, **19**, 560–563.
- J. S. Langer and J. D. Reppy (1970), Intrinsic critical velocities in superfluid helium, in *Progress in Low Temperature Physics*, C. J. Gorter, ed., vol. 6, pp. 1–35, North-Holland, Amsterdam.
- D. M. Lee (1997), The extraordinary phases of liquid ^3He , *Reviews of Modern Physics*, **69**, 645–665.
- A. J. Leggett (1975), A theoretical description of the new phases of liquid ^3He , *Reviews of Modern Physics*, **47**, 331–414.
- A. J. Leggett (2004), Nobel Lecture: Superfluid ^3He : the early days as seen by a theorist, *Reviews of Modern Physics*, **76**(3), 999.

- A. J. Leggett (2006), *Quantum Liquids: Bose condensation and Cooper pairing in condensed matter systems*, Oxford University Press, Oxford.
- J. Lubliner (1990), *Plasticity Theory*, Macmillan, New York.
- A. S. Monin and A. M. Yaglom (1971–1975), *Statistical Fluid Mechanics; Mechanics of Turbulence*, MIT Press, Cambridge MA.
- S. K. Nemirovskii and W. Fiszdon (1995), Chaotic quantized vortices and hydrodynamic processes in superfluid helium, *Reviews of Modern Physics*, **67**, 37–84.
- P. Nozières and D. Pines (1988), *The Theory of Quantum Liquids*, vol. 2, Addison-Wesley, Redwood City, CA.
- A. Oron, S. H. Davis, and S. G. Bankoff (1997), Long-scale evolution of thin liquid films, *Reviews of Modern Physics*, **69**, 931–980.
- D. D. Osheroff (1997), Superfluidity in ^3He : Discovery and understanding, *Reviews of Modern Physics*, **69**, 667–681.
- D. D. Osheroff, R. C. Richardson, and D. M. Lee (1972), Evidence for a new phase of solid He^3 , *Physical Review Letters*, **28**, 885–888.
- M. S. Paoletti, R. B. Fiorito, K. R. Sreenivasan, and D. P. Lathrop (2008), Visualization of superfluid helium flow, *Journal of the Physical Society of Japan*, **77**, 111 007/1–7.
- V. P. Peshkov (1946), Determination of the velocity of propagation of second sound in helium II, *Journal of Experimental and Theoretical Physics (U.S.S.R.)*, **16**, 1000.
- D. Pines (1961), *The Many-Body Problem*, W. A. Benjamin, Reading, MA.
- R. C. Richardson (1997), The Pomeranchuk effect [superfluid ^3He], *Reviews of Modern Physics*, **69**, 683–690.
- R. C. Richardson and E. N. Smith, eds. (1988), *Experimental Techniques in Condensed Matter Physics at Low Temperatures*, Addison-Wesley, Redwood City, CA.
- P. E. Rouse (1953), A theory of the linear viscoelastic properties of dilute solutions of polymers, *Journal of Chemical Physics*, **21**, 1272–1280.
- M. M. Salomaa and G. E. Volovik (1987), Quantized vortices in superfluid ^3He , *Reviews of Modern Physics*, **59**, 533–613.
- P. Schiffer and D. D. Osheroff (1995), Nucleation of the AB transition in superfluid ^3He : Surface effects and baked Alaska, *Reviews of Modern Physics*, **67**, 491–501.
- E. B. Sonin (1987), Vortex oscillations and hydrodynamics of rotating superfluids, *Reviews of Modern Physics*, **59**, 87–155.
- G. G. Stokes (1851), On the effect of internal friction of fluids on the motion of pendulums, *Cambridge Transactions*, **9**, 8.
- G. Stolovitzky and K. R. Sreenivasan (1994), Kolmogorov’s refined similarity hypotheses for turbulence and general stochastic processes, *Reviews of Modern Physics*, **66**, 229–240.
- E. C. Svensson, V. F. Sears, A. D. B. Woods, and P. Martel (1980), Neutron-diffraction study of the static structure factor and pair correlations in liquid ^4He , *Physical Review B*, **21**, 3638–3651.
- H. L. Swinney and J. P. Gollub (1978), The transition to turbulence, *Physics Today*, **31**(8), 41–44.
- D. R. Tilley and J. Tilley (1990), *Superfluidity and Superconductivity*, Adam Hilger, Bristol.
- W. F. Vinen (1961), The detection of single quanta of circulation in liquid helium II, *Proceedings of the Royal Society of London*, **A260**, 218–234.
- J. C. Wheatley (1975), Experimental properties of superfluid ^3He , *Reviews of Modern Physics*, **47**, 415–470.
- J. Wilks (1967), *The Properties of Liquid and Solid Helium*, Clarendon Press, Oxford.
- B. H. Zimm (1956), Dynamics of polymer molecules in dilute solution: Viscoelasticity, flow, birefringence, and dielectric loss, *Journal of Chemical Physics*, **24**, 269–278.

Part IV

ELECTRON TRANSPORT

16. Dynamics of Bloch Electrons

16.1 Introduction

Condensed matter physics provides an enormously successful account of the electrical properties of solids. The reason for this success is not so much because agreement between theory and experiment is better in this area than in any other, but because many surprising and productive qualitative concepts have emerged. The central idea is that response of a solid to weak electric and magnetic fields is determined by the energy band curves $\mathcal{E}_{n\vec{k}}$. First derivatives of these curves give effective velocities of electrons, while second derivatives give effective masses. When the second derivatives are negative, the solid can behave as if filled with particles with positive charge, called holes. All these dynamical phenomena result in fact from interactions between electrons and the lattice potential, but the simple ideas are so powerful that it is possible to forget all the theoretical underpinnings and adopt a few apparently classical dynamical rules. Much of modern electronics is built on this foundation.

16.1.1 Drude Model

The electron was only a few years old when the first theories of electrical conduction of metals appeared, by Drude (1900), Thomson (1907), and Lorentz (1909). The *Drude model* imagines that a metal contains a population of electrons that are accelerated by external electrical and magnetic fields, and are damped by some sort of frictional force. They obey

$$m\dot{\vec{v}} = -e\vec{E} - e\frac{\vec{v}}{c} \times \vec{B} - m\frac{\vec{v}}{\tau}, \quad (16.1)$$

where τ is a coefficient describing the damping and is called the *relaxation time*. It acquires this name because if an electron is given an initial velocity \vec{v}_0 and let loose in a solid without either electrical or magnetic fields present, the electron's subsequent behavior is

$$\vec{v}(t) = \vec{v}_0 e^{-t/\tau}. \quad \tau \text{ gives the characteristic time for any fluctuation to decay.} \quad (16.2)$$

In the presence of an electrical field \vec{E} , an initial velocity \vec{v}_0 develops instead to

$$\vec{v}(t) = -\frac{\tau e}{m}\vec{E} + \left[\vec{v}_0 + \frac{\tau e}{m}\vec{E}\right]e^{-t/\tau} \quad \text{Assume a solution of the form } A + Be^{-t/\tau} \text{ and solve for the unknown constants.} \quad (16.3)$$

so that at times much longer than τ one obtains

$$\vec{v} = -\frac{\tau e}{m} \vec{E} \quad \text{Equivalent to observing that at long times } \vec{v} \text{ will stop changing, so one can just set } \dot{\vec{v}} \text{ to zero in Eq. (16.1) and solve for } \vec{v}. \quad (16.4)$$

If the density of mobile electrons is n , then the current density \vec{j} arising in response to \vec{E} is

$$\vec{j} = -ne\vec{v} = \frac{ne^2\tau}{m} \vec{E} \quad (16.5)$$

$$\Rightarrow \sigma = \frac{ne^2\tau}{m}, \quad (16.6)$$

where the *electrical conductivity* σ is defined to be the linear coefficient relating current flow to electrical field.

Measurements of electrical conductivity are usually reported in terms of its inverse, the resistivity ρ , in terms of which the relaxation time can be expressed as

$$\tau = \frac{m}{ne^2\rho} = \frac{3.55 \cdot 10^{-13} \text{ s}}{n/[10^{22} \text{ cm}^{-3}] \rho/[\mu\Omega \text{ cm}]} \quad (16.7)$$

Using the resistivities from the periodic table inside the front cover in Eq. (16.7) shows that the relaxation time is on the order of 10^{-14} s. By itself, this calculation does not seem to make any real predictions, because it determines electrical conductivity only at the expense of introducing another unknown, the relaxation time. It does, however, frame electrical conductivity in the terms that will be used later for more detailed calculation, as a balance between the force $-e\vec{E}$ causing electrons to accelerate, with the damping from scattering events encoded in τ that causes them to decelerate.

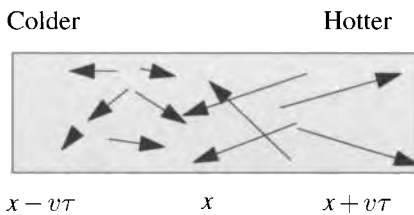


Figure 16.1. Flow of energy from a hot to a cold region carried by colliding electrons.

Drude's equation acquires more substance when the same framework is used to calculate some transport property in addition to the electrical conductivity, so that the unknown τ can be eliminated. Drude (1900) calculated the thermal conductivity of the electrons, which may roughly be estimated as follows: Thermal conductivity is the coefficient κ giving the flux of energy \vec{j}_E opposite to a thermal gradient $\vec{\nabla}T$. Pick some point x in a solid with a thermal gradient, depicted in Figure 16.1. Electrons arriving from the right with velocity in the x direction v_x have characteristically traveled a distance $v\tau$ since last colliding with the scattering forces that produce thermal equilibrium, and carry energy $\mathcal{E}(x + v_x\tau)$, while those

coming from the left carry energy $\mathcal{E}(x - v_x\tau)$. The density of electrons arriving from the right is something like $n/2$ because half the electrons to the right have positive velocities. So the net flux of energy is roughly

$$j\mathcal{E} = \frac{n}{2}v_x [\mathcal{E}(x - v_x\tau) - \mathcal{E}(x + v_x\tau)] \approx -nv_x^2\tau \frac{\partial\mathcal{E}}{\partial x} = -nv_x^2\tau \frac{\partial\mathcal{E}}{\partial T} \frac{\partial T}{\partial x} \quad (16.8)$$

$$= -\frac{2n}{m} \frac{1}{2}mv_x^2c_V\tau \frac{\partial T}{\partial x} = -\frac{\tau n}{m} \frac{3k_B^2T}{2} \frac{\partial T}{\partial x} \quad (16.9)$$

Specific heat is $\partial\mathcal{E}/\partial T$, classically equal to $3k_B/2$, while average x kinetic energy is $k_B T/2$.

$$\Rightarrow \frac{\kappa}{\sigma T} = \frac{3}{2} \left(\frac{k_B}{e} \right)^2 = 1.24 \cdot 10^{-13} \text{erg cm}^{-1} \text{K}^{-2}. \quad (16.10)$$

Through what was arguably a logical error, Drude originally obtained twice this value, in rather good agreement with experiment.

The argument used here to obtain the thermal conductivity does not stand up at all to close inspection. It pretends that electrons all traveling with mean velocity v_x carry differing amounts of kinetic energy. The most that can be said for it is that it is dimensionally sound and makes an essentially correct prediction, which is that the thermal conductivity divided by electrical conductivity and temperature yields a constant for metals. This fact was observed by Wiedemann and Franz (1853), and the experimental constant is around $2.3 \cdot 10^{-13} \text{erg cm}^{-1} \text{K}^{-2}$.

Producing a theory substantially better than these crude estimates requires a fair amount of effort, and will occupy the next two chapters. The first point to address is the fact that distinct energy bands, indexed by n , are dynamically separate. Under influence of weak and slowly varying fields, an electron that begins in one band can easily move about among energy states in the same band, but is exponentially unlikely to move into another. Next, by constructing an effective Lagrangian for wave packets, it will be shown how electrons can act like classical particles despite being described by Bloch's theory as waves. Finally, Boltzmann's general framework for describing electrical and thermal transport of classical particles will be used to predict the thermoelectric properties of metals.

16.2 Semiclassical Electron Dynamics

Rules of Semiclassical Dynamics. For many purposes, electrons in periodic solids act like classical particles with slightly unfamiliar laws of motion. Before beginning the lengthy process of deriving, justifying, and analyzing these laws, it is best to begin simply by stating what they are.

1. The band index n is a constant of the motion. An electron that begins its life in one band remains in it thereafter. For this reason, the band index n can be omitted from energies and wave functions in the following discussion.
2. The position of an electron in a crystal with inversion symmetry evolves according to

$$\dot{\vec{r}} = \frac{1}{\hbar} \frac{\partial \mathcal{E}_{\vec{k}}}{\partial \vec{k}}. \quad (16.11)$$

3. The electron's wave vector obeys

$$\hbar \dot{\vec{k}} = -e\vec{E} - \frac{e}{c} \dot{\vec{r}} \times \vec{B} \quad (16.12)$$

where \vec{E} and \vec{B} are electric field and magnetic induction and may be spatially varying. Because all energy functions and wave functions are periodic functions of \vec{k} , \vec{k} is physically indistinguishable from $\vec{k} + \vec{K}$, where \vec{K} is any reciprocal lattice vector.

16.2.1 Bloch Oscillations

Although representing a semiclassical picture, many quantum-mechanical effects are retained in Eqs. (16.11) and (16.12). These result from the fact that $\mathcal{E}_{n\vec{k}}$ is a periodic function of \vec{k} , as well as from the fact that the electron states are occupied according to the Fermi distribution rather than according to classical statistical mechanics.

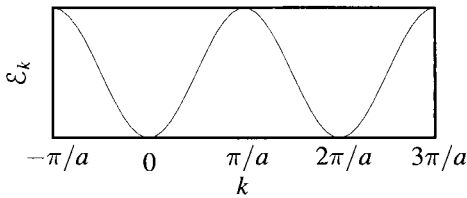


Figure 16.2. Energy of a tight-binding band, Eq. (16.13). Electrons have negative effective masses at $k = \pi/a$ and positive effective masses at $k = 0$.

As an example, consider the semiclassical dynamics of electrons whose energy is given by the tight-binding model, Eq. (8.72). For simplicity, specialize to a one-dimensional lattice of lattice constant a and write the energy functional as

$$\mathcal{E}_k = -2t \cos ak, \quad (16.13)$$

as shown in Figure 16.2. In the presence of a uniform electric field E , one has

$$\hbar \dot{k} = -eE \quad \text{From Eq. (16.12).} \quad (16.14)$$

$$\Rightarrow k = -eEt/\hbar \quad (16.15)$$

$$\Rightarrow \dot{r} = -\frac{2ta}{\hbar} \sin\left(\frac{aeEt}{\hbar}\right) \quad \text{From Eq. (16.11).} \quad (16.16)$$

$$\Rightarrow r = \frac{2t}{eE} \cos\left(\frac{aeEt}{\hbar}\right). \quad (16.17)$$

The location of the electron oscillates in time; this behavior is called *Bloch oscillation*. Despite the fact that \vec{k} increases without bound, the mean position of the electron is fixed. If this phenomenon were commonly seen, it would mean that under sufficiently intense electric fields electrons would start to oscillate rather than travel, and metals would become insulators. This simply does not happen. As shown in Problem 2, small amounts of damping added to Eq. (16.14) destroy the phenomenon, and electric fields in metals cannot practically be made large enough to overcome it. However, under special circumstances, Bloch oscillation can be observed, as shown in Figure 16.3.

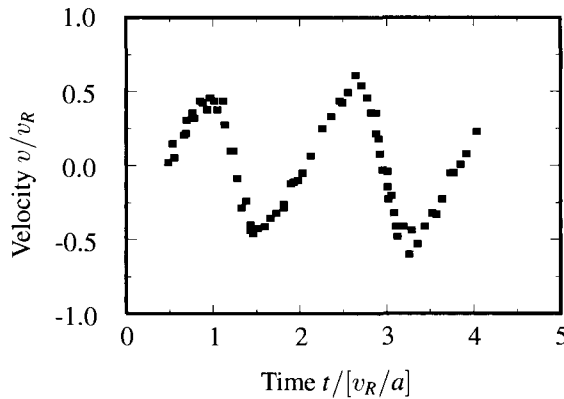


Figure 16.3. Experimental observation of Bloch oscillations. These are not observed for electrons in a solid, but are observed for cesium atoms trapped in potentials created by standing waves of laser light. Atoms are attracted to regions of high field density. The potential is made to undergo uniform acceleration, but the atoms oscillate rather than following the potential. Time is measured in units of v_R/a , where $v_R = 0.35 \text{ cm s}^{-1}$ is the recoil velocity of a cesium atom after being hit by a single photon, and the a is the imposed acceleration, $a = 0.85 \text{ m s}^{-2}$. [Source: ben Dahan et al. (1996), p. 4510.]

16.2.2 $\vec{k} \cdot \hat{P}$ Method

A first derivation of Eq. (16.11) follows from asking carefully what it means for the band index to be a constant of motion. Under the action of weak static fields, electrons remain trapped within a single band. In drawing pictures it is usually clear what this statement means; the eye naturally connects energy levels together. In solving equations, the matter is less clear. The effective Hamiltonian in Eq. (7.47) poses the solution of Bloch’s equation for each value of \vec{k} as a new and independent problem. As illustrated in Figure 16.4, there is no label on an energy eigenvalue telling which band it belongs to. The identity of bands is determined by continuity. Therefore, in order to determine how electrons stick to bands, it is necessary to begin by asking how energy eigenvalues $\mathcal{E}_{n\vec{k}}$ respond to extremely small changes in the Bloch index \vec{k} .

To find the answer, note that the large k -space matrix in Table 7.1, used to prove Bloch’s theorem, is made up of a series of blocks along the diagonal. Each of these

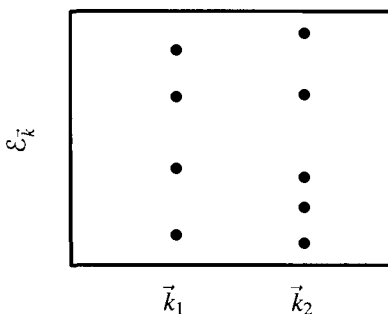


Figure 16.4. If one finds energy eigenvalues at two isolated values of \vec{k} , it is impossible to tell which eigenvalues belong to the same band.

blocks, which has a dimension equal to the number of reciprocal lattice vectors, is the same size as all the others. Therefore, if one restricts attention to any one of the blocks, uses it as a Hamiltonian, and finds the eigenfunctions, then one can use those eigenfunctions as a complete set with which to discuss the eigenfunctions of any of the other blocks. That is, one can describe the eigenfunctions indexed by $\vec{k} + d\vec{k}$ using for basis functions the eigenfunctions with index \vec{k} . This calculation gives a systematic way of approaching the question of how wave functions and eigenvalues deform into each other as \vec{k} changes.

Return to Eq. (7.47), and imagine solving it for some value of \vec{k} , finding all the energy eigenvalues corresponding to the different bands. Now increase \vec{k} slightly to $\vec{k} + \delta\vec{k}$. The equation to be solved is now

$$\hat{\mathcal{H}}_{\vec{k}+\delta\vec{k}} = \frac{\hbar^2}{2m} [-\vec{\nabla}^2 - 2i(\vec{k} + \delta\vec{k}) \cdot \vec{\nabla} + |\vec{k} + \delta\vec{k}|^2] u(\vec{r}) + U(\vec{r}) u(\vec{r}) = \mathcal{E} u(\vec{r}). \quad (16.18)$$

View this problem as a problem in perturbation theory, with the unperturbed Hamiltonian $\hat{\mathcal{H}}^0 = \hat{\mathcal{H}}_{\vec{k}}$ and the perturbation

$$\hat{\mathcal{H}}_{\vec{k}}^{(1)} = -\frac{\hbar^2}{2m} \left[-\delta k^2 - 2\delta\vec{k} \cdot \vec{k} + 2i\delta\vec{k} \cdot \vec{\nabla} \right]. \quad \text{Just expand out Eq. (16.18)} \quad (16.19)$$

The energy eigenvalues change as

$$\mathcal{E}_{n,\vec{k}+\delta\vec{k}} = \mathcal{E}_{n\vec{k}} + \mathcal{E}_{n\vec{k}}^{(1)} + \mathcal{E}_{n\vec{k}}^{(2)} + \dots \quad \text{Successive terms are successively higher order in } \delta\vec{k}. \quad (16.20)$$

The first-order change in the energy under this perturbation is

$$\mathcal{E}_{n\vec{k}}^{(1)} = \langle u_{n\vec{k}} | \left(\frac{\hbar^2}{m} \delta\vec{k} \cdot (\vec{k} - i\vec{\nabla}) \right) | u_{n\vec{k}} \rangle. \quad \begin{array}{l} \text{The first term on the right of} \\ \text{Eq. (16.19) is second order} \\ \text{in } \delta\vec{k} \text{ and can be neglected.} \end{array} \quad (16.21)$$

To simplify Eq. (16.21) it is valuable to notice the handy operator identity

$$(\vec{k} - i\vec{\nabla}) e^{-i\vec{k} \cdot \vec{r}} = -i e^{-i\vec{k} \cdot \vec{r}} \vec{\nabla}. \quad \begin{array}{l} \text{When the gradient acts on} \\ \text{the exponential it eliminates} \\ \text{the term proportional to } \vec{k}. \end{array} \quad (16.22)$$

Because $u_{n\vec{k}} = \exp[-i\vec{k} \cdot \vec{r}] \psi_{n\vec{k}}$, Eq. (16.21) simplifies to

$$\mathcal{E}_{n\vec{k}}^{(1)} = \frac{\hbar}{m} \langle \psi_{n\vec{k}} | \delta\vec{k} \cdot \hat{P} | \psi_{n\vec{k}} \rangle \quad (16.23)$$

Write (16.21) out as an integral, substitute ψ for u using (7.45), use $\hat{P} = -i\hbar\vec{\nabla}$ and rewrite as a matrix element. This expression explains the title of this subsection.

$$\Rightarrow \frac{\partial \mathcal{E}_{n\vec{k}}}{\partial \vec{k}} = \frac{\hbar}{m} \langle \psi_{n\vec{k}} | \hat{P} | \psi_{n\vec{k}} \rangle \quad \text{Because of Eq. (16.20).} \quad (16.24)$$

$$\Rightarrow \frac{\partial \mathcal{E}_{n\vec{k}}}{\partial \hbar \vec{k}} = \langle \hat{v} \rangle \equiv \vec{v}_{n\vec{k}}. \quad \text{Defining } \hat{v} = \hat{P}/m. \quad (16.25)$$

As in Section 7.2.4, Eqs. (16.25) and Eq. (16.11) show that the group velocity of an electron wave packet, $\partial\omega/\partial\vec{k}$, equals its mean velocity.

16.2.3 Effective Mass

External electric and magnetic fields accelerate electrons, forcing them to glide along the energy bands. Suppose that these fields are very weak and that the change in \vec{k} is accordingly very slow. If it is sufficiently slow, then one can invoke stationary perturbation theory, as in the previous section, and argue that

$$\frac{d}{dt} \langle \hat{v}_\alpha \rangle = \sum_\beta \frac{\partial \langle \hat{v}_\alpha \rangle}{\partial k_\beta} \frac{\partial k_\beta}{\partial t} \quad \hat{v}_\alpha \text{ is the } \alpha\text{th component of } \hat{v}. \quad (16.26)$$

$$\Rightarrow \frac{d}{dt} \langle \hat{v} \rangle = \hbar \mathbf{M}^{-1} \dot{\vec{k}}, \quad (16.27)$$

where

$$(\mathbf{M}^{-1})_{\alpha\beta} \equiv \frac{1}{\hbar^2} \frac{\partial^2 \mathcal{E}_{n\vec{k}}}{\partial k_\alpha \partial k_\beta}. \quad \text{From Eq. (16.25).} \quad (16.28)$$

The tensor \mathbf{M} defined in Eq. (16.28) is called the *effective mass tensor*. Because the energy $\mathcal{E}_{n\vec{k}}$ is in general not isotropic, acceleration will not in general be parallel to \vec{k} . However, that is not the most interesting feature of the effective mass. Because $\mathcal{E}_{n\vec{k}}$ is a periodic function in \vec{k} , its second derivatives will sometimes be positive and sometimes negative. For example, in Figure 16.2, the inverse effective mass is negative at $k = \pi/a$ and positive at $k = 0$. According to Eq. (16.12), the index k always increases in the direction of decreasing electric fields. However, when the effective mass is negative, the velocity of electrons is in the direction opposite to \vec{k} . Rather than thinking of these electrons as having negative mass, one thinks of them as having positive charge and calls them *holes*.

Additional information on the effective mass tensor can be obtained by continuing the perturbation expansion of Eq. (16.20) to second order. Problem 3 shows that it can be written as

$$(\mathbf{M}^{-1})_{\alpha\beta} = \frac{1}{m} \delta_{\alpha\beta} + \frac{1}{m^2} \sum_{n' \neq n} \frac{\langle \psi_{n\vec{k}} | \hat{P}_\alpha | \psi_{n'\vec{k}} \rangle \langle \psi_{n'\vec{k}} | \hat{P}_\beta | \psi_{n\vec{k}} \rangle + \text{c.c.}}{\mathcal{E}_{n\vec{k}} - \mathcal{E}_{n'\vec{k}}} \quad (16.29)$$

“c.c.” means “add the complex conjugate of the previous term.” The sum is carried out only over n' —not over n .

One can interpret Eq. (16.29) as saying that the effective mass of an electron arises from virtual transitions between bands. The closer the energy $\mathcal{E}_{n'\vec{k}}$ of band n' is to the energy $\mathcal{E}_{n\vec{k}}$ of band n , the larger the deviation of the inverse effective mass from $1/m$ will be. A nearby band of higher energy tends to make the effective mass negative, while a nearby band of lower energy tends to make the effective mass positive.

16.3 Noninteracting Electrons in an Electric Field

Understanding why electrons obey the semiclassical equations and why they are not able to change band index requires considering the behavior of noninteracting electrons placed in a weak electric field. This calculation is plagued with technical

difficulties. Periodic boundary conditions have played an important role in simplifying the mathematics of the electrons, but it appears that when a uniform electric field is turned on, one must abandon them. The electrostatic potential $V(\vec{r}) = -\vec{E} \cdot \vec{r}$ of a uniform electric field grows linearly in space, and so it must be larger at one side of the sample than at the other. As a reflection of this fact, if one actually places a finite sample of metal in an electric field, surface charges build up and cancel out the field in the interior altogether.

There are two solutions to this difficulty. The method to be pursued in this section recasts the problem so that the linear potential is eliminated altogether. This technique allows great formal progress, including a calculation of the rate of transitions between bands, but is hard to generalize so as to include magnetic fields. The following section proceeds instead by restricting attention to a subset of all wave functions, which are localized in space and therefore cannot see the divergences in the electrical potential.

To recast the problem, eliminating the scalar potential V , note that one is interested in electric fields under conditions where electrons flow continually around in a loop, and charge does not build up at the edges of the sample. A trick permitting such a calculation follows from recalling that electric fields are generated by time-dependent vector potentials according to Maxwell's equation

$$\vec{E} = -\frac{1}{c} \frac{\partial \vec{A}}{\partial t} - \vec{\nabla}V. \quad \text{Use } \vec{B} = \vec{\nabla} \times \vec{A} \text{ in Eq. (20.5b), and observe that if the curl of a function vanishes, it equals the gradient of a scalar.} \quad (16.30)$$

By introducing a time-dependent vector potential $\vec{A}(t)$, one can generate an electric field even when the scalar potential V vanishes. The advantage of employing \vec{A} rather than V is that it remains perfectly legitimate to work with periodic boundary conditions. A convenient one-dimensional geometry is illustrated in Figure 16.5. Mathematically, there is no difficulty at all in passing a thin tube of magnetic flux through the middle of a loop of wire, although experimentally it is difficult to achieve this feat without having some magnetic induction escape the thin tube and impinge upon the wire.

Rather than focus upon details of a loop of wire, it is simplest to pose a one-

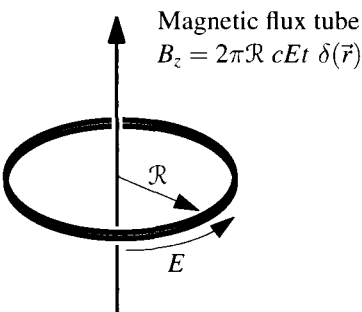


Figure 16.5. A thin tube of increasing magnetic flux through a loop of wire, so thin that no magnetic induction is visible in the wire, generates a constant electromotive force around the loop. The magnetic flux tube corresponds to a vector potential \vec{A} parallel to the wire and of strength $-cEt$, allowing an electric field to coexist with periodic boundary conditions. This geometry is the setting for the definition of the Houston states.

dimensional problem, making use of Eq. (16.30). The Hamiltonian is

$$\hat{\mathcal{H}} = \frac{1}{2m} \left(\hat{P} + \frac{e}{c} A \right)^2 + \hat{U}(\hat{R}), \quad (16.31)$$

where

$$A = -cEt. \quad (16.32)$$

Notice that the potential and hence the Hamiltonian are explicitly time-dependent. This is the price one pays for the ability to impose periodic boundary conditions. In order to solve (16.31), define

$$\left[\frac{1}{2m} \left(\hat{P} + \frac{e}{c} A \right)^2 + \hat{U} \right] \tilde{\phi}(x, t) = \mathcal{E}_t \tilde{\phi}(x, t). \quad \text{The subscript } t \text{ on } \mathcal{E} \text{ serves as a reminder that } \mathcal{E} \text{ is time-dependent.} \quad (16.33)$$

The function $\tilde{\phi}(x, t)$ is an eigenfunction of the Hamiltonian at any given time, viewing time as a parameter. Because it resides on the loops shown in Figure 16.5, it must be a periodic function and obey

$$\tilde{\phi}(x + L) = \tilde{\phi}(x). \quad \text{Taking } L \text{ to be the circumference of the loop.} \quad (16.34)$$

Glancing back at Eq. (16.22) shows that by multiplying wave functions with a phase factor, constants added to gradients can be induced to disappear. In fact, one can eliminate the vector potential A from Eq. (16.33) altogether by defining

$$\tilde{\phi}(x, t) = e^{-ieAx/\hbar c} \phi(x, t). \quad (16.35)$$

Using Eq. (16.22) shows that Eq. (16.33) becomes

$$\left[\frac{\hat{P}^2}{2m} + \hat{U} \right] \phi(x, t) = \mathcal{E}_t \phi(x, t). \quad (16.36)$$

Equation (16.36) is nothing but Bloch's equation and its solutions are Bloch eigenstates

$$\phi_{nk(t)}(x) = e^{ik(t)x} u_{nk(t)}(x). \quad \text{Where } u_{nk} \text{ is a periodic function, and } k, \text{ like } \mathcal{E}, \text{ depends upon time.} \quad (16.37)$$

Disturbingly, the electric field appears to have vanished from the problem altogether. Where did it go, and why are the energies and wave vectors shown depending upon t ? The answer is quite subtle. The electric field cannot really have disappeared from the problem, and because the only part of the mathematical problem not dealt with carefully so far is the imposition of boundary conditions, that is where the electric field must reside. Inserting Eqs. (16.35) and (16.37) into the boundary condition (16.34) and recalling that $u_{nk(t)}$ is periodic gives immediately that

$$e^{-ieA(x+L)/\hbar c} e^{ik(t)(x+L)} u_{nk(t)}(x+L) = e^{-ieAx/\hbar c + ik(t)x} u_{nk(t)}(x) \quad (16.38)$$

$$\Rightarrow \frac{-eA}{\hbar c} + k_{(t)} = \frac{2\pi l}{L}. \quad \begin{array}{l} \text{Because} \\ u_{nk(t)}(x+L) = u_{nk(t)}(x). \quad l \text{ is} \\ \text{some integer.} \end{array} \quad (16.39)$$

$$\Rightarrow \frac{eEt}{\hbar} + k_{(t)} = \frac{2\pi l}{L}. \quad (16.40)$$

$$(16.41)$$

It follows from Eq. (16.40) that if the boundary conditions are to be obeyed, the wave vectors k are indeed time-dependent, obeying

$$\hbar \dot{k} = -eE. \quad (16.42)$$

Despite the influence of the periodic potential \hat{U} , the index \vec{k} obeys classical equations of motion for an electron in an electric field. The identical semiclassical result is derived by another route in Problem 7.

The functions $\tilde{\phi}$ are called *Houston functions*. The Houston functions are orthonormal wave functions, but they are not exact solutions of Schrödinger's equation, because as soon as eigenvalues are time-dependent, the connection between the time-dependent Schrödinger equation and an eigenvalue problem such as Eq. (16.33) has been lost. If one starts an electron in a particular Houston state at $t = 0$ and follows its time evolution, it begins to deviate from a perfect Houston state in two ways. First, as it evolves, the amplitudes of Houston states with nearby \vec{k} become nonzero and grow, as shown in Problem 8. This behavior is typical of wave packets, and it corresponds to the spread of the wave packet under the influence of Schrödinger's equation. The spread cannot be prevented, although its effects can be minimized by starting the electron in a superposition of states with nearby \vec{k} . In addition to this gradual spread of wave vectors within a band, there is a more interesting phenomenon where the electron jumps from one band to another, a phenomenon known as *Zener tunneling*.

16.3.1 Zener Tunneling

Rough Calculation. One way to explain Zener tunneling is to observe that the effect of an electric field is to change electrons' energy by $e\vec{E} \cdot \vec{r}$, so that the band energy $\mathcal{E}_{n\vec{k}}$ shifts up and down with position, as shown in Figure 16.6. Suppose that an electron sits at the top of a valence band, \mathcal{E}_v , and the bottom of a conduction band \mathcal{E}_c sits a distance \mathcal{E}_g above it. If the electron can jump over a distance \mathcal{E}_g/eE , then without changing energy, it can enter the conduction band. The problem is that during this voyage, it will need to have an energy lying in the gap between valence and conduction bands.

It is not precisely true to say that states with energies lying in the energy gap are forbidden. They exist, but only if one permits complex values of the Bloch index \vec{k} . Because these solutions grow exponentially, they cannot uniformly fill a macroscopic crystal. According to the WKB approximation, introduced in Eq. (4.9), the amplitude for an electron to tunnel from one band to another should roughly be of the form

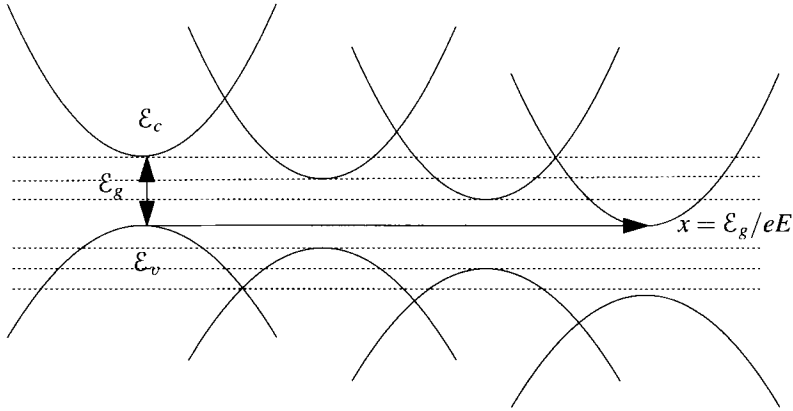


Figure 16.6. An electric field can be thought of as shifting energy bands up and down as a function of spatial location. An electron that tunnels through the energy gap over a distance x can succeed in changing bands.

$$\exp \left[\frac{i}{\hbar} \int_0^x dx' \sqrt{2m \sqrt{(\mathcal{E}_c - \mathcal{E})(\mathcal{E}_v - \mathcal{E})}} \right] \quad \text{Want something with dimensions of energy that is negative in the gap, and that vanishes at } \mathcal{E}_c \text{ and } \mathcal{E}_v. \quad (16.43)$$

$$\sim \exp \left[-x \sqrt{\frac{2m\mathcal{E}_g}{\hbar^2}} \right] \quad \text{Very rough estimate.} \quad (16.44)$$

$$\sim \exp \left[-\frac{\mathcal{E}_g}{eE} \sqrt{\frac{2m\mathcal{E}_g}{\hbar^2}} \right]. \quad (16.45)$$

This simple estimate is borne out surprisingly well by the detailed calculation that follows.

Detailed Calculation. A solution of Schrödinger’s equation with Bloch index \vec{k} must be some linear combination of Houston states with the same index:

$$|\psi(t)\rangle = \sum_{n'} C_{n'}(t) |\tilde{\phi}_{n'k(t)}\rangle. \quad (16.46)$$

So

$$i\hbar \frac{\partial |\psi\rangle}{\partial t} = \hat{\mathcal{H}} |\psi\rangle \quad (16.47)$$

implies that

$$\hat{\mathcal{H}} |\psi\rangle = \sum_{n'} C_{n'}(t) \mathcal{E}_{n'k(t)} |\tilde{\phi}_{n'k(t)}\rangle \quad \text{Because } \tilde{\phi} \text{ obeys Eq. (16.33).} \quad (16.48)$$

$$= i\hbar \sum_{n'} \frac{\partial C_{n'}}{\partial t} |\tilde{\phi}_{n'k(t)}\rangle + C_{n'}(t) \frac{\partial}{\partial \vec{k}} |\tilde{\phi}_{n'k(t)}\rangle \dot{\vec{k}} \quad (16.49)$$

Using Schrödinger’s equation, and the fact that $\tilde{\phi}$ depends upon t only through \vec{k} .

$$\Rightarrow \langle \tilde{\phi}_{nk(t)} | \hat{\mathcal{H}} | \psi \rangle = C_n(t) \mathcal{E}_{nk(t)} \quad (16.50)$$

$$= i\hbar \frac{\partial C_n}{\partial t} - \sum_{n'} iC_{n'} \langle \tilde{\phi}_{nk(t)} | \frac{\partial \tilde{\phi}_{n'k(t)}}{\partial k} \rangle eE. \quad (16.51)$$

For simplicity, restrict attention to a two-band model so that there are only two coefficients C_1 , and C_2 . The first of these begins at amplitude 1 when $t = 0$; the second begins at 0, and the goal is to see how fast it will grow. To leading order one has

$$C_1 \mathcal{E}_{1k(t)} = i\hbar \frac{\partial C_1}{\partial t} \quad (16.52)$$

$$\Rightarrow C_1 = \exp \left[-\frac{i}{\hbar} \int_0^t dt' \mathcal{E}_{1k(t')} \right]. \quad (16.53)$$

Now look at the equation for C_2 . Defining

$$\alpha_2(t) = C_2(t) \exp \left[\frac{i}{\hbar} \int_0^t dt' \mathcal{E}_{2k(t')} \right], \quad \text{Because } \alpha \text{ and } C \text{ are related by a phase factor,} \quad (16.54)$$

they can be used equally well to determine the probability that the electron arrives in band 2.

one has

$$\dot{\alpha}_2 = \langle \tilde{\phi}_{2k(t)} | \frac{\partial \tilde{\phi}_{1k(t)}}{\partial k} \rangle \frac{eE}{\hbar} \exp \left[\frac{i}{\hbar} \int_0^t dt' (\mathcal{E}_{2k(t')} - \mathcal{E}_{1k(t')}) \right]. \quad (16.55)$$

Equation (16.55) is sufficiently difficult to solve exactly that the greatest benefit comes from evaluating its leading behavior. Krieger and Iafate (1986) evaluated the matrix element between $\partial \tilde{\phi} / \partial k$ and $\tilde{\phi}$ and found that it was of order L/N , where L is the system length and N is the number of lattice points. This matrix element is largest when k is near the Brillouin zone boundary, and oscillates as a function of k . However, variations in the matrix element are unimportant in comparison with much more rapid oscillations of the exponential that make α exponentially small. It is reasonable to treat the matrix element as a constant, and to estimate the rate of tunneling from band 1 to band 2 after time \mathcal{T} as

$$\alpha_2(\mathcal{T}) \approx \frac{L}{N} \int_0^{\mathcal{T}} dt \frac{eE}{\hbar} \exp \left[\frac{i}{\hbar} \int_0^t dt' (\mathcal{E}_{2k(t')} - \mathcal{E}_{1k(t')}) \right]. \quad (16.56)$$

Take \mathcal{T} to be the time needed for k to advance by one reciprocal lattice vector $K = 2\pi N/L$. Changing the variable of integration from t to k gives

$$\alpha_2(\mathcal{T}) \approx \frac{L}{N} \int_0^{2\pi N/L} dk \exp \left[\frac{-i}{eE} \int_0^k dk' (\mathcal{E}_{2k'} - \mathcal{E}_{1k'}) \right]. \quad \text{Use Eq. (16.42) for the change of} \quad (16.57)$$

variables.

Assume, as in Figure 16.6, that the tunneling is to take place between two parabolic bands, the lower of the form $\mathcal{E} = \mathcal{E}_v - \hbar^2 k^2 / 2m_v^*$ and the upper of the form $\mathcal{E} = \mathcal{E}_c + \hbar^2 k^2 / 2m_c^*$. Then defining the reduced mass

$$\frac{1}{m^*} = \left[\frac{1}{m_v^*} + \frac{1}{m_c^*} \right] \quad (16.58)$$

gives

$$\mathcal{E}_{2k'} - \mathcal{E}_{1k'} = \mathcal{E}_g + \frac{\hbar^2 k'^2}{2m^*}. \tag{16.59}$$

Placing Eq. (16.59) into Eq. (16.57) produces an integral that is impossible to perform exactly, but that easily can be estimated by the method of steepest descents (Appendix B.4). Let q be the point in the complex plane where

$$\mathcal{E}_g + \frac{\hbar^2 q^2}{2m^*} = 0. \tag{16.60}$$

Then the method of steepest descents gives immediately that

$$\alpha_2(\mathcal{J}) \sim \exp \left[\frac{-i}{eE} \int_0^q dk' \mathcal{E}_g + \frac{\hbar^2 k'^2}{2m^*} \right]. \tag{16.61}$$

$$\sim \exp \left[\frac{-2i}{3eE} q \mathcal{E}_g \right] \tag{16.62}$$

$$\sim \exp \left[\frac{-2\mathcal{E}_g^{3/2}}{3eE} \sqrt{\frac{2m^*}{\hbar^2}} \right] \tag{16.63}$$

In the original calculation by Zener (1932), the energy bands did not have the form in Eq. (16.59), but were instead linear except for a small region where they avoid one another. The tunneling rate is then $\exp[-2\pi \mathcal{E}_g^2 / (eE d(\mathcal{E}_1 - \mathcal{E}_2)/dk)]$.

$$\sim \exp \left[-3.41 \cdot 10^7 [\mathcal{E}_g/\text{eV}]^{3/2} [m^*/m]^{1/2} / [E \cdot \text{cm V}^{-1}] \right]. \tag{16.64}$$

Equation (16.64) shows that because band gaps are typically 1 eV for metals, and because it is difficult to obtain voltages larger than 10^4 V cm^{-1} , the probability for an electron to tunnel from one band to another is on the order of $\exp[-10^3]$. This probability is negligible. In semiconductors, on the other hand, electric fields can reach 10^6 V cm^{-1} , effective masses may be one-tenth of the electron mass, band gaps are typically less than 1 eV, and Zener tunneling is therefore a common feature in the reverse bias of heavily doped diodes, as discussed by Sze (1981), pp. 516–536.

16.4 Semiclassical Equations from Wave Packets

16.4.1 Formal Dynamics of Wave Packets

As pointed out in Section 7.2.4, in any situation described by a wave equation where one wishes to speak of “particles,” in fact one is referring to wave packets. The most powerful and general way to derive a semiclassical equation of motion for electrons is to consider carefully how wave packets evolve.

While formal analysis essentially recovers the results of Section 7.2.4, it does not exactly reproduce them. The dynamical equations for electrons acquire terms not presented in Eqs. (16.11) or (16.12). These extra terms should in principle always be used to describe electron dynamics. In practice, they are frequently neglected, for two reasons. First, they vanish by symmetry in any centrosymmetric crystal. Second, they are unfamiliar and difficult to compute.

Sundaram and Niu (1999) discuss a formal method that can be used systematically to find electron dynamics. It is the same as the one used in Section 15.5.4 to

find an equation of motion for the wave function of superfluid helium, the effective Lagrangian of Appendix B.

It is first necessary to define carefully a wave packet $W_{\vec{r}_c, \vec{k}_c}(\vec{r})$ centered in space at \vec{r}_c and dominated by wave vector \vec{k}_c . In the presence of a magnetic induction whose vector potential is \vec{A} , the proper definition is

$$W_{\vec{r}_c, \vec{k}_c}(\vec{r}) = \frac{1}{\sqrt{N}} \sum_{\vec{k}} w_{\vec{k}\vec{k}_c} e^{-ie\vec{A}(\vec{r}_c)\cdot\vec{r}/\hbar c - i\vec{k}\cdot\vec{r}_c} \psi_{\vec{k}}(\vec{r}).$$

N is the number of unit cells in the system. \vec{k} is summed over a single Brillouin zone. $\psi_{\vec{k}}$ are solutions of Schrödinger's equation, all sharing band index n .

(16.65)

The phase factors in (16.65) are needed in order to ensure that W vary slowly as \vec{r}_c and \vec{k}_c vary. Bloch functions naturally oscillate with phase factor $e^{i\vec{k}\cdot\vec{r}}$ and, in the presence of a magnetic field, acquire an additional phase factor $e^{-ie \int d\vec{r} \cdot \vec{A}(\vec{r})/\hbar c}$; by incorporating these phase factors into the definition of the wave packet, the hope is to eliminate wild oscillations in W . The wave packet must be normalized, so

$$1 = \langle W_{\vec{r}_c, \vec{k}_c} | W_{\vec{r}_c, \vec{k}_c} \rangle = \frac{1}{N} \sum_{\vec{k}, \vec{k}'} \int d\vec{r} e^{i(\vec{k}' - \vec{k})\cdot\vec{r}_c} w_{\vec{k}\vec{k}_c} w_{\vec{k}'\vec{k}_c}^* \psi_{\vec{k}'}^*(\vec{r}) \psi_{\vec{k}}(\vec{r}) = \sum_{\vec{k}, \vec{k}'} w_{\vec{k}\vec{k}_c} w_{\vec{k}'\vec{k}_c}^* \delta_{\vec{k}\vec{k}'}$$

(16.66)

$$\Rightarrow 1 = \sum_{\vec{k}} |w_{\vec{k}\vec{k}_c}|^2. \quad \psi_{\vec{k}} \text{ is normalized over the volume } \mathcal{V} \text{ of the crystal.}$$

(16.67)

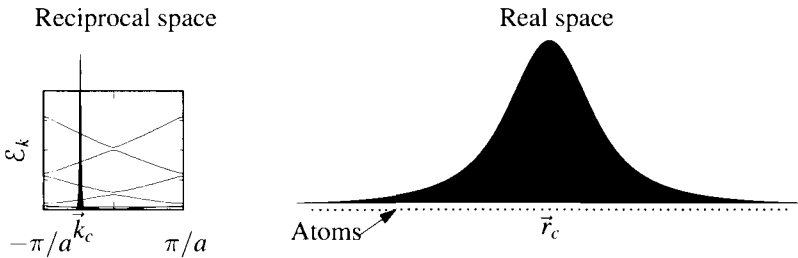


Figure 16.7. A wave packet involves a range of wave vectors that is considerably smaller than the width of the Brillouin zone, so the spatial extent of the wave packet is much larger than an atomic spacing. By taking the spatial extent to be on the order of 100 Å, it is possible to have the packet tightly localized in comparison with external potentials, making it possible to speak simultaneously of the wave number \vec{k}_c and position \vec{r}_c of an electron.

The shape of the wave packet is dictated by the weighting function w , which in addition to being normalized, must be taken to have a rather special form. Its amplitude $|w|_{\vec{k}-\vec{k}_c}$ depends only upon $\vec{k} - \vec{k}_c$. This amplitude determines the range $\Delta\vec{k}$ of wave numbers involved in the wave packet, and also determines its spatial extent $\Delta r \sim 1/\Delta k$. One should think of Δk extending about 1% of the spacing of the reciprocal lattice, which implies that Δr extends over about 100 unit cells

as shown in Figure 16.7. Electrical fields, magnetic fields, and other external potentials must therefore vary slowly on a scale of around 100 \AA , a limitation being violated more and more frequently in modern electronics.

The phase of w carries information about the actual spatial location of the wave packet, and it must be chosen carefully if it truly is to be centered at \vec{r}_c . In particular,

$$w_{\vec{k}\vec{k}_c} = |w|_{\vec{k}-\vec{k}_c} e^{i(\vec{k}-\vec{k}_c) \cdot \vec{\mathcal{R}}_{\vec{k}_c}}, \quad (16.68)$$

where $\mathcal{R}_{\vec{k}_c}$ is precisely the Berry connection of Eq. (8.59),

$$\vec{\mathcal{R}}_{\vec{k}_c} = i \int_{\Omega} d\vec{r} u_{\vec{k}_c}^*(\vec{r}) \frac{\partial}{\partial \vec{k}_c} u_{\vec{k}_c}(\vec{r}). \quad (16.69)$$

The demonstration that such a wave packet truly is centered at \vec{r}_c follows from the computation

$$\langle W_{\vec{r}_c \vec{k}_c} | \vec{r} - \vec{r}_c | W_{\vec{r}_c \vec{k}_c} \rangle = \langle W_{\vec{r}_c \vec{k}_c} | \vec{r} | W_{\vec{r}_c \vec{k}_c} \rangle - r_c \quad \begin{array}{l} \text{Because the packet is} \\ \text{normalized.} \end{array} \quad (16.70)$$

$$= \int \frac{d\vec{r}}{N} \sum_{\vec{k}'\vec{k}} w_{\vec{k}\vec{k}_c}^* w_{\vec{k}'\vec{k}_c} e^{i(\vec{k}'-\vec{k}) \cdot (\vec{r}-\vec{r}_c)} u_{\vec{k}}^*(\vec{r}) u_{\vec{k}'}(\vec{r}) [\vec{r} - \vec{r}_c] \quad (16.71)$$

Use Eq. (7.45) for the periodic function u to replace ψ in (16.65). (16.72)

$$= \int \frac{d\vec{r}}{N} \sum_{\vec{k}'\vec{k}} w_{\vec{k}\vec{k}_c}^* w_{\vec{k}'\vec{k}_c} u_{\vec{k}}^*(\vec{r}) u_{\vec{k}'}(\vec{r}) \frac{\partial}{\partial i\vec{k}'} e^{i(\vec{k}'-\vec{k}) \cdot (\vec{r}-\vec{r}_c)} \quad (16.73)$$

$$= - \int \frac{d\vec{r}}{N} \sum_{\vec{k}'\vec{k}} w_{\vec{k}\vec{k}_c}^* u_{\vec{k}}^*(\vec{r}) e^{i(\vec{k}'-\vec{k}) \cdot (\vec{r}-\vec{r}_c)} \frac{\partial}{\partial i\vec{k}'} [w_{\vec{k}'\vec{k}_c} u_{\vec{k}'}(\vec{r})] \quad (16.74)$$

Change the \vec{k}' sum to an integral with (6.11), integrate by parts, and return to the sum.

$$= - \int_{\Omega} d\vec{r} \sum_{\vec{k}'\vec{k}} \delta_{\vec{k}'\vec{k}} w_{\vec{k}\vec{k}_c}^* u_{\vec{k}}^*(\vec{r}) \frac{\partial}{\partial i\vec{k}'} [w_{\vec{k}'\vec{k}_c} u_{\vec{k}'}(\vec{r})] \quad (16.75)$$

As in Eq. (7.26), \int_{Ω} indicates integration over a single unit cell. No reciprocal lattice vectors \vec{K} needed because \vec{k} and \vec{k}' lie in a single zone.

$$= - \int_{\Omega} d\vec{r} \sum_{\vec{k}} |w|_{\vec{k}-\vec{k}_c}^2 u_{\vec{k}}^*(\vec{r}) \frac{1}{w_{\vec{k}\vec{k}_c}} \frac{\partial}{\partial i\vec{k}} [w_{\vec{k}\vec{k}_c} u_{\vec{k}}(\vec{r})] \quad (16.76)$$

$$= \int_{\Omega} d\vec{r} i u_{\vec{k}_c}^*(\vec{r}) \frac{\partial}{\partial \vec{k}_c} u_{\vec{k}_c}(\vec{r}) - \frac{\partial}{\partial i\vec{k}} \ln w_{\vec{k}\vec{k}_c} \Big|_{\vec{k}=\vec{k}_c} = \mathcal{R}_{\vec{k}_c} - \mathcal{R}_{\vec{k}_c} = 0 \quad (16.77)$$

$|u|^2$ integrates to 1; $|w|^2$ sums to 1; and $\partial |w|_{\vec{k}-\vec{k}_c} / \partial \vec{k} = 0$ because of the maximum at \vec{k}_c .

$$\Rightarrow \langle W_{\vec{r}_c \vec{k}_c} | \vec{r} | W_{\vec{r}_c \vec{k}_c} \rangle = \vec{r}_c \quad \begin{array}{l} \text{Hence the definition in} \\ \text{(16.69).} \end{array} \quad (16.78)$$

16.4.2 Dynamics from Lagrangian

Given this wave packet, one can obtain equations of motion for \vec{r}_c and \vec{k}_c by evaluating the Lagrangian

$$\mathcal{L} = \langle W_{\vec{r}_c \vec{k}_c} | i\hbar \frac{\partial}{\partial t} | W_{\vec{r}_c \vec{k}_c} \rangle - \langle W_{\vec{r}_c \vec{k}_c} | \hat{\mathcal{H}} - eV(\vec{r}) | W_{\vec{r}_c \vec{k}_c} \rangle \quad (16.79)$$

$$\hat{\mathcal{H}} = \frac{1}{2m} \left[\hat{\mathbf{p}} + \frac{e\vec{A}(\vec{r})}{c} \right]^2 + U(\vec{r}) \quad (16.80)$$

$$\left[\frac{\hat{\mathbf{p}}^2}{2m} + U(\vec{r}) \right] \psi_{\vec{k}} = \mathcal{E}_{\vec{k}} \psi_{\vec{k}}. \quad \text{Suppress the band index } n. \quad (16.81)$$

Magnetic fields are included through the vector potential \vec{A} , and electric fields are included through the scalar potential V . Because the focus is on wave packets, which are localized in space, one does not have to worry about the impossibility of incorporating the scalar potential rigorously into periodic boundary conditions.

Evaluation of the expectation values needed to find the Lagrangian (16.79) is a matter of evaluating various integrals. Whenever $|w|_{\vec{k}-\vec{k}_c}^2$ appears, it should be treated as a delta function centered at \vec{k}_c . Details are left to Problem 5, and the results are

$$\langle W_{\vec{r}_c \vec{k}_c} | i\hbar \frac{\partial}{\partial t} | W_{\vec{r}_c \vec{k}_c} \rangle = \frac{e\vec{r}_c}{c} \cdot \frac{d\vec{A}(\vec{r}_c)}{dt} + \hbar \vec{k}_c \cdot \dot{\vec{r}}_c + \hbar \vec{k}_c \cdot \vec{\mathcal{R}}_{\vec{r}_c} \quad (16.82a)$$

$$\langle W_{\vec{r}_c \vec{k}_c} | \hat{\mathcal{H}} - eV(\vec{r}) | W_{\vec{r}_c \vec{k}_c} \rangle = \mathcal{E}_{\vec{k}_c} - \vec{B} \cdot \vec{m}_{\vec{k}_c} - eV(\vec{r}_c) \quad (16.82b)$$

To obtain this result in the presence of the magnetic field requires the phase factor involving \vec{A} in Eq. (16.65), and it requires that the wave packet not be spatially extended on scales where the electric and magnetic fields vary noticeably. The term $\vec{m}_{\vec{k}}$ is an intrinsic magnetic moment of the wave function and comes formally from expanding \vec{A} about \vec{r}_c . c.c. below is “complex conjugate.”

with the orbital magnetic moment of the wave packet $m_{\vec{k}_c}$ given by

$$\vec{m}_{\vec{k}_c} = -\frac{e\hbar}{2mc} \frac{1}{2} \int_{\Omega} d\vec{r} \left[\frac{\partial u_{\vec{k}_c}^*}{\partial i\vec{k}_c} - \vec{\mathcal{R}}_{\vec{k}_c} u_{\vec{k}_c}^* \right] \times \left[\frac{\partial}{\partial i\vec{r}} + \vec{k}_c \right] u_{\vec{k}_c} + \text{c.c.} \quad (16.82c)$$

Finally, employing Lagrange’s equations, one obtains

$$\frac{\partial \mathcal{L}}{\partial \vec{r}_c} = \frac{d}{dt} \frac{\partial \mathcal{L}}{\partial \dot{\vec{r}}_c} \quad \text{and} \quad \frac{\partial \mathcal{L}}{\partial \vec{k}_c} = \frac{d}{dt} \frac{\partial \mathcal{L}}{\partial \dot{\vec{k}}_c}. \quad (16.83)$$

Problem 6 shows that after dropping the subscript c on \vec{k} and \vec{r} , one has the semi-classical equations of motion

$$\hbar \dot{\vec{k}} = -e\vec{E} - \frac{e}{c} \dot{\vec{r}} \times \vec{B} \quad (16.84a)$$

$$\dot{\vec{r}} = \frac{1}{\hbar} \frac{\partial \tilde{\mathcal{E}}_{\vec{k}}}{\partial \vec{k}} - \dot{\vec{k}} \times \vec{\Omega}, \quad (16.84b)$$

where

$$\tilde{\mathcal{E}}_{\vec{k}} = \mathcal{E}_{\vec{k}} - \vec{B} \cdot \vec{m}_{\vec{k}}, \quad (16.85a)$$

$$\vec{B}(\vec{r}) = \frac{\partial}{\partial \vec{r}} \times \vec{A}(\vec{r}), \quad \text{and} \quad (16.85b)$$

$$\vec{\Omega}(\vec{k}) = \frac{\partial}{\partial \vec{k}} \times \vec{\mathcal{R}}(\vec{k}). \quad (16.85c)$$

The terms involving the *anomalous velocity* $\vec{\Omega}$ and wave packet magnetic moment $\vec{m}_{\vec{k}}$, can sometimes be omitted from semiclassical equations of motion for electrons. One reason is that they often vanish by symmetry. In particular, they vanish for crystals that have both time-inversion symmetry, and spatial inversion symmetry. Under time inversion, \vec{k} , $\partial/i\partial\vec{r}$, \vec{r} , and \vec{B} flip sign while \vec{E} and $\vec{\mathcal{R}}_{\vec{k}}$ are unchanged; therefore $\vec{\Omega}(\vec{k}) = -\vec{\Omega}(-\vec{k})$ and $\vec{m}_{\vec{k}} = -\vec{m}_{-\vec{k}}$. Under spatial inversion, \vec{r} , \vec{k} , $\vec{\mathcal{R}}_{\vec{k}}$ and \vec{E} flip sign while \vec{B} does not, so $\vec{\Omega}(\vec{k}) = \vec{\Omega}(-\vec{k})$ and $\vec{m}_{\vec{k}} = \vec{m}_{-\vec{k}}$. These two symmetries are only compatible if $\vec{\Omega}$ and $\vec{m}_{\vec{k}}$ vanish for all \vec{k} . Thus the terms can be omitted for many monatomic solids. However, they should not be omitted in crystals without inversion symmetry, such as GaAs, or in crystals with spontaneous magnetic moments such as iron. The existence of such terms has been known for a long time, since work of Karplus and Luttinger (1954) and Blount (1962), and the fact that they nevertheless have often been left off is due to a desire for simplicity. The careful development of spintronics (Section 26.5) will however require these terms to provide an accurate account of how spin currents respond to external fields.

Limitations of Semiclassical Dynamics. Validity of the semiclassical equations of motion requires four conditions:

1. The spatial scales of all external potentials must be much larger than interatomic spacing, making it possible to construct wave packets spanning many unit cells, but seeing the external potentials as very slowly varying.
2. The magnitudes of the electric fields cannot be too large, or else they induce Zener tunneling between bands. To prevent this tunneling in a solid with band gap \mathcal{E}_g , one must require, according to Eq. (16.64),

$$\frac{eE}{k_F} \ll \mathcal{E}_g \sqrt{\frac{\mathcal{E}_g}{\mathcal{E}_F}}. \quad (16.86)$$

Electric fields this large are impossible to obtain in metals except near points of degeneracy where band gaps shrink to zero. With energy gaps on the order of 1 eV, and $1/k_F$ on the order of 1 Å, the electric field needs to be on the order of 1 V/Å, or 10^{10} V/m. The largest fields that actually can be generated in a metal are six orders of magnitude smaller, because electrons are quite effective in screening external fields out of existence.

3. The magnitudes of magnetic fields cannot be too large. The characteristic energy of electrons in magnetic fields is derived from their orbital period \mathcal{T} and is $2\pi\hbar/\mathcal{T}$. For free electrons, as shown in Section 21.2, $\mathcal{T} = 2\pi mc/eB$, which can be used to obtain the estimate $2\pi\hbar/\mathcal{T} \sim 1.16 \cdot 10^{-4} [B/\text{T}] \text{eV}$, measuring the magnetic induction in Tesla. By analogy with Eq. (16.86), estimate that magnetic fields will not induce interband transitions so long as

$$2\pi\hbar/\mathcal{T} \ll \mathcal{E}_g \sqrt{\frac{\mathcal{E}_g}{\mathcal{E}_F}}. \quad (16.87)$$

In magnetic fields of 10 T, electrons are therefore able to jump across band gaps on the order of 0.1eV.

4. As will be shown in Section 23.4, when incoming electrical fields oscillate at frequencies ω such that $\hbar\omega = \mathcal{E}_g$, they excite electrons between bands. Therefore semiclassical electron dynamics only applies in the presence of slowly varying external fields.

Hamiltonian Dynamics. Whenever classical dynamics are described by a Lagrangian $\mathcal{L}(\vec{Q}, \dot{\vec{Q}})$, it is possible to derive also a Hamiltonian, using the formulae

$$\mathcal{H} = \sum_l \dot{Q}_l P_l - \mathcal{L}; \quad P_l = \frac{\partial \mathcal{L}}{\partial \dot{Q}_l}. \quad \text{The } Q\text{'s here are the three components of } \vec{r}_c \text{ and the three components of } \vec{k}_c. \quad (16.88)$$

In the present case, dropping the subscript c from \vec{r}_c and \vec{k}_c , one has the canonical momenta \vec{p} and $\vec{\pi}$

$$\vec{p} = \frac{\partial \mathcal{L}}{\partial \dot{\vec{r}}} = \hbar \vec{k} - \frac{e\vec{A}}{c} \Rightarrow \hbar \vec{k} = \vec{p} + e\vec{A}/c \quad (16.89a)$$

$$\vec{\pi} = \frac{\partial \mathcal{L}}{\partial \dot{\vec{k}}} = \hbar \vec{\mathcal{R}}_{\vec{k}}, \quad (16.89b)$$

and from Eq. (16.88) obtains the Hamiltonian

$$\mathcal{H} = \mathcal{E}_{\vec{k}} - eV(\vec{r}) + (e/2mc)\vec{B} \cdot \vec{\mathcal{L}}_{\vec{k}} \equiv \mathcal{E}(\vec{p} + e\vec{A}/c) - eV(\vec{r}) + (e/2mc)\vec{B} \cdot \vec{\mathcal{L}}_{\vec{k}}. \quad (16.90)$$

The Hamiltonian is a constant of the motion, a fact that is especially useful in visualizing electron dynamics when the electrical potential V and \vec{L} vanish. One simply draws contours on the energy surface $\mathcal{E}_{n\vec{k}}$ and concludes that \vec{k} travels along these contours. *Closed orbits* are those for which \vec{k} is periodic in the repeated zone scheme, and *open orbits* are those for which \vec{k} continually increases in the repeated zone scheme, as illustrated in Figure 16.8.

16.5 Quantizing Semiclassical Dynamics

Having gone to all the trouble of coercing quantum mechanics into a classical form, it is interesting to move slightly backwards and quantize the semiclassical dynamics. This task may be accomplished by considering the overall phase of the wave packet.

A solution of Schrödinger's equation should obey

$$i\hbar \frac{\partial}{\partial t} |W\rangle = \hat{\mathcal{H}} |W\rangle. \quad (16.91)$$

Because wave packets are not exact solutions of Schrödinger's equation, they do not exactly obey Eq. (16.91). However, they should approximately obey

$$i\hbar \frac{\partial}{\partial t} |W\rangle = \mathcal{H} |W\rangle, \quad (16.92)$$

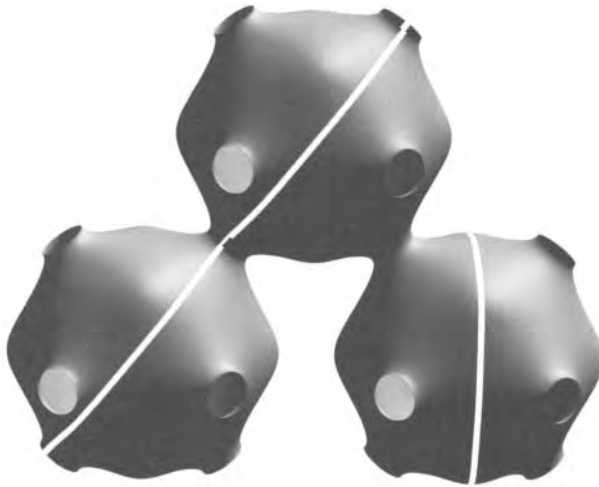


Figure 16.8. Energy contours on the Fermi surface of copper, showing open and closed orbits.

where \mathcal{H} is the Hamiltonian of Eq. (16.90), so that as time evolves, the wave packet acquires an additional phase

$$e^{-i\mathcal{H}t/\hbar}. \quad \text{Because } \mathcal{H} \text{ is a constant of the motion.} \quad (16.93)$$

Consider now a case in which after some time $t = \mathcal{T}$ the dynamics of the wave packet brings it back to its location at time $t = 0$; the position $\vec{r}(\mathcal{T})$ returns to $\vec{r}(0)$, and the wave number $\vec{k}(\mathcal{T})$ arrives at $\vec{k}(0) + \vec{K}$, where \vec{K} is any reciprocal lattice vector. If the phase factor in (16.93) differs from 1, the wave packet interferes destructively with its past self, but if it equals 1, the packet reinforces itself and can establish a resonant standing wave. The condition for this resonance to occur should roughly be of the form

$$\mathcal{H}\mathcal{T} = 2\pi\hbar j. \quad \text{Where } j \text{ is some integer.} \quad (16.94)$$

More careful examination of the resonance conditions for wave packets, provided by Littlejohn (1986), leads instead to the Bohr–Sommerfeld quantization condition of the “old” quantum mechanics, a good approximation for large quantum numbers j ,

$$2\pi\hbar(j + \nu) = \int dt \sum_l P_l \frac{\partial \mathcal{H}}{\partial P_l} = \oint \sum_l dQ_l P_l. \quad (16.95)$$

The *Maslov index* ν is a constant, frequently 1/2. This additional constant does not lead to any physical consequences in any of the following arguments, and it can be viewed as absorbed into Γ in all the formulae following Eq. (16.98).

Employing the canonical momenta calculated in Eq. (16.89) gives the quantization condition

$$\oint d\vec{k} \cdot \vec{\mathcal{R}}_{\vec{k}} + d\vec{r} \cdot \left[\vec{k} - \frac{e\vec{A}}{\hbar c} \right] = 2\pi j \quad (16.96)$$

$$\Rightarrow \oint d\vec{k} \cdot (\vec{\mathcal{R}}_{\vec{k}} - \vec{r}) - d\vec{r} \cdot \frac{e\vec{A}}{\hbar c} = 2\pi j. \quad \text{Integrating by parts.} \quad (16.97)$$

16.5.1 Wannier–Stark Ladders

One way in principle to send electrons into closed orbits is to consider a system with uniform electric field $\vec{E} = -\nabla V$ and no magnetic field. The wave vector \vec{k} evolves linearly in time as $\dot{\vec{k}} = -e\vec{E}t/\hbar$. Because $\dot{\vec{r}} = \partial\mathcal{E}/\partial\hbar\vec{k}$ flips sign when $\vec{k} \rightarrow \vec{K} - \vec{k}$, so long as \vec{E} points in the direction of a reciprocal lattice vector, the electron is supposed to execute periodic motion. Defining

$$\Gamma = \oint d\vec{k} \cdot \vec{\mathcal{R}}_{\vec{k}}, \quad \text{Because } \vec{k} \text{ returns to itself by increasing by a reciprocal lattice vector, the integral is a line integral from } 0 \text{ to } \vec{K}. \quad (16.98)$$

Eq. (16.97) becomes

$$2\pi j = \oint d\vec{k} \cdot (\vec{\mathcal{R}}_{\vec{k}} - \vec{r}) = \Gamma - \int_0^K d\vec{k} \cdot \vec{r} = \Gamma - K \langle \vec{r} \rangle \quad (16.99)$$

$\langle \vec{r} \rangle$ is defined to be the time average of \vec{r} , and gives the center of the orbit.

$$\Rightarrow \langle \vec{r} \rangle = \frac{\Gamma - 2\pi j}{K}. \quad (16.100)$$

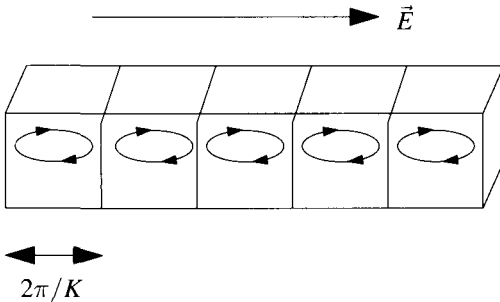


Figure 16.9. The Wannier–Stark ladder is a collection of electrons trapped in Bloch oscillations by an intense electric field, and spaced at intervals of $2\pi/K$, where \vec{K} is a reciprocal lattice vector.

In a pure metal at very low temperatures, Eq. (16.100) predicts no electrical conductivity. Each electron should circle around its unit cell in a closed orbit, as shown in Figure 16.9. The reason this result is never observed in practice is that electrons cannot execute even one oscillation before undergoing a scattering event that ruins the necessary quantum coherence, and the huge electric fields would produce Zener tunneling. Problem 1 is devoted to estimating orders of magnitude that show how difficult it would be to observe the phenomenon in a metal like copper.

Wannier–Stark ladders have been observed by Mendez et al. (1988) in GaAs superlattices, although the experiments are difficult, and the results not entirely in accord with the simplest theoretical account. Cleaner results are reported in optical lattices by Wilkinson et al. (1996).

16.5.2 de Haas–van Alphen Effect

A second and considerably more important case in which electrons execute closed orbits occurs when the electric field vanishes, but a uniform magnetic induction \vec{B} , derived from vector potential

$$\vec{A} = \frac{1}{2} \vec{B} \times \vec{r}, \quad \text{This gauge is not unique, but is convenient for this calculation.} \quad (16.101)$$

is present. The wave vector evolves according to

$$\dot{\vec{k}} = \frac{-e\vec{r}}{\hbar c} \times \vec{B} \Rightarrow \vec{k}(t) - \vec{k}(0) = \frac{-e}{\hbar c} [\vec{r}(t) - \vec{r}(0)] \times \vec{B} \quad (16.102)$$

$$\Rightarrow \vec{B} \times (\vec{k}(t) - \vec{k}(0)) = \frac{-e}{\hbar c} [\vec{r}(t) - \vec{r}(0)] B^2 + \frac{e}{\hbar c} \vec{B} \cdot [\vec{r}(t) - \vec{r}(0)] \vec{B}. \quad (16.103)$$

Because $\vec{A} \times (\vec{B} \times \vec{C}) = \vec{B}(\vec{A} \cdot \vec{C}) - \vec{C}(\vec{A} \cdot \vec{B})$.

Some orbits in \vec{k} space are pictured in Figure 16.8. De Haas and van Alphen (1930) measured the magnetization of bismuth in a field of 20 kG and found that magnetization oscillated as a function of magnetic field. The original measurements observed only two periods of oscillation, but with improvements in technique, many due to Shoenberg (1984), hundreds of periods (including periods of one frequency superposed upon another) became visible, as shown in Figure 16.10. Over two decades separated the first observation of this effect from the realization by Onsager (1952) and Lifshitz and Kosevich (1956) that the oscillations are sensitive probes of a simple geometrical property of the Fermi surface. From the period of oscillation one can directly determine the areas of extremal electron orbits. With this understanding in hand, de Haas–van Alphen oscillations become an experimental tool capable of deciphering the Fermi surface of most elements and compounds to surprising accuracy.

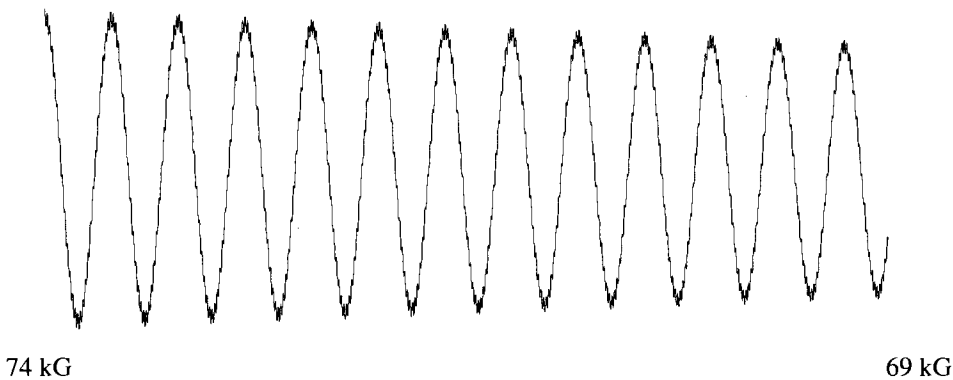


Figure 16.10. Sketch of de Haas–van Alphen oscillations of magnetization M in gold similar to those measured by Shoenberg and Vanderkooy (1970). The external magnetic field H points 8.5° away from (111). Large-scale oscillations are due to extremal orbits around the thin neck, while small-scale oscillations, barely resolved, are due to extremal orbits about the thick belly.

Origin of Oscillations in Quantization. The quantization condition (16.97) when only a magnetic induction B is present becomes

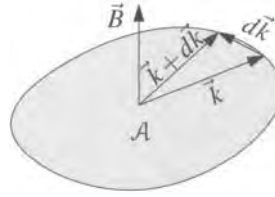
$$2\pi j = \Gamma - \int_0^{\mathcal{J}} dt \left[\frac{e\vec{A}}{c\hbar} \cdot \dot{\vec{r}} - \frac{e}{\hbar c} (\dot{\vec{r}} \times \vec{B}) \cdot \vec{r} \right] \quad \begin{array}{l} \text{Using the definition of } \Gamma \text{ from} \\ \text{Eq. (16.98), and inserting} \\ \text{(16.84a) for } \dot{\vec{k}}. \end{array} \quad (16.104)$$

$$= \Gamma + \int_0^{\mathcal{J}} dt \frac{e}{2\hbar c} \vec{r} \cdot (\dot{\vec{r}} \times \vec{B}) \quad (16.105)$$

$$= \Gamma + \int_0^{\mathcal{J}} dt \frac{\hbar c}{2eB} \left(\frac{\vec{B}}{B} \times \vec{k} \right) \cdot \dot{\vec{k}} \quad \begin{array}{l} \text{Use Eqs. (16.84a) and (16.103).} \\ \text{Constant offsets in } \vec{k} \text{ or } \vec{r} \text{ vanish.} \end{array} \quad (16.106)$$

$$= \Gamma + \oint d\vec{k} \cdot \frac{\hbar c}{2eB} \left(\frac{\vec{B}}{B} \times \vec{k} \right) \quad (16.107)$$

$$\Rightarrow 2\pi j = \Gamma + \mathcal{A} \frac{\hbar c}{eB}, \quad \begin{array}{l} d\vec{k} \cdot (\hat{n} \times \vec{k}) \text{ is twice} \\ \text{the area element.} \end{array} \quad (16.108)$$



where \mathcal{A} is the area in \vec{k} space enclosed by the orbit $\vec{k}(t)$.

The geometrical significance of Eq. (16.108) is illustrated in Figure 16.11. As the amplitude of the magnetic induction B increases, orbits move along the Fermi surface, increasing the area they enclose to keep the product $\mathcal{A}\hbar c/eB$ constant. With each integer j there is associated not just one orbit, but a range of them; all satisfy (16.108) and are within the small energy range $d\mathcal{E} = k_B T$ of the Fermi surface. This range is also depicted in Figure 16.11. Another way to think of Eq. (16.108) is that it restricts electrons to a series of concentric cylinders in \vec{k} space. The intersection of these cylinders with the Fermi surface shown in Figure 16.11 selects the electrons that can be active in transport measurements. The number of such active electrons is maximal whenever their orbits coincide with an extremal section \mathcal{A}_e of the Fermi surface, where $\partial\mathcal{A}/\partial k_z = 0$. The current loops of these electrons produce peaks in the magnetization, and thus the condition to see these peaks is

$$\frac{\mathcal{A}}{B} \frac{\hbar c}{2\pi e} = 1.05 \cdot 10^4 \frac{\mathcal{A} \cdot \text{\AA}^2}{[B/\text{T}]} = j - \Gamma/2\pi \quad (16.109a)$$

$$\Rightarrow \mathcal{A} = 9.52 \cdot 10^{-5} \frac{1}{\Delta(1/B)} [\text{\AA}^{-2}/\text{T}]. \quad \begin{array}{l} \Delta(1/B) \text{ is the change in } 1/B \\ \text{needed to see one complete} \\ \text{period of oscillation.} \end{array} \quad (16.109b)$$

16.5.3 Experimental Measurements of Fermi Surfaces

The simplest Fermi surfaces to decipher are those of the alkali metals, Na, K, and Rb (lithium undergoes a martensitic transition that has prevented its Fermi surface from being measured at the 1 K temperature where oscillations generally are measured). These metals have d -bands far removed from the half-filled s -band at the Fermi surface. As a consequence the Fermi surface is contained entirely within the first Brillouin zone and is very nearly spherical, as in the upper left entry

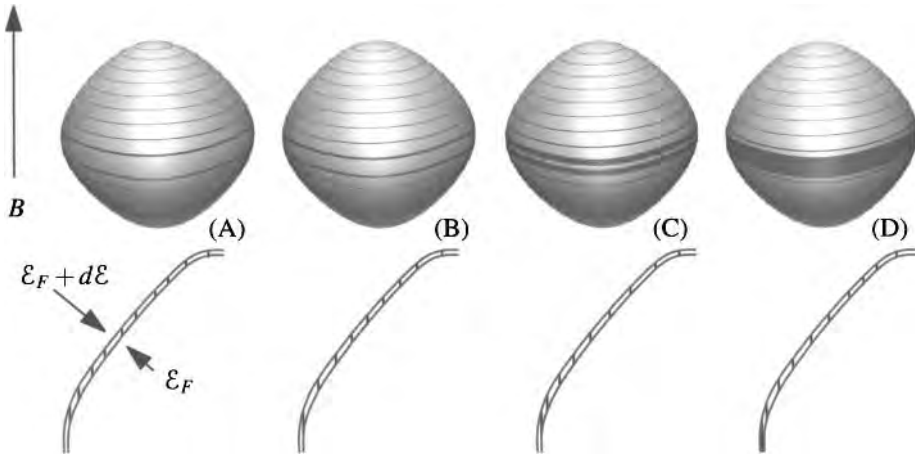


Figure 16.11. Resonantly oscillating electrons sit on the Fermi surface, move perpendicular to the magnetic field, and enclose an area in \vec{k} space $\mathcal{A} = (2\pi l - \Gamma)eB/\hbar c$. These electrons occupy the intersection of the Fermi surface with a set of concentric cylinders. The density of states satisfying these conditions is indicated by the thicknesses of the orbits, and is given by the number of states both obeying the quantization condition and lying between \mathcal{E}_F and $\mathcal{E}_F + d\mathcal{E}$, where $d\mathcal{E} = k_B T$. The lower part of the figure shows cross-sections of the surfaces in the upper part. Whenever electron orbits lie along an extremal point of the Fermi surface, as in (D), the density of states becomes very large. The figure is deceptive because the number of orbits pictured is around 20, while experimentally the number is around 10^4 .

of Figure 8.7. The experiments are so accurate that they can detect tiny deviations from the perfect sphere, on the scale of tenths of a percent.

The next simplest Fermi surfaces belong to the monovalent noble metals, Cu, Ag, and Au. Although the nearly free electron picture applies reasonably well to these elements, Figure 10.7 shows that the d -bands lie sufficiently close to the Fermi surface that the surface is distorted and cuts through the Brillouin zone, as illustrated in in Figure 16.12. Therefore a number of qualitatively different types of orbits is possible, and these show up as multiple frequencies in Figure 16.10.

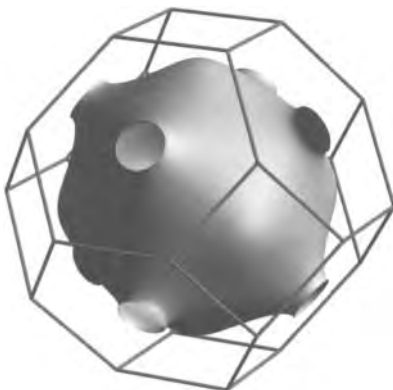


Figure 16.12. Fermi surface of copper, as measured by the de Haas van Alphen effect, employing data of Shoenberg (1984).

One way to interpret the experimental data is to write down a tight-binding model with a number of free parameters and vary them until the extremal Fermi surface orbits match those seen experimentally.

Three of the divalent metals (Ca, Sr, Ba) would be insulators if the Fermi surface did not cut across the first Brillouin zone, creating isolated pockets of electrons. The hexagonal divalents (Be, Mg, Zn, and Cd) have the unpleasant feature that important aspects of their band structure are produced by spin-orbit coupling, and the fields applied to measure the de Haas-van Alphen effect are sufficient to cause magnetic breakdown. The net effect is that the Fermi surface changes before one's eyes during the measurements, essentially from the second column of Figure 8.8 to the third column of Figure 8.8, and this fact must be taken into account in interpreting the measurements.

Elements with more than one or two mobile electrons per unit cell sometimes continue to be described by the nearly free electron picture, as in the case of aluminum. More commonly, however, the nearly free-electron picture breaks down altogether. For example, in the transition metals, the *d*-bands reach right up to the Fermi surface, and the surfaces bear no particular resemblance to free electron surfaces. It is difficult to interpret their de Haas-van Alphen oscillations without theoretical guidance from band structure calculations about the shapes of the surfaces, but with the aid of sufficient trial and error, surfaces such as tungsten, shown in Figure 16.13, have been worked out. Landolt and Börnstein (New Series) vol. 13c, provides a compendium of the results.



Figure 16.13. The Fermi surface of tungsten, as deciphered by Girvan et al. (1968).

The most accurate probes of the Fermi surface are provided by oscillations in magnetization, but because the effect results from changes in the density of states at the Fermi surface, magnetization is by no means the only quantity that oscillates. Careful measurements of sound speeds, specific heat, ultrasonic attenuation, and other quantities all exhibit oscillations with the same period in $1/B$. These probes are discussed at greater length in Cracknell and Wong (1973).

Problems

1. **Bloch oscillations:** Consider whether it should be possible to observe Bloch oscillations.
 - (a) Take the relaxation time in copper to be approximately $20 \cdot 10^{-14}$ s. How strong an electric field would be needed in order to have a Bloch oscillation in less than a relaxation time?
 - (b) Assuming a characteristic band gap of 2 eV, how large is this field compared to one that could induce Zener tunneling?
 - (c) Suppose the electric field of part (a) were applied, and the electrons produced a current according to the Drude formula rather than becoming localized. Estimate how much power would be dissipated per volume, and how fast the copper would heat up.
 - (d) Consider next GaAs, where at low temperatures relaxation times can rise to $3 \cdot 10^{-10}$ s, and where it is possible to build artificial structures for which the unit cell is on the order of $a = 100 \text{ \AA}$. How large an electric field would be needed to see Bloch oscillations in this case?
 - (e) Estimate the energy difference between two energy states in a Wannier–Stark ladder when such a field is applied.
2. **Damped dynamics:** Suppose that a small amount of damping changes the semiclassical equations of motion for tightly bound electron in one dimension to

$$\dot{r} = \frac{2\mathcal{E}_0 a}{\hbar} \sin ka \quad (16.110a)$$

$$\hbar \dot{k} = -eE - \frac{m\dot{r}}{\tau}. \quad (16.110b)$$

Take $\mathcal{E}_0 = 1 \text{ eV}$, $a = 2 \text{ \AA}$, $E = 10^6 \text{ V/cm}$, and $\tau = 10^{-14} \text{ s}$.

- (a) Put the equations into dimensionless form, measuring distance in units of a , and measuring time in units of τ .
- (b) Integrate the equations (16.110) numerically and examine the effect of the damping upon the electron dynamics.
- (c) Describe the final state of the system analytically.

3. Effective mass theorem:

- (a) Show that to second order in $\vec{\delta k}$, one has from Eqs. (16.19) and (16.20)

$$\mathcal{E}^{(2)} = \frac{\hbar^2}{2m} \delta k^2 + \frac{\hbar^2}{m^2} \sum_{n' \neq n} \frac{|\langle \psi_{n\vec{k}} | \vec{\delta k} \cdot \hat{P} | \psi_{n'\vec{k}} \rangle|^2}{\mathcal{E}_{n\vec{k}} - \mathcal{E}_{n'\vec{k}}}. \quad (16.111)$$

Second order contributions come both from second order in perturbation theory, as well as the fact that Eq. (16.19) contains a second order term.

(b) Show, therefore, that the effective mass tensor is given by Eq. (16.29).

4. **Tight-binding model:** Consider the tight-binding Hamiltonian for a spinless particle on a square lattice:

$$\hat{\mathcal{H}} = \sum_{\vec{R}} U|\vec{R}\rangle\langle\vec{R}| + t \sum_{\langle\vec{R}\vec{R}'\rangle} |\vec{R}\rangle\langle\vec{R}'| + |\vec{R}'\rangle\langle\vec{R}|, \quad (16.112)$$

where the sum in the second term is over distinct nearest-neighbor pairs.

(a) Write down the energy eigenvalues of this Hamiltonian.

(b) Find the effective mass tensor of a particle in one of these energy eigenstates. How does the effective mass vary with t ? Why?

5. **Effective Lagrangian:**

(a) Writing

$$\frac{\partial}{\partial t} = \dot{\vec{r}}_c \cdot \frac{\partial}{\partial \vec{r}_c} + \dot{\vec{k}}_c \cdot \frac{\partial}{\partial \vec{k}_c} \quad (16.113)$$

use Eq. (16.65) to evaluate Eq. (16.82a).

(b) Show that for any polynomial function f ,

$$f(\hat{P})\psi_{\vec{k}}(\vec{r}) = e^{i\vec{k}\cdot\vec{r}} f(\hat{P}_{\vec{k}})u_{\vec{k}}(\vec{r}), \quad (16.114)$$

where

$$\hat{P}_{\vec{k}} \equiv \hat{P} + \hbar\vec{k}. \quad (16.115)$$

The Bloch functions $\psi_{\vec{k}}$ and $u_{\vec{k}}$ are related by Eq. (7.45), and \hat{P} is the momentum operator.

(c) Begin the evaluation of Eq. (16.82b). Show that the matrix element equals

$$\int \frac{d\vec{r}}{N} \sum_{\vec{k}\vec{k}'} w_{\vec{k}\vec{k}'}^* e^{i(\vec{k}-\vec{k}')\cdot(\vec{r}_c-\vec{r})} u_{\vec{k}}^*(\vec{r}) \left\{ \begin{aligned} & [\hat{P}_{\vec{k}'} + \frac{e}{c}(\vec{A}(\vec{r}) - \vec{A}(\vec{r}_c))]^2/2m \\ & + U(\vec{r}) - eV(\vec{r}) \end{aligned} \right\} u_{\vec{k}'}(\vec{r}) w_{\vec{k}'\vec{k}_c} \quad (16.116)$$

(d) Separate off the terms independent of \vec{A} and show that they produce $\mathcal{E}_{\vec{k}_c} - eV(\vec{r}_c)$. Use the approximation that $V(\vec{r}) = V(\vec{r}_c) + (\vec{r} - \vec{r}_c) \cdot \partial V(\vec{r}_c)/\partial \vec{r}_c$.

(e) Discard the terms proportional to A^2 , and take $\vec{A} = -\vec{r} \times \vec{B}/2$. Show that the terms proportional to \vec{A} can be written as

$$\frac{e}{4mc} \vec{B} \cdot \int \frac{d\vec{r}}{N} \sum_{\vec{k}\vec{k}'} w_{\vec{k}\vec{k}'}^* u_{\vec{k}}(\vec{r}) \left[-\frac{\partial}{\partial i\vec{k}} e^{i(\vec{k}-\vec{k}')\cdot(\vec{r}_c-\vec{r})} \right] \times \hat{P}_{\vec{k}'} u_{\vec{k}'}(\vec{r}) w_{\vec{k}'\vec{k}_c} + \text{c.c.} \quad (16.117)$$

(f) Integrating by parts in \vec{k} , and following the steps that lead from Eq. (16.70) to Eq. (16.77), verify the remainder of Eq. (16.82).

6. Equations of motion:

(a) Show that if $\vec{C}_{\vec{r}}$ is a vector function of \vec{r} and \vec{D} is independent of \vec{r} then

$$\vec{D} \times \left(\frac{\partial}{\partial \vec{r}} \times \vec{C}_{\vec{r}} \right) = \frac{\partial}{\partial \vec{r}} (\vec{D} \cdot \vec{C}_{\vec{r}}) - (\vec{D} \cdot \frac{\partial}{\partial \vec{r}}) \vec{C}_{\vec{r}}. \quad (16.118)$$

(b) Using this identity both for the term involving \vec{A} , and the one involving $\vec{\mathcal{P}}_{\vec{k}_c}$, apply Eqs. (16.83) to Eqs. (16.82) to obtain equations of motion for \vec{k}_c and \vec{r}_c .

7. **Alternate view of Bloch states in weak electric fields:** Show that if one begins with a true Bloch state and subjects it to a weak electric field, that it evolves into a new Bloch state with wave vector obeying

$$\hbar \dot{\vec{k}} = -e \vec{E}. \quad (16.119)$$

In order to carry out the demonstration,

(a) Take a Bloch state and evolve it by a small amount forward in time dt , using the Hamiltonian

$$\hat{\mathcal{H}} = \frac{\hat{P}^2}{2m} + U(\hat{R}) + e \vec{E} \cdot \hat{R}. \quad (16.120)$$

(b) Then apply the translation operator $T_{\vec{R}}^\dagger$, which generates translations through Bravais lattice vectors. Interpret the result to show that one still has a Bloch state, but with a new \vec{k} vector, to first order in dt .

8. Houston states:

(a) Write the Schrödinger equation for a free electron in an electric field in terms of a basis of Houston states.

(b) Find the rate at which such an electron initially in a Houston state departs from the Houston state.

9. **Alternate view of Bloch states in weak fields:** Show that if a Bloch state ψ is subjected to a very weak magnetic induction B , then it evolves into a new Bloch state, and that the \vec{k} vector evolves according to

$$\hbar \dot{\vec{k}} = -\frac{e}{c} (\vec{v} \times \vec{B}). \quad (16.121)$$

(a) Suppose one has a wave packet $|W_{\vec{r}\vec{k}}\rangle$ that obeys

$$e^{i\hat{P}\cdot\vec{R}/\hbar} |W_{\vec{r}\vec{k}}\rangle \approx e^{i\vec{k}\cdot\vec{R}} |W_{\vec{r}\vec{k}}\rangle \quad (16.122)$$

and

$$\langle \vec{r} \rangle = \langle W_{\vec{r}\vec{k}} | \hat{R} | W_{\vec{r}\vec{k}} \rangle. \quad (16.123)$$

Adopt the gauge

$$\vec{A} = \frac{1}{2} \vec{B} \times (\vec{r} - \langle \vec{r} \rangle) \quad (16.124)$$

Because \vec{k} depends upon time, $\langle \vec{r} \rangle$ as given by Eq. (16.123) is time-dependent, and therefore the choice of gauge (16.124) describes a system with both magnetic induction \vec{B} and an electric field.

Argue therefore that in order to describe a system with magnetic induction B only, one must write the Hamiltonian

$$\hat{\mathcal{H}} = \frac{1}{2m} (\hat{P} + \frac{e}{c} \vec{A}(t))^2 + U(\vec{r}) - \frac{e}{2c} \vec{r} \cdot \vec{B} \times \vec{v}_{\vec{k}}. \quad (16.125)$$

- (b) Use this Hamiltonian to evolve $W_{\vec{r}\vec{k}}$ through a small amount of time, dt . Before the time evolution the wave function is described approximately by eigenvalue \vec{k} . After the evolution, the wave function is still approximately an eigenfunction of the operator $\hat{T}_{\vec{r}}^\dagger$, but the eigenvalue \vec{k} has shifted slightly. Use this fact to deduce an equation of motion for \vec{k} .

References

- M. ben Dahan, E. Peik, J. Reichel, Y. Castin, and C. Salomon (1996), Bloch oscillations of atoms in an optical potential, *Physical Review Letters*, **76**, 4508–4511.
- E. Blount (1962), Formalisms of band theory, *Solid State Physics: Advances in Research and Applications*, **13**, 305–373.
- M. Chang and Q. Niu (1996), Berry phase, hyperorbits, and the Hofstadter spectrum: Semiclassical dynamics in magnetic Bloch bands, *Physical Review B*, **53**, 7010–7023.
- A. P. Cracknell and K. C. Wong (1973), *The Fermi Surface; Its Concept, Determination, and Use in the Physics of Metals*, Clarendon Press, Oxford.
- P. Drude (1900), On the electron theory of metals, *Annalen der Physik*, **1**, 566–613. In German.
- R. F. Girvan, A. V. Gold, and R. A. Phillips (1968), The de Haas-van Alphen effect and the Fermi surface of tungsten, *Journal of Physics and Chemistry of Solids*, **29**, 1485–1502.
- R. Karplus and J. M. Luttinger (1954), Hall effect in ferromagnetics, *Physical Review*, **95**, 1154–1160.
- J. B. Krieger and G. J. Iafrate (1986), Time evolution of Bloch electrons in a homogeneous electric field, *Physical Review B*, **33**, 5494–5500.
- H. Landolt and R. Börnstein (New Series), *Numerical Data and Functional Relationships in Science and Technology*, New Series, Group III, Springer-Verlag, Berlin.
- I. M. Lifshitz and A. M. Kosevich (1956), Theory of magnetic susceptibility in metals at low temperatures, *Soviet Physics JETP*, **2**, 636–645.
- R. G. Littlejohn (1986), The semiclassical evolution of wave packets, *Physics Reports*, **138**, 193–291.
- H. A. Lorentz (1909), *The Theory of Electrons and its Applications to the Phenomena of Light and Radiant Heat*, Teubner, Leipzig.
- E. E. Mendez, F. Agulló-Rueda, and J. M. Hong (1988), Stark localization in GaAs-GaAlAs superlattices under an electric field, *Physical Review Letters*, **60**, 2426–2429.
- E. E. Mendez and G. Bastard (1993), Wannier-Stark ladders and Bloch oscillations in superlattices, *Physics Today*, **46**(6), 34–42.
- G. Nenciu (1991), Dynamics of band electrons in electric and magnetic fields: Rigorous justification of the effective hamiltonians, *Reviews of Modern Physics*, **63**, 91–127.

- L. Onsager (1952), Interpretation of the de Haas-van Alphen effect, *Philosophical Magazine*, **43**, 1006–1008.
- A. B. Pippard (1988), *Magnetoresistance in Metals*, Cambridge University Press, Cambridge.
- M. Raizen, C. Salomon, and Q. Niu (1997), New light on quantum transport, *Physics Today*, **50**(7), 30–34.
- D. Shoenberg (1984), *Magnetic Oscillations in Metals*, Cambridge, Cambridge University Press.
- D. Shoenberg and J. Vanderkooy (1970), Absolute amplitudes in the de Haas-van Alphen effect, *Journal of Low Temperature Physics*, **2**, 483–497.
- G. Sundaram and Q. Niu (1999), Wave-packet dynamics in slowly perturbed crystals: Gradient corrections and Berry-phase effects, *Physical Review B*, pp. 14 915–14 925.
- S. M. Sze (1981), *Physics of Semiconductor Devices*, 2nd ed., John Wiley and Sons, New York.
- J. J. Thomson (1907), *The Corpuscular Theory of Matter*, Charles Scribner's Sons, New York.
- G. Wiedemann and R. Franz (1853), On the thermal conductivity of metals, *Annalen der Physik*, **89**, 497–531. in German.
- S. R. Wilkinson, C. F. Bharucha, K. W. Madison, Q. Niu, and M. G. Raizen (1996), Observation of atomic Wannier–Stark ladders in an accelerating optical potential, *Physical Review Letters*, **76**, 4512–4515.
- J. Zak (1972), The kq -representation in the dynamics of electrons in solids, *Solid State Physics: Advances in Research and Applications*, **27**, 1–62.
- C. Zener (1932), Non-adiabatic crossing of energy levels, *Proceedings of the Royal Society of London*, **A137**, 696–702.

17. Transport Phenomena and Fermi Liquid Theory

17.1 Introduction

The Boltzmann equation and Fermi liquid theory are two phenomenological descriptions of how particles and energy move through condensed matter. The Boltzmann equation is a more general description of transport, describing any particles that obey Hamilton's equations. Fermi liquid theory focuses specifically upon the properties of interacting Fermi particles. In both cases, the theory makes it possible to describe macroscopic experiments in terms of a few well-chosen parameters while bypassing the microscopic information contained in principle within Schrödinger's equation.

17.2 Boltzmann Equation

It is exceedingly difficult to solve any microscopic Hamiltonian that provides a realistic account of the response of solids to external electromagnetic or thermal fields. For example, according to Eq. (16.42), the momentum of electrons in a loop of wire at constant voltage would increase without bound. In a real wire a variety of different processes prevents this increase from happening; the electrons scatter off impurities, or off vibrations in the lattice. To write down a Hamiltonian containing such processes and make substantial progress toward its solution is a challenging task. Fortunately, in many cases the problem can be studied through techniques that preceded quantum mechanics and can make detailed solutions irrelevant.

The *Boltzmann equation* describes transport properties of any particles obeying Hamilton's equations:

$$\dot{\vec{r}} = \frac{\partial \mathcal{H}}{\partial \vec{p}}, \quad \dot{\vec{p}} = -\frac{\partial \mathcal{H}}{\partial \vec{r}}, \quad (17.1)$$

where the Hamiltonian function \mathcal{H} describes the particles' interactions with electric field \vec{E} and magnetic induction \vec{B} in the form

$$\mathcal{H}(\vec{r}, \vec{p}) = \mathcal{E}(\vec{p} + \vec{A}e/c) - eV(\vec{r}), \quad \text{The result derived in Eq. (16.90) is now being postulated as a starting point.} \quad (17.2)$$

leading to

$$\dot{\vec{r}} = \frac{\partial \mathcal{E}}{\partial \hbar \vec{k}} \equiv \vec{v} \quad (17.3a)$$

$$\dot{\vec{k}} = -e\vec{E} - \frac{e\vec{v}}{c} \times \vec{B}, \quad (17.3b)$$

where $\hbar\vec{k}$ is defined by

$$\hbar\vec{k} = \vec{p} + e\vec{A}/c. \quad (17.3c)$$

Electron wave packets in centrosymmetric crystals obey these equation, with all effects of the periodic crystal lattice disappearing into the function $\mathcal{E}_{\vec{k}}$.

The aim now is to use these equations as a tool to describe the behavior of an ensemble of electrons subject to external fields. An ensemble means an ideal Fermi gas of electrons, taken to be noninteracting, but with the effects of Fermi statistics and temperature taken into account. The calculations are not true equilibrium calculations, because the presence of external fields is allowed to induce currents, but the system is supposed always to be close to thermal equilibrium.

Take $g_{\vec{r}\vec{k}}(t)$ to be the occupation number of electrons (wave packets) at position \vec{r} , indexed by wave vector \vec{k} and at time t . It gives the probability, lying between zero and one, that a state will be occupied, so the actual number of electrons in a box of size $d\vec{r}$, and whose wave number lies within a volume element in reciprocal space of size $d\vec{k}$, is

$$g_{\vec{r}\vec{k}}(t) d\vec{r} D_{\vec{k}} d\vec{k} = 2 \frac{d\vec{k} d\vec{r}}{(2\pi)^3} g_{\vec{r}\vec{k}}(t). \quad (17.4)$$

This expression is a straightforward application of the definition of the density of \vec{k} states, $D_{\vec{k}}$, using $\mathcal{V} = d\vec{r}$.

The way to use g is to begin with any function $G_{\vec{r}\vec{k}}$ that depends upon the location and wave number of electrons. Then the average value of $G_{\vec{r}\vec{k}}$ in a large volume is

$$G = \int [d\vec{k}] d\vec{r} g_{\vec{r}\vec{k}} G_{\vec{r}\vec{k}}. \quad (17.5)$$

Integration over $[d\vec{k}]$ defined in Eq. (6.15).

Phenomenological Form of g . It is possible to guess the form that g should have. In the presence of weak applied fields, the occupation number of electrons should differ only slightly from its value in their absence. Therefore,

$$g_{\vec{r}\vec{k}} = f_{\vec{r}\vec{k}} + \text{corrections}, \quad (17.6)$$

where f is the Fermi function.

Because under no circumstances can occupation numbers rise above unity or drop below zero, these corrections must all occur in an energy range of width $k_B T$ near the chemical potential μ . The function $\partial f / \partial \mu$ is nonzero only in this vicinity, so it is reasonable to suppose that all corrections will be proportional to it. Electrons with energies much less than the chemical potential μ cannot speed up because all states are occupied. Electrons with energies much greater than the chemical potential could speed up easily enough, but none are present to do it, leaving those in the vicinity of μ to provide all the action. Consider what should happen in an applied electric field \vec{E} . Because of their negative charge, the electrons that move against the field speed up, while those that move along it slow down, increasing the population moving against the field, and decreasing the population moving with it. Therefore, one expects a correction to the occupation number

for wave number \vec{k} of the form $-e\vec{v}_k \cdot \vec{E}$. Forming the product of the two terms mentioned so far, one has

$$g_{\vec{r}\vec{k}} \approx f_{\vec{r}\vec{k}} - \tau e \frac{\partial f}{\partial \mu} \vec{v}_k \cdot \vec{E}. \tag{17.7}$$

The right side of Eq. (17.7) needs to be dimensionless; for this reason it has been necessary to multiply by a phenomenological constant τ , representing a time for electrons to come to equilibrium, in order to bring the dimensions into order. These rough arguments exactly reproduce a more exact analysis that now follows.

17.2.1 Boltzmann Equation

Because the number of electrons is conserved, and positions and wave numbers change continuously, g obeys the continuity equation, Eq. (5.5), which in the present case applies to both positions and momenta and reads

$$\frac{\partial g}{\partial t} = -\frac{\partial}{\partial \vec{r}} \cdot \dot{\vec{r}}g - \frac{\partial}{\partial \vec{k}} \cdot \dot{\vec{k}}g. \tag{17.8}$$

It follows from Eqs. (17.3) that one can write

$$\frac{\partial g}{\partial t} = -\dot{\vec{r}} \cdot \frac{\partial}{\partial \vec{r}} g - \dot{\vec{k}} \cdot \frac{\partial}{\partial \vec{k}} g. \tag{17.9}$$

$\dot{\vec{r}}$ does not depend upon \vec{r} , and \vec{E} does not depend upon \vec{k} . $\frac{\partial}{\partial \vec{k}} \cdot \vec{v} \times \vec{B} = \vec{B} \cdot \frac{\partial}{\partial \vec{k}} \times \vec{v}$ vanishes because \vec{v} is the gradient of $\mathcal{E}_{\vec{r}}$.

Boltzmann added to Eq. (17.8) an additional term

$$\frac{\partial g}{\partial t} = -\dot{\vec{r}} \cdot \frac{\partial}{\partial \vec{r}} g - \dot{\vec{k}} \cdot \frac{\partial}{\partial \vec{k}} g + \left. \frac{dg}{dt} \right|_{\text{coll}}, \tag{17.10}$$

where

$$\left. \frac{dg}{dt} \right|_{\text{coll}} \tag{17.11}$$

is called the *collision term*. The added term acknowledges that particle momenta change not only in simple ways due to smooth externally applied forces, but also because of a host of additional complications that in principle should be incorporated in the Hamiltonian, such as impurities and thermal fluctuations that cause large and sudden momentum transfers. In the form of (17.10), the equation of motion for electron distribution functions is known as the *Boltzmann equation*.

There is a basic division in statistical mechanics between systems of particles whose motion can be understood analytically and those whose motion is consistent with the laws of thermal equilibrium. Systems in which particles are scattered sufficiently to explore phase space and come to thermal equilibrium are precisely those in which the trajectories of individual particles are too complicated to follow in detail. Roughly speaking, when dynamics of particles are simple, dynamics of distribution functions can be elaborate, while when dynamics of individual particles become too complex to follow in detail, dynamics of distributions can simplify. Accordingly, rather than trying to incorporate increasingly complex terms into the equations of motion (17.3) and solve for dynamics of individual particles, one hopes that the collision term can be chosen as something simple that drives (17.8) to be consistent with basic facts of statistical mechanics.

17.2.2 Including Anomalous Velocity

In crystals that are not centrosymmetric, the semi-classical equations of motion include the anomalous velocity of Eqs. (16.84). Xiao et al. (2005) showed a way to modify the Boltzmann equation to include these dynamical effects. The reason one cannot just write down the Boltzmann equation with new equations for the evolution of \vec{r} and \vec{k} is that \vec{r} and \vec{k} no longer obey Hamiltonian's equation in the form Eq. (17.1). However, this turns out not to be a fatal problem. Essentially, the result is to change the density of states.

The calculation is exact except that terms involving products of

$$\frac{\partial \vec{m}_{\vec{k}}}{\partial \vec{k}} \text{ times } \frac{\partial \vec{B}(\vec{r})}{\partial \vec{r}} \rightarrow 0 \quad \begin{array}{l} \vec{m}_{\vec{k}}, \text{ defined in Eq. (16.82c) is the intrinsic magnetic mo-} \\ \text{ment of the wave function. This expression is meant to} \\ \text{indicate that one should neglect any product involving} \\ \text{spatial derivatives of } \vec{B} \text{ and } \vec{k} \text{ derivatives of } \vec{m}. \end{array} \quad (17.12)$$

will be regarded as second order in two small quantities and neglected.

The modification of Boltzmann's equation proceeds by rewriting the semiclassical equations (16.84). First, define

$$\vec{v} \equiv \frac{\partial \vec{\mathcal{E}}_{\vec{k}}}{\partial \hbar \vec{k}} \quad (17.13)$$

and also the magnetic flux quantum

$$\Phi_0 \equiv \frac{hc}{e} \quad \begin{array}{l} \text{See Eq. (25.52) to observe this quantity aris-} \\ \text{ing in a historically more familiar context.} \end{array} \quad (17.14)$$

Next, substitute Eq. (16.84a) into Eq. (16.84b), obtaining

$$\dot{\vec{r}} = \vec{v} + \frac{1}{\hbar} \left[\vec{E} + \frac{e}{c} \dot{\vec{r}} \times \vec{B} \right] \times \vec{\Omega} \quad (17.15)$$

$$\Rightarrow \dot{\vec{r}} \left(1 + \frac{2\pi \vec{B} \cdot \vec{\Omega}}{\Phi_0} \right) = \vec{v} + \frac{e}{\hbar} \vec{E} \times \vec{\Omega} + \frac{2\pi}{\Phi_0} (\vec{v} \cdot \Omega) \vec{B}. \quad (17.16)$$

Use the identity $(\vec{A} \times \vec{B}) \times \vec{C} = (\vec{A} \cdot \vec{C})\vec{B} - (\vec{B} \cdot \vec{C})\vec{A}$ and also the fact that $\dot{\vec{r}} - \vec{v} \perp \vec{\Omega}$

Similarly, substituting Eq. (16.84b) into Eq. (16.84a) gives

$$\dot{\vec{k}} \left(1 + \frac{2\pi \vec{B} \cdot \vec{\Omega}}{\Phi_0} \right) = -\frac{e}{\hbar} \vec{E} - \frac{e}{\hbar c} \vec{v} \times \vec{B} - \frac{e^2}{\hbar c} (\vec{E} \cdot \vec{B}) \vec{\Omega}. \quad (17.17)$$

Recasting the electron equations of motion in this way suggests defining

$$\mathcal{D}(\vec{r}, \vec{k}, t) \equiv \left(1 + \frac{2\pi \vec{B}(\vec{r}, t) \cdot \vec{\Omega}(\vec{k})}{\Phi_0} \right). \quad (17.18)$$

Employing this definition, brief calculations of Problem 3 show that

$$\frac{\partial}{\partial \vec{r}} \cdot \mathcal{D} \dot{\vec{r}} = \frac{e}{\hbar} \frac{\partial}{\partial \vec{r}} \cdot (\vec{E} \times \Omega) \quad \begin{array}{l} \text{Use Maxwell's equation Eq. (20.5a) } \vec{\nabla} \cdot \vec{B} = \\ \text{0. There is some dependence on } \vec{r} \text{ buried inside } \vec{v} \\ \text{because of the appearance of } \vec{B}(\vec{r}, t) \text{ in} \\ \text{Eq. (16.85a). This is where the approximation} \\ \text{(17.12) comes in.} \end{array} \quad (17.19)$$

$$= \frac{e}{\hbar} \vec{\Omega} \cdot \left(\frac{\partial}{\partial \vec{r}} \times \vec{E} \right) = -\frac{e}{c\hbar} \Omega \cdot \frac{\partial \vec{B}}{\partial t} \quad \begin{array}{l} \text{Use Maxwell's} \\ \text{equation Eq. (20.5b).} \end{array} \quad (17.20)$$

Similarly,

$$\frac{\partial}{\partial \vec{k}} \cdot \dot{\vec{k}} \mathcal{D} = 0. \quad \text{No approximations needed here.} \quad (17.21)$$

Assembling Eqs. (17.20) and (17.21) gives

$$\frac{\partial \mathcal{D}}{\partial t} + \frac{\partial}{\partial \vec{r}} \cdot \mathcal{D} \dot{\vec{r}} + \frac{\partial}{\partial \vec{k}} \cdot \mathcal{D} \dot{\vec{k}} = 0 \quad \Omega \text{ depends explicitly on } \vec{k} \text{ but not on } t. \quad (17.22)$$

While $g(\vec{r}, \vec{k}, t)$ obeys the continuity equation Eq. (17.8), it does not obey (17.9) when all terms are included in the semi-classical equations of motion. However, one can define \tilde{g} by

$$g = \mathcal{D} \tilde{g}. \quad (17.23)$$

Multiplying Eq. (17.22) by \tilde{g}/\mathcal{D} , and subtracting it from Eq. (17.8) using Eq. (17.23),

$$\frac{\partial \tilde{g}}{\partial t} = -\dot{\vec{r}} \cdot \frac{\partial}{\partial \vec{r}} \tilde{g} - \dot{\vec{k}} \cdot \frac{\partial}{\partial \vec{k}} \tilde{g}. \quad (17.24)$$

Therefore, Boltzmann's equation (17.10) will continue to hold so long as one replaces g with \tilde{g} .

In summary, here is how to view the consequences of anomalous velocities for Boltzmann's equation. In any given problem, solve Eq. (17.10) using the full semi-classical equations of motion to obtain \tilde{g} . Then, when computing any observable, as in Eq. (17.5), write instead

$$G = \int [d\vec{k}] d\vec{r} \mathcal{D} \tilde{g}_{\vec{r}\vec{k}} G_{\vec{r}\vec{k}}. \quad (17.25)$$

Thus $\mathcal{D}(\vec{r}, \vec{k}, t)$ can be viewed as a modification of the density of states. There is no reason not to use the notation g for \tilde{g} just so long as one remembers to use the modified density of states \mathcal{D} . Thus \tilde{g} will not appear again explicitly, but if the anomalous velocity cannot be neglected, that is what g should mean.

17.2.3 Relaxation Time Approximation

Ask what properties the collision term must have. The basic property is that it must cause the distribution g to relax toward thermal equilibrium. The *relaxation time approximation* consists of nothing more or less than the simplest functional form of the collision term with this property. It is

$$\left. \frac{dg}{dt} \right|_{\text{coll.}} = -\frac{1}{\tau} [g_{\vec{r}\vec{k}} - f_{\vec{r}\vec{k}}], \quad (17.26)$$

where

$$f_{\vec{r}\vec{k}} = \frac{1}{e^{\beta_r(\mathcal{E}_{\vec{k}} - \mu_r)} + 1} \quad \begin{array}{l} \text{One might want to replace } \mathcal{E}_{\vec{k}} \text{ by } \mathcal{E}_{\vec{k}} - eV_r. \\ \text{Doing so amounts to a redefinition of } \mu \text{ and} \\ \text{is not necessary if } \mu_r \text{ is defined to be the constant} \\ \text{that produces the correct density } n(\vec{r}). \end{array} \quad (17.27)$$

is the Fermi function appropriate for the density and temperature at position \vec{r} .

The effect of the collision term is to make g rise wherever it is smaller than f , and make it shrink wherever it is greater. Allowing f to depend upon position through μ and β allows study of systems that are slightly out of equilibrium, such as bars of metal with uniform temperature gradients. The distribution g will try to relax everywhere to the local equilibrium distribution f . However, the dependence of f on position through density and temperature must be included. Otherwise there is no reason to expect g to be close to f even for very small external fields and temperature gradients, because total changes in temperature and density over large distances may be large. The constant out front, τ , is the relaxation time.

The relaxation time provides an approximate but effective way to incorporate a variety of complicated processes tending to bring condensed matter toward equilibrium. In the simplest possible approximation, τ is simply a constant, and all electrons decay toward zero velocity at the same rate, regardless of their energy or direction. This approximation is useful for simple estimates, but does not survive careful comparison either with experiment or calculation. For example, theoretical calculations in Section 18.2.1 show that above the Debye temperature, the relaxation time of an electron with energy \mathcal{E} is proportional to $\mathcal{E}^{-3/2}$. In general, there is no reason why the relaxation time of an electron with Bloch index \vec{k} should not depend in detail upon \vec{k} , but the balance between simplicity and accuracy recommends allowing τ to depend upon \vec{k} only through $\mathcal{E}_{\vec{k}}$, and $\tau_{\mathcal{E}}$ will generally be understood to depend upon \mathcal{E} in what follows.

Method of Characteristics. Once the relaxation time approximation is employed, the Boltzmann equation has a simple formal solution. Because g depends upon t , \vec{k} , and \vec{r} , the total time derivative of g is

$$\frac{dg}{dt} = \frac{\partial g}{\partial t} + \dot{\vec{r}} \cdot \frac{\partial g}{\partial \vec{r}} + \dot{\vec{k}} \cdot \frac{\partial g}{\partial \vec{k}}, \quad (17.28)$$

and Boltzmann's equation (17.10) becomes

$$\frac{dg}{dt} = -\frac{g-f}{\tau_{\mathcal{E}}} \quad (17.29)$$

$$\Rightarrow g_{\vec{r}\vec{k}}(t) = \int_{-\infty}^t dt' f(t') \frac{e^{-(t-t')/\tau_{\mathcal{E}}}}{\tau_{\mathcal{E}}}. \quad (17.30)$$

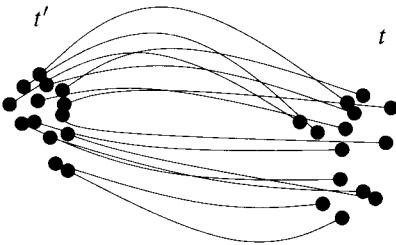


Figure 17.1. The distribution function g results from time averages over the histories of electrons that at time t end up at \vec{r} and \vec{k} .

In Eq. (17.30), $f(t')$ is shorthand for $f(\vec{r}(t'), \vec{k}(t'))$, in which $\vec{r}(t')$ and $\vec{k}(t')$ are solutions of the semiclassical equations of motion (17.3). They evolve in time in

such a way that right at $t' = t$ they become equal to \vec{r} and \vec{k} . What Eq. (17.30) says is that to find how many electrons are at $\vec{r}\vec{k}$ now, go back in time and find how many were destined to evolve to this point, as in Figure 17.1, obeying the semiclassical equations. But there is no need to go back too far, because the longer electrons have to travel, the more likely they are to be deflected from their trajectory by collisions. Integrating Eq. (17.30) by parts gives

$$g_{\vec{r}\vec{k}}(t) = f_{\vec{r}\vec{k}} - \int_{-\infty}^t dt' e^{-(t-t')/\tau_\varepsilon} \frac{d}{dt'} f(t'). \quad (17.31)$$

This form has the virtue of writing the solution of the Boltzmann equation as a sum of the unperturbed part of the distribution plus a correction. Recalling that f is the Fermi function evaluated at local temperature and chemical potential one can carry out the derivatives in the case where the Hamiltonian is given by Eq. (17.2) to find

$$g_{\vec{r}\vec{k}} = f_{\vec{r}\vec{k}} - \int_{-\infty}^t dt' e^{-(t-t')/\tau_\varepsilon} \left[\vec{r}_{t'} \cdot \frac{\partial}{\partial \vec{r}} + \vec{k}_{t'} \cdot \frac{\partial}{\partial \vec{k}} \right] f(t'). \quad (17.32)$$

Using Eq. (17.27) to write

$$\frac{\partial f}{\partial \vec{r}} = \frac{\partial f}{\partial \varepsilon} \left[-\vec{\nabla} \mu - (\varepsilon - \mu) \frac{\vec{\nabla} T}{T} \right], \quad \text{Although the indices } \vec{k} \text{ and } \vec{r} \text{ are being dropped, they are implicitly still present.} \quad (17.33)$$

and

$$\frac{\partial f}{\partial \vec{k}} = \frac{\partial f}{\partial \varepsilon} \frac{\partial \varepsilon}{\partial \vec{k}} = \frac{\partial f}{\partial \varepsilon} \hbar \vec{v}, \quad (17.34)$$

with Eq. (17.3) for \vec{k} gives the path integral expression due to Chambers (1957),

$$g = f - \int_{-\infty}^t dt' e^{-(t-t')/\tau_\varepsilon} \vec{v}_{\vec{k}} \cdot \left\{ e\vec{E} + \vec{\nabla} \mu + \frac{\varepsilon_{\vec{k}} - \mu}{T} \vec{\nabla} T \right\} \frac{\partial f(t')}{\partial \mu}. \quad (17.35)$$

Use $-\partial f / \partial \varepsilon = \partial f / \partial \mu$. The magnetic induction does not appear explicitly because $\vec{v} \cdot \vec{v} \times \vec{B} = 0$.

In cases where the semiclassical dynamics are slow compared to the relaxation time τ_ε , one can carry out the time integral, neglecting the time dependence of everything but the exponential factor, giving

$$g = f - \tau_\varepsilon \vec{v}_{\vec{k}} \cdot \left\{ e\vec{E} + \vec{\nabla} \mu + \frac{\varepsilon_{\vec{k}} - \mu}{T} \vec{\nabla} T \right\} \frac{\partial f}{\partial \mu}. \quad (17.36)$$

17.2.4 Relation to Rate of Production of Entropy

The various terms entering Eq. (17.36) appear quite complicated, but can be put in more elegant form when it is realized that they represent the creation of entropy. First write the first law of thermodynamics in the form

$$T \frac{\partial S}{\partial t} = \frac{\partial \mathcal{E}}{\partial t} - \mu \frac{\partial N}{\partial t}. \quad (17.37)$$

Defining

$$\vec{J}_N = N\vec{v} \text{ and } \vec{J}_E = \mathcal{E} \frac{\vec{J}_N}{N} \quad (17.38)$$

to be particle current and energy current, one has

$$\frac{\partial N}{\partial t} + \vec{\nabla} \cdot \vec{J}_N = 0 \quad (17.39)$$

and

$$\frac{\partial \mathcal{E}}{\partial t} + \vec{\nabla} \cdot \vec{J}_E = \vec{F} \cdot \vec{J}_N, \quad (17.40)$$

where \vec{F} is the external set of forces upon particles. It follows from combining Eqs. (17.37), (17.39), and (17.40) that

$$T \frac{\partial S}{\partial t} - \mu \vec{\nabla} \cdot \vec{J}_N + \vec{\nabla} \cdot \vec{J}_E = \vec{F} \cdot \vec{J}_N \quad (17.41)$$

so the rate \dot{S} at which entropy is generated is

$$\dot{S} \equiv \frac{\partial S}{\partial t} + \vec{\nabla} \cdot \left[\frac{\vec{J}_E - \mu \vec{J}_N}{T} \right] = \frac{\vec{F} \cdot \vec{J}_N}{T} - \vec{\nabla} \cdot \left(\frac{\mu}{T} \right) \cdot \vec{J}_N + \vec{\nabla} \cdot \left(\frac{1}{T} \right) \cdot \vec{J}_E \quad (17.42)$$

$$\Rightarrow \dot{Q} \equiv T \frac{\dot{S}}{V} = \left[-e\vec{E} - \vec{\nabla}\mu - \frac{\vec{\nabla}T}{T} \left(\frac{\mathcal{E}}{N} - \mu \right) \right] \cdot \frac{\vec{J}_N}{V}. \quad (17.43)$$

Identifying the external force \vec{F} with $-e\vec{E} - e\vec{v}/c \times \vec{B}$, and combining terms from the right-hand side of Eq. (17.42).

The right hand side of Eq. (17.43) describes heat produced per time \dot{Q} , because the left-hand side of Eq. (17.42) is a continuity equation for entropy of type Eq. (5.5). Define

$$\dot{Q}_{\vec{r}\vec{k}} = \left[-e\vec{E} - \vec{\nabla}\mu - \frac{\vec{\nabla}T}{T} (\mathcal{E}_{\vec{k}} - \mu) \right] \cdot \vec{v}_{\vec{k}} f_{\vec{k}} \quad \begin{array}{l} \mathcal{E}_{\vec{k}} \text{ is the energy of one particle} \\ \text{with wave number } \vec{k}. \end{array} \quad (17.44)$$

to be heat production per wavenumber per volume. Then Eq. (17.35) may be written as

$$g_{\vec{r}\vec{k}} = f_{\vec{r}\vec{k}} + \int_{-\infty}^t dt' e^{-(t-t')/\tau_E} \dot{Q}(t') \frac{\partial}{\partial \mu} \ln f(t') \quad \begin{array}{l} \text{Both } \dot{Q}(t') \text{ and } f(t') \text{ are evaluated along tra-} \\ \text{jectories } \vec{r}(t'), \vec{k}(t'). \end{array} \quad (17.45)$$

17.3 Transport Symmetries

The solution of the Boltzmann equation is now in a form that reveals the natural symmetries of transport phenomena.

The question to answer is the following. Suppose one applies a weak forcing field to a system, perhaps an electric or magnetic field or a thermal gradient. What response should be associated with that force? For example, applying a heat gradient will in general induce an electric current as well. Should one define “heat

current” to include some electric current? The answer is that one should define the flux induced by a force to be the derivative of heat (entropy times temperature) generation with respect to that force. The reason for this definition is that it leads to symmetries.

In general, define the flux X_α associated with the force x_α to be

$$X_\alpha = \frac{d\dot{Q}}{dx_\alpha}. \tag{17.46}$$

Examples of Forces and Fluxes. Take the force \vec{x} in Eq. (17.46) to be the electric field \vec{E} . Going to Eq. (17.43) and taking the gradient of \dot{Q} with respect to \vec{E} gives

$$-e \frac{\vec{J}_N}{\mathcal{V}} = \vec{j}. \tag{17.47}$$

So the flux conjugate to an applied electric field is the electrical current. Or, take the force to be a temperature gradient $\vec{\nabla}T$. Then the flux is

$$-\frac{1}{T}(\mathcal{E} - \mu) \frac{\vec{J}_N}{\mathcal{V}}. \tag{17.48}$$

The product of a flux with its force always has dimensions of energy per time per volume.

17.3.1 Onsager Relations

Suppose now that a system is subjected to several forces simultaneously. If each of them is sufficiently weak, then the fluxes which are induced should be linearly proportional to what has been applied. However, the results are not obvious. For example, a temperature gradient will in general induce an electrical current. Therefore, one has to consider a general *linear response* of the form

$$X_\alpha = \sum_\beta L_{\alpha\beta} x_\beta. \text{ The coefficients } L_{\alpha\beta} \text{ are arbitrary for the moment.} \tag{17.49}$$

The *Onsager relations* state that

$$L_{\alpha\beta}(B) = L_{\beta\alpha}(-B). \tag{17.50}$$

The flux of β in response to force α is the same as the flux of α in response to force β , provided that one also reverses the sign of the magnetic induction B .

The Onsager relations can be derived by computing $L_{\alpha\beta}$. Starting with Eq. (17.5) for total heat production, evaluating the occupation number of \vec{r} and \vec{k} states with Eq. (17.45), Problem 4 shows that

$$L_{\alpha\beta} = \int [d\vec{k}_i] d\vec{r}_i \int_{-\infty}^t dt' \frac{d\dot{Q}(t)}{dx_\alpha} e^{-(t-t')/\tau_\mathcal{E}} \left[\frac{\partial}{\partial \mu} \ln f(t') \right] \frac{d\dot{Q}(t')}{dx_\beta}. \tag{17.51}$$

From Eq. (17.51), one can see the origin of Onsager’s symmetries, as well as the conditions under which they fail. The main ideas are as follows:

As a consequence of Liouville’s theorem, one can choose to integrate either with respect to \vec{k}_t and \vec{r}_t or with respect to $\vec{k}_{t'}$ and $\vec{r}_{t'}$; the integration measures are the same. Therefore, if it were not for the troublesome term $\partial f(t')/\partial\mu$, the integrand of Eq. (17.51) would be quite symmetrical. The condition for Onsager reciprocity is therefore that it not matter whether $\partial f/\partial\mu$ is evaluated at \vec{k}, \vec{r} or at $\vec{k}_{t'}, \vec{r}_{t'}$.

This requirement permits Onsager’s symmetries to survive large magnetic fields, because although magnetic fields make $\vec{k}_{t'}$ rotate, they do it in such a way that the energy of the particle does not change, and

$$\mathcal{E}_{\vec{k}} = \mathcal{E}_{\vec{k}_{t'}} \Rightarrow f(t) = f(t'). \tag{17.52}$$

By contrast, electric fields conserve $\mathcal{E} - eV$ rather than \mathcal{E} , so electric fields are not allowed to be too large. However, one only has to worry about times on the order of the relaxation time $\tau_\mathcal{E}$, or electron motions through a mean free path, because otherwise the exponential becomes small. So the condition for the symmetries (17.50) to hold is that all externally imposed electrical and thermal potentials must vary negligibly on the scale of the electron mean free path. Under these conditions, the integrand of Eq. (17.51) has the following symmetries. Send

$$\begin{aligned} t &\rightarrow t'; \quad t' \rightarrow t; \\ \vec{B} &\rightarrow -\vec{B} \end{aligned} \tag{17.53a}$$

$$\begin{aligned} \vec{k}_{t'} &\rightarrow -\vec{k}_{-t'} \\ \vec{r}_{t'} &\rightarrow \vec{r}_{-t'} \end{aligned}, \quad \begin{array}{l} \text{If one starts out with some initial condition } \vec{k}, \vec{r}, \text{ then} \\ \text{running it forwards in time by } t - t' \text{ is the same as reversing} \\ \text{the sign of } \vec{B} \text{ and } \vec{k}, \text{ and running it backward in time by} \\ \text{amount } t - t'. \end{array} \tag{17.53b}$$

Using the symmetries Eq. (17.53) and switching to an integral over $\vec{k}_{t'}, \vec{r}_{t'}$ in Eq. (17.51) results in the Onsager symmetry (17.50).

17.4 Thermoelectric Phenomena

Boltzmann’s equation in the form of (17.36) provides everything needed to explore the response of solids to electrical, magnetic, and thermal fields. In what follows, all electrons are assumed to belong to some particular band n , and therefore the band index n will not be written explicitly. When more than one band crosses the Fermi surface, contributions of the several bands would need to be summed together.

17.4.1 Electrical Current

Consider first a solid immersed only in a uniform electrical field. The electrical current per volume \vec{j} is

$$\vec{j} = \frac{\vec{J}}{V} = -e \int [d\vec{k}] \vec{v}_{\vec{k}} g_{\vec{k}}. \tag{17.54}$$

This integral will find the current contributed by electrons in the n th band, and accordingly the integral is over the first Brillouin zone, not all of \vec{k} space. $[d\vec{k}]$ defined in Eq. (6.15).

The conductivity tensor σ is defined by

$$\frac{\partial j_\alpha}{\partial E_\beta} \equiv \sigma_{\alpha\beta} \quad (17.55)$$

$$= e^2 \int [d\vec{k}] \tau_\varepsilon v_\alpha v_\beta \frac{\partial f}{\partial \mu}. \quad \text{Using Eq. (17.36) and differentiating (17.54) with respect to } E_\beta. \text{ Dependence of } \vec{v}_\vec{k} \text{ on } \vec{k} \text{ is not displayed explicitly.} \quad (17.56)$$

There are two interesting ways to develop this expression.

1. The first emphasizes the connection with the free electron result. Assuming that the relaxation time τ_ε can be taken as constant,

$$\sigma_{\alpha\beta} = e^2 \tau \int [d\vec{k}] v_\alpha \left(-\frac{\partial f_\vec{k}}{\partial \hbar k_\beta} \right) \quad \text{Differentiating } f \text{ with respect to } \mu \text{ is the same as differentiating with respect to } -\mathcal{E}_\vec{k}, \text{ and } v_\beta(\vec{k}) = \partial \mathcal{E}_\vec{k} / \partial \hbar k_\beta \quad (17.57)$$

$$\Rightarrow \sigma_{\alpha\beta} = e^2 \tau \int [d\vec{k}] f_\vec{k} \frac{\partial v_\alpha}{\partial \hbar k_\beta} \quad \text{Using the fact that } \vec{v} \text{ is periodic in } \vec{k} \text{ across the first Brillouin zone to perform integration by parts.} \quad (17.58)$$

$$= e^2 \tau \int [d\vec{k}] f_\vec{k} (\mathbf{M}^{-1})_{\alpha\beta}. \quad \text{The effective mass tensor was defined in Eq. (16.28).} \quad (17.59)$$

In crystals of cubic symmetry, it is clear from Eq. (17.56) that the conductivity tensor is diagonal. The diagonal component is

$$\sigma = \frac{ne^2\tau}{m^*}, \quad (17.60)$$

with

$$\frac{1}{m^*} = \frac{1}{3n} \int [d\vec{k}] f_\vec{k} \text{Tr}(\mathbf{M}^{-1}). \quad \text{The factor of } 1/3 \text{ out front cancels the three terms produced by the trace of the matrix.} \quad (17.61)$$

2. On the other hand, using in Eq. (17.56) the fact that $\partial f / \partial \mu \approx \delta(\mathcal{E} - \mathcal{E}_F)$ in metals, and using Eq. (7.73) to obtain an integral $d\Sigma$ over the Fermi surface gives

$$\sigma_{\alpha\beta} = e^2 \int \frac{d\Sigma}{4\pi^3 \hbar v} \tau_\varepsilon v_\alpha v_\beta, \quad \text{Use Eq. (6.15) to write out } [d\vec{k}]. \quad (17.62)$$

so the conductivity can be understood as an average of velocities and relaxation time over the Fermi surface. Because of the assumption that a derivative of the Fermi function can be replaced by a delta function, Eq. (17.62) holds in metals but not in semiconductors.

Filled Bands Conduct No Current. Suppose that the Fermi energy lies above the highest energy in the band under consideration. Then for temperatures much less than the Fermi temperature, one can safely replace f by 1. In this case Eq. (17.58) shows that σ vanishes because $\vec{v}_\vec{k}$, like $\mathcal{E}_\vec{k}$ from which it derives, is a periodic function of \vec{k} . Carrying out the integral in the k_β direction, Eq. (17.58) gives zero

immediately. Equation (17.62) incorporates the same lesson. The integral $d\Sigma$ must be carried out over the Fermi surface, and if there is no Fermi surface, it vanishes.

Thus completely filled bands contribute nothing to electrical current. The reason is that in order to carry current, electrons must accelerate slightly in the presence of an electric field, which means that their index \vec{k} must increase slightly. However, in a filled band, all the \vec{k} are occupied, the rate of Zener tunneling out of the band is tremendously low, and the Pauli principle prevents electrons from altering their states at all.

17.4.2 Effective Mass and Holes

If the Fermi energy lies somewhere in the middle of the energy band under consideration, then f equals 1 up to some energy, and then zero thereafter. One can rewrite Eq. (17.59) as

$$\sigma_{\alpha\beta} = e^2\tau \int_{\text{occupied levels}} [d\vec{k}] (\mathbf{M}^{-1})_{\alpha\beta} \quad (17.63)$$

$$= -e^2\tau \int_{\text{unoccupied levels}} [d\vec{k}] (\mathbf{M}^{-1})_{\alpha\beta}. \quad (17.64)$$

Because f in Eq. (17.59) can be replaced by $1 - (1 - f)$. The term resulting from 1 vanishes, and $(1 - f)$ is nonzero (and equal to 1) only for the unoccupied levels.

When the Fermi level lies near the bottom of an energy band, $\mathcal{E}_{\vec{k}}$ may be approximately quadratic in \vec{k} . A particularly simple form $\mathcal{E}_{\vec{k}}$ might take is

$$\mathcal{E}_{\vec{k}} \approx \mathcal{E}_c + \frac{\hbar^2 k^2}{2m_n^*}. \quad (17.65)$$

From this form of $\mathcal{E}_{\vec{k}}$ follows an effective mass tensor that is diagonal and whose diagonal elements are equal to m_n^* . Using Eq. (17.63), and noting that the integral $[d\vec{k}]$ over occupied levels just gives the density of electrons n , one finds for the conductivity

$$\sigma = \frac{ne^2\tau}{m_n^*}. \quad (17.66)$$

Conversely, if the Fermi level lies near to the top of an energy band, in the simplest isotropic case one obtains

$$\mathcal{E}_{\vec{k}} \approx \mathcal{E}_v - \frac{\hbar^2 k^2}{2m_p^*}. \quad (17.67)$$

Equation (17.64) is the most convenient formula for computation of the conductivity in this case, and it gives

$$\sigma = \frac{pe^2\tau}{m_p^*}. \quad p \text{ is the density of holes, defined in Eq. (17.107).} \quad (17.68)$$

Energy levels that are not occupied—absences of electrons—act like particles with positive charge, and are called holes. Because conductivity involves the square of

the charge, conductivity cannot reveal the sign of the charge carrier. In a magnetic field, electrons and holes orbit in opposite directions, allowing experiments in crossed electrical and magnetic fields to distinguish between them.

The discussion of Bloch oscillations and Wannier–Stark ladders may have left the impression that it is not realistic to expect electrons to travel in unexpected directions against applied fields. This impression is wrong. Electron mean free paths rarely permit them to travel far enough to complete a Bloch oscillation. But in solids where the Fermi level lies near the top of an energy band rather than near the bottom, the mobile electrons do move opposite the expected direction, leading to their interpretation as holes. Such solids are extremely common.

17.4.3 Mixed Thermal and Electrical Gradients

Solids subject to simultaneous electrical and thermal gradients often act little like free-electron gases. Appreciating that strong interactions with the lattice can change the dynamics of electrons near the Fermi surface is the key to understanding qualitatively why this is so.

In accord with the Onsager symmetries (17.50), one needs to begin by defining pairs of fluxes and forces. There are three forces considered in Eq. (17.43), \vec{E} , $\vec{\nabla}\mu$, and $\vec{\nabla}T$. Because \vec{E} and $\vec{\nabla}\mu$ only enter in the combination $e\vec{E} + \vec{\nabla}\mu$, it is sensible to define the electrochemical force

$$\vec{G} = \vec{E} + \frac{\vec{\nabla}\mu}{e} \tag{17.69}$$

and is conventional to take $-\vec{\nabla}T/T$ as a second force. Taking the derivative of Eq. (17.43) with respect to $-\vec{\nabla}T/T$ and \vec{G} gives the conventional force–flux pairs

<i>Force</i>	<i>Flux</i>	
\vec{G}	$\vec{j} = -e\vec{J}_N/\mathcal{V}$	$= -e \int \frac{d\vec{r}}{\mathcal{V}} \int [d\vec{k}] \vec{v}_{\vec{r}\vec{k}} g_{\vec{r}\vec{k}}$
$\frac{-\vec{\nabla}T}{T}$	$\vec{j}_Q = (\vec{J}_\varepsilon - \mu\vec{J}_N)/\mathcal{V}$	$= \int \frac{d\vec{r}}{\mathcal{V}} \int [d\vec{k}] (\varepsilon_{\vec{k}} - \mu) \vec{v}_{\vec{r}\vec{k}} g_{\vec{r}\vec{k}}$

Define the matrices of linear relations between these fluxes and forces to be

$$\vec{j} = \mathbf{L}^{11}\vec{G} + \mathbf{L}^{12}\left(\frac{-\vec{\nabla}T}{T}\right) \tag{17.71}$$

$$\vec{j}_Q = \mathbf{L}^{21}\vec{G} + \mathbf{L}^{22}\left(\frac{-\vec{\nabla}T}{T}\right). \tag{17.72}$$

Inserting Eq. (17.36) into Eqs. (17.54) and (17.70) gives

$$\mathbf{L}^{11} = \mathcal{L}^{(0)}, \quad \mathbf{L}^{12} = \mathbf{L}^{21} = -\frac{1}{e}\mathcal{L}^{(1)}, \quad \mathbf{L}^{22} = \frac{1}{e^2}\mathcal{L}^{(2)}, \tag{17.73}$$

The equality of L^{12} and L^{21} follows from the Onsager relations, (17.50).

where

$$\mathcal{L}_{\alpha\beta}^{(\nu)} = e^2 \int [d\vec{k}] \tau_\varepsilon \frac{\partial f}{\partial \mu} v_\alpha v_\beta (\varepsilon_{\vec{k}} - \mu)^\nu. \tag{17.74}$$

Defining

$$\sigma_{\alpha\beta}(\mathcal{E}) = \tau_{\mathcal{E}} e^2 \int [d\vec{k}] v_{\alpha} v_{\beta} \delta(\mathcal{E} - \mathcal{E}_{\vec{k}}), \quad (17.75)$$

one has

$$\mathcal{L}_{\alpha\beta}^{(\nu)} = \int d\mathcal{E} \frac{\partial f}{\partial \mu} (\mathcal{E} - \mu)^{\nu} \sigma_{\alpha\beta}(\mathcal{E}). \quad (17.76)$$

Using the fact that at temperatures well below the Fermi temperature in metals

$$\frac{\partial f}{\partial \mu} \approx \delta(\mathcal{E} - \mathcal{E}_F) \quad (17.77)$$

one can evaluate $\mathcal{L}^{(\nu)}$ and find

$$\mathcal{L}_{\alpha\beta}^{(0)} = \sigma_{\alpha\beta}(\mathcal{E}_F) \quad (17.78)$$

$$\mathcal{L}_{\alpha\beta}^{(1)} = \frac{\pi^2}{3} (k_B T)^2 \sigma'_{\alpha\beta}(\mathcal{E}_F) \quad (17.79)$$

To find a nonvanishing contribution, one must take the Taylor expansion of σ about \mathcal{E}_F ; hence $\sigma' = d\sigma/d\mathcal{E}$ appears. The resulting integral was evaluated in Eq. (6.67).

$$\mathcal{L}_{\alpha\beta}^{(2)} = \frac{\pi^2}{3} (k_B T)^2 \sigma_{\alpha\beta}(\mathcal{E}_F). \quad (17.80)$$

The relevant integral was evaluated in Eq. (6.67).

17.4.4 Wiedemann–Franz Law

It is now possible to analyze various physical cases in which thermal and electrical gradients are mixed. First, notice that a pure electrochemical gradient causes heat flow, and a pure thermal gradient causes current to flow. The thermal conductivity is given by

$$\vec{j}_Q = \kappa (-\vec{\nabla} T) \quad (17.81)$$

under conditions where no current flows. So

$$0 = \mathbf{L}^{11} \vec{G} + \mathbf{L}^{12} \left(\frac{-\vec{\nabla} T}{T} \right) \quad (17.82)$$

$$\Rightarrow \vec{G} = (\mathbf{L}^{11})^{-1} \mathbf{L}^{12} \frac{\vec{\nabla} T}{T}, \quad \text{Set } \vec{j} = 0 \text{ in Eq. (17.71).} \quad (17.83)$$

showing that a weak field is necessary to oppose the current; in a finite sample, it would automatically result from charge buildup at the boundaries. So

$$\vec{j}_Q = \left[\mathbf{L}^{21} (\mathbf{L}^{11})^{-1} \mathbf{L}^{12} - \mathbf{L}^{22} \right] \left(\frac{\vec{\nabla} T}{T} \right) \quad \text{Put Eq. (17.83) into Eq. (17.72).} \quad (17.84)$$

$$\Rightarrow \kappa = \frac{\mathbf{L}^{22}}{T} + \mathcal{O}\left(\frac{k_B T}{\mathcal{E}_F}\right)^2 \quad \mathbf{L}^{21} \text{ and } \mathbf{L}^{12} \text{ go as } (k_B T / \mathcal{E}_F)^2, \text{ and the term they produce can be neglected relative to } \mathbf{L}^{22}. \quad (17.85)$$

$$\Rightarrow \kappa_{\alpha\beta} = \frac{\pi^2}{3} \frac{k_B^2 T}{e^2} \sigma_{\alpha\beta}. \quad \text{Assembling Eqs. (17.80) and (17.73).} \quad (17.86)$$

In this way, the Wiedemann–Franz law, Eq. (16.10), is recovered for Bloch electrons, giving for the constant of proportionality, the *Lorenz number*,

$$L_0 = \frac{\pi^2}{3} \frac{k_B^2}{e^2} = 2.72 \cdot 10^{-13} \text{ erg cm}^{-1} \text{ K}^{-2} = 2.43 \cdot 10^{-8} \text{ W} \cdot \Omega \cdot \text{K}^{-2} \quad (17.87)$$

This simple relation between thermal and electrical conductivity applies component by component to electrical and thermal conductivity so long as the relaxation time approximation is valid. As shown in Table 17.1, it describes many metals rather well at 300 K. The comparison of theory and experiment is considerably less successful at 20 K, because at low temperatures the relaxation time approximation is less reliable.

17.4.5 Thermopower—Seebeck Effect

It follows from Eqs. (17.71) and (17.72) that it should be possible to measure a potential drop across the ends of a sample between which there exists a temperature gradient. Actually to measure this temperature gradient requires a clever choice of geometry, as shown in Figure 17.2. Two separate metals are required, because otherwise a temperature gradient across one’s measuring device will induce additional potential drops within the voltmeter and distort the measurement. It should be pointed out that although the leads to which the voltmeter is attached have the same temperature, so there is no thermal gradient across the voltmeter, the chemical potentials of different metals at the same temperature are in general different, and contribute to current flow. This argument explains why the electrochemical force in Eq. (17.69) was defined to contain both electric field and chemical potential gradient. The *thermopower* or *absolute Seebeck coefficient* α is defined by

$$\vec{G} = \alpha \vec{\nabla} T$$

(17.88)

An ideal voltmeter permits no current to flow, so one has only to return to Eq. (17.71) and set \vec{j} to zero. Despite being named a coefficient, α is properly a tensor.

$$\Rightarrow \alpha = (\mathbf{L}^{11})^{-1} \frac{\mathbf{L}^{12}}{T} = -\frac{\pi^2 k_B^2 T}{3 e} \sigma^{-1} \sigma'$$

(17.89)

Using Eqs. (17.79), (17.80), and Eq. (17.73) in Eq. (17.71).

The fact that Eq. (17.89) involves $\sigma^{-1} \sigma'$ suggests that the relaxation time might cancel out, just as in the ratio of electrical to thermal conductivity, and make the Seebeck coefficient a good testing ground for theory. In fact, it is very sensitive to the derivative of the relaxation time with respect to energy, a quantity that is very difficult to calculate with precision, so experimental values of the Seebeck coefficient are hard to predict or interpret.

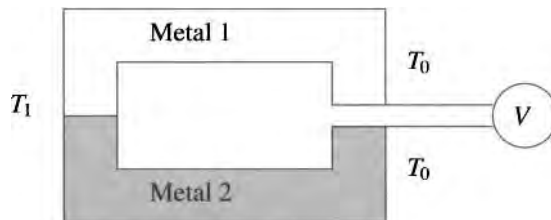


Figure 17.2. In order to measure thermopower, it is necessary to create a temperature gradient across two separate metals, so as to avoid temperature gradients across the leads of the voltmeter.

Typical measured values of the thermopower are on the order of microvolts per degree, and some values are listed in Table 17.1. The table does not go into great detail. For example, the thermopower of bismuth is highly anisotropic; thermopower parallel to the main symmetry axis is $-110 \mu\text{V K}^{-1}$ while that perpendicular to it is $-54 \mu\text{V K}^{-1}$.

17.4.6 Peltier Effect

The Peltier effect occurs when current flows in a bimetallic circuit without temperature gradients. The flow of electrical current induces a heat flow defined to have magnitude

$$\vec{j}_Q = \Pi \vec{j}. \quad (17.90)$$

One sees from Eq. (17.72) that

$$\Pi = \mathbf{L}^{21} (\mathbf{L}^{11})^{-1} = T\alpha. \quad (17.91)$$

The matrices \mathbf{L}^{11} and \mathbf{L}^{21} must commute to obtain the relation to the Seebeck coefficient α .

This result applies to a single metal. If two metals are arranged in series, then different heat currents will flow in each, and the junctions will either emit or absorb heat. This heat must be extracted or absorbed if temperature gradients are not to build up, so the Peltier effect can be used for heating and refrigeration. Problem 7 shows how heat transport is related to Peltier coefficients, and it shows that the usefulness of a piece of material either for refrigeration or for generating electric current from thermal gradients is characterized by a figure of merit:

$$Z = \frac{\alpha^2}{\rho\kappa}, \quad (17.92)$$

The figure of merit in the problem is defined in terms of two materials in a junction. The quantity here is loosely inspired by Eq. (17.197), and it can be used to discuss the merits of a single material.

where ρ is its resistivity and κ is its thermal conductivity. Z has dimensions of inverse kelvin, and sometimes ZT is reported instead. A few materials with particularly high figures of merit are Bi_2Te_3 with $ZT \approx 0.6$ at room temperature (used for refrigerators), and SiGe with $ZT \approx 0.5$ at 1000 K (converts heat to electric power in space satellites). The highest figure of merit at room temperature and pressure is 1.14 in the alloy $(\text{Bi}_2\text{Te}_3)_{0.25}(\text{Sb}_2\text{Te}_3)_{0.72}(\text{Sb}_2\text{Se}_3)_{0.033}$ Ettenberg et al. (1996), but an even higher figure of merit is found in superlattices. These are $5 \mu\text{m}$ thick films in which crystals of Bi_2Te_3 and Sb_2Te_3 alternate with a period on the order of 50 \AA Venkatasubramanian et al. (2001), and the figure of merit reaches 2.4.

17.4.7 Thomson Effect

The Thomson effect is the name given to the fact that heat dissipation is different in a wire where electric currents flow along with a temperature gradient than it is in the same wire when the direction of the current is reversed. The effect is the subject of Problem 8. The final result is that the contribution to heat evolution which is influenced by a current reversal is

$$-T \frac{d\alpha}{dT} \vec{\nabla} T \cdot \vec{j} \equiv -\mu \vec{\nabla} T \cdot \vec{j}, \quad (17.93)$$

Table 17.1. Thermoelectric data for selected elements

Element	Z	L/L_0		α (μVK^{-1})		R_{Hnec}	
		300 K	20 K	300 K	100 K	300 K	100 K
Li	1	0.90	0.22	10.6	4.3	-1.02	-0.16
Na	1	0.91	0.30	-5.8	-2.6	-0.54	-0.50
K	1	0.92		-13.7	-5.2	-0.89	-0.95
Rb	1			-10.2	-3.6	-0.86	-0.91
Cs	1			-0.9		-0.99	
Cu	1	0.91	0.31	1.9	1.2	-0.72	-0.78
Ag	1	0.96	0.70	1.5	0.7	-0.84	-0.84
Au	1	0.96	0.76	1.9	0.8	-0.69	-0.68
Be	2	0.97	0.23	1.7	-2.5	-30.49	-30.49
Mg	2	0.97	0.78	-1.5	-2.1	-1.15	
Ca	2			10.3	1.1		
Sr	2			1.1	-3.0		
Ba	2			12.1	-4.0		
Zn	2	0.92	0.67	2.4	0.7	3.03	3.89
Cd	2	0.97	0.65	2.6	-0.1	2.06	1.48
Hg	2	1.49	0.65			-1.97	
Al	3	0.89	0.72	-1.7	-2.2	-0.96	-0.84
Ga	3			1.8	0.5	-0.96	
In	3			1.7	0.6	-1.00	-0.50
Sn	4			-0.9	-0.0	-0.05	
Pb	4			-1.3	-0.6	0.21	
Sb	5	1.58					
Bi	5	1.07					
Mn	4			-10.0	-2.5	4.41	-23.51
Fe	2	1.36	0.98	16.2	11.6		
Co	2			-30.8	-8.4		
Ni	2	0.83		-19.2	-8.5		

The Lorenz number is compared to Sommerfeld's value L_0 given in Eq. (17.87). The Hall coefficient is compared to the ideal value $-nec$ given after Eq. (17.108). The Seebeck coefficient α does not compare well with free electron theory. Measurements at 300 K encompass those taken from 290-300; those at 100 K range from 80K-100K. In some cases samples are single crystals, and measurements are reported parallel to c axis. Measurements along other axes may differ by factors of 2, and may even have opposite sign. Other samples are polycrystalline, and results depend upon grain size. Details should be sought in the sources, which are Burkov and Vedernikov (1995) p. 390, Landolt and Börnstein (1959) p. 97, and Grigoriev and Meilkhov (1997) p. 692.

where μ is the Thomson coefficient, equal to

$$T \frac{d\alpha}{dT}, \tag{17.94}$$

a measure of the temperature derivative of the thermopower. Thomson coefficients are on the order of hundredths of microvolts per degree. Wilson (1954) shows that the coefficients can be calculated to about 50 percent accuracy on the basis of free-electron theory for the alkali metals.

17.4.8 Hall Effect

The effect found by Hall (1879) determines the sign of charge carriers in metals, and showed that holes are as real for transport purposes as electrons. The original experiment was carried out in a strip of metal, with a magnetic field \vec{H} of several kilogauss in the \hat{z} direction, and an electric field pointing along \hat{x} , as in Figure 17.3. The electric field drives a current along \hat{x} , $\vec{j}_x = \sigma \vec{E}$. The magnetic field needs to be large enough, the samples pure enough, and the temperature low enough that the time required for an electron to execute an orbit around the Fermi surface is smaller than the relaxation time τ . This high-field limit produces electron orbits such as those shown in Figure 17.4. What happens next depends upon the boundaries in the y direction. If current can flow across them, then the electric field along x induces a transverse current j_y along y indefinitely. If current cannot flow across them, then charge builds up on the y boundaries, creating an electric field E_y that eliminates the transverse current. Hall's results can be deduced from either of these measurements.

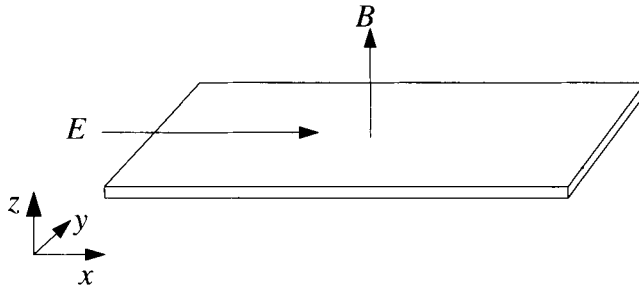


Figure 17.3. Geometry of the Hall effect.

In the presence of crossed electric and magnetic fields, electrons obey

$$\hbar \dot{\vec{k}} = -e \frac{\vec{v}}{c} \times \vec{B} - e \vec{E} \tag{17.95}$$

$$\Rightarrow \vec{B} \times \hbar \dot{\vec{k}} + e \vec{B} \times \vec{E} = -e \vec{B} \times \left(\frac{\vec{v}}{c} \times \vec{B} \right) = -\frac{e}{c} \vec{v}_\perp B^2 \quad \text{Where } \vec{v}_\perp \text{ is the component of } v \text{ perpendicular to } \vec{B}. \tag{17.96}$$

$$\Rightarrow \vec{v}_\perp = -\frac{\hbar c}{e} \frac{\vec{B} \times \dot{\vec{k}}}{B^2} - c \frac{\vec{B} \times \vec{E}}{B^2} \quad \text{Only this component of } v \text{ contributes to current.} \tag{17.97}$$

With this relation between velocity and wave vector, it is possible to evaluate the path integral solution (17.35) of Boltzmann's equation, giving

$$g - f = \int_{-\infty}^t dt' e^{-(t-t')/\tau_\epsilon} \left[\frac{c\hbar \vec{B} \times \dot{\vec{k}}}{e B^2} \right] \cdot e\vec{E} \frac{\partial f}{\partial \mu} \tag{17.98}$$

$$= \int_{-\infty}^t dt' e^{-(t-t')/\tau_\epsilon} \frac{c\hbar \dot{\vec{k}}}{B^2} \cdot [\vec{E} \times \vec{B}] \frac{\partial f}{\partial \mu} \frac{(\vec{A} \times \vec{B}) \cdot \vec{C}}{(\vec{C} \times \vec{A}) \cdot \vec{B}} \tag{17.99}$$

$$= \frac{c\hbar}{B^2} (\vec{k} - \langle \vec{k} \rangle) \cdot [\vec{E} \times \vec{B}] \frac{\partial f}{\partial \mu} \tag{17.100}$$

where

$$\langle \vec{k} \rangle = \frac{1}{\tau_\epsilon} \int_{-\infty}^t dt' e^{-(t-t')/\tau_\epsilon} \vec{k}(t'). \tag{17.101}$$

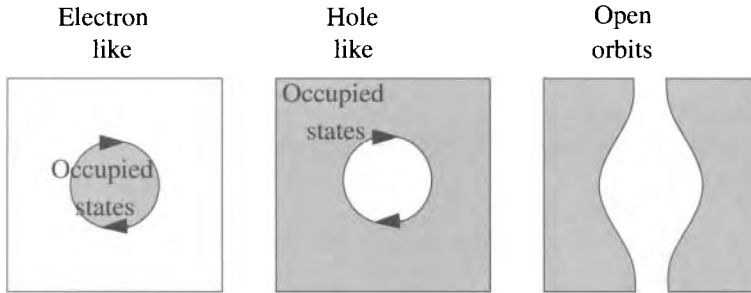


Figure 17.4. Electron-like, hole-like, and open orbits for the Hall effect.

There now are two cases to consider, shown in Figure 17.4, depending upon whether \vec{k} describes a closed or open orbit. In a closed orbit, \vec{k} traverses a circular closed path; the integral of \vec{k} over one cycle vanishes, and $\langle \vec{k} \rangle$ must be smaller than \vec{k} by a typical factor of \mathcal{T}/τ , where \mathcal{T} is the period of an orbit. So when all orbits at the Fermi surface are closed, one can neglect $\langle \vec{k} \rangle$ and write as in Eq. (17.54) that

$$\vec{j} = -e \int [d\vec{k}] \vec{v}_{\vec{k}} \frac{\partial f}{\partial \mu} \frac{\hbar c}{B^2} \vec{k} \cdot (\vec{E} \times \vec{B}) \tag{17.102}$$

$$= e \int [d\vec{k}] \frac{\partial f}{\partial \hbar \vec{k}} \frac{\hbar c}{B^2} \vec{k} \cdot (\vec{E} \times \vec{B}) \tag{17.103}$$

$$= \left\{ \frac{ec}{B^2} \int [d\vec{k}] \frac{\partial}{\partial \vec{k}} (f \vec{k} \cdot (\vec{E} \times \vec{B})) \right\} - \frac{nec}{B^2} (\vec{E} \times \vec{B}) \tag{17.104}$$

Since $\vec{\nabla}(AB) = A\vec{\nabla}B + B\vec{\nabla}A$, $\frac{\partial}{\partial \vec{k}} \vec{k} \cdot \vec{A} = \vec{A}$, and $n = \int [d\vec{k}] f$

Because all orbits at the Fermi surface are closed, the Brillouin zone boundaries can be located in such a way that no orbits pass through the boundaries. Choosing the Brillouin zone in this fashion, either all states at the zone boundary are occupied or all are unoccupied. If all are unoccupied, f vanishes there, and the first integral in Eq. (17.104) vanishes, giving

$$\vec{j} = -\frac{nec}{B^2} (\vec{E} \times \vec{B}). \tag{17.105}$$

If on the other hand all states at the Brillouin zone edge are occupied, replace f in Eq. (17.103) by $(f - 1)$ and repeat the argument, obtaining

$$\vec{j} = \frac{pec}{B^2}(\vec{E} \times \vec{B}), \quad (17.106)$$

where

$$p = \int [d\vec{k}] (1 - f_{\vec{k}}) \quad (17.107)$$

is the density of holes.

The *Hall coefficient* R_H is defined to be

$$R_H = -\frac{E_x}{B j_y}. \quad (17.108)$$

It equals $-1/nec$ in the case of Eq. (17.105), where transport is electron-like, and it equals $1/pec$ for Eq. (17.106), where transport is hole-like. Some values of the Hall coefficient appear in Table 17.1.

17.4.9 Magnetoresistance

In the presence of open orbits, such as shown in Figure 16.8 for copper, matters become complicated, because $\langle \vec{k} \rangle$ can no longer be neglected in Eq. (17.100), and orbits must pass through the Brillouin zone boundary. Rather than trying to perform a calculation in this case, the section will close with a comment upon magnetoresistance. The *resistivity tensor* ρ is the inverse of the conductivity tensor σ and satisfies

$$\vec{E} = \rho \vec{j} \quad (17.109)$$

In strong magnetic fields with all orbits at the Fermi surface closed, the conductivity tensor relating currents and fields along in the plane perpendicular to the magnetic field has the form

$$\sigma \propto \begin{pmatrix} \mathcal{C} \frac{\mathcal{J}}{\tau_\varepsilon} \frac{R_H}{B} & \frac{R_H}{B} \\ -\frac{R_H}{B} & \mathcal{C} \frac{\mathcal{J}}{\tau_\varepsilon} \frac{R_H}{B} \end{pmatrix} \quad (17.110)$$

The off-diagonal components are given by the definition (17.108). The diagonal components, as argued after Eq. (17.100), are roughly $\mathcal{J}/\tau_\varepsilon$ smaller; \mathcal{C} is an unknown constant.

Because \vec{k} should be proportional to B for large B , $\mathcal{J}/\tau_\varepsilon \sim 1/B$, and the diagonal components of the conductivity decrease as $1/B^2$. Inverting this matrix in the large B limit gives the curious result that the diagonal components of the resistivity tensor, the *magnetoresistance*, become independent of B and equal $B\mathcal{C}\mathcal{J}/R_H\tau_\varepsilon$.

In the presence of open orbits, $\langle \vec{k} \rangle$ cannot be neglected in Eq. (17.100), and the result is that both diagonal and off-diagonal components of (17.110) are of the same order of magnitude, going as $1/B$. The magnetoresistance therefore diverges as B . The noble metals have such open orbits, shown in Figure 16.8. Their magnetoresistance is highly anisotropic, as shown in Figure 17.5, and grows without bound as the magnetic field becomes stronger.

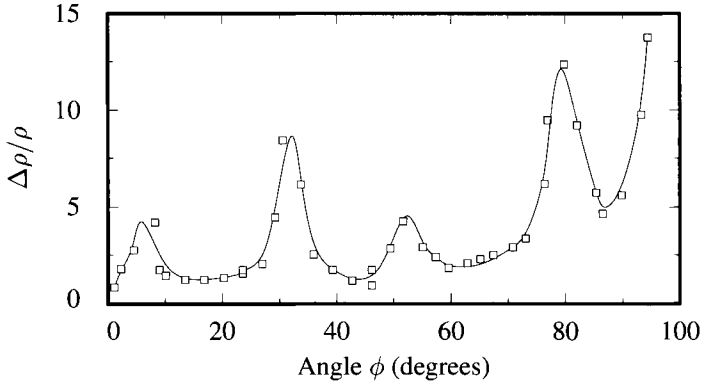


Figure 17.5. Magnetoresistance of crystalline silver at $T = 4.2$ K with a magnetic field of 2.35 T pointing along [001]. On the y axis is the change $\Delta\rho$ in the resistivity divided by the zero-field resistivity. Peaks correspond to open orbits. [Source: Alekseevskii and Gaidukhov (1960), p. 673.]

17.4.10 Anomalous Hall Effect

In materials with spontaneous magnetic moments M , no external field is needed in order to produce a Hall current. An electric field along \hat{x} leads to an electrical current pointing along \hat{y} . This phenomenon is the *anomalous Hall effect*.

For many years it was debated whether the effect was intrinsic and present in perfect crystals, as first proposed by Karplus and Luttinger (1954), or whether it required impurities as proposed by Smit (1955). The resolution of the debate is that both mechanisms appear simultaneously in practical experiments, but intrinsic contributions to the anomalous Hall conductivity are indeed possible.

The intrinsic part of the anomalous Hall effect comes from the anomalous velocity in Eq. (16.84). With a uniform non-zero electric field \vec{E} and no magnetic field, the electron velocity is

$$\vec{v} = \frac{\partial \mathcal{E}_{\vec{k}}}{\partial \hbar \vec{k}} + \frac{e\vec{E}}{\hbar} \times \vec{\Omega}_{\vec{k}}. \tag{17.111}$$

The first term on the right hand side of Eq. (17.111) leads to currents parallel to \vec{E} . The second term however produces a contribution

$$\vec{j} = -\frac{e^2}{\hbar} \vec{E} \times \int [d\vec{k}] \vec{\Omega}_{\vec{k}}^z f_{\vec{k}}, \tag{17.112}$$

Since \vec{E} is already a small quantity, there is no need to keep track also of the difference between $g_{\vec{k}}$ and $f_{\vec{k}}$. Sum over multiple bands if necessary.

and an anomalous Hall conductivity when \vec{j} is along x and \vec{E} is along y of

$$\sigma_{AH} = -\frac{e^2}{\hbar} \int [d\vec{k}] \vec{\Omega}_{\vec{k}}^z f_{\vec{k}}. \tag{17.113}$$

The integrand must also be summed over all occupied bands.

It is not immediately obvious that Eq. (17.113) describes an anomalous Hall effect that is proportional to the strength of spontaneous magnetization \vec{M} . In

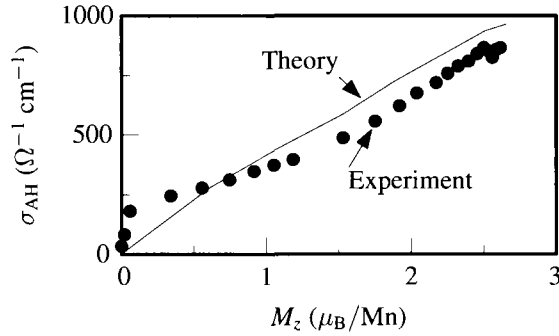


Figure 17.6. Comparison of experimental and theoretical values for the anomalous Hall conductivity σ_{AH} in ferromagnetic thin films of Mn_5Ge_3 . The variation of temperature from 2 to 400 K causes the spontaneous magnetic moment M^z to vary, and causes σ_{AH} to vary as well. Contributions from impurity scattering known as side jump scattering have been removed from the data. The theory appears to be a simple straight line, but in fact results from elaborate band structure calculations without adjustable parameters. [Source: Zeng et al. (2006), p. 3.]

a centrosymmetric crystal, the anomalous velocity $\Omega_{\vec{k}}$ vanishes (Section 16.4.2); spontaneous magnetization breaks the symmetry and allows the Berry connection and anomalous velocity to develop. Demonstrating this idea in a quantitative way requires the full machinery of band structure calculations.

Computation of $\Omega_{\vec{k}}$ leading to a prediction for anomalous Hall currents was first carried out by Jungwirth et al. (2002). Figure 17.6 shows a comparison of theory and experiment for the anomalous Hall effect in thin films of Mn_5Ge_3 . The spontaneous magnetization M^z varies strongly as a function of temperature, and the spontaneous Hall coefficient varies with it nearly linearly. Additional values of computed and measured anomalous Hall coefficients appear in Table 17.2.

Table 17.2. Anomalous Hall conductivity at low temperature for selected ferromagnets.

	bcc Fe	fcc Ni	hcp Co
Computation (S/cm)	753	-2203	447
Experiment (S/cm)	1032	-646	408

[Source: Wang et al. (2007), p. 7.]

17.5 Fermi Liquid Theory

17.5.1 Basic Ideas

Fermi liquid theory was developed by Landau (1956) for the purpose of explaining ^3He , but it has a significance that reaches beyond this particular application. It explains why a system of strongly interacting particles might continue to act in

accord with the single-particle approximation, and it provides a way to quantify the changes produced by interactions. The basic idea is that one should focus on excitations of the strongly interacting system, without worrying about the precise nature of the ground state. These *elementary excitations* act like particles, and therefore are also called *quasi-particles*. Their energies are nearly additive, and one can build complicated excited states by adding together many quasi-particles. Quasi-particles do interact with each other, but less strongly than the original particles from which they are constructed.

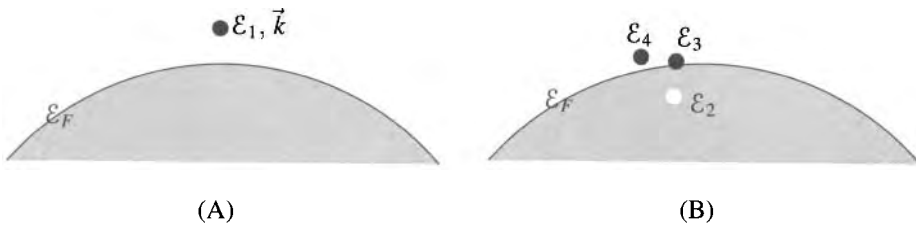


Figure 17.7. (A) An excited state of a collection of fermions, where precisely one fermion is given an energy above ϵ_F . (B) In order for the fermion sitting outside the Fermi sea to interact with those inside it, it must create a final state in which some particle has been ejected from below ϵ_F to above ϵ_F .

Here is a thought experiment to show where the quasi-particles come from. Build a metal, or a jar of ${}^3\text{He}$ with a knob on one side. When the knob is at zero, all of the interparticle interactions of the system are turned off. For a metal, the Coulomb interaction between electrons is set to zero, and for helium the short-range repulsion between helium atoms vanishes. When the knob is at 1, the interactions between particles reach full strength. Placing the knob at zero creates a noninteracting Fermi gas. Consider this gas in its ground state, except that one particle is given wave vector \vec{k} at energy ϵ_1 a tiny bit above the Fermi surface, as shown in Figure 17.7(A). All the excited states of the noninteracting system can be described by exciting one or more particles above the Fermi surface in this way.

Now imagine turning the knob slowly to 1, so that all the particles below the Fermi surface, in the *Fermi sea*, begin to interact with each other and with the particle sitting above. According to the adiabatic theorem [see Landau and Lifshitz (1977), p. 148, or Schiff (1968), p. 289], if the knob turns slowly enough, the system evolves continuously into an eigenstate of the interacting Hamiltonian. However, this is not the situation of interest to Fermi liquid theory. Instead, to construct Fermi liquid theory, imagine turning the knob at a rate that is rapid compared to the scattering time τ of \vec{k} states near the Fermi surface. The result of turning the knob will be a state that still has eigenvalue \vec{k} , which means that it has eigenvalue $\exp[i\vec{k} \cdot \vec{R}]$ when translated through \vec{R} . However, it will not be an energy eigenstate, and will decay in time.

The essential point is that for states lying very close to the Fermi surface, the scattering time τ goes to infinity as $(\epsilon_1 - \epsilon_F)^{-2}$, which means that one can turn the knob arbitrarily slowly and still end up with \vec{k} states after the knob reaches 1.

It is possible to explain the divergence of τ by examining the structure of the electron scattering problem, without performing a detailed calculation. As shown in Appendix C, when particles interact with two-body interactions, the interaction Hamiltonian takes the form

$$\hat{U}_{\text{int}} = \sum_{\substack{\vec{k}'\vec{q}\vec{k} \\ \sigma\sigma'}} U_{\vec{k}'\vec{q}\vec{k}} \hat{c}_{\vec{k}'-\vec{q},\sigma'}^\dagger \hat{c}_{\vec{k}+\vec{q},\sigma}^\dagger \hat{c}_{\vec{k},\sigma} \hat{c}_{\vec{k}',\sigma'}. \quad (17.114)$$

According to Fermi's Golden Rule, Eq. (13.99), the rate at which a particle leaves state \vec{k} and goes to some other state is proportional to the number of final states available after the scattering process. Possible final states are determined by asking for what states $\langle\Psi^f|$ the matrix element $\langle\Psi^f|\hat{U}_{\text{int}}|\Psi^i\rangle$ is nonzero. Only one particle, with wave number \vec{k} , lies above the Fermi surface in the initial state, so \vec{k}' in Eq. (17.114) must lie below the Fermi surface. If $\vec{q} = 0$ or $\vec{q} = \vec{k}' - \vec{k}$, the final state is the same as the initial state, and the wave number of the particle has not changed. The only other possibility is for the final state to consist of two particles above the Fermi surface, with wave vectors $\vec{k}' - \vec{q}$ and $\vec{k} + \vec{q}$, and a hole of wave vector \vec{k}' below it, as shown in Figure 17.7(B). As the particle with wave number \vec{k} descends closer and closer to the Fermi surface, it becomes more and more difficult to find acceptable final states. Equation (13.99) becomes

$$\mathcal{P}(\vec{k} \rightarrow \vec{k}') = \int \left(\prod_{l=2}^4 d\mathcal{E}_l D(\mathcal{E}_l) \right) \frac{2\pi}{\hbar} \delta(\mathcal{E}_1 + \mathcal{E}_2 - \mathcal{E}_3 - \mathcal{E}_4) |\langle\Psi^f|\hat{U}_{\text{int}}|\Psi^i\rangle|^2. \quad (17.115)$$

Taking into account the fact that \mathcal{E}_3 and \mathcal{E}_4 must be greater than \mathcal{E}_F , while $\mathcal{E}_2 < \mathcal{E}_F$, and taking the matrix element to be constant when all energies lie very close to the Fermi surface, Eq. (17.115) becomes

$$\mathcal{P}(\vec{k} \rightarrow \vec{k}') \propto \int_{2\mathcal{E}_F - \mathcal{E}_1}^{\mathcal{E}_F} d\mathcal{E}_2 \int_{\mathcal{E}_F}^{\mathcal{E}_1 + \mathcal{E}_2 - \mathcal{E}_F} d\mathcal{E}_3 \propto (\mathcal{E}_1 - \mathcal{E}_F)^2 \propto \tau^{-1}. \quad (17.116)$$

As claimed, the scattering time of \vec{k} states diverges near the Fermi surface.

To summarize: There exists a set of wave functions that are in one-to-one correspondence with low-lying excited states of the noninteracting Fermi gas and behave under translations like noninteracting particles with index \vec{k} . One can also construct states in correspondence with low-energy holes of the noninteracting gas. These states are not true energy eigenfunctions, but they decay very slowly near the Fermi surface.

17.5.2 Statistical Mechanics of Quasi-Particles

Energy Functional. Landau (1956) proposed a phenomenological description of a quantum state inhabited by many quasi-particles. Let $f_{\vec{k}}$ describe the occupation number of state \vec{k} . In the ground state all $f_{\vec{k}}$ below the Fermi surface are 1; all above are 0. Next, let $\delta f_{\vec{k}}$ describe the difference between the occupation of state \vec{k} and its

occupation in the ground state; in the ground state, all $\delta f_{\vec{k}}$ are 0. Suppose that the energy of the quantum state can be expanded in terms of the occupation numbers $\delta f_{\vec{k}}$ (the spin state σ will not be shown explicitly on $\delta f_{\vec{k}}$ unless necessary):

$$\mathcal{E}[\delta f] = \mathcal{E}_0 + \sum_{\vec{k}\sigma} \mathcal{E}_{\vec{k}}^{(0)} \delta f_{\vec{k}} + \frac{1}{2} \sum_{\substack{\vec{k}, \vec{k}' \\ \sigma, \sigma'}} \delta f_{\vec{k}} u_{\vec{k}\vec{k}'} \delta f_{\vec{k}'} + \dots \quad (17.117)$$

The function $\mathcal{E}_{\vec{k}}^{(0)}$ gives the energy of noninteracting particles. For a metal, it is the energy of Bloch wave functions, while for helium it is $\hbar^2 k^2 / 2m$. The function $u_{\vec{k}\vec{k}'}$ describes interactions between the quasi-particles.

Zero Temperature. The energy needed to add one quasi-particle $\delta f_{\vec{k}}$ above the Fermi surface is

$$\mathcal{E}_{\vec{k}} \equiv \mathcal{E}_{\vec{k}}^{(0)} + \sum_{\vec{k}'\sigma'} u_{\vec{k}\vec{k}'} \delta f_{\vec{k}'}. \quad (17.118)$$

If the chemical potential μ rises, the system will fill with quasi-particles until the cost of adding them rises above μ . Similarly, if the chemical potential drops, states will empty out until $\mathcal{E}_{\vec{k}} = \mu$. Therefore, in equilibrium at zero temperature where $\mu = \mathcal{E}_F$, the occupation numbers f are

$$f_{\vec{k}}^{(0)} \equiv \theta(\mathcal{E}_F - \mathcal{E}_{\vec{k}}). \quad (17.119)$$

For an isotropic system the Fermi wave vector is defined by $\mathcal{E}_{k_F} = \mathcal{E}_F$. Because indexing of the quasi-particles is in one-to-one correspondence with free particles, relationships for free particles are preserved, such as

$$N = \sum_{\vec{k}\sigma} f_{\vec{k}} \Rightarrow n = \frac{N}{\mathcal{V}} = \frac{1}{3\pi^2} k_F^3. \quad (17.120)$$

Low Temperatures. The grand partition function of the Fermi liquid is

$$Z_{\text{gr}} = \sum_{\delta n_{\vec{k}_1} \dots \delta n_{\vec{k}_N}} \exp \left\{ -\beta \left[\sum_{\vec{k}\sigma} (\mathcal{E}_{\vec{k}}^{(0)} - \mu) \delta n_{\vec{k}} + \frac{1}{2} \sum_{\substack{\vec{k}\vec{k}' \\ \sigma\sigma'}} \delta n_{\vec{k}} u_{\vec{k}\vec{k}'} \delta n_{\vec{k}'} \right] \right\}. \quad (17.121)$$

The integers $\delta n_{\vec{k}}$ take values 0 and 1 above the Fermi surface, and -1 and 0 below it, and are distinct from the occupation probabilities $\delta f_{\vec{k}}$, which are the thermal averages of the δn 's. This partition function cannot be summed exactly, but at low temperatures its properties can be obtained with excellent accuracy from a *mean field* approximation. To carry out the mean-field approximation, replace δn everywhere by

$$\delta n_{\vec{k}} = \delta f_{\vec{k}} + (\delta n_{\vec{k}} - \delta f_{\vec{k}}) \quad \text{To learn why this approximation is called mean field theory, see Section 24.4.} \quad (17.122)$$

and keep only up to linear order in the second term of (17.122), regarded as small. The grand partition function becomes

$$Z_{\text{gr}} = \sum_{\delta n_{\vec{k}_1}=0,1,\dots} e^{-\beta[\sum_{\vec{k}\sigma} \mathcal{E}_{\vec{k}}^{(0)} - \mu + \sum_{\vec{k}'\sigma'} u_{\vec{k}\vec{k}'} \delta f_{\vec{k}'}] \delta n_{\vec{k}} + \beta \frac{1}{2} \sum_{\vec{k}\vec{k}'\sigma\sigma'} \delta f_{\vec{k}} u_{\vec{k}\vec{k}'} \delta f_{\vec{k}'}} \quad (17.123)$$

$$= \prod_{\substack{\vec{k}\vec{k}' \\ \sigma\sigma'}} e^{\frac{1}{2}\beta\delta f_{\vec{k}} u_{\vec{k}\vec{k}'} \delta f_{\vec{k}'}} \sum_{\delta n_{\vec{k}_1} \dots} \prod_{\vec{k}\sigma} e^{-\beta[\mathcal{E}_{\vec{k}} - \mu] \delta n_{\vec{k}}} \quad (17.124)$$

$$= \prod_{\substack{\vec{k}\vec{k}' \\ \sigma\sigma'}} e^{\frac{1}{2}\beta\delta f_{\vec{k}} u_{\vec{k}\vec{k}'} \delta f_{\vec{k}'}} \prod_{\vec{k}\sigma} (1 + e^{-\beta[\mathcal{E}_{\vec{k}} - \mu] h_{\vec{k}}}), \quad (17.125)$$

where $h_{\vec{k}} = -1$ if state \vec{k} lies below the Fermi surface, and $h_{\vec{k}} = 1$ otherwise.

The expectation value $\delta f_{\vec{k}}$ of occupying state \vec{k} is given by

$$\delta f_{\vec{k}} = \prod_{\substack{\vec{k}\vec{k}' \\ \sigma\sigma'}} e^{\frac{1}{2}\beta\delta f_{\vec{k}} u_{\vec{k}\vec{k}'} \delta f_{\vec{k}'}} \left[\sum_{\delta n_{\vec{k}_1}=0,1,\dots} \right] \delta n_{\vec{k}} \prod_{\vec{k}'\sigma'} e^{-\beta[\mathcal{E}_{\vec{k}'} - \mu] \delta n_{\vec{k}'}} / Z_{\text{gr}}, \quad (17.126)$$

and because most terms cancel between numerator and denominator it is

$$\delta f_{\vec{k}} = \frac{h_{\vec{k}}}{e^{\beta h_{\vec{k}}(\mathcal{E}_{\vec{k}} - \mu)} + 1} = \frac{1}{e^{\beta(\mathcal{E}_{\vec{k}} - \mu)} + 1} - f_{\vec{k}}^{(0)}. \quad f^{(0)} \text{ defined in Eq. (17.119)}. \quad (17.127)$$

So the quasi-particle states are occupied with a probability that is given by the Fermi function. However, because $\mathcal{E}_{\vec{k}}$ depends upon the occupation probabilities through Eq. (17.118), Eq. (17.127) is a complicated implicit expression.

17.5.3 Effective Mass

The effective mass m^* of quasi-particles is defined by

$$v_F \equiv \left| \frac{\partial \mathcal{E}_{\vec{k}}}{\partial \hbar \vec{k}} \right|_{k_F} \equiv \frac{\hbar k_F}{m^*}. \quad (17.128)$$

Because of the interactions $u_{\vec{k}\vec{k}'}$, the effective mass and bare particle mass differ. The method employed to calculate the change is a generalization of the technique used in Section 16.2.2. The idea is to compute the total particle current of a system with quasi-particles in two different ways and, by comparing them, deduce the effective mass.

First Calculation of Particle Current. The quasi-particle states were specially chosen so as to be eigenfunctions of momentum, so evaluating the total flow of particles \vec{J}_N is easy. For helium it is

$$\vec{J}_N = \sum_{\alpha} \langle \Psi | \frac{\hat{p}_{\alpha}}{m} | \Psi \rangle \quad (17.129)$$

$$= \sum_{\vec{k}\sigma} \frac{\vec{k}\hbar}{m} f_{\vec{k}} = \sum_{\vec{k}\sigma} \frac{\vec{k}\hbar}{m} \delta f_{\vec{k}}. \quad \text{The difference between } f \text{ and } \delta f \text{ is spherically symmetrical.} \quad (17.130)$$

For a metal, the matrix element (17.129) would be evaluated as following Eq. (16.24), and it would give an effective mass due to interactions with the lattice, rather than simply m .

Second Calculation of Particle Current. However, the current carried by a collection of particles can also be calculated by calculating how their energy changes when all their momenta change by a small amount.

To see why, consider the operator that generates small changes in momentum \vec{p} ,

$$1 + \sum_l \vec{p} \cdot \frac{\partial}{\partial \vec{P}_l} = 1 + i \sum_l \vec{p} \cdot \hat{R}_l / \hbar. \quad (17.131)$$

Acting on a general Hamiltonian $\hat{\mathcal{H}}$ with this operator gives

$$[1 - i \sum_l \vec{p} \cdot \hat{R}_l / \hbar] \left\{ \sum_l \frac{\hat{P}_l^2}{2m} + \frac{1}{2} \sum_\beta \hat{U}_{\text{int}}(\hat{R}_l, \hat{R}_\beta) \right\} [1 + i \sum_l \vec{p} \cdot \hat{R}_l / \hbar] \quad (17.132)$$

$$= \hat{\mathcal{H}} + \sum_l \vec{p} \cdot \frac{\hat{P}_l}{m}. \quad (17.133)$$

So particle current can be calculated by taking a collection of quasi-particles, increasing all their momenta by $\vec{p} = \hbar d\vec{k}$, finding the change in their mean energy, and dividing through by $\hbar d\vec{k}$, just as in Eq. (16.24).

To apply this idea to the energy function of Eq. (17.117), note that if the index \vec{k} of all quasi-particles increases by $d\vec{k}$, then the occupation probability $f_{\vec{k}}$ is replaced by $f_{\vec{k}-d\vec{k}}$. Increasing the momenta of all quasi-particles by $\hbar d\vec{k}$ changes their energy to

$$\sum_{\vec{k}\sigma} \mathcal{E}_{\vec{k}}^{(0)} [f_{\vec{k}-d\vec{k}} - f_{\vec{k}}^{(0)}] + \frac{1}{2} \sum_{\substack{\vec{k}\vec{k}' \\ \sigma\sigma'}} [f_{\vec{k}-d\vec{k}} - f_{\vec{k}}^{(0)}] u_{\vec{k}\vec{k}'} [f_{\vec{k}'-d\vec{k}} - f_{\vec{k}'}^{(0)}] \quad (17.134)$$

$$= d\vec{k} \cdot \sum_{\vec{k}\sigma} f_{\vec{k}} \frac{\partial \mathcal{E}_{\vec{k}}}{\partial \vec{k}} + \sum_{\vec{k}\sigma} \mathcal{E}_{\vec{k}}^{(0)} \delta f_{\vec{k}} + \frac{1}{2} \sum_{\substack{\vec{k}\vec{k}' \\ \sigma\sigma'}} \delta f_{\vec{k}} u_{\vec{k}\vec{k}'} \delta f_{\vec{k}'}. \quad (17.135)$$

See Eq. (17.127). Multiply out the interaction term, whenever $\vec{k} - d\vec{k}$ appears, change the summation index sending $\vec{k} \rightarrow \vec{k} + d\vec{k}$, use $u_{\vec{k}\vec{k}'} = u_{\vec{k}'\vec{k}}$, and expand out to first order in $d\vec{k}$.

Differentiating the change in energy by $\hbar d\vec{k}$ gives

$$\vec{J}_N = \sum_{\vec{k}\sigma} v_{\vec{k}} f_{\vec{k}} \quad (17.136)$$

with

$$\vec{v}_{\vec{k}} = \frac{\partial \mathcal{E}_{\vec{k}}}{\partial \hbar \vec{k}}. \quad \text{Derivatives of } \mathcal{E}_{\vec{k}} \text{ give the group velocity.} \quad (17.137)$$

To express Eq. (17.136) in terms of δf rather than f , write

$$\vec{J}_N = \sum_{\vec{k}\sigma} \frac{\partial \mathcal{E}_{\vec{k}}^{(0)}}{\partial \hbar \vec{k}} f_{\vec{k}} + \sum_{\substack{\vec{k}\vec{k}' \\ \sigma\sigma'}} f_{\vec{k}} \frac{\partial}{\partial \hbar \vec{k}} u_{\vec{k}\vec{k}'} \delta f_{\vec{k}'} \quad (17.138)$$

$$= \sum_{\vec{k}\sigma} \frac{\partial \mathcal{E}_{\vec{k}}^{(0)}}{\partial \hbar \vec{k}} \delta f_{\vec{k}} + \sum_{\substack{\vec{k}\vec{k}' \\ \sigma\sigma'}} [\delta f_{\vec{k}} + f_{\vec{k}}^{(0)}] \frac{\partial}{\partial \hbar \vec{k}} u_{\vec{k}\vec{k}'} \delta f_{\vec{k}'} \quad (17.139)$$

$$= \sum_{\vec{k}\sigma} \frac{\partial \mathcal{E}_{\vec{k}}}{\partial \hbar \vec{k}} \delta f_{\vec{k}} - \sum_{\substack{\vec{k}\vec{k}' \\ \sigma\sigma'}} \frac{\partial f_{\vec{k}}^{(0)}}{\partial \hbar \vec{k}} u_{\vec{k}\vec{k}'} \delta f_{\vec{k}'} \quad \text{Regroup integrals, then integrate by parts.} \quad (17.140)$$

$$= \sum_{\vec{k}\sigma} \vec{v}_{\vec{k}} \delta f_{\vec{k}} + \sum_{\substack{\vec{k}\vec{k}' \\ \sigma\sigma'}} u_{\vec{k}\vec{k}'} \vec{v}_{\vec{k}'} \delta (\mathcal{E}_{\vec{k}'}^{(0)} - \mathcal{E}_F) \delta f_{\vec{k}}. \quad (17.141)$$

The second term on the right of Eq. (17.141) is interpreted as a *backflow*, a reverse flow of the medium around each particle, which inevitably accompanies it whenever one tries to drive the particle to create a current.

Comparing the Two Expressions. Comparing Eqs. (17.130) and (17.141) in the case where just one $\delta f_{\vec{k}}$ is nonzero provides now an expression for the effective mass induced by interactions,

$$\frac{\hbar \vec{k}}{m} = \vec{v}_{\vec{k}} + \sum_{\vec{k}'\sigma'} u_{\vec{k}\vec{k}'} \vec{v}_{\vec{k}'} \delta (\mathcal{E}_{\vec{k}'}^{(0)} - \mathcal{E}_F). \quad (17.142)$$

$$= \frac{\hbar \vec{k}}{m^*} + \sum_{\vec{k}'\sigma'} u_{\vec{k}\vec{k}'} \frac{\hbar \vec{k}'}{m^*} \delta (\mathcal{E}_{\vec{k}'}^{(0)} - \mathcal{E}_F) \quad \text{Using definition (17.128).} \quad (17.143)$$

$$\frac{m^*}{m} = 1 + \sum_{\vec{k}'\sigma'} u_{\vec{k}\vec{k}'} \frac{\vec{k}' \cdot \vec{k}}{k_F^2} \delta (\mathcal{E}_{\vec{k}'}^{(0)} - \mathcal{E}_F) \quad \begin{array}{l} \text{Take dot product of both sides with } \vec{k}. \\ \text{Assuming the Fermi surface spherical,} \\ \text{both } \vec{k} \text{ and } \vec{k}' \text{ must have magnitude } k_F \\ \text{because Fermi liquid theory is only} \\ \text{valid near the Fermi surface.} \end{array} \quad (17.144)$$

$$= 1 + \mathcal{V} \int dk' D_{\vec{k}'} d\Sigma \delta (\mathcal{E}_{\vec{k}'}^{(0)} - \mathcal{E}_F) u_{\vec{k}\vec{k}'} \hat{k} \cdot \hat{k}' \quad \begin{array}{l} \text{The angular integral } d\Sigma \text{ is} \\ \text{performed over the Fermi} \\ \text{surface.} \end{array} \quad (17.145)$$

$$= 1 + \mathcal{V} \int d\Sigma \frac{D(\mathcal{E}_F)}{4\pi} u_{\vec{k}\vec{k}'} \cos \theta \quad \begin{array}{l} \text{The density of states normally includes the} \\ \text{angular integral, and because that integral is} \\ \text{being performed separately, } D(\mathcal{E}_F) \text{ is divided} \\ \text{by } 4\pi. \theta \text{ is the angle between } \vec{k} \text{ and } \vec{k}'. \end{array} \quad (17.146)$$

$$= 1 + \mathcal{V} D(\mathcal{E}_F) \frac{1}{2} \int_{-1}^1 d(\cos \theta) u_{\vec{k}\vec{k}'} \cos \theta. \quad \begin{array}{l} u \text{ only depends on the angle} \\ \text{between } \vec{k} \text{ and } \vec{k}', \text{ and could be} \\ \text{written as a function of } \theta. \end{array} \quad (17.147)$$

So the effective mass m^* increases over the bare mass m according to a weighted average of the interactions $u_{\vec{k}\vec{k}'}$ over the Fermi surface.

17.5.4 Specific Heat

The specific heat at low temperatures is related to the density of states at the Fermi surface $D(\mathcal{E}_F)$. To calculate the specific heat, note that

$$C_V = \frac{\partial \mathcal{E}}{\partial T} \Big|_V = \frac{\partial}{\partial T} \left[\sum_{\vec{k}\sigma} \mathcal{E}_{\vec{k}}^{(0)} \delta f_{\vec{k}} + \frac{1}{2} \sum_{\substack{\vec{k}\vec{k}' \\ \sigma\sigma'}} \delta f_{\vec{k}} u_{\vec{k}\vec{k}'} \delta f_{\vec{k}'} \right] \quad (17.148)$$

$$= \sum_{\vec{k}\sigma} \mathcal{E}_{\vec{k}} \frac{\partial \delta f_{\vec{k}}}{\partial T}. \quad (17.149)$$

Using Eq. (17.127) for $\delta f_{\vec{k}}$ gives

$$\frac{\partial \delta f_{\vec{k}}}{\partial T} = \frac{h_{\vec{k}} e^{\beta h_{\vec{k}}(\mathcal{E}_{\vec{k}} - \mu)}}{[e^{h_{\vec{k}}\beta(\mathcal{E}_{\vec{k}} - \mu)} + 1]^2} \left\{ \frac{h_{\vec{k}}}{k_B T^2} (\mathcal{E}_{\vec{k}} - \mu) - \frac{h_{\vec{k}}}{k_B T} \sum_{\vec{k}'\sigma'} u_{\vec{k}\vec{k}'} \frac{\partial \delta f_{\vec{k}'}}{\partial T} + \frac{h_{\vec{k}}}{k_B T} \frac{\partial \mu}{\partial T} \right\}. \quad (17.150)$$

At low temperatures, the first term in curly brackets is much larger than the others in Eq. (17.150), so

$$C_V = \mathcal{V} \int [d\vec{k}] \frac{1}{k_B T^2} (\mathcal{E}_{\vec{k}} - \mu)^2 \frac{e^{\beta(\mathcal{E}_{\vec{k}} - \mu)}}{[e^{\beta(\mathcal{E}_{\vec{k}} - \mu)} + 1]^2} \quad \begin{array}{l} \text{Everything is even in} \\ \mathcal{E}_{\vec{k}} - \mu, \text{ so } h_{\vec{k}} \text{ goes away.} \end{array} \quad (17.151)$$

$$= \mathcal{V} \int d\mathcal{E} D(\mathcal{E}) \frac{1}{k_B T^2} (\mathcal{E} - \mu)^2 \frac{e^{\beta(\mathcal{E} - \mu)}}{[e^{\beta(\mathcal{E} - \mu)} + 1]^2} \quad (17.152)$$

$$\Rightarrow c_V = \frac{\pi^2}{3} k_B^2 T D(\mathcal{E}_F). \quad \begin{array}{l} \text{The integral over } \mathcal{E} \text{ is performed as in Eq. (6.67). This} \\ \text{equation is identical to Eq. (6.77).} \end{array} \quad (17.153)$$

Because the density of states at the Fermi surface is also given by

$$D(\mathcal{E}_F) = \int [d\vec{k}] \delta(\mathcal{E}_F - \mathcal{E}_{\vec{k}}) = \int d\mathcal{E} \frac{k^2 \delta(\mathcal{E}_F - \mathcal{E})}{\pi^2 \hbar |\partial \mathcal{E}_{\vec{k}} / \partial \hbar \vec{k}|} = \frac{k_F^2}{\pi^2 \hbar v_F} = \frac{m^* k_F}{\pi^2 \hbar^2}, \quad (17.154)$$

the specific heat can be used to measure the effective mass.

17.5.5 Fermi Liquid Parameters

Moments of $u_{\vec{k}\vec{k}'}$ over the Fermi surface provide the most important information about interactions. There is a conventional notation for these moments, the *Landau parameters*. This notation takes into account the possibility that particles with the same spin have an interaction that differs from the interaction between particles with different spin, so

$$u_{\vec{k}\uparrow\vec{k}'\uparrow} = u_{\vec{k}\downarrow\vec{k}'\downarrow} = u_{\vec{k}\vec{k}'}^s + u_{\vec{k}\vec{k}'}^a \quad (17.155)$$

$$u_{\vec{k}\uparrow\vec{k}'\downarrow} = u_{\vec{k}\downarrow\vec{k}'\uparrow} = u_{\vec{k}\vec{k}'}^s - u_{\vec{k}\vec{k}'}^a, \quad (17.156)$$

where the *s* stands for “symmetric,” and the *a* stands for “antisymmetric.” Then one defines

$$u_{\vec{k}\vec{k}'}^s = \sum_{l=0}^{\infty} u_l^s P_l(\cos \theta) \quad P_l \text{ is a Legendre polynomial.} \quad (17.157)$$

$$u_{\vec{k}\vec{k}'}^a = \sum_{l=0}^{\infty} u_l^a P_l(\cos \theta). \quad (17.158)$$

The formulae may be inverted:

$$u_l^s = \frac{2l+1}{2} \int_{-1}^1 d(\cos \theta) P_l(\cos \theta) \frac{u_{\vec{k}\uparrow\vec{k}'\uparrow} + u_{\vec{k}\uparrow\vec{k}'\downarrow}}{2} \quad (17.159)$$

$$u_l^a = \frac{2l+1}{2} \int_{-1}^1 d(\cos \theta) P_l(\cos \theta) \frac{u_{\vec{k}\uparrow\vec{k}'\uparrow} - u_{\vec{k}\uparrow\vec{k}'\downarrow}}{2}. \quad (17.160)$$

The parameters u all have dimensions of energy. To make them dimensionless, multiply by the density $\mathcal{V}D(\mathcal{E}_F)$ of energy states at the Fermi surface, to get

$$F_l^a \equiv \mathcal{V}D(\mathcal{E}_F) u_l^a, \quad F_l^s \equiv \mathcal{V}D(\mathcal{E}_F) u_l^s. \quad (17.161)$$

Example: Effective Mass Relation. The integral appearing in Eq. (17.147) is

$$\mathcal{V}D(\mathcal{E}_F) \frac{1}{2} \int_{-1}^1 d(\cos \theta) \cos \theta u_{\vec{k}\vec{k}'} \quad (17.162)$$

$$= \left(\frac{1}{3}\right) \left(\frac{3}{2}\right) \int_{-1}^1 d(\cos \theta) P_1(\cos \theta) \mathcal{V}D(\mathcal{E}_F) \frac{u_{\vec{k}\uparrow\vec{k}'\uparrow} + u_{\vec{k}\uparrow\vec{k}'\downarrow}}{2} \quad (17.163)$$

$$= \frac{1}{3} F_1^s. \quad (17.164)$$

So the effective mass relation (17.147) takes the form

$$\frac{m^*}{m} = 1 + \frac{1}{3} F_1^s. \quad (17.165)$$

17.5.6 Traveling Waves

The critical observer may complain that Fermi liquid theory is vacuous. It begins with some unknown quantities, such as specific heat and effective mass, and in attempting to improve matters it defines an infinite number of other unknown quantities—the interaction parameters—and then relates new unknowns to the old unknowns. Nothing has really been learned unless there are some cross-checks.

Landau provided a check by calculating the speeds of two different sorts of traveling waves in ${}^3\text{He}$. The first of them is ordinary sound, which is a traveling pressure wave where the liquid remains in local thermal equilibrium as pressure oscillates up and down. The second is *zero sound*, a traveling wave moving at frequencies so high that thermal equilibrium has no time to establish itself.

Ordinary First Sound. The speed of sound c in a liquid or gas is given by

$$c^2 = \left. \frac{\partial P}{\partial \rho} \right|_S. \quad (17.166)$$

In liquid ${}^3\text{He}$, the interest is in temperatures below 1 K. The difference between isothermal and adiabatic derivatives is proportional to $\partial S/\partial n|_T$, which vanishes at $T = 0$ because S does. Therefore one can replace the adiabatic derivative in Eq. (17.166) by an isothermal one and write

$$c^2 = \left. \frac{\mathcal{V}}{m} \frac{\partial P}{\partial N} \right|_{T\mathcal{V}} = - \frac{\mathcal{V}}{m} \frac{\partial}{\partial N} \frac{\partial F}{\partial \mathcal{V}} = \left. \frac{-\mathcal{V}}{m} \frac{\partial \mu}{\partial \mathcal{V}} \right|_N \quad (17.167)$$

$$= \left. \frac{N}{m} \frac{\partial \mu}{\partial N} \right|_{\mathcal{V}} = \frac{N}{m} \frac{\partial^2 F}{\partial N^2}. \quad (17.168)$$

The motion of sound involves sloshing of mass back and forth; there should be no doubt that the mass density $\rho = mN/\mathcal{V}$ involves the bare helium mass, not an effective mass. This argument would not, however, work for a metal, where sound also involves motion of the ions.

Equation (17.168) provides one explanation of why Fermi liquid theory expands the energy out to quadratic order in quasi-particle densities; the second derivatives needed to find sound speeds could not be obtained correctly otherwise.

Because μ is the natural independent variable, the easiest quantity to calculate in Eq. (17.168) is $\partial N/\partial\mu$. At very low temperatures, where the sound speed is being computed, one obtains

$$\delta f_{\vec{k}} = \theta(\mu - \mathcal{E}_{\vec{k}}) - \theta(\mathcal{E}_F - \mathcal{E}_{\vec{k}})|_{\mu=\mathcal{E}_F} \quad (17.169)$$

$$\Rightarrow \frac{\partial \delta f_{\vec{k}}}{\partial \mu} = \delta(\mathcal{E}_{\vec{k}} - \mu) \left(1 - \frac{\partial \mathcal{E}_{\vec{k}}}{\partial \mu}\right) \quad (17.170)$$

μ is oscillating around some equilibrium value as the wave passes by, and the occupation numbers δf are given by subtracting from f the occupation number appropriate in equilibrium.

$$= \delta(\mathcal{E}_{\vec{k}} - \mu) \left[1 - \sum_{\vec{k}'\sigma'} u_{\vec{k}\vec{k}'} \frac{\partial \delta f_{\vec{k}'}}{\partial \mu}\right]. \quad (17.171)$$

Now define

$$A = \sum_{\vec{k}'\sigma'} u_{\vec{k}\vec{k}'} \frac{\partial \delta f_{\vec{k}'}}{\partial \mu}. \quad (17.172)$$

Equation (17.171) guarantees that \vec{k}' lies on the Fermi surface, and because \vec{k} also lies on the Fermi surface, while $u_{\vec{k}\vec{k}'}$ depends only on the angle between \vec{k} and \vec{k}' , A is independent of \vec{k} . Then using Eqs. (17.171) and (17.172), one obtains

$$A = \int [d\vec{k}'] u_{\vec{k}\vec{k}'} \delta(\mathcal{E}_{\vec{k}'} - \mu) (1 - A) \quad (17.173)$$

$$= B (1 - A), \quad \text{where } B = \sum_{\vec{k}'\sigma'} u_{\vec{k}\vec{k}'} \delta(\mathcal{E}_{\vec{k}'} - \mu) = F_0^s \quad (17.174)$$

$$\Rightarrow A = \frac{B}{1+B} = \frac{F_0^s}{1+F_0^s}. \quad (17.175)$$

The total number of particles N in the system differentiated by μ is therefore

$$\frac{\partial N}{\partial \mu} = \sum_{\vec{k}\sigma} \frac{\partial \delta f_{\vec{k}}}{\partial \mu} \quad (17.176)$$

$$= \sum_{\vec{k}\sigma} \delta(\mathcal{E}_{\vec{k}} - \mu) (1 - A) \quad (17.177)$$

$$= \mathcal{V}D(\mathcal{E}_F) \frac{1}{1+F_0^s} \quad (17.178)$$

$$\Rightarrow c = \sqrt{\frac{n}{mD(\mathcal{E}_F)} (1+F_0^s)} \quad (17.179)$$

$$= v_F \sqrt{\frac{m^*}{3m} (1+F_0^s)}. \quad \text{Use Eqs. (17.120), (17.128), and (17.154).} \quad (17.180)$$

Zero Sound. When the frequency of oscillation is very fast compared to the scattering time of quasi-particles, the population of quasi-particles has no time to arrive locally at the equilibrium described by Eq. (17.169). To describe traveling waves in this limit, one can turn to the Boltzmann equation (17.10), interpreting $g = f_{\vec{k}}$ as the occupation number of quasi-particle excitations and using Eq. (17.118) as the energy functional corresponding to Eq. (17.2).

It is enough to consider cases in which deviations of the distribution function from equilibrium are small, and then linearize in the deviations. Letting $f_{\vec{k}}^{(0)}$ from Eq. (17.119) denote the equilibrium distribution and then expanding to first order, one finds immediately

$$\frac{\partial \delta f_{\vec{k}}}{\partial t} + \vec{v}_{\vec{k}} \cdot \frac{\partial}{\partial \vec{r}} \left\{ \delta f_{\vec{k}} - \frac{\partial f_{\vec{k}}^{(0)}}{\partial \mathcal{E}_{\vec{k}}} \mathcal{E}_{\vec{k}} \right\} = \left. \frac{dg}{dt} \right|_{\text{coll.}} \quad (17.181)$$

If $\delta f_{\vec{k}}$ varies in space, so does $\mathcal{E}_{\vec{k}}$ through its dependence on δf , but the variation of $\mathcal{E}_{\vec{k}}$ with \vec{r} is a small quantity.

The point of focusing upon time scales short compared with the scattering time (near the Fermi surface), is that the scattering term becomes negligible. To proceed, carry out a Fourier transform in time and space, going over to variables ω and \vec{q} respectively, to obtain

$$(\omega - \vec{q} \cdot \vec{v}_{\vec{k}}) \delta f_{\vec{k}} - \delta(\mathcal{E}_{\vec{k}} - \mathcal{E}_F) \vec{q} \cdot \vec{v}_{\vec{k}} \left(\sum_{\vec{k}'\sigma'} u_{\vec{k}\vec{k}'} \delta f_{\vec{k}'} \right) = 0. \quad \text{Because } \partial f_{\vec{k}}^{(0)} / \partial \mathcal{E}_{\vec{k}} = -\delta(\mathcal{E}_{\vec{k}} - \mathcal{E}_F). \quad (17.182)$$

All of the action is at the Fermi surface, and δf behaves as a delta function near there. To make this fact explicit, define

$$\phi_{\vec{k}} \delta(\mathcal{E}_F - \mathcal{E}_{\vec{k}}) = \delta f_{\vec{k}}. \quad (17.183)$$

Then

$$(\omega - \vec{q} \cdot \vec{v}_{\vec{k}}) \phi_{\vec{k}} - \vec{q} \cdot \vec{v}_{\vec{k}} \sum_{\vec{k}'\sigma'} u_{\vec{k}\vec{k}'} \phi_{\vec{k}'} = 0. \quad (17.184)$$

To simplify matters at this point, assume that $D(\mathcal{E}_F) u_{\vec{k}\vec{k}'}$ is spherically symmetric and can be replaced by F_0^s . The assumption is not reasonable: F_1^s must be included as well, but the additional algebra is left for Problem 12. Proceeding as if F_0^s were enough, one obtains

$$(\omega - \vec{q} \cdot \vec{v}_{\vec{k}}) \phi_{\vec{k}} - \vec{q} \cdot \vec{v}_{\vec{k}} F_0^s \int \frac{d\Sigma}{4\pi} \phi_{\vec{k}'} = 0. \quad \text{The integral is a surface integral over the Fermi sphere.} \quad (17.185)$$

$$\Rightarrow \phi_{\vec{k}} = \frac{\vec{q} \cdot \vec{v}_{\vec{k}}}{\omega - \vec{q} \cdot \vec{v}_{\vec{k}}} F_0^s \int \frac{d\Sigma}{4\pi} \phi_{\vec{k}'}. \quad (17.186)$$

Equation (17.186) shows that $\phi_{\vec{k}}$ depends only on the angle between \vec{q} and $\vec{v}_{\vec{k}}$ (which points along \vec{k}) and can be written as $\phi(\cos \theta)$. Let

$$\phi(\cos \theta) = \sum_{l=0}^{\infty} P_l(\cos \theta) \phi_l \quad \text{Legendre polynomials, again.} \quad (17.187)$$

$$\Rightarrow \phi(\cos \theta) = -\left[1 - \frac{\omega}{\omega - qv_F \cos \theta}\right] F_0^s \phi_0 \quad (17.188)$$

$$\Rightarrow \phi_0 = -F_0^s \phi_0 \frac{1}{2} \int_{-1}^1 d(\cos \theta) \left[1 - \frac{\omega}{\omega - qv_F \cos \theta}\right] \quad (17.189)$$

$$= -F_0^s \phi_0 \left[1 + \frac{1}{2} \frac{\omega}{qv_F} \ln \left(\frac{\omega - qv_F}{\omega + qv_F}\right)\right] \quad (17.190)$$

$$\Rightarrow 1 + F_0^s \left[1 + \frac{1}{2} \frac{\omega}{qv_F} \ln \left(\frac{\omega - qv_F}{\omega + qv_F}\right)\right] = 0. \quad (17.191)$$

If $F_0^s > 0$, there is always a solution of Eq. (17.191) for some value of ω/qv_F . In other words, there is a linear dispersion relation between ω and q . Unfortunately Eq. (17.191) does not compare well with experiment, because F_1^s does not turn out to be small. Including F_1^s in the analysis gives instead (Problem 12)

$$\left\{ F_0^s \left(1 + \frac{1}{3} F_1^s\right) + \left(\frac{\omega}{qv_F}\right)^2 F_1^s \right\} \left[1 + \frac{1}{2} \frac{\omega}{qv_F} \ln \left(\frac{\omega - qv_F}{\omega + qv_F}\right)\right] + 1 + \frac{F_1^s}{3} = 0. \quad (17.192)$$

A numerical solution of Eq. (17.192) gives the dispersion relation $c_0 = \omega/q$ for zero sound.

17.5.7 Comparison with Experiment in ³He

The Fermi liquid parameters that enter into Eq. (17.192) were measured in ³He by Greywall (1983) and are listed in Table 17.3. Abel et al. (1966) studied sound induced by a quartz crystal at 15.4 and 45.5 MHz, and they measured sound speed and attenuation as a function of temperature. Ideally the experiment would be conducted as a function of frequency, showing that at low frequencies sound propagates with the first sound velocity of Eq. (17.180) and that at higher frequencies it propagates at a new velocity given by solving Eq. (17.192). In the absence of tunable crystals to create sound of arbitrary frequency in the tens of megahertz range, the experiment was conducted as a function of temperature. The reasoning was that at sufficiently low temperature one should see zero sound, but at higher temperatures additional scattering should bring about thermal equilibrium more rapidly, and the velocity should cross over to first sound. The scattering time for quasi-particles varies as T^{-2} , and it was estimated that for $T = 1$ K the scattering time is of order 10^{-12} s. Therefore sound at 10 MHz should begin to travel as zero sound when the temperature is on the order of 10 mK. Precisely such a transition is demonstrated in Figure 17.8.

Table 17.3. Fermi liquid parameters for ³He

$P(\text{bar})$	F_0^s	F_1^s	F_0^a	F_1^a	m^*/m	$v_F (\text{m s}^{-1})$
0	9.15	5.27	-0.700	-0.55	2.76	59.7
3	15.83	6.40	-0.725	-0.73	3.13	54.3

Source: Greywall (1983).

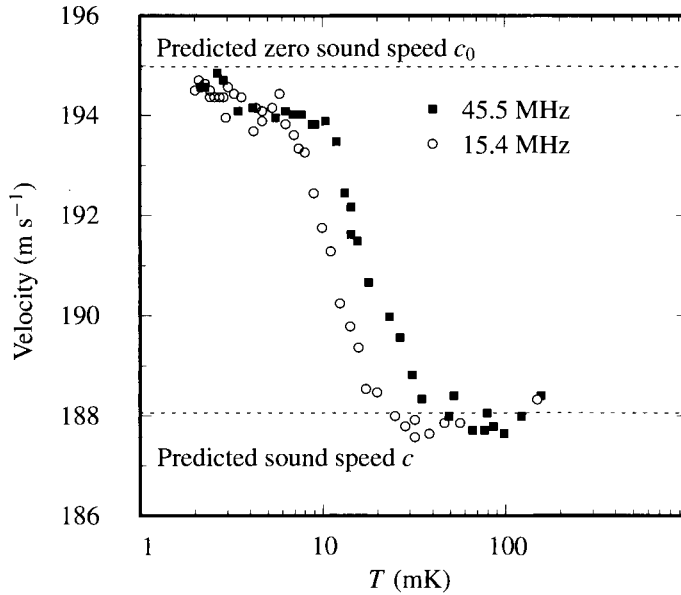


Figure 17.8. Sound propagation velocity as a function of temperature in ^3He , at a pressure of 0.32 bar. [Source: Abel et al. (1966), p. 76.]

The experiment was conducted at a pressure $P = 0.32$ bar, somewhat different from any for which the Fermi liquid parameters were measured directly. Using linear interpolation to estimate the values of the various parameters at this pressure, one finds that for ordinary sound from Eq. (17.180) $c = 188 \text{ m s}^{-1}$, while for zero sound, Eq. (17.192) has a solution at $\omega/qv_F = 3.3$ which predicts a zero sound velocity $c_0 = 195 \text{ m s}^{-1}$. These values compare well with the measurements in Figure 17.8. The test is not trivial, because Fermi liquid theory has predicted the existence of a new high-frequency mode, whose properties are to be found solely on the basis of specific heat and low-frequency sound measurements. Abel et al. (1966) also performed another test of the theory by measuring sound attenuation. Sound attenuation can be calculated within the context of the relaxation time approximation to the Boltzmann equation, using the relaxation time τ as an additional phenomenological parameter. Attenuation should increase as T^2 for zero sound, then decay as T^{-2} for regular sound. This behavior is seen as well, with the crossover occurring at the same temperature as the crossover in sound speed.

Problems

- Boltzmann statistics:** Calculate the analog of Eq. (17.60), proceeding from Eq. (17.56), assuming that the probability f of occupying a state is given by Boltzmann rather than Fermi statistics, and verify that the final answer is unchanged.
- Semiclassical equations:** Use Eq. (17.1) to derive Eq. (17.3b). Remember

that the vector potential \vec{A} may be time dependent and contribute to the electric field.

3. Boltzmann equation with anomalous velocity:

- (a) Demonstrate that Eq. (17.22) follows from Eqs. (17.16) and (17.17).
- (b) Verify Eq. (17.24)

4. Onsager relations:

- (a) Derive Eq. (17.51). Use the fact that $T\dot{S}$ is linear in the forces, and also use the fact that $\vec{v}_{\vec{k}} = -\vec{v}_{-\vec{k}}$.
- (b) Show that Eq. (17.51) leads to the symmetry Eq. (17.50).

5. AC conductivity: Use the Boltzmann equation to find the response of a free Fermi electron gas to an electric field which oscillates in time at frequency ω .

6. Current driven by thermal gradient: Consider a metal subject to a constant temperature gradient $\partial T/\partial x$. Assume energy near the Fermi surface to be isotropic and of the form $\epsilon_{\vec{k}} = m^*v_{\vec{k}}^2/2$. Show that the electric current j_x is nonzero and is proportional to

$$e\tau_{\epsilon_F} \frac{1}{m^*} c_{\mathcal{V}} \frac{\partial T}{\partial x}, \tag{17.193}$$

where $c_{\mathcal{V}}$ is the specific heat. Find the dimensionless constant of proportionality.

7. Thermoelectric figure of merit:

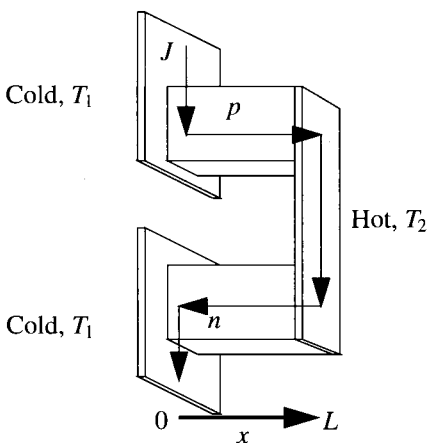


Figure 17.9. A thermoelectric refrigerator operates by passing current through a first element p with positive Peltier coefficient, and into a second n with negative Peltier coefficient, causing transport of heat from 0 to L .

Consider the operation of the thermoelectric refrigerator shown in Figure 17.9.

- (a) Argue that the thermal currents J_Q^p and J_Q^n flowing along x in the p and n elements are

$$J_Q^p = \Pi_p J - A_p \kappa_p \frac{\partial T}{\partial x} \quad (17.194a)$$

$$J_Q^n = -\Pi_n J - A_n \kappa_n \frac{\partial T}{\partial x}, \quad (17.194b)$$

where J is the electrical current, κ_p and κ_n are the thermal conductivities of the two elements, Π_p and Π_n are the Peltier coefficients of the two elements, and A_p and A_n are the cross-sectional areas.

- (b) The temperature gradients are not uniform, because the current flow produces Joule heating per unit length $J^2 R_{p,n}/L$, where R_p and R_n are the resistances of the two elements. Assume that the Peltier coefficients are independent of temperature. Solve for the temperature field in each element, and show that the flow of heat at $x = 0$ is

$$J_Q^p = \Pi_p J - A_p \kappa_p \frac{T_2 - T_1}{L} - \frac{J^2 R_p}{2} \quad (17.195a)$$

$$J_Q^n = -\Pi_n J - A_n \kappa_n \frac{T_2 - T_1}{L} - \frac{J^2 R_n}{2}. \quad (17.195b)$$

- (c) Find for any given temperature difference $T_2 - T_1$ the value of the current J_m producing the greatest total heat flux $J_Q = J_Q^p + J_Q^n$.
- (d) Show that the maximum temperature difference $T_2 - T_1$ that the refrigerator can sustain is

$$\frac{(\Pi_p - \Pi_n)^2}{2R\kappa}; \quad (17.196)$$

along the way, define R and κ . It is conventional to define a figure of merit

$$Z = \frac{(\Pi_p - \Pi_n)^2}{R\kappa T^2}, \quad T = (T_1 + T_2)/2. \quad (17.197)$$

which has dimensions of inverse kelvin. Sometimes the dimensionless ZT is also reported.

8. **Thomson coefficient:** The Thomson effect is the name given to the fact that heat dissipation is different in a wire where electric currents flow with a temperature gradient than it is in the same wire when the direction of the current is reversed. Derive the effect first by noting that the flow of entropy may be given by

$$T \frac{\partial S}{\partial t} = -\vec{\nabla} \cdot \vec{J}_Q + \vec{G} \cdot \vec{J}. \quad (17.198)$$

Use the general equations of linear transport theory to eliminate \vec{G} everywhere in favor of \vec{J} . As a result, find an equation for entropy generation just in terms

of electron current and temperature gradients. From this expression, isolate the term that will change when the relative direction of heat and temperature flow is altered. Relate this term to the temperature derivative of the thermopower, and describe an experiment that would allow one to measure this term.

The simple result of Eq. (17.93) is only correct if \mathbf{L}^{21} and \mathbf{L}^{11} commute.

9. **Hall effect—elementary argument:** A simple treatment of the Hall effect begins by assuming that electrons obey the equation of motion

$$m\dot{\vec{v}} = -e \left(\vec{E} + \frac{\vec{v}}{c} \times \vec{B} \right) - \frac{m\vec{v}}{\tau}. \quad (17.199)$$

- (a) Assume that current is not permitted to pass the y boundaries in Figure 17.3, so that charge builds up there and creates an electric field E_y in the y direction. Assume that when the electron current reaches steady state, electrons drift in the x direction at a constant rate. Furthermore, in steady state the y component of all electron velocities must vanish, or else more charge would build up on the boundaries, and the electric field along y would continue to change. Rewrite Eq. (17.199) so as to take into account these two observations.
- (b) Solve the resulting equations to find the Hall coefficient, defined to be

$$R_H = \frac{E_y}{B j_x}, \quad (17.200)$$

where j_x is the current in the x direction.

10. **Hall effect—Boltzmann equation:** In order to find the Hall coefficient in the context of the Boltzmann equation, one may proceed in the following way:

Begin with

$$\frac{\partial g}{\partial t} = -\vec{v}(\vec{r}) \frac{\partial}{\partial \vec{r}} g - \dot{\vec{k}} \frac{\partial}{\partial \vec{k}} g - \frac{g - f}{\tau}. \quad \text{Combining Eqs. (17.9) and (17.26).} \quad (17.201)$$

In steady state, $\partial g / \partial t$ vanishes, so one has

$$\vec{v}(\vec{r}) \frac{\partial}{\partial \vec{r}} g + \dot{\vec{k}} \frac{\partial}{\partial \vec{k}} g = -\frac{g - f}{\tau}. \quad (17.202)$$

When a magnetic induction \vec{B} is present, one obtains

$$\dot{\vec{k}} = -e(\vec{E} + \vec{v} \times \vec{B}/c). \quad (17.203)$$

- (a) Guess a solution of this equation in the form

$$g = f + [\mathcal{D} - \vec{k} \cdot \vec{\mathcal{C}}] \frac{\partial f}{\partial \mu}. \quad (17.204)$$

Find expressions for \mathcal{D} and $\vec{\mathcal{C}}$, assuming that \vec{E} lies in the plane of the metal, and \vec{B} is perpendicular to it. Neglect a term involving $\partial^2 f / \partial \mu^2$.

- (b) Compute currents along x and y for arbitrary values of B and \vec{E} , and find the electric field strength E_y necessary to guarantee that J_y , the current in the y direction vanishes.
- (c) As a result, find the Hall coefficient

$$R_H = \frac{E_y}{BJ_x}. \quad (17.205)$$

11. **Temperature dependence of μ :** In the context of Fermi liquid theory, find the leading temperature dependence of μ at low temperatures. Begin by writing the temperature derivative of the total number of particles, and by requiring it to be zero, find $\partial\mu/\partial T$.
12. **Higher-order expression for zero sound:** Verify that if all Fermi liquid parameters except for F_1^s and F_0^s vanish, then the dispersion relation for zero sound is

$$\left\{ F_0^s \left(1 + \frac{1}{3} F_1^s \right) + \left(\frac{\omega}{qv_F} \right)^2 F_1^s \right\} \left[1 + \frac{1}{2} \frac{\omega}{qv_F} \ln \left(\frac{\omega - qv_F}{\omega + qv_F} \right) \right] + 1 + \frac{F_1^s}{3} = 0. \quad (17.206)$$

References

- W. R. Abel, A. C. Anderson, and J. C. Wheatley (1966), Propagation of zero sound in liquid He^3 at low temperatures, *Physical Review Letters*, **17**, 74–78.
- N. E. Alekseevskii and Y. P. Gaidukhov (1960), The anisotropy of magnetoresistance and the topology of Fermi surfaces of metals, *Soviet Physics JETP*, **10**, 481–484.
- G. Baym and C. Pethick (1991), *Fermi-Liquid Theory: Concepts and Applications*, John Wiley and Sons, New York.
- A. T. Burkov and M. V. Vedernikov (1995), Thermoelectric properties of metallic materials, in *CRC Handbook of Thermoelectrics*, D. M. Rowe, ed., pp. 387–399, CRC Press, Boca Raton, FL.
- R. G. Chambers (1957), Magneto-resistance effects in the group I metals at high field, *Proceedings of the Royal Society of London*, **A238**, 344–357.
- M. H. Ettenberg, W. A. Jesser, and F. D. Rosi (1996), ??, in *Proceedings of the 15th International Conference on Thermoelectrics*, T. Caillat, ed., IEEE, Piscataway NJ.
- D. S. Greywall (1983), Specific heat of normal liquid ^3He , *Physical Review B*, **27**, 2747–2766.
- I. S. Grigoriev and E. Z. Meilkhov, eds. (1997), *Handbook of Physical Quantities*, CRC Press, Boca Raton, FL.
- E. H. Hall (1879), On a new action of the magnet on electric currents, *American Journal of Mathematics*, **2**, 287–292.
- R. P. Heubener (1972), Thermoelectricity in metals and alloys, *Solid State Physics: Advances in Research and Applications*, **27**, 63–134.
- A. Isihara (1993), *Electron Liquids*, Springer-Verlag, Berlin.
- T. Jungwirth, Q. Niu, and A. H. MacDonald (2002), Anomalous hall effect in ferromagnetic semiconductors, *Physical Review Letters*, **88**(20), 207 208.
- R. Karplus and J. M. Luttinger (1954), Hall effect in ferromagnetics, *Physical Review*, **95**, 1154–1160.

- L. D. Landau (1956), The theory of a Fermi liquid, *Journal of Experimental and Theoretical Physics (U.S.S.R.)*, **30**, 1058–1064. Reprinted in Pines (1961), pp. 260–265.
- L. D. Landau and E. M. Lifshitz (1977), *Quantum Mechanics (Non-relativistic Theory)*, 3rd ed., Pergamon Press, Oxford.
- H. Landolt and R. Börnstein (1959), *Numerical Data and Functional Relationships in Science and Technology*, II, Springer-Verlag, Berlin.
- G. Mahan, B. Sales, and J. Sharp (1997), Thermoelectric materials: new approaches to an old problem, *Physics Today*, **50**(3), 42–47.
- J. E. Parrot and A. D. Stuckes (1975), *Thermal Conductivity of Solids*, Pion, London.
- D. Pines (1961), *The Many-Body Problem*, W. A. Benjamin, Reading, MA.
- D. Pines and P. Nozières (1966), *The Theory of Quantum Liquids*, vol. 1, Benjamin, New York.
- A. B. Pippard (1988), *Magnetoresistance in Metals*, Cambridge University Press, Cambridge.
- L. Schiff (1968), *Quantum Mechanics*, 3rd ed., McGraw-Hill, New York.
- J. Smit (1955), The spontaneous Hall effect in ferromagnetics I, *Physica*, **55**, 877–887.
- R. Venkatasubramanian, E. Sivola, T. Colpitts, and B. O’Quinn (2001), Thin-file thermoelectric devices with high room-temperature figures of merit, *Nature*, **413**, 597–602.
- D. Vollhardt (1984), Normal ^3He : An almost localized Fermi liquid, *Reviews of Modern Physics*, **56**, 99–120.
- X. Wang, D. Vanderbilt, J. R. Yates, and I. Souza (2007), Fermi-surface calculation of the anomalous Hall conductivity, *Physical Review B*, **76**, 195 109/1–11.
- A. H. Wilson (1954), *The Theory of Metals*, Cambridge University Press, Cambridge.
- D. Xiao, J. Shi, and Q. Niu (2005), Berry phase correction to electron density of states in solids, *Physical Review Letters*, **95**(13), 137 204.
- C. Zeng, Y. Yao, Q. Niu, and H. Weitering (2006), Linear magnetization dependence of the intrinsic anomalous Hall effect, *Physical Review Letters*, **96**, 037 204/1–4.
- J. M. Ziman (1960), *Electrons and Phonons: The Theory of Transport Phenomena in Solids.*, Clarendon Press, Oxford.

18. Microscopic Theories of Conduction

18.1 Introduction

This chapter is devoted to exploring the difference between electrical conductors and insulators. Electrical resistance arises from the scattering of electrons as electric fields drag them through a sample. To connect electrical resistivity with the underlying physics at the atomic scale, it is necessary to grapple with the scattering problem directly. The simplest version of this theory treats impurities and thermal fluctuations as weak scattering sites, amenable to the same techniques that solve the problem of inelastic neutron scattering.

As the strength and density of impurities that scatter electrons increases, it is natural to expect the resistance of the solid to increase as well. What might not be expected is that past a certain density of impurities, the solid undergoes a qualitative change. It no longer can support traveling waves, and it turns from a conductor to an insulator. This mechanism is a subtle quantum-mechanical effect, valid at low temperatures. It is only one in a series of ways that qualitative shifts from conductors to insulators can occur. The essential difference between insulators and conductors is more than a question of filled versus unfilled bands in perfect crystals, and the most general explanation has probably not yet been formulated.

18.2 Weak Scattering Theory of Conductivity

18.2.1 General Formula for Relaxation Time

Although the calculation of electronic states in disordered materials is an extremely difficult problem, there is one fairly straightforward case, which is an extension of the nearly-free electron picture to the case of disordered metals or random alloys. Imagine that a collection of electrons sits in a weak but no longer periodic potential. If the effects of the potential may safely be treated to low order in perturbation theory, then its interactions with electrons may be solved in the same way that X-ray scattering in amorphous structures can be solved. As first noted by Bhatia and Krishnan (1948), the same correlation function governs the two cases, because the electrons, like the X-rays, are simply waves bouncing off weak scatterers.

The starting point is Section 10.2.1, which showed that in some cases, particularly the alkali metals, Schrödinger's equation for the conduction electrons in the presence of a periodic potential can be recast as a problem for plane waves in weak potentials. Formally, these weak potentials are nonlocal and energy-dependent, because the fact that they are so weak results from the cooperative screening provided by all the different electrons. All one needs to know, however, is that there

are cases where regarding a metal as free electrons in weak potentials has hope of quantitative success. Take $U(\vec{R})$ to be an appropriate pseudopotential, centered at \vec{R} . In the case of a liquid metal or metallic glass, the locations \vec{R} label all the sites inhabited by atoms. In the case of a random alloy, or a metal with impurities, the locations \vec{R} label all the places where the second species or impurity has been placed, and $U(\vec{R})$ describes the difference between the pseudopotential of the original metal and the pseudopotential of the impurity.

The Collision Term. The collision term $dg/dt|_{\text{coll}}$ is central to the Boltzmann equation. It has been treated so far in the relaxation time approximation. The first step in a microscopic theory of resistance is the attempt to calculate the relaxation time from an underlying picture of electron collisions.

The relaxation time approximation is based upon the view that there are effectively random processes causing electrons to alter their wave vectors. What form should these processes have? The question can be answered in a purely formal manner, using techniques to be presented in Section 20.4. The formal derivation can obscure the physical meaning of the various terms that arise, so the presentation in this section will emphasize physical arguments over formal ones.

Consider a collection of electrons described by the distribution function $g_{\vec{k}}$. There is no need for the index \vec{r} , so it will not be displayed explicitly. If an electron scatters off nonmagnetic impurities, the probability \mathcal{P} for it to make a transition from state \vec{k} and spin σ to state \vec{k}' with spin σ' must have the form

$$\mathcal{P}(\vec{k} \rightarrow \vec{k}', t) = g_{\vec{k}} \left[1 - g_{\vec{k}'} \right] \delta_{\sigma\sigma'} W_{\vec{k}\vec{k}'}. \quad (18.1)$$

Because the scattering potential is nonmagnetic, the jump can only occur if the electron spin σ does not change. The rate must be proportional to the number g of electrons occupying state \vec{k} , proportional to the number $1 - g$ of vacancies at destination \vec{k}' , and finally proportional to a rate $W_{\vec{k}\vec{k}'}$ that is independent of the occupation number g . Accounting both for electrons that jump into \vec{k} by these processes and for those that jump out gives

$$\left. \frac{dg}{dt} \right|_{\text{coll.}} = \frac{\mathcal{V}}{2} \int [d\vec{k}'] g_{\vec{k}'} [1 - g_{\vec{k}}] W_{\vec{k}'\vec{k}} - g_{\vec{k}} [1 - g_{\vec{k}'}] W_{\vec{k}\vec{k}'}. \quad (18.2)$$

The leading $1/2$ is due the fact that the spin state of the electron cannot change, effectively cutting the density of states in half. $[d\vec{k}']$ defined in Eq. (6.15).

Equation (18.2) is equivalent to the relaxation time approximation when the following conditions obtain:

1. Scattering potentials into which electrons collide are spherically symmetrical, and can be treated as weak.
2. The energies of occupied electronic states $\mathcal{E}_{\vec{k}}$ are isotropic, and they depend only upon the magnitude of \vec{k} .

The first assumption allows one to write the potential seen by electrons as

$$\hat{U}_{\text{tot}} \equiv \sum_{\vec{R}} U(r - \vec{R}). \quad (18.3)$$

The functions U are spherically symmetrical scattering potentials, centered at sites \vec{R} . They are best thought of as pseudopotentials of impurity atoms added to a perfect crystal, or else as atoms of the crystals out of place.

Adopting this form of scattering potential, and retracing steps starting with Fermi's Golden Rule that led to Eq. (13.104) gives

$$W_{\vec{k}\vec{k}'} = \sum_{\text{final states}} \frac{2\pi}{\hbar} \delta(\mathcal{E}^f - \mathcal{E}^i) |\langle \Psi^f | \hat{U}_{\text{tot}} | \Psi^i \rangle|^2 \quad (18.4)$$

$$= 2\pi S^i(\vec{q}, \omega_e) |U(\vec{q})|^2 \frac{N_s}{V^2}. \quad (18.5)$$

Here $\vec{q} = \vec{k} - \vec{k}'$ is the change in wave number of the electron upon scattering, and $\hbar\omega_e = \mathcal{E}_{\vec{k}} - \mathcal{E}_{\vec{k}'}$ gives its change in energy. The inelastic structure factor S^i appears just as for neutron scattering from phonons, now depending upon the change in electron energy. The number of scatterers N_s may refer to a dilute impurity with strong scattering properties, or to every atom in a liquid metal.

Because the potential $U(\vec{r})$ is spherically symmetrical, $U(\vec{q})$ is symmetric in \vec{k} and \vec{k}' and indeed only depends upon the angle θ between them. The inelastic structure factor is not in general insensitive to interchange of \vec{k} and \vec{k}' , but if scattering is nearly elastic and ω_e is very small, then one sees from Eq. (13.104) $S^i(\vec{q}, 0) = S^i(-\vec{q}, 0)$, and assuming one can use this approximation then

$$W_{\vec{k}\vec{k}'} = W_{\vec{k}'\vec{k}}. \quad (18.6)$$

Next assume that the solution of the Boltzmann equation has the form

$$g_{\vec{k}} = f_{\vec{k}} + \vec{C} \cdot \vec{k}. \quad (18.7)$$

Here \vec{C} is a vector that either is constant, or is a function of $\mathcal{E}_{\vec{k}}$; it cannot otherwise depend upon \vec{k} or \vec{r} .

This form is general enough to encompass spatially uniform electric fields, uniform temperature gradients, and uniform magnetic fields. Putting Eqs. (18.6) and (18.7) into Eq. (18.2) gives

$$\left. \frac{dg}{dt} \right|_{\text{coll.}} = -\vec{C} \cdot \frac{1}{2} \mathcal{V} \int [d\vec{k}'] (\vec{k} - \vec{k}') W_{\vec{k}\vec{k}'}, \quad (18.8)$$

and so

$$\left. \frac{dg}{dt} \right|_{\text{coll.}} = -\frac{g-f}{\tau_E}, \quad (18.9)$$

Because $W_{\vec{k}\vec{k}'}$ depends only on the angle between \vec{k} and \vec{k}' , only the component of \vec{k}' parallel to \vec{k} survives the integration. If one takes $\vec{k} = k\hat{z}$, W depends only on k'_z , and it is easy to see that the integrals of k'_x and k'_y vanish by symmetry. Note that $\vec{C} \cdot \vec{k} = g - f$.

with

$$\frac{1}{\tau_E} = \frac{1}{2} \mathcal{V} \int [d\vec{k}'] W_{\vec{k}\vec{k}'} (1 - \hat{k} \cdot \hat{k}'). \quad (18.10)$$

Inserting Eq. (18.5) into Eq. (18.10), noting that

$$(1 - \hat{k} \cdot \hat{k}') = 2 \left(\frac{q}{2k_F} \right)^2, \quad (18.11)$$

Table 18.1. Mean free paths of electrons in liquid metals

Metal:	Li	Na	Cu	Ag	Au	Zn	Hg	Al	Ga	Sn	Pb	Sb	Bi	Fe
l_T (Å):	45	157	34	51	27	15	5	20	17	5	6	4	4	3

Values obtained by treating the metals as free electron gases where $l_T = v_F \tau$, and the relaxation time τ is obtained from the resistivity ρ at the melting point through $\tau = m/e^2 n \rho$. Source: Cusack (1987) and Grigoriev and Meilkhov (1997) p. 555.

and averaging over initial phonon states as discussed prior to Eq. (13.113) gives

$$\frac{1}{\tau_\varepsilon} = \frac{\pi N_s}{2 \mathcal{V}} \int [d\vec{q}] S(\vec{q}, \omega_e) |U(\vec{q})|^2 \frac{q^2}{k_F^2}. \quad (18.12)$$

In this way, the relaxation time may be related to an integral over the inelastic structure factor and the pseudopotential $U(\vec{q})$.

Resistivity of Liquid Metals. A liquid metal is as disordered as a metal can be, yet somewhat surprisingly the weak scattering limit is often appropriate, and Eq. (18.12) allows quantitative description of resistivity. As evidence, one can use the measured resistivity of liquid metals to deduce the characteristic mean free path $l_T = v_F \tau$ electrons travel between scattering events. As shown in Table 18.1, this distance is tens of angstroms in the noble metals, although it shrinks to atomic dimensions in iron or bismuth.

For liquid metals, the static structure factor is spherically symmetric. Purely elastic electron scattering from such a disordered array of atoms leads to nonzero electrical resistivity. So it is enough to consider the limit $\omega_e = 0$ where change in electron energy can be neglected and write from Eqs. (3.55) and (13.104),

$$S(\vec{q}, \omega_e = 0) = S(\vec{q}) \hbar \delta(\mathcal{E}_F - \mathcal{E}(|\vec{k} - \vec{q}|)). \quad (18.13)$$

In writing this expression, make use of the fact that transport formulas such as Eq. (17.54) use \vec{k} only on the Fermi surface where $\mathcal{E}_{\vec{k}} = \mathcal{E}_F$. For elastic scattering, $\mathcal{E}_{\vec{k}'}$ must lie on the Fermi surface as well.

To continue the evaluation of Eq. (18.12), insert Eq. (18.13). Doing the angular integral over \vec{q}

$$\int_{-1}^1 d(\cos \theta) \delta(\mathcal{E}_F - \mathcal{E}(\sqrt{k_F^2 + q^2 - 2k_F q \cos \theta})) = \frac{\theta(2k_F - q)}{q \partial \mathcal{E} / \partial k_F} \quad (18.14)$$

gives finally an expression due to Ziman (1961),

$$\frac{1}{\tau_\varepsilon} = \frac{1}{4\pi \hbar^2 k_F^2 v_F} \frac{N_s}{\mathcal{V}} \int_0^{2k_F} dq q^3 S(q) |U(q)|^2 \quad \begin{array}{l} N_s \text{ is number of} \\ \text{scatterers.} \end{array} \quad (18.15)$$

$$\Rightarrow \rho = \frac{m}{ne^2 \tau_\varepsilon} = \frac{3\pi}{e^2 \hbar v_F^2} \left(\frac{N_s}{\mathcal{V}} \right) \frac{1}{4k_F^4} \int_0^{2k_F} dq q^3 S(q) |U(q)|^2. \quad (18.16)$$

The final expression uses free-electron relations between the electron density, the Fermi wave vector, and the Fermi velocity v_F . So in the weak scattering limit, the resistivity is just given by an integral over the static scattering structure factor S and the pseudopotential U .

In order to evaluate Eq. (18.16), it is necessary to know both the static structure function $S(\vec{q})$ and the pseudopotential $U(\vec{q})$. The former can be measured by X-ray scattering, and the latter can be obtained either from the density functional calculations described in Section 10.2.1, from de Haas–van Alphen measurements, or else from optical data to be described in Section 23.4. An example of assembling these various ingredients to determine the resistivity of liquid aluminum is provided as Problem 1. The calculation outlined in the problem should not be expected to be accurate to more than around 50%, but the more careful evaluation of Ashcroft and Guild (1965) duplicated experimental values within a few percent. Other properties of liquid metals are reviewed by Ashcroft and Stroud (1978) and March (1990).

Application to Phonons.

Calculation of the resistance of crystals proceeds in a slightly different way. An absolutely perfect crystal has almost no electrical resistance, as Bloch first realized [Section 7.1]. Formally this fact emerges without the need for any calculation from Eq. (18.12). The leading term Eq. (13.129) in the inelastic structure function is a product of delta functions restricting \vec{q} to the reciprocal lattice, and a delta function restricting \vec{k} and \vec{k}' to the Fermi surface. These two delta functions are incompatible: when \vec{k} and \vec{k}' are on the Fermi surface there is vanishing chance that $\vec{q} = \vec{k} - \vec{k}'$ is in the reciprocal lattice.

For metallic crystals resistivity comes from phonons, which means employing Eq. (13.134) to take into account the creation or destruction of one phonon in each electron scattering event.

To simplify matters, keep only longitudinal phonons corresponding to acoustic modes, for which the polarization $\epsilon_{\vec{q}} \parallel \vec{q}$. This type of interaction is called *normal scattering* (*N-process*). The contribution of other phonon bands is not necessarily negligible. when they enter in this context it is called called *Umklapp scattering* [*U-process*; Umklapp is German for “flopping over” and was introduced by Peierls (1929)]. It is hard to see without detailed calculation whether normal or Umklapp processes should be more important, and both should be included for accurate results. In the interests of simplicity, the calculation that follows will keep only the contribution from acoustic phonons, which is sufficient to give a good idea of how the general procedure runs, but not to achieve comparison with experiment on the order of 1% that is possible in the most ruthlessly correct calculations, presented by Bass et al. (1990).

Returning to Eq. (13.134), there are two terms to inspect. In one of them, proportional to $\delta(\omega_{\vec{q}} + \omega_e)$, the phonon of energy $\hbar\omega_{\vec{q}}$ steals energy from the electron. This requires the final electron state to have energy lower than the initial state. Looking now at Eq. (18.1), one sees that since \vec{k} is on the Fermi surface, both terms on the right hand side of Eq. (18.1) vanish unless the final state is higher in

energy than the initial state; the electron must scatter from occupied to unoccupied states. Terms where the phonon takes energy from the electron must be negligible at temperatures low compared with the Debye temperature. In the second process described by Eq. (13.134), proportional to $\delta(\omega_{\vec{q}} - \omega_e)$, the phonon gives energy to the electron. This process is allowed because the electron moves from occupied to unoccupied states. The main effect of keeping track of the energy associated with phonons is to decide which scattering process is allowed; otherwise the phonon energy is negligible in comparison with the electron energies. Thus one can write

$$S(\vec{q}, \omega) \approx \frac{\hbar^2 q^2}{2M\hbar\omega_{\vec{q}}} n_q \hbar \delta(\mathcal{E}_F - \mathcal{E}(|\vec{k} - \vec{q}|)) \quad \begin{array}{l} \text{Keep only the phonon absorption term of} \\ \text{Eq. (13.134); once this is done it is all} \\ \text{right to neglect the phonon energy inside} \\ \text{the delta function. } n_q \text{ is a phonon} \\ \text{occupation number.} \end{array} \quad (18.17)$$

Thus

$$\frac{1}{\tau_e} = \frac{\pi N_s}{2 \mathcal{V}} \int [d\vec{q}] \frac{\hbar^2 q^2}{2M\hbar\omega_{\vec{q}}} \hbar n_q \delta(\mathcal{E}_F - \mathcal{E}(|\vec{k} - \vec{q}|)) \left(\frac{q}{k_F}\right)^2 \quad (18.18)$$

$$\Rightarrow \rho = \frac{3\pi}{e^2 \hbar v_F^2} \left(\frac{N_s}{\mathcal{V}}\right) \frac{1}{4k_F^4} \int_0^{2k_F} dq q^3 \frac{\hbar q^2}{2M\omega_{\vec{q}}} n_q |U(q)|^2, \quad \text{Use Eq. (18.14)} \quad (18.19)$$

$$= \frac{3\pi}{e^2 \hbar v_F^2} \left(\frac{N_s}{\mathcal{V}}\right) \frac{1}{4k_F^4} \frac{\hbar}{2Mc} \left(\frac{k_B T}{\hbar c}\right)^5 \int_0^{2\Theta/T} dz z^4 \frac{1}{e^z - 1} \left|U\left(\frac{k_F z T}{\Theta}\right)\right|^2, \quad (18.20)$$

where c is the longitudinal wave speed, M is ion mass, $\Theta = \hbar k_F c / k_B$ is a Debye temperature, and $z = \Theta q / k_F T$. At temperatures T large compared with the Θ , Eq. (18.20) is linear in T , while at much lower temperatures the resistivity is predicted to vanish as T^5 , the *Bloch T^5 law*.

Comparison with Experiment. The most careful comparison of these predictions with experiment has been carried out for the alkali metals. As shown in Figure 18.1, the resistivity is linear to high accuracy at temperatures over 100 K, and it begins crossing over to a decay as T^5 at temperatures on the order of 20 K. By a temperature of 2 K, there is yet another crossover to a decay of resistivity as T^2 . The origin of this behavior is electron–electron scattering, as described in Section 17.5. Computing the coefficient of T^2 is difficult, and it is discussed by Bass et al. (1990).

18.2.2 Matthiessen's Rule

Comparison of theory and experiment for the alkali metals relies upon extremely pure crystalline samples. A piece of wire pulled from the shelf follows predictions of Eq. (18.20) down to around 100 K, but at lower temperatures it begins to differ. Grain boundaries, dislocations, and various trace elements scatter electrons, and therefore all contribute additively to resistivity according to Eq. (18.16). *Matthiessen's rule* states that separate sources of resistivity, such as phonons and impurities, sum linearly to produce the total resistivity of a sample just as resistors

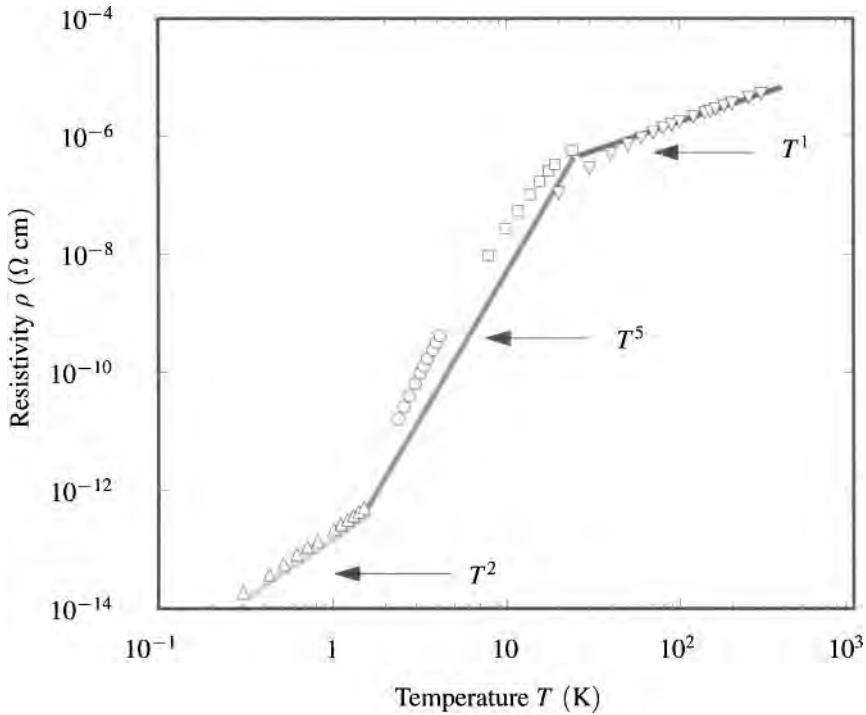


Figure 18.1. Resistivity of potassium from 0.1 to 300 K. At the lowest temperatures, the resistance varies as T^2 , from 2 to 20 K, it varies as T^5 , and from 100 K upwards, it varies as T^1 . [Source: Bass et al. (1990).]

in a series sum linearly. In any but the purest samples, resistivity is therefore the sum of two pieces: a temperature-dependent part resulting from Eq. (18.16), and a temperature-independent part that depends exclusively upon preparation and purity of the sample. The size of the temperature-independent resistivity is in fact used to define the purity of electrical samples. A common figure of merit is the *residual resistivity ratio* (RRR) which is the ratio of resistivity at 300 K to resistivity at 4 K. A “typical” sample of aluminum is 99.5% pure and has $RRR \approx 11$. A “pure” sample of aluminum is six nines (99.9999%) pure and might have $RRR = 2500$.

Matthiessen’s rule is no more than a good rule of thumb. It relies upon the linearity inherent in the weak scattering approximation, and when this approximation fails, so may Matthiessen’s rule as well.

18.2.3 Fluctuations

At any temperature above zero, resistance is never entirely constant, but fluctuates in time. These fluctuations are conventionally separated into three components

Thermal noise. Thermal noise consists of current fluctuations that are present whether a current is flowing or not. When the thermal noise signal is Fourier transformed, its root mean square amplitude is independent of frequency, and

the magnitude of voltage fluctuations in frequency interval $d\omega$ for a wire of resistance R is

$$\langle \delta V^2 \rangle = 4k_B T R d\omega. \quad (18.21)$$

These noise properties were identified by Johnson (1927) and were explained by Nyquist (1928).

Shot noise. Shot noise is an additional source of noise that is proportional to mean current. The current fluctuations δJ it produces have strength per frequency interval $d\omega$

$$\langle \delta J^2 \rangle = 2eJd\omega. \quad (18.22)$$

1/f or flicker noise. 1/f noise is an additional noise source whose amplitude grows with decreasing frequency f roughly as $1/f$. It is fairly ubiquitous, yet the specific mechanism that produces it varies from one system to another. Dutta and Horn (1981) provide a general explanation of how it might arise.

18.3 Metal–Insulator Transitions in Disordered Solids

18.3.1 Impurities and Disorder

No crystal produced in the laboratory is ever completely perfect. In the case of silicon that has been prepared for use in electronics, the degree of perfection is very high. Atoms such as silver and gold whose presence would disrupt electronic circuitry are excluded to better than one part in 10^{12} , and wafers of tens of centimeters in diameter are regularly prepared without a single dislocation or grain boundary disrupting the crystalline order. However, silicon binds very easily to oxygen, and silicon wafers used in electronics typically contain 10^{18} atoms/cm³ oxygen, which is tolerated and rarely mentioned as it does not disrupt electrical properties. Other materials such as aluminum or iron cannot be made nearly as pure, and in addition to traces of other metals and oxygen contain many dislocations. Small mixtures of other elements in a nearly perfect crystals are called *impurities*, and when one wants to call attention to the ways a solid differs from a perfect crystal one calls it *disordered*.

Disorder destroys crystalline regularity, and the conditions for Bloch's theorem no longer apply. One must ask whether the corrections to Bloch's picture are minor, or whether they produce qualitative changes in the nature of the solid. Both outcomes are possible, depending on how strongly electrons interact with the disorder. Sufficiently strong interactions can turn metals into insulators. Much of the work in this area was instigated by Mott, and is reviewed in Mott (1990).

An important class of scattering sites in solids are *point defects* produced either by *vacancies*, sites where atoms simply are missing, or else by substitutional atoms, replacing their hosts on randomly selected lattice sites. The effects of point defects divide into several different classes. Sometimes they have magnetic moments and can flip the spin of passing electrons. Discussion of this case is deferred to Section 26.6. The nonmagnetic impurities fall into two additional groups.

An impurity is called *compensated* or *isoelectronic* when it comes from the same column of the periodic table as the host crystal. Germanium or tin dissolved in silicon, or silver dissolved in gold, provide examples. Adding an atom of this sort amounts to a very localized perturbation on the crystal. The impurity carries a different number of electrons with it from the host. However, the extra (or missing) electrons are entirely confined to core states that are tightly bound to the nucleus, localized in space, and largely inert. Section 18.4 will be dedicated to studying the properties of electrons in such random potentials.

18.3.2 Non-Compensated Impurities and the Mott Transition

When impurities are not compensated, the electrons they carry cannot all be swept into a static potential. The effect is as if one has scattered throughout the solid atomic-sized spots of extra charge. All the conduction electrons in the solid interact strongly with these extra charges. Simple physical considerations based upon classical electrostatics make it possible to explain some of the main experimental results in a simple fashion.

Consider adding an atom of phosphorus to silicon. Phosphorus lies just to the right of silicon in the periodic table, and the perturbation it produces is best described by adding a single proton to a silicon atom, resulting in a long-range potential, falling off as $1/r$. The phosphorus comes accompanied by an extra electron as well, but this electron must be viewed as a member of the population of conduction electrons, responding to the potential. Its wave function spreads over hundreds of adjacent lattice sites.

Precisely because the spread is so large, the nature of the phosphorus impurity may be captured by a simple semiclassical argument, as shown by Kohn (1957). The static dielectric constant of silicon ϵ , like that of other semiconductors, is large and, according to Table 19.1, equals 11.8. The phosphorus nucleus is therefore strongly screened. In addition, as shown in Figures 10.10 and 23.16, silicon is technically an insulator. The valence band is filled, and any extra electron must enter a superposition of states from the conduction band. The lowest-lying states behave approximately like free electrons, with the provision that the mass of the electron be replaced by an effective mass m^* , which, according to Table 19.1, is on the order of 0.2. A proton in empty space binds an electron at radius $a_0 = \hbar^2/me^2$ with binding energy $\mathcal{E}_b = e^2/2a_0$ (this is a hydrogen atom). For phosphorus in silicon, the screening of the proton replaces e^2 by e^2/ϵ , where ϵ is the static dielectric constant, and the binding energy becomes instead

$$a_* = \frac{\epsilon \hbar^2}{m^* e^2} \quad \text{and} \quad \mathcal{E}_b = \frac{e^2}{2\epsilon a_*} = \frac{m^*}{m} \frac{1}{\epsilon^2} \cdot 13.6 \text{ eV}. \quad (18.23)$$

Because $m^*/m \sim 0.1$ and $\epsilon \sim 10$, a_* is approximately 100 times larger than the Bohr radius, and the binding energy is approximately 1000 times smaller than the binding energy of hydrogen. Some comparisons of Eq. (18.23) with actual binding energies appear in Table 19.2, showing that it successfully captures orders of magnitude despite simplifications such as assuming effective masses to be isotropic.

The large size of a_* retroactively justifies using concepts such as dielectric constant and effective mass that are only valid on scales much larger than a lattice spacing. Because of its small binding energy, phosphorus is called a *shallow impurity*, and because it adds an electron to the conduction band, it is called a *donor*. Elements to the left of silicon in the periodic table, such as boron or aluminum, come with one less electron than the host and may be treated as a weakly bound positronium atom, where a delocalized hole, built from states at the top of the valence band, is attracted to a screened $-1/r$ potential. These elements are called *acceptors*. Other impurities, such as gold, produce much more violent changes in the local electronic environment of silicon than do phosphorus or boron and cannot be described as hydrogen atoms. They are called *deep impurities*.

Metal–Insulator Transition in Si:P. The subtleties of impurity potentials, as well as the difficulty of precisely defining the difference between metals and insulators, are both well illustrated by examining the behavior of silicon as the density of phosphorus impurities increases. Take phosphorus-doped silicon (Si:P) down to a temperature on the order of 1 K, so that the chance of thermally exciting a phosphorus electron out of its bound state becomes negligible. At low densities of phosphorus, the material is nothing but pure silicon, an excellent insulator, and bound phosphorus electrons, also insulating. As the density of phosphorus increases, the bound electron wave functions begin to interact, and at a critical density the doped semiconductor turns into a metal.

This transition cannot be explained by the view that insulators are solids with filled Bloch bands, while metals have unfilled bands. From such a point of view, Si:P should always be a metal. Even at low densities, the phosphorus atoms could be arranged in a periodic way throughout the silicon. Bloch's theorem could then be brought to bear on the rather large resulting unit cell, which would produce bands nearly identical to those of silicon, but with the Fermi level moved upwards to populate the bottom of the conduction band with extra electrons provided by phosphorus.

However a dilute arrangement of phosphorus in silicon is no more likely to produce a metal than a lattice of silver atoms, spaced one meter apart. Coulomb repulsion between distant localized electrons produces an insulator that one-electron theory cannot explain. In fact many of the crystalline compounds predicted by one-electron density functional theory to be metals are in fact insulators. A prototype of these compounds is CuO, which will be the subject of further discussion in Section 23.6.3.

Experimental realizations of Si:P do not actually array the phosphorus in a crystalline array, but the basic physics is believed to be similar whether the arrangement of the phosphorus is regular or random, with a simple semiclassical analysis providing a simple picture of how an insulator gives way to a metal.

Polarization Argument for Mott Transition. View Si:P as a cubic lattice of phosphorus, treating the silicon as a continuous dielectric medium of dielectric constant ϵ . When an external electric field is applied to the sample, the phosphorus atoms

polarize slightly in response. Continuing to view the phosphorus as producing a weakly bound hydrogen-like state, its polarizability is

$$\alpha = \frac{9}{2} a_*^3. \quad \text{See, for example, Landau and Lifshitz (1977) pp. 286 and 290.} \quad (18.24)$$

The Clausius–Mossotti relation (Section 22.2.3) relates the polarizability α of the phosphorus to the dielectric constant of Si:P through

$$\frac{\epsilon - 1}{\epsilon + 2} = \frac{4\pi}{3} n_p \alpha \quad (18.25)$$

$$\Rightarrow \epsilon = \frac{3 + 8\pi n_p \alpha}{3 - 4\pi n_p \alpha}, \quad (18.26)$$

where n_p is the density of the phosphorus.

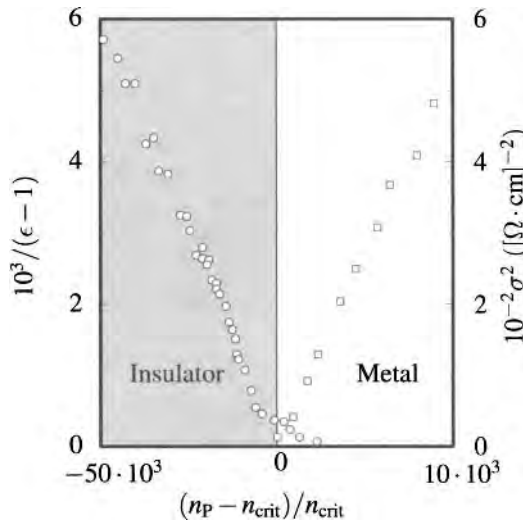


Figure 18.2. Metal–insulator transition in silicon doped with phosphorus. Enough phosphorus is added to bring the material to the verge of become metallic at low temperatures, so that application of slight uni-axial pressure, slightly increasing the density, is enough to push it over the edge. Dielectric susceptibility is measured on the insulating side, and metallic conductivity on the conducting side of the transition. [Source: Rosenbaum (1985), p. 3.]

Defining a dielectric constant makes it possible to discuss long-range interactions in a particularly simple way. It is plain from Eq. (18.26) that when the density n_p rises to

$$n_{\text{crit}} = \frac{3}{4\pi\alpha} = \frac{0.053}{a_*^3} \Rightarrow n_{\text{crit}}^{1/3} a_* = 0.38, \quad (18.27)$$

there is a *polarization catastrophe* in which the dielectric constant diverges. Further increase of the density would seem to send the dielectric constant negative, but in fact the whole basis of the calculation breaks down beyond this point, and the

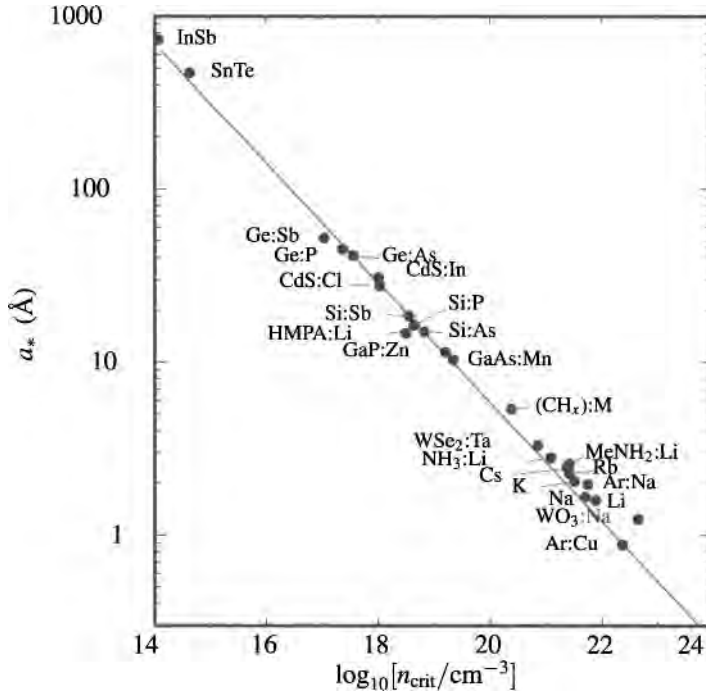


Figure 18.3. A host of different systems displays metal–insulator transitions when the condition $a_* n^{1/3} = 0.26$ obtains, as found by Edwards and Sienko (1982), p. 92. Note the large range of length scales covered by these data.

system becomes a metal rather than an insulator with local dipole moments. This *metal–insulator transition* is also known as the *Mott transition*.

Using $a_* = 48 a_0$ for silicon gives a value of $\alpha = 1.02 \cdot 10^{-19} \text{ cm}^3$; Eq. (18.27) predicts a critical density of $n_{\text{crit}} = 2.33 \cdot 10^{18} \text{ cm}^{-3}$. A measurement of this transition by Rosenbaum (1985), displayed in Figure 18.2, finds that the transition actually occurs at $3.74 \cdot 10^{18} \text{ cm}^{-3}$, rather good agreement for such a simple argument.

Edwards and Sienko (1982) find empirically that a whole host of metal–insulator transitions can be described by this simple theory, with the constant in Eq. (18.27) slightly altered. A summary of their results is presented in Figure 18.3. In none of these experiments is the impurity arrayed in a crystalline fashion, but the results seem insensitive to this detail.

18.4 Compensated Impurity Scattering and Green’s Functions

18.4.1 Tight-Binding Models of Disordered Solids

Compensated impurities can be treated as static potentials in a single-electron problem. They do not carry extra charge, and electrostatics is no longer a guide to what they do. Compensated impurities have a very large effect upon electronic motion when they are sufficiently numerous, and perturbation theory is frequently not ade-

quate to understand their effect upon electronic states. In trying to understand such processes, simple models have proved particularly useful. The most basic of these is the tight-binding model, introduced in Section 8.4.4.

Tight-Binding Hamiltonian. The tight-binding Hamiltonian may be dismissed by lovers of accuracy and realism, but it provides a simple starting point for conceptual advances. Following Eq. (8.67), it can be written

$$\hat{\mathcal{H}}_{\text{TB}} = \sum_{\vec{R}} U_{\vec{R}} |\vec{R}\rangle \langle \vec{R}| + \sum_{\langle \vec{R}\vec{R}' \rangle} t |\vec{R}\rangle \langle \vec{R}'| + t |\vec{R}'\rangle \langle \vec{R}|, \quad (18.28)$$

where the sum over $\langle \vec{R}\vec{R}' \rangle$ is over nearest-neighbor pairs only. Notice that the diagonal components $U_{\vec{R}}$ depend upon \vec{R} , allowing the possibility that different sites have different energies. By allowing $U_{\vec{R}}$ to vary randomly from site to site one models a disordered solid.

It is convenient to ask questions of the tight-binding Hamiltonian that are more difficult in a general context. For example, one can ask what happens after adding an impurity to one site in a crystal, altering the energy U_0 at the origin. This problem can be solved exactly. The impurity Hamiltonian is

$$\hat{\mathcal{H}}_1 = U_0 |0\rangle \langle 0|. \quad \text{Without loss of generality, take the disturbance to be at the origin.} \quad (18.29)$$

Taking $\hat{\mathcal{H}}_0$ to be the tight-binding Hamiltonian (18.28) with all diagonal energies $U_{\vec{R}} = 0$, the goal is to solve

$$\mathcal{E} |\psi\rangle = (\hat{\mathcal{H}}_0 + \hat{\mathcal{H}}_1) |\psi\rangle. \quad (18.30)$$

To solve this problem requires a certain amount of formal development, so it is useful to summarize the main results in advance.

One dimension. Adding an impurity to a one-dimensional chain always produces precisely one bound state, localized about the impurity.

Two dimensions. Adding an impurity to a two-dimensional net also always produces precisely one bound state. However, if the impurity potential is weak, the binding energy is exponentially small.

Three dimensions. Adding an impurity to a three-dimensional crystal produces a bound state only if the impurity is strong enough. A weak impurity warps the traveling waves in its vicinity but does not change them qualitatively.

To verify these claims, it is necessary to introduce some formalism concerning Green's functions.

18.4.2 Green's Functions

Green's functions originate in the question, "Starting with a particle at site $|0\rangle$ at time 0, what is the amplitude for finding it at site $|\vec{R}\rangle$ at time t ?" The answer to this question is that the amplitude is

$$\langle \vec{R} | \hat{G}(t) | 0 \rangle = \langle \vec{R} | e^{-i\hat{\mathcal{H}}t/\hbar} | 0 \rangle. \quad (18.31)$$

It is more convenient to work with Fourier transform of this operator, so define

$$\hat{G}(\mathcal{E}) = \frac{1}{i\hbar} \int_0^\infty dt e^{i\mathcal{E}t/\hbar} \hat{G}(t) \quad (18.32)$$

$$\Rightarrow \hat{G}(\mathcal{E}) = (\mathcal{E} - \hat{\mathcal{H}})^{-1}. \quad (18.33)$$

Equation (18.32) can only be expected to converge if \mathcal{E} has a positive imaginary part; this fact signals that \mathcal{E} must be allowed to vary in the complex plane, and warns that the physical significance of Green's functions may depend in an important way on the complex part of the energy, even when it is very small. The operator defined in Eq. (18.32) obtains its information from the future of a particle, starting at $t = 0$; if instead one had chosen to look at the past history of the particle, then one would have defined

$$\hat{G}(\mathcal{E}) = \frac{i}{\hbar} \int_{-\infty}^0 dt e^{i\mathcal{E}t/\hbar} \hat{G}(t), \quad (18.34)$$

which is in fact identical to Eq. (18.33) except that now \mathcal{E} must have a negative imaginary part in order for the integral to converge. So Green's function contains full information about the time evolution of a particle: When \mathcal{E} has a positive imaginary part, the information is about the future, and when \mathcal{E} has a negative imaginary part, the information is about the past. From Eq. (18.33), it should be clear that Green's function has a pole whenever $\hat{\mathcal{H}}$ has an eigenvalue, because if $|\mathcal{E}_n\rangle$ are the eigenstates of $\hat{\mathcal{H}}$ with energies \mathcal{E}_n , then

$$\hat{G} = (\mathcal{E} - \hat{\mathcal{H}})^{-1} = \sum_n (\mathcal{E} - \hat{\mathcal{H}})^{-1} |\mathcal{E}_n\rangle \langle \mathcal{E}_n| = \sum_n \frac{|\mathcal{E}_n\rangle \langle \mathcal{E}_n|}{\mathcal{E} - \mathcal{E}_n}. \quad (18.35)$$

The poles of \hat{G} identify all the energy eigenvalues of $\hat{\mathcal{H}}$. Letting $\mathcal{E} = \mathcal{E}_r \pm i\eta$, with \mathcal{E}_r and η real, in the neighborhood of one of the poles gives

$$\hat{G}^\pm(\mathcal{E}) \sim \frac{|\mathcal{E}_n\rangle \langle \mathcal{E}_n| (\mathcal{E}_r - \mathcal{E}_n)}{(\mathcal{E}_r - \mathcal{E}_n)^2 + \eta^2} \mp \frac{i\eta |\mathcal{E}_n\rangle \langle \mathcal{E}_n|}{(\mathcal{E}_r - \mathcal{E}_n)^2 + \eta^2} \quad \begin{array}{l} \text{In the vicinity of } \mathcal{E}_n \text{ only.} \\ \mathcal{E}_r \text{ and } \eta \text{ are real. The} \\ \text{superscript on } \hat{G} \text{ tells which} \\ \text{sign for } \eta \text{ was chosen.} \end{array} \quad (18.36)$$

$$= |\mathcal{E}_n\rangle \langle \mathcal{E}_n| \left\{ \frac{1}{\mathcal{E}_r - \mathcal{E}_n} \mp i\pi\delta(\mathcal{E}_r - \mathcal{E}_n) \right\}. \quad \begin{array}{l} \text{If } \eta \text{ is very small and} \\ \text{positive,} \\ \pi\delta(x) = \eta/(x^2 + \eta^2). \end{array} \quad (18.37)$$

The delta function resulting from the imaginary part of \hat{G} keeps track of the density of states. In particular,

$$\mp \frac{1}{\pi} \text{Im}[\langle \vec{R} | \hat{G}^{\pm}(\mathcal{E}) | \vec{R} \rangle] = \sum_n \delta(\mathcal{E}_r - \mathcal{E}_n) |\langle \vec{R} | n \rangle|^2 \quad (18.38)$$

defines the *local density of states* at position \vec{R} . This function can be employed to find the probability that an electron is localized at some point in space; Problem 7 in Chapter 26 provides an example.

Green's Function in One Dimension. Green's functions can be determined explicitly for tight-binding models when they are perfectly crystalline, and all the diagonal elements $U_{\vec{R}}$ vanish. Denoting Green's function in this case by \hat{G}_0 , return to the solution of the tight-binding Hamiltonian given in Section 8.4. Making use of the exact eigenfunctions and eigenvalues from Eq. (8.72) gives

$$\langle R | \hat{G}_0 | R' \rangle = \sum_k \frac{\langle R | k \rangle \langle k | R' \rangle}{\mathcal{E} - \mathcal{E}_0(k)} \quad \text{Assume the lattice spacing is unity.} \quad (18.39)$$

$$= \sum_l \frac{1}{N} \frac{e^{2\pi i l(R-R')/N}}{\mathcal{E} - 2t \cos(2\pi l/N)} \rightarrow \int_0^{2\pi} \frac{dk}{2\pi} \frac{e^{ik(R-R')}}{\mathcal{E} - 2t \cos(k)}. \quad (18.40)$$

Without loss of generality, let $R > R'$. Equation (18.40) can be transformed into a contour integral about the unit circle by defining

$$z = e^{ik} \Rightarrow dk = \frac{e^{-ik}}{i} dz \quad (18.41)$$

so that $\langle R | \hat{G}_0 | R' \rangle$ becomes

$$\oint \frac{dz}{2\pi i} \frac{z^{R-R'}}{z(\mathcal{E} - t(z + z^{-1}))} \quad (18.42)$$

$$= \oint \frac{dz}{2\pi i} \frac{z^{R-R'}}{\mathcal{E}z - tz^2 - t}. \quad (18.43)$$

The denominator has two roots:

$$z = \frac{\mathcal{E} \pm \sqrt{\mathcal{E}^2 - 4t^2}}{2t} \equiv z_- \text{ or } z_+, \quad (18.44)$$

where z_- is the smaller of the two in absolute value, while z_+ is the larger. Observing that the product of z_- and z_+ equals 1, one sees that z_- always lies within the unit circle, while z_+ lies out of it (unless both lie on it, a singular case). The result is that

$$\langle R | \hat{G}_0(\mathcal{E}) | R' \rangle = \frac{\mathcal{E}}{|\mathcal{E}|} \frac{1}{\sqrt{\mathcal{E}^2 - 4t^2}} \left[\frac{\mathcal{E}}{2t} - \frac{\mathcal{E}}{|\mathcal{E}|} \sqrt{\left(\frac{\mathcal{E}}{2t}\right)^2 - 1} \right]^{|R-R'|}, \quad (18.45)$$

if $|\mathcal{E}| > 2t$, and otherwise

$$\langle R | \hat{G}_0(\mathcal{E}_r \pm i\eta) | R \rangle = \frac{(-) \pm i}{\sqrt{4t^2 - \mathcal{E}_r^2}} \left[\left(\frac{\mathcal{E}_r}{2t} \right) \pm \frac{1}{i} \sqrt{1 - \left(\frac{\mathcal{E}_r}{2t} \right)^2} \right]^{|R-R'|} \quad (18.46)$$

Notice the branch cut between $-2t$ and $2t$. This branch cut represents a line of poles that have merged together (Problem 4 of Chapter 20). The diagonal element of this operator is plotted in Figure 18.4.

Two and Three Dimensions. Pictures of $\langle 0 | \hat{G}_0 | 0 \rangle$ for two- and three-dimensional square crystals appear in Figure 18.4. The computations involve elliptic integrals and are somewhat cumbersome, but the main feature that will be needed for the impurity problem is the behavior near the band edge, which is easily estimated. In a two-dimensional array with N sites, for \mathcal{E} near the band edge at $-4t$,

$$\langle 0 | \hat{G}_0(\mathcal{E}) | 0 \rangle = \frac{1}{N} \sum_{k_1 k_2} \frac{1}{\mathcal{E} - 2t [\cos 2\pi k_1 / \sqrt{N} + \cos 2\pi k_2 / \sqrt{N}]} \quad (18.47)$$

$$= \frac{1}{(2\pi)^2} \int_0^{2\pi} dk_1 \int_0^{2\pi} dk_2 \frac{1}{\mathcal{E} - 2t [\cos k_1 + \cos k_2]} \quad (18.48)$$

$$= \frac{1}{(2\pi)^2} \int dk_1 dk_2 \frac{1}{\delta\mathcal{E} - 4t - 2t [\cos k_1 + \cos k_2]} \quad (18.49)$$

$$\sim \frac{1}{(2\pi)} \int k dk \frac{1}{\delta\mathcal{E} - t k^2} \quad \begin{array}{l} \text{Defining } \delta\mathcal{E} = \mathcal{E} + 4t, \text{ moving to polar} \\ \text{coordinates, and expanding the cosines} \\ \text{around } k_1 = k_2 = \pi \text{ to obtain the} \\ \text{leading singularity.} \end{array} \quad (18.50)$$

$$\sim \frac{\ln(-\delta\mathcal{E}/t)}{4\pi t} \quad (18.51)$$

In a three-dimensional crystal, Green’s function goes to a constant near the band edge, as shown in Figure 18.4.

Perturbation Theory. One of the most important properties of Green’s functions is the way they change when a Hamiltonian is perturbed. If

$$\hat{\mathcal{H}} = \hat{\mathcal{H}}_0 + \hat{\mathcal{H}}_1, \quad (18.52)$$

then defining

$$\hat{G}_0 = (\mathcal{E} - \hat{\mathcal{H}}_0)^{-1} \quad (18.53)$$

gives

$$\hat{G} = (\mathcal{E} - \hat{\mathcal{H}})^{-1} = (\mathcal{E} - \hat{\mathcal{H}}_0 - \hat{\mathcal{H}}_1)^{-1} \quad (18.54)$$

$$= ((\mathcal{E} - \hat{\mathcal{H}}_0)(1 - (\mathcal{E} - \hat{\mathcal{H}}_0)^{-1} \hat{\mathcal{H}}_1))^{-1} = (1 - \hat{G}_0 \hat{\mathcal{H}}_1)^{-1} \hat{G}_0 \quad (18.55)$$

$$= \sum_{j=0}^{\infty} (\hat{G}_0 \hat{\mathcal{H}}_1)^j \hat{G}_0 = \hat{G}_0 + \hat{G}_0 \hat{\mathcal{H}}_1 \hat{G}_0 + \hat{G}_0 \hat{\mathcal{H}}_1 \hat{G}_0 \hat{\mathcal{H}}_1 \hat{G}_0 + \dots \quad (18.56)$$

$$= \hat{G}_0 + \hat{G}_0 \hat{\mathcal{H}}_1 \hat{G} = \hat{G}_0 + \hat{G} \hat{\mathcal{H}}_1 \hat{G}_0. \quad (18.57)$$

The \hat{T} matrix is defined to be the operator satisfying the equality

$$\hat{G} \equiv \hat{G}_0 + \hat{G}_0 \hat{T} \hat{G}_0. \quad (18.58)$$

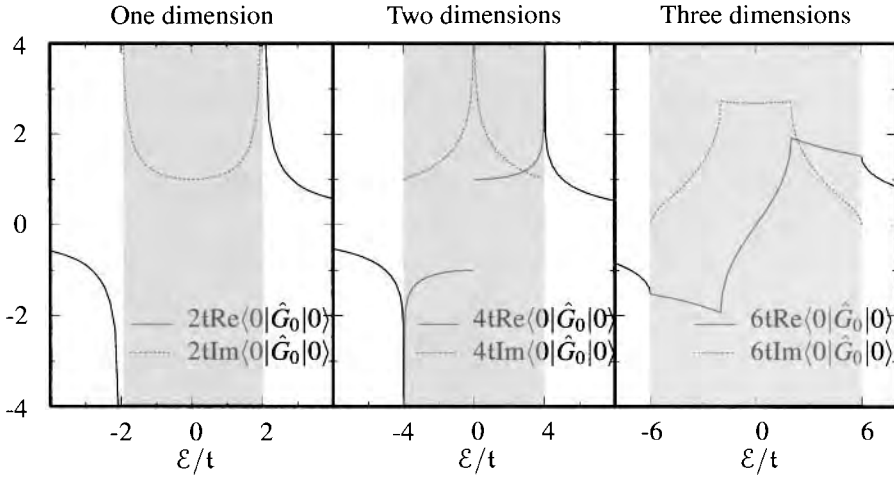


Figure 18.4. Green's functions for perfect square tight-binding lattice in one, two and three dimensions. The band of energies where propagating extended states are possible is shaded in each case. Because the imaginary part of Green's function gives the density of states, the singularities appearing in it are the van Hove singularities described in Section 7.2.5. The curves were determined from equations of Economou (1983), p. 82.

18.4.3 Single Impurity

All the formalism now is in place to find the effect of an impurity placed at site 0. Equation (18.29) states that $\hat{\mathcal{H}}_1 = U_0|0\rangle\langle 0|$, so Green's function corresponding to the Hamiltonian of Eq. (18.30) is

$$\hat{G} = \hat{G}_0 + \hat{G}_0|0\rangle U_0\langle 0|\hat{G}_0 + \hat{G}_0|0\rangle U_0\langle 0|\hat{G}_0|0\rangle U_0\langle 0|\hat{G}_0 + \dots \quad \text{See Eq. (18.56).} \quad (18.59)$$

$$= \hat{G}_0 + \hat{G}_0|0\rangle U_0\langle 0|\hat{G}_0 \sum_{p=0}^{\infty} \left(U_0\langle 0|\hat{G}_0|0\rangle \right)^p \quad \begin{array}{l} \text{Only one matrix element ever} \\ \text{appears in the sum.} \end{array} \quad (18.60)$$

$$= \hat{G}_0 + \frac{\hat{G}_0|0\rangle U_0\langle 0|\hat{G}_0}{1 - U_0\langle 0|\hat{G}_0|0\rangle}. \quad \begin{array}{l} \text{Recognizing the infinite sum to} \\ \text{be a Taylor expansion.} \end{array} \quad (18.61)$$

The simplicity of Eq. (18.61) illustrates the usefulness of Green's functions. By carrying out perturbation theory infinitely far, the effect of a single impurity is determined exactly.

Recall that the poles of (18.61) give the energy eigenvalues of $\hat{\mathcal{H}}$. Do any of the original poles of \hat{G}_0 remain poles of \hat{G} once the perturbation is applied? No: Consider what happens when \mathcal{E} approaches \mathcal{E}_{n0} , some pole of \hat{G}_0 . Then \hat{G}_0 begins to diverge, and

$$\hat{G}_0 \sim \frac{|\mathcal{E}_{n0}\rangle\langle \mathcal{E}_{n0}|}{\mathcal{E} - \mathcal{E}_{n0}} \quad (18.62)$$

$$\Rightarrow \hat{G} \sim \frac{|\mathcal{E}_{n0}\rangle\langle \mathcal{E}_{n0}|}{\mathcal{E} - \mathcal{E}_{n0}} - \frac{|\mathcal{E}_{n0}\rangle\langle \mathcal{E}_{n0}|0\rangle\langle 0|\mathcal{E}_{n0}\rangle\langle \mathcal{E}_{n0}|}{(\mathcal{E} - \mathcal{E}_{n0})\langle 0|\mathcal{E}_{n0}\rangle\langle \mathcal{E}_{n0}|0\rangle}, \quad \begin{array}{l} \text{Put Eq. (18.62) into} \\ \text{Eq. (18.61).} \end{array} \quad (18.63)$$

so that the pole cancels. The only poles of (18.61) remaining are those due to the vanishing of

$$1 - U_0 \langle 0 | \hat{G}_0(\mathcal{E}) | 0 \rangle = 0. \quad (18.64)$$

Equation (18.64) determines the energy eigenvalues of the impurity Hamiltonian. With the energy eigenvalues \mathcal{E}_n in hand, the eigenfunctions can be extracted from (18.35) by choosing \mathcal{E} to be near to some energy eigenvalue \mathcal{E}_n satisfying (18.64). Return to Eq. (18.61) and write

$$1 - U_0 \langle 0 | \hat{G}_0(\mathcal{E}) | 0 \rangle \approx -U_0 \langle 0 | \hat{G}'_0(\mathcal{E}_n) | 0 \rangle (\mathcal{E} - \mathcal{E}_n) \quad (18.65)$$

with

$$\hat{G}'_0 = \frac{\partial \hat{G}_0}{\partial \mathcal{E}}, \quad (18.66)$$

$$\Rightarrow \frac{|\mathcal{E}_n\rangle \langle \mathcal{E}_n|}{\mathcal{E} - \mathcal{E}_n} \sim \frac{\hat{G}_0(\mathcal{E}_n) | 0 \rangle \langle 0 | \hat{G}_0(\mathcal{E}_n)}{-\langle 0 | \hat{G}'_0(\mathcal{E}_n) | 0 \rangle} \frac{1}{\mathcal{E} - \mathcal{E}_n} \quad (18.67)$$

$$\Rightarrow |\mathcal{E}_n\rangle = \frac{\hat{G}_0(\mathcal{E}_n) | 0 \rangle}{\sqrt{-\langle 0 | \hat{G}'_0(\mathcal{E}_n) | 0 \rangle}}. \quad \text{This is an explicit expression for the eigenfunction.} \quad (18.68)$$

The term inside the square root is positive for bound states.

Impurities in One Dimension. The effects of impurities depend upon whether they are added to one-, two-, or three-dimensional systems. Begin with one dimension. In one dimension the unperturbed Hamiltonian has a continuous band of states stretching in energy from $-2t$ to $2t$. Green's function \hat{G}_0 in Eq. (18.40) can be viewed as a tightly grouped collection of N poles (see Problem 4 in Chapter 20), spaced at distance on the order of $1/N$. Around each of these N poles the Green function varies from $-\infty$ to ∞ , and somewhere in this range, for each pole, Eq. (18.64) must be satisfied. Therefore, after the impurity is added there is still a continuous band of states stretching in energy from $-2t$ to $2t$. Although somewhat distorted near the impurity, these states look like plane waves far from it. They are *extended* and can carry electrical current from one end of the system to the other.

However, a qualitatively different type of state exists as well. From Eq. (18.45), outside the band $\langle 0 | \hat{G}_0 | 0 \rangle = 1/\sqrt{\mathcal{E}^2 - 4t^2}$, and (18.64) can be satisfied when

$$\mathcal{E} = \pm \sqrt{4t^2 + U_0^2}. \quad \text{The + sign applies for } U_0 > 0 \text{ and the - sign applies for } U_0 < 0; \text{ see Figure 18.4.} \quad (18.69)$$

So, in one dimension, adding an impurity to a crystal always produces an energy eigenstate outside the band. If the impurity potential is attractive, there is a bound state below the band; even if it is repulsive, there is still a bound state, but now above the band. Because the energy of the bound state lies outside the conduction band, one finds by combining Eqs. (18.68) and (18.45) that the bound state is *localized*. It falls off in amplitude exponentially away from the location of the impurity at $|0\rangle$, because the matrix elements of G_0 fall off in this way. Localized electrons cannot easily contribute to electrical conduction because they do not extend across the sample.

Single Impurity in Two Dimensions. The addition of a single impurity does not remove the band of extended states stretching from $-4t$ to $4t$. As in one dimension the addition of an impurity always leads to the creation of a localized state. However, the binding is extraordinarily weak, because Green's function goes as a logarithm near the band edge. For $\delta\mathcal{E} < 0$, (18.50) is real and diverges logarithmically. Using Eq. (18.51) to solve (18.64) with $U_0 < 0$ gives

$$\mathcal{E} = -4t - te^{-4\pi t/|U_0|}. \quad (18.70)$$

The exponentially small binding energy appearing in Eq. (18.70) ends up appearing in unexpected places, such as the binding energy of Cooper pairs in superconductivity or the binding energies of magnetic impurities in the Kondo problem. These problems become effectively two-dimensional because they concern the interactions of a collection of interactions restricted to the Fermi surface, a nearly two-dimensional subset of the original collection of electrons.

Three Dimensions. In three dimensions, the unperturbed Green function is finite at the band edge, as shown in Figure 18.4. A sufficiently small impurity does not lead to the creation of a bound state because $1 - U_0\langle 0|\hat{G}_0(\mathcal{E})|0\rangle$ does not have any zeros. For a simple cubic lattice, the smallest value of U_0 leading to a bound state is approximately $U_0 = 1.5 \times 6t$. If a weaker impurity is added, all the extended plane-wave eigenstates deform slightly, but they are not affected qualitatively. This special feature of three-dimensional space is one of the reasons that it is so often legitimate to treat scattering potentials as weak.

Why then does a noncompensated impurity always create a bound state in three dimensions, no matter how weak it may be? To model a single noncompensated potential in the context of the tight-binding model, one would need to set an infinite number of energies $U_{\vec{R}}$ nonzero and to have them fall off in amplitude as $1/R$ moving away from the origin. The long range of this potential always produces a bound state.

18.4.4 Coherent Potential Approximation

The *coherent potential approximation* is an elaborate approximation scheme that describes disordered systems in which the impurities are too numerous or too strong for weak scattering theory to be satisfactory, but not strong enough, in three dimensions, to produce large numbers of localized states. The starting point is the idea of an effective medium surrounding each site that is spatially uniform but represents the average effect of disorder. To model this situation, write

$$\hat{\mathcal{H}} = \mathcal{H}_0 + \sum_m (U_m - \Sigma)|m\rangle\langle m| + \Sigma, \quad (18.71)$$

which for the moment is just an identity, but will be chosen later to make approximations as good as possible. The energies U_m will be viewed as random variables, characterized by a probability distribution $\mathcal{P}(U_m)$. Define

$$\hat{\mathcal{H}}_0^\Sigma = \mathcal{H}_0 + \Sigma, \quad \hat{\mathcal{H}}_1^\Sigma = \sum_m (U_m - \Sigma)|m\rangle\langle m| \quad (18.72)$$

so that

$$\hat{G}_0^\Sigma(\mathcal{E}) = \hat{G}_0(\mathcal{E} - \Sigma). \quad (18.73)$$

In general, Σ will turn out to be a function of the energy \mathcal{E} and will also be complex. An equation for the full Green function is now

$$\hat{G} = \hat{G}_0^\Sigma + \hat{G}_0^\Sigma \hat{T}^\Sigma \hat{G}_0^\Sigma, \quad (18.74)$$

where \hat{T}^Σ is the T -matrix appropriate to the perturbation \mathcal{H}_1^Σ , as defined in Eq. (18.58).

So far everything is exact. The only approximation is to put

$$\hat{T}^\Sigma \approx \sum_m \hat{T}_m^\Sigma, \quad (18.75)$$

where \hat{T}_m^Σ is the T matrix that would result if the only nonzero part of \hat{H}_1^Σ were at m . The problem of a single impurity has already been solved, and from Eq. (18.61) one sees immediately that the T matrix in this case is given by

$$\hat{T}_m^\Sigma = \frac{|m\rangle\langle U_m - \Sigma| \langle m|}{1 - (U_m - \Sigma)\langle m|\hat{G}_0^\Sigma|m\rangle} \quad (18.76)$$

There is still the task of choosing Σ . In order to do it effectively, write

$$\hat{G} = \hat{G}_0^\Sigma + \hat{G}_0^\Sigma \hat{T}^\Sigma \hat{G}_0^\Sigma. \quad (18.77)$$

and average both sides over disorder potentials U_m . Choose Σ by requiring that the difference between \hat{G}_0^Σ and \hat{G} vanish on average:

$$\overline{\hat{G}} = \hat{G}_0^\Sigma(\mathcal{E}) = \hat{G}_0(\mathcal{E} - \Sigma), \quad \text{The bar means to average all the potentials } U_m \text{ with probability distribution } \mathcal{P}(U_m). \quad (18.78)$$

with the consequence from Eq. (18.77) that

$$\overline{\hat{T}_m^\Sigma} = 0 \quad (18.79)$$

$$\Rightarrow \int dU \mathcal{P}(U) \frac{(U - \Sigma)}{1 - (U - \Sigma)\langle 0|\hat{G}_0^\Sigma|0\rangle} = 0. \quad (18.80)$$

Equation (18.80) is the basic equation of the coherent potential approximation. From it one calculates $\Sigma(\mathcal{E})$, and then the average of \hat{G} from Eq. (18.78). This formalism replaces Eq. (18.16) when scattering is not weak; Ziman (1979) discusses results obtained from this approximation.

18.5 Localization

The study of electronic states in random lattices was initiated by Anderson (1958). Adding a single impurity at a single site can lead to the creation of a single localized state. Life would be simple, and the ultimate conclusions correct, if one could

only argue that adding two impurities creates two bound states, three impurities three, and so on. One would conclude in this way that when an impurity is added to every site in one dimension, all states are localized. In two dimensions, they should also be localized, although the binding energies and decay lengths might be exponentially small. In three dimensions, only if the disordering wells had a height on the order of $9t$ might one expect all states to be localized, and one would have to consider the possibility that some states might be localized, and others not.

All these conclusions are correct, although the arguments are very imprecise. In fact, the conclusions can break down when one has added as few as two impurities to a system. Two impurities in a one-dimensional system do not necessarily create two bound states. If they are close together, they may merge into a single well, leaving still a single bound state. Nevertheless, for typical samples, the consensus has it that the situation in one, two, and three dimensions stands as just mentioned. In three dimensions, the dividing line between localized and extended states is called the *mobility edge*, and as a function of energy \mathcal{E} and disorder strength W it looks as in Figure 18.5.

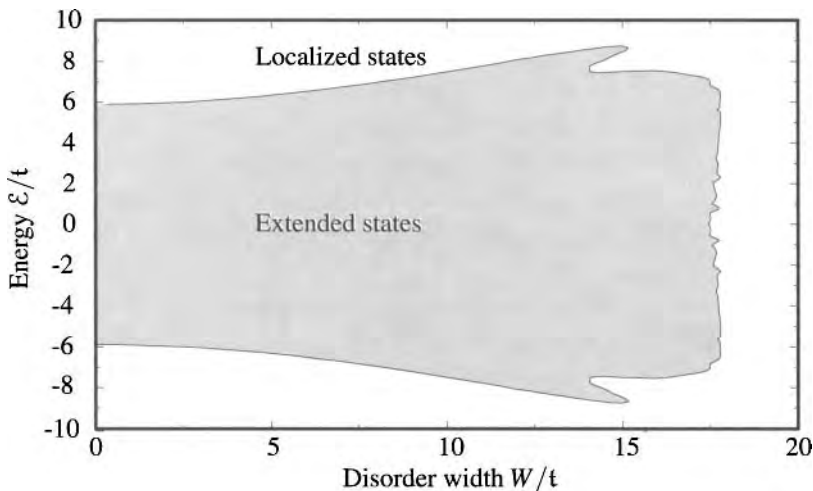


Figure 18.5. Calculation of the mobility edge, the dividing line between extended and localized states for a tight-binding model on a square lattice in three dimensions, where the energy U varies randomly between $-W/2$ and $W/2$ as in Eq. (18.81). The calculation was carried out using the method of Section 18.5.2, comparing the resistance of $3 \times 3 \times 3$ with $4 \times 4 \times 4$ sized systems.

It may seem that the results on localization are rather obvious. If so, reflect that if an impurity of identical energy is placed at each and every site, the problem remains completely periodic, and there is no localization, just a shift of all the energy levels. If there is any periodic pattern involved in the placing of impurities, states will always be extended, no matter what the dimension.

18.5.1 Exact Results in One Dimension

In the simplified setting of one spatial dimension, one can actually prove that all states are localized and can find explicit expressions for the *localization length*, which is the characteristic distance over which wave functions decay.

Consider the Hamiltonian Eq. (18.28) again. Now, however, take all the energies U_m to be random variables, distributed with some probability $\mathcal{P}(U)$. When a specific form of \mathcal{P} is needed, take

$$\mathcal{P}(U) = \frac{1}{W} \theta\left(\frac{W}{2} - U\right) \theta\left(\frac{W}{2} + U\right). \quad \text{So the onsite potential adopts with equal probability all values between } -W/2 \text{ and } W/2. \quad (18.81)$$

Instead of treating the impurity potentials U_m as small, treat the hopping matrix element t as small instead. Then the unperturbed Green function is

$$\langle l | \hat{G}_0 | m \rangle = \frac{\delta_{lm}}{\mathcal{E} - U_l}; \quad (18.82)$$

the overlap between adjacent sites induced by t will be the perturbation.

Definition of Localization Length. The localization length is defined to be

$$\lambda^{-1} \equiv \lim_{m \rightarrow \infty} -\frac{1}{2m} \overline{\ln |\langle 0 | \hat{G} | m \rangle|^2}, \quad (18.83)$$

where the bar means that one must average over the random potentials U_m on each site, using the probability distribution function \mathcal{P} .

In order to explain why the localization length has been defined in this manner, it is necessary to explain the physical significance of $\langle 0 | \hat{G} | m \rangle$ and to explain why quantities that are easier to calculate from a formal point of view yield no physical information.

Suppose that the eigenfunctions in the vicinity of some energy \mathcal{E} are localized. This statement means that each eigenfunction is peaked somewhere in the lattice, while away from the peak it falls off exponentially as $\exp[-m/\lambda]$, where m is the distance from the peak. Green's function is given by Eq. (18.35), so

$$\langle m | \hat{G}(\mathcal{E} - i\eta) | 0 \rangle = \sum_n \frac{\langle m | \mathcal{E}_n \rangle \langle \mathcal{E}_n | 0 \rangle}{\mathcal{E} - \mathcal{E}_n - i\eta}. \quad (18.84)$$

Because the peaks of the wave function move about randomly, only a small fraction of the wave functions, order $1/N$ where N is the number of sites in the lattice, will be peaked at 0; the rest will be negligible because their overlap with site 0 is so small. So

$$\langle m | \hat{G}(\mathcal{E} - i\eta) | 0 \rangle = \mathcal{V} \int d\mathcal{E}' D(\mathcal{E}') \frac{\langle m | \mathcal{E}' \rangle \langle \mathcal{E}' | 0 \rangle}{\mathcal{E} - \mathcal{E}' - i\eta} \quad (18.85)$$

$$\approx \frac{\mathcal{V}\lambda}{N} D(\mathcal{E}) i\pi \langle m | \mathcal{E} \rangle \quad \text{If the wave functions have width } \lambda, \text{ then a fraction } \lambda/N \text{ have overlap of order unity with site 0, and all the rest can be neglected.} \quad (18.86)$$

$$\approx \frac{\mathcal{V}\lambda}{N} D(\mathcal{E}) i\pi e^{i\phi} e^{-m/\lambda}, \quad \text{Because the wave functions fall off over distance } \lambda. \quad (18.87)$$

where ϕ describes the phase of the matrix element.

The presence of the phase in Eq. (18.87) causes difficulties. When one sets out to calculate some quantity such as electrical resistance in a disordered solid, it is not possible analytically to carry out the calculation for any particular set of randomly chosen energies U_m . The only practical calculation averages over them. The problem is that $\langle m|\hat{G}|0\rangle$ is guaranteed to be zero. The phase ϕ is a random function of the potentials U , and it will send $\langle m|\hat{G}|0\rangle$ to zero on average, even though all quantities being averaged over have the same order of magnitude. To eliminate the problem, the localization length is defined by Eq. (18.83); squaring the matrix element eliminates the phase problem, and taking the logarithm pulls out $1/\lambda$.

Perturbation Theory in Terms of Paths. The perturbation series Eq. (18.56) has a geometrical interpretation, in which electrons hop between sites of the lattice. In this case, the perturbation $\hat{\mathcal{H}}_1$ equals

$$t \sum_{\langle l'm'\rangle} |l'\rangle\langle m'|, \tag{18.88}$$

where l' and m' are nearest neighbors so Eq. (18.56) directs one to compute $\langle l|\hat{G}|m\rangle$ by summing over all paths that connect sites, n and m . The expansion is

$$\langle l|\hat{G}|m\rangle = \langle l|\hat{G}_0|m\rangle + \langle l|\hat{G}_0 \sum_{\langle l_1 m_1\rangle} |l_1\rangle t \langle m_1|\hat{G}_0|m\rangle + \dots \tag{18.89}$$

Because \hat{G}_0 is diagonal, a term in this expansion is only nonzero if

$$l = l_1 \rightarrow m_1 = l_2 \rightarrow m_2 \dots \rightarrow m \tag{18.90}$$

is a path which reaches from l to m . Each such path appears in the perturbation expansion exactly once. For each link between two neighboring sites one puts down a factor of t , and each time one reaches a site l' during the walk, one puts down a factor of $\langle l'|\hat{G}_0|l'\rangle$.

In one dimension, these formulas are particularly useful, because the number of possible paths is so limited. For example, for $l < m$, the first nonzero contribution to $\langle l|\hat{G}|m\rangle$, describing the amplitude for traveling from site l to site m , is the straight-line path

$$\langle l|\hat{G}_0|l\rangle t \langle l+1|\hat{G}_0|l+1\rangle t \dots t \langle m|\hat{G}_0|m\rangle. \tag{18.91}$$

The complete expression for $\langle l|\hat{G}|m\rangle$ must supplement (18.91) with higher-order terms that involve some wiggling forward and backward before ending up at m .

Renormalized Perturbation Expansion. One can write the perturbation expansion in a more compact way. The sum of all paths that begin at l and ends at m can be constructed as the product of *all paths that begin at l and end at l* with *all paths that begin at $l+1$ and end at m , but without ever coming back to l again*. The restriction is necessary, or else the path would already have been included in the first

set of paths. Denote by \hat{G}^l a Green function in which electrons are forbidden to visit site l . \hat{G}^l is the Green function resulting from the Hamiltonian $\hat{\mathcal{H}} + U^+ |m\rangle\langle m|$, with U^+ such a large energy that electrons are guaranteed to keep away from m . Then

$$\langle l | \hat{G} | m \rangle = \langle l | \hat{G} | l \rangle t \langle l + 1 | \hat{G}^l | m \rangle. \tag{18.92}$$

However, the set of paths traveling from $l + 1$ to m never visiting l again is the same as the set that travels from $l + 1$ to $l + 1$, never visiting l , and then hops from $l + 1$ to $l + 2$ to m , never visiting $l + 1$ again (a requirement that also rules out visiting l again.) Proceeding recursively in this way, one has

$$\langle l | \hat{G} | m \rangle = \langle l | \hat{G} | l \rangle t \langle l + 1 | \hat{G}^l | l + 1 \rangle t \langle l + 2 | \hat{G}^{l+1} | l + 2 \rangle \dots t \langle m | \hat{G}^{m-1} | m \rangle. \tag{18.93}$$

Equation (18.93) is depicted schematically in Figure 18.6.



Inserting Eq. (18.93) into Eq. (18.83), one finds immediately that to leading order in $1/m$,

$$\lambda^{-1} = -\ln[\langle l + 1 | t \hat{G}^l | l + 1 \rangle]; \tag{18.94}$$

The product of m terms cancels the factor of m out front. The first matrix element is different from all the rest, but its contribution becomes negligible as $m \rightarrow \infty$.

any value of l will do, because once the average is applied, all sites are equivalent.

Thus finding the localization length reduces to finding the probability of remaining at some site, assuming one never visits the site to the left. To evaluate this quantity, note that the set of paths starting at $l + 1$ and ending at $l + 1$ without ever visiting l consists of the following:

1. The path that just stays at $l + 1$ the whole time, plus
2. Paths obtained by hopping to $l + 2$, times all paths that end back at $l + 2$ without touching $l + 1$, and finally times all paths that go from $l + 1$ to $l + 1$ without visiting l .

In equation form,

$$\langle l + 1 | \hat{G}^l | l + 1 \rangle = \langle l + 1 | \hat{G}_0 | l + 1 \rangle + \left[\begin{array}{l} \langle l + 1 | \hat{G}_0 | l + 1 \rangle \\ \times t \langle l + 2 | \hat{G}^{l+1} | l + 2 \rangle \\ \times t \langle l + 1 | \hat{G}^l | l + 1 \rangle \end{array} \right] \tag{18.95}$$

$$\Rightarrow \langle l + 1 | \hat{G}^l | l + 1 \rangle = \frac{1}{\mathcal{E} - U_{l+1} - t^2 \langle l + 2 | \hat{G}^{l+1} | l + 2 \rangle}. \tag{18.96}$$

Using Eq. (18.82); see Figure 18.7.

Because all sites are equivalent, take $l = 0$. The probability distribution of $\langle 1 | t \hat{G}^0 | 1 \rangle$ can now be obtained from the probability distribution \mathcal{P} for U_l . All one

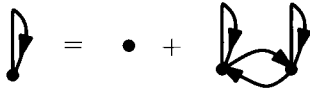


Figure 18.7. Diagram corresponding to Eq. (18.96).

needs is Eq. (18.96). The probability \mathcal{F} that $t\hat{G}^0$ will adopt some value g is

$$\mathcal{F}(g, \mathcal{E}) = \int \prod_m [dU_m \mathcal{P}(U_m)] \delta(g - \langle 1 | t\hat{G}^0(\mathcal{E}) | 1 \rangle) \tag{18.97}$$

$$= \int \prod_m [dU_m \mathcal{P}(U_m)] \delta\left(g - \frac{t}{\mathcal{E} - U_1 - t^2 \langle 2 | \hat{G}^1 | 2 \rangle}\right) \text{ Use Eq. (18.96).} \tag{18.98}$$

$$= \int \frac{t}{g^2} \prod_{m \neq 1} [dU_m \mathcal{P}(U_m)] \mathcal{P}\left(\mathcal{E} - \frac{t}{g} - t^2 \langle 2 | \hat{G}^1 | 2 \rangle\right) \tag{18.99}$$

The only appearance of U_1 is now made explicit, so one can integrate over it. Next, reintroduce the integral over U_1 to find....

$$= \frac{t}{g^2} \int \prod_m [dU_m \mathcal{P}(U_m)] \int dg' \mathcal{P}\left(\mathcal{E} - \frac{t}{g} - tg'\right) \delta(g' - t \langle 2 | \hat{G}^1 | 2 \rangle) \tag{18.100}$$

$$= \frac{t}{g^2} \int dg' \mathcal{P}\left(\mathcal{E} - \frac{t}{g} - tg'\right) \mathcal{F}(g', \mathcal{E}). \text{ The last term in Eq. (18.100) just gives the definition of } \mathcal{F}. \tag{18.101}$$

In general, the integral equation (18.101) must be solved numerically, but in the limit of weak disorder, where the standard deviation of the distribution \mathcal{P} is much smaller than t , one can obtain definite results. The details are assigned to problem 8, and the result is that for $\mathcal{E} = 0$

$$\lambda^{-1} = 0.1142 \frac{\overline{U^2}}{t^2}. \tag{18.102}$$

When the probability distribution takes the form of Eq. (18.81),

$$\lambda = \frac{105.045t^2}{W^2}. \text{ } W \text{ is the width of the disorder.} \tag{18.103}$$

18.5.2 Scaling Theory of Localization

The most powerful theory of localization is a scaling theory of Abrahams et al. (1979). It bypasses the obvious sort of calculation, such as extracting conductivities from some microscopic model, and instead derives advantage from a deceptively simple physical postulate. The resulting theory provides a framework in which to organize theoretical, numerical, and experimental data.

The physical idea behind the scaling theory is very simple. Suppose one has a bag filled with resistors. Assume that no matter how one hooks the resistors together, any two with the same resistance are indistinguishable. One resistor might obtain its large resistance from a small density of states, another by having the Fermi energy sit near the band edge, another by being very highly disordered,

another by being very long, but no matter. The resistance is all that counts for any circuit of which they are a part.

Consequences flow from this assumption as soon as one begins hooking resistors together to form other resistors on larger scales. First imagine hooking l identical resistors of resistance r in series. The resistance of the assembly can depend upon the number of resistors l and the resistance of the individual units r , but nothing else, so the total resistance is a function of the form $f(l, r)$. To simplify matters further, take whatever resistive material is at hand and shave it down or build it up until its resistance equals the basic quantum of resistance

$$R_H \equiv h/e^2 = 25\,813\ \Omega. \quad (18.104)$$

Let the length of material needed to have this resistance be L_0 . Then the resistance of any other length L of the same material is

$$R_1(l) = R_1(L/L_0). \quad (18.105)$$

The hypothesis of the scaling theory is that there is only one function $R_1(l)$, and the resistance of every quantum resistor changes with length according to Eq. (18.105). To appreciate the power of this statement, suppose one knows the function $R_1(l)$. Then whatever material one takes, it is enough to measure the resistance of one sample, and then the resistance of a sample of any other length is known.

The same hypothesis extends to two and three dimensions. In two dimensions, one hooks resistors together to form a square grid. This geometry is quite different from hooking them together in series, but one still guesses that the resistance of a square size L on the side is

$$R_2(l) = R_2(L/L_0), \quad (18.106)$$

where R_2 is a universal function appropriate to two-dimensional assemblies, but bears no relation to R_1 . Similarly, for three-dimensional cubes of material, one supposed the existence of a third universal function R_3 .

The most intuitive way to form a guess about the shapes of these scaling functions is to ask how resistance ought to scale for weak and strong resistors, where weak resistors have resistance much less than (18.104) and strong resistors have much greater. Very weak resistors have only occasional scattering sites and should obey the familiar macroscopic theory of resistivity. In the macroscopic theory, materials have a resistivity ρ , and the resistance is proportional to their length along the direction of current and is inversely proportional to their area perpendicular to it. Thus, the resistance of a bar of cross-sectional area A and length L is $\rho L/A$, the resistance of a rectangle of thickness t , length L , and height L is $\rho L/(tL)$, and the resistance of a cube of side length L is $\rho L/L^2$. In dimension d ,

$$R_d \sim L^{2-d} \quad \text{Ordinary macroscopic scaling of resistance,} \quad (18.107)$$

which applies when R is near zero.

must give the behavior of R_d when R is close to zero. Conversely, when R is very large, one should expect all states to be localized and should also expect R to rise exponentially with sample length as

$$R \sim e^{A_d L/L_0}. \quad A_d \text{ is some dimensionless constant depending upon dimensionality.} \quad (18.108)$$

In $d = 1$ and $d = 2$, there is no problem supposing that R rises monotonically with L . However, in $d = 3$, R shrinks as a function of L when it is small, and it grows when it is large. Rather than making guesses about the shapes of R_d , Abrahams et al. (1979) proposed that one focus on the functions

$$\beta_d(R) = \frac{L}{R} \frac{\partial R}{\partial L} = \frac{\partial \ln R}{\partial \ln L} = L \frac{\partial \ln R_d(L/L_0)}{\partial L} \quad (18.109)$$

and guessed that $\beta_d(R)$ is a smooth, monotonically increasing function. That is, the change of resistors with scale increases continuously as their resistance increases. This guess is not obvious, and it emerged in part as a compact way to sum up a variety of seemingly disconnected theoretical results. It is at least consistent with their asymptotic behavior. For resistors R near zero,

$$\beta_d(R) \sim 2 - d, \quad \text{From Eq. (18.107).} \quad (18.110)$$

while for large R

$$\beta_d(R) \sim \frac{A_d L}{L_0} \sim \ln R. \quad (18.111)$$

A schematic view of $\beta_d(R)$ appears in Figure 18.8.

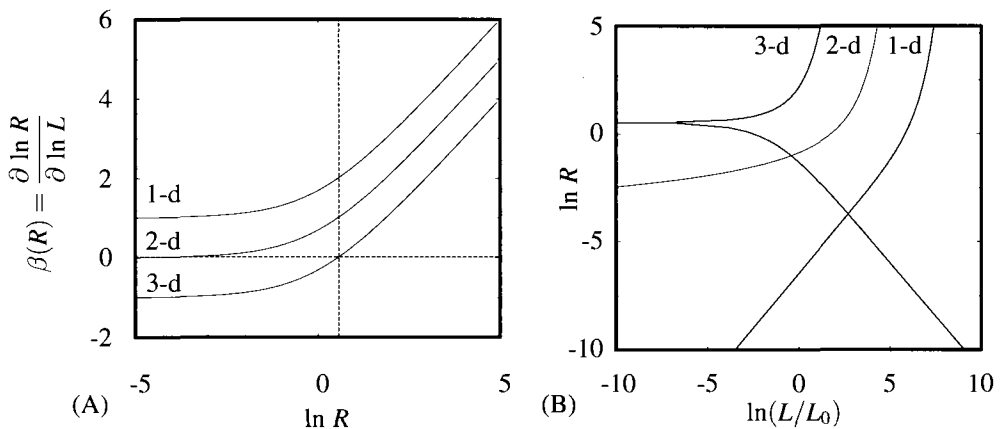


Figure 18.8. (A) Sketch of qualitative behavior of the three functions $\beta_d(R)$, given the asymptotic behavior in Eqs. (18.110) and (18.111) and assuming smooth interpolation between these two limits. (B) Three scaling functions $\ln R$ versus $\ln L/L_0$ resulting from the three functions β . At the point where the three-dimensional β function crosses 0, the resistance has a logarithmic singularity.

In one dimension, β is a smooth positive function. In two dimensions, it is always positive, but approaches zero along the negative $\ln R$ axis. In three dimensions, β must cross through zero. As a result, the scaling functions

$$\ln(L/L_0) = \int \frac{d \ln R}{\beta_d(\ln R)} \quad (18.112)$$

The point of this expression is to view $\ln L/L_0$ as a function of $\ln R$, and guess the shape of this function by guessing that $\beta_d(\ln R)$ has the form shown in Figure 18.8.

have singularities in two and three dimensions. In two dimensions the singularity occurs for $R \rightarrow 0$, while in three dimensions it occurs at a finite value of R . In two dimensions, the prediction of Figure 18.8 is that the larger a system gets, the larger its resistance gets. In other words, in the macroscopic limit, all states in two dimensions should be localized. In three dimensions the prediction is that for resistance below a universal critical value, making a system larger continually reduces its resistance, while for any system with resistance above this critical value, making it larger makes the resistance grow. The scaling theory recovers in this way the prediction of the mobility edge, and furthermore it states that to know whether a system lies on the localized or extended side of the edge, it is sufficient to measure its resistance at any scale.

These scaling ideas are particularly well suited to guide interpretation of numerical work. It would seem easy to investigate localization numerically. All one has to do is to write down a Hamiltonian with randomly chosen diagonal matrix elements, calculate the eigenfunctions, and classify them according to whether they are localized or extended. There is in fact no difficulty in carrying out such a calculation for lattices on the order of $13 \times 13 \times 13$. However, the results are extremely difficult to interpret. As the degree of randomness increases, the eigenfunctions all become bumpier and bumpier in a continuous way. There is no sign of a transition at some value of randomness, and there is no simple function that can be applied to the randomly oscillating wave functions to indicate whether they can carry current or not. In an infinite system, localized wave functions rise above zero only in the neighborhood of a limited number of lattice sites, but for the relatively small systems that can be solved numerically, localization is not visible.

Using the ideas of the scaling theory produces a completely unambiguous determination of localization. Rather than examining the properties of any single wave function or any single Hamiltonian, attention shifts to how the solutions alter with change of scale.

Figure 18.9 illustrates the process for a cubic lattice in three dimensions, described by Eq. (18.28) and with the probability distribution of impurity potentials described by Eq. (18.81). Problems 5 through 7 describe how to compute its resistance. Fluctuations of resistance are extremely large from one sample to another. Indeed, they are so large that \bar{R} , the average of resistance over many realizations of the disorder, cannot be computed. A criterion for determining when such an average has converged is that $\overline{\delta R^2} \equiv \overline{R^2} - \bar{R}^2$ should fall below some specified tolerance. When monitoring $\overline{\delta R^2}$, one will find that it never converges to zero. However, $\overline{\ln R}$ does converge; $\overline{[\ln R]^2} - [\overline{\ln R}]^2$ can be made as small as desired by

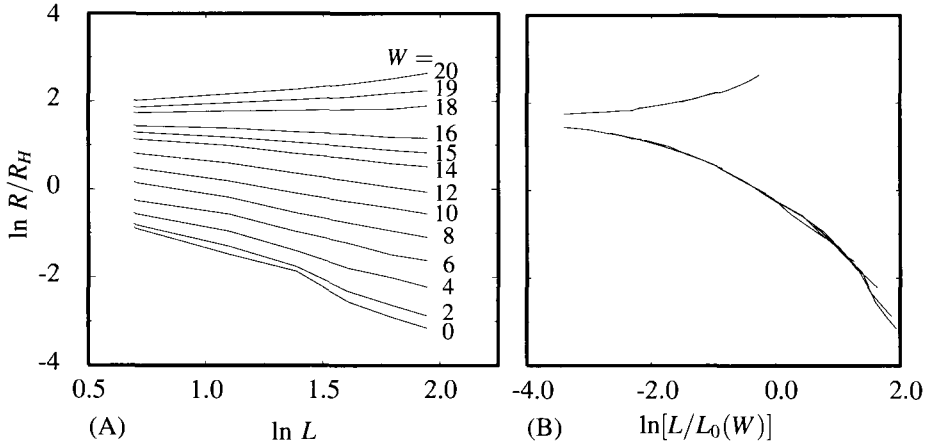


Figure 18.9. Three-dimensional scaling function for square lattice with diagonal disorder. (A) $\ln R/R_H$ ($R_H = h/e^2$) is plotted versus $\ln L$ for systems ranging from 2^3 to 7^3 in size, and disorder W ranging from 0 to 20. The transition from localized to extended states occurs around $W = 17$. (B) Each curve is displaced horizontally so as to overlap with the other curves, forming the scaling function $R_3(L/L_0)$.

sampling enough systems. An additional reason to define the localization length as in Eq. (18.83) is that Green’s functions fluctuate too much for their averages to be well-defined, but averages of logarithms converge.

Figure 18.9(A) shows plots of $\ln R$ as a function of $\ln L$. Averages over around 10^5 systems are required to obtain 1% accuracy. According to the basic scaling hypothesis, for any given level of disorder W , $\overline{\ln R}$ versus $\ln L$ should lie on a universal curve once L is appropriately scaled, meaning that each curve in Figure 18.9(A) must be shifted horizontally until it touches the curve below. The result is displayed in Figure 18.9(B), which shows the universal function $R_3(l)$. There is a transition between metals and insulators at a disorder W of around 17. If the disorder is larger than this critical value, resistance increases continually with L , and macroscopic samples of the material must be insulating. If the disorder is less, resistance decreases with sample size, and the material is a metal. The distinction between metals and insulators is apparent in very small systems; one can distinguish between them by monitoring the change in $\overline{\ln R}$ when passing from $2 \times 2 \times 2$ systems to $3 \times 3 \times 3$ systems. Figure 18.5 shows the result of comparing $\overline{\ln R}$ for 800 values of W and \mathcal{E} , for systems of size $3 \times 3 \times 3$ and $4 \times 4 \times 4$, identifying localized states as those where the resistance increases for the larger system, and identifying extended states as those where it decreases.

18.5.3 Comparison with Experiment

According to Figure 18.9, the resistance of an insulating solid grows exponentially as its size increases. Two 30 000 Ω resistors hooked in series should give much more than 60 000 Ω . These predictions are of course false. Macroscopic resistors

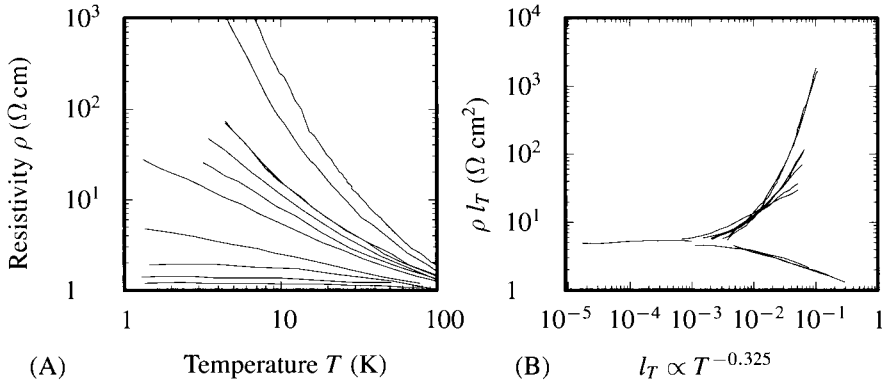


Figure 18.10. (A) Measurement of resistivity versus temperature for 10 samples of the conducting polymer PPV, disordered in varying degrees so as to transform from insulator to metal. [Source: Ahlskog et al. (1997), p. 6779.] (B) Data transformed using Eq. (18.114), assuming l_T to be a power law. The fourth curve from the bottom in (A) is fairly straight, and it will remain straight on a log-log plot after multiplication by any power of T . The only segment of the function R_3 that is straight is the horizontal segment right at the critical resistance dividing conductors and insulators. Therefore the power law $l_T \propto T^{-0.325}$ is chosen to make this line become horizontal. All the resistance curves are divided by $T^{-0.325}$, all are expressed as functions of $T^{0.325}$, and all curves are displaced horizontally until they overlap. The vertical scale is arbitrary up to an overall multiplicative factor. The results are similar to Figure 18.9.

obey Ohm’s law. The theory of localization describes effects of quantum mechanics that apply only at zero temperature. At any given finite temperature, there is some inelastic mean free path l_T above which predictions of localization theory fail.

A rough theory of the effect of temperature can be obtained by considering a three-dimensional sample of size l_T . Its resistance R is

$$R = R_3 \left(\frac{l_T}{L_0} \right). \tag{18.113}$$

If the sample is made any larger, however, Ohm’s law takes over. Because the resistance of ordinary three-dimensional resistors scales as $1/L$, resistance for $L > l_T$ is

$$R = R_3 \left(\frac{l_T}{L_0} \right) \frac{l_T}{L}. \tag{18.114}$$

Granted, this expression is a crude way to account for a transition from one sort of behavior to another. It is constructed so that resistance goes as $1/L$, but agrees with Eq. (18.113) when $l_T = L$.

Because l_T is an inelastic mean free path, it diminishes at high temperatures and diverges at low temperatures. In this sense, by changing the temperature of a sample from large to small, one scans from small to large extents of quantum coherence.

Figure 18.10 shows an application of Eq. (18.114) to obtain an experimental measurement of the three-dimensional scaling function also shown in Figure 18.9. Equation (18.114) requires knowledge of the function l_T . Rather than use an elaborate function to optimize accord with predictions, analysis in the figure proceeds

on the assumption that l_T is a power of T . The results are in satisfactory agreement with theory.

Localization in Other Systems. Localization is a phenomenon involving wave motion in a random medium, and it is not particular to the Schrödinger equation. Many of the first calculations arose from studies of phonons in disordered solids, as discussed by Ziman (1979) and Economou (1983). John (1991) discusses the localization of light in random dielectric media, and Störzer et al. (2006) have obtained the best evidence to date that random media can indeed cause light to localize.

18.6 Luttinger Liquids

One of the persistent questions in the study of many electrons is when the Fermi surface exists. Impurities and disorder can disrupt the ability of electrons to carry charge over long distances, but there is a more worrisome issue, which is whether interactions between electrons themselves, even in the perfect crystal, can cause the whole picture of independent electrons traveling near a Fermi surface to break down.

There are few exact results available to provide guidance. The hope has long been for a soluble and realistic model of many electrons. One of the few candidates is a model due to Tomonaga (1950) and Luttinger (1963), which however can only be solved in one dimension. Luttinger's solution of the model was partly incorrect, and the right answer was found by Mattis and Lieb (1965). Recent development of the subject is best sought in Giamarchi (2003).

One way to express the basic idea of the model is to look at a generic energy band diagram for one-dimensional electrons, Figure 18.11(A). A parabolic band occupied up to the Fermi surface is replaced by two linear bands, one for electrons moving to the left near the Fermi surface, the other for electrons moving to the right. This model should generically capture the low-energy behavior of electrons in one dimension.

Luttinger's model features electrons of two types, living in a one dimensional space of length L subject to periodic boundary conditions. The two types of electrons are sometimes called left-moving and right-moving electrons, but really they are defined by the fact that the first have an energy that increases linearly with wave number k , and the second have an energy that decreases linearly with wave number k . Thus the Hamiltonian begins with a first contribution

$$\hat{\mathcal{H}}_0 = \hbar v_F \sum_k k (\hat{c}_{lk}^\dagger \hat{c}_{lk} - \hat{c}_{rk}^\dagger \hat{c}_{rk}). \quad (18.115)$$

Think of $\hbar v_F = \partial \mathcal{E} / \partial k_F$ as coming from a linearization of the electron energy at the Fermi surface.

Here \hat{c}_{lk}^\dagger creates a left-moving electron with wave number k and \hat{c}_{rk}^\dagger creates a right-moving electron with wave number k . The linear dependence of energy on electron wave number was inspired by Dirac's theory for relativistic electrons, although in this case it can be thought of as resulting from linearizing electron energies

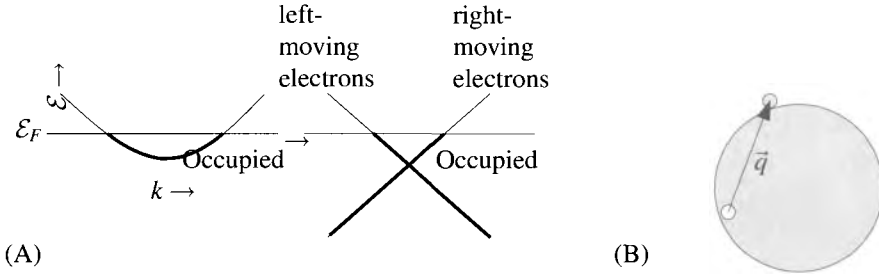


Figure 18.11. (A) A characteristic one-dimensional electron energy band on the left is replaced by the schematic model on the right for the purposes of the Luttinger model. One can view the Luttinger model as one that has generically correct features near the Fermi surface. (B) Illustration of the fact that in two dimensions, creating a particle-hole pair of momentum \vec{q} need not involve a large change of energy. The particle sits just above the Fermi surface, the hole just below.

near the Fermi surface. For Hamiltonian (18.115) as in Dirac’s theory, there is a problem because in the limit $L \rightarrow \infty$, the energy of the system can be made infinitely negative by populating many right-going states with $k \gg 0$ and many left-going states with $k \ll 0$. And as in Dirac’s theory, there is a cure that consists in imagining all these negative energy states to have been filled with electrons, paying attention only to excitations above this state.

The Luttinger Hamiltonian is completed with a second term that describes interactions between left- and right-moving electrons. The model can be solved for a very general interaction function $\sum_{ij} V(\hat{R}_{li} - \hat{R}_{rj})$, where \hat{R}_{li} is the operator corresponding to the position of the i ’th left-moving electron, and \hat{R}_{rj} corresponds to the j ’th right-moving electron. In second quantized notation one has (see Eq. (C.10))

$$\hat{\mathcal{H}}_1 = \sum_{kk'k''k'''} \hat{c}_{lk}^\dagger \hat{c}_{rk'}^\dagger \hat{c}_{rk''} \hat{c}_{lk'''} \langle kk' | V(\hat{R}_l - \hat{R}_r) | k''k''' \rangle \quad (18.116)$$

$$= \sum_{kk'k''k'''} \hat{c}_{lk}^\dagger \hat{c}_{rk'}^\dagger \hat{c}_{rk''} \hat{c}_{lk'''} \int \frac{dR_l dR_r}{L^2} e^{i(k''-k)R_l + i(k'''-k')R_r} V(R_l - R_r) \quad (18.117)$$

$$= \frac{1}{L} \sum_{kk'q} v(q) \hat{c}_{lk}^\dagger \hat{c}_{rk'}^\dagger \hat{c}_{r,k'+q} \hat{c}_{l,k-q} \quad \text{Where } v(q) = \int \exp[-iqx] V(x) \text{ and } q = k - k'' = k''' - k'. \quad (18.118)$$

Solution of the Luttinger model is possible because of an array of dazzling technical tricks, but a simple physical picture suggested by Haldane (1981) lurks behind them. Consider an excitation that creates a particle-hole pair, where the particle has momentum $\hbar\vec{q}$ more than the hole it leaves behind. In two or more dimensions, it is possible for this change in momentum to involve arbitrarily small amounts of energy, as shown in Figure 18.11(B). In one dimension, however, a small change q of momentum cannot take place perpendicular to the Fermi surface. It necessarily involves a change of energy equal to $\hbar^2 k_F |q| / 2m$. Therefore, in one dimension and only in one dimension, particle-hole pairs involve a definite relation

between energy and momentum. In this respect they themselves are like particles. Because these virtual particles are made from a pair of Fermions, they are bosons.

Thus the Luttinger model can be solved by *bosonization*, which means rewriting the Hamiltonian in terms of operators that correspond to creation of particle-hole pairs. This may be accomplished by defining density operators for $q > 0$:

$$\rho_l(q) = \sum_{-\frac{\pi}{a} < k}^{\frac{\pi}{a}-q} \hat{c}_{l,k+q}^\dagger \hat{c}_{lk}; \quad \rho_l(-q) = \sum_{-\frac{\pi}{a} < k}^{\frac{\pi}{a}-q} \hat{c}_{l,k}^\dagger \hat{c}_{l,k+q} \quad \text{Note, } q > 0. \quad (18.119a)$$

$$\rho_r(q) = \sum_{-\frac{\pi}{a} < k}^{\frac{\pi}{a}-q} \hat{c}_{r,k+q}^\dagger \hat{c}_{r,k}; \quad \rho_r(-q) = \sum_{-\frac{\pi}{a} < k}^{\frac{\pi}{a}-q} \hat{c}_{r,k}^\dagger \hat{c}_{r,k+q} \quad (18.119b)$$

The subtlety lies in the choice of upper and lower limits for the sum over k . Ordinarily, k is viewed as periodic, and when k reached the top of the Brillouin zone, $k + q$ would flip over to the bottom. With the definitions in Eq. (18.119), the top and bottom of the Brillouin zone are kept completely separate, and the system takes the form of a filled Fermi sea.

For the sake of definiteness take $q > q'$ and compute

$$[\hat{\rho}_l(-q), \hat{\rho}_l(q')] = \sum_{-\frac{\pi}{a} < k}^{\frac{\pi}{a}-q} \sum_{-\frac{\pi}{a} < k'}^{\frac{\pi}{a}-q'} [\hat{c}_{l,k}^\dagger \hat{c}_{l,k+q}, \hat{c}_{l,k'+q'}^\dagger \hat{c}_{lk'}] \quad (18.120)$$

$$= \sum_{-\frac{\pi}{a} < k}^{\frac{\pi}{a}-q} \sum_{-\frac{\pi}{a} < k'}^{\frac{\pi}{a}-q'} \hat{c}_{l,k'}^\dagger \hat{c}_{lk} \delta_{k+q,k'+q'} - \hat{c}_{l,k'+q'}^\dagger \hat{c}_{l,k+q} \delta_{k,k'} \quad \text{Use Eqs. (C.3) repeatedly.} \quad (18.121)$$

$$= \left(\sum_{k=-\frac{\pi}{a}}^{\frac{\pi}{a}-q'} - \sum_{k=-\frac{\pi}{a}-q}^{\frac{\pi}{a}-(q-q')} \right) \hat{c}_{lk}^\dagger \hat{c}_{l,k+q-q'} \quad \text{Requires about a page of algebra. It is helpful to write the limits on the sums as products of theta functions, and then use the delta function to eliminate } k' \text{ in terms of } k. \quad (18.122)$$

The operators in Eq. (18.122) have canceled out completely except when k is near the top or the bottom of the Brillouin zone. Suppose one is interested only in low-energy excitations; that is, $q \ll \pi/a$. One can restrict attention to the space of wave functions where all the k states down at $-\pi/a$ are completely filled, and all the states up at π/a are completely empty. In this space the first sum in Eq. (18.122) can be replaced by $\sum_{k=-\pi/a}^{-\pi/a+q} \delta_{qq'}$ and the second vanishes. One arrives at the same result, by a slightly different route, if $q < q'$. Thus one has finally

$$[\hat{\rho}_l(-q), \hat{\rho}_l(q')] = \sum_{-\frac{k=\pi}{a}}^{-\frac{\pi}{a}+q} \delta_{qq'} = \frac{L}{2\pi} q \delta_{qq'} \quad (18.123)$$

Similarly

$$[\hat{\rho}_r(q), \hat{\rho}_r(-q')] = \sum_{-\frac{k=\pi}{a}}^{-\frac{\pi}{a}+q} \delta_{qq'} = \frac{L}{2\pi} q \delta_{qq'} \quad (18.124)$$

while $\hat{\rho}_l$ and $\hat{\rho}_r$ commute. Mattis and Lieb (1965) comment about the temptation to think Eq. (18.122) vanishes that

there is a large difference between very large determinants and *infinite* ones....It was first observed by Julian Schwinger... that the very fact that one postulates the existence of a ground state (i.e. the filled Fermi sea) *forces* certain commutators to be nonvanishing even though in first quantization they automatically vanish. The “paradoxical contradictions” of which Schwinger speaks seem to anticipate the difficulties of the Luttinger model. —Mattis and Lieb (1965), p. 304

Comparing with Eq. (13.44), note that $\hat{\rho}_l$ and $\hat{\rho}_r$ obey the commutation relations for boson creation and annihilation operators once one rescales them as

$$\hat{a}_q = \sqrt{\frac{2\pi}{Lq}} \hat{\rho}_r(q), \quad \hat{a}_{-q} = \sqrt{\frac{2\pi}{Lq}} \hat{\rho}_l(-q) \quad (18.125a)$$

$$\hat{a}_q^\dagger = \sqrt{\frac{2\pi}{Lq}} \hat{\rho}_r(-q), \quad \hat{a}_{-q}^\dagger = \sqrt{\frac{2\pi}{Lq}} \hat{\rho}_l(q). \quad (18.125b)$$

The goal is now to rewrite the Luttinger Hamiltonian in terms of these new operators. The interaction term (18.118) is easy to rewrite. Inserting the density operators from Eq. (18.119) gives

$$\hat{\mathcal{H}}_1 = \frac{1}{L} \sum_{q>0} v(q) \hat{\rho}_l(q) \hat{\rho}_r(-q) + v(-q) \hat{\rho}_l(-q) \hat{\rho}_r(q) \quad (18.126)$$

$$= \sum_{q>0} \frac{q}{2\pi} v(q) \left[\hat{a}_{-q}^\dagger \hat{a}_q^\dagger + \hat{a}_{-q} \hat{a}_q \right] \quad \text{Remember assumption that } v(q) \text{ is even.} \quad (18.127)$$

The noninteracting Hamiltonian is less straightforward to represent in terms of the density operators, but the task can be accomplished by computing that

$$[\hat{\mathcal{H}}_0, \hat{\rho}_l(\pm q)] = \pm q \hat{\rho}_l(\pm q) \quad (18.128)$$

$$[\hat{\mathcal{H}}_0, \hat{\rho}_r(\pm q)] = \mp q \hat{\rho}_r(\pm q), \quad (18.129)$$

which means that

$$[\hat{\mathcal{H}}_0, \hat{a}_{\pm q}^\dagger] = q \hat{a}_{\pm q}^\dagger \quad (18.130)$$

$$[\hat{\mathcal{H}}_0, \hat{a}_{\pm q}] = -q \hat{a}_{\pm q} \quad (18.131)$$

Thus $\hat{\mathcal{H}}_0$ has the same commutation relations as $\sum_{q>0} q (\hat{a}_q^\dagger \hat{a}_q + \hat{a}_{-q}^\dagger \hat{a}_{-q})$. Identifying this quantity with $\hat{\mathcal{H}}_0$, up to an additive constant which can be neglected, the Luttinger Hamiltonian equals

$$\hat{\mathcal{H}} = \sum_{q>0} q \left(\hbar v_F \left[\hat{a}_q^\dagger \hat{a}_q + \hat{a}_{-q}^\dagger \hat{a}_{-q} \right] + \frac{v(q)}{2\pi} \left[\hat{a}_{-q}^\dagger \hat{a}_q^\dagger + \hat{a}_{-q} \hat{a}_q \right] \right) \quad (18.132)$$

This Hamiltonian can be made diagonal through the type of transformation used by Bogoliubov in the theories of superfluidity (Problem 15.7) and superconductivity (Section 27.3.4). Define new Bose operators

$$\hat{a}_q^\dagger = \hat{b}_q^\dagger \cosh \phi_q + \hat{b}_{-q} \sinh \phi_q \quad \begin{array}{l} \text{The inverse relations look like} \\ \hat{b}_q = \hat{a}_q \cosh(\phi_q) - \hat{a}_{-q}^\dagger \sinh(\phi_q), \text{ assuming} \\ \phi_q = \phi_{-q}. \end{array} \quad (18.133a)$$

$$\hat{a}_q = \hat{b}_q \cosh \phi_q + \hat{b}_{-q}^\dagger \sinh \phi_q \quad \begin{array}{l} \text{It is easy to verify that this transformation} \\ \text{preserves Bose commutation relations.} \end{array} \quad (18.133b)$$

Inserting Eqs. (18.133) into the Hamiltonian (18.132), using $v(q) = v(-q)$, the Hamiltonian becomes diagonal under the condition that

$$\hbar v_F \sinh(2\phi_q) + \frac{v(q)}{2\pi} \cosh(2\phi_q) = 0 \quad (18.134)$$

and apart from more additive constants one has

$$\hat{\mathcal{H}} = \sum_{q>0} q \sqrt{\hbar^2 v_F^2 - (v(q)/2\pi)^2} (\hat{b}_q^\dagger \hat{b}_q + \hat{b}_{-q}^\dagger \hat{b}_{-q}), \quad (18.135)$$

which finally puts the Hamiltonian into diagonal form.

18.6.1 Density of States

The Hamiltonian for the Luttinger model has now been diagonalized, and it remarkably has turned into a quadratic Hamiltonian for non-interacting bosons, although it began as a Hamiltonian for interacting electrons. Computing quantities of physical interest is however surprisingly difficult, since the transformations leading from the fermionic to the bosonic representation are complicated, and it is not clear given the bose operators \hat{b} how one can get the fermion operators \hat{c} back again.

Luther and Peschel (1974) showed how to accomplish this task. Observe that

$$[\hat{\rho}_l(q), \hat{c}_{lk}] = -\hat{c}_{l,k-q}. \quad \begin{array}{l} \text{This computation is a straightforward exercise} \\ \text{in anti-commuting } \hat{c}_{lk} \text{ past the operators} \\ \text{in Eq. (18.119).} \end{array} \quad (18.136)$$

Therefore, defining the spatial destruction operator

$$\hat{\psi}_l(x) = \sum_k \frac{e^{ikx}}{\sqrt{L}} \hat{c}_k, \quad (18.137)$$

one finds that

$$[\hat{\rho}_l(q), \hat{\psi}_l(x)] = -e^{iqx} \hat{\psi}_l(x). \quad (18.138)$$

Now consider

$$\hat{\Psi} = e^{\sum_{q'>0} \frac{2\pi}{q'L} \left(e^{iq'x} \hat{\rho}_l(-q') - e^{-iq'x} \hat{\rho}_l(q') \right)}. \quad (18.139)$$

Using the result from Messiah (1999) p. 208 for any two operators \hat{A} and \hat{B} whose commutator is a scalar that $[\hat{A}, f(\hat{B})] = f'(\hat{B})[\hat{A}, \hat{B}]$, one computes that

$$[\hat{\rho}_l(q), \hat{\Psi}] = \sum_{q'} \frac{2\pi}{q'L} e^{iq'x} \hat{\Psi} [\hat{\rho}_l(q), \hat{\rho}_l(-q')] \quad (18.140)$$

$$= -e^{iqx} \hat{\Psi}. \quad \text{Using Eq. (18.123).} \quad (18.141)$$

Problem 9 shows that the same relation applies to commutation with $\hat{\rho}_l(-q)$. Since $\hat{\Psi}$ and $\hat{\psi}_l(x)$ have the same commutation relation with $\hat{\rho}_l(q)$ and $\hat{\rho}_l(-q)$, they can be identified with one another up to overall constants, and

$$\hat{\psi}_l(x) = \frac{1}{\sqrt{\alpha}} \exp \left[\sum_{q' > 0} \frac{2\pi e^{-q'\alpha/2}}{q'L} \left(e^{iq'x} \hat{\rho}_l(-q') - e^{-iq'x} \hat{\rho}_l(q') \right) \right]. \quad (18.142)$$

Note sneaky introduction of convergence factor α ; the factor in front is needed to normalize results later. See Haldane (1981) for a much more careful derivation, including some terms needed to correct the fact that the right hand side leaves the number of fermions constant, and the left side does not.

It follows immediately with use of Eq. (18.125) that

$$\hat{c}_{lk} = \int \frac{dx}{\sqrt{L\alpha}} e^{-ik(x-i\alpha) + \sum_q \sqrt{\frac{2\pi}{qL}} (e^{iqx} \hat{a}_{-q} - e^{-iqx} \hat{a}_{-q}^\dagger)}. \quad (18.143)$$

The density of single-particle states for left-moving particles is

$$\hat{n}_{lk} = \hat{c}_{lk}^\dagger \hat{c}_{lk}. \quad (18.144)$$

The goal is to find the expectation of \hat{n}_{lk} in the ground state. Following computations that are the subject of Problem 9, one has

$$\langle \hat{n}_{lk} \rangle = \int \frac{dx}{\alpha} e^{-ikx} + \int_0^\infty \frac{e^{-\alpha q}}{q} ([e^{iqx} - 1] \sinh^2(\phi_q) + [e^{-iqx} - 1] \cosh^2(\phi_q)). \quad (18.145)$$

The computation can now follow different paths, depending upon assumptions about the electron interaction $v(q)$. The simplest assumption is that the interaction is very short range in space, meaning that $v(q) = v_0$ is constant. The convergence factor α is now needed to control integrals that would otherwise diverge, but this is all right given the understanding that α is really standing in for the decay at large wave number of $v(q)$. With some more manipulations, one finds

$$\langle \hat{n}_{lk} \rangle = \int_0^L dx \frac{e^{-ikx}}{\alpha + ix} \left(\frac{\alpha^2}{\alpha^2 + x^2} \right)^{u_0^2} \quad (18.146)$$

$$\Rightarrow \langle \hat{n}_{lk} \rangle \propto k^{2u_0^2} \quad \text{This expression for the power law in } k \text{ should} \quad (18.147)$$

be good so long as $k\alpha$ is small.

where

$$u_0^2 = \frac{1}{2} \left[\frac{\hbar v_F}{\sqrt{\hbar^2 v_F^2 - (v_0/(2\pi))^2}} - 1 \right]. \quad (18.148)$$

For noninteracting electrons $v_0 = 0$, $u_0 = 0$, and the density of states is constant outside the Fermi surface, where in fact it vanishes. For interacting electrons, the density of states vanishes approaching the Fermi surface as a power of k that is given by the strength of the interactions between electrons. Interactions between electrons have fundamentally changed electron excitations near the Fermi surface.

Despite the host of detailed theoretical results concerning one-dimensional electron systems, thought to constitute a whole class of materials called *Luttinger liquids*, experimental confirmation has come very slowly. Clean one-dimensional systems are hard to create, and hard to connect to three-dimensional measuring devices. One indication of Luttinger liquid behavior comes from experiments designed to allow electrons to tunnel across an insulating barrier into a carbon nanotube. The nanotubes are essentially one-dimensional conductors, and good candidates for Luttinger liquid behavior. Because the density of states vanishes as a power law for energies near the Fermi surface, Kane et al. (1997) show one should expect the current to vanish as a power law either as a function of temperature or of bias voltage. Figure 18.12 shows data indicating this is in fact the case.

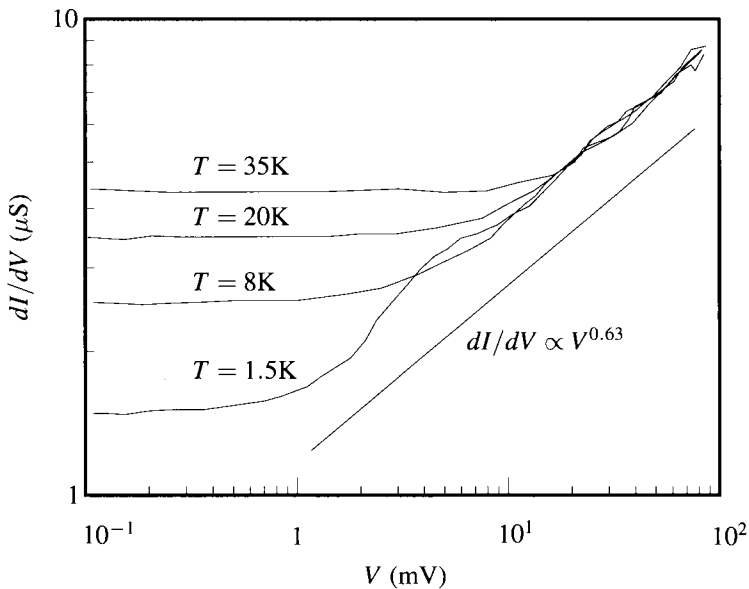
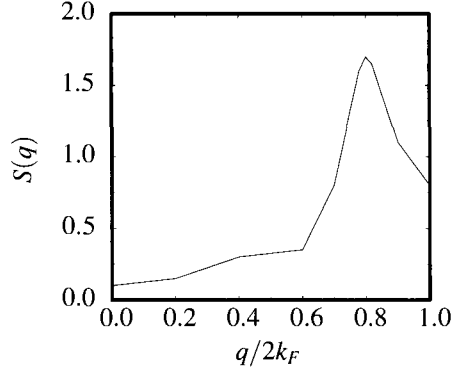


Figure 18.12. Differential conductance measured at various temperatures for current injected into a rope of carbon nanotubes. As the temperature decreases, the data appear to approach a power law, as predicted by Luttinger liquid theory. [Source: Bockrath et al. (1999) p. 599].

Problems

1. **Resistance of liquid aluminum:** The structure function $S(q)$ has been measured for molten aluminum at 700°C , and is shown below.



Use these data, and the pseudopotential of Eq. (10.38), with the values listed after it, to compute the resistivity of aluminum at 700°C , and compare with the experimental result of $24.7 \mu\Omega \cdot \text{cm}$. Note that the potential $U(\vec{q})$ in Eq. (18.16) differs from the pseudopotential $U_{\vec{q}}$ in Eq. (10.38) by a factor of Ω , the volume per atom.

2. **Electron in an incommensurate potential:** Consider the Hamiltonian

$$\hat{\mathcal{H}} = t \sum_l \left\{ \frac{1}{2} (|l\rangle\langle l+1| + |l\rangle\langle l-1|) + \cos(2\pi l\tau) |l\rangle\langle l| \right\}. \quad (18.149)$$

The problem becomes particularly interesting when the potential $\cos(2\pi l\tau)$ is incommensurate with the lattice sites $|l\rangle$, which happens when τ is irrational. For example, one might take τ to be the golden mean,

$$\tau = \frac{\sqrt{5} + 1}{2}. \quad (18.150)$$

- (a) Suppose that instead of taking τ to be exactly the golden mean, one replaces it by rational approximants to the golden mean:

$$\tau_n = \frac{F_{n+1}}{F_n}, \quad (18.151)$$

where F_n is the n th Fibonacci number, $F_n = F_{n-1} + F_{n-2}$,

$$F_0 = 1, F_1 = 1, F_2 = 2, F_3 = 3, F_4 = 5, F_5 = 8 \dots \quad (18.152)$$

How many bands does (18.149) have when one uses τ_n for τ (compare with Problem 7 in Chapter 8).

- (b) For τ now given by Eq. (18.150), the wave functions of the Hamiltonian are a curious intermediate between localized and extended. Demonstrate this fact by assuming that there is an eigenstate at $\mathcal{E} = 0$, taking $\psi_0 = \langle 0|\psi\rangle = 1$ and $\psi_1 = \langle 1|\psi\rangle = 1$. Then use Eq. (18.149) to compute $\psi_m = \langle m|\psi\rangle$ for m on the order of 10^4 and observe how the magnitude of ψ_m scales with m .

One way to do this is to plot the *participation ratio*

$$P(m) = \frac{\sum_{l=1}^m \psi_l^4}{(\sum_{l=1}^m \psi_l^2)^2}. \quad (18.153)$$

In order to calculate $P(m)$, make use of quantities calculated in order to find $P(m-1)$; do not carry out a sum starting at 0 and going up to m for each individual $P(m)$.

Compare the behavior of the participation ratio with what would be expected for localized states, and what would be expected for extended states.

3. **Introduction to transfer matrices:** Consider a tight-binding model for a one-dimensional chain of atoms with random impurities scattered along it:

$$\hat{\mathcal{H}} = \sum_l |l\rangle U_l \langle l| + t|l\rangle \langle l+1| + t|l+1\rangle \langle l|. \quad (18.154)$$

Take U_l to be a random variable occupying all values between $-W/2$ and $W/2$.

- (a) Show that a solution $|\psi\rangle$ of Schrödinger's equation with energy \mathcal{E} satisfies

$$\begin{pmatrix} \psi_{l+1} \\ \psi_l \end{pmatrix} = \mathbf{T} \begin{pmatrix} \psi_l \\ \psi_{l-1} \end{pmatrix} \quad (18.155)$$

and find the 2×2 transfer matrix \mathbf{T} making Eq. (18.155) true.

- (b) Suppose that $\psi_0 = 0$ and $\psi_1 = 1$. Using Eq. (18.155) in a numerical routine, find how $|\psi_l|^2$ behaves for large l for $\mathcal{E} = 0$, $W/t = 10$, and $W/t = 1$. Plot $|\psi_l|^2$ versus l on a linear-log plot.
- (c) What conclusion can one draw about solutions of Schrödinger's equation? It is helpful to suppose that $U_l = U_{-l}$.

4. **Tight-binding Hamiltonian in two dimensions:**

- (a) Consider a square lattice in two dimensions. Write down the tight-binding Hamiltonian, with nearest-neighbor hopping t and onsite energies U_l .
- (b) Prepare a numerical routine that takes a wave function ψ on an 8×8 square lattice with periodic boundary conditions and computes $\hat{\mathcal{H}}\psi$. $\hat{\mathcal{H}}$ is a 64×64 matrix, and ψ is a 64-component vector. Set up the routine so that it is easy to change the size of the lattice. The components of ψ must be allowed to be complex numbers.

- (c) Set the onsite energy U_l to zero. Set $\psi_{(0,0)} = 1$ and all other components of ψ to zero. Set $\mathbf{t}dt/\hbar = 0.01$. Compute the time evolution of ψ by

$$\psi^{(n)} = \left[1 - \frac{i\mathbf{t}dt}{\hbar} \hat{\mathcal{H}} \right] \psi^{(n-1)}. \quad (18.156)$$

Actually, this is not a good way to solve Schrödinger's equation, because it does not preserve normalization and is not accurate to high order, but it will do for the present. Find $\psi_{0,0}^{(n)}$ for 4096 values of n , and prepare a plot of the real and imaginary parts of $\psi_{(0,0)}$ as a function of time.

- (d) Multiply $\psi(t)$ by $\exp[-0.1t/(\hbar/t)]$, take the fast Fourier transform of the result, and plot real and imaginary parts. To what function computed in this chapter should the result correspond?

5. Scaling theory of localization I:

- (a) Consider a three-dimensional tight-binding model on a square lattice. Show that solutions ψ of Schrödinger's equation must obey the equation

$$\begin{pmatrix} \psi_{l+1} \\ \psi_l \end{pmatrix} = \mathbf{T} \begin{pmatrix} \psi_l \\ \psi_{l-1} \end{pmatrix}, \quad (18.157)$$

where

$$\mathbf{T} = \begin{pmatrix} -\hat{\mathcal{H}}_2 & -1 \\ 1 & 0 \end{pmatrix}. \quad (18.158)$$

Here $\hat{\mathcal{H}}_2$ is the tight-binding Hamiltonian for the two-dimensional square lattice, and ψ_l is condensed notation for $\psi_{j,k,l}$. The three indices on ψ label the three-dimensional sites of the tight-binding model. ψ_l is a vector (whose values can be indexed by j and k) with as many components as a two-dimensional tight-binding model and where the final index l is being treated separately for use with the transfer matrix \mathbf{T} .

- (b) The transfer matrix for a 2×2 two-dimensional Hamiltonian with periodic boundary conditions in which all the diagonal elements vanish is

$$\begin{pmatrix} 0 & -1 & -1 & 0 & -1 & 0 & 0 & 0 \\ -1 & 0 & 0 & -1 & 0 & -1 & 0 & 0 \\ -1 & 0 & 0 & -1 & 0 & 0 & -1 & 0 \\ 0 & -1 & -1 & 0 & 0 & 0 & 0 & -1 \\ 1 & 0 & 0 & 0 & 0 & 0 & 0 & 0 \\ 0 & 1 & 0 & 0 & 0 & 0 & 0 & 0 \\ 0 & 0 & 1 & 0 & 0 & 0 & 0 & 0 \\ 0 & 0 & 0 & 1 & 0 & 0 & 0 & 0 \end{pmatrix}. \quad (18.159)$$

Generate an automatic procedure to create this matrix.

- (c) Print the matrix for a 3×3 two-dimensional system.

6. **Scaling theory of localization II:** Let \mathbf{T} be the transfer matrix for a tight-binding Hamiltonian on an $L \times L$ square lattice,

$$\mathbf{T}_l = \begin{pmatrix} \mathcal{E} - \hat{\mathcal{H}}_l & -1 \\ 1 & 0 \end{pmatrix}. \quad (18.160)$$

The subscript l is needed because the matrices $\hat{\mathcal{H}}_l$ have random diagonal elements, chosen with equal probability to lie within $[-W/2, W/2]$. Let

$$\mathbf{Q} = \prod_{l=1}^L \mathbf{T}_l. \quad (18.161)$$

Then according to Pichard and André (1986), the conductance G of an $L \times L \times L$ cube, in units of e^2/h , is

$$G = \frac{1}{R} = \text{Tr} \left[\frac{2}{\mathbf{Q}\mathbf{Q}^* + (\mathbf{Q}\mathbf{Q}^*)^{-1} + 2} \right]. \quad (18.162)$$

- Rewrite the expression for G in terms of the eigenvalues of the matrix $\mathbf{Q}\mathbf{Q}^*$.
- Calculate the resistance of a $3 \times 3 \times 3$ block at $W = 0$ and $\mathcal{E} = 0$ and find $\ln R = 1.4818$.
- Find the resistance of a single $3 \times 3 \times 3$ block at $W = 10$ and $\mathcal{E} = 0$.
- The resistance found in the previous part will depend greatly upon the particular values of the random disorder. To obtain a more meaningful result, carry out averages over many realizations of the randomness. That is, compute $\ln R$ for one $3 \times 3 \times 3$ block, obtaining $\ln R_1$. Without initializing the random number generator, find the resistance of a second $3 \times 3 \times 3$ block, obtaining $\ln R_2$. Continue in this way, generating the series of resistances $\ln R_l$. The fluctuations in resistance are so large that \bar{R} is not well defined, but $\overline{\ln R}$ will average well. Let $\overline{\ln R}_l$ be the average of $\ln R$ after l computations. Keep computing until the fluctuations in $\overline{\ln R}_l$ settle down to within around 4%.

7. **Scaling theory of localization III:**

Use the numerical routine of problem 6 to compute the conductance G , defined in Eq. (18.162), and therefore find the scaling function for localization in three dimensions. That is, reproduce Figure 18.9. This figure was produced by using tens of thousands of cubes of size up to $7 \times 7 \times 7$, but if systems this size are too time-consuming, an adequate figure can be produced with cubes of size up to $5 \times 5 \times 5$.

8. **Weak localization:** The goal of this problem is to carry out the calculations leading from Eq. (18.101) to Eq. (18.103). Specialize to the center of the band, $\mathcal{E} = 0$, and write $\mathcal{F}(g, \mathcal{E} = 0) = \mathcal{F}(g)$.

- (a) Show that

$$\lambda^{-1} = - \int dg \mathcal{F}(g) \ln |g|. \quad (18.163)$$

- (b) Show that if $\mathcal{P}(U)$ is very narrow and centered on zero, then to leading order in W/t one obtains

$$\mathcal{F}(g) = \frac{1}{g^2} \mathcal{F}(-1/g). \quad (18.164)$$

- (c) Verify that Eq. (18.164) has solution

$$\mathcal{F} = \frac{C}{\sqrt{1+g^4}}, \quad (18.165)$$

where C is a constant.

- (d) Show that to normalize \mathcal{F} , $C = 0.2696 \dots$

- (e) Equation (18.165) is completely independent of the probability distribution \mathcal{P} . From Eq. (18.101), an approximate form for \mathcal{F} that involves \mathcal{P} is

$$\mathcal{F}(g) = \frac{t}{g^2} \int dg' \mathcal{P}\left(-\frac{t}{g} - tg'\right) \frac{C}{\sqrt{1+g'^4}}. \quad (18.166)$$

Iterating Eq. (18.101) further would produce even better approximations for \mathcal{F} , but to leading order in W/t it is not necessary.

- (f) Inserting Eqs. (18.166) and (18.81) into Eq. (18.163), and working to leading order in W/t , verify Eq. (18.103).

9. Luttinger Liquids:

- (a) Verify that

$$[\hat{\rho}_l(-q), \hat{\Psi}] = - \sum_{q'} \frac{2\pi}{q'L} e^{-iq'x} \hat{\Psi} [\hat{\rho}_l(-q), \hat{\rho}_l(q')] \quad (18.167)$$

$$= -e^{iqx} \hat{\Psi}. \quad (18.168)$$

- (b) Verify Eq. (18.145). Use Eq. (13.119) to treat averages of exponentials of Bose operators. Keep only terms that survive the expectation value in the ground state.

- (c) Verify Eq. (18.146).

References

- E. Abrahams, P. W. Anderson, D. C. Licciardello, and T. V. Ramakrishnan (1979), Scaling theory of localization: Absence of quantum diffusion in two dimensions, *Physical Review Letters*, **42**, 673–676.
- M. Ahlskog, R. Menon, A. J. Heeger, T. Noguchi, and T. Ohnishi (1997), Metal-insulator transition in oriented poly(*p*-phenylenevinylene), *Physical Review B*, **55**, 6777–6787.
- B. L. Al'tshuler and P. A. Lee (1988), Disordered electronic systems, *Physics Today*, **41**(12), 36–44.
- P. W. Anderson (1958), Absence of diffusion in certain random lattices, *Physical Review*, **109**, 1492–1505.

- N. W. Ashcroft and L. J. Guild (1965), The resistivity of liquid aluminium, *Physics Letters*, **14**, 23–24.
- N. W. Ashcroft and D. Stroud (1978), Theory of the thermodynamics of simple liquid metals, *Solid State Physics: Advances in Research and Applications*, **33**, 1–81.
- J. Bass, W. P. Pratt, and P. A. Schroeder (1990), The temperature-dependent electrical resistivities of the alkali metals, *Reviews of Modern Physics*, **62**, 645–744.
- D. Belitz and T. R. Kirkpatrick (1994), The Anderson-Mott transition, *Reviews of Modern Physics*, **66**, 261–380.
- A. B. Bhatia and K. S. Krishnan (1948), “Diffuse scattering” of the Fermi electrons in monovalent metals in relation to their electrical resistivities, *Proceedings of the Royal Society of London, A* **194**, 185–205.
- M. Bockrath, D. H. Cobden, J. Lu, A. G. Rinzler, R. E. Smalley, L. Balents, and P. L. McEuen (1999), Luttinger-liquid behaviour in carbon nanotubes, *Nature*, **397**, 598–601.
- A. R. Bulsara and L. Gammaitoni (1996), Tuning in to noise, *Physics Today*, **49**(3), 39–45.
- D. Chattopadhyay and H. J. Queisser (1981), Electron scattering by ionized impurities in semiconductors, *Reviews of Modern Physics*, **53**, 745–768.
- N. E. Cusack (1987), *The Physics of Structurally Disordered Matter*, Adam Hilger, Bristol.
- P. Dean (1972), The vibrational properties of disordered systems: Numerical studies, *Reviews of Modern Physics*, **44**, 127–168.
- P. Dutta and P. M. Horn (1981), Low-frequency fluctuations in solids: $1/f$ noise, *Reviews of Modern Physics*, **53**, 497–516.
- E. N. Economou (1983), *Green’s Functions in Quantum Physics*, Springer-Verlag, Berlin.
- P. P. Edwards and M. J. Sienko (1982), The transition to the metallic state, *Accounts of Chemical Research*, **15**, 87–93.
- R. J. Elliott, J. A. Krumhansl, and P. L. Leath (1974), The theory and properties of randomly disordered crystals and related physical systems, *Reviews of Modern Physics*, **46**, 465–543.
- H. Fritzsche (1984), Noncrystalline semiconductors, *Physics Today*, **37**(10), 34–41.
- T. Giamarchi (2003), *Quantum Physics in One Dimension*, Oxford University Press, Oxford.
- I. S. Grigoriev and E. Z. Meilkhov, eds. (1997), *Handbook of Physical Quantities*, CRC Press, Boca Raton, FL.
- F. D. M. Haldane (1981), ‘Luttinger liquid theory’ of one-dimensional quantum fluids. I. Properties of the Luttinger model and their extension to the general 1D interacting spinless Fermi gas, *Journal of Physics C: Solid State Physics*, **14**(19), 2585–2609.
- S. John (1991), Localization of light (in dielectric microstructures), *Physics Today*, **44**(5), 32–40.
- J. B. Johnson (1927), Thermal agitation of electricity in conductors, *Physical Review*, **29**, 367–368. The complete text of the article reads: Ordinary electric conductors are sources of random voltage fluctuations, as a result of thermal agitation of the electric charges in the conductor. The average effect of the fluctuations has been measured by means of a vacuum tube amplifier, where it manifests itself as a component of the phenomenon commonly called “tube noise.” A part of the “tube noise” arises in the first tube and other elements of the apparatus; the remainder in the input resistance, with a mean square voltage fluctuation $(V^2)_m$ which is proportional to the resistance R of that conductor. The ratio $(V^2)_m/R$, of the order of 10^{-18} watt at room temperature, is independent of the material and shape of the conductor, but is proportional to its absolute temperature. In the range of audio frequencies, at least, the noise contains all frequencies at equal amplitudes. The noise of an input resistance of only 5000 ohms may exceed that of the rest of the circuit, so that the limit of useful amplification is at times set by the thermal agitation of charges in the input resistance of the amplifier.
- C. Kane, L. Balents, and M. P. A. Fisher (1997), Coulomb interactions and mesoscopic effects in carbon nanotubes, *Physical Review Letters*, **79**, 5086–5089.
- A. Kawabata (2007), Electron conduction in one-dimension, *Reports on Progress in Physics*, **70**,

- 219–254.
- W. Kohn (1957), Shallow impurity states in silicon and germanium, *Solid State Physics: Advances in Research and Applications*, **5**, 257–320.
- B. Kramer and A. MacKinnon (1993), Localization: Theory and experiment, *Reports on Progress in Physics*, **56**, 1469–1564.
- L. D. Landau and E. M. Lifshitz (1977), *Quantum Mechanics (Non-relativistic Theory)*, 3rd ed., Pergamon Press, Oxford.
- A. Luther and I. Peschel (1974), Single-particle states, Kohn anomaly, and pairing fluctuations in one dimension, *Physical Review B*, **9**, 2911–2919.
- J. M. Luttinger (1963), An exactly soluble model of a many-fermion system, *Journal of Mathematical Physics*, **4**, 1154–1162.
- N. March (1990), *Liquid Metals: Concepts and Theory*, Cambridge University Press, Cambridge.
- D. C. Mattis and E. H. Lieb (1965), Exact solution of a many-Fermion system and its associated boson field, *Journal of Mathematical Physics*, **6**, 304–312.
- R. Menon, C. O. Yoon, D. Moses, A. J. Heeger, and Y. Cao (1993), Transport in polyaniline near the critical regime of the metal-insulator transition, *Physical Review B*, **48**, 17 685–17 694.
- A. Messiah (1999), *Quantum Mechanics*, Dover, New York.
- N. F. Mott (1978), Metal-insulator transitions, *Physics Today*, **31**(11), 42–47.
- N. F. Mott (1990), *Metal-Insulator Transitions*, 2nd ed., Taylor and Francis, London.
- N. F. Mott and E. A. Davis (1979), *Electronic Processes in Non-Crystalline Materials*, 2nd ed., Clarendon Press, Oxford.
- H. Nyquist (1928), Thermal agitation of electric charge in conductors, *Physical Review*, **32**, 110–113.
- S. T. Pantelides (1978), The electronic structure of impurities and other point defects in semiconductors, *Reviews of Modern Physics*, **50**, 797–858.
- R. E. Peierls (1929), On the kinetic theory of heat transport in crystals, *Annalen der Physik*, **3**, 1055–1101. In German.
- J. L. Pichard and G. André (1986), Many-channel transmission: Large volume limit of the distribution of localization lengths and one-parameter scaling, *Europhysics Letters*, **2**, 477–486.
- T. F. Rosenbaum (1985), The disordered insulator: Electron glasses and crystals, in *Localization and Metal-Insulator Transitions*, H. Fritzsche and D. Adler, eds., pp. 1–8, Plenum, New York.
- M. V. Sadovskii (1981), Electron localization in disordered systems: Critical behavior and macroscopic manifestations, *Soviet Physics Uspekhi*, **24**, 96–115.
- P. Sheng (1995), *Introduction to Wave Scattering, Localization, and Mesoscopic Phenomena*, Academic Press, San Diego.
- M. Störzer, P. Gross, C. M. Aegerter, and G. Maret (2006), Observation of the critical regime near Anderson localization of light, *Physical Review Letters*, **96**(6), 063 904.
- A. P. Sutton (1993), *Electronic Structure of Materials*, Clarendon Press, Oxford.
- S. Tomonaga (1950), Remarks on Bloch's method of sound waves applied to many-fermion problems, *Progress of Theoretical Physics*, **5**, 544–569.
- R. A. Webb and S. Washburn (1988), Quantum interference fluctuations in disordered metals, *Physics Today*, **41**(12), 46–53.
- J. M. Ziman (1961), A theory of the electrical properties of liquid metals. I The monovalent metals, *Philosophical Magazine*, **6**, 1013–1034.
- J. M. Ziman (1979), *Models of Disorder : The Theoretical Physics of Homogeneously Disordered Systems*, Cambridge University Press, Cambridge.
- A. Zunger (1986), Electronic structure of 3d transition-atom impurities in semiconductors, *Solid State Physics: Advances in Research and Applications*, **39**, 275–464.

19. Electronics

19.1 Introduction

Electronics is the art of controlling the flow of electrons. It began with the discovery of the ancient Greeks that a piece of amber ($\eta\lambda\epsilon\kappa\tau\rho\omicron\nu$) could attract and hold small objects after being rubbed. The path leading to electrons' controlled removal from matter included the observation early in the eighteenth century that the electrical conductivity of air increases in the vicinity of a hot poker, continued with Franklin's kite experiment relating lightning to static electricity, and culminated in the middle of the nineteenth century with experiments of Crookes who passed electricity between high-voltage plates in evacuated tubes. Edison noticed in 1883 that if he placed a metal plate inside a light bulb, current would flow to the plate if it was at a positive voltage with respect to the filament, but not otherwise. Edison did not think this observation of *rectification* particularly significant, but it has turned out to have as many consequences as his electric lights.

Credit for the discovery of the electron is given to J. J. Thomson, whose experiments on the flow of electricity from heated filaments in evacuated tubes isolated it as a particle with a definite ratio of charge to mass. The name "electron" was proposed by G. J. Stoney in 1894 for the unit of charge equal to 10^{-19} coulombs, and this term gradually superseded Thomson's term "corpuscle" for the new particle. The first practical electronic device was built by J. A. Fleming, who built upon the work of Thomson and Edison to create a *cathode ray tube* with a heated filament capable of rectifying oscillating currents. He called it a "valve," but it is now better known as the *diode*, and is depicted in Figure 19.1. Commercial radio

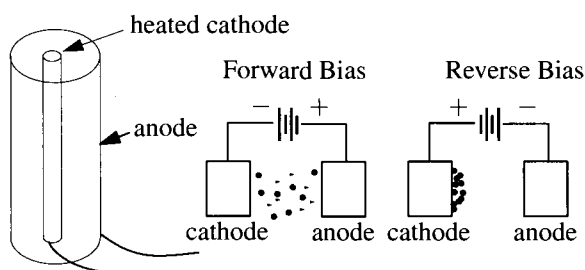


Figure 19.1. The essential action of a diode is to send current in one direction in response to an applied voltage, and not the other. The origin of this asymmetry is the fact that metals at elevated temperatures emit electrons long before they emit positively charged ions. A heated cathode therefore sends off an appreciable current toward a positively charged anode, but almost none toward a negatively charged anode.

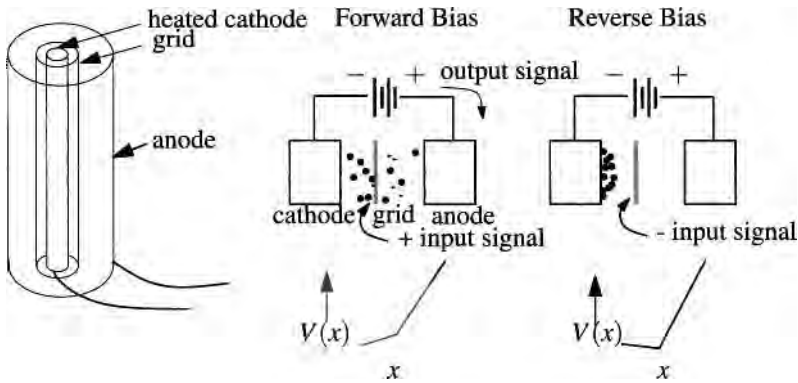


Figure 19.2. The triode serves not only to rectify current, but also to amplify small signals. It accomplishes this task through the interposition of a grid between cathode and anode. The potential between cathode and grid determines whether electrons begin the journey between cathode and grid at all. However, once electrons arrive at the grid, they discover that a much larger positive potential awaits them at the anode and accelerate toward it. Because only a small proportion of the electrons enters the grid, small grid currents control large cathode→anode currents.

transmission became feasible soon after with the invention by L. De Forest of the *triode*, shown in Figure 19.2. Rectification is essential to practical radio transmission because the time average electrical field of a propagating radio wave is zero, and even if the amplitude of such a wave is modulated to encode sound, it cannot directly drive a speaker. Once the signal is passed through a rectifier, time averages no longer vanish, and the signal can easily be decoded. The triode was essential not only because it allowed amplification of weak signals, but also because by feeding a portion of the output back in to the control grid, it could be made into a powerful and stable source of radio-frequency oscillations.

Up through the 1970s much of electronics consisted in the study of cathode ray tubes. They have now almost entirely been superseded by semiconductor devices, which are much more reliable, and have slowly managed to capture even high-power and high-frequency applications that at first seemed out of reach. However, the basic concepts of controlling current, rectification, amplification, and switching all first developed in the context of cathode ray tubes and were then taken over and further developed by semiconductor descendants. Even the basic physics of the various devices has many points of similarity. For this reason, it is advisable to begin the study of electronics with the physics that made the cathode ray tubes possible.

19.2 Metal Interfaces

As sketched in Figure 19.1, the cathode ray tube diode relies upon the fact that a heated piece of metal emits electrons, but not positively charged ions. This effect becomes most clearly visible when air is evacuated from the region in which the

electrons are to travel, and for this reason cathode ray tubes are also known as *vacuum tubes* or *electron tubes*. The physical question that needs to be answered is how a metal surface in contact with vacuum emits electrons as a function of temperature and electrical potential.

19.2.1 Work Functions

All the calculations of electronic energy levels up until now have been carried out relative to one another. For example, the Fermi level was sometimes calculated relative to the energy of the lowest single-particle electronic level, and in the band structure diagrams of Section 10.4, the Fermi level was defined to be zero. None of these calculations answers the question of the amount of energy needed to remove an electron from an electrically neutral solid in vacuum. This energy is defined to be the *work function* and is often denoted by ϕ . It can be measured by optical methods to be discussed in Section 23.6.1, or by properties of thermal emission to be discussed immediately below. To calculate it requires understanding what happens when an electron is dragged through the interface between metal and vacuum.

The work function must be contrasted with the chemical potential, which is the energy required to take an electron from the bulk and remove it to infinity. Inspection of Table 23.2 shows that the experimentally measured energy required to pass an electron through one crystal surface typically differs by 10–20% from the energy required to move it through an inequivalent one. As the energy required for transit from bulk to infinity cannot depend upon path, it is necessary to establish carefully what the experiments actually determine.

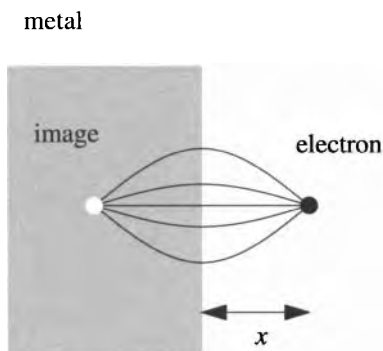


Figure 19.3. An electron at a distance x from a metal surface is attracted to the surface by an image charge of opposite sign which guarantees that electric field lines will be normal to the surface.

The electrostatic potentials contributing to the work function operate on three separate length scales:

Atomic. In passing through the surface of a crystal, an electron passes through a highly inhomogeneous environment where the crystal terminates. Although the surface is almost completely electrically neutral, there is always a strong dipole layer. The electron is buffeted by strong forces as it passes through this layer, but the range over which these forces operate is only on the order of a few lattice spacings, due to the effectiveness of screening in a metal.

Micron. After the electron exits the metal, it interacts with an image charge, whose presence enforces the boundary condition that the tangential electric field vanish on the surface, as shown in Figure 19.3. The force F at distance x from the surface is

$$F = \frac{e^2}{(2x)^2}, \quad (19.1)$$

which implies that the electron has a potential energy

$$U(x) = -\frac{e^2}{4x} = -\frac{1}{x} 3.6 \cdot 10^{-4} \mu\text{m eV}. \quad (19.2)$$

Work functions are on the order of several electron volts, and therefore further changes due to the image charge energy become negligible by the time an electron has traveled a few microns from the surface.

Macroscopic. Because different crystal faces have different dipole layers, the regions outside them must be at different electrical potentials, produced by minute shifts in electron density near the crystal surface. The existence of this potential is absolutely necessary, because there is no other way to bring an electron out of the bulk through one surface, return it through another surface, and have it return to the original bulk energy. The spatial scale for the variation of this potential is the size of the crystal itself.

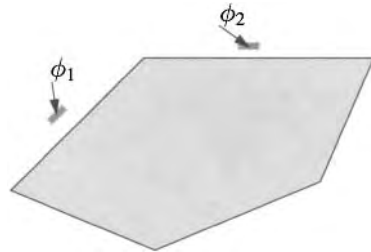


Figure 19.4. The work function is defined as the energy needed to remove an electron from the bulk of a metal, and bring it within about a micron of a particular surface.

Therefore, as indicated in Figure 19.4 the work function is defined to be the energy of electrons brought out to distances on the order of microns from crystals whose dimensions are larger than microns. Hölzl and Schulte (1979) describe many additional complications that can arise in attempting to calculate or to measure work functions, such as what happens when surfaces are rough, or contain a layer of adsorbate atoms.

19.2.2 Schottky Barrier

Equation (19.2) fails when an electron is too close to the crystal surface, because the potential energy U diverges, and more realistic calculations require explicit description of the electronic surface states of a metal. However, it is adequate for the purpose of estimating the effect of an externally applied electrical potential on the work function. Suppose that a positively charged metal plate is placed at a large

distance to the right of the metal surface, creating a linear electric field of strength $-E$. Now the potential energy $U(x)$ of the electron is

$$U(x) = -\frac{e^2}{4x} - e|E|x, \tag{19.3}$$

which creates a barrier, shown in Figure 19.5, at distance

$$x_0 = \sqrt{\frac{e}{4|E|}} \Rightarrow U(x_0) = -e\sqrt{e|E|}. \tag{19.4}$$

Therefore an externally applied electric field changes the barrier restraining an electron within the metal by $e\sqrt{e|E|}$.

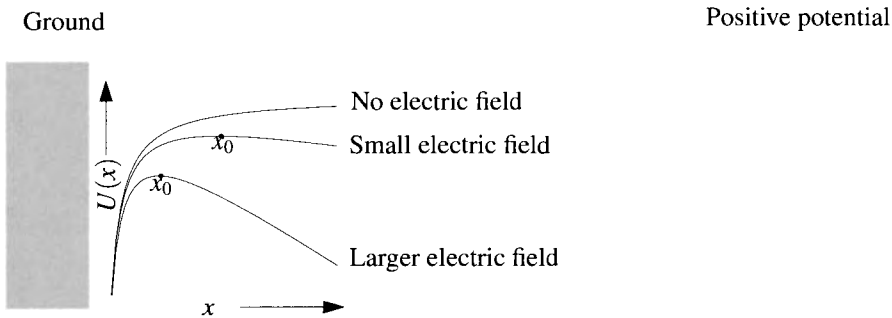


Figure 19.5. An externally applied electric field, created by placing at a distance a large plate at an elevated voltage, lowers the barrier an electron must surpass in order to exit a metal.

Having first found the effect of applied electric fields, the next goal is to examine the *thermionic emission* of electrons that results from heating the metal. This task is accomplished by considering the electrons in the metal to be in equilibrium with a dilute gas of electrons hovering outside it. For simplicity the electrons are treated within the semiclassical approximation, which makes it possible to speak of the probability for an electron to have wave number \vec{k} at position x outside the metal

$$f_{x\vec{k}} = \frac{1}{e^{\beta(\mathcal{E}_{\vec{k}}^0 + U(x) - \mu)} + 1}. \tag{19.5}$$

Compare with Eq. (17.27). Here it is more convenient to keep μ constant and describe the spatial change in potential through $U(\vec{r})$.

The probability of finding electrons does not vanish as x travels far from the metal. Finding the vacuum full of electrons may seem unacceptable, but is an inevitable consequence of the fact that no solid or liquid can ever be in equilibrium with a vacuum at nonzero temperature. Entropy always favors total evaporation. However, a solid can exist in equilibrium with a dilute vapor of a particular concentration, and that is what Eq. (19.5) implies for the electrons in a metal. The properties of the electron vapor are fixed by the observation that because it is in equilibrium with the metal, the two must have the same chemical potential. Taking “far from the

metal” to denote distances on the order of a micron, the chemical potential must be replaced by the negative of the work function, $\phi = -\mu > 0$. Work functions are typically on the order of several electron volts, as shown in Table 23.2, so for temperatures much less than 10 000 K, Eq. (19.5) can be replaced by

$$f_{x\vec{k}} \approx e^{-\beta(\mathcal{E}_k^0 + U(x) + \phi)}. \quad (19.6)$$

In order to find the current drawn from the metal in the presence of an applied electric field, one should write down the Boltzmann equation and calculate the nonequilibrium function $g_{x\vec{k}}$. However, it is adequate to consider a simple approximation, which is to assume that the electron gas is in equilibrium at all points to the left of x_0 and that all electrons that reach x_0 and are traveling to the right escape over the barrier and run off as a current. This idea predicts a current

$$j = -e \exp \{-\beta[\phi + U(x_0)]\} \int [d\vec{k}] \frac{\hbar k_x}{m} \theta(k_x) e^{-\beta \hbar^2 k^2 / 2m} \quad \text{For } [d\vec{k}], \text{ see Eq. (6.15)}. \quad (19.7)$$

$$= -AT^2 \exp \left\{ -\beta \left[\phi - e\sqrt{e|E|} \right] \right\}, \quad \text{From Eq. (19.4)}. \quad (19.8)$$

where

$$A = \frac{em}{2\pi^2 \hbar^3} k_B^2 = 120.2 \text{ A cm}^{-2} \text{ K}^{-2}. \quad (19.9)$$

Equation (19.8) is called the *Richardson–Dushman* equation when used for $E = 0$, while the reduction of the work function by the square root of an applied field is called the *Schottky* effect. The current does not vanish when the electric field E goes away, which means that if one places a cold grounded plate at some distance from the heated metal and provides a path for the electrons departing from the metal to return to it, current will flow through the vacuum even in the absence of a voltage difference. The factors outside the exponential in Eq. (19.8) are not particularly to be trusted, but the exponential scaling with temperature and electric field can be verified experimentally and can be used to measure the work function ϕ . Equation (19.9) was derived by Schottky (1938), and it provided theoretical underpinning for the development of cathode-ray tube electronics.

19.2.3 Contact Potentials

Whenever two dissimilar materials are brought together, charge moves between them. The reason is that they have in general different work functions, and electrons from the material with the smaller work function rush into the material with the larger one. As this process occurs, charge builds up in the second material, and at some point Coulomb repulsion brings the charge transfer to a halt. The effects of Coulomb repulsion can, however, be minimized if the electrons that flow to the second material are located as close as possible to the (positive) holes flowing to the first material. For this reason, the electrons and holes arrange themselves as surface charges along the interface between the two materials, the electrons on the side of the second material, the holes on the side of the first. Variations on this basic scenario follow mainly from the widths of the regions with surface charge. When two

metals are brought in contact, the regions with excess charge have atomic dimensions. When semiconductors are brought into contact, charge densities are much smaller than in metals, and the length scales over which charges build up turn out to be much larger, as will be shown in Section 19.4.2.

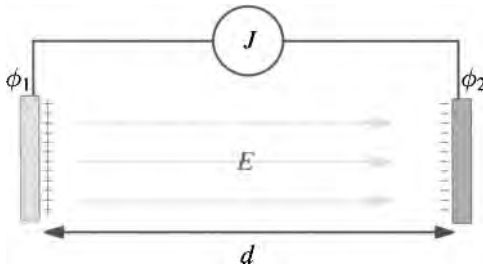


Figure 19.6. Two metals with work functions $\phi_1 < \phi_2$ are arrayed as plates of a capacitor, and charge is allowed to pass between them through an ammeter. By measuring the current J and from it deducing the total charge transferred, the difference between the metals' work functions is determined using Eq. (19.11).

For now, consider the case of two metals in contact. To bring an electron from one metal to its neighbor costs energy ϕ_1 , but recovers energy $-\phi_2$, where ϕ_1 is the work function of the first metal, and ϕ_2 is the work function of the second. Assuming $\phi_2 > \phi_1$, electrons continue to flow from metal 1 to metal 2, until the Coulomb repulsion of the additional charges added to metal 2 cancels out the advantages of the difference in work function. This difference in electrical potential is called a *contact potential*. As shown in Figure 19.6, by using two different metals as two plates of a capacitor and then connecting them with a wire, one can measure the difference in their work functions. Because the metals are arrayed as a capacitor, the electrical potential difference V between them is

$$V = Ed = 4\pi\sigma d, \quad (19.10)$$

where σ is the magnitude of the surface charge on each of the metals, and d is the spacing between them. In equilibrium, the potential energy $-eV$ needed to bring an electron from one plate to another equals the difference in work functions, so

$$\phi_2 - \phi_1 = 4\pi e\sigma d. \quad (19.11)$$

One way to measure the difference in work functions is simply to measure the total current that flows between two metals at known spacing after they are connected by a wire. A more accurate procedure is to find an external potential difference imposed between the two metals so that no current flows when the spacing between the two metals is changed slightly. This potential difference must be just the difference in work functions shown in Eq. (19.11).

Double Layers and Reconstruction. Expressions (19.4) and (19.11) provide relations for metals in contact with vacuum or each other by cleverly evading questions of what happens at short length scales. Equation (19.4) must break down when electrons come within a few angstroms of a metal surface, while Eq. (19.11) should fail when two metals come closer than within a few angstroms of each other. Qualitatively, however, each of them is correct. For angstrom-scale separations between metals, Eq. (19.11) predicts that a *double layer* of charge will build up, with

charge density on the order of $5 \cdot 10^{-3}$ electrons/Å². Compared to the the normal density of electrons along any surface of a metal, this number is not particularly large. However, the electric fields involved are on the order of 1eV/Å, and they are enormous compared to fields normally generated in the laboratory. The double layer of surface charges is a dipole layer, and one can view the work function of a metal generally as arising from the presence of such layers at the surface.

Band structure programs are able to calculate detailed properties of surfaces with a fair degree of success, and they find such quantities as work functions. Early work along these directions was described by Lang (1973) and Appelbaum and Hamann (1976), and a more recent review is given by Zangwill (1988). Because the computer programs depend upon using Bloch's theorem, they must have a periodic crystal in which to carry out the calculations. One solution of this difficulty is to carry out calculations with a unit cell such as depicted in Figure 19.7.

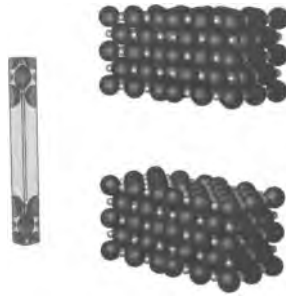


Figure 19.7. Band structure programs study surfaces by creating a unit cell (left) that upon repetition in all directions produces an array of slabs (right). The thicker the slabs, the more realistic an account of surface and bulk states the program can provide. The figure does not show any surface reconstruction, which often occurs and whose analysis is a frequent aim in the calculations.

19.3 Semiconductors

The beginnings of modern electronics lay in the control of current rectification by the cathode-ray diode. However, the cathode-ray tube did not provide the first case in which rectification was observed. It was seen independently by Braun (1874) and by Schuster (1874). Braun conducted experiments in which a crystal such as ferrous sulfide was contacted with a very thin wire, and the resistance was measured as a function of the direction in which current was flowing. Such point junctions do rectify current, although the effect is quite small and had no immediate practical consequences.

The first diodes were produced by placing a whisker of metal in contact with a semiconductor crystal, and are described by Henisch (1957). Early devices could rarely compete with cathode-ray tubes, because they were still comparatively inefficient and unpredictable. In order to make them work at all, it was sometimes necessary to slide the whisker around until a region of good contact was found at

random. The progress of basic research into solid-state physics in the 1930s and late 1940s found the cause of the apparent unpredictability of semiconductors: the presence of certain crucial impurities in extremely small quantities. Once the role of these impurities was understood, and methods developed to control them, diodes and triodes based upon semiconductors took part in a remarkable development that eventually displaced the cathode-ray tubes that had inspired them, and they led electronics to a level of extraordinary complexity.

The discussion will begin with the simplest basic physics, and gradually decorate it with additional effects, until the mechanisms responsible for semiconductor electronics emerge. The starting point is the statistical mechanics of pure semiconductor crystals, followed by statistical mechanics of semiconductor crystals doped with small quantities of impurities, and finally the theory of conductivity in junctions between differently doped semiconductors.

19.3.1 Pure Semiconductors

Preliminaries. Semiconductors are bad insulators. At zero temperature all electrons lie within completely filled valence bands separated from conduction bands by an energy gap of magnitude \mathcal{E}_g . Important features of the bands of silicon, germanium, and gallium arsenide appear in Figure 19.8. One would expect these materials simply to be insulators, except that the energy gap is small, on the order of 2 eV or less. At room temperature the occupation of the conduction band is proportional to

$$e^{-\beta\mathcal{E}_g/2} \sim 10^{-9}. \quad \text{For } \beta = 1/k_B T = 40 \text{ eV}^{-1} \text{ and } \mathcal{E}_g = 1 \text{ eV. The factor of } 1/2 \text{ is a bit surprising, but will emerge from analysis.} \quad (19.12)$$

Because thermal excitation provides exponentially growing numbers of mobile charge carriers, the electrical conductivity of semiconductors grows exponentially

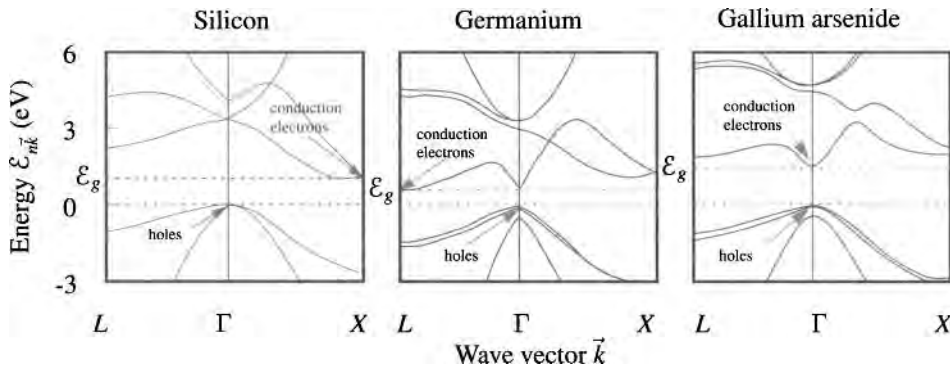


Figure 19.8. Essential features of band structures of silicon, germanium, and gallium arsenide. All have band gaps on the order of 1 eV. The bottom of the conduction band for silicon and germanium does not lie at Γ , so these materials have an indirect gap. Gallium arsenide, by contrast, has a direct gap. These diagrams are extracted from Figures 23.15 and 23.16, which contain information on how they were obtained.

with temperature, in contrast with metals where scattering generally reduces conductivity as temperature goes up. As the band gap \mathcal{E}_g sinks below 1 eV, thermal excitation becomes a sufficiently important source of carriers that the semiconductors conduct at room temperature. More important is the fact that the electrical properties of semiconductors are enormously sensitive to the presence of certain types of impurities, which make their presence felt even at concentrations on the order of one part in 10^{10} . Before the role of impurities was understood, semiconductors seemed capricious and unreliable. Now that they are not only understood but can be controlled, the impurities are employed to give semiconductors tremendously interesting and variable electrical transport properties, with which the electronics industry has developed and grown for over four decades. The word “impurity” connotes something undesirable, so one stops using it in reference to elements intentionally added to semiconductors and refers to “dopants” and “doping” instead.

Band Structure of Semiconductors. Because of the great importance of the energy gap in semiconductors, a few words are in order on how it is measured and calculated. In fact, neither experimental measurement nor theoretical calculation is straightforward. The most precise experimental technique is optical absorption. According to a simple band-theory picture, light falling upon a semiconductor should pass through unimpeded until the energy of a photon is adequate to create an excitation of energy \mathcal{E}_g , after which absorption should rapidly increase. The actual story of what happens in such experiments is sufficiently complex and interesting that it is deferred to Chapters 21 and 22. Some of the effects should, however, be mentioned now.

1. Any transition involving a photon must conserve not only energy but also momentum. The momentum carried by a photon turns out to be negligible compared with that of typical electron states. In Figure 19.8, the lowest-energy spot in the conduction band of silicon lies at about 8/10 of the way toward X , while the highest-energy spot in the valence band lies at Γ . An electron occupying a state near X cannot transfer to Γ simply by emitting a photon. The transition is therefore comparatively rare, with phonons supplying the missing momentum. For this reason, silicon is called an *indirect semiconductor*, as it has an *indirect gap*. Germanium is also an indirect semiconductor, and the bottom of its conduction band lies at L . Many optical applications demand a *direct semiconductor*, where the lowest point of the conduction band lies directly above the highest point of the valence band. For these applications, GaAs is the most important material.
2. Near the band edge, where optical absorption is supposed to vanish, it usually displays one or more thin sharp peaks. These peaks are signatures of *excitons*, which are bound electron–hole pairs whose energy can sit slightly below any states describable in the one-electron picture.
3. Photons whose energy lies below the band gap and out of range of excitons continue to be absorbed, at a rate that decreases exponentially the farther they lie below the band edge. This absorption is due to impurities and fluctuations.

Table 19.1. Semiconductor data

Com- pound	\mathcal{E}_g (eV)	$d\mathcal{E}_g/dT$ (eV/K)	n_i (cm^{-3})	ϵ^0	m_n^* (m)	m_{ph}^* (m)	m_{pl}^* (m)	μ_n ($\text{cm}^2/\text{V s}$)	μ_p ($\text{cm}^2/\text{V s}$)
Si	i 1.11	$-9.0 \cdot 10^{-5}$	$1.02 \cdot 10^{10}$	11.9	1.18	0.54	0.15	1350	480
Ge	i 0.74	$-3.7 \cdot 10^{-4}$	$2.33 \cdot 10^{13}$	16.5	0.55	0.3	0.04	3900	1800
GaAs	d 1.43	$-3.9 \cdot 10^{-4}$	$2 \cdot 10^6$	12.5	0.067	0.50	0.07	7900	450
SiC	i 2.2	$-5.8 \cdot 10^{-4}$		9.7	0.82	1		900	50
AlAs	i 2.14	$-4 \cdot 10^{-4}$	$2 \cdot 10^{17}$	10.0	0.5	0.5	0.26	294	
AlSb	i 1.63	$-4 \cdot 10^{-4}$		12.0	0.3	1	0.5	200	400
GaN	d 3.44	$-6.7 \cdot 10^{-4}$	$2 \cdot 10^{17}$	12.0	0.3	1		440	
GaSb	d 0.7	$-3.7 \cdot 10^{-4}$	10^{14}	15.7	0.05	0.3	0.04	7700	1600
InP	d 1.34	$-2.9 \cdot 10^{-4}$	$1.2 \cdot 10^8$	15.2	0.073	0.6	0.12	5400	150
InAs	d 0.36	$-3.5 \cdot 10^{-4}$	$1.3 \cdot 10^{15}$	15.2	0.027	0.4	0.03	30 000	450
InSb	d 0.18	$-2.8 \cdot 10^{-4}$	$2.0 \cdot 10^{16}$	16.8	0.013	0.4	0.02	77 000	850

Data on whether a compound has a direct (d) or indirect (i) gap, energy gap, static dielectric constant, effective masses, and mobilities, for some semiconductors. The electron effective mass m_n^* is the density of states effective mass defined in Eq. (19.23). The data refer to room temperature, and to samples with donor and acceptor impurities at densities of 10^{15} cm^{-3} or less. Source: Landolt and Börnstein (New Series) vol. 17 and Pierret (1996).

Despite these experimental complications the experimental determination of band gaps can be made rather precisely. Not only the energy gap, but also the structure of the energy bands in the neighborhood of valence band maxima and conduction band minima, is important. One can fit the energy to a quadratic form and write

$$\mathcal{E}_{\vec{k}} = \mathcal{E}_c + \frac{\hbar^2}{2} \vec{k}^* \mathbf{M}^{-1} \vec{k} \quad \text{For electrons in the conduction band.} \quad (19.13a)$$

$$\mathcal{E}_{\vec{k}} = \mathcal{E}_v - \frac{\hbar^2}{2} \vec{k}^* \mathbf{M}^{-1} \vec{k}, \quad \text{For holes in the valence band.} \quad (19.13b)$$

where \mathbf{M} is the effective mass tensor. For silicon, germanium, and gallium arsenide, the bands at the valence maximum would be threefold degenerate in the absence of spin. The spin-orbit interaction splits off one of the bands, leaving two above it that still are degenerate at Γ . The two bands have, however, different curvatures near Γ , leading to *heavy holes* (low curvature) and *light holes* (high curvature), both of which contribute to the transport properties of semiconductors. Because of the great degree of symmetry associated with Γ , the energy surfaces of these holes are spherically symmetrical, and the effective mass tensors are multiples of the unit matrix.

The conduction band minimum in gallium arsenide is nondegenerate and spherical. In silicon and germanium, the conduction band minima are quite anisotropic, and consist in a number of symmetrically arrayed pockets of electrons, as shown in Figure 19.9. The effective mass tensors have been measured by the technique of cyclotron resonance, to be discussed in Section 21.2.

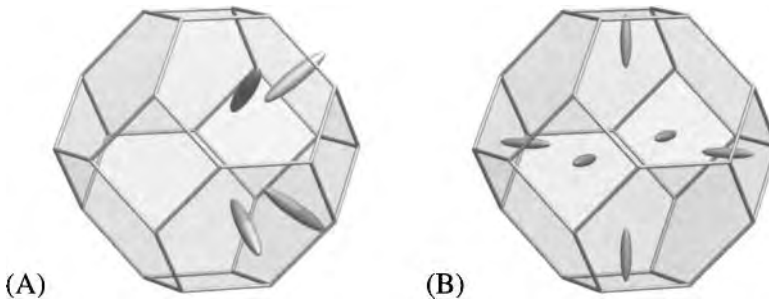


Figure 19.9. (A) The conduction band minima in germanium lie along (111) and straddle the zone boundary, producing four inequivalent pockets of electrons with a highly anisotropic effective mass. (B) In silicon, the conduction band minima lie 8/10 of the way toward (100), producing six pockets of electrons, but only three with distinct symmetries.

19.3.2 Semiconductor in Equilibrium

Electron and Hole Densities. In equilibrium, the numbers of mobile charge carriers in a semiconductor are given by the Fermi function. The volume density of electrons n above the conduction band edge is given by

$$n = \int_{\mathcal{E}_c}^{\infty} d\mathcal{E} D(\mathcal{E}) \frac{1}{e^{\beta(\mathcal{E}-\mu)} + 1}, \quad (19.14)$$

while the density of holes p below the valence band edge is

$$p = \int_{-\infty}^{\mathcal{E}_v} d\mathcal{E} D(\mathcal{E}) \left\{ 1 - \frac{1}{e^{\beta(\mathcal{E}-\mu)} + 1} \right\} \quad (19.15a)$$

$$= \int_{-\infty}^{\mathcal{E}_v} d\mathcal{E} D(\mathcal{E}) \frac{1}{e^{-\beta(\mathcal{E}-\mu)} + 1}. \quad (19.15b)$$

Nondegenerate Semiconductors. These expressions simplify for a *nondegenerate semiconductor*, which is one for which the probability of occupying states near the band edge is exponentially small: that is,

$$\mathcal{E}_c - \mu \gg k_B T \quad \text{and} \quad \mu - \mathcal{E}_v \gg k_B T. \quad \text{A practical criterion is } \mathcal{E}_c - \mu > 3k_B T. \quad (19.16)$$

When these conditions hold, the semiconductor is quite different from most metals. Whereas in metals carrier concentrations are on the order of 10^{22} electrons per cubic centimeter, for nondegenerate semiconductors carrier concentrations are on the order of 10^{19} cm^{-3} or less. Whether a semiconductor lies in the nondegenerate limit or not will depend upon the density of dopants (impurities) added to it. In semiconductor devices, dopant densities are frequently great enough to cause violation of inequalities (19.16). Nevertheless, the nondegenerate limit is of great utility because the transport properties of semiconductor devices are largely determined by the regions with light doping, while the regions with heavy doping act like short circuits and can often be ignored.

Given conditions (19.16), the Fermi functions (19.14) and (19.15) can be replaced by Boltzmann factors, and the equations for electron and hole concentration in the nondegenerate case become

$$n = \mathcal{N}_c e^{-\beta(\mathcal{E}_c - \mu)}, \quad p = \mathcal{N}_v e^{-\beta(\mu - \mathcal{E}_v)} \quad (19.17)$$

with

$$\mathcal{N}_c = \int_{\mathcal{E}_c}^{\infty} d\mathcal{E} D(\mathcal{E}) e^{-\beta(\mathcal{E} - \mathcal{E}_c)} \quad (19.18a)$$

$$\mathcal{N}_v = \int_{-\infty}^{\mathcal{E}_v} d\mathcal{E} D(\mathcal{E}) e^{-\beta(\mathcal{E}_v - \mathcal{E})}. \quad (19.18b)$$

Effective Masses. With reasonable approximations, one can calculate \mathcal{N}_c and \mathcal{N}_v . It is not sufficient to take the density of states $D(\mathcal{E})$ just to be a constant. In Eq. (19.18) the exponential factor places heavy emphasis on states just at the edges of the bands where the density of states vanishes, so there is an interplay between the two terms in the integrand. Still, only states within a narrow strip near the valence maximum or conduction minimum are important, and one can use the quadratic approximations (19.13) to evaluate the density of states. For the conduction band, one has

$$D(\mathcal{E}) = \int [d\vec{k}] \delta\left(\mathcal{E} - \mathcal{E}_c - \frac{1}{2} \hbar^2 \vec{k}^* \mathbf{M}^{-1} \vec{k}\right) \quad \text{For } [d\vec{k}], \text{ see Eq. (6.15).} \quad (19.19)$$

$$= \int [d\vec{k}] \delta\left(\mathcal{E} - \mathcal{E}_c - \frac{1}{2} \hbar^2 \sum_l k_l^2 / m_l\right). \quad \begin{array}{l} \text{Changing to a } \vec{k} \text{ basis in which } \mathbf{M} \\ \text{is diagonal, with elements } m_l. \end{array} \quad (19.20)$$

Defining

$$m_n^* = [m_1 m_2 m_3]^{1/3} \quad \text{and} \quad \vec{q} = (k_1 / \sqrt{m_1}, k_2 / \sqrt{m_2}, k_3 / \sqrt{m_3}) \quad (19.21)$$

gives

$$D(\mathcal{E}) = 2 \int m_n^{*3/2} \frac{d\vec{q}}{(2\pi)^3} \delta\left(\mathcal{E} - \mathcal{E}_c - \frac{1}{2} \hbar^2 q^2\right) \quad (19.22)$$

$$= \sqrt{2(\mathcal{E} - \mathcal{E}_c)} \frac{m_n^{*3/2}}{\hbar^3 \pi^2} \mathcal{M}_c. \quad \begin{array}{l} \text{Where } \mathcal{M}_c \text{ is the number of} \\ \text{symmetrically equivalent minima in the} \\ \text{conduction band, equaling six for} \\ \text{silicon and eight for germanium.} \end{array} \quad (19.23)$$

Because m_n^* is defined so as to bring the density of states $D(\mathcal{E})$ into a simple form, it is called the *density of states effective mass*; experimental values for several semiconductors appear in Table 19.1. In the case of holes, one can repeat the steps leading to Eq. (19.23) for heavy and light holes separately and define $m_p^{*3/2}$ to be the sum $(m_{pl}^*)^{3/2} + (m_{ph}^*)^{3/2}$ of the light and heavy effective hole masses. Then

$$\mathcal{N}_c = \frac{1}{4} \left(\frac{2m_n^* k_B T}{\pi \hbar^2} \right)^{3/2} \mathcal{M}_c \quad (19.24a)$$

$$\mathcal{N}_v = \frac{1}{4} \left(\frac{2m_p^* k_B T}{\pi \hbar^2} \right)^{3/2}. \quad (19.24b)$$

In order to find equilibrium densities of electrons and holes from Eq. (19.17), one needs to determine the chemical potential μ . However, there is a convenient relation independent of it, the *law of mass action*, obtained by multiplying together the expressions for n and p , to find

$$np = \mathcal{N}_c \mathcal{N}_v e^{-\beta \mathcal{E}_g}. \quad \text{The energy gap } \mathcal{E}_g = \mathcal{E}_c - \mathcal{E}_v. \quad (19.25)$$

19.3.3 Intrinsic Semiconductor

An *intrinsic semiconductor* is a pure single crystal. For every electron excited into the conduction band, a hole must be left behind in the valence band, so the intrinsic electron density n_i is

$$n_i = \sqrt{\mathcal{N}_c \mathcal{N}_v} e^{-\beta \mathcal{E}_g/2} \quad \text{From Eq. (19.25), setting } n = p. \quad (19.26a)$$

$$= 2.510 \cdot 10^{19} \text{ cm}^{-3} \left(\frac{m_n^* m_p^*}{m^2} \right)^{3/4} \mathcal{M}_c^{1/2} \left(\frac{T}{300 \text{ K}} \right)^{3/2} e^{-\beta \mathcal{E}_g/2}. \quad (19.26b)$$

Solving Eq. (19.17) for the chemical potential gives immediately the intrinsic chemical potential μ_i

$$\mu_i = k_B T \ln \frac{n_i}{\mathcal{N}_c} + \mathcal{E}_c = \mathcal{E}_v + \frac{\mathcal{E}_g}{2} + \frac{3}{4} k_B T \ln(m_p^*/m_n^*) - \frac{1}{2} k_B T \ln \mathcal{M}_c. \quad (19.27)$$

Table 19.2. Binding energies of common donors and acceptors in some semiconductors at room temperature

		Group V donors, $\mathcal{E}_c - \mathcal{E}_d$ (meV)								
Host	Eq. (18.23)	N	P	As	Sb	Bi				
Si	113	140	45	53.7	42.7	70.6				
Ge	28		12.9	14.2	10.3	12.8				
		Group III acceptors, $\mathcal{E}_a - \mathcal{E}_v$ (meV)								
Host	Eq. (18.23)	B	In	Ga	Al	Tl				
Si	48	45	155	74	67	25				
Ge	15	9.73	12.0	11.3	10.8	13.5				
		Donors, $\mathcal{E}_c - \mathcal{E}_d$ (meV)								
Host	Eq. (18.23)	Pb	Se	Si	S	Ge	C			
GaAs	5.8	5.8	5.8	5.8	5.9	5.9	5.9			
		Acceptors, $\mathcal{E}_a - \mathcal{E}_v$ (meV)								
Host	Eq. (18.23)	Be	Mg	Zn	Cd	C	Si	Ge	Sn	Mn
GaAs	23	28	29	31	35	27	35	40	167	113
InP	21	31	31	46	57	41		210		270

Apart from the case of donors in GaAs, the simple theory of Eq. (18.23) gives no more than the order of magnitude of the binding energy. Improvements on the theory, more properly incorporating anisotropy of the effective mass, and corrections due to the strong potential in the central cell near the impurity are discussed by Yu and Cardona (1996), Chapter 4. Source: Landolt and Börnstein (New Series), vol. 17.

The logarithm in Eq. (19.27) is of order unity or even zero if holes and electrons have the same effective mass, so because $k_B T \sim 1/40$ eV at room temperature and band gaps are around 1 eV for semiconductors, the chemical potential sits smack in the middle of the band gap. Thus it cooperates in enforcing (19.17), making the semiconductor as nondegenerate as possible by staying away from the band edges.

Compact Expressions. Combining Eqs. (19.26) and (19.25) puts the law of mass action in the general compact form

$$np = n_i^2 \quad (19.28)$$

and allows rewriting Eqs. (19.17) for electron and hole densities as

$$n = n_i e^{-\beta(\mu_i - \mu)}, \quad p = n_i e^{-\beta(\mu - \mu_i)}. \quad (19.29)$$

19.3.4 Extrinsic Semiconductor

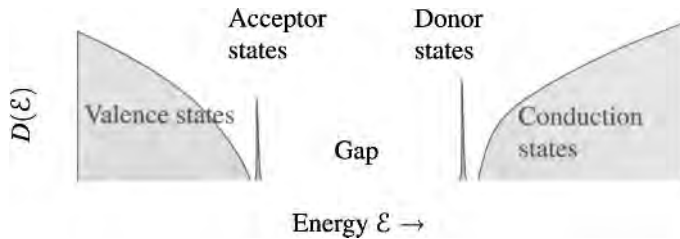


Figure 19.10. The effect of adding donors to a semiconductor is to create a population of bound states sitting just below the conduction band, while adding acceptors creates bound states just above the valence band. At room temperature, almost all the bound states break apart; each donor gives an electron to the conduction band, while each acceptor gives a hole to the valence band.

When certain sorts of impurities are used to dope a semiconductor, the physics changes rather dramatically. The most interesting impurities are noncompensated, lying one column to the right or one column to the left of a semiconductor in the periodic table. Examples of common dopants appear in Table 19.2. As discussed in Section 18.3, addition of these impurities creates a population of bound states. Atoms from column V added to a semiconductor of column IV create states just below the conduction band edge called donors, while atoms from column III added to a semiconductor of column IV create states just above the valence band edge called acceptors (Figure 19.10). However, at room temperature, these bound states are not occupied; they are almost completely ionized. Thus the practical effect of adding a donor is to add a single mobile electron, while the practical effect of adding an acceptor is to add a single mobile hole.

The energies in Table 19.2 do not make it obvious that impurity states should be ionized completely. The thermal energy at room temperature is around 25 meV, which is at best comparable to the binding energies. It is entropy more than energy that ionizes the impurities. For the purposes of a rough estimate, let the density

of impurity sites per volume be \mathcal{N}_d , and denote by \mathcal{N}_c the density of conduction states per volume into which an electron could choose to move. In a system of volume \mathcal{V} , the number of different ways to arrange electrons originally bound on the impurities among the conduction states is roughly $(\mathcal{N}_c/\mathcal{N}_d)^{\mathcal{V}\mathcal{N}_d}$, leading to entropy $k_B \mathcal{V} \mathcal{N}_d \ln \mathcal{N}_c/\mathcal{N}_d$. Therefore the temperature at which ionization occurs is not $k_B T \approx \mathcal{E}_b$, but $k_B T \ln \mathcal{N}_c/\mathcal{N}_d \approx \mathcal{E}_b$. The fewer impurities there are, the more mobile their electrons become. In practice, for doping levels of $\mathcal{N}_d \leq 10^{18} \text{ cm}^{-3}$, ionization is probably complete, but if doping rises higher the approximation must be checked, because $\mathcal{N}_c \approx 10^{22} \text{ cm}^{-3}$.

Verifying these claims requires a simple statistical calculation. Consider a crystal with a valence band, a conduction band lying at energy $\mathcal{E}_g = \mathcal{E}_c - \mathcal{E}_v$ higher, and donor states with maximum binding energy \mathcal{E}_d just below the bottom of the conduction band. Because the impurity potential is weak, the probability of an electron being trapped in anything but the “ground state” of the effective hydrogen atom problem is negligible. In addition to occupying the conduction and valence bands, electrons can also occupy the donor bound states. The donor occupation number can be zero, and the donor can trap an electron with either spin up or spin down, but it cannot bind simultaneously two electrons of opposite spin. Therefore, in the grand canonical ensemble conventionally used for the Fermi gas, the occupation probability f_d of the donor levels is

$$f_d = \frac{0 \times 1 + 1 \times 2 \times e^{-\beta(\mathcal{E}_d - \mu)}}{1 + 2 \times e^{-\beta(\mathcal{E}_d - \mu)}} \quad (19.30)$$

$$= \frac{1}{1 + \frac{1}{2} e^{\beta(\mathcal{E}_d - \mu)}} \ll 1. \quad (19.31)$$

Equation (19.38) will show that μ lies typically in the middle of the gap, so that at room temperature $\mathcal{E}_d - \mu$ is much larger than $k_B T$, and f_d is nearly zero.

Similarly, if acceptor impurities are placed at an energy \mathcal{E}_a above the valence band, the probability that a hole, spin up or spin down, will be localized on them is

$$f_a = \frac{1}{\frac{1}{4} e^{\beta(\mu - \mathcal{E}_a)} + 1} \ll 1. \quad (19.32)$$

The factor of 1/4 appears in the denominator because the valence maximum is fourfold degenerate, including spin degeneracy. Again, Eq. (19.38) shows that typically this occupation number is much less than 1.

The way that entropy ionizes impurities is hidden in the value of the chemical potential, and the chemical potential is determined simply by the total number of mobile electrons. Suppose that a density of \mathcal{N}_d donors per volume is added to the semiconducting crystal, which otherwise contains n_t electrons per volume in the valence and conduction bands. The total density of electrons is then

$$n_t + \mathcal{N}_d = \int_{\mathcal{E}_c} d\mathcal{E} D(\mathcal{E}) \frac{1}{1 + e^{\beta(\mathcal{E} - \mu)}} + \int^{\mathcal{E}_v} d\mathcal{E} D(\mathcal{E}) \frac{1}{1 + e^{\beta(\mathcal{E} - \mu)}} + \mathcal{N}_d f_d. \quad (19.33)$$

Because the integral of $D(\mathcal{E})$ over the valence band gives n_t , and assuming f_d is negligible,

$$\mathcal{N}_d = \int_{\mathcal{E}_c} d\mathcal{E} D(\mathcal{E}) \frac{1}{1 + e^{\beta(\mathcal{E} - \mu)}} - \int^{\mathcal{E}_v} d\mathcal{E} D(\mathcal{E}) \frac{1}{1 + e^{\beta(\mathcal{E} - \mu)}} \quad (19.34)$$

$$\Rightarrow \mathcal{N}_d = n - p = n_i e^{-\beta(\mu_i - \mu)} - n_i e^{-\beta(\mu - \mu_i)}. \quad (19.35)$$

When both donors and \mathcal{N}_a acceptors per volume are present, then similarly

$$n - p = \mathcal{N}_d - \mathcal{N}_a. \quad (19.36)$$

Using the law of mass action Eq. (19.28), one now easily solves for n and p , and finds

$$n = \frac{1}{2}[\mathcal{N}_d - \mathcal{N}_a] + \frac{1}{2} [(\mathcal{N}_d - \mathcal{N}_a)^2 + 4n_i^2]^{1/2} \quad (19.37a)$$

$$p = \frac{1}{2}[\mathcal{N}_a - \mathcal{N}_d] + \frac{1}{2} [(\mathcal{N}_d - \mathcal{N}_a)^2 + 4n_i^2]^{1/2}. \quad (19.37b)$$

To check that everything is consistent, one needs to make sure that the chemical potential is in fact in the middle of the gap, making f_d and f_a small. From Eq. (19.29)

$$n - p = 2n_i \sinh \beta(\mu - \mu_i) \Rightarrow \mu = \mu_i + k_B T \sinh^{-1} ([\mathcal{N}_d - \mathcal{N}_a]/2n_i). \quad (19.38)$$

Thus dopants must exceed by many orders of magnitude the intrinsic carrier density before the chemical potential departs far enough from the center of the gap to endanger the conditions for nondegeneracy in (19.16).

Equation (19.37) simplifies when $\mathcal{N}_d \gg \mathcal{N}_a$, and it becomes

$$n \approx \mathcal{N}_d \quad \text{The number of mobile electrons is essentially the number of donors.} \quad (19.39a)$$

$$p \approx \frac{n_i^2}{\mathcal{N}_d}. \quad \text{Holes are the minority carrier.} \quad (19.39b)$$

There is a similar result when the number of acceptors exceeds the number of donors; in this case,

$$p \approx \mathcal{N}_a \quad \text{The number of mobile holes is essentially the number of acceptors.} \quad (19.40a)$$

$$n \approx \frac{n_i^2}{\mathcal{N}_a}. \quad \text{Electrons are the minority carrier.} \quad (19.40b)$$

19.4 Diodes and Transistors

The first semiconductor device was the *point-contact rectifier* or *Schottky diode*, in which a metal whisker was placed against a semiconducting crystal. The contact of metal with semiconductor remains an important element in electronic design, and it is worth understanding the conditions under which this junction rectifies current.

Ideal Schottky Diode. Suppose that an ideal contact between semiconductor and metal is possible, in which the atoms of the metal join seamlessly with those of the semiconductor. Such a joint is actually extremely difficult to create in practice for numerous reasons. Immediately after cleaving, semiconductor surfaces acquire oxide layers; any sort of mechanical polishing produces surfaces that are far from atomically flat; and even conventional molecular beam epitaxy often fails to lay

metal smoothly down upon a semiconductor surface, producing instead blobs and islands. Nevertheless, suppose that a smooth contact has been achieved. After examining this ideal case, the consequences of a defective interface will also be mentioned.

Figure 19.11 shows the equilibrium behavior of an n -doped semiconductor brought into contact with a metal. The work function of the semiconductor is taken to be less than the work function of the metal; if the reverse is the case, the junction may have little or no rectifying power, and the contact is called *ohmic*, as in Problem 2. Because of the higher chemical potential, electrons rush from the semiconductor to the metal, lowering the voltage of the metal until electrostatic forces prevent further motion of charge. The resulting potential profile is depicted in the lower parts of Figure 19.11. The representation of the junction in Figure 19.11 explains why the electrostatic potential is said to cause *band bending*.

When an external voltage V_A is applied to raise the metal relative to the semiconductor, the situation changes qualitatively as in Figure 19.12(A). The barrier for

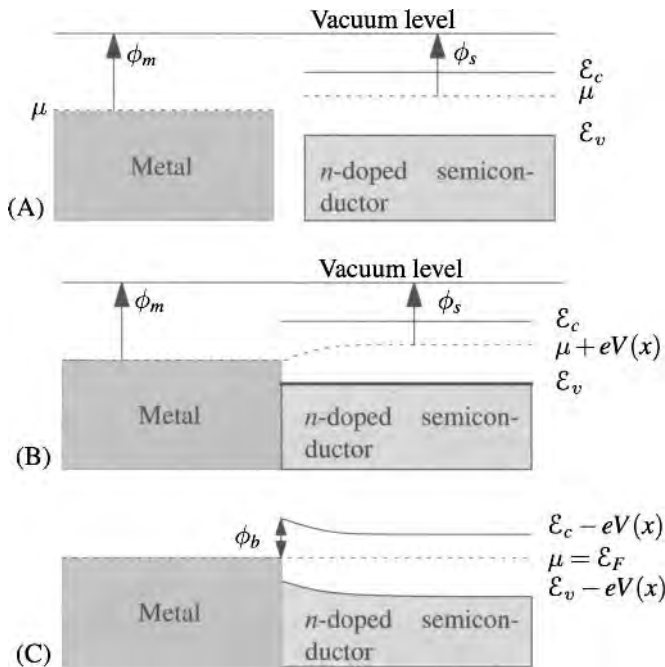


Figure 19.11. (A) In the first instant that a metal and semiconductor are brought together, their chemical potentials do not coincide. (B) Very quickly, however, charge moves from the solid with higher chemical potential to the one with lower chemical potential—in this case, from the n -doped semiconductor to the metal—until the rise in voltage of the semiconductor compensates for the difference in chemical potential. (C) The customary representation of the potentials experienced by the electrons and holes shows the chemical potential μ as constant, and it adds the electrostatic potential $-eV$ to the conduction and valence band levels. The bands have been bent by the potentials which form across the junction. The chemical potential is often referred to as the Fermi energy \mathcal{E}_F .

electrons is lowered, and the electrons flow into the metal from the semiconductor as a current. However, if the voltage changes in the opposite fashion, as in Figure 19.12(B), the barrier seen by electrons in the metal does not change, and therefore current does not increase in the opposite direction.

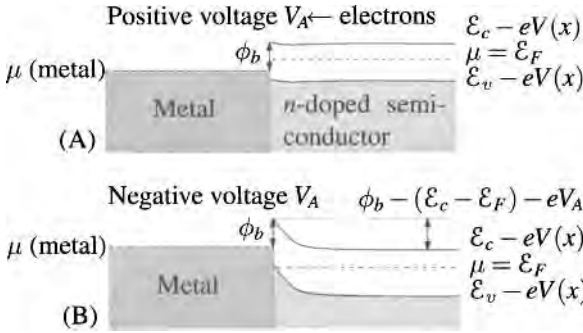


Figure 19.12. (A) When the voltage of the metal is raised relative to the semiconductor by eV_A , electrons flow to the metal. (B) However, when the voltage of the metal is lowered, the barrier perceived by the electrons does not change, and little current flows.

Quantitative Theory. The quantitative theory for rectification in the Schottky diode is almost identical to the theory of thermionic emission from metals. The electrons in the semiconductor with enough energy to travel to the metal are those in the conduction band whose velocity toward the metal is large enough that they can cross the barrier between semiconductor and metal. According to Figures 19.11(C), and 19.12, the height of this barrier in the presence of an applied voltage V_A is $\phi_b - (\mathcal{E}_c - \mu) - eV_A$, so the condition is

$$\frac{\hbar^2 k_x^2}{2m_n^*} > \phi_b - (\mathcal{E}_c - \mu) - eV_A. \quad \text{Using the density of states effective mass in an approximation for the (anisotropic) kinetic energy.} \quad (19.41)$$

The current density $j_{s \rightarrow m}$ due to this collection of electrons is

$$j_{s \rightarrow m} = \int [d\vec{k}] \theta\left(\frac{\hbar^2 k_x^2}{2m_n^*} - [\phi_b - (\mathcal{E}_c - \mu) - eV_A]\right) \frac{e\hbar k_x}{m_n^*} e^{-\beta(\hbar^2 k^2/2m_n^* + \mathcal{E}_c - \mu)} \quad (19.42)$$

Using the nondegenerate limit of the Fermi function and assuming the electrons to travel in the $-x$ direction, with the minus canceling the sign of the charge. $[d\vec{k}]$ defined in Eq. (6.15).

$$= \frac{2}{(2\pi)^3} \frac{2m_n^* \pi k_B T}{\hbar^2} \frac{e}{\hbar} \int_{\phi_b - \mathcal{E}_c + \mu - eV_A}^{\infty} d\left(\frac{\hbar^2 k_x^2}{2m_n^*}\right) e^{-\beta(\hbar^2 k_x^2/2m_n^* + \mathcal{E}_c - \mu)} \quad (19.43)$$

Doing the integrals over k_y and k_z .

$$= \frac{m_n^*}{m} AT^2 \exp\{-\beta[\phi_b - eV_A]\}. \quad \mathcal{A} = 120 \text{ A K}^{-2} \text{ cm}^{-2} \text{ was given in Eq. (19.9).} \quad (19.44)$$

When $V_A = 0$, the reverse current $j_{m \rightarrow s}$ flowing from metal to semiconductor must equal the one calculated in Eq. (19.44), and because the barrier seen from the metal does not change with V_A , the current flowing in this reverse direction will be independent of applied voltage. So the total current in the junction is

$$j = \frac{m_n^*}{m} AT^2 [\exp\{-\beta[\phi_b - eV_A]\} - \exp\{-\beta\phi_b\}]. \quad (19.45)$$

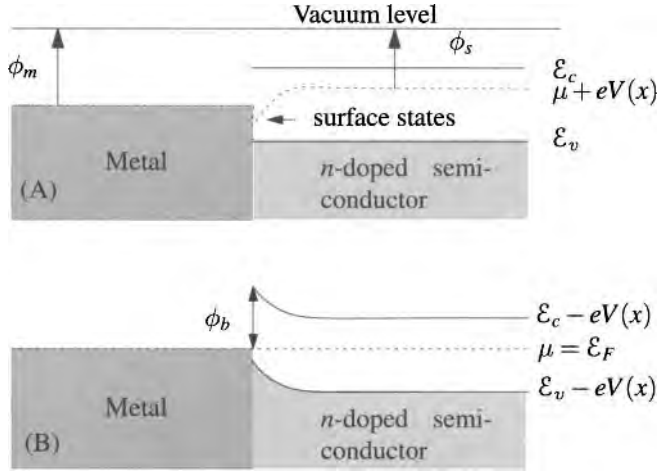


Figure 19.13. Effect of surface states on metal–semiconductor junction. (A) The electrochemical potential $\mu + eV$ at the surface of the semiconductor is fixed at a particular location in the gap independent of doping. (B) The bands are bent so that the barrier between metal and semiconductor is a constant ϕ_b that depends mainly upon properties of the semiconductor surface, and only slightly upon either metal or semiconductor work functions.

19.4.1 Surface States

Experimental measurements confirm Eq. (19.45), but with one troubling discrepancy. The constant ϕ_b does not equal $\phi_m - \phi_s + (\mathcal{E}_c - \mu)$ as it should according to Figure 19.11, and it is almost independent of the metal or doping level of the semiconductor involved in the contact. For example, *n*-type GaAs almost always appears to have $\phi_b \approx 2\mathcal{E}_g/3 = 0.95\text{eV}$, while *p*-type GaAs almost always appears to have $\phi_b \approx \mathcal{E}_g/3 = 0.47\text{eV}$. The explanation, proposed by Bardeen (1947), is that the surface of the semiconductor joins the metal in a rough fashion. At the interface there is a high density (10^{15} cm^{-2}) of *dangling bonds*—that is, atoms eagerly expecting to join onto neighbors to form a perfect diamond lattice, but frustrated by the presence of the surface. It is energetically favorable to steal charge from the nearby bulk and to place electrons on the dangling bonds, leaving a positively charged region several hundred angstroms thick below the semiconductor surface. In addition, there is a large density of propagating surface states with energies lying right within the gap and localized states due to defects. A schematic representation of the consequences for energy bands appears in Figure 19.13. When the metal and semiconductor come into contact, the chemical potentials equilibrate as charge moves from the metal into the surface states, creating a dipole layer at the interface. Because the charge density needed to create this layer is often small compared to the density of dangling bonds, the space charge distribution within the semiconductor is not much altered by the approach of the metal.

Semiconductor electronics avoids the problem of surface states by building junctions out of single crystals. Instead of preparing two separately doped crystals,

polishing the surfaces, and gluing them together, the dopants are injected into a single sample at desired locations, either as an ion beam or by diffusion.

19.4.2 Semiconductor Junctions

Junction in Equilibrium. Consider a junction between an n -doped and a p -doped region. Electrons move from the n -type region to the p -type region until charge buildup cancels out the advantage of populating lower energy levels. Figures 19.14 and 19.15 help in visualizing why.

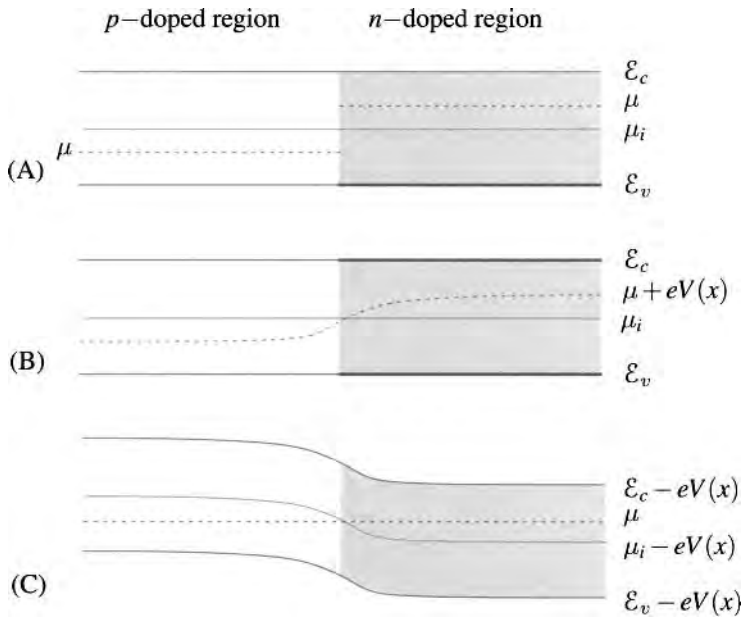


Figure 19.14. (A) In the first instant that n - and p -doped semiconductors are brought together, their chemical potentials do not coincide. (B) Therefore, electrons move from the region with higher chemical potential into the region with lower chemical potentials leaving holes behind. As electrons move in and holes move out, the voltage of the p -doped region begins to decrease, while that of the n -doped region begins to increase, raising the electrostatic potential energy of the electrons and holes. When the ensemble comes to equilibrium, the electrochemical potential $\mu + eV$ has the form depicted. (C) The customary representation of the potentials experienced by the electrons and holes shows the chemical potential μ as constant, and it adds the electrostatic potential $-eV$ to the conduction and valence band levels. The bands have been bent by the potentials that form across the junction.

To obtain a quantitative theory, observe that in the presence of an electrical potential $V(x)$, the densities of electrons n and holes p in a nondegenerate semiconductor are given by

$$n(x) = n_i e^{\beta(\mu + eV(x) - \mu_i)} \quad \text{Generalize Eqs. (19.29) to include spatial variations; valid if spatial gradients are small enough that the semiconductor is locally in equilibrium.} \quad (19.46a)$$

$$p(x) = n_i e^{\beta(\mu_i - eV(x) - \mu)}. \quad (19.46b)$$

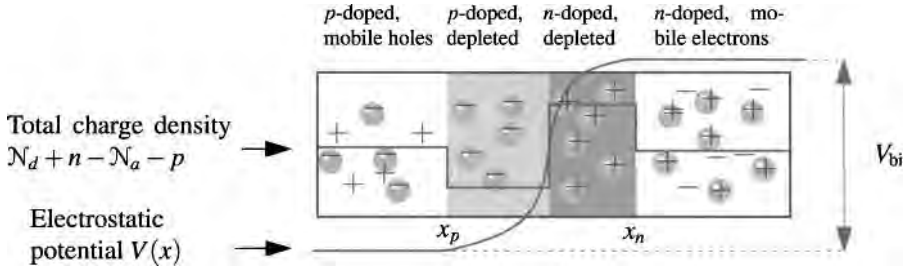


Figure 19.15. Illustration of the redistribution of mobile charges near a p - n junction. The mobile carriers abandon the region between x_n and x_p , leaving nonzero ionic charge density behind.

Far to the left of the junction ($x \rightarrow -\infty$), on the p -doped side, the total charge density must vanish, which requires $p = N_a$. Similarly, $n = N_d$ far to the right of the junction ($x \rightarrow \infty$). Multiplying Eq. (19.46a) for $x \rightarrow \infty$ by Eq. (19.46b) for $x \rightarrow -\infty$ gives

$$n(\infty)p(-\infty) = N_d N_a = n_i^2 e^{\beta(eV(\infty) - eV(-\infty))} \tag{19.47}$$

$$\Rightarrow eV_{bi} \equiv e[V(\infty) - V(-\infty)] \tag{19.48}$$

$$= k_B T \ln \frac{N_d N_a}{n_i^2} = \mathcal{E}_g + k_B T \ln \left[\frac{N_d N_a}{N_c N_v} \right], \tag{19.49}$$

where V_{bi} is the *built-in voltage* across the junction, an intrinsic potential difference due to the fact that the electrons of the n -doped region combine with the holes of the p -doped region.

Charge Distribution. Real junctions have complicated three-dimensional forms, but the essential features are captured in a one-dimensional calculation, as a function of the spatial index x . The tricky part of the calculation comes from the fact that the potential $V(x)$ is produced by the charge densities $n(x)$ and $p(x)$, so the problem must be solved self-consistently, using Poisson’s equation. The charge density is the sum of a number of terms. The impurity states are fully ionized, leaving behind charged ions that contribute

$$en_{ions} = e[N_d(x) - N_a(x)]. \tag{19.50}$$

In addition, one has to consider the contributions from the electrons $n(x)$ in the conduction band and the holes $p(x)$ in the valence band, so Poisson’s equation reads

$$\frac{\partial^2 V}{\partial x^2} = -4\pi e [N_d(x) - n(x) - N_a(x) + p(x)] / \epsilon^0, \tag{19.51}$$

with ϵ^0 the dielectric constant.

For the junction depicted in Figure 19.15 there is an abrupt transition between an n -type semiconductor and a p -type semiconductor, so

$$N_a(x) = N_a \theta(-x) \quad \theta(x) \text{ is a Heaviside step function.} \tag{19.52a}$$

$$N_d(x) = N_d \theta(x). \tag{19.52b}$$

Junctions are not actually infinitely sharp, but they can certainly be less than 100 Å, which is going to be the scale of the *depletion regions* in which charge builds up.

Equation (19.46) shows that once the potential begins to deviate from its value at infinity, the number of carriers n or p drops below \mathcal{N}_d or \mathcal{N}_a like a stone. It is therefore reasonable to construct an approximation in which the charge density is zero everywhere up to $x_p < 0$, at which point the charge density abruptly changes to $-e\mathcal{N}_a$. At $x = 0$ the charge density rises to $e\mathcal{N}_d$, and finally at some $x_n > 0$, it falls abruptly back to zero. The potential produced by such a charge density is

$$V(x) = \begin{cases} V(-\infty) & \text{for } x < x_p \\ V(-\infty) + 2\pi e \frac{\mathcal{N}_a}{\epsilon_0} (x - x_p)^2 & \text{for } 0 > x > x_p \\ V(\infty) - 2\pi e \frac{\mathcal{N}_d}{\epsilon_0} (x - x_n)^2 & \text{for } 0 < x < x_n \\ V(\infty) & \text{for } x > x_n. \end{cases} \quad (19.53)$$

Equation (19.53) is obviously a solution of Eq. (19.51), and the only thing left to check is that the solution and its first derivative are continuous at $x = 0$. Continuity of (19.53) at 0 demands that

$$V(-\infty) + 2\pi e \frac{\mathcal{N}_a}{\epsilon_0} x_p^2 = V(\infty) - 2\pi e \frac{\mathcal{N}_d}{\epsilon_0} x_n^2, \quad (19.54)$$

while continuity of the derivative requires that

$$\mathcal{N}_d x_n = -\mathcal{N}_a x_p. \quad (19.55)$$

Solving Eq. (19.54) and Eq. (19.55) for the lengths x_n and x_p gives

$$x_n = \sqrt{\frac{\epsilon_0 \mathcal{N}_a V_{bi}}{2\pi e \mathcal{N}_d [\mathcal{N}_a + \mathcal{N}_d]}} \quad (19.56a)$$

$$x_p = -\sqrt{\frac{\epsilon_0 \mathcal{N}_d V_{bi}}{2\pi e \mathcal{N}_a [\mathcal{N}_a + \mathcal{N}_d]}} \quad (19.56b)$$

using again the built-in voltage V_{bi} defined in Eq. (19.48). Placing typical numerical values into Eq. (19.56), dopant densities on the order of 10^{18} cm^{-3} , and potential differences eV_{bi} on the order of 0.1 eV gives depletion layers on the order of a few hundred angstroms. Because the depletion region has no mobile charge, its resistance is considerably greater than that of the doped regions to either side.

When an external voltage V_A is applied to such a junction, the net effect depends greatly upon the direction in which it happens. If the potential of the left-hand side is raised relative to the right-hand side, electrons are attracted to the left, and holes are attracted to the right. As a consequence, x_n moves further to the left, and x_p moves further to the right. Conversely, if the potential is lowered to the left, electrons are repelled from the left, and the size of the depletion region

increases. Quantitatively, applying a voltage corresponds to a case in which the system departs slightly from equilibrium, so that the chemical potential μ is no longer constant, but instead changes by amount eV_A from one end of the sample to the other. Most of the voltage drop occurs in the depletion region. One does not need to determine the spatial profile to observe, however, that because μ is now different on the two sides of the sample, the potentials $V(\infty)$ and $V(-\infty)$ must also change accordingly so as to maintain charge neutrality, and the difference between them also changes by V_A . According to Eq. (19.56), the effect of applied voltage is to send $V_{bi} \rightarrow V_{bi} - V_A$ and thereby change the lengths of x_n and x_p by a factor of $\sqrt{1 - V_A/V_{bi}}$.

The applied voltage V_A is taken positive if it raises the voltage of the p -doped region with respect to the n -doped region in Figure 19.15. As the size of the depletion region varies, the amount of current that flows through the junction changes dramatically, increasing exponentially as V_A increases. The reason for the exponential rise is that for an electron to flow through the depletion region, it must be a mobile carrier on the left side of Figure 19.15 with enough thermal energy to surmount the potential barrier eV_{bi} ; the number of such electrons is proportional to $\exp[-\beta eV_{bi}]$ and changes in response to external voltages as $\exp[\beta eV_A]$. When the external voltage is zero, the number of electrons returning from the left must exactly equal the number jumping over the potential barrier from the right; electrons in the p -doped region are always attracted back to the n -doped region and have no barrier to cross. This electron current from left to right should not change much while external voltage rises from zero, so the total current J has the form

$$J \propto e^{\beta eV_A} - 1, \quad (19.57)$$

showing the exponential dependence upon external voltage that characterizes rectification.

19.4.3 Boltzmann Equation for Semiconductors

Once an external voltage V_A is applied across a junction and current begins to flow, equilibrium equations such as (19.46) no longer directly apply. One must return to the Boltzmann equation, Section 17.2, and solve for the distribution function $g_{\vec{r}\vec{k}}$. The most convenient form of the Boltzmann equation for semiconductors is somewhat different from the most convenient form for metals because:

1. It is valuable to write the equations in a form that emphasizes the separate roles of electrons and holes.
2. It is useful to simplify the equations by averaging over wave vectors \vec{k} .

Using the Hamiltonian structure (17.1), rewrite Eq. (17.10) in the relaxation time approximation as

$$\frac{\partial g}{\partial t} = -\frac{\partial}{\partial \vec{r}} \cdot \dot{\vec{r}}g - \frac{\partial}{\partial \vec{k}} \cdot \dot{\vec{k}}g + \frac{f-g}{\tau}. \quad (19.58)$$

The density n of electrons at position \vec{r} is defined by

$$n = \int [d\vec{k}] g_{\vec{r}\vec{k}}, \quad \begin{array}{l} \text{The integral is over the first Brillouin zone,} \\ \text{and } [d\vec{k}] \text{ is defined in Eq. (6.15).} \end{array} \quad (19.59)$$

with g giving the occupation probability of states in the conduction band. Integrating $d\vec{k}$ over both sides of Eq. (19.58) gives

$$\frac{\partial n}{\partial t} = -\frac{\partial}{\partial \vec{r}} \cdot \langle \dot{\vec{r}} \rangle n + \frac{n^{(0)} - n}{\tau_n}, \quad \begin{array}{l} \text{The relaxation time } \tau \text{ should be independent} \\ \text{of } \vec{k} \text{ to pass through the averaging process;} \\ \text{otherwise, use a constant } \tau_n \text{ that gives the} \\ \text{best approximation to the averaged collision} \\ \text{term.} \end{array} \quad (19.60)$$

where $n^{(0)}$ is the equilibrium density of electrons in the conduction band, and $\langle \dot{\vec{r}} \rangle$ is the velocity $\vec{v}_{\vec{k}}$ averaged over the Brillouin zone,

$$\langle \dot{\vec{r}} \rangle = \frac{1}{n} \int [d\vec{k}] g_{\vec{r}\vec{k}} \vec{v}_{\vec{k}} \quad (19.61)$$

$$= \frac{1}{n} \int [d\vec{k}] \left[f - \tau \vec{v}_{\vec{k}} \cdot \left\{ e\vec{E} \frac{\partial f}{\partial \mu} + \frac{\partial f}{\partial \vec{r}} \right\} \right] \vec{v}_{\vec{k}} \quad \begin{array}{l} \text{Using Eq. (17.36), employing} \\ \text{Eq. (17.34) to simplify some of} \\ \text{the terms.} \end{array} \quad (19.62)$$

$$\approx \frac{1}{n} \int [d\vec{k}] \left[-\tau \vec{v}_{\vec{k}} \cdot \left\{ e\vec{E} \beta g + \frac{\partial g}{\partial \vec{r}} \right\} \right] \vec{v}_{\vec{k}} \quad \begin{array}{l} \text{The first term vanishes by} \\ \text{symmetry. } \partial f / \partial \mu = \beta f \text{ in the} \\ \text{nondegenerate limit. Finally,} \\ \text{replace } f \text{ by } g, \text{ because the two} \\ \text{differ only by small quantities.} \end{array} \quad (19.63)$$

$$= -\mu_n \vec{E} - \frac{\mathcal{D}_n}{n} \frac{\partial n}{\partial \vec{r}} \quad (19.64)$$

with the mobility μ_n ,

$$\mu_n = \frac{e}{3} \beta \langle \tau v_k^2 \rangle \quad \begin{array}{l} \text{Assuming that the conductivity tensor of Eq. (17.62)} \\ \text{is diagonal. Otherwise, mobility and diffu-} \\ \text{sion are tensors.} \end{array} \quad (19.65)$$

and the diffusion constant \mathcal{D}_n giving the Einstein relation,

$$\mathcal{D}_n = \frac{1}{3} \langle \tau v_k^2 \rangle = \frac{k_B T \mu_n}{e}. \quad \begin{array}{l} \text{The factor of } 1/3 \text{ appears because only the} \\ \text{component of } \vec{v} \text{ along } \vec{E} \text{ survives the average} \\ \text{in Eq. (19.63).} \end{array} \quad (19.66)$$

Therefore currents of electrons and holes are

$$\vec{j}_n = e\mu_n n \vec{E} + e\mathcal{D}_n \vec{\nabla} n \quad \text{Multiply Eq. (19.64) by } -ne. \quad (19.67a)$$

$$\vec{j}_p = e\mu_p p \vec{E} - e\mathcal{D}_p \vec{\nabla} p, \quad \text{Working in an analogous fashion.} \quad (19.67b)$$

and the equations of motion for the electron and hole distributions are

$$\frac{\partial n}{\partial t} = \frac{1}{e} \vec{\nabla} \cdot \vec{j}_n + \frac{n^{(0)} - n}{\tau_n} \quad (19.68a)$$

$$\frac{\partial p}{\partial t} = -\frac{1}{e} \vec{\nabla} \cdot \vec{j}_p + \frac{p^{(0)} - p}{\tau_p}, \quad (19.68b)$$

with the electric field determined from

$$\vec{\nabla} \cdot \vec{E} = \frac{4\pi e(p - n + n_{\text{ions}})}{\epsilon^0}. \quad (19.69)$$

Recombination and Generation. Several different physical processes may be encompassed by the relaxation times τ_n and τ_p . In addition to scattering off impurities, electrons and holes can collide and recombine; they can also be generated by very energetic collision events. Therefore, the collision term in semiconductors is thought of as a *recombination and generation current*. The relaxation times τ_p and τ_n are impossible to tabulate, because they depend sensitively upon sample purity and temperature, and can vary from 10^{-9} to 10^{-14} s. They can be measured in any given sample—for example, by exposing the crystal to a flash of light that excites electrons into the conduction band and by then measuring the decay of the conductivity.

19.4.4 Detailed Theory of Rectification

Solving Eqs. (19.67)–(19.69) poses numerous difficulties. The equations are nonlinear, because they involve products of n and p with the electric field \vec{E} . Exact analytical solution is out of the question, even in the simplified one-dimensional situation upon which attention is now focused. Numerical solution is also not entirely straightforward because of the wide range of scales over which the various quantities vary. For example, the characteristic scale of depletion layers is from 10^{-6} to 10^{-4} cm, while the characteristic scale for variation of n and p outside the depletion layers turns out to be on the order of 10^{-2} cm. In addition, the magnitudes of the charge distributions vary over many orders of magnitude.

Ideal Diode Equation. The best approach to these difficulties is a conventional solution, the *ideal diode equation*. As in the equilibrium case, the diode is divided into three regions, indicated in Figure 19.16:

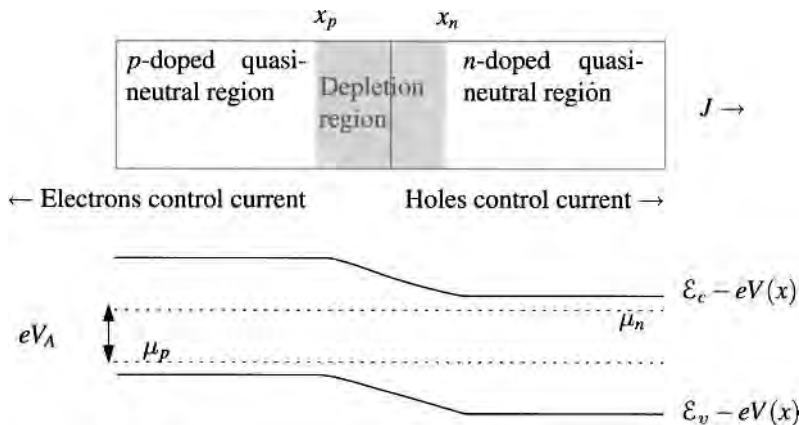


Figure 19.16. Sketch of p - n junction in forward bias, with voltage of the p side raised by voltage V_A above n side of the junction. Because the junction is out of equilibrium, the chemical potentials μ_n and μ_p in the n and p regions are not equal. The depletion region is compressed by the voltage difference, and current increases exponentially with V_A .

A quasi-neutral n -doped region where the electric field is extremely small and the density of mobile electrons is close to \mathcal{N}_d .

A depletion region where the electric field rises rapidly to large values and where consequently the concentrations of charge carriers rapidly fall below their values in homogeneously doped samples. In the midst of this depletion region, the doping changes from n to p type.

A quasi-neutral p -doped region where the electric field drops back to zero and the density of mobile holes is close to \mathcal{N}_a .

The vast majority of mobile charge carriers in the quasi-neutral n -doped region are electrons. However, there is also a small population of holes. Similarly there is a small population of electrons in the p -doped region. These two populations are called *minority carriers*, and the operation of the diode can be understood by carefully analyzing their behavior, because whichever of them is least mobile constitutes the main bottleneck restraining charge flow through the diode.

Further progress rests upon two simplifications:

1. The boundary between the depletion region and the quasi-neutral regions is sharp. In the quasi-neutral regions, the electric field is very small, and the drift currents $e\mu_n nE$ (p -region) and $e\mu_p pE$ of the minority carriers are negligible. That is, in regions where carriers are unlikely, they obey the purely linear equations

$$j_n = e\mathcal{D}_n \vec{n}' \quad \begin{array}{l} \text{Electrons, specializing to one dimension; the} \\ \text{prime means spatial derivative.} \end{array} \quad (19.70a)$$

$$j_p = -e\mathcal{D}_p \vec{p}' \quad \text{Holes.} \quad (19.70b)$$

This approximation is excellent.

2. Recombination and generation of charge carriers is neglected in the depletion region. This assumption is made for mathematical convenience only. The faster the charges sweep through the depletion region, the more appropriate it will be, but for low current flow it leads to appreciable deviation from experiment.

Solution in Depletion Region. The value of the second assumption lies in the fact that it makes possible an analytical relation for n and p in the depletion region, allowing the behavior of the diode to be obtained in closed form. Because recombination and generation are neglected, the currents of electrons and holes are separately conserved, and both j_n and j_p are constant in space. Using Eqs. (19.67), one can quickly find a solution for n and p which according to Problem 4 is

$$n(x) = \mathcal{N}_d e^{\beta e[V(x) - V(x_n)]} \left[1 + \frac{j_n}{e\mathcal{N}_d \mathcal{D}_n} \int_{x_n}^x dx' e^{-\beta e[V(x') - V(x_n)]} \right] \quad (19.71a)$$

$$p(x) = \mathcal{N}_a e^{-\beta e[V(x) - V(x_p)]} \left[1 - \frac{j_p}{e\mathcal{N}_a \mathcal{D}_p} \int_{x_p}^x dx' e^{\beta e[V(x') - V(x_p)]} \right] \quad (19.71b)$$

Under equilibrium conditions, where no current flows, the second terms on the right-hand side of Eqs. (19.71) vanish. Ignoring this second term is very convenient, because use of the first term requires only knowledge of the total change in potential across the depletion region, while the second would require knowledge of details of the profile of $V(x)$. Fortunately, for most cases of interest the second term remains negligible relative to the first, even out of equilibrium. Looking ahead to Eq. (19.77), one can estimate its size in the presence of applied voltage V_A to be

$$\frac{n_i^2}{\mathcal{N}_a \mathcal{N}_d} \frac{x_p - x_n}{L_n} e^{\beta e V_A} \approx 10^{-10} e^{\beta e V_A}. \quad \text{Junction widths are typically } 10^2 \text{ times smaller than diffusion lengths, and } n_i^2 / \mathcal{N}_d \mathcal{N}_a \sim 10^{-8}. \quad (19.72)$$

Therefore, Eq. (19.71) can be replaced by the *law of the junction*:

$$n(x) = \mathcal{N}_d e^{\beta e [V(x) - V(x_n)]} \quad (19.73a)$$

$$p(x) = \mathcal{N}_a e^{-\beta e [V(x) - V(x_p)]} \quad (19.73b)$$

$$\Rightarrow n(x_p) = \mathcal{N}_d e^{\beta e [V_A - V_{bi}]} = \frac{n_i^2}{\mathcal{N}_a} e^{\beta e V_A} \quad \text{See Eq. (19.49), and use approximation Eq. (19.40). Note that the density of minority carriers on the left side of the junction is being set by the density } \mathcal{N}_d \text{ of donors on the right side.} \quad (19.73c)$$

$$p(x_n) = \mathcal{N}_a e^{\beta e [V_A - V_{bi}]} = \frac{n_i^2}{\mathcal{N}_d} e^{\beta e V_A}. \quad (19.73d)$$

Solution in Quasi-Neutral Region. Equations (19.73) constitute a complete solution for the charge carriers in the depletion region. They cannot be used alone to find the current flowing through the diode, because Eqs. (19.73) produce a complete cancellation of diffusion and drift currents, and putting back in the tiny corrections of Eqs. (19.71) to obtain nonzero current means adding back in terms proportional to j_n and j_p which are still unknown. In this sense, Eqs. (19.73) are compatible with a huge range of currents through the diode. However, by using Eqs. (19.73) to impose a boundary condition upon the solutions of Eqs. (19.68), the currents are rapidly determined.

Using the expressions for current (19.70) in Eqs. (19.68) gives in steady state

$$0 = \mathcal{D}_p \frac{d^2 p}{dx^2} - \frac{p - p^{(0)}}{\tau_p} \quad \text{Applies only to minority carriers, and only in quasi-neutral regions. } p^{(0)} \text{ and } n^{(0)} \text{ are the equilibrium minority carrier densities, given by Eqs. (19.39) or (19.40).} \quad (19.74a)$$

$$0 = \mathcal{D}_n \frac{d^2 n}{dx^2} - \frac{n - n^{(0)}}{\tau_n}, \quad (19.74b)$$

which have solution

$$p - p^{(0)} = [p(x_n) - p^{(0)}] e^{-(x-x_n)/L_p} \quad \text{Applies where } p \text{ is the minority carrier, to the right of } x_n. \quad (19.75a)$$

$$n - n^{(0)} = [n(x_p) - n^{(0)}] e^{(x-x_p)/L_n} \quad \text{Applies where } n \text{ is the minority carrier, to the left of } x_p. \quad (19.75b)$$

where

$$L_n = \sqrt{\mathcal{D}_n \tau_n} \quad \text{and} \quad L_p = \sqrt{\mathcal{D}_p \tau_p} \quad (19.76)$$

are the *diffusion lengths* of electrons in the p -doped region, and of holes in the n -doped region, respectively. The currents due to these minority carriers are, from Eqs. (19.67),

$$j_n = e \frac{\mathcal{D}_n}{L_n} [n(x_p) - n^{(0)}] \quad \text{Evaluate Eq. (19.75a) at } x_p. \quad (19.77a)$$

$$= e \frac{\mathcal{D}_n}{L_n} \frac{n_i^2}{\mathcal{N}_a} [e^{\beta e V_A} - 1] \quad \text{Use Eqs. (19.73c) and (19.40b).} \quad (19.77b)$$

$$j_p = e \frac{\mathcal{D}_p}{L_p} [p(x_n) - p^{(0)}], \quad (19.77c)$$

$$= e \frac{\mathcal{D}_p}{L_p} \frac{n_i^2}{\mathcal{N}_d} [e^{\beta e V_A} - 1], \quad \text{Use Eqs. (19.73d) and (19.39b).} \quad (19.77d)$$

producing a total current per volume given by the *ideal diode* or *Shockley equation*,

$$j = en_i^2 [e^{\beta e V_A} - 1] \left[\frac{\mathcal{D}_n}{L_n \mathcal{N}_a} + \frac{\mathcal{D}_p}{L_d \mathcal{N}_d} \right]. \quad (19.78)$$

Doping must be heavy enough that Eqs. (19.39) and (19.40) hold.

One of the most important features of Eq. (19.78) is that because \mathcal{N}_a and \mathcal{N}_d appear in denominators, current flow is set by the side of the diode that is most lightly doped. The heavily doped side acts like a short circuit. This fact is particularly important for the design of the transistor.

19.4.5 Transistor

By the 1920s numerous scientists realized that because electronics was based upon the diode and the triode, and because semiconductor diodes could be created (although unreliably), it would be valuable to create a semiconductor analog of the triode. Twenty-five years elapsed between the first ideas, and the first practical implementation, called the *transistor* by Bardeen and Brattain (1948). The first working transistor involved contact between thin metal whiskers and semiconductors, rather like the Schottky diodes. It was unable to carry large currents and never developed into a commercial device, but the research project in which the point-contact transistor was created uncovered much of the basic physics of semiconductor junctions, particularly the fact that transport in diodes is dominated by minority carriers. The *bipolar junction transistor* followed not long after and served as the foundation for the first developments of semiconductor electronics.

The basic idea of the bipolar junction transistor is to take advantage of the large disparity between electron and hole currents in a diode where one side is much more heavily doped than the other. Consider, for example, a p^+n junction, where the superscript $+$ indicates heavy doping, on the order of 10^{18} cm^{-3} , so that the assumption the semiconductor is nondegenerate breaks down. For steady current flow under forward bias, a tiny electron current flows into the n region, and a large hole current flows in to the p^+ region. In a diode, the hole current would be drawn to the n region and out of the semiconductor, but in the transistor the hole

current is diverted by making the n region much narrower than the diffusion length L_p of the minority carriers and placing it in contact with a second pn junction, which is under reverse bias. The reverse bias means that in the depletion region electric fields propel holes toward the p region and repel electrons. Whenever a hole diffusing about in the n region wanders into this second depletion region, it is trapped and sent off to the collector. The net effect is to split the current traveling into the emitter into its constituent components, with almost all the holes going out the collector and almost all the electrons coming in from the base. The large ratio between these two currents, along with the fact that they are linearly related according to Eqs. (19.77), means that the transistor can function as a linear amplifier. On the other hand, if the current to the base is reversed, the current out the collector does not follow it linearly but drops to very low values. Thus the transistor also rectifies current and can be used as a binary switch.

The mathematical analysis of the binary junction transistor involves no ideas or assumptions not already present in the case of the ideal diode. The only difficulty is that there is now a large number of different regions, so the notation becomes confusing. Once again the basic idea is to assume steady-state conditions and

1. Separate the device into quasi-neutral and depletion regions.
2. Ignore recombination–generation in depletion regions.

Also as before, the strategy is to focus upon the minority carriers in each region. The fields that need to be found are $n_E(x)$, the electron concentration in the *emitter*, $p_B(x)$, the hole concentration in the *base*, and $n_C(x)$, the electron concentration in the *collector*, regions labeled in Figure 19.17.

The concentrations of the minority carriers at the edges of each depletion region are determined by precisely the considerations that produced the ideal diode equation. So, in analogy with Eqs. (19.73c) and (19.73d),

$$n_E(x_a) = \frac{n_i^2}{N_E} e^{\beta e V_{EB}} \quad \begin{array}{l} N_E \text{ is the acceptor concentration in the emitter} \\ \text{region, } V_{EB} > 0 \text{ (for active bias) is the} \\ \text{voltage of emitter over base.} \end{array} \quad (19.79a)$$

$$p_B(x_b) = \frac{n_i^2}{N_B} e^{\beta e V_{EB}} \quad N_B \text{ is the donor concentration in the base region.} \quad (19.79b)$$

$$p_B(x_c) = \frac{n_i^2}{N_B} e^{\beta e V_{CB}} \quad \begin{array}{l} V_{CB} < 0 \text{ (for active bias) is the voltage of} \\ \text{the collector relative to the base; when } V_{CB} \text{ is} \\ \text{negative, collector voltage is below base.} \end{array} \quad (19.79c)$$

$$n_C(x_d) = \frac{n_i^2}{N_C} e^{\beta e V_{CB}} \quad \begin{array}{l} N_C \text{ is the acceptor concentration in the collector} \\ \text{region.} \end{array} \quad (19.79d)$$

These boundary equations are coupled to the diffusion equations in the three quasi-neutral regions, which are unchanged from Eqs. (19.70). The currents of electrons and holes in the emitter and collector can then be calculated from

$$j_{En} = e \mathcal{D}_E n'_E(x_a) \quad (19.80a)$$

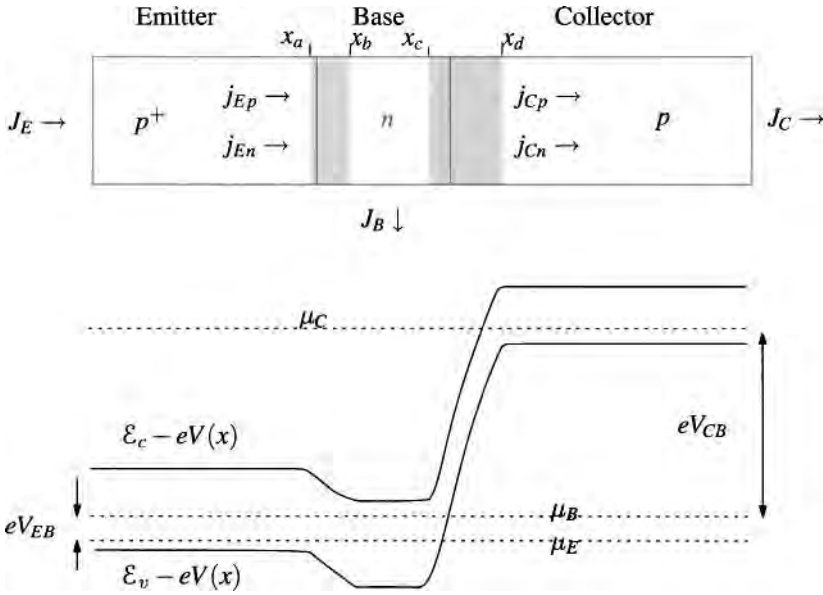


Figure 19.17. The binary junction transistor can be made from two back-to-back p - n junctions. When actively biased, the voltage of the emitter is raised by V_{EB} over the voltage of the base, and the voltage of the base is raised by $|V_{CB}| = -V_{CB}$ over the voltage of the collector. The chemical potential of electrons in the three regions is indicated by dotted lines. The left-hand depletion region shrinks relative to equilibrium while the right-hand one grows. The currents J are positive.

$$j_{Ep} = -e\mathcal{D}_B p'_B(x_b) \tag{19.80b}$$

$$j_{Cp} = -e\mathcal{D}_B p'_B(x_c) \tag{19.80c}$$

$$j_{Cn} = e\mathcal{D}_C n'_C(x_d). \tag{19.80d}$$

Solving the diffusion equations analogous to (19.74) in the three quasi-neutral regions subject to the boundary conditions (19.79) results in total currents J_E and J_C to the emitter and from the collector

$$J_E = J_{FO}(e^{\beta eV_{EB}} - 1) - \alpha_R J_{RO}(e^{\beta eV_{CB}} - 1) \tag{19.81a}$$

$$J_C = \alpha_F J_{FO}(e^{\beta eV_{EB}} - 1) - J_{RO}(e^{\beta eV_{CB}} - 1) \tag{19.81b}$$

with

$$J_{FO} = eA \left(\frac{\mathcal{D}_E}{L_E} \frac{n_i^2}{N_E} + \frac{\mathcal{D}_B}{L_B} \frac{n_i^2}{N_B} \coth\left(\frac{x_c - x_b}{L_B}\right) \right) \tag{19.81c}$$

A is the area perpendicular to current flow in the transistor. L_B is the diffusion length in the base; see Eq. (19.76).

$$J_{RO} = eA \left(\frac{\mathcal{D}_C}{L_C} \frac{n_i^2}{N_C} + \frac{\mathcal{D}_B}{L_B} \frac{n_i^2}{N_B} \coth\left(\frac{x_c - x_b}{L_B}\right) \right) \tag{19.81d}$$

$$\alpha_F J_{FO} = \alpha_R J_{RO} = eA \frac{\mathcal{D}_B}{L_B} \frac{n_i^2}{N_B} \operatorname{cosech}\left(\frac{x_c - x_b}{L_B}\right). \tag{19.81e}$$

Equations (19.81) are the Ebers–Moll equations; they form one of the bases for practical circuit design, and their detailed derivation is the subject of Problem 5.

Note that the diffusion length of the base L_B must be comparable to or greater than $x_c - x_b$, or else control of the collector current by the base is lost.

19.5 Inversion Layers

19.5.1 Heterostructures

The earliest electronic devices depended upon the contact between metal and vacuum, the next generation depended upon contact between metal and semiconductor, and the next industry depended upon junctions between regions of different doping, as well as junctions between semiconductors and insulators. A new generation of semiconductor devices is now evolving that depends upon junctions between different semiconductor alloys. The advantage of these is that they make possible the creation of *heterostructures* where the band gap varies in ways that would never occur spontaneously in nature.

A widely employed example is GaAlAs. Aluminum replaces gallium substitutionally in the alloy, lying right above it in column IIIA of the periodic table. The lattice constant of GaAs is 5.63 \AA , that of AlAs, 5.62 \AA , both adopting the zincblende structure, so there is no appreciable lattice distortion incurred by placing, say, a layer of $\text{Ga}_{0.7}\text{Al}_{0.3}\text{As}$ upon GaAs. However, the band gap of $\text{Ga}_{0.7}\text{Al}_{0.3}\text{As}$ is 1.82 eV , compared to 1.42 eV for GaAs. The technique of molecular beam epitaxy, described in Section 4.3, makes it possible to alternate layers of one alloy with another with atomic scale precision.

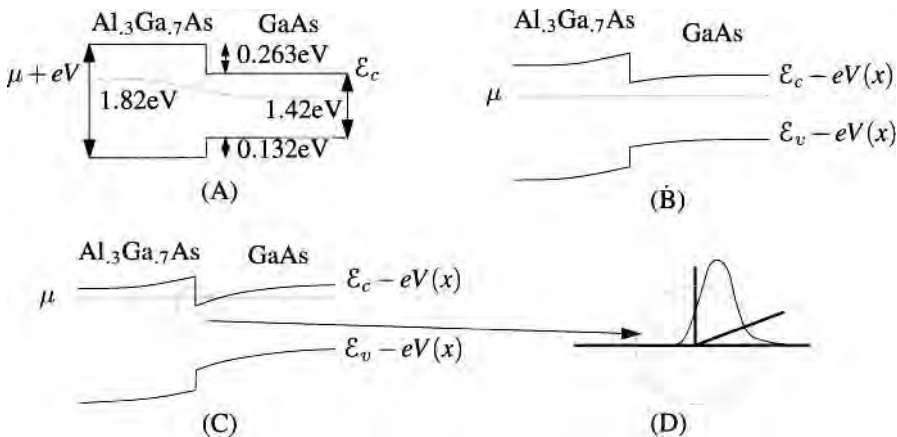


Figure 19.18. (A) Schematic picture of junction between two semiconductors with different band gaps, illustrated with numbers appropriate to $\text{Ga}_{0.7}\text{Al}_{0.3}\text{As}$. Calculating the band offsets is difficult and is discussed by Yu et al. (1992). (B) Same as (A), but drawing different quantities to illustrate band bending. (C) In case of heavy enough doping, the chemical potential can rise above the conduction band edge in a small notch-like region. (D) Enlargement of the conduction band region that would remain occupied even at temperature $T = 0$, with a sketch of a bound-state wave function trapped in the potential.

The formulas describing the profiles of charge around heterostructure junctions are not dramatically different from those of Section 19.4.2, and the main physical results can be deduced from diagrams in the spirit of Figs. 19.11 and 19.14, as displayed in Figure 19.18. The electron bands are discontinuous in the vicinity of the junction, which permits some interesting possibilities. A notch in the bands, such as shown in Figure 19.18(C), creates a small region that is occupied even at zero temperature, called an *inversion layer*.

Metal–Oxide–Silicon Junctions.

A similar notched potential can be created in a layered structure with a thin insulating coating separating metal and semiconductor, as illustrated in Figure 19.19. When the semiconductor is silicon and the insulator is silicon oxide, the junction is known by the acronym *MOS*. This combination can be used to create very compact, fast transistors, with low power dissipation, and has therefore become the most important technology in the creation of integrated circuits. The acronym *CMOS* refers to *complementary metal–oxide–silicon*, which means that both *p*- and *n*-type structures are built on the same chip. These structures are discussed in texts on semiconductor devices, such as Sze (1981) and Sze (1998).

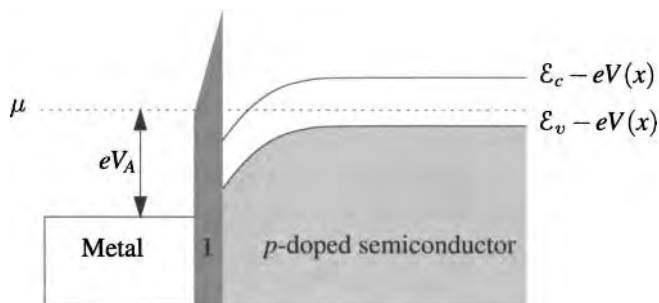


Figure 19.19. Metal–insulator–semiconductor (MIS), and, more particularly, metal–oxide–silicon (MOS) junctions provide an alternative to heterojunctions in forming inversion layers. By raising the voltage of the metal by V_A above the silicon, electrons are pulled over to the interface with the insulator, and the Fermi level μ can be pulled above the conduction band edge.

Two-Dimensional Electron Gas. Some of the most interesting physical discoveries in heterostructures have been built upon the *two-dimensional electron gas* (2DEG), the principle behind which was illustrated in Figures 19.18 and 19.19. By doping both sides of a heterojunction sufficiently, the chemical potential can be made to rise until it intersects a small corner of the conduction band, as shown in Figures 19.18(C) and 19.18(D). Even at the very lowest temperatures, electronic states must be populated in the vicinity of the corner. One way to view Figure 19.18(D) is that it sets up a one-dimensional problem of elementary quantum mechanics, which is to find the eigenstates of a particle in a triangular potential. As shown in Section 18.4.3, a one-dimensional attractive potential always has at least one bound state, no matter how shallow and small it may be. The potential barriers

in the vicinity of the heterojunction are on the order of 0.1 eV. At room temperature, electrons would escape the restraining potential, and in fact the region to the right of the junction in Figure 19.18 would constitute an n -doped semiconductor in the degenerate limit. However, at temperatures of a few kelvin or less where experiments are characteristically performed, only the ground state has measurable occupation. This restriction to low temperatures is clearly a disadvantage. To overcome this restriction, it is not sufficient to find materials so that the energy scale of Figure 19.18 is multiplied by 100. The great mobility of electrons at low temperatures and the great purity achievable in semiconductors are equally important.

Figure 19.18 may lead to a mental picture in which electrons are trapped in one-dimensional potentials. The trapping is only in the z direction, as shown in Figure 19.20. Along x and y the electrons are free to move; the atomic sharpness of the heterojunction, the extreme purity of the samples, and the subkelvin temperatures all conspire to give electrons exceptionally high mobilities in the remaining two dimensions. For a GaAs–Al_{0.29}Ga_{0.71}As interface, the electron mobility reaches $10^5 \text{ cm}^2 \text{ V}^{-1} \text{ s}^{-1}$, while the relaxation time τ can reach $4 \cdot 10^{-12} \text{ s}$. This relaxation time is two orders of magnitude larger than the characteristic values emerging from Eq. (16.7).

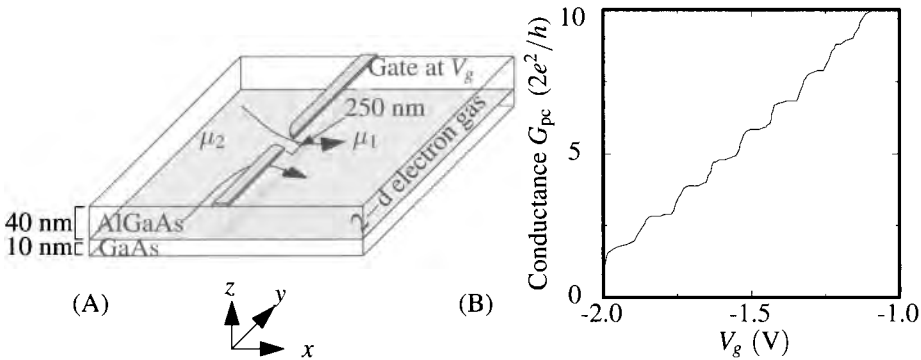


Figure 19.20. (A) Geometry of quantum point contact. Electrons can only pass through the region between the gates, which is shaped more like a blunted arrow than a long narrow channel. By raising and lowering the gate voltage V_g , the effective width of the constriction can be controlled. (B) Quantized conductance across the constriction, using Eq. (19.90) to process the raw data, observed by van Wees et al. (1988), p. 849.

The two-dimensional electron gas is the setting for many remarkable experiments, including the quantum Hall effect to be discussed in Section 25.5. In the context of electronic devices, it constitutes the starting point for building more elaborate structures.

19.5.2 Quantum Point Contact

To create a *quantum point contact*, two metal layers are deposited on top of a two-dimensional electron gas, as shown in Figure 19.20. By applying a negative voltage

of around -0.5 V to the strips of metal, the Fermi level underneath them is driven downwards, and the electron gas completely depleted. The only path the electrons can follow is through the narrow channel left behind. As discussed by Beenakker (1997) and van Houten and Beenakker (1996), conductance through a channel of this type is quantized in units of $2e^2/h$.

Demonstrating this claim requires a fairly careful consideration of what electrical conductance really means. The quantum point contact is just a static quantum mechanical potential, through which wave functions travel or from which they reflect. Wave propagation conserves energy. Yet any wire with resistivity greater than zero must dissipate energy. How are these two views compatible? Landauer (1957) gave a conceptual resolution. He pointed out that experiments measuring conductivity contain the ingredients shown in Figure 19.21. Saying that there is a voltage difference between two points in a circuit really means that there are two reservoirs of electrons independently in thermal equilibrium, and with different chemical potentials, and that they have been connected by the channel whose conductance is to be measured. Any electron transmitted across the channel must give up energy, on average, once it arrives at the second reservoir, because the second reservoir is at lower potential than the first, and the arriving electron comes to equilibrium with its fellow electrons. All dissipation occurs in the reservoirs, not in the channel, but the dissipation is inevitable because of the way that voltage differences are defined.

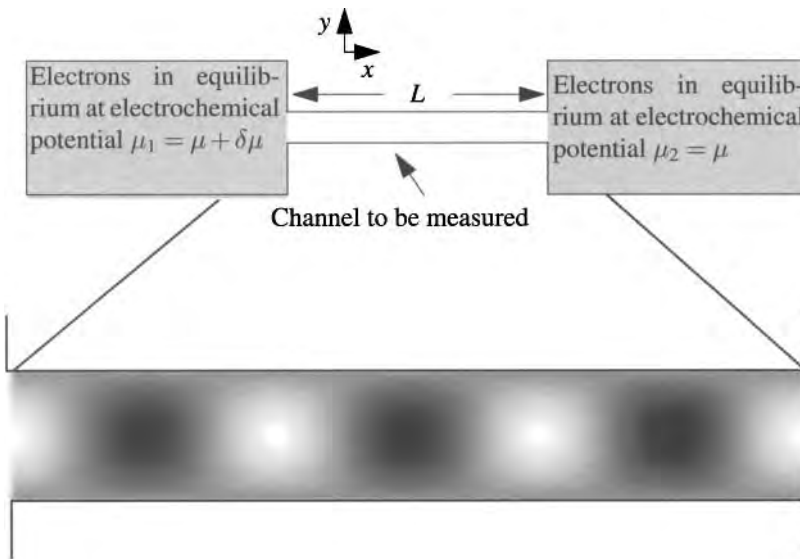


Figure 19.21. Two reservoirs at electrochemical potential $\mu_1 = \mu + \delta\mu$ and $\mu_2 = \mu$ are connected by a channel so narrow that quantization of waves in the y direction becomes important.

The channel depicted in Figure 19.21 is so narrow that quantization in the y direction becomes important; when this experiment is performed, channel widths are on the order of tens to hundreds of nanometers. The energy levels in the channel

therefore have the form

$$\mathcal{E}_{lk_x} = \mathcal{E}_l^y + \frac{\hbar^2 k_x^2}{2m}. \quad \begin{array}{l} l \text{ is a discrete index. In fact, one does not even have to} \\ \text{assume the free-electron form along } x, \text{ just that energies} \\ \text{in the two directions are additive.} \end{array} \quad (19.82)$$

For $\delta\mu > 0$, reservoir 1 will populate quantum levels in the channel that cause electrons to move down the channel along x , with no corresponding current coming back because those levels are empty in reservoir 2. The net current flowing through the channel is therefore

$$J = \frac{1}{L} \sum_{lk_x} -ev_{lk_x} [f_1(\mathcal{E}_{lk_x}) - f_2(\mathcal{E}_{lk_x})] \quad (19.83)$$

v_{lk_x} is the velocity of an electron along the channel, and f_1 and f_2 are the Fermi functions of the two reservoirs. Summing over \vec{k} counts all the particles in the channel, so multiply by v/L to get the flux.

$$= -e \sum_l \int dk_x D_{k_x} \frac{\partial \mathcal{E}_{lk_x}}{\partial \hbar k_x} [\theta(\mu + \delta\mu - \mathcal{E}_{lk_x}) - \theta(\mu - \mathcal{E}_{lk_x})] \quad (19.84)$$

Specialize to low temperatures, and change the sum over k_x to an integral using the one-dimensional density of states D_{k_x} .

$$= -e \frac{2}{2\pi\hbar} \sum_l \int_{\mathcal{E}_l^y}^{\infty} d\mathcal{E} [\theta(\mu + \delta\mu - \mathcal{E}) - \theta(\mu - \mathcal{E})] \quad (19.85)$$

$$= -e \frac{2}{2\pi\hbar} \delta\mu \sum_l \theta(\mu - \mathcal{E}_l^y) \quad \begin{array}{l} \text{Ignore the rare values of } \mu \text{ where } \mu + \delta\mu > \\ \mathcal{E}_l^y \text{ and } \mu < \mathcal{E}_l^y. \end{array} \quad (19.86)$$

$$= \frac{2Ne^2}{h} V \quad \begin{array}{l} \text{Where } N = \sum_l \theta(\mu - \mathcal{E}_l^y) \text{ is the number of} \\ \text{occupied quantum states along } y, \text{ and } V = \\ -\delta\mu/e \text{ is the voltage.} \end{array} \quad (19.87)$$

$$\Rightarrow G_{\text{pc}} = \frac{2Ne^2}{h}. \quad \begin{array}{l} G_{\text{pc}} \text{ is the conductance of the quantum point} \\ \text{contact.} \end{array} \quad (19.88)$$

Thus each quantum level l and each spin degree of freedom contribute e^2/h to the conductance. The form of the energy \mathcal{E}_{lk_x} is irrelevant, just so long as it is a sum of contributions from x and y directions. This quantized conductance has been observed, as shown in Figure 19.20. The quantization of conductance was first predicted by Imry (1987), but the subject remained controversial until matters were settled by experiment.

To explain the experimental observations, it is necessary also to observe that the quantum point contact is always in series with other resistors R in a circuit. The complete relation between current J and voltage V is

$$V = J \left(R + \frac{1}{G_{\text{pc}}} \right) \quad \text{Conductance is the inverse of resistance.} \quad (19.89)$$

$$\Rightarrow G_{\text{pc}} = \frac{J}{V - JR}. \quad (19.90)$$

The resistance R can be treated as a single free parameter to make the steps in G_{pc} of equal height.

19.5.3 Quantum Dot

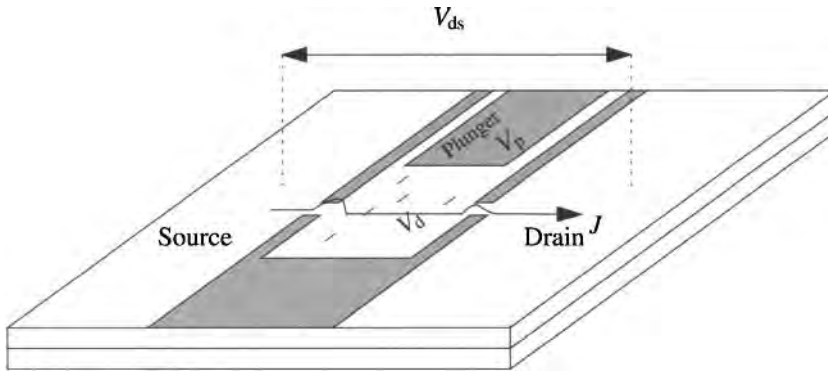


Figure 19.22. The quantum dot is a puddle of charge trapped between two quantum point contacts. Because of the micron-scale dimensions of the trapping region, the number of trapped electrons can be very small. One side of the trap is a plunger whose voltage can be raised and lowered to alter the electrostatic properties of the dot. The current J flowing from source to drain is the main experimental observable.

The *quantum dot*, as shown in Figure 19.22, is a structure one level more complex than the quantum point contact. It mainly consists of two quantum point contacts in series, but there is an additional interesting twist. The region between the point contacts is rather small, an area on the order of $0.5\mu\text{ m}\times 0.5\mu\text{ m}$. In rough analogy with the gate region of a transistor, there is also a metallic contact called the *plunger* whose voltage can be raised and lowered in order to affect the number of electrons in the central region.

Although named the quantum dot, the basic operation of this device is in large part curiously classical. The kinetic energies of electrons, so decisive in metals, are relatively small in this case. Consider, for example, placing N electrons into a quantum dot with area d^2 . The single-electron quantum states would have energies approximately

$$\frac{\hbar^2 k^2}{2m} = 1.5 \cdot 10^{-6} \frac{\text{eV}}{d^2/[\mu\text{m}]^2}. \quad (19.91)$$

This energy should be compared with the Coulomb repulsion of two electrons at distance d , which is

$$\frac{e^2}{d} = 1.4 \cdot 10^{-3} \frac{\text{eV}}{d/[\mu\text{m}]}. \quad (19.92)$$

The difference in scale between the two energies is overstated by Eq. (19.92), because the Coulomb repulsion is diminished by screening effects to be discussed next, but it is still correct to start with Coulomb repulsion as the main physical effect and then add kinetic energy later as a small perturbation. The energy of electrons in the quantum dot can be treated as a purely classical problem of adding particles to a box, because no matter what the shape of their wave functions, only the Coulomb integral has much importance.

Screening and Capacitance. To begin, suppose that the quantum point contacts to the left and right of the dot are impenetrable barriers, and investigate how the energy of the dot would vary as a function of the number of electrons placed in it. The electrons in the dot cannot be taken independent of the rest of the universe. They are in close proximity to the various metal gates, and charge must flow in and out of these gates so as to maintain them at externally applied voltages whenever electrons enter or leave the dot. Classical electrostatics handles this screening problem by defining a capacitance matrix $C_{\alpha\beta}$ which posits that the charge $Q_{\alpha\beta}$ on any of the gates, or in the dot, is a linear function of the electrostatic potentials V_{α} of the gates and the dot. To make things simple, suppose that the charge on the dot Q_d depends only upon the potential within the dot, V_d , and the potential of the plunger, V_p . Write the charge on the dot and plunger as

$$Q_d = C_d V_d - C_{dp} V_p, \quad \begin{array}{l} \text{The minus sign in front of } C_{dp} \text{ is conventional,} \\ \text{and it ensures that } C_{dp} \text{ will be positive.} \end{array} \quad (19.93)$$

$$Q_p = -C_{pd} V_d + C_p V_p. \quad (19.94)$$

Because the possibility of electron motion through the junctions is being neglected for the moment, the only feature of the outside world with which electrons in the dot interact is the plunger. Therefore the charge on the dot must be a function of $V_d - V_p$, which means that

$$C_d = C_{dp} = C_{pd}. \quad \begin{array}{l} \text{The capacitance matrix must be symmetric, because it is given by second derivatives of the energy } U \text{ in Eq. (19.96) with respect to potential, and therefore } C_{pd} = C_{dp}. \end{array} \quad (19.95)$$

The plunger is not similarly isolated. It is connected to a large reservoir of electrons at potential V_p that enables it to remain at potential V_p no matter what happens on the dot. The electrostatic energy of the system is therefore

$$U_{\text{electrostatic}} = \frac{1}{2} [Q_d V_d + Q_p V_p] + [Q_{\text{reservoir}} - Q_p] V_p. \quad (19.96)$$

$$= \frac{Q_d^2}{2C_d} + V_p Q_d + \dots \quad \begin{array}{l} \text{The remaining terms depend only upon } V_p, \\ \text{are independent of } Q_d, \text{ and so can be dropped.} \end{array} \quad (19.97)$$

Make use of Eqs. (19.93), (19.94), and (19.95).

The number of electrons preferred on the dot in equilibrium is given by minimizing Eq. (19.97) with respect to Q_d and is

$$N \equiv \frac{Q_d}{-e} = \frac{C_d V_p}{e}. \quad (19.98)$$

If C_d were a capacitance on the order of 1 farad, this equilibrium number would be immense. The point of the quantum dot is to generate capacitances C_d so small that the equilibrium occupation is of order unity—that is, capacitances on the order of $\text{aF} = 10^{-18} \text{ F}$ (attofarad). In terms of this unit, Eq. (19.98) can be rewritten as

$$N = 0.625 \frac{C_d}{100 \text{ aF}} \frac{V_p}{10^{-3} \text{ V}}, \quad (19.99)$$

showing that voltages on the order of millivolts applied to the plunger should produce changes of order unity in the number of electrons sitting on the dot. For such small numbers of electrons, one must take into account the fact that N is an integer. What Eqs. (19.98) and (19.99) in fact predict is that the number of electrons N increases in steps, with a transition occurring whenever states with N and $N + 1$ electrons have the same energy, at a voltage

$$V_p = [N + 1/2] \frac{e}{C_d}. \quad \text{Set Eq. (19.97) equal to itself evaluated at } -Q_d/e = N \text{ and } N + 1, \text{ using Eq. (19.98), and solve for } V_p. \quad (19.100)$$

Having established the energetics of the problem in a simple classical fashion, quantum features begin to creep into the interpretation of the results. The theory based upon Eq. (19.98) is the theory of the *Coulomb blockade*, and it makes three main predictions.

1. If a very small voltage is applied across the quantum dot, from source to drain, the current from source to drain should show sharp narrow peaks as a function of the plunger voltage V_p , with the peaks spaced in voltage by a distance e/C_d .
2. For fixed plunger voltage V_p , current from source to drain should be relatively tiny until the voltage from source to drain exceeds a critical threshold, either positive or negative. The gap in voltage between the negative and positive thresholds is e/C_d .
3. The characteristic energy scale on which temperature fluctuations should destroy these effects is $k_B T \sim e^2/2C_d$, which works out to be a few kelvin.

The logic behind these predictions has to do with imagining physically how electrons will manage to traverse the quantum dot in the presence of a voltage between source and drain. In order to do so, an electron must tunnel across the first quantum point contact, dwell for some time on the dot, and then tunnel across the second quantum point contact. If according to Eq. (19.98) the electrostatic energy of the dot goes up when an extra electron hops on, tunneling will be made difficult. There are three ways around. First, whenever the plunger voltage sits at one of the values indicated by Eq. (19.100), the energies of having N and $N + 1$ electrons on the dot are degenerate. There is no energy penalty preventing an electron from flowing in and out of the dot, so for these special plunger voltages the dot has a high conductivity, leading to prediction 1. Second, for an arbitrary plunger voltage, the voltage between source and drain can be made large enough that it supplies the energy needed to hop on and off the dot. Hence a prediction that current through the dot will rapidly increase after a critical threshold no matter what the plunger voltage. Third, thermal fluctuations may be large enough to supply the missing energy, leading to the final prediction of a temperature scale on which the quantum effects disappear.

All three of these predictions are beautifully verified by experiment. Figure 19.23 shows both (A) the periodic current peaks as a function of plunger voltage, and (B) the very nonlinear relation between current and source–drain voltage.

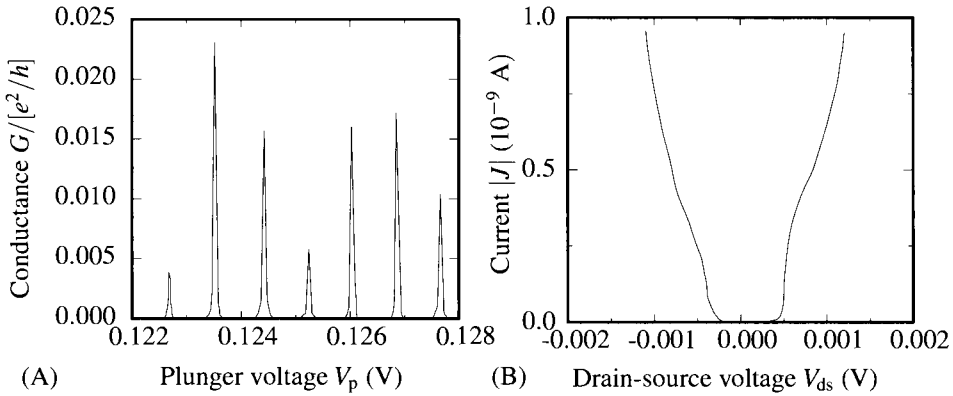


Figure 19.23. (A) Conductance as a function of plunger voltage displaying sharp, equally spaced peaks. (B) Current across a quantum dot plunger versus the voltage V_{ds} across the dot. [Source: Meirav and Foxman (1996), p. 257.]

Problems

1. **Chemical potential in intrinsic semiconductor:** Consider a crystal of silicon, with a very low level of doping, but a slight excess of acceptors over donors.
 - (a) At sufficiently low temperatures, the chemical potential moves far away from the center of the gap. At what temperature does this happen, and why?
 - (b) Next, consider the same situation, but with a slight excess of donors over acceptors, and answer the same questions.
2. **Ohmic junction:** Diagrams of electronic circuits frequently show wires connected to portions of semiconductors. These connections are supposed to be ohmic, to conduct current with equal ease in either direction, and in linear proportion to applied voltage. Because metal–semiconductor junctions have intrinsic rectifying properties, ohmic response cannot be taken for granted.
 - (a) To have a sense of ways to obtain such junctions, copy the three parts of Figure 19.11, but assuming that the work function of the semiconductor is greater than the work function of the metal.
 - (b) Argue from the graphical construction that the rectifying powers of the junction are plausibly diminished, by considering as in Figure 19.12 how the band bending is affected by an applied voltage.
3. **Thermopower of semiconductors:**
 - (a) Consider an n -doped semiconductor, where transport is dominated by electrons in the conduction band. Measure all energies \mathcal{E} relative to the bottom of the conduction band, so $\mathcal{E}_c = 0$. Assume that $\mathcal{E} = m^*v^2/2$, that $D(\mathcal{E}) \propto \sqrt{\mathcal{E}}$, that $\tau_{\mathcal{E}} = a\mathcal{E}^{-s}$, and that the matrices of Eq. (17.73) are all diagonal. Equation

(17.74) is still valid, but for semiconductors the approximation in Eq. (17.77) cannot be used. Show that the thermopower α is given by

$$\alpha = -\frac{k_B}{e} \left[\frac{5}{2} - s - \frac{\mu}{k_B T} \right]. \quad \text{The identity } \Gamma(1+x) = x\Gamma(x) \text{ is helpful.} \quad (19.101)$$

- (b) Now consider a p -doped semiconductor, where transport is dominated by holes. How does Eq. (19.101) change in this case?
4. **Carriers in depletion region:** Using Eqs. (19.67), verify Eqs. (19.71). Notice that because (19.71) is obtained from expressions for the current, it cannot be used directly to predict it.
5. **Ebers–Moll equations:**
- (a) Write down the three equations analogous to Eqs. (19.74) for minority carriers in the three quasi-neutral regions of the transistor.
- (b) Write down the solutions of these equations; in the collector and emitter regions, the solutions are immediately determined up to an overall constant, while in the base region, there are two unknown constants to calculate.
- (c) Find the unknown constants by imposing boundary conditions (19.79), and show that the currents described by (19.80) can be put in the form (19.81).

References

- J. A. Appelbaum and D. R. Hamann (1976), The electronic structure of solid surfaces, *Reviews of Modern Physics*, **48**, 479–496.
- J. Bardeen (1947), Surface states and rectification at a metal semi-conductor contact, *Physical Review*, **71**, 717–727.
- J. Bardeen and W. H. Brattain (1948), The transistor, a semi-conductor triode, *Physical Review*, **74**, 230–231.
- J. C. Bean (1986), The growth of novel silicon materials, *Physics Today*, **39**(10), 36–42.
- C. W. J. Beenakker (1997), Random-matrix theory of quantum transport, *Reviews of Modern Physics*, **69**, 731–808.
- F. Braun (1874), On current flow in metallic sulfides, *Annalen der Physik und Chemie*, **229**, 556–563. In German.
- L. L. Chang and L. Esaki (1992), Semiconductor quantum heterostructures, *Physics Today*, **45**(10), 36–43.
- L. F. Eastman (1986), Compound-semiconductor transistors, *Physics Today*, **39**(10), 77–83.
- P. M. Fahey, P. B. Griffin, and J. D. Plummer (1989), Point defects and dopant diffusion in silicon, *Reviews of Modern Physics*, **61**, 289–384.
- F. J. Feigl (1986), VLSI technology and dielectric film science, *Physics Today*, **39**(10), 47–54.
- D. K. Ferry and H. L. Grubin (1995), Modeling of quantum transport in semiconductor devices, *Solid State Physics: Advances in Research and Applications*, **49**, 283–448.
- A. Fowler (1997), On some modern uses of the electron in logic and memory, *Physics Today*, **50**(10), 50–54.
- A. B. Fowler (1993), A semicentury of semiconductors, *Physics Today*, **46**(10), 59–62.
- J. M. Gibson (1997), Reading and writing with electron beams, *Physics Today*, **50**(10), 56–61.
- N. C. Greenham and R. H. Friend (1995), Semiconductor device physics of conjugated polymers, *Solid State Physics: Advances in Research and Applications*, **49**, 1–149.

- H. K. Henisch (1957), *Rectifying Semi-Conductor Contacts*, Clarendon Press, Oxford.
- J. Hölzl and F. K. Schulte (1979), Work function of metals, in *Solid Surface Physics*, vol. 85 of *Springer Tracts in Modern Physics*, Springer-Verlag, Berlin.
- Y. Imry (1987), Quantum interference effects in submicron systems, *Philosophical Magazine B*, **56**, 969–970.
- M. A. Kastner (1992), The single-electron transistor, *Reviews of Modern Physics*, **64**, 849–858.
- M. A. Kastner (1993), Artificial atoms, *Physics Today*, **46**(1), 24–31.
- R. W. Keyes (1989), Physics of digital devices, *Reviews of Modern Physics*, **61**, 279–287.
- R. Landauer (1957), Spatial variation of currents and fields due to localized scatterers in metallic conduction, *IBM Journal of Research and Development*, **1**, 223–231.
- H. Landolt and R. Börnstein (New Series), *Numerical Data and Functional Relationships in Science and Technology*, New Series, Group III, Springer-Verlag, Berlin.
- N. D. Lang (1973), Density-functional formalism and the electronic structure of metal surfaces, *Solid State Physics: Advances in Research and Applications*, **28**, 225–300.
- B. G. Levi (1988), Very small tunnel junctions sense the effect of single electrons, *Physics Today*, **41**(5), 19–22.
- U. Meirav and E. B. Foxman (1996), Single-electron phenomena in semiconductors, *Semiconductor Science and Technology*, **10**, 255–284.
- A. Miller, A. MacKinnon, and D. Weaire (1981), Beyond the binaries — the chalcopyrite and related semiconducting compounds, *Solid State Physics: Advances in Research and Applications*, **36**, 119–275.
- R. F. Pierret (1996), *Semiconductor Device Fundamentals*, Addison-Wesley, Reading, MA.
- R. C. Pond and J. P. Hirth (1994), Defects at surfaces and interfaces, *Solid State Physics: Advances in Research and Applications*, **47**, 287–365.
- J. Rammer (1991), Quantum transport theory of electrons in solids: A single-particle approach, *Reviews of Modern Physics*, **63**, 781–817.
- W. Schottky (1938), Theory of semiconductor bandgaps, *Die Naturwissenschaften*, **26**, 843. In German.
- A. Schuster (1874), On unilateral conductivity, *Philosophical Magazine*, **48**, 251–257.
- W. Shockley (1950), *Electrons and Holes in Semiconductors, with Applications to Transistor Electronics*, Van Nostrand, New York.
- R. W. Siegel (1993), Exploring mesoscopia: the bold new world of nanostructures, *Physics Today*, **46**(10), 64–68.
- H. I. Smith and H. G. Craighead (1990), Nanofabrication, *Physics Today*, **43**(2), 24–30.
- B. G. Streetman (1995), *Solid State Electronic Devices*, 4th ed., Prentice Hall, Englewood Cliffs, NJ.
- S. M. Sze (1981), *Physics of Semiconductor Devices*, 2nd ed., John Wiley and Sons, New York.
- S. M. Sze (1998), *Modern Semiconductor Device Physics*, John Wiley and Sons, New York.
- H. van Houten and C. W. J. Beenakker (1996), Quantum point contacts, *Physics Today*, **49**(7), 22–27.
- H. van Houten, C. W. J. Beenakker, and B. J. van Wees (1992), Quantum point contacts, in *Semiconductors and Semimetals*, M. Reed, ed., vol. 35, pp. 9–112, Academic Press, Boston.
- B. J. van Wees, H. van Houten, C. W. J. Beenakker, J. G. Williamson, L. P. Kouwenhoven, D. van der Marel, and C. T. Foxon (1988), Quantized conductance of point contacts in a two-dimensional electron gas, *Physical Review Letters*, **60**, 848–850.
- J. H. Weaver (1986), Metal-semiconductor interfaces, *Physics Today*, **39**(1), 24–30.
- E. T. Yu, J. O. McCaldin, and T. C. McGill (1992), Band offsets in semiconductor heterojunctions, *Solid State Physics: Advances in Research and Applications*, **46**, 1–146.
- P. Y. Yu and M. Cardona (1996), *Fundamentals of Semiconductors*, Springer-Verlag, Berlin.
- A. Zangwill (1988), *Physics at Surfaces*, Cambridge University Press, Cambridge.

Condensed Matter Physics, Second Edition
by Michael P. Marder
Copyright © 2010 John Wiley & Sons, Inc.

Part V

OPTICAL PROPERTIES

20. Phenomenological Theory

20.1 Introduction

Experiments with light provide unexpected ways to illuminate the inner workings of solids. Oscillating electrical and magnetic fields can explore the immense range of length and time scales sketched out in Figure 20.1, a range so large that the interaction of light with matter is impossible to treat thoroughly inside any single framework. The theoretical starting point that is appropriate for infrared radiation falling on an ionic insulator has nothing to say about soft X-rays knocking core electrons out of a metal. The underlying equations, Schrödinger's equation for the solid coupled to the quantized radiation field, are too complicated to be of much use. However, there is a collection of simple ideas that makes it possible to understand most experiments. The main effect of incoming light is to make electrons oscillate. Their response depends upon interactions with the atomic solid in which they live and with each other. Fortunately, the interaction of an electron with a lattice can often be modeled by a simple idea—the effective mass—and the interaction of electrons with each other can often be explained with the classical idea of a dielectric function.

Drude's model, Section 16.1.1, provides a simple initial description for the optical response of metals. Rewriting Eq. (16.1) with $\vec{B} = 0$ as

$$m\dot{\vec{v}} = -e\vec{E} - m\frac{\vec{v}}{\tau}, \quad (20.1)$$

and supposing that \vec{E} and \vec{v} have time dependence of the form $\exp[-i\omega t]$ gives

$$-i\omega m\vec{v} = -e\vec{E} - m\frac{\vec{v}}{\tau} \quad (20.2)$$

$$\Rightarrow \vec{j} = -ne\vec{v} = \frac{ne^2\tau/m}{1 - i\omega\tau}\vec{E} \quad (20.3)$$

$$\Rightarrow \sigma(\omega) = \frac{ne^2\tau/m}{1 - i\omega\tau}. \quad (20.4)$$

Therefore for frequencies much smaller than the relaxation rate $2\pi/\tau$, current is in phase with applied electric fields, and the conductivity is given by the low-frequency form, Eq. (16.6). At higher frequencies, current and field fall out of phase, and the low-frequency relation no longer applies. Many features of the optical response of metals can be explained in this way.

However, there are types of optical response that Eq. (20.4) does not capture. The *photoelectric effect* was discovered by Hertz (1887) and Thomson (1897).

Light impinges upon a piece of metal, and a current of electrons emerges in exchange. The intensity of the current is proportional to the intensity of the incoming light, but there is a cutoff frequency below which no electrons emerge, no matter what the intensity. Einstein (1905) explained this experiment by supposing that light could be viewed as a stream of particles carrying quanta of energy, an idea that marks the origin of quantum mechanics.

Two sets of ideas come together to make an enlightened study of matter possible. The first is the study of how electrons in a solid respond to external electrical and magnetic fields, dealt with in Chapter 16. The second is the phenomenological description of matter immersed in electromagnetic fields known as Maxwell's equations.

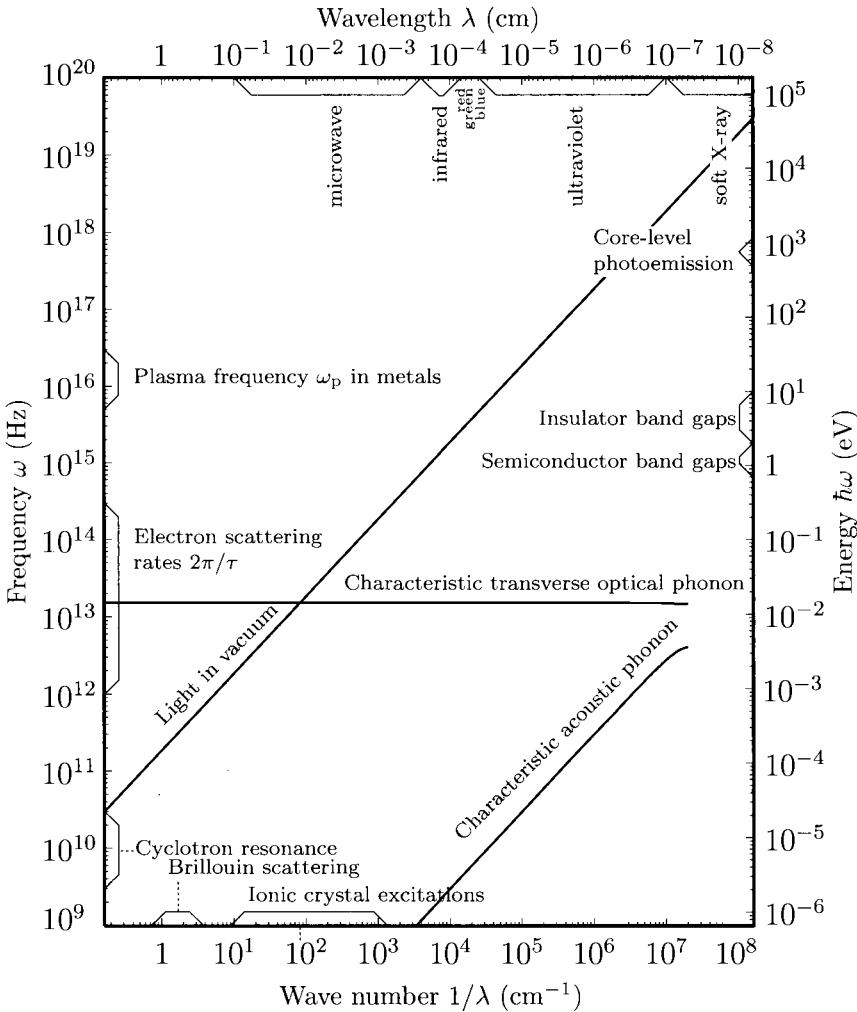


Figure 20.1. Overview of length and energy scales important for the interaction of light with condensed matter.

20.2 Maxwell's Equations

Maxwell's equations are classical, and therefore they describe a quantum-mechanical bath of photons in the limit where the number of photons is very large. For a diamond in sunlight or a semiconductor sample in a beamline, this limit is sensible. The main failure of this semiclassical approximation is its inability to predict the spontaneous emission of photons. Even for lasers, spontaneous emission is of relatively minor importance, and it can fully be taken into account without resorting to the full machinery of quantized photon fields, as will be demonstrated in Section 21.5.2.

There are really two versions of Maxwell's equations in common use. One of them describes the fundamental interactions of charged particles and propagating waves. The other is phenomenological, and it sweeps complicated long-range interactions between vast numbers of particles into continuous functions such as index of refraction or conductivity. This second form of Maxwell's equations is of much greater value in condensed matter physics than the first. It provides not only the best way to account for the interaction of light with solids, but also the best way to find the effective interactions of electrons and phonons with one another and themselves.

Maxwell's equations for electromagnetic waves interacting with a density n of electrons were obtained by Heaviside (1892) and are

$$\vec{\nabla} \cdot \vec{E} = -4\pi en \quad \vec{\nabla} \cdot \vec{B} = 0 \quad (20.5a)$$

$$\vec{\nabla} \times \vec{E} = -\frac{1}{c} \frac{\partial \vec{B}}{\partial t} \quad \vec{\nabla} \times \vec{B} = \frac{4\pi \vec{j}}{c} + \frac{1}{c} \frac{\partial \vec{E}}{\partial t}. \quad (20.5b)$$

These equations are microscopic in the sense that response of all charged matter to the fields is treated explicitly. Maxwell had developed alongside the original equations a phenomenological counterpart where microscopic field and material response are bundled together. The easiest way to find the phenomenological equations proceeds in three steps.

First, distinguish charges outside the system n_{ext} from those inside n_{int} . In what follows, charges and currents will usually not carry a subscript and should be understood to be the internal charges and currents, $n_{\text{int}} = n$, $j_{\text{int}} = j$. The external charges control or drive the system, while the internal charges respond.

Second, define the polarization \vec{P} by

$$\vec{P} = \int^t dt' \vec{j}_{\text{int}}(t'). \quad (20.6)$$

Employ the continuity equation

$$-e \frac{\partial n_{\text{int}}}{\partial t} = -\vec{\nabla} \cdot \vec{j}_{\text{int}} \quad (20.7)$$

$$\Rightarrow en_{\text{int}} = \vec{\nabla} \cdot \vec{P}, \quad (20.8)$$

The arbitrary constant of integration in Eq. (20.6) can be used to eliminate the arbitrary constant here. But see Section 22.2— at a microscopic level, \vec{P} is not well-defined.

so one can define

$$\vec{D} = \vec{E} + 4\pi\vec{P}. \quad (20.9)$$

When one uses Eqs. (20.6) and (20.9), Maxwell's equations become

$$\vec{\nabla} \cdot \vec{D} = -4\pi en_{\text{ext}} \quad \vec{\nabla} \cdot \vec{B} = 0 \quad (20.10a)$$

$$\vec{\nabla} \times \vec{E} = -\frac{1}{c} \frac{\partial \vec{B}}{\partial t} \quad \vec{\nabla} \times \vec{B} = \frac{4\pi \vec{j}_{\text{ext}}}{c} + \frac{1}{c} \frac{\partial \vec{D}}{\partial t}. \quad (20.10b)$$

So long as attention is restricted to the interior of a sample, the external charge densities vanish. However, the external charges cannot be neglected completely because they establish boundary conditions for material within the interior. Often all fields would vanish were it not for the driving influence of external charges.

Third, find a relationship between current \vec{j} and electric field \vec{E} . Suppose that the material is homogeneous and that current is a linear functional of the field. The most general possible relation is then

$$\vec{j}(\vec{r}, t) = \int dt' d\vec{r}' \sigma(\vec{r} - \vec{r}', t - t') \vec{E}(\vec{r}', t') \quad (20.11a)$$

$$\equiv \sigma * \vec{E}(\vec{r}, t). \quad \text{See Appendix A.5.} \quad (20.11b)$$

σ is in general a 3×3 tensor. "Homogeneity" means that the relation between \vec{j} and \vec{E} is unchanged if both \vec{j} and \vec{E} are displaced by a constant vector, implying $\sigma(\vec{r}, \vec{r}') = \sigma(\vec{r} - \vec{r}')$.

One interpretation of the conductivity tensor is that it describes the current \vec{j} that would flow in a sample following a delta-function pulse of electric field \vec{E} at $t = 0$. The assumption of homogeneity means that one can only employ Eq. (20.11) on length scales much larger than a lattice spacing, or other microstructure if it is present. Given this restriction, there is no need to define spatial averages of \vec{E} and \vec{B} as is often conventionally done.

Equation (20.11) simplifies in form if one takes a Fourier transform with respect to $\int d\vec{r} dt \exp[i\omega t - i\vec{q} \cdot \vec{r}]$ to find

$$\vec{j}(\vec{q}, \omega) = \sigma(\vec{q}, \omega) \vec{E}(\vec{q}, \omega). \quad \text{See Appendix A.5.} \quad (20.12)$$

Once the conductivity has been defined, other quantities follow. The dielectric tensor ϵ is defined by

$$\vec{D}(\vec{r}, t) = \epsilon * \vec{E}(\vec{r}, t) \Rightarrow \vec{D}(\vec{q}, \omega) = \epsilon(\vec{q}, \omega) \vec{E}(\vec{q}, \omega). \quad \text{In general } \epsilon \text{ is a } 3 \times 3 \text{ tensor.} \quad (20.13)$$

Combining Eqs. (20.6), (20.9), (20.12), and (20.13) gives

$$\epsilon(\vec{q}, \omega) = 1 + \frac{4\pi i}{\omega} \sigma(\vec{q}, \omega). \quad (20.14)$$

Relation (20.14) is surprisingly powerful. Calculating currents is a favorite activity of theorists, who theoretically follow how all charges respond to electrical

fields and thereby obtain conductivities. Experimentalists have trouble following the motion of charge in detail, particularly at optical frequencies. However, the dielectric tensor is a classic experimental quantity, governing dispersion and absorption of waves. Connecting conductivity and dielectric constant with (20.14) constitutes a connection between theoretical and experimental viewpoints.

Arbitrary Divisions. Maxwell's equations conventionally are presented in another way. Charge is divided into two groups, bound and free. The bound charges produce dielectric behavior, while the free charges participate in conductivity. In addition, materials have a magnetic permeability μ that relates the microscopic field \vec{B} to a macroscopic field \vec{H} .

Il'inskii and Keldysh (1994) emphasize that all these different phenomena are in fact hidden within Eq. (20.11). The divisions between bound and free charge are not fundamental. There is more than one possible way to define the polarization, conductivity, and dielectric constant. Sometimes it may seem natural to divide electrons into more than one group, bundling some in with the polarization and dielectric constant and leaving others free. For example, the currents \vec{j}_{core} due to core electrons might be written as $\vec{P} = \int dt' \vec{j}_{\text{bound}}(t')$ but currents due to conduction electrons left as \vec{j}_{free} . There is nothing necessary about such a division between free and bound charges, although in a given experimental context it may seem natural.

For example, such a point of view was adopted to discuss impurities in semiconductors in Section 18.3.1. The impurities, whether localized or conducting, were placed in a medium with dielectric constant $\epsilon^0 = 11.8$. This dielectric constant is actually due to the polarization of the valence electrons of silicon, but it is very convenient to treat these valence electrons separately from the impurity electrons and refer only to a dielectric constant.

Magnetic permeability seems to be missing. Where has it gone? The question will arise again in Chapter 24. Magnetic permeability consists in the tendency of incoming fields to excite current traveling in closed loops. The conductivity tensor of (20.11) can describe such response, but only when the conductivity is nonlocal. In Fourier space, the magnetic parts of the conductivity tensor will vary as q^2 , while the dielectric parts are independent of q .

20.2.1 Traveling Waves

The quantities actually measured in experiment are closely related to the dielectric function ϵ . From Eqs. (20.10b) and (20.13) one finds that

$$\vec{\nabla} \times \vec{\nabla} \times \vec{E} = -\frac{1}{c} \frac{\partial}{\partial t} \vec{\nabla} \times \vec{B} = -\frac{1}{c^2} \frac{\partial^2 \epsilon * \vec{E}}{\partial t^2} \tag{20.15}$$

$$\Rightarrow q^2 \vec{E} - \vec{q}(\vec{q} \cdot \vec{E}) = \epsilon(\vec{q}, \omega) \frac{\omega^2}{c^2} \vec{E}. \tag{20.16}$$

Take the Fourier transform, and use identity
 $\vec{q} \times \vec{q} \times \vec{A} = \vec{q}(\vec{q} \cdot \vec{A}) - q^2 \vec{A}.$

In the general case where ϵ is a tensor, Eq. (20.16) becomes a 3×3 matrix equation that must be diagonalized. Frequently, however, the dielectric medium can be

treated as isotropic, which means that ϵ is a multiple of the unit matrix and can be treated as a scalar. Not only fluids and polycrystals are isotropic, but all cubic crystals as well, because the only 3×3 matrix able to survive the cubic symmetry operations is a multiple of the unit matrix (Problem 3). In this case, the medium supports precisely two sorts of waves, transverse and longitudinal.

Transverse. For transverse waves, \vec{E} is perpendicular to \vec{q} , and so Eq. (20.16) becomes

$$q^2 \vec{E} = \epsilon(\vec{q}, \omega) \frac{\omega^2}{c^2} \vec{E} \quad \epsilon \text{ is now a scalar.} \quad (20.17)$$

$$\Rightarrow q = \omega \tilde{n}/c; \quad \tilde{n}(\vec{q}, \omega) = \sqrt{\epsilon(\vec{q}, \omega)}, \quad (20.18)$$

and the amplitude of light traveling in the sample varies in space and time as

$$\vec{E}_0 e^{i\omega[\tilde{n}x/c - t]}. \quad \text{For a wave traveling along } x. \quad (20.19)$$

The real part of the dielectric constant is customarily denoted ϵ_1 , and the imaginary part ϵ_2 , while the real part of \tilde{n} is the *index of refraction* \bar{n} , which gives the phase velocity of the electromagnetic waves as c/\bar{n} , and the imaginary part of \tilde{n} is called the *extinction coefficient* κ . These quantities are related by

$$\epsilon_1 = \bar{n}^2 - \kappa^2 \quad (20.20a)$$

$$\epsilon_2 = 4\pi \text{Re}[\sigma]/\omega = 2\bar{n}\kappa. \quad (20.20b)$$

An experimental quantity that can be measured directly is the rate at which the intensity of light decays as it passes through a sample; intensity goes as the square of amplitude, so the *absorption coefficient* α is defined by

$$\alpha = \frac{2\omega}{c} \kappa = \frac{\omega \epsilon_2}{\bar{n}c}. \quad \alpha \text{ gives the rate of spatial decay, and has units of inverse length.} \quad (20.21)$$

Longitudinal. For longitudinal waves, \vec{E} is parallel to \vec{q} , and Eq. (20.16) becomes

$$\epsilon(\vec{q}, \omega) \frac{\omega^2}{c^2} \vec{E} = 0 \quad (20.22)$$

$$\Rightarrow \epsilon(\vec{q}, \omega) = 0. \quad \text{Assuming } \epsilon \text{ is a scalar.} \quad (20.23)$$

20.2.2 Mechanical Oscillators as Dielectric Function

Before proceeding to more elaborate calculations, it will be helpful to present a simple mechanical model for dielectric functions in insulators and metals. Note that a typical wavelength of light passing through a solid is 100 Å or more, while all microscopic dimensions such as unit cell dimensions, or mean free paths of

electrons, tend to be substantially less. Therefore, one can safely take applied electric fields to be of the form

$$\vec{E}(\vec{r}, t) = \vec{E}e^{-i\omega t}, \quad (20.24)$$

set $\vec{q} = 0$ in dielectric and conductivity tensors, and then drop reference to \vec{q} altogether. For this reason, in the ensuing discussion the various response functions will depend upon ω alone.

In an insulator, charges cannot flow indefinitely in response to a static electric field. A simple model consistent with this fact regards the insulator as composed of a collection of charged particles bound to particular sites in a solid, with the particles oscillating about the sites in response to external fields. Oscillators of type l , with mass m_l , charge $-e$, oscillatory frequency ω_l , and damping time τ_l obey

$$m_l \ddot{\vec{r}} = -m_l \omega_l^2 \vec{r} - m_l \dot{\vec{r}}/\tau_l - e\vec{E}(\vec{r}, t) \quad (20.25)$$

$$\Rightarrow \vec{r}(\omega) = -\frac{e\vec{E}}{m_l(\omega_l^2 - i\omega/\tau_l - \omega^2)} \quad \begin{array}{l} \text{Assuming that } \vec{E} \text{ has the form} \\ \text{given in Eq. (20.24).} \end{array} \quad (20.26)$$

If the density of charges of this type is n_l , the current associated with this motion is

$$\vec{j}(\omega) = \frac{-i\omega n_l e^2 \vec{E}}{m_l(\omega_l^2 - i\omega/\tau_l - \omega^2)}, \quad (20.27)$$

so the conductivity is

$$\sigma(\omega) = \frac{-i\omega n_l e^2}{m_l(\omega_l^2 - i\omega/\tau_l - \omega^2)}. \quad (20.28)$$

Making use of Eq. (20.14), the dielectric constant of a material with many different types of oscillators is

$$\epsilon(\omega) = 1 + \sum_l \frac{4\pi n_l e^2 / m_l}{\omega_l^2 - \omega^2 - i\omega/\tau_l}. \quad (20.29)$$

In the subsequent discussion, dielectric functions of the form Eq. (20.29) will appear frequently. Sometimes the oscillators will be isolated impurity atoms, other times they will be phonons, and they may also be electrons jumping between bands.

From the vantage point of dielectric constants, a conductor is actually just a special type of insulator, one where charges are free to move large distances, and one of the oscillation frequencies ω_l equals zero. Focusing upon this term in Eq. (20.28), dropping the index l , gives for the conductivity and dielectric constant

$$\sigma(\omega) = \frac{ne^2\tau}{m(1 - i\omega\tau)} \quad \text{The same as Eq. (20.4).} \quad (20.30)$$

$$\epsilon(\omega) = 1 - \frac{\omega_p^2}{\omega(\omega + i/\tau)}, \quad (20.31)$$

where the *plasma frequency* ω_p is defined by

$$\omega_p = \sqrt{\frac{4\pi n e^2}{m}}. \quad (20.32)$$

The dielectric function Eq. (20.29) has both real and imaginary parts, which are

$$\epsilon_1(\omega) = \text{Re}[\epsilon(\omega)] = 1 + \sum_l \frac{4\pi n_l e^2 (\omega_l^2 - \omega^2)/m_l}{(\omega_l^2 - \omega^2)^2 + (\omega/\tau_l)^2} \quad (20.33a)$$

$$\epsilon_2(\omega) = \text{Im}[\epsilon(\omega)] = \sum_l \frac{4\pi n_l e^2 \omega / (\tau_l m_l)}{(\omega_l^2 - \omega^2)^2 + (\omega/\tau_l)^2}, \quad (20.33b)$$

and individual terms in the sum have the characteristic shapes depicted in Figure 20.2.

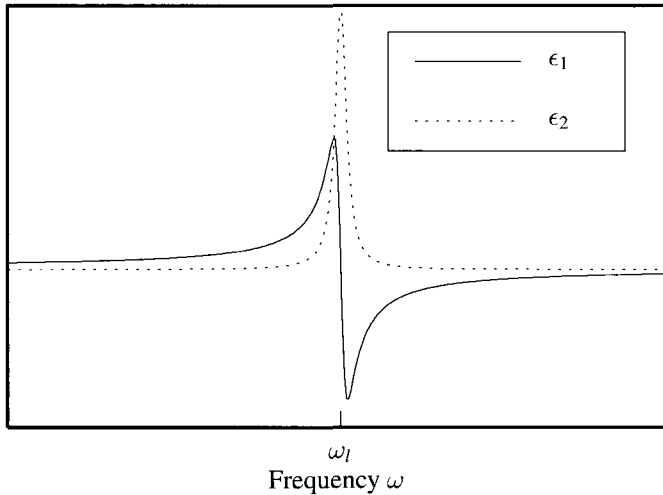


Figure 20.2. Characteristic shapes of the real and imaginary parts of the dielectric function described in Eq. (20.33). Only one term in the sum over l is depicted.

20.3 Kramers–Kronig Relations

Causality. The expression for the dielectric function in Eq. (20.33) was obtained from a simplified mechanical model of solids, but it is a rather general expression of the forms that dielectric constants are allowed to have. There is a constraint upon dielectric constants, not considered until now, that of *causality*.

The electric displacement D is related to the electric field by

$$\vec{D}(\omega) = \epsilon(\omega)\vec{E}(\omega) \Rightarrow \vec{D}(t) = \int dt' \epsilon(t')\vec{E}(t-t'). \quad (20.34)$$

The electric displacement is produced in response to external fields, so one can be certain that if the electric field vanishes up until $t = 0$, the displacement $D(t)$ must

do so as well. In particular, suppose that $\vec{E}(t) = t_0 \vec{E}_0 \delta(t)$ is a brief intense pulse of electric field at $t = 0$, where t_0 is a constant with dimensions of time characterizing the duration of the pulse. Then Eq. (20.34) becomes

$$\vec{D}(t) = \epsilon(t) t_0 \vec{E}_0. \tag{20.35}$$

Because $D(t)$ must vanish for all $t < 0$, it follows that

$$\epsilon(t) = 0 \text{ for } t < 0. \tag{20.36}$$

This requirement continues to hold if ϵ is a tensor, or if the dependence of ϵ on wave number \vec{q} is retained.

The only property of ϵ needed in order to obtain Eq. (20.36) is that it linearly relates two quantities that must be causally connected. A host of other functions have the same property. Some examples are the electric conductivity, which relates current to electric field, the complex reflectivity, which relates light bouncing off a sample to the light coming in, the flow of a fluid being stirred in a rheometer, the vibration of a solid being pulled in a tensile testing apparatus, or the temperature rise of a glass being injected with periodic pulses of heat. Somewhat surprising consequences will flow from Eq. (20.36), and similar consequences should be understood to apply to all these other cases as well.

From Eq. (20.36) it follows that

$$\epsilon(\omega) = \int_0^\infty dt e^{i\omega t} \epsilon(t). \tag{20.37}$$

Allow ω to range over the complex plane. So long as the imaginary part of ω is greater than zero, the exponential function multiplying $\epsilon(t)$ decays as t becomes large, and the integral must be finite; this conclusion follows both because ϵ vanishes for $t < 0$ and because as a response to an impulse at $t = 0$, one cannot expect it to grow exponentially in time thereafter. Therefore $\epsilon(\omega)$ cannot have any poles when ω lies in the upper half of the complex plane. From Cauchy’s theorem, one might write

$$\epsilon(\omega) = \oint \frac{d\omega'}{2\pi i} \frac{\epsilon(\omega')}{\omega' - \omega - i\eta}. \tag{20.38}$$

Close the contour in the upper half-plane. The only pole is at $\omega + i\eta$, where η is very small, and the contribution of this residue gives the result.

However, Eq. (20.38) is not quite right, because in order for Cauchy’s theorem to be valid, the function inside the integral must drop off faster than ω' for large ω' . To get the proper result, it is necessary to have some idea of the form of $\epsilon(\omega)$; all the approximate expressions derived so far behave as $\epsilon^\infty + \mathcal{O}(1/\omega')^2$. The correct version of Eq. (20.38) is therefore

$$\epsilon(\omega) - \epsilon^\infty = \oint \frac{d\omega'}{2\pi i} \frac{\epsilon(\omega') - \epsilon^\infty}{\omega' - \omega - i\eta}. \tag{20.39}$$

ϵ^∞ is the value of ϵ as $\omega \rightarrow \infty$.

The Kramers–Kronig relations are completely contained in Eq. (20.39), but to appreciate them, one must separate the equation into real and imaginary parts. The

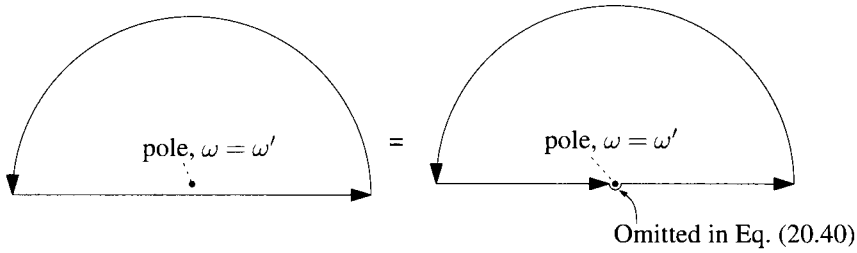


Figure 20.3. The integral at distance η above the real axis can be deformed into a contour integral on the real axis, with a contribution from a half-circuit around the pole at $\omega = \omega'$.

easiest way to accomplish this task is to rewrite Eq. (20.39) so that all the terms in the integrand multiplying $\epsilon(\omega')$ are purely imaginary. Figure 20.3 shows a change in integration contour which makes it possible to send η to zero and which gives

$$\epsilon(\omega) - \epsilon^\infty = \mathcal{P} \int \frac{d\omega' \epsilon(\omega') - \epsilon^\infty}{\pi i \omega' - \omega} \quad \text{To take the principal part } \mathcal{P} \text{ of the integral, keep } \omega' \text{ on the real axis, but integrate on the domain } (-\infty, \omega - \eta] \cup [\omega + \eta, \infty), \text{ finally allowing } \eta \rightarrow 0. \text{ The factor of 2 relative to Eq. (20.39) is needed because the small lower half-circle in Figure 20.3 is omitted.} \quad (20.40)$$

One can now take the real and imaginary parts of Eq. (20.40) immediately, finding

$$\text{Re}[\epsilon(\omega) - \epsilon^\infty] = \mathcal{P} \int \frac{d\omega' \text{Im}[\epsilon(\omega') - \epsilon^\infty]}{\pi \omega' - \omega} \quad (20.41a)$$

$$\text{Im}[\epsilon(\omega) - \epsilon^\infty] = -\mathcal{P} \int \frac{d\omega' \text{Re}[\epsilon(\omega') - \epsilon^\infty]}{\pi \omega' - \omega}. \quad (20.41b)$$

Because $\epsilon(t)$ is real, one must have $\epsilon(\omega) = \epsilon^*(-\omega)$, which implies that the real part of $\epsilon(\omega)$ is even and that the imaginary part is odd. Therefore, using ϵ_1 for the real and ϵ_2 for the imaginary part of ϵ it is conventional to rewrite Eq. (20.41) as

$$\epsilon_1(\omega) - \epsilon^\infty = \mathcal{P} \int_0^\infty \frac{2\omega' d\omega' \epsilon_2(\omega')}{\pi \omega'^2 - \omega^2}. \quad (20.42a)$$

$$\epsilon_2(\omega) = -\mathcal{P} \int_0^\infty \frac{2\omega d\omega' \epsilon_1(\omega') - \epsilon^\infty}{\pi \omega'^2 - \omega^2}. \quad (20.42b)$$

Equations (20.42) constitute the *Kramers–Kronig relation*.

20.3.1 Application to Optical Experiments

The Kramers–Kronig relation has important application to the optical behavior of solids, because it means that measurements of the imaginary part of the dielectric constant—absorption—can be used to find the real part—dispersion—or vice versa. Suppose, for example, that one wishes to find the absorption of light in metals or semiconductors at photon energies lying above the band gap. At these frequencies, the absorption coefficient α is on the order of 10^6 cm^{-1} , and light penetrates only around 100 \AA into the sample. Exceedingly thin samples would be

needed to measure absorption. An alternative is to measure light reflection from a thick sample. If the penetration depth is very small, the sample’s surface will have to be exceedingly flat and free of impurities to provide meaningful results, but such surface preparation may well be easier than creating a 100-Å-thick slice.

Reflection. Reflection from surfaces has its own Kramers–Kronig relation. The amplitude and phase of light bouncing in normal incidence off a flat surface is obtained by multiplying the incoming wave by the *complex reflectivity*

$$\tilde{r} = \frac{\tilde{n} - 1}{\tilde{n} + 1} \equiv \rho e^{i\theta}. \quad \text{The amplitude of reflected wave is } \rho; \theta \text{ contains phase information. See Jackson (1999), Eq. (7.42).} \quad (20.43)$$

The amplitude ρ is what is measured in experiment. Instead of applying Eqs. (20.42) to the dielectric constant ϵ , one can apply it instead to the logarithm of the reflectivity:

$$\ln\left(\frac{\tilde{r}(\omega)}{\tilde{r}(0)}\right) = \ln(\rho(\omega)/\rho(0)) + i(\theta(\omega) - \theta(0)), \quad (20.44)$$

obtaining

$$\theta(\omega) - \theta(0) = -\frac{1}{\pi} \mathcal{P} \int d\omega' \ln \left[\frac{\rho(\omega')}{\rho(0)} \right] \left[\frac{1}{\omega' - \omega} - \frac{1}{\omega'} \right] \quad (20.45)$$

This intermediate form is recorded to make clear that the integrand vanishes quickly enough as $\omega' \rightarrow \infty$ to legitimize the changes in the contour of integration.

$$\Rightarrow \theta(\omega) = -\frac{2\omega}{\pi} \mathcal{P} \int_0^\infty d\omega' \frac{\ln \rho(\omega')}{\omega'^2 - \omega^2}. \quad \text{Because } \rho(\omega) \text{ is even, and } \theta(\omega) \text{ as an odd continuous function must vanish at the origin.} \quad (20.46)$$

In this way, absorption can be determined by measuring reflection.

Ellipsometry. In general, linearly polarized light reflected from a surface at an angle other than 0° or 90° leaves with elliptical polarization. Using polarized light in this way to measure optical constants is called *ellipsometry*, and the basic formulae are described by Yu and Cardona (1996), p. 239.

Sum Rules. A benefit of the Kramers–Kronig relations is that they permit conclusions about physical properties in one frequency range to be drawn from measurements in an entirely different frequency range. As an example of how such information is to be extracted, it is helpful to present two sum rules. The first follows from Eq. (20.42a) simply by setting ω to zero, and it reads

$$\epsilon_1(0) - 1 = \frac{2}{\pi} \int_0^\infty d\omega' \frac{\epsilon_2(\omega')}{\omega'}. \quad (20.47)$$

So the static dielectric constant is related to an integral over all dissipative processes.

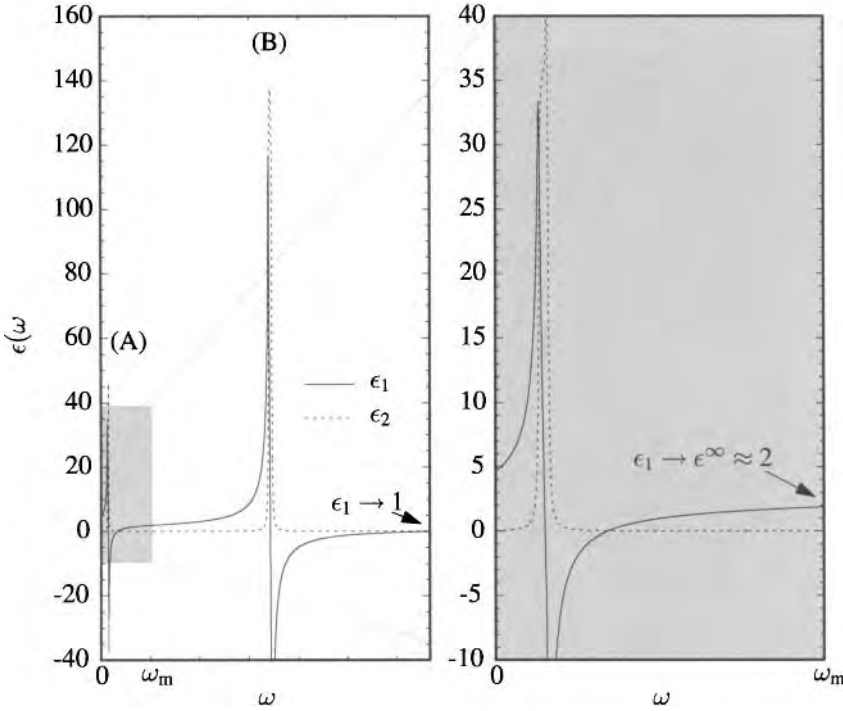


Figure 20.4. Schematic view of dielectric constant resulting from two groups (A) and (B) of modes, widely separated in frequency. In the vicinity of ω_m the imaginary part of the dielectric constant nearly vanishes, and the real part goes to a constant ϵ^∞ , but $\epsilon^\infty \neq 1$ because of the additional structure above ω_m . The left panel shows the complete dielectric function, while the right panel focuses upon a low-frequency region that would be described as a resonant band embedded in dielectric medium of constant ϵ^∞ .

As a second example, set $\omega \approx \omega_m$ in Eq. (20.42a) and refer to Figure 20.4. Because $\omega \gg \omega'$ whenever ϵ_2 is nonzero in region (A) and $\omega \ll \omega'$ whenever ϵ_2 is nonzero in region (B), Eq. (20.42a) becomes

$$\text{Re}[\epsilon(\omega)] = 1 - \frac{2}{\pi\omega^2} \int_0^{\omega_m} d\omega' \omega' \epsilon_2(\omega') + \frac{2}{\pi} \int_{\omega_m}^{\infty} d\omega' \frac{\epsilon_2(\omega')}{\omega'} \quad (20.48)$$

$$= \epsilon^\infty - \frac{\omega_p^2}{\omega^2}, \quad \text{Using Eq. (20.47), extending the integration past region (B).} \quad (20.49)$$

where

$$\epsilon^\infty = 1 + \frac{2}{\pi} \int_{\omega_m}^{\infty} d\omega' \frac{\epsilon_2(\omega')}{\omega'} \quad (20.50)$$

and

$$\omega_p^2 \equiv \frac{4\pi n e^2}{m_{\text{opt}}} = \frac{2}{\pi} \int_0^{\omega_m} d\omega' \omega' \epsilon_2(\omega') \quad (20.51)$$

Take this expression to define the optical mass m_{opt} , which will be calculated from a microscopic viewpoint in Eq. (23.26).

$$\Rightarrow \int_0^{\omega_m} d\omega' \omega' \epsilon_2(\omega') = \frac{2\pi^2 n e^2}{m_{\text{opt}}} \quad (20.52)$$

The frequency ω_p is the plasma frequency, and it generalizes the quantity defined by Eqs. (20.31) and (20.32). The *optical mass* m_{opt} is defined by Eq. (20.52). Thus general lessons to learn from Eq. (20.49) are as follows:

1. A collection of absorbing modes whose frequency lies well below the probe frequency ω_m acts like a collection of unbound electrons, and its influence falls off as $1/\omega^2$.
2. A collection of absorbing modes whose frequency lies well above the probe frequency ω_m acts like a high-frequency dielectric constant ϵ^∞ .

20.4 The Kubo–Greenwood Formula

One of the most important quantum-mechanical calculations in the theory of solids concerns the *linear response* of a collection of electrons to an externally applied electromagnetic field. Not only does this calculation permit one to find the electrical conductivity of solids, it describes their interaction with light and also permits a self-consistent description of the interaction of electrons with one another. The strength of the calculation is that it starts from quantum-mechanical principles, introducing few phenomenological assumptions. This feature is also its greatest weakness, and for the purposes of studying thermoelectric properties of solids the Boltzmann equation is more powerful.

The setting of this calculation is quite general. Consider a collection of electrons occupying states of energy

$$\mathcal{E}_l = \hbar\omega_l \quad \text{The calculation is within the independent electron approximation.} \quad (20.53)$$

with probability f_l . Usually f_l will be a Fermi factor, which means essentially that states up to the Fermi energy are occupied, while those above are unoccupied. However, the calculation continues to function when f_l has other forms, a fact of particular importance for lasers. Apply an external electromagnetic field, and ask for the expectation value of the current that results in response. The calculation has two steps. First, one has to work out the response to first order of an arbitrary quantum-mechanical state to a potential $\hat{U}(t)$ with time dependence $\cos \omega t$. Next, one finds the expectation value of the current in this state.

20.4.1 Born Approximation

Begin with the Born approximation, which states that an eigenstate $|l\rangle$ of $\hat{\mathcal{H}}$ that comes in contact with a weak time-dependent potential $\hat{U}(t)$ evolves into

$$|\tilde{l}(t)\rangle \approx \mathcal{N} \left[e^{-i\hat{\mathcal{H}}t/\hbar} |l\rangle + \int_{-\infty}^t dt' e^{-i\hat{\mathcal{H}}(t-t')/\hbar} \frac{\hat{U}(t')}{i\hbar} e^{-i\hat{\mathcal{H}}t'/\hbar} |l\rangle \right] \quad (20.54)$$

The eigenstates of \mathcal{H} are denoted by $|l\rangle$, while the time-dependent state evolving from $|l\rangle$ under the combined action of \mathcal{H} and \hat{U} is called $|\tilde{l}(t)\rangle$. \mathcal{N} is a normalization constant.

$$= \mathcal{N} \left[e^{-i\omega_l t} |l\rangle + \sum_{l'} \int_{-\infty}^t dt' |l'\rangle e^{-i\omega_{l'}(t-t')} \frac{\langle l' | \hat{U} | l \rangle}{i\hbar} e^{-i\omega_l t' - i\omega_{l'} t'} \right] \quad (20.55)$$

Take $\hat{U}(t')$ to have time dependence $\exp(-i\omega_l t')$; ω must have a small positive imaginary part η for the time integral converge, or else take $\omega_{l'}$ to have an imaginary part $-\gamma_{l'}$.

$$= \left\{ |l\rangle + \sum_{l' \neq l} |l'\rangle \frac{\langle l' | \hat{U} | l \rangle e^{-i\omega_l t}}{\hbar(\omega_l - \omega_{l'} + \omega)} \right\} e^{-i\omega_l t}. \quad \text{Excluding } l \text{ from the sum takes care of the normalization.} \quad (20.56)$$

If, on the other hand, the time dependent potential were to have the form $U^* \exp[i\omega^* t]$, then one would have instead

$$|\tilde{l}(t)\rangle = \left\{ |l\rangle + \sum_{l' \neq l} |l'\rangle \frac{\langle l' | \hat{U}^* | l \rangle e^{i\omega^* t}}{\hbar(\omega_l - \omega_{l'} - \omega^*)} \right\} e^{-i\omega_l t}. \quad (20.57)$$

Imaginary Frequencies. For purely formal reasons, so that the integrals in (20.56) converge, it is necessary to take the frequencies ω or $\omega_{l'}$ to have imaginary parts; ω needs a small positive imaginary part η , while $\omega_{l'}$ needs an imaginary part $-\gamma_{l'}$. The constant η does not have much physical interest. It corresponds to turning on the interaction potential U very slowly, a long time in the past, so that the interacting system can adiabatically adjust itself to the new potential and reach a steady state. The constants $\gamma_{l'}$ are more important. By making them nonzero, one is able to describe transitions into metastable states. The initial state of a system is usually very stable; the system has been there for a long time, and it would remain if not perturbed by U . However, the intermediate states indexed by l' are usually not true eigenstates. In a formally exact description of a quantum system, the eigenvalues and frequencies should all be real. The common situation is, however, that the quantum states l' used in describing excited states of a system are not exact, both because one has only an approximate solution of the Hamiltonian and because the Hamiltonian actually has many more degrees of freedom than one is able to describe. Not being exact eigenstates, these states decay, and the decay can be modeled by giving them complex energies. All Bloch states $\psi_{n\vec{k}}$ should really be described in this way; they decay because electron–electron interactions have not been treated exactly, because the real wave functions involve many electrons not one, because the crystal in which they live has impurities, or because of interactions with phonons. Localized states, described for example by Wannier functions, should be taken to decay for the same sorts of reasons. The important point is that many different types of ignorance and error can be accommodated with a few constants $\gamma_{l'}$, and only in this way does detailed comparison with experiment become possible. The initial states $|l\rangle$ usually do not decay. They are, after all, states the system chose to go to itself in the absence of outside interference.

Interaction with Electromagnetic Field. The next step is to use Eq. (20.56) to describe a situation in which a collection of electrons interacts with an electromagnetic field. As in Section 16.3 the sensible way for an electrical field to coexist with periodic boundary conditions is to introduce it through a vector potential. Specializing to the case described by Eq. (20.24) where the wavelength of light is much greater than unit cell dimensions or electron mean free paths, one can treat the light

as a spatially uniform oscillating field with

$$\vec{A} = \frac{c\vec{E}}{i\omega}e^{-i\omega t} + \text{c.c.} \quad \text{c.c. means "complex conjugate."} \tag{20.58}$$

The next task is to find the expectation value of the current in such a state \tilde{l} . When an electromagnetic field is described classically by a vector potential \vec{A} , \hat{P} must be understood as the canonical momentum, where classically $\vec{p} = m\vec{v} - e\vec{A}/c$. So the current operator is

$$\hat{j} = -\frac{e}{m}\left[\hat{P} + \frac{e}{c}\vec{A}\right], \quad \text{See Goldstein (1980), pp. 341-342.} \tag{20.59}$$

and the Hamiltonian changes also because

$$\hat{P} \rightarrow \hat{P} + \frac{e}{c}\vec{A}, \tag{20.60}$$

so the kinetic energy becomes

$$\frac{(\hat{P} + \frac{e}{c}\vec{A})^2}{2m} \tag{20.61}$$

$$= \frac{\hat{P}^2}{2m} + \frac{e}{2mc}[\vec{A} \cdot \hat{P} + \hat{P} \cdot \vec{A}] + \dots \quad \text{Terms of order } A^2 \text{ are irrelevant in a theory of linear response.} \tag{20.62}$$

$$= \frac{\hat{P}^2}{2m} + \frac{e}{mc}[\vec{A} \cdot \hat{P}] + \dots \quad \text{It is conventional to specialize to the transverse gauge } \vec{\nabla} \cdot \vec{A} = 0 \text{ so as to obtain this simplification.} \tag{20.63}$$

To linear order in applied fields, the Hamiltonian is changed by addition of a term

$$\hat{U}(t) = \frac{e}{mi\omega}[\vec{E} \cdot \hat{P}]e^{-i\omega t} - \frac{e}{mi\omega^*}[\vec{E} \cdot \hat{P}]e^{i\omega^*t}. \tag{20.64}$$

The contribution to the current of state $|\tilde{l}\rangle$ is therefore .

$$\vec{J} = \mathcal{V}\vec{j} = -\frac{e}{m}\langle\tilde{l}|\hat{P} + \frac{e}{c}\vec{A}|\tilde{l}\rangle \tag{20.65}$$

Using Eq. (20.58) for the the vector potential and using Eq. (20.56) for the state $|\tilde{l}\rangle$.

$$= -\frac{e}{m}\langle l|\hat{P}|l\rangle - \left\{ \frac{e^2\vec{E}}{im\omega}e^{-i\omega t} + \text{c.c.} \right\} \langle l|\hat{j}|l\rangle. \quad \text{This term comes from the expectation value } \langle l|\hat{j}|l\rangle. \text{ The next two lines result from the terms proportional to } \vec{E} \text{ in } |\tilde{l}\rangle \text{ acting on left and right-hand sides.}$$

$$\begin{aligned} & -\frac{e^2}{i\hbar m^2} \sum_{l' \neq l} \langle l|\hat{P}|l'\rangle \langle l'|\vec{E} \cdot \hat{P}|l\rangle \left\{ \frac{e^{-i\omega t}}{\omega(\omega_l - \omega_{l'} + \omega)} - \frac{e^{i\omega^*t}}{\omega^*(\omega_l - \omega_{l'} - \omega^*)} \right\} \\ & -\frac{e^2}{i\hbar m^2} \sum_{l' \neq l} \langle l|\vec{E} \cdot \hat{P}|l'\rangle \langle l'|\hat{P}|l\rangle \left\{ \frac{e^{-i\omega t}}{\omega(\omega_l^* - \omega_{l'}^* - \omega)} - \frac{e^{i\omega^*t}}{\omega^*(\omega_l^* - \omega_{l'}^* + \omega^*)} \right\}. \end{aligned} \tag{20.66}$$

The conductivity tensor $\sigma(\omega)$ is defined as the coefficient of $e^{-i\omega t}$ that relates the current \vec{j} to the applied electric field. Assuming that state $|l\rangle$ is occupied with

probability f_l , assuming that the ground state had no net current, and summing over all states l gives the *Kubo–Greenwood formula*

$$\begin{aligned} & \sigma_{\alpha\beta}(\omega) \\ &= \frac{-e^2}{im\omega\mathcal{V}} \sum_l \left[f_l \delta_{\alpha\beta} + \sum_{l'} \frac{f_l}{\hbar m} \left\{ \frac{\langle l|\hat{P}_\alpha|l'\rangle\langle l'|\hat{P}_\beta|l\rangle}{\omega_l - \omega_{l'} + \omega} + \frac{\langle l|\hat{P}_\beta|l'\rangle\langle l'|\hat{P}_\alpha|l\rangle}{\omega_l^* - \omega_{l'}^* - \omega} \right\} \right]. \end{aligned} \quad (20.67)$$

This expression simplifies if all the ω_l are real. Then exchanging l and l' in the second term gives

$$\sigma_{\alpha\beta}(\omega) = \frac{-e^2}{im\omega\mathcal{V}} \left[\sum_l f_l \delta_{\alpha\beta} + \sum_{l'} \frac{f_l - f_{l'}}{\hbar m} \frac{\langle l|\hat{P}_\alpha|l'\rangle\langle l'|\hat{P}_\beta|l\rangle}{\omega_l - \omega_{l'} + \omega + i\eta} \right]. \quad (20.68)$$

Adding a small imaginary part $i\eta$ to ω explicitly.

Absorption of incoming energy is given by the real part of the conductivity tensor, and is worth writing out separately. When all the decay rates $\gamma_{l'} = -\text{Im } \omega_{l'}$ are zero, the real part is entirely induced by the small imaginary term η in the denominator of Eq. (20.68), and is

$$\text{Re } [\sigma_{\alpha\beta}(\omega)] = -\text{Im} \frac{e^2}{m\omega\mathcal{V}} \left[\sum_{ll'} \frac{f_l - f_{l'}}{\hbar m} \frac{\langle l|\hat{P}_\alpha|l'\rangle\langle l'|\hat{P}_\beta|l\rangle}{\omega_l - \omega_{l'} + \omega + i\eta} \right] \quad (20.69)$$

$$= \frac{\pi}{\omega\mathcal{V}} \sum_{ll'} (f_l - f_{l'}) \langle l|\frac{e\hat{P}_\alpha}{m}|l'\rangle\langle l'|\frac{e\hat{P}_\beta}{m}|l\rangle \delta(\mathcal{E}_{l'} - \mathcal{E}_l - \hbar\omega). \quad (20.70)$$

Recall $\text{Im}[1/(x - i\eta)] = \pi\delta(x)$.

More generally, if decay rates $\gamma_l = -\text{Im } \omega_l$ are not zero,

$$\text{Re } [\sigma_{\alpha\beta}(\omega)] = \frac{e^2\pi}{\hbar\omega m^2\mathcal{V}} \sum_{ll'} (f_l - f_{l'}) \langle l|\hat{P}_\alpha|l'\rangle\langle l'|\hat{P}_\beta|l\rangle F_{ll'}(\omega), \quad (20.71)$$

where $F_{ll'}(\omega) = (\gamma_{l'} - \gamma_l) / (\pi[(\omega - \omega_{l'} + \omega_l)^2 + \gamma_{l'}^2])$ is the *lineshape*, a Lorentzian of width $\gamma_{l'} - \gamma_l$ centered at $\omega_l - \omega_{l'}$.

Expression (20.71) can be simplified slightly with some additional assumptions. First assume that the occupation numbers f_l are either 1 for occupied states or 0 for unoccupied states. Then the only terms contributing to the conductivity are those where l or l' is occupied, but not both. Since the occupied states are stable, take $\gamma_l = 0$ for occupied states. Finally, choose $\omega > 0$ and suppose that $F_{ll'}$ is negligibly small whenever l' is an occupied state and l is not. Under these conditions one can write

$$\text{Re } [\sigma_{\alpha\beta}(\omega)] = \frac{e^2}{\hbar\omega m^2\mathcal{V}} \sum_{\substack{l \text{ occupied} \\ l' \text{ unoccupied}}} \gamma_{l'} \frac{\langle l|\hat{P}_\alpha|l'\rangle\langle l'|\hat{P}_\beta|l\rangle}{[\omega - (\omega_{l'} - \omega_l)]^2 + \gamma_{l'}^2}. \quad (20.72)$$

Equation (20.67) has a dual interpretation. For sufficiently small values of ω it reduces to Eq. (16.29), and it describes the motion of electrons within a single band with an effective mass. However, as ω rises toward optical frequencies, the effective mass picture breaks down, and Eq. (20.67) now describes transitions between levels that become possible whenever there is a resonance such that $\omega_{l'} - \omega_l = \omega$. For a material in equilibrium, only low-lying states are occupied, higher-lying states are empty, and the real part of the conductivity tensor (20.71) describes the absorption of energy from incoming waves. However, if a material can be prepared out of equilibrium, with higher-lying states occupied and low-lying states empty, the sign of energy absorption reverses, and Eq. (20.71) describes stimulated emission. Therefore, this equation describes the basic operation of the laser.

20.4.2 Susceptibility

A slight variant on the preceding calculation is valuable in order to produce estimates of the interactions of electrons with one another. The calculation differs from the previous one in several respects. First and most important, electrical potentials created by electrons in solids have wavelengths on the order of interatomic spacings. The $\vec{q} \rightarrow 0$ limit employed until now is not legitimate, and the perturbing potential \hat{U} must be taken to behave as

$$U(\vec{q}, \omega) e^{i\vec{q}\cdot\vec{r} - i\omega t} + c.c. \tag{20.73}$$

In compensation for the difficulties introduced by the extra spatial dependence of U , it is customary to take the unperturbed electron states $|l\rangle$ simply to be plane waves, not so much because the approximation is carefully justified as because otherwise the expressions become unwieldy. The calculation is also simplified by focusing upon the expectation value of the charge density rather than upon the current, making expressions somewhat more compact.

The electron density n is defined to be

$$n(\vec{r}, t) = \sum_l f_l \langle \tilde{l}(t) | \vec{r} \rangle \langle \vec{r} | \tilde{l}(t) \rangle. \tag{20.74}$$

If one uses the simplification that $|l\rangle$ is a plane wave, takes the potential U to be an electrical potential

$$U(\vec{q}, \omega) = -eV(\vec{q}, \omega), \tag{20.75}$$

and proceeds in just the fashion that leads to Eq. (20.68), Problem 5 shows that

$$-en(\vec{q}, \omega) = \chi_c(\vec{q}, \omega)V(\vec{q}, \omega) \tag{20.76}$$

with

$$\chi_c(\vec{q}, \omega) = e^2 \sum_{\vec{k}\sigma} \frac{1}{\hbar V} \frac{(f_{\vec{k}+\vec{q}} - f_{\vec{k}})}{\omega_{\vec{k}+\vec{q}} - \omega_{\vec{k}} - \omega}. \tag{20.77}$$

χ_c is not the dielectric susceptibility. It relates charge density to applied field, rather than dipole moments to field. Its relation to the dielectric constant ϵ is determined by writing

$$\nabla^2 V = \nabla^2 V_{\text{ext}} + 4\pi en = 4\pi en_{\text{ext}} + 4\pi en \quad \text{See Eq. (20.10).} \quad (20.78)$$

$$\Rightarrow \nabla^2 V = -\vec{\nabla} \cdot \vec{D} + 4\pi en \quad (20.79)$$

$$\Rightarrow -q^2 V(\vec{q}, \omega) = -i\vec{q} \cdot \vec{D} + 4\pi en(\vec{q}, \omega) \quad (20.80)$$

$$\Rightarrow -q^2 V(\vec{q}, \omega) = -i\vec{q} \cdot \vec{D} - 4\pi \chi_c(\vec{q}, \omega) V(\vec{q}, \omega) \quad (20.81)$$

$$\Rightarrow (4\pi \chi_c - q^2) V(\vec{q}, \omega) = -i\vec{q} \cdot \vec{D} \quad (20.82)$$

$$\Rightarrow (q^2 - 4\pi \chi_c) \vec{E} = \vec{q}(\vec{q} \cdot \vec{D}) \quad \text{Because } \vec{E} = -i\vec{q}V. \quad (20.83)$$

For longitudinal vibrations, where $\vec{q} \cdot \vec{D} = qD$, one therefore has

$$\epsilon(\vec{q}, \omega) = 1 - \frac{4\pi \chi_c}{q^2} \quad (20.84)$$

In this form, $\epsilon(\vec{q}, \omega)$ is called the *dynamic Lindhard dielectric function*.

20.4.3 Many-Body Green Functions

The Born approximation is only the first step in formal schemes that track the effects of perturbations. The most powerful formal methods employ Green's functions similar to those in Section 18.4.2, but generalized to describe many interacting electrons. These methods make it possible to obtain a variety of results, including expressions for electrons interacting with light and with each other. Many of the results can also be obtained by more elementary means, although the elementary derivations are not as systematic and are sometimes less convincing. Some of the many books describing many-body Green functions are Kadanoff and Baym (1962), Abrikosov et al. (1965), and Fetter and Walecka (1971).

Problems

1. **Numerical evaluation of Kramers–Kronig relations:** While the Kramers–Kronig relations in the form (20.39) are valuable for analytical work, they are almost useless for practical evaluation of response functions. The integrals are very singular and are hard to evaluate accurately.

One practical way to employ these relations is by returning to the arguments from which they originally were derived. To illustrate the process, suppose that the imaginary part of a dielectric constant has been measured and that the experimental data give

$$\text{Im}\epsilon(\omega) = \epsilon_2(\omega) \approx \frac{\omega}{\omega_1} [2e^{-((\omega/\omega_1)^2 - 1)^2/3} + 10e^{-((\omega/\omega_2)^2 - 1)^2/5}] \quad (20.85)$$

with

$$\omega_1 = 4 \text{ Hz} \quad \text{and} \quad \omega_2 = 13 \text{ Hz}. \quad (20.86)$$

The goal is to find $\text{Re}[\epsilon(\omega)] = \epsilon_1(\omega)$.

- (a) Recall that $\epsilon(t)$ is real. Show that $\epsilon_1(\omega)$ is an even function of ω and that $\epsilon_2(\omega)$ is an odd function of ω .
- (b) Show that the inverse Fourier transform of $\epsilon_1(\omega)$ is an even function of t , and that the inverse Fourier transform of $\epsilon_2(\omega)$ is an odd function of t .
- (c) Given

$$\epsilon_2(t) \equiv \int \frac{d\omega}{2\pi} e^{-i\omega t} \epsilon_2(\omega), \quad (20.87)$$

how can

$$\epsilon_1(t) \equiv \int \frac{d\omega}{2\pi} e^{-i\omega t} \epsilon_1(\omega) \quad (20.88)$$

be determined, using the fact that $\epsilon(t) = 0$ for $t < 0$?

- (d) Making use of these suggestions and employing numerical fast Fourier transforms, find the real part of the dielectric constant given by Eq. (20.85)

2. **Connection between Kubo formula and Boltzmann equation:** It is reassuring to verify that the Boltzmann equation does indeed emerge as the low-frequency limit of the Kubo formula for the conductivity. Expression (20.67) becomes somewhat problematic in this limit, because from Eq. (20.58) the vector potential and hence the current diverge as $\omega \rightarrow 0$. The dissipative processes preventing this growth can be represented by taking $\omega \rightarrow \omega + i/\tau$. Making this substitution and sending the real part, ω , to zero, verify that Eq. (20.67) coincides with a result of the Boltzmann approach.
3. **Cubic symmetry:** Show that if a conductivity tensor $\sigma_{\alpha\beta}$ is invariant under the cubic symmetry operations, then it must be a multiple of the unit tensor.
4. **Sums of poles:** Consider the function

$$f(\omega) = \sum_{l=1}^{30} \frac{1}{\omega - \omega_l - i\eta}. \quad (20.89)$$

- (a) Plot this function for $\omega \in [-1, 2]$ when $\omega_l = l/30$ for $\eta = 10^{-4}$, $\eta = 10^{-2}$, and $\eta = 0.1$.
- (b) What integral does the sum correspond to for the larger values of η ? What is the value of the integral, and does it compare well with the sum?
- (c) The function f makes a qualitative transition between one type of behavior for small η and another type of behavior for large η . What determines the value of η at which the transition takes place?
- (d) What does this problem reveal about the relation between eigenvalues of a quantum mechanical Hamiltonian and the idea of a density of states? What is the significance of η ?

5. Susceptibility of the electron gas:

(a) Writing the electron density n defined in Eq. (20.74) in \vec{k} space, show that

$$n(\vec{q}, t) \equiv \int d\vec{r} e^{-i\vec{q}\cdot\vec{r}} n(\vec{r}, t) = \sum_{l, \vec{q}_1} f_l \langle \vec{l} | \vec{q}_1 \rangle \langle \vec{q} + \vec{q}_1 | \vec{l} \rangle \quad (20.90)$$

(b) Consider a potential of the form

$$U(\vec{r}, t) = U(\vec{q}, \omega) e^{i\vec{q}\cdot\vec{r} - i\omega t} / \mathcal{V}. \quad (20.91)$$

Take the unperturbed states $|l\rangle$ to be plane waves. Show that Eq. (20.56) produces for n

$$\frac{eU(\vec{q}, \omega)}{\mathcal{V}} \sum_{\vec{k}\sigma} \frac{1}{\hbar} \left[\frac{e^{i\omega t} f_{\vec{k}}}{\omega_{\vec{k}} - \omega_{\vec{k}+\vec{q}} + \omega} - \frac{e^{-i\omega t} f_{\vec{k}+\vec{q}}}{\omega_{\vec{k}} - \omega_{\vec{k}+\vec{q}} - \omega} \right]. \quad (20.92)$$

To obtain this result, drop a term proportional to $\delta_{\vec{q},0}$ in order to focus upon spatially nonuniform conditions.

(c) Consequently, derive Eqs. (20.76) and (20.77).

6. Static Lindhard dielectric function:

(a) By relabeling the first sum in Eq. (20.77), show that for $\omega = 0$,

$$\chi_c = -\frac{e^2}{\mathcal{V}} \sum_{\vec{k}\sigma} 2f_{\vec{k}} \frac{1}{\hbar^2 \left[\frac{\vec{q}\cdot\vec{k}}{m} + \frac{q^2}{2m} \right]}. \quad (20.93)$$

(b) Transform Eq. (20.93) into an integral over \vec{k} in polar coordinates. First integrate over $\cos \theta$, and next integrate over k , from 0 to k_F . The answer should be

$$\chi_c = -\frac{me^2}{\pi^2 \hbar^2} \frac{(4k_F^2 - q^2) \log \left(\frac{2k_F + q}{2k_F - q} \right) + 4k_F q}{8q}. \quad (20.94)$$

(c) Take the limit $q \rightarrow 0$ and show that

$$\chi_c = -\frac{me^2 k_F}{\pi^2 \hbar^2}. \quad (20.95)$$

7. Screening of bare nuclei: The Lindhard dielectric function, Eq. (20.84), can be used in a wide variety of physical contexts, both dynamic and static, to solve problems involving the interaction of many electrons. Consider, for example, a nucleus of charge Z surrounded by a cloud of Z electrons, which produces a potential U for the purposes of Eq. (20.73) equal to

$$U_{\text{ext}}(\vec{q}) = -\frac{4\pi Z e^2}{q^2}. \quad \text{This is the Fourier transform of the Coulomb potential } -Ze^2/r. \quad (20.96)$$

(a) Show that Eq. (20.83) can be rewritten as

$$U(\vec{q}, \omega) = \frac{U_{\text{ext}}(\vec{q}, \omega)}{1 - 4\pi\chi_c/q^2}, \quad (20.97)$$

where U is the total potential produced by the nucleus together with the cloud of surrounding electrons.

(b) Using the result of Problem 6, show that

$$\frac{1}{\Omega}U(q=0) = -\frac{2}{3}\mathcal{E}_F, \quad (20.98)$$

where Ω is the volume of the unit cell, and \mathcal{E}_F is the Fermi energy $\hbar^2 k_F^2/2m$ appropriate for Z free electrons per unit cell.

References

- A. A. Abrikosov, L. P. Gor'kov, and I. Y. Dzyaloshinskii (1965), *Quantum Field Theoretical Methods in Statistical Physics*, 2nd ed., Pergamon Press, Oxford.
- A. Einstein (1905), The production and transformation of light: A heuristic point of view, *Annalen der Physik (Leipzig)*, **17**, 132–148. In German.
- A. Fetter and J. D. Walecka (1971), *Quantum Theory of Many-Particle Systems*, McGraw-Hill, San Francisco.
- H. Goldstein (1980), *Classical Mechanics*, 2nd ed., Addison-Wesley, Reading, MA.
- O. Heaviside (1892), *Electrical Papers*, London, Macmillan.
- H. Hertz (1887), The effect of ultraviolet light on an electrical discharge, *Annalen der Physik (Leipzig)*, **31**, 983–1000. in German.
- Y. Il'inskii and L. V. Keldysh (1994), *Electromagnetic Response of Material Media*, Plenum Press, New York.
- J. D. Jackson (1999), *Classical Electrodynamics*, 3rd ed., John Wiley and Sons, New York.
- L. P. Kadanoff and G. Baym (1962), *Quantum Statistical Mechanics; Green's Function Methods in Equilibrium and Nonequilibrium Problems*, W. A. Benjamin, New York.
- J. J. Thomson (1897), Cathode rays, *Philosophical Magazine*, **44**, 293–316.
- P. Y. Yu and M. Cardona (1996), *Fundamentals of Semiconductors*, Springer-Verlag, Berlin.

21. Optical Properties of Semiconductors

21.1 Introduction

Chapter 19 made extensive use of the band theory of crystals to describe the transport properties of semiconductors. It relied upon accurate values for energy gaps, as well as upon effective masses of electrons and holes in the vicinities of band maxima and minima. However, although the electrical properties of semiconductors depend crucially upon these quantities, the dependence is indirect. The most accurate experimental determinations come from optical measurements, where photons drive electrons between various Bloch states. These measurements are not nearly so simple as they sound. Apart from the difficulties of obtaining clean surfaces and pure samples, the process of optical absorption usually demands understanding some physics beyond the simple band theory. In the case of silicon and germanium, the lowest-energy optical transitions are indirect, and they cannot proceed without aid from phonons. Even in the semiconductors with a direct optical gap, the absorption process is almost always complicated by excitons, excitations resulting from the attraction between an electron and the hole it has left behind. These observations confirm that no simple model such as the one-electron picture of energy bands in a crystal will completely capture experimental phenomena in solids and that the more precise experiments become, the more apparent will be the discrepancies.

21.2 Cyclotron Resonance

In principle, once the band structure of the semiconductor is known, so are the effective masses, because they are nothing but second derivatives of the band energy \mathcal{E} with respect to the Bloch wave vector \vec{k} as in Eq. (16.28). This definition provides a way to find effective masses from band structure calculations, but is almost useless if they are to be determined experimentally. Experimental determination of effective masses requires a physical probe that tests dynamics directly, a service provided in semiconductors by the technique of *cyclotron resonance*.

Effective masses enter into expressions for conductivity such as $\sigma = ne^2\tau/m^*$, but always in conjunction with the relaxation time, making it difficult to separate the two. Cyclotron resonance solves this problem by introducing a magnetic field, as shown in Figure 21.1. Classically, an electron moving at velocity v in a magnetic induction of strength B experiences a force perpendicular to the direction of motion

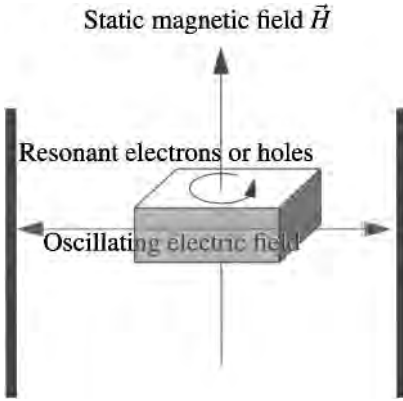


Figure 21.1. Cyclotron resonance is produced in a semiconductor by applying a static magnetic field and then applying microwave radiation at the orbital frequency of the electrons or holes.

of magnitude evB/c . Assuming it travels in a circular orbit of radius R and setting the centripetal force equal to the magnetic force

$$\frac{m^*v^2}{R} = \frac{evB}{c} \quad (21.1)$$

predicts an orbital frequency

$$\omega_c = \frac{v}{R} = \frac{eB}{m^*c} = 17.6 \frac{m}{m^*} \left[\frac{B}{\text{kG}} \right] \text{ GHz.} \quad (21.2)$$

Because this oscillation frequency is independent of the radius of the orbit, by applying a perpendicular electric field with frequency ω_c , electrons can be excited to large orbits and resonantly absorb incoming radiation. The relaxation time enters nowhere in the resonance condition, although it plays a crucial role in determining when the resonance is practically observable.

Calculation of Absorption. It is not too cumbersome to work out a detailed expression for the absorption of microwave radiation so long as the effective mass m^* of an electron (or hole) can be taken to be a scalar. In the semiclassical approximation the dynamics of electrons are given by

$$\dot{\vec{v}} + \frac{\vec{v}}{\tau} = -\frac{e\vec{E}}{m^*} - \frac{e}{m^*c} \vec{v} \times \vec{B}. \quad \tau \text{ is the relaxation time.} \quad (21.3)$$

Taking the static \vec{B} field to point along the \hat{z} direction, and allowing both \vec{E} and \vec{v} vary in time as $e^{-i\omega t}$, one has that

$$\left(-i\omega + \frac{1}{\tau} \right) \vec{v} = -\frac{e\vec{E}}{m^*} - \omega_c (\hat{x}v_y - \hat{y}v_x) \quad (21.4)$$

$$\Rightarrow \left(-i\omega + \frac{1}{\tau} \right) \vec{v} = -\frac{e\vec{E}}{m^*} - \omega_c \begin{pmatrix} 0 & 1 & 0 \\ -1 & 0 & 0 \\ 0 & 0 & 0 \end{pmatrix} \vec{v}. \quad (21.5)$$

Therefore

$$\vec{j} = -ne\vec{v} \equiv \sigma\vec{E}, \quad \vec{j} \text{ is the current density, and } n \text{ is the conduction electron density.} \quad (21.6)$$

where

$$\sigma = \begin{pmatrix} \sigma_{xx} & \sigma_{xy} & 0 \\ -\sigma_{xy} & \sigma_{xx} & 0 \\ 0 & 0 & \sigma_{zz} \end{pmatrix} \quad (21.7)$$

$$\sigma_{xx} = \frac{\sigma_0(1 - i\omega\tau)}{(1 - i\omega\tau)^2 + \omega_c^2\tau^2} \quad (21.8a)$$

$$\sigma_{xy} = -\frac{\sigma_0\tau\omega_c}{(1 - i\omega\tau)^2 + \omega_c^2\tau^2} \quad (21.8b)$$

and

$$\sigma_{zz} = \frac{\sigma_0}{1 - i\omega\tau}, \quad (21.8c)$$

with

$$\sigma_0 = \frac{ne^2\tau}{m^*}. \quad (21.8d)$$

If the applied electric field is along \hat{x} , then the time-averaged power absorbed by the sample, $\langle \vec{E} \cdot \vec{j} \rangle / 2$, is proportional to the real part of σ_{xx} , which is

$$\text{Re}[\sigma_{xx}] = \sigma_0 \frac{\omega_c^2\tau^2 + \omega^2\tau^2 + 1}{(\omega_c^2\tau^2 - \omega^2\tau^2 + 1)^2 + 4\omega^2\tau^2}. \quad (21.9)$$

A plot of Eq. (21.9) appears in Figure 21.2 for several values of $\omega\tau$.

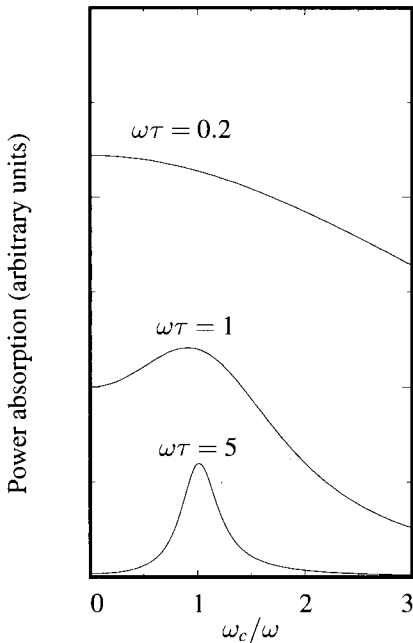


Figure 21.2. Plot of Eq. (21.9) for three values of $\omega\tau$. The frequency ω is the frequency of the oscillating electric field \vec{E} —in contrast with ω_c , which is the resonant frequency of electrons governed by \vec{B} . When $\omega\tau \ll 1$, collisions damp the motion of the electron before it has time to complete one cycle and absorb much energy. No resonance is visible. By the time $\omega\tau = 1$ the relaxation time has become large enough to permit observation of a resonance. Varying ω_c is carried out by varying the strength of the static magnetic field, while the oscillating electric field frequency ω remains fixed.

Practical Considerations. It was a substantial achievement by Dresselhaus et al. (1953) and Lax et al. (1954) to turn cyclotron resonance into a practical tool, because for the experiment to work four competing requirements must be satisfied simultaneously.

1. One must guarantee that the semiclassical approximation be valid for the dynamics of the electrons or holes. This condition rules out optical frequencies where $\hbar\omega \gtrsim 1$ eV and interband transitions become possible.
2. The oscillating electric field must be able to penetrate the sample. This requirement is equivalent to demanding that $\omega > \omega_p$, the plasma frequency of Eq. (20.32). For undoped silicon and germanium at a temperature of 4 K, with free carrier densities on the order of 10^{13} cm⁻³, this condition can be satisfied, but already by a temperature of 70 K the carrier densities have risen high enough that plasma oscillations mask the cyclotron resonance. This condition rules out use of this technique in metals.
3. The relaxation time must be long enough that $\omega\tau \gtrsim 1$, according to Figure 21.2, requiring (a) very pure samples to reduce impurity scattering and (b) low temperatures to avoid phonon scattering.
4. The free carrier density must be high enough that electrons and holes are available to absorb radiation. Although the density of free carriers is exponentially small at low temperatures, this problem can be overcome by irradiating samples with photons at the energy of the band gap.

21.2.1 Electron Energy Surfaces

Data from a cyclotron resonance experiment in germanium appear in Figure 21.3. There is a large number of peaks present. Because germanium is an indirect gap semiconductor, its conduction band minimum does not lie atop $\vec{k} = 0$, but instead consists of four pockets of electrons straddling the zone boundaries in the (111) direction: these electron pockets were shown in Figure 19.9(A). The constant energy surfaces in the neighborhood of the conduction band minima are not at all spherical, but instead have the form

$$\mathcal{E} = \frac{\hbar^2}{2} \left[\frac{k_1^2}{m_1^*} + \frac{k_2^2}{m_2^*} + \frac{k_3^2}{m_3^*} \right] \quad (21.10)$$

Every symmetric quadratic form can be diagonalized; the energy is being expressed here in the basis where the effective mass tensor is diagonal. In the case of germanium, k_1 is along (111), and for silicon it is along (100).

where $m_1^* = 1.64 m$ and $m_2^* = m_3^* = 0.082 m$. For arbitrary directions of the magnetic field, there is a separate peak from each pocket of electrons, although for certain symmetry directions the peaks coalesce. For silicon, the situation is similar [Figure 19.9(B)], except that the conduction band minimum lies along the line between 0 and (100), providing three rather than four distinct pockets of electrons. The effective masses for silicon are $m_1^* = 0.9 m$ and $m_2^* = m_3^* = 0.19 m$.

When the effective mass tensor is not diagonal, one must return to Eq. (21.4) to see how the resonance condition changes. Rather than finding again the shape of the absorption line, it is enough to ask for the frequencies at which resonances occur. Resonances are located by searching for solutions of Eq. (21.4) which, in

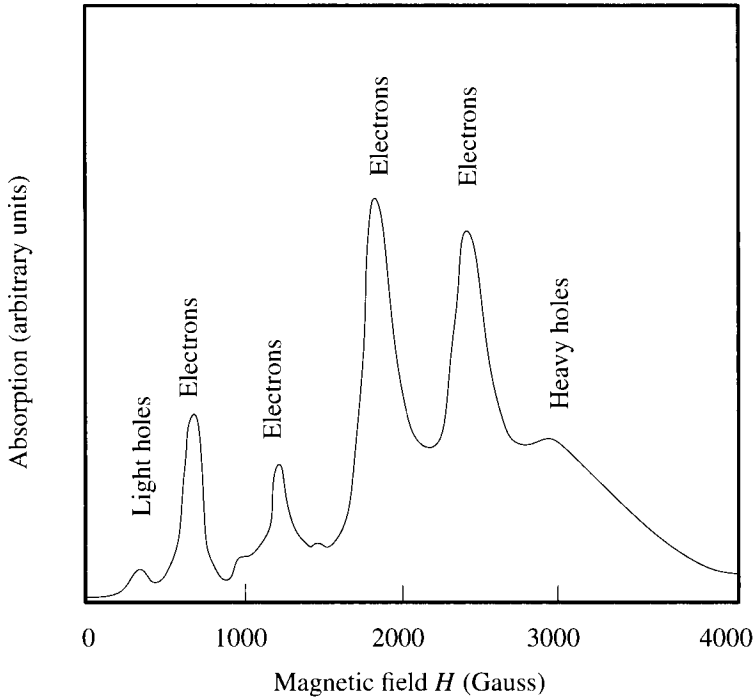


Figure 21.3. Data from cyclotron resonance in germanium. The magnetic field is oriented at 10° from the (110) plane and 30° from the [100] direction. Each of the four pockets of electrons in Figure 19.9 contributes a peak, as well as the light and the heavy holes. Because the applied electric field is not perfectly sinusoidal, but has a small frequency components of 2ω , 3ω . . . , higher harmonics of electron resonances are also visible. [Source: Dexter et al. (1956), p. 642.]

the absence of damping ($\tau = 0$), can exist when $\vec{E} = 0$. If one adopts coordinates where \mathbf{M} is diagonal, then

$$0 = i\omega\vec{v} - \frac{e}{c} \begin{pmatrix} \frac{1}{m_1^*} & 0 & 0 \\ 0 & \frac{1}{m_2^*} & 0 \\ 0 & 0 & \frac{1}{m_3^*} \end{pmatrix} \begin{pmatrix} 0 & B_3 & -B_2 \\ -B_3 & 0 & B_1 \\ B_2 & -B_1 & 0 \end{pmatrix} \vec{v} \quad (21.11)$$

$$\Rightarrow \omega = \frac{e}{c} \sqrt{\sum_{\alpha=1}^3 \frac{B_\alpha^2 m_\alpha^*}{m_1^* m_2^* m_3^*}} \quad \text{Find when the determinant of the right-hand side of Eq. (21.11) vanishes.} \quad (21.12)$$

Effective masses are determined by changing the direction of the magnetic field and by observing changes in locations of the resonance peaks according to Eq. (21.12).

Hole Energy Surfaces. The valence band maxima of silicon and germanium are found at $\vec{k} = 0$. However, matters are still somewhat complicated, because these bands are twofold degenerate right at $\vec{k} = 0$, allowing two separate effective masses

for holes. The heavy hole in germanium has $m_H^* \approx 0.28 m$ and the light hole has $m_L^* \approx 0.044 m$, while the corresponding numbers for silicon are $m_H^* \approx 0.49 m$ and $m_L^* \approx 0.16 m$.

21.3 Semiconductor Band Gaps

21.3.1 Direct Transitions

Direct gap semiconductors, as defined in Section 19.3.1, have a maximum of the valence band sitting directly below the minimum energy state of the conduction band in k space.

The theory for optical transitions in this case starts with Eq. (20.70), which shows a contribution to absorption whenever the energy $\hbar\omega$ of an incoming photon equals the difference $\mathcal{E}_{n'} - \mathcal{E}_n$ between two energy states. In order to place the theoretical result in the most convenient form, it is helpful to recall Eq. (20.14) and rewrite (20.70) as

$$\text{Im}[\epsilon_{\alpha\beta}] = \frac{4e^2\pi^2}{m^2\omega^2\mathcal{V}} \sum_{ll'} (f_l - f_{l'}) \langle l | \hat{P}_\alpha | l' \rangle \langle l' | \hat{P}_\beta | l \rangle \delta(\mathcal{E}_{l'} - \mathcal{E}_l - \hbar\omega) \quad (21.13)$$

$$= \left(\frac{2\pi e}{m\omega} \right)^2 \frac{1}{\mathcal{V}} \sum_{\vec{k}n_1n_2} \langle \vec{k}n_1 | \hat{P}_\alpha | \vec{k}n_2 \rangle \langle \vec{k}n_2 | \hat{P}_\beta | \vec{k}n_1 \rangle \delta(\mathcal{E}_{n_2\vec{k}} - \mathcal{E}_{n_1\vec{k}} - \hbar\omega) \quad (21.14)$$

Labeling the states now by Bloch index \vec{k} and band indices n_1 and n_2 . The Bloch indices \vec{k} of the initial and final states must be the same or else the matrix element vanishes. The sum is understood to include only cases where $n_1\vec{k}$ is occupied, and $n_2\vec{k}$ is unoccupied.

$$= \left(\frac{2\pi e}{m\omega} \right)^2 |P_{\alpha\beta}(\omega)|^2 D_j(\hbar\omega), \quad (21.15)$$

where

$$|P_{\alpha\beta}(\omega)|^2 \equiv \frac{\sum_{n_1n_2\vec{k}} \langle \vec{k}n_1 | \hat{P}_\alpha | \vec{k}n_2 \rangle \langle \vec{k}n_2 | \hat{P}_\beta | \vec{k}n_1 \rangle \delta(\mathcal{E}_{n_2\vec{k}} - \mathcal{E}_{n_1\vec{k}} - \hbar\omega)}{\sum_{n_1n_2\vec{k}} \delta(\mathcal{E}_{n_2\vec{k}} - \mathcal{E}_{n_1\vec{k}} - \hbar\omega)} \quad (21.16)$$

and

$$D_j(\hbar\omega) \equiv \frac{1}{\mathcal{V}} \sum_{n_1n_2\vec{k}} \delta(\mathcal{E}_{n_2\vec{k}} - \mathcal{E}_{n_1\vec{k}} - \hbar\omega). \quad (21.17)$$

The absorption has been expressed as a product of an average matrix element $|P|$ and the *joint density of states* D_j . The reason to place the expression in this form is that the averaged matrix element has no particular reason to exhibit sharp changes as a function of frequency and can often be approximated as a constant, but the joint density of states D_j is extremely sensitive to details of the band structure and depends strongly upon frequency. The joint density of states carries all the information about whether there exist pairs of occupied and unoccupied states with the right energy separation so that the photon can excite an electron between them. It vanishes when this condition is not met. In addition, whenever the band energies $\mathcal{E}_{n_2\vec{k}}$ and $\mathcal{E}_{n_1\vec{k}}$ run parallel to one another as a function of \vec{k} , D_j exhibits van Hove singularities, as defined in Section 7.2.5.

For direct band gap semiconductors to which Eq. (21.14) applies, one must turn to alloys, such as GaAs, or InSb. It is natural to expect that right at the threshold of absorption, where $\hbar\omega \geq \mathcal{E}_g$, the matrix element $|P_{\alpha\beta}|$ has no reason to vary rapidly, so optical absorption should be proportional to the joint density of states $D_j(\hbar\omega)$. Because both valence and conduction bands have parabolic extrema around $\vec{k} = 0$, $\mathcal{E}_c(\vec{k}) - \mathcal{E}_v(\vec{k}) - \mathcal{E}_g$ is a parabolic function vanishing at $\vec{k} = 0$, and D_j must therefore exhibit the van Hove singularity discussed in Section 7.2.5; that is, D_j should vanish for $\hbar\omega < \mathcal{E}_g$, and then should rise as $\sqrt{\hbar\omega - \mathcal{E}_g}$.

There are few cases where such behavior is actually observed. One of them appears in Figure 21.4. More frequently, the onset of optical absorption displays the behavior shown in Figure 21.5. The expected square root shape has been overridden by an additional process, the formation of excitons, to be described in Section 21.4.

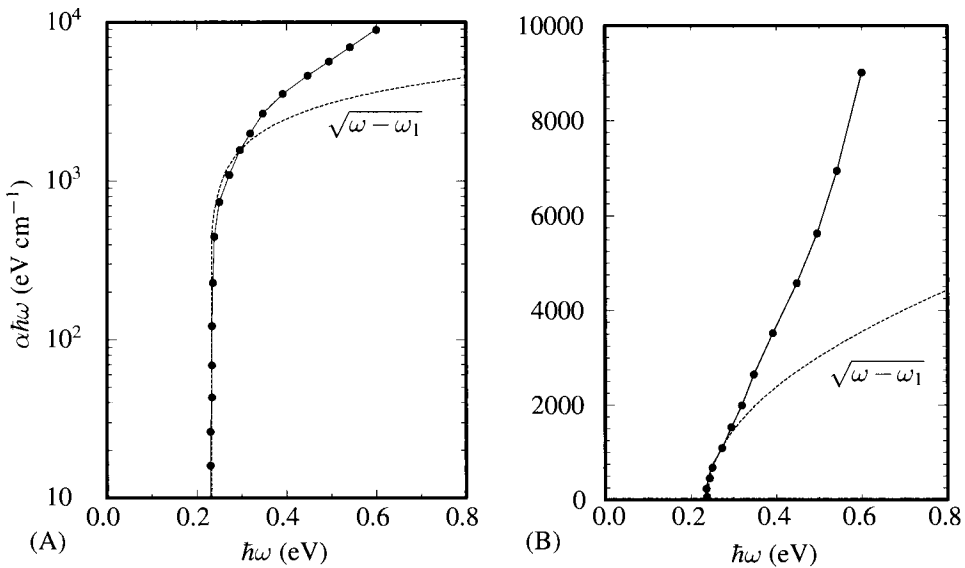


Figure 21.4. Measurement of absorption coefficient α times $\hbar\omega$, showing a van Hove singularity at onset of optical absorption in the direct gap semiconductor InSb. Data taken at a temperature of 5 K by Goebli and Fan and reported by Johnson (1967), p. 171, are compared with the expected square root form. The y axis is multiplied by $\hbar\omega$ because of the ω dependence predicted by Eq. (20.21) in combination with Eq. (21.16). (A) shows the data on a linear-log scale, while (B) shows the same data replotted on a linear scale, making the agreement look less impressive. Deviations from square root form due to variation of the matrix element $|P_{\alpha\beta}|$ produce better agreement with the experiment and were calculated by Kane (1957).

21.3.2 Indirect Transitions

As mentioned in Section 19.3.1, the elemental semiconductors germanium and silicon have indirect gaps, meaning that the conduction band minima are at different

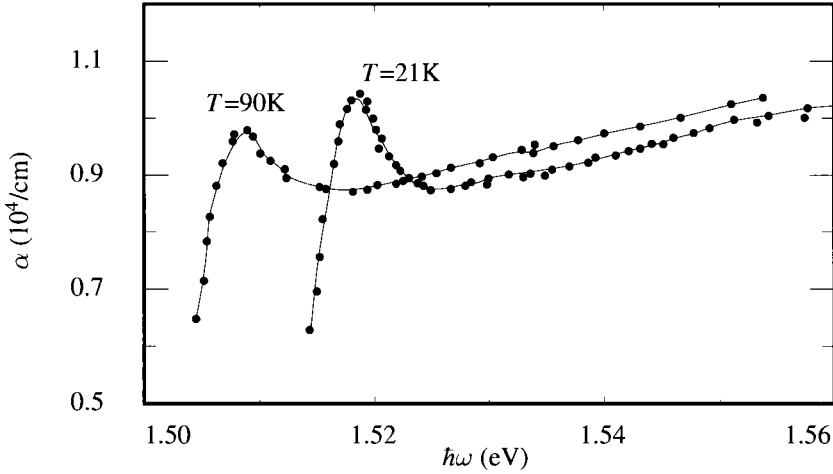


Figure 21.5. Measurement of absorption coefficient α in gallium arsenide, showing modification of absorption due to excitons. [Source: Sturge (1962), p. 771.]

locations in k space from the valence band maxima. It is possible for light to excite electrons between the valence band maximum and conduction band minimum, but only with the assistance of phonons so as to permit conservation of momentum. The microscopic theory of such transitions is therefore rather involved. The initial and final states of the system differ not only because an electron has moved to a new state, but also because the number of phonons has changed. The interaction Hamiltonian between photons and solid does not include a term for phonons, so any matrix element with the interaction Hamiltonian in the middle and with such initial and final states on either side must vanish. These transitions show up only at second order in perturbation theory. Fortunately, it is possible to guess the form of the final result without going through detailed calculations, using only conservation laws. In order for the Bloch index of an electron to change by $\delta\vec{k}$, either a phonon of wave vector $-\delta\vec{k}$ and energy $\hbar\omega_{\text{ph}}(\delta\vec{k})$ must be created, or a phonon of wave vector $\delta\vec{k}$ and energy $\hbar\omega_{\text{ph}}(\delta\vec{k})$ must be destroyed, in order to conserve crystal momentum. In order for energy to be conserved, one must have

$$\hbar\omega = \mathcal{E}_c - \mathcal{E}_v \pm \hbar\omega_{\text{ph}}(\delta\vec{k}). \quad \mathcal{E}_c \text{ is the energy of an electron in the conduction band, and } \mathcal{E}_v \text{ is the energy of an electron in the valence band.} \quad (21.18)$$

At temperatures much lower than the Debye temperature, there will be very few phonons residing naturally in the sample, and the negative term in Eq. (21.18) where a phonon is destroyed should cease to provide transitions. So according to Eq. (21.18), optical absorption in silicon and germanium should appear in two stages, at a first and a second frequency, with the strength of the absorption at the first frequency diminishing steadily with temperature.

The shape of the absorption curve can similarly be estimated. A complete formula will have to involve various matrix elements, sums over intermediate states,

and so on. Assuming that the energy dependence of all these can be neglected, the extinction coefficient κ should be proportional to

$$\kappa \propto \sum_{\vec{k}_c, \vec{k}_v} \delta \left(\mathcal{E}_c(\vec{k}_c) - \mathcal{E}_v(\vec{k}_v) - \hbar\omega \pm \hbar\omega_{\text{ph}}(\vec{\delta k}) \right) \quad (21.19)$$

$$= \int d\mathcal{E}_c \int d\mathcal{E}_v D_c(\mathcal{E}_c) D_v(\mathcal{E}_v) \delta \left(\mathcal{E}_c - \mathcal{E}_v - \hbar\omega \pm \hbar\omega_{\text{ph}} \right) \quad (21.20)$$

Neglect the $\vec{\delta k}$ dependence of ω_{ph} .

$$\propto \int_{\mathcal{E}_g} d\mathcal{E}_c \int^0 d\mathcal{E}_v \sqrt{\mathcal{E}_c - \mathcal{E}_g} \sqrt{-\mathcal{E}_v} \delta \left(\mathcal{E}_c - \mathcal{E}_v - \hbar\omega \pm \hbar\omega_{\text{ph}} \right) \quad (21.21)$$

Letting \mathcal{E}_g be the band gap, setting the valence band maximum to zero, and using the generic three-dimensional forms of the density of states near a band maximum or minimum.

$$= \int_{\mathcal{E}_g}^{\hbar\omega \mp \hbar\omega_{\text{ph}}} d\mathcal{E}_c \sqrt{\mathcal{E}_c - \mathcal{E}_g} \sqrt{\hbar\omega - \mathcal{E}_c \mp \hbar\omega_{\text{ph}}} \quad (21.22)$$

$$= (\hbar\omega \mp \hbar\omega_{\text{ph}} - \mathcal{E}_g)^2 \int_0^1 dy \sqrt{y} \sqrt{1-y}. \quad (21.23)$$

Letting $y = (\mathcal{E}_c - \mathcal{E}_g) / (\hbar\omega \mp \hbar\omega_{\text{ph}} - \mathcal{E}_g)$. From Eq. (21.22), the result vanishes, however, unless $\hbar\omega > \mathcal{E}_g \mp \hbar\omega_{\text{ph}}$. The value of the integral is not important, just the fact that it is constant.

This prediction is only in moderate accord with experiment, as shown in Figure 21.6. It is possible to pick out the two frequencies $\mathcal{E}_g \mp \hbar\omega_{\text{ph}}$. However, at low energies the curve does not have the expected form, nor does the onset of absorption at $\mathcal{E}_g + \hbar\omega_{\text{ph}}$. Both of these discrepancies are attributed to excitons.

21.4 Excitons

When a photon excites an electron into the conduction band, it inevitably leaves behind a hole in the valence band as well. In the context of the single-particle band theory, the energies of these two excitations should simply be added together. However, it is easy to imagine that because the electron and hole are charged particles and because at low temperatures there will not be enough free carriers to screen them, they can lower their energy by approaching one another and binding together. Such bound electron–hole pairs are called *excitons* (Figure 21.7).

The exciton can be considered in two limits. In the first case, the binding is sufficient weak that the hole and electron orbit at a large distance from one another. Then one has a Mott–Wannier exciton. In the second case, the hole and electron are so tightly bound that they sit on the same site. Then one has a Frenkel exciton.

21.4.1 Mott–Wannier Excitons

Excitons are comparatively easy to understand in semiconductors. Because of the large static dielectric constant, the Coulomb interaction between electron and hole is greatly reduced, and their mean separation when bound together is much larger

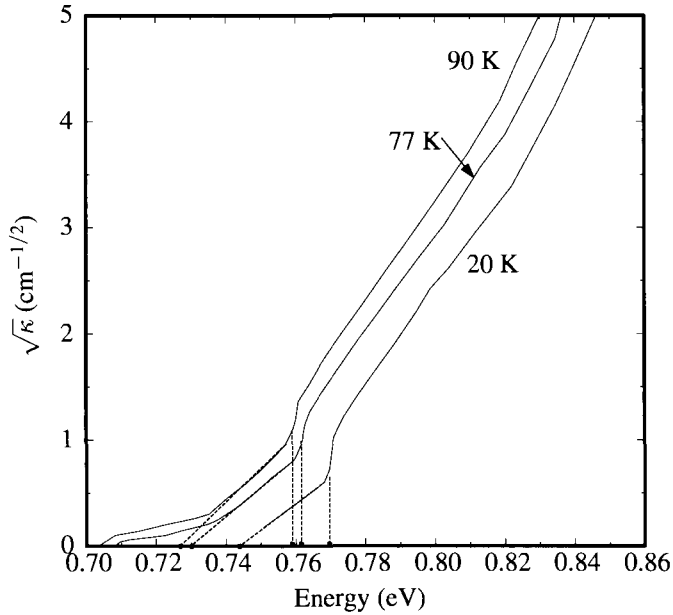


Figure 21.6. Onset of optical absorption in germanium. The square root of the extinction coefficient κ is plotted as a function of incoming photon energy, in the expectation that the experiment will behave according to the prediction of Eq. (21.23). The measurements should look like a straight line, followed by a smooth transition into another straight line of steeper slope. Extrapolation of the first straight line to zero (sloped dotted lines) should give $\mathcal{E}_g - \hbar\omega_{\text{ph}}$, while the transition point should give $\mathcal{E}_g + \hbar\omega_{\text{ph}}$ (vertical dotted lines). At the very lowest temperature, this prediction is obeyed partly, although there is a cusp at the transition point. At the two higher temperatures, there is also a low-energy tail in the absorption that does not fit the predictions. These discrepancies have been explained quantitatively as consequences of excitons. [Source: Macfarlane et al. (1957), p. 1379.]

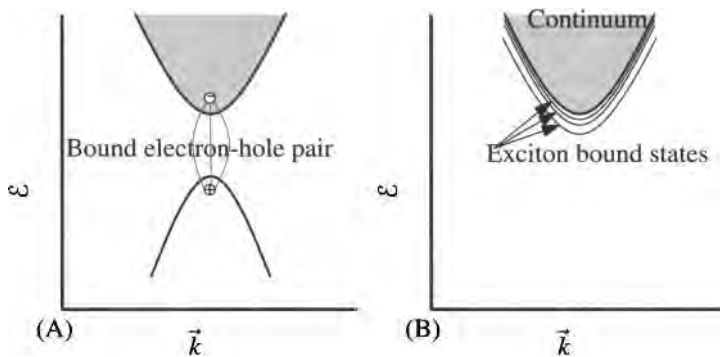


Figure 21.7. Schematic view of energy levels resulting from exciton formation. In (A) an electron and hole bind together. (B) shows the energy levels of the bound pair consisting of an infinite series of discrete levels below the one-electron conduction band that vary with \vec{k} because of their center-of-mass motion, along with a continuum of states above.

than a lattice spacing. In this limit, the exciton is called a *Mott–Wannier exciton*. The same arguments used in Section 18.3.1 to discuss interaction of electrons with weak impurity potentials apply again. Assume that the characteristic distance between electron and hole is much larger than a lattice spacing, so that the wave functions for both electron and hole can be constructed as products of Bloch waves with wave vector \vec{k} near 0. Then the interactions of electron and hole with the periodic ionic potential can be eliminated from the Hamiltonian, provided that their masses are replaced by the appropriate effective masses. That is, the electron and hole obey

$$\left[\frac{-\hbar^2}{2m_n^*} \nabla_{\vec{r}_n}^2 + \frac{-\hbar^2}{2m_p^*} \nabla_{\vec{r}_p}^2 - \frac{e^2}{\epsilon^0 |\vec{r}_n - \vec{r}_p|} - \mathcal{E} \right] \Psi(\vec{r}_n, \vec{r}_p) = 0. \quad \epsilon^0 \text{ is the static dielectric constant.} \quad (21.24)$$

Equation (21.24) is exactly the equation obeyed by the electron and proton in forming the hydrogen atom. It can be separated into two equations, one describing the center-of-mass motion of the exciton and the other describing the binding by defining

$$\vec{R} = \frac{m_n^* \vec{r}_n + m_p^* \vec{r}_p}{m_n^* + m_p^*} \quad (21.25)$$

$$\vec{r} = \vec{r}_n - \vec{r}_p \quad (21.26)$$

to give

$$0 = \left[\frac{-\hbar^2}{2(m_n^* + m_p^*)} \nabla_{\vec{R}}^2 - \mathcal{E}_{\text{cm}} \right] \Psi_{\text{cm}}(\vec{R}) \quad \text{cm= center of mass.} \quad (21.27)$$

$$0 = \left[\frac{-\hbar^2}{2\mu} \nabla_{\vec{r}}^2 - \frac{e^2}{\epsilon^0 r} - \mathcal{E}_b \right] \Psi_b(\vec{r}), \quad \text{b=binding.} \quad (21.28)$$

with the reduced mass μ given by

$$\mu = \frac{m_n^* m_p^*}{m_n^* + m_p^*}. \quad (21.29)$$

There is no need to repeat the solution of the hydrogen atom any further. The bound states of Eq. (21.28) have energies

$$\mathcal{E}_l = -\frac{\mu e^4}{2\hbar^2 \epsilon^0{}^2 l^2} = -\frac{\mu}{m\epsilon^0{}^2} \cdot 13.6 \text{ eV} \quad l = 1 \dots \infty. \quad (21.30)$$

and are characterized by a radius

$$a_0^* = \frac{\epsilon^0 \hbar^2}{e^2 \mu} = \frac{m\epsilon^0}{\mu} \cdot 0.529 \text{ \AA}. \quad (21.31)$$

Because μ is typically half an electron mass or less, while ϵ for a semiconductor may be around 10, the scale on which the bound state lives is 20 times larger than the usual hydrogen atom; therefore, the picture of the electron and hole sitting in a classical background dielectric is consistent. Binding energies are on the order of a

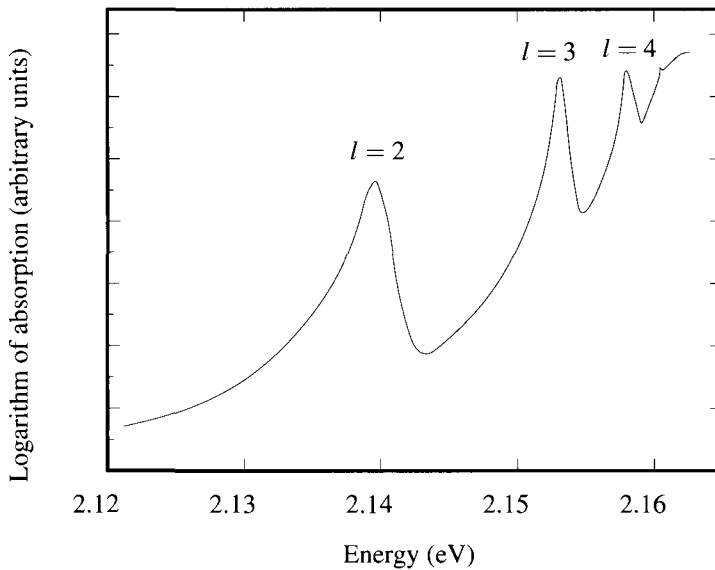


Figure 21.8. Absorption measured in Cu_2O . Cuprous oxide is an indirect gap semiconductor, and absorption begins to increase as a square root, at an energy of 2.045 eV. This square root form is predicted by Elliott (1957) for phonon-assisted transitions to the lowest-lying exciton state; direct transitions are forbidden by symmetry. At about 0.1 eV higher in energy a series of peaks corresponding to electron transitions between the top of the valence band and excited exciton states begins. The first ($l = 2$), second, and third excited states are clearly visible. [Experiments performed at 77 K by Baumeister (1961), p 361.]

hundredth of a Rydberg, or 0.1 eV. The dispersion relations of excitons have been measured with great accuracy, as reported by Ueta et al. (1986).

According to Eq. (21.30), the presence of excitons produces a sequence of discrete energy states sitting near the conduction band edge. Usually these peaks are not resolved individually, but merge into a bump centered around $\hbar\omega = \mathcal{E}_g$. However, at low temperatures in Cu_2O , a sequence of distinct absorption peaks can be measured, as shown in Figure 21.8. In these measurements, an electron makes a transition from the valence band to various excited states of the excitons. In addition, just like the hydrogen atom, Eq. (21.28) must have a continuous collection of unbound solutions, which enhance the absorption for $\hbar\omega > \mathcal{E}_g$. Why are such effects observed in GaAs (Figure 21.5) but not InSb (Figure 21.4)? The static dielectric constant of InSb, recorded in Table 22.2, is 17.88, and the effective mass m^* is $0.01m$, reducing the energy scale of the excitons to $3 \cdot 10^{-4}$ eV and making them invisible even at temperatures as low as 5 K.

21.4.2 Frenkel Excitons

The *Frenkel exciton* consists of a bound state of electrons and holes in insulators, where the spatial extent of the exciton is on the scale of angstroms, and the continuum approximation that served the Mott–Wannier exciton fails. These excitons

have excited states, just like more conventional molecules, and transitions between these excited states allow optical absorption in insulators. In addition, these excitons are mobile and can travel through the lattice as particles. A calculation of their properties, using the Hartree-Fock approximation, appears as Problems 4 and 5.

21.4.3 Electron–Hole Liquid

When a sufficiently large density of excitons is created in a semiconductor, by strong illumination, the excitons can condense into a liquid-like state that manifests itself as an *electron–hole drop*, first predicted by Keldysh and Kozlov (1967) and reviewed by Hensel et al. (1977) and Rice (1977).

21.5 Optoelectronics

Semiconductor electronics can be made to interact with light in numerous different ways, ranging from the conversion of photons into electrical energy to the conversion of electrical energy to laser beams. These various applications are largely implicit in the Kubo formula, Eq. (20.70), but great ingenuity continues to be expended in obtaining efficient performance.

21.5.1 Solar Cells

A solar cell is essentially a diode that has been fabricated so as to absorb as much light as possible in the neighborhood of the junction. Every photon that is absorbed generates an electron–hole pair. The pairs that are generated inside the depletion region are immediately ripped apart by the enormous electric fields and sent to opposite sides. Because the depletion region is very narrow, the formation of pairs in the quasi-neutral regions is more important. Minority carriers formed within a distance L_p or L_n of the depletion zone can diffuse there and are then swept across to the other side of the junction. This picture predicts that shining light of intensity I on a diode will produce a current density

$$j = -I\mathcal{G}(L_p + L_n) \quad \mathcal{G} \text{ is some constant of proportionality taking into account the efficiency of absorption, and making the units come out right.} \quad (21.32)$$

Because the sizes of the quasi-neutral regions are independent of the voltage across the diode, the main effect of light is simply to lower the current–voltage curve of the diode downwards, as shown in Figure 21.9. When the solar cell is under illumination but not connected to a circuit, the separation of electron–hole pairs causes the voltage across it to rise until the current–voltage curve intersects the point where current vanishes, at a voltage on the order of $k_B T/e$, or around 0.025 V. Connected to a load, the voltage drops slightly and current begins to flow, generating power. There is an ideal load at which power generation is maximum, while if the cell is connected across an open circuit the voltage across it drops to zero, and it again generates no power. Solar cells can convert sunlight to power

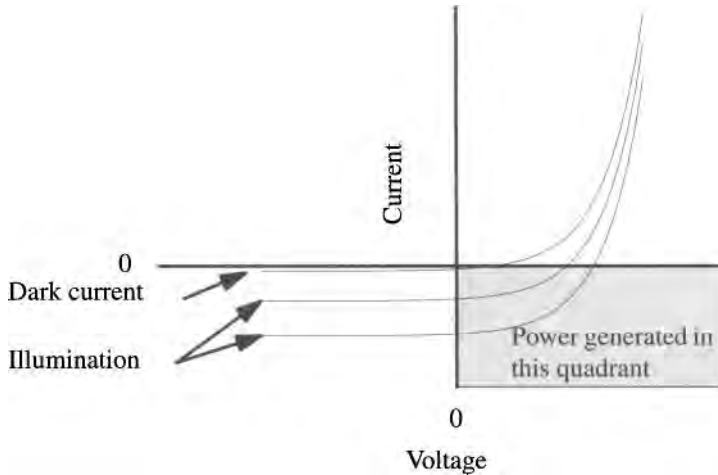


Figure 21.9. The current–voltage characteristic for a solar cell is essentially the ideal diode equation (19.78) shifted vertically downwards. In the lower right quadrant the diode is forward biased, but current flows in the opposite direction, generating power.

with an efficiency of over 25%, but are not yet an economical source of energy under most conditions.

21.5.2 Lasers

The laser is based upon the idea of *stimulated emission*, first conceived by Einstein (1916) and first measured by Ladenburg (1928). Three decades followed the first experimental observations before a coherent beam of radiation was actually produced, and several more decades followed before this “solution in search of a problem” became important commercially. Possible applications of the laser were, however, evident right from the outset.

Hecht (1992) describes the complicated history of the race to complete the laser. G. Gould eventually won extensive patent rights to the laser based upon personal notes written in 1957, but it was an influential paper of Schawlow and Townes (1958) that started the international scramble to build a working device, won by Maiman (1960). The basic idea is fairly simple. If an excited electronic state that should be nearly empty in thermal equilibrium is somehow given a macroscopic occupation of electrons, then as soon as the electrons begin to travel to the ground state the process can proceed explosively. The light emitted by electrons as they jump down the energy levels triggers other electrons to jump down simultaneously, and light emission grows exponentially. To see why, go back to Einstein’s original argument.

Stimulated and Spontaneous Emission. Einstein (1916) deduced stimulated emission from deceptively simple arguments about thermal equilibrium. Consider an isolated cavity filled with material whose index of refraction is \bar{n} , and focus upon two electronic states 1 and 2, of energies \mathcal{E}_1 and $\mathcal{E}_1 + \mathcal{E}_{12}$. Einstein first ob-

served that all systems prepared in an excited state decay at some rate, and he took the *spontaneous transition rate* R_{sp} from state 2 to 1 to be

$$R_{sp} = A_{21}f_2(1 - f_1) \quad \begin{array}{l} \text{The transition rate is proportional to the proba-} \\ \text{bility that state 2 be occupied and that state 1 be} \\ \text{empty. } f_2 \text{ and } f_1 \text{ are Fermi factors for the respec-} \\ \text{tive states.} \end{array} \quad (21.33)$$

Next suppose the cavity to be so well isolated that the material inside is in complete equilibrium with a bath of photons at temperature T . Whenever a photon of the right frequency collides with an electron in state 1, it has the chance to be absorbed and bring the electron to state 2. The rate R_{12} at which electrons make transitions from the lower to the upper state is proportional to the probability f_1 that the lower state is occupied, to the probability $(1 - f_2)$ that the upper state is unoccupied, and to the number of photons $N_{\mathcal{E}_{12}}$ of energy \mathcal{E}_{12} in the cavity. As noted in Eq. (20.72), transitions between electronic states are never completely restricted to a single energy, but can be produced by photons in some small range $d\mathcal{E}$. Accordingly, the number of photons producing the transition is proportional to $N_{\mathcal{E}_{12}}D_{ph}(\mathcal{E}_{12})$, where D_{ph} is the energy density of photon states. Because the density of photon states will depend upon the index of refraction of the medium, complicated electron–electron interactions are subtly being included with almost no increase in the complexity of the theory. Thus

$$R_{12} = B_{12}f_1(1 - f_2)N_{\mathcal{E}_{12}}D_{ph}(\mathcal{E}_{12}) \quad \begin{array}{l} B_{12} \text{ is a temperature-independent coefficient} \\ \text{to be determined later.} \end{array} \quad (21.34)$$

The reverse rate, R_{21} , at which an electron jumps down from an excited state, producing photons, must at least be as large as R_{sp} . Einstein guessed that the rate would also rise in proportion to the number of photons in the cavity. Choosing a coefficient B_{21} defined to correspond closely to the coefficient in Eq. (21.34) gives

$$R_{21} = B_{21}f_2(1 - f_1)N_{\mathcal{E}_{12}}D_{ph}(\mathcal{E}_{12}) + A_{21}f_2(1 - f_1). \quad (21.35)$$

The transition rate is the sum of the spontaneous transition rate, independent of the photons, and a term proportional to the photon number.

The contribution proportional to $N_{\mathcal{E}_{12}}$ is the *stimulated emission rate*. Why photons should cause such transitions is not immediately clear, but considering how thermal equilibrium is maintained shows that these transitions must be present.

In thermal equilibrium the population of electrons is stationary, and R_{12} and R_{21} must be equal. Because

$$\frac{f_2(1 - f_1)}{f_1(1 - f_2)} = e^{-\beta\mathcal{E}_{12}}, \quad \begin{array}{l} \text{Just put in Fermi functions to verify. Equivalent} \\ \text{to the statement that the probability of occupying} \\ \text{any quantum state in equilibrium is proportional} \\ \text{to } e^{-\beta\mathcal{E}}. \end{array} \quad (21.36)$$

one has

$$R_{12} = R_{21} \quad (21.37)$$

$$\Rightarrow B_{12}N_{\mathcal{E}_{12}}D_{ph}(\mathcal{E}_{12}) = e^{-\beta\mathcal{E}_{12}} [B_{21}N_{\mathcal{E}_{12}}D_{ph}(\mathcal{E}_{12}) + A_{21}] \quad (21.38)$$

$$\Rightarrow D_{\text{ph}}(\mathcal{E}_{12})B_{12} - A_{21} = e^{-\beta\mathcal{E}_{12}} [D_{\text{ph}}(\mathcal{E}_{12})B_{21} - A_{21}] \frac{N_{\mathcal{E}_{12}}}{1/(\exp[\beta\mathcal{E}_{12}] - 1)} \quad (21.39)$$

$$\Rightarrow A_{21} = D_{\text{ph}}(\mathcal{E}_{12})B_{21} \quad \text{and} \quad B_{12} = \quad (21.40)$$

If Eq. (21.39) is to hold independent of temperature.

Equation (21.40) can also be written as

$$R_{21} = B_{21}f_2(1 - f_1)(N_{\mathcal{E}_{12}} + 1)D_{\text{ph}}(\mathcal{E}_{12}). \quad (21.41)$$

In this form, change in electron energies by emission and absorption of photons reveals a perfect parallel with the change in neutron energies by emission and absorption of phonons described in Eq. (13.134). The probability of transitions where electron energy increases is proportional to $N_{\mathcal{E}_{12}}$, while the probability of transitions where it decreases is proportional to $N_{\mathcal{E}_{12}} + 1$, with the trailing factor of 1 responsible for spontaneous emission.

Einstein's argument is completed by asserting that in nonequilibrium situations, as when a stream of light energy hits electrons and is ultimately dispersed as heat, the occupation probabilities f_1 and f_2 need not have the values used to obtain Eq. (21.36), but the transition rates R_{12} and R_{21} will continue to depend upon f_1 and f_2 in the ways indicated by Eqs. (21.34) and (21.41). Thus, away from equilibrium, the absorption of energy by electrons from photons will be proportional to

$$R_{12} - R_{21} = B_{21}[(f_1 - f_2) N_{\mathcal{E}_{12}} - f_2(1 - f_1)]D_{\text{ph}}(\mathcal{E}_{12}). \quad (21.42)$$

The absorption of energy is given by the difference between absorption and emission, as given by Eqs. (21.34) and (21.41).

The coefficient B_{12} is the only remaining unknown of the theory, and it can be determined by comparison with the Kubo–Greenwood formula. When the photon density $N_{\mathcal{E}_{12}}$ is very large, spontaneous emission becomes negligible, and Eq. (21.42) must coincide with the results of the semiclassical theory of absorption. Therefore, turn to Eq. (20.71), which predicts that if one is considering only the the two quantum states 1 and 2, then the conductivity is

$$\text{Re}[\sigma_{\alpha\beta}(\omega)] = \frac{e^2\pi}{\hbar\omega m^2\mathcal{V}}(f_1 - f_2)F_{12}(\omega)\langle 1|\hat{P}_\alpha|2\rangle\langle 2|\hat{P}_\beta|1\rangle. \quad (21.43)$$

$F_{12}(\omega)$ is the lineshape, a function with unit area, and peaked at $\omega_2 - \omega_1$.

In practical situations, there will not simply be two levels 1 and 2, but instead a large number N of atoms or impurities that can be excited from one level to another. Summing over these many atoms will have the effect of averaging over all possible spatial orientations of the excited state $|2\rangle$ and replacing the matrix elements by their spatial average $\sum_\beta |\langle 1|\hat{P}_\beta|2\rangle|^2/3$. Using Eqs. (20.14) and (20.21) to relate conductivity to the attenuation constant $\alpha = -g$ shows that radiation intensity I grows as $\exp[gx]$ where the *gain* is

$$g(\omega) = \frac{N}{\mathcal{V}} \frac{4\pi^2 c^2}{\omega \bar{n}} \left(\frac{e^2}{\hbar c} \right) F_{12}(\omega)(f_2 - f_1) \frac{\sum_\beta |\langle 1|\hat{P}_\beta|2\rangle|^2}{3m^2 c^2}. \quad (21.44)$$

The net rate $R_{21} - R_{12}$ at which electrons travel between states 2 and 1 equals the rate at which photons are produced per time. To find the total number of photons, multiply g in Eq. (21.44) by c/\bar{n} to find the time rate of change of light intensity I . Next recall that light intensity is proportional to photon number through $I = N_{\mathcal{E}_{12}} \hbar\omega$, and finally that in a medium with macroscopic index of refraction \bar{n} , the density of photon states per volume is

$$D_{\text{ph}}(\omega) = \frac{\bar{n}^3 \omega^2}{\pi^2 c^3}. \quad (21.45)$$

This is density of states per volume; a factor of \mathcal{V} is needed to find total numbers of photons.

Multiplying Eq. (21.44) by Eq. (21.45), multiplying by $\mathcal{V}c/\bar{n}$, and integrating over ω gives

$$R_{21} - R_{12} = \frac{\partial}{\partial t} N_{\mathcal{E}_{12}} = -N \frac{\mathcal{E}_{12}}{\hbar} \bar{n} \left(\frac{e^2}{\hbar c} \right) 4(f_1 - f_2) \sum_{\beta} \frac{|\langle 1 | \hat{P}_{\beta} | 2 \rangle|^2}{3m^2 c^2} N_{\mathcal{E}_{12}} \quad (21.46)$$

N is the number of host atoms or impurity sites, while $N_{\mathcal{E}_{12}}$ is the number of photons. B_{12} can be determined from Eqs. (21.42) and (21.45) if desired, but this rate equation for photons is more useful than B_{12} . The lineshape $F_{12}(\omega)$ integrates to 1.

Equation (21.44) contains a theoretical motivation for building a laser. If it is possible to construct an initial state in which $f_2 > f_1$, then the attenuation will be negative, and light will grow exponentially as it passes through the medium until state 2 is depleted. Under these circumstances, $-\alpha = g$ as computed in Eq. (21.44) is renamed the gain, and the symbol α is reserved for sources of attenuation and loss that compete with the growth from population inversion.

In order to obtain a laser, it is not enough for the intensity of a beam of light passed into the system to grow. It must be possible for external light sources to be turned off, while light emission from the system continues to grow spontaneously. This condition can be achieved by placing material in a cavity with reflecting ends, as shown in Figure 21.10. If the reflection coefficient of the two ends is \mathcal{R} , then the condition for amplification in the laser cavity is

$$\mathcal{R} \exp[x(g - \alpha)] > 1. \quad (21.47)$$

Light has to be able to make a round trip in the cavity and end up stronger than at the beginning. The gain g due to stimulated emission competes with loss processes summarized in the coefficient α .

Pumping. The discussion has hinged upon the assumption of *population inversion*: that an excited state has been populated so that $f_2 > f_1$. Occupying an excited state preferentially at the expense of one lying lower in energy is easy to describe, but violates conditions of thermal equilibrium, so it is not immediately obvious how to achieve it in practice.

Lasers can be created in numerous different ways and in many different types of materials, including liquids and gases. The following discussion will focus upon *solid-state lasers*, which does not refer exclusively to lasers formed of semiconductors, but includes any case in which the laser material is solid. The most important ideas are *metastable states* and *pumping*. For the purposes of laser physics,

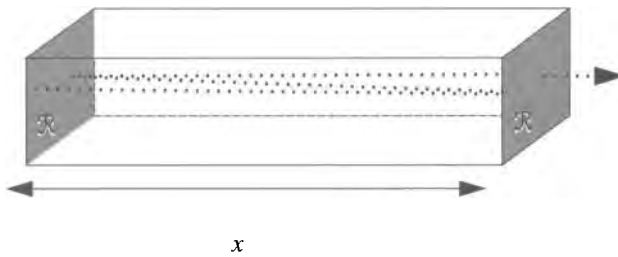


Figure 21.10. Light in a laser cavity reflects several times back and forth from mirrored ends of reflection coefficient \mathcal{R} so as to stimulate more light emission before exiting.

a metastable state is an excited energy level with a lifetime on the order of 10^{-5} to 10^{-3} s. Characteristic *non-radiative decay* times of excited states in solids are usually on the order 10^{-8} to 10^{-11} s, because this is the time that phonons typically require in order to transfer energy from an excited level. A first requirement of a solid-state laser is therefore to find an excited state that cannot be depleted by single phonons, either because available transitions exceed the maximum phonon frequency or because symmetry causes matrix elements [analogous to the ones in Eqs. (13.99) or (20.70)] between initial and final states to vanish. Transitions driven by multiple phonons are still possible, but sufficiently unlikely that emission of photons has a chance to win.

A metastable state has a long lifetime, and by the energy uncertainty principle it can only be excited from the ground state by energy lying in a very narrow range. Because only a laser can produce light with such a narrow linewidth, it would seem that a laser is required to populate the levels upon which laser action is to rely. This difficulty is overcome by pumping, illustrated in Figure 21.11. Rather than occupying the metastable state directly, one pushes electrons into one or more states with short lifetimes that lie above the desired metastable state, and that rapidly decay to it in non-radiative fashion.

Solid-State Ionic Lasers. One way to make a laser is by employing the discrete energy levels provided by color centers in insulating crystals (Section 22.4). The first laser, built from a crystal of ruby by Maiman (1960), was a *three-state* laser involving pump states and a metastable state decaying to the ground state, as shown in Figure 21.12(A). In order to occupy the 2E state upon which the laser relied, the crystal was illuminated with a powerful flashlamp that succeeded in placing more electrons into 2E than were left in the ground state. Numerous researchers realized that a *four-state* laser would have considerable advantages because if the state at the bottom of the laser transition was normally unoccupied, constraints upon the occupation of the upper level become less severe. Three-state lasers typically operate in pulsed fashion, with bursts of laser radiation following flashes of pumping light, while four-state lasers can operate continuously. The energy levels of Nd in yttrium aluminum garnet (YAG), the impurity in one of the most important solid-state lasers appear in Figure 21.12(B).

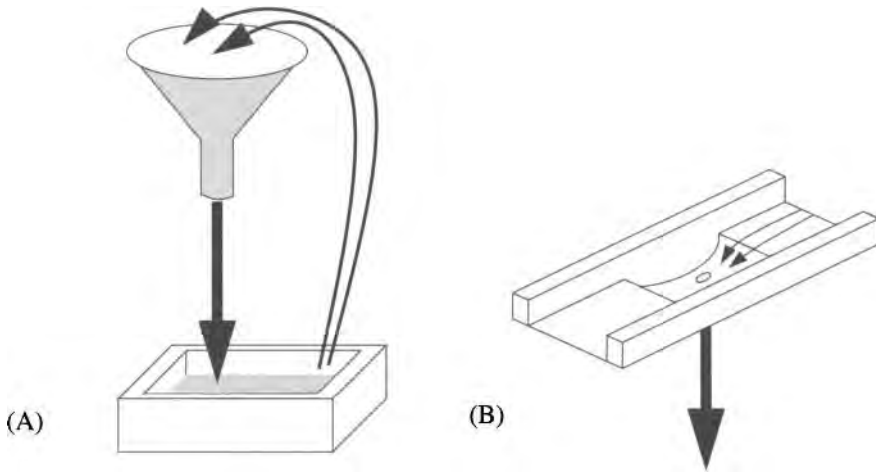


Figure 21.11. (A) The problem of occupying a metastable atomic state is a bit like pumping water from a trough into a funnel. The pumping action can be sloppy and erratic, but the water nevertheless exits the funnel in a narrow steady beam. (B) For a semiconductor laser, the pumping scheme is a bit different. As electrons travel along, they pass into a region where the doping has changed, and the Fermi level drops precipitously from conduction to valence band, leading to a laser transition somewhat like water falling through a drain. The double heterostructure laser ensures that the optical transitions take place in a confined spatial region by trapping the electrons with an additional slight drop in Fermi level of the conduction band that resembles a basin.

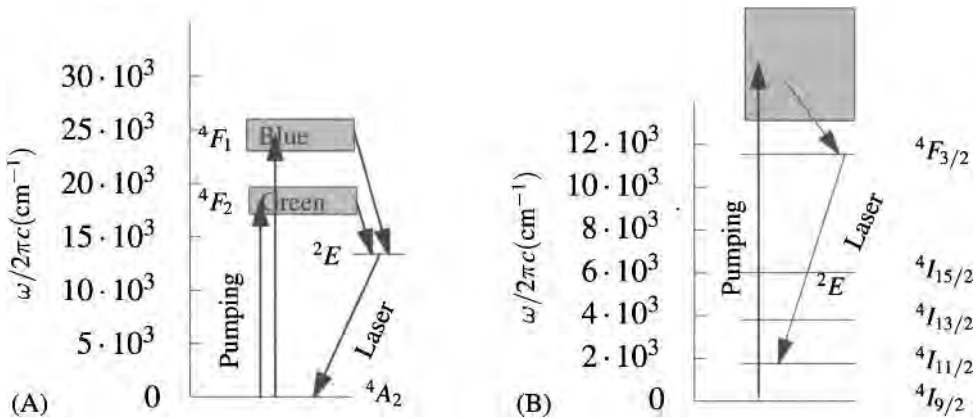


Figure 21.12. (A) Energy levels of Cr^{3+} in Al_2O_3 (ruby). Electrons are pumped to high levels, and they quickly decay to metastable state 2E . The laser transition then occurs to 4A_2 . (B) Energy levels of Nd in $\text{Y}_3\text{Al}_5\text{O}_{12}$ (Nd:YAG). The metastable state is ${}^4F_{3/2}$, and the laser transition occurs to state ${}^4I_{11/2}$. Transitions to other states also occur, but the transition to ${}^4I_{11/2}$ is the most likely, at 60% probability. Energy levels are being described in LS coupling, as described by Schiff (1968), p. 435, or Landau and Lifshitz (1977), p. 250, where the superscript gives $2S + 1$, the subscript gives J , and the capital letter indicates L .

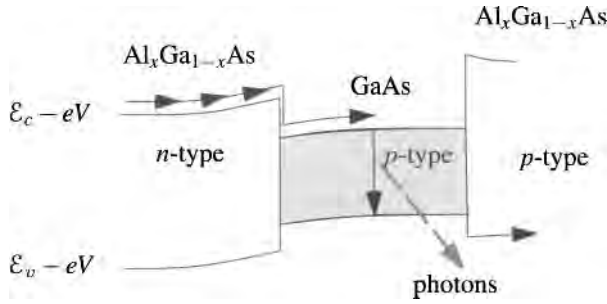


Figure 21.13. A double heterojunction structure makes use of two junctions to trap electrons and force them into radiative transitions in a small region. Electrons arriving from the n -doped region on the left find themselves trapped in a p -type region and hemmed in on both sides. The central layer also has a higher index of refraction than the surrounding regions, confining light in a cavity.

Light-Emitting Diodes and Semiconductor Lasers. The light-emitting diode and semiconductor laser exploit the fact that electrons in n -type material traveling in the conduction band must rapidly fall to the valence band after entering p -type material. In the process, they emit photons whose energy equals the band gap. The light-emitting diode simply extracts this radiation. To obtain a laser, it is necessary to obtain a high spatial density of recombining electrons and holes, and to trap the light they emit in a cavity. Practical devices are based upon the double heterojunction structure shown in Figure 21.13. The central region acts like a trap where electrons collect in large numbers and recombine with high efficiency.

If an indirect gap semiconductor such as silicon were used in this application, electrons would collect at the lowest point in the conduction band but then find themselves unable to make the transition to the valence band without assistance from phonons. The efficiency of the device would be unacceptable. That is why direct gap semiconductors such as GaAs are needed for optical applications.

Problems

1. Optical measurements:

- Use the locations of the peaks for light and heavy holes to estimate the frequency ω at which the experiment in Figure 21.3 was conducted.
- The data in Figure 21.6 allow one to estimate $\omega_{\text{ph}}(\vec{\delta}k)$. Using the data at 20 K, what are ω_{ph} and $\vec{\delta}k$?

- Lifetime of hydrogen excited state:** Many of the quantities appearing in the theory of lasers can be evaluated explicitly for hydrogen. Consider transitions between the 2P and 1S states, using the wave functions

$$\psi_1 = \frac{\exp[-r/a_0]}{\sqrt{\pi a_0^3}} \quad \text{and} \quad \psi_2 = \frac{x \exp[-r/2a_0]}{\sqrt{2^5 \pi a_0^5}}. \quad (21.48)$$

- (a) Evaluate the integral $P_{12} \equiv \langle 1 | \hat{p}_x | 2 \rangle$.
- (b) Evaluate ω for the $2P \rightarrow 1S$ transition.
- (c) How must Eq. (21.44) be generalized to account for the sixfold degeneracy of the $2P$ state?
- (d) Show that in a box with N hydrogen atoms, the transition rate A_{21} from one of the six $2P$ states to one of the two $1S$ states is given by

$$A_{21}(\omega)(f_2 - f_1) = \frac{1}{6N} g(\omega) \frac{c}{\bar{n}}. \quad (21.49)$$

- (e) Set $\bar{n} = 1$, and find A_{21} by integrating $A_{21}(\omega) D_{\text{ph}}(\omega)$ over ω .
- (f) Put A_{21} into a final form involving e , m , \hbar , and c . The numerical answer is $6.268 \cdot 10^8 \text{ s}^{-1}$.

3. **Gunn effect:** The conduction band of gallium arsenide has the form shown in Figure 19.8. In the central minimum, electrons have a small effective mass ($m^* = 0.07m$), leading to a mobility on the order of $7500 \text{ cm}^2 \text{ V}^{-1} \text{ s}^{-1}$. However, once the electron acquires a \vec{k} in the minimum on the right, its effective mass increases to around $m^* = 0.4m$, and its mobility decreases to $200 \text{ cm}^2 \text{ V}^{-1} \text{ s}^{-1}$. The result is that electron velocity as a function of electric field E looks as shown in Figure 21.14.

When a sufficiently large electrical field ($\sim 3000 \text{ V/cm}$) is applied to GaAs, the crystal begins to emit pulses, typically at frequencies in the 50 GHz range. The physical origin of the pulses lies in the fact that as electrons become more energetic, it is favorable for them to jump from the center valley at Γ to the left valley at L in Figure 19.8. However, when they do so, their mobility decreases, and they slow down. This leads to a traffic jam of charge, which travels through the sample as a localized pulse. The goal of this problem is to calculate properties of these moving pulses.

Model electron velocity versus field by

$$v(E) = \begin{cases} \mu_1 E & \text{for } E < E_c \\ \mu_2 E & \text{for } E > E_c, \end{cases} \quad (21.50)$$

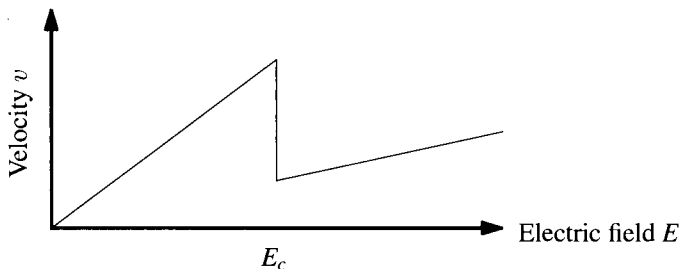


Figure 21.14. Schematic view of velocity as a function of field for electrons in gallium arsenide. Electron mobility decreases for fields greater than the critical E_c .

with $\mu_1 > \mu_2$, as shown in Figure 21.14. Denote net charge density as a function of length x along the sample by $n(x)$; $n(x)$ vanishes far from the pulse. Denote current by j , and take it to be of the form

$$j = nev(E) - eD \frac{\partial n}{\partial x}, \quad (21.51)$$

where e is the electron charge and D is a diffusion constant.

- (a) Write down Poisson's equation for the electric field, and an equation relating the current j and the time rate of change of the charge density n . In order to describe a pulse moving at velocity v^* , assume that all spatially varying fields are moving in steady state at velocity v^* , and use this assumption to simplify the relation between current and charge density.
- (b) Look for a solution such that charge density vanishes for large negative x and large positive x . Assume that for large negative x the electric field approaches a low value $E_1 < E_c$, and for large positive x it approaches a larger value $E_2 > E_c$. Find an expression for $\partial n / \partial E$, and integrate it to find charge as a function of electric field.
- (c) Assume that

$$\mu_1 E_1 = \mu_2 E_2 = v^*. \quad (21.52)$$

Adding to these equations the condition that charge density vanish when the field reaches E_2 , find v^* in terms of the mobilities μ_1 , μ_2 , and E_c .

- (d) Find the electric field $E(x)$ for $E < E_c$.
- (e) As a pulse of this type moves across a sample, what happens to the potential drop from one end of the sample to the other? Suppose that one demands that the potential drop across the sample remain constant as the pulse moves in its interior. Draw a sketch indicating how one could construct solutions that would make it possible to satisfy this condition.

4. Frenkel exciton I: To model the Frenkel exciton, consider a variant of the tight-binding model. At each site of a lattice there is an electron, which can occupy one of two states, an atomic ground state and an atomic excited state. Denote the Wannier states by $w_g(\vec{r} - \vec{R})$ and $w_e(\vec{r} - \vec{R})$; suppose they are real functions and are localized near the atomic sites.

When the atoms are assembled into a crystal, the ground state is given to good approximation by a Hartree–Fock state, consisting of an antisymmetrized product for N electrons of $w_g(\vec{r}_i - \vec{R})$, the product being taken over all N sites in the lattice. In second-quantized notation, the ground state of the system is

$$|\Phi_0\rangle = \prod_{\vec{R}} \hat{c}_{\vec{R},g}^\dagger |0\rangle. \quad (21.53)$$

$\hat{c}_{\vec{R},g}^\dagger$ creates an electron in the atomic ground state at site \vec{R} .

Suppose now that the only quantum states of importance are the ground state and the excited states where one electron at one site moves from the ground to the excited state; such a state is

$$|\vec{R}\rangle \equiv \hat{c}_{\vec{R}e}^\dagger \hat{c}_{\vec{R}g} |\Phi_0\rangle. \quad (21.54)$$

- (a) Choose the zero of energy so that $\langle \vec{R} | \hat{\mathcal{H}} | \Phi_0 \rangle = 0$. If the states in Eqs. (21.53) and (21.54) are all that matter, then the Hamiltonian is given by

$$\hat{\mathcal{H}} = |\Phi_0\rangle \langle \Phi_0 | \hat{\mathcal{H}} | \Phi_0 \rangle \langle \Phi_0 | + \sum_{\vec{R}\vec{R}'} |\vec{R}\rangle \langle \vec{R} | \hat{\mathcal{H}} | \vec{R}' \rangle \langle \vec{R}' |. \quad (21.55)$$

Show that

$$|\Phi_{\vec{k}}\rangle = \frac{1}{\sqrt{N}} \sum_{\vec{R}} e^{i\vec{k}\cdot\vec{R}} |\vec{R}\rangle \quad (21.56)$$

is an eigenstate, and find the eigenvalue. Use the fact that $\langle \vec{R} + \vec{R}' | \hat{\mathcal{H}} | \vec{R} \rangle$ depends only upon \vec{R}' .

- (b) Now proceed to evaluate the matrix elements $\langle \vec{R} | \hat{\mathcal{H}} | \vec{R}' \rangle$ that determine this eigenvalue. The Hamiltonian $\hat{\mathcal{H}}$ contains kinetic energy and Coulomb interaction terms. There are many contributions to $\langle \vec{R} | \hat{\mathcal{H}} | \vec{R}' \rangle$; however, this matrix element causes something proportional to the unit operator to be added to the Hamiltonian, is equivalent to a constant shift in energy, and can be neglected. Therefore, focus on evaluating $\langle \vec{R} | \hat{\mathcal{H}} | \vec{R}' \rangle$ for $\vec{R} \neq \vec{R}'$. Assuming that Coulomb interaction leads to the largest interaction between sites, take

$$\hat{\mathcal{H}} = \frac{e^2}{2} \sum_{l \neq l'} \frac{1}{|\vec{r}_l - \vec{r}_{l'}|}. \quad (21.57)$$

This is the Schrödinger representation; do not confuse the independent variable \vec{r}_l with the wave function centered at \vec{R} , which is denoted by $|\vec{R}\rangle$.

Write the Hamiltonian (21.57) in second quantized notation, using Eq. (C.10).

- (c) Show that

$$\langle \vec{R} | \hat{\mathcal{H}} | \vec{R}' \rangle = e^2 \int \frac{d\vec{r}_1 d\vec{r}_2}{|\vec{r}_1 - \vec{r}_2|} \left[\begin{array}{l} w_g(\vec{r}_1 - \vec{R}') w_e(\vec{r}_2 - \vec{R}) w_e(\vec{r}_1 - \vec{R}') w_g(\vec{r}_2 - \vec{R}) \\ - w_e(\vec{r}_1 - \vec{R}) w_g(\vec{r}_2 - \vec{R}') w_e(\vec{r}_1 - \vec{R}') w_g(\vec{r}_2 - \vec{R}) \end{array} \right]. \quad (21.58)$$

- (d) Argue from localization of the wave functions that the second term in Eq. (21.58) can be neglected, and

$$\langle \vec{R} | \hat{\mathcal{H}} | \vec{R}' \rangle \approx e^2 \int \frac{d\vec{r}_1 d\vec{r}_2}{|\vec{r}_1 - \vec{r}_2|} w_g(\vec{r}_1 - \vec{R}') w_e(\vec{r}_2 - \vec{R}) w_e(\vec{r}_1 - \vec{R}') w_g(\vec{r}_2 - \vec{R}). \quad (21.59)$$

5. Frenkel exciton II:

- (a) Continuing the study of the Frenkel exciton, let $\delta\vec{R} \equiv \vec{R} - \vec{R}'$, $\delta\vec{r}_1 = \vec{r}_1 - \vec{R}'$ and $\delta\vec{r}_2 = \vec{r}_2 - \vec{R}$. Show that

$$\frac{\delta R}{|\vec{r}_1 - \vec{r}_2|} \approx 1 + \frac{1}{2} \left[\frac{2(\delta\vec{r}_1 - \delta\vec{r}_2) \cdot \delta\vec{R}}{\delta R^2} - \frac{(\delta\vec{r}_1 - \delta\vec{r}_2)^2}{\delta R^2} \right] + \frac{3}{8} \left[\frac{2(\delta\vec{r}_1 - \delta\vec{r}_2) \cdot \delta\vec{R}}{\delta R^2} \right]^2 \dots \quad (21.60)$$

- (b) Define the dipole moment

$$\vec{p} = e \int d\vec{r} w_g(\vec{r}) w_e(\vec{r}) \vec{r}. \quad (21.61)$$

Show that

$$\langle \vec{R} | \hat{J} | \vec{R}' \rangle \approx \frac{p^2}{\delta R^3} - 3 \frac{(\vec{p} \cdot \delta\vec{R})^2}{\delta R^5} \quad (21.62)$$

$$= -\vec{p} \cdot \left[\vec{\nabla} \left(\vec{p} \cdot \vec{\nabla} \frac{1}{\delta R} \right) \right]. \quad (21.63)$$

- (c) Using Eq. (21.63), find the energy of state $\Phi_{\vec{k}}$. Convert sums over $\delta\vec{R}$ to integrals to find the final expression.

References

- P. W. Baumeister (1961), Optical absorption of cuprous oxide, *Physical Review*, **121**, 359–362.
- W. F. Brinkman, T. M. Rice, P. W. Anderson, and S. T. Chui (1972), Metallic state of the electron-hole liquid, particularly in germanium, *Physical Review Letters*, **28**, 961–964.
- J. L. Bromberg (1988), The birth of the laser, *Physics Today*, **41**(10), 26–33.
- M. L. Cohen and J. R. Chelikowsky (1989), *Electronic Structure and Optical Properties of Semiconductors*, 2nd ed., Springer-Verlag, Berlin.
- R. N. Dexter, H. J. Zeiger, and B. Lax (1956), Cyclotron resonance experiments in silicon and germanium, *Physical Review*, **104**, 637–644.
- G. Dresselhaus, A. F. Kip, and C. Kittel (1953), Observation of cyclotron resonance in germanium crystals, *Physical Review*, **92**, 827.
- G. Dresselhaus, A. F. Kip, and C. Kittel (1955), Cyclotron resonance of electrons and holes in silicon and germanium crystals, *Physical Review*, **98**, 368–384.
- I. Egri (1985), Excitons and plasmons in metals, semiconductors and insulators: A unified approach, *Physics Reports*, **119**, 363–402.
- H. Ehrenreich and J. H. Martin (1979), Solar photovoltaic energy, *Physics Today*, **32**(9), 25–32.
- A. Einstein (1916), Quantum theory of radiation, *Mitteilungen der Physikalischen Gesellschaft, Zürich*, **16**, 47–62. In German. Translated in van der Waerden (1967), pp. 63–77.
- R. J. Elliott (1957), Intensity of optical absorption by excitons, *Physical Review*, **108**, 1384–1389.
- M. A. Green (1998), Solar cells, in *Modern Semiconductor Device Physics*, S. M. Sze, ed., pp. 473–530, John Wiley and Sons, New York.
- J. Hecht (1992), *Laser Pioneers*, revised ed., Academic Press, Boston.
- J. C. Hensel, T. G. Phillips, and G. A. Thomas (1977), The electron-hole liquid in semiconductors: experimental aspects, *Solid State Physics: Advances in Research and Applications*, **32**, 87–314.

- E. J. Johnson (1967), Absorption near the fundamental edge, in *Semiconductors and Semimetals*, R. K. Willardson and A. C. Beer, eds., vol. 3, pp. 153–258, Academic Press, New York.
- E. O. Kane (1957), Band structure of indium antimonide, *Journal of Physics and Chemistry of Solids*, **1**, 249–261.
- L. V. Keldysh and A. N. Kozlov (1967), Collective properties of large-radius excitons, *JETP Letters*, **5**, 190–194.
- L. C. Kimerling, K. D. Kolenbrander, J. Michel, and J. Palm (1997), Light emission from silicon, *Solid State Physics: Advances in Research and Applications*, **50**, 333–381.
- C. F. Klingshirn (1995), *Semiconductor Optics*, Springer-Verlag, Berlin.
- R. C. Knox (1963), *Theory of Excitons*, Academic Press, New York.
- W. Koechner (1992), *Solid-state Laser Engineering*, 3rd ed., Springer-Verlag, Berlin.
- R. Ladenburg (1928), Research on the anomalous dispersion of gases, *Physikalische Zeitschrift*, **48**, 1525. In German.
- L. D. Landau and E. M. Lifshitz (1977), *Quantum Mechanics (Non-relativistic Theory)*, 3rd ed., Pergamon Press, Oxford.
- B. Lax, H. J. Zeiger, R. N. Dexter, and E. S. Rosenblum (1954), Directional properties of the cyclotron resonance in germanium, *Physical Review*, **93**, 1418–1420.
- R. Loudon (1973), *The Quantum Theory of Light*, Clarendon Press, Oxford.
- G. G. Macfarlane, T. P. McLean, J. E. Quarrington, and V. Roberts (1957), Fine structure in the absorption-edge spectrum of Ge, *Physical Review*, **108**, 1377–1383.
- T. H. Maiman (1960), Stimulated optical radiation in ruby, *Nature*, **187**, 493–494.
- P. Mieghem (1992), Theory of band tails in heavily doped semiconductors, *Reviews of Modern Physics*, **64**, 755–793.
- G. F. Neumark, R. M. Park, and J. M. DePuydt (1994), Blue-green diode lasers, *Physics Today*, **47**(6), 26–32.
- A. V. Nurmikko and R. L. Gunshor (1995), Physics and device science in II-VI semiconductor visible light emitters, *Solid State Physics: Advances in Research and Applications*, **49**, 205–282.
- D. C. Reynolds and T. C. Collins (1981), *Excitons, their Properties and Uses*, Academic Press, New York.
- T. M. Rice (1977), The electron-hole liquid in semiconductors: theoretical aspects, *Solid State Physics: Advances in Research and Applications*, **32**, 1–86.
- A. L. Schawlow and C. H. Townes (1958), Infrared and optical masers, *Physical Review*, **112**, 1940–1949.
- L. Schiff (1968), *Quantum Mechanics*, 3rd ed., McGraw-Hill, New York.
- J. Singh (1984), The dynamics of excitons, *Solid State Physics: Advances in Research and Applications*, **38**, 295–370.
- J. L. Stone (1993), Photovoltaics: unlimited electrical energy from the sun, *Physics Today*, **46**(9), 22–29.
- M. D. Sturge (1962), Optical absorption of gallium arsenide between 0.6 and 2.75 eV, *Physical Review*, **127**, 768–773.
- Y. Suematsu (1985), Advances in semiconductor lasers, *Physics Today*, **38**(5), 32–39.
- M. Ueta, H. Kanzaki, K. Kobayashi, Y. Toyozawa, and E. Hanamura (1986), *Excitonic Processes in Solids*, Springer-Verlag, Berlin.
- B. L. van der Waerden (1967), *Sources of Quantum Mechanics*, North-Holland, Amsterdam.
- J. P. Wolfe (1982), Thermodynamics of excitons in semiconductors, *Physics Today*, **35**(3), 46–54.

22. Optical Properties of Insulators

22.1 Introduction

Insulators do not allow charge to travel long distances at low frequencies, but that does not mean that their response to electric fields is simple. Even the response of insulators to static fields is complicated, expressed in terms of quantities that are difficult to define, and hard to calculate precisely. As the frequency of incoming radiation increases, insulators become difficult to distinguish from metals, because radiation passes through both in similar ways.

Almost all optically transparent materials are insulators. Insulators have no free electrons to interact with light, and phonons provide the main way for insulating crystals to interact with radiation. If phonons provided the only mechanism, insulating crystals would generally be transparent. However, very small concentrations of impurities and vacancies create localized states that have a large effect on optical properties. The study of these color centers is one of most important topics in the optical properties of insulators, and it has had an impact on applications ranging from photography to the laser.

22.2 Polarization

Polarization is Ill-Defined. As defined by Eq. (20.6) the polarization is not precisely determined. Changes in the polarization are given by the current \vec{j} , but the actual value of the polarization at any given time is rather arbitrary. This uncertainty is unavoidable, as indicated in Figure 22.1. Depending upon how charges are grouped together, the polarization can have any value desired. Measurable quantities are not affected by changes in the definition of the polarization, because every change in definition of bulk polarization simultaneously implies changing the amount of surface charge. However, Figure 22.1 actually understates the difficulty of defining polarization, because charge distributions are not point-like, but distributed continuously as in Figure 11.1. By changing the origin of the unit cell continuously, the dipole moment of the cell can also be made to vary continuously. So long as one consistently keeps track of polarization and surface charge, there should not ultimately be any difficulties.

22.2.1 Ferroelectrics

The need to define polarization becomes especially acute for the *pyroelectric* and *ferroelectric* materials. Pyroelectric solids develop an electric field upon heating and cooling. Any free charge in the environment quickly rushes to mask it, but until then the field is measurable. Heating and cooling produce electric fields because

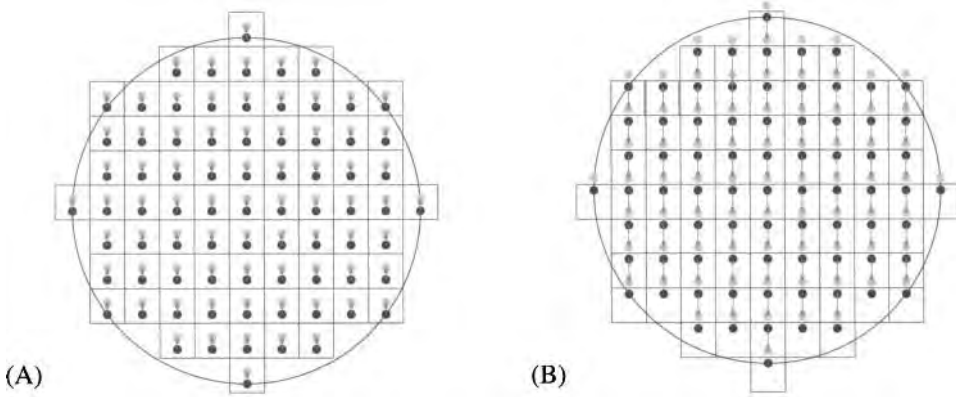


Figure 22.1. When charges are distributed throughout a solid, the polarization density depends upon how they are grouped. In (A), positive and negative charges have been grouped with their nearest neighbors. In (B), they have been grouped so that the polarization now points in the opposite direction. In compensation, there is now a substantial surface charge.

they cause expansion and contraction of the crystal along various axes. Each unit cell is electrically polarized, and as the dipole moment changes, an electric field develops. The ferroelectric crystals have an additional property, which is that each unit cell can choose between two symmetrical forms where the dipole moments point in opposite directions. The crystal can be caused to flip between one and the other by application of an external field. Usually, a ferroelectric has a transition temperature T_c above which the polarization vanishes, and the substance becomes *paraelectric*. External electric fields easily cause ferroelectrics to flip between the two equivalent stable states just below the transition temperature, whereas far below the transition temperature, electric fields powerful enough to cause the polarization to flip may not be available in the laboratory.

The explanation of ferroelectrics in terms of dipole moments in each unit cell seems intuitively clear, but is thrown into question to the extent that this dipole moment cannot be defined. Because thousands of ferroelectric compounds have been created, measured, and tabulated (for example, in Landolt and Börnstein (New Series) vols. 16 and 28), the best definition of the polarization is in terms of the actual operations performed in experiment.

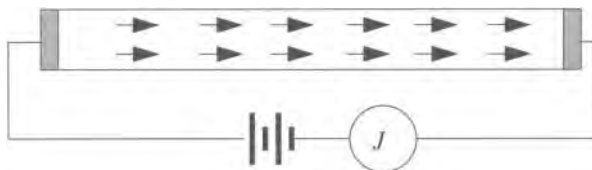


Figure 22.2. The spontaneous electric polarization of a sample is measured by cooling it below the ferroelectric transition temperature in an electric field, and then measuring the total charge that flows between the ends.

The experiments depend upon being able to access the paraelectric phase above T_c , where the polarization can safely be taken to be zero. As indicated in Figure 22.2, the experiment begins with an insulating sample in the paraelectric phase, with electrical contacts at the ends. The aim is to measure all the charge that flows between ends of the sample, so the electrical contacts at the ends must be very good and are often obtained with liquid electrolytes. An electric field is applied to the sample, and the temperature is then lowered through the ferroelectric transition. The applied field ensures that the sample forms a single domain of dipoles all pointing in the same direction. Finally, the applied electric field can be turned off. The total charge Q that has flowed from one end of the sample to the other since the beginning of the experiment gives the total polarization through $P = Q/A$, following Eq. (20.6). It is really the change in polarization between two states of the solid that is being measured, and nothing else can precisely be defined.

22.2.2 Berry phase theory of polarization

With the advent of band structure calculations, considerable effort has been expended in learning how to calculate ferroelectric polarizations or, more precisely, to find the difference in polarization between the two symmetrical states of the ferroelectric.

The computations are based conceptually upon the experimental procedure of starting in a paraelectric phase without polarization and adiabatically changing the temperature T until spontaneous polarization appears. This process corresponds exactly to the situation in which the geometric phases of Section 8.4.3 should arise, as pointed out by Resta (1994) and King-Smith and Vanderbilt (1993).

Suppose that at time $t = 0$, one has an insulating crystal without any bulk polarization. Suppose that a long time later, by slowly changing a parameter such as temperature, a polarization appears. Denote the Wannier functions at the later time by $w_n(\vec{r})$. The dipole moment per unit cell changes from 0 to

$$\vec{P} = -\frac{e}{\Omega} \sum_n \int d\vec{r} \vec{r} |w_n(\vec{r})|^2. \quad \text{Sum only over occupied bands } n. \quad (22.1)$$

As discussed at the beginning of Section 8.4.4, Wannier functions in insulators are localized, and the integral in Eq. (22.1) should converge. Indeed, the integral in Eq. (22.1) was defined in Eq. (8.56), making it possible to rewrite in terms of the Berry connection, Eq. (8.54), as

$$\vec{P} = -\frac{e}{\Omega} \sum_n \vec{r}_n = -\frac{e}{\Omega} \sum_{n\vec{k}} \vec{\mathcal{R}}_{n\vec{k}}. \quad (22.2)$$

A comparison of theory and experiment for some crystals appears in Table 22.1.

22.2.3 Clausius–Mossotti Relation

The Clausius–Mossotti relation is the classic link between atomic polarization and dielectric constants. Suppose one takes a single unit cell out a solid, subjects it to

Table 22.1. Comparison of theory and experiment for spontaneous polarization P of selected perovskite crystals.

	KNbO ₃	PbZr _{1/2} Ti _{1/2} O ₃	BaTiO ₃
Theory (C/m ²)	0.35 ^a	0.74 ^b	0.2-0.4 ^d
Experiment (C/m ²)	0.37	0.75 ^c	0.27 ^d

Sources: (a) Resta et al. (1993), (b) Sághi-Szabó et al. (1999) (c) Berlincourt and Krueger (1959) (d)Wahl et al. (2008)

a uniform electric field of strength \vec{E} , and finds that it responds by developing a dipole moment $\vec{p} = \alpha\vec{E}$. The question is how a periodic solid tiled with such unit cells will respond to an external electric field. The dipole moment in each unit cell creates electric fields that affect all other unit cells, so the problem must be solved self-consistently. It is tricky because the sums that arise are divergent and must be handled carefully. In fact, the field created within a solid by a collection of dipoles depends upon the way the sum is cut off far away; that is, it depends upon the macroscopic shape of the sample. The field also depends upon details of how dipoles are arranged at the atomic level. The influence of local arrangement simplifies considerably in the case of a crystal of cubic symmetry, so the following discussion will focus on this special case.

Consider a sphere of dielectric material. The reasons to focus upon a sphere are as follows:

1. When a sphere of dielectric material is placed into a uniform external electric field of strength \vec{E}_0 , classical electrostatics shows that the polarization \vec{P} and electric field \vec{E} inside the sphere are uniform, as shown in Figure 22.3 and related by

$$\vec{E} = \vec{E}_0 - \frac{4\pi}{3}\vec{P}. \quad (22.3)$$

Therefore, one should expect that all the unit cells in a sample of this shape develop the same microscopic polarization \vec{p} . In a sample of arbitrary shape, electrostatics would predict that fields and dipole moments should vary macroscopically in a complicated way throughout the sample, making it difficult to relate microscopic and macroscopic behavior.

2. In a cubic crystal, the unit cell at the center of a sphere sees fields with cubic symmetry, a fact that can be used to resolve conclusively the value of divergent sums.

Focus on the unit cell at the center of the sphere. The field \vec{E}_{cell} acting upon it is due to two sources. First, this unit cell sees the external field \vec{E}_0 . Second, it sees the field

$$\vec{E}_1 = - \sum_{\vec{R} \neq 0} \nabla_{\vec{R}} \frac{\vec{p} \cdot \vec{R}}{R^3} = \sum_{\vec{R} \neq 0} 3 \frac{\vec{R}(\vec{R} \cdot \vec{p})}{R^5} - \frac{\vec{p}}{R^3} \quad (22.4)$$

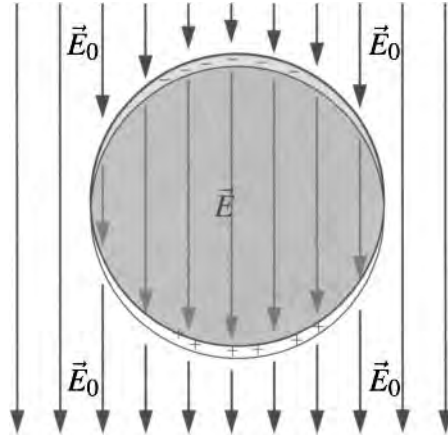


Figure 22.3. A dielectric sphere placed in a uniform electric field \vec{E}_0 counteracts the field by developing a uniform polarization in the opposite direction, as if rigid spheres of positive and negative charge move slightly apart. The reduction of \vec{E}_0 to \vec{E} results from the uniform field created by the surface charges at the top and bottom of the sphere.

due to all the dipole moments of the other unit cells. By symmetry, \vec{E}_1 must vanish, as shown in Problem 1, so $\vec{E}_{\text{cell}} = \vec{E}_0$. But if this result holds for the center of the sphere, it must hold elsewhere as well, because all parts of the sphere have the same dipole moment. The polarization \vec{p} in each unit cell is

$$\vec{p} = \alpha \vec{E}_{\text{cell}} \Rightarrow \vec{p} = \alpha \vec{E}_0. \quad \text{The susceptibility } \alpha \text{ is defined to be the coefficient of proportionality in this relation.} \quad (22.5)$$

So when the spatial density of dipoles is n ,

$$\vec{P} = n\alpha \vec{E}_0. \quad \text{The ambiguities about choice of unit cell and definition of } \vec{P} \text{ are resolved by requiring } \vec{P} \text{ to vanish when } \vec{E}_0 \text{ vanishes.} \quad (22.6)$$

To adopt the language of dielectric media, one must consider the electric field and polarization density on scales very large compared to the lattice spacing. The spatial average of the polarization is \vec{P} , while the spatial average of the electric field \vec{E} is given by Eq. (22.3) and is the sum of the external field \vec{E}_0 with the field $-4\pi\vec{P}/3$ produced by surface charges. Finally, to compute the dielectric constant, one has to find the ratio of $\vec{E} + 4\pi\vec{P}$ to \vec{E} . This ratio is

$$\frac{E + 4\pi P}{E} = \frac{E_0 - \frac{4\pi}{3}P + 4\pi P}{E_0 - \frac{4\pi}{3}P} \quad (22.7)$$

$$\Rightarrow \epsilon = \frac{3 + 8\pi n\alpha}{3 - 4\pi n\alpha}. \quad \text{Using Eq. (22.6).} \quad (22.8)$$

Equation (22.8) is the Clausius–Mossotti relation.

A sphere is not the only shape that adopts a uniform internal electric field when placed in a uniform external electric field. Any ellipsoid has the same property, as does a thin slab. In general, the electric field inside one of these samples has the form

$$\vec{E} = \vec{E}_0 - \mathcal{N}\vec{P}, \quad (22.9)$$

where \mathcal{N} is the *depolarization factor* and equals $4\pi/3$ for a sphere, equals 4π for a slab, and vanishes for a long thin rod whose axis lies along the field. The electric field \vec{E}_{cell} acting upon a unit cell in one of these samples must equal the electric field it would have seen if the sample had been a sphere, plus the additional field due to the different arrangement of surface charges. So the field acting upon a unit cell is

$$\vec{E}_{\text{cell}} = \vec{E}_0 - \mathcal{N}\vec{P} + \frac{4\pi}{3}\vec{P} = \vec{E} + \frac{4\pi}{3}\vec{P} \quad \text{The field on the cell varies according to Eq. (22.9), but must equal } \vec{E}_0 \text{ for a sphere when } \mathcal{N} = 4\pi/3. \quad (22.10)$$

$$\Rightarrow \vec{E}_{\text{cell}} = \frac{4\pi}{3} \frac{\epsilon + 2}{\epsilon - 1} \vec{P} \quad \text{Use } \vec{E} = 4\pi\vec{P}/(\epsilon - 1). \quad (22.11)$$

$$= \frac{4\pi}{3} \frac{\epsilon + 2}{\epsilon - 1} n\alpha \vec{E}_{\text{cell}} \quad (22.12)$$

$$\Rightarrow \alpha = \frac{3}{4\pi n} \left(\frac{\epsilon - 1}{\epsilon + 2} \right) \quad (22.13)$$

$$\Rightarrow \epsilon = \frac{3 + 8\pi n\alpha}{3 - 4\pi n\alpha}. \quad \text{Reproducing Eq. (22.6) as expected.} \quad (22.14)$$

22.3 Optical Modes in Ionic Crystals

In modeling the phonon dispersion relations of silicon in Section 13.2.4, ions were taken to interact only with nearest neighbors. Despite the fact that models of this type may produce good agreement with experiment, they are misleading. Whenever an ion moves, it interacts with other ions throughout the crystal with a force that dies off only as $1/r^2$. In an insulator, the absence of free charge means that these long-range interactions are not screened. Therefore a realistic calculation of phonon frequencies in an insulator should take long-range electrostatic effects into account. Furthermore, because ionic motion and the accompanying motion of charge are inseparable, the phonons should strongly couple to external electromagnetic radiation. Optical phonons acquired their name for a reason.

A truly realistic calculation would be very difficult to perform, but a good approximate calculation can be obtained by mixing together three ingredients.

1. Nearby ions interact through short-range forces, needed to stabilize the crystal. These forces will be modeled as linear forces between nearest neighbors.
2. Ions also interact through long-range Coulomb forces that will be treated by using the Clausius–Mossotti relation.

- The individual ions are polarizable, and they develop internal dipole moments in response to electric fields.

Mechanical Model for Near Neighbors. As a mechanical model for nearest neighbors, imagine that every unit cell contains two ions, of mass M_1 and M_2 , at positions \vec{u}_1 and \vec{u}_2 relative to equilibrium. This problem has already been studied in Section 13.2.1. The equation of motion for the ions is Eq. (13.7), and the frequency with which they oscillate is given by Eq. (13.9). According to Figure 20.1, when the frequency of light is in the vicinity of 10 THz characteristic of optical phonons, its wavelength is on the order of 10^6 \AA , so only the $\vec{k} \rightarrow 0$ limit given by Eq. (13.10) is important. In the long-wavelength limit, the ions have two dynamical modes. In the acoustic mode, shown in Figure 13.4, the ions within the unit cell move together. The polarization in the unit cell does not change, so electromagnetic radiation will not easily excite this mode, and it can be neglected. In the optical mode, however, the ions move in opposite directions, creating oscillating dipole moments that can be excited by oscillating electric fields. To describe this interaction, let

$$\vec{u} = \vec{u}_1 - \vec{u}_2 \quad \text{Normal modes are found by inverting a matrix described by Eqs. (13.10).} \quad (22.15)$$

be the normal mode described by Eq. (13.10b). It has a resonance frequency of

$$\bar{\omega} \equiv \sqrt{\frac{2\mathcal{K}}{M}}, \quad \text{where } M = \frac{M_1 M_2}{(M_1 + M_2)}. \quad \mathcal{K} \text{ is the spring constant of nearest neighbors defined in Eq. (13.7).} \quad (22.16)$$

In the presence of an oscillating electric field of strength \vec{E}_{cell} , suppose that the optical mode oscillates according to

$$M\ddot{\vec{u}} = -M\bar{\omega}^2\vec{u} - M\dot{\vec{u}}/\tau + e^*\vec{E}_{\text{cell}}. \quad (22.17)$$

$$\Rightarrow \vec{u} = -\frac{e^*}{M(\omega^2 - \bar{\omega}^2 + i\omega/\tau)}\vec{E}_{\text{cell}}. \quad \text{Fourier transforming with } \int dt \exp[i\omega t]. \quad (22.18)$$

The relaxation time τ describes how long ions keep oscillating once the external field is turned off. A reason to employ an effective charge e^* is that relative motion of the ions may well be accompanied by a readjustment in the electron clouds around them, so that the net motion of charge is less or greater than one would expect based on the distance the ions have moved.

Dipole Moments. The dipole moment in each cell is made of two contributions. First, ionic motion produces a dipole moment $e^*\vec{u}$. Second, the electron cloud around each of the ions can polarize, producing a second moment of size $\alpha^\infty \vec{E}_{\text{cell}}$. The electrons adjust much more quickly than the ions to external fields. The total polarization is therefore

$$\vec{p} = e^*\vec{u} + \alpha^\infty \vec{E}_{\text{cell}}. \quad \alpha^\infty \text{ comes from redistribution of charge around individual ions, and is different from } \alpha \text{ caused by ionic motion in Eq. (22.14).} \quad (22.19)$$

The long-range interactions between dipoles can be described by the same arguments that lead to the Clausius–Mossotti relation. In particular, the field \vec{E}_{cell} acting on the dipole in each cell is given by Eq. (22.10). Therefore

$$\vec{P} = n \left[\frac{(e^*)^2}{M(\bar{\omega}^2 - \omega^2 - i\omega/\tau)} + \alpha^\infty \right] \vec{E}_{\text{cell}} \quad \text{Put Eq. (22.18) in Eq. (22.19).} \quad (22.20)$$

$$\Rightarrow \frac{3}{4\pi} \frac{\epsilon(\omega) - 1}{\epsilon(\omega) + 2} = n \left[\frac{(e^*)^2}{M(\bar{\omega}^2 - \omega^2 - i\omega/\tau)} + \alpha^\infty \right]. \quad (22.21)$$

The quantity on the right is just P/E_{cell} , while the left comes from Eq. (22.13).

There are four phenomenological quantities in Eq. (22.21): e^* , τ , α^∞ , and $\bar{\omega}$. Figure 22.4 shows that the dielectric function $\epsilon(\omega)$ has definite low- and high-frequency limits, and these can be used to eliminate two of the phenomenological constants. For frequencies ω much greater than $\bar{\omega}$, but still small enough that electron charge responds quasi-statically, one can use Eq. (22.21) with $\vec{u} \approx 0$. Denoting the dielectric function in this limit by ϵ^∞ , Eq. (22.21) gives

$$\alpha^\infty = \frac{3}{4\pi n} \left(\frac{\epsilon^\infty - 1}{\epsilon^\infty + 2} \right). \quad (22.22)$$

On the other hand, for frequencies ω much less than $\bar{\omega}$ one can take

$$\vec{u} = \frac{e^* \vec{E}_{\text{cell}}}{M\bar{\omega}^2} \quad (22.23)$$

and find

$$(e^*)^2 = \frac{9M\bar{\omega}^2}{4\pi n} \left(\frac{\epsilon^0 - \epsilon^\infty}{(\epsilon^0 + 2)(\epsilon^\infty + 2)} \right). \quad (22.24)$$

With these values for e^* and α^∞ , one can now solve Eq. (22.21) for $\epsilon(\omega)$ and obtain

$$\epsilon(\omega) = \epsilon^\infty + \frac{\epsilon^\infty - \epsilon^0}{\left(\frac{\omega^2}{\bar{\omega}^2} + i \frac{\omega}{\tau\bar{\omega}^2} \right) \left(\frac{\epsilon^0 + 2}{\epsilon^\infty + 2} \right) - 1}. \quad (22.25)$$

Equation (22.25) goes to the correct limits as $\omega \rightarrow 0$ and $\omega \rightarrow \infty$.

22.3.1 Polaritons

To simplify the dispersion relation (22.25), it is useful to define the *transverse optical* frequency ω_T by

$$\omega_T^2 = \bar{\omega}^2 \left(\frac{\epsilon^\infty + 2}{\epsilon^0 + 2} \right) \quad (22.26)$$

and the *longitudinal optical* frequency ω_L by

$$\omega_L^2 = \omega_T^2 \left[\frac{\epsilon^0}{\epsilon^\infty} \right] \tag{22.27}$$

$$\Rightarrow \epsilon(\omega) = \epsilon^\infty \left[\frac{\omega^2 + i\omega/\tau - \omega_L^2}{\omega^2 + i\omega/\tau - \omega_T^2} \right]. \tag{22.28}$$

The relationship (22.27) between ω_L and ω_T is called the *Lyddane–Teller–Sachs* equation.

The dispersion relation Eq. (22.28) allows both transverse and longitudinal propagating modes within the crystal. According to Eq. (20.17), the transverse modes satisfy

$$\frac{\omega^2 \epsilon(\omega)}{c^2} = q^2, \tag{22.29}$$

while according to Eq. (20.23) the longitudinal mode satisfies

$$\epsilon(\omega) = 0. \tag{22.30}$$

In the limit $\tau \rightarrow \infty$, the dielectric function vanishes for $\omega = \omega_L$, explaining the name given to ω_L .

The dielectric function of CdS has been measured by Balkanski (1972) from reflectance and absorption measurements, and the results are shown in Figure 22.4. The data match so well to Eq. (22.28) for the parameter values listed in the caption that it is sufficient just to plot the theoretical formula. Employing this dielectric

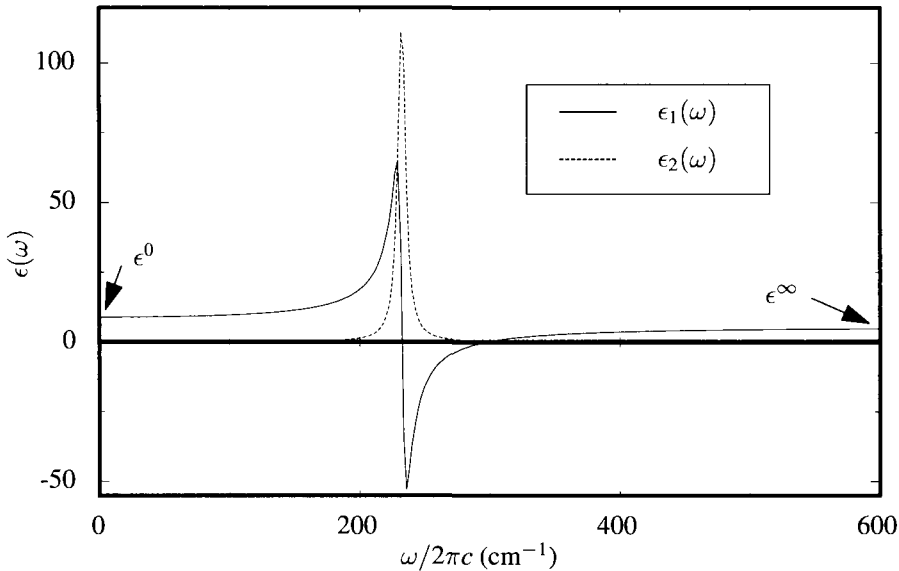


Figure 22.4. Dielectric function for CdS, deduced from reflection data by Balkanski (1972). The data fit Eq. (22.28) with $\epsilon^\infty = 5.4$, $\epsilon^0 = 8.9$, $\omega_T/2\pi c = 232 \text{ cm}^{-1}$, $1/2\pi\tau c = 6.9 \text{ cm}^{-1}$. Most data in the infrared are reported for ω in units of cm^{-1} , referring to $1/\lambda = \omega/2\pi c$, with c the speed of light in vacuum.

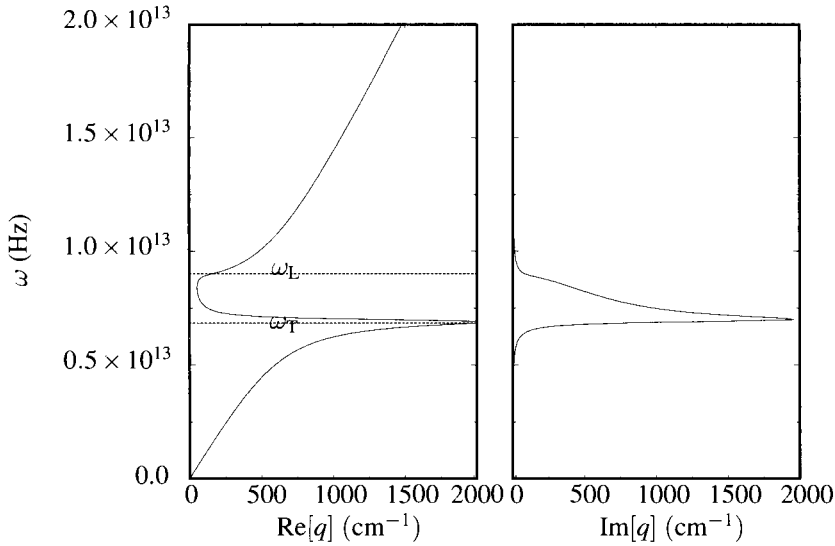


Figure 22.5. Frequency ω of transverse waves as a function of complex wave vector q resulting from data of Figure 22.4.

function in Eq. (22.29) produces the plot of ω versus real and imaginary parts of q that appears in Figure 22.5.

The dispersion relation has three branches, which are most easily distinguished by sending $\tau \rightarrow \infty$ to identify the physical significance of ω_L and ω_T :

Lower Branch: At low wave numbers, light behaves as if traveling in an ordinary dielectric medium of dielectric constant ϵ^0 . As q increases, the dispersion curve bends over and finally approaches the transverse frequency ω_T . The dielectric function becomes very large along this branch, which means that a small amplitude of external electromagnetic radiation is accompanied by an extremely large polarization. Purely light-like at low frequencies, the radiation becomes almost completely phonon-like near ω_T . The mode created by the coupling of light and phonons is called a *polariton*.

Central Branch: Between ω_T and ω_L , propagating modes are heavily damped, and any incident radiation is almost completely reflected from the crystal. The central region is fairly narrow, and collecting radiation reflected from a crystal transforms broadband radiation into a fairly monochromatic *residual* or *Restrahl* band. Einstein (1907) used this frequency in calculating the specific heat of diamond, as mentioned in Section 13.3.1.

Upper Branch: Well above ω_L light propagates as if in a medium of dielectric constant ϵ^∞ . There are propagating modes in the vicinity of frequency ω_L that are transverse modes and should not be confused with the distinct longitudinal mode that exists right at ω_L .

Values of dielectric constants and transverse and longitudinal frequencies appear in Table 22.2.

22.3.2 Polarons

Electromagnetic radiation traveling in the vacuum is always transverse, so it tends to generate transverse waves when it impinges upon a crystal. It provides no opportunity to excite the longitudinal mode where $\epsilon = 0$. If, however, an electron flies into a polar crystal, it excites mainly the longitudinal modes, while it pushes charge out of the way like a snow plow. A polarization cloud surrounds the electron as it travels, changing its effective mass. The resulting quasi-particle is called a *polaron*.

The polaron is not an easy particle to find experimentally. The theoretical attention it has received might therefore seem difficult to understand. One explanation is that the interaction between electrons and phonons needed to attack the polaron problem is also the basic interaction lying behind superconductivity of metals and alloys. Superconductivity brings new layers of complexity to the problem, so there is value in studying the simpler case of the polaron first.

Relation between Polarization and Displacement. Because the interaction between electrons and phonons excites longitudinal modes, it is useful to begin by finding a relation between the polarization \vec{P} and ionic displacement \vec{u} for the longitudinal mode. Start with

$$\vec{P} = n[e^*\vec{u} + \alpha^\infty \vec{E}_{\text{cell}}]. \quad \text{From Eq. (22.19).} \quad (22.31)$$

Then

$$\vec{E} = -4\pi\vec{P}, \quad \text{Because } \epsilon = 0 \Rightarrow \vec{D} = 0. \quad (22.32)$$

which holds for the longitudinal mode implies in conjunction with Eq. (22.10) that

$$\vec{E}_{\text{cell}} = \frac{2}{3}\vec{E} = -\frac{8\pi}{3}\vec{P} \quad (22.33)$$

$$\Rightarrow \vec{P} = \frac{ne^*}{1 + n\alpha^\infty 8\pi/3} \vec{u}. \quad \text{Put Eq. (22.33) in Eq. (22.31).} \quad (22.34)$$

The expressions (22.22) and (22.24) for e^* and α^∞ give

$$\frac{ne^*}{1 + n\alpha^\infty 8\pi/3} = n \sqrt{\frac{9M\bar{\omega}^2}{4\pi n} \frac{\epsilon^0 - \epsilon^\infty}{(\epsilon^0 + 2)(\epsilon^\infty + 2)}} \quad (22.35)$$

$$= \sqrt{\frac{M\omega_L^2 n}{4\pi} \left(\frac{1}{\epsilon^\infty} - \frac{1}{\epsilon^0} \right)}. \quad (22.36)$$

Therefore

$$\vec{P} = \beta\vec{u}, \quad (22.37)$$

Table 22.2. Dielectric properties of ionic crystals

Compound	ϵ^∞	ϵ^0	$\frac{\omega_T}{2\pi c}$ (cm^{-1})	$\frac{\omega_L}{2\pi c}$ (cm^{-1})	$\frac{m^*}{m}$	α_p	$\frac{m^*}{m}(1 + \frac{\alpha_p}{6})$	$\frac{m_{\text{pol}}^*}{m}$
LiF	1.93	8.50	318	667				
LiCl	2.79	10.83	221	435				
LiBr	3.22	11.95	187	360				
LiH	3.60	12.90	590	1116				
NaF	1.75	4.73	262	431				
NaCl	2.35	5.43	178	271				
NaBr	2.64	5.78	146	216				
NaI	3.08	6.60	124	182				
KF	1.86	5.11	202	334				
KCl	2.20	4.49	142	216	0.434	3.45	0.683	0.920
KBr	2.39	4.52	114	169	0.390	3.14	0.594	0.700
KI	2.68	4.68	102	144	0.325	2.51	0.461	0.540
RbF	1.94	5.99	163	286				
RbCl	2.20	4.58	117	180	0.432	3.84	0.708	1.030
RbBr	2.36	4.51	95	131				
RbI	2.61	4.55	76	108	0.368	3.16	0.562	0.720
CsF	2.17	7.27	134	245				
CsCl	2.67	6.68	107	168				
CsBr	2.83	6.38	78	118				
CsI	3.09	6.32	66	94	0.420	3.67	0.677	0.960
GaAs	10.90	12.83	273	296	0.066	0.07	0.067	0.066
GaSb	14.40	15.69	231	240	0.047	0.03	0.047	0.047
GaP	8.46	10.28	365	403	0.338	0.20	0.349	0.350
InAs	11.80	14.61	219	243	0.023	0.05	0.023	0.023
InSb	15.68	17.88	185	197	0.014	0.02	0.014	0.013
CdS	5.27	8.42	244	308	0.155	0.53	0.169	0.170
CdSe	6.10	9.30	174	214	0.130	0.46	0.140	0.140
CdTe	7.21	10.23	141	168	0.091	0.32	0.096	0.096
ZnS	5.14	8	282	352	0.280	0.65	0.310	0.313
ZnSe	5.90	8.33	207	246	0.171	0.43	0.183	0.184
ZnTe	7.28	9.86	177	205	0.160	0.33	0.169	0.169
ZnO	4	8.15	414	591	0.240	0.85	0.274	0.279
PbS	18.50	190	67	214	0.082	0.32	0.086	0.087
PbSe	25.20	280	44	147	0.047	0.21	0.049	0.049
PbTe	36.90	450	32	110	0.034	0.15	0.035	0.035
AlSb	9.88	11	323	344	0.011	0.011	0.02	0.011
InP	9.56	12.29	308	350	0.077	0.076	0.11	0.077
SnTe	45	177	22	140				
CdF ₂	2.40	7.78	224	403	0.900	0.450	3.19	0.690
SiC	6.65	10	793	972	0.240	0.230	0.26	0.240

The experiments were performed on single crystals at liquid helium temperatures. To check polaron theory, compare m_{pol}^*/m with $m^*/m(1 + \alpha_p/6)$. The approximation is excellent for $\alpha_p \ll 1$. Source: Kartheuser (1972).

with

$$\beta = \sqrt{\frac{M\omega_L^2 n}{4\pi} \left(\frac{1}{\epsilon^\infty} - \frac{1}{\epsilon^0} \right)}. \quad (22.38)$$

Interaction between Electron and Polarization. When an electron interacts with a polarized medium, the energy of interaction is

$$\hat{U}_{\text{el-phonon}} = e \int d\vec{r}' \vec{P}(\vec{r}') \cdot \nabla_{\vec{r}'} \frac{1}{|\hat{R} - \vec{r}'|}. \quad \hat{R} \text{ is the position operator for the electron.} \quad (22.39)$$

Making use of Eq. (13.43a), which expresses \hat{u} in terms of creation and annihilation operators, and Eq. (22.37), which gives the polarization in terms of the lattice displacements \hat{u} , leads to

$$\hat{U}_{\text{el-phonon}} = e\beta \int d\vec{r}' \sqrt{\frac{\hbar}{2M\omega_L N}} \sum_{\vec{k}} \frac{\vec{k}}{k} \cdot \left[\nabla_{\vec{r}'} \frac{1}{|\vec{r}' - \hat{R}|} \right] [e^{i\vec{k}\cdot\vec{r}'} \hat{a}_{\vec{k}} + e^{-i\vec{k}\cdot\vec{r}'} \hat{a}_{\vec{k}}^\dagger] \quad (22.40)$$

$$= -e\beta \int d\vec{r}' \sqrt{\frac{\hbar}{2M\omega_L N}} \sum_{\vec{k}} \frac{i\vec{k}\cdot\vec{k}}{k} \frac{1}{|\vec{r}' - \hat{R}|} [e^{i\vec{k}\cdot\vec{r}'} \hat{a}_{\vec{k}} - e^{-i\vec{k}\cdot\vec{r}'} \hat{a}_{\vec{k}}^\dagger]. \quad (22.41)$$

In Eq. (22.40), only the longitudinal mode, where the polarization equals \vec{k}/k , was retained. The reason is that this mode is the only one to survive the dot product with \vec{k} that emerges in Eq. (22.41). Electrons moving through a charged medium naturally push at material in front of them, creating compression waves, and are less likely to induce the side to side wiggling of transverse waves. Finally carrying out the integral over \vec{r}' the electron-phonon interaction becomes

$$\hat{U}_{\text{el-phonon}} = e\beta 4\pi i \sum_{\vec{k}} \sqrt{\frac{\hbar}{2M\omega_L N}} \frac{1}{k} [e^{-i\vec{k}\cdot\hat{R}} \hat{a}_{\vec{k}}^\dagger - e^{i\vec{k}\cdot\hat{R}} \hat{a}_{\vec{k}}]. \quad (22.42)$$

To characterize the strength of the electron-phonon interaction, define a dimensionless parameter comparing the typical energy of phonons, $\hbar\omega_L$, to a characteristic electrostatic energy. Forming a distance from $\sqrt{\hbar/2m^*\omega_L}$, where m^* is the electron effective mass gives a dimensionless ratio α_p of electron energy to phonon energy defined by Fröhlich (1952):

$$\alpha_p \equiv \frac{e^2}{2} \sqrt{\frac{2m^*\omega_L}{\hbar}} \frac{1}{\hbar\omega_L} \left(\frac{1}{\epsilon^\infty} - \frac{1}{\epsilon^0} \right) = 1.44 \cdot 10^8 \left(\frac{1}{\epsilon^\infty} - \frac{1}{\epsilon^0} \right) \sqrt{\frac{m^*/m}{\omega_L \cdot s}}. \quad (22.43)$$

Finally, the ion mass M cancels between Eqs. (22.42) and (22.38), so

$$\hat{U}_{\text{el-phonon}} = i\sqrt{4\pi\alpha_p} \frac{1}{\sqrt{V}} \left(\frac{\hbar^5 \omega_L^3}{2m^*} \right)^{1/4} \sum_{\vec{k}} \frac{1}{k} [e^{-i\vec{k}\cdot\hat{R}} \hat{a}_{\vec{k}}^\dagger - e^{i\vec{k}\cdot\hat{R}} \hat{a}_{\vec{k}}]. \quad (22.44)$$

The second quantized form of (22.44) will be useful. It is obtained through the identity (C.7),

$$\hat{U}_{\text{el-phon}} = \sum_{\vec{q}\vec{q}'} \hat{c}_{\vec{q}'}^\dagger \langle \vec{q}' | \hat{U}_{\text{el-phon}} | \vec{q} \rangle \hat{c}_{\vec{q}} \quad \text{The } c\text{'s are creation and annihilation operators for electrons in plane wave states.} \quad (22.45)$$

and is

$$\hat{U}_{\text{el-phon}} = i\sqrt{4\pi\alpha_p} \frac{1}{\sqrt{\mathcal{V}}} \left(\frac{\hbar^5 \omega_L^3}{2m^*} \right)^{1/4} \sum_{\vec{q}''\vec{k}} \frac{1}{k} [\hat{c}_{\vec{q}''-\vec{k}}^\dagger \hat{c}_{\vec{q}''} \hat{a}_{\vec{k}}^\dagger - \hat{c}_{\vec{q}''+\vec{k}}^\dagger \hat{c}_{\vec{q}''} \hat{a}_{\vec{k}}]. \quad (22.46)$$

Polaron Dispersion Relation. The operator for electron–phonon interactions can be used to search for the change in effective mass of an electron moving through an ionic crystal. If the coupling parameter α_p is small, then this task may be accomplished by finding the change in energy of an electron to leading order in perturbation theory. To make things simple, assume that in the absence of polarization effects, the electron would travel as a plane wave with energy $\hbar^2 q^2/2m^*$. The effective mass here results from interactions of the electrons with the static lattice, as in Section 16.2.3, and must be distinguished from the additional effective mass the electron will acquire when it drags around a cloud of phonons.

At first order in perturbation theory, the expectation value of (22.46) vanishes, so to obtain a nonzero result one must move to the second-order term, which is

$$\Delta\mathcal{E}^{(2)} = \sum_{\Phi'\vec{q}'} \frac{|\langle \vec{q} | \langle \Phi_0 | \hat{U}_{\text{el-phon}} | \Phi' \rangle | \vec{q}' \rangle|^2}{\mathcal{E}(\vec{q}, \Phi_0) - \mathcal{E}(\vec{q}', \Phi')}. \quad \text{\(\Phi_0\) refers to the ground state of the phonons, and \(\Phi'\) is a state with longitudinal optical phonons present; \(\vec{q}\) and \(\vec{q}'\) are electron wave numbers.} \quad (22.47)$$

Placing Eq. (22.46) into Eq. (22.47), the only intermediate phonon state Φ' that survives is the one with precisely one phonon of wave number $\vec{k} = \vec{q} - \vec{q}'$ and energy $\hbar\omega_L$. All possible electron momenta \vec{q}' are allowed, but states \vec{q} and \vec{q}' must have the same spin, so when the sum over \vec{q} is converted into an integral, the density of states is $\mathcal{V}/(2\pi)^3$, not $2\mathcal{V}/(2\pi)^3$. One has

$$\Delta\mathcal{E}^{(2)} = 4\pi\alpha_p \frac{1}{\mathcal{V}} \sqrt{\frac{\hbar^5 \omega_L^3}{2m^*}} \sum_{\vec{q}'} \frac{1}{|\vec{q} - \vec{q}'|^2} \left[\frac{1}{\frac{\hbar^2 q^2}{2m^*} - \left(\frac{\hbar^2 q'^2}{2m^*} + \hbar\omega_L \right)} \right] \quad (22.48)$$

$$= 4\pi\alpha_p \frac{1}{\mathcal{V}} \sqrt{\frac{\hbar^5 \omega_L^3}{2m^*}} \int d\vec{q}' \frac{d(\cos\theta)}{(2\pi)^3} \frac{2\pi\mathcal{V}}{\frac{\hbar^2 q^2}{2m^*} - \left(\frac{\hbar^2 |\vec{q}' + \vec{q}|^2}{2m^*} + \hbar\omega_L \right)} \quad (22.49)$$

$$= \frac{\alpha_p}{\pi} \sqrt{\frac{\hbar^5 \omega_L^3}{2m^*}} \int_{-1}^1 ds \int_0^\infty dq' \frac{1}{\frac{\hbar^2 q^2}{2m^*} - \left(\frac{\hbar^2 (q'^2 + q^2 + 2qq's)}{2m^*} + \hbar\omega_L \right)} \quad (22.50)$$

$$= -\alpha_p \sqrt{m^* \hbar \omega_L^3} \frac{\sqrt{2}}{q} \sin^{-1} \sqrt{\frac{\hbar^2 q^2}{2m^* \hbar \omega_L}}. \quad (22.51)$$

Perform first the q' integral, and then s . q' can safely be integrated to infinity because the integral is convergent. One of the terms following the q' integral looks hopeless, but it is odd in s and vanishes by symmetry.

The interaction of the electron with the phonons lowers the energy of the interacting system. For low momenta $\hbar\vec{q}$, the change in energy is $-\alpha_p\hbar\omega_L$. As the electron energy rises toward the phonon energy, the energy gain increases. For small q one finds that

$$\Delta\mathcal{E}^{(2)} = -\alpha_p\hbar\omega_L - \alpha_p\frac{\hbar^2q^2}{12m^*}. \quad (22.52)$$

Even in the absence of interaction with polarized ions, the electron already has an effective mass m^* due to interaction with the periodic crystal potential. Interaction with the polarization cloud raises the effective mass to a new value, m_{pol}^* .

When one adds Eq. (22.52) on to the original kinetic energy of the electron, $\hbar^2q^2/2m^*$, to lowest order in α_p the effective mass of the electron is changed by the interaction with the phonons and equals

$$\frac{m_{\text{pol}}^*}{m^*} = 1 + \frac{\alpha_p}{6}. \quad (22.53)$$

This result is sensible, because the electron has to drag phonons around with it as it moves, and therefore becomes heavier. The stronger the coupling with the phonons, the heavier it becomes.

When the electron kinetic energy is larger than $\hbar\omega_L$, then rather than simply being surrounded by a cloud of phonons, the electron emits them in a shower. According to Eq. (22.51), the change in electron energy becomes imaginary and is

$$\Delta\mathcal{E}^{(2)} = -\alpha_p\sqrt{m^*\hbar\omega_L^3}\frac{\sqrt{2}}{q}\left[\pi/2 + i\cosh^{-1}\sqrt{\frac{\hbar^2q^2}{2m^*\hbar\omega_L}}\right]. \quad (22.54)$$

The meaning of an imaginary energy is that the probability of finding the electron in state q decays exponentially in time. The electron wave function behaves in time as

$$\exp\left[-\frac{i}{\hbar}(\mathcal{E}^{(0)} + \Delta\mathcal{E}^{(2)})t\right], \quad (22.55)$$

so that the probability of finding the electron in its initial state decays as

$$\exp\left[\frac{2}{\hbar}\text{Im}(\Delta\mathcal{E}^{(2)})t\right]. \quad (22.56)$$

The decay rate is

$$2\alpha_p\sqrt{m^*\hbar\omega_L^3}\frac{\sqrt{2}}{\hbar q}\cosh^{-1}\sqrt{\frac{\hbar^2q^2}{2m^*\hbar\omega_L}}. \quad (22.57)$$

The same computation can be carried out using time-dependent perturbation theory (Problem 3), and it gives the same answer, because time-dependent and stationary perturbation theory are really just different views of the same calculation.

22.3.3 Experimental Observations of Polarons

Polaron theory has been checked rather carefully, although the experiments are difficult and not exceptionally accurate. A serious check requires independent measurement of all the parameters in Eq. (22.43). One of the parameters in Eq. (22.43) is the electron effective mass m^* in the absence of polaron effects, so experimental techniques must be devised that can turn off polaron physics to find m^* , then turn it back on to measure m_{pol}^* and compare with (22.53).

Information on how this task may be accomplished is contained in Eq. (22.57). When the electron kinetic energy is larger than $\hbar\omega_L$, its effective mass is no longer altered by polaron physics, and furthermore its interaction with polar ions decreases as q becomes larger. Equivalently, if the electrons are excited by an experimental probe at frequencies well above ω_L , the electrons will display an effective mass m^* , while at frequencies below ω_L they display an effective mass m_{pol}^* . *Faraday rotation*, discussed in Problem 2, is a probe of electron effective masses at infrared frequencies, around 10^{14} Hz, while cyclotron resonance, discussed in Section 21.2, operates in the microwave regime at around 10^{10} Hz, so the two effective masses can be measured independently.

An additional experimental problem lies in the fact that it is difficult to coerce an electron into the conduction band of an insulator. In some cases, such as ZnO, the problem can be solved by doping with suitable impurities. In other cases, the solution is to blast the crystal with light of such a frequency as to excite electrons from valence to conduction band. Cyclotron resonance can be performed in either case, but Faraday rotation measurements have been restricted to the doped crystals, so the number of cases where a complete check of the polaron theory is available is limited. However, as can be seen from the final columns of Table 22.2, agreement between theory and experiment is quite good. Where the coupling constant α_p is larger than one, lowest-order perturbation becomes questionable, and in fact the measured polaron effective mass is roughly double the prediction of Eq. (22.53), but for those compounds where $\alpha_p < 1$ the agreement is excellent. Feynman (1972) discusses on pp. 234–241 how to improve the theory so as to handle larger values of α_p . The strong-coupling limit, $\alpha_p \rightarrow \infty$, has also been reviewed by Peeters and Devreese (1984).

A related area of study considers charged localized excitations in polymers such as polyacetylene, and it has been reviewed by Heeger et al. (1988).

22.4 Point Defects and Color Centers

The coloration of ionic crystals provided a subject of intense interest for decades. The transverse and longitudinal frequencies listed in Table 22.2 all lie below the frequency of visible light. Figure 22.5 shows that visible light should pass almost unchanged through the ionic crystals. Yet they frequently have distinct colors. For example, sodium chloride can have either a bluish or a yellowish tint. The blue tint is naturally present in salt, and it is due to the presence of small aggregates of excess sodium. Röntgen (1921) showed that the yellow color could be produced either

by heating a salt crystal in sodium vapor or by irradiation by X-rays, and he also showed that the photoelectric effect was greatly enhanced by radiation. The yellow coloration had earlier been ascribed to the precipitation of small metal particles within the crystal, but Röntgen showed that it was most intense in cases where no traces of precipitates were to be found. The defect responsible for discoloration was too small to detect with any microscope.

The center of research into these phenomena in the 1920s and 1930s was in Göttingen, directed by R. W. Pohl. The nature of the localized *color centers* responsible for optical absorption and emission peaks was slowly teased out of a variety of experiments, involving irradiation, electrical conductivity, and mechanical stresses. Mollwo (1933), for example, showed that the density of a crystal decreased in direct proportion to the strength of its absorption peak. A decrease in density can be explained by observing that each metal ion entering the crystal wants to divest itself of an outer electron and deliver it to a corresponding halogen ion. In the absence of the halogen, it is thermodynamically favorable for an empty site to diffuse into the crystal and absorb the extra electron. Mott and Gurney (1940) made the connection between the theoretical idea of the vacancy and the color centers observed by Pohl.

The significance of research into color centers goes beyond explaining the yellow tint of salt. Understanding the role of defects in determining optical properties of ionic crystals provided the background for explaining the physics of photography and the physics behind photocopying. The same body of knowledge also played an important role in finding materials suitable for creating the laser. The alkali halide crystals themselves have few practical applications as optical materials, but they provided the testing ground where optical effects of defects could be explained in detail.

22.4.1 Vacancies

The simplest defect in a crystal is a *vacancy*, which is simply a lattice site from which an atom is missing. The energy cost of introducing a vacancy into a crystal is related to the cohesive energy. As shown in Table 22.3, these two energies are of the same order of magnitude, but never identical. The reason for the difference is that atoms in the vicinity of a vacancy relax, lowering the energy below what it would be after the atom had instantaneously been plucked out of the solid. Because the energy cost of a vacancy is finite, every equilibrium crystal contains a finite density, given by Eq. (5.21), that increases exponentially with temperature. In the ionic crystals, the density of vacancies can be increased enormously by introduction of alkali metals, rising to as high as one part in a thousand. Visible coloration is produced by vacancy densities on the order of one part in ten thousand.

Frenkel and Schottky Pairs. In ionic solids there are common defects more elaborate than a vacancy. Because the ions carry charges, defects must form in such a way as to maintain charge neutrality. An ion that abandons a site (leaving a vacancy) and climbs into an interstitial location is called a *Frenkel pair*. The

Table 22.3. Cohesive energy versus vacancy energy for selected elements

Crystal	Cohesive Energy \mathcal{E}/N (eV)	Vacancy Energy (eV)
Na	1.16	0.42
Au	3.8	0.97
Al	3.4	0.76
Pt	5.3	1.4
Ne	0.021	0.020
Kr	0.11	0.077
Ge	3.9	2.0

Source: Flynn (1972), p. 7.

vacancy and interstitial are bound together because of the Coulomb attraction between them, and they occupy neighboring sites. A *Schottky pair*, by contrast, occurs when nearby vacancies develop, one where a cation should be, and the other where an anion should be.

22.4.2 F Centers

The vacancy is thermodynamically the most likely defect, and it therefore leads to the dominant type of optical absorption in the alkali halides, called the *F center* (after Farbe, “color” in German). A vacancy binds an electron, as shown in Figure 22.6, with the electron density largest at the center of the vacancy and diminishing rapidly far away. Optical absorption results from driving the trapped electron to a localized excited state lying approximately 2 eV above the ground state. The peaks of the absorption and emission bands at low temperature are tabulated in Table 22.4. A striking feature of these bands is the large difference between the

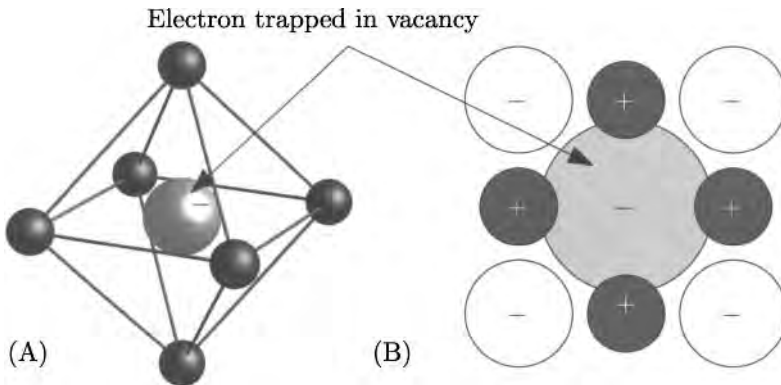


Figure 22.6. The F center is a halogen ion vacancy that has trapped an electron. (A) A three-dimensional view of ions around the vacancy. (B) Diagram showing the density of the trapped electron in a two-dimensional section passing through the vacancy.

Table 22.4. Absorption and emission peaks from F centers in alkali halide crystals at low temperatures

Compound	\mathcal{E}_{abs} (eV)	\mathcal{E}_{em} (eV)	Compound	\mathcal{E}_{abs} (eV)	\mathcal{E}_{em} (eV)
NaF	3.72	1.67	RbCl	2.05	1.09
NaCl	2.77	0.98	RbBr	1.86	0.87
KF	2.85	1.66	RbI	1.71	0.81
KCl	2.31	1.22	CsF	1.89	1.42
KBr	2.06	0.92	CsCl	2.17	1.26
KI	1.87	0.83	CsBr	1.96	0.91
RbF	2.43	1.33	CsI	1.68	0.74

Notice that the energy of absorption \mathcal{E}_{abs} and emission \mathcal{E}_{em} are substantially different. Source: Pick (1972), p. 659, and Fowler (1968), p. 627.

frequencies of absorption and emission, called the *Stokes shift*. The phenomenon is called the Franck–Condon effect, and will be discussed in the next section.

22.4.3 Electron Spin Resonance and Electron Nuclear Double Resonance

The final controversies over the structure of color centers were laid to rest by spin resonance experiments. In *electron spin resonance* (ESR), a static magnetic field \vec{H}_0 is applied to the sample, producing an induction $B_0 = H_0$. The two spin levels of the trapped electron are split in energy by an amount $2\mu_B B_0$, where μ_B is the Bohr magneton. This energy splitting can be measured by applying an additional oscillating magnetic field at frequencies ω of order 10^{10} Hz and then detecting resonant absorption whenever $\hbar\omega = 2\mu_B B_0$. The technique gives information about

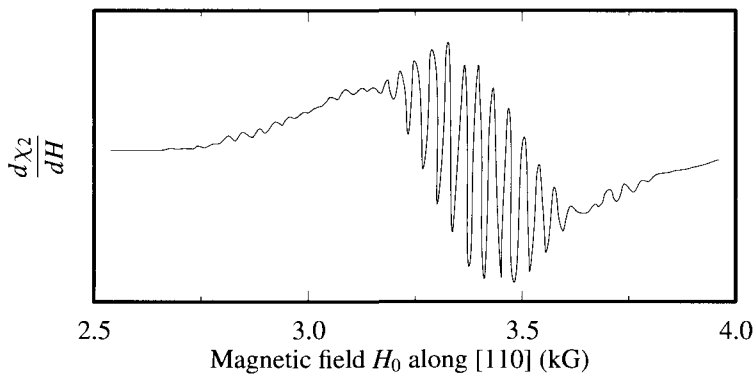


Figure 22.7. Electron spin resonance in RbCl F centers at a temperature of 90 K. The oscillating magnetic field is applied at a fixed frequency of $\nu = 9.38 \cdot 10^9$ Hz, while the static magnetic field is increased from 2.5 to 4 kG. The imaginary part χ_2 of the magnetic susceptibility is proportional to absorption, and the change of this quantity with applied field H_0 is plotted on the y axis. The width of the peaks is approximately 36 G. [Source: Pick (1972), p. 666.]

color centers because the absorption resonance can be split into multiple peaks by the hyperfine interaction of the trapped electron with the nuclei of the surrounding ions. A simple way to model this interaction is to observe that the static magnetic field experienced by a trapped electron is the sum of two pieces,

$$\vec{B} = \vec{B}_0 + \sum_l \vec{B}_l, \quad (22.58)$$

where \vec{B}_l is the magnetic field due to the nuclei of the nearby ions. In the case of RbCl, the positive ions are ^{85}Rb , which has magnetic moment $1.35 \mu_N$ ($\mu_N = e\hbar/2m_n c$ is the nuclear magneton) and nuclear spin $I = 5/2$. Nuclear spins do not equilibrate quickly with the applied field \vec{B}_0 , so nuclei of the six near neighbors of a trapped electron can be in any of their quantum eigenstates, and the total spin with which the electron interacts ranges from $-15\hbar$ to $15\hbar$. Thus the hyperfine interaction with near neighbors should split the electron spin resonance into 31 levels: The most likely level corresponds to total nuclear spin 0, and other levels appear with diminishing probability. Measurements are not in precise accord with the prediction, as shown in Figure 22.7, because next-nearest and other neighbors cannot be neglected, and the resonance lines are accordingly broadened. The measurements are made more precise by proceeding to *electron nuclear double resonance* (ENDOR), invented by Feher (1959), where at the same time the electron oscillates between spin levels a second oscillating field in the range of 1 MHz is applied to search for resonant oscillations of the surrounding nuclei. As discussed by Seidel and Wolf (1968), this technique measures the trapped electron probability density at distances up to eight nearest neighbors from the vacancy. The density distribution of a trapped electron measured in this way is shown in Figure 22.8.

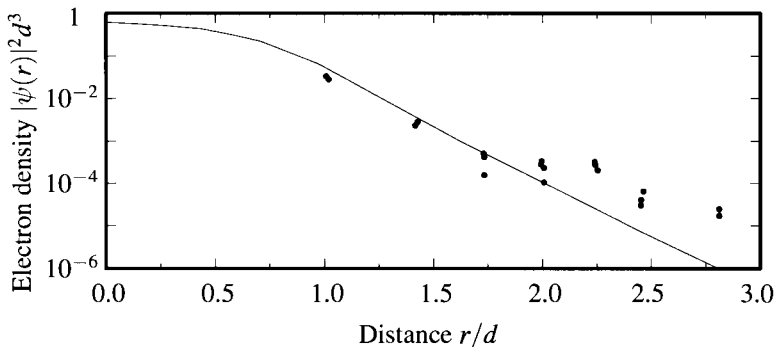


Figure 22.8. Compilation of electron density versus distance from vacancy center, measured in KF, NaCl, KBr, and KI using electron nuclear double resonance. The solid line is a theoretical curve, assuming the electron wave function is hydrogen-like, decaying exponentially on scale $0.4a_0$. Distance is measured in units of nearest-neighbor spacing d . [Source: Seidel and Wolf (1968), p. 566.]

22.4.4 Other Centers

Exposing ionic crystals to alkali vapor produces almost nothing but F centers. Bombarding the crystals with X-rays produces F centers as well, but also a host of other color centers. A variety of composite color centers can also be produced by irradiating a crystal full of F centers with light. It is energetically favorable for F centers to cluster near to one another, so when their density becomes high enough, they form bound pairs and triplets, much like atoms combining into molecules.

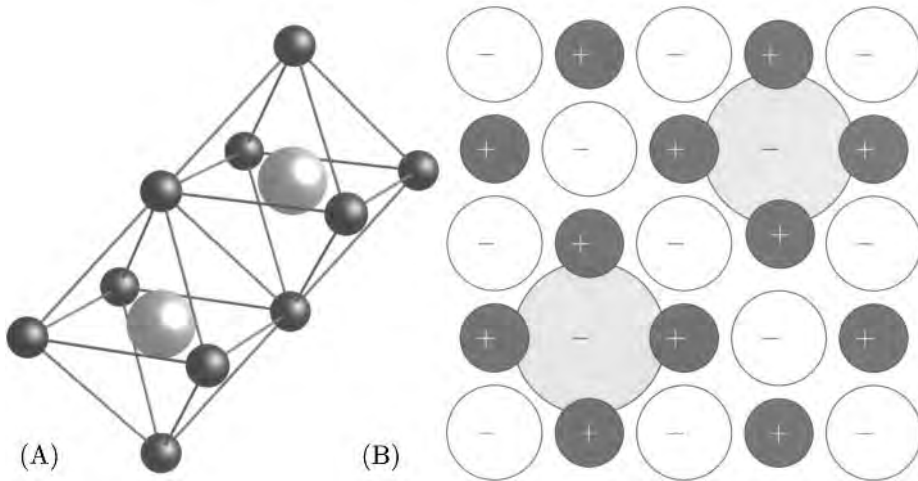


Figure 22.9. The F_2 or M center consists of two adjacent F centers, bound together like a hydrogen molecule. (A) A three-dimensional view. (B) A projection onto the x - y plane.

The F_2 or M center (Figure 22.9) consists of two neighboring anion vacancies that bind two electrons, and behave a bit like a helium atom, while the F_3 or R center [Figure 22.10(A)] is constituted by three neighboring anion vacancies binding an electron. If an anion is stripped of an electron, by irradiation at low temperatures, the result is a V_K center, [Figure 22.10(B)] which can be thought of as a hole bound to two negative ions in an otherwise perfect lattice. The perfect antimorph of the F center, a hole bound to a single alkali ion vacancy, does not exist. Holes are well-defined particles on length scales that are large compared to the lattice spacing, but concepts such as effective mass from which holes derive are not clearly applicable on scales as small as a single vacancy.

22.4.5 Franck–Condon Effect

One of the surprising features of F centers, as shown in Figure 22.11, is that absorption and emission of light occurs at different frequencies and is highly temperature-dependent. This phenomenon is the *Franck–Condon effect*. The basic physical reason is that ions near a trapped electron relax so as to optimize their interaction with it, but the way they relax for the ground energy state is different from the way they relax for each excited state. During an optical transition, the ions do not have time to move; the transition frequency should be calculated in a frozen lattice. If

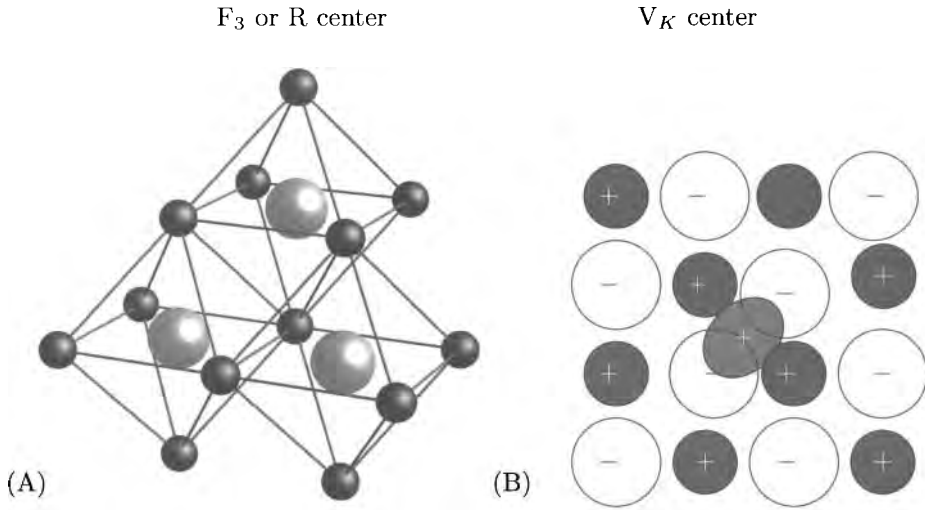


Figure 22.10. (A) shows a three-dimensional view of the F₃ center, where three F centers have grouped together. (B) shows a cross-sectional view of the V_K center, which is produced by ejecting an electron from a metal ion.

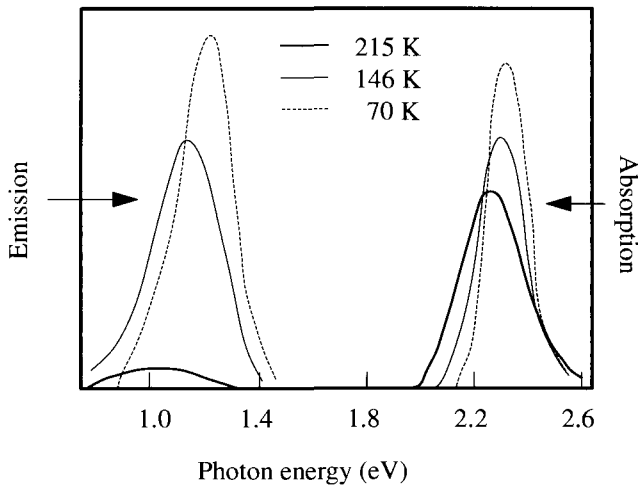


Figure 22.11. The absorption and emission lines of an F center in KCl are peaked about different energies and are strong functions of temperature. [Source: Lüty (1961), p. 247.]

the excited state is long-lived, however, the ions have time to adjust, the excess energy is dissipated in phonons, and by the time the trapped electron returns to its ground state, the transition frequency is diminished. Therefore, the difference in photon energies between absorption and emission of F centers directly measures the relaxation energy of nearby ions as an F center electron jumps to an excited state.

Computation of Transition Probabilities for the Franck–Condon Effect. A simple model allows one to explore the phenomena occurring in the Franck–Condon

effect. The idea of the model is first to treat the F center and ion neighbors separately, then couple them, and finally to include interactions with incoming photons.

The starting point is a Hamiltonian $\hat{\mathcal{H}}_F$ describing the electronic levels of an F center. All one needs to know about this Hamiltonian is that the ground-state energy is $\mathcal{E}_0 = 0$, and it has an excited state $|F_1\rangle$ of energy \mathcal{E}_1 , so

$$\hat{\mathcal{H}}_F|F_0\rangle = \mathcal{E}_0|F_0\rangle = 0 \quad (22.59a)$$

$$\hat{\mathcal{H}}_F|F_1\rangle = \mathcal{E}_1|F_1\rangle. \quad (22.59b)$$

To model the process of interaction with ions, it is sufficient to fix upon a single ion coordinate \hat{x} , called a *configuration coordinate*, governed by the harmonic oscillator Hamiltonian

$$\hat{\mathcal{H}}_{\text{ion}} = \frac{\hat{P}^2}{2M} + \frac{M\omega_1^2}{2}\hat{x}^2. \quad (22.60)$$

The idea behind the Franck–Condon effect is that the energy of the F center is coupled to the position of the ion. This effect may be captured simply through the interaction Hamiltonian

$$\hat{\mathcal{H}}_{\text{int}} = g\hat{x}\hat{\mathcal{H}}_F, \quad g \text{ is a coupling constant.} \quad (22.61)$$

so that the eigenvalue equation to solve is

$$\left\{ \hat{\mathcal{H}}_F(1 + g\hat{x}) + \hat{\mathcal{H}}_{\text{ion}} \right\} |\psi\rangle = \mathcal{E}_{\text{tot}}|\psi\rangle. \quad (22.62)$$

It is fairly simple to find the eigenvalues of (22.62) exactly in terms of the eigenvalues of $\hat{\mathcal{H}}_F$. Let

$$\phi_l(x) \equiv \langle x, \mathcal{E}_l | \psi \rangle. \quad (22.63)$$

Acting from the left with $\langle x, \mathcal{E}_l |$ on Eq. (22.62) gives

$$\left\{ \mathcal{E}_l(1 + gx) + \frac{-\hbar^2\nabla^2}{2M} + \frac{M\omega_1^2}{2}x^2 \right\} \phi_l(x) = \mathcal{E}_{\text{tot}}\phi_l(x). \quad \text{The index } l \text{ equals 0 or 1.} \quad (22.64)$$

Equation (22.64) describes a harmonic oscillator whose x coordinate has been shifted by

$$\mathcal{D}_l = \frac{\mathcal{E}_l g}{M\omega_1^2}. \quad (22.65)$$

It can be rewritten as

$$\left\{ \mathcal{E}_l + \frac{-\hbar^2\nabla^2}{2M} + \frac{M\omega_1^2}{2} \left[(x + \mathcal{D}_l)^2 - \mathcal{D}_l^2 \right] \right\} \phi_l(x) = \mathcal{E}_{\text{tot}}\phi_l(x). \quad (22.66)$$

The solutions of Eq. (22.66) are just the harmonic oscillator eigenfunctions ϕ_l , but evaluated at the argument $x + \mathcal{D}_l$ rather than at x , and the eigenenergies of (22.66) are

$$\mathcal{E}_{l,n} = \mathcal{E}_l + \hbar\omega_1(n + \frac{1}{2}) - \frac{1}{2}\mathcal{D}_l^2 M\omega_1^2. \quad (22.67)$$

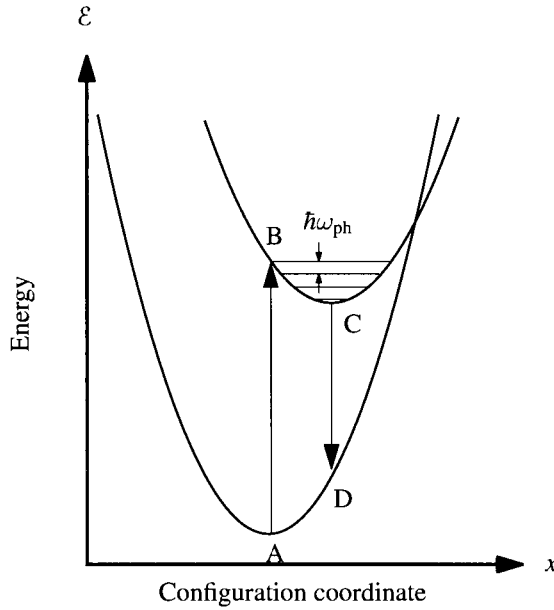


Figure 22.12. In the Franck–Condon effect, frequencies of absorption and emission of an impurity are different. The difference is called the Stokes shift. The reason for the difference is that once the trapped electron has absorbed a photon and moved to an excited state, the ions around it slowly adjust, lowering the energy of the state.

Now consider the influence of incoming radiation of frequency ω upon this system. According to Eq. (20.70), the real part of the conductivity and hence the optical absorption is proportional to

$$\sum_{\text{final}} \delta(\mathcal{E}_{\text{tot,final}} - \mathcal{E}_{\text{tot,0}} - \hbar\omega) |\langle \psi_0 | \hat{U}_{\text{int}} | \psi_{\text{final}} \rangle|^2, \quad (22.68)$$

where \hat{U}_{int} is the interaction Hamiltonian of the F center with the photons. To make matters simple, take \hat{U}_{int} to act only on the F center electron, and not to affect the ion coordinate x . In this case, the transition rate from the ground state to a state where the F center has energy \mathcal{E}_1 and the ion is in state n , absorbing a photon of energy

$$\hbar\omega = \mathcal{E}_1 + n\hbar\omega_1 - \frac{1}{2}\mathcal{D}_1^2 M\omega_1^2, \quad (22.69)$$

is proportional to

$$\left| \int dx \phi_0(x) \phi_n(x + \mathcal{D}_1) \right|^2. \quad (22.70)$$

In the final state, the F center is in state 1, which means that the oscillator wave functions must be evaluated with argument $x + \mathcal{D}_1$.

There are two interesting limits in which to evaluate Eq. (22.70). The first is that in which \mathcal{D}_1 is small compared to the natural spatial extent of the harmonic

oscillator wavefunction,

$$x_0 = \sqrt{\frac{\hbar}{M\omega_i}} \gg \mathcal{D}_1 \quad \text{See Schiff (1968), p. 67.} \quad (22.71)$$

$$\Rightarrow 1 \gg \frac{\mathcal{E}_1 g}{\sqrt{\hbar M \omega_i^3}}. \quad (22.72)$$

This limit corresponds to weak coupling of the ion to the center, or high ω_i , which means that the ion can respond rapidly to the photon. The functions in Eq. (22.70) overlap best when $n = 0$, which means that the dominant transition is one that goes straight from the ground state at A to the lowest excited state C in Figure 22.12. The opposite limit is

$$\mathcal{D}_1 \gg x_0, \quad (22.73)$$

which corresponds to weak coupling or to slowly responding ions. Now the maximum overlap in Eq. (22.70) occurs for a large value of n . The integral appearing there can be evaluated exactly, and defining $\chi = x/x_0$ gives

$$\int dx \phi_0(x) \phi_n(x + \mathcal{D}_1) \quad (22.74)$$

$$= \int d\chi \sqrt{\frac{1}{\pi 2^n n!}} e^{\chi \mathcal{D}_1/x_0 - (\mathcal{D}_1/x_0)^2/2} (-1)^n \frac{d^n}{d\chi^n} e^{-\chi^2} \quad \begin{array}{l} \text{Use the standard} \\ \text{expressions for harmonic} \\ \text{oscillator wave} \\ \text{functions—for example,} \\ \text{Schiff (1968) p. 71, or} \\ \text{Landau and Lifshitz} \\ \text{(1977), p. 70.} \end{array} \quad (22.75)$$

$$= \int d\chi \sqrt{\frac{1}{\pi 2^n n!}} \left(\frac{\mathcal{D}_1}{x_0}\right)^n e^{\chi \mathcal{D}_1/x_0 - (\mathcal{D}_1/x_0)^2/2} e^{-\chi^2} \quad \text{Integrating by parts } n \text{ times.} \quad (22.76)$$

$$= \sqrt{\frac{1}{2^n n!}} \left(\frac{\mathcal{D}_1}{x_0}\right)^n e^{-(\mathcal{D}_1/x_0)^2/4}. \quad (22.77)$$

As a function of n , (22.77) is largest when

$$n = \frac{1}{2} (\mathcal{D}_1/x_0)^2. \quad (22.78)$$

Just as drawn in the path from A to B in Figure 22.12, the most likely final energy of the system is a quadratic function of the displacement coordinate \mathcal{D}_1 . If the excited state is long-lived, the ion will slowly relax down to C, and emission will take place from C to D.

22.4.6 Urbach Tails

If the optical gap of a solid is \mathcal{E}_g , then one should expect no measurable absorption for incoming light with $\hbar\omega < \mathcal{E}_g$. However, some absorption does occur, and in a wide range of solids including ionic crystals, insulators with F centers, and amorphous semiconductors, optical absorption takes the form

$$\alpha \propto \exp \left[-\frac{(\mathcal{E}_g - \hbar\omega)}{k_B T} \right]. \quad (22.79)$$

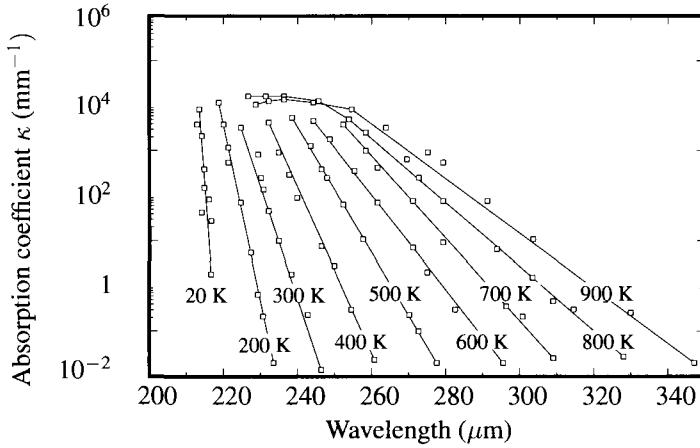


Figure 22.13. Attenuation constant versus wavelength for radiation incident upon a KI crystal at a variety of temperatures. The range of exponential decay spans six decades. [Source: Haupt (1959), p. 239.]

In the range where Eq. (22.79) is valid, α can vary by six orders of magnitude or more, as first found by Urbach (1953). Data from high-quality KI crystals are displayed in Figure 22.13.

Problems

1. Clausius–Mossotti relation

- Using elementary electrostatics, verify Eq. (22.3).
- Verify that (22.4) vanishes for dipoles arranged in any structure with cubic symmetry.

- Faraday rotation:** In a Faraday rotation experiment, infrared radiation passes through a thin sample, along the direction of an applied magnetic field. If the light is linearly polarized, then the angle of polarization rotates. The Faraday rotation θ per unit length along the sample is defined by

$$\theta = \frac{\omega}{2c} [\bar{n}_- - \bar{n}_+], \quad (22.80)$$

where \bar{n}_+ and \bar{n}_- are the indices of refraction for right and left circularly polarized light.

- Consider a population of electrons obeying

$$\ddot{\vec{r}} + \frac{\dot{\vec{r}}}{\tau} + \frac{e}{m^*c} \dot{\vec{r}} \times \vec{B} = -\frac{e}{m^*} \vec{E} e^{-i\omega t}. \quad (22.81)$$

Take the magnetic field to point along \hat{z} . Find the current, and therefore the conductivities σ^\pm , for right- and left-polarized fields \vec{E} .

- (b) Assume that the frequency ω is large, which means $\omega\tau \gg 1$ and $eB/m^*c \ll \omega$. Expand the conductivities to leading order in ω_c and $1/\tau$.
- (c) Find the dielectric constant and index of refraction to leading order in these same quantities. Assume $\omega \gg \omega_p$, and find an expression for θ .
3. **Polaron decay:** Assume that the energy $\hbar^2 q^2/2m^*$ of an electron in a polar solid is greater than the energy $\hbar\omega_L$ of a longitudinal optical phonon. Employing Fermi's Golden Rule, Eq. (13.99), show that the rate at which an electron of wave number q decays is given by Eq. (22.57). Perform the angular integral over $\cos\theta$ before the momentum integral, and recall that $\cosh^{-1}x = \ln[x \pm \sqrt{x^2 - 1}]$.

4. Franck–Condon effect:

Consider an F center sitting in the excited state at position C in Figure 22.12, described by the Hamiltonian

$$\hat{\mathcal{H}}_F + \hat{\mathcal{H}}_{\text{ion}} + \hat{\mathcal{H}}_{\text{int}}, \quad (22.82)$$

where the three portions of the Hamiltonian are described by Eqs. (22.59), (22.60), and (22.61).

In the case where the distance

$$\mathcal{D}_1 = \frac{\mathcal{E}_1 g}{M\omega_1^2} \quad (22.83)$$

is large compared to the quantum zero-point fluctuations of the ion coordinate x_0 , find the quantum number n characterizing the most likely final state indicated in Figure 22.12 by position D.

5. **Urbach tails:** Theoretical calculations tend not to reproduce Eq. (22.79) exactly, but to find functional forms that fall off more rapidly as $\hbar\omega$ falls below \mathcal{E}_g . As an illustration, one can use the configuration coordinate model for the Franck–Condon effect.

- (a) Write down Eq. (20.70) for the real part of the conductivity, and relate it to the optical absorption.
- (b) Take the initial state to be the state of energy $\mathcal{E}_{0,n}$ from Eq. (22.67), occupied with probability $f_n = \exp[-\beta\mathcal{E}_{0,n}]$, and take the final state to be the one with energy $\mathcal{E}_{1,0}$: The electron is excited to state $|F_1\rangle$, but the ionic coordinate is relaxed. Rewrite Eq. (20.70), assuming that

$$\langle F_0, n | \hat{P} | F_1, 0 \rangle = \langle F_0 | \hat{P} | F_1 \rangle \langle F_0, n | F_1, 0 \rangle. \quad (22.84)$$

- (c) Convert the sum over n to an integral, and perform the integral. Show that the temperature dependence of the result is correct, but that the absorption falls off too quickly as a function of $\mathcal{E}_g - \hbar\omega$.

References

- W. S. Baer (1967), Faraday rotation in ZnO: Determination of the electron effective mass., *Physical Review*, **154**, 785–789.
- M. Balkanski (1972), Photon-phonon interactions in solids, in *Optical Properties of Solids*, F. Abelès, ed., pp. 529–652, North-Holland, Amsterdam.
- B. Bendow (1978), Multiphonon infrared absorption in the highly transparent frequency regime of solids, *Solid State Physics: Advances in Research and Applications*, **33**, 249–316.
- D. Berlincourt and H. H. A. Krueger (1959), Domain processes in lead titanate zirconate and barium titanate ceramics, *Journal of Applied Physics*, **30**, 1804–1810.
- A. Einstein (1907), Planck's theory of radiation and the theory of specific heat, *Annalen der Physik (Leipzig)*, **22**, 180–190. In German.
- A. Einstein (1911), A relation between the elastic constants and specific heat of solid bodies made from atoms of a single type, *Annalen der Physik (Leipzig)*, pp. 170–174. In German.
- D. Emin (1982), Small polarons, *Physics Today*, **35**(6), 34–40.
- G. Feher (1959), Observation of nuclear magnetic resonances via the electron spin resonance line, *Physical Review*, **103**, 834–835.
- R. P. Feynman (1972), *Statistical Mechanics*, Addison-Wesley, Redwood City, CA.
- C. P. Flynn (1972), *Point Defects and Diffusion*, Clarendon Press, Oxford.
- W. B. Fowler, ed. (1968), *Physics of Color Centers*, Academic Press, New York.
- H. Fröhlich (1952), Interaction of electrons with lattice vibrations, *Proceedings of the Royal Society of London*, **A215**, 291–298.
- B. Gerlach and H. Lowen (1991), Analytical properties of polaron systems or: Do polaronic phase transitions exist or not?, *Reviews of Modern Physics*, **63**, 63–90.
- U. Haupt (1959), On the temperature dependence and form of the long wavelength excitation band in KI crystals, *Zeitschrift für Physik*, **157**, 232–246.
- A. J. Heeger, S. Kivelson, J. R. Schrieffer, and W. P. Su (1988), Solitons in conducting polymers, *Reviews of Modern Physics*, **60**, 781–850.
- J. W. Hodby (1971), Cyclotron resonance of the polaron in the alkali and silver halides. iii, *Journal of Physics C*, **4**, L8–L11.
- E. Kartheuser (1972), Dielectric properties of polar crystals, in *Polarons in Ionic Crystals and Polar Semiconductors*, J. T. Devreese, ed., North Holland, Amsterdam.
- R. D. Kingsmith and D. Vanderbilt (1993), Theory of Polarization of Crystalline Solids, *Physical Review B*, **47**(3), 1651–1654.
- L. D. Landau and E. M. Lifshitz (1977), *Quantum Mechanics (Non-relativistic Theory)*, 3rd ed., Pergamon Press, Oxford.
- H. Landolt and R. Börnstein (New Series), *Numerical Data and Functional Relationships in Science and Technology*, New Series, Group III, Springer-Verlag, Berlin.
- M. E. Lines and A. M. Glass (1977), *Principles and Applications of Ferroelectrics and Related Materials*, Clarendon Press, Oxford.
- F. Lüty (1961), Electronic transitions in color centers, *Halbleiter Probleme*, **6**, 238–278.
- E. Mollwo (1933), On the color centers of alkali halide crystals, *Zeitschrift für Physik*, **85**, 56–67. In German.
- N. F. Mott and R. W. Gurney (1940), *Electronic Processes in Ionic Crystals*, Oxford University Press, Oxford.
- F. M. Peeters and J. T. Devreese (1984), Theory of polaron mobility, *Solid State Physics: Advances in Research and Applications*, **38**, 81–133.
- H. Pick (1972), Structure of trapped electron and trapped hole centers in alkali halides: "Color centers", in *Optical Properties of Solids*, F. Abelès, ed., pp. 654–747, North-Holland, Amsterdam.
- R. Resta (1994), Macroscopic polarization in crystalline dielectrics: The geometric phase approach,

- Reviews of Modern Physics*, **66**, 899–915.
- R. Resta, M. Posternak, and A. Baldereschi (1993), Towards a quantum theory of polarization in ferroelectrics: The case of $knbo_3$, *Physical Review Letters*, **70**, 1010–1013.
- W. C. Röntgen (1921), On the electrical conductivity of single crystals, and on the influence of radiation, *Annalen der Physik*, **64**, 1–195. In German.
- G. Sághi-Szabó, R. E. Cohen, and H. Krakauer (1999), First-principles study of piezoelectricity in tetragonal $pbtio_3$ and $pbzr_1/2ti_1/2o_3$, *Physical Review B*, **59**(20), 12 771–12 776.
- G. A. Samara and P. S. Peercy (1981), The study of soft-mode transitions at high pressure, *Solid State Physics: Advances in Research and Applications*, **36**, 1–118.
- L. Schiff (1968), *Quantum Mechanics*, 3rd ed., McGraw-Hill, New York.
- H. Seidel and H. C. Wolf (1968), ESR and ENDOR spectroscopy of color centers in alkali halide crystals, in *Physics of Color Centers*, W. B. Fowler, ed., pp. 537–624, Academic Press, New York.
- F. Urbach (1953), The long-wavelength edge of photographic sensitivity and the electronic absorption of solids, *Physical Review*, **92**, 1324.
- B. E. Vugmeister and M. D. Glinchuk (1990), Dipole glass and ferroelectricity in random-site electric dipole systems, *Reviews of Modern Physics*, **62**, 993–1026.
- R. Wahl, D. Vogtenhuber, and G. Kresse (2008), Srtio[sub 3] and batio[sub 3] revisited using the projector augmented wave method: Performance of hybrid and semilocal functionals, *Physical Review B*, **78**, 104 116.
- I. S. Zheludev (1971), Ferroelectricity and symmetry, *Solid State Physics: Advances in Research and Applications*, **26**, 429–464.

23. Optical Properties of Metals and Inelastic Scattering

23.1 Introduction

The interaction of electromagnetic radiation with metals divides between low and high frequencies. Low frequency refers to frequencies too small to induce transitions from one Bloch band to another. The energies involved in hopping between bands are characteristically around 1 eV, so the dividing line is around

$$1 \text{ eV} \Rightarrow \omega \sim 10^{15} \text{ Hz} \Rightarrow \lambda \sim 1 \text{ } \mu\text{m}. \quad (23.1)$$

For frequencies below this point, the absence of transitions between bands means that the behavior of electrons is semiclassical and can be treated by the formalism of Section 17.2. This is not to say that there are no quantum-mechanical effects; the response of electrons even to static electric fields has many quantum-mechanical features, but classical notions of electrons wiggling back and forth in response to oscillating fields provide the right starting point. At frequencies above the cutoff (23.1), the language and mode of thought in discussing the problem begin to alter. Although the incoming light will still be treated classically, and there is no need to quantize the electromagnetic field, the effects of the light waves are most easily understood as a beam of photons whose absorption is able to induce transitions between various quantum mechanical states. For energies of 10–100 eV, light has become the most powerful probe of electronic structure in metals and semiconductors, making possible in some cases a direct experimental investigation of the one-electron picture, including quantitative measurements of the energy bands.

23.1.1 Plasma Frequency

In the Drude model, a metal consists of a gas of noninteracting mobile electrons. The response of such electrons to external electric fields was described in Eqs. (20.4) and (20.31), which showed that

$$\epsilon(\omega) = 1 - \frac{\omega_p^2}{\omega(\omega + i/\tau)} \quad \begin{array}{l} \text{To compare with experiment, the constant 1} \\ \text{often must be replaced by } \epsilon^\infty. \end{array} \quad (23.2)$$

$$\omega_p = \sqrt{\frac{4\pi n e^2}{m}} = 5.64 \cdot 10^{15} \text{ Hz} \left[\frac{n}{10^{22} \text{ cm}^{-3}} \right]^{1/2}. \quad (23.3)$$

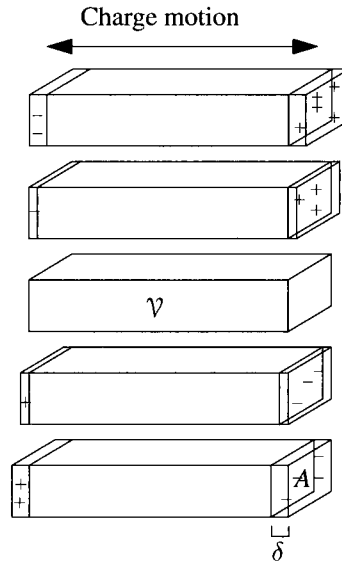


Figure 23.1. Plasma oscillations result from the bulk motion of charge in a solid.

The definition of the plasma frequency ω_p is motivated by the limit $\omega\tau \gg 1$, which leads to

$$\epsilon(\omega) = 1 - \left(\frac{\omega_p}{\omega}\right)^2. \quad (23.4)$$

It has a very simple physical interpretation, illustrated in Figure 23.1. Consider a slab of electrons sitting on top a slab of neutralizing positive charge. If the whole slab of electrons is moved a distance δ , then positive charge develops on one side of the slab, negative charge on the other. The charge, say, on the positive side is $enA\delta$, where A is the area of the slab, and n the density of charged particles. A uniform electric field $E = 4\pi en\delta$ develops between two such slabs of charge. If the total volume of the system is \mathcal{V} , then the force on all of the electrons is

$$en\mathcal{V}E = 4\pi n^2 e^2 \mathcal{V} \delta. \quad (23.5)$$

Setting this force equal to mass, $mn\mathcal{V}$, times acceleration $\ddot{\delta}$ gives

$$\ddot{\delta} = -\frac{4\pi ne^2}{m} \delta. \quad (23.6)$$

So the frequency of plasma oscillations is

$$\omega_p^2 = \frac{4\pi ne^2}{m}. \quad (23.7)$$

This result is correct only for free electrons. In the presence of a periodic potential, the plasma frequency is modified. Conventionally, the electron mass m is replaced by an effective mass called the optical mass; see Eq. (23.27).

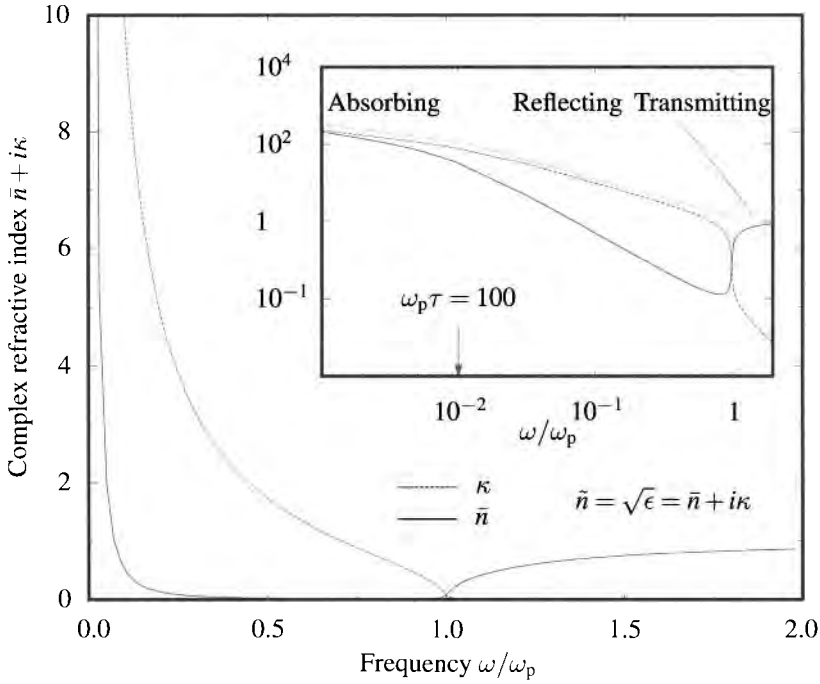


Figure 23.2. Index of refraction \bar{n} and extinction coefficient κ for metal obeying Eq. (23.2), with $\omega_p\tau = 100$, showing absorbing, reflecting, and transmitting frequency ranges.

Three Regimes for Metallic Response. The product $\omega_p\tau$ can be estimated from Eqs. (16.7) and (23.3) and can range from 10 to 100. Therefore, according to Eq. (23.2), the optical absorption of metals should pass through three phases, shown in Figure 23.2.

Absorbing: For $0 < \omega\tau \lesssim 1$ the metal absorbs the incident radiation, because

$$\epsilon \approx 1 + i\tau \frac{\omega_p^2}{\omega} (1 + i\omega\tau) \Rightarrow \bar{n} \approx \kappa \approx \sqrt{\tau\omega_p^2/2\omega}. \tag{23.8}$$

The index of refraction \bar{n} and extinction coefficient κ were defined in Eqs. (20.18) and (20.20).

Reflecting: For $1 \lesssim \omega\tau \lesssim \omega_p\tau$ the real part of ϵ is negative, equaling approximately

$$\frac{(\omega^2 - \omega_p^2)}{\omega^2} \tag{23.9}$$

and resulting in

$$\kappa \approx \sqrt{\omega_p^2/\omega^2 - 1} \text{ and } \bar{n} \approx \frac{\omega_p^2}{2\tau\omega^2 \sqrt{\omega_p^2 - \omega^2}}. \tag{23.10}$$

According to Eq. (20.43), because the index of refraction \bar{n} is small in comparison with the extinction coefficient κ , almost all radiation incident upon the metal in this range of frequencies will be reflected.

Transparent: For $\omega \gtrsim \omega_p$ the real part of the dielectric constant first vanishes and then becomes positive as ω increases. The metal becomes nearly transparent to the incoming radiation, with index of refraction and extinction coefficient given by

$$\bar{n} \approx \sqrt{1 - \omega_p^2/\omega^2} \quad \kappa \approx \frac{\omega_p^2}{2\tau\omega^2 \sqrt{\omega^2 - \omega_p^2}}. \quad (23.11)$$

23.2 Metals at Low Frequencies

When the frequency of radiation is low enough that the semiclassical approach is valid, a restriction that was the subject of Problem 20.2, the population of electrons is described by the Boltzmann equation (Section 17.2), which, in the absence of thermal gradients reads

$$\frac{\partial g}{\partial t} = -\vec{v} \cdot \nabla g - e\vec{E} \cdot \vec{v} \frac{\partial g}{\partial \mu} - \frac{g}{\tau}. \quad (23.12)$$

Use $\partial f / \partial \vec{k} = \partial \mathcal{E} / \partial \vec{k} \partial f / \partial \mathcal{E} N = -\hbar \vec{v} \partial f / \partial \mu$,
starting with Eq. (17.10) in the relaxation time approximation.

Suppose the electric field to have the form

$$\vec{E} = \vec{E}(\vec{q}, \omega) e^{i\vec{q} \cdot \vec{r} - i\omega t}. \quad (23.13)$$

Then Eq. (23.12) is easily solved by taking

$$g_{\vec{k}} = g_{\vec{k}}(\vec{q}, \omega) e^{i\vec{q} \cdot \vec{r} - i\omega t} \quad (23.14)$$

The label \vec{k} describes the Bloch index of an electron, while the label \vec{q} describes the wave vector of the electromagnetic wave.

so that

$$g_{\vec{k}}(\vec{q}, \omega)[-i\omega] = [-i\vec{v} \cdot \vec{q} - 1/\tau] g_{\vec{k}}(\vec{q}, \omega) - e\vec{E} \cdot \vec{v} \frac{\partial f}{\partial \mu} \quad (23.15)$$

$$\Rightarrow g_{\vec{k}}(\vec{q}, \omega) = -e \frac{\partial f}{\partial \mu} \frac{\vec{E}(\vec{q}, \omega) \cdot \vec{v}}{1/\tau - i(\omega - \vec{q} \cdot \vec{v})}. \quad (23.16)$$

Remember that \vec{v} is a function of \vec{k} according to Eq. (7.59).

The current associated with the distribution function (23.16) is determined by an integral over \vec{k} , and from it can be obtained the conductivity σ through

$$\vec{j} = -e \int [d\vec{k}] \vec{v} g_{\vec{k}} \quad [d\vec{k}] \text{ defined in Eq. (6.15)}. \quad (23.17)$$

$$= e^2 \int [d\vec{k}] \frac{\partial f}{\partial \mu} \frac{\vec{v} [\vec{v} \cdot \vec{E}(\vec{q}, \omega)]}{1/\tau - i(\omega - \vec{q} \cdot \vec{v})} \quad (23.18)$$

$$\Rightarrow \sigma_{\alpha\beta} = e^2 \int [d\vec{k}] \frac{\partial f}{\partial \mu} \frac{v_\alpha v_\beta}{1/\tau - i(\omega - \vec{q} \cdot \vec{v})} \quad \text{The subscript on } v \text{ is a Cartesian coordinate.} \quad (23.19)$$

$$= e^2 \int \frac{d\Sigma}{4\pi^3 \hbar v} \frac{v_\alpha v_\beta}{1/\tau - i(\omega - \vec{q} \cdot \vec{v})} \quad \text{The integral is over the Fermi surface, as in Eq. (7.73). Use Eq. (6.15).} \quad (23.20)$$

$$\Rightarrow \epsilon_{\alpha\beta} = \delta_{\alpha\beta} + \frac{4\pi i e^2}{\omega} \int \frac{d\Sigma}{4\pi^3 \hbar v} \frac{v_\alpha v_\beta}{1/\tau - i(\omega - \vec{q} \cdot \vec{v})} \quad \text{Using Eq. (20.14) to relate conductivity to dielectric constant.} \quad (23.21)$$

The wave vector \vec{q} of transverse propagating electromagnetic waves can now be determined from

$$q = \frac{\sqrt{\epsilon}\omega}{c} = (\bar{n} + i\kappa) \frac{\omega}{c}. \quad (23.22)$$

Because \vec{q} appears in the middle of the integral (23.21), this task is not particularly simple.

Recovery of Drude Formula. Often, the \vec{q} dependence of (23.21) can be neglected. The conditions needed to neglect it are that $\vec{q} \cdot \vec{v}$ be small compared to other terms in the denominator of (23.21), which means that

$$\frac{1}{\tau} - i\omega + i(\bar{n} + i\kappa) \frac{\omega v_F}{c} \approx \frac{1}{\tau} - i\omega \quad (23.23a)$$

The largest $\vec{q} \cdot \vec{v}$ can be is qv_F , where v_F is the largest velocity of an electron on the Fermi surface; the factor of $\partial f / \partial \mu$ restricts v to the Fermi surface. Use Eq. (23.22) for q .

$$\Rightarrow \frac{\bar{n} v_F}{c} \ll 1 \quad (23.23b)$$

and

$$\kappa \omega v_F \tau / c \ll 1 \quad \text{or equivalently} \quad l_T \ll \delta, \quad (23.23c)$$

where $l_T = v_F \tau$ is the electron mean free path, and

$$\delta \equiv \frac{c}{\kappa \omega} \quad (23.24)$$

is the *skin depth*, the characteristic distance that electromagnetic waves penetrate into a metal, according to Eq. (20.19). Condition (23.23b) is almost always satisfied, because Fermi velocities are two orders of magnitude smaller than the speed of light. Condition (23.23c) is satisfied by typical metals at room temperature, where mean free paths are on the order of 100 Å and where for frequencies up to the cutoff in (23.1) the skin depth is 1000 Å or greater, as will be shown below. It is violated by pure metals at temperatures on the order of 10 K, because the mean free path can rise as high as 10^{-2} cm.

Assuming that the conditions of (23.23) hold, σ does not depend upon \vec{q} . In an isotropic solid or a cubic crystal, the dielectric tensor can be treated as a scalar and equals

$$\epsilon = 1 - \frac{\omega_p^2}{\omega(\omega + i/\tau)} \quad (23.25)$$

with

$$\omega_p^2 = \frac{4\pi n e^2}{m_{\text{opt}}}, \quad (23.26)$$

the optical mass m_{opt} being defined by

$$\frac{1}{m_{\text{opt}}} = \frac{1}{m} \frac{\int [d\vec{k}] \frac{\partial f}{\partial \mu} m v_x^2}{\int [d\vec{k}] f_k} = \int \frac{d\Sigma}{12\pi^3 \hbar n} v. \quad \text{Averages of } v_x^2 \text{ equal averages of } v^2/3. \text{ Denominator equals } n. \quad (23.27)$$

The Drude results (20.31) and (20.32) have emerged unchanged from this analysis, except that the electron mass is replaced by the effective mass m_{opt} resulting from an average over the Fermi surface.

23.2.1 Anomalous Skin Effect

When the conditions of (23.23) do not hold, determining the dispersion relation for a metal rapidly becomes quite complicated. In the limit where the second of the conditions is reversed and the skin depth δ is much smaller than the mean free path, the complications are worth pursuing slightly further. The integral appearing in Eq. (23.21) changes from an average over the entire Fermi surface into an integral very sharply peaked on a line running around the Fermi surface. For this reason, the *anomalous skin effect* can be used to measure geometrical properties of the Fermi surface, and Pippard (1957) employed it to obtain the first experimental determination of the Fermi surface of copper.

Pippard's experiments were carried out at frequencies $\omega \approx 10^{11}$ Hz and at temperatures on the order of 10 K, where the relaxation time τ in copper rises from its room temperature value of 10^{-14} s to 10^{-10} s. The dielectric tensor changes very rapidly in this frequency regime, so one cannot simply speak of an index of refraction, but roughly speaking $\bar{n} \sim 10^4$, so that $q \sim \bar{n}\omega/c \sim 10^5 \text{ cm}^{-1}$. Because the Fermi velocity of copper is around $1.5 \cdot 10^8 \text{ cm/sec}$ it follows that $\omega \ll qv_F$, and ω can be neglected in the denominator of (23.21). The evaluation of Eq. (23.21) continues with the observation that because $\tau v_F q \gg 1$, the integral will be dominated by occasions where $\vec{q} \cdot \vec{v}_F = 0$ —that is, where the wave vector \vec{q} is perpendicular to the direction of electron propagation \vec{v} , as shown in Figure 23.3. As radiation passes through the surface of the metal, it decays rapidly. Because the mean free path of electrons is much larger than the skin depth, electrons traveling parallel to the surface and perpendicular to \vec{q} are excited into large amplitude oscillations.

To estimate the value of (23.20), suppose that radiation is arriving along $\vec{q} = q\hat{z}$, that it is polarized along x , and that the portion of the Fermi surface where $\vec{v} \cdot \vec{q} = 0$ can be approximated by two radii of curvature, \mathcal{R}_ϕ and \mathcal{R}_θ , describing the curvature along the θ and ϕ directions depicted in Figure 23.3. Then

$$d\Sigma \approx \mathcal{R}_\phi \mathcal{R}_\theta d\theta d\phi, \quad v_x \approx v_F \cos \phi \quad (23.28)$$

and

$$\sigma_{xx} = e^2 \int \frac{\mathcal{R}_\phi \mathcal{R}_\theta d\theta d\phi}{4\pi^3 \hbar v_F} \frac{v_F^2 \cos^2 \phi}{1/\tau + iqv_F \theta} \quad \text{Replacing } \vec{q} \cdot \vec{v}_F \text{ by } qv_F \theta \text{ is fine because the integrand drops off very rapidly away from } \theta = 0. \quad (23.29)$$

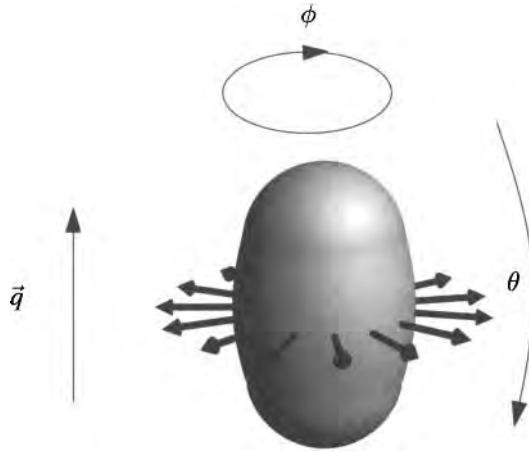


Figure 23.3. The electrons responsible for the anomalous skin effect have velocities perpendicular to the incoming radiation \vec{q} . Recall from Section 7.2.5, and Problem 1 in Chapter 7, that electron velocity vectors are normal to the Fermi surface.

$$= \frac{e^2}{4\pi\hbar q} \mathcal{R}_\phi \mathcal{R}_\theta. \quad \text{Extending the limits of } \theta \text{ integration from } -\infty \text{ to } \infty \text{ is also fine because } qv_F\tau \gg 1. \quad (23.30)$$

Without following the analysis further, it is clear that the relaxation time τ and Fermi velocity v_F have dropped out of the expression for the conductivity, which is governed by the curvature of the Fermi surface. Detailed calculation of absorption requires studying a highly dispersive wave as it enters the surface of the metal, and it will not be pursued further here. However, the geometrical information in Eq. (23.30) is enough to determine shapes of Fermi surfaces, and it was the first method used to obtain Figure 16.12.

23.3 Plasmons

The plasma frequency ω_p in Figure 23.2 where $\epsilon = 0$, $\bar{n} = \kappa$, and the metal passes from reflecting to transparent is worth examining further. Oscillations at frequency ω_p are only the longest wavelength limit of a whole family of oscillating modes. The general condition for a longitudinal propagating mode is $\epsilon(\vec{q}, \omega) = 0$, and the excitations obeying this condition above the plasma frequency are called *plasmons*. To calculate their properties one can turn to the dielectric function of the electron gas defined by Eqs. (20.84) and (20.77).

First look for a resonance at small \vec{q} . One can rewrite the susceptibility χ_c as

$$\chi_c = \frac{e^2}{\hbar\mathcal{V}} \sum_{\vec{k}} f_{\vec{k}} \left[\frac{1}{\omega_{\vec{k}} - \omega_{\vec{q}+\vec{k}} - \omega} + \frac{1}{\omega_{\vec{k}} - \omega_{\vec{q}+\vec{k}} + \omega} \right] \quad (23.31)$$

$$= \frac{e^2}{\hbar\mathcal{V}} \sum_{\vec{k}} \frac{2f_{\vec{k}}(\omega_{\vec{k}} - \omega_{\vec{k}+\vec{q}})}{(\omega_{\vec{k}} - \omega_{\vec{k}+\vec{q}})^2 - \omega^2} \quad (23.32)$$

$$= \frac{e^2}{\mathcal{V}} \sum_{\vec{k}} \frac{2f_{\vec{k}} \left[\frac{q^2}{2m} + \frac{\vec{q} \cdot \vec{k}}{m} \right]}{\omega^2 - \hbar^2 \left[\frac{\vec{q} \cdot \vec{k}}{m} + \frac{q^2}{2m} \right]^2}. \quad (23.33)$$

Because the goal is to find long-wavelength propagating modes in the vicinity of the plasma frequency ω_p , it is logical to treat \vec{q} as small and expand (23.33) in powers of \vec{q} . Keeping the first two orders gives

$$\chi_c(\vec{q}, \omega) \approx \frac{e^2}{\mathcal{V}} \sum_{\vec{k}} \frac{f_{\vec{k}}}{\omega^2} \frac{q^2}{m} \left[1 + \frac{3(\vec{q} \cdot \vec{k})^2 \hbar^2}{m^2 \omega^2} \right]. \quad (23.34)$$

Carrying out an angular average, the factor of 3 disappears, leaving

$$\chi_c(\vec{q}, \omega) = \frac{e^2}{\mathcal{V}} \sum_{\vec{k}} \frac{f_{\vec{k}}}{\omega^2} \frac{q^2}{m} \left[1 + \frac{(qk)^2 \hbar^2}{m^2 \omega^2} \right]. \quad (23.35)$$

The sum over \vec{k} includes a sum over all angles of \vec{k} , so the result cannot change if terms are replaced by their angular average.

Recall that

$$N = \sum_{\vec{k}\sigma} f_{\vec{k}} = \mathcal{V} \int \frac{dk}{4\pi^3} 4\pi k^2 f_{\vec{k}}. \quad (23.36)$$

So one must have that

$$\sum_{\vec{k}\sigma} f_{\vec{k}} k^2 = \frac{3}{5} N k_F^2. \quad (23.37)$$

Using Eqs. (23.35) and (23.37) in Eq. (20.84) gives

$$\epsilon(\vec{q}, \omega) = 1 - \frac{4\pi n e^2}{m\omega^2} \left[1 + \frac{3}{5} \frac{\hbar^2 k_F^2 q^2}{m^2 \omega^2} \right]. \quad (23.38)$$

So longitudinal modes propagate when $\epsilon = 0$, which means

$$1 = \frac{\omega_p^2}{\omega^2} \left[1 + \frac{3}{5} \frac{\hbar^2 k_F^2 q^2}{m^2 \omega^2} \right] \quad (23.39)$$

$$\Rightarrow \omega^2 = \omega_p^2 + \frac{6}{5} \frac{\mathcal{E}_F q^2}{m}. \quad (23.40)$$

Equation (23.40) is the dispersion relation for plasmons.

23.3.1 Experimental Observation of Plasmons

Plasmons are fairly long-lived until they achieve a wave vector at which it is possible for a plasmon to transfer some of its energy to a single moving electron. At this point, the plasma waves decay rapidly, in a phenomenon known as *Landau damping*. The condition for Landau damping may be obtained by examining when it becomes possible for the denominator in Eq. (23.33) to vanish with ω and q related by Eq. (23.40), and \vec{k} within the Fermi surface.

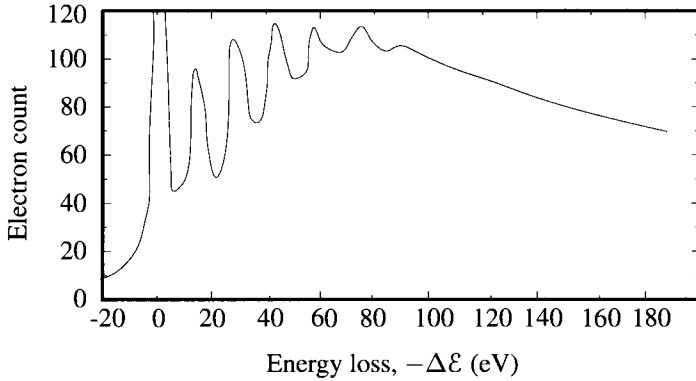


Figure 23.4. Number of scattered electrons as a function of energy loss. The peaks correspond to creation of zero, one, two, or more plasmons. [Source: Lang (1948), p. 241.]

The classic experiments measuring such plasma oscillations in metals were performed simultaneously by Ruthemann (1948) and Lang (1948). A monoenergetic electron beam with an energy in the kilovolt range was passed through a 500-Å aluminum film. In aluminum $\hbar\omega_p$ is 15.8 eV, and collision events involving the creation of one or a few plasmons appear as energy loss peaks in multiples of this quantum after the electron beam exits the film. A sample of such data appears in Figure 23.4.

Just as in the cases of neutron scattering for the measurement of phonon dispersion relations, or photoemission for the measurement of electronic band structure, the dispersion of plasmons can be measured through an inelastic scattering experi-

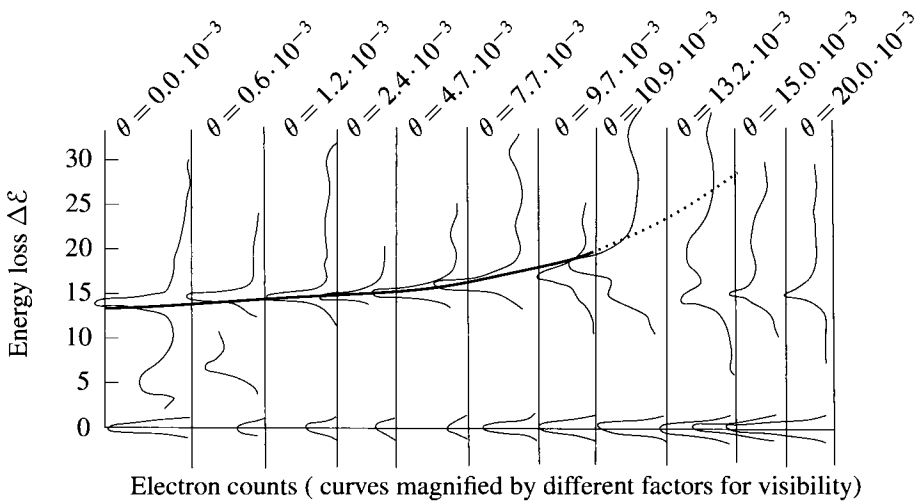


Figure 23.5. Energy loss versus number of scattered electrons for numerous scattering angles θ . Only a single plasmon peak is visible, and it disappears when the conditions for Landau damping are met. The line through the peaks shows the plasmon dispersion relation $\hbar\omega(\theta)$. [Source: Kunz (1962) p. 59.]

Table 23.1. Comparison of measured and predicted plasmon dispersion relations

Element	Be	Al	Mg	Sb	Na
α_{pl} [from Eq. (23.43)]	0.47	0.44	0.39	0.44	0.32
α_{pl} (experiment)	0.42	0.35	0.39	0.37	0.29

Source: Platzman and Wolff (1973) p. 71.

ment. Plasmons are excited by electrons injected into samples. Inelastic scattering with electrons is called *electron energy loss spectroscopy* (EELS), and is reviewed by Schnatterly (1979). Equations (13.93) can be used to analyze data of the type shown in Figure 23.5.

In particular, suppose that an electron enters a sample, losing energy $\Delta\mathcal{E}$, and changing direction from \vec{k} to \vec{k}' , differing by a small angle θ . Then conservation of energy and momentum require that

$$\hbar\omega(\vec{k} - \vec{k}') = \Delta\mathcal{E} \quad (23.41)$$

$$\Rightarrow \hbar\omega(2k \sin \theta/2) \approx \hbar\omega_p + \alpha_{\text{pl}} \frac{\hbar^2 k^2}{m} \theta^2 \quad (23.42)$$

Use Eq. (23.40), the fact that θ is small and Eq. (3.8); the change in electron angle θ is twice the Bragg angle of Eq. (3.8).

where

$$\alpha_{\text{pl}} = \frac{3}{5} \frac{\hbar^2 k_F^2}{2m\hbar\omega_p}. \quad (23.43)$$

The results are satisfactory, as shown in Table 23.1.

23.4 Interband Transitions

As the frequency of incoming photons increases toward 1 eV, so does the probability that light will induce transitions where electrons hop between bands. Actually, there is no reason in a metal why the such transitions cannot occur for arbitrarily small photon energies, but the minimum jump tends to be on the order of 1 eV. The dominant optical transition in such a case is described by the same equation, Eq. (21.14), that was employed to discuss direct transitions in semiconductors.

Example: Sodium. Interband transitions in the alkali metals are particularly simple, because the conduction band electrons behave very nearly like free non-interacting electrons, and have energies well above any of the core electrons. The Fermi surface is nearly spherical, and deviations from the completely free electron model can be attributed to a weak pseudopotential. These claims result from band structure calculations, and are also in excellent agreement with the optical measurements to be discussed below, as well as with de Haas–van Alphen measurements of the type discussed in Section 16.5.2.

All of the alkali metals adopt the bcc crystal structure in their ground state. The relation of the Fermi surface to the edges of the Brillouin zone is given approximately by the upper left image in Figure 8.7. The closest approach to the zone edge

is at point N , labeled in Figure 7.9, which is at distance $2\pi/\sqrt{2}a = 4.44/a$ from the origin, while the Fermi surface is at distance $[6\pi^2]^{1/3}/a = 3.89/a$. Figure 23.6 shows the computed band structure of sodium along the line $\Gamma - N$. At the location of the Fermi surface, the energy bands are extremely close to the free electron values, and therefore the wave functions are accurately given by Eq. (8.14).

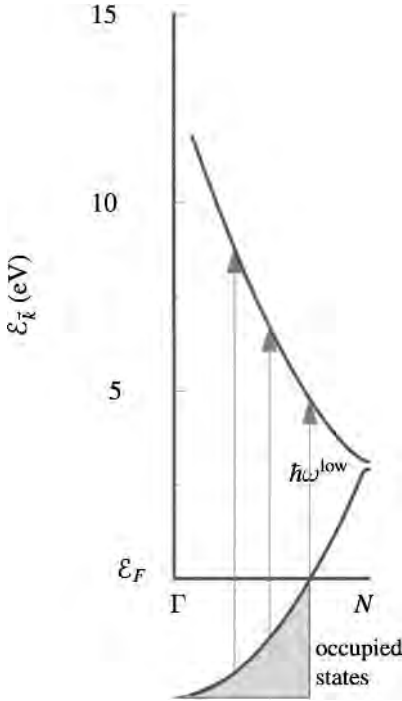


Figure 23.6. The sodium electron bands are nearly indistinguishable from free electron bands except near zone edges, and the Fermi level lies sufficient distance away that the nearly free electron approximation is excellent. The smallest interband transition, $\hbar\omega^{\text{low}}$, takes an electron from the Fermi surface up to the next band.

In order to evaluate Eq. (21.16), one needs to find the matrix elements

$$\langle n_1 \vec{k} | \hat{P}_\alpha | n_2 \vec{k} \rangle. \tag{23.44}$$

There is only one occupied band n_1 , but there are 12 reciprocal lattice vectors equivalent to (110) providing upper bands n_2 that must be considered. Their contributions are simply additive, so it is enough to deal with one at a time. According to (8.15), which dealt with two bands at a time in the extended zone representation, the wave functions of electrons in the lower and upper bands are

$$\psi_{\vec{k}}^{\text{low}}(\vec{r}) \approx \frac{1}{\sqrt{V}} \left[e^{i\vec{k}\cdot\vec{r}} + \frac{e^{i(\vec{k}-\vec{K})\cdot\vec{r}} U_{-\vec{K}}}{\mathcal{E}_{\vec{k}}^0 - \mathcal{E}_{\vec{k}-\vec{K}}^0} \right] \tag{23.45}$$

This is the wave function corresponding to the lower branch in Figure 23.6. In employing Eq. (8.15), \vec{K} has been replaced by $-\vec{K}$.

$$\psi_{\vec{k}}^{\text{high}}(\vec{r}) \approx \frac{1}{\sqrt{V}} \left[e^{i(\vec{k}-\vec{K})\cdot\vec{r}} + \frac{e^{i\vec{k}\cdot\vec{r}} U_{\vec{K}}}{\mathcal{E}_{\vec{k}-\vec{K}}^0 - \mathcal{E}_{\vec{k}}^0} \right]. \tag{23.46}$$

This is the wave function corresponding to the upper branch in Figure 23.6.

Most details are left to Problem 2. In brief, (20.70) becomes

$$\operatorname{Re}[\sigma_{\alpha\beta}](\omega) = \frac{\pi}{\omega} \frac{e^2 \hbar^2}{m^2} \frac{1}{\mathcal{V}} \sum_{\vec{k}, \vec{K} \in \langle 110 \rangle} f_{\vec{k}} \frac{|U_{\vec{K}}|^2 K_{\alpha} K_{\beta}}{(\mathcal{E}_{\vec{k}-\vec{K}}^0 - \mathcal{E}_{\vec{k}}^0)^2} \delta(\mathcal{E}_{\vec{k}-\vec{K}}^0 - \mathcal{E}_{\vec{k}}^0 - \hbar\omega) \quad (23.47)$$

\vec{k} is summed over the Brillouin zone, and \vec{K} ranges over the vectors equivalent to $\langle 110 \rangle$ under cubic symmetry operations.

$$\Rightarrow \sigma(\omega) = \frac{4e^2 \pi}{m^2 \omega^3} K^2 |U_{\vec{K}}|^2 D_j(\hbar\omega), \quad (23.48)$$

where the joint density of states D_j defined in Eq. (21.17) takes the form

$$D_j(\hbar\omega) = \frac{1}{\mathcal{V}} \sum_{\vec{k}, \vec{K} \in \langle 110 \rangle} f_{\vec{k}} \delta(\mathcal{E}_{\vec{k}-\vec{K}}^0 - \mathcal{E}_{\vec{k}}^0 - \hbar\omega) \quad (23.49)$$

$$= \frac{m^3}{4\pi^2 \hbar^4 K^3} (\omega^{\text{high}} - \omega)(\omega - \omega^{\text{low}}) \quad \sigma \text{ vanishes for } \omega > \omega^{\text{high}} \text{ and } \omega < \omega^{\text{low}}. \quad (23.50)$$

with

$$\omega^{\text{high}} = \frac{\hbar^2 K(K + 2k_F)}{2\hbar m} \quad \omega^{\text{low}} = \frac{\hbar^2 K(K - 2k_F)}{2\hbar m}. \quad (23.51)$$

Figure 23.7 shows experimental measurements of absorption in the alkali metals. The onset of absorption is in accord with the theoretical results, and it can be used to estimate the size of the pseudopotential $U_{\vec{K}}$, as shown in Problem 2.

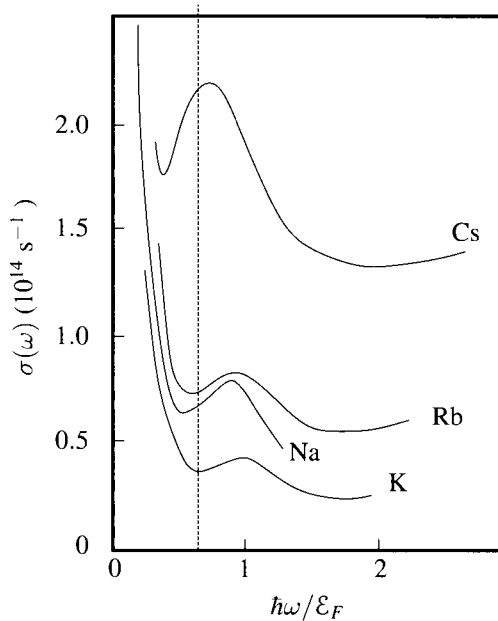


Figure 23.7. Optical absorption of alkali metals, showing quadratic peak due to onset of interband absorption. The minimum in absorption at ω^{high} lies at higher frequencies than those shown and it would likely be masked by transitions between additional bands. [Source: Smith (1970), p. 3664.]

Noble Metals. The noble metals differ from the alkalis because the filled d band lies comparatively close to the Fermi surface, as shown in Figure 10.7. This fact has two consequences. First, it means that in the frequency range where the dielectric constant is dominated by the s electrons, ϵ^∞ is quite large, on the order of 7, because the d electrons provide a highly polarizable environment, roughly as depicted in Figure 20.4. Second, the first interband transitions are not between electrons at the Fermi surface and unoccupied bands above. Instead, the lowest-energy jumps are between the d bands and the Fermi surface, as predicted by Figure 10.7(A). Experimental measurements of absorption in the three noble metals appear in Figure 23.8, showing that absorption begins at the expected frequencies.

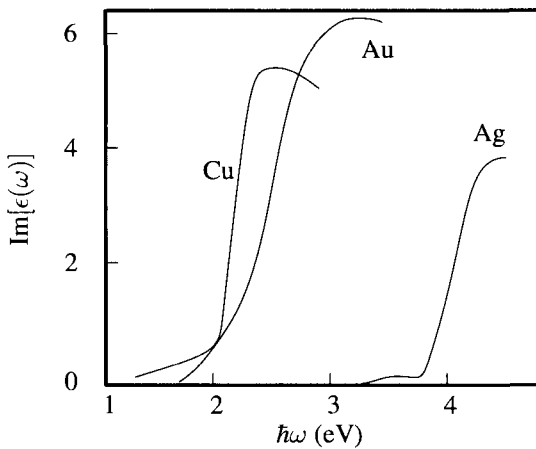


Figure 23.8. Imaginary part of the dielectric constant measured for copper, silver and gold. The absorption edge occurs close to the energy of around 2 eV predicted for copper in Figure 10.7(A), although it is not completely sharp. [Data of Thèye (1968), published by Abelès (1972) p. 138.]

23.5 Brillouin and Raman Scattering

Electromagnetic waves impinging upon samples have so far been presumed to pass through with their frequency unchanged. Brillouin (1922) proposed that photons entering a sample with energy $\hbar\omega_0$ could leave with energy $\hbar(\omega_0 - \omega_1)$ if an excitation of energy $\hbar\omega_1$ were created in the process. Raman (1928) was the first to measure this phenomenon directly. The excitations responsible for changing the frequency of light can be phonons, magnons, or any of the more elaborate quasi-particles such as excitons or polaritons.

Just as for inelastic neutron scattering, two conservation laws control the inelastic scattering of light, and photons can either lose or gain energy depending upon whether an excitation is created or destroyed. Conservation of energy obviously requires that the energy change of the excitation match the energy change of the light. In the case where an excitation is created, conservation of crystal momentum requires that

$$\vec{k}_f = \vec{k}_0 - \vec{k}_1. \quad \begin{array}{l} \vec{k}_f \text{ is the final wave vector of the light, } \vec{k}_0 \text{ is the} \\ \text{initial wave vector, and } \vec{k}_1 \text{ is the wave vector of} \\ \text{the excitation.} \end{array} \quad (23.52)$$

In a medium with index of refraction \bar{n} , light obeys the dispersion relation $\omega = ck/\bar{n}$, so the two conservation laws can be combined to read

$$\frac{c}{\bar{n}}(k_f - k_0) = \mp \omega_1 \left(\mp (\vec{k}_f - \vec{k}_0) \right). \quad (23.53)$$

The minus sign creates an excitation, while the positive sign destroys one. $\omega_1(\vec{k})$ is the dispersion relation of the excitation. Compare with Eq. (13.93).

Light whose frequency is reduced is *Stokes scattered light*, while light whose frequency increases is *anti-Stokes scattered light*, and the frequency change is called the *Raman shift*.

Brillouin's theory concerned the scattering of light from sound waves, so when inelastic light scattering creates and destroys acoustic phonons it is known as *Brillouin scattering*, while Raman's experiments involved optical phonons, and inelastic scattering from these excitations is called *Raman scattering*. Because of the high photon fluxes available from synchrotrons, X-rays can be employed as well as visible light, leading to the technique of *inelastic X-ray scattering*.

Referring to Figure 20.1, the wave number of visible photons is several orders of magnitude smaller than the wave number of phonons near the zone edge. For this reason, Raman and Brillouin scattering are only able to look at phonons near the zone center. Inelastic X-ray scattering, however, is able to explore phonon dispersion relations through the entire Brillouin zone.

23.5.1 Brillouin Scattering

In the case of acoustic phonons,

$$\omega_1 = c_p k. \quad c_p \text{ is the sound speed of a transverse or longitudinal phonon.} \quad (23.54)$$

Adopting the case of Stokes scattering—the minus sign in Eq. (23.53)—and taking θ to be the angle between incoming and outgoing light, one has

$$(k_f - k_0) = -\frac{\bar{n}c_p}{c} \sqrt{k_f^2 + k_0^2 - 2k_f k_0 \cos \theta} \quad (23.55)$$

$$\Rightarrow k_0 - k_f \approx k_0 \frac{2\bar{n}c_p}{c} \sqrt{\frac{1 - \cos \theta}{2}}. \quad \text{Because } c_p/c \ll 1, k_f \text{ and } k_0 \text{ can be set equal to leading approximation on the right-hand side.} \quad (23.56)$$

$$\Rightarrow \omega_0 - \omega_f = \frac{2\bar{n}\omega_0 c_p}{c} \sin \theta / 2 \quad (23.57)$$

The data shown in Figure 23.9 show Brillouin scattering from longitudinal and transverse phonons in germanium. The phonon frequencies were already known from acoustic measurements, so the data were used to extract the complex dielectric constant \tilde{n} of germanium, with the width of the peaks providing a measure of the extinction coefficient κ .

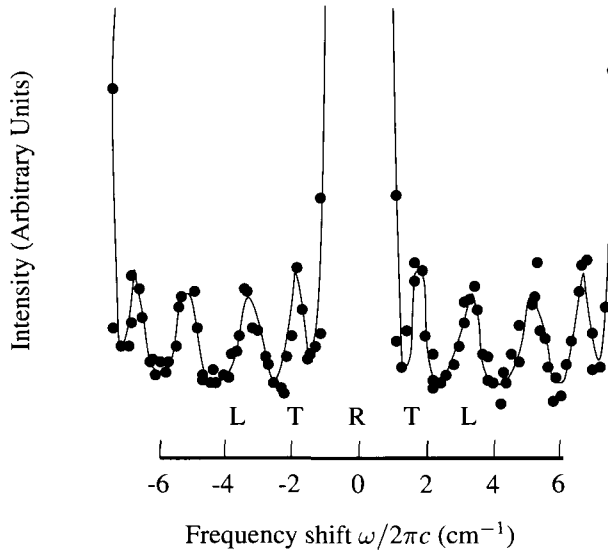


Figure 23.9. Brillouin scattering from the (111) surface of germanium around a wavelength of 6328 Å. The transverse (T) and longitudinal (L) frequencies, as well as multiples of the longitudinal and transverse phonon frequencies due to multiple phonon absorption or emission are visible around the central Rayleigh (R) peak. [Source: Sandercock (1972), p. 239.]

23.5.2 Raman Scattering

In scattering off optical phonons, the frequency ω_1 is nearly constant near the zone center; Raman scattering is frequently used to determine this constant. A more elaborate use of the technique is the measurement of the polariton dispersion relation shown in Figure 23.10. Because large variations in this dispersion relation occur for very small wave numbers, Raman scattering has an advantage over neutron scattering in this situation.

23.5.3 Inelastic X-Ray Scattering

The feasibility of using inelastic X-ray scattering to measure phonon spectra was demonstrated by Dörner et al. (1987), and their measurements of the phonon dispersion relation of beryllium appear in Figure 23.11.

23.6 Photoemission

23.6.1 Measurement of Work Functions

As photon energies rise toward 4 eV, a new sort of transition becomes possible, one in which a photon not only excites an electron to a higher energy band, but ejects it from the sample altogether. The physics governing the ejection of electrons by photons is essentially the same that governs ejection by elevated temperature, as in the Richardson–Dushman equation, Eq. (19.8). Because a photon of frequency ω

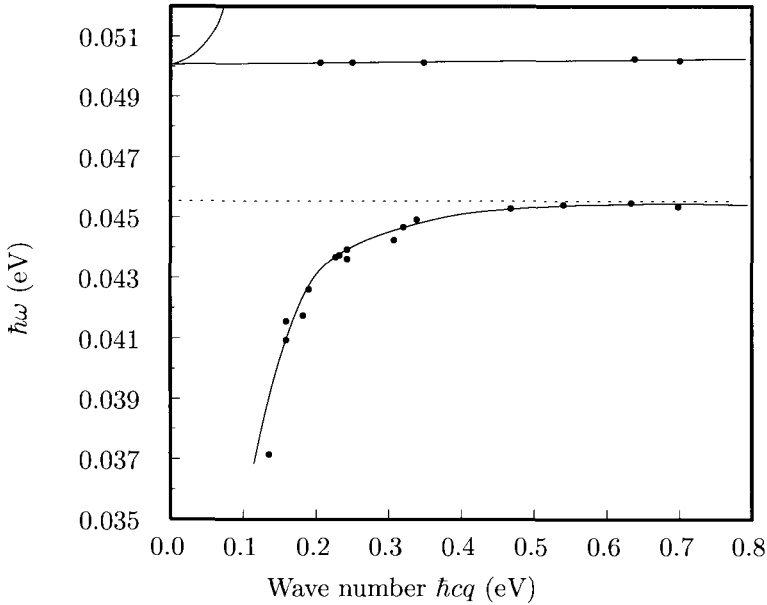


Figure 23.10. Dispersion relation of polaritons in GaP measured with Raman scattering. The data are taken in (100) and (111) directions, and also in polycrystals. To scan through the dispersion relation, one frequency of incoming laser light was used, but outgoing light intensity was measured as a function of energy for a range of angles θ . Compare with Figure 22.5, where a similar dispersion relation was obtained indirectly from absorption measurements. [Source: Henry and Hopfield (1965), p. 965.]

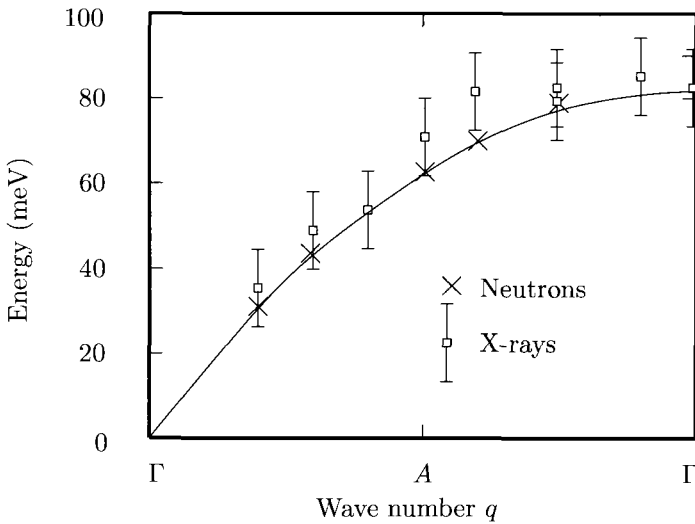


Figure 23.11. Dispersion relation of longitudinal phonons in beryllium along the c axis, comparing inelastic X-ray scattering with neutron scattering. Prior to this experiment, such measurements with X-rays had been thought impractical; the situation changed because of the large photon flux possible at a synchrotron. [Source: Dorner et al. (1987), p. 182.]

can supply energy $\hbar\omega$ to an electron, the effect of light upon a sample is to reduce the work function to $\phi - \hbar\omega$, and when $\hbar\omega > \phi$, electrons are free to flow out, in proportion to the incoming photon density. A plot of photoelectron current versus photon energy appears in Figure 23.12, and a table of work functions measured in this way appears in Table 23.2.

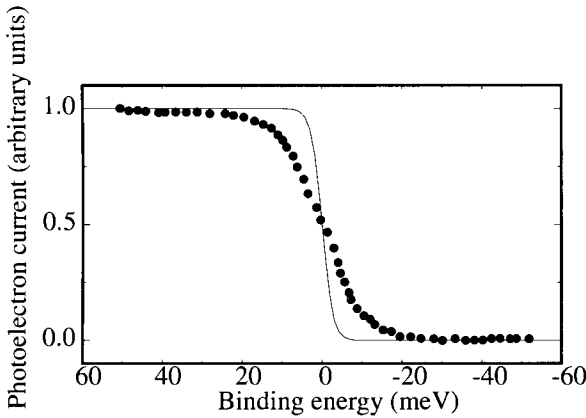


Figure 23.12. Electron current versus photon energy relative to energy of work function of silver at 15 K. The measurement is sensitive enough that the profile of the Fermi function is visible. The data are somewhat broader than the appropriate Fermi function; the deviation is a measure of divergences in the experimental system from the one-electron picture. [Source: Patthey et al. (1990), p. 8872.]

Table 23.2. Work functions of selected metals and compounds

Compound	Surface	ϕ (eV)	Compound	Surface	ϕ (eV)
Ag	(100)	4.64	Na	(110)	2.9
	(110)	4.52	Nb	(100)	4.02
	(111)	4.74		(110)	4.87
Al	(100)	4.20	(111)	4.36	
	(110)	4.06	Ni	(100)	5.22
	(111)	4.26		(110)	5.04
Au	(100)	5.47	(111)	5.35	
	(110)	5.37	Pt	(100)	5.84
	(111)	5.31		Si	(111) 2×1
Be	(0001)	5.1	(111) 7×7	4.50	
Cu	(100)	5.10	(100) 2×1	4.87	
	(110)	4.48	W	(100)	4.63
	(111)	4.94		(110)	5.25
Fe	(100)	4.67	(111)	4.47	
Ge	(111) 2×1	4.68	SiC	(0001)	4.6
	(111) 2×8	4.53	AlN	(100)	5.35
K	(110)	2.39	GaAs	(110)	5.56
Mg	(100)	3.71	GaSb	(110)	4.91
Mo	(100)	4.53	InP	(110)	5.85
	(110)	4.95			
	(111)	4.55			

Values are obtained mainly by photoemission, but also from thermal emission using Eq. (19.9), and by measuring currents emitted under strong electric fields. Source: Landolt and Börnstein (New Series) vol. 17 and Hölzl and Schulte (1979), p. 86.

23.6.2 Angle-Resolved Photoemission

Because of the close association of photoemission experiments with the work function and because the work function is connected with transitions between solid and vacuum, for a long time it was thought that photoemission could measure only properties of solid surfaces. It can be used very effectively for that purpose, but has even more important application in measuring bulk energy bands. *Angle-resolved photoemission spectroscopy* (ARPES) has become the most important experimental tool for probing the electronic properties of solids, and makes it possible to map out energy bands directly.

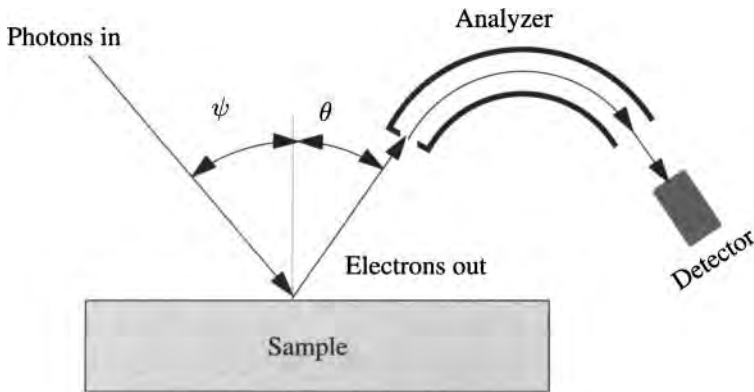


Figure 23.13. Schematic view of angle-resolved photoemission experiment. Photons are incident upon a surface at angle ψ , and electrons are collected at angle θ . Passing the electrons through a curved chamber with an electric field that sends the electrons in a curved path, only those in a narrow range of kinetic energies survive to impact upon the detector. Varying the electric field allows a measurement of photoelectron current as a function of kinetic energy.

A schematic view of the experiment is presented in Figure 23.13. Photons are directed toward the surface of a sample at an angle ψ , electrons emitted along angle θ are collected, and the amplitude of the photocurrent is measured as a function of the electrons' kinetic energy. There is a wide range of variables to vary; the angles of incoming photons and outgoing electrons, the energies of the incoming photons and outgoing electrons, and the Miller index of the crystal surface. A single experiment will rarely vary all of these, and a characteristic set of data appears in Figure 23.14, where both electrons and photons travel normal to the crystal, and photocurrent is measured versus final electron energy for a range of incident photon energies.

To understand the significance of this technique, it is useful to make a comparison with two other types of experiment, optical absorption, and neutron scattering. According to Eq. (20.70), optical absorption is produced by sums over electron transitions between a ground state and all final states compatible with energy conservation. Angle-resolved photoemission breaks the sum into constitutive components by finding the transition rate to states where an outgoing electron has known

energy and momentum. Ideally one would like to think of the experiment as being entirely analogous to neutron scattering, with the photon taking the place of the incoming neutron, while the outgoing electron takes the place of the outgoing neutron. Just as neutron scattering contained enough information to obtain phonon dispersion relations, angle-resolved photoemission should contain enough information to obtain electron band dispersion relations. In the spirit of Section 13.4.1, one can write down the consequences of energy and momentum conservation. Energy conservation demands

$$\phi + \mathcal{E}_{\text{kin}} - (-\mathcal{E}_B) = \hbar\omega, \quad (23.58)$$

where \mathcal{E}_B , the *binding energy* is the negative of the electron's energy before impact by the photon, and $\phi + \mathcal{E}_{\text{kin}}$, work function plus kinetic energy, is its energy after being ejected. Because photon momentum is negligible, crystal momentum conservation would demand that the final wave vector \vec{k}_f of the ejected electron be equal to its initial wave vector up to the inevitable addition or subtraction of a reciprocal lattice vector so as to lie in the first Brillouin zone. So Eq. (23.58) would become

$$\mathcal{E}_B(\vec{k}_{\text{final}}) = \hbar\omega - \phi - \mathcal{E}_{\text{kin}}, \quad \text{Map } \vec{k}_f \text{ back into the first Brillouin zone if necessary.} \quad (23.59)$$

and energy levels $\mathcal{E}_B(\vec{k}_{\text{final}})$ could be mapped out as a function of \vec{k}_{final} . In fact this is almost exactly how the experiments are interpreted, but there are considerable grounds for worry. The old view that photoemission should be tremendously sensitive to the surface was not all wrong, and the difficulty manifests itself in the fact that momentum of the electron in the direction perpendicular to the sample surface has no reason to be conserved. Right at the onset of photoemission this claim is very easy to understand. A photon travels into the sample and transfers energy to an electron that most likely already has some momentum $\hbar k_{\perp}$ in the direction of the surface. On its way out of the sample the electron decelerates, and finally emerges with almost no momentum at all, so $\hbar k_{\perp}$ is certainly not conserved. Momentum parallel to the sample surface is conserved because the symmetry that produces the conservation law still holds; the system remains invariant when translated through a lattice vector parallel to the surface. It clearly does not remain invariant when displaced perpendicular to the surface, so the conservation law in this direction is lost.

In principle the missing information about the original momentum of the electron can be recovered by conducting experiments with different crystal surfaces, and then combining the information from the multiple experiments. While such experiments have been done, there is an easier solution in practice. A classical particle passing rapidly through a short-ranged force loses very little momentum. To be more precise, a particle traveling along \hat{x} through a potential that varies by amount ΔU in a short distance experiences a change in momentum

$$\Delta p = \int -\frac{\partial U}{\partial x} dt \approx -\frac{\Delta U}{v}, \quad \text{Assuming that the velocity } v \text{ can be taken nearly constant.} \quad (23.60)$$

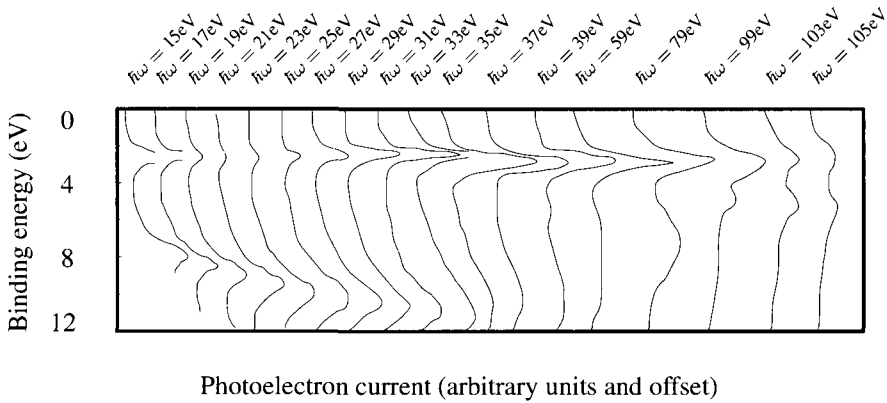


Figure 23.14. Characteristic raw data from a photoemission experiment, for photon injection and electron emission in beryllium along [0001]. The curves show photoelectron current as a function of energy for a large number of photon energies $\hbar\omega$. The curves are offset from one another horizontally so as all to be visible. The upper peak, with a binding energy of around 2.5 eV is independent of incident photon energy and is therefore likely to be a surface state. The lower peak is dispersive, and likely to correspond to a bulk band. [Source: Jensen et al. (1984), p. 5502.]

where v is its velocity, so the faster the particle moves the less momentum it loses. For this reason, angle-resolved photoemission spectroscopy is carried out with photons in the range of 10–1000 eV (*ultraviolet photoemission spectroscopy*, UPS) or above 1000 eV (*X-ray photoelectron spectroscopy*, XPS). A bit of uncertainty about k_{\perp} remains, but can be resolved by identifying critical points where $\partial\mathcal{E}_B/\partial k$ vanishes and changes sign with zone edges.

Example: Beryllium. Radiation at the necessary frequencies and intensities became available with the advent of the synchrotron. Figure 23.14 illustrates the type of data that photoemission provides. Photons impact a beryllium surface along [0001], and electrons are detected returning in the same direction and sorted as a function of their kinetic energy. There are two separate bands visible in the figure. The upper one is nondispersive; the binding energy is independent of the incoming photon energy. Frequently, such nondispersive bands are surface states. The initial momentum $\hbar\vec{k}_{\perp}$ perpendicular to the surface is guaranteed to be zero, and the momenta \vec{k}_{\parallel} parallel to the surface can be measured without uncertainty (they too are zero in the present case). So the upper band is simply reporting the energy of a surface state at $\vec{k} = 0$. The lower band is dispersive, and therefore it results from a bulk electron energy band. To a first approximation, one can assume that the final momentum of the electron equals $\hbar\vec{k}_{\perp}$, but in addition there are clues within the data that help improve upon this approximation. Notice that the lower band has maxima and minima. They should correspond to cases where k_{\perp} reaches points of symmetry in the Brillouin zone. Referring to Figure 7.10, the minimum at $\hbar\omega = 35$ eV is point A, while the maximum at around 103 eV is probably Γ . In this fashion the data provide a direct measurement of $\mathcal{E}_{n\vec{k}}$ as a function of \vec{k} .

Semiconductors. Some of the most careful studies of this type have been carried out to investigate the band structures of silicon, germanium, and gallium arsenide. Figures 23.15 and 23.16 show theoretically computed band structures compared with photoemission data. In addition to mapping out bands below the Fermi surface, *inverse photoemission* can be used to map out bands above the Fermi surface. Inverse photoemission consists in passing electrons of known energy into a sample, and measuring the ejected photons. The electrons must go into unoccupied states, which is why the information provided by inverse photoemission is complementary to the information given by photoemission.

The theoretical band structures are best viewed as collaborations between theory and experiment. In order to ensure that band gaps agree with experiment, innovative terms carrying information about electron–electron interaction are added to the calculations. The band structures assembled in Section 10.4 already represent complicated calculations, but the one in Figures 23.16 and 23.15 are even more difficult to reproduce. The validation of the one-electron picture of electronic structure is nevertheless remarkable. The one-electron approximation has real experimental meaning, and electronic excitations of the solid behave as theory says they should.

There are many interesting complications associated with the interpretation of photoemission spectra. The intensity peaks always have a width of several electron volts, a width that is considerably greater than experimental resolution. The width is a result of *many-body effects*—that is, the scattering of electrons off of

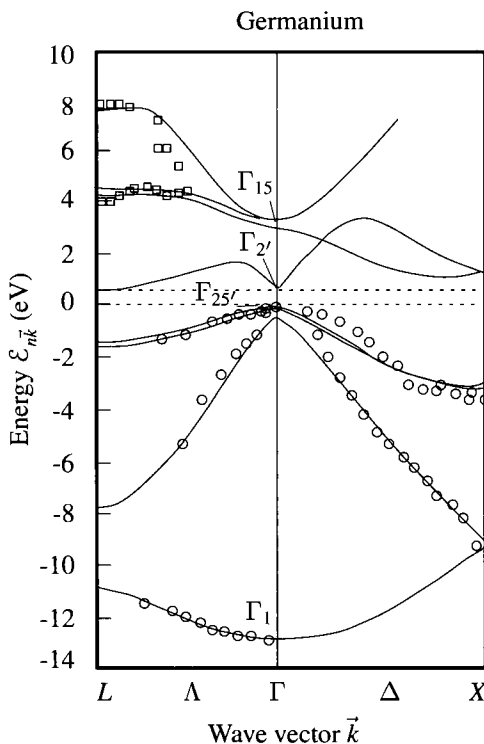


Figure 23.15. Theoretical energy bands of germanium compared with direct and inverse photoemission data. The theoretical calculations are due to Louie (1992), p. 79; they consist of density functional calculations supplemented with information from the theory of electron interaction. The photoemission experiments are due to Wachs et al. (1985) and Straub et al. (1986).

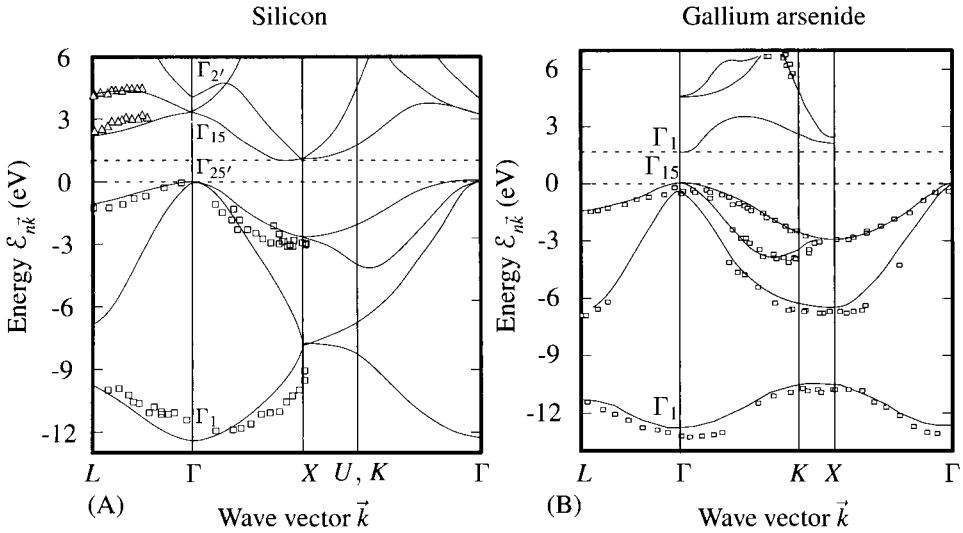


Figure 23.16. (A) Theoretical energy bands of silicon calculated with semiempirical pseudopotentials by Chelikowsky and Cohen (1976) compared with photoemission studies of Straub et al. (1986) and Rich et al. (1989). Notation for the symmetries of wave functions along Γ given in Table 7.4. (B) Theoretical energy bands of gallium arsenide calculated with semiempirical pseudopotentials by Pandey and Phillips (1974) compared with photoemission studies of Chiang et al. (1980) and Williams et al. (1986).

one another and the resulting decay of the single-particle states. There is much formalism to deal with this problem, but it is not easy to get practical information out of it. Matters are further complicated by the fact that interactions between surface and bulk states can move peaks around in a manner that falls outside the simple description used here.

23.6.3 Core-Level Photoemission and Charge-Transfer Insulators

Core-level photoemission is a curiously indirect technique. The incoming photons are much more energetic than in the photoemission experiments described so far, with typical photon energies on the order of 1000 eV, which places them in the X-ray range and giving the method also the name *X-ray photoelectron spectroscopy*. The requirement of a powerful coherent source of X-rays means that experiments of this type did not become possible before the availability of synchrotron radiation (Section 3.4.2.) The photons enter the atom, bypass the valence electrons, and knock out a core electron whose binding energy is approximately equal to that of the incoming photon. Nevertheless, the experiment is not conducted in the expectation of learning anything about the core electrons. Valence electrons still provide the object of study. Knocking out a core electron has the effect of suddenly adding a positive charge e to the core of an atom, as if an extra proton had somehow been injected into the nucleus, and the interest of the experiment lies in discovering how the valence electrons nearby will respond. The spatially localized nature of the per-

turbation naturally leads to information about the solid with a localized character. The type of information that can be extracted and the way it is interpreted is best illustrated with a particular example.

Transition Metal Oxides. Even during the first days that the single-electron band theory of solids was being constructed, it was realized that there existed solids that violated its predictions in a qualitative way. The prototypical example is NiO, as discussed by Mott (1949). The transition metal oxides, from VO through ZnO, have many features in common. Most of them adopt the NaCl structure (Figure 2.7). Density functional theory predicts them to be metals. In fact, they are all insulators, with an optical band gap of 1–4 eV, and all antiferromagnetic (Figures 3.14 and 24.6). The difficulty presented by these compounds is particularly evident for VO, MnO, and CoO, which have an odd number of electrons in each unit cell. The valence bands are not filled, so one can state with certainty in the single-electron approximation that they must be metals. Optical absorption of CoO appears in Figure 23.17, which clearly shows an optical gap of 4 eV. In the case of TiO, CrO, Fe, and NiO, the number of electrons per unit cell is even, so these compounds could in principle be insulators. However, the valence bands are built from the $3d4s$ shells, which, after lending two electrons to form O^{-II} , are incomplete. Detailed calculations almost always find these compounds to be metals. Density functional calculations for NiO do find it to be insulating once antiferromagnetic ground states are explored, but the calculated gap is much smaller than the one measured experimentally.

Among these transition metal compounds, CuO is both the most complicated and the most interesting. It stands alone in adopting a complicated crystal structure, which is monoclinic, and has four coppers and four oxygens in each unit cell, as shown in Figure 23.18. Density functional calculations of Ching et al. (1989)

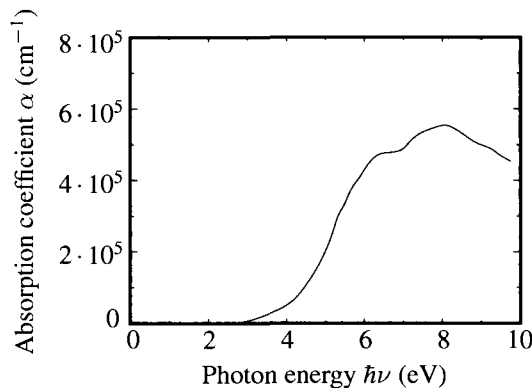


Figure 23.17. Optical absorption of CoO. The first traces of absorption appear at 3 eV, but these are attributed either to impurities or to excitonic effects. The steep linear rise, which extrapolates back to zero absorption at 4 eV, is thought to be more significant, and therefore the optical gap of CoO is conventionally said to be 4 eV. [Source: Powell and Spicer (1970), p. 2188.]

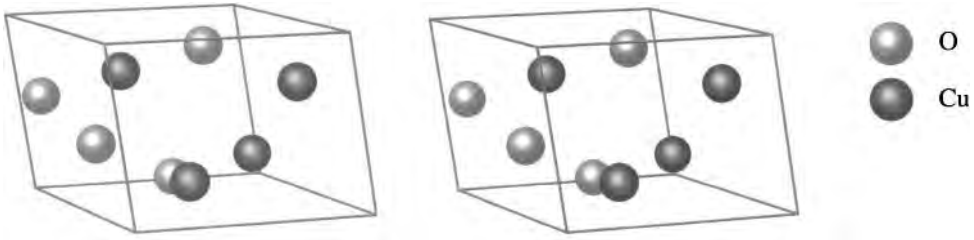


Figure 23.18. The structure of CuO, as determined by Åsbrink and Norrby (1970). The monoclinic unit cell contains 4 oxygens and 4 coppers. Stereo pair.

unambiguously predict CuO to be metallic, but in fact it is a semiconductor with a gap of 1.4 eV.

A great deal of research has been devoted to the transition metal oxides without resolving the essential difficulty. The general belief is that band theory fails because the d electrons are rather closely localized on the nickel atoms, and the density functional approximation underestimates the consequences of Coulomb repulsion between them. Copper oxide is on the insulating side of the metal–insulator transitions discussed in Section 18.3. The qualitative failure of single-electron band theory does not mean that there is no means to predict the results of experiments in CuO. A wide variety of experimental results can be described through the use of simple models to be described below. The use of these simple models is, however, predicated upon the knowledge that CuO is an insulator. They cannot predict that it belongs to the insulating class, nor explain why it does so.

The models used to explain CuO are *local*, which means essentially that they view the solid as a large molecule, where most of the physics can be understood by analyzing a tiny cluster of atoms, and the more remote atoms provide tiny additional perturbations. The starting points of these calculations are the energy levels of isolated copper and oxygen atoms, and they proceed by then considering what happens when the atoms are brought together in pairs. There is no trace of the wide range of propagating states, indexed by \vec{k} , that should characterize a metal.

These observations partially provide an explanation for why such a large number of core-level photoemission studies has been devoted to the transition metal oxides. A probe with a highly localized character is devoted to solids where the excitations have a similarly localized character. X-rays directed at copper are able to eject electrons from the $2p$ core state, which because of the spin–orbit interaction splits into $2p_{1/2}$ and $2p_{3/2}$ levels. In pure copper, the binding energy of $2p_{3/2}$ is $\mathcal{E}_{\text{core}} = 923.3$ eV. In CuO, not one but two peaks are found near this energy, but neither of the peaks has quite the expected energy. The differences in energies between the core binding energy $\mathcal{E}_{\text{core}}$ and the observed peak locations are due to changes in state of the valence electrons, and the fact that extra peaks are observed is due to the existence of multiple metastable valence states.

What are these different valence states? The answer is provided by a phenomenological form of quantum mechanics in which one uses a small number of

matrix elements as free parameters to fit the experimental data, guided mainly by energy levels of isolated atoms. The phenomenology of Fermi liquid theory began with the observation that metals exist, and it supposes that the actual quantum states remain in one-to-one correspondence with quantum states of the free Fermi gas. The logic in the case of CuO is similar, except that now by observing the solid to be an insulator, one makes the supposition that the actual quantum states will be in one-to-one correspondence with states of $\text{Cu}^{\text{II}}\text{O}^{-\text{II}}$ molecules.

Begin by considering quantum states of isolated atoms. Let $|d^{10}\rangle$ and $|d^9\rangle$ be the lowest-energy wave functions of a copper atom with 10 and 9 electrons in the d shell. In its ground state, copper has ten $3d$ electrons and one $4s$ electron, but oxygen is always able to steal at least the $4s$ electron from the copper. Similarly, let $|\text{O}^{-1}\rangle$, and $|\text{O}^{-\text{II}}\rangle$ be oxygen wave functions where the oxygen has acquired one or two extra electrons. A point that particularly needs to be emphasized is that these wave functions are many-electron wave functions. In particular, they take fully into account the energetic penalties that Coulomb repulsion imposes every time an additional electron is added to the atom. In the single-electron picture, adding two electrons of opposite spin to a solid costs the same energy for each, while adding two electrons of opposite spin to an atom can never act in that way.

Supposing these wave functions to be known, pass now to the CuO solid, but focus down on just a single adjoining copper and oxygen pair. Guess that the quantum states of the solid relevant for core-level photoemission are in one-to-one correspondence with quantum states of this molecule, and that the quantum states of the molecule can be constructed from linear combinations of the atomic wave functions. Considering only the wave functions where the total valence charge shared between copper and oxygen is conserved at 11 electrons, there are two states, $|d^9\text{O}^{-\text{II}}\rangle$ and $|d^{10}\text{O}^{-1}\rangle$. Let $\hat{\mathcal{H}}$ be the Hamiltonian for the cupric oxide solid, and take the expectation values of the Hamiltonian in these states to be

$$\langle d^9\text{O}^{-\text{II}}|\hat{\mathcal{H}}|d^9\text{O}^{-\text{II}}\rangle \equiv 0 \quad \begin{array}{l} \text{Energies are always arbitrary up to an} \\ \text{overall constant, so set this one to zero,} \\ \text{corresponding to the ground-state} \\ \text{energy of copper oxide.} \end{array} \quad (23.61a)$$

$$\langle d^{10}\text{O}^{-1}|\hat{\mathcal{H}}|d^{10}\text{O}^{-1}\rangle \equiv \Delta. \quad \text{Charge transfer energy.} \quad (23.61b)$$

The matrix element in Eq. (23.61b) is the *charge transfer energy*, the energy cost involved in moving an electron from oxygen to copper. Denote the off-diagonal component of $\hat{\mathcal{H}}$ in these states by

$$\langle d^9\text{O}^{-\text{II}}|\hat{\mathcal{H}}|d^{10}\text{O}^{-1}\rangle = \langle d^{10}\text{O}^{-1}|\hat{\mathcal{H}}|d^9\text{O}^{-\text{II}}\rangle \equiv T, \quad (23.62)$$

so that the low-energy excitations of CuO are given by the eigenvalues and eigenvectors of the matrix

$$\begin{pmatrix} 0 & T \\ T & \Delta \end{pmatrix}. \quad (23.63)$$

Problem 5 shows that the ground state is

$$|\Psi_{i0}\rangle = \cos \theta_i |d^9\text{O}^{-\text{II}}\rangle - \sin \theta_i |d^{10}\text{O}^{-1}\rangle \quad (23.64a)$$

where

$$\tan 2\theta_i = \frac{2T}{\Delta}. \quad \text{When } T \text{ is much less than } \Delta, \text{ the ground state is almost pure } d^9, \text{ but as } T \text{ and } \Delta \text{ become comparable the two states mix.} \quad (23.64b)$$

Now imagine that an incoming photon knocks a $2p_{3/2}$ electron out of the core of the copper, and construct again the low-lying states of the valence electrons

$$\langle c^I d^9 O^{-II} | \hat{f} | c^I d^9 O^{-II} \rangle \equiv \mathcal{E}_{\text{core}} \quad \begin{array}{l} \text{The energy needed to eject} \\ \text{a core electron.} \end{array} \quad (23.65a)$$

$$\langle c^I d^{10} O^{-I} | \hat{f} | c^I d^{10} O^{-I} \rangle \equiv \mathcal{E}_{\text{core}} + \Delta - U_{cd}. \quad \begin{array}{l} \text{Charge transfer energy} \\ \text{minus attraction to core} \\ \text{hole.} \end{array} \quad (23.65b)$$

The matrix elements of Eq. (23.65) are raised by the energy $\mathcal{E}_{\text{core}}$ needed to eject the core electron. In addition, each electron jumping onto the copper gains an energy U_{cd} through its Coulomb interaction with the positive charge in the core. Therefore U_{cd} displays in the simplest possible way the effect of electron correlation. In the single-electron picture, removing an electron from the core state could not change the relative energies of two other states, it would just shift them together.

Assuming off-diagonal terms of the Hamiltonian to be the same as before implies that valence states in the presence of the core hole are given by diagonalizing the matrix

$$\begin{pmatrix} \mathcal{E}_{\text{core}} & T \\ T & \mathcal{E}_{\text{core}} + \Delta - U_{cd} \end{pmatrix}. \quad (23.66)$$

Denote the eigenstates by

$$|\Psi_{f0}\rangle = \cos \theta_f |c^I d^9 O^{-II}\rangle - \sin \theta_f |c^I d^{10} O^{-I}\rangle \quad (23.67a)$$

$$|\Psi_{f1}\rangle = \sin \theta_f |c^I d^9 O^{-II}\rangle + \cos \theta_f |c^I d^{10} O^{-I}\rangle, \quad (23.67b)$$

where the label f indicates final states of the valence electrons and

$$\tan 2\theta_f = \frac{2T}{\Delta - U_{cd}}. \quad (23.67c)$$

To make use of the eigenvectors obtained from these matrices, consider the calculation of transition rates for the core-level photoemission experiment. The rate at which the process occurs is given by Eq. (20.72). The initial state of the system is given by the lowest-energy eigenstate of (23.63), and the final states are given by the eigenstates of (23.66). The matrix elements needing to be evaluated are

$$\langle c^0 | \hat{P} | c^I \rangle \langle \Psi_{i0} | \Psi_{f0,1} \rangle \quad \begin{array}{l} \text{Because it is the core electron being ejected, the momen-} \\ \text{tum operator acts upon the core electron, not on the va-} \\ \text{lence electrons. The first matrix element places } \hat{P} \text{ in be-} \\ \text{tween core states with and without the ejected electron.} \end{array} \quad (23.68)$$

The energy difference between the two eigenstates in Eq. (23.67) is

$$\Delta \mathcal{E} = \sqrt{(\Delta - U_{cd})^2 + 4T^2}, \quad (23.69)$$

and this energy should correspond to the peak splitting of CuO in Figure 23.19. From Eq. (23.68) one can estimate that the ratio of the heights of the two peaks in

Figure 23.19 should be (Problem 5)

$$\frac{|\langle \Psi_{i0} | \Psi_{f1} \rangle|^2}{|\langle \Psi_{i0} | \Psi_{f0} \rangle|^2} = \tan^2(\theta_i - \theta_f). \quad (23.70)$$

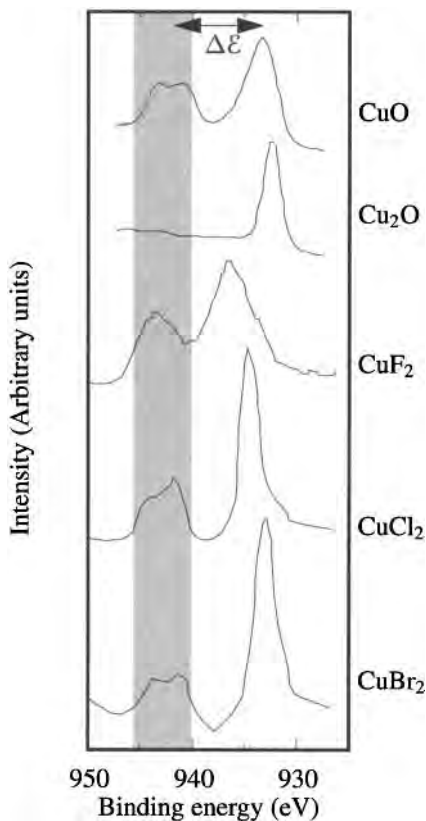


Figure 23.19. Core-level photoemission from CuO, Cu₂O, and copper dihalides, in the vicinity of the $2p_{3/2}$ state. As shown by the gray bar, the satellite line stays fixed for all compounds except Cu₂O, where it is absent, while the main line jumps about. [Source: Ghijssen et al. (1988), p. 11 324 and van der Laan et al. (1981), p. 4371.]

Completing the description of CuO consists in determining the parameters T , Δ , and U_{cd} that specify its low-energy excitations. This task cannot be accomplished through experiments on CuO alone. Core-level photoemission in the vicinity of $2p_{3/2}$ appears in the upper panel of Figure 23.19. Two peaks are visible. But how are they to be identified? For example, how can one tell whether $\langle c^1 d^{10} O^{-1} |$ (d^{10} for short) or $\langle c^1 d^9 O^{-II} |$ (d^9 for short) lies lower in energy? These questions can be answered by comparing core-level photoemission of CuO with core-level spectra of other copper compounds such as Cu₂O and the copper dihalides CuF₂, CuCl₂, and CuBr₂.

Begin by comparing the photoemission intensity of CuO and Cu₂O. The essential difference between these two compounds is that in Cu₂O coppers can satisfy oxygen's longing for two electrons by donating one each from the $4s$ states, leaving the $3d^{10}$ bands intact. Only one peak appears in the photoemission spectrum of Cu₂O, and it must be identified with a predominantly $3d^{10}$ final state of copper. The left-hand peak in all the other compounds must then be identified with a predominantly $3d^9$ final state. In the processes that create the left-hand peak, an

X-ray photon hits a $2p_{3/2}$ core electron of a copper atom whose outer shell is in state $3d^9$, and the outer shell remains in state $3d^9$ as the electron is ejected. This process should be insensitive to the atoms surrounding the copper, and accordingly the energy of this peak changes little as one moves from compound to compound. For the right-hand peak, ejection of the core electron is accompanied by capture of an electron from a neighboring oxygen to form $3d^{10}$. This second process depends upon the interaction with neighbors, and therefore should vary in energy from compound to compound. The rightmost peak in Figure 23.19 does in fact move about in energy more noticeably than the satellite.

Having determined the nature of the peaks in Figure 23.19, there still remains the problem that the three parameters Δ , T , and U_{cd} cannot be determined uniquely from the two equations (23.69) and (23.70). Problem 6 shows how to combine information from the different compounds to provide a plausible solution. Assuming that T and U_{cd} are approximately the same for all compounds while Δ varies, one can determine that $U_{cd} \approx 9$ eV, $T \approx 2.5$ eV, and that for CuO, $\Delta \approx 1.5$ eV.

Problems

1. Qualitative optical properties:

- What is the frequency of electromagnetic radiation at which aluminum should become transparent, according to the Drude theory?
- What is the frequency of electromagnetic radiation at which very pure silicon, at 300 K, should become transparent according to the Drude theory?
- Pure silicon has a silvery mirror-like surface. Provide a qualitative explanation for why it is not transparent.
- Draw a sketch of the absorption coefficient of silicon from $\omega = 0$ up to the visible.

2. Optical absorption of alkali metals: The aim of this problem is to verify Eq. (23.48). The calculation is straightforward, except that expressions such as Eq. (20.70) have a very condensed notation, and it can be confusing to untangle them.

- Verify that Eqs. (23.45) and (23.46) follow from Eq. (8.14) when one focuses upon a single Bragg vector \vec{K} .
- In the present case, one really needs to consider the 12 equivalent vectors $\langle 110 \rangle$. How should Eqs. (23.45) and (23.46) be generalized?
- Show that Eq. (23.47) follows from Eq. (20.70).
- Carry out the integrals needed to verify Eqs. (23.50) and (23.51).
- Find numerical values for ω^{low} and ω^{high} in the case of sodium, in units of Hz, and also evaluate the joint density of states in units of $1/[\text{eV cm}^3]$.

(f) Referring to Figure 23.7, estimate the pseudopotential energy $|U_{\vec{K}}|$ for $\vec{K} = (110)$.

3. **Helicon waves:** Plasma oscillations constitute the sloshing back and forth of a cloud of electrons. In the presence of a static magnetic field, the calculation becomes more complicated. Assume a magnetic field \vec{B}_0 is present in a conducting material, pointing along the \hat{z} axis, and one passes an electromagnetic wave along the same axis. An analog of the purely classical calculation of the plasma frequency may be obtained as follows:

(a) Begin with Maxwell's equations

$$\nabla \times \vec{E} = -\frac{1}{c} \frac{\partial \vec{B}}{\partial t} \quad (23.71)$$

$$\nabla \times \vec{B} = \frac{1}{c} \frac{\partial \vec{E}}{\partial t} + \frac{4\pi}{c} \vec{j}, \quad (23.72)$$

with

$$\vec{j}(\omega) = \sigma(\omega) \vec{E}(\omega). \quad (23.73)$$

Assume that the electric field propagates along the \hat{z} axis as

$$\vec{E} = \vec{E}_0 e^{i\vec{k} \cdot \vec{r} - i\omega t} \quad (23.74)$$

with

$$\vec{k} = (0, 0, k). \quad (23.75)$$

Define

$$k_0 = \frac{\omega}{c}. \quad (23.76)$$

Show first that

$$\vec{k} \times \vec{k} \times \vec{E}_0 + k_0^2 \epsilon \vec{E}_0 = 0 \quad (23.77)$$

and find an expression for the dielectric tensor ϵ in terms of the conductivity tensor σ .

(b) Assuming rotational symmetry around the \hat{z} axis, so that x and y are equivalent, and assuming further that

$$\epsilon_{xz} = \epsilon_{yz} = 0 \quad (23.78)$$

because electrons move in circles in the x - y plane only, show that Eq. (23.77) becomes

$$\left(\frac{k^2}{k_0^2} - \epsilon_+ \right) \left(\frac{k^2}{k_0^2} - \epsilon_- \right) \epsilon_{zz} = 0 \quad (23.79)$$

and find ϵ_+ and ϵ_- in terms of ϵ_{xx} and ϵ_{xy} .

(c) Take

$$\vec{j} = -ne\vec{v} \quad (23.80)$$

and

$$m\dot{\vec{v}} = -e \left[\vec{E} + \frac{\vec{v}}{c} \times \vec{B}_0 \right] - \frac{m\vec{v}}{\tau}. \quad (23.81)$$

Recall that \vec{B}_0 is the static field along the \hat{z} axis. Solve Eqs. (23.73), (23.80), and (23.81) for the dielectric tensor, and as a consequence find the frequency of the helicon modes. You should find along the way that

$$\epsilon_{xx} = 1 - \frac{\omega_p^2}{\omega\tilde{\omega}} \frac{1}{[1 - (\omega_c/\tilde{\omega})^2]}, \quad (23.82)$$

where

$$\omega_c = \frac{eB_0}{mc} \quad (23.83)$$

and

$$\tilde{\omega} = \omega + i/\tau. \quad (23.84)$$

- (d) Find the values of ω_c and ω_p for aluminum in $B_0 = 10^4 G$. For ω comparable to the cyclotron frequency, show that the first term on the right-hand side of Eq. (23.82) can be neglected.
- (e) Find the dispersion relation for helicon waves, and say whether they propagate when ω is less than or greater than the cyclotron frequency

4. Landau damping:

- (a) The susceptibility of an electron gas is given by Eq. (23.33). Argue that χ will acquire an imaginary part when the denominator of Eq. (23.33) can vanish, and find an expression for the smallest value of \vec{q} for which it is possible.
- (b) Evaluate this expression for aluminum

5. Core-level photoemission I:

- (a) Verify Eqs. (23.64) and (23.67).
- (b) Verify Eqs. (23.69) and (23.70).

6. Core-level photoemission II:

- (a) For each of the copper dihalides in Figure 23.19, take T to be a free parameter, and using Eqs. (23.69) and (23.70), plot U_{cd} versus T . Make use of the energy gap $\Delta\mathcal{E}$ and the ratio of peak heights in order to determine Δ as a function of T . Show that the curves intersect for $U_{cd} \approx 9$ eV; therefore, give U_{cd} this value.
- (b) Find Δ for CuO.
- (c) The optical band gap of CuO can now be estimated based upon a property of the matrix (23.63). Decide what calculation should correspond to this physical quantity, and find the optical band gap.

References

- F. Abelès, ed. (1972), *Optical Properties of Solids*, North-Holland, Amsterdam.
- S. Åsbrink and L.-J. Norrby (1970), A refinement of the crystal structure of copper (II) oxide with a discussion of some exceptional e.s.d.'s, *Acta Crystallographica B*, **26**, 8–15.
- L. Brillouin (1922), Scattering of light and X-rays by a transparent homogeneous body: Influence of thermal agitation, *Annales de Physique*, **17**, 88–122. In French.
- J. R. Chelikowsky and M. L. Cohen (1976), Nonlocal pseudopotential calculations for the electronic structure of eleven diamond and zinc-blende semiconductors, *Physical Review B*, **14**, 556–582.
- T.-C. Chiang, J. A. Knapp, M. Aono, and D. E. Eastman (1980), Angle-resolved photoemission, valence-band dispersions $E(k)$, and electron and hole lifetimes for GaAs, *PRB*, **21**, 3513–3522.
- W. Y. Ching, Y.-N. Xu, and K. W. Wong (1989), Ground-state and optical properties of Cu_2O and CuO crystals, *Physical Review B*, **40**, 7684–7695.
- B. Dorner, E. Burkel, T. Illini, and J. Peisl (1987), First measurement of a phonon dispersion curve by inelastic X-ray scattering, *Zeitschrift für Physik B*, **69**, 179–183.
- J. Ghijsen, H. Tjeng, J. van Elp, H. Eskes, J. Westerink, G. A. Sawatzky, and M. T. Czyzyk (1988), Electronic structure of Cu_2 and CuO , *Physical Review B*, **38**, 11 322–11 330.
- M. Glicksman (1971), Plasmas in solids, *Solid State Physics: Advances in Research and Applications*, **26**, 275–427.
- V. Heine (1980), Electronic structure from the point of view of the local atomic environment, *Solid State Physics: Advances in Research and Applications*, **35**, 1–127.
- C. H. Henry and J. J. Hopfield (1965), Raman scattering by polaritons, *Physical Review Letters*, **15**, 964–966.
- F. J. Himpsel and N. V. Smith (1985), Photoelectron spectroscopy, *Physics Today*, **38**(12), 60–66.
- J. Hölzl and F. K. Schulte (1979), Work function of metals, in *Solid Surface Physics*, vol. 85 of *Springer Tracts in Modern Physics*, Springer-Verlag, Berlin.
- S. Hüfner (1994), Electronic structure of NiO and related 3d-transition-metal compounds, *Advances in Physics*, **43**, 183–356.
- E. D. Isaacs and P. M. Platzman (1996), Inelastic X-ray scattering in condensed matter systems, *Physics Today*, **49**(2), 40–45.
- E. Jensen, R. A. Bartynski, T. Gustafsson, E. W. Plummer, M. Y. Chou, M. L. Cohen, and G. B. Hoflund (1984), Angle-resolved photoemission study of the electronic structure of beryllium: Bulk band dispersions and many-electron effects, *Physical Review B*, **30**, 5500–5507.
- C. Kunz (1962), On the angular dependence of characteristic energy loss in Al, Si, Ag, *Zeitschrift für Physik*, **167**, 53–71. In German.
- H. Landolt and R. Börnstein (New Series), *Numerical Data and Functional Relationships in Science and Technology*, New Series, Group III, Springer-Verlag, Berlin.
- W. Lang (1948), Velocity loss of medium speed electrons during passage through thin metal foils, *Optik (Stuttgart)*, **3**, 233–246. In German.
- S. G. Louie (1992), Quasiparticle excitations and photoemission, in *Angle-Resolved Photoemission: Theory and Current Practice*, S. D. Kevan, ed., vol. 74 of *Studies in Surface Science and Catalysis*, pp. 33–98, Elsevier, Amsterdam.
- S. T. Manson and A. F. Starace (1982), Photoelectron angular distributions: Energy dependence for s subshells, *Reviews of Modern Physics*, **54**, 389–405.
- G. Margaritondo (1988), 100 years of photoemission, *Physics Today*, **41**(4), 66–72.
- E. G. McRae (1979), Electronic surface resonances of crystals, *Reviews of Modern Physics*, **51**, 541–568.
- N. F. Mott (1949), The basis of the electron theory of metals with special reference to the transition metals, *Proceedings of the Physical Society (London)*, **62 A**, 416–422.
- K. Ohtaka and Y. Tanabe (1990), Theory of the soft-X-ray edge problem in simple metals: Historical

- survey and recent developments, *Reviews of Modern Physics*, **62**, 929–991.
- K. C. Pandey and J. C. Phillips (1974), Nonlocal pseudopotentials for Ge and GaAs, *Physical Review B*, **9**, 1552–1559.
- F. Patthey, J. M. Imer, W. D. Schneider, H. Beck, Y. Baer, and B. Delly (1990), High-resolution photoemission study of the low-energy excitations in 4*f*-electron systems, *Physical Review B*, **42**, 8864–8881.
- A. B. Pippard (1957), An experimental determination of the Fermi surface in copper, *Philosophical Transactions of the Royal Society of London*, **A250**, 325–357.
- A. B. Pippard (1988), *Magnetoresistance in Metals*, Cambridge University Press, Cambridge.
- P. M. Platzman and P. A. Wolff (1973), *Waves and Interactions in Solid State Plasmas*, Academic Press, New York.
- R. J. Powell and W. E. Spicer (1970), Optical properties of NiO and CoO, *Physical Review B*, **2**, 2182–2193.
- C. V. Raman (1928), A change of wavelength in light scattering, *Nature*, **121**, 619–620.
- D. H. Rich, T. Miller, G. E. Franklin, and T.-C. Chiang (1989), Sb-induced bulk band transitions in Si(111) and Si(001) observed in synchrotron photoemission studies, *Physical Review B*, **39**, 1438–1441.
- G. Ruthemann (1948), Discrete energy loss of medium velocity electrons during passage through thin foils, *Annals of Physics*, **2**, 114–134. In German.
- J. R. Sandercock (1972), Brillouin-scattering measurements on silicon and germanium, *Physical Review Letters*, **28**, 237–240.
- S. E. Schnatterly (1979), Inelastic electron scattering spectroscopy, *Solid State Physics: Advances in Research and Applications*, **34**, 275–358.
- N. V. Smith (1970), Photoemission studies of the alkali metals. ii: Rubidium and cesium, *Physical Review B*, **3**, 3662–3670.
- D. Straub, L. Ley, and F. J. Himpsel (1986), Inverse-photoemission study of unoccupied electronic states in Ge and Si: Bulk energy bands, *Physical Review B*, **33**, 2607–2614.
- M. L. Thèye (1968), Ph.D. thesis, University of Paris VI. In French.
- G. van der Laan, C. Westra, C. Haas, and G. A. Sawatzky (1981), Satellite structure in photoelectron and Auger spectra of copper dihalides, *Physical Review B*, **23**, 4369–4380.
- A. L. Wachs, T. Miller, T. C. Hsieh, A. P. Shapiro, and T.-C. Chiang (1985), Angle-resolved photoemission studies of Ge(111)-(2×8), Ge(111)-(1×1)H, Si(111)-(7×7), and Si(100)-(2×1), *Physical Review B*, **32**, 2326–2333.
- G. P. Williams, F. Cerrina, G. J. Lapeyre, J. R. Anderson, R. J. Smith, and J. Hermanson (1986), Experimental study of the band structure of GaP, GaAs, GaSb, InP, InAs, and InSb, *Physical Review B*, **34**, 5548–5557.

Part VI

MAGNETISM

24. Classical Theories of Magnetism and Ordering

24.1 Introduction

The ancient Greeks knew of the attraction between lodestone and iron; magnets receive brief mention from Plato and Aristotle. Curious statements echo back from antiquity, that “a loadstone rubbed with garlic does not attract iron...” [Gilbert (1600), p. 2], but the practical use of lodestone as a magnetic compass is also quite old, dating at least before 1000 A.D. Unlike electrified amber, a lodestone’s attractive force is permanent, but strangely selective. It attracts iron, but not other metals such as silver or gold. A magnet split in half produces two weaker magnets. And “[a]pply a red-hot iron rod to a magnetized needle and the needle stands still, not turning to the iron; but as soon as the temperature has fallen somewhat it at once turns to it” [Gilbert (1600), p. 107].

If magnetism is the oldest great mystery of solids, it has also remained one of the most difficult to explain. One reason is that the origin of magnetism is relentlessly quantum mechanical. No solid built of charged particles could have magnetic properties in a world completely ruled by classical physics. Most magnetic effects result from quantum-mechanical interactions of electrons with one another, interactions that cannot even be accommodated within the single-electron theory that has dominated study so far. To make matters even more interesting, magnetic ions interact with each other over large distances, and their response to external stimuli tend to be hysteretic and spatially complex. Some of the very simplest questions one can possibly pose in the subject of magnetism are still unsolved.

24.2 Three Views of Magnetism

24.2.1 From Magnetic Moments

The macroscopic theory of magnetic media can begin with the claim that within the solid there lives a population of magnetic moments \vec{M} , whirling loops of charge producing currents according to

$$\vec{j}_{\text{mag}} = c\vec{\nabla} \times \vec{M}. \quad (24.1)$$

When one defines

$$\vec{H} \equiv \vec{B} - 4\pi\vec{M} \quad (24.2)$$

and separates \vec{j}_{mag} from other currents, the second of Eqs. (20.10b) becomes

$$\nabla \times \vec{B} = \frac{4\pi \vec{j}_{\text{mag}}}{c} + \frac{4\pi \vec{j}_{\text{ext}}}{c} + \frac{1}{c} \frac{\partial \vec{D}}{\partial t} \quad \text{Currents are separated into "external" and "magnetic."} \quad (24.3)$$

$$= 4\pi \vec{\nabla} \times \vec{M} + \frac{4\pi \vec{j}_{\text{ext}}}{c} + \frac{1}{c} \frac{\partial \vec{D}}{\partial t} \quad (24.4)$$

$$\Rightarrow \nabla \times \vec{H} = \frac{4\pi \vec{j}_{\text{ext}}}{c} + \frac{1}{c} \frac{\partial \vec{D}}{\partial t}. \quad (24.5)$$

The rest of Maxwell's equations remain unchanged, featuring \vec{B} as before. In a linear magnetic medium, the magnetic induction \vec{B} and magnetic field \vec{H} are related by

$$\vec{B} = \mu \vec{H}, \quad (24.6)$$

where μ is the *magnetic permeability*, and the material is called *paramagnetic* if $\mu > 1$ and *diamagnetic* is $\mu < 1$. The *magnetic susceptibility* is defined to be

$$\chi = \frac{\partial M}{\partial H}. \quad \text{In general, } \chi \text{ is a tensor.} \quad (24.7)$$

When magnetic response is linear, $4\pi\chi = \mu - 1$, so paramagnets have $\chi > 0$, and diamagnets have $\chi < 0$. Because χ is dimensionless in both SI and cgs systems of units, one must be warned that the susceptibility in SI is defined to be 4π greater than the susceptibility in cgs. Unit conversions provide no warning of this convention.

24.2.2 From Conductivity

The magnetic dipole density \vec{M} seems to be a new physical addition to the problem of electromagnetics, but so long as it is linearly related to \vec{B} , it can be derived from a special case of the phenomenology introduced by Eq. (20.11) relating current \vec{j} to electric field \vec{E} . The argument has a weakness, but it is nevertheless interesting to watch magnetism emerge from this point of view. Working in the space of Fourier transform variables \vec{q} and ω , divide the electric field into longitudinal and transverse components according to

$$\vec{E}_L = \frac{\vec{q}(\vec{E} \cdot \vec{q})}{q^2}, \quad \vec{E}_T = \vec{E} - \vec{E}_L. \quad (24.8)$$

Then a medium with magnetic permeability μ is one in which the relation between current and field is

$$\vec{j} = \frac{c^2 q^2}{4\pi i \omega} \left(1 - \frac{1}{\mu}\right) \vec{E}_T \quad (24.9)$$

$$\Rightarrow \frac{\partial \vec{j}}{\partial t} = -\frac{c^2}{4\pi} \left(1 - \frac{1}{\mu}\right) \vec{\nabla} \times \vec{\nabla} \times \vec{E} \quad \begin{array}{l} \text{Reexpressed in real space, using} \\ \text{the identity} \\ \vec{\nabla} \times \vec{\nabla} \times \vec{E} = \vec{\nabla} \vec{\nabla} \cdot \vec{E} - \nabla^2 \vec{E}. \end{array} \quad (24.10)$$

$$= \frac{c}{4\pi} \left(1 - \frac{1}{\mu}\right) \vec{\nabla} \times \frac{\partial \vec{B}}{\partial t} \quad \text{From Eq. (20.10b).} \quad (24.11)$$

$$\Rightarrow \vec{j} = \frac{c}{4\pi} \left(1 - \frac{1}{\mu}\right) \vec{\nabla} \times (\vec{B} - \vec{B}_0) \quad \vec{B}_0 \text{ is a time-independent field.} \quad (24.12)$$

$$\Rightarrow \vec{\nabla} \times \vec{B} = \left(1 - \frac{1}{\mu}\right) \vec{\nabla} \times \vec{B} + \frac{1}{c} \frac{\partial \vec{D}}{\partial t} \quad \text{From Eq. (20.10b), and setting } \vec{B}_0 \text{ to zero; the need to set } \vec{B}_0 \text{ to zero is the technical flaw in this derivation.} \quad (24.13)$$

$$\Rightarrow \vec{\nabla} \times \frac{\vec{B}}{\mu} = \vec{\nabla} \times \vec{H} = \frac{1}{c} \frac{\partial \vec{D}}{\partial t}. \quad (24.14)$$

24.2.3 From a Free Energy

The weakness in deriving Eq. (24.14) from Eq. (24.8) appears in Eq. (24.12); a time-independent magnetic field \vec{B}_0 arises, and it must arbitrarily be set to zero to obtain the conventional form of magnetic response. In addition, the derivation assumes a linear relation between \vec{B} and \vec{H} . The goals of a proper thermodynamic account of magnetism are first to remove this ambiguity, and second to deal with the fact that many important magnetic phenomena are not linear. Without placing magnetism on such a foundation, it is not possible to describe some of the more interesting forms of magnetic response such as formation of ferromagnetic domains, or superconductivity.

Begin by supposing the existence of an energy functional

$$\mathcal{E}\{\vec{B}(\vec{r})\} \quad (24.15)$$

that gives the energy of a magnetic system when the magnetic induction $\vec{B}(\vec{r})$ is specified. In addition to isolated systems, it is often useful to consider a system such as the one sketched in Figure 24.1. A sample is placed within a large box, surrounded by current-carrying wires that constitute its only contact with the external world. The contents of the box do work on the outside world only if an electric field \vec{E} arises. If so, the field does work at a rate $\int d\vec{r} \vec{E} \cdot \vec{j}_{\text{ext}}$; equivalently, the external world does work on the box at the rate

$$\frac{d\mathcal{E}}{dt} = - \int d\vec{r} \vec{E}(\vec{r}) \cdot \vec{j}_{\text{ext}}(\vec{r}). \quad \text{The integral is taken over the box containing both sample and wires. The box needs to be large enough that at its outer edges the interaction between wires and sample has become very small.} \quad (24.16)$$

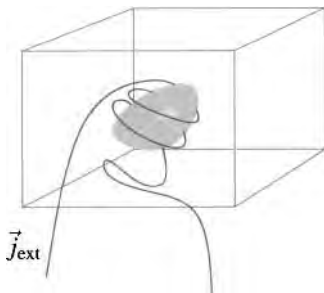


Figure 24.1. A sample is placed within a box and influenced by the outside world only through currents \vec{j}_{ext} that are created by wires passing into the box and that are physically separated from the sample.

Supposing, however, that energy \mathcal{E} as a functional of induction \vec{B} in the box is known, the change in energy can be computed in another way. Define

$$\vec{H}(\vec{r}) = 4\pi \frac{\delta \mathcal{E}\{\vec{B}\}}{\delta \vec{B}(\vec{r})}. \quad \text{See Appendix B for the definition of functional derivatives.} \quad (24.17)$$

Then for any small change in $\vec{B}(\vec{r})$, the change in energy is

$$\delta \mathcal{E} = \frac{1}{4\pi} \int d\vec{r} \vec{H}(\vec{r}) \cdot \delta \vec{B}(\vec{r}). \quad \text{There is no need to assume that } \vec{H} \text{ is a linear function of } \vec{B}. \quad (24.18)$$

In particular,

$$\frac{\partial \mathcal{E}}{\partial t} = \frac{1}{4\pi} \int d\vec{r} \vec{H}(\vec{r}) \cdot \frac{\partial \vec{B}(\vec{r})}{\partial t} \quad (24.19)$$

$$= -\frac{c}{4\pi} \int d\vec{r} \vec{H} \cdot \vec{\nabla} \times \vec{E} \quad (24.20)$$

$$= -\frac{c}{4\pi} \int d\vec{r} \left[\vec{E} \cdot \vec{\nabla} \times \vec{H} - \vec{\nabla} \cdot (\vec{H} \times \vec{E}) \right] \quad \begin{array}{l} \text{Use } \vec{\nabla} \cdot (\vec{A} \times \vec{B}) \\ = (\vec{\nabla} \times \vec{A}) \cdot \vec{B} - (\vec{\nabla} \times \vec{B}) \cdot \vec{A}. \end{array} \quad (24.21)$$

$$= -\frac{c}{4\pi} \int d\vec{r} \vec{E} \cdot \vec{\nabla} \times \vec{H}. \quad \begin{array}{l} \text{The second term of Eq. (24.21) can be converted} \\ \text{to a surface integral of energy radiated out of the} \\ \text{box. For a large enough box, and slow enough} \\ \text{variation of all fields it is negligible.} \end{array} \quad (24.22)$$

Comparing Eqs. (24.22) and (24.16) and requiring them to be equal for arbitrary fields \vec{E} imposes on $\mathcal{E}\{\vec{B}\}$ the constraint

$$\vec{\nabla} \times \vec{H}(\vec{r}) = \frac{4\pi}{c} \vec{j}_{\text{ext}}. \quad (24.23)$$

Although \vec{H} is produced by the external currents, it cannot be computed by pretending the sample to be altogether absent and finding the field that would be produced without it. The sample imposes boundary conditions on this equation, and the solution depends upon them.

From this starting point the rest of magnetostatics can be recovered. The magnetization is defined by

$$\vec{M}(\vec{r}) \equiv \frac{1}{4\pi} \left(\vec{B}(\vec{r}) - \vec{H}(\vec{r}) \right); \quad (24.24)$$

for linear materials the permeability and susceptibility can be defined as before.

Equilibrium States. An isolated system in equilibrium at temperature T and with specified induction $\vec{B}(\vec{r})$ will choose a state that minimizes

$$\mathcal{F}(T, \vec{B}) = \mathcal{E}(\vec{B}) - TS. \quad (24.25)$$

Using Eq. (24.24), changes in the free energy can be written

$$\delta \mathcal{F} = -S \delta T + \int d\vec{r} \vec{H}(\vec{r}) \cdot \delta \vec{M}(\vec{r}) + \frac{1}{8\pi} \int d\vec{r} \delta H^2(\vec{r}). \quad (24.26)$$

If the system is connected to the world by external currents, as in Figure 24.1, \mathcal{F} is no longer the appropriate thermodynamic potential. By altering its magnetization, the system can extract energy from the sources that maintain the current \vec{j}_{ext} fixed. Under these circumstances the thermodynamic potential to minimize is not \mathcal{F} , but instead $\tilde{\mathcal{G}}$, where

$$\tilde{\mathcal{G}} = \mathcal{F} - \frac{1}{4\pi} \int d\vec{r} \vec{B}(\vec{r}) \cdot \vec{H}(\vec{r}). \quad (24.27)$$

A brief calculation to verify this claim is the subject of Problem 3. Small changes in external currents produce changes in $\tilde{\mathcal{G}}$

$$\delta\tilde{\mathcal{G}} = -\frac{1}{4\pi} \int d\vec{r} \vec{B}(\vec{r}) \cdot \delta\vec{H}(\vec{r}) \quad (24.28)$$

$$= -\int d\vec{r} \vec{M}(\vec{r}) \cdot \delta\vec{H}(\vec{r}) - \frac{1}{4\pi} \int d\vec{r} \vec{H}(\vec{r}) \cdot \delta\vec{H}(\vec{r}). \quad (24.29)$$

When the field \vec{H} is employed as an independent variable, then thermodynamic equilibrium is given also by minima of

$$\mathcal{G} = \tilde{\mathcal{G}} + \frac{1}{8\pi} \int d\vec{r} H^2(\vec{r}) \quad (24.30)$$

for which

$$\delta\mathcal{G} = -S\delta T - \int d\vec{r} \vec{M} \cdot \delta\vec{H}. \quad (24.31)$$

The thermodynamic potential \mathcal{G} , which describes an ensemble at fixed temperature T and field \vec{H} , is a common starting point for studies of magnetic systems.

\vec{B} versus \vec{H} . A source of confusion is the question of when to employ \vec{B} and when to employ \vec{H} . There are two competing considerations. As indicated in Eq. (24.23), the source for \vec{H} is external currents. Experiments that control external currents therefore control \vec{H} more directly than \vec{B} , and they are frequently reported in terms of \vec{H} . In particular, for a long thin cylindrical sample with its axis pointing along \vec{B} , Eq. (24.23) implies that no matter how the sample responds to \vec{B} , the field \vec{H} is constant everywhere in space, because the component of H tangential to the surface is continuous, and the normal component vanishes everywhere except at the ends. It is natural in this case to speak of \vec{H} as the experimentally applied field. On the other hand, the microscopic field perceived by nuclei or localized electrons is clearly \vec{B} . Thus experimental results should feature \vec{H} , while microscopic Hamiltonians should employ \vec{B} . The fact that this convention is not standard is probably due to the fact that the magnetic permeability of many metals differs from 1 only by parts in 10^5 (Table 25.4), so that in these materials \vec{B} and \vec{H} are equal for all practical purposes.

24.3 Magnetic Dipole Moments

The magnetic dipole moment density \vec{M} is really just a convenient way of viewing closed loops of current, but it is worth exploring the properties of these dipoles a

bit further to find their energy in external magnetic fields. The magnetic dipole moment of a current distribution can be defined as

$$\vec{m} = \int d\vec{r} \frac{1}{2c} \vec{r} \times \vec{j}(\vec{r}). \quad \text{In order for the magnetic moment to be independent of the choice of origin, the integral of the current over space must vanish.} \quad (24.32)$$

The Lorentz force on any current distribution is

$$\vec{F} = \frac{1}{c} \int d\vec{r} \vec{j}(\vec{r}) \times \vec{B}(\vec{r}). \quad (24.33)$$

If the current distribution \vec{j} forms a closed loop and then vanishes except in the vicinity of some point, say the origin, then it makes sense to expand the magnetic induction \vec{B} as a Taylor series about that point, obtaining

$$\vec{F} = \frac{1}{c} \int d\vec{r} \vec{j}(\vec{r}) \times [\vec{B}(0) + (\vec{r} \cdot \vec{\nabla}) \vec{B}(0) + \dots] \quad (24.34)$$

$$= 0 + (\vec{m} \times \vec{\nabla}) \times \vec{B} \quad \text{See Problem 1 to verify this claim.} \quad (24.35)$$

$$= \vec{\nabla}(\vec{m} \cdot \vec{B}) \quad \text{See Problem 1 to verify this claim.} \quad (24.36)$$

$$\Rightarrow U = -\vec{m} \cdot \vec{B}. \quad U \text{ is the potential energy of the dipole in an external field.} \quad (24.37)$$

According to Eq. (24.37), magnetic dipoles should tend to align along external fields to minimize their energy, and solids should all be paramagnetic. However,

Table 24.1. Susceptibilities of insulating elements near 290 K

Element	χ ($10^{-6} \text{ cm}^3 \text{ mole}^{-1}$)	Element	χ ($10^{-6} \text{ cm}^3 \text{ mole}^{-1}$)
Ar	-19.18	N2	-12.04
As	-5.24	Ne	-7.02
B	-6.70	P	-26.63
C	-5.88	S	-15.39
Cl	-20.18	Se	-23.69
Ge	-7.99	Si	-3.09
H2	-4.00	Te	-37.00
He	-1.88	Tl	-43.42
I	-45.68	Xe	-43.33
Kr	-28.49		

All entries are diamagnetic. The data are in cgs; susceptibilities in SI are defined to be 4π times greater. The recorded values are obtained by dividing the dimensionless susceptibility χ by moles per cm^3 . Source: Landolt and Börnstein (1959), vol. 2, part 9 and Grigoriev and Meilkhov (1997).

the calculation assumes that somehow the current \vec{j} flowing through the dipole remains constant as the dipole orients itself in an external field, and it neglects the work involved in maintaining the current.

In fact, a free charge circling in a magnetic field is diamagnetic. A positively charged particle under the influence of a magnetic field in the positive \hat{z} direction circles in a clockwise direction, and according to Eq. (24.32), or the right-hand rule, it produces a magnetic moment in the negative \hat{z} direction.

Both diamagnetism and paramagnetism are possible because some magnetic moments really are permanent, while others arise only in response to applied fields. The internal current loops of electrons are fixed by quantum mechanics, and they cannot be altered by external fields. Therefore electrons orient their intrinsic magnetic moments in the direction of applied inductions and enhance them, producing paramagnetic behavior with $\mu > 1$. However, placing electrons in a box and considering the magnetic contributions due to their circular orbits in the external fields tends to lead to diamagnetic behavior, $\mu < 1$. Examples of diamagnetic materials appear in Table 24.1.

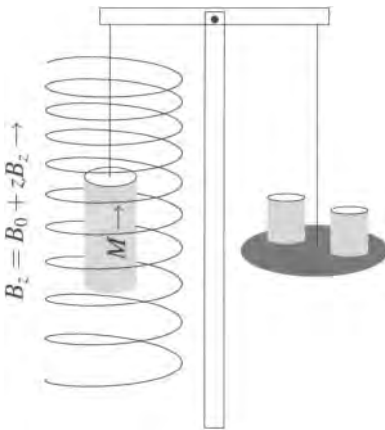


Figure 24.2. Schematic view of Faraday balance. A cylindrical sample is placed within a coil whose windings increase in density to produce a magnetic induction with both constant and linearly increasing components. The resulting force on the sample is measured as a change in its weight.

Experimental Phenomena. Measuring the magnetic properties of materials usually comes down to the ability to make an accurate measurement of magnetic moments, either those that arise in response to an external applied field or those that arise spontaneously. One classic technique is the *Faraday balance*, shown in Figure 24.2. A long cylindrical sample is placed inside a coil where the density of the windings increases linearly in the vertical direction, so that when current flows through the coil it produces a magnetic induction of the form

$$B_z(z) = B_0 + zB_1. \quad \text{The component of the magnetic field in the vertical direction increases linearly in the vertical direction.} \quad (24.38)$$

The constant part of the induction, B_0 , induces a magnetic moment m in the sample, while the gradient in the induction, $dB_z/dz = B_1$, produces a force mB_1 , according to Eq. (24.36).

24.3.1 Spontaneous Magnetization of Ferromagnets

So long as the response of a solid to magnetic fields remains linear, magnetism is captured by Eq. (24.14). Most condensed matter specimens are either diamagnetic or paramagnetic, particularly at elevated temperature. However, the study of magnetism gains new interest when it begins to focus upon a set of spectacular phenomena in which magnetic dipoles take on a life of their own and cannot be described by any function of the instantaneous magnetic field, let alone a linear one.

Below a critical temperature T_c of 1042 K, iron develops a spontaneous magnetization, which rises continuously to a maximum value at very low temperatures. This magnetization can be measured by conventional means, such as the Faraday balance, but it is also possible to measure directly the intense magnetic fields seen at each iron nucleus that are a signature of the magnetic order. Two separate experimental techniques are employed. The first is the Mössbauer effect, and data of this type from which the internal magnetic fields were extracted appeared in Figure 13.20. The second is *nuclear magnetic resonance* (NMR), the analog of electron spin resonance discussed in Section 22.4.3. The magnetic field at the nucleus is deduced by using the known magnetic moment m_I of the nucleus and then searching for resonant absorption of oscillatory radiation when the nucleus is driven between two spin states in a static magnetic field. Because the mass of nuclei is much larger than the mass of electrons, the characteristic frequency for resonant absorption is in the megahertz for nuclei, as opposed to gigahertz for electrons, but the principle of the two resonant absorption experiments is the same. Resulting measurements of the internal field in iron versus temperature appear in Figure 24.3.

The natural unit for discussing magnetic moments is the *Bohr magneton*

$$\mu_B = \frac{e\hbar}{2mc}, \quad (24.39)$$

whose value is

$$\mu_B = 9.27 \cdot 10^{-21} \text{ cm esu} = 9.27 \cdot 10^{-21} \text{ erg G}^{-1}. \quad (24.40)$$

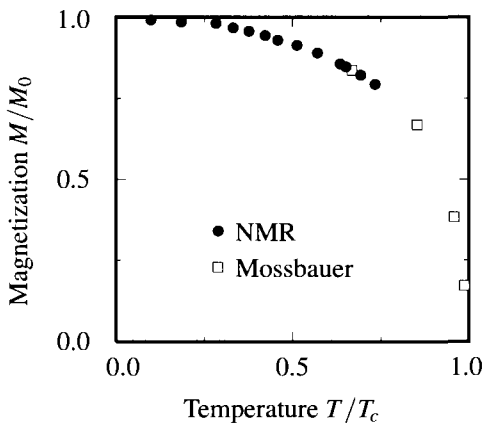


Figure 24.3. Internal magnetic fields in iron, with temperature measured in terms of the Curie temperature $T_c = 1042$ K, and internal fields in terms of their room temperature value H_0 . The magnetization falls off in a similar but not identical fashion, disappearing at the same temperature. [Source: Preston et al. (1962).]

Magnetic moments for selected elements and compounds appear in Table 24.2.

Ferromagnets exhibit a specific heat peak in the vicinity of the critical temperature T_c where ferromagnetism first appears, called the *Curie temperature* and shown in Figure 24.4(A). This peak is characteristic of second-order phase transitions, and will be discussed further in Section 24.6. Above the transition temperature, they are paramagnets with magnetic susceptibility, as shown in Figure 24.4(B) obeying

$$\chi \propto \frac{1}{T - \Theta}; \quad (24.41)$$

Θ is sometimes called the *Curie–Weiss temperature*, and is intended to provide an accurate description of susceptibility at high temperatures. It does not necessarily coincide with the Curie temperature, although the two are always of the same order of magnitude.

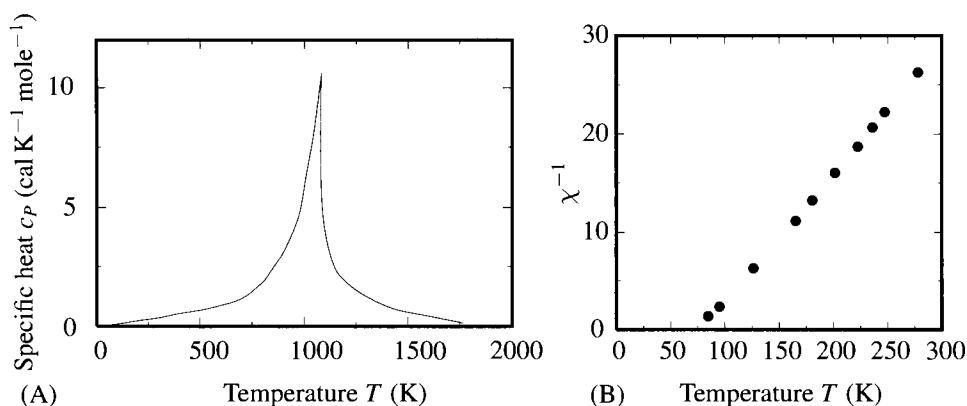


Figure 24.4. (A) Specific heat of iron attributed to magnetic effects in the vicinity of the ferromagnetic transition temperature. [Source: Hofmann et al. (1956) p. 53.] (B) Magnetic susceptibility χ of EuO. $1/\chi$ is plotted and is linear, showing that $\chi \propto 1/(T - T_c)$, and the Curie–Weiss and Curie temperatures coincide. Source: Matthias et al. (1961), p. 160.]

Iron's neighbors in the periodic table, nickel and cobalt, are also ferromagnetic. The outermost electrons of these elements are two $4s$ electrons forming a conduction band. Right below them in energy is an incomplete d shell, the electrons of which group together to produce a large magnetic moment. The interatomic interactions are large enough that the d electrons form a narrow band of mobile electrons, but simultaneously they display features of localized moments. Sections 26.4 and 26.7 will introduce some of the theoretical models used in such cases.

Several of the rare earths are also ferromagnetic, but the localization of the associated moments is more complete, so the difficulties in understanding these elements are less severe than it is for the transition metals.

24.3.2 Ferrimagnets

While the magnetization of iron drops smoothly and continuously to zero as temperature T approaches T_c from below, some rare earth magnets have a more compli-

Table 24.2. Properties of magnetically ordered materials

Compound		T_c (K)	Θ (K)	m_I (μ_B)	Compound		T_c (K)	m_I (μ_B)
Cr	a	312		0.59	FeFe ₂ O ₄	fi	858	4.1
CoO	a	291	-330	3.8	(magnetite)			
CuO	a	230	-745	0.5	FeNiFeO ₄	fi	858	2.3
Mn	a	100		0.5	FeLiFeO ₄	fi	943	2.6
MnO	a	122	-610	5	FeCuFeO ₄	fi	728	1.3
NiO	a	523	-2470	2	FeCoFeO ₄	fi	793	3.7
O ₂	a	23.9		2				
Co	f	1394	1415	1.72				
Dy	f	85	157	10.65				
Eu	f	289	108	7.12				
Fe	f	1043	1100	2.2				
Gd	f	302	289	7.97				
Ho	f	20	87	10.9				
Ni	f	628	650	0.6				
Tb	f	20	87	10.9				

The symbols a and f refer to antiferromagnets and ferromagnets, and the ferrites labeled fi are ferrimagnetic. m_I refers to magnetic moment per atom and is measured in units of the Bohr magneton, $\mu_B = e\hbar/2mc$ [Eq. (24.39)] at 0 K. The rare earth ferromagnets do not become paramagnets at their ferromagnetic Curie temperature, but instead make a transition to antiferromagnetism, and become paramagnets above a second critical temperature. Source: Landolt and Börnstein (1959), vol. 2, part 9, Slick (1980), and Grigoriev and Meilkhov (1997).

cated behavior, shown in Figure 24.5. At a *compensation temperature*, the magnetization reaches zero, but it passes through this value and out the other side before eventually reaching zero for good at T_c . The interpretation of this behavior is that unit cells contain magnetic moments pointing in competing directions, and tending to diminish as temperature increases at different rates. This view is confirmed explicitly by neutron scattering. Materials of this type are called *ferrimagnets*; at the compensation temperature the two moments exactly balance.

The magnets known through the centuries such as magnetite (lodestone) are of this type. The thermodynamics of ferrimagnets is different from that of ferromagnets. In the high-temperature paramagnetic phase, the magnetic susceptibility is observed to behave as

$$\chi = \frac{1}{T + |\Theta|}. \quad \text{That is, ferrimagnets are distinguished by a negative Curie-Weiss temperature.} \quad (24.42)$$

The idea of compensating magnetic moments within each unit cell is due to Néel (1948), and the magnetic transition temperature T_c of ferrimagnets is called the *Néel temperature*.

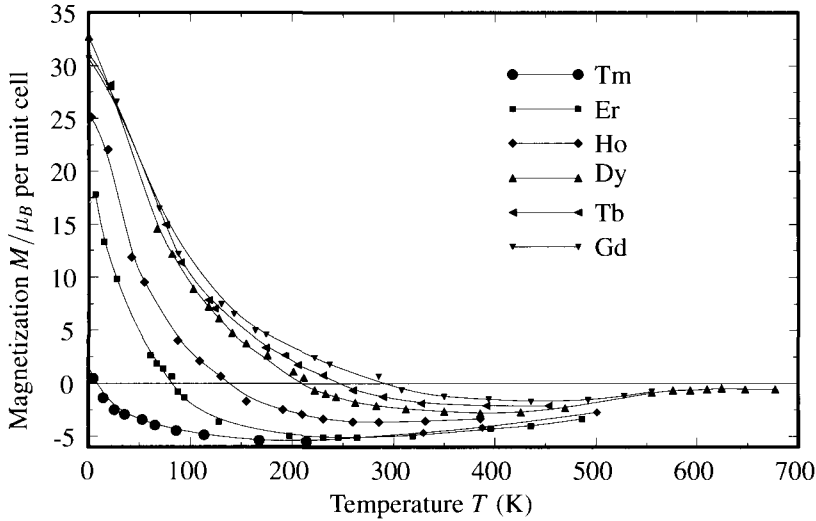


Figure 24.5. Spontaneous magnetization of rare earth iron garnets $5\text{Fe}_2\text{O}_3 \cdot \text{R}_2\text{O}_2$, where R stands for one of the rare earths in the figure. The spontaneous magnetization passes through zero at the compensation temperature, below the temperature where magnetic order disappears altogether. Experiments actually measure only the absolute value of the magnetization; the magnetization is shown negative to make the slope of the magnetization curve continuous. [Source: Bertaut and Pauthenet (1957), p. 262.]

24.3.3 Antiferromagnets

A particular type of ferrimagnet is the *antiferromagnet*, where competing moments within a unit cell cancel each other out entirely. Chromium and manganese are elemental antiferromagnets. The oxides of the transition metals also tend to be antiferromagnets. The existence of antiferromagnets was deduced by Néel on the basis of the temperature dependence of the susceptibility, Eq. (24.42), well before the neutron scattering data in Figure 3.14 revealed extra lines. One possible arrangement of spins in antiferromagnetic compounds is illustrated in Figure 24.6. Magnetic ordering in rare earth alloys can become even more complicated. It is possible to have interesting helical arrangements, also known as *canted*.

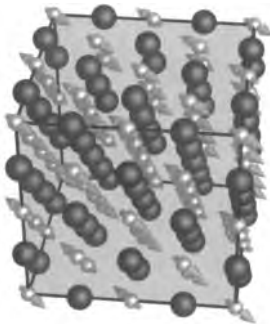


Figure 24.6. Spin structure of transition metal oxides such as CoO or NiO. The structures are determined by neutron scattering, as in Figure 3.14. Spins point along and against $[110]$ directions, and they are aligned within (111) planes.

24.4 Mean Field Theory and the Ising Model

The simplest model of ferromagnetism, of the transition between order and disorder, is the *Ising model*, created by Ising's adviser, Lenz. Consider a collection of spins located at sites on a regular lattice. Ferromagnets tend to be anisotropic; there is an *easy axis* along which the energy is lower than in other directions. In the Ising model, this tendency is taken to extremes, and the spins can point only along this direction, either up or down. The spins are, however, classical and are represented by the integers ± 1 . Neighboring spins interact through a coupling constant J , and the energy of the collection of spins is

$$\mathcal{E} = - \sum_{\langle \vec{R}\vec{R}' \rangle} J \sigma_{\vec{R}} \sigma_{\vec{R}'} - \sum_{\vec{R}} H \mu_B \sigma_{\vec{R}}, \quad (24.43)$$

$\langle \vec{R}\vec{R}' \rangle$ means that one should sum over all distinct nearest-neighbor pairs. The variables $\sigma_{\vec{R}}$ are integers taking values ± 1 . The strength of the interaction with the magnetic field is proportional to the Bohr magneton μ_B .

so the probability of a certain spin configuration at temperature T is

$$\mathcal{P}(\sigma_{\vec{R}}) \propto \exp \left\{ \beta \sum_{\langle \vec{R}\vec{R}' \rangle} J \sigma_{\vec{R}} \sigma_{\vec{R}'} + \beta \sum_{\vec{R}} H \mu_B \sigma_{\vec{R}} \right\}. \quad (24.44)$$

Ising computed the free energy and magnetization of spins obeying Eq. (24.43) for a one-dimensional array. His results were disappointing, for there is no phase transition, and the average magnetization vanishes at all temperatures in the one-dimensional chain. Therefore, following Ising's calculation, the question was still open as to whether statistical mechanics could explain phase transformations. At a conference on statistical mechanics held in 1937, experts were evenly divided when asked to vote on the question, "Does the partition function contain the information necessary to describe a sharp phase transition" [Pais (1982), p. 432]. The matter was settled definitively by Onsager (1944). He found an analytical solution of the two-dimensional version of Ising's model, with a phase transformation between order and disorder at a temperature T_c obeying $\tanh[J/k_B T_c] = \sqrt{2} - 1$. Below this temperature, there is long-range ferromagnetic order, with all spins pointing on average in the same direction. Above this temperature, the average magnetization vanishes. Techniques similar to those found by Onsager have permitted the complete solution of a small number of additional models, discussed by Baxter (1982), but do not, unfortunately, constitute a general approach to ordering problems. For example, it has not proved possible to extend such methods to dimensions higher than two, and the Ising model still has no complete solution in three dimensions.

Mean field theory, first introduced by Weiss (1907), provides a valuable approximate solution to ordering problems. It has the advantage of simplicity and clarity, even accuracy for certain ranges of temperature, despite the disadvantage of producing qualitatively incorrect answers right where the problem becomes most

interesting, in the vicinity of the phase transition. The idea is to replace a system of interacting spins by a single spin sitting in the mean, or average, magnetic field produced by all its neighbors. This average magnetic field is calculated self-consistently by asking what magnetic field the single spin must produce when it sits in a uniform external field and by demanding that the two fields agree. The qualitative error in this calculation is the neglect of correlations. For example, near a phase transition, magnetic spins aggregate into blobs of spins pointing in the same direction, while different blobs point in different ways. The average magnetic field may be zero while simultaneously the chance of a spin and its near neighbors pointing in the same direction is very high. Mean field theory cannot correctly characterize this situation, because if the average field is zero, mean field theory predicts no correlation between a spin and its neighbors.

Formally, mean field theory proceeds by observing that the difficulty in computing a partition function resulting from Eq. (24.43) lies in the products of spins $\sigma_{\vec{R}}\sigma_{\vec{R}'}$, and that the partition function could immediately be summed if only a single power of the spin appeared. Write

$$\sigma_{\vec{R}} = \bar{\sigma} + (\sigma_{\vec{R}} - \bar{\sigma}), \quad \bar{\sigma} \text{ is the average spin.} \tag{24.45}$$

and treat $(\sigma_{\vec{R}} - \bar{\sigma})$ as formally a small quantity. Then, keeping up to first order in this supposedly small quantity, one obtains

$$\sigma_{\vec{R}}\sigma_{\vec{R}'} = [\bar{\sigma} + (\sigma_{\vec{R}} - \bar{\sigma})][\bar{\sigma} + (\sigma_{\vec{R}'} - \bar{\sigma})] \approx \bar{\sigma}(\sigma_{\vec{R}} + \sigma_{\vec{R}'}) - \bar{\sigma}^2. \tag{24.46}$$

Let z , the coordination number, be the number of nearest neighbors with which each spin interacts, and N be the total number of spins. Then

$$- \sum_{\langle \vec{R}\vec{R}' \rangle} J \sigma_{\vec{R}}\sigma_{\vec{R}'} - \sum_{\vec{R}} H \mu_B \sigma_{\vec{R}} \approx NzJ\bar{\sigma}^2/2 - \sum_{\vec{R}} (H + \bar{H}) \mu_B \sigma_{\vec{R}} \tag{24.47}$$

Use Eq. (24.46) for $\sigma_{\vec{R}}\sigma_{\vec{R}'}$. \bar{H} is the mean field seen by each spin, produced by its neighbors. The factor of $1/2$ in the first term comes from the restriction to distinct nearest-neighbor pairs.

with

$$\bar{H} = \frac{zJ\bar{\sigma}}{\mu_B}. \tag{24.48}$$

The partition function Z for the spin system can therefore be written

$$Z \approx \sum_{\sigma_1 \dots \sigma_N} \exp \left[-\beta(NzJ\bar{\sigma}^2/2 - \sum_{\vec{R}} (H + \bar{H}) \mu_B \sigma_{\vec{R}}) \right] \tag{24.49}$$

$$= e^{-\beta NzJ\bar{\sigma}^2/2} \left[\exp[\beta(H + \bar{H})\mu_B] + \exp[-\beta(H + \bar{H})\mu_B] \right]^N \tag{24.50}$$

$$\Rightarrow \mathcal{F} = -k_B T \ln Z = NzJ\bar{\sigma}^2/2 - Nk_B T \ln[2 \cosh \beta \mu_B (H + \bar{H})]. \tag{24.51}$$

To close the mean field theory, one has to determine the mean field \bar{H} , or equivalently the mean spin $\bar{\sigma}$. The mean spin is

$$\bar{\sigma} = \frac{1}{Z} \sum_{\sigma_1 \dots \sigma_N} \frac{1}{N} \sum_{\vec{R}'} \sigma_{\vec{R}'} \exp[-\beta \mathcal{E} \{ \sigma_{\vec{R}} \}] \tag{24.52}$$

$$= \frac{1}{Z} \sum_{\sigma_1 \dots \sigma_N} \frac{1}{\beta N \mu_B} \frac{\partial}{\partial H} \exp[-\beta \mathcal{E} \{ \sigma_{\vec{R}} \}] \quad \text{See Eq. (24.43).} \quad (24.53)$$

$$= -\frac{1}{N} \frac{1}{\mu_B} \frac{\partial \mathcal{F}}{\partial H} \quad \text{Because } \mathcal{F} = -k_B T \ln Z. \quad (24.54)$$

$$= \tanh \beta \mu_B (H + \bar{H}) \quad \text{Employing the approximation of Eq. (24.51).} \quad (24.55)$$

$$\Rightarrow \bar{\sigma} = \tanh \beta [zJ\bar{\sigma} + \mu_B H]. \quad (24.56)$$

The solutions of Eq. (24.56) are best illustrated by the graphical construction of Figure 24.7. For external field $H = 0$, solutions of Eq. (24.56) divide into two regions.

High-temperature phase. For $k_B T \geq zJ$ there is no net magnetization. $\bar{\sigma} = 0$ is the only solution. If one plots a graph of free energy versus magnetization, there is a single minimum at $\sigma = 0$.

Low-temperature phase. For $k_B T < zJ$ Eq. (24.56) has three solutions. One of these is still $\bar{\sigma} = 0$, while the other two are at values that approach ± 1 as the temperature approaches zero. Now, the free energy has three extrema and two minima, as in Figure 5.5. The free energy of the solutions with $\bar{\sigma} \neq 0$ is lower than the free energy of the solution with $\bar{\sigma} = 0$, so they are preferred in thermal equilibrium. In magnetic systems, these two solutions are related by symmetry and are degenerate; the system chooses between them randomly in a process of *spontaneous symmetry breaking*.

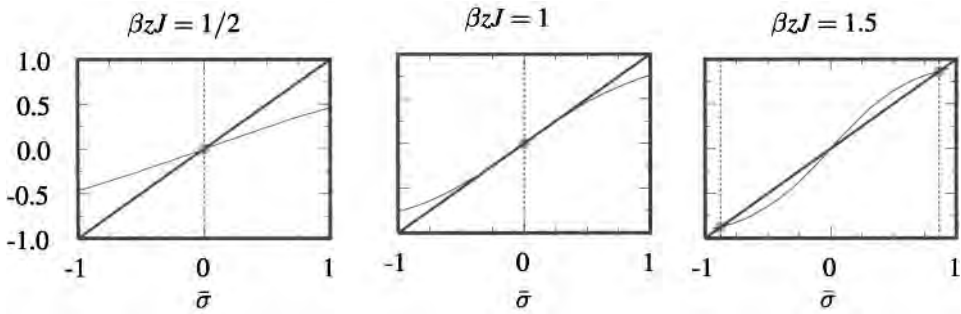


Figure 24.7. One solves Eq. (24.56) graphically by drawing $\bar{\sigma}$ and $\tanh \beta zJ\bar{\sigma}$ on top of one another and looking for where they cross. For $\beta zJ < 1$, the only crossing is at $\bar{\sigma} = 0$. However, for βzJ greater than the critical value of 1, there are three crossings.

24.4.1 Domains

The lessons of this simple calculation are somewhat puzzling when one applies them to the transition metal ferromagnets. As shown in Table 24.2, iron, nickel, and cobalt have transition temperatures $T_c = zJ/k_B$ on the order of 1000 K. Taking the case of iron, with $z = 8$, one estimates an exchange coupling $J \approx 0.01$ eV and a mean field \bar{H} , from Eq. (24.48), at each ion to be $7 \cdot 10^6$ G. Direct measurements

of the field were discussed in Section 13.5, and they are in fact about $3 \cdot 10^5$ G. But even after adopting the smaller number, such fields seem exceptionally large on two counts. First, the magnetization of iron can be made to alter through application of external fields that are comparatively small, only on the order of 1 G. It is hard to understand how iron could be affected by such small fields when vastly larger ones are operating internally. Second, referring back to Section 22.2, it is somewhat hard to see how spontaneous magnetization is supposed to arise at all. According to the calculations of that section, in a spherical region filled with a cubic array of dipoles, the net field acting upon each dipole due to all the other dipoles is zero. The arguments referred to electrical dipoles, but nothing changes if magnetic dipoles appear instead. Ferromagnetic order is supposed to arise because of interactions between nearby spins, but if the interactions have the form of dipole fields they cancel each other out completely.

The explanation of these two puzzles is that two rather different types of forces operate between magnetic moments. At very short distances, on the order of atomic spacings, magnetic order is induced by powerful *exchange forces* that arise quantum mechanically from the competition of Coulomb repulsion with Fermi statistics. This local ordering can be ferromagnetic, antiferromagnetic, ferrimagnetic, or of a more complicated canted type. Simultaneously, at distances large compared with atomic spacings, magnetic moments interact as dipoles, with an energy that falls off as $1/r^2$ between any two dipoles, but that can diverge if one sums over all the interactions between a large population.

In order to accommodate these two competing interactions, ferromagnets organize into *domains*, as depicted in Figure 24.8. The first theory for the size and shape of the domains is due to Landau and Lifshitz (1935). The simplest context in which to study them is a model similar to the Ising model. In the Ising model, spins can point only along the easy axis, a condition too restrictive to permit the study of domains. However, domain structures, as shown in Figure 24.8(B), can be captured by spins pointing along four directions, \hat{x} , $-\hat{x}$, \hat{y} , and $-\hat{y}$. Suppose that the easy axis is still present, and also suppose that spins pointing along $\pm\hat{x}$ have an energy α per spin greater than spins pointing along $\pm\hat{y}$. Finally, because domains emerge from the competition between long- and short-range forces, the magnetic induction B created by all the spins needs to be included as well. The energy of the spins is therefore

$$\mathcal{E} = - \sum_{\langle \vec{R}\vec{R}' \rangle} J \vec{\sigma}_{\vec{R}} \cdot \vec{\sigma}_{\vec{R}'} + \sum_{\vec{R}} \left[\alpha (\vec{\sigma}_{\vec{R}} \cdot \hat{x})^2 - \mu_B \vec{B} \cdot \vec{\sigma}_{\vec{R}} \right] + \frac{1}{8\pi} \int d\vec{r} \vec{B} \cdot \vec{B}. \quad (24.57)$$

$\vec{\sigma} = \pm\hat{x}$ or $\pm\hat{y}$, and \vec{B} is the spatially varying magnetic induction created by the magnetization $\vec{M} = \mu_B \vec{\sigma}$.

Because $\vec{H} = \vec{B} - 4\pi\vec{M}$, $4\pi \delta\mathcal{E}/\delta\vec{B} = \vec{H}$ as it should according to Eq. (24.17), if the sum over \vec{R} is interpreted as an integral for the purposes of computing the functional derivative.

Depending upon the size of the coupling constant J , the system will minimize its energy in different ways. When the coupling constant J is large and the system

is sufficiently small, it is favorable for all spins to point in the same direction. The sample will create an overall induction \vec{B} extending outside it, because the price to be paid for this field is less than the cost of creating an interface between spins pointing in opposite directions.

In the opposite limit of large samples and small coupling J the system is willing to create many interfaces in order to eliminate the energy penalty of the magnetic induction. To leading approximation, in this limit, energy is minimized by requiring $4\pi\delta\mathcal{E}/\delta\vec{B} = \vec{H} = 0$. Because $\vec{\nabla} \cdot \vec{B} = 0$ is one of Maxwell's equations, one must have $\vec{\nabla} \cdot \vec{M} = 0$ within the sample, and $\hat{n} \cdot \vec{M} = 0$ at the boundaries, where \hat{n} is a unit normal. Figure 24.8(A) shows an arrangement of spins that obeys these conditions. Magnetic field lines within the sample follow the spins. All trajectories created by integrating along the spin vector field form closed loops inside the sample; no magnetic field leaks out. To ensure that $\vec{\nabla} \cdot \vec{M}$ equal zero, it is enough to require the normal component of \vec{M} at the interfaces between domains to be continuous.

The scale of domains in Figure 24.8(A) is determined by noting that the energy cost of forming interfaces of horizontal length L is JL/la per length along y , where a is the spacing between spins. If $L \gg l$, the cost of forming the extra triangular interfaces is small, but the anisotropy energy cost of forming the regions with horizontal magnetization is $\alpha l^2/la^2$ per length along y . As a function of l , the domain energy is

$$\mathcal{E} = \frac{JL}{la} + \frac{\alpha l}{a^2} \quad \text{This is energy per length in the } y \text{ direction.} \quad (24.58)$$

$$\Rightarrow \frac{\partial \mathcal{E}}{\partial l} = \frac{\alpha}{a^2} - \frac{JL}{l^2 a} \quad (24.59)$$

$$\Rightarrow l = a \sqrt{\frac{JL}{\alpha a}} \quad \text{The value of } l \text{ that minimizes } \mathcal{E}. \quad (24.60)$$

$$\Rightarrow \frac{\mathcal{E}_{\min}}{L} = 2 \frac{\sqrt{\alpha J}}{a^2} \sqrt{\frac{a}{L}}. \quad \text{This is energy per area.} \quad (24.61)$$

The domain scale l depends upon the macroscopic scale of the sample, as well as on the ratio between the coupling J and the anisotropy energy α . Assuming J and α to be roughly the same order of magnitude, Eq. (24.59) predicts that the size of domains will be given by the geometric mean of the sample dimensions and the lattice spacing. The energy of the system per volume is smaller by a factor of $\sqrt{L/a}$ than the scale set by J and α .

In cubic crystals such as iron, the form of magnetic anisotropy described by Eq. (24.57) is too simple, because the anisotropy shares the symmetries of the cubic system. In real crystals the pattern of domain magnetizations frequently resembles Figure 24.8(B) rather than Figure 24.8(A), or it forms even more elaborate patterns when the edges of the sample do not coincide with symmetry axes.

Dynamical problems in which magnetic spins evolve while interacting with each other and with external fields belong to the study of *micromagnetics*. An introduction is provided by Aharoni (1996).

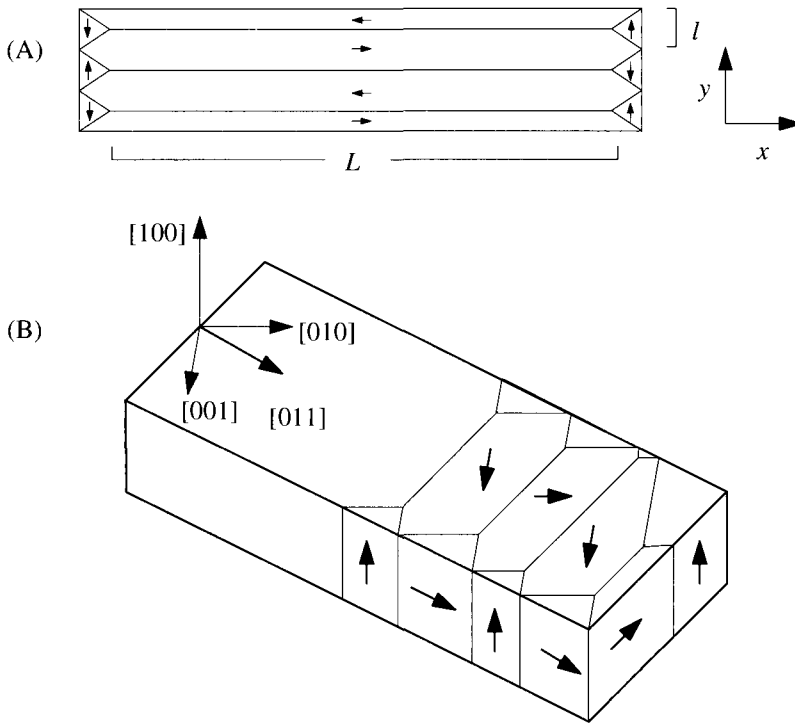


Figure 24.8. (A) Domain formation in a rectangular bar magnet. Notice that the flux lines form closed loops, so no flux escapes from the bar, because the normal component of the magnetic induction is continuous across the domain boundaries. (B) In an anisotropic crystal, domain structures become more complicated. While domains orient themselves so as to reduce the amount of flux that escapes the crystal, they also follow crystalline axes, and some small domains produce magnetic fields outside the sample.

24.4.2 Hysteresis

As shown in Figure 24.9, changing an external magnetic field by 0.05 G can alter the induction of a ferromagnetic sample by 0.1 T. Compared to internal fields of 300 kG, the applied field seems negligible. The reason for the large measurable effect is that external fields cause changes in the sizes and orientations of domains, rather than ripping apart the local magnetic order. The dynamics of the domains are complicated, and their states depend in detail upon the particular history of fields that has been applied to them. Figure 24.9 illustrates the hysteretic relation between \vec{B} and \vec{H} as an applied field is increased or decreased in various ways.

An interesting phenomenon illustrated in Figure 24.9 is *return-point memory*. If H is increasing and then the direction is reversed at H_1 , the magnetic field B decreases along a shallower path than it had during the initial rise. Reversing H at H_2 so that it rises again, B follows yet a third path until H reaches H_1 again, where B changes slope to follow the original curve. One explanation for this phenomenon appears in Problem 8.

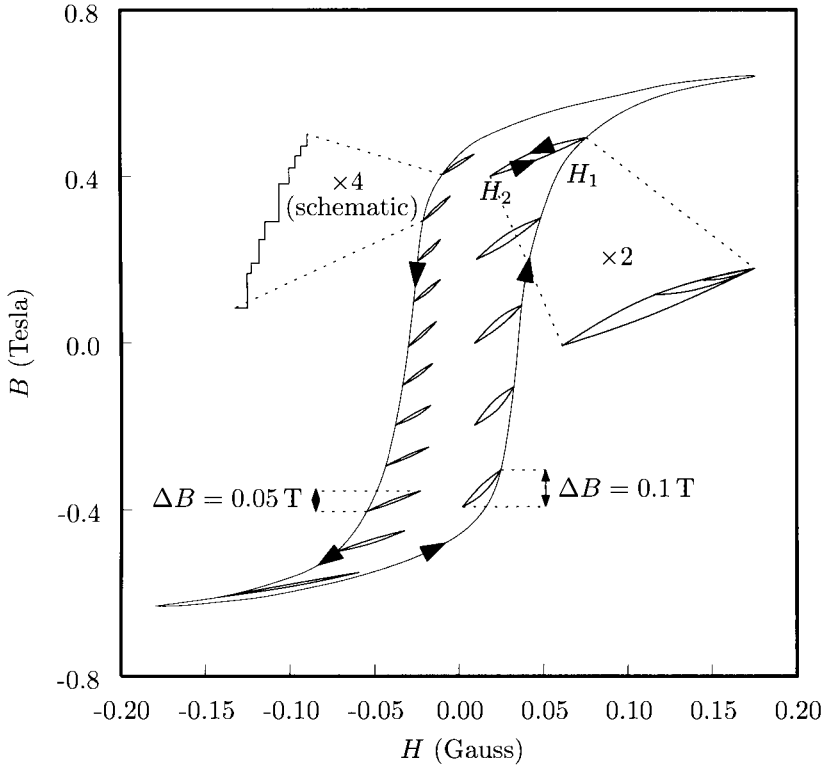


Figure 24.9. Hysteresis in the magnetization curve of Permalloy. Discrete steps are visible in the magnetization curve only when it is traversed slowly; each of the steps in fact consists of hundreds of smaller discrete events, down eventually to minute level at which individual magnetic domains reverse. [Source: Bozorth (1951), p. 542.]

24.5 Other Order–Disorder Transitions

24.5.1 Alloy Superlattices

The appearance of ferromagnetic order at a definite temperature is an example of the competition between energetic advantages of placing spins in their ground state, and the entropic advantage of randomizing them. The same conflict between two basic impulses is the same in the ordering of alloys, or in the transformation of solids into liquids. Therefore, all of these processes can be described at the conceptual level by Ising models. To demonstrate the generality of this approach, and to show how mean field theory may be extended to deal with increasingly complicated circumstances, the discussion will now focus upon the ordering of alloys into superlattices.

The superlattices described in Section 5.3.3 undergo an order–disorder transition at temperatures on the order of 400°C. At first the problem appears to bear little resemblance to the ordering of magnetic spins, but in fact the two problems are almost identical. A description of the superlattice problem in the grand canon-

ical ensemble is indistinguishable from a description of the magnetic problem in the canonical ensemble.

To show why, begin with two species of atom occupying every site of a lattice. The essential features of the superlattice transformation are contained in models where the energy of the system depends only upon interactions between very nearby atoms, and in the simplest models, only interactions between nearest neighbors are retained.

Suppose that when atom *A* is next to atom *B* the energy of interaction between them is $\epsilon_{AB} < 0$, and also suppose that the interactions of atoms *A* and *B* with neighbors of their own kind are ϵ_{AA} and ϵ_{BB} respectively. Because every site of the lattice is occupied by one type of atom or the other, the state of the system is completely specified by creating a variable $\sigma_{\vec{R}}$, which adopts values ± 1 at every lattice site. When $\sigma_{\vec{R}} = -1$, an atom of type *A* is at site \vec{R} , and when $\sigma_{\vec{R}} = 1$, an atom of type *B* is there. To express the energy of the system in terms of $\sigma_{\vec{R}}$, one needs to find a function *f* of two variables such that

$$f(-1, -1) = \epsilon_{AA}, \quad f(1, -1) = f(-1, 1) = \epsilon_{AB}, \quad \text{and} \quad f(1, 1) = \epsilon_{BB}. \quad (24.62)$$

A simple choice is

$$f(\sigma_{\vec{R}}, \sigma_{\vec{R}'}) = C_1 + C_2(\sigma_{\vec{R}} + \sigma_{\vec{R}'}) + C_3\sigma_{\vec{R}}\sigma_{\vec{R}'}, \quad (24.63)$$

leading to

$$f(\sigma_{\vec{R}}, \sigma_{\vec{R}'}) = \frac{\epsilon_{BB} + \epsilon_{AB}}{2}(\sigma_{\vec{R}} + \sigma_{\vec{R}'}) - \epsilon_{AB}\sigma_{\vec{R}}\sigma_{\vec{R}'}. \quad (24.64)$$

In order to obtain this expression, require Eq. (24.63) to satisfy Eq. (24.62), obtaining three equations in three unknowns, for C_1 , C_2 , and C_3 . In addition, because energies are always arbitrary up to an overall constant, set $C_1 = 0 \Rightarrow \epsilon_{AA} + 2\epsilon_{AB} + \epsilon_{BB} = 0$ to simplify the result.

Experiments are carried out with the overall composition of the alloy fixed. However, technical features of the statistical mechanics are simpler if one allows the relative concentrations of atoms to vary and adopts a grand canonical ensemble and chemical potential μ instead. The probability \mathcal{P} of encountering some configuration $\sigma_{\vec{R}}$ is therefore

$$\mathcal{P}(\sigma_{\vec{R}}) = \exp \left\{ \beta\mu \sum_{\vec{R}} \sigma_{\vec{R}} - \beta \sum_{\langle \vec{R}\vec{R}' \rangle} f(\sigma_{\vec{R}}, \sigma_{\vec{R}'}) \right\} \quad \begin{array}{l} \mu \text{ is the chemical potential} \\ \text{for replacing an atom of} \\ \text{type } A \text{ with an atom of type} \\ B; \text{ the total number of} \\ \text{atoms remains fixed.} \end{array} \quad (24.65)$$

$$= \exp \left\{ \beta\mu_B H \sum_{\vec{R}} \sigma_{\vec{R}} + \beta J \sum_{\langle \vec{R}\vec{R}' \rangle} \sigma_{\vec{R}}\sigma_{\vec{R}'} \right\} \quad \begin{array}{l} \text{Sum over distinct} \\ \text{nearest-neighbor pairs } \vec{R}\vec{R}'. \end{array} \quad (24.66)$$

where

$$\mu_B H = \mu - \frac{\epsilon_{BB} + \epsilon_{AB}}{2} z \quad \text{and} \quad J = \epsilon_{AB}. \quad (24.67)$$

μ_B is the Bohr magneton, not to be confused if possible with the chemical potential μ . z is the coordination number—that is, the number of nearest neighbors of each atomic site.

Equations (24.67) and (24.44) are identical. Nevertheless, the path through mean field theory needs to be traced through again because of some differences in the underlying physical problems. Superlattice ordering occurs because it is favorable for atoms of different types to be neighbors. Thus ϵ_{AB} and therefore J are negative. The superlattice is like an antiferromagnet, not a ferromagnet. In addition, the relative concentration of atoms A and B is specified experimentally, so the chemical potential (equivalently the field H) must be adjusted at the end of the calculation to ensure that the proper concentration has been obtained.

Bragg and Williams (1934) showed how to address these problems. Mean field theory requires one to anticipate some features of the solution, using a guess about the most likely configurations of $\sigma_{\vec{R}}$ in order to calculate estimates of (24.66) in a self-consistent fashion. Take, for example, the case of CuZn in one-to-one ratio (β -brass). Experiment indicates that when this alloy forms a superlattice, every atom tends to be surrounded by near neighbors of the opposite type, in the CsCl structure (Figure 2.8). The atoms are segregated into two *sublattices*. This observation leads to the guess that for all those configurations $\sigma_{\vec{R}}$ that have high probability according to Eq. (24.66), almost all neighbors of $\sigma_{\vec{R}} = 1$ will have $\sigma_{\vec{R}'} = -1$, with occasional exceptions that grow in number as one approaches the transition temperature of 400°C.

The formal way to employ this idea is to write

$$\sigma_{\vec{R}_A} = \sigma_A + (\sigma_{\vec{R}_A} - \sigma_A), \quad \sigma_{\vec{R}_B} = \sigma_B + (\sigma_{\vec{R}_B} - \sigma_B) \quad \begin{array}{l} \text{Think of } \sigma_A \text{ and } \sigma_B \text{ as values close to } -1 \text{ and} \\ \text{1, respectively. They will equal the mean values} \\ \text{of the alloy variable } \sigma \text{ on the } A \text{ and } B \\ \text{sublattices.} \end{array} \quad (24.68)$$

and to treat the cross-term $(\sigma_{\vec{R}_A} - \sigma_A)(\sigma_{\vec{R}_B} - \sigma_B)$ as negligibly small in Eq. (24.66). With this approximation, (24.66) becomes

$$\mathcal{P} = \exp \left\{ \beta \mu_B H \sum_{\vec{R}} \sigma_{\vec{R}} + \beta J \sum_{\langle \vec{R}_A \vec{R}_B \rangle} (\sigma_A \sigma_{\vec{R}_B} + \sigma_B \sigma_{\vec{R}_A} - \sigma_A \sigma_B) \right\}, \quad (24.69)$$

Here \vec{R}_A ranges over all sites on the A sublattice, and \vec{R}_B ranges over all neighbors of \vec{R}_A on the B sublattice.

$$= \prod_{\vec{R}_A} \exp \left\{ \beta \mu_B H \sigma_{\vec{R}_A} + \beta J z (\sigma_B \sigma_{\vec{R}_A} - \sigma_A \sigma_B / 2) \right\} \prod_{\vec{R}_B} \exp \left\{ \beta \mu_B H \sigma_{\vec{R}_B} + \beta J z (\sigma_A \sigma_{\vec{R}_B} - \sigma_A \sigma_B / 2) \right\}. \quad \begin{array}{l} z \text{ is the coordination} \\ \text{number.} \end{array} \quad (24.70)$$

The probability of any configuration is therefore given approximately by multiplying the independent probabilities of all the individual variables $\sigma_{\vec{R}}$. Because σ_A and σ_B are the mean values of σ on the two sublattices, one can use (24.70) to calculate

them self-consistently. For example, the mean value of any variable $\sigma_{\vec{R}_A}$ is

$$\sigma_A = \left\langle \sigma_{\vec{R}_A} \right\rangle = \frac{e^{\{\beta\mu_B H + \beta J z \sigma_B\}} - e^{\{-\beta\mu_B H - \beta J z \sigma_B\}}}{e^{\{\beta\mu_B H + \beta J z \sigma_B\}} + e^{\{-\beta\mu_B H - \beta J z \sigma_B\}}}. \quad \text{The probability that } \sigma_{\vec{R}_A} = 1 \text{ times } 1 \text{ plus the probability it equals } -1 \text{ times } -1. \quad (24.71)$$

Thus

$$\sigma_A = \tanh[\beta\mu_B H + \beta z \sigma_B J] \quad (24.72a)$$

$$\sigma_B = \tanh[\beta\mu_B H + \beta z \sigma_A J]. \quad (24.72b)$$

The chemical potential μ is determined by the requirement that atoms A and B be present in equal proportion, which implies that

$$\sigma_A + \sigma_B = 0. \quad \text{If } N_A \text{ and } N_B \text{ are the numbers of } A \text{ and } B \text{ sublattice sites, then } \sum_{\vec{R}} \sigma_{\vec{R}} = N_B - N_A = \sum_{\vec{R}_A} \sigma_{\vec{R}} + \sum_{\vec{R}_B} \sigma_{\vec{R}} = N_A \sigma_A + N_B \sigma_B. \quad (24.73)$$

One can only achieve Eq. (24.73) if $\mu_B H = \mu - z(\epsilon_{BB} + \epsilon_{AB})/2 = 0$, so finally one has

$$\sigma_A = -\tanh(\beta J z \sigma_A) = \tanh(\beta |J| z \sigma_A). \quad \text{Remember that superlattice ordering only happens when } J = \epsilon_{AB} < 0. \quad (24.74)$$

Because Eq. (24.74) is identical to Eq. (24.56), it can be solved by the method indicated in Figure 24.7.

24.5.2 Spin Glasses

Spin glasses were discovered by Jacobs and Schmitt (1959). They occur when the interactions between spins have random sign or magnitude. There are typically huge numbers of nearly degenerate states separated by energy barriers of many different sizes. Edwards and Anderson (1975) wrote down the analog of the Ising model for these systems, and it was solved by Parisi (1987).

24.6 Critical Phenomena

Mean field theory is a crude approximation, but it describes the physics of phase transitions rather well, except near one special location on the phase diagram, the *critical point*, sketched in Figure 24.10. What makes this point so critical? As particularly emphasized by Fisher (1974) a comparison of phenomena applicable to magnets and to fluids provides some explanation.

- The critical point is a unique location in the phase diagram. In a magnetic system, the critical point occurs for zero external magnetic field and at the critical temperature T_c , which is the lowest temperature at which the spontaneous magnetization vanishes. In a fluid, for any given pressure there is a temperature below which fluid and gas can coexist, and above which fluid and gas merge into a single phase. The critical point occurs at the pressure for which this critical temperature is as high as possible. In CO_2 , for example, the critical point is at 72 atm and a temperature of 31.04°C .

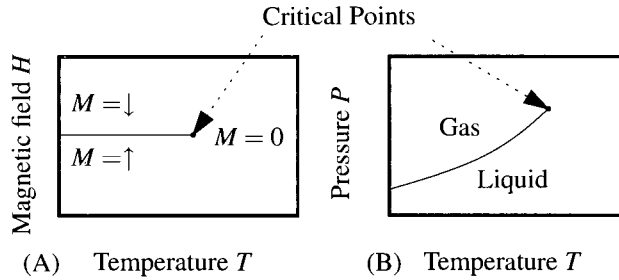


Figure 24.10. (A) Schematic phase diagram for a ferromagnet. The critical point lies at the highest temperature where there is spontaneous magnetization in zero field. (B) Schematic phase diagram of liquid–gas system. Beyond the critical point, fluid and gas phases merge and cannot be distinguished as pressure varies. The two phases of the magnet are related by symmetry, but this is not true in the liquid–gas system.

- The specific heat both of magnets and fluids diverges approaching the critical point. The divergence takes the form of a power law.
- The magnetic susceptibility diverges in magnetic systems, and the compressibility diverges in fluids. These divergences also take the forms of power laws.
- The divergences result from large fluctuations: large correlated domains of spins flipping back and forth in magnets, and large regions altering between one density and another in fluids. Fluids that normally are transparent become milky, displaying *critical opalescence*.

Investigating these phenomena led to two important ideas:

Universality. Divergences near the critical point are identical in a variety of apparently different physical systems and also in a collection of simple models. Systems group into a small number of *universality classes*. For example, ferromagnetic salts, carbon dioxide, and the Ising model all behave identically near the critical point, and belong to the same class. However, two-dimensional magnetic films are essentially different from three-dimensional magnetic systems, and they belong to a different class.

Scaling. The key to understanding the critical point lies in understanding the relationship between systems of different sizes. Scaling functions, such as those used to describe localization in Section 18.5.2, are the key to encoding the universal features of the critical point. Formal development of this idea led to the *renormalization group* of Wilson (1975).

24.6.1 Landau Free Energy

In order to see that mean field theory fails near the critical point, it is necessary to analyze its predictions and compare them with experiment. This task could be carried out by starting with Eq. (24.56). However, it is preferable to adopt a

framework developed by Landau (1937) that exhibits clearly the minimal set of assumptions needed to obtain the results of mean field theory.

Suppose that the free energy of a magnetic system is *analytic* in the vicinity of the critical point, and that all physical quantities can be expressed as a Taylor series in the magnetization and temperature. This assumption seems reasonable, because the magnetization vanishes right at the critical point, and one only needs to know how the free energy depends upon it when it is small. So

$$\mathcal{F}(M, T) = A_0(T) + A_2(T)M^2 + A_4(T)M^4 + HM. \quad \text{The coupling between the small magnetization } M \text{ and the external field } H \text{ is given by Eq. (24.26).} \quad (24.75)$$

The coefficients $A_0(T) \dots A_4(T)$ are undetermined functions of temperature. The reason that only even terms in M appear is that the system must be invariant under $M \rightarrow -M, H \rightarrow -H$; terms odd in M alone must vanish.

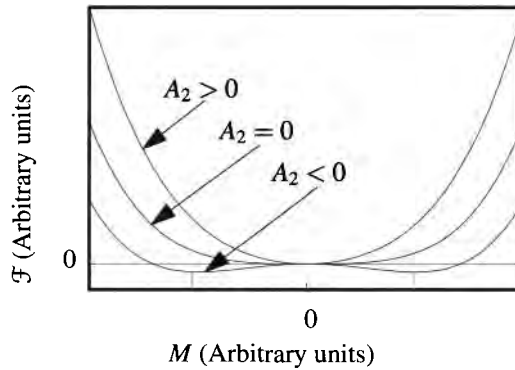


Figure 24.11. Form of Landau's free energy, Eq. (24.75), for $A_2 > 0, A_2 = 0,$ and $A_2 < 0$. Energies are measured relative to A_0 .

Let T_c be the critical temperature, and define the *reduced temperature*

$$t \equiv \frac{T - T_c}{T_c}, \quad (24.76)$$

which is a dimensionless variable designed to vanish right at the critical temperature. Phase separation begins when \mathcal{F} develops a concave structure. A_4 must always be positive or else \mathcal{F} is minimized by sending M to infinity. A_0 sets the zero of energy and has little significance. Therefore the onset of nonzero magnetization is governed by $A_2(T)$. As shown in Figure 24.11, the shape of \mathcal{F} changes when A_2 passes through zero, so the critical point must be the place where A_2 vanishes. Measure energies relative to $A_0(T_c)$, and let a_2 and a_4 be constants. The form of the free energy in the vicinity of the critical point must be

$$\mathcal{F} = a_2 t M^2 + a_4 M^4 + HM. \quad (24.77)$$

Spontaneous Magnetization. The equilibrium magnetization is determined by minimizing the free energy. Therefore, it must satisfy

$$H + 2ta_2M + 4a_4M^3 = 0. \quad (24.78)$$

When $H = 0$, $M = 0$ always satisfies Eq. (24.78). However, for $t < 0$ there are two more solutions:

$$M = \begin{cases} \pm \sqrt{\frac{2|t|a_2}{4a_4}} & \text{for } t < 0 \\ 0 & \text{for } t > 0. \end{cases} \quad (24.79)$$

Figure 24.11 shows that for $t < 0$ these values of M give a lower value of the free energy than $M = 0$, and therefore correspond to equilibrium.

Specific Heat. With the behavior of M in hand it is possible to evaluate a collection of other quantities. The specific heat is determined by the identity

$$C_V = \frac{\partial \mathcal{E}}{\partial T} = \frac{\partial}{\partial T} \frac{\partial \beta \mathcal{F}}{\partial \beta} \quad (24.80)$$

For a derivation from thermodynamics, see for example, Landau and Lifshitz (1980) pp. 47–48. The relation for \mathcal{E} also is easily derived by writing out the expression for \mathcal{E} in the canonical ensemble.

$$= -\frac{1}{T_c} \frac{\partial}{\partial t} (1+t)^2 \frac{\partial}{\partial t} \left(\frac{\mathcal{F}}{1+t} \right) \quad (24.81)$$

Use Eq. (24.76).

$$\approx -\frac{1}{T_c} \frac{\partial^2 \mathcal{F}}{\partial t^2} \quad (24.82)$$

Focusing on small t .

$$= \begin{cases} \frac{1}{T_c} \frac{a_2^2}{2a_4} & \text{for } t < 0 \\ 0 & \text{for } t > 0. \end{cases} \quad (24.83)$$

Insert Eq. (24.79) into Eq. (24.77).

Magnetic Susceptibility. Turning on an external field H changes the equilibrium magnetization. For $t < 0$, take

$$M = \sqrt{\frac{2|t|a_2}{4a_4}} + qH, \quad (24.84)$$

where q is to be determined. Placing Eq. (24.84) into Eq. (24.78) and expanding to first order in H , one finds that

$$q = -\frac{1}{4a_2|t|}. \quad (24.85)$$

Expanding similarly about $M = 0$ for $t > 0$ gives

$$\frac{\partial M}{\partial H} \approx \begin{cases} -\frac{1}{4|t|a_2} & \text{for } t < 0 \\ -\frac{1}{2ta_2} & \text{for } t > 0. \end{cases} \quad (24.86)$$

Critical Isotherm. Finally, right on the critical isotherm at $t = 0$, one has that

$$H + 4a_4M^3 = 0 \Rightarrow M \propto H^{1/3}. \quad (24.87)$$

The suppositions of the Landau theory are entirely reasonable, yet experiments prove them wrong. The assumption that fails is the assumption that the free energy can be expanded in a Taylor series about the critical point.

Correspondence between Liquids and Magnets. Experiments on critical point phenomena have been conducted both in magnets, and in liquid–gas systems. The two systems act almost identically in the vicinity of the critical point, once corresponding variables have been identified.

A correspondence between magnetic and liquid–gas systems can be constructed in a manner similar to that used for superlattices in Section 5.3.3. Imagine that the material of type *A* in that section is a fluid, while the material of type *B* is gas. Then the equations describing the superlattice can immediately be interpreted as describing liquid–gas phase transitions. At temperatures below the transition, fluid prefers to group with fluid and gas prefers to group with gas, meaning that the energy ϵ_{AB} is positive, and the fluid–gas system corresponds to a ferromagnet, with positive J in Eq. (24.43). Above the transition temperature, fluid and gas mix together, forming a single homogeneous phase, while below the transition, gas and liquid phase separate.

Based on this discussion, one forms the following correspondence: The magnetization M corresponds to the difference in particle density Δn between liquid and gas. The thermodynamic variable conjugate to M is the magnetic field H , so the variable conjugate to Δn , which is the chemical potential μ , must correspond to magnetic field. The chemical potential is hard to measure directly. However, according to the Gibbs–Duhem relation

$$dP = sdT + nd\mu, \quad \text{See Landau and Lifshitz (1980), p. 72; } s \text{ is the entropy per volume.} \quad (24.88)$$

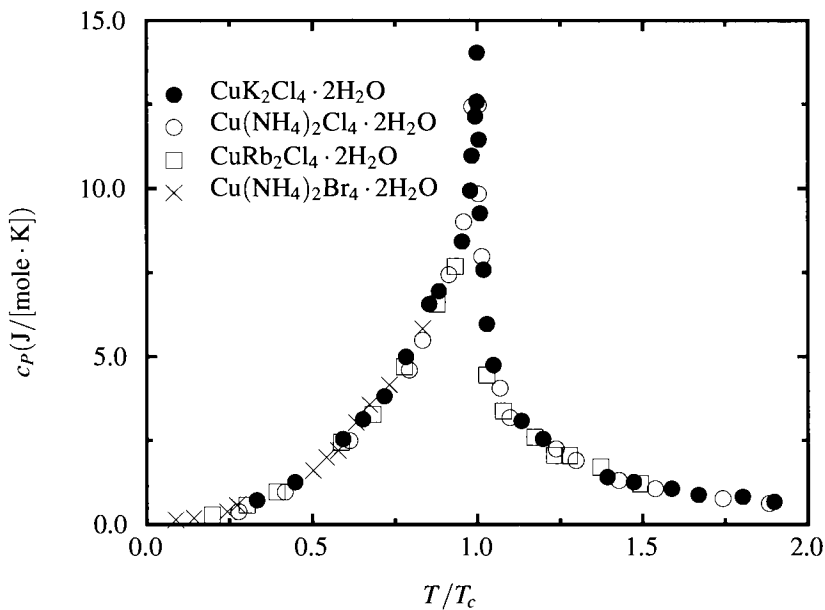


Figure 24.12. Molar heat capacities of four ferromagnetic copper salts versus scaled temperature T/T_c . [Source Jongh and Miedema (1974).]

so that if temperature is fixed, pressure is proportional to chemical potential, and pressure can therefore be used instead of chemical potential as the analog of magnetic field.

Six exponents are conventionally defined to characterize various quantities that become singular near the critical point.

Specific Heat— α . The specific heat both in fluids and in magnets diverges as

$$C_V(t) \sim |t|^{-\alpha}; \quad (24.89)$$

data for magnets appear in Figure 24.12. Mean field theory predicts a discontinuity in the specific heat, not a divergence.

Magnetization and Density— β . Figure 24.13(A) displays experimental measurements of temperature versus magnetization near the critical point. According to Eq. (24.79), T should approach T_c as M^2 . The data however show that T approaches T_c as M^3 . Figure 24.13(B) shows that temperature versus density at constant pressure for a collection of liquid–gas systems is characterized by the same exponent. So

$$M \sim |t|^\beta \quad \text{and} \quad \Delta n \sim |t|^\beta. \quad (24.90)$$

Letting n_c be the density at the critical point, one can take Δn to be $n_{\text{liquid}} - n_c$, $n_c - n_{\text{gas}}$, or $n_{\text{liquid}} - n_{\text{gas}}$.

Compressibility and Susceptibility— γ . The isothermal compressibility of fluids diverges near the critical point:

$$K_T = \frac{1}{n} \frac{\partial n}{\partial P} \sim \frac{1}{n_c} \frac{\partial \Delta n}{\partial P} \sim |t|^{-\gamma}. \quad (24.91)$$

The analogous divergence for a magnet is

$$\frac{\partial M}{\partial H} = \chi \sim |t|^{-\gamma}. \quad (24.92)$$

Mean field theory predicts $\gamma = 1$, but the measurements find a slightly larger exponent.

Critical Isotherm— δ . A next critical exponent occurs by making measurements right at T_c on the critical isotherm

$$P \sim |\Delta n|^\delta, \quad (24.93)$$

and for a magnet

$$|M| \sim |H|^{1/\delta}. \quad (24.94)$$

The mean field prediction is $\delta = 3$, but the measurements find $\delta \approx 5$.

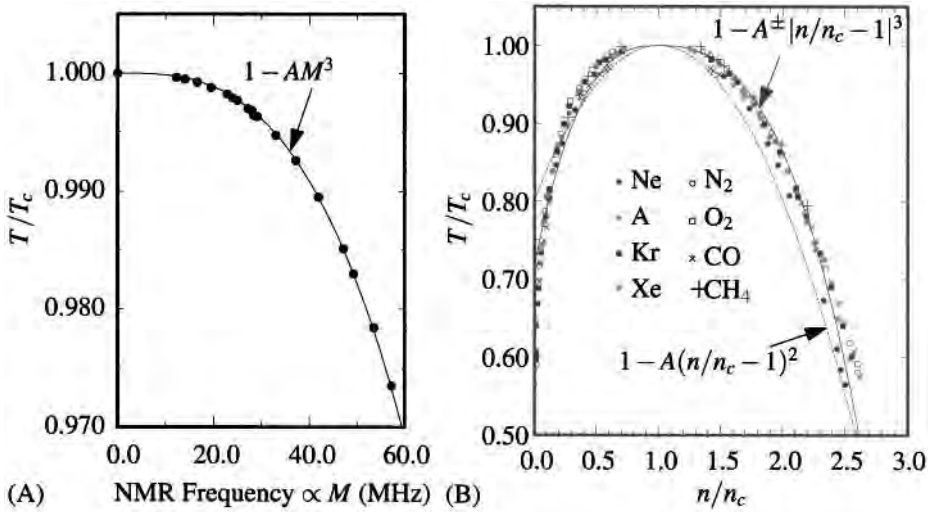


Figure 24.13. (A) Temperature versus magnetization, measured using nuclear magnetic resonance by Heller and Benedek (1962) for the antiferromagnet MnF_2 , near the critical temperature $T = 67.336$ K. The data are fit well by $T/T_c = 1 - A|M|^3$. (B) Coexistence curve for eight fluids, measured by Guggenheim (1945). The data can be fit reasonably well by curves of the form $T/T_c = 1 - A^\pm |n/n_c - 1|^3$, where A^\pm is a constant taking different values depending on whether n is greater or less than n_c . The best quadratic fit is also shown, but it suits the data less well.

Correlation Length — ν . A final pair of exponents relates to light scattering experiments that probe the correlation function of fluids. According to Eq. (5.48) the two-particle correlation function g is closely related to the scattering function S . Near the critical point, $g(r)$ is observed to behave as

$$g(r) - 1 \sim e^{-r/\xi} \quad \text{There are power-law corrections given in Eq. (24.99),} \quad (24.95)$$

so $\exp[-r/\xi]/r^{1+\eta}$ is more accurate.

where $\xi(T)$ is called the *correlation length*. The implication for scattering experiments is that

$$S(\vec{q}) - 1 = n \int d\vec{r} e^{i\vec{q}\cdot\vec{r}} [g(r) - 1] \quad (24.96)$$

$$\sim \int d\vec{r} e^{-r/\xi + i\vec{q}\cdot\vec{r}} \sim \frac{1}{1 + \xi^2 q^2}. \quad (24.97)$$

The correlation length ξ diverges approaching the critical point, with

$$\xi \sim |t|^{-\nu}. \quad (24.98)$$

This divergence can be measured by plotting $1/S(q)$ versus q^2

Power-Law Decay at Critical Point— η . Right at the critical point, the correlation function g decays as a power and not as an exponential. The rate at which it decays is

$$g(r) \sim r^{-1-\eta}, \quad (24.99)$$

Table 24.3. Summary of critical exponents, showing correspondence between fluid-gas systems, magnetic systems, and the three-dimensional Ising model

Exponent	Fluid	Magnet	Mean Field Theory	Experiment	3d Ising
α	$C_V \sim t ^{-\alpha}$	$C_V \sim t ^{-\alpha}$	discontinuity	0.11–0.12	0.110
β	$\Delta n \sim t ^\beta$	$M \sim t ^\beta$	$\frac{1}{2}$	0.35–0.37	0.325
γ	$K_T \sim t ^{-\gamma}$	$\chi \sim t ^{-\gamma}$	1	1.21–1.35	1.241
δ	$P \sim \Delta n ^\delta$	$ H \sim M ^\delta$	3	4.0–4.6	4.82
ν	$\xi \sim t ^{-\nu}$	$\xi \sim t ^{-\nu}$		0.61–0.64	0.63
η	$g(r) \sim r^{-1-\eta}$	$g(r) \sim r^{-1-\eta}$		0.02–0.06	0.032

Source: Vicentini-Missoni (1972) p. 67, Cummins (1971), p. 417, and Goldenfeld (1992) p. 384.

and this equation defines the exponent η .

Table 24.3 presents a summary of the six exponents and gives their values in mean field theory and experiment.

24.6.2 Scaling Theory

The Landau theory of phase transitions makes no assumption more severe than that the free energy could be expanded as a Taylor series in the neighborhood of the critical point. Because the Landau theory fails, this assumption must fail, and the question is what should replace it.

A full theory of the critical point is extremely elaborate. The concept of universality makes it possible to construct a theory by focusing upon simple models, such as the Ising model, whose critical behavior is identical to that of the experimental systems. Yet even for these model systems, the analysis is extremely involved. The most accurate determination of critical behavior for the Ising models is given by power-series expansions of the partition function, discussed by Domb (1974).

Rather than developing the theory, the discussion will focus upon developing the language needed to describe experimental observations. The basic observation is that near the critical point, physical quantities behave as power laws, that these power laws are universal, but that the exponents are far from obvious. It has become commonplace to claim that natural phenomena behave as power laws, but the standard set in the field of critical phenomena, where precise power-law scaling is observed over many decades, has rarely been matched.

Widom (1965) showed that many experimental observations could be described by assuming a particular type of scaling relation between thermodynamic variables. The scaling theory can take a number of different forms, one of which is to make an hypothesis about the manner in which variables appear within the free energy.

Consider the power-law divergence of the specific heat, shown in Figure 24.12. Because the specific heat is obtained from the free energy as in Eq. (24.80), the free energy $\mathcal{G}(T, H)$ must have a singular piece. Separate the singularity out in the

form

$$\frac{\mathcal{G}}{\nu k_B T} = |t|^{x_1} G(t, H), \tag{24.100}$$

where the exponent x_1 has been chosen so that when $H = 0$, G is a smooth function of t . At $H = 0$ the specific heat must diverge as $|t|^{-\alpha}$, so one has that

$$C_V = \frac{\partial}{\partial T} \frac{\partial \beta \mathcal{G}}{\partial \beta} \sim t^{-\alpha} \tag{24.101}$$

$$\Rightarrow x_1 = 2 - \alpha. \tag{24.102}$$

Notice that differentiating by T lowers the power of t , but multiplying by T does not raise the power of t ; it multiplies by the constant T_c .

Scaling Form for Free Energy. The main difficulty posed by a form such as Eq. (24.101) lies in the experimental fact that when $H \neq 0$, there are no singular quantities as t passes through zero. The specific heat is only singular right at the critical point. With a nonzero magnetic field, the specific heat displays a peak as a function of temperature, but varies smoothly. Choosing a form for G in accord with this experimental observation proceeds in two steps.

First, assume that the magnetic field and temperature enter G only in the combination

$$G(t, H) = G \left(\frac{H}{H_0 |t|^\Delta} \right). \tag{24.103}$$

H_0 is some constant, and Δ is some exponent.

One way to express the idea behind this functional form is to say that the importance of the magnetic field to the free energy can only be judged by comparing it to some reference value, and it is supposed that this reference value scales as a power law with the reduced temperature.

Second, assume that G itself behaves as a power when its argument becomes extremely large:

$$\lim_{y \rightarrow \infty} G(y) \sim y^{x_2}. \tag{24.104}$$

Making this assumption, one has for small $|t|$ but nonzero H that

$$\frac{\mathcal{G}}{\nu k_B T} \sim |t|^{2-\alpha} \left(\frac{H}{H_0 |t|^\Delta} \right)^{x_2} \sim |t|^{2-\alpha-\Delta x_2}. \tag{24.105}$$

Thus the free energy can be made nonsingular whenever $H \neq 0$, provided that

$$x_2 = \frac{2 - \alpha}{\Delta}. \tag{24.106}$$

The exponent Δ can be expressed entirely in terms of exponents that have already been defined by examining the spontaneous magnetization. One has

$$-M = \frac{\partial \mathcal{G}}{\partial H} = |t|^{2-\alpha} \frac{1}{H_0 |t|^\Delta} G' \left(\frac{H}{H_0 |t|^\Delta} \right). \tag{24.107}$$

See Eq. (24.31).

When $H \rightarrow 0$, the magnetization must vanish as $|t|^\beta$, so

$$|t|^{2-\alpha-\Delta} \sim |t|^\beta \quad (24.108)$$

$$\Rightarrow \Delta = 2 - \alpha - \beta. \quad (24.109)$$

Notice one peculiarity. Above the critical temperature, the spontaneous magnetization must vanish, yet it is predicted to have the same power law divergence above as below. These two facts are consistent if one observes that the coefficients of the power-law can be different above and below T_c : the coefficient above T_c is just zero.

Relations Among Exponents. Having determined the singular parts of the free energy in terms of the exponents α and β , it is possible to continue calculating the various singular quantities that are found experimentally. All the remaining singularities can now be related to the ones that have already been found.

For example, the magnetic susceptibility is

$$\left. \frac{\partial M}{\partial H} \right|_{H=0} = \chi \sim \frac{|t|^{2-\alpha}}{H_0^2 |t|^{2\Delta}} G'' \left(\frac{H}{H_0 |t|^\Delta} \right) \Big|_{H=0} \quad (24.110)$$

$$\Rightarrow |t|^{2-\alpha-2\Delta} \sim |t|^{-\gamma} \quad (24.111)$$

$$\Rightarrow \gamma = \alpha + 2\Delta - 2. \quad (24.112)$$

Combining Eq. (24.112) with Eq. (24.109) gives

$$2 = \alpha + 2\beta + \gamma. \quad (24.113)$$

This relation among exponents, the *Widom relation*, is a consequence of the scaling assumption, and it is obeyed in all known cases.

The exponent δ describes the relation of the magnetization to the magnetic field on the critical isotherm. As $t \rightarrow 0$,

$$M \sim \frac{1}{H_0 |t|^\Delta} |t|^{2-\alpha} \left(\frac{H}{H_0 |t|^\Delta} \right)^{x_2-1} \quad (24.114)$$

$$\sim H^{x_2-1} = H^{(2-\alpha-\Delta)/\Delta} \quad (24.115)$$

$$\Rightarrow \frac{1}{\delta} = \frac{2-\alpha-\gamma}{2-\alpha+\gamma} \quad (24.116)$$

$$\Rightarrow \delta = 1 + \frac{\gamma}{\beta}, \quad \text{Use Eq. (24.113).} \quad (24.117)$$

which is the *Rushbrooke relation*.

The final exponents, ν and η , relate to properties of the correlation function $g(r)$, so the connection between the correlation function and the free energy needs to be determined. The relation is provided by observing that fluctuations in particle number are related to the compressibility K_T through

$$\langle \Delta N^2 \rangle = -\frac{k_B T N^2}{\mathcal{V}^2} \frac{\partial \mathcal{V}}{\partial P} = k_B T n^2 \mathcal{V} K_T \quad \text{See Landau and Lifshitz (1980), p. 342.} \quad (24.118)$$

$$= \left[\int d\vec{r} d\vec{r}' \langle n(\vec{r}) n(\vec{r}') \rangle \right] - \langle N \rangle^2 \tag{24.119}$$

$$= \mathcal{V} n \left\{ 1 + n \int d\vec{r} (g(r) - 1) \right\}. \tag{24.120}$$

Follows steps similar to those around Eq. (3.51), and use Eq. (5.45) for g .

Because near the critical point

$$g(r) \sim \frac{e^{-r/\xi}}{r^{1+\eta}}, \tag{24.121}$$

one has

$$K_T \sim \int d\vec{r} g(r). \tag{24.122}$$

Changing variables to $\vec{s} = \vec{r}/\xi$ and using Eq. (24.121), one obtains

$$K_T \sim \xi^3 \xi^{-1-\eta} \int d\vec{s} \frac{e^{-s}}{s^{1+\eta}} \tag{24.123}$$

$$\sim \xi^{2-\eta} \sim |t|^{-\nu(2-\eta)}. \tag{24.124}$$

However, the compressibility must diverge as $|t|^{-\gamma}$, so

$$(2 - \eta)\nu = \gamma, \tag{24.125}$$

the *Fisher–Essam relation*. Finally, there is an apparently improbable argument that because $G = \mathcal{G}/k_B T \mathcal{V}$ has dimensions of inverse length to the third power, but the only length in the system that should be important near the critical point is the correlation length ξ , one must have that

$$\frac{\mathcal{G}}{k_B T \mathcal{V}} \sim |t|^{2-\alpha} \sim \xi^{-3} \tag{24.126}$$

$$\Rightarrow 2 - \alpha = 3\nu, \tag{24.127}$$

the *Josephson or hyperscaling relation*. All of these scaling relations are obeyed within a few percent by the experimental values listed in Table 24.3.

Scaling Form for Magnetization. Some of the most detailed experimental results are expressed using an alternate form of the scaling hypothesis, one that relates the magnetic field and magnetization through

$$|H| = |M|^\delta h \left(\frac{t}{|M|^{1/\beta}} \right). \tag{24.128}$$

The function h can be measured by choosing temperature T and field H , measuring M , and then constructing the ratio $|H|/|M|^\delta$ and plotting it versus the variable

$$x = \frac{t}{|M|^{1/\beta}}. \tag{24.129}$$

When the external magnetic field H vanishes, $h(x)$ must vanish. Because $|M| \sim t^\beta$ for $H = 0$, the conclusion is that in vanishing field $x = t/|M|^{1/\beta} = -x_0$ is a constant, and $h(-x_0) = 0$.

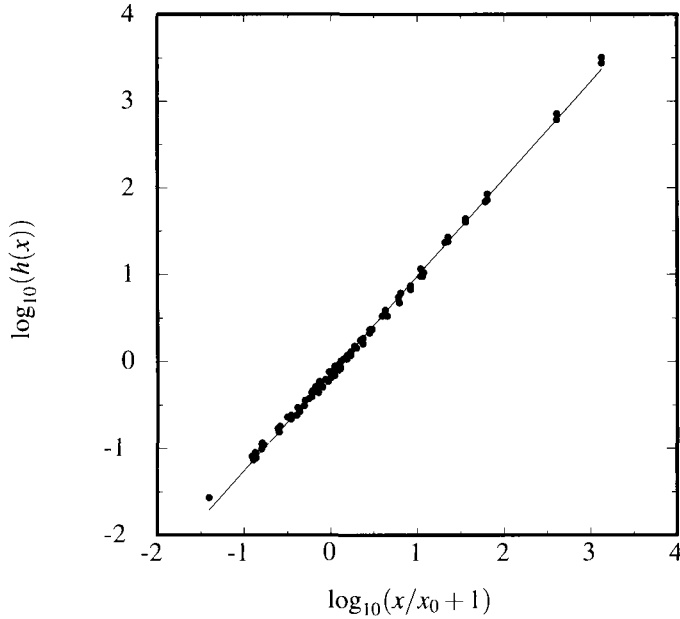


Figure 24.14. Log–log plot of scaling function $h = |H|/|M|^\delta$ versus $x = t/|M|^{1/\beta}$, using $\delta = 4.32$, $\beta = 0.364$, and $x_0 = 0.596$ for CrBr_3 . The exponents and the critical temperature $T_c = 32.841$ K are determined together as part of the process of trying to ensure that data taken at different temperatures lie on top of a single scaling curve. [Source: Vicentini-Missoni (1972), p. 68.]

If the scaling hypothesis is correct, then measurements of $|H|/|M|^\delta$ versus $x + x_0$ should fall on a single line. As shown in Figure 24.14, the data do collapse in this way, and furthermore the function h takes the form of a power law over a large range of temperature near the critical point.

Problems

1. **Magnetic dipole moment:** Consider a small loop of wire in the x – y plane with area A , and current J flowing through it. Show that the vector potential \vec{A} far from the loop is given by

$$\vec{A} = \frac{\vec{m} \times \vec{r}}{r^3}, \quad (24.130)$$

where \vec{r} is a vector from the middle of the loop of wire to an observation point.

2. **Magnetic dipole energies:** Verify Eqs. (24.36) and (24.37):

- (a) Consider a distribution of current $\vec{j}(\vec{r})$ that is localized and is in steady state, which means that $\vec{\nabla} \cdot \vec{j} = 0$. By considering

$$\int d\vec{r} r_\alpha r_\beta \vec{\nabla} \cdot \vec{j} = 0, \quad (24.131)$$

show that

$$\int d\vec{r} (r_\alpha j_\beta + r_\beta j_\alpha) = 0. \quad (24.132)$$

(b) Using Eq. (24.132), show that for any vector \vec{C} ,

$$\int d\vec{r} \vec{j}\vec{r} \cdot \vec{C} = \frac{1}{2} \int d\vec{r} [\vec{r} \times \vec{j}] \times \vec{C}. \quad (24.133)$$

(c) Verify Eqs. (24.36) and (24.37).

3. **Thermodynamic potential:** Show that Eq. (24.27) describes the thermodynamic potential appropriate for a system where external currents $\vec{j}_{\text{ext}}(\vec{r})$ rather than magnetic induction $\vec{B}(\vec{r})$ are specified. Write \vec{B} as the curl of a vector potential. Show that for fixed temperature, any changes in \mathcal{G} can be written as an integral over changes in $\vec{j}_{\text{ext}}(\vec{r})$, and find the thermodynamic variable conjugate to \vec{j}_{ext} .

4. **Mean field theory:** Consider a two-dimensional Ising model on a square lattice. Suppose that

$$\mathcal{E} = - \sum_{\langle \vec{R}\vec{R}' \rangle} J \sigma_{\vec{R}} \sigma_{\vec{R}'} - \sum_{\vec{R}} H \mu_B \sigma_{\vec{R}} \quad (24.134)$$

and that J is negative.

(a) Let the mean value of spins on alternating sites be denoted by σ_\uparrow and σ_\downarrow . Find the free energy corresponding to this Hamiltonian within mean field theory.

(b) Find the self-consistent equations that determine the mean spins σ_\uparrow and σ_\downarrow within mean field theory.

(c) Above the transition temperature, $\sigma_\uparrow = \sigma_\downarrow$. Find the high-temperature form of the magnetic susceptibility, reproducing an equation in this chapter. Relate the unknown quantity in that equation to J .

5. **One-dimensional Ising model:** The goal of this problem is to analyze the statistical mechanics of the one-dimensional Ising model.

(a) Let $f(\sigma_1, \sigma_2) = \exp[\beta J \sigma_1 \sigma_2]$. Show that

$$f(\sigma_1, \sigma_2) = \cosh \beta J + \sigma_1 \sigma_2 \sinh \beta J. \quad (24.135)$$

(b) The partition function for an Ising chain with N spins is

$$\sum_{\sigma_1, \dots, \sigma_N \in \{-1, 1\}} \prod_{l=1}^{N-1} f(\sigma_l, \sigma_{l+1}). \quad (24.136)$$

Inserting Eq. (24.135), show that only one term survives the sum over $\sigma_1 \dots \sigma_N$.

- (c) Evaluate the free energy, and establish that it is a smooth, analytic function, ruling out any phase transition.
- (d) What is the thermal average of σ_1 as a function of temperature?

6. **Superlattices:** Consider a 3:1 mixture of atoms A and B in the structure depicted in Figure 5.4.

Construct a mean field theory analogous to Eq. (24.72) for atoms in this geometry.

- (a) Find two self-consistent equations for σ_A and σ_B . One of the equations should be

$$\sigma_A = \tanh(\beta\mu_B H + \epsilon_{AB}\beta[4\sigma_B + 8\sigma_A]). \quad (24.137)$$

- (b) Write down the simple linear relation between σ_A and σ_B which follows from requiring atoms A and B to be in 3:1 ratio.
- (c) Inverting the tanh in the two equations and subtracting them to eliminate H , obtain a single self-consistent equation for σ_A .
- (d) Draw a picture illustrating the solution of this equation. Carefully trace out the solutions as a function of temperature, looking closely at the onset of order. According to mean field theory, is the transition first or second order?

7. **Properties of scaling function h :** Consider the scaling function h defined in Eq. (24.128).

- (a) Send $T \rightarrow T_c$. What is the behavior of $h(x)$ in the vicinity of $x = 0$? Does it have some type of singularity, or not?
- (b) While holding t fixed away from zero, send M toward zero. How must $h(x)$ behave in this limit?
- (c) Obtain the Rushbrooke relation, Eq. (24.117), employing h .
- (d) $h(x)$ vanishes as a power of $x + x_0$ for $x + x_0$ close to but greater than zero. Find the power.

8. **Preisach model:** The Preisach model views a magnet as a large collection of noninteracting hysteretic domains. Each domain can be described by the hysteretic function $\mu_{H_1, H_2}(H)$. The way μ works is this: If $\mu = 0$, it remains so until H exceeds H_2 . Then μ jumps to μ_B . It remains at μ_B until H drops below H_1 , at which point it returns to 0. If \mathcal{N} is the probability density of domains with lower and upper fields H_1 and H_2 , then the total response of a ferromagnet is given by

$$\vec{M} = \int_{-\infty}^{\infty} dH_1 \int_{H_1}^{\infty} dH_2 \mathcal{N}(H_1, H_2) \mu_{H_1, H_2}(H) \quad (24.138)$$

Argue that any magnet described by Eq. (24.138) exhibits *return-point memory*, as shown in Figure 24.9. That is, suppose field H is changed as follows:

- H is initially made large and negative.
- H increases monotonically to some value H_0 , where the magnetization is M_0 .
- H next decreases below H_0 .
- Finally, it increases back up to H_0 . What needs to be argued is that the magnetization has returned to M_0 .

References

- A. Aharoni (1996), *Introduction to the Theory of Ferromagnetism*, Clarendon Press, Oxford.
- G. Ahlers (1980), Critical phenomena at low temperature, *Reviews of Modern Physics*, **52**, 489–503.
- R. J. Baxter (1982), *Exactly Solved Models in Statistical Mechanics*, Academic Press, London.
- F. Bertaut and R. Pauthenet (1957), Crystalline structure and magnetic properties of ferrites having the general formula $5\text{Fe}_2\text{O}_3 \cdot 3\text{M}_2\text{O}_3$, *Proceedings of the Institution of Electrical Engineering*, Part B, **104**, Supplement 5, 261–264.
- H. N. Bertram and J. G. Zhu (1992), Fundamental magnetization processes in thin-film recording media, *Solid State Physics: Advances in Research and Applications*, **46**, 271–371.
- K. Binder and A. P. Young (1986), Spin glasses: Experimental facts, theoretical concepts and open questions, *Reviews of Modern Physics*, **58**, 801–976.
- R. M. Bozorth (1951), *Ferromagnetism*, van Nostrand, New York.
- W. L. Bragg and E. J. Williams (1934), The effect of thermal agitation on atomic arrangement in alloys, *Proceedings of the Royal Society of London*, **A145**, 699–730.
- A. Corciovei, G. Costache, and D. Vamanu (1972), Ferromagnetic thin films, *Solid State Physics: Advances in Research and Applications*, **27**, 237–350.
- H. Z. Cummins (1971), Light scattering spectroscopy of critical phenomena, in *Critical Phenomena*, M. S. Green, ed., Proceedings of the International School of Physics “Enrico Fermi”, pp. 380–444, Academic Press, New York.
- C. Domb (1974), Ising model, in *Phase Transitions and Critical Phenomena*, C. Domb and M. S. Green, eds., vol. 3, pp. 357–484, Academic Press, London.
- S. F. Edwards and P. W. Anderson (1975), Theory of spin glasses, *Journal of Physics F*, **5**, 965–974.
- E. Fawcett, H. L. Alberts, V. Y. Galkin, and D. R. Noakes (1994), Spin-density-wave antiferromagnetism in chromium alloys, *Reviews of Modern Physics*, **66**, 25–127.
- D. S. Fisher, G. M. Grinstein, and A. Khurana (1988), Theory of random magnets, *Physics Today*, **41**(12), 56–67.
- M. E. Fisher (1974), The renormalization group in the theory of critical behaviour, *Reviews of Modern Physics*, **46**, 597–616.
- W. Gilbert (1600), *On the Loadstone and Magnetic Bodies, and on the Great Magnet the Earth*, John Wiley and Sons, New York. Translated by P. F. Mottelay, 1893
- N. Goldenfeld (1992), *Lectures on Phase Transitions and the Renormalization Group*, Addison-Wesley, Reading, MA.
- I. S. Grigoriev and E. Z. Meilkhov, eds. (1997), *Handbook of Physical Quantities*, CRC Press, Boca Raton, FL.
- E. A. Guggenheim (1945), The principle of corresponding states, *Journal of Chemical Physics*, **13**, 253–261.
- P. Heller and G. B. Benedek (1962), Nuclear magnetic resonance in MnF_2 near the critical point, *Physical Review Letters*, **8**, 428–432.
- J. F. Herbst (1991), $\text{R}_2\text{Fe}_{14}\text{B}$ materials: Intrinsic properties and technological aspects, *Reviews of Modern Physics*, **63**, 819–898.
- L. L. Hirst (1997), The microscopic magnetization: Concept and application, *Reviews of Modern Physics*, **69**, 607–627.
- J. A. Hofmann, A. Paskin, K. J. Tauer, and R. J. Weiss (1956), Analysis of ferromagnetic and antiferromagnetic second-order transitions, *Journal of Physics and Chemistry of Solids*, **1**, 45–60.

- P. C. Hohenberg and B. I. Halperin (1977), Theory of dynamic critical phenomena, *Reviews of Modern Physics*, **49**, 435–479.
- I. S. Jacobs and R. W. Schmitt (1959), Low-temperature electrical and magnetic behavior of dilute alloys: Mn in Cu and Co in Cu, *Physical Review*, **113**, 459–463.
- D. Jiles (1991), *Introduction to Magnetism and Magnetic Materials*, Chapman and Hall, London.
- L. J. Jongh and A. R. Miedema (1974), Experiments on simple magnetic model systems, *Advances in Physics*, **23**, 1–260.
- L. D. Landau (1937), On the theory of phase transitions, *Physikalische Zeitschrift der Sowjetunion*, **11**, 26 and 545. In German. Translated in Landau (1965), p. 193–216
- L. D. Landau (1965), *Collected Papers of L D Landau*, D. ter Haar, ed., Gordon and Breach, New York.
- L. D. Landau and E. M. Lifshitz (1935), On the theory of the dispersion of magnetic permeability in ferromagnetic bodies, *Physikalische Zeitschrift der Sowjetunion*, **8**, 153–168. In German. Translated in Landau (1965), pp. 101–116
- L. D. Landau and E. M. Lifshitz (1980), *Statistical Physics, Part I*, 3rd ed., Pergamon Press, Oxford.
- H. Landolt and R. Börnstein (1959), *Numerical Data and Functional Relationships in Science and Technology*, II, Springer-Verlag, Berlin.
- B. T. Matthias, R. M. Bozorth, and J. H. van Vleck (1961), Ferromagnetic interactions in EuO, *Physical Review Letters*, **7**, 160–161.
- L. Néel (1948), Magnetic properties of ferrites: Ferrimagnetism and antiferromagnetism, *Annales de Physique*, **3**, 137–198. In French.
- A. S. Oja and O. V. Lounasmaa (1997), Nuclear magnetic ordering in simple metals at positive and negative nanokelvin temperatures, *Reviews of Modern Physics*, **69**, 1–136.
- L. Onsager (1944), Crystal statistics I: A two-dimensional model with an order-disorder transition, *Physical Review*, **65**, 117–149.
- A. Pais (1982), *Subtle is the Lord*, Oxford University Press, New York.
- G. E. Pake (1993), Nuclear magnetic resonance in bulk matter, *Physics Today*, **46**(10), 46–50.
- G. Parisi (1987), Spin glasses, in *Proceedings of the International School of Physics 'Enrico Fermi' Course 92: Elementary Particles*, N. Cabibbo, ed., pp. 404–421, North Holland, Amsterdam.
- R. S. Preston, S. S. Hanna, and J. Heberle (1962), Mössbauer effect in metallic iron, *Physical Review*, **128**, 2207–2218.
- J. S. Rigden (1986), Quantum states and precession: The two discoveries of NMR, *Reviews of Modern Physics*, **58**, 433–448.
- C. P. Slichter (1963), *Principles of Magnetic Resonance*, Harper and Row, New York.
- P. I. Slick (1980), Ferrites for non-microwave applications, in *Ferromagnetic Materials*, E. P. Wohlfarth, ed., vol. 2, pp. 190–241, North-Holland, Amsterdam.
- K. H. Stewart (1954), *Ferromagnetic Domains*, Cambridge University Press, Cambridge.
- M. Vicentini-Missoni (1972), Equilibrium scaling in fluids and magnets, in *Phase Transitions and Critical Phenomena*, C. Domb and M. S. Green, eds., vol. 2, pp. 39–77, Academic Press, London.
- P. Weiss (1907), The molecular field hypothesis and the ferromagnetic phenomenon, *Journal de Physique*, **6**, 661–690.
- M. B. Weissman (1988), $1/f$ noise and other slow, nonexponential kinetics in condensed matter, *Reviews of Modern Physics*, **60**, 537–571.
- M. B. Weissman (1993), What is a spin glass? A glimpse via mesoscopic noise, *Reviews of Modern Physics*, **65**, 829–839.
- B. Widom (1965), Equation of state in the neighborhood of the critical point, *Journal of Chemical Physics*, **43**, 3898–3905.
- K. G. Wilson (1975), The renormalization group: Critical phenomena and the Kondo problem, *Reviews of Modern Physics*, **47**, 773–840.

25. Magnetism of Ions and Electrons

25.1 Introduction

As late as the first quarter of the twentieth century, the magnetism of solids remained a great mystery. The assumption that magnetic solids were assemblies of vast numbers of smaller magnets was an hypothesis that could successfully be studied from mechanical and statistical points of view. However, the origin of the microscopic magnets was not explained.

The greatest difficulty was presented by a theorem of Bohr (1911) and van Leeuwen (1921), which stated that if one considers a collection of classical charged particles interacting with each other and with external potentials, their partition function must be completely insensitive to the presence of any applied magnetic field. The simple proof of this statement is the subject of Problem 2. Therefore, no solid in thermal equilibrium should have any magnetic properties. Indeed “when one attempts to apply classical statistics to electronic motions within the atom, the less said, the better” [van Vleck (1932), p. 104].

If one thinks of a collection of electrons in a box, moving with various velocities, this result at first seems strange, because upon introduction of a magnetic field the electrons will begin to circle in orbits and thus generate magnetic moments. However, the magnetism of electrons turning in circles in the middle of a sample is exactly compensated by electrons at the boundaries, as illustrated in Problem 1. Only with the appearance of quantum mechanics could one explain how solids could have magnetic properties at all.

In part, the answer given by quantum mechanics is the simple assertion that electrons possess a magnetic moment of strength μ_B , together with the directive that one must not question its origin in classical terms. The magnetism of solids does not end, however, with the primitive magnetic moments of the elementary particles, but continues to emerge in new ways from assemblies of particles. The unfilled inner shells of the transition metals and rare earth metals have a strong paramagnetic response. They sometimes have permanent magnetic moments, and even filled atomic shells are weakly diamagnetic. An ensemble of free electrons in a box is diamagnetic.

The existence of magnetism is due to quantum-mechanical restrictions on the orbits of charged particles that prevent the perfect classical cancellation from occurring. Many details of how the magnetic response works out are best viewed as attempts by tightly packed electrons to minimize Coulomb repulsion. Two electrons circling a nucleus reduce their Coulomb interaction by adopting an antisymmetric wave function that vanishes whenever they come near each other. The Pauli

principle demands that the overall wave function be antisymmetric, so the spin wave function must be symmetric. That is, the electrons lower their energy by adopting the same spin state and developing a local magnetic moment. This tendency to develop ferromagnetism fights against other energies that tend the opposite way and that are of the same general size. The helium atom does not have a ground state with total spin $S = 1$, but instead has $S = 0$. The reason is that the lowest-energy state for a single electron is a nondegenerate $n = 0, l = 0$ state. To build a spatially antisymmetric wave function, there is no choice but to have at least one electron in an excited state, $n = 1, l = 1$, and this excited state costs enough in energy to outweigh the benefits of antisymmetry. In fact, it can be proved in general that the ground state of any two-electron system has total spin $S = 0$, which shows that filling atomic shells in the proper order is the most important first step in placing electrons in their ground state.

No general statements will be true in all cases because magnetism results frequently from competition between delicately balanced competing effects. However, it may be helpful to indicate some of the energies that are likely to be involved.

Shell energies 1–10 eV: To good approximation, electrons fill up each atom with ascending values of index n and angular momentum quantum number l , as described in the periodic table, and rarely employ states with quantum number n until all states with number $n - 1$ have been filled. The closed inner shells of the atoms have no net magnetic moment and are weakly diamagnetic. Exceptions to this rule in the transition metals and rare earths can produce metals with spontaneous magnetic moments.

Hund's rules 1–10 eV: Within an incompletely filled atomic shell, electrons try to minimize Coulomb repulsion by choosing total spin and angular momentum in accord with Hund's rules, to be described in more detail below. For unfilled f shells of the rare earth solids, the energy to be gained from Hund's rules overrides any interaction with neighboring atoms.

Band energies 1–10 eV: In Fe, Ni, and Co, delocalized electrons acquire a net magnetic moment, essentially also as a means of reducing Coulomb repulsion.

Crystal field splitting 0.1–1 eV: The presence of neighboring atoms in a crystal breaks the spherical symmetry of the individual atomic nucleus. For iron compounds, this effect is often large enough that Hund's rules no longer apply, and the total spatial angular momentum L equals 0.

Interatomic exchange 10^{-2} –0.1 eV: Just as the combination of Coulomb repulsion and Fermi statistics produces magnetic correlations within the atom, it also creates them between neighboring atoms. Whether the effect produces ferromagnetic or antiferromagnetic correlations is extremely difficult to calculate or predict, because it typically results from the near cancellation of terms whose energy might be ~ 1.0 eV.

Indirect exchange, superexchange 10^{-2} –0.1 eV: Magnetic atoms can induce mag-

netic moments in their surroundings, and the induced moments can interact with other magnetic atoms, producing a net indirect interaction. The surrounding might include a sea of otherwise nonmagnetic conduction electrons or neighboring nonmagnetic atoms.

Interaction with magnetic fields 10^{-4} – 10^{20} eV: The energy of a single magnetic moment in a 1-T magnetic field is only around 10^{-4} eV. The interaction energy of magnetic moments with the magnetic fields produced by other moments therefore appears to be small. However, the interaction is so long ranged that the number of relevant interactions is enormous, and it effectively grows without bound as samples grow in size. For this reason, magnetic samples spontaneously develop elaborate domain structures in which magnetic correlations on large scales are quite different from the magnetic correlations on short scales. It is also for this reason that magnetic fields of a strength achievable in the laboratory are able to flip the moments in permanent magnets.

25.2 Atomic Magnetism

Isolated atoms have magnetic properties, and the goal of this section is to lay out the combination of semiempirical wisdom and quantum mechanics that permits them to be calculated. Speaking of isolated atoms may raise thoughts of dilute gases, but magnetic experiments on dilute vapors of rare elements are difficult and rarely performed, partly because magnetic measurements so often rely upon measuring torques or forces created when magnetic fields are applied to large solid samples. What is referred to theoretically as an isolated atom is more likely a rare magnetic atom dissolved in a largely nonmagnetic host, in which case the possibility that the magnetic atom is influenced by the host has to be considered. Nevertheless, the discussion begins with the assumption that any desired atom can be isolated and its magnetic properties can be measured.

The interaction of isolated atoms with external magnetic fields occurs in two ways. First, there is the interaction of the orbital magnetic momentum with the magnetic induction. This contribution is found by including the vector potential \vec{A} in the momentum operator for the electron motion. Second, one must include the interaction of \vec{B} with the electron spin. One has therefore a Hamiltonian of the form

$$\hat{\mathcal{H}} = \frac{1}{2m} \sum_l \left[\hat{P}_l + \frac{e}{c} \vec{A}(\hat{R}_l) \right]^2 + 2\mu_B B \hat{S}_l^z, \quad (25.1)$$

The factor of 2 sitting in front of μ_B is a consequence of Dirac's relativistic theory of the electron. The positive sign of the term results from the negative charge of the electron, the convention that e be positive, and the interaction energy (24.37).

where μ_B is the Bohr magneton defined in Eq. (24.39).

The sum is taken over all electrons in the atom. Two additional comments are in order. The first is that all of the magnetic interactions involve the inverse of

the electron mass. This fact is significant, because it demonstrates why nuclear contributions to magnetism can be ignored in this context. These would involve the inverse of the nuclear mass instead and are therefore negligible by comparison.

In order to obtain definite results from the Hamiltonian, assume that

$$\vec{A}(\hat{R}) = -\frac{1}{2}\hat{R} \times B\hat{z}, \quad (25.2)$$

which describes a uniform induction \vec{B} , taken to point in the \hat{z} direction. Define the angular momentum operator

$$\hbar\hat{L} = \sum_j \hat{R}_j \times \hat{P}_j \quad (25.3)$$

$$\Rightarrow \hat{P}_j \cdot \vec{A} = -\frac{1}{2}\hat{P}_j \cdot \hat{R} \times \vec{B} = \frac{1}{2}\vec{B} \cdot \hat{R}_j \times \hat{P}_j \quad \begin{array}{l} \hat{R} \text{ and } \hat{P} \text{ can be treated here as commuting} \\ \text{operators, because the cross product always} \\ \text{multiplies different components together.} \end{array} \quad (25.4)$$

$$\Rightarrow \hat{\mathcal{H}} = \frac{1}{2m} \sum_l \hat{P}_l^2 + \mu_B (\hat{L} + 2\hat{S}) \cdot \vec{B} + \frac{e^2}{8mc^2} B^2 \sum_j (\hat{X}_j^2 + \hat{Y}_j^2). \quad (25.5)$$

\hat{L} and \hat{S} denote the total orbital and spin angular momenta of the atom, and have integer and half-integer eigenvalues respectively. If the states $|l\rangle$ index the electronic orbital states in the absence of the magnetic interaction, then keeping all terms up to quadratic order in the induction B , perturbation theory to second order gives

$$\Delta\mathcal{E}_l = \mu_B \vec{B} \cdot \langle l | \hat{L} + 2\hat{S} | l \rangle + \sum_{l' \neq l} \frac{|\langle l | \mu_B \vec{B} \cdot (\hat{L} + 2\hat{S}) | l' \rangle|^2}{\mathcal{E}_l - \mathcal{E}_{l'}} + \frac{e^2 B^2}{8mc^2} \langle l | \sum_j (\hat{X}_j^2 + \hat{Y}_j^2) | l \rangle. \quad (25.6)$$

The first term on the right hand side of Eq. (25.6) is linear, and it dominates magnetic response unless the relevant matrix element vanishes. The reason is that the natural dimensionless parameter in terms of which to discuss the strength of the magnetic interactions is the ratio of a typical magnetic to a typical atomic energy. The typical magnetic energy is

$$\mu_B B = 5.79 \cdot 10^{-5} [B/\text{Tesla}] \text{ eV}. \quad (25.7)$$

On the other hand, a typical separation between atomic energy levels is on the order of 1 eV, so the magnetic energies are small by comparison.

25.2.1 Hund's Rules

In order to determine whether the first term of Eq. (25.6) vanishes or not, it is necessary to find the properties of the atom in its ground state. The ground states are described for all but the very heaviest atoms by Hund's rules, which originated in spectroscopic observation. They are easy to describe, but could only rigorously be justified by full solution of the quantum-mechanical problem of many electrons circling the nucleus. In order to express the rules, it must first be observed that

electrons organize themselves into shells. The filled shells are relatively inert, and Hund's rules concern themselves only with the organization of electrons in incompletely filled shells. Electrons in these shells can be indexed by quantum numbers L , L_z , S , and S_z . In fact, only $\hat{J} = \hat{L} + \hat{S}$ is a true constant of the motion. Use of \hat{L} and \hat{S} as independent quantum numbers is predicated upon assuming that spin and angular momentum do not interact strongly with one another, which means that the atom does not interact strongly with the magnetic field it generates itself. Formally, the spin-orbit coupling, proportional to $\hat{S} \cdot \hat{L}$, needs to be a small perturbation. Given this assumption of *Russel-Saunders coupling*, Hund's rules are as follows:

1. Electrons in the incomplete shell first choose to maximize the total spin S . For example, for an atom with two valence electrons in a shell with $l > 1$, the electrons can choose either to occupy the same L_z state, in which case they must have opposite spins, or different L_z states (all degenerate in energy), in which case the spins can do what they want. If the electrons occupy different orbitals and adopt a triplet spin state, which is symmetric, then they may also have an antisymmetric spatial state. The Coulomb repulsion between the electrons is then reduced because the wave function automatically vanishes as they approach each other. For this reason, the two electrons prefer to stick to different orbitals, and they take the triplet over the singlet state. One can think of this rule as specifying that atoms on a single site develop ferromagnetic correlation and want their spins to point together.
2. Once S has been determined, the electrons choose the largest value of L consistent with putting electrons in different orbitals whenever possible. For example, when the shell is half full, all possible values of l_z are occupied, and the total L must be zero. This rule may be understood classically as a second consequence of the desire to reduce Coulomb interactions. If one were required to set two electrons spinning about an atom with the same total angular momentum, but otherwise as far apart as possible, one would put them in the same orbit, but 180° out of phase. In this case, the electrons would actually be in the same state quantum mechanically, just differing by a phase factor; the Coulomb repulsion between them would be enormous, and such a state is not favored. The electrons have to be in states of different L_z . So the next guess is that they rotate classically in the same direction, and about axes that differ as little as possible. If, for example, they were to rotate in opposite directions, they would encounter each other twice per orbit.
3. Once L and S have been determined, the space of $(2L + 1)(2S + 1)$ states is split by the spin-orbit interaction, which has a magnitude on the order of electronic orbital energies times $(Z\alpha)^2$, where Z is the atomic number and α is the fine structure constant. The electrons choose as the ground state

$$J = |L - S| \quad (25.8a)$$

if the shell is less than half full, and they choose

$$J = L + S \quad \text{See Landau and Lifshitz (1977), p. 267 for a discussion.} \quad (25.8b)$$

if the shell is more than half full. When the shell is half full, $L = 0$, so there is no jump in J at half filling. For a shell that is one electron shy of half filling, one has $S = L$, which implies $J = 0$ (see Figure 25.1).

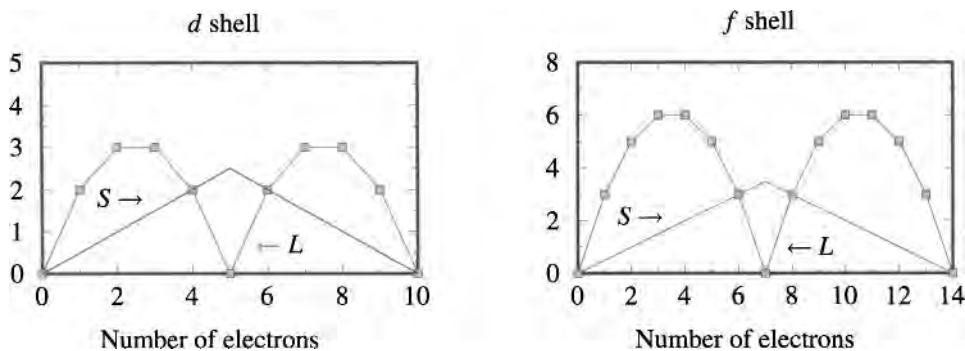


Figure 25.1. Hund’s rules for d and f shells predict values for spin angular momentum S and orbital angular momentum L as indicated.

The groundwork has now been laid to calculate the matrix elements constituting the first term on the right-hand side of Eq. (25.6),

$$\langle l | \hat{L}_z + 2\hat{S}_z | l \rangle. \quad (25.9)$$

The reason to refer to “elements” is that the state $|l\rangle$ is always degenerate, so one must use first-order degenerate perturbation theory. Hund’s rules first specify S , then L , and finally J , but this subspace is still $2J + 1$ -fold degenerate in the absence of applied magnetic fields. A more detailed description of the quantum numbers involved in these states is provided by writing

$$\langle JLSJ_z | \hat{L}_z + 2\hat{S}_z | JLSJ_z \rangle. \quad (25.10)$$

A physical description of what is involved in calculating (25.10) appears in Figure 25.2. The magnitude and direction of \vec{J} are conserved, the magnitudes of \vec{L} and \vec{S} are conserved, but not their directions, and $\vec{L} + 2\vec{S}$ needs to be calculated. Its expectation value lies along \vec{J} .

The formal evaluation of Eq. (25.10) is made possible by the Wigner–Eckart theorem, according to which the matrix elements of any vector operator \hat{V} are proportional to the matrix elements of \hat{J} :

$$\langle JLSJ_z | \hat{V} | JLSJ_z \rangle = g(JLS) \langle JLSJ_z | \hat{J} | JLSJ_z \rangle, \quad (25.11)$$

where g is independent of J_z and J_z' , although it depends upon everything else, including the operator \hat{V} . The particular application needed in the case of magnetism is

$$\langle JLSJ_z | \hat{L}_z + 2\hat{S}_z | JLSJ_z \rangle = g(JLS) \langle JLSJ_z | \hat{J}_z | JLSJ_z \rangle \quad (25.12)$$

$$= g(JLS) J_z \delta_{J_z J_z'}. \quad (25.13)$$

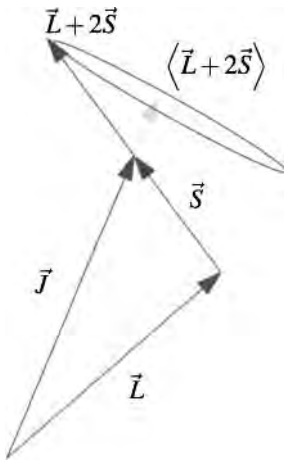


Figure 25.2. View the spin and orbital angular momentum of an atom as two gyroscopes, linked end to end. The total angular momentum $\vec{J} = \vec{L} + \vec{S}$ is conserved, but \vec{L} and \vec{S} precess about one another. The expectation value of $\vec{L} + \vec{S}$ lies along \vec{J} .

Evaluation of $g(JLS)$. The problem of finding the splitting induced by the magnetic field is therefore reduced to the problem of finding the *Landé g factor* $g(JLS)$. A trick enabling the evaluation begins by considering

$$\langle JLSJ_z | \hat{L} + 2\hat{S} | JLSJ_z' \rangle = g(JLS) \langle JLSJ_z | \hat{J} | JLSJ_z' \rangle \quad (25.14)$$

$$\Rightarrow \langle JLSJ_z | \hat{L} + 2\hat{S} | J'L'S'J_z' \rangle = g(JLS) \langle JLSJ_z | \hat{J} | J'L'S'J_z' \rangle \quad (25.15)$$

Both matrix elements vanish unless $J = J'$ and $L = L'$ and $S = S'$.

$$\begin{aligned} &\Rightarrow \sum_{L'J'S'J_z'} \langle JLSJ_z | \hat{L} + 2\hat{S} | J'L'S'J_z' \rangle \cdot \langle J'L'S'J_z' | \hat{J} | J''L''S''J_z'' \rangle \\ &= g(JLS) \sum_{L'J'S'J_z'} \langle JLSJ_z | \hat{J} | J'L'S'J_z' \rangle \cdot \langle J'L'S'J_z' | \hat{J} | J''L''S''J_z'' \rangle. \end{aligned} \quad (25.16)$$

Because the sum in Eq. (25.16) is taken over a complete set of states, it becomes

$$\langle JLSJ_z | (\hat{L} + 2\hat{S}) \cdot \hat{J} | JLSJ_z' \rangle = g(JLS) \langle JLSJ_z | \hat{J}^2 | JLSJ_z' \rangle. \quad (25.17)$$

All of the matrix elements in (25.17) can be evaluated because

$$\hat{S}^2 = (\hat{J} - \hat{L})^2 = \hat{J}^2 + \hat{L}^2 - 2\hat{L} \cdot \hat{J} \quad (25.18)$$

$$\hat{L}^2 = (\hat{J} - \hat{S})^2 = \hat{J}^2 + \hat{S}^2 - 2\hat{S} \cdot \hat{J}. \quad (25.19)$$

Therefore

$$g(JLS) = \frac{1}{2} \frac{[3J(J+1) - L(L+1) + S(S+1)]}{J(J+1)}. \quad (25.20)$$

The final result is that an external magnetic field splits the $2J + 1$ -fold ground state of an isolated atom into $2J + 1$ separate levels, and the energy difference between them is

$$\frac{\mu_B B}{2} \frac{[3J(J+1) - L(L+1) + S(S+1)]}{J(J+1)}. \quad (25.21)$$

25.2.2 Curie's Law

Room temperature corresponds to an energy of 0.025 eV, much larger than the basic energy scale of magnetic ions given in Eq. (25.7). Therefore magnetic spins at room temperature find themselves in a statistical distribution of states. States with spin up and spin down are almost equally populated, so the net magnetic moments are fairly small.

It is usually, although not always, adequate to assume that only the lowest-lying spin multiplet contributes to statistical mechanical sums. Making this assumption, the partition function for a single magnetic ion is given by

$$Z_{\text{ion}} = \sum_{J_z=-J}^J e^{-\beta g \mu_B B J_z} \quad (25.22)$$

$$= \frac{e^{\beta g \mu_B B (J+1/2)} - e^{-\beta g \mu_B B (J+1/2)}}{e^{\beta g \mu_B B / 2} - e^{-\beta g \mu_B B / 2}}. \quad (25.23)$$

The free energy is

$$\mathcal{F} = -k_B T \ln Z_{\text{ion}} + \frac{1}{8\pi} \int d\vec{r} B^2. \quad (25.24)$$

In this thermodynamic ensemble, the energy of the external field must be included. If the potential \mathcal{G} were used instead, the integral over the external field could be omitted.

According to Eq. (24.26), with a density of n magnetic ions in a volume \mathcal{V} , one can now find the magnetization from

$$H = \frac{4\pi}{\mathcal{V}} \frac{\partial \mathcal{F}}{\partial B} \Rightarrow M = \frac{B}{4\pi} - \frac{1}{\mathcal{V}} \frac{\partial \mathcal{F}}{\partial B} \quad (25.25)$$

$$\Rightarrow M = nk_B T \frac{\partial}{\partial B} \ln Z_{\text{ion}} \quad (25.26)$$

$$= n \mu_B g J \mathcal{B}_J(\beta \mu_B g J B), \quad (25.27)$$

where

$$\mathcal{B}_J(x) = \frac{2J+1}{2J} \coth\left(\frac{2J+1}{2J}x\right) - \frac{1}{2J} \coth\left(\frac{x}{2J}\right). \quad (25.28)$$

So long as $\mu_B B \ll k_B T$, one has

$$\coth x \approx \frac{1}{x} + \frac{x}{3} + \dots \quad (25.29)$$

$$\Rightarrow \mathcal{B}_J = \frac{1}{3} \frac{J+1}{J} \beta \mu_B g J B, \quad (25.30)$$

so that

$$\bar{M} \approx n g^2 (\mu_B)^2 \frac{B}{k_B T} \frac{J(J+1)}{3}. \quad (25.31)$$

Equation (25.31) is Curie's law. It holds so long as the magnetic ions may be treated as noninteracting and in isotropic environments. The law breaks down once interactions between the different ions become important; even at high temperatures, interacting ions are better described by Eq. (24.41).

Comparison with Experiment. Curie's law can be tested for a variety of magnetic ions in nonmagnetic hosts. The comparison is particularly successful for lanthanide compounds, where a rare earth ion sits in a nonmagnetic host. For example, cerium compounds include CeCl_3 , CeF_3 , and $\text{Ce}_2\text{Mg}_3(\text{NO}_3)_{12} \cdot 24\text{H}_2\text{O}$. Properties of a magnetic ion vary by around 5% from one host to another.

Comparison with experiment is accomplished by writing the susceptibility in the form

$$\chi = n \frac{1}{3k_B T} \mu_{\text{eff}}^2, \quad (25.32)$$

where according to Eq. (25.31),

$$\mu_{\text{eff}} = g(JLS) \sqrt{J(J+1)} \cdot \mu_B \quad \text{For dilute magnetic systems, ignore the difference between } \vec{B} \text{ and } \vec{H}. \quad (25.33)$$

Equation (25.33) is to be compared to an experimental measurement of

$$\mu_{\text{exp}} = \sqrt{\frac{3k_B T \chi}{n}}. \quad (25.34)$$

This comparison is performed for the lanthanides in Table 25.1. The agreement with theory is impressive, except in the case of europium and samarium, where magnetic multiplets lying above the ground state play a measurable role. Bohr says that “[o]n the whole a consideration of the magnetic properties of the elements within the long periods gives us a vivid impression of how a wound in the otherwise symmetrical inner structure is first developed and then healed as we pass from one element to another.” [Bohr (1922), p. 107]

For magnetic transition metal ions the comparison is much less successful, as shown in Table 25.2. d electron wave functions have a longer range than the f electron wave functions, and transition metal ions interact more strongly with their environment than the lanthanides, so the third of Hund's rules is no longer correct. However, the theory can be improved substantially by postulating that the orbital angular momentum L is *quenched* by interactions with the crystal. Intuitively, one can think of interactions with crystal fields causing \hat{L} to precess, so that all matrix elements of \hat{L} vanish, although \hat{L}^2 still has value $L(L+1)$. In this case, Hund's third rule is replaced by $J = S$. Table 25.2 shows that this new rule is fairly successful in explaining the experimental observations.

Larmor Diamagnetism and Van Vleck Paramagnetism. The leading contribution to the susceptibility in Eq. (25.6) vanishes when $J = 0$, because $J = 0$ leads to $g(JLS) = 0$. J can vanish either for filled shells, or for shells that are one electron shy of half filling, because in the latter case $L = S$, and $J = |L - S| = 0$ according to the third of Hund's rules. The ground state $|0\rangle$ with $J = 0$ is nondegenerate, and its change in energy with magnetic induction B is

$$\Delta \mathcal{E} = \frac{e^2}{8mc^2} B^2 \langle 0 | \sum_j (\hat{X}_j^2 + \hat{Y}_j^2) | 0 \rangle - \sum_{l' \neq 0} \frac{|\langle l' | \mu_B \vec{B} \cdot (\hat{L} + 2\hat{S}) | 0 \rangle|^2}{\mathcal{E}_{l'} - \mathcal{E}_0}. \quad (25.35)$$

Table 25.1. Effective magneton numbers μ_{eff} calculated from Eq. (25.33) and compared with experiment at 300 K

Element	Term	μ_{eff} , Eq. (25.33) (μ_B)	μ_{exp} , Eq. (25.34) (μ_B)
La ³⁺	$4f^0 1S$	0	Diamagnetic
Ce ³⁺	$4f^1 2F_{5/2}$	2.5	2.3
Pr ³⁺	$4f^2 3H_4$	3.6	3.4
Nd ³⁺	$4f^3 4I_{9/2}$	3.6	3.5
Pm ³⁺	$4f^4 5I_4$	2.7	Radioactive
Sm ³⁺	$4f^5 6H_{5/2}$	0.9	1.6
Eu ³⁺	$4f^6 7F_0$	0	3.4
Gd ³⁺	$4f^7 8S_{7/2}$	7.9	7.9
Tb ³⁺	$4f^8 7F_6$	9.7	9.5
Dy ³⁺	$4f^9 6H_{15/2}$	10.6	10.4
Ho ³⁺	$4f^{10} 5I_8$	10.6	10.4
Er ³⁺	$4f^{11} 4I_{15/2}$	9.6	9.4
Tm ³⁺	$4f^{12} 3H_6$	7.6	7.1
Yb ³⁺	$4f^{13} 2F_{7/2}$	4.5	4.9
Lu ³⁺	$4f^{14} 1S$	0	0

The rare earth atoms are dissolved in compounds such as $\text{Ce}_2\text{I}_2\text{O}_{11} \cdot 4\text{H}_2\text{O}$, where they give up the two 6s electrons and one of the 4f electrons. The particularly strong discrepancies for europium and samarium are due to the presence of additional low-lying states neglected by the simple theory. Source: van Vleck (1932) p. 243 and Boudreaux and Mulay (1976), p. 276.

Table 25.2. Effective magneton numbers μ_{eff} calculated from Eqs. (25.33) and (25.34) and compared with experiment at 300 K

Element	Term	μ_{eff} , Eq. (25.33) (μ_B)	μ_{eff} , $J = S$ (μ_B)	μ_{exp} , Eq. (25.34) (μ_B)
Ti ³⁺	$3d^1 2D_{3/2}$	1.6	1.7	1.8
V ³⁺	$3d^2 3F_2$	1.6	2.8	2.7
Cr ³⁺	$3d^3 4F_{3/2}$	0.8	3.9	3.8
Mn ³⁺	$3d^4 5D_0$	0.0	4.9	4.9
Fe ³⁺	$3d^5 6S_{5/2}$	5.9	5.9	5.9
Fe ²⁺	$3d^6 5D_4$	6.7	4.9	5.3
Co ²⁺	$3d^7 4F_{9/2}$	6.5	3.9	4.0
Ni ²⁺	$3d^8 3F_4$	5.6	2.8	2.9–3.5
Cu ²⁺	$3d^9 2D_{5/2}$	3.6	1.7	1.7–1.9

The quenching of orbital angular momentum means that Eq. (25.33) is best evaluated with $J = S$, rather than Eq. (25.8). Source: Boudreaux and Mulay (1976), p. 54.

Table 25.3. Susceptibilities of noble gases compared with Eq. (25.36)

Element:	He	Ne	Ar	Kr	Xe
$-\chi$, experiment (10^{-6} cm ³ mole ⁻¹):	1.88	7.02	19.18	28.49	43.33
χ , Eq. (25.36) $\times 0.35$ (10^{-6} cm ³ mole ⁻¹):	0.99	14.82	20.54	23.74	27.95

The very rough agreement is slightly improved by multiplying Eq. (25.36) by 0.35. For helium, the factor of 6 in Eq. (25.36) is eliminated and a radius of 1 Å is employed. Otherwise, radii come from Table 11.1. Experimental data from Table 24.1.

Because the magnetic susceptibility $\chi = -\partial^2 \mathcal{G} / \partial H^2 \approx -\partial^2 \Delta \mathcal{E} / \partial B^2$, the first term on the left hand side of Eq. (25.35) leads to a magnetization against the applied field and is therefore diamagnetic, *Larmor diamagnetism*. The second term on the right-hand side of Eq. (25.35) is negative, because the denominator is negative and therefore produces magnetic response that is paramagnetic—*van Vleck paramagnetism*. The second term vanishes for closed shells, where not only J but L and S are all separately zero; however, for shells one electron short of half filling, both terms on the right of Eq. (25.35) may compete. Aside from observing that both are very small, no general statement can be added. Curie paramagnetism, Larmor diamagnetism, and van Vleck paramagnetism all feature a small magnetic susceptibility proportional to μ_B^2 . However, the mechanisms are quite different. Curie's law results from a matrix element that is linear in the magnetic field, and the susceptibility would vanish if it were not for the way that magnetic fields change the statistical occupation of states at nonzero temperature.

The susceptibility of the noble gases can be estimated by employing atomic radii from Table 11.1 and writing

$$\chi \approx -n \frac{e^2}{4mc^2} 6 \frac{2}{3} r^2. \quad (25.36)$$

r is the atomic radius, the factor of 6 comes from the fact that there are 6 electrons in the outer shell, and the factor of $2/3$ comes from estimating $x^2 + y^2 = 2r^2/3$.

As shown in Table 25.3, the comparison with experiment is only partially successful; agreement is improved by arbitrarily multiplying Eq. (25.36) by 0.35, presumably because it is not legitimate to treat all electrons as occupying the outer radius.

25.3 Magnetism of the Free-Electron Gas

Having determined the magnetic properties of electrons when strongly bound within ions, it is valuable to consider the opposite extreme and examine their magnetic properties as they move about nearly free in a metal.

There are essentially three terms in the response of free fermions to an external magnetic field. The first is called *Pauli paramagnetism*, and it results from the action of the magnetic field on the spins of the electrons. The second is called *Landau diamagnetism*, after Landau (1930), and results from the moments created by the circular motions of the electrons. The third (a series) was also calculated by

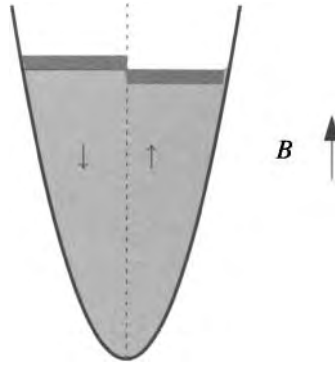


Figure 25.3. When subject to a magnetic induction B , the number of spin-down electrons increases and the number of spin-up electrons decreases, to minimize the total free energy. Landau (1939) and predicts the oscillations of magnetization with magnetic field that lead to the de Haas–van Alphen effect.

25.3.1 Pauli Paramagnetism

Pauli paramagnetism can be understood as follows: In the absence of a magnetic field, the ground state of a free electron gas has equal numbers of spin-up and spin-down electrons. An induction B pointing up raises the energies of spin-up electrons by the amount

$$\mathcal{E}_{\vec{k}} = \mathcal{E}_{\vec{k}}^0 + \mu_B B. \quad \text{The energy } \mathcal{E}_{\vec{k}}^0 \text{ is the energy of electrons in the absence of a magnetic field. The } g\text{-factor, which equals almost exactly 2, cancels the factor of } 1/2 \text{ from the spin-}1/2 \text{ quantum number.} \quad (25.37)$$

Now consider a very weak magnetic induction B applied to the electron gas, as shown in Figure 25.3, and calculate the net magnetic moment it induces. Remembering that the definition of $D(\mathcal{E})$ assumes up- and down-spin states to be equivalent, and must be divided by two if they are considered separately, the number of spin-up electrons is

$$N_{\text{up}} = \mathcal{V} \int d\mathcal{E}^0 \frac{D(\mathcal{E}^0)}{2} f(\mathcal{E}^0 + \mu_B B), \quad (25.38)$$

$D(\mathcal{E}^0)$ denotes the density of states in the absence of a magnetic field, and $f(\mathcal{E})$ is defined in Eq. (6.49). It is not clear that the density of states D should not change to first order with the magnetic field, but this guess will be verified in later calculations.

and the number of spin down electrons is

$$N_{\text{down}} = \mathcal{V} \int d\mathcal{E}^0 \frac{D(\mathcal{E}^0)}{2} f(\mathcal{E}^0 - \mu_B B). \quad (25.39)$$

Expanding in the small quantity B gives

$$N_{\text{up}} \approx \frac{N}{2} - \frac{\mu_B B}{2} \frac{\partial N}{\partial \mu}, \quad (25.40)$$

Notice that differentiating f with respect to $\mu_B B$ is the same as differentiating with respect to \mathcal{E}^0 , which in turn is the same as differentiating by the negative of the chemical potential, $-\mu$. The derivative with respect to the chemical potential can then be brought outside the integral.

while

$$N_{\text{down}} \approx \frac{N}{2} + \frac{\mu_B B}{2} \frac{\partial N}{\partial \mu}. \quad (25.41)$$

The magnetization M points in the direction opposite to the spins, because the electron is negatively charged. Therefore, the magnetization per volume is

$$M = \frac{\mu_B}{\mathcal{V}} (N_{\text{down}} - N_{\text{up}}) = \frac{(\mu_B)^2}{\mathcal{V}} \frac{\partial N}{\partial \mu} B \quad (25.42)$$

and the magnetic susceptibility χ is

$$\chi = \frac{\partial M}{\partial H} \approx \frac{\partial M}{\partial B} = (\mu_B)^2 \frac{1}{\mathcal{V}} \frac{\partial N}{\partial \mu}, \quad (25.43)$$

which at temperatures well below the Fermi temperature becomes

$$\chi = \mu_B^2 D(\mathcal{E}_F). \quad (25.44)$$

This expression makes use of the Sommerfeld expansion—for example, by differentiating the expression for N exhibited in Eq. (6.72).

In the particular case of the free Fermi gas, the density of states at the Fermi surface is given by Eq. (6.24), resulting in

$$\chi = \frac{\mu_B^2 k_F m}{\pi^2 \hbar^2} = 4.757 \cdot 10^{-7} (n/[10^{22} \cdot \text{cm}^{-3}])^{1/3}. \quad (25.45)$$

This expression is in cgs. For SI, multiply by $\frac{1}{4\pi}$.

25.3.2 Landau Diamagnetism

A collection of noninteracting electrons would change their energy in response to an applied magnetic field even if they did not have spin. This effect, first calculated by Landau (1930), is entirely quantum mechanical in origin, because it vanishes in any classical calculation. For classical electrons, electrons bouncing off boundaries cancel effects of electrons in the bulk. However, for quantum electrons, the quantization of electron orbits destroys the perfect cancellation and allows an effect to remain. When thermal energies are large compared with magnetic energies the resulting effect is diamagnetic, and precisely one-third as large as the Pauli paramagnetism in magnitude.

Electron Energy Levels in a Magnetic Field. To calculate this effect, one must find the energy levels and density of states for electrons in a magnetic field. This task is left as Problem 4, and the results are as follows: The problem has a characteristic frequency, the cyclotron frequency defined in Section 21.2,

$$\omega_c = \frac{eB}{mc}, \quad (25.46)$$

that gives the rate at which electrons spin about in their orbits. Energy states are indexed by three quantum numbers: k_z , a wave vector parallel to the field; k_y , a

wave vector perpendicular to the field which is related to the x coordinate of the center of the orbit through

$$x_0 = \frac{-\hbar k_y}{m\omega_c}; \quad (25.47)$$

and an index ν that describes how energetically the electron rotates about the center of the orbit. The integer ν labels *Landau levels*. In a box of side length L with periodic boundary conditions, the allowed values of k_y and k_z are given by Eq. (6.7).

The energy levels corresponding to these three quantum numbers are

$$\mathcal{E}_{\nu, k_z, k_y} = \frac{\hbar^2 k_z^2}{2m} + (\nu + \frac{1}{2})\hbar\omega_c. \quad (25.48)$$

The rotation rates of the electrons are quantized in units of ω_c , and the energy is independent of k_y , which corresponds physically to the center of the orbit. There really should be an extra term in this expression, $\sigma\mu_B B/2$, with σ taking values ± 1 according to the spin of the electron. The effects of the term have already been included in the previous section, so drop it to simplify things a bit.

By requiring that x_0 lie between 0 and the end of the sample at L , one can determine the degeneracy of an energy state with given ν and k_z . One has that

$$0 < x_0 < L \Rightarrow 0 < \frac{-\hbar 2\pi l_2}{m\omega_c L} < L \quad \text{Using Eq. (6.7) for the allowed values of } k_y, \text{ where } l_2 \text{ is an integer, and Eq. (25.47) for } x_0. \quad (25.49)$$

$$\Rightarrow 0 > l_2 > -\frac{m\omega_c L^2}{2\pi\hbar}. \quad \text{The absolute value of the right-hand side gives the number of allowed values of } l_2. \quad (25.50)$$

$$\Rightarrow N = \frac{BA}{\Phi_0} = \frac{\Phi}{\Phi_0} \quad (25.51)$$

with

$$\Phi_0 \equiv \frac{hc}{e} = 4.14 \cdot 10^{-7} \text{ G cm}^2; \quad N \text{ is the total number of degenerate states, } \Phi \text{ is the total magnetic flux, and } A = L^2 \text{ is the total area.} \quad (25.52)$$

the number of degenerate electron states N in a Landau level is given by the ratio of the total magnetic flux to the magnetic flux quantum Φ_0 .

The density of k_z states is $L/2\pi$. Therefore for each ν , the density of states including spin degeneracy is

$$D(k_z, \nu) = 2 \frac{m\omega_c}{2\pi\hbar} \frac{1}{2\pi}. \quad (25.53)$$

The first factor of two comes from spin degeneracy, the next factor comes from Eq. (25.49), and the final factor comes from the density of k_z states. The spin degeneracy comes from the fact that a spin-up electron in one level has the same energy as a spin-down electron in an adjacent level.

Instead of the density of k_z states, one can instead consider the density of energy states and obtains

$$D(\mathcal{E}, \nu) = \frac{2}{(2\pi)^2} \frac{\hbar\omega_c}{2} \left(\frac{2m}{\hbar^2}\right)^{3/2} \left[\mathcal{E} - (\nu + \frac{1}{2})\hbar\omega_c\right]^{-1/2} \quad \text{Using Eq. (25.48).} \quad (25.54)$$

$$\equiv \hbar\omega_c G \left[\mathcal{E} - \left(\nu + \frac{1}{2}\right)\hbar\omega_c \right], \tag{25.55}$$

with

$$G(x) = \frac{1}{(2\pi)^2} \left(\frac{2m}{\hbar^2} \right)^{3/2} x^{-1/2}. \tag{25.56}$$

The density of states is all that is needed in order to obtain the grand canonical potential in the presence of a magnetic field, and thereby magnetic response. In general the expression cannot easily be simplified, but when the cyclotron energy $\hbar\omega_c$ is much less than the typical thermal energy $k_B T$ a compact result can be obtained.

The grand canonical potential of the electron gas is

$$\Pi = -k_B T \mathcal{V} \int d\mathcal{E} \sum_{\nu} D(\mathcal{E}, \nu) \ln[1 + e^{\beta(\mu - \mathcal{E})}] \tag{25.57}$$

$$= -k_B T \hbar\omega_c \mathcal{V} \int d\mathcal{E} \sum_{\nu=0}^{\infty} G(\mathcal{E}) \ln[1 + e^{\beta[\mu - (\mathcal{E} + (\nu + 1/2)\hbar\omega_c])}]. \tag{25.58}$$

Using Eq. (25.55), and sending \mathcal{E} to $\mathcal{E} + (\nu + \frac{1}{2})\hbar\omega_c$.

Using the assumption that the magnetic energy $\hbar\omega_c$ is much less than the thermal energy $k_B T$, one can convert the sum over ν into an integral. The relevant formula is a version of the Euler–Maclaurin theorem which states

$$\sum_{\nu=0}^{\infty} F \left(\nu + \frac{1}{2} \right) \approx \int_0^{\infty} F(x) dx + \frac{1}{24} F'(0). \tag{25.59}$$

Using this result, one has

$$\begin{aligned} \Pi &= -\mathcal{V} \int d\mathcal{E} k_B T \hbar\omega_c G(\mathcal{E}) \int d\nu \ln[1 + e^{\beta\mu - \beta(\mathcal{E} + \nu\hbar\omega_c)}] \\ &\quad + \frac{\mathcal{V}}{24} \int d\mathcal{E} (\hbar\omega_c)^2 G(\mathcal{E}) \frac{1}{e^{\beta\mathcal{E} - \beta\mu} + 1} \end{aligned} \tag{25.60}$$

$$= \Pi_0 + \frac{\mathcal{V}}{24} (\hbar\omega_c)^2 \int d\mathcal{E} G(\mathcal{E}) f(\mathcal{E}), \tag{25.61}$$

with

$$\Pi_0 = -\mathcal{V} \int d\mathcal{E} \int_0^{\infty} dx k_B T G(\mathcal{E}) \ln [1 + e^{\beta(\mu - \mathcal{E} - x)}]. \text{ The variable } x = \nu\hbar\omega_c. \tag{25.62}$$

Because Π_0 does not depend upon the magnetic field, it must be nothing other than the grand canonical potential Π in the absence of the magnetic field. Furthermore, the second term of Eq. (25.61) can be obtained by taking derivatives of Π_0 , because

$$\mathcal{V} \int d\mathcal{E} G(\mathcal{E}) f(\mathcal{E}) = -\frac{\partial^2 \Pi_0}{\partial \mu^2}. \tag{25.63}$$

Taking a first derivative of Eq. (25.62) with respect to μ brings βf into the integrand. Note that the second derivative with respect to μ can be rewritten as $-\partial/\partial x$ and used to eliminate the integral over x .

Therefore

$$\Pi = \Pi_0 - \frac{1}{6}(B\mu_B)^2 \frac{\partial^2 \Pi_0}{\partial \mu^2} \quad \text{From the definitions (24.39) and (25.46), } 2B\mu_B = \hbar\omega_c. \quad (25.64)$$

$$\Rightarrow M = -\frac{\partial \Pi}{\partial H} \Big|_{\mu} \approx -\frac{\partial \Pi}{\partial B} \Big|_{\mu} = -\frac{1}{3}B\mu_B^2 \frac{\partial N}{\partial \mu} \quad (25.65)$$

$$\Rightarrow \chi = -\frac{1}{3}\mu_B^2 \frac{\partial N}{\partial \mu}. \quad \text{One can show that it does not matter whether one holds } \mu \text{ or } N \text{ constant in this derivative, because } \mu \text{ varies only quadratically with } B. \quad (25.66)$$

Notice that this contribution to the susceptibility is opposite in sign to the Pauli contribution in Eq. (25.45), and one-third of it in magnitude.

Therefore, the total magnetic susceptibility of the free-electron gas, including the contributions both of Pauli and Landau, is

$$\chi = \frac{2}{3}\mu_B^2 \frac{\partial N}{\partial \mu} \quad \text{Adding (25.66) to (25.45).} \quad (25.67)$$

$$= \frac{2}{3} \frac{\mu_B^2 k_F m}{\pi^2 \hbar^2}. \quad \text{Compare with Eq. (25.45).} \quad (25.68)$$

There are grounds for worrying about the validity of Eq. (25.66). The effects of boundaries have been treated in a casual, somewhat intuitive way. Landau (1930) argued that because “the number of trajectories colliding at the walls can be considered as small, with an adequately large container, then we can assume this requirement [Eq. (25.49)] gives us practically all the existing trajectories.” However, the perfect vanishing of magnetic response in classical physics is only apparent when boundary electrons are treated carefully; they cancel out exactly the immense diamagnetic response of electrons in the interior. Van Vleck (1932) discusses these issues in Section 81, and Problem 5 shows one way to perform the calculation with boundaries included.

The series (25.60) begins to oscillate once cyclotron energies and thermal energies become comparable. These oscillations are precisely the de Haas–van Alphen effect studied in Section 16.5.2. Although Landau had seen these oscillations in his calculations as early as 1930, he thought that magnetic fields uniform enough to observe them could not practically be created in the laboratory. The experimental phenomenon was discovered without the aid of theory.

Actual Susceptibilities. The free-electron model does a rather bad job of describing the magnetic susceptibilities of the metallic elements, as shown in Table 25.4. The reason is that the valence electrons surrounding the ions make large contributions to magnetic response that have been ignored, and which are impossible to separate cleanly from the contributions of the conduction electrons. For the purposes of magnetism, treating metals as boxes full of free electrons is inadequate.

25.3.3 Aharonov–Bohm Effect

Aharonov and Bohm (1959) pointed out that because the vector potential \vec{A} appears in Schrödinger’s equation, not the induction \vec{B} , there exist circumstances

Table 25.4. Magnetic susceptibilities of metals near 290 K

Metal	Z	χ [Eq. (25.68)] (10^{-6} cm ³ mole ⁻¹)		χ (Experimental) (10^{-6} cm ³ mole ⁻¹)
Li	1	6.90	p	25.00
Na	1	10.26	p	14.00
K	1	15.83	p	18.00
Rb	1	18.16	p	17.00
Cs	1	21.33	p	30.00
Cu	1	4.59	d	-5.46
Ag	1	5.87	d	-20.00
Au	1	5.84	d	-28.00
Be	2	4.50	d	-9.00
Mg	2	9.08	p	6.00
Ca	2	13.69	p	44.00
Sr	2	16.59	p	92.00
Ba	2	17.78	p	20.00
Zn	2	6.86	d	-9.15
Cd	2	8.66	d	-20.23
Hg	2	5.96	d	-17.10
Al	3	8.32	p	16.40
Ga	3	9.29	d	-21.68
In	3	11.24	d	-10.33
Sn	4	12.65	d	-29.68
Pb	4	13.68	d	-22.79
Sb	5	14.70	d	-97.40
Bi	5	16.40	d	-271.67

The data are in cgs; susceptibilities in SI are defined to be 4π times greater. They are obtained by dividing the dimensionless susceptibility χ by moles per cm³. The symbols d and p refer to whether the metal is actually diamagnetic or paramagnetic. Source: Landolt and Börnstein (1959) vol. 2, parts 9 and 10.

where knowledge of \vec{B} alone in some region of space is insufficient to describe the behavior of electrons. They imagined electrons traveling in the vicinity of a thin solenoid with uniform induction \vec{B} inside, and no induction outside, as shown in Figure 25.4. Note that because

$$\Phi = \int d^2r B_z = \oint d\vec{r} \cdot \vec{A}, \quad (25.69)$$

the vector potential of a flux tube with flux Φ pointing along \hat{z} is azimuthal, and in cylindrical coordinates (r, ϕ) it has value

$$A_\phi = \frac{\Phi}{2\pi r}. \quad (25.70)$$

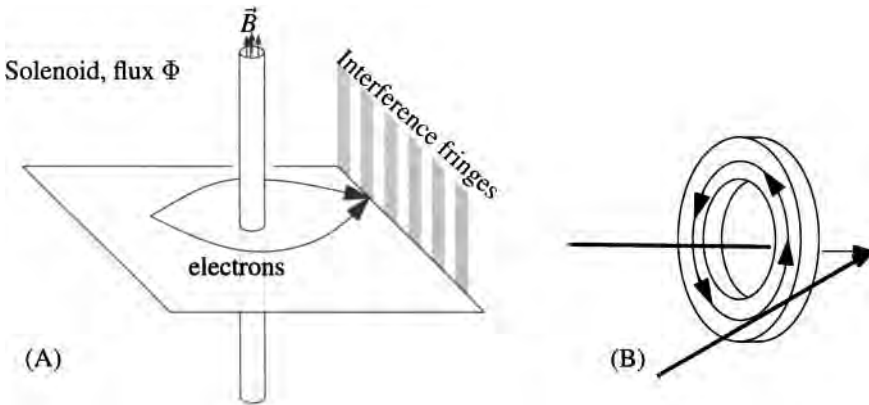


Figure 25.4. (A) Electrons traveling around a flux tube suffer a phase change and can interfere with themselves even if they only travel through regions where $\vec{B} = 0$. (B) An open flux tube is not experimentally realizable, but a small toroidal magnet with no flux leakage can be constructed instead.

Therefore while the magnetic induction vanishes outside the flux tube, the vector potential does not.

Electrons traveling in the presence of this flux tube must obey

$$\frac{1}{2m} \left[\frac{\hbar}{i} \vec{\nabla} + \frac{e}{c} \vec{A} \right]^2 \psi = \mathcal{E} \psi \quad (25.71)$$

$$\Rightarrow \psi \propto \exp \left[i \vec{k} \cdot \vec{r} - i \frac{e}{\hbar c} \int^{\vec{r}} d\vec{r}' \cdot \vec{A}(\vec{r}') \right]. \quad \text{Just substitute into Eq. (25.71).} \quad (25.72)$$

In this context one can view position in space as the adiabatic parameter $\vec{\lambda}$ appearing in Section 8.4.3 on geometric phases. Then the Berry connection and Berry phase are

$$\vec{\mathcal{R}}_{\vec{r}} = i \langle \psi | \vec{\nabla}_{\vec{r}} | \psi \rangle = \frac{e}{\hbar c} \vec{A}(\vec{r}) \quad \text{and} \quad \Gamma = \frac{e}{\hbar c} \oint d\vec{r} \cdot \vec{A} = 2\pi \frac{\Phi}{\Phi_0} \quad (25.73)$$

Thus an electron traveling in a complete circuit about a flux tube of flux Φ acquires a phase $\Phi e / \hbar c$ and can interfere with itself. Referring back to Eq. (25.51), this phase can be written as $2\pi \Phi / \Phi_0$. In particular, for a flux tube whose strength is a multiple of the flux quantum Φ_0 , the interference effect vanishes.

After years of controversy, Tonomura et al. (1986) carried out decisive experiments. An infinitely long solenoid is not experimentally realizable, but a perfect toroidal magnet from which no flux leaks out was constructed by enclosing a thin ferromagnetic ring within a superconducting casing and enclosing the superconductor in copper. Flux leakage was unmeasurable, incident electrons were completely shielded from the region of magnetic field, but a phase change depending upon whether electrons went through or around the torus could be measured. Electron holograms illustrating the effect appear in Figure 25.5.

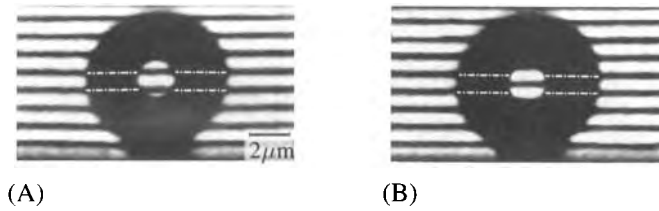


Figure 25.5. Electron hologram showing interference fringes of electrons passing through small toroidal magnet. The magnetic flux passing through the torus is quantized so as to produce an integer multiple of π phase change in the electron wave functions. The electron is completely screened from the magnetic induction in the magnet. In (A) the phase change is 0, while in (B) the phase change is π . [Source: Tonomura (1993), p. 67.]

25.4 Tightly Bound Electrons in Magnetic Fields

The energy levels of nearly free electrons are changed substantially by magnetic fields. What of the opposite limit, tightly bound electrons? Their energy levels are profoundly affected as well. This subject can be investigated by incorporating magnetic fields into the tight-binding model.

The appropriate generalization of the tight-binding Hamiltonian in the presence of a magnetic field is the subject of Problem 3. One can heuristically obtain the desired result, using an illegitimate argument, as follows: If one had a vector potential \vec{A} that was constant in space, then one could create the canonical momentum by

$$\hat{P} - \frac{e}{c}\vec{A} = e^{ie\vec{A}\cdot\hat{R}/\hbar c} \hat{P} e^{-ie\vec{A}\cdot\hat{R}/\hbar c} \tag{25.74}$$

and could therefore include a vector potential in a Hamiltonian by employing the *Peierls substitution*

$$\hat{J} \zeta \rightarrow e^{ie\vec{A}\cdot\hat{R}/\hbar c} \hat{J} \zeta e^{-ie\vec{A}\cdot\hat{R}/\hbar c}. \tag{25.75}$$

If one carries out this replacement on the tight-binding Hamiltonian, (18.37), it becomes

$$\sum_{\vec{R}\vec{\delta}} e^{-ie\vec{A}\cdot\vec{\delta}/\hbar c} |\vec{R}\rangle \langle \vec{R} + \vec{\delta}| + \sum_{\vec{R}} |\vec{R}\rangle U \langle \vec{R}|. \tag{25.76}$$

Although this argument is inadequate when \vec{A} is not constant, it is precisely (25.76) that appears as the result of Problem 3.

Formal Calculation of Energy Levels. Problem 3 also shows that the eigenvalue problem for Hamiltonian (25.76) may be transformed into the following one-dimensional problem, depending upon index l :

$$2\psi_l \cos(2\pi lb - \kappa) + \psi_{l+1} + \psi_{l-1} = \mathcal{E}\psi_l, \tag{25.77}$$

where

$$b = \frac{Ba^2}{\Phi_0} \quad \Phi_0 \text{ is the magnetic flux quantum.} \tag{25.78}$$

and

$$\kappa = ak_x. \quad k_x \text{ is a Bloch wave-vector; the energy eigenvalues will be indexed by } \kappa. \quad (25.79)$$

Suppose that $b = p/q$ is rational. Then Bloch's theorem implies that the energy levels should split into q bands, because the potential in Eq. (25.81) is periodic with period q . The reason is that, according to Bloch's theorem,

$$\psi_{l+q} = e^{ikq} \psi_l. \quad (25.80)$$

Thus only q of the coefficients ψ_l in Eq. (25.77) are independent, and Eq. (25.77) is therefore a $q \times q$ matrix equation with q energy bands depending upon k . This result is peculiar, because changing the magnetic induction from $b = 1/2$ to $b = 5001/10000$ changes the number of bands from 2 to 10000. Nevertheless, it is correct.

To proceed in calculating these energy bands, rewrite Eq. (25.80) in transfer matrix form:

$$\begin{pmatrix} \psi_{l+1} \\ \psi_l \end{pmatrix} = \begin{pmatrix} \mathcal{E} - 2 \cos(2\pi lb - \kappa) & -1 \\ 1 & 0 \end{pmatrix} \begin{pmatrix} \psi_l \\ \psi_{l-1} \end{pmatrix}. \quad (25.81)$$

From Bloch's theorem,

$$e^{iqk} \begin{pmatrix} \psi_1 \\ \psi_0 \end{pmatrix} = \begin{pmatrix} \psi_{q+1} \\ \psi_q \end{pmatrix} = \mathbf{Q}(\mathcal{E}, \kappa) \begin{pmatrix} \psi_1 \\ \psi_0 \end{pmatrix} \quad (25.82)$$

with

$$\mathbf{Q} = \prod_{l=1}^q \begin{pmatrix} \mathcal{E} - 2 \cos(2\pi lb - \kappa) & -1 \\ 1 & 0 \end{pmatrix} \quad (25.83)$$

$$\Rightarrow \text{Det} \left| \mathbf{Q}(\mathcal{E}, \kappa) - e^{iqk} \right| = 0. \quad (25.84)$$

\mathbf{Q} is only a 2×2 matrix, and multiplying out Eq. (25.84) gives

$$\text{Det} \{ \mathbf{Q}(\mathcal{E}, \kappa) \} + e^{2iqk} - \text{Tr} \{ \mathbf{Q}(\mathcal{E}, \kappa) \} e^{iqk} = 0. \quad (25.85)$$

Because $\mathbf{Q}(\mathcal{E}, \kappa)$ is the product of matrices of determinant 1, it has determinant 1 as well, from which follows that

$$\text{Tr} \{ \mathbf{Q}(\mathcal{E}, \kappa) \} = 2 \cos qk, \quad (25.86)$$

for any given value of κ .

Consider $\text{Tr} \{ \mathbf{Q}(\mathcal{E}, \kappa) \}$ as a function of κ . If one replaces κ by $\kappa' = \kappa + 2\pi/q$, then

$$\text{Tr} \{ \mathbf{Q}(\mathcal{E}, \kappa) \} = \text{Tr} \{ \mathbf{Q}(\mathcal{E}, \kappa') \} \quad (25.87)$$

because from Eq. (25.83) one sees that $\mathbf{Q}(\mathcal{E}, \kappa + 2\pi/q)$ is built from a product of exactly the same matrices that make up $\mathbf{Q}(\mathcal{E}, \kappa)$, although in a different order, but the trace is invariant under cyclic permutation. Thus

$$\text{Tr} \{ \mathbf{Q}(\mathcal{E}, \kappa) \} = \sum_{l=-\infty}^{\infty} F_l e^{iq\kappa l}. \quad (25.88)$$

On the other hand the highest Fourier component $e^{iq\kappa}$ that can appear in \mathbf{Q} is $e^{iq\kappa}$, by inspecting Eq. (25.83). So

$$\text{Tr} \{ \mathbf{Q}(\mathcal{E}, \kappa) \} = F_0(\mathcal{E}) + F_1(\mathcal{E})e^{iq\kappa} + F_1^*(\mathcal{E})e^{-iq\kappa}. \quad (25.89)$$

By inspection of Eq. (25.83) one can pick out the terms which involve maximal powers of $e^{iq\kappa}$. These are contained in

$$\prod_{l=1}^q (-) \left[e^{i(2\pi lb - \kappa)} + e^{-i(2\pi lb - \kappa)} \right] \quad (25.90)$$

and can be seen to give

$$F_1(\mathcal{E}) = (-1)^q \prod_{l=1}^q e^{-2\pi ilb} \quad (25.91)$$

$$= (-1)^q e^{-2\pi biq(q+1)/2}. \quad (25.92)$$

In order to find F_0 , observe that if one can find a value κ_0 such that the terms involving F_1 vanish, then

$$F_0(\mathcal{E}) = \text{Tr} \{ \mathbf{Q}(\mathcal{E}, \kappa_0) \}. \quad (25.93)$$

From Eqs. (25.92) and (25.89) one finds that the sum of terms depending upon κ is

$$(-1)^q 2 \cos \left[2\pi b \left(q^2 + q \right) / 2 - q\kappa \right]. \quad (25.94)$$

Because the argument of the cosine can be rewritten

$$\pi p(q+1) - q\kappa, \quad (25.95)$$

the cosine can be made to vanish by choosing

$$\kappa_0 = \frac{\pi}{2q}. \quad (25.96)$$

Thus it follows from Eq. (25.86) that

$$\text{Tr} \{ \mathbf{Q}(\mathcal{E}, \kappa) \} = 2 \cos qk = \text{Tr} \{ \mathbf{Q}(\mathcal{E}, \pi/2q) \} + 2 \cos \left[\pi b(q^2 + q) + \pi q - q\kappa \right]. \quad (25.97)$$

Because k and κ can be varied freely, \mathcal{E} is an allowed eigenvalue so long as

$$\left| \text{Tr} \{ \mathbf{Q}(\mathcal{E}, \pi/2q) \} \right| \leq 4. \quad (25.98)$$

The spectrum of allowed energy levels predicted by Eq. (25.98) was first calculated by Hofstadter (1976) and appears in Figure 25.6. Minute changes in B produce great changes in the effective periodicity of the electron problem and cause rapid changes in the number of distinct energy bands.

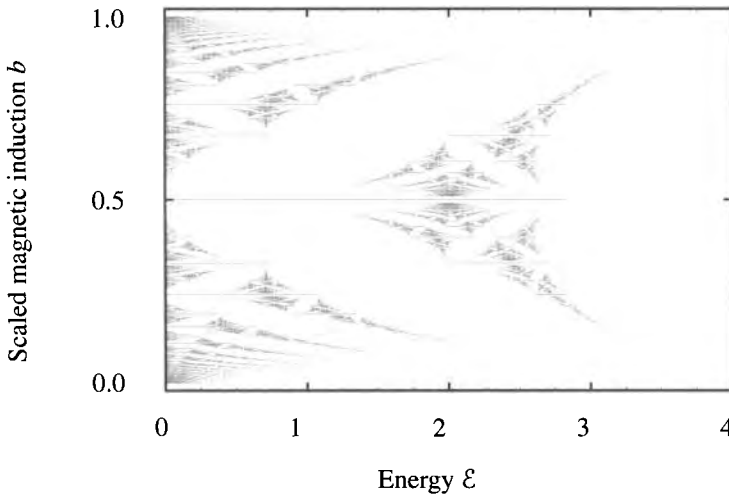


Figure 25.6. This picture was produced by testing Eq. (25.98) for all $p < q$, $q \leq 50$, for 500 values of ε for each pair of p and q , and then drawing a dot at all allowed energy levels. The number of bands is a thoroughly discontinuous function of the dimensionless magnetic induction $b = p/q$, yet the picture as a whole has some sort of underlying continuity.

25.5 Quantum Hall Effect

25.5.1 Integer Quantum Hall Effect

The quantum Hall effect was first observed von Klitzing, Dorda, and Pepper (1980). The experiments were carried out in a two-dimensional electron gas formed by an inversion layer at a Si/SiO₂ interface (Section 19.5). At temperatures on the order of a few kelvin and at fields on the order of a few Tesla, von Klitzing, Dorda, and Pepper observed that the transverse conductivity σ_{xy} was quantized, with values

$$\sigma_{xy} = \frac{\nu}{R_K}, \quad (25.99)$$

where ν is an integer and the *von Klitzing constant*

$$R_K = \frac{h}{e^2} = 25\,813 \, \Omega. \quad \text{Just as defined in Eq. (18.104).} \quad (25.100)$$

As shown in Figure 25.7, long plateaus at these values are separated by very steep rises. The value of the conductivity in the plateau is equal to its theoretical value to at least one part in 10^8 , and reproducible to one part in 10^{10} , so the Hall effect is now employed to correct drift in the international standards of electrical resistance.

First Explanation: Current Loops and Moments. The geometry of the integer quantum Hall effect is depicted schematically in Figure 25.8. Figure 25.8(A) shows the density of states of a quantum Hall device with some density of localized states created by impurities. In an absolutely perfect sample, when the induction

B increased, as soon as one Landau level became empty the next would instantly begin to lose its first electrons. The situation is different when localized states are present. After the chemical potential falls below the lowest-lying extended state in some Landau level, there remains a range of B for which the chemical potential moves through the localized states, and all extended states in lower-lying Landau levels remain completely filled. The field strengths for which extended states in all Landau levels are either completely empty or completely filled will correspond to the Hall plateaus, so the presence of some density of disorder-induced localized states is important in explaining the origin of the integer Hall effect. Figure 25.8(B) shows a simplified geometry for studying the effect. By driving a current J in one direction and measuring the voltage difference V in the perpendicular direction, one measures the transverse conductivity σ_{xy} . A simple argument due to Streda (1982) shows why σ_{xy} should be quantized.

Consider any closed contour \mathcal{C} in the sample. Imagine changing the external induction \vec{B} slightly, so the total magnetic flux Φ within the contour increases at rate $\dot{\Phi}$. The contour experiences an electromotive force

$$\oint_{\mathcal{C}} d\vec{l} \cdot \vec{E} = -\frac{1}{c} \frac{\partial \Phi}{\partial t}. \quad \text{Lenz's law, or see Eq. (20.5b).} \quad (25.101)$$

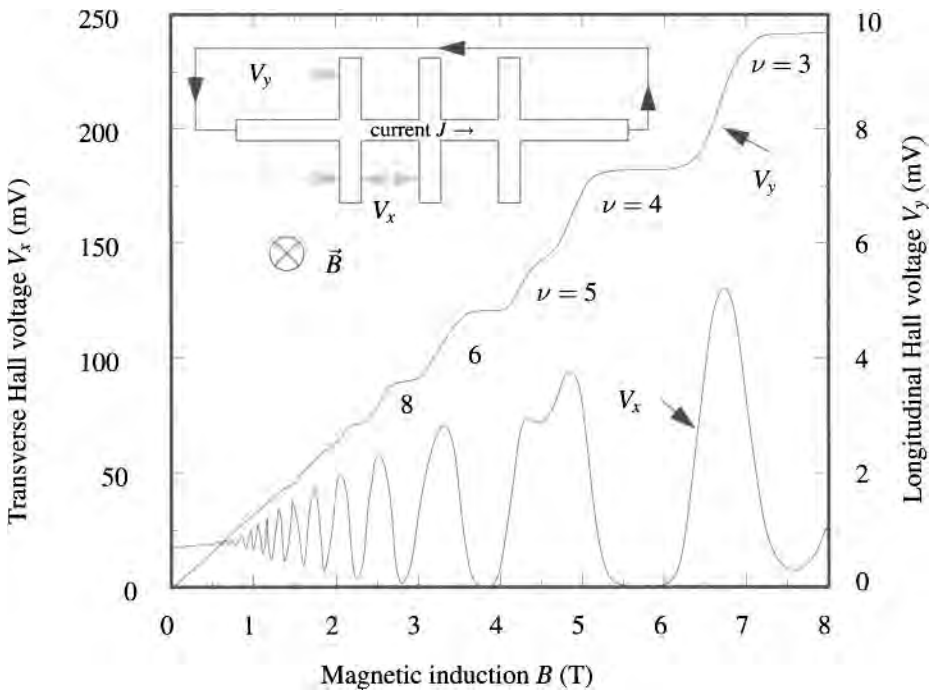


Figure 25.7. Experimental observation of the integer quantum Hall effect. A constant current of $J = 28 \mu\text{A}$ runs around the upper loop; the current between the terminals separated by V_y is much smaller. The voltage plateaus correspond to Hall resistances of R_K/ν , where ν is an integer. [Source: Cage (1987), p. 44.]

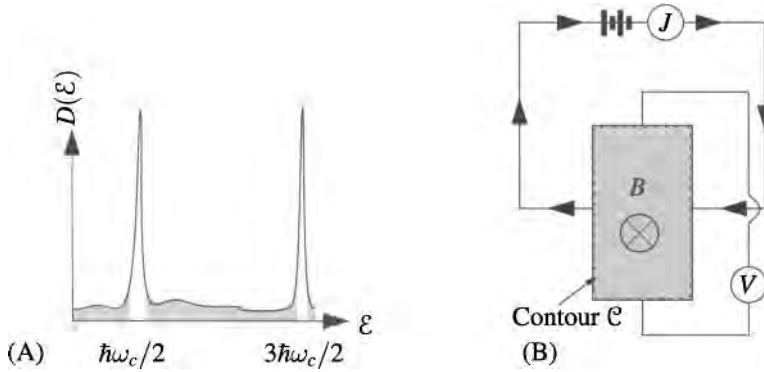


Figure 25.8. (A) The density of states of a quantum Hall device contains large numbers of states at energies $\hbar\omega_c(\nu + 1/2)$, but also contains localized states (shaded) in between the sharp peaks. (B) The quantized Hall effect is observed by creating a two-dimensional electron gas, immersing it in a strong field \vec{B} , driving a current J through in one direction, and observing the transverse voltage V .

The current j_{\perp} traveling normal to the contour is given by

$$j_{\perp} = \sigma_{xy} E_{\parallel}, \quad (25.102)$$

where E_{\parallel} is the component of the electric field parallel to \mathcal{C} . Therefore, Eq. (25.101) can be written

$$\frac{1}{\sigma_{xy}} \oint_{\mathcal{C}} dl j_{\perp} = \frac{-1}{c} \frac{\partial \Phi}{\partial t} \quad (25.103)$$

$$\Rightarrow \frac{\partial Q}{\partial t} = -\frac{\sigma_{xy}}{c} \frac{\partial \Phi}{\partial t} \quad \text{Here } Q \text{ is the total charge within contour } \mathcal{C}. \quad (25.104)$$

$$\Rightarrow \sigma_{xy} = -c \frac{\partial Q}{\partial \Phi}. \quad (25.105)$$

If ν Landau levels are occupied, then according to Eq. (25.51), the total charge Q in the Landau levels is

$$Q = -e\nu \frac{\Phi}{\Phi_0} \quad (25.106)$$

$$\Rightarrow \sigma_{xy} = \frac{ec\nu}{\Phi_0} = \frac{\nu e^2}{h} = \frac{\nu}{R_K}. \quad \text{Using Eq. (25.51)}. \quad (25.107)$$

Because Eq. (25.107) was derived for ideal noninteracting electrons, it should not yet be clear why it still may be employed to 10-place accuracy when describing realistic, dirty, interacting experimental samples. An explanation is provided by making two plausible assumptions.

1. The number of quantum energy states in a Landau level is not affected by interactions between electrons or disorder. Referring to Figure 25.8(A), assume that the total number of energy levels contained in the broadened peak around

$\hbar\omega_c/2$ remains Φ/Φ_0 even after impurities and electron–electron interactions are considered. The large energy gap between the first and second Landau levels makes this assumption increasingly plausible as the induction strength B increases.

2. Assume that the densities of localized states constituting the shaded regions in Figure 25.8(A) are rigid and do not change as B changes.

As B increases, the total number of states in the Landau level increases in proportion. If the numbers of localized states in the tail of the Landau level do not change, virtually all of the increase occurs through a rise in the number of extended states at the center of the level. So long as μ lies within the region of localized states, changes in the total number of charges N contained in the current loop must continue to be given by Eq. (25.51). The accuracy with which the Hall conductivity is quantized depends upon the accuracy with which the two assumptions about energy levels are obeyed; experimentally, the accuracy is at the level of parts per billion.

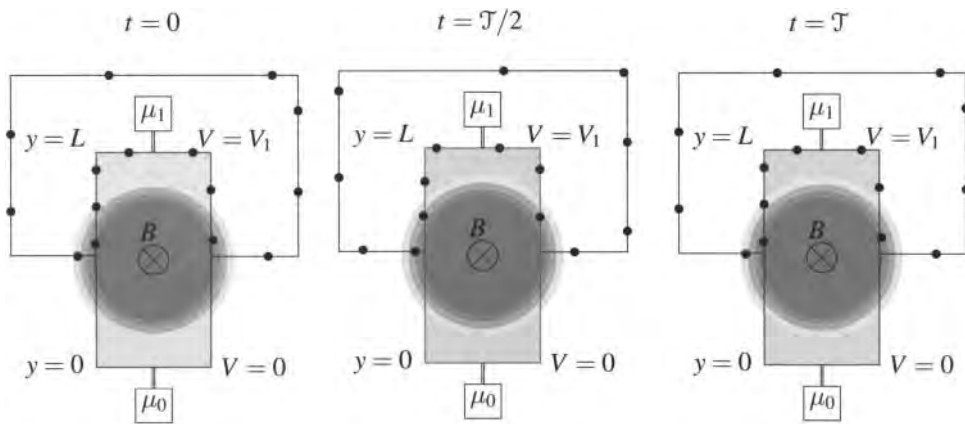


Figure 25.9. If the electric field across a sample is expressed as a time-dependent vector potential, it can be made to disappear from everything but the boundary conditions, and the boundary conditions return to their starting values at time intervals \mathcal{T} . Dots indicate electrons traveling around wire, while reservoirs at μ_0 and μ_1 maintain voltages 0 and V_1 .

Second Explanation: Gauge Invariance. A different way to think about the quantum Hall effect was proposed by Laughlin (1981). Consider a single electron moving in a thin strip and in a strong uniform magnetic induction B , shown in Figure 25.9. The strip should be large enough so that its outer edges in the y direction are out of the range of B . Draw an imaginary perfect rectangle within the strip but at the top and bottom passing beyond the magnetic induction, and consider the quantum-mechanical problem restricted to the area within the rectangle. In the absence of any potential difference along y , specializing to the gauge

$$\vec{A} = \hat{y}xB, \tag{25.108}$$

Schrödinger's equation is

$$\left[\frac{-\hbar^2}{2m} \frac{\partial^2}{\partial x^2} + \frac{1}{2m} \left(\frac{\hbar}{i} \frac{\partial}{\partial y} + \frac{exB}{c} \right)^2 + U(\vec{r}) - \mathcal{E} \right] \psi(\vec{r}) = 0. \quad (25.109)$$

$U(\vec{r})$ is a potential that includes effects of the crystal, and impurities.

Now introduce a slight complication that for the moment will seem artificial. There is some boundary condition that must be imposed when solving the Schrödinger equation; whatever it may be, it can be indicated as a linear condition

$$\mathcal{B}[\psi(x, L)] = 0, \quad (25.110)$$

where \mathcal{B} is some operator that gives the boundary conditions. Now define $\psi^\gamma(\vec{r})$ to be eigenfunctions of the equation such that

$$\mathcal{B}[\psi^\gamma(x, L)e^{i\gamma}] = 0. \quad (25.111)$$

These eigenfunctions can certainly be found for any applied field and any γ , although it is not clear why one should care.

Now put an electric field $E(\vec{r})$ onto the sample, and assume it points only in the \hat{y} direction. This field is not just the applied field, but could also include the field generated by Coulomb charges within the strip. Employ the method of Section 16.3, which derives electron fields from time-dependent vector potentials, as in Eq. (16.30). The Hamiltonian becomes

$$\left[\frac{-\hbar^2}{2m} \frac{\partial^2}{\partial x^2} + \frac{1}{2m} \left(\frac{\hbar}{i} \frac{\partial}{\partial y} + \frac{exB}{c} + eE_y(\vec{r})t \right)^2 + U(\vec{r}) - \mathcal{E} \right] \psi(\vec{r}) = 0. \quad (25.112)$$

Because of the explicit time dependence in the vector potential, this equation does not follow from the time-dependent Schrödinger equation. However, as in Section 16.3, the errors introduced in this way are exponentially small.

The electric field can be eliminated formally from the problem by writing

$$\psi = e^{ieVt/\hbar} \tilde{\psi}, \quad (25.113)$$

where V is the electric potential defined by

$$\vec{E} = -\vec{\nabla}V. \quad (25.114)$$

Because near $y = 0$ (the bottom of the rectangle) and $y = L$ (the top of the rectangle) there is no magnetic field and the strip is metallic, the voltage is constant in space to high accuracy. In particular, the electric potential at the top of the strip, $V(L) = V_1$ is independent of x . The function $\tilde{\psi}$ therefore obeys precisely the same equation as ψ in the absence of a field, but it obeys boundary condition

$$\mathcal{B}[e^{-ietV_1/\hbar} \tilde{\psi}(x, L)] = 0. \quad (25.115)$$

In other words, $\tilde{\psi}$ is of the form indicated in Eq. (25.111) with

$$\gamma = -\frac{eV_1 t}{\hbar}. \quad (25.116)$$

Now consider what happens when

$$\frac{eV_1 t}{\hbar} = 2\pi. \quad (25.117)$$

This condition occurs after a time

$$\mathcal{T} = \frac{\hbar}{eV_1}. \quad (25.118)$$

The boundary condition has returned to its value at $t = 0$, so all the single-particle states $\tilde{\psi}$ are the same as the states ψ . The occupation of the states might be different. That is, as time progresses from 0 to \mathcal{T} , each state l must evolve until finally at time \mathcal{T} it turns into some other state l' . All the quantum states at $t = \mathcal{T}$ must be identical to those at $t = 0$, but they are not necessarily occupied in the same way. In fact, if some Landau level is incompletely filled, the occupation of states should be expected to change. However, if the Fermi level lies within the region of localized states between Landau levels, the occupation of states at $t = \mathcal{T}$ must be precisely what it was at $t = 0$. First consider the localized states. They are trapped in potential wells, with wave functions that are exponentially small at the system boundaries, so as the boundary condition indicated by Eq. (25.116) changes, they change exponentially little. Next consider the extended states within a filled Landau level. All of these states are occupied at $t = 0$, and when t arrives at \mathcal{T} they must all remain occupied.

In short, one can be quite sure that the system at $t = \mathcal{T}$ is indistinguishable from the system at $t = 0$. Because the voltage at top and bottom is imposed without allowing current to flow along y , the most that could have happened is that an integer number ν of electrons was transported through the sample in the x direction, as indicated in Figure 25.9. The current that has passed through the system is therefore

$$J_x = \frac{\nu e}{\mathcal{T}} = \frac{\nu e^2 V_1}{h}, \quad (25.119)$$

which means that the conductance is

$$\sigma_{xy} = \nu \frac{e^2}{h} = \frac{\nu}{R_K}. \quad (25.120)$$

25.5.2 Fractional Quantum Hall Effect

The integer quantum Hall effect depends crucially upon the presence of disorder, which allows the Fermi level to lie in a gap between extended states and thereby produces plateaus in the transverse conductivity. Tsui et al. (1982) created two-dimensional electron gases in GaAs–AlGaAs with electron mobilities [Eq. (19.65)] on the order of $5 \cdot 10^5 \text{ cm}^2 \text{ V}^{-1} \text{ s}^{-1}$, 100 times larger than the mobilities in samples where the integer Hall effect was observed. The importance of impurities was

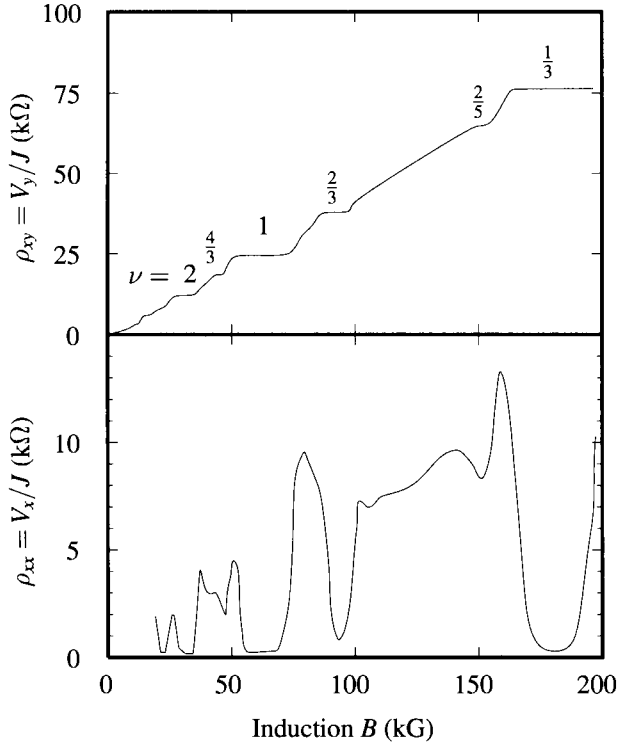


Figure 25.10. Measurement of fractional quantum Hall effect in GaAs/GaAlAs heterostructure with mobility of $4 \cdot 10^5 \text{ cm}^2 \text{ V}^{-1} \text{ s}^{-1}$ and electron density of $1.45 \cdot 10^{11} \text{ cm}^{-2}$ at a temperature of 150 mK. [Data of Boebinger, Chang, Störmer, and Tsui, published by Chang (1990), p. 185.]

correspondingly less, but instead of eliminating plateaus in the Hall voltage, a host of new plateaus appeared, as illustrated by the data in Figure 25.10.

The physics underlying the fractional quantum Hall effect is in some ways quite different from the physics underlying the integer effect. Locking the voltage V_y into plateaus is due to the formation of a *quantum liquid*, in which the electrons form a highly correlated state to minimize the effects of Coulomb repulsion.

A general explanation of the fractional quantum Hall effect can be found by returning to the second argument used for the integer effect. Suppose that the electron ground state is a sum of many determinantal wave functions and that for any given boundary condition of the type described in Eq. (25.115) there exist q degenerate ground state solutions. Suppose furthermore that at every time interval \mathcal{T} the ground-state wave function travels between these degenerate states in sequence. Then the ground-state wave function does not return to itself completely until after a time $q\mathcal{T}$. Repeating the argument that led to Eq. (25.120), the conductivity will be

$$\frac{p e^2}{q h}, \quad (25.121)$$

where p is the integer number of electrons that leaves the sample in time $q\mathcal{T}$.

It is obvious to ask in the wake of the argument about the type of microscopic state which supports this degeneracy. In addition, with few exceptions, only odd denominators p have ever been seen. This fact also calls out for a microscopic explanation.

Laughlin Wave Function. Laughlin (1983) proposed a generalization of the free-electron state in which the density of states within filled levels is eB/phc , and which therefore has conductivity p times less than that of the single Landau level. A first observation leading to this state is that in a strong magnetic field, the Coulomb interaction between electrons becomes increasingly unimportant. The characteristic minimum distance between electrons is $1/\sqrt{n} = \sqrt{hc/eB}$, so the ratio of Coulomb to magnetic energies is

$$\frac{e^2\sqrt{n}}{\epsilon^0\hbar\omega_c} = \frac{m^*ce^2}{\epsilon^0\hbar\sqrt{eBhc}} = \frac{m^*}{\epsilon^0m} 1.93 \cdot 10^2 / \sqrt{B/\text{T}}. \quad \epsilon^0 \text{ is the static dielectric constant.} \quad (25.122)$$

In a metal, the Coulomb energy would be much larger than the magnetic energy at any realistic field strength, but in gallium arsenide, with $\epsilon^0 = 12.5$ and $m^* = .067m$, magnetic fields of a few Tesla are sufficient for the magnetic energy to dominate. The significance of reaching the high-field limit is that the true ground state of the system of interacting electrons can accurately be written using only states in the lowest Landau level as basis functions. States in higher Landau levels cost energy $\hbar\omega_c$, and Coulomb repulsion is too small an energy to force any electron to make the transition.

In preparation for constructing the ground state of the interacting electrons, it is useful to write the Schrödinger equation for free electrons in a magnetic field in the symmetric gauge, with \vec{B} pointing along $-\hat{z}$:

$$\left[\frac{1}{2m} \left(\frac{\hbar}{i} \frac{\partial}{\partial y} - \frac{exB}{2c} \right)^2 + \frac{1}{2m} \left(\frac{\hbar}{i} \frac{\partial}{\partial x} + \frac{eyB}{2c} \right)^2 - \mathcal{E} \right] \psi(\vec{r}) = 0. \quad (25.123)$$

Define the magnetic length

$$l_B = \sqrt{\frac{2\hbar c}{eB}}, \quad \text{and define variables } \tilde{y} = \frac{y}{l_B} \text{ and } \tilde{x} = \frac{x}{l_B}. \quad (25.124)$$

The Hamiltonian becomes

$$\frac{\hbar\omega_c}{4} \left[\left(\frac{1}{i} \frac{\partial}{\partial \tilde{y}} - \tilde{x} \right)^2 + \left(\frac{1}{i} \frac{\partial}{\partial \tilde{x}} + \tilde{y} \right)^2 \right] \psi = \psi \mathcal{E}. \quad (25.125)$$

Let

$$z = \tilde{x} + i\tilde{y}, \quad \text{and define } \psi = e^{-|z|^2/2} \phi(z, \bar{z}). \quad (25.126)$$

Then the eigenvalue equation for ϕ is

$$\hbar\omega_c \left\{ \frac{\partial \phi}{\partial \bar{z}} \bar{z} - \frac{\partial^2 \phi}{\partial z \partial \bar{z}} + \frac{1}{2} \phi \right\} = \mathcal{E} \phi. \quad (25.127)$$

In the partial derivatives, z and its complex conjugate \bar{z} are treated as independent variables. Therefore it is easy to construct the many degenerate wave functions that constitute the first Landau level by writing

$$\phi(z, \bar{z}) = f(z) \Rightarrow \psi(z, \bar{z}) = f(z)e^{-|z|^2/2}, \quad (25.128)$$

where f is an arbitrary power series in z . Because $\partial f(z)/\partial \bar{z} = 0$, all functions of the form (25.128) have eigenvalue $\mathcal{E} = \hbar\omega_c/2$.

Because the ground state of the true many-body Hamiltonian, with Coulomb interactions included, can be constructed out of functions living in the first Landau level, the many-electron wave function must be of the form

$$\Psi = f(z_0 \dots z_{N-1})e^{-\sum_{l=0}^{N-1} |z_l|^2/2}, \quad (25.129)$$

where f is an analytic function of all its arguments. Laughlin (1983) proposed that one examine a many-body wave function of a simpler form, called a *Jastrow wave function*, similar to Eq. (15.114) for the theory of liquid helium, and similar to the wave function that describes the ground state of superconductors. The form is

$$\Psi = \prod_{l < l'} f_2(z_l - z_{l'})e^{-\sum_{l=0}^{N-1} |z_l|^2/2}. \quad (25.130)$$

The function f_2 can be determined by considering constraints imposed by rotational symmetry. The Hamiltonian commutes with the angular momentum operators

$$\hat{L}_l = -i\frac{\partial}{\partial \theta_l} = \left[z_l \frac{\partial}{\partial z_l} - \bar{z}_l \frac{\partial}{\partial \bar{z}_l} \right], \quad (25.131)$$

and all of these, for different l , commute with one another. Therefore the eigenstates can be taken to be eigenfunctions of these operators, which means that

$$z \frac{\partial f_2(z)}{\partial z} = q f_2(z) \Rightarrow f_2(z) = z^q. \quad \text{Where } q \text{ is an integer, if } f_2 \text{ is to remain infinitely differentiable at the origin.} \quad (25.132)$$

So

$$\Psi = \prod_{l < l'} (z_l - z_{l'})^q e^{-\sum_{l=0}^{N-1} |z_l|^2/2}. \quad (25.133)$$

The wave function must be odd under interchange of particles, so q must be odd. This consequence of Fermi statistics thus explains why odd denominators are most easily observed in the Hall plateaus. The wave function (25.133) is a plausible candidate for the ground state of electrons in a strong magnetic field because it is constructed purely from wave functions in the lowest Landau level, and it vanishes whenever two particles come close together so as to reduce the effects of Coulomb repulsion. Guessing the form in Eq. (25.130) is enough to fix the wave function, even without inserting it into Schrödinger's equation and varying parameters.

When $q = 1$, Eq. (25.133) is precisely an antisymmetric product of N states in the lowest Landau level:

$$\Psi = \begin{vmatrix} 1 & 1 & \dots & 1 \\ z_0 & z_1 & \dots & z_{N-1} \\ \cdot & \cdot & \dots & \cdot \\ \cdot & \cdot & \dots & \cdot \\ \cdot & \cdot & \dots & \cdot \\ z_0^{N-1} & z_1^{N-1} & \dots & z_{N-1}^{N-1} \end{vmatrix} e^{-\sum_{l=0}^{N-1} |z_l|^2/2}. \quad \begin{array}{l} \text{Vertical lines indicate taking the} \\ \text{determinant of this matrix.} \\ \text{Subscripts on } z \text{ label particle} \\ \text{number, while superscripts are} \\ \text{exponents.} \end{array} \quad (25.134)$$

To see that Eqs. (25.134) and (25.133) are equal, recall that a determinant is unchanged when one column is subtracted from another. For example, subtract column 1 from column 2. All the vertical entries are of the form

$$z_2^m - z_1^m = (z_2 - z_1) \sum_{l=0}^{m-1} z_2^l z_1^{m-l-1}. \quad (25.135)$$

So $z_2 - z_1$ is a factor of the determinant. Similarly, $z_l - z_{l'}$ is a factor for all $l \neq l'$. The largest power of z_0 to appear in Eq. (25.133) is z_0^{N-1} , and the largest power of z_0 to appear in Eq. (25.134) is the same. The prefactors of Eqs. (25.133) and (25.134) are polynomials of the same degree and sharing all the same factors, so they must be equal up to an overall constant.

When q equals an odd integer, the wave function describes a correlated state where electrons fill a fraction $1/q$ of the states in the lowest Landau level. This claim may be demonstrated by considering how to find the degeneracy of a Landau level using functions of the type $z^m \exp[-|z|^2/2]$. Suppose that the N single-particle states

$$e^{-|z|^2/2}, z e^{-|z|^2/2}, z^2 e^{-|z|^2/2} \dots z^{N-1} e^{-|z|^2/2} \quad (25.136)$$

are occupied. The density $|z^m \exp[-|z|^2/2]|^2$ has a maximum at $|z|^2 = m$, so the functions in (25.136) describe a series of concentric rings of charge, filling an area uniformly out to a radius of $|z|^2 = N - 1 \approx N$. The units of length in Eq. (25.124) are l_B , so the area A filled by charge is

$$A = \pi N l_B^2 = \frac{2\pi N \hbar c}{eB} \Rightarrow N = \frac{BA}{\Phi_0}. \quad \text{Use Eq. (25.124) for the magnetic length } l_B, \text{ and compare result with Eq. (25.51).} \quad (25.137)$$

Thus the area occupied by electrons in a wave function of the form (25.133) can be determined by finding the radius of maximum density when all but one of the variables is set to some small value near zero, and the remaining one is allowed to become large. Set all but z_0 to values near zero, and search for the maximum density as a function of z_0 . For general values of q the maximum occurs for

$$|z_0|^2 = q(N - 1) \Rightarrow N = \frac{BA}{q\Phi_0}. \quad \text{Replace } N \text{ by } Nq \text{ in Eq. (25.137).} \quad (25.138)$$

In particular, when $q = 3$, the Landau level is filled one-third of the way to the top, and the filling fraction ν equals $1/3$.

Fractional Charge. Laughlin furthermore proposed that the excitations of the fractional quantum Hall state carry fractional charge. Imagine constructing an extremely thin solenoid with uniform induction B inside and no induction outside, and passing it through the two-dimensional electron gas. Imagine beginning with no flux through the solenoid, and then slowly increasing B until finally the total flux in the solenoid is Φ_0 . According to the discussion of Section 25.3.3, an electron traveling a circuit around an infinitely thin flux tube with flux of Φ_0 will undergo a phase change of 2π , and no physical measurement can detect the presence of the tube. Therefore the electron gas after the tube reaches flux Φ_0 must be in an eigenstate of the original Hamiltonian. This state cannot be the ground state because turning on the flux tube at the origin drives charge away from the origin, and so one has constructed an excited state.

To see that charge is driven away from the origin, and to calculate how much, note that turning on the flux tube creates an azimuthal electric field,

$$E_\phi = -\frac{1}{c} \frac{1}{2\pi r} \frac{\partial \Phi}{\partial t}. \quad (25.139)$$

Traveling far from the flux tube, the current produced by this electric field is perpendicular to it, because only σ_{xy} is nonzero, and the total charge Q transported away from the flux tube is

$$Q = \int dt \, 2\pi r \, j_\perp = - \int dt \, \sigma_{xy} \frac{1}{c} \frac{\partial \Phi}{\partial t} \quad (25.140)$$

$$= -\frac{1}{c} \frac{\nu}{R_K} \Phi_0 = -\nu e. \quad (25.141)$$

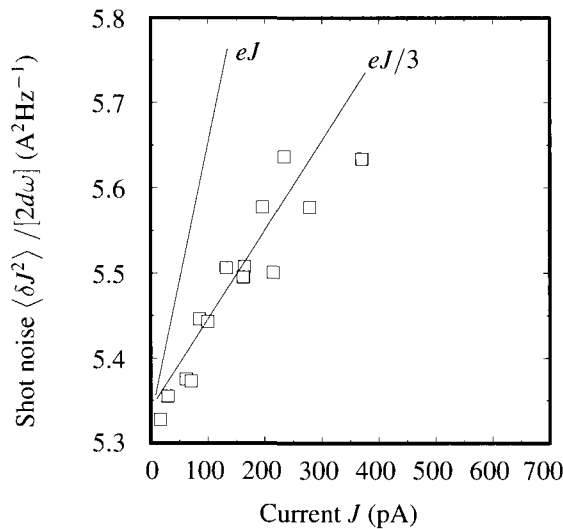


Figure 25.11. Shot noise in GaAs/GaAlAs heterostructure in magnetic field that puts the system in the $\nu = 1/3$ plateau. The magnitude of the shot noise is consistent with a system where current is carried by particles of charge $e/3$, and it is inconsistent with one where the carriers have charge e . [Source: Saminadayar et al. (1997), p. 2528.]

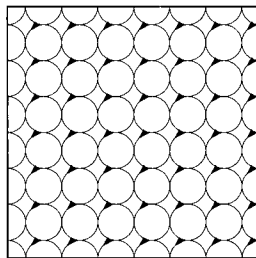
So for filling fraction $\nu = 1/3$, this argument constructs an excited state of the Hamiltonian in which a charge of precisely $e/3$ is transported through any large loop surrounding the origin, and therefore the charge carriers are predicted to have charge $e/3$.

Experimental Observation of Fractional Charge. Saminadayar et al. (1997) tested this idea experimentally. The test is based upon Eq. (18.22), which predicts that current fluctuations in any current-carrying system contain shot noise proportional to the current, proportional to twice the particle charge, and proportional to the frequency bandwidth. The results clearly support the claim that charge carriers in systems with filling fraction $\nu = 1/3$ have charge $e/3$, and they are displayed in Figure 25.11.

Problems

1. **Classical electrons in a magnetic field—mechanics:** Consider a population of classical electrons in a two-dimensional box of side length L , all of which are moving in some direction at velocity v . When a magnetic field is turned on, the electrons in the center of the box begin to rotate, leading to a diamagnetic response. However, those electrons within reach of the boundary bounce off it, ultimately traveling around in the opposite direction. Find the net magnetic response of the whole system; according to Problem 3.2, it should vanish.

Assume that the centers of the electrons' orbits sit on a finely spaced grid. Discuss the electrons whose orbits hit the boundary separately from those whose orbits do not. Use drawings and geometrical arguments rather than complicated analytical formulae.



2. **Classical electrons in a magnetic field—statistical mechanics:** Show that the free energy of a collection of classical electrons in a box must be independent of any static applied magnetic field.
 - (a) Write down the classical partition function Z for N particles. The particles interact with each other according to an arbitrary potential U that depends only upon their positions.

- (b) Show how a spatially uniform static magnetic field is to be included in the partition function.
- (c) Show finally that with a change of integration variables the magnetic field can be eliminated from the partition function and therefore cannot affect any thermodynamic variable.

3. **Tightly bound electrons in two dimensions and in a strong magnetic field:** Suppose that one has a Hamiltonian for a two-dimensional system on a square lattice of spacing a ,

$$\hat{\mathcal{H}}_0 = \frac{\hat{P}^2}{2m} + U(\hat{R}). \tag{25.142}$$

Suppose that in a basis of Wannier functions, $w(\vec{R}, \vec{r})$, $\hat{\mathcal{H}}_0$ takes the form given in Eq. (8.67),

$$\hat{\mathcal{H}}_0 \approx \sum_{\vec{R}\vec{\delta}} |\vec{R}\rangle \mathfrak{t}(\vec{R} + \vec{\delta}) | \text{Measure energies relative to the on-site energy } U; \text{ recall that } \vec{\delta} \text{ is the set of nearest neighbors of } \vec{R}. \tag{25.143}$$

Now turn on a magnetic field. The Hamiltonian becomes

$$\hat{\mathcal{H}} = \frac{(\hat{P} + e\vec{A}/c)^2}{2m} + U(\hat{R}). \tag{25.144}$$

Take the vector potential to be $\vec{A} = (0, x, 0)B$.

Expand eigenfunctions of $\hat{\mathcal{H}}$ in the form

$$\psi(\vec{r}) = \frac{1}{\sqrt{N}} \sum_{\vec{R}} e^{-ieyBR_x/\hbar c} C_{\vec{R}} w(\vec{R}, \vec{r}). \tag{25.145}$$

$w(\vec{R}, \vec{r})$ is a Wannier function, and $C_{\vec{R}}$ is a coefficient that needs to be determined in the remainder of the problem.

- (a) For Wannier functions very well localized compared to the scale on which the vector potential varies, show that to leading order,

$$\hat{\mathfrak{t}}\psi(\vec{r}) = \frac{1}{\sqrt{N}} \sum_{\vec{R}} C_{\vec{R}} e^{-ieByR_x/\hbar c} \hat{\mathcal{H}}_0 w(\vec{R}, \vec{r}). \tag{25.146}$$

- (b) Show that

$$\mathfrak{t} \left[\begin{array}{l} C_{\vec{R}+a\hat{x}} e^{-ieBaR_y/\hbar c} + C_{\vec{R}-a\hat{x}} e^{ieBaR_y/\hbar c} \\ + C_{\vec{R}+a\hat{y}} + C_{\vec{R}-a\hat{y}} \end{array} \right] = \mathcal{E} C_{\vec{R}}. \tag{25.147}$$

- (c) Reduce Eq. (25.147) to a one-dimensional equation. First define

$$n = \frac{R_x}{a}, \quad m = \frac{R_y}{a}, \quad \kappa = ak_x, \quad \text{and} \quad \tilde{\mathcal{E}} = \frac{\mathcal{E}}{\mathfrak{t}}. \tag{25.148}$$

Suppose that

$$C_{\vec{R}} = \psi_m e^{in\kappa}. \quad (25.149)$$

Show that

$$2\psi_m \cos(2\pi mb - \kappa) + \psi_{m+1} + \psi_{m-1} = \tilde{\mathcal{E}}\psi_m, \quad (25.150)$$

where

$$b = \frac{ea^2B}{2\pi\hbar c} = \frac{a^2B}{\Phi_0}. \quad (25.151)$$

4. **Quantum electrons in a magnetic field:** Work through the energy levels of an electron in a magnetic field. Beginning with the Hamiltonian

$$\hat{\mathcal{H}} = \frac{1}{2m} \left(\hat{P} + \frac{e}{c} \vec{A} \right)^2, \quad (25.152)$$

adopt the Landau gauge

$$\vec{A} = (0, Bx, 0). \quad (25.153)$$

Show for wave functions proportional to $\exp[iyk_y]$ that Eq. (25.152) becomes the Hamiltonian for a harmonic oscillator centered about

$$x_0 = -\frac{\hbar k_y}{m\omega_c}, \quad (25.154)$$

where ω_c is given by Eq. (25.46). Show that the energy levels are given by Eq. (25.48).

5. **Careful derivation of Landau diamagnetism:** Consider noninteracting electrons confined by a potential $\rho^2 \mathcal{E}_0 / 2R_0^2$, where ρ is the radius in cylindrical coordinates, with a magnetic field of strength H pointing in the \hat{z} direction. Schrödinger's equation is

$$-\frac{\hbar^2}{2m} \left[\frac{1}{\rho} \frac{\partial}{\partial \rho} \rho \frac{\partial \psi}{\partial \rho} + \frac{\partial^2 \psi}{\partial z^2} + \frac{1}{\rho^2} \frac{\partial^2 \psi}{\partial \phi^2} \right] - \frac{1}{2} i\hbar\omega_c \frac{\partial \psi}{\partial \phi} + \left[\frac{m\omega_c^2}{8} + \frac{\mathcal{E}_0}{2R_0^2} \right] \rho^2 \psi = \mathcal{E} \psi. \quad (25.155)$$

(a) Define

$$\psi = \frac{1}{\sqrt{2\pi}} R(\rho) e^{il\phi + ik_z z} \quad (25.156)$$

and

$$\xi = \frac{m\omega_c}{2\hbar} \rho^2 \quad (25.157)$$

Show that after substituting ξ for ρ one obtains

$$\xi R'' + R' - \left[\frac{\hbar^2 k_z^2}{2m\hbar\omega_c} + \frac{\mathcal{E}_0 \xi}{mR_0^2 \omega_c^2} + \frac{\xi}{4} + \frac{l^2}{4\xi} + \frac{l}{2} - \frac{\mathcal{E}}{\hbar\omega_c} \right] R = 0. \quad (25.158)$$

(b) Show that R behaves as $\exp[-\nu\xi/2]$ for large ξ and as $\xi^{|l|/2}$ for small ξ . Find the constant ν .

(c) Now define

$$\exp[-\nu\xi/2]\xi^{|l|/2}w(\xi) = R(\xi) \quad (25.159)$$

and

$$\xi = \frac{\zeta}{\nu}. \quad (25.160)$$

Show that

$$\zeta w'' - w'\zeta + (|l| + 1)w' + \left[\frac{(\mathcal{E} - \hbar^2 k_z^2 / 2m)}{\hbar\omega_c \nu} - \frac{(|l| + 1)\nu + l}{2\nu} \right] w = 0 \quad (25.161)$$

(d) The confluent hypergeometric function $F(\alpha, \gamma; \zeta)$ solves

$$\zeta F'' + (\gamma - \zeta)F' - \alpha F = 0 \quad (25.162)$$

and is well-behaved at infinity only if α is a negative integer. Find the energy levels of the electron.

(e) Repeat the arguments leading to Eq. (25.66) and show that they are unchanged in the limit $\nu - 1 \ll 1$.

References

- Y. Aharonov and D. Bohm (1959), Significance of electromagnetic potentials in quantum theory, *Physical Review*, **115**, 485–491.
- T. Ando, A. B. Fowler, and F. Stern (1982), Electronic properties of two-dimensional systems, *Reviews of Modern Physics*, **54**, 437–672.
- G. Boebinger (1996), Correlated electrons in a million gauss, *Physics Today*, **49**(6), 36–42.
- N. Bohr (1911), Ph.D. thesis, Copenhagen.
- N. Bohr (1922), *The Theory of Spectra and Atomic Constitution*, Cambridge University Press, Cambridge.
- E. A. Boudreaux and L. N. Mulay (1976), *Theory and Applications of Molecular Paramagnetism*, John Wiley and Sons, New York.
- M. E. Cage (1987), Experimental aspects and metrological applications, in *The Quantum Hall Effect*, R. E. Prange and S. M. Girvin, eds., pp. 37–68, Springer-Verlag, New York.
- A. M. Chang (1990), Experimental aspects, in *The Quantum Hall Effect*, R. E. Prange and S. M. Girvin, eds., pp. 175–232, Springer-Verlag, New York.
- D. R. Hofstadter (1976), Energy levels and wave functions of Bloch electrons in rational and irrational magnetic fields, *Physical Review B*, **14**, 2239–2249.
- L. D. Landau (1930), Diamagnetism of metals, *Zeitschrift für Physik*, **64**, 629–637. In German. Translated in Landau (1965), pp. 31–38.
- L. D. Landau (1939), On the de Haas-van Alphen effect, *Proceedings of the Royal Society of London*, **A170**, 363–364. Appendix to paper by Shoenberg. Reprinted in Landau (1965), pp. 268–270.
- L. D. Landau (1965), *Collected Papers of L D Landau*, D. ter Haar, ed., Gordon and Breach, New York.

- L. D. Landau and E. M. Lifshitz (1977), *Quantum Mechanics (Non-relativistic Theory)*, 3rd ed., Pergamon Press, Oxford.
- L. D. Landau and E. M. Lifshitz (1980), *Statistical Physics, Part 1*, 3rd ed., Pergamon Press, Oxford.
- H. Landolt and R. Börnstein (1959), *Numerical Data and Functional Relationships in Science and Technology*, II, Springer-Verlag, Berlin.
- R. B. Laughlin (1981), Quantized Hall conductivity in two dimensions, *Physical Review B*, **23**, 5632–5633.
- R. B. Laughlin (1983), Anomalous quantum Hall effect: An incompressible quantum fluid with fractionally charged excitations, *Physical Review Letters*, **50**, 1395–1398.
- A. V. Nurmikko and A. Pinczuk (1993), Optical probes in the quantum Hall regime, *Physics Today*, **46**(6), 24–32.
- R. E. Prange and S. M. Girvin, eds. (1987), *The Quantum Hall Effect*, Springer-Verlag, New York.
- L. Saminadayar, D. C. Glattli, Y. Jin, and B. Etienne (1997), Observation of the $e/3$ fractionally charged Laughlin quasiparticle, *Physical Review Letters*, **79**, 2526–2529.
- S. L. Sondhi, S. M. Girvin, J. P. Carini, and D. Shahar (1997), Continuous quantum phase transitions, *Reviews of Modern Physics*, **69**, 315–333.
- P. Streda (1982), Theory of quantised Hall conductivity in two dimensions, *Journal of Physics C*, **15**, L717–L721.
- A. Tonomura (1993), *Electron Holography*, Springer-Verlag, Berlin.
- A. Tonomura, N. Osakabe, T. Matsuda, T. Kawasaki, J. Endo, S. Yano, and H. Yamada (1986), Evidence for the Aharonov-Bohm effect with magnetic field completely shielded from electron wave, *Physical Review Letters*, **56**, 792–795.
- D. C. Tsui, H. L. Störmer, and A. C. Gossard (1982), Two-dimensional magnetotransport in the extreme quantum limit, *Physical Review Letters*, **45**, 1559–1562.
- H.-J. van Leeuwen (1921), Problems in the electronic theory of magnetism, *Journal de Physique*, pp. 361–377. In French.
- J. H. van Vleck (1932), *The Theory of Electric and Magnetic Susceptibilities*, Oxford University Press, London.
- K. von Klitzing (1986), The quantized Hall effect, *Reviews of Modern Physics*, **58**, 519–531.
- K. von Klitzing, G. Dorda, and M. Pepper (1980), New method for high-accuracy determination of the fine-structure constant based on quantum Hall resistance, *Physical Review Letters*, **45**, 1545–1547.
- D. R. Yennie (1987), Integral quantum Hall effect for nonspecialists, *Reviews of Modern Physics*, **59**, 781–824.

26. Quantum Mechanics of Interacting Magnetic Moments

26.1 Introduction

Permanent magnetic moments could not exist in a world of charges ruled by classical electromagnetism. Quantum mechanics solves this difficulty through the quantization of orbits. However, there is a second difficulty that quantum mechanics must also be called upon to solve, and that is the strength with which adjacent magnetic moments interact.

Nearby magnetic dipoles do interact with each others' magnetic fields. Yet magnetic fields are so naturally weak that even at distances characteristic of the atomic scale, magnetic dipoles are too small to explain magnetism. The induction produced by a magnetic dipole \vec{m}_1 is

$$\vec{B} = \vec{\nabla} \left[\vec{m}_1 \cdot \vec{\nabla} \frac{1}{r} \right] = \frac{3\hat{r}(\vec{m}_1 \cdot \hat{r}) - \vec{m}_1}{r^3}, \quad (26.1)$$

and so according to Eq. (24.37) the energy of two dipoles separated by \vec{r}_{12} and interacting with each others' fields is

$$\frac{\vec{m}_1 \cdot \vec{m}_2 - 3(\vec{m}_2 \cdot \hat{r}_{12})(\vec{m}_1 \cdot \hat{r}_{12})}{r_{12}^3}, \quad (26.2)$$

which has a maximum magnitude of $2m_1m_2/r_{12}^3$ when $\vec{m}_1 \parallel \vec{m}_2 \parallel \vec{r}_{12}$. The energy scale for the dipole interactions is

$$\frac{1}{4} \frac{m_1}{\mu_B} \frac{m_2}{\mu_B} \left(\frac{2a_0}{r_{12}} \right)^3 \frac{\mu_B^2}{a_0^3} = 0.9 \cdot 10^{-4} \text{ eV} \cdot \frac{m_1}{\mu_B} \frac{m_2}{\mu_B} \left(\frac{2a_0}{r_{12}} \right)^3. \quad a_0 \text{ is the Bohr radius.} \quad (26.3)$$

Because this energy scale equals $k_B T$ for a temperature of 1 K, magnetic dipole interactions would have difficulty explaining a solid whose ferromagnetic transition temperature was 10 K, let alone iron for which it is over 1000 K. Apart from their role in large-scale phenomena such as domains, the magnetic fields produced by electrons and ions are usually negligible.

26.2 Origin of Ferromagnetism

26.2.1 Heitler–London Calculation

The physical effect that produces magnetic ordering of adjacent magnetic moments is the same that leads to magnetic ordering within an ion and produces Hund's

rules. Magnetic fields are irrelevant; what matters is the effort by electrons to choose a spin state that will minimize the Coulomb repulsion between them once Fermi statistics are taken into account. Interactions between spins are actually just a convenient way to record the end result of electrostatic repulsion.

The emergence of interactions between spins from Coulomb forces is most clearly illustrated by a calculation of Heitler and London (1927) (Figure 26.1). Consider two adjacent atoms separated by distance $\vec{R}_{12} = \vec{R}_1 - \vec{R}_2$, and let $\phi_1(\vec{r})$ and $\phi_2(\vec{r})$ be spatial wave functions of the outermost electrons on atoms 1 and 2, respectively. These wave functions should be determined when the atoms are infinitely far apart, not interacting, and the Coulomb forces between the two atoms will be treated as a perturbation.

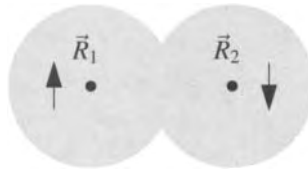


Figure 26.1. Setting for the calculation of Heitler and London (1927). Two electrons, possibly of different spin, surround nuclei at locations \vec{R}_1 and \vec{R}_2 . Correlations between the spins are induced by the overlap of the wave functions.

Because the wave functions ϕ_1 and ϕ_2 are determined when the atoms are far separated, they will not be orthogonal when the atoms come close together; the overlap integral

$$I \equiv \left\| \int d\vec{r} \phi_1^*(\vec{r})\phi_2(\vec{r}) \right\| \quad (26.4)$$

is not zero.

So long as the excited states of the two atoms remain irrelevant, the two-electron wave function when the two electrons approach one another will consist of linear combinations of antisymmetric products of ϕ_1 and ϕ_2 . It is not enough, however, to consider only the spatial dependence of the electron wave functions. The electrons employ spin degrees of freedom as part of the strategy of lowering their energy, and spin must be included explicitly.

Spin Singlets and Triplets. The Hamiltonian does not depend upon spin explicitly, so all spin operators commute with the Hamiltonian, and the eigenfunctions can be chosen as eigenfunctions of the commuting operators \hat{S}^2 and \hat{S}^z . The spin eigenfunctions are first

$$\frac{1}{\sqrt{2}} (\chi_1(\sigma_1)\chi_1(\sigma_2) - \chi_1(\sigma_1)\chi_1(\sigma_2)), \quad (26.5a)$$

which has eigenvalues $S = S_z = 0$ and is a *spin singlet*. Second, there is the *triplet*

$$\begin{aligned}
\chi_{\uparrow}(\sigma_1)\chi_{\uparrow}(\sigma_2) & S = 1; S_z = 1 \\
\frac{1}{\sqrt{2}} (\chi_{\uparrow}(\sigma_1)\chi_{\downarrow}(\sigma_2) + \chi_{\downarrow}(\sigma_1)\chi_{\uparrow}(\sigma_2)) & S = 1; S_z = 0 \\
\chi_{\downarrow}(\sigma_1)\chi_{\downarrow}(\sigma_2) & S = 1; S_z = -1.
\end{aligned} \tag{26.5b}$$

Spatial Wave Functions. The product of spatial and spin wave functions must be antisymmetric under exchange of particle numbers. Because the singlet wave function is odd, it must multiply a spatial wave function that is even, while the triplet wave functions must multiply something odd. From the two functions ϕ_1 and ϕ_2 , only one even and one odd function can be constructed, and when one takes into account the overlap integral in Eq. (26.4) the normalized combinations are

$$\phi_s(\vec{r}_1, \vec{r}_2) = \frac{1}{\sqrt{2+2I^2}} [\phi_1(\vec{r}_1)\phi_2(\vec{r}_2) + \phi_1(\vec{r}_2)\phi_2(\vec{r}_1)], \text{ Even, multiply by spin singlet.} \tag{26.6a}$$

$$\phi_t(\vec{r}_1, \vec{r}_2) = \frac{1}{\sqrt{2-2I^2}} [\phi_1(\vec{r}_1)\phi_2(\vec{r}_2) - \phi_1(\vec{r}_2)\phi_2(\vec{r}_1)]. \text{ Odd, multiply by spin triplet and get three more wave functions.} \tag{26.6b}$$

The Hamiltonian is diagonal in the space spanned by the four wave functions produced by the allowed products of Eqs. (26.5) and (26.6), because the Hamiltonian is independent of spin, but all the spin functions are orthogonal to one another. These four wave functions must be eigenfunctions of that subspace, although not necessarily of the full Hamiltonian. What remains is to calculate the expectation value of the Hamiltonian in each of them, and to find an approximation for the wave function of the ground state.

Evaluation of Energies. Let \mathcal{E}_0 be the energies of each atom when the two atoms are infinitely separated, so that

$$\left[\frac{\hat{p}_1^2}{2m} - \frac{e^2}{|\vec{r}_1 - \vec{R}_1|} \right] \phi_1(\vec{r}_1) = \mathcal{E}_0 \phi_1(\vec{r}_1). \tag{26.7}$$

When the two atoms come together, the full Hamiltonian is

$$\begin{aligned}
\hat{\mathcal{H}} = & \frac{\hat{p}_1^2}{2m} - \frac{e^2}{|\vec{r}_1 - \vec{R}_1|} + \frac{\hat{p}_2^2}{2m} - \frac{e^2}{|\vec{r}_2 - \vec{R}_2|} \\
& + \frac{e^2}{|\vec{r}_1 - \vec{r}_2|} + \frac{e^2}{|\vec{R}_1 - \vec{R}_2|} - \frac{e^2}{|\vec{r}_1 - \vec{R}_2|} - \frac{e^2}{|\vec{r}_2 - \vec{R}_1|}.
\end{aligned} \tag{26.8}$$

Then

$$\begin{aligned}
& \int d\vec{r}_1 d\vec{r}_2 \phi_1^*(\vec{r}_1)\phi_2^*(\vec{r}_2)\hat{\mathcal{H}}\phi_1(\vec{r}_1)\phi_2(\vec{r}_2) \\
& = \int d\vec{r}_1 d\vec{r}_2 \phi_2^*(\vec{r}_1)\phi_1^*(\vec{r}_2)\hat{\mathcal{H}}\phi_2(\vec{r}_1)\phi_1(\vec{r}_2)
\end{aligned} \tag{26.9}$$

$$= 2\mathcal{E}_0 + U, \tag{26.10}$$

where

$$U = \int d\vec{r}_1 d\vec{r}_2 \left[\frac{|\phi_1(\vec{r}_1)|^2}{|\phi_2(\vec{r}_2)|^2} \right] \left[\frac{e^2}{|\vec{r}_1 - \vec{r}_2|} + \frac{e^2}{|\vec{R}_1 - \vec{R}_2|} - \frac{e^2}{|\vec{r}_1 - \vec{R}_2|} - \frac{e^2}{|\vec{r}_2 - \vec{R}_1|} \right], \quad (26.11)$$

and

$$\begin{aligned} & \int d\vec{r}_1 d\vec{r}_2 \phi_2^*(\vec{r}_1) \phi_1^*(\vec{r}_2) \hat{\mathcal{H}} \phi_1(\vec{r}_1) \phi_2(\vec{r}_2) \\ &= \int d\vec{r}_1 d\vec{r}_2 \phi_1^*(\vec{r}_1) \phi_2^*(\vec{r}_2) \hat{\mathcal{H}} \phi_2(\vec{r}_1) \phi_1(\vec{r}_2) \end{aligned} \quad (26.12)$$

$$= 2\mathcal{E}_0 l^2 + V, \quad \text{Notice that the Coulomb interactions appearing in Eq. (26.14) are not the same as those appearing in Eq. (26.12); because } \vec{r}_1 \text{ and } \vec{r}_2 \text{ have been exchanged, the Coulomb terms are grouped differently.} \quad (26.13)$$

with

$$V = \int d\vec{r}_1 d\vec{r}_2 \left[\frac{\phi_1^*(\vec{r}_1) \phi_2^*(\vec{r}_2)}{\phi_2^*(\vec{r}_1) \phi_1^*(\vec{r}_2)} \right] \left[\frac{e^2}{|\vec{r}_1 - \vec{r}_2|} + \frac{e^2}{|\vec{R}_1 - \vec{R}_2|} - \frac{e^2}{|\vec{r}_1 - \vec{R}_1|} - \frac{e^2}{|\vec{r}_2 - \vec{R}_2|} \right]. \quad (26.14)$$

Finally,

$$\mathcal{E}_s = \langle \phi_s | \hat{\mathcal{H}} | \phi_s \rangle = 2 \frac{2\mathcal{E}_0 + U + 2l^2 \mathcal{E}_0 + V}{2 + 2l^2} = 2\mathcal{E}_0 + \frac{U + V}{1 + l^2} \quad (26.15a)$$

and

$$\mathcal{E}_t = \langle \phi_t | \hat{\mathcal{H}} | \phi_t \rangle = 2 \frac{2\mathcal{E}_0 + U - 2l^2 \mathcal{E}_0 - V}{2 - 2l^2} = 2\mathcal{E}_0 + \frac{U - V}{1 - l^2} \quad (26.15b)$$

and the difference between triplet and singlet energies is

$$\mathcal{E}_t - \mathcal{E}_s = \frac{2l^2 U - 2V}{1 - l^4} \equiv -J. \quad (26.16)$$

The sign of the triplet–singlet energy difference can vary according to the magnitudes of the three integrals l , U , and V . In the particular case of the helium atom, Heitler and London (1927) found that Eq. (26.16) is positive, so the singlet is of lower energy. Spins on the two atoms point in opposite directions, providing a two-atom example of antiferromagnetism.

Lieb–Mattis Theorem. While Eq. (26.16) is very suggestive of how varying overlap integrals can lead sometimes to ferromagnetism and other times to antiferromagnetism, it results from approximations, and in at least one case where it can be checked thoroughly it is wrong. Lieb and Mattis (1962) proved that the true ground state of any two-electron system is always a singlet. Equation (26.16) can predict that the triplet ground state is lower, but such a prediction must be wrong.

The argument is one earlier used by Feynman (1953) to discuss properties of the ground state of helium, and it is based upon observing that the ground state must be free of nodes. In brief, the argument proceeds as follows: Consider any

Hamiltonian for two electrons, and suppose one has found the ground-state wave function $\phi(\vec{r}_1, \vec{r}_2)$. The function $\phi^*(\vec{r}_1, \vec{r}_2)$ must have the same energy, as does $\phi + \phi^*$, so one may as well take ϕ to be real. Using the variational principle of Appendix B.2, ϕ minimizes the functional

$$\mathcal{F}\{\phi\} = \frac{\int d\vec{r}_1 d\vec{r}_2 \left[\frac{\hbar^2}{2m} |\nabla_1 \phi|^2 + \frac{\hbar^2}{2m} |\nabla_2 \phi|^2 + U(\vec{r}_1, \vec{r}_2) |\phi(\vec{r}_1, \vec{r}_2)|^2 \right]}{\int d\vec{r}_1 d\vec{r}_2 |\phi(\vec{r}_1, \vec{r}_2)|^2}. \quad (26.17)$$

Suppose that $\phi(\vec{r}_1, \vec{r}_2)$ is an odd function of its arguments. In some places it is positive, in other places it is negative, and somewhere it must pass through zero, so it has at least one node. Next consider the absolute value of ϕ , $|\phi(\vec{r}_1, \vec{r}_2)|$. Placed into Eq. (26.17), $|\phi|$ gives the same value as ϕ ; tiny regions around the nodes of ϕ where derivatives of $|\phi|$ might be ambiguous can be excluded from the integral without changing it appreciably. However, deforming ϕ near the cusp in Figure 26.2 is guaranteed to lower the energy functional (26.17), as shown in Problem 1. Therefore ϕ cannot be a ground state, and consequently it cannot have nodes. The singlet is guaranteed to lie lower than the triplet for all potentials U .

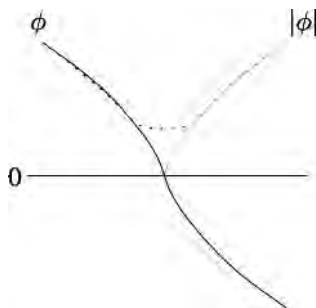


Figure 26.2. The energy of a wave function with a cusp is always lowered by smoothing out the cusp. If ϕ has a node it has the same energy as $|\phi|$, but the energy of $|\phi|$ can be lowered by deforming to the dotted line, so ϕ cannot be a ground state.

Generalizing from this argument, it would be hard to see how ferromagnetism could occur at all. The conclusions that can be obtained for two electrons are actually quite particular to problems involving only two electrons. Consider the ground state of the ion Pr^{3+} , which consists essentially of two $4f$ electrons sitting outside a xenon core. If the Lieb–Mattis theorem could be applied, Pr^{3+} would be in a state with $S = 0$ and nonmagnetic. In fact, Hund's first rule predicts, and experiment confirms, that the ground state is the triplet $S = 1$. The theorem fails because the two $4f$ electrons must be orthogonal to the inner shells of electrons, and the $4f$ electrons are consequently required to have nodes. The theorem based upon avoidance of nodes is irrelevant, and in returning to the Heitler–London approximation, one finds that it does not do such a bad job after all. Equation (26.16) can be applied, roughly, to Pr^{3+} by allowing \vec{R}_2 and \vec{R}_1 to coalesce and letting ϕ_1 and ϕ_2 be two orthogonal wave functions in the $4f$ shell. The overlap integral l vanishes, and

Eq. (26.16) predicts that the triplet will lie lower than the singlet by $2U$, predicting ferromagnetic correlations, and correctly recovering Hund's first rule.

26.2.2 Spin Hamiltonian

Because the symmetric and antisymmetric spatial states of two electrons are unshakeably correlated with the spin wave functions, Dirac (1926) and Heisenberg (1926) showed that the original Hamiltonian (26.8), which acts only on spatial degrees of freedom, can be replaced by a new Hamiltonian acting only upon the spin degrees of freedom. This new Hamiltonian is constructed to give results identical to the old one within the subspace of states spanned by the wave functions in Eqs. (26.5) and (26.6). It would not, of course, remain correct if excited atomic states were to become important.

The four electronic states created by the products of Eqs. (26.5) and (26.6) have two energies. The three triplet states sharing the same energy are related to each other by symmetry. Their energies are invariant when the spins of the two electrons, \vec{S}_1 and \vec{S}_2 , rotate simultaneously by the same amount. This observation suggests the Hamiltonian

$$\hat{\mathcal{H}} = a + b\hat{S}_1 \cdot \hat{S}_2 \quad a \text{ and } b \text{ are constants.} \quad (26.18)$$

$$= a + b \left(\hat{S}_1^z \hat{S}_2^z + \frac{1}{2} [\hat{S}_1^+ \hat{S}_2^- + \hat{S}_2^+ \hat{S}_1^-] \right). \quad (26.19)$$

See Schiff (1968), pp. 200-201,
or Landau and Lifshitz (1977),
p. 85. The raising and lowering
operators are defined by
 $\hat{S}^\pm = \hat{S}^x \pm i\hat{S}^y$.

When this Hamiltonian acts on the triplet state it gives $a + b/4$, while when it acts on the singlet state it gives $a - 3b/4$. The difference J between singlet and triplet energies defined in Eq. (26.16) equals $-b$, and evaluating a gives

$$\hat{\mathcal{H}} = 2\mathcal{E}_0 + \frac{U - V}{1 - I^2} + \left(\frac{1}{4} - \hat{S}_1 \cdot \hat{S}_2 \right) J. \quad (26.20)$$

A positive value of J causes the two spins to point in the same direction in the ground state.

26.3 Heisenberg Model

The *Heisenberg model* supposes that when a large collection of magnetic ions is placed in a lattice, Eq. (26.20) remains a guide to the form of the energy, and

$$\hat{\mathcal{H}} = - \sum_{\langle l l' \rangle} J_{ll'} \hat{S}_l \cdot \hat{S}_{l'}. \quad (26.21)$$

Drop additive contributions to the energy, and allow the possibility that J depends in a general fashion upon the particular pair of spins that is interacting. Carry out the sum over distinct pairs of spins at l and l' .

Equation (26.21) cannot easily be derived in a controlled fashion, and it is not necessarily the form that realistic accounts of interactions between electrons will take. It has, however, formed the basis for almost all studies of the organization

and dynamics of spins, at either the quantum-mechanical or classical level, which makes it worthwhile to sketch a brief derivation.

Consider a lattice of ions, and describe the electronic states in this lattice in terms of Wannier functions $w(\vec{R}, \vec{r})$, chosen because of their convenient ability to describe electrons localized on atomic sites \vec{R} , and with functions at different sites orthogonal to one another. The lesson from studying two electrons is that even when the spatial wave functions of all electrons are fixed, the system can adopt various energies according to the way that spin and space degrees of freedom interact to conform to Fermi statistics. Therefore, consider the space of states spanned by a fixed collection of Wannier functions and all possible spin states of the many electrons. For N electrons the Hamiltonian is

$$\sum_{l=1}^N \frac{\hat{p}_l^2}{2m} + \hat{U} = \hat{\mathcal{H}}_{\text{kinetic}} + \hat{\mathcal{H}}_{\text{int}}, \quad (26.22)$$

where \hat{U} can either be the Coulomb interaction or else some more elaborate effective two-body potential such as a screened Coulomb interaction. Focus on the interaction term, which contains all the magnetic effects, and rewrite it in second quantized form using the Wannier functions as basis functions. Use $|\vec{R}_l\rangle$ for the state vector such that $\langle \vec{r} | \vec{R}_l \rangle = w(\vec{R}_l, \vec{r})$, and denote the creation and annihilation operators for these states by \hat{c}_l^\dagger and \hat{c}_l . According to Eq. (C.10), the Hamiltonian in second quantized form is

$$\hat{\mathcal{H}}_{\text{int}} = \sum_{\substack{l'l''l'''' \\ \sigma\sigma'}} \langle \vec{R}_l \vec{R}_{l'} | \hat{U} | \vec{R}_{l''} \vec{R}_{l''''} \rangle \hat{c}_{l\sigma}^\dagger \hat{c}_{l'\sigma'}^\dagger \hat{c}_{l''\sigma''} \hat{c}_{l'''\sigma'''} \quad (26.23)$$

The spin states of \vec{R}_l and $\vec{R}_{l''}$ must be the same, as must be those of $\vec{R}_{l'}$ and $\vec{R}_{l''''}$, or else the matrix element vanishes because \hat{U} is independent of spin.

The approximation that leads Eq. (26.23) to reproduce the Heisenberg Hamiltonian assumes either that $\vec{R}_{l''} = \vec{R}_{l'}$ and $\vec{R}_{l'''} = \vec{R}_l$ or that $\vec{R}_{l''} = \vec{R}_l$ and $\vec{R}_{l'''} = \vec{R}_{l'}$. This approximation can be motivated either by pointing out that the Wannier functions are localized within a unit cell, so the matrix elements are small unless the wave functions group in pairs, or else by pointing out that these are the unique groupings of Wannier function indices that allow (26.23) to produce a nonzero result at lowest order in perturbation theory. Adopting in any event this approximation,

$$\hat{\mathcal{H}}_{\text{int}} = \sum_{\substack{l'l' \\ \sigma\sigma'}} \langle \vec{R}_l \vec{R}_{l'} | \hat{U} | \vec{R}_l \vec{R}_{l'} \rangle \hat{c}_{l\sigma}^\dagger \hat{c}_{l'\sigma'}^\dagger \hat{c}_{l\sigma} \hat{c}_{l'\sigma'} + \sum_{\substack{l'l' \\ \sigma\sigma'}} \langle \vec{R}_l \vec{R}_{l'} | \hat{U} | \vec{R}_{l'} \vec{R}_l \rangle \hat{c}_{l\sigma}^\dagger \hat{c}_{l'\sigma'}^\dagger \hat{c}_{l'\sigma'} \hat{c}_{l\sigma} \quad (26.24)$$

$$= \sum_{\substack{l'l' \\ \sigma\sigma'}} \langle \vec{R}_l \vec{R}_{l'} | \hat{U} | \vec{R}_l \vec{R}_{l'} \rangle \hat{c}_{l\sigma}^\dagger \hat{c}_{l'\sigma'}^\dagger \hat{c}_{l\sigma} \hat{c}_{l'\sigma'} + \sum_{\substack{l'l' \\ \sigma\sigma'}} \langle \vec{R}_l \vec{R}_{l'} | \hat{U} | \vec{R}_{l'} \vec{R}_l \rangle [\hat{n}_{l\sigma} \delta_{ll'} - \hat{c}_{l\sigma}^\dagger \hat{c}_{l'\sigma'} \hat{c}_{l'\sigma'}^\dagger \hat{c}_{l\sigma}]. \quad (26.25)$$

The final term of Eq. (26.25) is called the *exchange term*, and it can be put in the form of an interaction between spins. To do so, note the identities

$$\hat{S}^z = \frac{1}{2} [\hat{c}_\uparrow^\dagger \hat{c}_\uparrow - \hat{c}_\downarrow^\dagger \hat{c}_\downarrow] = \frac{1}{2} [\hat{n}_\uparrow - \hat{n}_\downarrow] \quad (26.26a)$$

$$\hat{S}^+ = \hat{c}_\uparrow^\dagger c_\downarrow; \quad \hat{S}^- = \hat{c}_\downarrow^\dagger c_\uparrow. \quad (26.26b)$$

In addition, by supposition every Wannier state \vec{R} is occupied either by a spin-up or spin-down electron, which means that

$$\hat{n}_{l\uparrow}\hat{n}_{l'\uparrow} + \hat{n}_{l\downarrow}\hat{n}_{l'\downarrow} \quad \text{The number operator } \hat{n} = \hat{c}^\dagger \hat{c}. \quad (26.27)$$

$$= \frac{1}{2} \{ (\hat{n}_{l\uparrow} + \hat{n}_{l\downarrow})(\hat{n}_{l'\uparrow} + \hat{n}_{l'\downarrow}) + (\hat{n}_{l\uparrow} - \hat{n}_{l\downarrow})(\hat{n}_{l'\uparrow} - \hat{n}_{l'\downarrow}) \} \quad (26.28)$$

$$= \frac{1}{2} \{ 1 + 4\hat{S}_l^z \cdot \hat{S}_{l'}^z \}. \quad \text{Use Eq. (26.26a)}. \quad (26.29)$$

Performing explicitly the spin sums in the exchange term from Eq. (26.24) gives therefore

$$\hat{\mathcal{H}}_{\text{exch}} = -\langle \vec{R}_l \vec{R}_{l'} | \hat{U} | \vec{R}_{l'} \vec{R}_l \rangle \left\{ \begin{array}{l} \hat{n}_{l\uparrow}\hat{n}_{l'\uparrow} + \hat{c}_{l\uparrow}^\dagger \hat{c}_{l\downarrow} \hat{c}_{l'\downarrow}^\dagger \hat{c}_{l'\uparrow} \\ + \hat{c}_{l\downarrow}^\dagger \hat{c}_{l\uparrow} \hat{c}_{l'\uparrow}^\dagger \hat{c}_{l'\downarrow} + \hat{n}_{l\downarrow}\hat{n}_{l'\downarrow} \end{array} \right\} \quad (26.30)$$

$$= -2\langle \vec{R}_l \vec{R}_{l'} | \hat{U} | \vec{R}_{l'} \vec{R}_l \rangle \left\{ \frac{1}{4} + \hat{S}_l^z \hat{S}_{l'}^z + \frac{1}{2} [\hat{S}_l^+ \hat{S}_{l'}^- + \hat{S}_l^- \hat{S}_{l'}^+] \right\} \quad (26.31)$$

$$= -2\langle \vec{R}_l \vec{R}_{l'} | \hat{U} | \vec{R}_{l'} \vec{R}_l \rangle \left\{ \frac{1}{4} + \hat{S}_l \cdot \hat{S}_{l'} \right\}, \quad \text{See Eq. (26.19)}. \quad (26.32)$$

which means that the Hamiltonian contains the term

$$-4 \sum_{\langle ll' \rangle} \langle \vec{R}_l \vec{R}_{l'} | \hat{U} | \vec{R}_{l'} \vec{R}_l \rangle \hat{S}_l \cdot \hat{S}_{l'} \quad (26.33)$$

as claimed in Eq. (26.21). The remaining term of Eq. (26.24) does not depend upon the spin states of particles, so Eq. (26.33) alone is responsible for magnetic ordering.

26.3.1 Indirect Exchange and Superexchange

Direct overlap of wave functions is not the only way for two magnetic ions to interact. They can also affect each through *indirect exchange*, in which the interaction between two ions is mediated by conduction electrons. Roughly speaking, the electrons belonging to an ion flip a conduction electron which then travels to another site and interacts with the spin of the ion on the second site. The calculations of Section 26.6 will provide a specific illustration of how conduction electrons interact with a localized spin. A second way for separated spins to interact is through *superexchange*, a similar process, but where the mediating influence comes from a neutral atom sitting between the magnetic ions. Whatever the source of the interaction between spins, the leading term in the Hamiltonian is often of the Heisenberg form.

26.3.2 Ground State

Ferromagnet. The ground state of the Heisenberg model is easy to construct so long as all the constants $J_{ll'}$ are positive. Any state where all spins point in the same direction, say along z , has energy

$$\langle \uparrow \uparrow \uparrow \dots | \hat{\mathcal{H}} | \uparrow \uparrow \uparrow \dots \rangle = - \sum_{\langle ll' \rangle} \frac{J_{ll'}}{4}. \quad \text{For spin } 1/2, \text{ with } S^2 \text{ replacing } 1/4 \text{ if the spins have different magnitude.} \quad (26.34)$$

Proving that this simple state is actually the ground state is the subject of Problem 2.

Antiferromagnet. When some constants J are negative, the problem of finding the ground state is much more difficult. Quantum states in which alternating spins point in opposite directions are not eigenstates. For the case where there is only one negative constant J that multiplies interactions between nearest neighbors, the ground state wave function was found by Bethe (1931) and was developed further by Orbach (1958).

26.3.3 Spin Waves

The excited states of the Heisenberg Hamiltonian have the same significance for magnetic behavior that phonons have for elastic behavior. They determine magnetic contributions to specific heat, and as they grow in amplitude with increasing temperature, they determine the location of phase transitions between magnetic and nonmagnetic states.

The ferromagnetic ground state is degenerate, because while spins all need to point in the same direction, there is no preference for precisely what that direction should be. Many of the low-energy excitations are *spin waves*, which are constructed by slowly twisting the local spin orientation while passing through the crystal. These deformations of the local spin ordering can propagate through the crystal like plane waves and are called *magnons*.

The energy of very long-wavelength spin waves vanishes, just like the energy of very long-wavelength phonons; both are Goldstone modes. Goldstone (1963), p. 163 explained that “Whenever the original Lagrangian has a continuous symmetry group, the new solutions have a reduced symmetry and contain massless bosons.” “The massless particles . . . correspond to ‘spin-wave’ excitations in which only the direction of [phase angle] ϕ makes infinitesimal oscillations. The mass must be zero because when all the $\phi(x)$ rotate in phase there is no gain in energy because of the symmetry.”

Schwinger Representation. A formal theory of spin waves, effective both for ferromagnets and antiferromagnets, begins with a representation of quantum spin operators due to Schwinger (1965). The Heisenberg Hamiltonian arose from products of fermion creation and annihilation operators, but in this new representation the spins are represented by Bose operators.

Let \hat{a}_1^\dagger and \hat{a}_2^\dagger be two Bose creation operators. Let σ^α be the Pauli spin matrices, with $\alpha = x, y, z$. Consider

$$\hat{S}^\alpha = \frac{1}{2} \sum_{ll'} a_l^\dagger \sigma_{ll'}^\alpha a_{l'}. \quad \sigma^x = \begin{pmatrix} 0 & 1 \\ 1 & 0 \end{pmatrix}; \sigma^y = \begin{pmatrix} 0 & -i \\ i & 0 \end{pmatrix}; \sigma^z = \begin{pmatrix} 1 & 0 \\ 0 & 1 \end{pmatrix}. \quad (26.35)$$

Writing the components out explicitly, one has

$$\hat{S}^z = \frac{1}{2} (\hat{a}_1^\dagger \hat{a}_1 - \hat{a}_2^\dagger \hat{a}_2) \quad (26.36a)$$

$$\hat{S}^x = \frac{1}{2} (\hat{a}_1^\dagger \hat{a}_2 + \hat{a}_2^\dagger \hat{a}_1) \quad (26.36b)$$

$$\hat{S}^y = i \frac{1}{2} (\hat{a}_2^\dagger \hat{a}_1 - \hat{a}_1^\dagger \hat{a}_2). \quad (26.36c)$$

One can verify that the operators in Eq. (26.36) obey the commutation relations for angular momentum operators. For example,

$$\begin{aligned} [\hat{S}^x, \hat{S}^y] &= i \frac{1}{4} [\hat{a}_1^\dagger \hat{a}_2 + \hat{a}_2^\dagger \hat{a}_1, \hat{a}_2^\dagger \hat{a}_1 - \hat{a}_1^\dagger \hat{a}_2] \\ &= i \hat{S}^z. \end{aligned} \quad (26.37)$$

One also has that

$$\hat{S}^+ = \hat{a}_1^\dagger \hat{a}_2; \quad \hat{S}^- = \hat{a}_2^\dagger \hat{a}_1. \quad (26.38)$$

Angular momentum operators can describe particles of any integer or half-odd-integer spin. If one wants to describe particles of spin S , then one has to work in a space where

$$\frac{1}{2} (\hat{a}_1^\dagger \hat{a}_1 + \hat{a}_2^\dagger \hat{a}_2) = S. \quad (26.39)$$

Holstein and Primakoff (1940) found an improbable formal device to ensure that Eq. (26.39) will be satisfied, by writing

$$\hat{a}_2^\dagger \hat{a}_2 = 2S - \hat{a}_1^\dagger \hat{a}_1 \quad (26.40)$$

and then taking the square root of both sides to obtain

$$\hat{a}_2 = \sqrt{2S - \hat{a}_1^\dagger \hat{a}_1}. \quad (26.41)$$

It seems incorrect to take the square root of the left hand side like this, but the identity stands up to inspection.

The result is

$$\hat{S}^+ = \hat{a}_1^\dagger \sqrt{2S - \hat{a}_1^\dagger \hat{a}_1} \quad (26.42a)$$

$$\hat{S}^- = \sqrt{2S - \hat{a}_1^\dagger \hat{a}_1} \hat{a}_1 \quad (26.42b)$$

$$\hat{S}^z = (\hat{a}_1^\dagger \hat{a}_1 - S). \quad (26.42c)$$

Neglecting the peculiar derivation of these relations, one can verify without much apparent trouble that all the necessary commutation relations continue to be satisfied. For example,

$$[\hat{S}^+, \hat{S}^-] = 2\hat{S}^z. \quad \text{The calculation occupies about four lines, and relies upon the fact that } \hat{a}^\dagger \hat{a} \text{ commutes with any function of itself.} \quad (26.43)$$

The subscript on \hat{a}_1 has been dropped. An obvious problem with this representation is that it allows the eigenvalue of $\hat{a}^\dagger \hat{a}$ to be greater than $2S$, which would correspond to negative eigenvalues of $\hat{a}_2^\dagger \hat{a}_2$ —an impossibility. This representation of the rotation operators allows the creation of states that were not permitted by the original representation. In the correct subspace the representation creates no difficulties, but one must be aware of the possibility that the representation will create unphysical states.

Now return to the Heisenberg Hamiltonian. It can be solved in an approximate way by taking S to be large and by expanding in powers of $1/S$. This approximation begins with a classical account of the lowest-energy configuration and proceeds with a quantum-mechanical calculation of the fluctuations about it. The expansion is known as the $1/S$ expansion and is related to a host of similar approximations called $1/N$ expansions, discussed by Bickers (1987). First write

$$\hat{S}_l \cdot \hat{S}_{l'} = \frac{1}{2} (\hat{S}_l^+ \hat{S}_{l'}^- + \hat{S}_{l'}^+ \hat{S}_l^-) + \hat{S}_l^z \hat{S}_{l'}^z \quad (26.44)$$

$$= \frac{1}{2} \hat{a}_l^\dagger \sqrt{2S - \hat{a}_l^\dagger \hat{a}_l} \sqrt{2S - \hat{a}_{l'}^\dagger \hat{a}_{l'}} \hat{a}_{l'} + \frac{1}{2} \hat{a}_{l'}^\dagger \sqrt{2S - \hat{a}_{l'}^\dagger \hat{a}_{l'}} \sqrt{2S - \hat{a}_l^\dagger \hat{a}_l} \hat{a}_l + (S - \hat{a}_l^\dagger \hat{a}_l)(S - \hat{a}_{l'}^\dagger \hat{a}_{l'}). \quad (26.45)$$

The semiclassical approximation involves supposing that S becomes very large. In this limit, guess that the operators \hat{a} can be written as

$$\hat{a}_l = \sqrt{S} b_l + (\hat{a}_l - \sqrt{S} b_l), \quad (26.46)$$

with the second term taken to be small. The values of the constants b_l will be determined by minimizing the Hamiltonian, and expansion in the remainder produces a series in $1/S$. To leading order, one then has

$$\hat{\mathcal{H}} = - \sum_{ll'} J_{ll'} S^2 \left[\frac{1}{2} (b_l b_{l'}^* + b_{l'} b_l^*) \sqrt{2 - |b_l|^2} \sqrt{2 - |b_{l'}|^2} + (1 - |b_l|^2)(1 - |b_{l'}|^2) \right]. \quad (26.47)$$

The general procedure is to minimize this Hamiltonian with respect to all the parameters b_l . If the $J_{ll'}$'s are random variables or very long range, this task may be insoluble. Assume that all of the $J_{ll'}$ are positive, that they are only nonzero if ll' are a nearest neighbor pair, and that all the nonzero elements are the same and equal to J . It is therefore natural to guess that all the b_l are equal. Taking this to be the case, the ground-state energy is

$$\mathcal{E}_0 = -JNzS^2 (|b|^2(2 - |b|^2) + (1 - |b|^2)^2) = -JNzS^2, \quad (26.48)$$

where z is the coordination number of each lattice site, and N is the total number of sites. The ground-state energy is independent of the particular value of b , because the spins can rotate in any direction so long as they all point together. Imposing an external magnetic field would favor a particular spin direction, and therefore a particular value of b , but for the present, one can choose $b = 0$. Continuing with the expansion of the Hamiltonian means treating the operators \hat{a} formally as small. Working to next order gives

$$\hat{\mathcal{H}} \approx -NJzS^2 - 2J \sum_{\langle ll' \rangle} S \left(\hat{a}_l^\dagger \hat{a}_{l'} + \hat{a}_{l'}^\dagger \hat{a}_l - \hat{a}_l^\dagger \hat{a}_l - \hat{a}_{l'}^\dagger \hat{a}_{l'} \right). \quad (26.49)$$

The sum over $\langle ll' \rangle$ is a sum over distinct nearest-neighbor pairs. A factor of two is needed because each pair appears twice in Eq. (26.47).

This Hamiltonian is essentially the tight-binding Hamiltonian of Eq. (8.67), and the solution obtained for (8.67) can be used again. The Hamiltonian is diagonalized by the operators

$$\hat{a}_l = \frac{1}{\sqrt{N}} \sum_{\vec{k}} \hat{a}_k e^{-i\vec{k} \cdot \vec{r}_l} \quad (26.51)$$

in terms of which it becomes

$$\hat{\mathcal{H}} = -NJzS^2 - 2JS \sum_{\vec{k}} \sum_{\vec{\delta}} \left[\cos(\vec{k} \cdot \vec{\delta}) - 1 \right] \hat{a}_k^\dagger \hat{a}_{\vec{k}} \quad (26.52)$$

$$= -NJzS^2 + \sum_{\vec{k}} \hbar\omega_{\vec{k}} \hat{n}_{\vec{k}}, \quad (26.53)$$

where

$$\hbar\omega = 2SJ \sum_{\vec{\delta}} \left(1 - \cos(\vec{\delta} \cdot \vec{k}) \right), \quad (26.54)$$

and $\vec{\delta}$ are the nearest-neighbor vectors. Equation (26.54) gives the spin wave dispersion relation. It should be kept in mind that this dispersion relation is only the approximate result of the $1/S$ expansion, but it describes the behavior of the Heisenberg model fairly well even for small S .

Bound States. The approximate analysis of Holstein and Primakoff incorrectly predicts the qualitative nature of the lowest-energy excitations of the Heisenberg model. Mattis (1988), Section 5.4, shows that on a one-dimensional chain, two magnons can form a bound state, and propagating structures of this sort lie lower in energy, for any value of k , than individual magnons. Wortis (1965) has shown that the situation is more complicated in higher dimensions. In two dimensions there is again a bound state for every \vec{k} , although the difference in energy between the bound state and the lowest-energy magnon is exponentially small. In three dimensions there are no bound states at all for small values of \vec{k} , although at higher \vec{k} there may be one, two, or three.

26.3.4 Spin Waves in Antiferromagnets

If the coupling J between spins is chosen negative, then all features of the quantum problem become more difficult. Neighboring spins do tend to be antiparallel,

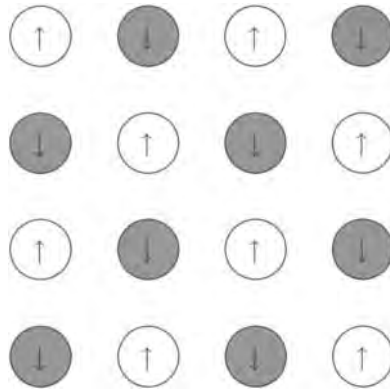


Figure 26.3. In the the Néel state, neighboring spins belong to separate sublattices, pointing up and down respectively. This spin configuration provides only an approximate solution of the quantum-mechanical Hamiltonian.

although the actual ground-state wave function is very complicated. To capture the tendency of neighbors to point in opposite directions, called the *Néel state*, divide the spins into two interpenetrating sublattices, A and B, so that the neighbors of the A spins are all on the B sublattice and vice versa (Figure 26.3). One way to remove the inconvenience of keeping track of the change in spin direction when moving from site to site is to transform the Hamiltonian. Subject all the spin operators on the B sublattice to a 180° rotation about the x axis, so $x \rightarrow x$, $y \rightarrow -y$, and $z \rightarrow -z$, and the spin operators transform as

$$S_{l'}^{\pm} \rightarrow S_{l'}^{\mp} \quad S_{l'}^z \rightarrow -S_{l'}^z. \tag{26.55}$$

Following this transformation, a ferromagnetic state where all spins point in the same direction will have precisely the same energy as the Néel state had before the transformation. The transformation does not by itself solve the problem, because the ferromagnetic state is no more an eigenstate of the new Hamiltonian than the Néel state was of the old one, but it simplifies the algebra. Assuming that only spins that are nearest neighbors interact, the Heisenberg Hamiltonian becomes

$$\hat{\mathcal{H}} = 2|J| \sum_{\langle ll' \rangle} \frac{1}{2} \left[\hat{S}_l^+ \hat{S}_{l'}^+ + \hat{S}_l^- \hat{S}_{l'}^- \right] - \hat{S}_l^z \hat{S}_{l'}^z \tag{26.56}$$

$$= 2|J| \sum_{\langle ll' \rangle} \left[\frac{1}{2} \hat{a}_l^\dagger \sqrt{2S - \hat{a}_l^\dagger \hat{a}_l} \hat{a}_{l'}^\dagger \sqrt{2S - \hat{a}_{l'}^\dagger \hat{a}_{l'}} + \frac{1}{2} \sqrt{2S - \hat{a}_l^\dagger \hat{a}_l} \hat{a}_l \sqrt{2S - \hat{a}_{l'}^\dagger \hat{a}_{l'}} \hat{a}_{l'} - (\hat{a}_l^\dagger \hat{a}_l - S)(\hat{a}_{l'}^\dagger \hat{a}_{l'} - S) \right]. \tag{26.57}$$

Adopt again the expression for the creation and annihilation operators in Eq. (26.46), and expand in powers of the second term. Taking b to be uniform in space, the leading term in the Hamiltonian is

$$\hat{\mathcal{H}} \approx -Nz|J|S^2 \left[(1 - b^2)^2 - b^2 (2 - b^2) \right], \tag{26.58}$$

which reaches a local minimum for

$$b = 0. \quad \begin{array}{l} \text{Eq. (26.58) can be made arbitrarily negative by taking } b \text{ large, but large values} \\ \text{of } b \text{ do not provide legitimate points about which to expand the Hamiltonian.} \end{array} \quad (26.59)$$

Expanding next to quadratic order in the creation and annihilation operators,

$$\hat{\mathcal{H}} \approx 2|J| \sum_{\langle l'l' \rangle} \left[-S^2 + S \left\{ \hat{a}_l^\dagger \hat{a}_l + \hat{a}_{l'}^\dagger \hat{a}_{l'} + \hat{a}_l^\dagger \hat{a}_{l'}^\dagger + \hat{a}_l \hat{a}_{l'} \right\} \right]. \quad (26.60)$$

Because Eq. (26.60) once again resembles the tight-binding model, it is natural to define

$$\hat{a}_{\vec{k}} = \frac{1}{\sqrt{N}} \sum_l e^{i\vec{k} \cdot \vec{R}_l} \hat{a}_l \quad \text{Compare with Eq. (8.68)}. \quad (26.61)$$

and rewrite Eq. (26.60) in terms of $\hat{a}_{\vec{k}}$ and $\hat{a}_{\vec{k}}^\dagger$ in the hopes that it will become diagonal. The hopes are temporarily dashed, because

$$\hat{\mathcal{H}} = -|J|NzS^2 + |J|S \sum_{\vec{k}, \vec{\delta}} \left[\left(\hat{a}_{\vec{k}}^\dagger \hat{a}_{-\vec{k}}^\dagger + \hat{a}_{\vec{k}} \hat{a}_{-\vec{k}} \right) \cos(\vec{k} \cdot \vec{\delta}) + 2\hat{a}_{\vec{k}}^\dagger \hat{a}_{\vec{k}} \right]. \quad \begin{array}{l} \vec{\delta} \text{ are nearest-neighbor} \\ \text{vectors.} \end{array} \quad (26.62)$$

This Hamiltonian is not diagonal, but it only mixes \vec{k} , and $-\vec{k}$. It can finally be made diagonal through a transformation to new variables of the form

$$\hat{a}_{\vec{k}} = \cosh(\alpha_{\vec{k}}) \hat{\gamma}_{\vec{k}} + \sinh(\alpha_{\vec{k}}) \hat{\gamma}_{-\vec{k}}^\dagger, \quad (26.63)$$

with α real. Problem 4 shows that substituting Eq. (26.63) into Eq. (26.62) diagonalizes the Hamiltonian, provided that

$$\tanh 2\alpha_{\vec{k}} = -\frac{1}{z} \sum_{\vec{\delta}} \cos(\vec{k} \cdot \vec{\delta}). \quad \begin{array}{l} z \text{ is the number of nearest neighbors of each} \\ \text{site.} \end{array} \quad (26.64)$$

In terms of the operators $\hat{\gamma}$, the Hamiltonian becomes

$$\hat{\mathcal{H}} = -Nz|J|S(S+1) + 2|J|zS \sum_{\vec{k}} \left(\hat{\gamma}_{\vec{k}}^\dagger \hat{\gamma}_{\vec{k}} + \frac{1}{2} \right) \sqrt{1 - \tanh^2 2\alpha_{\vec{k}}}. \quad (26.65)$$

While Eq. (26.65) was constructed in order to search for excited states of the antiferromagnet, it provides as a bonus an estimate of the ground-state energy. Write the ground-state energy in the form

$$-NS^2|J|z \left(1 + \frac{\Gamma}{zS} \right). \quad (26.66)$$

For a one-dimensional chain of spin-1/2 particles, Eq. (26.65) gives $\Gamma = 2 - 4/\pi = 0.726$, while the exact result is $\Gamma = 0.773$.

The energy of a magnon with wave number \vec{k} is predicted to be

$$\mathcal{E}_{\vec{k}} = 2|J|S \sqrt{z^2 - \left(\sum_{\vec{\delta}} \cos \vec{k} \cdot \vec{\delta} \right)^2}. \quad \text{Combine Eqs. (26.65) and (26.64)}. \quad (26.67)$$

Unlike ferromagnetic magnons, the energy of antiferromagnetic magnons rises linearly for small \vec{k} .

The approximate prediction in Eq. (26.67) compares well with the exact one-dimensional results for single magnon excitations. However, the lowest-energy excitations for any given \vec{k} are once again bound states, as shown by Fadeev and Takhtajan (1981).

26.3.5 Comparison with Experiment

Figure 3.14 showed that spin-polarized neutrons are capable of detecting magnetic structures. Inelastic neutron scattering can be used to detect magnons in magnetic systems, exactly as it is used to measure phonons. Measurements of ferromagnetic and antiferromagnetic magnon dispersion relations gathered in this way are shown in Figure 26.4. The crude model used for the exchange constants $J_{ll'}$ precludes quantitative comparison of Eqs. (26.54) or (26.64) with the data, but the ferromagnetic dispersion does rise from zero quadratically, and the antiferromagnetic dispersion does rise linearly, as predicted.

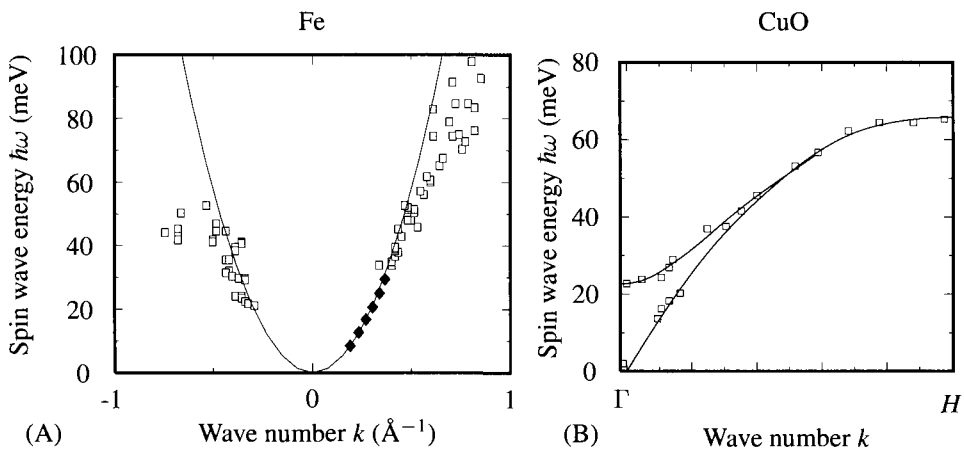


Figure 26.4. (A) Dispersion relation for ferromagnetic magnons in iron obtained with inelastic neutron scattering. [Source: Yethiraj et al. (1991), p. 2571, and Lynn (1975), p. 2629.] (B) Dispersion relation for antiferromagnetic magnons in CuO obtained with inelastic neutron scattering. Two modes are visible, one acoustic and one optical. Solid lines have expected theoretical form. [Source: Aïn et al. (1989), p. 1279.]

26.4 Ferromagnetism in Transition Metals

26.4.1 Stoner Model

The magnetism of the transition metals and their alloys sits in an uneasy relation to the Heisenberg model. The Heisenberg model conjures up an image of isolated magnetic spins interacting with neighboring spins at short range. In metals such as

iron, the conduction electrons participate in the magnetism; they are *itinerant* and carry a net magnetic moment, although they are spread throughout the crystal.

Stoner (1934) showed how to think about the coexistence of magnetism with one-electron band theory. The two are not in conflict. A collection of Bloch electrons can display a net magnetic moment if it is energetically favorable to occupy one spin direction more heavily than the other. Depopulating one spin direction in favor of another is guaranteed to incur a cost in kinetic and potential energy. The size of the penalty is indicated by the inverse of the density of states $D(\mathcal{E}_F)$. If the density of states is large, many electrons can be moved into higher-energy states that sit only a tiny bit above (what was thought to be) the Fermi energy; but if it is small, the energies of electrons rapidly rise as they transfer from one spin direction to the other. The exchange interaction between overlapping electrons favors ferromagnetism, so the question is which of the two effects wins.

As observed in Section 8.4.4, Wannier functions for metals can be defined, but cannot necessarily be localized at atomic sites, and may interact with other atoms over a long range. Writing down the exchange interaction (26.21), one should expect very large numbers of spins to interact with each other; in the extreme case, the interaction could become something like $-J[\sum_l \hat{S}_l]^2$. Because the sum over all spin operators is a macroscopic quantity, the total magnetic moment of a crystal, it should behave classically. Under these conditions, it should be appropriate to replace the quantum spin operators by their average value $\langle S \rangle$.

To construct the *Stoner model*, suppose that one has a collection of mobile electrons whose energy per volume is described by a density of states $D(\mathcal{E})$. Further suppose that when the mean spin per electron is $\langle S \rangle$, the energy per volume of the electrons is changed by $-Jn \langle S \rangle^2 / 2$, with some effective constant J taking into account the actual range of interaction between spins. The competition between one-particle energies and exchange energies can be evaluated by supposing that up- and down-spin states are occupied equally up to energy $\mathcal{E}_F - \Delta_1$, and that from there up to an energy $\mathcal{E}_F + \Delta_2$, only spin-up states are occupied. For the moment restrict attention to energies Δ sufficiently small that the density of states may be treated as constant. Then if the number of particles in the system is to be conserved, $\Delta_1 = \Delta_2 = \Delta$. So one can write that the total energy per volume of the electrons is

$$\mathcal{E} = \int_0^{\mathcal{E}_F - \Delta} d\mathcal{E}' D(\mathcal{E}') \mathcal{E}' + \frac{1}{2} \int_{\mathcal{E}_F - \Delta}^{\mathcal{E}_F + \Delta} d\mathcal{E}' D(\mathcal{E}') \mathcal{E}' - \frac{1}{2} nJ \langle S \rangle^2, \quad (26.68)$$

where the average spin per particle is

$$\langle S \rangle = \frac{1}{2n} \int_{\mathcal{E}_F - \Delta}^{\mathcal{E}_F + \Delta} d\mathcal{E}' \frac{1}{2} D(\mathcal{E}') = \frac{1}{2n} D(\mathcal{E}_F) \Delta. \quad (26.69)$$

The leading factor of 1/2 assumes spin 1/2 electrons, while the second comes from the fact that the density of states includes both spin directions.

A brief calculation shows that

$$\left. \frac{\partial \mathcal{E}}{\partial \Delta} \right|_{\mathcal{E}_F} = \Delta D(\mathcal{E}_F) - \frac{J}{4n} D(\mathcal{E}_F)^2 \Delta, \quad (26.70)$$

which means that the system is unstable to ferromagnetism when

$$\left. \frac{\partial \mathcal{E}}{\partial \Delta} \right|_{\mathcal{E}_F} = 0 \Rightarrow \frac{J}{n} D(\mathcal{E}_F) = 4. \quad \begin{array}{l} \text{This is the condition for linear instability of} \\ \text{the unmagnetized state. It predicts that the} \\ \text{net spin runs away from zero, but does not} \\ \text{say what the spin will become.} \end{array} \quad (26.71)$$

The value of $\langle S \rangle$ does not necessarily increase until it saturates at $1/2$. The details depend entirely upon the shape of the density of states. If

$$\mathcal{E} = \int_0^{\mathcal{E}_F - \Delta_1} d\mathcal{E}' D(\mathcal{E}') \mathcal{E}' + \frac{1}{2} \int_{\mathcal{E}_F - \Delta_1}^{\mathcal{E}_F + \Delta_2} d\mathcal{E}' D(\mathcal{E}') \mathcal{E}' - \frac{1}{2} J n \langle S \rangle^2, \quad (26.72)$$

then

$$\frac{\partial \Delta_2}{\partial \Delta_1} = \frac{D(\mathcal{E}_F - \Delta_1)}{D(\mathcal{E}_F + \Delta_2)}, \quad \begin{array}{l} \text{This condition results from conserving the num-} \\ \text{ber of electrons.} \end{array} \quad (26.73)$$

and magnetization tends to increase so long as

$$\frac{\partial \mathcal{E}}{\partial \Delta_1} \leq 0 \quad (26.74)$$

$$\Rightarrow \Delta_1 + \Delta_2 \leq \frac{J}{4n} \int_{\mathcal{E}_F - \Delta_1}^{\mathcal{E}_F + \Delta_2} d\mathcal{E}' D(\mathcal{E}'). \quad (26.75)$$

26.4.2 Calculations Within Band Theory

The magnetic moments of the transition metals can be calculated with almost astonishing reliability by the combination of density functional theory and band calculations. The flavor of how these calculations proceed can be obtained by returning to the Hartree-Fock description of the uniform electron gas. The calculations of Section 9.2.4 assumed that up- and down-spin states were populated equally, but it is easy to relax this assumption and see what comes out. Returning to Eq. (9.50), the energy of N_\uparrow up-spin electrons and N_\downarrow down-spin electrons would be

$$\mathcal{E} = \mathcal{E}_\uparrow + \mathcal{E}_\downarrow \quad (26.76)$$

where

$$\mathcal{E}_\uparrow = N_\uparrow \left[\frac{3}{5} \mathcal{E}_{F\uparrow} - \frac{3}{4} \frac{e^2 k_{F\uparrow}}{\pi} \right], \quad \text{An identical expression holds for } \mathcal{E}_\downarrow. \quad (26.77)$$

$$\mathcal{E}_{F\uparrow} = \frac{\hbar^2 k_{F\uparrow}^2}{2m}, \quad \text{and} \quad \frac{4\pi}{3} \frac{1}{(2\pi)^3} k_{F\uparrow}^3 = \frac{N_\uparrow}{V}. \quad (26.78)$$

If the energy (26.76) can be lowered at all by creating nonzero net spin, then the energy is minimized by putting all N electrons into a single spin direction. The energy of such a state is

$$\mathcal{E}_{\text{polarized}} = N \left[\frac{3}{5} \frac{\hbar^2}{2m} (6\pi^2 n)^{2/3} - \frac{3}{4\pi} e^2 (6\pi^2 n)^{1/3} \right], \quad (26.79)$$

and it must be compared with the unpolarized state

$$\mathcal{E}_{\text{unpolarized}} = N \left[\frac{3 \hbar^2}{5 2m} (3\pi^2 n)^{2/3} - \frac{3}{4\pi} e^2 (3\pi^2 n)^{1/3} \right]. \quad (26.80)$$

After a bit of algebra, the criterion for the ferromagnetically polarized state to have lower energy can be put in the form

$$\begin{aligned} \frac{2\pi\hbar^2}{5m} \left(\frac{1}{2^{1/3}} + 1 \right) &< e^2 (6\pi^2 n)^{-1/3} \\ \Rightarrow \frac{r_W}{a_0} &> \frac{2\pi}{5} \left(\frac{1}{2^{1/3}} + 1 \right) \left(\frac{9\pi}{2} \right)^{1/3} = 5.45. \end{aligned} \quad (26.82)$$

See Eq. (11.48) for the definition of r_W ; a_0 is the Bohr radius, \hbar^2/me^2 .

The prediction of (26.82) that ferromagnetism is preferred at low electron densities is not confirmed by any experimental results. Only cesium among the elements should be ferromagnetic according to this criterion, and cesium is nonmagnetic. The validity of the approach is not, however, fairly judged by such a crude version of the calculation. A more reasonable test is to ask what happens when the full apparatus of density functional theory is set loose on the magnetic problem, allowing populations of up- and down-spin electrons to vary freely and letting the exchange and correlation functional \mathcal{E}_{xc} from Eq. (9.103) battle kinetic energy terms over magnetic structures.

The 3d transition metals present the most important test case, because the metallic ferromagnets iron, cobalt, and nickel are in this group. In rough terms, these elements are magnetic because many partly filled d bands are clustered about the Fermi surface, providing a large density of states and allowing the Stoner criterion (26.71) to be satisfied. Quantitative calculations along these lines are summarized by Moruzzi and Marcus (1993), and some results are presented in Table 26.1.

The predictive power of the band structure calculations is somewhat hampered by their great sensitivity to changes in lattice structure. Band structure calculations

Table 26.1. Magnetic moment per ion in the ground state for the 3d transition metals in fcc and bcc minimum energy states

Element:	Sc	Ti	V	Cr	Mn	Fe	Co	Ni
Calculated m/μ_B (bcc):	0	0	0	0	0.70	2.15	1.68	0.38
Experimental m/μ_B (bcc):				0		2.12		
Calculated m/μ_B (fcc):	0	0	0	0	0	0	1.56	0.60
Experimental m/μ_B (fcc):							1.61	0.61

Results are from density functional calculations of Moruzzi and Marcus (1993). The calculations are not always capable of deciding between the fcc and bcc structures, but given the correct structure they correctly predict the magnetic moment.

usually fail to predict experimental lattice constants to better than a few percent, and they may have trouble correctly deciding which of several candidate lattices is the true ground state. Equilibrium magnetic properties can vary quickly with small changes in lattice constant, so if experiment and calculation disagree on what the lattice constant should be, it is not clear what should be used to find the magnetic moment. Some remarkable predictions are nevertheless possible. Iron is bcc at room temperature, but calculations predict that if it were fcc, and if its lattice constant were expanded by around 5% above equilibrium, it should become ferromagnetic with a moment of $2\mu_B$ per ion. Pescia et al. (1987) tested this prediction by depositing a thin epitaxial layer of iron on fcc copper, and they found that it was indeed ferromagnetic.

26.5 Spintronics

Conventional electronics depends upon the manipulation of charge. Switches control the flow of charge currents, and the currents carry information. One hope for the future of information processing is to move from control of charge to spin. In one respect, spin has long been used to hold information; domains of aligned spin form bits in magnetic recording. The vision of *spintronics* is to move beyond control of domains with external fields to new devices, where packets of spin travel through wires, carrying bits as packets of charge do now. The hope is that these devices will have lower dissipation and faster switching times than ones now used.

26.5.1 Giant Magnetoresistance

In one respect, the hope of technological advance through control of spin has already been realized. Binasch et al. (1989) and Baibich et al. (1988) discovered *giant magnetoresistance* in layered magnetic materials. Figure 26.5(A) shows the change of in-plane resistivity for three layers of Fe, Cr, and Fe as a function of magnetic field applied perpendicular to the layers. The effect is around one percent, which is much greater than the change in resistance of crystalline iron alone. The magnetic coupling between the two iron layers is antiferromagnetic; absent an external field, they point opposite to each other. Thus the large resistance is due to forcing electrons through a layered structure where spins point opposite to one another in the different layers. Theories for the origins of the change in resistance are reviewed by Žutić et al. (2004).

Combining many iron and chromium layers together, as shown in Figure 26.5(B), the fractional change in resistivity climbs to 80%. Devices optimized for applications, such as *spin valves*, have an intermediate structural complexity, and might consist of four layers: an antiferromagnetic top layer, a ferromagnetic layer, a conducting layer, and a final thin ferromagnetic layer, as described by Wolf et al. (2001).

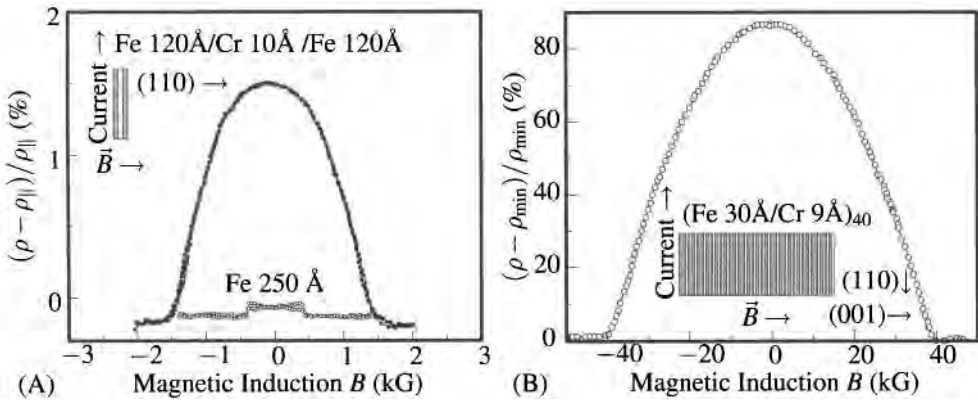


Figure 26.5. First measurements of giant magnetoresistance in magnetic multilayers. (A) Change in resistivity as a function of magnetic induction for a three-layer structure of Fe and Cr. The reference resistivity $\rho_{||}$ is the saturation resistivity $B \rightarrow \infty$ along the easy axis (001). The data from the magnetic multilayer are compared with a reference film of pure iron. [Source: Binasch et al. (1989), p. 4829.] (B) Change in resistivity as a function of magnetic induction for an 80-layer structure of Fe and Cr at 4.2K. [Source: Baibich et al. (1988), p. 2473.]

26.5.2 Spin Torque

Slonczewski (1996) and Berger (1996) observed that since spins carry angular momentum, currents containing an excess population of one type of spin should be able to flip magnetic domains. Freitas and Berger (1985) had already observed domain-wall motion triggered by currents of several amperes, but the prediction was that modest spin current densities in nanometer scale channels could flip domains as well.

A spin current describes the rate of spin transport. Classically, if particles carrying spin \vec{S} are moving with velocity \vec{v} , then the current describing component j of the spin moving in direction i is

$$Q_{ij} = v_i S_j. \quad (26.83)$$

Quantum mechanically, the definition stays essentially the same. The spin current density at point \vec{r} carried by state $|\psi\rangle$ is

$$Q_{ij}(\vec{r}) = \text{Re}\langle\psi|\delta(\vec{r}-\hat{R})\hat{S}_j\frac{\hat{P}_i}{m}|\psi\rangle \quad \text{Be careful and work with } (\hbar/m)\text{Im}(\psi^*\vec{\nabla}\psi). \quad (26.84)$$

Suppose a current of spin $\frac{1}{2}$ particles is flowing along \hat{x} with a wave function of the form

$$\psi(x) = \frac{e^{ikx}}{\sqrt{\mathcal{N}}}(a|\uparrow\rangle + b|\downarrow\rangle). \quad (26.85)$$

The spin operators \hat{S}_j are given by $\hbar/2$ times the Pauli matrices of Eq. (26.35), so Eq. (26.84) becomes

$$Q_{xx} = \frac{k\hbar^2}{2\mathcal{N}m}(a^*b + b^*a) \quad (26.86a)$$

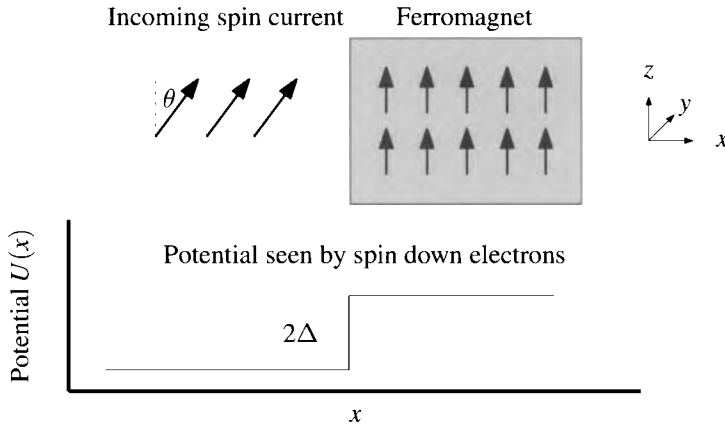


Figure 26.6. A spin current incident upon a ferromagnet creates a spin torque. This schematic diagram illustrates model calculations.

$$Q_{xy} = \frac{\hbar^2}{2V_m} i(b^*a - a^*b) \tag{26.86b}$$

$$Q_{xz} = \frac{\hbar^2}{2V_m} (|a|^2 - |b|^2) \tag{26.86c}$$

Specializing further, suppose that a spin current whose spin axis points at angle θ away from \hat{z} in the $x-z$ plane impinges upon a ferromagnet where all spins point along \hat{z} (Figure 26.6). Use a very simple model of the ferromagnet, in the spirit of the Stoner model, where the highest occupied spin up states have kinetic energy 2Δ more than the highest occupied spin down states. Thus assume that down spins see an energy barrier of height 2Δ , while up spins pass into the ferromagnet with kinetic energy unchanged. That is, when spin down electrons with $\hbar^2 k^2 / 2m > 2\Delta$ enter the ferromagnet, their wave vector changes from k to

$$k_{\downarrow} = \sqrt{k^2 - 4m\Delta/\hbar^2} \quad \text{while for spin up} \quad k_{\uparrow} = k. \tag{26.87}$$

Computing transmission and reflection coefficients t and r as is customary in barrier penetration problems

$$t_{\downarrow} = \frac{2k}{k+k_{\downarrow}}; \quad r_{\downarrow} = \frac{k-k_{\downarrow}}{k+k_{\downarrow}}. \quad \text{For spin down, } r=0 \text{ and } t=1. \tag{26.88}$$

The main point is that up- and down-spin electrons have different transmission and reflection coefficients upon entering the ferromagnet; fine details of the coefficients' values are less significant.

The result is that outside the ferromagnet there is a wave function

$$\psi^{\text{out}} = \frac{e^{ikx}}{\sqrt{V}} (\cos \theta/2 | \uparrow \rangle + \sin \theta/2 | \downarrow \rangle) + \frac{e^{-ikx}}{\sqrt{V}} r_{\downarrow} \sin \theta/2 | \downarrow \rangle$$

Rotation matrices applied to spin 1/2 particles produce half the rotation one would expect for a vector.

$$\tag{26.89}$$

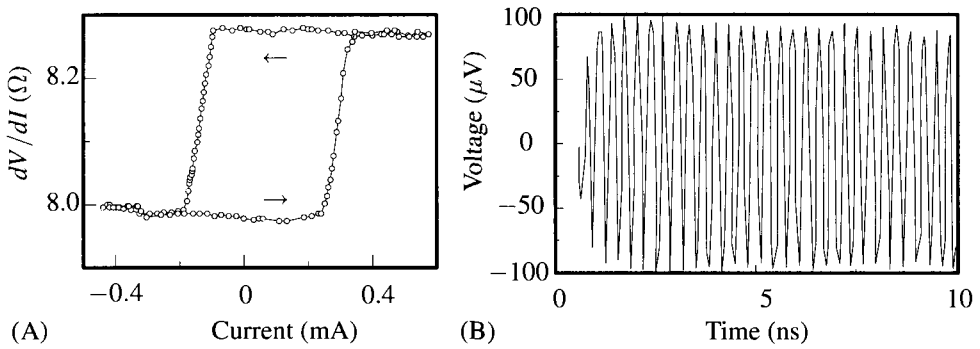


Figure 26.7. Domain flipping and precession induced by spin torques. (A) Magnetization flip in room-temperature layered metallic system consisting of 20nm $\text{Ni}_{81}\text{Fe}_{19}$ /12nm $\text{Cu}/4.5\text{nm Ni}_{81}\text{Fe}_{19}$. A constant external magnetic field is used to maintain zero net magnetic field on the thinner magnetic layer, which flips and changes the magnetoresistance. (B) Magnetization precession in a 8nm $\text{Ir}_{20}\text{Mn}_{80}$ /4nm $\text{Ni}_{80}\text{Fe}_{20}$ /8nm $\text{Cu}/4\text{nm Ni}_{80}\text{Fe}_{20}$ layered structure at a temperature of 40K. [Source: Ralph and Stiles (2008), p. 1192.]

and inside the ferromagnet

$$\psi^{\text{in}} = \frac{e^{ikx}}{\sqrt{\mathcal{V}}} \left(\cos \theta/2 | \uparrow \rangle + t_{\downarrow} e^{i(k_{\perp} - k)} \sin \theta/2 | \downarrow \rangle \right). \quad (26.90)$$

Returning to Eqs. (26.86), one can compute the spin currents inside and out. Outside, they are

$$Q_{xx}^{\text{out}} = \frac{k\hbar^2}{2\mathcal{V}m} \sin \theta \quad \text{In principle there are terms going as } e^{2ikx} \text{ and } e^{-2ikx}, \text{ but they oscillate so rapidly they can be neglected.} \quad (26.91a)$$

$$Q_{xy}^{\text{out}} = 0 \quad (26.91b)$$

$$Q_{xz}^{\text{out}} = \frac{k\hbar^2}{2\mathcal{V}m} \left(\cos \theta + r_{\downarrow}^2 \sin^2 \theta/2 \right) \quad (26.91c)$$

Inside the ferromagnet, the spin current is

$$Q_{xx}^{\text{in}} = \frac{\hbar^2}{2\mathcal{V}m} t_{\downarrow} \frac{k+k_{\perp}}{2} \sin \theta \cos(k_{\perp} - k)x \quad \text{Return to Eq. (26.84); remember to take real part.} \quad (26.92a)$$

$$Q_{xy}^{\text{in}} = \frac{\hbar^2}{2\mathcal{V}m} t_{\downarrow} \frac{k+k_{\perp}}{2} \sin \theta \sin(k - k_{\perp})x \quad (26.92b)$$

$$Q_{xz}^{\text{in}} = \frac{\hbar^2}{2\mathcal{V}m} \left(k \cos^2 \theta/2 - k_{\perp} t_{\downarrow}^2 \sin^2 \theta/2 \right) \quad (26.92c)$$

Define the current

$$I_k = \frac{A \hbar k}{\mathcal{V} m} e. \quad (26.93)$$

The components of the spin current are discontinuous at the edge of the ferromagnet, $x = 0$, and this discontinuity integrated over the area A of its surface is the

torque \vec{N} :

$$N_x = \frac{\hbar I k}{2 e} \sin \theta (1 - t_{\downarrow}) \quad \text{Use Eq. (26.88).} \quad (26.94a)$$

$$N_y = 0 \quad (26.94b)$$

$$N_z = \frac{\hbar I k_{\perp} - k}{2 e} t_{\downarrow}^2 \sin^2 \theta / 2. \quad \text{Use } t_{\uparrow}^2 + r_{\uparrow}^2 = 1. \quad (26.94c)$$

A qualitative conclusion to draw from Eq. (26.92) is that once spin currents enter a ferromagnet they will precess in space with a wavelength $2\pi/(k_{\perp} - k)$. A qualitative conclusion from Eq. (26.94) is that each excess spin-up electron entering the ferromagnet does bring with it a change in angular momentum on the order of $\hbar/2$. A spin polarized current I will thus deliver a torque on the order of $I\hbar/e$. Assuming this current arrives in a sample containing N atoms with spin angular momentum $\hbar N$, the characteristic time to make the sample flip or precess will be Ne/I . For $N \sim 10^6$ and currents on the order of mA, this works out to 10^{-10} s.

Figure 26.7 shows the results of two different experiments. In the first, a current pulse flips a magnetic domain. In the second, the arrival of a polarized spin current causes the spins in a device to precess.

26.6 Kondo Effect

Resistance Minima. According to Matthiessen's rule, Section 18.2.2, the resistivity of a metal should consist of two additive pieces. The first, due to phonons, decreases with temperature, dropping as T^5 at low temperatures. The second, due to impurities, is temperature-independent. A puzzling exception to this rule was observed by de Haas et al. (1934), while measuring the resistance of gold. Its resistance dropped to a minimum at a temperature of 4 K, and then proceeded to rise at lower temperatures. Some feature of the solid became more effective at scattering electrons as its temperature decreased. It was clear to Wilson (1954) that small traces of impurities were responsible, because the resistance minimum could be moved about by varying their concentration, but there was no explanation beyond this, and he believed that "some new physical principle seems to be involved." Some characteristic resistance measurements appear in Figure 26.8.

The explanation lies in the magnetic character of the impurities. At high temperatures, the spin of an isolated magnetic impurity flips about freely, presenting a small isotropic scattering potential to incoming electrons. At low temperatures, by pointing in a definite direction, the magnetic impurity becomes more effective in scattering electrons. Some experimental evidence along these lines was obtained by Sarachik et al. (1964), and the first theory is due to Kondo (1964). His calculation followed the influence of single magnetic moment upon a collection of conduction electrons out to third order in perturbation theory. It appeared to explain the resistance minima observed at temperatures of a few kelvin, but could not be the full story, because it predicted that at 0 kelvin the resistance should become infinite, something neither observed experimentally nor believed to be true. An

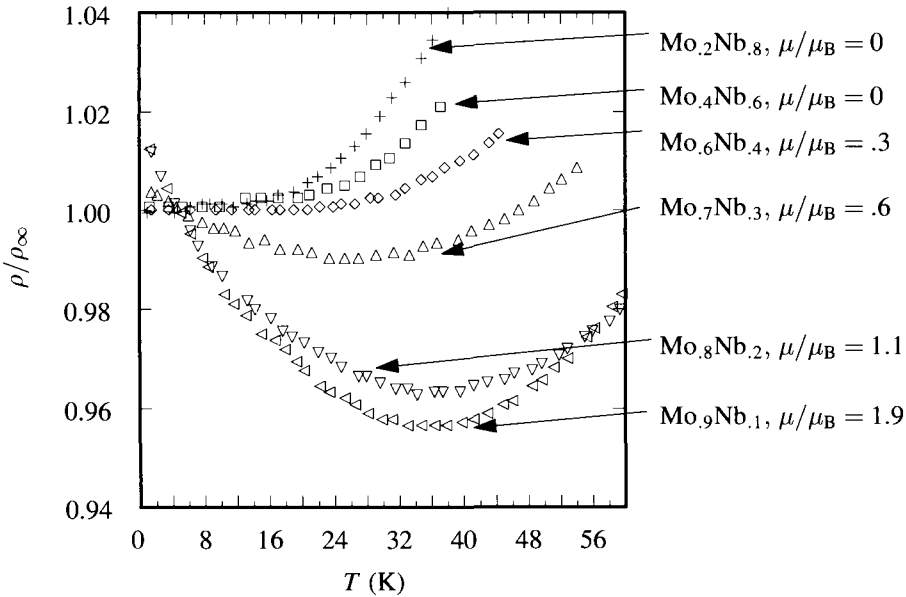


Figure 26.8. Resistivity data for $\text{Mo}_x\text{Nb}_{1-x}$ alloys, showing that depth and location of a minimum of resistivity at low temperatures is correlated with the strength of magnetic moments in the sample. [Source: Sarachik et al. (1964), p. A1043.]

intense search for the solution to this problem over the next decade led to many valuable new ideas, and eventually even exact analytical solutions of Wiegmann (1980) and Andrei (1982), reviewed by Hewson (1997).

From the host of approaches to this problem it is only possible to choose a small sample. First it will be demonstrated why a sea of conduction electrons interacting with an impurity can behave as though interacting with a magnetic moment. The half-bandwidth \mathcal{W} will denote the range of energy states inhabited by the electrons; their energies will range from $-\mathcal{W}$ to \mathcal{W} . Next it will be shown that the band of conduction electrons interacting with a magnetic moment of strength J is indistinguishable from an equivalent system in which the bandwidth $2\mathcal{W}$ diminishes a bit, while J slightly increases. This rescaling of the problem, due to Anderson et al. (1970); Anderson (1970) and Wilson (1975), provides a simple introduction to how ideas from the renormalization group can be employed for systems of interacting electrons.

Anderson Model. To begin, consider a model due to Anderson (1961) which describes a collection of conduction electrons in contact with a single impurity site (Figure 26.9). The Hamiltonian is

$$\hat{\mathcal{H}} = \epsilon_0[\hat{n}_{0\uparrow} + \hat{n}_{0\downarrow}] + U\hat{n}_{0\uparrow}\hat{n}_{0\downarrow} + \sum_{\vec{k}\sigma} [\epsilon_{\vec{k}}\hat{c}_{\vec{k}\sigma}^\dagger\hat{c}_{\vec{k}\sigma} + v_{\vec{k}}\hat{c}_{0\sigma}^\dagger\hat{c}_{\vec{k}\sigma} + v_{\vec{k}}^*\hat{c}_{\vec{k}\sigma}^\dagger\hat{c}_{0\sigma}]. \quad (26.95)$$

The first two terms describe the impurity; placing one electron there costs an energy ϵ_0 , but placing two there costs $2\epsilon_0 + U$, with U representing the repulsion that two localized electrons are expected to feel for one another. The remaining terms

describe the conduction electrons and provide terms proportional to $v_{\vec{k}}$ that allow them to interact with the impurity. In actual physical contexts, the impurity is likely to be an atom with an unfilled outer d or f shell, and the shell will usually have more than one orbital state available. Because the spin degrees of freedom included in Eq. (26.95) are quite enough to produce many interesting effects, additional orbital degeneracy can be neglected on a first pass through the theory.

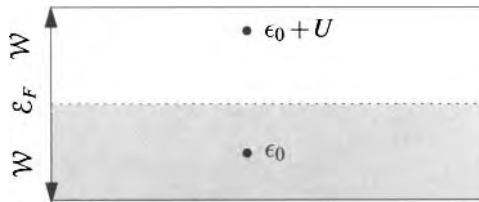


Figure 26.9. A band of conduction electrons, bandwidth $2W$, is placed in contact with an impurity site, where the energy to add a first electron is ϵ_0 , and the additional energy to add a second is $\epsilon_0 + U$. If the first energy lies below the Fermi surface while the second energy lies above the Fermi surface, it is an excellent approximation to say that the impurity is singly occupied.

To make the impurity potential in (26.95) start acting like a magnetic moment, suppose that

- the Fermi level \mathcal{E}_F of the conduction electrons lies well above ϵ_0 , so the impurity state is almost sure to be occupied,
- but $\epsilon_0 + U$ is much greater than the Fermi level, so double occupation is very unlikely, and
- the couplings $v_{\vec{k}}$ between the impurity and the conduction electrons can be treated as small.

Rather than simply carrying out perturbation theory to some order in $v_{\vec{k}}$, the goal is instead to have a general idea how the presence of the impurity affects properties of the system at low temperature. At low temperatures, only states near the ground state enter, so the way the impurity affects the whole collection of low-lying excitations needs to be analyzed. What results is an effective Hamiltonian for low-lying excitations that results from eliminating high-energy states.

The meaning of the last statement is best clarified by proceeding immediately to show how it is done. First, break the Hamiltonian up so that it is possible to keep track of whether the impurity site is unoccupied ($n_0 = 0$), singly occupied ($n_0 = 1$) or doubly occupied ($n_0 = 2$). Toward this end, define \hat{P}_0 , \hat{P}_1 , and \hat{P}_2 to be projection operators. \hat{P}_0 acting on any quantum state where the impurity is occupied gives zero, but if the impurity is unoccupied, \hat{P}_0 returns the state unchanged. \hat{P}_1 and \hat{P}_2 similarly project out the $n_0 = 1$ and $n_0 = 2$ spaces. Formally, one can write

$$\hat{P}_0 = (1 - \hat{n}_{0\downarrow})(1 - \hat{n}_{0\uparrow}), \quad (26.96)$$

with similar expressions for the other operators.

Next, letting $|\psi\rangle$ be some quantum state of many electrons, let

$$|\psi_0\rangle = \hat{P}_0|\psi\rangle, \quad |\psi_1\rangle = \hat{P}_1|\psi\rangle, \quad \text{and } |\psi_2\rangle = \hat{P}_2|\psi\rangle. \quad (26.97)$$

Also, define

$$\hat{\mathcal{H}}_{ll'} = \hat{P}_l \hat{\mathcal{H}} \hat{P}_{l'}, \quad (26.98)$$

For example, $\hat{\mathcal{H}}_{l_0}$ gives the action of the Hamiltonian on whatever piece of a wave function has the impurity state empty, and it selects from the result whatever part is singly occupied.

so $\hat{\mathcal{H}}|\psi\rangle = \mathcal{E}|\psi\rangle$ can be rewritten as

$$\begin{pmatrix} \hat{\mathcal{H}}_{00} & \hat{\mathcal{H}}_{01} & 0 \\ \hat{\mathcal{H}}_{10} & \hat{\mathcal{H}}_{11} & \hat{\mathcal{H}}_{12} \\ 0 & \hat{\mathcal{H}}_{21} & \hat{\mathcal{H}}_{22} \end{pmatrix} \begin{pmatrix} |\psi_0\rangle \\ |\psi_1\rangle \\ |\psi_2\rangle \end{pmatrix} = \mathcal{E} \begin{pmatrix} |\psi_0\rangle \\ |\psi_1\rangle \\ |\psi_2\rangle \end{pmatrix} \quad (26.99)$$

The reason that $\hat{\mathcal{H}}_{02} = \hat{\mathcal{H}}_{20} = 0$ is that the various terms in the Hamiltonian can leave the occupation of the impurity by 1, or leave it alone, but cannot change it by 2.

Having broken the Hamiltonian apart to describe its action on different states of the impurity separately, it is now possible to transform (26.99) so that it is a problem posed for $|\psi_1\rangle$ alone, eliminating from the problem the subspaces where $n_0 = 0$ or $n_0 = 2$. Simply write

$$\hat{\mathcal{H}}_{00}|\psi_0\rangle + \hat{\mathcal{H}}_{01}|\psi_1\rangle = \mathcal{E}|\psi_0\rangle \quad \text{The top equation in (26.99).} \quad (26.100)$$

$$\Rightarrow |\psi_0\rangle = (\mathcal{E} - \hat{\mathcal{H}}_{00})^{-1} \hat{\mathcal{H}}_{01}|\psi_1\rangle \quad (26.101)$$

$$\text{and } |\psi_2\rangle = (\mathcal{E} - \hat{\mathcal{H}}_{22})^{-1} \hat{\mathcal{H}}_{21}|\psi_1\rangle; \quad \text{Similarly from the bottom equation of (26.99). Now substitute Eqs. (26.102) and (26.101) into the middle equation of (26.99) to obtain} \quad (26.102)$$

$$\left\{ \hat{\mathcal{H}}_{10} (\mathcal{E} - \hat{\mathcal{H}}_{00})^{-1} \hat{\mathcal{H}}_{01} + (\hat{\mathcal{H}}_{11} - \mathcal{E}) + \hat{\mathcal{H}}_{12} (\mathcal{E} - \hat{\mathcal{H}}_{22})^{-1} \hat{\mathcal{H}}_{21} \right\} |\psi_1\rangle = 0. \quad (26.103)$$

By eliminating $|\psi_0\rangle$ and $|\psi_2\rangle$, Eq. (26.103) recasts the original problem entirely in terms of states where the impurity is singly occupied. This formulation is appropriate when one expects on physical grounds that single occupation is to be expected.

To proceed further, it is necessary to obtain explicit expressions for the entries in the matrix on the left-hand side of Eq. (26.99). Consider $\hat{\mathcal{H}}_{l_0}$. It needs to act on a state where the impurity is unoccupied and subsequently produce one where it is singly occupied. The only piece of $\hat{\mathcal{H}}$ that works that way is

$$\sum_{\vec{k}\sigma} v_{\vec{k}} \hat{c}_{0\sigma}^\dagger \hat{c}_{\vec{k}\sigma}. \quad (26.104)$$

However, (26.104) does not annihilate states where the impurity is singly occupied as it should; one needs to add a projection operator on the right, to get

$$\hat{\mathcal{H}}_{l_0} = \sum_{\vec{k}\sigma} v_{\vec{k}} \hat{c}_{0\sigma}^\dagger \hat{c}_{\vec{k}\sigma} \hat{P}_0 \quad (26.105)$$

$$\begin{aligned}
&= \sum_{\vec{k}\sigma} v_{\vec{k}} \hat{c}_{0\sigma}^\dagger \hat{c}_{\vec{k}\sigma} (1 - \hat{n}_{0\downarrow}) (1 - \hat{n}_{0\uparrow}) \quad \text{See Eq. (26.96).} \quad (26.106) \\
&= \sum_{\vec{k}\sigma} v_{\vec{k}} \hat{c}_{0\sigma}^\dagger \hat{c}_{\vec{k}\sigma} (1 - \hat{n}_{0,-\sigma}). \quad \text{The term } (1 - \hat{n}_{0\sigma}) \text{ is superfluous, because (26.107)} \\
&\quad \text{if the state with spin } \sigma \text{ is occupied, } \hat{c}_{0\sigma}^\dagger \text{ will} \\
&\quad \text{annihilate it anyway.}
\end{aligned}$$

Because $\hat{\mathcal{H}}$ is Hermitian,

$$\hat{\mathcal{H}}_{01} = \hat{\mathcal{H}}_{10}^* = \sum_{\vec{k}\sigma} (1 - \hat{n}_{0,-\sigma}) v_{\vec{k}}^* \hat{c}_{\vec{k}\sigma}^\dagger \hat{c}_{0\sigma}. \quad (26.108)$$

Other terms can be worked out similarly, such as

$$\hat{\mathcal{H}}_{11} = \hat{P}_1 [\epsilon_0 + \sum_{\vec{k}\sigma} \epsilon_{\vec{k}} \hat{c}_{\vec{k}\sigma}^\dagger \hat{c}_{\vec{k}\sigma}]; \quad \hat{\mathcal{H}}_{00} = \hat{P}_0 \sum_{\vec{k}\sigma} \epsilon_{\vec{k}} \hat{c}_{\vec{k}\sigma}^\dagger \hat{c}_{\vec{k}\sigma} \quad (26.109)$$

and

$$\hat{\mathcal{H}}_{21} = \hat{\mathcal{H}}_{12}^* = \sum_{\vec{k}\sigma} v_{\vec{k}} \hat{c}_{0\sigma}^\dagger \hat{c}_{\vec{k}\sigma} \hat{n}_{0,-\sigma}. \quad (26.110)$$

From Impurity to Local Moment. With these formal developments as prelude, it can now be demonstrated that Eq. (26.103) approximately describes conduction electrons interacting with a magnetic moment at the impurity site. Consider the first term,

$$\hat{\mathcal{H}}_{10} (\mathcal{E} - \hat{\mathcal{H}}_{00})^{-1} \hat{\mathcal{H}}_{01} |\psi_1\rangle \quad (26.111)$$

$$= \hat{\mathcal{H}}_{10} \sum_{\vec{k}\sigma} (1 - \hat{n}_{0,-\sigma}) v_{\vec{k}}^* \hat{c}_{\vec{k}\sigma}^\dagger \hat{c}_{0\sigma} (\mathcal{E} - [\hat{\mathcal{H}}_{11} - \epsilon_0 + \epsilon_{\vec{k}}])^{-1} |\psi_1\rangle. \quad (26.112)$$

Use Eq. (26.109) to get rid of $\hat{\mathcal{H}}_{00}$, and add $\epsilon_{\vec{k}}$ because in moving $(\mathcal{E} - \hat{\mathcal{H}}_{00})^{-1}$ to the right of $\hat{c}_{\vec{k}\sigma}^\dagger$, $\hat{\mathcal{H}}_{00}$ acts on an empty state \vec{k} that is populated to the left.

As Eq. (26.108) shows, (26.111) is of order $|v_{\vec{k}}|^2$ and very small. To leading order Eq. (26.103) can be replaced by $(\hat{\mathcal{H}}_{11} - \mathcal{E})|\psi_1\rangle = 0$. Up to order $|v_{\vec{k}}|^2$, $\mathcal{E} - \hat{\mathcal{H}}_{11}$ can be replaced by 0 in (26.112). Thus Eq. (26.103) can be interpreted as describing a situation where the impurity is singly occupied, but makes virtual transitions to the unoccupied or doubly occupied states and immediately jumps back. Furthermore, if one restricts attention to excited states \vec{k} near the Fermi surface, then $\epsilon_{\vec{k}}$ can be replaced whenever it appears by \mathcal{E}_F . Equation (26.112) now becomes

$$\frac{\hat{\mathcal{H}}_{10}}{\epsilon_0 - \mathcal{E}_F} \sum_{\vec{k}\sigma} v_{\vec{k}}^* (1 - \hat{n}_{0,-\sigma}) \hat{c}_{\vec{k}\sigma}^\dagger \hat{c}_{0\sigma} |\psi_1\rangle \quad (26.113)$$

$$= \sum_{\vec{k}\vec{k}'\sigma\sigma'} \frac{v_{\vec{k}'} v_{\vec{k}}^*}{\epsilon_0 - \mathcal{E}_F} \hat{c}_{0\sigma'}^\dagger \hat{c}_{\vec{k}'\sigma'} (1 - \hat{n}_{0,-\sigma'}) (1 - \hat{n}_{0,-\sigma}) \hat{c}_{\vec{k}\sigma}^\dagger \hat{c}_{0\sigma} |\psi_1\rangle \quad (26.114)$$

$$= \sum_{\vec{k}\vec{k}'\sigma\sigma'} \frac{v_{\vec{k}'} v_{\vec{k}}^*}{\mathcal{E}_F - \epsilon_0} \hat{c}_{0\sigma'}^\dagger \hat{c}_{\vec{k}\sigma}^\dagger \hat{c}_{\vec{k}'\sigma'} \hat{c}_{0\sigma} |\psi_1\rangle. \quad (26.115)$$

The two terms that have been omitted always just give 1, unless everything vanishes anyway. Reversing two of the operators reverses the sign and produces spin-independent constant.

In the $n_0 = 1$ subspace, the impurity has two possible states, \uparrow and \downarrow , which can be identified with the states of a spin 1/2 particle. Thinking in these terms, $\hat{c}_{0\uparrow}^\dagger \hat{c}_{0\downarrow}$ can be identified with \hat{S}^+ , the raising operator for the spin, while $\hat{c}_{0\downarrow}^\dagger \hat{c}_{0\uparrow} = \hat{S}^-$. For the z component of the spin, $\hat{S}^z = (\hat{n}_{0\uparrow} - \hat{n}_{0\downarrow})/2$, use the identity

$$\hat{n}_{0\uparrow} \hat{c}_{k\uparrow}^\dagger \hat{c}_{k'\uparrow} + \hat{n}_{0\downarrow} \hat{c}_{k\downarrow}^\dagger \hat{c}_{k'\downarrow} \quad \text{This is what shows up in (26.115).} \quad (26.116)$$

$$= \frac{1}{2}(\hat{n}_{0\uparrow} - \hat{n}_{0\downarrow})(\hat{c}_{k\uparrow}^\dagger \hat{c}_{k'\uparrow} - \hat{c}_{k\downarrow}^\dagger \hat{c}_{k'\downarrow}) + \frac{1}{2}(\hat{n}_{0\uparrow} + \hat{n}_{0\downarrow})(\hat{c}_{k\uparrow}^\dagger \hat{c}_{k'\uparrow} + \hat{c}_{k\downarrow}^\dagger \hat{c}_{k'\downarrow}) \quad (26.117)$$

$$= \hat{S}^z(\hat{c}_{k\uparrow}^\dagger \hat{c}_{k'\uparrow} - \hat{c}_{k\downarrow}^\dagger \hat{c}_{k'\downarrow}) + \frac{1}{2} \sum_{\sigma} \hat{c}_{k\sigma}^\dagger \hat{c}_{k'\sigma}. \quad \text{In the } n_0 = 1 \text{ subspace, } \hat{n}_{0\uparrow} + \hat{n}_{0\downarrow} \text{ always gives 1.} \quad (26.118)$$

Therefore, Eq. (26.115) can be rewritten as

$$\sum_{\vec{k}\vec{k}'} \frac{v_{\vec{k}'} v_{\vec{k}}^*}{\mathcal{E}_F - \epsilon_0} \left[\hat{S}^+ \hat{c}_{k\downarrow}^\dagger \hat{c}_{k'\uparrow} + \hat{S}^- \hat{c}_{k\uparrow}^\dagger \hat{c}_{k'\downarrow} + \hat{S}^z(\hat{c}_{k\uparrow}^\dagger \hat{c}_{k'\uparrow} - \hat{c}_{k\downarrow}^\dagger \hat{c}_{k'\downarrow}) + \frac{1}{2} \sum_{\sigma} \hat{c}_{k\sigma}^\dagger \hat{c}_{k'\sigma} \right] |\psi_1\rangle. \quad (26.119)$$

The first three terms in the bracket of (26.119) represent electron spins interacting with a spin-1/2 magnetic moment. The last term is a small correction to the energies of the conduction electrons that does not involve the spin. Treating the third term of (26.103) in a fashion similar to the first term finally transforms (26.103) into an effective Hamiltonian, only to be used on states of type ψ_1 . The effective Hamiltonian is

$$\hat{\mathcal{H}}_{\text{eff}} = \hat{\mathcal{H}}_{11} + \sum_{\vec{k}\vec{k}'} J_{\vec{k}\vec{k}'} \left[\hat{S}^+ \hat{c}_{k\downarrow}^\dagger \hat{c}_{k'\uparrow} + \hat{S}^- \hat{c}_{k\uparrow}^\dagger \hat{c}_{k'\downarrow} + \hat{S}^z(\hat{c}_{k\uparrow}^\dagger \hat{c}_{k'\uparrow} - \hat{c}_{k\downarrow}^\dagger \hat{c}_{k'\downarrow}) \right] + K_{\vec{k}\vec{k}'} \sum_{\sigma} \hat{c}_{k\sigma}^\dagger \hat{c}_{k'\sigma} \quad (26.120a)$$

with

$$J_{\vec{k}\vec{k}'} = v_{\vec{k}'} v_{\vec{k}}^* \left[\frac{1}{\mathcal{E}_F - \epsilon_0} + \frac{1}{U + \epsilon_0 - \mathcal{E}_F} \right]. \quad (26.120b)$$

Completing the derivation of Eq. (26.120) and finding $K_{\vec{k}\vec{k}'}$ is the subject of Problem 6. Under the conditions depicted in Figure 26.9, the conduction electrons are coupled antiferromagnetically to the local moment, because $J_{\vec{k}\vec{k}'}$ is positive.

26.6.1 Scaling Theory

The previous section demonstrated that by eliminating states far above and below the Fermi level from a Hamiltonian, an impurity potential can be revealed as a magnetic moment. Putting matters this way leads to an additional suggestion: The states being eliminated might not have to be impurity states. They could also be conduction electron states. This suggestion is correct. By eliminating states at the band edges in just the fashion that occupancies of the impurity were eliminated

before, the coupling between conduction electrons and a local magnetic moment can be made to grow. A whole family of different Hamiltonians is thereby shown to be equivalent, some with strong coupling to the spin and a small bandwidth, others with a weak coupling to the spin and a large bandwidth. The final result is quite simple, and it appears in Eq. (26.129).

The starting Hamiltonian is a simplified version of the Hamiltonian found in Eq. (26.120):

$$\hat{\mathcal{H}} = \sum_{\substack{\vec{k}\sigma \\ \epsilon_{\vec{k}} < \mathcal{W}}} \epsilon_{\vec{k}} \hat{c}_{\vec{k}\sigma}^\dagger \hat{c}_{\vec{k}\sigma} + \sum_{\vec{k}\vec{k}'} J \left\{ \hat{S}^- \hat{c}_{\vec{k}\uparrow}^\dagger \hat{c}_{\vec{k}'\downarrow} + \hat{S}^+ \hat{c}_{\vec{k}\downarrow}^\dagger \hat{c}_{\vec{k}'\uparrow} + \hat{S}^z \left[\hat{c}_{\vec{k}\uparrow}^\dagger \hat{c}_{\vec{k}'\uparrow} - \hat{c}_{\vec{k}\downarrow}^\dagger \hat{c}_{\vec{k}'\downarrow} \right] \right\}. \quad (26.121)$$

Proceed as in the previous section, except that now \hat{P}_2 is a projection operator demanding that $\mathcal{W} - |\delta\mathcal{W}| < \epsilon_{\vec{k}} < \mathcal{W}$, \hat{P}_1 projects on states with $-\mathcal{W} + |\delta\mathcal{W}| < \epsilon_{\vec{k}} < \mathcal{W} - |\delta\mathcal{W}|$, while \hat{P}_0 insists that $-\mathcal{W} < \epsilon_{\vec{k}} < -\mathcal{W} + |\delta\mathcal{W}|$, as shown in Figure 26.10.

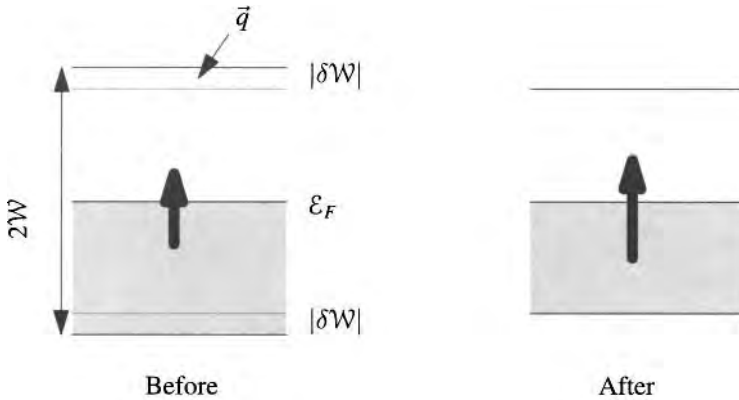


Figure 26.10. A small band of states, of width $|\delta\mathcal{W}|$ is eliminated from the upper and lower band edges. Accounting for the virtual transitions that would have been possible to these states makes the coupling to the magnetic moment stronger.

Using \vec{k} or \vec{k}' to denote states obeying $-\mathcal{W} + |\delta\mathcal{W}| < \epsilon_{\vec{k}} < \mathcal{W} - |\delta\mathcal{W}|$, and using \vec{q} or \vec{q}' to denote states obeying $\mathcal{W} - |\delta\mathcal{W}| < \epsilon_{\vec{q}} < \mathcal{W}$, then

$$\hat{\mathcal{H}}_{12} = J \sum_{\vec{k}\vec{q}} \hat{S}^- \hat{c}_{\vec{k}\uparrow}^\dagger \hat{c}_{\vec{q}\downarrow} + \hat{S}^+ \hat{c}_{\vec{k}\downarrow}^\dagger \hat{c}_{\vec{q}\uparrow} + \hat{S}^z \left[\hat{c}_{\vec{k}\uparrow}^\dagger \hat{c}_{\vec{q}\uparrow} - \hat{c}_{\vec{k}\downarrow}^\dagger \hat{c}_{\vec{q}\downarrow} \right], \quad (26.122a)$$

$$\hat{\mathcal{H}}_{21} = J \sum_{\vec{k}'\vec{q}'} \hat{S}^- \hat{c}_{\vec{q}'\uparrow}^\dagger \hat{c}_{\vec{k}'\downarrow} + \hat{S}^+ \hat{c}_{\vec{q}'\downarrow}^\dagger \hat{c}_{\vec{k}'\uparrow} + \hat{S}^z \left[\hat{c}_{\vec{q}'\uparrow}^\dagger \hat{c}_{\vec{k}'\uparrow} - \hat{c}_{\vec{q}'\downarrow}^\dagger \hat{c}_{\vec{k}'\downarrow} \right]. \quad (26.122b)$$

In the previous section, $\hat{\mathcal{H}}_{02}$ was zero, something that is no longer true. However, so long as $\mathcal{W}/J \gg 1$, processes in which an electron scatters from $-\mathcal{W}$ to \mathcal{W} are unimportant. Not all the following discussion is restricted to this limit, so setting $\hat{\mathcal{H}}_{02} = \hat{\mathcal{H}}_{20} = 0$ should be regarded as an approximation that is usually, but not always, well-justified.

As in Eq. (26.103), one needs to examine $\hat{\mathcal{H}}_{11} - \mathcal{E}$ plus two extra terms, one of which is

$$\hat{\mathcal{H}}_{12}(\mathcal{E} - \hat{\mathcal{H}}_{22})^{-1}\hat{\mathcal{H}}_{21}|\psi_1\rangle \quad (26.123)$$

$$\approx \hat{\mathcal{H}}_{12}\hat{\mathcal{H}}_{21}(\mathcal{E} - \hat{\mathcal{H}}_{22} - [\mathcal{W} - \mathcal{E}_F])^{-1}|\psi_1\rangle \quad (26.124)$$

A particle from the occupied states is destroyed, and one is created in the narrow region near \mathcal{W} . The highest-energy states that can be destroyed have energy around \mathcal{E}_F , and these make the most important contribution to all physical processes; hence $\mathcal{W} - \mathcal{E}_F$.

$$\approx \hat{\mathcal{H}}_{12}\hat{\mathcal{H}}_{21}(-\mathcal{W})^{-1}|\psi_1\rangle. \quad (26.125)$$

Restrict attention to low-energy excitations, which means $\mathcal{E} \approx \mathcal{E}_F$, and measure all energies as a distance from \mathcal{E}_F . In acting upon $|\psi_1\rangle$, $\hat{\mathcal{H}}_{22}$ can be taken to vanish, because the states up near \mathcal{W} are empty.

All that remains is the somewhat painful task of multiplying out $\hat{\mathcal{H}}_{12}\hat{\mathcal{H}}_{21}$. Details are left to Problem 8, and the result is

$$\hat{\mathcal{H}}_{12}\hat{\mathcal{H}}_{21} = J^2 D(\mathcal{W})[-\delta\mathcal{W}] \sum_{\bar{k}\bar{k}'} \frac{3}{4} \sum_{\sigma} \hat{c}_{\bar{k}\sigma}^{\dagger} \hat{c}_{\bar{k}'\sigma} - \left\{ \hat{S}^{-} \hat{c}_{\bar{k}\uparrow}^{\dagger} \hat{c}_{\bar{k}'\downarrow} + \hat{S}^{+} \hat{c}_{\bar{k}\downarrow}^{\dagger} \hat{c}_{\bar{k}'\uparrow} + \hat{S}^z \left[\hat{c}_{\bar{k}\uparrow}^{\dagger} \hat{c}_{\bar{k}'\uparrow} - \hat{c}_{\bar{k}\downarrow}^{\dagger} \hat{c}_{\bar{k}'\downarrow} \right] \right\}. \quad (26.126)$$

Eliminating the lower band of states near $-\mathcal{W}$ leads to an equal contribution, and doubles (26.125). Therefore, from Eqs. (26.125) and (26.126), the effective Hamiltonian produced by Eq. (26.103) has the same form as Eq. (26.121), but with a new value $J + \delta J$ of J ,

$$J + \delta J = J - 2 \frac{J^2}{\mathcal{W}} D(\mathcal{W}) \delta\mathcal{W}, \quad \delta\mathcal{W} \text{ is negative, because the bandwidth is being reduced.} \quad (26.127)$$

and the energies of the conduction electrons are altered by addition of a term

$$\frac{3}{2} J^2 D(\mathcal{W}) \frac{\delta\mathcal{W}}{\mathcal{W}} \sum_{\bar{k}\bar{k}'\sigma} \hat{c}_{\bar{k}\sigma}^{\dagger} \hat{c}_{\bar{k}'\sigma}. \quad (26.128)$$

The renormalization of J in Eq. (26.127) can be used repeatedly to find how J changes for large changes of \mathcal{W} . One has

$$\frac{dJ}{d\mathcal{W}} = -2 \frac{J^2}{\mathcal{W}} D(\mathcal{W}). \quad (26.129)$$

The density of states $D(\mathcal{W})$ will of course vary with \mathcal{W} , but as \mathcal{W} becomes smaller and smaller, driving J to larger and larger values, $D(\mathcal{W})$ must approach D_0 , the density of states at the Fermi level. To see the basic structure of Eq. (26.129), set $D(\mathcal{W})$ to this value, so that it can be integrated, giving

$$\mathcal{W} \exp \left[-\frac{1}{2D_0 J} \right] = \text{constant} \equiv k_B T_K, \quad (26.130)$$

where T_K is defined to be the *Kondo temperature*. Two Hamiltonians with different values of \mathcal{W} and J should have the same low-temperature behavior so long as \mathcal{W} and J are related by Eq. (26.130). In addition, as \mathcal{W} changes, the Hamiltonian must acquire an additional term given by Eq. (26.128), but this additional term does not directly involve the magnetic moment.

Two limits of Eq. (26.130) are particularly useful. Imagine fixing T_K , but varying \mathcal{W} and J . In one limit, J is small and \mathcal{W} is exponentially large. This limit describes a very large population of electrons interacting very weakly with a magnetic moment, and because the interaction is weak, perturbation theory should be applicable. In the other limit, J is large and \mathcal{W} is small. In this limit, a small number of conduction electrons interacts very strongly with a magnetic moment. It is natural to assume that the strong interaction will produce a strong antiferromagnetic correlation between the electrons and the moment at temperatures below the Kondo temperature, and that this correlation is destroyed as the temperature rises.

Scaling of Resistivity. To obtain physical consequences from the scaling relation (26.130), assume that physical properties of a system will depend on temperature only in the form $\mathcal{F}(T/T_K)$, and that two systems with the same T_K are essentially indistinguishable. Take the particular case of resistivity;

$$\rho = \mathcal{F}\left(\frac{T}{T_K}\right). \quad (26.131)$$

If all else in the problem is fixed, and the coupling J to the magnetic moment is made very small, the resistivity ρ should vanish as J^2 ; this conclusion follows for example from Eq. (18.16), which shows rather generally that scattering from a potential vanishes as the square of the potential's strength. The way to obtain such behavior for small J is to guess something like

$$\mathcal{F}(x) = \left[\frac{1}{\ln(x)} \right]^2 \quad (26.132)$$

$$\Rightarrow \mathcal{F}\left(\frac{T}{T_K}\right) = \rho = \left[\frac{2D_0J}{1 + 2D_0J \ln(k_B T/\mathcal{W})} \right]^2 \quad (26.133)$$

$$\sim 4D_0^2 J^2 (1 - 4D_0J \ln(k_B T/\mathcal{W})) . \quad \text{Catch the leading trends for small } J \text{ by Taylor expanding.} \quad (26.134)$$

The prediction is that the contribution to resistivity from magnetic impurities should begin to rise in a logarithmic fashion as temperature approaches T_K . The total resistivity is the sum of this magnetic contribution and the contribution from phonons that according to Bloch's law Eq. (18.20) drops as T^5 . Taking the density of magnetic impurities to be n_{mi} , the low-temperature resistivity should behave as

$$\rho \sim \mathcal{A}T^5 - \mathcal{B}n_{mi} \ln(k_B T/\mathcal{W}), \quad \mathcal{A} \text{ and } \mathcal{B} \text{ are constants.} \quad (26.135)$$

and a minimum in resistivity occurs when

$$\frac{d\rho}{dT} = 0 \Rightarrow T_{\min} = \left(\frac{\mathcal{B}n_{mi}}{5\mathcal{A}} \right)^{1/5} \quad (26.136)$$

The shape of the resistivity minimum in Figure 26.8 and the movement of the minimum with magnetic impurity density n_{mi} are well accounted for by Eq. (26.135).

The form guessed in Eq. (26.132) for the resistivity has the unfortunate property of diverging when $T \rightarrow T_K$. The divergence may be eliminated by choosing instead, for example,

$$\mathcal{F}\left(\frac{T}{T_K}\right) = \left[\frac{1}{\cosh^{-1}(T/T_K)} \right]^2, \quad (26.137)$$

which rises to some finite value as $T \rightarrow 0$, but produces the proper J^2 behavior for small J . Hewson (1997) describes several calculations that make the behavior indicated by Eq. (26.137) more compelling than a plausible guess.

Specific Heat. The heavy fermion compounds mentioned in Section 6.5.1 are roughly modeled as lattices of Kondo spins. Compounds such as UPt_3 and UPe_{13} have low-temperature specific heats whose linear term is up to 1000 times larger than would be anticipated from free-electron theory. If the low-temperature specific heat is linear in temperature, the scaling theory suggests that

$$C_V \propto n \frac{T}{T_K} = n \frac{k_B T}{\mathcal{W}} \exp\left[\frac{1}{2D_0 J}\right]. \quad (26.138)$$

While this equation does not allow an immediate connection with experiment, it does show how small reductions in the density of states D_0 or coupling constant J can be expected to produce exponentially large increases in the linear term of the specific heat.

Figure 26.11 shows the specific heat as a function of temperature for UPe_{13} , one of the heavy fermion compounds. The large values of C_V/T at low temperatures are due to the peak at around 0.75 K, which has to decay rapidly in order to drop to zero at 0 K. If the scaling theory associated with Eq. (26.130) is applicable, then at very low temperatures conduction electrons have spins pointing opposite the uranium local moments, while above the Kondo temperature this correlation disappears. Therefore, the entropy $S = \int dT C_V/T$ associated with the peak should be $k_B \ln 2$ or $5.8 \text{ J mole}^{-1} \text{ K}^{-1}$. Performing the integral over the peak in Figure 26.11 actually gives $1.2 \text{ J mole}^{-1} \text{ K}^{-1}$, of the same order of magnitude as the simple prediction.

26.7 Hubbard Model

Hubbard (1963, 1964a,b) proposed a seemingly simple extension of the tight-binding model intended to explore the electronic correlations leading to magnetism. To the ordinary tight-binding model Hubbard added a term that provides an energy penalty U for any atomic site occupied by more than one electron. Hubbard argued that the diagonal piece of the Coulomb interaction has magnitude of around 20 eV, while the off-diagonal terms are all at least 10 times smaller; therefore he included

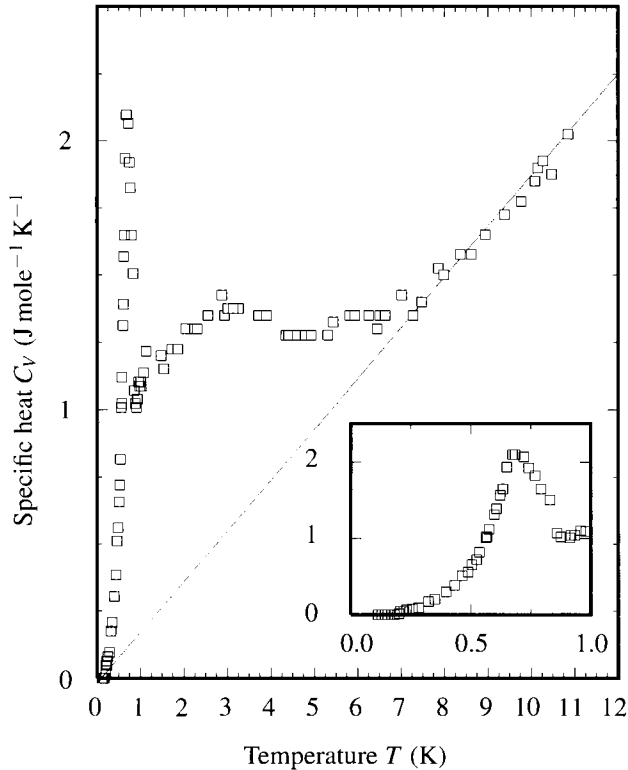


Figure 26.11. Low-temperature specific heat of the heavy fermion compound UBe_{13} . The very large slope in C_V at low temperatures is due to the peak at around 0.75 K; were it not for this peak, C_V/T would have a value comparable to that of the free electron metals. [Source Ott et al. (1983, 1984).]

only the repulsion between electrons at the same site. The Hubbard Hamiltonian in second quantized notation is conventionally

$$\hat{\mathcal{H}} = \sum_{\langle ll' \rangle} -t \left[\hat{c}_{l\sigma}^\dagger \hat{c}_{l'\sigma} + \hat{c}_{l'\sigma}^\dagger \hat{c}_{l\sigma} \right] + U \sum_l \hat{c}_{l\uparrow}^\dagger \hat{c}_{l\uparrow} \hat{c}_{l\downarrow}^\dagger \hat{c}_{l\downarrow}, \quad (26.139)$$

where the sum $\langle ll' \rangle$ is taken over distinct nearest-neighbor pairs.

26.7.1 Mean-Field Solution

An exact solution of the Hubbard model is available in one dimension, due to Lieb and Wu (1968). The ground state has spin zero, with antiferromagnetic correlations between neighboring spins. These results do not carry over to two or three dimensions. The only simple thing to do in three dimensions is to employ mean field theory, which is generally believed to be wrong in most aspects, but which illustrates the competing effects. To carry out the mean field theory, write

the model as

$$\hat{\mathcal{H}} = \sum_{\langle ll' \rangle} -t \left[\hat{c}_{l\sigma}^\dagger \hat{c}_{l'\sigma} + \hat{c}_{l'\sigma}^\dagger \hat{c}_{l\sigma} \right] + U \sum_l \hat{n}_{l\uparrow} \hat{n}_{l\downarrow}. \quad (26.140)$$

The difficulty resides in the last term, which is quartic in fermion operators. In the standard steps of mean field theory, try

$$\hat{n}_{l\sigma} = n_\sigma + (\hat{n}_{l\sigma} - n_\sigma). \quad (26.141)$$

Choosing the average value of n to be the same on all sites prejudices matters in favor of ferromagnetism, which Hubbard had devised the model to explain. Expanding to quadratic order, one finds that

$$\hat{\mathcal{H}} \approx \sum_{\langle ll' \rangle} -t \left[\hat{c}_{l\sigma}^\dagger \hat{c}_{l'\sigma} + \hat{c}_{l'\sigma}^\dagger \hat{c}_{l\sigma} \right] + U \sum_l \hat{n}_{l\uparrow} n_\downarrow + n_\uparrow \hat{n}_{l\downarrow} - n_\uparrow n_\downarrow. \quad (26.142)$$

Going into \vec{k} space, the Hamiltonian becomes diagonal, and equals

$$\sum_{\vec{k}\vec{\delta}\sigma} -t \hat{c}_{k\sigma}^\dagger \hat{c}_{\vec{k}+\vec{\delta}\sigma} \cos \vec{\delta} \cdot \vec{k} + U \sum_{\vec{k}} \hat{n}_{\vec{k}\uparrow} n_\downarrow + n_\uparrow \hat{n}_{\vec{k}\downarrow} - n_\uparrow n_\downarrow. \quad \vec{\delta} \text{ are nearest-neighbor vectors.} \quad (26.143)$$

The mean field theory is closed by setting the mean occupancy of up and down electrons equal to n_\uparrow and n_\downarrow , respectively. Further progress depends upon choosing a particular lattice and dimension in which to work. It is easiest to work in one dimension, where all the algebra is simple. Because the up and down electrons can have different densities, one must suppose that they are described by two separate Fermi levels. If a is the lattice spacing and N is the total number of lattice sites, then

$$Nn_\uparrow = Na \int_{-k_{F\uparrow}}^{k_{F\uparrow}} \frac{dk}{2\pi} \quad (26.144)$$

$$\Rightarrow \pi n_\uparrow = ak_{F\uparrow}. \quad (26.145)$$

Doing the integral in Eq. (26.143), the ground-state energy is

$$\mathcal{E}_0 = \frac{N}{\pi} [-2t] [\sin \pi n_\uparrow + \sin \pi n_\downarrow] + NU n_\uparrow n_\downarrow. \quad (26.146)$$

The total number of electrons in the metal is always fixed; assume that the band is half filled, so that $n_\uparrow + n_\downarrow = 1$. Then the ground-state energy becomes

$$\mathcal{E}_0 = \frac{-4tN}{\pi} \sin \pi n_\uparrow + UN n_\uparrow (1 - n_\uparrow). \quad (26.147)$$

Minimizing this expression, one finds that for

$$\frac{U}{t} > \frac{16}{\pi}, \quad (26.148)$$

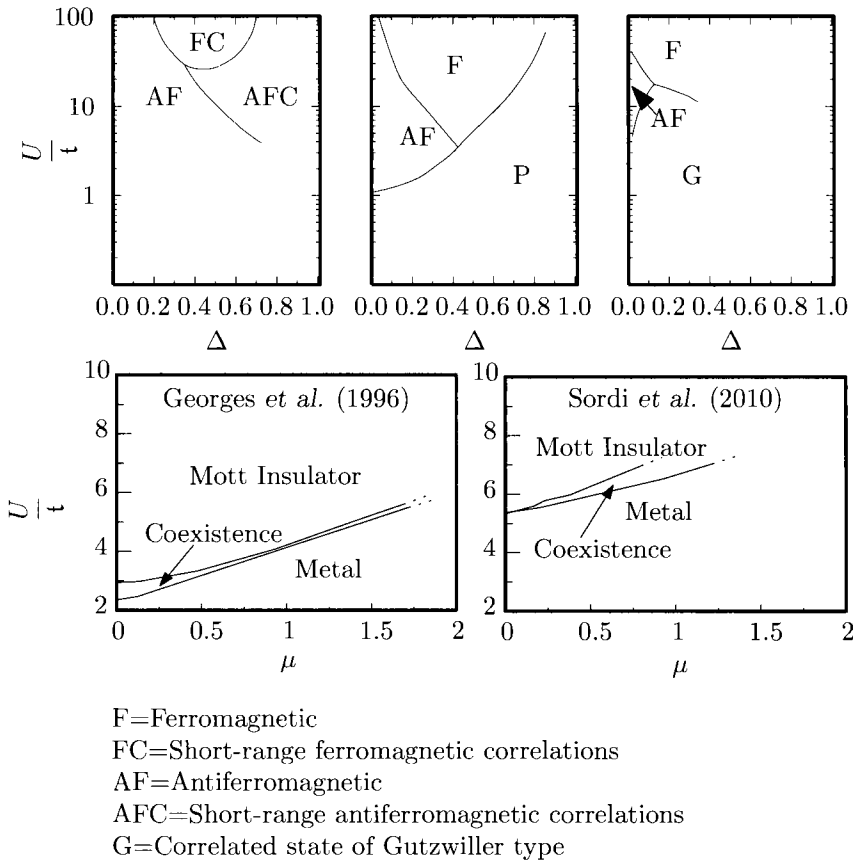


Figure 26.12. Five representative phase diagrams of the two-dimensional Hubbard model, as a function of on-site repulsion U over hopping parameter t , and filling fraction Δ , which tells the fraction of sites that has more than one electron, or chemical potential μ , which enters by adding $(\mu - U/2) \sum_i n_i$ to Eq. (26.139). Early approximations differed dramatically; more recently, the phase diagrams have started to converge, although the problem is still not definitively solved. [Results of Kaxiras and Manousakis (1988) Coppersmith and Yu (1989), Richter et al. (1978), Georges et al. (1996) (hopping energies t made random variables here), and Sordi et al. (2010). There are also predictions of superconducting regions, as in Giamarchi and Lhuillier (1991).]

$n_\uparrow = 1$ and $n_\downarrow = 0$ (or the roles may be reversed), so that the Coulomb repulsion leads to ferromagnetic ordering. Otherwise, one has $n_\uparrow = n_\downarrow = 1/2$, and the system is an ordinary metal.

This calculation illustrates the physics of the Hubbard model in an uncomfortable way. By using mean field theory, one obtains simple expressions that illustrate the competition between kinetic energy and magnetic ordering that the model was designed to explore. Unfortunately, in one dimension this solution is known to be qualitatively incorrect. The exact analytical solution has no sharp transition in any physical quantity as U/t varies. The correlations between neighboring spins are antiferromagnetic, not ferromagnetic.

In two and three dimensions, there is only one point of general agreement. At half filling, where the number of electrons precisely equals the number of lattice sites, and for large enough U , the ground state is antiferromagnetic. Some reasons for this conclusion are explored in Problem 9. This conclusion has considerable physical importance, because it provides the simplest way to see how solids like CuO (Section 23.6.3) that should be metals according to band theory actually turn out to be antiferromagnetic insulators, called *Mott-Hubbard* or *Mott* insulators. Even this statement needs to be qualified, because charge transfer between oxygen and copper as discussed in Section 23.6.3 is not included in the Hubbard model, which is hard enough to solve without it. Away from half filling, the problem is not completely solved. Figure 26.12 displays five characteristic phase diagrams describing the ground state of the Hubbard model as a function of U/t and of Δ or chemical potential μ ; Δ gives the fraction of electrons per site in excess of half filling, so there is one electron per site when $\Delta = 0$, and two electrons per site when $\Delta = 1$. The chemical potential μ enters the model by adding $(\mu - U/2) \sum_i n_i$ to Eq. (26.139).

The fact that the properties of the two-dimensional Hubbard model are not yet known with certainty is unsatisfactory because the Hubbard model is widely viewed as the simplest context in which to try to obtain exact results for many interacting electrons; this model has been investigated with a ferocious intensity since the discovery of high-temperature superconductors. There is no better illustration of the difficulties involved in progressing systematically beyond the one-electron pictures of solids.

Problems

1. **Wave functions with cusps:** Show that the energy of $|\phi\rangle$ in Figure 26.2 can certainly be lowered by smoothing out the cusp. One way to perform the demonstration is to flatten out the wave function as shown in the figure throughout some small volume v and then estimate the effect on kinetic and potential energies.
2. **Ferromagnetic ground state:** Consider the Hamiltonian (26.21) with all J positive, and take $\hat{S}_{\vec{R}}$ to describe spin 1/2 particles.
 - (a) Show with the aid of the identity in Eq. (26.19) that the state where all spins are eigenvalues of \hat{S}^z with eigenvalue 1/2 is an eigenfunction of the Hamiltonian.
 - (b) Show that the largest value that $\langle \Psi | \hat{S}_{\vec{R}} \cdot \hat{S}_{\vec{R}'} | \Psi \rangle$ can assume for $\vec{R} \neq \vec{R}'$ in any wave function Ψ is less than or equal to the largest eigenvalue of $\hat{S}_{\vec{R}} \cdot \hat{S}_{\vec{R}'}$. By expanding out the square of $\hat{S}_{\vec{R}} + \hat{S}_{\vec{R}'}$, show that the largest eigenvalue of this operator is 1/4.
 - (c) Therefore show that the ferromagnetic state provides the ground state of the Heisenberg Hamiltonian.

3. **Magnetic susceptibility of Fermi liquids:** Extend the Stoner model to Fermi liquids and find their magnetic susceptibility.

- (a) Write the energy of a Fermi liquid in the presence of a magnetic field.
- (b) Assume that all $\delta f_{\vec{k}\uparrow}$ are occupied only for energies $\mathcal{E}^0 < \mathcal{E}_F - \Delta$, while all $\delta f_{\vec{k}\downarrow}$ are occupied for $\mathcal{E}^0 < \mathcal{E}_F + \Delta$. Assume that the density of states $D(\mathcal{E})$ can be taken constant and that the $\vec{k}\vec{k}'$ dependence of the parameters $u_{\vec{k}\sigma\vec{k}'\sigma'}$ can be ignored. Rewrite the total energy in terms of integrals over energy.
- (c) Find the value of Δ by minimizing the total energy, and show that the susceptibility is

$$\chi = \frac{\mu_B^2 D(\mathcal{E}_F)}{1 + F_0^a}. \tag{26.149}$$

4. **Diagonalizing spin waves:** Show that Eq. (26.63) diagonalizes (26.62) using Eq. (26.64).

5. **Projection operators:**

- (a) Find expressions analogous to Eq. (26.96) for \hat{P}_1 and \hat{P}_2 .
- (b) Verify that $\hat{P}_0 \dots \hat{P}_2$ satisfy the requirement of all projection operators

$$\hat{P}^2 = \hat{P}. \tag{26.150}$$

(c) Why is Eq. (26.99) true?

6. **Local moment:** Derive Eq. (26.120), and find an expression for $K_{\vec{k}\vec{k}'}$.

7. **Mean field treatment of magnetic moments:** Consider the Anderson model given in Eq. (26.95). An approximate solution can be obtained through the mean field replacement

$$U \hat{n}_{0\uparrow} \hat{n}_{0\downarrow} \approx U \langle \hat{n}_{0\uparrow} \rangle \hat{n}_{0\downarrow} + U \hat{n}_{0\uparrow} \langle \hat{n}_{0\downarrow} \rangle - U \langle \hat{n}_{0\uparrow} \rangle \langle \hat{n}_{0\downarrow} \rangle. \tag{26.151}$$

The brackets mean that one finds the expectation value, or mean occupancy, of the impurity states. Neglect the final term on the right-hand side of Eq. (26.151), which leads to a constant energy shift, and define

$$\epsilon_{0\sigma} = \epsilon_0 + U \langle \hat{n}_{0,-\sigma} \rangle. \tag{26.152}$$

One has then to solve the Hamiltonian

$$\hat{\mathcal{H}} = \sum_{\sigma} \hat{\mathcal{H}}_{\sigma} \tag{26.153a}$$

where

$$\hat{\mathcal{H}}_{\sigma} = \epsilon_{0\sigma} \hat{c}_{0\sigma}^{\dagger} \hat{c}_{0\sigma} + \sum_{\vec{k}} [\epsilon_{\vec{k}} \hat{c}_{\vec{k}\sigma}^{\dagger} \hat{c}_{\vec{k}\sigma} + v_{\vec{k}} \hat{c}_{0\sigma}^{\dagger} \hat{c}_{\vec{k}\sigma} + v_{\vec{k}}^* \hat{c}_{\vec{k}\sigma}^{\dagger} \hat{c}_{0\sigma}]. \tag{26.153b}$$

(a) Define the Green function

$$\hat{G}_\sigma(\mathcal{E}) = [\mathcal{E} - \hat{\mathcal{H}}_\sigma + i\eta]^{-1}. \quad \eta \text{ is very small.} \quad (26.154)$$

Let $|\emptyset\rangle$ be the vacuum state, and let

$$|0\rangle = \hat{c}_{0\sigma}^\dagger |\emptyset\rangle \quad \text{and} \quad |\vec{k}\rangle = \hat{c}_{\vec{k}\sigma}^\dagger |\emptyset\rangle. \quad (26.155)$$

Show that

$$[\mathcal{E} - \epsilon_{0\sigma} + i\eta] \langle 0 | \hat{G}_\sigma | 0 \rangle - \sum_{\vec{k}} v_k \langle \vec{k} | \hat{G}_\sigma | 0 \rangle = 1 \quad (26.156a)$$

$$[\mathcal{E} - \epsilon_{\vec{k}} + i\eta] \langle \vec{k} | \hat{G}_\sigma | 0 \rangle - v_k^* \langle 0 | \hat{G}_\sigma | 0 \rangle = 0. \quad (26.156b)$$

(b) Show that

$$\langle 0 | \hat{G}_\sigma | 0 \rangle = \frac{1}{\mathcal{E} - \epsilon_{0\sigma} + i\eta - \delta\epsilon + i\Delta}, \quad (26.157a)$$

where

$$\delta\epsilon = \sum_{\vec{k}} \frac{|v_{\vec{k}}|^2}{\mathcal{E} - \epsilon_{\vec{k}}} \quad \text{and} \quad \Delta = \pi \sum_{\vec{k}} |v_{\vec{k}}|^2 \delta(\mathcal{E} - \epsilon_{\vec{k}}). \quad (26.157b)$$

(c) Recall from Eq. (18.38) that

$$n_{0\sigma}(\mathcal{E}) d\mathcal{E} = -\frac{1}{\pi} \text{Im} \langle 0 | \hat{G}_\sigma(\mathcal{E}) | 0 \rangle d\mathcal{E} \quad (26.158)$$

gives the probability that the impurity state with spin σ will be occupied in the energy range $[\mathcal{E}, \mathcal{E} + d\mathcal{E}]$. Take the limit $\eta \rightarrow 0$, assume that $\delta\epsilon$ is negligibly small, and assume that Δ can be treated as a constant. Find two self-consistent expressions for $\langle \hat{n}_{0\uparrow} \rangle$ and $\langle \hat{n}_{0\downarrow} \rangle$ by employing

$$\langle \hat{n}_{0\sigma} \rangle = \int_{-\infty}^{\mathcal{E}_F} d\mathcal{E} n_{0\sigma}(\mathcal{E}). \quad (26.159)$$

Assume $\epsilon_{0\sigma} > \mathcal{E}_F$. The expressions should be in the form $\langle \hat{n}_{0\uparrow} \rangle = f(\langle \hat{n}_{0\downarrow} \rangle)$ for some function f .

(d) Take $\mathcal{E}_F - \epsilon_0 = U/2$ and $U/\Delta = 1$. Plot $f(\langle \hat{n}_{0\downarrow} \rangle)$ and $f^{-1}(\langle \hat{n}_{0\downarrow} \rangle)$ versus $\langle \hat{n}_{0\downarrow} \rangle$ on a graph where x and y axes range between 0 and 1. The crossings of these two curves give possible values for the spin occupation of the impurity. There is only one solution. What magnetic moment is predicted for the impurity?

(e) Repeat the previous part of this problem for $U/\Delta = 5$. There is more than one solution. What magnetic moment is predicted for the impurity?

8. Renormalization of J :

(a) In multiplying (26.122a) and (26.122b), to be applied to $|\psi_1\rangle$, one can take $\hat{c}_{\bar{q}\sigma}\hat{c}_{\bar{q}'\sigma}^\dagger = \delta_{\bar{q}\bar{q}'}$. Why?

(b) Using identities such as

$$\hat{S}^z\hat{S}^- = -\frac{1}{2}\hat{S}^- \quad \text{or} \quad \hat{S}^-\hat{S}^+ = \frac{1}{2} - \hat{S}^z, \quad (26.160)$$

verify Eq. (26.126).

9. **The t - J model:** Consider the Hubbard model at half filling:

$$\sum_{\langle ll'\rangle} -t \left[\hat{c}_{l\sigma}^\dagger \hat{c}_{l'\sigma} + \hat{c}_{l'\sigma}^\dagger \hat{c}_{l\sigma} \right] + U \sum_l \hat{c}_{l\uparrow}^\dagger \hat{c}_{l\uparrow} \hat{c}_{l\downarrow}^\dagger \hat{c}_{l\downarrow}. \quad (26.161)$$

The number of electrons and the number of lattice sites are both equal to N .

(a) What is the ground state of the model when $t = 0$ and $U > 0$? What is the degeneracy of the ground state? What are the energies of the excited states?

(b) Introduce the hopping term proportional to t as a perturbation. The task is to find the new ground state. Show that to second order in perturbation theory one must diagonalize an effective Hamiltonian of the form

$$J_{\text{eff}} \sum_{\langle ll'\rangle} \left(\hat{S}_l \cdot \hat{S}_{l'} - \frac{1}{4} \right), \quad (26.162)$$

and find the value of J_{eff} . This model is known as the t - J model.

(c) Describe physically why the ground state of the $t - J$ model, and therefore of the Hubbard model for large U , are antiferromagnetic at half filling.

References

- M. Aïn, W. Reichardt, B. Hennion, G. Pepy, and B. M. Wanklyn (1989), Magnetic excitations in CuO, *Physica C*, **162–164**, 1279–1280.
- P. W. Anderson (1961), Localized magnetic states in metals, *Physical Review*, **124**, 41–53.
- P. W. Anderson (1970), A poor man's derivation of scaling laws for the Kondo problem, *Journal of Physics C*, **3**, 2436–2441.
- P. W. Anderson (1997), When the electron falls apart, *Physics Today*, **50**(10), 42–47.
- P. W. Anderson, G. Yuval, and D. R. Hamann (1970), Exact results in the Kondo problem. II. scaling theory, qualitatively correct solution, and some new results on one-dimensional classical statistical models, *Physical Review B*, **1**, 4464–4473.
- N. Andrei (1982), Calculation of the magnetoresistance in the Kondo model, *Physics Letters*, **87A**, 299–302.
- N. Andrei, K. Furuya, and J. H. Lowenstein (1983), Solution of the Kondo problem, *Reviews of Modern Physics*, **55**, 331–402.

- A. G. Arnov and Y. V. Sharvin (1987), Magnetic flux effects in disordered conductors, *Reviews of Modern Physics*, **59**, 755–779.
- M. N. Baibich, J. M. Broto, A. Fert, et al. (1988), Giant magnetoresistance of (001)Fe/(001)Cr magnetic superlattices, *Physical Review Letters*, **61**(21), 2472–2475.
- L. Berger (1996), Emission of spin waves by a magnetic multilayer traversed by a current, *Physical Review B*, **54**(13), 9353–9358.
- H. Bethe (1931), On the theory of metals: I Eigenvalues and eigenfunctions of a linear atomic chain, *Zeitschrift für Physik*, **71**, 205–226. In German.
- N. E. Bickers (1987), Review of techniques in the large- N expansion for dilute magnetic alloys, *Reviews of Modern Physics*, **59**, 845–939.
- G. Binasch, P. Grünberg, F. Saurenbach, and W. Zinn (1989), Enhanced magnetoresistance in layered magnetic structures with antiferromagnetic interlayer exchange, *Physical Review B*, **39**, 4828–4830.
- S. N. Coppersmith and C. C. Yu (1989), Phase diagram of the Hubbard model: A variational wavefunction approach, *Physical Review B*, **39**, 11 464–11 474.
- M. C. Cross and D. S. Fisher (1985), Magnetism in solid ^3He : Confrontation between theory and experiment, *Reviews of Modern Physics*, **57**, 881–921.
- W. J. de Haas, J. H. de Boer, and G. J. van den Berg (1934), The electrical resistance of gold, copper, and lead, *Physica*, **1**, 1115–1124.
- P. A. M. Dirac (1926), On the theory of quantum mechanics, *Proceedings of the Royal Society of London*, **A112**, 661–677.
- L. D. Fadeev and L. A. Takhtajan (1981), What is the spin of a spin wave?, *Physics Letters A*, **85**, 375–377.
- R. P. Feynman (1953), Atomic theory of liquid helium near absolute zero, *Physical Review*, **91**, 1301–1308.
- P. P. Freitas and L. Berger (1985), Observation of s - d exchange force between domain walls and electric current in very thin Permalloy films, *Journal of Applied Physics*, **57**(4), 1266–1269.
- A. Georges, G. Kotliar, W. Krauth, and M. J. Rozenberg (1996), Dynamical mean-field theory of strongly correlated fermion systems and the limit of infinite dimensions, *Reviews of Modern Physics*, **68**, 13–25.
- T. Giamarchi and C. Lhuillier (1991), Phase diagrams of the two-dimensional Hubbard and t - J models by a variational Monte Carlo method, *Physical Review B*, **43**, 12 943–12 951.
- J. Goldstone (1963), Field theories with “superconductor” solutions, *Nuovo Cimento*, **19**, 155–164.
- G. Gruner (1994), The dynamics of spin-density waves, *Reviews of Modern Physics*, **66**, 1–24.
- A. J. Heeger (1969), Localized moments and nonmoments in metals: the Kondo effect, *Solid State Physics: Advances in Research and Applications*, **23**, 283–411.
- W. Heisenberg (1926), On the theory of ferromagnetism, *Zeitschrift für Physik*, **49**, 619–636.
- W. Heitler and F. London (1927), Interaction of neutral atoms and homopolar binding in quantum mechanics, *Zeitschrift für Physik*, **44**, 455–472. In German.
- A. C. Hewson (1997), *The Kondo Problem to Heavy Fermions*, Cambridge University Press, Cambridge.
- T. Holstein and H. Primakoff (1940), Field dependence of the intrinsic domain magnetization of a ferromagnet, *Physical Review*, **58**, 1098–1113.
- J. Hubbard (1963), Electron correlations in narrow energy bands, *Proceedings of the Royal Society of London*, **A266**, 238–257.
- J. Hubbard (1964a), Electron correlations in narrow energy bands II. The degenerate band case, *Proceedings of the Royal Society of London*, **A277**, 237–259.
- J. Hubbard (1964b), Electron correlations in narrow energy bands III. An improved solution, *Proceedings of the Royal Society of London*, **A281**, 401–419.
- B. Huckestein (1995), Scaling theory of the integer quantum Hall effect, *Reviews of Modern Physics*,

- 67, 357–396.
- I. Žutić, J. Fabian, and S. Das Sarma (2004), Spintronics: Fundamentals and applications, *Reviews of Modern Physics*, **76**(2), 323–410. , I.—I
- A. Isihara (1989), Electron correlations in two dimensions, *Solid State Physics: Advances in Research and Applications*, **42**, 271–402.
- E. Kaxiras and E. Manousakis (1988), Ground state of the strong-coupling Hubbard Hamiltonian: A numerical diagonalization study, *Physical Review B*, **37**, 656–659.
- C. Kittel (1968), Indirect exchange interactions in metals, *Solid State Physics: Advances in Research and Applications*, **22**, 1–26.
- E. B. Kolomeisky and J. P. Straley (1996), Phase diagram and correlation exponents for interacting fermions in one dimension, *Reviews of Modern Physics*, **68**, 175–214.
- J. Kondo (1964), Resistance minimum in dilute magnetic alloys, *Progress in Theoretical Physics*, **32**, 37–49.
- L. D. Landau and E. M. Lifshitz (1977), *Quantum Mechanics (Non-relativistic Theory)*, 3rd ed., Pergamon Press, Oxford.
- E. H. Lieb and D. Mattis (1962), Theory of ferromagnetism and the ordering of electronic energy levels, *Physical Review*, **125**, 164–172.
- E. H. Lieb and F. Wu (1968), Absence of Mott transition in an exact solution of the short-range, one-band model in one dimension, *Physical Review Letters*, **20**, 1445–1448.
- J. W. Lynn (1975), Temperature dependence of the magnetic excitations in iron, *Physical Review B*, **11**, 2624–2637.
- E. Manousakis (1991), The spin-1/2 Heisenberg antiferromagnet on a square lattice and its application to the cuprous oxides, *Reviews of Modern Physics*, **63**, 1–62.
- D. C. Mattis (1988), *The Theory of Magnetism*, vol. I, Springer-Verlag, New York.
- V. L. Moruzzi and P. M. Marcus (1993), Energy band theory of metallic magnetism in the elements, in *Handbook of Magnetic Materials*, K. H. J. Buschow, ed., vol. 7, pp. 97–137.
- F. C. Nix and W. Shockley (1938), Order-disorder transformations in alloys, *Reviews of Modern Physics*, **10**, 1–71.
- P. Nozières (1974), A “Fermi-liquid” description of the Kondo problem at low temperatures, *Journal of Low Temperature Physics*, **17**, 31–42.
- P. Nozières (1975), The Kondo problem: Fancy mathematical techniques versus simple physical ideas, in *Low Temperature Physics—LT14*, M. Krusius and M. Vuorio, eds., vol. 5, pp. 339–374, North-Holland, Amsterdam.
- R. Orbach (1958), Linear antiferromagnetic chain with anisotropic coupling, *Physical Review*, **112**, 309–316.
- H. R. Ott, H. Rudigier, Z. Fisk, and J. L. Smith (1983), UBe₁₃: An unconventional actinide superconductor, *Physical Review Letters*, **50**, 1595–1598.
- H. R. Ott, H. Rudigier, Z. Fisk, and J. L. Smith (1984), Superconducting ground state of a strongly interacting electron system: UBe₁₃, in *Moment Formation in Solids*, W. J. L. Buyers, ed., pp. 305–311, Plenum, New York.
- D. Pescia, M. Stambanoni, G. L. Bona, A. Vaterlaus, R. F. Willis, and F. Meier (1987), Magnetism of epitaxial fcc iron films on Cu (001) investigated by spin-polarized photoelectron emission, *Physical Review Letters*, **58**, 2126–2129.
- G. T. Rado and H. Suhl, eds. (1963–), *Magnetism*, Academic Press, New York.
- D. Ralph and M. Stiles (2008), Spin transfer torques, *Journal of Magnetism and Magnetic Materials*, **320**(7), 1190 – 1216.
- A. Richter, F. Goedsche, and G. Röpke (1978), Functional integral approach for the Hubbard model with arbitrary electron density, *Physica Status Solidi B*, **88**, 189–198.
- M. Roger, J. H. Hetherington, and J. M. Delrieu (1983), Magnetism in solid ³He, *Reviews of Modern Physics*, **55**, 1–64.

- M. Sarachik, E. Corenzwit, and L. D. Longinotti (1964), Resistivity of MoNb and MoRe alloys containing 1% Fe., *Physical Review*, **135**, A1041–A1045.
- L. Schiff (1968), *Quantum Mechanics*, 3rd ed., McGraw-Hill, New York.
- J. Schwinger (1965), On angular momentum, in *Quantum Theory of Angular Momentum*, L. Biedenharn and H. van Dam, eds., Academic, New York.
- R. Shankar (1994), Renormalization-group approach to interacting fermions, *Reviews of Modern Physics*, **66**, 129–192.
- K. S. Singwi and M. P. Tosi (1981), Correlations in electron liquids, *Solid State Physics: Advances in Research and Applications*, **36**, 177–266.
- J. C. Slonczewski (1996), Current-driven excitation of magnetic multilayers, *Journal of Magnetism and Magnetic Materials*, **159**(1-2), L1 – L7.
- G. Sordi, K. Haule, and A.-M. S. Tremblay (2010), Finite doping signatures of the mott transition in the two-dimensional hubbard model, *Physical Review Letters*, **104**(22), 226402.
- M. B. Stearns (1978), Why is iron magnetic?, *Physics Today*, **31**(4), 34–39.
- E. C. Stoner (1934), *Magnetism and Matter*, Methuen, London.
- H. Tsunetsugu, M. Sigrist, and K. Ueda (1997), The ground-state phase diagram of the one-dimensional Kondo lattice model, *Reviews of Modern Physics*, **69**, 809–863.
- P. B. Wiegmann (1980), Exact solution of *s-d* exchange model at $T = 0$, *JETP Letters*, **31**, 364–370.
- A. H. Wilson (1954), *The Theory of Metals*, Cambridge University Press, Cambridge.
- K. G. Wilson (1975), The renormalization group: Critical phenomena and the Kondo problem, *Reviews of Modern Physics*, **47**, 773–840.
- K. G. Wilson (1983), The renormalization group and critical phenomena, *Reviews of Modern Physics*, **55**, 583–600.
- S. A. Wolf, D. D. Awschalom, R. A. Buhrman, J. M. Daughton, S. von Molnár, M. L. Roukes, A. Y. Chtchelkanova, and D. M. Treger (2001), Spintronics: a spin-based electronics vision for the future, *Science*, pp. 1488–1495.
- M. Wortis (1965), Bound states of two spin waves in Heisenberg ferromagnet, *Physical Review*, **132**, 85–97.
- J. Yeomans (1988), The theory and application of axial Ising models, *Solid State Physics: Advances in Research and Applications*, **41**, 151–200.
- M. Yethiraj, R. A. Robinson, D. S. Sivia, J. W. Lynn, and H. A. Mook (1991), Neutron-scattering study of the magnon energies and intensities in iron, *Physical Review B*, **43**, 2565–2574.

27. Superconductivity

27.1 Introduction

Kamerlingh Onnes (1911) found that mercury loses all electrical resistance below a critical temperature of 4 K. In copper, a very good conductor at temperatures of 77 K, electrical currents decay with a characteristic time of $2 \cdot 10^{-13}$ s. But a superconductor is qualitatively better. Currents in a superconductor have been seen to persist for over a year. Since Kamerlingh Onnes' initial discovery, most metals and alloys have been found to exhibit superconductivity at some temperature, so the phenomenon is quite universal.

The phenomenon of superconductivity posed for many years a serious challenge to quantum mechanics. Perhaps the dense combination of many electrons really could not be described by the same equations that had been deduced from experiments on dilute systems; perhaps quantum mechanics was just an approximation to more complicated many-body equations, and superconductivity was the key to finding the true form. Sommerfeld and Bethe (1933) wrote that “[d]espite failure up to now, we may assert that superconductivity will be solved on the basis of our present quantum mechanical understanding.” This assertion remained a matter of faith for another 25 years as one microscopic theory after another collapsed until Bardeen, Cooper, and Schrieffer (1957) created a compelling quantum-mechanical model.

An important idea to grasp in understanding superconductivity is that it really is a macroscopic phenomenon, and corresponds to a definite macroscopic state of matter. The important feature of a superconductor is not how it responds to external electrical fields, but how it responds to external magnetic fields. Meissner and Ochsenfeld (1933) found that magnetic flux is completely expelled from a superconductor. Suppose one has a loop with a current flowing in it. Magnetic flux lines must thread the loop, as in Figure 27.1. In order for the current to diminish,

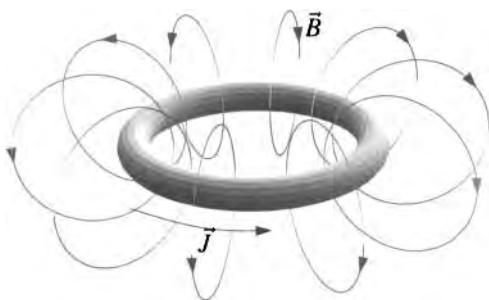


Figure 27.1. The flux lines threading a current loop have to pass through the current if the current is to diminish. But for a superconductor, that is impossible, and the current persists.

the total magnetic field it creates would have to be reduced as well. In the course of the reduction, a flux line would have to pass through the current loop, but for a superconductor that is nearly impossible. It is for this reason that currents in superconductors are so persistent. The impurity scattering sites in the metal and the collisions of electrons with phonons do not go away, but whenever an electron is slowed down by such a collision, a flux line heads toward the metal surface. The metal repels it, and in so doing pushes the tardy electron back up to speed.

27.2 Phenomenology of Superconductivity

Perfect Diamagnets. When a superconductor is placed in an external field \vec{H} , all the flux lines are expelled from it so \vec{B} is zero in its interior. The magnetic permeability μ described by Eq. (24.6) is zero, and the superconductor is a perfect diamagnet. This perfect diamagnetism can be explained phenomenologically by supposing superconductors to be solids in which electrons accelerate in the presence of electric fields without displaying any damping. Like magnets and dielectric media, they are captured by proposing a relation between electrical field and current, which is

$$m\dot{\vec{v}} = -e\vec{E} \quad (27.1)$$

$$\Rightarrow \frac{\partial \vec{j}}{\partial t} = \frac{ne^2}{m} \vec{E} \quad (27.2)$$

$$\Rightarrow \frac{\partial}{\partial t} \vec{\nabla} \times \vec{\nabla} \times \frac{\vec{B}}{\mu} = \frac{4\pi ne^2}{mc} \vec{\nabla} \times \vec{E} \quad (27.3)$$

Using Eq. (24.5) and restricting attention to slowly varying currents so that $\partial \vec{D} / \partial t$ can be ignored.

$$\Rightarrow \vec{\nabla} \times \vec{\nabla} \times \frac{\vec{B}}{\mu} = -\frac{4\pi ne^2}{mc^2} (\vec{B} - \vec{B}_0). \quad (27.4)$$

Using again Eq. (20.5b) and integrating in time, obtaining a constant of integration \vec{B}_0 .

This line of argument cannot determine the constant field \vec{B}_0 . Because of Meissner and Ochsenfeld's observation that all magnetic fields are expelled from a superconductor, London (1961) proposed that superconductivity could be explained by setting \vec{B}_0 to zero to obtain

$$\vec{B} + \lambda_L^2 \vec{\nabla} \times \vec{\nabla} \times \vec{B} = 0 \quad (27.5)$$

where the *London penetration depth* is

$$\lambda_L = \sqrt{\frac{mc^2}{4\pi\mu ne^2}}. \quad (27.6)$$

The assumption is that any features of magnetic response not captured explicitly by \vec{j} are captured by a coefficient μ .

Equation (27.5) is called the *London equation*. The length λ_L gets its name from the solutions of Eq. (27.5). Consider a superconductor which occupies all of space for $z > 0$. Look for solutions of Eq. (27.5) which are independent of x and y . Rewrite Eq. (27.5) as

$$\vec{B} + \lambda_L^2 \left(\vec{\nabla} (\vec{\nabla} \cdot \vec{B}) - \nabla^2 \vec{B} \right) = 0. \quad (27.7)$$

Taking the dot product of Eq. (27.7) with \hat{z} gives

$$B_z = 0. \quad \text{Because } B \text{ is independent of } x \text{ and } y, \text{ all the } x \text{ and } y \text{ derivatives vanish.} \quad (27.8)$$

The first conclusion is then that the normal component of the magnetic induction always vanishes at the surface of a superconductor. Taking next a dot product with respect to \hat{x} gives

$$B_x = \lambda_L^2 \frac{\partial^2 B_x}{\partial z^2} \Rightarrow B_x \propto e^{-z/\lambda_L}. \quad (27.9)$$

The second conclusion is that a component of the induction parallel to a superconducting surface dies off exponentially over length λ_L . This decay is the origin of the Meissner effect. Because the current within the superconductor is related to the induction by Eq. (24.3), one obtains two additional important conclusions:

1. The superconductor sustains currents in equilibrium.
2. These currents inhabit a strip of width λ_L near the superconductor's surface, and they vanish everywhere else.

27.2.1 Phenomenological Free Energy

Trying to explain superconductivity with Eq. (27.2) as the starting point creates two difficulties. First, the constant time-independent magnetic field \vec{B}_0 needs to be eliminated without explanation in the midst of the analysis. Second, it is not the most general relation leading to superconductivity. Both difficulties can be counteracted by recasting the phenomenological theory in terms of a free energy, rather than a linear relation between current and field.

Consider a material without macroscopic magnetic fields in equilibrium. Weinberg (1986) emphasizes the economy of beginning with a free energy whose magnetic-field-dependent part takes the form

$$\mathcal{F} = \int d\vec{r}d\vec{r}' \sum_{\alpha\beta} \frac{1}{2} A_\alpha(\vec{r}) G_{\alpha\beta}(\vec{r}-\vec{r}') A_\beta(\vec{r}') + \delta(\vec{r}-\vec{r}') \frac{1}{8\pi} \vec{B}(\vec{r}) \cdot \vec{B}(\vec{r}'). \quad (27.10)$$

G is an arbitrary phenomenological function. Because it is a function of $\vec{r}-\vec{r}'$, it describes a macroscopically homogeneous medium.

Equation (27.10) differs from the previous magnetic free energy (24.25) in two respects. It is less general, because Eq. (27.10) is only quadratic in \vec{A} , and therefore only suitable for small deviations from equilibrium. On the other hand, this form puts forward \vec{A} as the primary variable rather than \vec{B} . A technical point that should be mentioned is that Eq. (27.10) is therefore not gauge-invariant. This deficiency can be remedied by replacing \vec{A} wherever it appears by $\vec{A} - \vec{\nabla}\phi$, where a gauge change $\vec{A} \rightarrow \vec{A} + \vec{\nabla}\chi$ sends ϕ to $\phi + \chi$. The final results will all be expressed in terms of $\vec{B} = \vec{\nabla} \times \vec{A}$, and because $\vec{\nabla} \times \vec{\nabla}\phi = 0$ is a vector identity there is no need to carry ϕ along.

The minima of this free energy describe equilibrium states. Requiring the functional derivative of the free energy to be zero with respect to the vector potential gives

$$[\vec{\nabla} \times \vec{\nabla} \times \frac{\vec{A}(\vec{r})}{4\pi}]_{\alpha} = - \int d\vec{r}' \sum_{\beta} G_{\alpha\beta}(\vec{r} - \vec{r}') A_{\beta}(\vec{r}') \quad (27.11)$$

Write $\vec{B} = \vec{\nabla} \times \vec{A}$ before taking derivatives of Eq. (27.10).

$$\Rightarrow j_{\alpha}(\vec{r}) = \frac{c}{4\pi} [\vec{\nabla} \times \vec{B}]_{\alpha} = -c \int d\vec{r}' \sum_{\beta} G_{\alpha\beta}(\vec{r} - \vec{r}') A_{\beta}(\vec{r}'). \quad (27.12)$$

In Fourier space, Eq. (27.11) becomes

$$\sum_{\beta} \left\{ G_{\alpha\beta}(\vec{k}) + \frac{1}{4\pi} (k^2 \delta_{\alpha\beta} - k_{\alpha} k_{\beta}) \right\} A_{\beta} = 0. \quad (27.13)$$

A system displays paramagnetic or diamagnetic behavior with permeability μ if in the limit as $k \rightarrow 0$,

$$G_{\alpha\beta} \rightarrow \left(\frac{1}{\mu} - 1 \right) \frac{1}{4\pi} [k^2 \delta_{\alpha\beta} - k_{\alpha} k_{\beta}]. \quad \text{Not obvious—obtained by working backwards from the desired result.} \quad (27.14)$$

To see why, note that if G is taken to have this form, then the term involving G in the free energy is

$$\frac{1/\mu - 1}{8\pi} \int d\vec{r} d\vec{r}' \delta(\vec{r} - \vec{r}') \vec{A} \cdot \vec{\nabla} \times \vec{\nabla} \times \vec{A} \quad \text{Write } \sum_{\beta} [k^2 \delta_{\alpha\beta} - k_{\alpha} k_{\beta}] A_{\beta} = -[\vec{k} \times \vec{k} \times \vec{A}]_{\alpha}. \quad (27.15)$$

$$= \frac{1/\mu - 1}{8\pi} \int d\vec{r} B(\vec{r})^2. \quad \text{Use the identity in Eq. (24.21) to integrate by parts and turn the leftmost } \vec{A} \text{ into } \vec{B}. \quad (27.16)$$

Adding Eq. (27.16) to the second term in Eq. (27.10) gives a free energy

$$\mathcal{F} = \frac{1}{8\pi\mu} \int d\vec{r} B^2(\vec{r}), \quad (27.17)$$

which describes a conventional permeable magnetic substance.

A superconductor is produced by adding any term to $G_{\alpha\beta}$ that destroys the existence of solutions with spatially uniform magnetic fields. For example, suppose that

$$\lim_{k \rightarrow 0} G_{\alpha\beta} = \frac{1}{4\pi\lambda_L^2} \delta_{\alpha\beta}. \quad (27.18)$$

In this event, the free energy takes the form

$$\frac{1}{8\pi} \int d\vec{r} \frac{1}{\lambda_L^2} A^2(\vec{r}) + |\vec{\nabla} \times \vec{A}|^2, \quad (27.19)$$

which has an extremum when

$$\frac{1}{\lambda_L^2} \vec{A} + \vec{\nabla} \times \vec{\nabla} \times \vec{A} = 0. \quad (27.20)$$

Taking the curl of Eq. (27.20) to ensure that the final results are gauge-invariant gives

$$\vec{B} + \lambda_L^2 \vec{\nabla} \times \vec{\nabla} \times \vec{B} = 0, \quad (27.21)$$

recovering Eq. (27.5).

Equation (27.21) is not quite as general as Eq. (27.5) because the first involves \vec{B} while the second involves \vec{B}/μ . A magnetic permeability different from unity can be introduced if one takes $G_{\alpha\beta}$ to be the sum of two terms, one of the form (27.14) and the second of the form (27.18). The physical interpretation of adding these two terms together is that some electrons in a solid, such as the valence electrons, are confined to individual atoms and create a magnetic response μ . Another population of electrons creates superconductivity. Adding together these two responses continues to produce a superconductor, but the penetration depth changes and is given by Eq. (27.6).

27.2.2 Thermodynamics of Superconductors

Suppose one takes a long thin cylinder of superconducting material and places it in an external magnetic field of strength H that points along the cylinder axis. The long cylindrical shape is desirable because its demagnetizing factor is zero, and the normal component of the magnetic field automatically vanishes along most of its surface. Experimentally, Meissner and Ochsenfeld (1933) found that at a critical applied field H_c the superconductivity is destroyed and magnetic flux penetrates the sample. The transition is completely reversible, so right at this critical field the superconducting state and normal state of the material must be in equilibrium. The free energy per volume of the metal in the normal state must be just

$$\mathcal{F} = \mathcal{F}_{\text{normal}} + \frac{1}{8\pi\mu} B_c^2. \quad (27.22)$$

Because the superconducting state expels the magnetic induction, its free energy is just $\mathcal{F}_{\text{superconducting}}$.

There now appears to be a problem. The free energy of the normal state is greater than that of the superconducting one, and the magnetic field energy is also positive. Yet when the critical field H_c is applied, (27.22) is supposed to equal $\mathcal{F}_{\text{superconducting}}$. What has gone wrong? The answer is that thermodynamics is being used improperly. The reversible experiments are carried out by slowly varying external currents, not by controlling B directly. In the instant that the normal metal expels B and becomes superconducting, a host of magnetic flux lines blasts off to infinity. The work done during this instant must be accounted for; equivalently, one must choose to work with thermodynamic variables that really do vary smoothly during the change from normal metal to superconductor. The correct thermodynamic potential, as in Eq. (24.27), is

$$\tilde{\mathcal{G}} = \mathcal{F} - \vec{B} \cdot \frac{\delta \mathcal{F}}{\delta \vec{B}} = \mathcal{F}_{\text{normal}} - \frac{1}{8\pi\mu} B_c^2. \quad (27.23)$$

Therefore the difference in free energy per volume at any given temperature between superconducting and normal metal must be exactly

$$\Delta\mathcal{F} \equiv \mathcal{F}_{\text{normal}} - \mathcal{F}_{\text{superconducting}} = \frac{B_c^2}{8\pi\mu}. \quad (27.24)$$

Because $\mu \approx 1$ for superconducting metals, Eq. (27.24) is often written

$$\Delta\mathcal{F} = \frac{H_c^2}{8\pi}. \quad (27.25)$$

One should remember, as mentioned in Section 24.2.3, that the magnetic field H inside a long thin cylinder with axis along the field is always spatially uniform and equal to the externally applied field. It is magnetic induction B that is expelled from superconducting samples, not the magnetic field H .

By differentiating Eq. (27.25) with respect to temperature, one finds immediately that the excess entropy of normal metal relative to the superconductor must be

$$\Delta S = \frac{\partial}{\partial T} \Delta\mathcal{F} = \frac{H_c}{4\pi} \frac{\partial H_c}{\partial T}. \quad (27.26)$$

Meissner and Ochsenfeld determined that as temperature rises towards the critical temperature T_c where superconductivity vanishes in zero magnetic field, the critical field H_c also goes to zero. It follows immediately from Eq. (27.26) that the latent heat of transformation is zero, and therefore the transition is second order.

27.2.3 Landau–Ginzburg Free Energy

The most productive phenomenological description of superconductivity combines ideas from the free energy (27.10) with the idea that the superconductivity resides in a population of superconducting electrons whose density vanishes at a critical temperature T_c . Landau and Ginzburg (1950) described the superconducting state through a macroscopic wave function Ψ that plays a role for superconductivity identical to the role played by the wave function Ψ employed in Eq. (15.98) for superfluid helium. If the supercurrent density $n = |\Psi|^2$ vanishes at T_c , then it should be possible to expand $G_{\alpha\beta}$ (see Eq. (27.10)) in powers of $|\Psi|^2$. Landau and Ginzburg guessed the free energy to be

$$\mathcal{F} = \int \frac{d\vec{r}}{\mathcal{V}} \left[\alpha |\Psi|^2 + \frac{\beta}{2} |\Psi|^4 + \frac{1}{8\pi} B^2 + \frac{1}{2m^*} \left| \left[\frac{\hbar}{i} \vec{\nabla} + \frac{2e}{c} \vec{A}(\vec{r}) \right] \Psi(\vec{r}) \right|^2 \right]. \quad (27.27)$$

The first two terms in Eq. (27.27) are procured directly from Landau's general theory of second-order phase transformations, discussed in Section 24.6.1. The remaining terms provide a particular realization of Eq. (27.10) and were inspired by the idea that the superconducting electron wave function might interact with the vector potential like a single macroscopic particle. The effective charge $e^* =$

$2e$ multiplying \vec{A} is due to the fact that pairs of electrons are responsible for the superconductivity. Minimizing Eq. (27.27) with respect to \vec{A} leads to

$$\vec{\nabla} \times \vec{B} = \frac{4\pi}{c} \vec{j}, \quad (27.28)$$

with

$$\vec{j}(\vec{r}) = -\frac{2e\hbar}{2im^*} [\Psi^* \vec{\nabla} \Psi - \Psi \vec{\nabla} \Psi^*] - \frac{4e^2}{m^*c} \vec{A} \Psi^* \Psi. \quad (27.29a)$$

Minimizing with respect to Ψ^* leads to

$$0 = \left[\alpha + \beta |\Psi|^2 + \frac{1}{2m^*} \left(\frac{\hbar}{i} \vec{\nabla} + \frac{2e}{c} \vec{A} \right)^2 \right] \Psi. \quad (27.29b)$$

Integrate so that all spatial derivatives act on Ψ , then take functional derivative with respect to Ψ^* .

Equations (27.29) are the *Landau–Ginzburg equations*.

Boundary Condition. To solve problems in particular geometries, it is always necessary to specify the behavior of Ψ at the boundary of a sample. When a superconductor contacts vacuum no current can flow out of the boundary, so

$$\hat{n} \cdot \left(\frac{\hbar}{i} \vec{\nabla} + \frac{2e}{c} \vec{A} \right) \Psi = 0. \quad (27.30)$$

Here \hat{n} is normal to the boundary; see Landau and Ginzburg (1950), de Gennes (1992), p. 177, or Wertheim (1969), p. 327.

Landau and Ginzburg observe that “it is natural to demand that the wave function at the boundary of the metal should vanish” but such an additional boundary condition on the superconducting wave function would eliminate solutions in thin films except for quantized values of the film thickness. Because this phenomenon is not observed, the seemingly natural boundary condition $\Psi = 0$ must be rejected.

27.2.4 Type I and Type II Superconductors

The Landau–Ginzburg equations depend upon two lengths. The first is a *coherence length* ξ that sets the scale for spatial variations of the order parameter Ψ . This length is given by

$$\xi^2 = \frac{\hbar^2}{2m^*|\alpha|}. \quad (27.31)$$

The second length is the London penetration depth. In terms of Landau and Ginzburg’s parameters it is given by

$$\lambda_L^2 = \frac{m^*c^2\beta}{4\pi|\alpha|(2e)^2}. \quad (27.32)$$

The coherence length and penetration depth, as well as critical temperature and lower critical field are tabulated in Table 27.1.

Table 27.1. Properties of superconductors

Compound	T_c (K)	H_c (G)	ξ (Å)	λ_L (Å)
Al	1.18	105	13 000–16 000	160–500
As ($P = 14$ GPa)	0.5			
Ba ($P = 20$ GPa)	5.3			
Be	0.02			
Bi ($P = 8$ GPa)	8.55			
Cd	0.52	30	7600	1 100
Ce ($P = 5$ GPa)	1.7			
Cs ($P = 13$ GPa)	1.6			
Ga	1.09	58.9		
Hf	0.02			
Hg	3.95	340		380–450
In	3.41	289	2 400–3 500	390–640
Ir	0.10	20.1		
La	6.0	1096		
Lu	0.1			
Mg	0.0005			
Mo	0.92	98		
Nb	9.3	1980	380	390
P ($P = 17$ GPa)	5.8			
Pb	7.20	803	510–960	390–630
Ru	0.49	47		
Se ($P = 13$ GPa)	6.9			
Si ($P = 12$ GPa)	7.1			
Sn	3.7	308	1 000–3 000	340–750
Ta	4.46	831		
Tc	7.8	1410		
Te ($P = 8$ GPa)	4.3			
Th	1.37	162		
Ti	0.42	56		
Tl	2.4	180	4200	
U	1.8			
W	0.02	1.07		
Y ($P = 17$ GPa)	2.7			
Zn	0.85	52		
Zr	0.53	47		
Nb ₃ Sn	18.5	28	34	1 600
YBa ₂ Cu ₃ O _{7-x}	92	500	4–8	900–8 000
HgBa ₂ Ca ₂ Cu ₃ O _y	135			

Critical temperature T_c , lower critical magnetic field H_c where flux first penetrates sample at zero temperature, coherence length ξ and London penetration depth λ_L for selected superconductors. Measurements are at atmospheric pressure unless otherwise indicated. Source: Grigoriev and Meilkhov (1997), pp. 566-567 and Plakida (1995).

Calculation of Coherence Length ξ . These lengths emerge from some simple calculations based upon Eq. (27.29b). First, consider a case in which externally imposed magnetic fields vanish. One sees immediately from Eq. (27.29b) that the spatially uniform solutions are

$$|\Psi|^2 = \begin{cases} \Psi_0^2 \equiv -\frac{\alpha}{\beta} & \text{or} \\ 0. \end{cases} \quad (27.33)$$

The constant β must always be positive or else \mathcal{F} is minimized by sending $\Psi \rightarrow \infty$. The nonzero case in Eq. (27.33) is only possible if $\alpha < 0$, and it corresponds to a spatially uniform superconducting state. The free energy per volume of this state, from Eq. (27.27), is

$$\frac{\mathcal{F}}{\bar{V}} = -\frac{\alpha^2}{2\beta} \quad (27.34)$$

and comparing with Eq. (27.25) shows that

$$H_c^2 = \frac{4\pi\alpha^2}{\beta}. \quad (27.35)$$

When superconductivity is present, it makes sense to scale Ψ by this uniform value Ψ_0 and define

$$\psi = \frac{\Psi}{\Psi_0}, \quad (27.36)$$

in terms of which Eq. (27.29b) becomes

$$-\xi^2 \nabla^2 \psi - \psi + \psi|\psi|^2 = 0, \quad \text{When } \vec{A} = 0. \quad (27.37)$$

ξ being given by Eq. (27.31). Thus ξ is the characteristic scale on which ψ varies in the absence of magnetic fields.

One-Dimensional Interface. The physical significance of ξ is illustrated by examining the scale over which the wave function ψ varies. Take ψ to be real, and consider a one-dimensional interface. In one dimension one has

$$-\xi^2 \psi'' - \psi + \psi^3 = 0. \quad (27.38)$$

Multiplying Eq. (27.38) by ψ' and integrating, one has the first integral

$$-\xi^2 (\psi')^2 - \psi^2 + \frac{1}{2} \psi^4 = \text{Const.} \quad (27.39)$$

Equation (27.39) is only consistent with an asymptotic value of $\psi = 1$ if one takes the right hand side constant to be $-1/2$. In this case, one can then write

$$\psi' = \frac{1}{\sqrt{2}\xi} (1 - \psi^2) \quad (27.40)$$

which has a solution

$$\psi = \tanh \frac{x}{\sqrt{2}\xi}. \quad (27.41)$$

This solution describes a transition between two spatially uniform superconducting regions where the phase of the wave function changes sign across the interface. The coherence length ξ sets the spatial scale for this transition.

Penetration Depth. The second length, the penetration depth, arises when one considers a superconductor occupying the region, say, $x < 0$, in an exceedingly weak field. When the field is zero, one has the solution $\Psi = \Psi_0$ for $x < 0$. In the presence of a very weak field, Ψ will change to linear order in the field, but because it is nonzero without a field, to leading order one can continue to use $\Psi = \Psi_0$. Looking at Eq. (27.29a) and keeping only the leading terms gives

$$\vec{j} = \frac{c}{4\pi} \vec{\nabla} \times \vec{B} = -\frac{4e^2}{m^*c} \Psi_0^2 \vec{A}. \quad (27.42)$$

Taking the cross product of Eq. (27.42) gives

$$\vec{\nabla} \times \vec{\nabla} \times \vec{B} = -\frac{4\pi}{c} \frac{4e^2}{m^*c} \Psi_0^2 \vec{B} = -\lambda_L^{-2} \vec{B}. \quad (27.43)$$

Using Eq. (27.33) immediately gives Eq. (27.32) for the penetration depth.

The ratio of the penetration depth and coherence length

$$\kappa = \lambda_L / \xi = \frac{m^*c}{e\hbar} \sqrt{\frac{\beta}{8\pi}} \quad (27.44)$$

is in fact the only free parameter of the Landau–Ginzburg theory, because all other constants can be scaled out, by rescaling ψ , distance, and \vec{A} . To be specific, define

$$\vec{a} = \frac{4e\vec{A}}{c\sqrt{2m^*|\alpha|}} \quad (27.45)$$

and measure all distances in units of ξ . Then Eq. (27.29b) becomes

$$\psi - \psi|\psi|^2 - (-i\vec{\nabla} + \vec{a}/2)^2\psi = 0 \quad (27.46)$$

while Eq. (27.29a) becomes

$$\frac{\lambda_L^2}{\xi^2} \vec{\nabla} \times \vec{\nabla} \times \vec{a} = -\frac{1}{i} (\psi^* \vec{\nabla} \psi - \psi \vec{\nabla} \psi^*) - |\psi|^2 \vec{a}. \quad (27.47)$$

Surface Energies. A particularly important result of Landau and Ginzburg's theory is the calculation of the surface energy between normal and superconducting metals. For $\kappa < 1/\sqrt{2}$ the energy is positive; however, if $\kappa > 1/\sqrt{2}$, the surface energy is negative. Once one has a negative surface energy, it becomes favorable for magnetic flux to penetrate a superconductor and form interlocking regions of normal and superconducting metal. Superconductors for which this happens are called *type II*; those for which it does not are called *type I*. The way in which the flux penetrates was worked out by Abrikosov (1957).

In order to discover why the magnitude of κ plays such an important role, consider a superconductor in a magnetic field larger than H_c , so that the superconductivity is destroyed and $\Psi = 0$. Now begin to lower the field, and examine

the linear stability of the state $\Psi = 0$ by expanding everything to first order in Ψ . From Eq. (27.29a), one sees that the current \vec{j} vanishes to this order, and therefore one can take \vec{A} simply to be the vector potential associated with a uniform field H , pointing, say, along the \hat{z} axis. Writing Eq. (27.29b) to linear order then gives

$$\frac{1}{2m^*}(-i\hbar\vec{\nabla} + \frac{2e\vec{A}}{c})^2\Psi = -\alpha\Psi. \quad (27.48)$$

This equation is the same as the eigenvalue equation for an electron in a constant external magnetic field, and so one can immediately write down the solution by comparison with Eq. (25.48). Define H_{c_2} to be the largest magnetic field permitting a nonzero solution of Eq. (27.48). The lowest-energy eigenvalue is $\hbar\omega_c/2$, where in this case

$$\omega_c = \frac{2eH_{c_2}}{m^*c}, \quad (27.49)$$

because in Eq. (27.48) the charge carrier has charge $-2e$. The larger H becomes, the larger α would need to be in order for a solution to be possible. For a given α , the largest H at which Eq. (27.48) has nonzero solution is therefore

$$-\alpha = |\alpha| = \frac{e\hbar H_{c_2}}{m^*c}. \quad (27.50)$$

Using Eq. (27.35) to express the critical field H_c in terms of α and β , along with Eq. (27.44) to define κ , gives

$$\frac{H_{c_2}}{H_c} = \sqrt{2}\kappa. \quad (27.51)$$

Now one can see why $\kappa = 1/\sqrt{2}$ divides the two types of superconductors. If $\kappa > 1/\sqrt{2}$, then H_{c_2} lies above H_c . For applied magnetic fields between H_c and H_{c_2} , it is energetically unfavorable to expel all magnetic flux from the system, but favorable to form at least one superconducting vortex, corresponding to solutions of Eq. (27.48). Equation (27.48) predicts that a vortex will form, but is unable to describe its strength or final form; these can only be obtained from more elaborate calculations taking into account the nonlinear terms of Eq. (27.47). As the magnetic field descends below H_{c_2} toward H_c , more and more vortices fill the system, until at H_c they coalesce and expel all the magnetic flux. By contrast, if $\kappa < 1/\sqrt{2}$, forming a vortex does not become possible until the magnetic field has dropped below H_c . It is reasonable to guess, and possible to verify, that the system does not choose to form vortices when it has the option of expelling all the magnetic field and to become superconducting instead. The picture that led to Eq. (27.48), in which a normal metal in a magnetic field develops a superconducting wave function to order Ψ , is no longer valid. It is more favorable for Ψ to grow to size $-\alpha/\beta$ and take over the whole sample.

Interface Energies. Problem 2 describes the free energies of superconducting-metal interfaces in two limits. For $\kappa = 0$,

$$\frac{\tilde{g}}{A} = \frac{H_c^2}{4\pi} \sqrt{2} \xi \frac{2}{3}, \quad (27.52)$$

and forming the interface costs a finite positive energy per unit area A . For $\kappa \rightarrow \infty$,

$$\frac{\tilde{g}}{A} = -\frac{H_c^2}{8\pi} \lambda_L; \quad (27.53)$$

because this energy is negative, the system will respond by trying to form as much interface as it can. The result is the *Abrikosov lattice* of flux lines penetrating the sample depicted in Figure 27.2.

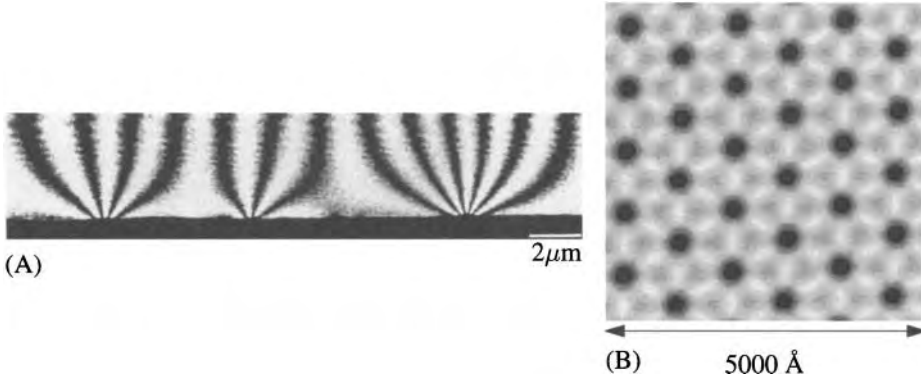


Figure 27.2. A Type II superconductor is unstable to the formation of flux tubes that penetrate the sample trying to generate a maximal area where superconductor and metal are in contact. The lowest free energy configuration is often a triangular lattice. (A) Electron hologram from the side of magnetic flux entering a lead film [Source: Tonomura et al. (1986), p. 93.] (B) Top view of an Abrikosov lattice of flux tubes in NbSe₂, taken with scanning tunneling microscopy. [Courtesy of S. Pan and A. de Lozanne, University of Texas.]

27.2.5 Flux Quantization

The Landau–Ginzburg equations have an effective charge $-2e$ seated in the spot one would expect to be occupied by the electron charge $-e$. This effective charge has a convoluted history. Ginzburg had guessed that the superconducting charge carriers might have an effective charge e^* . Landau objected that effective charges violate gauge invariance, and their paper takes the position that “ e is a charge, which there is no reason to consider as different from the electronic charge.” In fact, arguments based upon gauge invariance require only that charges be integral multiples of the electron charge; in two-dimensional space these arguments permit effective particles with arbitrary charge, as shown in Figure 25.11 and discussed by Wilczek (1990). Despite the fact that the microscopic theory of superconductivity involved pairing of electrons, the correct form of the Landau–Ginzburg equations was not clear, and the effective charge $-2e$ was a surprise when discovered experimentally by Deaver and Fairbank (1961) and Doll and Näbauer (1961) in studies of quantized magnetic fluxes.

The Landau–Ginzburg equations predict that the magnetic flux trapped within a superconductor is quantized (Figure 27.3). Suppose, however, that the effective

charge $-e^*$ and mass m^* of the superconducting particles were not known. The superconducting current associated with Ψ would be

$$\vec{j} = -\frac{e^*\hbar}{2im^*} [\Psi^*\vec{\nabla}\Psi - \Psi\vec{\nabla}\Psi^*] - \frac{e^{*2}}{m^*c}\vec{A}\Psi^*\Psi. \tag{27.54}$$

Letting

$$\Psi(\vec{r}) = \Psi_0 e^{i\phi(\vec{r})} \text{ Take } \phi \text{ to be real.} \tag{27.55}$$

gives

$$\vec{j} = -\frac{\Psi_0^2}{m^*} \left(\frac{e^{*2}}{c}\vec{A} + e^*\hbar\vec{\nabla}\phi \right) \tag{27.56}$$

$$\Rightarrow -\vec{\nabla}\phi = \frac{1}{\hbar} \left(\frac{m^*}{e^*\Psi_0^2}\vec{j} + \frac{e^*}{c}\vec{A} \right). \tag{27.57}$$

Simply demanding that the phase ϕ be differentiable is enough to prove that the magnetic flux is quantized, just as in Eq. (15.106). Because Ψ must return to itself when ϕ changes through 2π , one obtains

$$-\int d\vec{s} \cdot \vec{\nabla}\phi = 2\pi l, \text{ } l \text{ is an integer.} \tag{27.58}$$

As a result,

$$\int d\vec{s} \cdot \frac{1}{\hbar} \left[\frac{m^*}{e^*\Psi_0^2}\vec{j} + \frac{e^*}{c}\vec{A} \right] = 2\pi l. \tag{27.59}$$

Choosing a contour of integration that lies within the cylinder at a depth greater than the skin depth (Figure 27.3), \vec{j} is negligible, and

$$\frac{e^*}{c\hbar} \int d\vec{s} \cdot \vec{A} = 2\pi l \tag{27.60}$$

$$\Rightarrow \int d^2r B_z = \Phi = \frac{2\pi\hbar c}{e^*} = l \frac{e}{e^*} \Phi_0. \text{ See definition of } \Phi_0 \text{ in Eq. (25.51).} \tag{27.61}$$

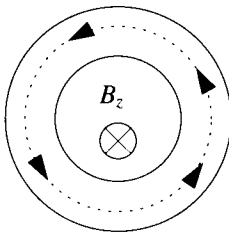


Figure 27.3. Magnetic flux that pierces a superconducting ring is quantized in units of $\Phi_0/2$. The integration contour in Eq. (27.59) is taken on the dotted line, which lies deep in the superconductor where \vec{j} vanishes.

So the integrated magnetic flux Φ that penetrates a hole through a superconductor is quantized in units of $(e/e^*)\Phi_0$, and can be used to measure the effective charge e^* . The measurements in Figure 27.4 show that $e^* = 2e$, leading to the conventional form of Eq. (27.27). The fact that the only phase changes observed in Figure 25.5 are 0 and π is another experimental demonstration of this same fact.

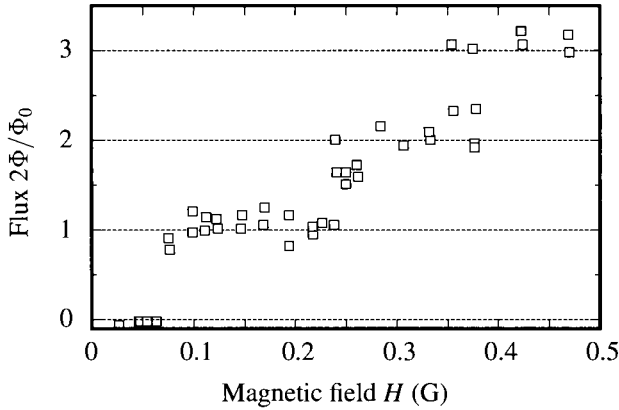


Figure 27.4. Trapped magnetic flux in a superconducting cylinder as a function of applied field. The dimensions of the cylinder are on the order of $10\ \mu\text{m}$, and it is made of tin. The flux is measured by moving the cylinder up and down at 100 Hz toward and away from a conducting coil and measuring the electromotive force induced in the coil. [Source: Deaver and Fairbank (1961), p. 44; a nearly identical experiment was published simultaneously by Doll and Näbauer (1961). Theoretical discussions by Byers and Yang and Onsager are sandwiched between these two experimental papers.]

27.2.6 The Josephson Effect

It takes a certain degree of courage to adopt a phenomenological function like Ψ , treat it as a physical entity, and predict new phenomena. Josephson (1962) predicted that the wave function could be induced to interfere with itself and oscillate if two superconductors were separated by a small strip of nonsuperconducting material. A qualitative derivation of Josephson's equations is presented at first; Section 27.2.9 obtains the basic results in a more careful way.

Consider two superconductors separated by a thin insulating layer. On the opposite sides of this *weak link*, the two superconductors interact only because of their exponentially small residues as they decay across the barrier into each others territory. The change in energy of two nearly independent systems due to tunneling is given in general by

$$\int d\vec{r} U(\vec{r}) (\Psi_1^*(\vec{r})\Psi_2(\vec{r}) + \Psi_1(\vec{r})\Psi_2^*(\vec{r})) \quad (27.62)$$

$$= \epsilon (\Psi_1^*\Psi_2 + \Psi_1\Psi_2^*) , \quad (27.63)$$

where the wave function without the argument \vec{r} refers to its value at some reference point inside the bulk, and ϵ is some very small quantity with dimensions of energy. Writing down a Schrödinger equation for two wave functions coupled by such an interaction leads to

$$\frac{\partial\Psi_1}{\partial t} = \frac{-i}{\hbar} [\mathcal{E}_1\Psi_1 + \epsilon\Psi_2] \quad (27.64a)$$

$$\frac{\partial\Psi_2}{\partial t} = \frac{-i}{\hbar} [\mathcal{E}_2\Psi_2 + \epsilon\Psi_1] . \quad (27.64b)$$

Taking each wave function now to be of the form

$$\Psi_l = \sqrt{n_l} e^{i\phi_l} \tag{27.65}$$

gives

$$\left(\frac{1}{2} \frac{\dot{n}_1}{\sqrt{n_1}} + i\sqrt{n_1} \dot{\phi}_1 \right) e^{i\phi_1} = \frac{-i}{\hbar} \left[\mathcal{E}_1 \sqrt{n_1} e^{i\phi_1} + \epsilon \sqrt{n_2} e^{i\phi_2} \right].$$

A similar equation holds with indices reversed.

(27.66)

The superconducting electron densities n_1 and n_2 within the superconducting regions are the same and constant, apart from some extremely small variations, so by taking the real and imaginary parts of Eq. (27.66), one finds

$$n_1 = 2 \frac{\epsilon n}{\hbar} \sin(\phi_2 - \phi_1) = -n_2 = \frac{j}{2e}$$

Superconducting particles are flowing from one superconductor to another; this time rate of change is the total current. (27.67a)

$$\dot{\phi}_2 - \dot{\phi}_1 = \frac{1}{\hbar} (\mathcal{E}_1 - \mathcal{E}_2) = 2e(V_2 - V_1)/\hbar.$$

The factor of two appears at the end because the energies correspond to energies of electron pairs. (27.67b)

In the presence of magnetic fields, Eqs. (27.67) are not correct because the phase of a wave function changes in the presence of a magnetic field. To make a wave function phase gauge-invariant, add $2e/(\hbar c) \int_0 d\vec{s} \cdot \vec{A}$ to the phase, where the line integral is taken from some arbitrary reference point. Incorporating this generalization, Josephson's equations become

$$\vec{j} = \vec{j}_0 \sin\left(\phi_2 - \phi_1 + \frac{2e}{\hbar c} \int_1^2 d\vec{s} \cdot \vec{A}\right) \tag{27.68a}$$

$$\frac{-1}{\hbar} (\mathcal{E}_2 - \mathcal{E}_1) = 2eV/\hbar = \frac{\partial}{\partial t} \left(\phi_2 - \phi_1 + \frac{2e}{\hbar c} \int_1^2 d\vec{s} \cdot \vec{A} \right). \tag{27.68b}$$

V is the voltage difference between the two superconductors, and the factor of two appears because the energies \mathcal{E}_i are energies of electron pairs.

Equations (27.68) have peculiar properties. If one places two superconductors at different voltages in contact ($\mathcal{E}_1 - \mathcal{E}_2 \neq 0$), then $\phi_2 - \phi_1$ drifts in time, so n_1 and n_2 oscillate about their mean values at $484 \text{ MHz}/\mu\text{V}$ —the *AC Josephson effect*. On the other hand, if $\mathcal{E}_1 - \mathcal{E}_2 = 0$, then $\phi_2 - \phi_1$ does not change in time, but does not have to vanish, so Eq. (27.68a) permits steady current flow—the *DC Josephson effect*. If a current source injects electrons into a Josephson junction, then the phase difference $\phi_2 - \phi_1$ simply adjusts to a nonzero value, up to a maximum value of $\pi/2$. Current flow in the absence of a voltage difference is a defining properties of superconductors.

The experiment that was decisive in bringing about acceptance of the Josephson effect was performed by Anderson and Rowell (1963). It consisted of measuring the relationship between current and voltage in a *Josephson junction* as a function of magnetic field. Later experiments probed more exotic interference effects; those shown in Figure 27.5 provide a clear demonstration that Eqs. (27.68) are sound. Calculation of the form of the interference is left to Problem 3.

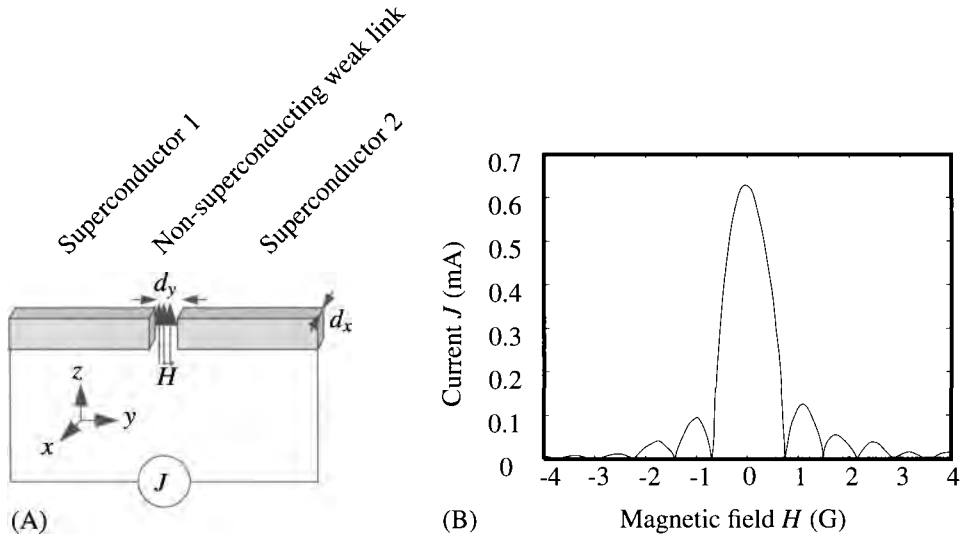


Figure 27.5. (A) Setting for Fraunhofer diffraction in a Josephson junction. (B) The critical Josephson current J_c is the maximum zero-voltage current that can flow through a Josephson junction. The data show a measurement of J_c in an Sn–SnO–Sn junction at $T = 1.9$ K. [Results of R. C Jaklevic, reported by Mercereau (1969), p. 402]

27.2.7 Circuits with Josephson Junction Elements

When used as a circuit element, the Josephson junction has both some resistance R and capacitance C . So the circuit element containing the Josephson junction is described by

$$\frac{V}{R} + J_0 \sin \phi + C\dot{V} = J, \quad \text{Leave out magnetic fields for the moment so as not to have to carry along the integrals of the vector potential.} \quad (27.69)$$

where $\phi = \phi_2 - \phi_1$. Eq. (27.69) constitutes the *resistively shunted junction (RSJ)* model. In the absence of magnetic fields

$$\dot{\phi} = 2eV/\hbar, \quad (27.70)$$

because the difference in Fermi energies between the two superconductors is just $2eV$. Therefore

$$J = \frac{\dot{\phi}\hbar}{2eR} + J_0 \sin \phi + \frac{C\hbar}{2e} \ddot{\phi} \quad (27.71)$$

$$\Rightarrow \frac{\hbar C}{2e} \ddot{\phi} + \frac{\hbar}{2eR} \dot{\phi} = -\frac{\partial}{\partial \phi} [-\phi J - J_0 \cos \phi]. \quad (27.72)$$

Equation (27.72) has a mechanical analog, the motion of a damped particle in a potential. The potential slopes downwards, but with periodic bumps as shown

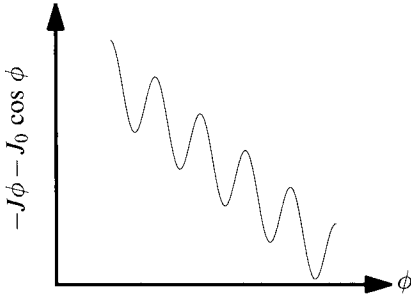


Figure 27.6. The washboard potential in Eq. (27.72).

in Figure 27.6: It is called a *tilted washboard potential*. One can understand the behavior of the Josephson junction based on the mechanical analogy without going through complicated analysis. First, make the equations dimensionless by measuring time in units of

$$t_0 = \frac{\hbar}{2eJ_0R}, \tag{27.73}$$

so that Eq. (27.72) becomes

$$\beta \ddot{\phi} + \dot{\phi} = -\frac{\partial}{\partial \phi} \left[-\phi \frac{J}{J_0} - \cos \phi \right], \tag{27.74}$$

where

$$\beta = \frac{J_0 R^2 C 2e}{\hbar}. \tag{27.75}$$

If $\beta \gg 1$, then the particle is very heavy, and the junction is hysteretic. To see why, suppose the current J to be less than J_0 . The particle sits in one of the basins, perhaps rocking back and forth slightly, meaning that the voltage oscillates weakly about zero. Next suppose the current J to be raised above J_0 . Then the particle rolls down the washboard. This continual motion corresponds to a voltage V . If the current is lowered again to its original value, the ball has acquired momentum, and because the damping is weak, it will continue to roll across the washboard. The nonzero voltage maintains itself, although the current is less than critical. This hysteretic behavior is prevented when the particle is overdamped, which corresponds to a small shunting resistance R .

27.2.8 SQUIDS

Superconducting quantum interference devices (SQUIDS) are Josephson junctions employed as very sensitive detectors of magnetic flux. DC SQUIDS consist of superconducting loops containing two junctions. Consider the contour depicted in Figure 27.7. Assuming that the superconductors are thicker than the penetration depth, along with Eq. (27.57), one obtains $\vec{\nabla} \phi = -4\pi \vec{A} / \Phi_0$ everywhere in the superconductor. Therefore

$$\oint d\vec{s} \cdot \vec{A} = \Phi = \int_4^1 d\vec{s} \cdot \vec{A} - \frac{\Phi_0}{4\pi} \int_1^2 d\vec{s} \cdot \vec{\nabla} \phi + \int_2^3 d\vec{s} \cdot \vec{A} - \frac{\Phi_0}{4\pi} \int_3^4 d\vec{s} \cdot \vec{\nabla} \phi \tag{27.76}$$

$$\Rightarrow \Phi = \frac{\Phi_0}{4\pi} (\gamma_{23} - \gamma_{14}), \tag{27.77}$$

where

$$\gamma_{14} = \phi_4 - \phi_1 + \frac{4\pi}{\Phi_0} \int_1^4 d\vec{s} \cdot \vec{A}. \text{ With an identical expression for } \gamma_{23}. \tag{27.78}$$

If the weak links were absent, the phase changes γ_{14} and γ_{23} would have to be multiples of 2π , giving back the flux quantization condition (27.61). The gaps between the superconductors allow arbitrary amounts of flux to creep into the loop, but then place a constraint on the phases of the wave function.

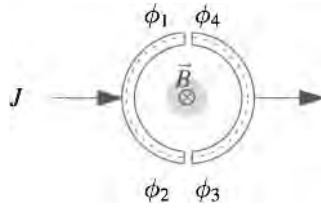


Figure 27.7. A DC SQUID consists of two Josephson junctions in parallel. The assembly is extremely sensitive to the enclosed magnetic flux. The dotted line is a contour used to calculate Eq. (27.76).

According to Eq. (27.68a), the total current passing through the DC SQUID is

$$J = J_0 \sin(\gamma_{14}) + J_0 \sin(\gamma_{23}) \tag{27.79}$$

$$= J_0 \left[\sin(\gamma_{23} - 4\pi\Phi/\Phi_0) + \sin(\gamma_{23}) \right]. \text{ Inserting Eq. (27.77).} \tag{27.80}$$

The current oscillates as a function of the phase Φ in the SQUID, and it can be used as a sensitive measure of magnetic fields. In practice, Eq. (27.69) must be used to describe the behavior of the phase, rather than Eq. (27.68a), and the junctions are resistively shunted so as to eliminate the hysteresis that would accompany the completely nondissipative case.

27.2.9 Origin of Josephson’s Equations

Section 27.2.1 described the derivation of superconductivity from hypotheses concerning a free energy. A broadening of this point of view to encompass dynamical phenomena allows for a very general derivation of Josephson’s equations.

The new point of view focuses upon the field ϕ appearing in the macroscopic wave function $\Psi_0 \exp i\phi$. According to Eq. (27.57), so long as Ψ_0 is constant, the current \vec{j} can be put in the form

$$\vec{j} = - \frac{|\Psi_0|^2 8\pi e\hbar}{m^* \Phi_0} \left[\frac{\Phi_0}{4\pi} \vec{\nabla} \phi + \vec{A} \right]. \text{ The magnetic flux quantum } \Phi_0 \text{ is defined in Eq. (25.51).} \tag{27.81}$$

Therefore $\chi = \Phi_0\phi/4\pi$ enters the theory in exactly the same fashion as the field χ in electrodynamics used to generate gauge transformations of the vector potential.

The most economical theory of superconductivity begins with two postulates:

1. The field χ generating phase changes has become a macroscopic field with physically measurable consequences. The vector potential always appears in combination with χ as $\vec{A} + \vec{\nabla}\chi$, while the scalar potential V always appears in combination with χ as $V - \dot{\chi}/c$.
2. When $\phi = 4\pi\chi/\Phi_0$ appears in the theory, it does so in the form $\exp[i\phi]$, so ϕ only has significance up to multiples of 2π .

These postulates describe a *spontaneous breaking of gauge symmetry*.

Having determined that the gauge potential χ should be part of the theory, one can write down a Lagrangian in the spirit of Section B.3 for superconductivity in the form

$$L = \int d\vec{r}dt \mathcal{L} = \int d\vec{r}dt \left\{ \frac{E^2 - B^2}{8\pi} - G(\vec{A} + \vec{\nabla}\chi, V - \dot{\chi}/c) \right\}. \quad \text{V is the scalar potential.} \quad (27.82)$$

Use

$$\vec{E} = -\vec{\nabla}V - \frac{1}{c} \frac{\partial \vec{A}}{\partial t}, \quad \text{and} \quad \vec{B} = \vec{\nabla} \times \vec{A}. \quad (27.83)$$

Problem 4 demonstrates through straightforward computations that

$$\frac{\delta L}{\delta V} = 0 \Rightarrow \frac{\partial G}{\partial V} = -ne \quad -ne \text{ is the charge density.} \quad (27.84a)$$

$$\frac{\delta L}{\delta \vec{A}} = 0 \Rightarrow \frac{\partial G}{\partial \vec{A}} = -\frac{\vec{j}}{c}. \quad (27.84b)$$

The Lagrangian must also vanish with respect to variations in χ , so

$$\frac{\delta L}{\delta \chi} = 0 \Rightarrow \vec{\nabla} \cdot \frac{\partial G}{\partial \vec{A}} - \frac{\partial}{\partial t} \frac{1}{c} \frac{\partial G}{\partial V} = 0 \quad (27.85)$$

$$\Rightarrow \frac{\partial}{\partial t} [-ne] = -\vec{\nabla} \cdot \vec{j}. \quad \text{This is just the equation of continuity, obtained by substituting in Eqs. (27.84).} \quad (27.86)$$

The Lagrangian depends upon the fields \vec{A} , V , and χ , as well as upon the time derivatives of \vec{A} and χ . Therefore, the Hamiltonian is

$$\mathcal{H} = \vec{A} \cdot \frac{\partial \mathcal{L}}{\partial \vec{A}} + \dot{\chi} \frac{\partial \mathcal{L}}{\partial \dot{\chi}} - \mathcal{L}. \quad \text{Just the definition of the Hamiltonian, as on p. 346 of Goldstein (1980).} \quad (27.87)$$

There is no need to calculate any properties of the Hamiltonian explicitly in order to derive the Josephson effect. One has only to observe that the Hamiltonian is conserved and must equal the energy of the system. According to Eq. (27.84a), the canonical momentum corresponding to χ is proportional to the charge density,

$$\frac{\partial \mathcal{L}}{\partial \dot{\chi}} = -\frac{ne}{c}. \quad (27.88)$$

Therefore Hamilton's equations for χ must be

$$\frac{\partial \mathcal{H}}{\partial \chi} = \frac{\dot{n}e}{c} \quad \text{Identify } Q \text{ with } \chi \text{ and } P \text{ with } -ne/c. \text{ This equation is } \frac{\partial \mathcal{H}}{\partial Q} = -\dot{P}. \quad (27.89a)$$

$$\frac{\partial \mathcal{H}}{\partial[-ne/c]} = \dot{\chi}. \quad \text{This equation is } \frac{\partial \mathcal{H}}{\partial P} = \dot{Q}. \quad (27.89b)$$

The derivative of the energy \mathcal{H} with respect to the electron density n is precisely the electron electrochemical potential μ . Finally,

$$\dot{\chi} = -\frac{c\mu}{e} \Rightarrow \dot{\phi} = -\frac{2\mu}{\hbar} = \frac{2eV}{\hbar}. \quad \text{Use } \chi = \phi\hbar c/2e. \quad (27.90)$$

If two points differ in voltage by an amount $\delta V = \delta\mu/(-e)$, then the phase difference $\delta\phi$ between these points changes at a rate $\delta\dot{\phi} = 2e\delta V/\hbar$. Because all physical quantities are periodic functions of $\phi + 4\pi \int d\vec{s} \cdot \vec{A}/\Phi_0$ with period 2π , the current must oscillate with frequency $2e\delta V/h$. The arguments leading to this conclusion depend only upon the assumption that ϕ is a physical field and that physical quantities depend upon $\exp[i\phi]$. Oscillations of Josephson junctions therefore provide the most precise measurement of the *Josephson constant* $K_J = 2e/h$.

While Eq. (27.68b) depends only upon fundamental constants, and is correct to very high accuracy, Eq. (27.68a) is less fundamental. The function $\sin \phi$ appearing in Eq. (27.68a) could be replaced by other functions, just so long as they had the same periodicity.

27.3 Microscopic Theory of Superconductivity

The phenomenological theories of superconductivity are in many respects quite complete. Yet there are certain types of questions that they cannot answer. Why are some materials superconducting and others not? What determines the critical temperature T_c and critical field H_c ? What sets the coherence length and penetration depth λ_L ? These are issues that a microscopic theory should address. Because the single-electron Hamiltonians that are amenable to exact or numerical solution do not produce superconductivity and because the full many-electron Hamiltonian is intractable, decades passed after the experimental discovery of superconductivity with little theoretical progress:

Bloch, in a famous theorem later extended by Bohm to many-body systems, showed that in the absence of a magnetic field the most stable state of an electron system is that of zero current. Because of the frustrations which the many theorists who worked on the problem encountered, Bloch jokingly proposed a second theorem—that “any theory of superconductivity can be refuted.”
—Bardeen (1963), p. 3

A crucial step on the path to a microscopic theory was the discovery of the isotope effect by Maxwell (1950) and Reynolds et al. (1950), shown in Figure 27.8.

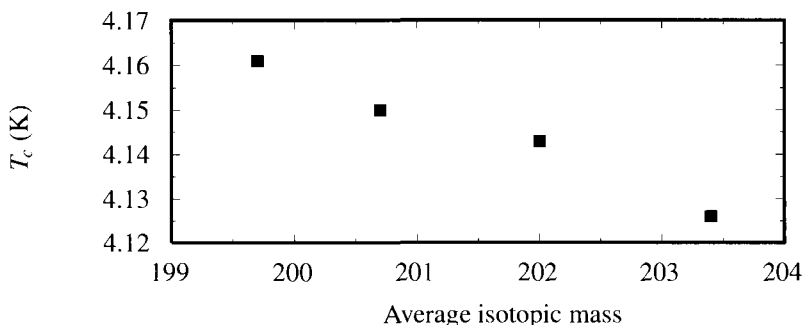


Figure 27.8. Superconducting transition temperature T_c versus average isotopic mass in four samples of mercury, showing decrease in T_c with increasing mass. [Source: Reynolds et al. (1950), p. 487.]

If the superconducting transition temperature could be depressed by changing the mass of the ions, then the interaction of electrons and ions must be crucial. The theory of polarons in Section 22.3.2 is based upon this same type of interaction. In fact, Fröhlich (1950) began a theory of superconductivity based upon an interaction between electrons and phonons prior to the experimental observations shown in Figure 27.8, and the Hamiltonian he deduced for this purpose is a starting point for successful microscopic models.

27.3.1 Electron–Ion Interaction

Fröhlich (1950) found that electrons could effectively attract each other because of an intermediate interaction with phonons. In rough terms, the motion of an electron with wave number \vec{k} through the lattice causes the ions to vibrate with the same wave number. It is then energetically favorable for a second electron, traveling in the opposite direction from the first but with the same wavelength, to synchronize its phase with the first electron so as to obtain the greatest energetic benefit from the ionic vibrations. This synchrony is an effective attraction between the two electrons. To see in detail how the attraction comes about requires bringing together results on the interaction of electrons with ions and with each other.

The most physically meaningful way to perform this task is by imagining that an electric field \vec{E} has been imposed on a metal and then finding the resulting motion of charge, including both (a) charge motion associated with conduction electrons and (b) charge motion associated with ions. From the total conductivity σ obtained in this way follows a dielectric function ϵ that contains information on all the charge carriers bundled together. This dielectric function shows how electrons and ions adjust in response to any electric field, but in particular it can be used to show how electrons and ions adjust in response to the electric field of a moving electron. It follows that the effective interaction of two electrons separated by distance r is $e^2/\epsilon r$, with ϵ carrying information about the cooperative motion both of ions and a sea of conduction electrons.

Conduction Electron Current. Equations (20.75) and (20.76) describe how conduction electrons move in response to external potentials V . Because $\sigma = \omega(\epsilon - 1)/4\pi i$ from (20.14), Eq. (20.84) says that for longitudinal waves, the conduction electron contribution to the conductivity is

$$\sigma_{\text{el}} = \frac{i\omega\chi_c}{q^2}. \quad (27.91)$$

Equation (27.91) looks simple until one contemplates writing χ_c out in its full splendor. Evaluation of Eq. (20.76) can be simplified in two steps:

1. Only the low-frequency susceptibility is needed. The reason is that electrons will only experience an attractive interaction when they oscillate at frequencies characteristic of phonons. As shown in Figure 20.1, characteristic phonon energies and frequencies are around two orders of magnitude less than characteristic electron energies and frequencies, so χ_c can be evaluated at $\omega = 0$, allowing the electrons to respond adiabatically to the phonons.
2. Only the long wavelength susceptibility is needed. When $\omega \rightarrow 0$, Problem 20.6 shows that χ_c takes the form

$$\chi_c = -\frac{me^2}{\pi^2\hbar^2} \frac{(4k_F^2 - q^2) \log\left(\frac{q + 2k_F}{2k_F - q}\right) + 4k_F q}{8q} \quad (27.92)$$

and that in the low q limit

$$\chi_c = -\frac{me^2 k_F}{\pi^2\hbar^2} \equiv -\frac{\kappa_c^2}{4\pi}. \quad (27.93)$$

There seems not to be much justification for going to the low q limit because the interest will be in q in the neighborhood of k_F . However, the plot of $\chi_c(q)/\chi_c(0)$ in Figure 27.9 shows that the error is hardly significant, because χ changes only by 10% by the time q reaches k_F .

The final result is that the contribution of electrons to the conductivity is

$$\sigma_{\text{el}} = \frac{\omega\kappa_c^2}{4\pi i q^2}. \quad (27.94)$$

Ion Current. Section 22.3.2 showed how an electron moving in a polar solid would cause ions to move. The analysis relevant for superconductivity is very similar, but it must be modified slightly because the important phonons are acoustic rather than optical.

Returning to Eq. (22.18), suppose that ionic displacements \vec{u} respond to applied electric fields by obeying

$$\vec{u} = \frac{-e^* \vec{E}}{M(\omega^2 - \bar{\omega}_q^2)}. \quad (27.95)$$

For small \vec{q} , \vec{E} should probably be replaced by \vec{E}_{cell} , but in view of other uncertainties the replacement is pedantic.

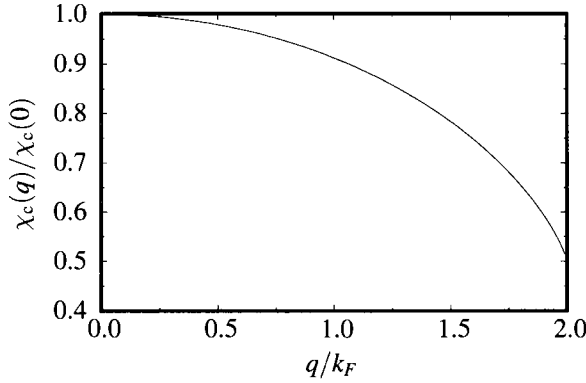


Figure 27.9. Charge susceptibility χ_c , showing that the large wavelength limit $q \rightarrow 0$ is a satisfactory approximation for q as large as k_F .

In Section 22.3.2 the bare phonon frequency $\bar{\omega}$ was constant; now take it to depend upon \vec{q} , and in particular to vanish for $\vec{q} = 0$. The function $\bar{\omega}_{\vec{q}}$ is assumed to be known, but its particular form will not be important in what follows here. Observing that

$$\vec{j}_{\text{ion}}(\vec{q}, \omega) = -i\omega ne^* \vec{u} \tag{27.96}$$

and defining

$$\omega_{\text{pi}}^2 = \frac{4\pi ne^{*2}}{M}, \quad \text{This is an ionic plasma frequency.} \tag{27.97}$$

the conductivity σ_{ion} of the ions is

$$\sigma_{\text{ion}} = -\frac{\omega}{4\pi i} \frac{\omega_{\text{pi}}^2}{\omega^2 - \bar{\omega}_{\vec{q}}^2}. \tag{27.98}$$

Electrons and Ions Together. When one finally combines electronic and ionic currents, the total conductivity is

$$\sigma(\vec{q}, \omega) = \frac{\omega}{4\pi i} \left[\frac{\kappa_c^2}{q^2} - \frac{\omega_{\text{pi}}^2}{\omega^2 - \bar{\omega}_{\vec{q}}^2} \right] \quad \text{Combine Eqs. (27.98) and (27.94).} \tag{27.99}$$

$$\Rightarrow \epsilon(\vec{q}, \omega) = 1 + \frac{\kappa_c^2}{q^2} - \frac{\omega_{\text{pi}}^2}{\omega^2 - \bar{\omega}_{\vec{q}}^2}. \quad \text{See Eq. (20.14).} \tag{27.100}$$

Just as in polar solids, $\bar{\omega}_{\vec{q}}$ does not correspond to an actual resonant frequency. The frequency $\omega_{\vec{q}}$ of longitudinal phonons is given by demanding that ϵ vanish, and it is

$$\omega_{\vec{q}}^2 = \bar{\omega}_{\vec{q}}^2 + \frac{q^2 \omega_{\text{pi}}^2}{q^2 + \kappa_c^2}. \quad \text{See Eq. (20.23). Notice that if electrons were not available to screen the ions, the longitudinal phonons would oscillate at the plasma frequency } \omega_{\text{pi}} \text{ as } \vec{q} \rightarrow 0, \text{ rather than producing the expected acoustic mode.} \tag{27.101}$$

Using this definition, a bit of algebra shows that

$$\frac{1}{\epsilon(\vec{q}, \omega)} = \frac{q^2}{q^2 + \kappa_c^2} \left[\frac{\omega^2 - \bar{\omega}_{\vec{q}}^2}{\omega^2 - \omega_{\vec{q}}^2} \right]. \quad (27.102)$$

Effective Interaction. Suppose now that two electrons move through a solid whose dielectric function is given by Eq. (27.102). If they have wave vectors \vec{k}_1 and \vec{k}_2 and energies \mathcal{E}_1 and \mathcal{E}_2 , then the charge density of the two of them oscillates as

$$|\psi_1 e^{i\vec{k}_1 \cdot \vec{r} - \mathcal{E}_1 t/\hbar} + \psi_2 e^{i\vec{k}_2 \cdot \vec{r} - \mathcal{E}_2 t/\hbar}|^2 \propto \text{const.} + \cos[(\vec{k}_1 - \vec{k}_2) \cdot \vec{r} - (\mathcal{E}_1 - \mathcal{E}_2)t/\hbar]. \quad (27.103)$$

Their effective interaction is therefore

$$U_{\text{eff}} = \frac{4\pi e^2}{\epsilon(\vec{q}, \omega) q^2} = \frac{4\pi e^2}{q^2 + \kappa_c^2} \left[1 + \frac{\omega_{\vec{q}}^2 - \bar{\omega}_{\vec{q}}^2}{\omega^2 - \omega_{\vec{q}}^2} \right] \quad (27.104a)$$

with

$$\vec{q} = \vec{k}_1 - \vec{k}_2 \quad \text{and} \quad \hbar\omega = \mathcal{E}_1 - \mathcal{E}_2. \quad (27.104b)$$

The essential point to observe in Eqs. (27.104) is that when $\bar{\omega}_{\vec{q}} < \omega < \omega_{\vec{q}}$, the effective interaction becomes negative, and the two electrons attract one another.

Second Quantized Interaction.

To see how to express the interaction of electrons in second quantized notation, suppose that electrons have an effective potential $U_{\text{eff}}(\vec{r} - \vec{r}')$ in position space. Use plane waves $\exp[i\vec{k} \cdot \vec{r}]/\sqrt{V}$ as the basis states in Eq. (C.10). Then the interaction becomes

$$\hat{U}_{\text{eff}} = \frac{1}{2} \sum_{\vec{k}\vec{k}'\vec{k}''\vec{k}'''} \hat{c}_{\vec{k}}^\dagger \hat{c}_{\vec{k}'}^\dagger \hat{c}_{\vec{k}''} \hat{c}_{\vec{k}'''} U_{\text{eff}}(\vec{r}_1 - \vec{r}_2) |\vec{k}''\vec{k}'''\rangle \quad (27.105)$$

The matrix element becomes

$$\frac{1}{V^2} \int d\vec{r} d\vec{r}' d\vec{r}'' d\vec{r}''' \left[e^{-i\vec{k} \cdot \vec{r} - i\vec{k}' \cdot \vec{r}' + i\vec{k}'' \cdot \vec{r}'' + i\vec{k}''' \cdot \vec{r}'''} U_{\text{eff}}(\vec{r} - \vec{r}') \right. \\ \left. \times \delta(\vec{r} - \vec{r}') \delta(\vec{r}'' - \vec{r}''') \right] \quad (27.106)$$

$$= \frac{(2\pi)^3}{V^2} \delta(\vec{k}'' + \vec{k}''' - \vec{k} - \vec{k}') U_{\text{eff}}(\vec{k}'' - \vec{k}) \quad (27.107)$$

$$= \frac{1}{V} \delta_{\vec{k}'' + \vec{k}''' - \vec{k} - \vec{k}'} U_{\text{eff}}(\vec{k}'' - \vec{k}) \quad \text{Viewing } \vec{k} \text{ states as discrete. See Eq. (6.12)} \quad (27.108)$$

The fact that the interaction depends only upon the distance $\vec{r}_1 - \vec{r}_2$ between particles enforces conservation of momentum when viewed in \vec{k} space. Thus, returning to Eq. (27.104), and including electron spin, one has the effective interaction

$$\hat{\mathcal{H}} = \frac{1}{2} \frac{1}{V} \sum_{\substack{\vec{q}\vec{k}\vec{k}' \\ \sigma\sigma'}} \frac{4\pi e^2}{q^2 + \kappa_c^2} \left[1 + \frac{\omega_{\vec{q}}^2 - \bar{\omega}_{\vec{q}}^2}{\omega^2 - \omega_{\vec{q}}^2} \right] \hat{c}_{\vec{k}\sigma}^\dagger \hat{c}_{\vec{k}'\sigma'}^\dagger \hat{c}_{\vec{k} - \vec{q}\sigma} \hat{c}_{\vec{k} + \vec{q}\sigma}. \quad (27.109)$$

27.3.2 Instability of the Normal State: Cooper Problem

Cooper (1956) performed the first calculation showing how a small attractive interaction between electrons destabilizes the conventional electronic ground state. The idea is the following. Consider a state containing N particles that occupy \vec{k} states up to a Fermi level. This state will be denoted by $|G\rangle$, and the first guess is that it is the ground state of the Hamiltonian, or at least close to it. Formally,

$$|G\rangle = \prod_{k < k_F} c_{\vec{k}}^\dagger |\emptyset\rangle. \tag{27.110}$$

Now imagine adding two new particles to $|G\rangle$. One possibility is that the two new particles seek out the lowest-lying unfilled \vec{k} states and occupy them. Solutions of this sort certainly exist. But in the case where the particles interact by an attractive potential, there is another possibility; they may form a bound state that in no respect resembles the independent particles. Such a Cooper pair is at the heart of superconductivity. The calculation will show that states of the form (27.110) are unstable. While identification of an instability is never sufficient to show where the unstable system will terminate its travels, the nature of the instability also gives sufficient clues that the problem can be recast and solved completely.

Consider first a simplified treatment that leaves open a few nagging questions, but makes the development much clearer than the proper formalism. The Schrödinger equation for two electrons added on top of a Fermi sea of N electrons, occupying \vec{k} states up to k_F is

$$\left[\frac{-\hbar^2 \nabla_1^2}{2m} + \frac{-\hbar^2 \nabla_2^2}{2m} + U(\vec{r}_1 - \vec{r}_2) \right] \Psi(\vec{r}_1, \vec{r}_2) = \mathcal{E} \Psi(\vec{r}_1, \vec{r}_2), \tag{27.111}$$

subject to the constraint that $\Psi(\vec{r}_1, \vec{r}_2)$ contain no Fourier components with \vec{k} less than k_F . To simplify matters, assume that the pair of electrons described by Ψ has no net momentum and can therefore be written in the form

$$\Psi(\vec{r}_1, \vec{r}_2) = \sum_{k' > k_F} \Psi_{\vec{k}'} e^{-i\vec{k}' \cdot (\vec{r}_1 - \vec{r}_2)}. \tag{27.112}$$

Placing Eq. (27.112) into Eq. (27.111), multiplying by $\exp[i\vec{k} \cdot (\vec{r}_1 - \vec{r}_2)]$ and integrating over $\vec{r}_1 - \vec{r}_2$ gives

$$(2\epsilon_{\vec{k}} - \mathcal{E}) \Psi_{\vec{k}} + \sum_{k' > k_F} U_{\vec{k}\vec{k}'} \Psi_{\vec{k}'} = 0. \tag{27.113}$$

$\epsilon_{\vec{k}} = \hbar^2 k^2 / 2m$ is the energy of a single-particle state. The potential $U_{\vec{k}\vec{k}'}$ is $\langle \vec{k} | \hat{U} | \vec{k}' \rangle$. Because $|\vec{k}\rangle$ is a normalized plane wave $\exp[i\vec{k} \cdot \vec{r}] / \sqrt{\mathcal{V}}$, $U_{\vec{k}\vec{k}'}$ is $1/\mathcal{V}$ times the conventional Fourier transform of the potential $U(\vec{r})$.

In order to make further analytical progress, one must make some assumption about the form of U . An assumption that is particularly suited to analytical progress is

$$U_{\vec{k}\vec{k}'} = -\frac{U_0}{\mathcal{V}} \theta(\hbar\omega - |\mathcal{E}_F - \epsilon_{\vec{k}}|) \theta(\hbar\omega - |\mathcal{E}_F - \epsilon_{\vec{k}'}|). \tag{27.114}$$

Technically, the form of potential U assumed in Eq. (27.111) is not consistent with this sort of behavior in \vec{k} space. One could retroactively modify Eq. (27.111) to avoid being upset by this. The constant U_0 has dimensions of energy times volume, and it is derived from the Fourier transform of the potential $U(\vec{r})$.

When one lets k_{\max} be the largest value of k for which $\hbar\omega - |\mathcal{E}_F - \epsilon_{\vec{k}}|$ is positive, Eq. (27.113) takes the form

$$(2\epsilon_{\vec{k}} - \mathcal{E})\Psi_{\vec{k}} = \frac{U_0}{\mathcal{V}} \sum_{\vec{k}' > k_F}^{k_{\max}} \Psi_{\vec{k}'}. \quad \text{True so long as } k < k_{\max}; \text{ otherwise the right hand side vanishes.} \quad (27.115)$$

One can construct a host of solutions to Eq. (27.115) by picking any two wave vectors \vec{k}_a and \vec{k}_b whose magnitudes (above k_F) are the same, setting

$$\mathcal{E} = 2\epsilon_{\vec{k}_a}, \quad (27.116)$$

and taking the only nonzero components of Ψ to be

$$\Psi_{\vec{k}_a} = -\Psi_{\vec{k}_b} = \frac{1}{\sqrt{2}}. \quad (27.117)$$

Solutions of this type correspond to adding two particles to a normal Fermi liquid. If, however, one assumes that $\mathcal{E} - 2\epsilon_{\vec{k}} \neq 0$, then by summing Eq. (27.115) over \vec{k} one gets

$$\sum_{\vec{k} > k_F}^{k_{\max}} \Psi_{\vec{k}} = \sum_{\vec{k} > k_F}^{k_{\max}} \frac{U_0}{\mathcal{V}} \frac{1}{(2\epsilon_{\vec{k}} - \mathcal{E})} \sum_{\vec{k}' > k_F}^{k_{\max}} \Psi_{\vec{k}'}. \quad (27.118)$$

$$\Rightarrow 1 = \sum_{\vec{k}}^{k_{\max}} \frac{U_0}{(2\epsilon_{\vec{k}} - \mathcal{E})\mathcal{V}} \quad (27.119)$$

$$\approx \int_{\mathcal{E}_F}^{\mathcal{E}_F + \hbar\omega} d\epsilon \frac{D(\mathcal{E}_F)}{2} \frac{U_0}{2\epsilon - \mathcal{E}} \quad \text{The factor of } 1/2 \text{ is needed because there is no sum over spin.} \quad (27.120)$$

$$\Rightarrow 1 = \frac{1}{4} D(\mathcal{E}_F) U_0 \ln\left(\frac{2\mathcal{E}_F + 2\hbar\omega - \mathcal{E}}{2\mathcal{E}_F - \mathcal{E}}\right). \quad (27.121)$$

Assuming that $U_0 D(\mathcal{E}_F)$ is much less than one, an approximate solution of Eq. (27.121) is

$$\mathcal{E} = 2\mathcal{E}_F - (2\mathcal{E}_{\max} - 2\mathcal{E}_F) \exp\left[-\frac{4}{D(\mathcal{E}_F)U_0}\right]. \quad (27.122)$$

The energy of the bound state is only slightly smaller than the energy of two additional particles at the Fermi level. However, the wave function is quite different from the form in Eq. (27.117); it is

$$\Psi_{\vec{k}} = \frac{U_0}{(2\epsilon_{\vec{k}} - \mathcal{E})\mathcal{V}} \sum_{\vec{k}' > k_F}^{k_{\max}} \Psi_{\vec{k}'}. \quad (27.123)$$

This wave function is rotationally invariant. Because the two electrons making up the wave function must be antisymmetric, they must be multiplied by an antisymmetric spin wave function in order to satisfy the Pauli principle. The conclusion

is that two electrons in an antisymmetric spin state, and with opposite \vec{k} vectors so as to have no net momentum, can form a bound pair if they are added on top of collection of other electrons that are assumed not to have formed pairs of this type.

But then the assumption that the other electrons have not already formed bound pairs is clearly wrong, and one has to start all over at the beginning. However, before doing so, it is worth recasting the Cooper problem in the language of second quantization, to set the stage for the Hamiltonian actually used to study superconductivity.

27.3.3 Self-Consistent Ground State

Model Hamiltonian. Given the observation that pairs of electrons with opposite wave vectors and spins seem capable of binding into pairs, Bardeen, Cooper, and Schrieffer (1957) proposed the *BCS model Hamiltonian*, which abstracts from all the preceding complicated discussion a simple solvable model. It is

$$\hat{\mathcal{H}}_{\text{BCS}} = \sum_{\vec{k}, \sigma} \epsilon_{\vec{k}} \hat{c}_{\vec{k}\sigma}^\dagger \hat{c}_{\vec{k}\sigma} + \sum_{\vec{k}\vec{k}'} U_{\vec{k}\vec{k}'} \hat{c}_{\vec{k}\uparrow}^\dagger \hat{c}_{-\vec{k}\downarrow}^\dagger \hat{c}_{-\vec{k}'\downarrow} \hat{c}_{\vec{k}'\uparrow}. \tag{27.124}$$

A glaring departure from Eq. (27.109) is the absence of the sum on \vec{q} . Nonzero values of \vec{q} correspond to electron pairs whose center of mass momentum is nonzero. These play no role in the ground state, so the \vec{q} sum can be omitted from this Hamiltonian. Later, when interaction with external fields is considered, the \vec{q} sum will have to be brought back.

The matrix elements $U_{\vec{k}\vec{k}'}$ will not be needed for some time. In model calculations they can freely be altered into any form that decays for large \vec{k} and that is negative for some \vec{k} and \vec{k}' near the Fermi surface. With use of Eq. (27.114), the problem can be solved exactly, and when need arises, this form of the potential will be adopted.

The Cooper problem suggests that the Fermi sea is unstable toward the creation of correlated pairs of electrons. How can one create a state that has definite numbers of electrons correlated in pairs? A simple guess is that the state is of the form

$$|\Phi_N\rangle = \left[\sum_{\vec{k}} \hat{c}_{\vec{k}\uparrow}^\dagger \hat{c}_{-\vec{k}\downarrow}^\dagger g_{\vec{k}} \right]^N |\emptyset\rangle, \tag{27.125}$$

which creates all possible pairs of $2N$ particles with various weights. If $g_{\vec{k}} = 1$ up to the Fermi surface and is zero thereafter, then the state Φ_N is precisely a Bloch state. The only terms in the product to survive are those that create precisely one sample of each type of particle; there are $N!$ such terms, so one must divide through by this factor to normalize the state. Bardeen, Cooper, and Schrieffer found that for formal reasons this type of state is inconvenient to work with. The difficulties are similar to those that arise in classical statistical mechanics. They make it advantageous to work in the grand canonical rather than the canonical ensemble, and are ameliorated by considering

$$|\Phi\rangle \equiv \sum_N \frac{1}{N!} |\Phi_N\rangle \tag{27.126}$$

$$= \sum_N \frac{1}{N!} \left[\sum_{\vec{k}} \hat{c}_{\vec{k}\uparrow}^\dagger \hat{c}_{-\vec{k}\downarrow}^\dagger g_{\vec{k}} \right]^N |\emptyset\rangle. \quad (27.127)$$

The constants $g_{\vec{k}}$ could also depend upon N . Neglecting this dependence is justified by noting that the sum will be dominated by a narrow range of N and assuming that $g_{\vec{k}}$ does not vary appreciably with N in this range.

Coherent States. Equation (27.127) can be rewritten as

$$|\Phi\rangle = \exp\left[\sum_{\vec{k}} g_{\vec{k}} \hat{c}_{\vec{k}\uparrow}^\dagger \hat{c}_{-\vec{k}\downarrow}^\dagger\right] |\emptyset\rangle. \quad (27.128)$$

(27.128) is a *coherent state*, similar to the states that allow one to find the classical limit of quantum optics. Coherent states have pleasant formal properties that offset the fact they they have indefinite particle number. For fermion operators, only the zero and first powers survive in the exponential, so one can finally rewrite Eq. (27.128) as

$$|\Phi\rangle = \prod_{\vec{k}} \left[1 + g_{\vec{k}} \hat{c}_{\vec{k}\uparrow}^\dagger \hat{c}_{-\vec{k}\downarrow}^\dagger \right] |\emptyset\rangle \equiv \hat{\Phi} |\emptyset\rangle. \quad (27.129)$$

The variational procedure of Section B.2 dictates that given a trial state and a Hamiltonian, one has to take the expectation value of the Hamiltonian and try to minimize it with respect to all of the parameters in the trial wave function. The wave function does not have definite particle number, which means that instead of enforcing the constraint that $|\Phi\rangle$ be normalized, it is necessary to enforce the constraint that the average particle number be maintained at N . This constraint is maintained by introducing a Lagrange multiplier that is easily identified as the chemical potential μ .

Here are several identities that make it possible to manipulate the coherent state.

1. The normalization of the state is given by

$$\langle \Phi | \Phi \rangle = \prod_{\vec{k}} \left(1 + |g_{\vec{k}}|^2 \right) = \mathcal{N}^2. \quad (27.130)$$

2. Taking the expectation of the operators which destroy a pair of electrons, one obtains

$$b_{\vec{k}} = \frac{1}{\mathcal{N}^2} \langle \Phi | \hat{c}_{-\vec{k}\downarrow} \hat{c}_{\vec{k}\uparrow} | \Phi \rangle = \frac{g_{\vec{k}}}{1 + |g_{\vec{k}}|^2}, \quad (27.131)$$

because one of the factors of $1 + |g_{\vec{k}}|^2$ disappears and is replaced by $g_{\vec{k}}$. Similarly,

$$\frac{1}{\mathcal{N}^2} \langle \Phi | \hat{c}_{\vec{k}\uparrow}^\dagger \hat{c}_{-\vec{k}\downarrow}^\dagger \hat{c}_{-\vec{k}'\downarrow} \hat{c}_{\vec{k}'\uparrow} | \Phi \rangle = b_{\vec{k}}^* b_{\vec{k}'}. \quad (27.132)$$

3. The number of particles of a given spin in the wave function equals the number of pairs containing that particle: formally, one has

$$\left[\sum_{\sigma} \hat{n}_{\vec{k}\sigma}, \hat{\Phi} \right] = \left[g_{\vec{k}} \hat{c}_{\vec{k}\uparrow}^\dagger \hat{c}_{-\vec{k}\downarrow}^\dagger + g_{-\vec{k}} \hat{c}_{-\vec{k}\uparrow}^\dagger \hat{c}_{\vec{k}\downarrow}^\dagger \right] \hat{\Phi}. \quad (27.133)$$

Expectation Value of Hamiltonian. Identities (27.130) through (27.133) make it possible to evaluate the expectation value of the Hamiltonian (27.124). The kinetic energy expectation value comes from Eq. (27.133), and then Eq. (27.131):

$$\frac{1}{\mathcal{N}^2} \langle \Phi | \sum_{\sigma} \hat{n}_{\vec{k}\sigma} | \Phi \rangle = \frac{1}{\mathcal{N}^2} \langle \Phi | \left(g_{\vec{k}} \hat{c}_{\vec{k}\uparrow}^{\dagger} \hat{c}_{-\vec{k}\downarrow}^{\dagger} + g_{-\vec{k}} \hat{c}_{-\vec{k}\uparrow}^{\dagger} \hat{c}_{\vec{k}\downarrow}^{\dagger} \right) | \Phi \rangle \quad (27.134)$$

$$\Rightarrow \sum_{\sigma} n_{\vec{k}\sigma} = g_{\vec{k}} b_{\vec{k}}^* + g_{-\vec{k}} b_{-\vec{k}}^*. \quad (27.135)$$

Equation (27.132) already records the matrix element needed for the potential term in the BCS Hamiltonian. Therefore, the expectation value of Eq. (27.124), including the Lagrange multiplier μ to enforce particle number, is

$$\langle \Phi | \hat{\mathcal{H}}_{\text{BCS}} - \mu N | \Phi \rangle = \sum_{\vec{k}} 2 (\epsilon_{\vec{k}} - \mu) g_{\vec{k}} b_{\vec{k}}^* + \sum_{\vec{k}\vec{k}'} U_{\vec{k}\vec{k}'} b_{\vec{k}}^* b_{\vec{k}'}. \quad (27.136)$$

Varying Parameters in Trial State. In order to minimize Eq. (27.136) with respect to the parameters $g_{\vec{k}}$, take the derivative with respect to $g_{\vec{q}}^*$. Noting that

$$\frac{\partial b_{\vec{k}}^*}{\partial g_{\vec{k}}^*} = \frac{1}{(1 + |g_{\vec{k}}|^2)^2}; \quad \frac{\partial b_{\vec{k}}}{\partial g_{\vec{k}}^*} = -\frac{g_{\vec{k}}^2}{(1 + |g_{\vec{k}}|^2)^2}, \quad (27.137)$$

one has

$$\frac{2(\epsilon_{\vec{q}} - \mu) g_{\vec{q}}}{(1 + |g_{\vec{q}}|^2)^2} + \sum_{\vec{k}\vec{k}'} \frac{U_{\vec{k}\vec{k}'}}{(1 + |g_{\vec{q}}|^2)^2} \left[b_{\vec{k}} \delta_{\vec{k}\vec{q}} - b_{\vec{k}}^* g_{\vec{q}}^2 \delta_{\vec{q}\vec{k}'} \right] = 0. \quad (27.138)$$

It is conventional to define the *gap function*

$$\Delta_{\vec{k}} = - \sum_{\vec{k}'} U_{\vec{k}\vec{k}'} b_{\vec{k}'}, \quad (27.139)$$

in terms of which Eq. (27.138) becomes

$$0 = 2 (\epsilon_{\vec{q}} - \mu) g_{\vec{q}} - \Delta_{\vec{q}} + g_{\vec{q}}^2 \Delta_{\vec{q}}^* \quad \text{Use the fact that } U_{\vec{k}\vec{k}'} = U_{\vec{k}'\vec{k}}^*. \quad (27.140)$$

$$\Rightarrow g_{\vec{k}} = \frac{\mathcal{E}_{\vec{k}} - (\epsilon_{\vec{k}} - \mu)}{\Delta_{\vec{k}}^*}, \quad (27.141)$$

with

$$\mathcal{E}_{\vec{k}} = \sqrt{(\epsilon_{\vec{k}} - \mu)^2 + |\Delta_{\vec{k}}|^2}. \quad (27.142)$$

The energy $\mathcal{E}_{\vec{k}}$ will emerge as the energy of an excitation above the ground state indexed by \vec{k} . It is always positive, and is shown in Figure 27.10. With a little algebra, it follows that

$$b_{\vec{k}} = \frac{g_{\vec{k}}}{1 + |g_{\vec{k}}|^2} = \frac{\Delta_{\vec{k}}}{2\mathcal{E}_{\vec{k}}}. \quad (27.143)$$

Chemical Potential. To calculate physical quantities, it is necessary to determine the chemical potential μ . Despite the fact that electrons occupy a complicated correlated state, the Fermi energy can still be defined by

$$N = 2 \sum_{\vec{k}} \theta(\mathcal{E}_F - \epsilon_{\vec{k}}) = \int_0^{\mathcal{E}_F} d\epsilon D(\epsilon), \quad (27.144)$$

and the chemical potential turns out to equal \mathcal{E}_F . To see why, recall that the chemical potential is determined implicitly from the constraint

$$N = \sum_{\vec{k}\sigma} g_{\vec{k}}^* b_{\vec{k}} = \sum_{\vec{k}\sigma} \frac{1}{2} \left[1 - \frac{\epsilon_{\vec{k}} - \mu}{\mathcal{E}_{\vec{k}}} \right] \quad \text{See Eq. (27.135), and Figure 27.10.} \quad (27.145)$$

$$= \sum_{\vec{k}\sigma} \frac{1}{2} \left[1 - \frac{\epsilon_{\vec{k}} - \mu}{\sqrt{(\epsilon_{\vec{k}} - \mu)^2 + |\Delta|^2}} \right] \quad (27.146)$$

$$= \int d\epsilon \frac{D(\epsilon)}{2} \left[1 - \frac{\epsilon - \mu}{\sqrt{(\epsilon - \mu)^2 + |\Delta|^2}} \right] \quad (27.147)$$

$$= \int d\epsilon \left[\int^{\epsilon} d\epsilon' D(\epsilon') \right] \frac{1}{2} \frac{\partial}{\partial \epsilon} \frac{\epsilon - \mu}{\sqrt{(\epsilon - \mu)^2 + |\Delta|^2}} \quad (27.148)$$

$$= \int d\epsilon \left[\int^{\mu} d\epsilon' D(\epsilon') \right] \frac{1}{2} \frac{\partial}{\partial \epsilon} \frac{\epsilon - \mu}{\sqrt{(\epsilon - \mu)^2 + |\Delta|^2}} + \mathcal{O}(\Delta/\mathcal{E}_F)^2 \quad (27.149)$$

See the Sommerfeld expansion in Section 6.5.

$$= \left[\int^{\mu} d\epsilon' D(\epsilon') \right] = N + D(\mathcal{E}_F)(\mu - \mathcal{E}_F) \quad (27.150)$$

$$\Rightarrow \mu = \mathcal{E}_F. \quad \text{Use Eq. (27.144).} \quad (27.151)$$

Gap Equation. From the definition of $\Delta_{\vec{k}}$ it follows that

$$\Delta_{\vec{k}} = - \sum_{\vec{k}'} U_{\vec{k}\vec{k}'} \frac{\Delta_{\vec{k}'}}{2\mathcal{E}_{\vec{k}'}}. \quad (27.152)$$

Equation (27.152) is the *gap equation* at zero temperature. It can be solved analytically if one assumes the simple separable potential given in Eq. (27.114). Then

$$\Delta_{\vec{k}} = \theta(\hbar\omega - |\epsilon_{\vec{k}} - \mathcal{E}_F|) \frac{U_0}{\mathcal{V}} \sum_{\vec{k}'} \frac{\Delta_{\vec{k}'}}{2\sqrt{(\epsilon_{\vec{k}'} - \mu)^2 + |\Delta_{\vec{k}'}|^2}}. \quad (27.153)$$

The step function inside the sum need not be written out explicitly, because the functional form of $\Delta_{\vec{k}}$ is

$$\Delta_{\vec{k}} = \Delta \theta(\hbar\omega - |\epsilon_{\vec{k}} - \mathcal{E}_F|). \quad (27.154)$$

To determine the remaining constant Δ , assume that $\Delta_{\vec{k}}$ is not zero for all \vec{k} , so that

$$1 = \sum_{\vec{k}} \frac{1}{V} \theta(\hbar\omega - |\epsilon_{\vec{k}} - \mathcal{E}_F|) \frac{U_0}{2\sqrt{(\epsilon_{\vec{k}} - \mu)^2 + |\Delta|^2}}. \tag{27.155}$$

$$= \int_{\mathcal{E}_F - \hbar\omega}^{\mathcal{E}_F + \hbar\omega} d\epsilon \frac{D(\epsilon)}{2} \frac{U_0}{2\sqrt{(\epsilon - \mathcal{E}_F)^2 + |\Delta|^2}} \quad \begin{array}{l} \text{Because } \mu = \mathcal{E}_F. \text{ Factor of } 1/2 \\ \text{in density of states because there} \\ \text{is no spin sum.} \end{array} \tag{27.156}$$

$$= U_0 \int_0^{\hbar\omega/\Delta} d\zeta \frac{D(\mathcal{E}_F)}{2\sqrt{\zeta^2 + 1}} \tag{27.157}$$

$$= \frac{U_0 D(\mathcal{E}_F)}{2} \sinh^{-1} \frac{\hbar\omega}{\Delta} \tag{27.158}$$

$$\Rightarrow \Delta = 2\hbar\omega \exp \left[-\frac{2}{D(\mathcal{E}_F)U_0} \right]. \quad \begin{array}{l} \text{Correct when } D(\mathcal{E}_F)U_0 \ll 1. \text{ Frequently, } D(\mathcal{E}_F) \\ \text{is denoted instead by } 2N(0), \text{ where } N(0) \text{ is} \\ \text{the density of states of a single spin direction} \\ \text{at the Fermi surface.} \end{array} \tag{27.159}$$

The binding energy Δ that emerges from this calculation differs from the one that appeared in Eq. (27.122) by a factor of 2 inside the exponential. This binding energy is exponentially larger than the binding of an isolated Cooper pair, because all N particles in the wave function are participating in the bound state in a consistent way.

27.3.4 Thermodynamics of Superconductors

The great advantage of working in the grand canonical ensemble is most evident when one wants to do thermodynamics. The grand partition function is

$$Z_{\text{gr}} = \text{Tr} e^{-\beta[\hat{\mathcal{H}}_{\text{BCS}} - \mu\hat{N}]}, \tag{27.160}$$

where the trace is over all sets of Fermi occupation numbers. Because $\hat{\mathcal{H}}_{\text{BCS}}$ is quartic in Fermi operators, the trace cannot be performed in closed form. However, one can get an excellent approximation to the thermodynamics employing a version of mean field theory that is designed to reproduce the results already obtained from coherent states at zero temperature. The expectation value $b_{\vec{k}} = \langle \hat{c}_{-\vec{k}\downarrow} \hat{c}_{\vec{k}\uparrow} \rangle$ is all one needs to understand the ground state. So guess that mean field theory is accomplished by setting

$$\hat{c}_{-\vec{k}\downarrow} \hat{c}_{\vec{k}\uparrow} = b_{\vec{k}} + \left(\hat{c}_{-\vec{k}\downarrow} \hat{c}_{\vec{k}\uparrow} - b_{\vec{k}} \right), \tag{27.161}$$

treating the second term as small, and expanding to first order only in the small quantities. The result of carrying out this procedure is the effective grand partition function

$$Z_{\text{gr}} = \text{Tr} e^{-\beta[\hat{\mathcal{J}}_{\text{eff}} - \mu N]}, \tag{27.162}$$

where

$$\hat{\mathcal{H}}_{\text{eff}} - \mu N = \sum_{\vec{k}\sigma} \hat{n}_{\vec{k}\sigma} (\epsilon_{\vec{k}} - \mu) + \sum_{\vec{k}\vec{k}'} b_{\vec{k}'} U_{\vec{k}\vec{k}'} \hat{c}_{\vec{k}\uparrow}^\dagger \hat{c}_{-\vec{k}\downarrow}^\dagger + b_{\vec{k}}^* U_{\vec{k}'\vec{k}}^* \hat{c}_{-\vec{k}'\downarrow} \hat{c}_{\vec{k}'\uparrow} - b_{\vec{k}}^* b_{\vec{k}'} U_{\vec{k}\vec{k}'} \quad (27.163)$$

$$\equiv \sum_{\vec{k}\sigma} \hat{n}_{\vec{k}\sigma} (\epsilon_{\vec{k}} - \mu) - \sum_{\vec{k}} [\Delta_{\vec{k}} \hat{c}_{\vec{k}\uparrow}^\dagger \hat{c}_{-\vec{k}\downarrow}^\dagger + \Delta_{\vec{k}}^* \hat{c}_{-\vec{k}\downarrow} \hat{c}_{\vec{k}\uparrow}] - \sum_{\vec{k}\vec{k}'} b_{\vec{k}}^* b_{\vec{k}'} U_{\vec{k}\vec{k}'} \quad (27.164)$$

In the ground state, this decomposition was exact; at nonzero temperature it is no longer exact, but provides a very good approximation except exceedingly close to the critical temperature. Because products of no more than two Fermi operators appear now in Eq. (27.164), the trace can be performed exactly by the means used to solve the ideal Fermi gas. First, however, it is necessary to diagonalize the Hamiltonian. The appropriate transformation was introduced by Bogoliubov (1958) and by Valatin (1958). Perform the canonical transformation

$$\hat{c}_{\vec{k}\uparrow} = u_{\vec{k}} \hat{\gamma}_{\vec{k}\uparrow} + v_{\vec{k}}^* \hat{\gamma}_{\vec{k}\downarrow}^\dagger \quad (27.165a)$$

$$\hat{c}_{-\vec{k}\downarrow}^\dagger = -v_{\vec{k}} \hat{\gamma}_{\vec{k}\uparrow} + u_{\vec{k}}^* \hat{\gamma}_{\vec{k}\downarrow}^\dagger. \quad (27.165b)$$

The new operators only obey the correct Fermi commutation relations if

$$|u_{\vec{k}}|^2 + |v_{\vec{k}}|^2 = 1. \quad (27.166)$$

Placing Eqs. (27.165) into Eq. (27.164), one finds

$$\hat{\mathcal{H}}_{\text{eff}} - \mu N = \sum_{\vec{k}} \left[\begin{aligned} & (\epsilon_{\vec{k}} - \mu) \left\{ \begin{aligned} & [u_{\vec{k}}^* \hat{\gamma}_{\vec{k}\uparrow}^\dagger + v_{\vec{k}} \hat{\gamma}_{\vec{k}\downarrow}] [u_{\vec{k}} \hat{\gamma}_{\vec{k}\uparrow} + v_{\vec{k}}^* \hat{\gamma}_{\vec{k}\downarrow}^\dagger] \\ & + [-v_{\vec{k}} \hat{\gamma}_{\vec{k}\uparrow} + u_{\vec{k}}^* \hat{\gamma}_{\vec{k}\downarrow}^\dagger] [-v_{\vec{k}}^* \hat{\gamma}_{\vec{k}\uparrow}^\dagger + u_{\vec{k}} \hat{\gamma}_{\vec{k}\downarrow}] \end{aligned} \right\} \\ & - \Delta_{\vec{k}} [u_{\vec{k}}^* \hat{\gamma}_{\vec{k}\uparrow}^\dagger + v_{\vec{k}} \hat{\gamma}_{\vec{k}\downarrow}] [-v_{\vec{k}} \hat{\gamma}_{\vec{k}\uparrow} + u_{\vec{k}}^* \hat{\gamma}_{\vec{k}\downarrow}^\dagger] \\ & - \Delta_{\vec{k}}^* [-v_{\vec{k}}^* \hat{\gamma}_{\vec{k}\uparrow}^\dagger + u_{\vec{k}} \hat{\gamma}_{\vec{k}\downarrow}] [u_{\vec{k}} \hat{\gamma}_{\vec{k}\uparrow} + v_{\vec{k}}^* \hat{\gamma}_{\vec{k}\downarrow}^\dagger] \\ & - \sum_{\vec{k}'} b_{\vec{k}}^* b_{\vec{k}'} U_{\vec{k}\vec{k}'} \end{aligned} \right] \quad (27.167)$$

Requiring the coefficients of the nondiagonal terms, for example, of $\hat{\gamma}_{\vec{k}\downarrow} \hat{\gamma}_{\vec{k}\uparrow}^\dagger$, to vanish leads to the condition

$$2u_{\vec{k}} v_{\vec{k}} (\epsilon_{\vec{k}} - \mu) + \Delta_{\vec{k}} v_{\vec{k}}^2 - \Delta_{\vec{k}}^* u_{\vec{k}}^2 = 0. \quad (27.168)$$

One has the freedom to choose one of $u_{\vec{k}}$ or $v_{\vec{k}}$ real; choose $u_{\vec{k}}$, so as to write

$$0 = 2\sqrt{1 - |v_{\vec{k}}|^2} v_{\vec{k}} (\epsilon_{\vec{k}} - \mu) + \Delta_{\vec{k}} v_{\vec{k}}^2 - \Delta_{\vec{k}}^* (1 - |v_{\vec{k}}|^2). \quad (27.169)$$

Write $v_{\vec{k}}$ as

$$v_{\vec{k}} = \frac{g_{\vec{k}}^*}{\sqrt{1 + |g_{\vec{k}}|^2}}, \quad (27.170)$$

thus defining $g_{\vec{k}}$. Then Eq. (27.169) becomes

$$0 = 2(\epsilon_{\vec{k}} - \mu)g_{\vec{k}} - \Delta_{\vec{k}} + g_{\vec{k}}^2 \Delta_{\vec{k}}^*. \quad (27.171)$$

So the definition of $g_{\vec{k}}$ is no accident: It satisfies Eq. (27.140) precisely as before. Once this condition is met, the Hamiltonian becomes diagonal. As before,

$$g_{\vec{k}} = \frac{\mathcal{E}_{\vec{k}} - (\epsilon_{\vec{k}} - \mu)}{\Delta_{\vec{k}}^*}. \quad (27.172)$$

For future reference, note that

$$|v_{\vec{k}}|^2 = \frac{\mathcal{E}_{\vec{k}} - (\epsilon_{\vec{k}} - \mu)}{2\mathcal{E}_{\vec{k}}}, \quad |u_{\vec{k}}|^2 = \frac{\mathcal{E}_{\vec{k}} + \epsilon_{\vec{k}} - \mu}{2\mathcal{E}_{\vec{k}}}, \quad v_{\vec{k}}u_{\vec{k}}^* = \frac{\Delta_{\vec{k}}^*}{2\mathcal{E}_{\vec{k}}}. \quad (27.173)$$

Writing out the Hamiltonian in terms of the new operators $\hat{\gamma}$, one finds that

$$\hat{\mathcal{H}}_{\text{eff}} - \mu N = \sum_{\vec{k}} \mathcal{E}_{\vec{k}} \left[\hat{\gamma}_{\vec{k}\uparrow}^\dagger \hat{\gamma}_{\vec{k}\uparrow} + \hat{\gamma}_{\vec{k}\downarrow}^\dagger \hat{\gamma}_{\vec{k}\downarrow} \right] + \sum_{\vec{k}} \left[\epsilon_{\vec{k}} - \mu - \mathcal{E}_{\vec{k}} - \sum_{\vec{k}'} b_{\vec{k}}^* b_{\vec{k}'} U_{\vec{k}\vec{k}'} \right]. \quad (27.174)$$

This expression clearly shows that $\mathcal{E}_{\vec{k}}$ give the energies of excitations above the ground state.

There is still one piece of the puzzle missing, because $\Delta_{\vec{k}}$ has been defined in terms of $b_{\vec{k}}$, but nothing has yet been done to fix $b_{\vec{k}}$. Write

$$b_{-\vec{k}}^* = b_{\vec{k}}^* = \langle \hat{c}_{\vec{k}\uparrow}^\dagger \hat{c}_{-\vec{k}\downarrow}^\dagger \rangle = \langle v_{\vec{k}} u_{\vec{k}}^* (\hat{\gamma}_{\vec{k}\downarrow}^\dagger \hat{\gamma}_{\vec{k}\downarrow}^\dagger - \hat{\gamma}_{\vec{k}\uparrow}^\dagger \hat{\gamma}_{\vec{k}\uparrow}^\dagger) \rangle + \text{terms with } \gamma\gamma \text{ or } \gamma^\dagger\gamma^\dagger. \quad (27.175)$$

This expectation value must be identical with what one expects for noninteracting fermions, because that is what Eq. (27.174) describes. Therefore

$$b_{\vec{k}}^* = v_{\vec{k}} u_{\vec{k}}^* (1 - 2f_{\vec{k}}), \quad (27.176)$$

where

$$f_{\vec{k}} = \frac{1}{e^{\beta\mathcal{E}_{\vec{k}}} + 1} \quad (27.177)$$

is the Fermi function. However, it is an unusual Fermi function. The denominator features $\exp[\beta\mathcal{E}_{\vec{k}}]$, rather than $\exp[\beta(\mathcal{E}_{\vec{k}} - \mu)]$. The formal reason is that although μ is buried inside the definition of $\mathcal{E}_{\vec{k}}$, it does not multiply the quantum operators in Eq. (27.174). Physically, the reason is that $\hat{\gamma}^\dagger$ creates an excited state, but does not change particle number. Because $\mathcal{E}_{\vec{k}}$ is always positive, $f_{\vec{k}}$ reaches its maximum value at the Fermi surface, and it decays to zero when \vec{k} lies either above or below, as shown in Figure 27.10. It describes the occupation probability of holes below the Fermi surface and electrons above the Fermi surface.

Using Eqs. (27.170), (27.166), and (27.172) to determine $u_{\vec{k}}$ and $v_{\vec{k}}$ gives finally that

$$b_{\vec{k}} = \frac{\Delta_{\vec{k}}}{2\mathcal{E}_{\vec{k}}} (1 - 2f_{\vec{k}}) \quad (27.178)$$

$$\Rightarrow \sum_{\vec{k}'} b_{\vec{k}'} U_{\vec{k}\vec{k}'} = -\Delta_{\vec{k}} = \sum_{\vec{k}'} \frac{\Delta_{\vec{k}'}}{2\mathcal{E}_{\vec{k}'}} (1 - 2f_{\vec{k}'}) U_{\vec{k}\vec{k}'}, \quad (27.179)$$

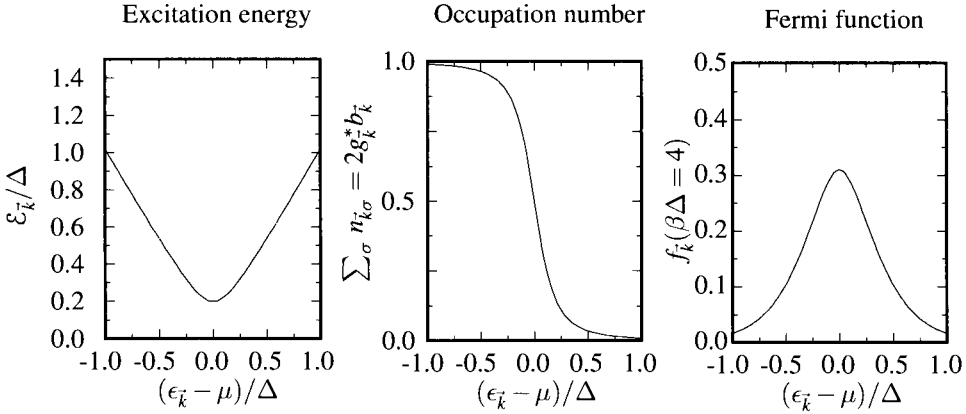


Figure 27.10. Sketches of the excitation energy, occupation number, and Fermi function for the BCS theory of superconductivity.

generalizing the BCS gap equation to nonzero temperatures.

The critical temperature is the highest one for which this equation has a solution for Δ nonzero. So the critical temperature should be given by the solution of the gap equation when Δ is infinitesimal. Using the same simple form of $U_{\vec{k}\vec{k}'}$ from Eq. (27.114) shows that if Δ is almost zero then

$$\Delta = \sum_{\vec{k}} \theta(\hbar\omega - |\mathcal{E}_F - \epsilon_{\vec{k}}|) \frac{\Delta}{2|\epsilon_{\vec{k}} - \mu|} \frac{U_0}{V} (1 - 2f_{\vec{k}}) \tag{27.180}$$

$$\Rightarrow 1 = \int_0^{\beta\hbar\omega} U_0 \frac{D(\mathcal{E}_F)}{2} \frac{dx}{x} \left[1 - \frac{2}{e^x + 1} \right] \quad x = \beta(\epsilon_{\vec{k}} - \mu). \tag{27.181}$$

$$\approx \frac{U_0 D(\mathcal{E}_F)}{2} \left\{ \ln \beta\hbar\omega \left[1 - \frac{2}{e^{\beta\hbar\omega} + 1} \right] + 2 \int_0^\infty dx \ln x \frac{\partial}{\partial x} \frac{1}{e^x + 1} \right\} \tag{27.182}$$

$$\approx \frac{U_0 D(\mathcal{E}_F)}{2} \left\{ \ln(\beta\hbar\omega) + \ln\left(\frac{2\gamma_E}{\pi}\right) \right\}, \tag{27.183}$$

Computations use approximation $\beta\hbar\omega \gg 1$; Eq. (27.184) shows that this is the same as $U_0 D(\mathcal{E}_F) \ll 1$.

where γ_E is Euler’s constant. The final result is that

$$k_B T_c = \hbar\omega \frac{2\gamma_E}{\pi} \exp\left[-\frac{2}{U_0 D(\mathcal{E}_F)}\right], \tag{27.184}$$

and comparing with Eq. (27.159) predicts that the ratio between the gap at zero temperature and the critical temperature takes the universal value

$$\Rightarrow \frac{2\Delta(T=0)}{k_B T_c} = \frac{2\pi}{\gamma_E} = 3.53. \tag{27.185}$$

When the gap Δ is measured by tunneling, this relationship is found to hold to about 30 %, displayed in Table 27.2. Considering the simplicity of the form assumed for $U_{\vec{k}\vec{k}'}$, the agreement is quite acceptable.

Table 27.2. Thermodynamic properties of a variety of superconducting materials

Element	$2\Delta/k_B T$	$(C_s - C_n)/C_n$	Element	$2\Delta/k_B T$	$(C_s - C_n)/C_n$
BCS	3.53	1.43			
Al	2.5–4.2	1.3–1.6	Pb	4.0–4.4	2.7
Cd	3.2–3.4	1.3–1.4	Sn	2.8–4.0	1.6
Ga	3.5	1.4	Ta	3.5–3.7	1.6
Hg	4.0–4.6	2.4	Tl	3.6–3.9	1.5
In	3.4–3.7	1.7	V	3.4–3.5	1.5
La	1.7–3.2	1.5	Zn	3.2–3.4	1.2–1.3
Nb	3.6–3.8	1.9–2.0			

Ratio of energy gap Δ to critical temperature $k_B T$ [Eq. (27.185)] as well as fractional change in specific heat from normal to superconducting state is compared with predictions of Bardeen, Cooper, and Schrieffer. Source: Meservey and Schwartz (1969).

27.3.5 Superconductor in External Magnetic Field

Bogoliubov Hamiltonian. In order to find the behavior of a superconductor placed in an external magnetic field, the model Hamiltonian must be altered: made more complex in one respect, and simpler in another. The complication arises in the form of the electron interactions. Comparing Eqs. (27.109) and (27.124), one sees that a sum over \vec{q} was dropped in moving from the first to the second. The interpretation of \vec{q} is that it corresponds to the center of mass momentum of Cooper pairs. In the superconducting ground state, all the Cooper pairs are stationary, but this assumption is invalid when external fields are applied and supercurrents result. The sum over \vec{q} must be added back in to the Hamiltonian. To keep formal complexity to the minimum, the potential $U_{\vec{k}\vec{k}'}$ will be simplified to the maximum degree and replaced by the constant value $-U_0/\mathcal{V}$. Might such a choice lead to divergences? Equation (27.155) shows that it will not. Instead of that integral being cut off at $\mathcal{E}_F + \hbar\omega$, it would be cut off at $W/2$, where W is the bandwidth, and describes the range of energies where $D(\epsilon)$ is nonzero.

The formulation of superconductivity due to Bogoliubov (1958) therefore begins with the Hamiltonian

$$\hat{H} = \sum_{\vec{k}\vec{k}'\sigma} \epsilon_{\vec{k}\vec{k}'} \hat{c}_{\vec{k}\sigma}^\dagger \hat{c}_{\vec{k}'\sigma} - \sum_{\vec{k}\vec{q}\vec{k}'} \frac{U_0}{\mathcal{V}} \hat{c}_{\vec{k}\uparrow}^\dagger \hat{c}_{\vec{q}-\vec{k}\downarrow}^\dagger \hat{c}_{\vec{q}-\vec{k}'\downarrow} \hat{c}_{\vec{k}'\uparrow}. \tag{27.186}$$

The energy $\epsilon_{\vec{k}\vec{k}'}$ depends upon \vec{k} and \vec{k}' in order to accommodate the possible addition of external potentials.

The pattern by which quartic Hamiltonians are changed to quadratic ones should now be clear. One replaces the product of four fermion operators in the last term with products of two operators times the expectation values of the other two. Let

N_k denote the total number of plane waves \vec{k} , and define

$$\Delta_{\vec{q}} = \sum_{\vec{k}'} \frac{U_0}{\mathcal{V}} \langle \hat{c}_{\vec{q}-\vec{k}'\downarrow} \hat{c}_{\vec{k}'\uparrow} \rangle. \quad (27.187)$$

Then

$$\hat{\mathcal{H}} - \mu N = \sum_{\vec{k}\vec{k}'\sigma} [\epsilon_{\vec{k}\vec{k}'} - \mu\delta_{\vec{k}\vec{k}'}] \hat{c}_{\vec{k}\sigma}^\dagger \hat{c}_{\vec{k}'\sigma} - \sum_{\vec{k}\vec{q}} [\Delta_{\vec{q}}^* \hat{c}_{\vec{q}-\vec{k}\downarrow} \hat{c}_{\vec{k}\uparrow} + \Delta_{\vec{q}} \hat{c}_{\vec{k}\uparrow}^\dagger \hat{c}_{\vec{q}-\vec{k}\downarrow}^\dagger]. \quad (27.188)$$

There should be an extra constant subtracted off, as in the nonzero temperature calculation, but it can be absorbed into the one-particle energy.

In order to focus upon external potentials, the Hamiltonian must be written in terms of \vec{r} rather than \vec{k} . Define

$$\hat{c}_{\vec{r}\sigma} = \sum_{\vec{k}} \frac{e^{-i\vec{k}\cdot\vec{r}}}{\sqrt{N_k}} \hat{c}_{\vec{k}\sigma}, \quad \Delta_{\vec{k}} = \frac{1}{N_k} \sum_{\vec{r}} e^{i\vec{k}\cdot\vec{r}} \Delta_{\vec{r}}, \quad \epsilon_{\vec{k}\vec{k}'} = \frac{1}{N_k} \sum_{\vec{r}\vec{r}'} e^{i\vec{k}\cdot\vec{r} - i\vec{k}'\cdot\vec{r}'} \epsilon_{\vec{r}\vec{r}'}. \quad (27.189)$$

The factor of $1/\sqrt{N_k}$ guarantees that $\hat{c}_{\vec{r}}$ has the right anticommutation relations.

Substituting the final two relations in Eq. (27.189) into Eq. (27.188) and then using the first gives

$$\hat{\mathcal{H}} = \sum_{\vec{r}\vec{r}'\sigma} [\epsilon_{\vec{r}\vec{r}'} - \mu\delta_{\vec{r}\vec{r}'}] \hat{c}_{\vec{r}\sigma}^\dagger \hat{c}_{\vec{r}'\sigma} - \sum_{\vec{r}} [\Delta_{\vec{r}}^* \hat{c}_{\vec{r}\downarrow} \hat{c}_{\vec{r}\uparrow} + \Delta_{\vec{r}} \hat{c}_{\vec{r}\uparrow}^\dagger \hat{c}_{\vec{r}\downarrow}^\dagger]. \quad (27.190)$$

Diagonalizing the Hamiltonian. This Hamiltonian is quadratic, so in principle it can be diagonalized. Let $\gamma_{l\sigma}$ be a linear combination of the \hat{c} 's which diagonalizes the Hamiltonian. In other words, the γ operators are defined by

$$\hat{\mathcal{H}} = \sum_l \mathcal{E}_l [\hat{\gamma}_{l\uparrow}^\dagger \hat{\gamma}_{l\uparrow} + \hat{\gamma}_{l\downarrow}^\dagger \hat{\gamma}_{l\downarrow}]. \quad (27.191)$$

A sufficiently general transformation of the \hat{c} 's is of the form

$$\begin{aligned} \hat{c}_{\vec{r}\uparrow} &= \frac{1}{\sqrt{N_k}} \sum_l u_l(\vec{r}) \hat{\gamma}_{l\uparrow} + v_l^*(\vec{r}) \hat{\gamma}_{l\downarrow}^\dagger \\ \hat{c}_{\vec{r}\downarrow} &= \frac{1}{\sqrt{N_k}} \sum_l u_l(\vec{r}) \hat{\gamma}_{l\downarrow} - v_l^*(\vec{r}) \hat{\gamma}_{l\uparrow}^\dagger. \end{aligned} \quad (27.192)$$

The general transformation would involve four separate functions, but one finds in the course of the calculations that only two of them are independent, and that signs must be chosen in this way for the diagonalization to work.

In order to find equations for u and v note that

$$\begin{aligned} [\mathcal{H}_B, \hat{\gamma}_{l\sigma}] &= -\mathcal{E}_l \hat{\gamma}_{l\sigma} \\ [\mathcal{H}_B, \hat{\gamma}_{l\sigma}^\dagger] &= \mathcal{E}_l \hat{\gamma}_{l\sigma}^\dagger. \end{aligned} \quad (27.193)$$

These are commutators, not anticommutators, and they work as indicated because the product of two identical $\hat{\gamma}$'s is zero.

Next note that

$$[\mathcal{H}_B, \hat{c}_{\vec{r}\uparrow}^\dagger] = \sum_{\vec{r}'} [\epsilon_{\vec{r}\vec{r}'}^* - \mu\delta_{\vec{r}\vec{r}'}] \hat{c}_{\vec{r}'\uparrow}^\dagger - \Delta_{\vec{r}}^* \hat{c}_{\vec{r}\downarrow} \quad \text{Do commutation with } \vec{r}', \text{ then} \quad (27.194a)$$

change \vec{r}' to \vec{r} .

$$[\mathcal{H}_B, \hat{c}_{\vec{r}\downarrow}^\dagger] = \sum_{\vec{r}'} [\epsilon_{\vec{r}\vec{r}'}^* - \mu\delta_{\vec{r}\vec{r}'}] \hat{c}_{\vec{r}'\downarrow}^\dagger + \Delta_{\vec{r}}^* \hat{c}_{\vec{r}\uparrow} \tag{27.194b}$$

$$[\mathcal{H}_B, \hat{c}_{\vec{r}\uparrow}] = - \sum_{\vec{r}'} [\epsilon_{\vec{r}\vec{r}'} - \mu\delta_{\vec{r}\vec{r}'}] \hat{c}_{\vec{r}'\uparrow} + \Delta_{\vec{r}} \hat{c}_{\vec{r}\downarrow}^\dagger \tag{27.194c}$$

Take the complex conjugate of the first two relations.

$$[\mathcal{H}_B, \hat{c}_{\vec{r}\downarrow}] = - \sum_{\vec{r}'} [\epsilon_{\vec{r}\vec{r}'} - \mu\delta_{\vec{r}\vec{r}'}] \hat{c}_{\vec{r}'\downarrow} - \Delta_{\vec{r}} \hat{c}_{\vec{r}\uparrow}^\dagger. \tag{27.194d}$$

Placing the expression for \hat{c} in terms of $\hat{\gamma}$ into any of these four expressions, one finds that the results are consistent only if the minus signs in relations between \hat{c} and $\hat{\gamma}$ are chosen as in Eq. (27.192); matching terms in γ requires that

$$\begin{aligned} u_l(\vec{r})\mathcal{E}_l &= \sum_{\vec{r}'} [\epsilon_{\vec{r}\vec{r}'} - \mu\delta_{\vec{r}\vec{r}'}] u_l(\vec{r}') + v_l(\vec{r})\Delta_{\vec{r}} \\ v_l(\vec{r})\mathcal{E}_l &= - \sum_{\vec{r}'} [\epsilon_{\vec{r}\vec{r}'}^* - \mu\delta_{\vec{r}\vec{r}'}] v_l(\vec{r}') + u_l(\vec{r})\Delta_{\vec{r}}^*. \end{aligned} \tag{27.195}$$

These coupled eigenvalue equations are the *Bogoliubov equations*. The pair potential Δ is given by

$$\Delta_{\vec{r}} = \frac{U_0}{\mathcal{V}} N_k \langle \hat{c}_{\vec{r}\downarrow} \hat{c}_{\vec{r}\uparrow} \rangle = \sum_l \frac{U_0}{\mathcal{V}} u_l(\vec{r}) v_l^*(\vec{r}). \tag{27.196}$$

Interaction with Electromagnetic Fields. The reason to pose the Bogoliubov equations in real space is that external potentials can be incorporated into the matrix $\epsilon_{\vec{r}\vec{r}'}$, which also contains kinetic energy and contains effects of interaction with a lattice or impurities. For a homogeneous system, with no external potential, they reduce exactly to what appeared before in Eq. (27.168). The functions u_l and v_l are just plane waves:

$$u_{\vec{k}}^{(0)}(\vec{r}) = u_{\vec{k}} e^{-i\vec{k}\cdot\vec{r}}, \quad v_{\vec{k}}^{(0)}(\vec{r}) = v_{\vec{k}} e^{-i\vec{k}\cdot\vec{r}}. \text{ Identify the index } l \text{ with } \vec{k}. \tag{27.197}$$

Treating these solutions as the zero-order starting point, the Meissner effect emerges from finding effects of a weak external vector potential. The calculation is a rather elaborate exercise in perturbation theory.

As the vector potential turns on, the plane waves are altered only slightly, so the solutions of the perturbed problem can be indexed by \vec{k} , which takes the place of index l . The problem to be solved is

$$u_{\vec{k}}(\vec{r})\mathcal{E}_{\vec{k}} = \left\{ \frac{1}{2m} \left(-i\hbar\vec{\nabla} + \frac{e\vec{A}}{c} \right)^2 - \mu \right\} u_{\vec{k}}(\vec{r}) + v_{\vec{k}}(\vec{r})\Delta_{\vec{r}} \tag{27.198a}$$

$$v_{\vec{k}}(\vec{r})\mathcal{E}_{\vec{k}} = - \left\{ \frac{1}{2m} \left(i\hbar\vec{\nabla} + \frac{e\vec{A}}{c} \right)^2 - \mu \right\} v_{\vec{k}}(\vec{r}) + u_{\vec{k}}(\vec{r})\Delta_{\vec{r}}^*. \tag{27.198b}$$

Let

$$u_{\vec{k}}(\vec{r}) = u_{\vec{k}}^{(0)}(\vec{r}) + u_{\vec{k}}^{(1)}(\vec{r}) = u_{\vec{k}} e^{-i\vec{k}\cdot\vec{r}} + \sum_{\vec{k}'} e^{-i\vec{k}'\cdot\vec{r}} u_{\vec{k}}^{(1)}(\vec{k}') \tag{27.199a}$$

$$v_{\vec{k}}(\vec{r}) = v_{\vec{k}}^{(0)}(\vec{r}) + v_{\vec{k}}^{(1)}(\vec{r}) = v_{\vec{k}} e^{-i\vec{k}\cdot\vec{r}} + \sum_{\vec{k}'} e^{-i\vec{k}'\cdot\vec{r}} v_{\vec{k}}^{(1)}(\vec{k}'). \tag{27.199b}$$

Treating the vector potential as small, and collecting terms to first order, one has

$$\left(\mathcal{E}_{\vec{k}} - \frac{\hbar^2}{2m} \nabla^2 - \mu\right) v_{\vec{k}}^{(1)}(\vec{r}) - \Delta^* u_{\vec{k}}^{(1)}(\vec{r}) = -\frac{ie\hbar}{2mc} \left(\vec{A} \cdot \vec{\nabla} + \vec{\nabla} \cdot \vec{A}\right) v_{\vec{k}}^{(0)}(\vec{r}) \quad (27.200a)$$

$$\left(\mathcal{E}_{\vec{k}} + \frac{\hbar^2}{2m} \nabla^2 + \mu\right) u_{\vec{k}}^{(1)}(\vec{r}) - \Delta v_{\vec{k}}^{(1)}(\vec{r}) = -\frac{ie\hbar}{2mc} \left(\vec{A} \cdot \vec{\nabla} + \vec{\nabla} \cdot \vec{A}\right) u_{\vec{k}}^{(0)}(\vec{r}). \quad (27.200b)$$

In order to write down Eqs. (27.200), some technical problems have to be solved. The first is that the energy $\mathcal{E}_{\vec{k}} = \mathcal{E}_{\vec{k}}^{(0)} + \mathcal{E}_{\vec{k}}^{(1)}$ might change to first order in \vec{A} , but a change was not included. Problem 6 shows that $\mathcal{E}_{\vec{k}}^{(1)}$ vanishes so long as $\vec{\nabla} \cdot \vec{A} = 0$. In addition, $\Delta_{\vec{r}}$ has been replaced by the constant Δ , although $\Delta_{\vec{r}} = \Delta^{(0)} + \Delta_{\vec{r}}^{(1)}$ should in principle acquire a spatially varying contribution at first order. The demonstration is not straightforward, but $\Delta_{\vec{r}}^{(1)} = 0$ so long as the vector potential is restricted to the *London gauge*, $\vec{\nabla} \cdot \vec{A} = 0$. It is unfortunately not easy to carry out the full calculation in a fashion that is manifestly gauge-invariant.

Substituting Eqs. (27.199) into Eqs. (27.200) and integrating by $\int d\vec{r} \exp[i\vec{k}' \cdot \vec{r}]/\mathcal{V}$, one finds

$$\left(\mathcal{E}_{\vec{k}} + \zeta_{\vec{k}'}\right) v_{\vec{k}}^{(1)}(\vec{k}') - \Delta^* u_{\vec{k}}^{(1)}(\vec{k}') = F_{\vec{k}'\vec{k}} v_{\vec{k}}^{(0)} \quad (27.201a)$$

$$\left(\mathcal{E}_{\vec{k}} - \zeta_{\vec{k}'}\right) u_{\vec{k}}^{(1)}(\vec{k}') - \Delta v_{\vec{k}}^{(1)}(\vec{k}') = F_{\vec{k}'\vec{k}} u_{\vec{k}}^{(0)}, \quad (27.201b)$$

with the unperturbed single-particle energies

$$\zeta_{\vec{k}} = \frac{\hbar^2 k^2}{2m} - \mu, \quad \text{so that } \mathcal{E}_{\vec{k}} = \sqrt{\zeta_{\vec{k}}^2 + |\Delta|^2}, \quad (27.202)$$

and

$$F_{\vec{k}'\vec{k}} = -\frac{e\hbar}{2mc} \int \frac{d\vec{r}'}{\mathcal{V}} e^{i(\vec{k}' - \vec{k}) \cdot \vec{r}'} (\vec{k} + \vec{k}') \cdot \vec{A}(\vec{r}') = F_{\vec{k}\vec{k}'}. \quad (27.203)$$

One can immediately find the explicit expressions

$$v_{\vec{k}}^{(1)}(\vec{k}') = \frac{F_{\vec{k}'\vec{k}}}{\mathcal{E}_{\vec{k}}^2 - \mathcal{E}_{\vec{k}'}^2} \left[(\mathcal{E}_{\vec{k}} - \zeta_{\vec{k}'}) v_{\vec{k}} + \Delta^* u_{\vec{k}} \right] \quad (27.204a)$$

$$u_{\vec{k}}^{(1)}(\vec{k}') = \frac{F_{\vec{k}'\vec{k}}}{\mathcal{E}_{\vec{k}}^2 - \mathcal{E}_{\vec{k}'}^2} \left[(\mathcal{E}_{\vec{k}} + \zeta_{\vec{k}'}) u_{\vec{k}} + \Delta v_{\vec{k}} \right]. \quad (27.204b)$$

The perturbation theory is now finished, but there remains the task of finding the change in physical quantities of interest.

27.3.6 Derivation of Meissner Effect

To see whether the quantum wave function exhibits the Meissner effect, one must look at the response of the current to the vector potential. If the current has a linear response, then the material is superconducting. The current is

$$\vec{j} = -2e \frac{N_k}{\mathcal{V}} \text{Re} \left\langle \hat{c}_{\vec{r}\uparrow}^\dagger \left(\frac{\hat{P}}{m} + \frac{e\vec{A}}{mc} \right) \hat{c}_{\vec{r}\uparrow} \right\rangle \quad (27.205)$$

The factor of 2 is for spin, and the factor of N_k/\mathcal{V} accounts for the fact that there are N_k values of \vec{k} , hence N_k values of \vec{r} which occupy a total volume \mathcal{V} , so each \vec{r} is associated with a volume \mathcal{V}/N_k .

$$= \frac{-e}{\mathcal{V}} \sum_{\vec{k}\vec{k}'} \left\langle \left(u_{\vec{k}'}^*(\vec{r}) \hat{\gamma}_{\vec{k}'\uparrow}^\dagger + v_{\vec{k}'}(\vec{r}) \hat{\gamma}_{\vec{k}'\downarrow} \right) \left(\frac{\hat{P}}{m} + \frac{e\vec{A}}{mc} \right) \left(u_{\vec{k}}(\vec{r}) \hat{\gamma}_{\vec{k}\uparrow} + v_{\vec{k}}^*(\vec{r}) \hat{\gamma}_{\vec{k}\downarrow}^\dagger \right) \right\rangle + \text{c.c.} \tag{27.206}$$

$$= \frac{-e}{\mathcal{V}} \sum_{\vec{k}} v_{\vec{k}}(\vec{r}) \left[\frac{\hbar \vec{\nabla}}{im} + \frac{e\vec{A}}{mc} \right] v_{\vec{k}}^*(\vec{r}) + \text{c.c.} \tag{27.207}$$

The only term that does not annihilate the ground state is $\hat{\gamma}\hat{\gamma}^\dagger$.

Note that

$$\sum_{\vec{k}} v_{\vec{k}} v_{\vec{k}}^* = \frac{1}{2} \sum_{\vec{k}} \frac{\mathcal{E}_{\vec{k}} - \zeta_{\vec{k}}}{\mathcal{E}_{\vec{k}}} = N/2, \tag{27.208}$$

Compare with Eqs. (27.145) and (27.173).

so the current becomes

$$\vec{j} = \vec{j}^1 - \frac{ne^2\vec{A}}{mc}, \tag{27.209}$$

n is the total density of electrons.

where

$$\vec{j}^1 = -e \frac{1}{\mathcal{V}} \sum_{\vec{k}} v_{\vec{k}} \frac{\hbar \vec{\nabla}}{im} v_{\vec{k}}^*(\vec{r}) + \text{c.c.} \tag{27.210}$$

\vec{j}^1 requires further evaluation. To first order in \vec{A} ,

$$\vec{j}^1 = -\frac{e\hbar}{\mathcal{V}m} \sum_{\vec{k}\vec{k}'} v_{\vec{k}} v_{\vec{k}}^{(1)*}(\vec{k}') (\vec{k} + \vec{k}') e^{i(\vec{k}' - \vec{k}) \cdot \vec{r}} + v_{\vec{k}}^* v_{\vec{k}}^{(1)}(\vec{k}') (\vec{k} + \vec{k}') e^{-i(\vec{k}' - \vec{k}) \cdot \vec{r}}. \tag{27.211}$$

Substituting the expression for $v_{\vec{k}}^{(1)}(\vec{k}')$ obtained in Eq. (27.204) and using Eq. (27.173) gives that

$$\vec{j}^1 = \frac{-e\hbar}{m\mathcal{V}} \sum_{\vec{k}\vec{k}'} \left(\vec{k} + \vec{k}' \right) e^{i(\vec{k}' - \vec{k}) \cdot \vec{r}} \frac{F_{\vec{k}'\vec{k}}}{\mathcal{E}_{\vec{k}}^2 - \mathcal{E}_{\vec{k}'}^2} \left[(\mathcal{E}_{\vec{k}} - \zeta_{\vec{k}'}') \left(\frac{\mathcal{E}_{\vec{k}} - \zeta_{\vec{k}}}{2\mathcal{E}_{\vec{k}}} \right) + \frac{\Delta^* \Delta}{2\mathcal{E}_{\vec{k}}} \right] + \left(\vec{k} + \vec{k}' \right) e^{-i(\vec{k}' - \vec{k}) \cdot \vec{r}} \frac{F_{\vec{k}'\vec{k}}^*}{\mathcal{E}_{\vec{k}}^2 - \mathcal{E}_{\vec{k}'}^2} \left[(\mathcal{E}_{\vec{k}} - \zeta_{\vec{k}}) \left(\frac{\mathcal{E}_{\vec{k}} - \zeta_{\vec{k}}}{2\mathcal{E}_{\vec{k}}} \right) + \frac{\Delta \Delta^*}{2\mathcal{E}_{\vec{k}}} \right] \tag{27.212}$$

$$= \frac{-e\hbar}{m\mathcal{V}} \sum_{\vec{k}\vec{k}'} \left(\vec{k} + \vec{k}' \right) e^{i(\vec{k}' - \vec{k}) \cdot \vec{r}} F_{\vec{k}'\vec{k}} L(\zeta_{\vec{k}}, \zeta_{\vec{k}'}'), \tag{27.213}$$

Interchanging \vec{k} and \vec{k}' in the second half of the right-hand side and doing a moderate amount of algebra.

where

$$L(\zeta_{\vec{k}}, \zeta_{\vec{k}'}') = \frac{\mathcal{E}_{\vec{k}} \mathcal{E}_{\vec{k}'}' - \zeta_{\vec{k}} \zeta_{\vec{k}'}' - \Delta^* \Delta}{2(\mathcal{E}_{\vec{k}} + \mathcal{E}_{\vec{k}'}') \mathcal{E}_{\vec{k}} \mathcal{E}_{\vec{k}'}'}. \tag{27.214}$$

Because L depends upon the absolute value of \vec{k} and \vec{k}' only through the energies $\zeta_{\vec{k}}$, one can do the angular integrals over \vec{k} and \vec{k}' . Define

$$\sigma_{\alpha\beta}(\zeta, \zeta', \vec{R}) = \frac{2\pi\hbar}{2\mathcal{V}^2} \left(\frac{e\hbar}{m} \right)^2 \sum_{\vec{k}\vec{k}'} \delta(\zeta_{\vec{k}} - \zeta) \delta(\zeta_{\vec{k}'} - \zeta') (k_\alpha + k'_\alpha) (k_\beta + k'_\beta) e^{i(\vec{k} - \vec{k}') \cdot \vec{R}}. \tag{27.215}$$

Then expanding out $F_{\vec{k}'\vec{k}}$ using Eq. (27.203) gives

$$\vec{j}_\alpha^1(\vec{r}) = \frac{1}{2\pi\hbar c} \sum_\beta \int d\vec{r}' d\zeta d\zeta' L(\zeta, \zeta') \sigma_{\alpha\beta}(\zeta, \zeta', \vec{r} - \vec{r}') A_\beta(\vec{r}'). \quad (27.216)$$

The conductivity σ can be evaluated by defining

$$Q(\zeta, \vec{r}) = \frac{1}{V} \sum_{\vec{k}} \delta(\zeta_{\vec{k}} - \zeta) e^{-i\vec{k}\cdot\vec{r}} \approx \frac{D(\mathcal{E}_F) \sin \sqrt{2m\zeta/\hbar^2} r}{2k_F r}, \quad (27.217)$$

Evaluate energy and wave vector at the Fermi surface, because this is the only place where the coherence factor $L(\zeta, \zeta')$ is much different from zero.

so that

$$\sigma_{\alpha\beta}(\zeta, \zeta', \vec{R}) = -\frac{2\pi\hbar}{2} \left(\frac{e\hbar}{m} \right)^2 \frac{\partial}{\partial a_\alpha} \frac{\partial}{\partial a_\beta} Q(\zeta, \vec{R} - \vec{a}) Q(\zeta', -(\vec{R} + \vec{a})) \Big|_{\vec{a}=0} \quad (27.218)$$

$$\approx e^2 \frac{v_F}{2\pi} D(\mathcal{E}_F) \frac{R_\alpha R_\beta}{R^4} \cos \left[\frac{(\zeta - \zeta')R}{\hbar v_F} \right]. \quad (27.219)$$

In taking the derivatives with respect to a_α or a_β , keep only the largest powers of $k_F R$, which is much larger than 1 for most important values of R .

Therefore, the first contribution to the current can now be written

$$j_\alpha^1(\vec{r}) = \sum_\beta \int d\vec{r}' S_{\alpha\beta}^1(\vec{r} - \vec{r}') A_\beta(\vec{r}'), \quad (27.220)$$

with

$$S_{\alpha\beta}^1(\vec{R}) = \frac{3ne^2}{4\pi^2 m c \hbar v_F} \frac{R_\alpha R_\beta}{R^4} \int d\zeta d\zeta' L(\zeta, \zeta') \cos \left[\frac{(\zeta - \zeta')R}{\hbar v_F} \right]. \quad (27.221)$$

The coherence length ξ is conventionally defined for the microscopic model as

$$\xi = \frac{\hbar v_F}{\pi \Delta}. \quad (27.222)$$

Upon evaluating the final integral in Eq. (27.221) (Problem 7) and summing both terms in Eq. (27.209) the current is

$$j_\alpha(\vec{r}) = \sum_\beta \int d\vec{r}' S_{\alpha\beta}(\vec{r} - \vec{r}') A_\beta(\vec{r}') \quad (27.223a)$$

with

$$S_{\alpha\beta}(\vec{R}) = \frac{-3ne^2}{4\pi m c \xi} \frac{R_\alpha R_\beta}{R^4} I(R) \quad (27.223b)$$

and

$$I(R) = \frac{1}{\pi} \int_{-\infty}^{\infty} \frac{dy'}{\cosh y'} \exp \left[-\frac{2R}{\pi \xi} \cosh y' \right]. \quad (27.223c)$$

When \vec{A} varies slowly on the scale of the coherence length ξ , it can be taken out of the spatial integral, and one finds that

$$\vec{j}(\vec{r}) = \frac{-ne^2}{mc} \vec{A}(\vec{r}). \tag{27.224}$$

If \vec{A} does not vary slowly, Eq. (27.223a) describes averages of \vec{A} over a ball the size of the coherence length ξ .

In either case, the microscopic theory predicts perfect diamagnetism. For example, operating with $4\pi/c\vec{\nabla} \times$ on both sides of Eq. (27.224) reproduces the London equation Eq. (27.5). More generally, the relation between current and vector potential in Eq. (27.223) meets the conditions laid down in Section 27.2.1 for production of the Meissner effect. The microscopic theory has predicted that superconductors will be perfect diamagnets, and it also shows how the coherence length ξ is related to the gap parameter Δ .

27.3.7 Comparison with Experiment

According to Bardeen, “In working out the properties of our simplified model and comparing with experimental results on real metals, the excellent agreement obtained was a continual source of amazement Everything fitted together neatly like the pieces of a jigsaw puzzle. Accordingly, the scepticism with which the theory was greeted in some quarters was surprising.” [Bardeen (1963), p. 7]. The resistance was rapidly conquered by several comparisons with experiment, including specific heat and nuclear spin relation. The predictions of how these two effects should vary with temperature was computed by methods similar to those used for the Meissner effect. Specific heat is obtained by differentiating the expectation value of the Hamiltonian with respect to temperature, while spin relaxation involves the expectation value $\langle \hat{c}_\uparrow^\dagger \hat{c}_\downarrow \rangle$. The forms of temperature dependence are different below T_c . Specific heat drops off rapidly as T drops below T_c , while spin relaxation at first rises when T goes down, eventually dropping to zero. These two predictions were confirmed experimentally, as shown in Figure 27.11, and played a decisive role in confirming the correctness of the basic model.

Improvements in photoemission have made it possible to observe directly changes in the electron density of states due to the superconducting transition. The density of electronic states in BCS theory should be

$$D(E_k) = \left(\frac{d\mathcal{E}_k}{dk} \right)^{-1} = \left(\frac{d\mathcal{E}_k}{d\epsilon_k} \right)^{-1} \left(\frac{d\epsilon_k}{dk} \right)^{-1} = D(\mathcal{E}_F) \operatorname{Re} \frac{|\mathcal{E}_k|}{\sqrt{\mathcal{E}_k^2 - \Delta^2}}. \tag{27.225}$$

Using Eq. (27.142)

Eq. (27.225) predicts that the density of states vanishes completely within a range $\pm\Delta$ around \mathcal{E}_F . This is not observed in photoemission experiments. Instead the density of states is smeared out by the finite lifetime of excitations. Dynes et al. (1978) proposed a simple modification of Eq. (27.225), adding an imaginary part

to the energy, so that the probability of interacting with a state of energy \mathcal{E} becomes

$$f(\mathcal{E})D(\mathcal{E}) = f(\mathcal{E})\text{Re}e^{\frac{\mathcal{E} - i\Gamma}{\sqrt{\mathcal{E} - i\Gamma + \Delta}\sqrt{\mathcal{E} - i\Gamma - \Delta}}}. \quad (27.226)$$

$f(\mathcal{E})$ is the Fermi function. The expression is set up to choose the correct branch of the square roots. Γ functions as an extra fitting parameter.

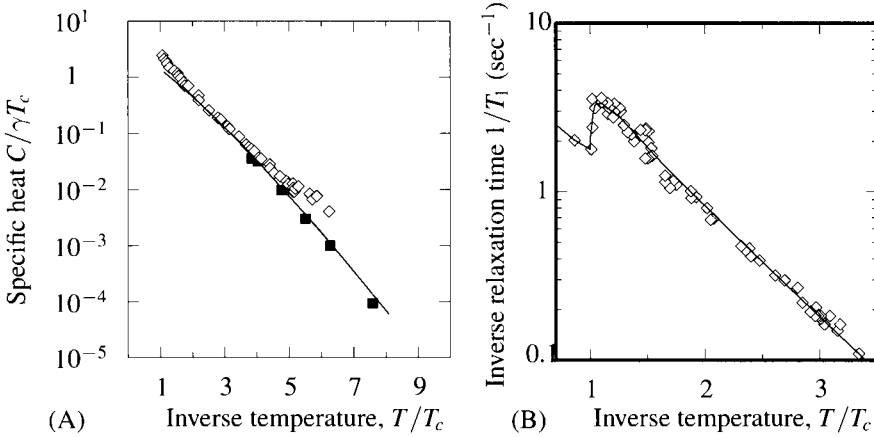


Figure 27.11. (A) Specific heat of aluminum and vanadium, relative to γT_c , where γ is the Sommerfeld parameter defined in Eq. (6.78), compared to the prediction of Bardeen, Cooper, and Schrieffer. [Source: Boorse (1959), p. 391.] (B) Inverse nuclear spin relaxation in aluminum compared with prediction of Bardeen, Cooper, and Schrieffer. Note the initial rise below T_c followed by an exponential drop. [Source: Masuda and Redfield (1962), p. 161.]

Some questions could not, however, be answered from the model Hamiltonian alone. So long as the effective electron–electron interaction $U_{\vec{k}}$ is negative, the model always predicts superconductivity, leaving much room for a more detailed explanation of which materials are superconducting, which are not, and what sets the critical temperature. To address such questions it is necessary to return to Eq. (27.104). A thorough discussion has been provided by McMillan (1968), building upon work of Eliashberg (1960). The calculations are very elaborate, but the flavor of what is accomplished can be captured by letting angular brackets denote averages with respect to \vec{k} and \vec{k}' over the Fermi surface, take $\vec{q} = \vec{k} - \vec{k}'$ and defining

$$\lambda_{\text{ep}} = -D(\mathcal{E}_F) \left\langle \frac{4\pi e^2}{q^2 + \kappa_c^2} \frac{\omega_{\vec{q}}^2 - \bar{\omega}_{\vec{q}}^2}{(\epsilon_{\vec{k}} - \epsilon_{\vec{k}'})^2/\hbar^2 - \omega_{\vec{q}}^2} \right\rangle, \quad \mu^* = D(\mathcal{E}_F) \left\langle \frac{4\pi e^2}{q^2 + \kappa_c^2} \right\rangle. \quad (27.227)$$

Thus μ^* is related to a product of the strength of the Coulomb interaction and the density of states at the Fermi surface, while λ_{ep} is roughly the electron–phonon interaction times the density of states at the Fermi surface. Physical quantities needed to evaluate these averages include the following:

- Electron energy bands near the Fermi surface.

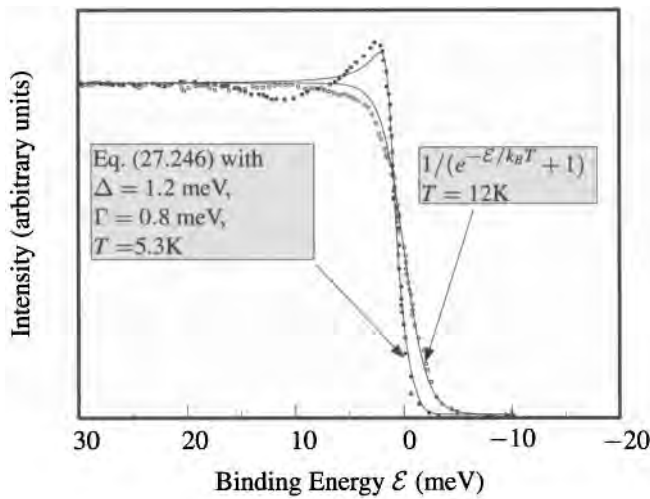


Figure 27.12. High-resolution photoemission from lead, above and below the superconducting transition. For temperatures $T > T_c$, the photoemission intensity is a Fermi function. Below T_c , the data are described by Eq. (27.226). Lines are theoretical expressions and circles are data. [Source: Yokoya et al. (2002), p. 102.]

- Phonon densities of states.
- Electron–phonon interaction matrix elements.

Following a sophisticated numerical analysis, McMillan finds that the superconducting transition temperature T_c is given approximately by

$$T_c = \frac{\Theta_D}{1.45} \exp \left\{ - \left[\frac{(1 + \lambda_{ep})}{\lambda_{ep} - \mu^*(1 + 0.62\lambda_{ep})} \right] \right\}, \quad (27.228)$$

with Θ_D the Debye temperature. According to Table 13.1, Debye temperatures are on the order of a few hundred kelvin. Following Eq. (22.42), one can estimate the order of magnitude of the electron–phonon coupling as $C \approx \sqrt{2\pi e^2 \hbar \omega / k_F^2}$. Using also Eq. (6.33) to estimate the density of states at the Fermi surface, and taking $\vec{k} = \vec{k}'$, gives finally the very rough estimate $\lambda_{ep} \approx 0.8 \cdot [10^{23} \text{ cm}^{-3} / n]^{1/3}$. A value of 0.8 for λ_{ep} should be an upper limit, because the average in Eq. (27.227) involves regions that are both positive and negative, and cancel against each other. Neglecting $\mu^* \approx 0.1$ and taking $\Theta_D = 400$ K gives a superconducting transition temperature of around 30 K. For many years, Nb₃Ge held the record as material with the highest superconducting transition temperature, with $T_c = 23$ K, and 30 K was widely suspected to be a theoretical upper bound.

27.3.8 High-Temperature Superconductors

Bednorz and Müller (1986) found that La_{2–x}Ba_xCuO₄ (LBCO) becomes superconducting at a temperature of 35 K, triggering a frenzied hunt for new superconduct-

ing materials. Soon afterwards Wu et al. (1987) found $\text{YBa}_2\text{Cu}_3\text{O}_{6+x}$ (*1-2-3 compound*, or *YBCO*) with a transition temperature of 92K, meaning that it could be driven superconducting by immersion in liquid nitrogen at 77K. Additional compounds were eventually found with superconducting transitions at temperatures over 100 K. The *high-temperature superconductors* are different from the compounds that set the previous records. They are not conventional metals. Instead, they are antiferromagnetic insulators, carefully doped so as to produce metallic and superconducting phases. Many of them are based upon layers of CuO_2 ; just as with CuO (Section 23.6.3) the insulating behavior is induced by electron correlations and cannot be explained in the single-electron picture. While there is no full consensus on the theoretical description of high-temperature superconductors, many experimental claims are now fairly well established.

Structure. The high-temperature superconductors are brittle ceramics. Figure 27.13 shows the structure of a well-studied member of the family, $\text{La}_{2-x}\text{Sr}_x\text{CuO}_4$, also called *LSCO* or *La214*. The superconductivity is due to motion of electrons on the copper-oxygen planes. The unit in the center of the crystal is perovskite (Section 2.3.6), explaining why the copper-oxide superconductors are also called perovskites. The crystal has both tetragonal and orthorhombic phases, which result from slight symmetry-breaking distortions of the structure shown in the figure.

The parent compound, La_2CuO_4 is an antiferromagnetic insulator. Superconductors are produced by substituting varying degrees of strontium for the lanthanum. Lanthanum has a single *d* electron in an outer shell, while strontium has a filled *s* shell, so the effect of substituting strontium for lanthanum is to dope the structure with holes. Some fraction of the positive charge from the holes makes its way to the copper-oxygen planes, and in range of concentrations produces superconductivity. The maximum T_c of 38K is reached for $x \approx 0.15$.

Phase Diagram.

The full array of experimental probes in condensed matter physics has been brought to bear on the high-temperature superconductors. One of the central conclusions is that the phase diagrams of a large number of the materials are essentially identical, once they have been scaled by the maximum transition temperature, and by the optimal dopant concentration. The result appears in Figure 27.14.

Antiferromagnetic Region When dopant concentration x is zero, all of the copper-oxide ceramic superconductors are anti-ferromagnetic insulators. This is remarkable. Superconductivity consists in the expulsion of magnetic flux from a solid, so magnetic ordering and superconductivity are naturally considered to be competing and incompatible forms of order. The Curie temperatures where antiferromagnetic order disappears are on the order of several hundred degrees Kelvin.

Superconducting Region Figure 27.14 shows that just when the doping x reaches the point where the antiferromagnetic transition temperature T_c drops to zero, superconductivity appears. As the dopant concentration x increases, and the hole

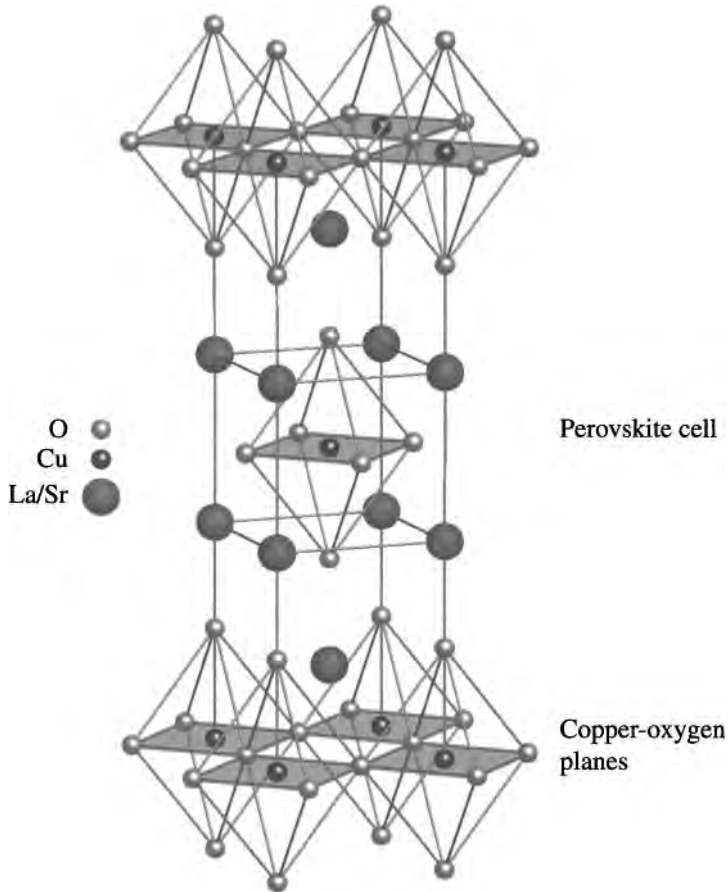


Figure 27.13. Structure of La_2CuO_4 , as reported by Yamada et al. (1988). There are both tetragonal and orthorhombic phases, which however cannot be distinguished on the scale of this figure. Superconductivity results from substitution of Sr for La to form $\text{La}_{2-x}\text{Sr}_x\text{CuO}_4$

density available to the copper-oxygen planes increases, and the superconducting transition temperature increases, reaching a maximum around $x = .15$ for LSCO and $x = .18$ for $\text{Bi}_2\text{Sr}_2\text{CaCu}_2\text{O}_{8+x}$ (Bi2212). Then the superconducting transition temperature decreases again, reaching 0 at around $x = 0.3$. For higher dopant concentrations, the ceramics are normal metals.

The coherence length ξ of the high-temperature superconductors is anisotropic, but small, on the order of 1 or 2 Å. The parameter κ defined in Eq. (27.44) is much larger than 1, so these superconductors are of type II. The usefulness of the materials would greatly be increased if they continued to act as superconductors for magnetic fields greater than H_{c2} where vortices first form. However, the small coherence length leads naturally to large numbers of vortices with narrow cores that are very hard to pin, and drift of the vortices creates dissipation.

Pseudogap Region Figure 27.14 shows another dividing line, detected in the high-temperature superconductors by a wide variety of probes. The dividing line is a crossover temperature T^* , as no thermodynamic quantity has yet shown an abrupt enough change to qualify as a true phase transition. However, below this line, there are many unusual properties. The region is often called the *pseudogap* phase

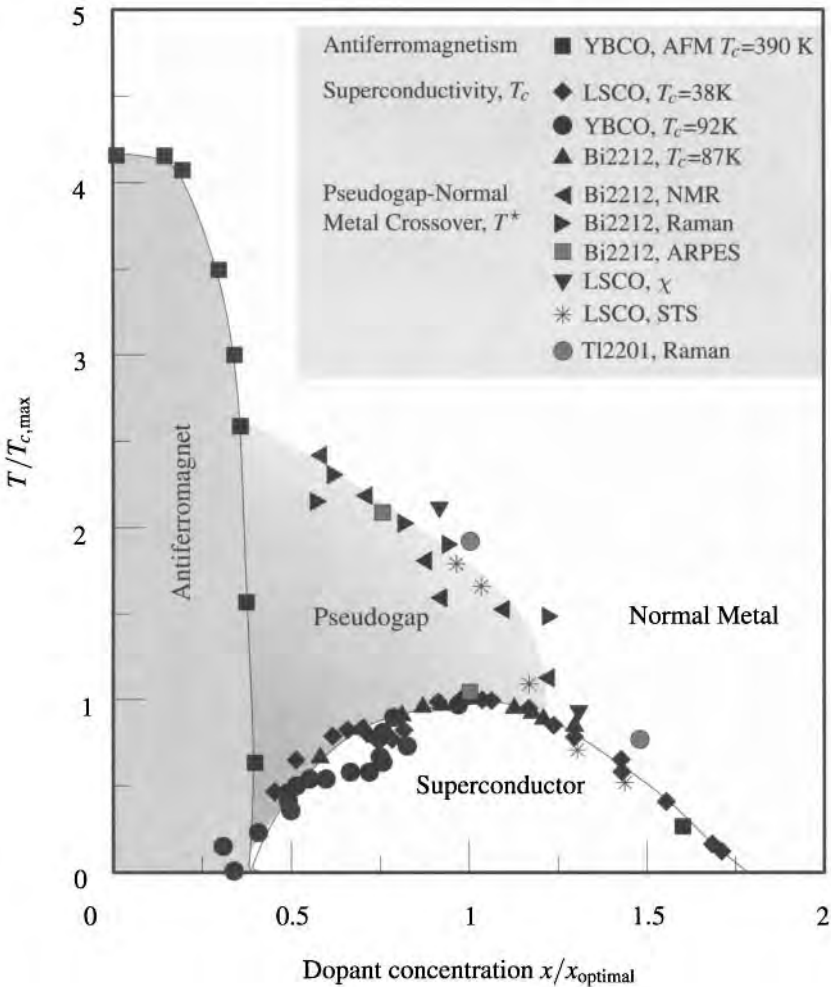


Figure 27.14. Phase diagram for a number of copper-oxide superconductors. The horizontal axis is scaled by the optimal hole concentration, which is on the order of 0.2 per unit cell. The vertical temperature axis is scaled by the maximum critical superconducting temperature, typically around 100 K. Scaled in this way, the phase diagrams of many different compounds collapse onto each other. Bi2212 is $\text{Bi}_2\text{Sr}_2\text{CaCu}_2\text{O}_{8+x}$ and Tl2201 is $\text{Tl}_2\text{Ba}_2\text{CuO}_{6+x}$. The crossover temperature T^* is detected by many different probes including nuclear magnetic resonance (NMR), Raman scattering, angle-resolved photoemission spectroscopy (ARPES), magnetic susceptibility (χ), and scanning tunneling spectroscopy (STS). [Source: Rossat-Mignod et al. (1990), Greene and Bagley (1990), p. 529 and Nakano et al. (1998) p. 2623.]

because as discussed by Damascelli et al. (2003), angle-resolved photoemission detects a superconducting gap, by techniques like that shown in Figure 27.12, along some but not all directions perpendicular to the Fermi surface. Investigations with scanning tunneling probes, reviewed by Fischer et al. (2007), tell a similar story. Almost any probe one chooses shows some sort of cross-over between two limiting behaviors at round T^* , and thus one can map out the line with Raman spectroscopy, nuclear magnetic resonance, or magnetic susceptibility as well.

Even the normal metal phase may be unusual. Electrical resistivity is surprisingly linear in temperature; in the case of YBCO, the linear behavior persists up to around 1000 K. The various competing contributions to resistivity, as for example in Figure 18.1, are mysteriously absent. A phenomenological account of this behavior is provided by Varma et al. (1989).

Theories While experimentalists have been busy mapping out the phase diagram, theorists have been busy trying to calculate it. No definitive answer has yet been reached. A very appealing theory is that the essence of the high-temperature superconductors is to be found in the Hubbard model of Section 26.7. The high-temperature superconductors are no more and no less than doped Mott-Hubbard insulators. The challenge faced by this point of view is that it has so far not proved possible to solve the Hubbard model exactly, nor has any method of approximation been found completely convincing. Thus, if some approximate solution is found that reproduces some feature of the experiments, it is hard to tell whether this feature really resulted from the Hubbard model itself, or from the choice of approximations. Lee et al. (2006) provide a confident case that Mott-Hubbard physics does indeed explain the main features of the copper-oxide ceramic superconductors. Chen et al. (2005) provide a careful presentation of some alternatives. If one theory does eventually emerge dominant, it will happen because the great majority of experimentalists finds it useful in interpreting their experiments. This has not yet happened with a single microscopic theory.

Symmetry of the Order Parameter.

The majority of experimental evidence supports the claim that the superconducting order parameter of the high T_c materials has d -wave character, while for most previous superconductors it had s -wave character. Before displaying the experimental evidence, it is necessary to establish what this claim means, which requires in turn asking about the relationship between the Landau–Ginzburg equation and the underlying microscopic theory of Bardeen, Cooper, and Schrieffer.

The theory of Landau and Ginzburg is built upon the order parameter Ψ . The most important properties of this order parameter are, first, that it becomes nonzero only in the presence of superconductivity and, second, that it alters under gauge transformations

$$\vec{A} \rightarrow \vec{A} + \vec{\nabla}\chi \text{ as } \Psi \rightarrow \Psi e^{-2ie\chi/\hbar c}. \quad (27.229)$$

The phase of Ψ then naturally satisfied the conditions outlined in Section 27.2.9 that lead to the Josephson effect.

The Bogoliubov equations feature a quantity that shares these two properties—the pair potential $\Delta_{\vec{r}}$. To see why, turn to Eqs. (27.198), and ask how u , v , and Δ transform after gauge transformations. To keep the form of the equations intact, they transform as

$$u_{\vec{k}}(\vec{r}) \rightarrow u_{\vec{k}}(\vec{r})e^{-ie\chi/\hbar c}, \quad v_{\vec{k}}(\vec{r}) \rightarrow v_{\vec{k}}(\vec{r})e^{ie\chi/\hbar c}, \quad \text{and} \quad \Delta_{\vec{r}} \rightarrow \Delta_{\vec{r}}e^{-2ie\chi/\hbar c}. \quad (27.230)$$

Very near the transition temperature T_c , Gor'kov (1959) showed that $\Delta_{\vec{r}}$ is in fact proportional to Ψ . At lower temperatures the correspondence is less certain, but the precise form of the Landau–Ginzburg equations is not necessarily correct in any event.

In searching for the form that a theory of high-temperature superconductivity might take, it is natural to ask how $\Delta_{\vec{r}}$ might generalize when the simplifying assumptions leading to Eq. (27.196) no longer apply. If the effective potential U is not isotropic, then

$$\Delta_{\vec{k}\vec{q}} = \sum_{\vec{k}'} \frac{U_{\vec{k}\vec{k}'}}{\mathcal{V}} \langle \hat{c}_{\vec{q}-\vec{k}'\downarrow} \hat{c}_{\vec{k}'\uparrow} \rangle. \quad (27.231)$$

Fourier transforming according to prescriptions as in Eq. (27.189) gives

$$\Delta_{\vec{r}\vec{r}'} = \sum_{\vec{r}''} \frac{U_{\vec{r}\vec{r}''}}{\mathcal{V}} \langle \hat{c}_{-\vec{r}''\downarrow} \hat{c}_{\vec{r}''-\vec{r}'\uparrow} \rangle. \quad (27.232)$$

The implication of this calculation is that in a general theory of superconductivity, the analog of Ψ should depend upon two arguments, becoming $\Psi(\vec{r}, \vec{r}')$. The calculations worked out so far assumed that the effective potential U was isotropic, and consequently that Ψ depended only upon the center-of-mass coordinate $(\vec{r} + \vec{r}')/2$. In a more general theory, $\Psi(\vec{r}, \vec{r}')$ might be expected to do the following:

$$\text{Vary slowly as a function of } (\vec{r} + \vec{r}')/2. \quad (27.233a)$$

$$\text{Decay rapidly as a function } R = |\vec{r} - \vec{r}'|. \quad (27.233b)$$

$$\text{Depend upon the direction of } \vec{R} = \vec{r} - \vec{r}'. \quad (27.233c)$$

A superconductor where Ψ is independent of the direction of \vec{R} is called *s-wave*. One where Ψ has the symmetry of $\vec{x} \cdot \vec{R} \propto \cos \theta$ is *p-wave*. Superfluid ^3He has an order parameter of this type. One with the symmetry of $(\vec{x} \cdot \vec{R})^2 - (\vec{y} \cdot \vec{R})^2 \propto \cos 2\theta$ is called *d-wave*. Problem 8 shows that under some simplifying assumptions, one should expect to measure

$$|\Delta_{\vec{k}}| \propto |\cos 2\phi| \quad \text{Where } \phi \text{ is the angle of the vector } (k_x, k_y). \quad (27.234)$$

Experimental investigations of the symmetry of the order parameter can be carried out without commitment to any particular microscopic theory of the interaction U , as discussed by Annett et al. (1996). Two particularly direct experiments provide evidence for *d-wave* pairing. The first is Josephson tunneling into superconducting samples from different angles, as performed by Wollman et al. (1995).

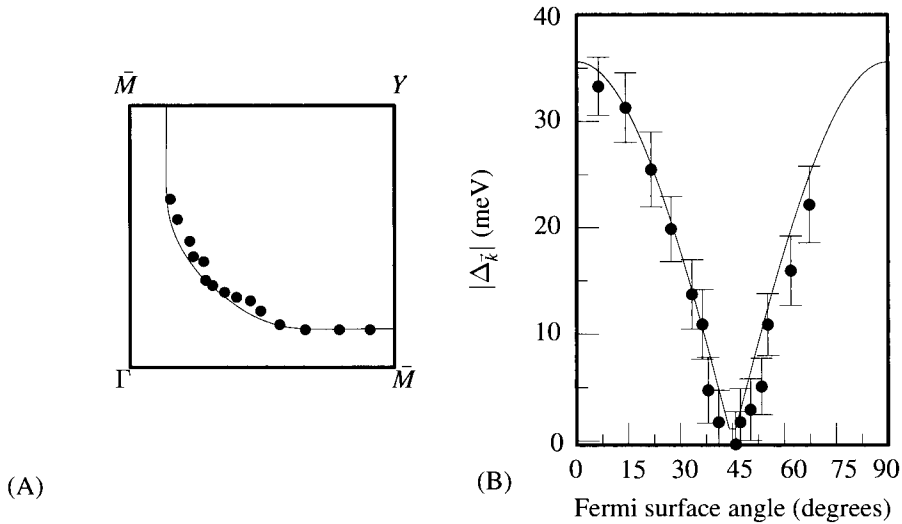


Figure 27.15. Experimental evidence for d -wave pairing in the high-temperature superconducting ceramic $\text{Bi}_2\text{Sr}_2\text{CaCu}_2\text{O}_{8+\delta}$ (Bi2212). (A) Experimental trace of the Fermi surface at 13K obtained from angle-resolved photoemission. (B) Measurement of the superconducting gap $\Delta_{\vec{k}}$ as a function of angle. The solid line is a plot of $|\cos(ak_x) - \cos(ak_y)|$. [Source: Ding et al. (1996), p. 799.]

Even more direct and convincing are results from angle-resolved photoemission spectroscopy, discussed by Damascelli et al. (2003). The methods employed are those shown in Figure 27.12. Opening a superconducting gap creates a small bump in the density of states below the Fermi surface, and the size and shape of the bump can be used to fit to the magnitude of the superconducting gap $|\Delta_{\vec{k}}|$. Figure 27.15 shows direct measurements of variations in the size of the superconducting gap $|\Delta_{\vec{k}}|$ consistent with Eq. (27.234).

Thus, a microscopic theory of high-temperature superconductivity needs to explain the coexistence of superconductivity and antiferromagnetism in the same material, reproduce the main features of the phase diagram in fig:ybco.thermo, and incorporate d -wave symmetry. The problem is not that there is no theory of the high-temperature superconducting materials. The problem is that there are many, and none has yet carried the day. The last word belongs to Anderson (1997): “the consensus is that there is absolutely no consensus on the theory of high T_c superconductivity.”

To those men of early times and, as it were, first parents of philosophy, to Aristotle, Theophrastus, Ptolemaeus, Hippocrates, Galen, be due honor rendered ever, for from them has knowledge descended to those that have come after them: but our age has discovered and brought to light very many things which they too, were they among the living, would cheerfully adopt. Wherefore we have had no hesitation in setting forth in hypothe-

ses that are provable, the things that we have through long experience discovered. Farewell.

— Gilbert (1600), p. li

Problems

1. **Superconducting sphere:** Consider a sphere of superconducting material of type I, whose critical field is H_c , in a uniform external magnetic field \vec{H} .

(a) Using the fact that normal magnetic fields must vanish at the surface of a superconductor, show that when the external field H reaches a value of $\frac{2}{3}H_c$, some portion of the sphere must make the transition to normal metal. Do not try to find the shape of the region that does so.

(b) At what external field will the entire sphere become normal?

2. **Energy of normal-superconducting interfaces:** Consider a half-space, $x < 0$, of normal metal in equilibrium with a superconductor filling $x > 0$. To allow the normal and superconducting metals to remain in equilibrium, the normal metal is permeated almost everywhere by a magnetic induction B_c .

(a) First consider the limit $\kappa \rightarrow 0$, where the penetration depth λ_L is small. Because superconductivity vanishes in the normal metal, it is reasonable to guess that one needs to look for a solution in the superconductor such that Ψ vanishes at $x = 0$, such as Eq. (27.41). Find the difference in free energy $\tilde{\mathcal{G}}$ between a superconductor where Ψ vanishes at $x = 0$, and one where the wave function Ψ fills the space $x > 0$ uniformly. Show that the interface energy is positive, and given by Eq. (27.52).

(b) Next consider the opposite limit, in which the coherence length ξ is small compared to the penetration depth λ_L . Now the gradients of Ψ can be neglected, and instead one has to consider the contributions of the magnetic field. First compute the free energy per area

$$\mathcal{F} = \int_0^\infty dx \Psi_0^2 \frac{4e^2}{2mc^2} A^2 + \frac{B^2}{8\pi}. \quad (27.235)$$

Simplify \mathcal{F} with the use of Eq. (27.9). Then compute $\tilde{\mathcal{G}}$ as defined in Eq. (24.27), and verify Eq. (27.53).

3. **Diffraction effects in Josephson junctions:** Referring to Figure 27.5, and employing Eq. (27.68a), show that the maximum zero-voltage current J_c able to flow through a rectangular Josephson junction in the presence of a magnetic field is given by

$$J_c \propto \left| \frac{\sin(2\pi\Phi/\Phi_0)}{(2\pi\Phi/\Phi_0)} \right|. \quad (27.236)$$

(a) Write down a vector potential \vec{A} that produces the desired field \vec{B}

(b) Assuming some phases ϕ_1 and ϕ_2 on the two sides of the junction, find the total current J by integrating (27.68a) across the area of the junction.

(c) Choose the phases ϕ_1 and ϕ_2 to maximize the zero-voltage current flow.

4. **Josephson Lagrangian:** Verify Eqs. (27.84).

5. **Properties of BCS coherent state:** Verify Eqs. (27.130) through (27.133).

6. **London gauge:**

(a) Show that if $\vec{\nabla} \cdot \vec{A} = 0$, then first-order changes in the energies $\mathcal{E}_{\vec{k}}$ do not appear in Eqs. (27.200).

(b) Verify that $\Delta_{\vec{r}}$ responds to a change in gauge χ as reported in Eq. (27.230).

(c) Physical properties of superconductors are functionals of the vector potential \vec{A} . For small vector potentials, the functional is linear, and in a homogeneous superconductor one must have

$$\Delta_{\vec{r}} = \Delta^{(0)} + \Delta_{\vec{r}}^{(1)} = \Delta^{(0)} + \int d\vec{r}' \vec{\mathcal{P}}(\vec{r} - \vec{r}') \cdot \vec{A}(\vec{r}'), \quad (27.237)$$

for some function $\vec{\mathcal{P}}$. Consider the particular case where $\vec{A} = \vec{\nabla}\chi$, and χ is very small. Linearizing Eq. (27.230) and comparing it with Eq. (27.237), show that

$$\vec{\mathcal{P}}(\vec{r}) = \frac{-ie\Delta^{(0)}}{2\pi\hbar c} \vec{\nabla} \left(\frac{1}{r} \right). \quad (27.238)$$

(d) Show as a consequence that in the London gauge, where $\vec{\nabla} \cdot \vec{A} = 0$, and if $\vec{A} \cdot \hat{n}$ vanishes at the outer reaches of the system, with \hat{n} is a unit normal, then $\Delta_{\vec{r}}^{(1)} = 0$, and $\Delta_{\vec{r}} = \Delta$. In other words, gauge invariance is used to choose a convenient gauge in which the problem simplifies.

7. **Meissner effect integral:** Evaluate

$$W(R) \equiv \int d\zeta d\zeta' L(\zeta, \zeta') \cos [(\zeta - \zeta')R/\hbar v_F]. \quad (27.239)$$

(a) Use Eq. (27.214) for $L(\zeta, \zeta')$ and Eq. (27.202) for $\mathcal{E}_{\vec{k}}$. Make the substitutions $\zeta = \Delta \sinh x$ and $\zeta' = \Delta \sinh x'$.

(b) Define $y = (x - x')/2$ and $y' = (x + x')/2$. Express the integral in terms of y and y' .

(c) Retain the variable y' , but make the substitution $p = \sinh y$. The integral over p can be performed to give

$$W(R) = \pi\hbar v_F \delta(R) - \pi\Delta \int dy' \frac{\exp[-2\Delta \cosh y'R/\hbar v_F]}{\cosh y'}. \quad (27.240)$$

8. ***d*-wave Superconductivity:** Suppose that the gap function $\Delta_{\vec{r}\vec{r}'}$ of Eq. (27.232) obeys the conditions of Eqs. (27.233); in fact, there is no dependence upon $(\vec{r} + \vec{r}')$. Suppose that the dependence on the direction of \vec{R} is of the *d*-wave form

$$(\vec{x} \cdot \vec{R})^2 - (\vec{y} \cdot \vec{R})^2 \propto \cos 2\theta. \quad (27.241)$$

Show that $\Delta_{\vec{k}\vec{k}'}$ takes the form for some function $f(k)$

$$\Delta_{\vec{k}\vec{k}'} = \delta_{\vec{k}\vec{k}'} \left(\frac{\partial^2}{\partial k_x^2} - \frac{\partial^2}{\partial k_y^2} \right) f(k), \quad (27.242)$$

resulting in a symmetry for the gap function given by Eq. (27.234).

References

- A. A. Abrikosov (1957), On the magnetic properties of superconductors of the second group, *Soviet Physics JETP*, **6**, 489–492.
- P. B. Allen and B. Mitrovic (1982), Theory of superconducting T_c , *Solid State Physics: Advances in Research and Applications*, **37**, 1–92.
- P. W. Anderson (1997), *The Theory of Superconductivity in the High- T_c Cuprates*, Princeton University Press, Princeton, NJ.
- P. W. Anderson and J. M. Rowell (1963), Probable observation of the Josephson superconducting tunneling effect, *Physical Review Letters*, **10**, 230–232.
- J. F. Annett, N. Goldenfeld, and A. J. Leggett (1996), Experimental constraints on the pairing state of the cuprate superconductors: An emerging consensus, in *Physical Properties of High Temperature Superconductors*, D. M. Ginsberg, ed., vol. V, pp. 375–461.
- J. Bardeen (1963), Development of concepts in superconductivity, in *Proceedings of the Eighth International Conference on Low Temperature Physics*, R. O. Davies, ed., pp. 3–8, Butterworths, London.
- J. Bardeen (1990), Superconductivity and other macroscopic quantum phenomena, *Physics Today*, **43**(12), 25–31.
- J. Bardeen, L. N. Cooper, and J. R. Schrieffer (1957), Theory of superconductivity, *Physical Review*, **108**, 1175–1204.
- B. Batlogg (1991), Physical properties of high- T_c superconductors, *Physics Today*, **44**(6), 44–50.
- G. Bednorz and K. A. Müller (1986), Possible high T_c superconductivity in the Ba-Ca-Cu-O system, *Zeitschrift für Physik*, **B64**, 189–193.
- J. G. Bednorz and K. A. Müller (1988), Perovskite-type oxides—the new approach to high- T_c superconductivity, *Reviews of Modern Physics*, **60**, 585–600.
- R. Beyers and T. M. Shaw (1989), The structure of yttrium barium copper oxide ($Y_1Ba_2Cu_3O_{7-\delta}$), *Solid State Physics: Advances in Research and Applications*, **42**, 135–212.
- G. Blatter, M. V. Feigel'man, V. B. Geshkenbein, A. I. Larkin, and V. M. Vinokur (1994), Vortices in high-temperature superconductors, *Reviews of Modern Physics*, **66**, 1125–1388.
- N. N. Bogoliubov (1958), A new method in the theory of superconductivity, *Soviet Physics JETP*, **7**, 41–46. Reprinted in Pines (1961), pp. 399–404.
- H. A. Boorse (1959), Superconducting electronic specific heats, the “exponential law,” and the Bardeen, Cooper, Schrieffer theory, *Physical Review Letters*, **2**, 391–393.
- J. P. Carbotte (1990), Properties of boson-exchange superconductors, *Reviews of Modern Physics*, **62**, 1027–1157.

- P. M. Chaikin and R. L. Greene (1986), Superconductivity and magnetism in organic metals, *Physics Today*, **39**(5), 24–32.
- Q. Chen, J. Stajic, S. Tan, and K. Levin (2005), Bcs-bec crossover: From high temperature superconductors to ultracold superfluids, *Physics Reports*, **412**(1), 1 – 88.
- L. N. Cooper (1956), Bound electron pairs in a degenerate Fermi gas, *Physical Review*, **104**, 1189–1190.
- D. L. Cox and M. B. Maple (1995), Electronic pairing in exotic superconductors, *Physics Today*, **48**(2), 32–40.
- G. W. Crabtree and D. R. Nelson (1997), Vortex physics in high-temperature superconductors, *Physics Today*, **50**(4), 38–45.
- E. Dagotto (1994), Correlated electrons in high-temperature superconductors, *Reviews of Modern Physics*, **66**, 763–840.
- A. Damascelli, Z. Hussain, and Z.-X. Shen (2003), Angle-resolved photoemission studies of the cuprate superconductors, *Reviews of Modern Physics*, **75**(2), 473–541.
- P.-G. de Gennes (1992), *Superconductivity of Metals and Alloys*, Addison-Wesley, Reading, MA.
- B. S. Deaver and W. M. Fairbank (1961), Experimental evidence for quantized flux in superconducting cylinders, *Physical Review Letters*, **7**, 43–46.
- H. Ding, M. R. Norman, J. C. Campuzano, et al. (1996), Angle-resolved photoemission spectroscopy study of the superconducting gap anisotropy in $\text{Bi}_2\text{Sr}_2\text{CaCu}_2\text{O}_{8+x}$, *Physical Review B*, **54**(14), R9678–R9681.
- R. Doll and M. Näbauer (1961), Experimental proof of magnetic flux quantization in a superconducting ring, *Physical Review Letters*, **7**, 51–52.
- R. C. Dynes, V. Narayanamurt, and J. P. Garno (1978), Direct measurement of quasiparticle-lifetime broadening in a strong-coupled superconductor, *Physical Review Letters*, **41**, 1509–1512.
- G. M. Eliashberg (1960), Interactions between electrons and lattice vibrations in a superconductor, *Soviet Physics JETP*, **11**, 696–702.
- L. Esaki (1974), Long journey into tunnelling, *Reviews of Modern Physics*, **46**, 237–244.
- O. Fischer, M. Kugler, I. Maggio-Aprile, C. Berthod, and C. Renner (2007), Scanning tunneling spectroscopy of high-temperature superconductors, *Reviews of Modern Physics*, **79**, 353–419.
- H. Fröhlich (1950), Isotope effect in superconductivity, *Proceedings of the Physical Society (London)*, **A63**, 778.
- T. H. Geballe (1993), Superconductivity: from physics to technology, *Physics Today*, **46**(10), 52–56.
- I. Giaever (1974), Electron tunnelling and superconductivity, *Reviews of Modern Physics*, **46**, 245–250.
- W. Gilbert (1600), *On the Loadstone and Magnetic Bodies, and on the Great Magnet the Earth*, John Wiley and Sons, New York. Translated by P. F. Mottelay, 1893
- H. Goldstein (1980), *Classical Mechanics*, 2nd ed., Addison-Wesley, Reading, MA.
- L. P. Gor'kov (1959), Microscopic derivation of the Ginzburg-Landau equations in the theory of superconductivity, *Soviet Physics JETP*, **9**, 1364–1367.
- L. H. Greene and B. G. Bagley (1990), Oxygen stoichiometric effects and related atomic substitutions in the high T_c cuprates, in *Physical Properties of High Temperature Superconductors*, D. M. Ginsberg, ed., vol. 2, pp. 509–569, World Scientific, Singapore.
- I. S. Grigoriev and E. Z. Meilkhov, eds. (1997), *Handbook of Physical Quantities*, CRC Press, Boca Raton, FL.
- O. Gunnarsson (1997), Superconductivity in fullerides, *Reviews of Modern Physics*, **69**, 575–606.
- A. V. Gurevich and R. G. Mints (1987), Self-heating in normal metals and superconductors, *Reviews of Modern Physics*, **59**, 941–999.
- J. Hansen and P. E. Lindelof (1984), Static and dynamic interactions between Josephson junctions, *Reviews of Modern Physics*, **56**, 431–459.

- K. C. Hass (1989), Electronic structure of copper-oxide superconductors, *Solid State Physics: Advances in Research and Applications*, **42**, 213–270.
- H. Hayakawa (1986), Josephson computer technology, *Physics Today*, **39**(3), 46–52.
- A. F. Hebard (1992), Superconductivity in doped fullerenes, *Physics Today*, **45**(11), 26–32.
- J. D. Jorgensen (1991), Defects and superconductivity in the copper oxides, *Physics Today*, **44**(6), 34–40.
- B. D. Josephson (1962), Possible new effects in superconductive tunneling, *Physics Letters*, **1**, 251–253.
- B. D. Josephson (1974), The discovery of tunnelling supercurrents, *Reviews of Modern Physics*, **46**, 251–254.
- H. Kamerlingh Onnes (1911), The resistance of platinum at helium temperature, *Communications from the Physical Laboratory at the University of Leiden*, **119b**, 19–26.
- L. D. Landau (1965), *Collected Papers of L D Landau*, D. ter Haar, ed., Gordon and Breach, New York.
- L. D. Landau and V. L. Ginzburg (1950), On the theory of superconductivity, *Journal of Experimental and Theoretical Physics (U.S.S.R.)*, **20**, 1064–1084. In Russian. Translated in Landau (1965), pp. 546–568.
- D. Larbalestier (1991), Critical currents and magnet applications of high- T_c superconductors, *Physics Today*, **44**(6), 74–82.
- P. A. Lee, N. Nagaosa, and X.-G. Wen (2006), Doping a mott insulator: Physics of high-temperature superconductivity, *Reviews of Modern Physics*, **78**(1), 17.
- C. M. Lieber and Z. Zhe (1994), Physical properties of metal-doped fullerene superconductors, *Solid State Physics: Advances in Research and Applications*, **48**, 349–384.
- K. K. Likharev (1979), Superconducting weak links, *Reviews of Modern Physics*, **51**, 101–159.
- F. London (1961), *Superfluids*, 2nd ed., Dover, New York.
- D. E. MacLaughlin (1976), Magnetic resonance in the superconducting state, *Solid State Physics: Advances in Research and Applications*, **31**, 1–69.
- M. B. Maple (1986), Novel types of superconductivity in f -electron systems, *Physics Today*, **39**(3), 72–80.
- Y. Masuda and A. G. Redfield (1962), Nuclear spin relaxation in superconducting aluminum, *Physical Review*, **125**, 159–163.
- E. Maxwell (1950), Isotope effect in the superconductivity of mercury, *Physical Review*, **78**, 477.
- W. McMillan (1968), Transition temperature of strong-coupled superconductors, *Physical Review*, **167**, 331–344.
- W. Meissner and R. Ochsenfeld (1933), A new effect in penetration of superconductors, *Die Naturwissenschaften*, **21**, 787–788. In German.
- J. E. Mercereau (1969), Macroscopic quantum phenomena, in *Superconductivity*, R. D. Parks, ed., vol. I, pp. 393–421, Marcel Dekker, New York.
- R. Meservey and B. B. Schwartz (1969), Equilibrium properties: Comparison of experimental results with predictions of the BCS theory, in *Superconductivity*, R. D. Parks, ed., vol. I, pp. 117–191, Marcel Dekker, New York.
- R. Micnas, J. Ranninger, and S. Robaszkiewicz (1990), Superconductivity in narrow-band systems with local nonretarded attractive interactions, *Reviews of Modern Physics*, **62**, 113–234.
- R. G. Mints and A. L. Rakhmanov (1981), Critical state stability in type-II superconductors and superconducting-normal-metal composites, *Reviews of Modern Physics*, **53**, 551–592.
- T. Nakano, N. Momono, M. Oda, and M. Ido (1998), Correlation between the doping dependences of superconducting gap magnitude 2Δ and pseudogap temperature T^* in high- T_c cuprates, *Journal of the Physical Society of Japan*, **67**, 2622–2625.
- J. Nobel and P. Lindenfeld (1996), The discovery of superconductivity, *Physics Today*, **49**(9), 40–42.

- R. D. Parks (1969), *Superconductivity*, Marcel Dekker, New York.
- W. E. Pickett (1989), Electronic structure of the high-temperature oxide superconductors, *Reviews of Modern Physics*, **61**, 433–512.
- D. Pines (1961), *The Many-Body Problem*, W. A. Benjamin, Reading, MA.
- N. M. Plakida (1995), *High-Temperature Superconductivity: Experiment and Theory*, Springer-Verlag, Berlin.
- M. Rasolt and Z. Tesanovic (1992), Theoretical aspects of superconductivity in very high magnetic fields, *Reviews of Modern Physics*, **64**, 709–754.
- B. Raveau (1992), Defects and superconductivity in layered cuprates, *Physics Today*, **45**(10), 53–58.
- C. A. Reynolds, B. Serin, W. H. Wright, and L. B. Nesbitt (1950), Superconductivity of isotopes of mercury, *Physical Review*, **78**, 487.
- J. Rossat-Mignod, J. X. Boucherie, P. Bulet, et al. (1990), Neutron scattering study of $\text{YBa}_2\text{Cu}_3\text{O}_x$ (magnetic properties), in *International Seminar on High Temperature Superconductivity*, V. L. Aksenov, N. N. Bogoliubov, and N. M. Plakida, eds., pp. 74–85, World Scientific, Singapore.
- J. M. Rowell (1988), Superconductivity research: a different view, *Physics Today*, **41**(11), 38–46.
- M. Sigrist and T. M. Rice (1995), Unusual paramagnetic phenomena in granular high-temperature superconductors—a consequence of d -wave pairing?, *Reviews of Modern Physics*, **67**, 503–513.
- M. Sigrist and K. Ueda (1991), Phenomenological theory of unconventional superconductivity, *Reviews of Modern Physics*, **63**, 239–311.
- R. Simon (1991), High- T_c thin films and electronic devices, *Physics Today*, **44**(6), 64–70.
- A. W. Sleight (1991), Synthesis of oxide superconductors, *Physics Today*, **44**(6), 24–30.
- A. Sommerfeld and H. Bethe (1933), Electron theory of metals, in *Handbuch der Physik*, H. Geiger and K. Sheel, eds., vol. 24, pp. 333–622, Springer-Verlag, Berlin.
- L. R. Testardi (1975), Structural instability and superconductivity in A-15 compounds, *Reviews of Modern Physics*, **47**, 637–648.
- M. Tinkham (1996), *Introduction to Superconductivity*, 2nd ed., McGraw-Hill, New York.
- M. Tinkham and C. J. Lobb (1989), Physical properties of the new superconductors, *Solid State Physics: Advances in Research and Applications*, **42**, 91–134.
- A. Tonomura, N. Osakabe, T. Matsuda, T. Kawasaki, J. Endo, S. Yano, and H. Yamada (1986), Evidence for the Aharonov-Bohm effect with magnetic field completely shielded from electron wave, *Physical Review Letters*, **56**, 792–795.
- J. G. Valatin (1958), Comments on the theory of superconductivity, *Il Nuovo Cimento*, **7**, 843–857.
- C. M. Varma, P. B. Littlewood, S. Schmitt-Rink, E. Abrahams, and A. E. Ruckenstein (1989), Phenomenology of the normal state of Cu-O high-temperature superconductors, *Physical Review Letters*, **63**, 1996–1999.
- S. Weinberg (1986), Superconductivity for particular theorists, *Progress of Theoretical Physics, Supplement* **86**, 43–53.
- N. R. Wertheim (1969), The Ginzburg Landau equations and their extensions, in *Superconductivity*, R. D. Parks, ed., vol. I, pp. 321–370, Marcel Dekker, New York.
- F. Wilczek (1990), *Fractional Statistics and Anyon Superconductivity*, World Scientific, Singapore.
- D. A. Wollman, D. J. van Harlingen, J. Giapintzakis, and D. M. Ginsberg (1995), Evidence for $d_{x^2-y^2}$ pairing from the magnetic field modulation of $\text{YBa}_2\text{Cu}_3\text{O}_{7-\text{Pb}}$ Josephson junctions, *Physical Review Letters*, **74**, 797–800.
- H. Won and K. Maki (1994), d -wave superconductor as a model of high- T_c superconductors, *Physical Review B*, **49**(2), 1397–1402.
- M. K. Wu, J. R. Ashburn, C. J. Torng, et al. (1987), Superconductivity at 93 K in a new mixed-phase y-ba-cu-o compound system at ambient pressure, *Physical Review Letters*, **58**(9), 908–910.
- K. Yamada, E. Kudo, Y. Endoh, et al. (1988), Determination of space group and refinement of structure parameters for $\text{La}_2\text{CuO}_4 - \delta$ crystals, *Japanese Journal of Applied Physics*, **27**, 1132–1137.

- Y. Yeshurun, A. P. Malozemoff, and A. Shaulov (1996), Magnetic relaxation in high-temperature superconductors, *Reviews of Modern Physics*, **68**, 911–949.
- T. Yokoya, T. Kiss, A. Chainani, and S. Shina (2002), Superconducting transitions studied by ultrahigh-resolution photoemission, *Journal of Electron Spectroscopy and Related Phenomena*, **124**, 99–105.

APPENDICES

A. Lattice Sums and Fourier Transforms

A.1 One-Dimensional Sum

The following sum arises in Section 3.2.4.

$$\Sigma_q = \sum_{l=0}^{N-1} e^{ilaq} \quad \text{There are } N \text{ terms in this sum.} \quad (\text{A.1})$$

$$\Rightarrow e^{iaq}\Sigma_q = \sum_{l=0}^{N-1} e^{i(l+1)aq} \quad (\text{A.2})$$

$$= \sum_{l=0}^{N-1} e^{ilaq} - 1 + e^{iNaq} \quad \text{Replacing } l \text{ by } l+1 \text{ is the same as removing} \\ \text{the first term in the sum, and adding an extra} \\ \text{term on at the end.} \quad (\text{A.3})$$

$$= \Sigma_q - 1 + e^{iNaq} \quad (\text{A.4})$$

$$\Rightarrow \Sigma_q = \frac{e^{iNaq} - 1}{e^{iaq} - 1} \quad \text{Solving Eq. (A.2) for } \Sigma_q. \quad (\text{A.5})$$

$$= \frac{e^{iNaq/2} \sin Naq/2}{e^{iaq/2} \sin aq/2} \quad \text{Using } \sin(x) = (e^{ix} - e^{-ix})/2i. \quad (\text{A.6})$$

$$\Rightarrow |\Sigma_q|^2 = \frac{\sin^2 Naq/2}{\sin^2 aq/2}. \quad (\text{A.7})$$

The result is plotted in Figure 3.3.

A.2 Area Under Peaks

Because Figure 3.3 looks like a sum of Dirac delta functions, it is useful to find the area under each of the peaks. In fact, both Σ_q and $|\Sigma_q|^2$ can be regarded as sums of delta functions. The area under a peak of Σ_q is obtained by integrating from $-\pi/a$ to π/a and is

$$\int_{-\pi/a}^{\pi/a} dq \frac{e^{iNaq} - 1}{e^{iaq} - 1} \quad \text{The limits of integration go from midway be-} \\ \text{tween one set of peaks to midway between} \\ \text{the next.} \quad (\text{A.8})$$

$$= \oint \frac{dz}{iaz} \frac{z^N - 1}{z - 1} \quad \text{Defining } z = \exp[iaq] \text{ and taking the unit cir-} \\ \text{cle as the integration contour.} \quad (\text{A.9})$$

$$= \frac{2\pi}{a} = N \frac{2\pi}{L}, \quad \text{The residue of the pole at } z = 0 \text{ is 1. Recall} \\ \text{that } L = aN \text{ is the length of the system.} \quad (\text{A.10})$$

and

$$\Sigma_q = \sum_{l'} N \frac{2\pi}{L} \delta(q - 2\pi l'/a) = \sum_{l'} 2\pi \delta(qa - 2\pi l'). \quad (\text{A.11})$$

The area under a peak of $|\Sigma_q|^2$ is found similarly.

$$\int_{-\pi/a}^{\pi/a} dq \left| \frac{e^{iNaq} - 1}{e^{iaq} - 1} \right|^2 \quad (\text{A.12})$$

$$= \oint \frac{dz}{iaz} \frac{z^N - 1}{z - 1} \frac{z^{-N} - 1}{z^{-1} - 1} \quad (\text{A.13})$$

$$= \oint \frac{dz}{ia} \frac{1 + z^{2N} - 2z^N}{z^N(1 - z)^2} \quad (\text{A.14})$$

$$= \oint \frac{dz}{ia} \frac{1}{z^N(1 - z)^2} \quad \text{There is no pole in the two discarded terms.} \quad (\text{A.15})$$

$$= \frac{2\pi N}{a} = 2\pi N \frac{N}{L} \quad \text{Using the residue theorem with aid of the Taylor expansion } 1/(1 - z)^2 = \sum_{l=0}^{\infty} (l + 1)z^l. \quad (\text{A.16})$$

So the area under a peak of $|\Sigma_q|^2$ is N times the area under a peak of Σ_q .

A.3 Three-Dimensional Sum

In the three-dimensional case, let $\vec{a}_1 \dots \vec{a}_3$ be primitive vectors, and consider the collection of lattice points of the form

$$\vec{R} = \sum_{\alpha=1}^3 l_{\alpha} \vec{a}_{\alpha} \quad \text{with} \quad 0 \leq l_{\alpha} < M. \quad (\text{A.17})$$

Then

$$\Sigma_{\vec{q}} = \sum_{\vec{R}} e^{i\vec{q} \cdot \vec{R}} \quad (\text{A.18})$$

$$= \prod_{\alpha=1}^3 \left[\sum_{l_{\alpha}} e^{il_{\alpha} \vec{q} \cdot \vec{a}_{\alpha}} \right] \quad (\text{A.19})$$

$$= \prod_{\alpha=1}^3 \frac{e^{iM\vec{a}_{\alpha} \cdot \vec{q}} - 1}{e^{i\vec{a}_{\alpha} \cdot \vec{q}} - 1} \quad \text{Using Eq. (3.13)} \quad (\text{A.20})$$

$$= \prod_{\alpha=1}^3 (2\pi) \sum_{m'_{\alpha}} \delta(\vec{q} \cdot \vec{a}_{\alpha} - 2\pi m'_{\alpha}). \quad \text{See Eq. (A.11).} \quad (\text{A.21})$$

The values of \vec{q} at which the delta functions peak are the reciprocal lattice vectors \vec{K} , obeying Eq. (3.18). If one integrates any of the delta functions by $d\vec{q}$, what is the result? Define the variables $Q_{\alpha} = \vec{q} \cdot \vec{a}_{\alpha}$. Then

$$\int d\vec{q} \prod_{\alpha} \delta(\vec{q} \cdot \vec{a}_{\alpha} - 2\pi m'_{\alpha}) \quad (\text{A.22})$$

$$= \int d\vec{Q} \frac{1}{\left| \frac{\partial \vec{Q}}{\partial \vec{q}} \right|} \prod_{\alpha} \delta(Q_{\alpha} - 2\pi m'_{\alpha}) \tag{A.23}$$

$$= \frac{1}{|\vec{a}_1 \cdot (\vec{a}_2 \times \vec{a}_3)|} = \frac{N}{\mathcal{V}}. \tag{A.24}$$

The matrix of derivatives of \vec{Q} by \vec{q} is a matrix whose rows are the Cartesian components of the three primitive vectors \vec{a} . The determinant of this matrix is the volume of the primitive cell defined by the three primitive vectors.

Therefore

$$\sum_{\vec{R}} e^{i\vec{q} \cdot \vec{R}} = \sum_{\vec{K}} N \left(\frac{2\pi}{L} \right)^3 \delta(\vec{q} - \vec{K}). \text{ With } L^3 = \mathcal{V}. \tag{A.25}$$

A.4 Discrete Case

Rather than choosing to evaluate Σ_q for all values of q , one often has reason to restrict q to the discrete values

$$q = \frac{2\pi l}{Na}. \text{ With } l \text{ an integer.} \tag{A.26}$$

It is clear from Eq. (A.1) that $\Sigma_q = N$ when $q = 0, q = 2\pi/a, q = 4\pi/a, \dots$, and it is clear from Eq. (A.5) that Σ_q vanishes otherwise. So with q restricted by Eq. (A.26) one has

$$\Sigma_q = N \sum_{l=-\infty}^{\infty} \delta_{q, 2\pi l/a} \tag{A.27}$$

$$= N \sum_K \delta_{q,K}. \tag{A.28}$$

Because $2\pi l/a$ are just the reciprocal lattice vectors in one dimension.

In three dimensions, (A.28) generalizes naturally to

$$\sum_{\vec{R}} e^{i\vec{q} \cdot \vec{R}} = N \sum_{\vec{K}} \delta_{\vec{q}, \vec{K}}. \tag{A.29}$$

N is the total number of elements in the sum over \vec{R} .

Equation (6.12) provided a correspondence between discrete and continuous delta functions, which says to multiply the discrete delta function by $(2\pi)^3/\mathcal{V}$. Using this rule turns Eq. (A.29) into

$$\sum_{\vec{R}} e^{i\vec{q} \cdot \vec{R}} = (2\pi)^3 \frac{N}{\mathcal{V}} \sum_{\vec{K}} \delta(\vec{q} - \vec{K}), \tag{A.30}$$

which is identical to Eq. (A.25).

An additional result in one dimension follows from computing

$$\sum_q e^{iqr} = \sum_{l=1}^N e^{2\pi i l r / Na} \tag{A.31}$$

$$= \frac{e^{2\pi i r/a} - 1}{e^{2\pi i r/Na} - 1} = aN \sum_l \delta(r - lNa) = L\delta(r). \text{ Since } r \in [0, L]. \tag{A.32}$$

Similarly, if \vec{q} lies in the first Brillouin zone, then

$$\sum_{\vec{q} \in B.Z.} e^{i\vec{q} \cdot \vec{r}} = \mathcal{V} \delta(\vec{r}). \quad (\text{A.33})$$

A.5 Convolution

The *convolution* of two functions $A(\vec{r})$ and $B(\vec{r})$ is

$$A * B(\vec{r}) \equiv \int d\vec{r}' A(\vec{r}') B(\vec{r} - \vec{r}'). \quad (\text{A.34})$$

Fourier transforms of convolutions give products:

$$\int d\vec{r} e^{i\vec{q} \cdot \vec{r}} A * B(\vec{r}) \quad (\text{A.35})$$

$$= \int d\vec{r} d\vec{r}' e^{i\vec{q} \cdot \vec{r}} A(\vec{r}') B(\vec{r} - \vec{r}') \quad (\text{A.36})$$

$$= \int d\vec{r} d\vec{r}' e^{i\vec{q} \cdot [(\vec{r} - \vec{r}') + \vec{r}']} A(\vec{r}') B(\vec{r} - \vec{r}') \quad (\text{A.37})$$

$$= \left[\int d\vec{r}' e^{i\vec{q} \cdot \vec{r}'} A(\vec{r}') \right] \left[\int d\vec{r} e^{i\vec{q} \cdot \vec{r}} B(\vec{r}) \right] \quad (\text{A.38})$$

$$= A(\vec{q}) B(\vec{q}). \quad (\text{A.39})$$

Similarly, Fourier transforms of products give convolutions:

$$\int d\vec{r} e^{i\vec{q} \cdot \vec{r}} A(\vec{r}) B(\vec{r}) = \int d\vec{r} d\vec{r}' \delta(\vec{r} - \vec{r}') e^{i\vec{q} \cdot \vec{r}} A(\vec{r}') B(\vec{r}) \quad (\text{A.40})$$

$$= \int d\vec{r} d\vec{r}' d\vec{q}' \frac{e^{-i\vec{q}' \cdot (\vec{r} - \vec{r}')}}{2\pi} e^{i\vec{q} \cdot \vec{r}} A(\vec{r}') B(\vec{r}) \quad (\text{A.41})$$

$$= \int \frac{d\vec{q}'}{2\pi} \left[\int d\vec{r}' e^{i\vec{q}' \cdot \vec{r}'} A(\vec{r}') \right] \left[\int d\vec{r} e^{i(\vec{q} - \vec{q}') \cdot \vec{r}} B(\vec{r}) \right] = \frac{A * B(\vec{q})}{2\pi}. \quad (\text{A.42})$$

A.6 Using the Fast Fourier Transform

The *fast Fourier transform* (FFT) is a rapid numerical algorithm for evaluating the sum

$$F_m = \sum_{l=0}^N e^{2\pi i l m / N} G_l. \quad (\text{A.43})$$

Press et al. (1992) describe the algorithm and provide source code; better and more elaborate routines can be obtained at <http://www.netlib.org>. Routines computing multidimensional generalizations of (A.43) are available as well.

There are many subtleties involved in relating a discrete sum such as (A.43) to a continuous integral; some are discussed by Brigham (1988) and Nussbaumer (1982). It is risky to use the discrete transform blindly, but in cases where it is appropriate, here is a prescription for relating it to continuous Fourier transforms.

Suppose that the goal is to use a discrete transform with N points to describe the Fourier transform of a continuous function $G(x)$, with the interval covered by the discrete transform corresponding to the interval $[-x_{\max}, x_{\max}]$. Define

$$dx = 2 \frac{x_{\max}}{N} \quad (\text{A.44})$$

and

$$dk = \frac{2\pi}{Ndx}. \quad (\text{A.45})$$

Also define a function l that shuffles the index of a Fourier transform in a conventional way:

```
function l(j)
  if ( j > (N+1)/2 )
    {
      return (j-N-1)
    } else {
      return (j-1)
    }
}
```

Next, fill an array $F(j)$ with values of the function $G(x)$ according to

```
for j=1 through N
  {
    x=l(j)*dx
    F(j)=G(x)*dx
  }
```

After invoking a fast Fourier transform routine on the array $F(j)$, the original $F(j)$ will be overwritten with its discrete Fourier transform, and the value of $F(j)$ will be the Fourier transform $G(k)$, where

$$k=l(j)*dk$$

If one begins instead with $G(k)$ rather than $G(x)$, one has instead

```
for j=1 through N
  {
    k=l(j)*dk
    F(j)=G(k)*dk/(2*pi)
  }
```

and uses an appropriate flag in the Fourier transform routine to obtain the inverse transform.

Fast Fourier transform routines exist also for multidimensional sums, and they obey conventions naturally generalized from those for the one-dimensional sums. For example, suppose one wants to carry out the sum in Eq. (7.33),

$$\sum_{\vec{K}} U_{\vec{K}} \psi(\vec{q} - \vec{K}). \quad (\text{A.46})$$

This sum is in the form of a convolution, so by far the fastest way to carry it out is to take the Fourier transform of $U_{\vec{k}}$, the transform of ψ , multiply the two, and then invert the transform. Put another way, the potential energy operator is diagonal in real space, so it should be computed there. The bookkeeping needed to compute $\vec{K}_{11,12,13}$, and load Fourier components of U and ψ into $N \times N \times N$ arrays is indicated by

```

for j1=1 through N
  {
  for j2=1 through N
    {
    for j3=1 through N
      {
      for m=1 through 3
        {
          K (m) = l (j1) * b1 (m) + l (j2) * b2 (m) + l (j3) * b3 (m)
                                                    Builds reciprocal lattice vector K

          kp (m) = q (m) - K (m)
        }
        uu (j1, j2, j3) = U (K)
                                                    Loads Fourier components of potential into
                                                    array uu.

        ps (j1, j2, j3) = psi (kp)
                                                    Loads Fourier components of  $\psi$  into array ps
      }
    }
  }
}

```

References

- E. O. Brigham (1988), *The Fast Fourier Transform and its Applications*, Prentice Hall, Englewood Cliffs, NJ.
- H. J. Nussbaumer (1982), *Fast Fourier Transform and Convolution Algorithms*, Springer-Verlag, Berlin.
- W. H. Press, S. A. Teukolsky, W. T. Vetterling, and B. P. Flannery (1992), *Numerical Recipes in C*, 2nd ed., Cambridge University Press, Cambridge.

B. Variational Techniques

B.1 Functionals and Functional Derivatives

A *functional* is a rule for obtaining a number from a function. For example, the rule might be “integrate the function ψ over all space,” in which case the functional is

$$F\{\psi\} = \int d\vec{r}' \psi(\vec{r}'). \quad (\text{B.1})$$

Other examples might involve multiplying the function ψ by $\exp(-r'^2/r_0^2)$ or by itself before integrating.

A *functional derivative* describes how a functional changes when the function placed into it changes by a small amount. Functional derivatives can be defined formally by a natural extension of the definition of ordinary differentiation. Given the functional $F\{\psi\}$, then the functional derivative describing how F responds to small alterations of ψ in the vicinity of \vec{r} is

$$\frac{\delta F\{\psi\}}{\delta\psi(\vec{r})} = \lim_{\epsilon \rightarrow 0} \frac{F(\psi(\vec{r}') + \epsilon\delta(\vec{r}' - \vec{r})) - F(\psi(\vec{r}'))}{\epsilon}. \quad (\text{B.2})$$

Alter ψ by adding a small function peaked around \vec{r} , and divide through by the integral of the added function.

Example. If

$$F\{\psi(\vec{r}')\} = \int d\vec{r}' g(\psi(\vec{r}')), \quad (\text{B.3})$$

where g is an ordinary function, then

$$\frac{\delta F\{\psi\}}{\delta\psi(\vec{r})} = \lim_{\epsilon \rightarrow 0} \frac{\int d\vec{r}' g(\psi(\vec{r}') + \epsilon\delta(\vec{r}' - \vec{r})) - g(\psi(\vec{r}'))}{\epsilon} \quad (\text{B.4})$$

$$= \lim_{\epsilon \rightarrow 0} \frac{\int d\vec{r}' g(\psi(\vec{r}')) + \epsilon g'(\psi(\vec{r}'))\delta(\vec{r}' - \vec{r}) - g(\psi(\vec{r}'))}{\epsilon} \quad (\text{B.5})$$

$$= g'(\psi(\vec{r})). \quad (\text{B.6})$$

Courage is needed to perform a Taylor expansion in powers of a delta function, which is infinitely large where its argument vanishes. More mathematically compelling accounts of this procedure can be found, for example, in Zeidler (1995) or Hassani (1999), Chapter 30, pp. 973–1002.

B.2 Time-Independent Schrödinger Equation

The time-independent Schrödinger equation is equivalent to a variational principle, a point of view that is particularly valuable in suggesting approximation schemes. To derive the variational rule, consider the functional

$$F_{\mathcal{H}}\{\psi\} = \langle \psi | \hat{\mathcal{H}} | \psi \rangle, \quad \text{A functional is a rule for obtaining a number from a function, in this case from the wave function } |\psi\rangle. \quad (\text{B.7})$$

and find its extrema subject to the constraint that

$$\langle \psi | \psi \rangle = 1. \quad (\text{B.8})$$

An extremum of a functional F is a function ψ causing functional derivatives $\delta F / \delta \psi(\vec{r})$ to vanish for all \vec{r} . A function that minimizes F will be an extremum, but so will be a function which maximizes F , or one for which F is at a saddle point, such as sketched in Figure 7.4.

There are two ways to enforce the constraint (B.8).

- Divide the functional $F_{\mathcal{H}}$ through by $\langle \psi | \psi \rangle$ and take functional derivatives of

$$\frac{\langle \psi | \hat{\mathcal{H}} | \psi \rangle}{\langle \psi | \psi \rangle}. \quad (\text{B.9})$$

If $|\psi\rangle$ is multiplied by any overall scale factor, (B.9) does not change, because the factor cancels between numerator and denominator. An extremum of (B.9) is therefore sensitive to the shape of ψ , but cannot depend upon its normalization. After finding an extremum of (B.9), one is free to set $\langle \psi | \psi \rangle = 1$.

- Use the method of Lagrange multipliers. In this method, one takes the constraint that is supposed to be imposed, multiplies it by an arbitrary constant, the Lagrange multiplier, and subtracts the product from the original functional. In the present case, that means finding extrema of

$$\langle \psi | \hat{\mathcal{H}} | \psi \rangle - \mathcal{E} \langle \psi | \psi \rangle. \quad \mathcal{E} \text{ is the Lagrange multiplier.} \quad (\text{B.10})$$

The simplest way to find extrema of $F_{\mathcal{H}}$ is by treating $\langle \psi |$ and $|\psi\rangle$ as independent variables, and requiring the variation of $F_{\mathcal{H}}$ to vanish simply by writing

$$0 = \frac{\partial}{\partial \langle \psi |} \frac{\langle \psi | \hat{\mathcal{H}} | \psi \rangle}{\langle \psi | \psi \rangle} = \frac{\hat{\mathcal{H}} | \psi \rangle}{\langle \psi | \psi \rangle} - |\psi\rangle \frac{\langle \psi | \hat{\mathcal{H}} | \psi \rangle}{\langle \psi | \psi \rangle^2} \quad (\text{B.11})$$

$$\Rightarrow \hat{\mathcal{H}} | \psi \rangle = \mathcal{E} | \psi \rangle \quad \text{with} \quad \mathcal{E} = \frac{\langle \psi | \hat{\mathcal{H}} | \psi \rangle}{\langle \psi | \psi \rangle} \quad \text{The method of Lagrange multipliers gives the same result.} \quad (\text{B.12})$$

Therefore the variational procedure is equivalent to Schrödinger's equation.

If the steps leading to Eq. (B.12) seem unjustified, it is easy to employ the definition of functional differentiation (B.2) on the functional $\int d\vec{r}' \psi^*(\vec{r}') [\hat{\mathcal{H}} - \mathcal{E}] \psi(\vec{r}')$ and show that

$$0 = \frac{\delta}{\delta \psi^*(\vec{r})} \int d\vec{r}' \psi^*(\vec{r}') [\hat{\mathcal{H}} - \mathcal{E}] \psi(\vec{r}') \tag{B.13}$$

$$\Rightarrow 0 = [\hat{\mathcal{H}} - \mathcal{E}] \psi(\vec{r}) \tag{B.14}$$

Anyone uncomfortable with treating ψ and ψ^* as independent functions is free to write everything out in terms of the real and imaginary parts of ψ , differentiate with respect to them, and verify that the same results are obtained again.

B.3 Time-Dependent Schrödinger Equation

The equivalence of the time-independent Schrödinger equation to extrema of the mean value of the Hamiltonian is well known. It is less commonly appreciated that the time-dependent Schrödinger equation can be obtained from a variational principle. Like so many other formal relations in quantum mechanics, the observation is due to Dirac.

The action L giving the time-dependent equation is simply

$$L = \int dt \mathcal{L}, \tag{B.15}$$

where

$$\mathcal{L} = \langle \psi | i\hbar \frac{\partial}{\partial t} | \psi \rangle - \langle \psi | \hat{\mathcal{H}} | \psi \rangle. \tag{B.16}$$

Lagrange's equation are

$$\frac{\delta L}{\delta \psi^*(\vec{r}, t)} = 0 \tag{B.17}$$

$$\Rightarrow \frac{d}{dt} \frac{\partial \mathcal{L}}{\partial \langle \dot{\psi} |} = \frac{\partial \mathcal{L}}{\partial \langle \psi |} \tag{B.18}$$

$$\Rightarrow i\hbar \frac{\partial}{\partial t} | \psi \rangle = \hat{\mathcal{H}} | \psi \rangle. \tag{B.19}$$

Because there is no dependence upon $\langle \dot{\psi} |$, everything comes from the right hand side.

A more detailed derivation of Eq. (B.19) can be obtained by using the methods of functional differentiation described at the beginning of this appendix. The approximation scheme suggested by this calculation is to substitute for $|\psi\rangle$ some restricted set of wave functions parameterized by a number of variables, and then to use Eqs. (B.16) and (B.18) to find equations of motion.

This variational principle has great advantages when one's goal is to obtain effective equations of motion for collective coordinates. Unlike an effective Hamiltonian, an effective Lagrangian \mathcal{L} makes few demands. There is no requirement that one identify canonical momenta conjugate to the coordinates. One can take any parameterization of ψ that seems handy, insert it into the Lagrangian, and obtain equations of motion for the parameters. This method is employed in Section 15.5.5 to find the dispersion relation for superfluid helium, and in Section 16.4 to find the equation of motion for electron wave packets.

B.4 Method of Steepest Descent

Many intractable integrals can be approximated well by the *method of steepest descent*. The integrals are of the form

$$\int dx e^{-\beta H(x)}, \quad (\text{B.20})$$

and the approximation becomes good in the limit where the parameter β becomes infinite. Find the point x_0 in the complex plane where $H(x_0)$ is minimized, and deform the integration contour so that instead of passing necessarily along the real axis, the contour heads off into the complex plane and passes through x_0 . If $H(x)$ is singular off the real axis and deforming the contour involves picking up large numbers of poles, it may be advisable to settle for the point x_1 on the real axis where $H(x)$ is minimized. In any event, write

$$H(x) \approx H(x_0) + \frac{(x - x_0)^2}{2} H''(x_0) + \dots \quad (\text{B.21})$$

$$\Rightarrow \int dx e^{-\beta H(x)} \approx e^{-\beta H(x_0)} \sqrt{\frac{2\pi}{|\beta H''(x_0)|}}. \quad \text{Do the Gaussian integral.} \quad (\text{B.22})$$

This method is employed in Section 16.3.1 on Zener tunneling.

References

- S. Hassani (1999), *Mathematical Physics: A Modern Introduction to Its Foundations*, Springer-Verlag, New York.
- E. Zeidler (1995), *Applied Functional Analysis: Applications to Mathematical Physics*, Springer-Verlag, New York.

C. Second Quantization

C.1 Rules

C.1.1 States

Begin with a complete orthonormal set of basis functions ψ_l . Any collection of identical particles can be described by sums of products of these functions. In the formalism of second quantization, one focuses upon many-body basis functions, which describe how many particles are in each state. For example,

$$|0, 2, 3, 10, \dots\rangle \quad (\text{C.1})$$

means that no particles are in state ψ_1 , two particles are in state ψ_2 , three are in state ψ_3 , and so on. The integers describing the numbers of particles are called *occupation numbers*.

C.1.2 Operators

The operators of second quantization change the numbers of particles in these quantum states. There is a *creation operator* with index l that adds one particle to state l and an *annihilation operator* with index l that takes one particle away from state l .

Fermions. The Pauli principle prohibits more than one electron from occupying any given quantum state, so the occupation numbers all are zero or one. The creation and annihilation operators are usually denoted by \hat{c}_l^\dagger and \hat{c}_l respectively. The way they operate is

$$\hat{c}_l |n_1 n_2 \dots n_l \dots\rangle = \begin{cases} 0 & \text{if } n_l = 0 \\ |n_1 n_2 \dots 0 \dots\rangle & \text{if } n_l = 1 \end{cases} \quad (\text{C.2a})$$

$$\hat{c}_l^\dagger |n_1 n_2 \dots n_l \dots\rangle = \begin{cases} 0 & \text{if } n_l = 1 \\ |n_1 n_2 \dots 1 \dots\rangle & \text{if } n_l = 0. \end{cases} \quad (\text{C.2b})$$

The operators anticommute:

$$\hat{c}_l^\dagger \hat{c}_{l'}^\dagger + \hat{c}_{l'}^\dagger \hat{c}_l^\dagger = 0 \quad (\text{C.3a})$$

$$\hat{c}_l \hat{c}_{l'} + \hat{c}_{l'} \hat{c}_l = 0 \quad (\text{C.3b})$$

$$\hat{c}_l \hat{c}_{l'}^\dagger + \hat{c}_{l'}^\dagger \hat{c}_l = \delta_{ll'}. \quad (\text{C.3c})$$

Bosons. Bosons can inhabit any quantum state as often as they please, so the occupation numbers range over all non-negative integers. The creation and annihilation operators are usually denoted by \hat{a}_l^\dagger and \hat{a}_l respectively. The way they operate is

$$\hat{a}_l |n_1 n_2 \dots n_l \dots\rangle = \sqrt{n_l} |n_1 n_2 \dots n_l - 1 \dots\rangle \quad (\text{C.4a})$$

$$\hat{a}_l^\dagger |n_1 n_2 \dots n_l \dots\rangle = \sqrt{n_l + 1} |n_1 n_2 \dots n_l + 1 \dots\rangle. \quad (\text{C.4b})$$

The operators commute:

$$\hat{a}_l^\dagger \hat{a}_{l'} - \hat{a}_{l'}^\dagger \hat{a}_l = 0 \quad (\text{C.5a})$$

$$\hat{a}_l \hat{a}_{l'} - \hat{a}_{l'} \hat{a}_l = 0 \quad (\text{C.5b})$$

$$\hat{a}_l \hat{a}_{l'}^\dagger - \hat{a}_{l'}^\dagger \hat{a}_l = \delta_{ll'}. \quad (\text{C.5c})$$

C.1.3 Hamiltonians

A Hamiltonian that is given as a sum of operators on single particles can be rewritten in second quantized notation as

$$\hat{\mathcal{H}} = \sum_j \hat{f}_j \quad \begin{array}{l} f_j \text{ means an operator such as } f(\vec{r}_j) \text{ that acts} \\ \text{in some identical fashion upon each particle} \\ j \text{ in turn.} \end{array} \quad (\text{C.6})$$

$$= \sum_{ll'} \hat{c}_l^\dagger \langle \psi_l(1) | \hat{f}_l | \psi_{l'}(1) \rangle \hat{c}_{l'}. \quad \begin{array}{l} \text{The wave functions } \psi_l \text{ and operator } \hat{f} \text{ all act} \\ \text{on particle 1. The expression for bose opera-} \\ \text{tors is identical.} \end{array} \quad (\text{C.7})$$

The notation $|\psi_{l'}(1)\rangle$ means that particle number 1 is in state $\psi_{l'}$. For example, if \hat{f} is the kinetic energy operator and ψ_l is the product of a Wannier function w_l and a spin function χ_l , then

$$\langle \psi_l(1) | \hat{f}_l | \psi_{l'}(1) \rangle = \delta_{\chi_l \chi_{l'}} \int d\vec{r}_1 w_l^*(\vec{r}_1) \frac{-\hbar^2 \nabla_1^2}{2m} w_{l'}(\vec{r}_1) \quad (\text{C.8})$$

The leading delta function requires the spins of the two states to be the same.
The Laplacian ∇_1^2 acts on variable \vec{r}_1 .

A Hamiltonian that is given as a sum of operators on pairs of particles can be rewritten in second quantized notation as

$$\hat{\mathcal{H}} = \sum_{j \neq j'} \hat{f}_{jj'} \quad \begin{array}{l} f_{jj'} \text{ means an operator such as } f(\vec{r}_j, \vec{r}_{j'}) \text{ that} \\ \text{acts in some identical fashion upon pairs of} \\ \text{particles.} \end{array} \quad (\text{C.9})$$

$$= \sum_{ll' l'' l'''} \hat{c}_l^\dagger \hat{c}_{l'}^\dagger \hat{c}_{l''} \hat{c}_{l'''} \langle \psi_l(1) \psi_{l'}(2) | \hat{f}_{l l'} | \psi_{l''}(1) \psi_{l'''}(2) \rangle \quad (\text{C.10})$$

For example, if $f_{l l'}$ is the Coulomb interaction and ψ_l is the product of some spatial wave function ϕ_l and a spin function χ_l , then

$$\begin{aligned} & \langle \psi_l(1) \psi_{l'}(2) | \hat{f}_{l l'} | \psi_{l''}(1) \psi_{l'''}(2) \rangle \\ &= \frac{1}{2} \delta_{\chi_l \chi_{l''}} \delta_{\chi_{l'} \chi_{l'''}} \int d\vec{r}_1 d\vec{r}_2 \phi_l^*(\vec{r}_1) \phi_{l'}^*(\vec{r}_2) \frac{e^2}{|\vec{r}_1 - \vec{r}_2|} \phi_{l''}(\vec{r}_1) \phi_{l'''}(\vec{r}_2). \end{aligned} \quad (\text{C.11})$$

Often one does not write down spin sums or spin delta functions explicitly and just multiplies the final answer by appropriate factors of two.

C.2 Derivations

C.2.1 Bosons

A collection of Bose particles can be described by a wave function of the form

$$|n_1 n_2 n_3 \dots\rangle = \sqrt{\frac{1}{N! n_1! n_2! \dots}} \sum_{\text{Permutations } s_j} \prod_{j=1}^N |\psi_{l(j)}(s_j)\rangle. \quad (\text{C.12})$$

The function s_j gives some permutation of the integers j , and by summing over all permutations the wave function is guaranteed to be symmetric under interchange of all indices.

The function $l(j)$ is some function into the positive integers. The idea is that the states ψ_l are numbered in a way that may be quite arbitrary. Suppose one decides to build a many-body state with one particle in state 1 and two particles in state 3. The function $l(j)$ could then be

$$l(1) = 3, \quad l(2) = 1 \quad l(3) = 3. \quad (\text{C.13})$$

Notation of the form $|\psi_2(6)\rangle$ means that particle number 6 is in state ψ_2 .

The number of times a certain integer $l(j)$ appears as j ranges from 1 to N is n_l , so n_l gives the number of particles in state l . The factors of $n_1! n_2! \dots$ account for the fact that any given term in the sum where n_1 particles are in state 1 appears $n_1!$ times. To illustrate that the factorials are correctly employed, suppose first of all that there is only one particle in each distinct state. Then there are $N!$ distinct orthogonal functions appearing in the sum (C.12), and the normalization must be $1/\sqrt{N!}$. On the other hand, suppose all particles are in state ψ_1 . Then all the $N!$ terms in the sum are identical, and the sum must be divided by $N!$ to produce a normalized wave function.

To study the behavior of this wave function, it is helpful to define the operator

$$\hat{E}_{l \leftarrow l'} = \sum_j |\psi_l(j)\rangle \langle \psi_{l'}(j)|. \quad (\text{C.14})$$

The effect of this operator is to search one at a time for each particle in state $\psi_{l'}$ and move it to state ψ_l .

To use this operator, consider a Hamiltonian of the form (C.6),

$$\hat{\mathcal{H}} = \sum_{j=1}^N \hat{f}_j = \sum_{l'l} |\psi_l(j)\rangle \langle \psi_l(j)| \hat{f}_j |\psi_{l'}(j)\rangle \langle \psi_{l'}(j)| \quad (\text{C.15})$$

$$= \sum_{l'l} \hat{E}_{l \leftarrow l'} \langle \psi_l(1)| \hat{f}_1 |\psi_{l'}(1)\rangle. \quad (\text{C.16})$$

The matrix elements of the one-particle operator \hat{f} do not depend upon which particle is involved, so the label 1 can be used instead of j .

Let $\hat{E}_{l \leftarrow l'}$ act upon $|n_1 n_2 \dots\rangle$. If state $\psi_{l'}$ is not occupied, the result is zero. If it is occupied, then in every term of (C.12), there will be precisely $n_{l'}$ values of j

for which there is a nonzero result, with the population of state l' being reduced by 1 and the population of state l being increased by 1. The result will not be properly normalized because $\sqrt{n_{l'}!n_l!}$ is in the denominator rather than $\sqrt{(n_{l'} - 1)!(n_l + 1)!}$, and a factor of $n_{l'}$ has been acquired along the way. So

$$\hat{E}_{l \leftarrow l'} |n_1 n_2 \dots\rangle = \sqrt{n_{l'}(n_l + 1)} | \dots n_{l'} - 1 \dots n_l + 1 \dots \rangle. \quad (\text{C.17})$$

For this reason, define

$$\hat{a}_l^\dagger |n_1, n_2 \dots\rangle = \sqrt{n_l + 1} | \dots n_l + 1 \dots \rangle \quad (\text{C.18a})$$

$$\hat{a}_l |n_1, n_2 \dots\rangle = \sqrt{n_l} | \dots n_l - 1 \dots \rangle \quad (\text{C.18b})$$

so that

$$\hat{E}_{l \leftarrow l'} = \hat{a}_l^\dagger \hat{a}_{l'}. \quad (\text{C.19})$$

It is easy from Eq. (C.18) to check the commutation relations (C.5) by allowing the creation and annihilation operators to act in various orders upon general states $|n_1 n_2 \dots\rangle$.

C.2.2 Fermions

The wave function describing a collection of fermions must be antisymmetric under interchange of arguments, and it consists of sums of terms of the form

$$\Psi = |n_1 n_2 \dots\rangle = \sqrt{\frac{1}{N!}} \sum_{\text{Permutations } s_j} (-1)^s \prod_{j=1}^N |\psi_{l(j)}(s_j)\rangle, \quad (\text{C.20})$$

where the sum is over all permutations s_j of $j = 1 \dots N$, with s the sign of the permutation. In order for Ψ not to equal zero, no more than one electron is allowed to inhabit each individual state. If an electron is in state l , then n_l is one and otherwise it is zero.

Given the occupation numbers n_l for each state ψ_l , the wave function that can be formed from the collection is almost unique. There is only one ambiguity, which has to do with the overall sign of the wave function. The ambiguity is avoided by requiring that $l(j)$ be an increasing function of j .

Consider again a Hamiltonian of the form (C.15), acting on antisymmetric wave functions Ψ as in Eq. (C.20). It is sufficient to examine the behavior of a single term in the sum (C.15). For example, look at

$$\langle \Psi_a | \psi_l(1) \rangle \langle \psi_{l'}(1) | \Psi_b \rangle. \quad (\text{C.21})$$

(C.21) is nonzero only if in $|\Psi_b\rangle$ $\psi_{l'}$ is occupied, ψ_l unoccupied, while in $|\Psi_a\rangle$ $\psi_{l'}$ is unoccupied, ψ_l is occupied, and otherwise Ψ_a and Ψ_b are identical. To be explicitly, let

$$|\Psi_a\rangle = \sum_s (-1)^s \frac{1}{\sqrt{3!}} |\psi_1(s_1)\rangle |\psi_2(s_2)\rangle |\psi_3(s_3)\rangle \quad (\text{C.22})$$

$$|\Psi_b\rangle = \sum_s (-1)^s \frac{1}{\sqrt{3!}} |\psi_1(s_1)\rangle |\psi_3(s_2)\rangle |\psi_4(s_3)\rangle \quad (\text{C.23})$$

and look at

$$\langle \Psi_a | \psi_2(1) \rangle \langle \psi_4(1) | \Psi_b \rangle. \quad (\text{C.24})$$

The parts of the wave functions that survive are

$$\frac{1}{3!} \left[\langle \psi_3(2) | \langle \psi_1(3) | - \langle \psi_1(2) | \langle \psi_3(3) | \right. \\ \left. \begin{array}{l} \langle \psi_2(1) | \psi_2(1) \rangle \\ \langle \psi_4(1) | \psi_4(1) \rangle \end{array} \right\} \quad (\text{C.25}) \\ \left[| \psi_1(2) \rangle | \psi_3(3) \rangle - | \psi_3(2) \rangle | \psi_1(3) \rangle \right]$$

$$= -\frac{1}{3}. \quad (\text{C.26})$$

The general lesson to learn from this example is that one must permute ψ_l past all the states below it in the ordering scheme to produce the term $|\psi_l(1)\rangle$, obtaining a factor of

$$(-1)^{\sum_{j=1}^{l-1} n_j}, \quad (\text{C.27})$$

where n_l is 1 if state l is occupied in Ψ_a and zero otherwise. One also has a factor

$$(-1)^{\sum_{j=1}^{l'-1} n_j} \quad (\text{C.28})$$

similarly, so that

$$\sum_{j=1}^N \langle \Psi_a | \psi_l(j) \rangle \langle \psi_{l'}(j) | \Psi_b \rangle = (-1)^{\sum_{j=1}^{l'-1} n_j} (-1)^{\sum_{j=1}^{l-1} n_j} \quad (\text{C.29})$$

if it is not zero.

Therefore, one can again define the operator $\hat{E}_{l \leftarrow l'}$ from Eq. (C.14). Write wave functions in the occupation number representation

$$|\Psi\rangle = |n_1 n_2 n_3 \dots\rangle, \quad (\text{C.30})$$

where each n_i can be either zero or one. In the example above,

$$|\Psi_a\rangle = |1110000 \dots\rangle \quad (\text{C.31})$$

$$|\Psi_b\rangle = |1011000 \dots\rangle. \quad (\text{C.32})$$

In acting on such a wave function

$$\hat{E}_{l \leftarrow l'} |n_1 n_2 n_3 \dots\rangle \quad (\text{C.33}) \\ = (-1)^{\sum_{j=1}^{l'-1} n_j} (-1)^{\sum_{j=1}^{l-1} n_j} \delta_{n_{l'} 1} \delta_{n_l 0} |n_1 n_2 n_3 \dots n_{l'} - 1 \dots n_l + 1 \dots\rangle.$$

The creation and annihilation operators are defined so that

$$\hat{E}_{l \leftarrow l'} = \hat{c}_l^\dagger \hat{c}_{l'}. \quad (\text{C.34})$$

More explicitly,

$$\hat{c}_l |n_1 n_2 n_3 \dots\rangle = \delta_{1, n_l} (-1)^{\sum_{j=1}^{l-1} n_j} |n_1 n_2 n_3 \dots n_{l-1} 0 n_{l+1} \dots\rangle \quad (\text{C.35a})$$

$$\hat{c}_l^\dagger |n_1 n_2 n_3 \dots\rangle = \delta_{0, n_l} (-1)^{\sum_{j=1}^{l-1} n_j} |n_1 n_2 n_3 \dots n_{l-1} 1 n_{l+1} \dots\rangle. \quad (\text{C.35b})$$

The anti-commutation relations in Eq. (C.3) can be verified explicitly from this definition.

A final relation that should be verified is Eq. (C.10). The special ordering of the creation and annihilation operators results from the condition $j \neq j'$ in the sum over particle numbers. Write

$$\begin{aligned} & \sum_{j \neq j'} \hat{f}_{jj'} \\ &= \sum_{\substack{l'l''l'''' \\ j \neq j'}} |\psi_l(j)\rangle |\psi_{l'}(j')\rangle \langle \psi_l(j) \psi_{l'}(j') | \hat{f}_{jj'} | \psi_{l''}(j) \psi_{l''''}(j') \rangle \langle \psi_{l''}(j) | \langle \psi_{l''''}(j') | \end{aligned} \quad (\text{C.36})$$

$$\begin{aligned} &= \sum_{\substack{l'l''l'''' \\ jj'}} [|\psi_l(j)\rangle \langle \psi_{l''}(j)|] [|\psi_{l'}(j')\rangle \langle \psi_{l''''}(j')|] \langle \psi_l(j) \psi_{l'}(j') | \hat{f}_{jj'} | \psi_{l''}(j) \psi_{l''''}(j') \rangle \\ &\quad - \sum_{\substack{l'l''l'''' \\ j}} \delta_{l'l''} [|\psi_l(j)\rangle \langle \psi_{l''}(j)|] \langle \psi_l(j) \psi_{l'}(j) | \hat{f}_{jj} | \psi_{l''}(j) \psi_{l''''}(j) \rangle \end{aligned} \quad (\text{C.37})$$

$$\begin{aligned} &= \sum_{l'l''l''''} \hat{E}_{l \leftarrow l''} \hat{E}_{l' \leftarrow l''''} \langle \psi_l(1) \psi_{l'}(2) | \hat{f}_{12} | \psi_{l''}(1) \psi_{l''''}(2) \rangle \\ &\quad - \sum_{l'l''l''''} \delta_{l'l''} \hat{E}_{l \leftarrow l''} \langle \psi_l(1) \psi_{l'}(2) | \hat{f}_{12} | \psi_{l''}(1) \psi_{l''''}(2) \rangle \end{aligned} \quad (\text{C.38})$$

$$\begin{aligned} &= \sum_{l'l''l''''} \hat{c}_l^\dagger \hat{c}_{l''} \hat{c}_{l'}^\dagger \hat{c}_{l''''} \langle \psi_l(1) \psi_{l'}(2) | \hat{f}_{12} | \psi_{l''}(1) \psi_{l''''}(2) \rangle \\ &\quad - \sum_{l'l''l''''} \delta_{l'l''} \hat{c}_l^\dagger \hat{c}_{l''} \langle \psi_l(1) \psi_{l'}(2) | \hat{f}_{12} | \psi_{l''}(1) \psi_{l''''}(2) \rangle \end{aligned} \quad (\text{C.39})$$

$$= \sum_{l'l''l''''} \hat{c}_l^\dagger \hat{c}_{l''} \hat{c}_{l'}^\dagger \hat{c}_{l''''} \langle \psi_l(1) \psi_{l'}(2) | \hat{f}_{12} | \psi_{l''}(1) \psi_{l''''}(2) \rangle. \quad (\text{C.40})$$

Index

Page numbers of references are in *italics*.

Page numbers of problems are in **bold**.

- α
- α_T , linear expansion, 363
 - Cartesian index, 325
 - critical exponent, 748
 - fine structure constant, 763
 - Landau–Ginzburg theory coefficient, 844
 - Madelung constant, 304
 - magnetic anisotropy, 737
 - optical absorption coefficient, 68, 616
 - polarizability, 299, 398
 - Seebeck coefficient, 497
- β
- β -brass, 742
 - $\beta = 1/k_B T$, 110
 - β_T , linear expansion, 363
 - Cartesian index, 325
 - critical exponent, 748
 - Landau–Ginzburg theory coefficient, 844
 - scaling function, 549
 - Siebert relation, 70
- Γ
- Brillouin zone symmetry point, 193
 - decay rate, 375
 - fracture energy, 401
- γ
- γ_T , Grüneisen parameter, 362
 - $\hat{\gamma}$, electron creation and annihilation operators, 870
 - Cartesian index, 325
 - critical exponent, 748
 - Sommerfeld parameter, 170
 - sum of Gaussians, 240
- Δ
- expansion parameter, 208
 - superconducting gap, 867
- δ
- $\delta(\vec{r})$ or $\delta_{ll'}$, delta function, 49
 - $\vec{\delta}$, nearest neighbor vectors, 226
- Cartesian index, 325
- critical exponent, 748
 - integer for stacking period, 79
- ϵ
- $\vec{\epsilon}$, phonon polarization, 347
 - dielectric function, 397
 - fraction for interplanar spacing, 79
 - Lennard-Jones energy, 299
- ζ
- complex variable, $\zeta = x + iy$, 403
- η
- critical exponent, 749
 - imaginary part of energy, 536
 - viscosity, 117
- Θ
- Θ solvent, 127, 423
 - Θ_D , Debye temperature, 359
 - Curie–Weiss temperature, 731
- θ
- angle, 47
 - Heaviside step function, 136
- κ
- κ_c , electron–ion screening length, 860
 - extinction coefficient, 616
 - flow stress, 425
 - ratio of superconducting penetration depth and coherence length, 848
 - thermal conductivity, 454
 - vorticity, 438
- λ
- λ point in liquid helium, 427
 - λ_L , London penetration depth, 840
 - λ_{ep} , electron–phonon interaction in McMillan theory of superconductivity, 880
 - eigenvalue, 272
 - Lamé constant, 328
 - wavelength, 71

- μ
- μ^* , Coulomb interaction in McMillan theory of superconductivity, 880
 - μ_B , Bohr magneton, 730
 - chemical potential, 86
 - Lamé constant, 328
 - magnetic permeability, 724
 - mobility, 591
- ν
- critical exponent, 749
 - Landau level, filling fraction, 772
 - Poisson's ratio, 330
- Ξ
- random vector, 111
- ξ
- $\vec{\xi}$, random force, 112
 - correlation length, 749
 - screening length, 258
 - superconducting coherence length, 845
- Π
- grand potential, 164
 - momentum tensor, 414
 - Peltier coefficient, 498
- π
- 3.14159 . . . , 9
 - canonical momentum, 470
- ρ
- mass density, 329
 - resistivity, 454
- Σ
- dimensionless stress, 403
 - sum, 48
- σ
- $\sigma_{\alpha\beta}$, conductivity tensor, 493
 - $\sigma_{\alpha\beta}$, stress tensor, 326
 - electrical conductivity, 454
 - Lennard-Jones radius, 299
 - scattering cross section, 46
 - spin index, 236
- τ
- τ_e , energy-dependent relaxation time, 488
 - golden mean, 135
 - relaxation time, 453
- Φ
- Φ , magnetic flux, 772
 - Φ_0 , magnetic flux quantum, 772
 - Phonon dynamical matrix, 346
- ϕ
- $\phi_{\mathcal{E}\vec{k}}$, augmented plane wave basis function, 275
 - analytic function, 403
 - Hartree Fock basis functions, 236
 - phase, 223
 - two body potential, 15
 - work function, 86
- χ
- χ_c , charge susceptibility, 627
 - dielectric susceptibility, 398
 - group character, 198
 - magnetic susceptibility, 724
 - spin eigenfunctions, 236
- Ψ
- wave function, 157
- ψ
- wave function, 157
- Ω
- $\vec{\Omega}$, anomalous velocity, 469
 - solid angle, 46
 - volume of unit cell, 181
- ω
- ω_c , cyclotron frequency, 634
 - ω_p , plasma frequency, 618
 - frequency, 46
- A
- A_I , cohesive energy lattice sum, 300
 - \vec{A} , vector potential, 460
 - scattering amplitude, 46
 - area, 379
 - Einstein A coefficient, 647
 - hexagonal Brillouin zone symmetry point, 194
- a
- \hat{a} , phonon annihilation operator, 352
 - a^{at} atomic wave functions, 219
 - lattice constant, 7
 - neutron scattering length, 367
 - primary lattice constant, 19
- \mathcal{A}
- Richardson–Dushman constant, 572
- B
- \vec{B} , magnetic induction, 456
 - bulk modulus, 301
 - Einstein B coefficient, 647
- b
- \vec{b} , Bravais lattice primitive vectors, 51
 - amplitude in BCS theory of superconductivity, 866
 - damping constant, 112
 - tertiary lattice constant, 19
- C
- $C_{\alpha\beta\gamma\delta}$, tensor for linear elasticity, 325
 - capacitance, 604
 - constant, 304
 - cyclic point group, 36
 - extensive specific heat, 354
- c
- \hat{c} , electron annihilation operator, 506
 - c_V , intensive specific heat, 168

- concentration, 101
- secondary lattice constant, 19
- speed of light, 61
- speed of sound, 332
- D*
 - $D_{\vec{k}}$, $D(\mathcal{E})$, densities of states, 159
 - \vec{D} , electric displacement, 614
 - dihedral point group, 36
- d*
 - $[d\vec{k}]$, integration incorporating density of states., 161
 - atomic orbital, 269
 - interplanar spacing, 79
 - nearest neighbor spacing, 43
- \mathcal{D}
 - diffusion constant, 98
- E*
 - E , Lagrangean strain tensor, 321
 - \vec{E} , electric field, 456
 - unit matrix, 193
- e*
 - 2.71828 . . . , 46
 - \hat{e} , unit vector, 272
 - $e_{\alpha\beta}$, strain tensor, 37, 325
 - electron charge (positive), 61
- \mathcal{E}
 - \mathcal{E}_F , Fermi energy, 162
 - \mathcal{E}_g , energy gap, 211
 - $\mathcal{E}_{n\vec{k}}$, band energies, 182
 - energy, 15
- F*
 - F_{HK} , Hohenberg-Kohn functional, 246
 - force, 112
 - Lindhard dielectric function, 244
 - scattering form factor, 54
- f*
 - 1/*f* noise, 530
 - $f(\mathcal{E})$, $f_{\vec{k}}$, Fermi function, 165
 - atomic orbital, 269
 - scattering form factor, 46
- \mathcal{F}
 - free energy, 101
- G*
 - conductance, 563
 - electrochemical force, 495
 - Gibbs free energy, 429
 - Green's function, 536
 - group element, 13
 - shear modulus, 330
 - wave number for ionic displacements, 310
- g*
 - g*, metric tensor, 321
 - amplitude in BCS theory of superconductivity, 866
- correlation function, 114
- gain in lasers, 648
- gravity, 379
- Landé *g* factor, 765
- probability distribution in Boltzmann equation, 484
- separation parameter for Ewald summation, 303
- H*
 - bcc Brillouin zone symmetry point, 194
 - hexagonal Brillouin zone symmetry point, 194
 - magnetic field, 473
- h*
 - \hbar , $h/2\pi$, 86
 - height, 379
 - number of elements in group representation, 198
 - Planck's constant, 64
- \mathcal{H}
 - Hamiltonian, 157
- I*
 - scattering intensity, 46
 - stress invariants, 424
- i*
 - $\sqrt{-1}$, 46
 - Miller index, 51
- J*
 - magnetic exchange coupling constant, 734
 - stress invariants, 425
 - total current, 87
- j*
 - \vec{j} , current density, 98
 - j_l , Bessel function, 276
 - integer, 68
 - Miller index, 51
- K*
 - K_J , Josephson constant, 858
 - K_T , isothermal compressibility, 748
 - \vec{K} , reciprocal lattice vector, 50
 - fcc Brillouin zone symmetry point, 193
 - hexagonal Brillouin zone symmetry point, 194
 - stress intensity factor, 405
- k*
 - \vec{k} space, 159
 - \vec{k} , Bloch wave vector, 182
 - $\vec{k} \cdot \hat{P}$ method, 457
 - k_B , Boltzmann's constant, 43
 - k_F , Fermi wave vector, 159
 - \vec{k} , wave vector, 46
 - Miller index, 51
- \mathcal{K}
 - spring constant, 43

L

- L_0 , Lorenz number, 496
- \mathbf{L} , thermoelectric transport matrix, 495
- diffusion length, 594
- fcc Brillouin zone symmetry point, 193
- hexagonal Brillouin zone symmetry point, 194
- system length, 158

l

- l_T , mean free path, 68
- integer, 48
- matrix dimensions group representation, 198
- Miller index, 53

M

- \mathbf{M} , effective mass tensor, 459
- hexagonal Brillouin zone symmetry point, 194
- ion mass, 155, 342
- large integer, 101
- magnetic dipole moment density, 723

m

- m^* , effective mass, 494
- electron mass, 86
- integer, 79

 \mathcal{M}

- multiplicity, 73

N

- N -process, 527
- bcc Brillouin zone symmetry point, 194
- number of particles, 48

n

- \hat{n} , director in liquid crystals, 121
- \hat{n} , unit normal, 187
- \bar{n} , index of refraction, 616
- n_i , Bose-Einstein factor, 356
- band index, 179
- electron density, 61
- integer, 12, 79
- particle density, 66

N

- depolarization factor, 664

O

- octahedral point group, 36

 \mathcal{O}

- order parameter, 113

P

- P_l , Legendre polynomial, 277
- \hat{P} , momentum operator, 182
- \vec{P} , polarization, 38
- bcc Brillouin zone symmetry point, 194
- polarization factor, 61
- pressure, 126
- stacking period, 79

P

- \vec{p} , dipole, 299
- atomic orbital, 269
- integer, 40

 \mathcal{P}

- probability, 124

Q

- charge, 604
- heat, 490

q

- integer, 40
- particle charge, 155
- wave vector, 47

R

- R_H , resistance quantum, 548
- R_h , muffin hole radius, 276
- R_{12} , transition rate, 647
- \hat{R} , position operator, 176
- \vec{R} , ionic position, 6
- R_K , von Klitzing constant, 780
- particle size, 109

r

- r_s , radius parameter, 162
- \vec{r} , position vector, 46
- radial coordinate, 46
- rational number, 40

 R_H

- Hall coefficient, 502

 \mathcal{R}

- polymer radius of gyration, 125
- radial wave function, 269
- rotation matrix, 13

S

- change of coordinates, 13
- entropy, 101
- spiegel point group, 36
- structure factor, 67

s

- atomic orbital, 269
- permutation index, 236

S

- applied stress, 330

T

- T matrix, 538
- $T[n]$, kinetic energy functional, 246
- T_c , Curie temperature, phase transition temperature, 730
- $\hat{T}_{\vec{R}}$, translation operator, 182
- temperature, 43
- tetragonal point group, 36

 \mathcal{T}

- time period, 469

t

- hopping term, 226

- t*
- t_c , reduced temperature, 745
 - time, 46
- U*
- U , periodic potential, 175
 - U -process, 527
 - fcc Brillouin zone symmetry point, 193
 - potential energy, 86
- u*
- \vec{u} , Bravais lattice vector, 53
 - \vec{u} , displacement vector, 37, 325
 - u_{nk} , periodic Bloch function, 182
 - amplitude in Bogoliubov theory of superconductivity, 870
- V*
- voltage, 87
- v*
- \vec{v} , basis vector, 9, 53
 - \vec{v}_{nk} , group velocity, 185
 - v_F , Fermi velocity, 162
 - amplitude in Bogoliubov theory of superconductivity, 870
- V*
- volume, 50
- W*
- $W_{kk'}$, scattering transition rate, 525
 - fcc Brillouin zone symmetry point, 193
 - plastic work, 426
 - wave packet, 185
 - width of disorder potential, 543
- w*
- Wannier function, 222
- W*
- half-bandwidth, 222, 820
- X*
- fcc Brillouin zone symmetry point, 193
- x*
- position component, 20
- Y*
- Y_{lm} , spherical harmonic, 268
 - Young's modulus, 43, 330
- y*
- position component, 20
- Z*
- conduction electrons per atom, 167
 - atomic number, 64
 - partition function, 164
 - thermoelectric figure of merit, 498
- z*
- coordination number, 114
 - position component, 20
- 1/*f* noise, 530
- 1/*N* expansion, 807
- 1–2–3 compound, 882
- 2DEG, *see* two-dimensional electron gas
- ab initio*, 257
- Abascal, J. L. F., 151
- Abel, W. R., 515, 516, 520
- Abelès, F., 686, 719
- Abrahams, E., 547, 564, 893
- Abrahams, S. C., 65, 73
- Abrikosov lattice, 850
- Abrikosov, A. A., 628, 631, 848, 890
- absorption coefficient, 616, 620, 626
- acceptors, 532
- table of binding energies, 580
- accidental degeneracy, 202
- acoustic branch, 344
- acoustic phonons, *see* phonons, acoustic
- acoustic waves, 331
- adiabatic change, 223
- adiabatic theorem, 505
- Adler, D., 566
- adsorption, 81
- Aegerter, C. M., 566
- Ag
- de Haas–van Alphen oscillations, 473
 - magnetoresistance, 503
 - photoemission from, 705
 - pseudopotential for, 268
 - specific heat, 156, 359
- AgCu phase diagram, 103
- Agulló-Rueda, F., 480
- Aharoni, A., *xxii*, 149, 738, 757
- Aharonov, Y., 223, 232, 774, 794
- Aharonov–Bohm effect, 774–776
- Ahlers, G., 757
- Ahlskog, M., 552, 564
- Aiñ, M., 811, 835
- Aksenov, V. L., 893
- Al
- band structure, 281
 - cohesive energy, 312, 313
 - plasmons, 697
 - pseudopotential for, 268, 286
 - residual resistivity ratio, 529
 - resistivity, 527, 560
 - specific heat, 363
 - superconducting specific heat, 880
 - superconducting spin relaxation, 880
 - thermal expansion, 363
- Al'tshuler, B. L., 564
- Albers, B. J., 94
- Alberts, H. L., 757
- Alder, B. J., 263
- Alekseevskii, N. E., 503, 520
- Alexander, H., 409

- Alexander, L. E., 73
 alkali halides
 cohesive energy, 301–305
 table of cohesive energies, 305
 table of optical F center properties, 677
 alkali metals
 band structure, 280
 cohesive energy, 305
 Fermi surfaces, 474
 optical absorption, 700, **716**
 pseudopotentials, 268
 resistivity, 528
 table of ionization potentials, 302
 Allen, P. B., 890
 Allen, S. M., 109, 149
 allotropic, 5
 alloys, 101–113
 interstitial, 102
 primary, 102
 secondary, 103
 substitutional, 102
 Allum, D. R., 435, 447
 Altman, E. I., 94
 alumina
 grains, 108
 amber, 567
 Amelinckx, S., 385, 409
 Ammann lines, 140
 amorphous materials, 116
 analytic continuation, 404, 619
 Anderson, A. C., 520
 Anderson, J. R., 720
 Anderson, P. W., 564, 656, 757, 835, 890
 Josephson effect, 853
 last word on high T_c , 887
 localization, 542
 magnetic impurity, 820
 scaling theory of Kondo problem, 820
 spin glasses, 743
 Ando, T., 794
 André, G., 566
 Andrei, N., 820, 835
 Andronikashvili, E. L., 427, 447
 Angell, C. A., 117, 149
 anion, 302
 annealing, 104
 Annett, J. F., 886, 890
 annihilation operator, 352, 907
 time evolution, 354
 anomalous dispersion, 65
 anomalous Hall effect, 503–504
 table, 504
 anomalous skin effect, 694–695
 anomalous velocity, 469, 486, 503, 504, **517**
 Boltzmann equation, 486
 anticommutation relation, 907
 antiferromagnetism, 733
 MnO, 63
 neutron scattering, 63
 table of data, 732
 antiphase boundaries, 106, 109
 anti-Stokes scattering, 702
 antisymmetric wave functions, 235
 Ao, P., 448
 Aono, M., 719
 Appelbaum, J. A., 574, 607
 APW, *see* linear augmented plane waves
 Ar, 116
 Armstrong, R. C., 447
 Arnov, A. G., 836
 ARPES, *see* photoemission, angle-resolved
 photoemission spectroscopy
 Asano, H., 893
 Åsbrink, S., 719
 Ashburn, J. R., 893
 Ashcroft empty core potential, *see*
 pseudopotentials, empty core
 Ashcroft, N. W., 267, 291, 301, 318, 527, 565
 atom trapping, 457
 atomic radii, 297, 769
 Au
 equilibrium crystals, 4
 resistance minimum, 819
 AuCu phase diagram, 103
 augmented plane waves, *see* linear augmented
 plane waves
 Averbach, B. L., 381, 409
 Avouris, Ph., 89, 95
 Awschalom, D. D., 838
 Axe, J. D., 73

 B2122, *see* $\text{Bi}_2\text{Sr}_2\text{CaCu}_2\text{O}_{8+x}$
 Börnstein, R., 41, 291, 339, 480, 521, 608,
 686, 719, 758, 795
 Ba
 Fermi surface, 281
 backflow, 510
 Baer, W. S., 686
 Baer, Y., 720
 Baerends, E. J., 318
 Baetzold, R. C., 94
 Bagley, B. G., 891
 Baibich, M. N., 836
 Baldereschi, A., 687
 Balents, L., 565
 Balents, L., 565
 Balkanski, M., 667, 686
 band bending, 584

- band gap, *see* energy gap
band index, 182, 183
band structure, 265–286, **287–290**
 alkali metals, 280
 aluminum, 281
 copper, 282
 ferromagnets, 813
 GaAs, 710
 germanium, 709
 graphene, 284
 krypton, 283
 noble gases, 282
 noble metals, 280
 rare earths, 286
 semiconductors, 283, 576–577
 silicon, 285, 710
 sodium, 699
 surfaces, 574
 transition metals, 284
 vanadium, 285
band structure energy, 309
bandwidth, 222
Bankoff, S. G., 449
Bardeen, J., 607, 858, 890
 semiconductor surface states, 586
 superconductivity, 839, 865, 879
 transistor, 595
Barker, J. A., 149
Barrett, C. S., 73
Bartynski, R. A., 719
base, 596
basis, *see* lattice with basis
Bass, J., 528, 565
Bastard, G., 480
Batchelor, G. K., 447
BaTiO₃, 662
Batlogg, B., 890
Baumeister, P. W., 644, 656
Baumeister, T., 380, 409
Baxter, R. J., 734, 757
Baykara M. Z., 94
Baym, G., 520, 631
bcc, *see* lattices, body-centered cubic
BCS, *see* superconductivity, Bardeen–Cooper–Schrieffer
Be
 Fermi surface, 281
 inelastic X-ray scattering, 703
 photoemission data, 708
Bean, J. C., 607
Beck, H., 720
Bednorz, J. G., 881, 890
Beenakker, C. W. J., 601, 607, 608
Beer, A. C., 657
Behringer, R. P., 150, 339
Belitz, D., 565
Bellman, A. F., 887, 891
ben Dahan, M., 457, 480
Bendow, B., 686
Benedek, G. B., 749, 757
Bensimon, D., 149
Berezinskii, V. L., 409
Berger, L., 816, 836
Bergman, D. J., 335, 339
Berlincourt, D., 686
Bernal model, 115
Bernal, J. D., 115, 149
Bernardes, N., 318
Berne, B. J., 74
Bernstein, N., 271
Bernu, B., 262
Berry connection, 224, 467, 504, 661, 776
Berry phase, 223–225, **230**, 776
Berry, M. V., 223, 232
Bertaut, F., 733, 757
Berthod, C., 891
Bertram, H. N., 757
Bethe ansatz, 805
Bethe, H., 805, 836, 893
 Mott–Bethe relation, **73**
 superconductivity, 839
Beyers, R., 890
Bharucha, C. F., 472
Bhatia, A. B., 523, 565
Bi
 de Haas–van Alphen oscillations, 473
 thermopower, 498
Bi₂Sr₂CaCu₂O_{8+δ}, 887
Bi₂Sr₂CaCu₂O_{8+x}, 884
Bi₂Te₃
 thermoelectric, 498
Bi2212, *see* Bi₂Sr₂CaCu₂O_{8+δ}
Bickers, N. E., 807, 836
Biedenharn, L., 838
Binasch, G., 836
Binder, K., 757
Binnig, G., 86, 91, 94
bipolar junction transistor, 595
Bird, R. B., 318, 447
Birge, N. O., 118, 149
Birgeneau, R. J., 149
Blase, X., 291
Blatter, G., 890
Blech, I., 151
Bloch T^5 law, 528
Bloch oscillations, 456, 457, **477**, 495
Bloch wave vector, 182
 number of distinct values, 184

- Bloch's theorem, 175–191, **230**, 532
 Fourier space, 181
 in one dimension, 176–180
 in three dimensions, 180–191
 statement of, 181, 183
 sub-bands in magnetic field, 778
 Bloch, F., 175, 206, 207, 232, 255, 262, 858
 Blount, E., 480
 Boatner, L. A., 109
 Bockrath, M., 565
 body-centered cubic, *see* lattices
 Boebinger, G., 786, 794
 Bogoliubov equations, *see* superconductivity,
 Bogoliubov equations
 Bogoliubov transformation, 447, 870
 Bogoliubov, N. N., 448, 890, 893
 superconductivity, 870, 873
 superfluidity, 446
 Bohm, D., 223, 232, 774, 794, 858
 Bohr magneton, 730, 761
 Bohr radius
 effective, in silicon, 531
 Bohr, N., 759, 767, 794
 Bohr–Sommerfeld quantization, 471
 Boltzmann equation, **443**, 483–504, **517**, **519**,
 623
 anomalous velocity, 486
 collision term, 485
 crossed electric magnetic fields, 501
 first stated, 485
 formal solution, 488
 founded on Hamilton's equations, 483
 incorporating spatial gradients, 487
 metallic absorption at low frequencies,
 692
 practical solution, 489
 semiconductors, 590–595
 Boltzmann factor, 165
 Boltzmann statistics, 165
 Bona, G. L., 837
 bond lengths
 table for selected molecules, 242
 bond-orientational order, 392
 Boorse, H. A., 880, 890
 Booth, T. J., 16
 Borchardt-Ott, W., 36, 41
 Born approximation, 623–624
 Born exponent, 299
 Born, M., 233, 262, 327, 339, 341, 377
 Born–Oppenheimer approximation, 233
 Bose gas, 435, **446**
 Bose-Einstein factor, 356
 Boseck, S., 94
 bosonization, 555
 Boucherie, J. X., 893
 Bouckaert, L. P., 201, 206
 Bouckaert–Smoluchowski–Wigner notation,
 201
 Boudreaux, E. A., 768, 794
 Bowley, R. M., 447
 Boyce, J. B., 74
 Bozorth, R. M., 757, 758
 Bradley, C. J., 36, 41, 193, 206
 Brady, G. S., 331, 339
 Bragg angle, 45, 47
 Bragg peaks, 49, **71**, 372
 Bragg planes, 50, 57
 Bragg, W. L., 104, 149, 742, 757
 braking radiation, 56
 branch cut, 404, 538
 branches, 344
 brass
 band structure energy, 311
 Brattain, W. H., 607
 Braun, E., 41
 Braun, F., 574, 607
 Braun, W., 85, 94
 Bravais lattices, 6
 enumerated, 30–32
 scattering, 48
 Bravais, A., 17, 41
 Brefeld, W., 74
 Breit–Wigner factor, 375
 Bremsstrahlung, 56
 Bridgeman, P., 424, 448
 Brigham, E. O., 900, 902
 Brillouin scattering, 702
 Brillouin zones, 184
 extended zone scheme, 188, 190, 209
 first mentioned, 179
 irreducible, 202
 nearly free electrons, bcc, 217
 nearly free electrons, fcc, 216
 nearly free electrons, hexagonal, 218
 of body-centered cubic lattice, 194
 of face-centered cubic lattice, 193
 of hexagonal lattice, 194
 phonons in one dimension, 343
 pictures of second and third, 213
 reduced zone scheme, 188, 190, 209
 repeated zone scheme, 189, 190
 second, third, and higher, 211
 symmetry of, 202
 Brillouin, L., 719
 Brinkman, W. F., 149, 656
 brittle, 379
 brittleness versus ductility, 400
 Brock, J. D., 149

- Brockhouse, B. N., 377
 Bromberg, J. L., 656
 Broto, J. M., 836
 Brovman, E. G., 374, 377
 Brown, R., 97, 149
 Brownian motion, 70
 Brueckner, K. A., 263
 BSW, *see* Bouckaert–Smoluchowski–Wigner notation
 Buhrman, R. A., 838
 built-in voltage, 587
 bulk modulus, 301, 328, **337**
 table for noble gases, 301
 Bullett, D. W., 291
 Bulsara, A. R., 565
 Burgers vector, 383, 394
 Burke, K., 263
 Burkel, E., 719
 Burkov, A. T., 499, 520
 Burlet, P., 893
 Burton, K., 384
 Buschow, K. H. J., 837
 Bustamante, C., 91, 94
 Buyco, E. H., 378
 Buyers, W. J. L., 837
- C**
 band structure, 284
 C₆₀, 143
 Cândido, L., 262
 Ca
 Fermi surface, 281
 Cabibbo, N., 758
 CaF₂
 structure, 26
 table of similar compounds, 27
 Cage, M. E., 781, 794
 Cahn, J. W., 109, 149, 151
 calcium fluoride, *see* CaF₂
 calcium titanate, *see* CaTiO₃
 Callaway, J., 262
 Campuzano, J. C., 887, 891
 Cao, Y., 566
 capacitance matrix, 604
 Car, R., 272, 291
 Carbotte, J. P., 890
 Cardona, M., 580, 598, 608, 621, 631
 Cargill, G. S., 116, 149
 Carini, J. P., 795
 Carlsson, A. E., 318, 400, 409
 Carra, P., 74
 Castin, Y., 480
 cathode ray tube, 567
 CaTiO₃
 structure, 28
 table of similar compounds, 29
 cation, 302
 Cauchy relation, 327
 Cauchy's theorem, 619
 Cauchy, A., 327
 causality, 618
 Cd
 Fermi surface, 281
 CdS
 dielectric function, 667
 polaritons, 667
 centered rectangular lattice, *see* lattices
 central forces, 327, 349
 central limit theorem, 124
 centrosymmetric, 38
 Ceperley, D. M., 262, 263, 448
 Cerrina, F., 720
 cesium chloride, *see* CsCl
 Chaikin, P. M., 123, 149, 335, 339, 891
 Chainani, A., 894
 Chainani, A., 881
 chalcogenide glasses, 120
 Chambers, R. G., 520
 Chandrasekhar, S., 123, 149, 335, 339
 Chang, A. M., 786, 794
 Chang, H., 94
 Chang, L. L., 607
 Chang, M., 480
 change of coordinates, 13
 chaotic versus integrable systems, 485
 character table, 199
 characteristics, 488
 characters, 198
 charge density wave, 311
 charge susceptibility, 627, **630**, 695, 860
 charge transfer energy, 713
 Charlier, J.-C., 291
 Chattopadhyay, D., 565
 Chazelas, J., 836
 Chelikowsky, J. R., 656, 710, 719
 chemical potential
 between different metals, 497
 doped semiconductors, 583
 driving force for superfluids, 429
 Josephson's equations, 858
 superconductivity, 868
 superlattices, 743
 temperature dependence for
 noninteracting electrons, 169
 versus work function, 569
 chemisorption, 81
 Chen, Q., 891
 Cheng, C., 82, 94

- Cherenkov–Landau criterion, 406, 434, 435
 Chew, N. G., 410
 Chiang, T., 710, 719, 720
 Ching, W. Y., 712, 719
 cholesterics, 121
 Chou, M. Y., 367, 378, 719
 Chtchelkanova, A. Y., 838
 Chu, C. W., 893
 Chui, S. T., 656
 citations
 maximum number of, 258
 Citrin, P. H., 74
 Cladis, P. E., 149
 classes, 198
 classical limit, 165
 classical statistics, 165
 Clauser, H. R., 331, 339
 Clausius–Mossotti relation, 533, 661, **684**
 climb, 383
 closed orbits, 470, 471, 501
 clouds, 128
 CMOS, *see* complementary metal–oxide–silicon
 CO, 241
 Co
 ferromagnetism, 731, 736, 814
 CO₂
 critical point, 743
 Cobden, D. H., 565
 Cochran, A. J., 36, 41, 61, 74
 coefficient of non-specificity, xx
 Cohen, E. G. D., 448
 Cohen, M. L., 291, 318, 656, 719
 GaAs calculations, 710
 pseudopotentials, 307
 Cohen, R. E., 687
 coherence length, *see* superconductivity,
 coherence length
 coherent potential approximation, 541–542
 coherent states, 866
 cohesive energy, 295–313
 band structure calculations, 312
 hydrogen-bonded solids, 312
 table for noble gases, 301
 collector, 596
 Collins, T. C., 657
 collision term, 485, 524–527
 colloidal suspensions, 393
 colloids, 128–133
 color centers, 674–684
 lasers, 650
 color groups, 36
 Colpitts, T., 521
 commutation relation, 908
 compensation temperature, 732
 complementary metal–oxide–silicon, 599
 complex energy, 624, **629**
 compound, 24
 conductance, *see* electrical conductivity
 conduction electron density
 table for selected metals, 167
 conductivity
 electrical, *see* electrical conductivity
 thermal, *see* thermal conductivity
 configuration coordinate, 681
 conformal mapping, 402–404, **409**
 conservation laws
 inelastic light scattering, 701
 optical absorption, 640
 phonons, 364
 photoemission, 707
 contact potentials, 572–573
 continuity equation, 108, 413, 414, 437, 485,
 613
 derivation, 98
 continuous random network, 119, **143**
 conventional unit cell, 20
 size of bcc, 22
 size of fcc, 21
 convolution theorem, 138
 CoO
 insulator, 711
 magnetic structure, 733
 optical absorption, 711
 Cooper problem, *see* superconductivity,
 Cooper problem
 Cooper, L. N., 839, 863, 865, 890, 891
 coordination number, 114, 119, **143**, 735
 copolymer, 123
 Coppersmith, S. N., 831, 836
 Corciovei, A., 757
 Corenzwit, E., 838
 corn starch, 417
 corpuscle, 567
 correlation, 67, 242, 714, 735
 correlation functions, 113
 liquids, 113–114
 radial, 114
 two-dimensional colloid, 393
 correlation length, 749
 Corrigan, D., 109
 Costache, G., 757
 Cottrell, A. H., 307, 308, 318
 Coulomb blockade, 605, 606
 Coulomb integral, 238
 Coulomb interaction, 234, 303
 Cowley, R. A., 367, 377
 Cox, D. L., 891

- Cr
 magnetic superlattices, 815
- Crabtree, G. W., 891
- Cracknell, A. P., 36, 41, 193, 206, 476, 480
- cracks, 399–406
 as branch cuts, 404
 in strip, 400
 lattice trapping, **408**
- Craighead, H. G., 608
- CrBr₃
 scaling data, 754
- creation operator, 352, 907
 time evolution, 354
- Creuzet, G., 836
- critical opalescence, 744
- critical phenomena, 743–754
 critical isotherm, 746
 experimental scaling function, 754
 exponents, 748–750
 magnetic susceptibility, 746
 scaling theory, 750–754
 specific heat, 746
 spontaneous magnetization, 745
 table of exponents, 750
- critical point, 743
- CRN, *see* continuous random network
- Cross, M. C., 836
- crystal
 essence of, 66
 two-dimensional, 6
- crystal habit
 first law of, 3
 second law of, 3, **40**
- crystal momentum, 179, 182, 365, 640
- crystal structures
 of elements, 19
 databases, 37
- crystal systems, 13
 cubic, 30
 enumerated, 30–32
 hexagonal, 32
 monoclinic, 32
 orthorhombic, 32
 rhombohedral, 32
 tetragonal, 30
 triclinic, 32
 trigonal, 32
- Cs
 Bloch oscillations, 457
 magnetism, 814
- CsCl
 structure, 26
 table of similar compounds, 26
- Cu
 anomalous skin effect, 694
 band structure, 282
 band structure energy, 311, **315**
 core binding energies, 712
 Fermi surface, 475
 Fermi surface orbits, 471
 optical properties, 282
- Cu₂O
 charge density, 296
 crystal habits, 5
 optical absorption, 644
- cubic close-packed, 20
- Cullis, A. B., 385, 410
- Cummins, H. Z., 750, 757
- CuO, 532
 base for superconductors, 882
 core-level data, 715
 core-level photoemission, 711–716
 Hubbard model, 832
 insulator, 279
 structure, *see* lattices, CuO
- CuO₂
 base for superconductors, 882
- Curie temperature, 731
- Curie's law, 766–767
 experimental tests, 767
- Curie–Weiss temperature, 731, 732
- current operator, 625
- Curtiss, C. F., 318, 447
- Curtiss, L. A., 257, 263
- Cusack, N. E., 117, 149, 526, 565
- cusp conditions, 254
- CuZn
 superlattice ordering, 742
- cyclotron frequency, 634, 771
- cyclotron resonance, 577, 633–638, **652**, 674
 data in germanium, 637
 sketch of setup, 634
- Czyzyk, M. T., 719
- Däweritz, L., 94
- Dagotto, E., 891
- Damascelli, A., 891
- dangling bonds, 586
- Das Sarma, S., 837
- Daughton, J. M., 838
- Davey, S. C., 410
- Davies, R. O., 890
- Davis, E. A., 566
- Davis, N. P., 86, 94
- Davis, S. H., 449
- Davisson, J., 82, 94
- de Boer, J. H., 836
- de Gennes, P.-G., 94, 116, 149, 339, 448, 891

- liquid crystals, 123, 335
- polymers, 417
- superconductivity, 845
- wetting, 81
- de Haas, W. J., 473, 819, 836
- de Haas–van Alphen effect, 473–476, 774
- de Lozanne, A. L., 94, 850
- Dean, P., 565
- Deaver, B. S., 850, 852, 891
- Debye frequency, 359
- Debye model, 358
- Debye temperature, 359, **377**
 - table, 360
- Debye, P., 355, 358, 377
- Debye–Scherrer method, 59
- Debye–Waller factor, 371, 372, **377**
- decay, 624, 626
- deflation rule, 135, 140
- degeneracy, 210
 - accidental, 202
- degenerate electron gas, 166
- Delly, B., 720
- Delrieu, J. M., 837
- delta function
 - Dirac and discrete related, 160
- Demircan, E., 439, 448
- dendrites, 108, 109
- dense random packing, 115
- density functional theory, 242, 244–252, 709, 711, 813
- density of states, 159–163, **172**
 - arbitrary dimensions, **173**
 - $D(\mathcal{E})$, 161
 - for free electrons, 161
 - for phonons, 356
 - for phonons in silicon, 357
 - from Green's functions, 536
 - in periodic potential, 185
 - joint, 638
 - $D_{\vec{k}}$, 160
 - local, 537
 - one and two dimensions, 163
- depletion region, 589, 592, 593, **607**
- depolarization factor, 664
- DePuydt, J. M., 657
- Desai, P. D., 378
- Desiraju, G., 318
- Devanarayanan, S., 378
- deviatoric stress, 425
- Devreese, J. T., 686
- Dexter, R. N., 637, 656, 657
- diamagnetism, 724, 729, 842
- diamond, 283
 - irreducible representations, 200
 - phonons, 349
 - residual ray, 668
 - scattering, 54
 - specific heat, 354, 355
 - structure, 24
 - two-body potentials, 314
- dielectric function, 614, 616–623
 - causality, 618
 - data for CdS, 667
 - high frequency, 666
 - insulators, 617
 - Kosterlitz–Thouless, 397
 - Lindhard, 628
 - low frequency, 666
 - metal–insulator transitions, 532, 533
 - metals, 617
 - sketch, 618
 - superconductivity, 862
 - table for ionic crystals, 670
 - table for semiconductors, 577
- differential scattering cross section, neutrons, 368
- diffusing-wave spectroscopy, 128
- diffusion, **147**
 - diffusion equation, 98
 - derivation, 99
- diffusion length, 594
- diffusion Monte Carlo, 253
- diffusion(, 97
- diffusion-limited aggregation, **93**
- Dimmock, J. O., 291
- Ding, H., 887, 891
- diode, 583–585
 - cathode ray, 567
 - solar cell, 645
- dipole interactions, 299
- dipole moments
 - table for selected molecules, 242
- Dirac equation, 277, 761
- Dirac, P. A. M., 234, 263, 368, 377, 802, 836
- direct gap, 576
- disbelief, suspension of, 157
- dislocations, 381–399, **406**
 - Burgers vector, 383
 - climb, 383
 - core, 395
 - edge, 382, 383
 - energy in two dimensions, 395
 - force to move, 386
 - glide plane, 383
 - imaged, 385
 - interacting in two dimensions, 395
 - screw, 382, 383
 - slip plane, 383

- spiral growth, 385
- surface growth, 384
- disorder, 530, 781
 - tight binding model, 535
- dispersion relations
 - ^4He , 434
 - excitons, 644
 - ferromagnetic spin waves, 808
 - light, 615, 702
 - phonons excited by cracks, 406
 - phonons in one dimension, 343, 345, **376**
 - phonons in silicon, 351, 367
 - phonons, from inelastic X-ray scattering, 703
 - plasmons, 696
 - polaritons, 666, 667, 704
 - polarons, 672
 - schematic for neutron scattering, 366
 - spin waves, antiferromagnetic, 811
 - spin waves, ferromagnetic, 811
- dissipation, 112, 415, 601
- divalent metals
 - Fermi surfaces, 476
- DLA, *see* diffusion-limited aggregation
- DNA, 71
- Doi, M., 417, 448
- Doll, R., 850, 852, 891
- Dolling, G., 357, 367, 377
- domains
 - energy of, 738
 - sketch, 739
- Domb, C., 750, 757, 758
- Donnelly, R. J., 438, 442, 448
- donors, 532
 - table of binding energies, 580
- Dorantes-Davila, J., 831
- Dorda, G., 780, 795
- Dorner, B., 703, 719
- double layer, 573
- Drazin, P. G., 448
- Dresselhaus, G., 232, 635, 656
- Dresselhaus, M. S., 232
- Drude model, 453, 611, 689, 694, **716**
- Drude, P., 453, 480
- Dubonos, S. V., 150
- ductile, 379
- Dulong and Petit, law of, 354, 357
- Durian, D. J., 74
- Dutta, P., 565
- dynamic light scattering, 68
- dynamic viscosity, 415
- Dynes, R. C., 891
- Dzyaloshinskii, I. Y., 631
- Eastman, D. E., 719
- Eastman, L. F., 607
- easy axis, 734
- Ebbesen, T. W., 143, 149
- Eberhart, J. P., 61, 74
- Ebers–Moll equations, 597, **607**
- Echenique, P. M., 263
- Economou, E. N., 539, 565
- Edison, T., 567
- Edwards, P. P., 534, 565
- Edwards, S. F., 417, 448, 743, 757
- EELS, *see* electron energy loss spectroscopy
- effective Hamiltonian, 183
- effective mass
 - cyclotron resonance, 636
 - density of states, 579
 - electrical transport, 494
 - Fermi liquid, 508
 - polaron, 673
 - semiconductors, 577
 - specific heat, 170
 - table for semiconductors, 577
 - theorem, 459, **477**
 - tight-binding model, 478
- effective particles, 170
- Egelstaff, P. A., 151
- Egri, I., 656
- Ehrenreich, H., 291, 656
- Einstein relation, **147**
- Einstein, A., 147, 149, 354, 378, 631, 656, 686
 - model for phonons, 358
 - photoelectric effect, 612
 - specific heat of crystals, 355, 358
 - transition probabilities, 373, 646
- Eisenberger, P., 74
- elastic modulus of rubber, 323
- elastic scattering, *see* scattering, elastic
- elasticity, 321–332
 - reference state, 321
- electrical conductivity
 - anomalous skin effect, 695
 - cubic symmetry, 493
 - cyclotron resonance, 635
 - Drude model, 454
 - electrons and ions combined, 861
 - fluctuations, 529
 - frequency dependent, 611
 - Maxwell's equations, 614
 - quantized, 600–602, 780, 785
 - scattering theory, 523–530
 - tensor, 493, 625, **629**
- electrochemical force, 495
- electron density, 627

- electron energy loss spectroscopy, 698
- electron hologram, 777, 850
- electron nuclear double resonance, 678
- electron spin resonance, 677
- electron tubes, 569
- electron–hole liquid, 645
- electrons
 - elastic scattering, 63
 - electron interactions, 233–258, 624, 627, 709, 880
 - group velocity, 458
 - in electric field, 459, **479**
 - in magnetic field, **479**, 769–791
 - in polarizable medium, *see* polarons
 - nearly free, 208–217
 - phonon interactions, 671, 859, 880
 - semiclassical dynamics, *see* semiclassical dynamics
 - tightly bound, 219–227
- elementary excitations, 505
- elements
 - table of cohesive energy versus density, 314
 - table of crystal structures, 19
 - table of Debye temperatures, 360
 - table of effective radii, 298
- Eliashberg, G. M., 880, 891
- Elliot, S. R., 149
- Elliott, R. J., 565, 656
- ellipsometry, 621
- Emin, D., 686
- emitter, 596
- empty core pseudopotential, *see* pseudopotentials
- Emsley, J., 5, 16, 302, 318
- Endo, J., 795, 893
- Endoh, Y., 893
- ENDOR, *see* electron nuclear double resonance
- energy bands, *see* band structure
- energy conservation
 - inelastic light scattering, 701
 - optical absorption, 640
 - phonons, 364
 - photoemission, 707
- energy current, 490
- energy density of states, 161
- energy gap, 277
 - CoO, 711
 - direct, 576
 - GaAs and GaAlAs, 598
 - indirect, 576, 636, 652
 - nearly free electrons, 211
 - semiconductors, 575, 638–641
 - table for semiconductors, 577
 - Urbach tails, 683
- entropy
 - Boltzmann equation, 489
 - generation rate, 490
 - ionizing impurities, 581
 - mixing, 101
 - polymer chains, 125
 - superconductivity, 844
 - two-dimensional dislocations, 396
- epitaxy, 78
- Ernst, F., 81, 94
- Ernzerhof, M., 263
- Erzan, A., 94
- Esaki, L., 607, 891
- Eskes, H., 719
- ESR, *see* electron spin resonance
- Etienne, B., 795
- Etienne, P., 836
- Ettenberg, M. H., 520
- Euler angles, 12
- Euler's equation, 413
- Euler–Maclaurin theorem, 773
- EuO
 - magnetic susceptibility, 731
- eutectic, 106
- Evans, A. G., 410
- Ewald construction, 55
 - in two dimensions, 83
- Ewald sphere, 55, 58
- Ewald summation, 302–304, **316**
 - for metals, 306
- Ewald, P. P., 17, 41, 43, 74
- EXAFS, *see* extended X-ray absorption fine structure
- exchange energy, 306
- exchange forces, 737
- exchange functionals, 258
- exchange integral, 238
- exchange interaction, 243, 803
- excitons, 576, 641–645
 - Frenkel, 644, **654**, **656**
 - GaAs, 640
 - Mott–Wannier, 641–644
- experiments
 - bad ideas for, 55, 86, 312, 413, 433
- extended states, 540
- extended X-ray absorption fine structure, 67
- extended zone scheme, 188, 209
- external charges, 613
- extinctions, 54, **71**, 218
- F centers, 676
 - absorption and emission peaks, 677

- charge density surrounding, 678
- F₂ center, 679
- Faber, T. E., 448
- Fabian, Jaroslav, 837
- face-centered cubic, *see* lattices
- faceting, **92**
- Fadeev, L. D., 836
- Fahey, P. M., 607
- Fairbank, W. M., 850, 852, 891
- Fan, Y., 639
- Faraday balance, 729
- Faraday rotation, 674, **684**
- fast Fourier transform, 274, 900–902
- Fawcett, E., 757
- fcc, *see* lattices, face-centered cubic
- Fe
 - ferromagnetism, 736, 814
 - Mössbauer effect, 375
 - magnetic anisotropy, 738
 - magnetic superlattices, 815
 - magnetic transition, 730
 - specific heat, 731
- Fe₃C, 102
- Fedorov, E., 17, 41
- Feher, G., 678, 686
- Feigel'man, M. V., 890
- Feigl, F. J., 607
- Fermi energy, 162
 - table for selected metals, 167
- Fermi function, 165, **173**
 - graph, 165
 - experimental measurement, 705
 - graph of derivative, 168
 - superconductivity, 872
- Fermi level, 162
- Fermi liquid parameters, 511–512
 - table for ³He, 515
- Fermi liquid theory, 504–516, **520**
 - backflow, 510
 - effective mass, 508
 - effective mass relation, 512
 - first sound, 512
 - Landau parameters, 511
 - magnetic susceptibility, **833**
 - scattering time, 506
 - specific heat, 510
 - zero sound, 514
- Fermi sea, 505, 863
- Fermi sphere, 159
- Fermi surface, 162, **228**
 - determined from Kohn anomalies, 374
 - determined from anomalous skin effect, 695
 - determined from de Haas–van Alphen effect, 474–476
 - divergence of scattering time, 506
 - extremal section, 474
 - nearly free electrons, 215
 - nearly free electrons, bcc, 217
 - nearly free electrons, fcc, 216
 - nearly free electrons, hexagonal, 218
 - open and closed orbits, 470, 471
- Fermi temperature, 166
 - table for selected metals, 167
- Fermi velocity, 162
 - table for selected metals, 167
- Fermi wave vector, 159
 - table for selected metals, 167
- Fermi's Golden Rule, 368, 506, 525
- Fermi–Dirac statistics, 166
- fermion sign problem, 253
- Ferrante, J., 318
- ferrimagnetism, 731–732
 - compensation in rare earth garnets, 733
 - table of data, 732
- ferroelectrics, 659–661
- ferromagnetism, 730–731
 - ground state, **832**
 - table of data, 732
 - transition metals, 811–815
- Ferry, D. K., 607
- Ferry, J. D., 423, 448
- Fert, A., 836
- Fetter, A., 628, 631
- Feynman, R. P., 448, 686, 836
 - nodeless ground states, 800
 - polaron theory, 674
 - superfluid structure factor, 442
 - superfluid wave function, 440
- FFT, *see* fast Fourier transform
- Fibonacci sequence, 134
- Fick's law, 98
- field ion microscopy, 85
- Field, S. B., 255, 263
- filled bands, 494
- filling fraction, 789
- FIM, *see* field ion microscopy
- Fineberg, J., 410
- Fiorito, R. B., 449
- Firsov, A. A., 150
- first Brillouin zone, 184
- first principles, 257
- first sound, 512
- Fischer, O., 891
- Fisher, D. S., 757, 836
- Fisher, M. E., 448, 757
 - critical phenomena, 743

- superfluid vortices, 439
- Fisher, M. P. A., 565
- Fisher–Essam relation, 753
- Fisk, Z., 837
- Fiszdon, W., 449
- Flannery, B. P., 902
- Fleming, J. A., 567
- flicker noise, 530
- flint, 233
- Flores, F., 263
- flow stress, 425
- fluctuation dissipation theorem, 112, 419
- fluids
 - critical phenomena, 749
 - dilute polymeric solutions, 417
 - incompressible, 414
 - mechanics, 413–443
 - Newtonian, 415
 - non-Newtonian, 417
 - table of critical exponents, 750
 - table of viscosities, 416
 - viscoelastic, 417
- fluorite, *see* CaF₂
- flux, 491
- flux tube, 460, 776
- Flynn, C. P., 102, 149, 686
- Fock, V., 235, 263
- force, 491
- form factor, 47
- form factors, 46, 61
- fountain effect, 428
- Fourier transform, 614
 - fast, 274, 900–902
- Fowler, A., 607
- Fowler, A. B., 607, 794
- Fowler, W. B., 677, 686, 687
- Foxman, E. B., 606, 608
- Foxon, C. T., 608
- fractional charge, 790
- fracture, *see* cracks
- Franck–Condon effect, 679–683, **685**
- Frank, C., 410
- Frank, F. C., 142, 149, 384
- Frank–Kasper phases, 142
- Franklin, B., 567
- Franklin, G. E., 720
- Franz, R., 455, 481, 496
- free energy
 - criterion for phase separation, 105
 - dilute mixtures, 101
 - double well, 105
 - elasticity of cubic solids, 326
 - elasticity of isotropic solids, 328
 - isolated ion in magnetic field, 766
 - magnetism derived from, 725–726
 - phase transitions, 745
 - polymer chains, 125
 - polymers with volume interactions, 127
 - rubber, 322
 - scaling form for critical phenomena, 751
 - superconductivity derived from, 841–843
- free Fermi gas, 158
- Freitas, P. P., 836
- Frenkel pair, 676
- Frenkel, J., 384, 386, 410
- Frenkel–Kontorova model, 386
- friction, 335
- Friedel model of *d* band metals, **317**
- Friedel, J., 410
- Friederich, A., 836
- Friedrich, W., 43, 74, 341
- Friedrichs transition, **338**
- Friend, R. H., 607
- Fritzsche, H., 565, 566
- Fröhlich, H., 686, 859, 891
- fullerenes, 143
- functional derivative, 236, 441, 726, 737, 842, 903
- functionals, 903
- Furnas, T. C., 73
- Furthmüller, J., *xxii*, 291, 318
- Furuya, K., 835
- GaAlAs
 - deposition, 85
 - fractional quantum Hall effect, 785, 790
 - heterostructures, 598
 - mobility, 600
- GaAs
 - Bloch oscillations, 477
 - data on optical absorption, 640
 - deposition, 85
 - direct gap, 576, 652
 - energy bands and photoemission, 710
 - excitons, 644
 - form of effective mass, 577
 - fractional quantum Hall effect, 785, 787, 790
 - growth oscillations, 85
 - Gunn effect, **653**
 - irreducible representations, 200
 - mobility, 600
 - optical absorption, 639
 - Wannier–Stark ladders, 472
- Gaidukhov, Y. P., 503, 520
- gain, 648
- Galkin, V. Y., 757
- Gammaitoni, L., 565

- gang of four, *see* Abrahams, E.
 Gao, L., 893
 GaP
 polaritons, 704
 Gardner, J., 109
 Gardner, M., 139, 149
 garlic
 magnetic properties, 723
 Garo, J. P., 891
 Garofalini, S. H., 74, 318
 gauge symmetry breaking, 857
 gauge transformations
 free electrons in electric field, 461
 integer Hall effect, 784
 superconductivity, 841, 850, 853, 876, 886
 Gaussians, 240
 Ge
 Brillouin scattering, 703
 charge density, 296
 cyclotron data, 637
 cyclotron resonance, 636
 data on optical absorption, 642
 energy bands and photoemission, 709
 form of effective mass, 577, 636
 holes, 638
 indirect gap, 576, 639
 irreducible representations, 200
 Geballe, T. H., 891
 Gehrenbeck, R. K., 74
 Geiger, H., 893
 Geim, A. K., 16, 150
 Gell-Mann, M. I., 263
 generalized dual method, 148
 generalized gradient approximations, 257
 geometrical phase, 223–225, 776
 Georges, A., 831, 836
 Gerber, Ch., 94
 Gerlach, B., 686
 Germer, L. H., 82, 94
 Geshkenbein, V. B., 890
 GGA, *see* generalized gradient approximations
 Ghijsen, J., 715, 719
 ghosts, 271
 Giaever, I., 891
 Giamarchi, T., 553, 565, 836
 giant magnetoresistance, 815
 Giapintzakis, J., 893
 Gibbs–Duhem relation, 430, 747
 Gibson, J. M., 607
 Gilbert, W., 757, 888, 891
 Gilman, J. J., 116, 150
 Ginsberg, D. M., 890, 891, 893
 Ginzburg, V. L., 844, 850, 892
 Girvan, R. F., 476, 480
 Girvin, S. M., 794, 795
 Gittings, A. S., 74
 Glaberson, W. I., 448
 glass
 chalcogenides, 120
 Glass, A. M., 686
 glasses, 116–120
 brittleness, 379
 coordination, 119
 fragile, 119
 metallic, 133, 524
 network, 119
 strong, 119
 transition temperature, 117
 Glattli, D. C., 795
 Glicksman, M., 719
 glide axis, 39
 glide line, 12
 glide plane, 36, 383
 Glinchuk, M. D., 687
 Glusker, J. P., 74
 Glyde, H. H., 442, 448
 Goedsche, F., 837
 Gold, A. V., 207, 232, 480
 Goldbart, P. M., 339
 golden mean, 135, 560
 Goldenfeld, N., 750, 757, 890
 Goldman, A. I., 150
 Goldstein, H., 12, 16, 631, 891
 Goldstone modes, 343, 805
 Goldstone, J., 343, 378, 805, 836
 Gollub, J. P., 449
 Golub, R., 378
 Gomer, R., 81, 94
 Gonze, X., 271, 291
 Goodby, J. W., 410
 Goodier, J. N., 339
 Gor'kov, L. P., 631, 886, 891
 Gordon, J. E., 410
 Gorter, C. J., 448
 Gossard, A. C., 795
 Gould, G., 646
 Grünberg, P., 836
 grain boundaries, 77, 106
 grains, 106
 picture, 108
 growth of, 145
 in isotropic solids, 328
 grand canonical ensemble
 alloys, 741
 electrons in magnetic field, 773
 noninteracting electrons, 164, 582

- superconductivity, 865
- grand orthogonality theorem, 198
- granular materials, 116
- graphene, **14**
 - band structure, 284
 - experimental image, 6
 - tight binding band structure, **229**
- graphite, 14, 90, 283
- Gratias, D., 151
- Green's functions, 536–542, **833**
 - many-body, 628
 - one dimension, 537
 - pictures, 539
 - two and three dimensions, 538
- Green, M. A., 656
- Green, M. S., 757, 758
- Greene, L. H., 891
- Greene, R. L., 891
- Greenham, N. C., 607
- Greywall, D. S., 515, 520
- Grier, D. G., 393, 410
- Griffin, P. B., 607
- Grigoriev, I. S., 331, 339, 381, 410, 448, 499, 520, 565, 728, 757, 846, 891
- Grigorievna, I. V., 150
- Grinstein, G. M., 757
- Grosberg, A. Y., 150, 417, 448
- Gross, P., 566
- Groth, P., 5, 16
- ground states, *see also* cohesive energy
 - electrons, as ions move, 313
 - Fermi liquid, 507
 - free Fermi gas, **172**
 - helium, 427
 - hydrogen atom, 251
 - magnetic structure of atom, 763
 - many noninteracting electrons, 158
 - normal state instability, 863
 - proved nondegenerate, 800
 - three dimensions, **39**
 - two dimensions, **15**
- group representations, 192–203, **205**
 - character table, 199
 - characters, 198
 - classes, 198
 - grand orthogonality theorem, 198
 - irreducible, 196
 - reducible, 196
 - test for reducibility, 199
- group theory, 12, 192–203
 - point group, 12
 - translation group, 12
- group velocity, 185, 458
 - divergence in Hartree–Fock, 244
- Grubin, H. L., 607
- Grüneisen parameter, 362
- Gruner, G., 311, 318, 836
- Guertler, P., 74
- Guggenheim, E. A., 749, 757
- Guild, L. J., 565
- Guinea, R., 318
- Gunn effect, **653**
- Gunnarsson, O., 263, 891
- Gunshor, R. L., 657
- Gurevich, A. V., 891
- Gurney, R. W., 675, 686
- Gustafsson, T., 719
- H (hydrogen)
 - bound states, 643
 - binding energy, 531
 - excited state lifetimes, **652**
 - stability of atom, 250
 - unbound states, 644
- Haas, C., 720
- Haasen, P., 150, 409
- habit, *see* crystal habit
- Häglund, J. H., 318
- Hafner, J., xxii, 281, 282, 285, 291, 313, 318
- Hahn, T., 36, 41, 61, 74
- Hakonen, P., 448
- Haldane, F. D. M., 565
- Hales, T. C., 115, 150
- halides
 - table of electron affinities, 302
- Hall coefficient, 502
- Hall effect, 500–504, **519**, *see also* quantum
 - Hall effect
 - anomalous, 503–504
- Hall, E. H., 500, 520
- Halperin, B. I., 392, 410, 758
- Hamann, D. R., 574, 607, 835
- Hamilton's equations, 483
- Hamilton, W. C., 73
- Hamiltonian
 - Anderson model for magnetic impurity, 820
 - atom in magnetic field, 761
 - Bardeen–Cooper–Schrieffer, 865
 - Bose gas, 446
 - correlated transition metal oxide, 713
 - Franck–Condon effect, 681
 - free electrons in magnetic field, 787
 - harmonic oscillator, 352
 - Heisenberg, 802
 - Heitler–London, 799
 - Hubbard, 829
 - Kondo, 825

- Kosterlitz–Thouless, 397
- localization, 544
- Mott–Wannier excitons, 643
- much of condensed matter physics, 155
- phonons, 353
- second quantized, 908
- semiclassical electron dynamics, 470
- single electron in periodic potential, 176
- single-electron model, 157
- tight-binding, 226, 535–551
- tight-binding in magnetic field, 777
- Hanmura, E., 657
- Hanna, S. S., 378, 758
- Hansen, J., 891
- Hansen, M., 103, 150
- hard spheres, 116
- Harrison construction, 215
- Harrison, W. A., 215
- Hartree equation, 234, **258**
- Hartree, D. R., 232, 234, 263
- Hartree–Fock equations, 235–244
- Hass, K. C., 892
- Hassager, O., 447
- Hassani, S., 903, 906
- Haüy, R. J., 16
- Haule, K., 831, 838
- Haupt, U., 684, 686
- Hauptman, H. A., 74
- Haüy, R. J., 3, 5
- Hayakawa, H., 892
- Hayes, T. M., 74
- hcp, *see* lattices, hexagonal close-packed
- ³He, *see also* Fermi liquid theory
 - first sound, 512, 515
 - scattering time, 515
 - superfluidity, 442
 - table of Fermi liquid parameters, 515
 - zero sound measured, 516
- ⁴He
 - λ point, 427
 - chemical potentials, 429
 - entropy, 429
 - equilibrium crystal, 4
 - first sound, 432
 - fountain effect, 428
 - ground state, 427
 - ions in, 435
 - neutron scattering, 434
 - phase as superfluid velocity, 437
 - rotation, 437
 - second sound, 431–434
 - second sound experiment, 433
 - structure factor, 442
 - superfluid, 427–442
 - thermal gradients, 430
 - two-fluid model, 428, 430–434
 - vortices, 435, 437
 - wave function, 435
- He II, *see* ⁴He
- Heaviside, O., 613, 631
- heavy atom, 64
- heavy fermions, 171, 828, 829
- Hebard, A. F., 892
- Heberle, J., 378, 758
- Hecht, J., 646, 656
- Heeger, A. J., 564, 566, 674, 686, 836
- Heine, V., 16, 268, 291, 307, 318, 719
- Heisenberg model, 802–804
 - antiferromagnetic ground state, 805
 - ferromagnetic ground state, 805, **832**
- Heisenberg uncertainty principle, 250
- Heisenberg, W., 175, 802, 836
- Heitler, W., 798, 800, 836
- Heitler–London calculation, 797–800
- helicon waves, **717**
- Heller, P., 749, 757
- Henderson, D., 149
- Henisch, H. K., 574, 608
- Hennion, B., 835
- Henry, C. H., 704, 719
- Henry, J. Y., 893
- Hensel, J. C., 645, 656
- Herbst, J. F., 757
- Hermanson, J., 720
- Hertz, H., 611, 631
- Hess, D., 271
- Hessel, J. F. C., 17, 41
- heterostructures, 598–605
- Hetherington, J. H., 837
- Hetler, W., 798, 800
- Heubener, R. P., 520
- Hewson, A. C., 820, 836
- hexagonal close-packed, *see* lattices
- hexagonal lattice, *see also* lattices
 - symmetry points of, 202, 203
- hexatics, 393
- Heyraud, J. C., 4, 16
- Hg (mercury)
 - superconductivity, 839
- Hidaka, Y., 893
- high-temperature superconductors(, 881
 - high-temperature superconductors), 887
- Hill, R., 426, 448
- Himpsel, F. J., 719, 720
- Hirschfelder, J. O., 318
- Hirst, L. L., 757
- Hirth, J. P., 410, 608
- Hockey, B., 108

- Hodby, J. W., 686
 Hoddeson, L., 17, 41
 Hölzl, J., 570, 608, 705, 719
 Hoffund, G. B., 719
 Hofmann, J. A., 731, 757
 Hofstadter, D. R., 779, 794
 Hohenberg, P. C., 244, 263, 758
 holes, 453, 459, 494, 500, 502
 heavy, 577, 638
 light, 577, 638
 Holstein, T., 806, 836
 Holstein-Primakoff representation, 806
 homopolymer, 123
 honeycomb lattice, *see* lattices
 Hong, J. M., 480
 Hopfield, J. J., 704, 719
 hopping term, 221, 227
 Hor, P. H., 893
 Horn, P. M., 565
 Hotop, H., 302, 318
 Houston functions, 462, **479**
 Howells, W. S., 151
 Hsieh, T. C., 720
 Huang, Z. J., 893
 Hubbard model, 828–832, **835**
 exact one-dimensional solution, 829
 half filling, 831
 mean field theory, 829–831
 two-dimensional phase diagrams, 831
 Hubbard, J., 828, 836
 Huckestein, B., 837
 Hufner, S. H., 719
 Huffman, D. R., 150
 Hume-Rothery, W., 318
 Humphreys, J., 385
 Hund's rules, 762–765, 767
 Hussain, Z., 891
 Hutchison, J. L., 410
 hydrogen-bonded solids, 312
 hyperscaling relation, 753

 Iafrate, G. J., 480
 ice, 115
 icosahedral symmetry, 133
 ideal diode equation, 595
 Ido, M., 892
 ignorance and error, 624
 Ijima, S., 143
 Il'inskii, Y., 615, 631
 Illini, T., 719
 Imer, J. M., 720
 impurities, 530
 compensated, 530, 534
 deep, 532
 in tight-binding model, 535
 non-compensated, 531, 541
 one dimension, 535, 540
 shallow, 532
 three dimensions, 535, 541
 two dimensions, 535, 541
 Imry, Y., 602, 608
 incommensurate potential, **560**
 indirect exchange, 804
 indirect gap, 576, 652
 inelastic scattering, *see* scattering, inelastic
 inelastic structure factor, 369, 525
 InSb
 excitons, 644
 optical absorption, 639
 insulators
 defined in single-electron theory, 277
 dielectric function, 617
 optical properties, 659–685
 table of magnetic properties, 728
 integrated circuits, 77, 599
 interfaces
 coherent, 78
 commensurate, 78
 geometrical description, 77–81
 intermetallic compound, 103
 international notation, 36
 interplanar spacing, 79, **91**
 interstitial alloy, 102
 Invar, 363, 364
 inversion layer, 599, 780
 ionic crystals
 cohesive energy, 301–305
 optical modes, 664–674
 table of cohesive energies, 305
 table of dielectric properties, 670
 ionization of dopants, 581
 ionization potentials
 table for selected molecules, 242
 Ipatova, I. P., 378
 irreducible zones, 202
 Isaacs, E. D., 719
 Ishimaru, A., 150
 Isihara, A., 520, 837
 Ising model, **755**
 exact solution in one dimension, **755**
 exact solution in two dimensions, 734
 mean field solution, 734–736
 no exact solution in three dimensions, 734
 table of critical exponents, 750
 isoelectronic, 530
 isothermal compressibility, 748
 isotropic solids, 328
 Izumi, F., 893

- J. Perrin, 151
 Jackson, J. D., 46, 61, 74, 631
 Jacobs, I. S., 743, 758
 Jaeger, H. M., 150, 335, 339
 Jaklevic, R. C., 854
 Janot, C., 143, 150
 Jastrow wave function, 254, 788
 jellium, 242
 density functional theory, 247
 ferromagnetism, 813
 Hartree–Fock theory, 243
 phase diagram, 256
 Jensen, E., 708, 719
 Jensen, L. H., 75
 Jesser, W. A., 520
 Jiang, D., 150
 Jiles, D., 758
 Jin, Y., 795
 Joannopoulos, J. D., 318
 John, S., 565
 Johnson noise, 530
 Johnson, E. J., 639, 657
 Johnson, J. B., 530, 565
 joint density of states, 638, 700
 Jones, R. O., 263
 Jongh, L. J., 747, 758
 Jorgensen, J. D., 892
 Josephson constant, 858
 Josephson effect, *see* superconductivity,
 Josephson effect
 Josephson junction, 854
 Josephson junction circuits, 854–856
 Josephson relation, 753
 Josephson, B. D., 852, 892
 Joshi, S. K., 378
 Jungwirth, T., 520
 Jurgens, J. M., 893
- $\vec{k} \cdot \hat{P}$ method, 457
 Kadanoff, L. P., 149, 150, 628, 631
 Kadowaki, K., 887, 891
 Kagan, Y. M., 374, 377
 Kahn, F. J., 150
 Kamerlingh Onnes, H., 839, 892
 Kane, C., 565
 Kane, E. O., 639, 657
 Kanzaki, H., 657
 Karn, P. W., 438, 448
 Karplus, R., 480, 520
 Kartheuser, E., 670, 686
 Kasper, J. S., 142, 149
 Kastner, M. A., 608
 Katsnelson, M. I., 16
 Kawabata, A., 566
 Kawasaki, T., 795, 893
 Kaxiras, E., 831, 837
 KCl
 absorption and emission data, 680
 Keesom, W. H., 427
 Keldysh, L. V., 615, 631, 645, 657
 Keller, D., 94
 Keller, D.t., 91
 Kelton, K. F., 108, 150
 Kelton, R. F., 150
 Kelvin, W. T., 354, 378
 Kepler’s conjecture, 114
 Kevan, S. D., 719
 key, 379
 Keyes, R. W., 608
 Khalatnikov, I. M., 448
 Khokhlov, A. R., 150, 417, 448
 Khurana, A., 757
 KI
 Urbach tail, 684
 Kim, M., 319
 Kimerling, L. C., 657
 Kincaid, B. M., 74
 King-Smith, R. D., 74, 318
 Kingsmith, R. D., 686
 Kip, A. F., 656
 Kirby, R. K., 378
 Kirkpatrick, T. R., 565
 Kiss, T., 881, 894
 Kittel, C., 656, 837
 Kivelson, S., 232, 686
 Kleinman, L., 266, 291
 Klingshirn, C. F., 657
 Knapp, J. A., 719
 KNbO₃, 662
 Knipping, P., 43, 74, 341
 Knox, R. C., 657
 Knudsen cells, 84
 Kobayashi, K., 657
 Koch, A. J., 150
 Koechner, W., 657
 Koenig, S. H., 378
 Körling, M. K., 318
 Kohler, J. S., 386, 410
 Kohn anomalies, 373
 Kohn, W., 232, 263, 378, 566
 analytic structure of bands, 226
 anomalies, 373
 density functional theory, 244
 Kohn–Sham equations, 255
 shallow impurity states, 531
 Kohn–Sham equations, 255–258, 268
 Kojima, T., 318
 Kokusho, K., 893

- Kolenbrander, K. D., 657
 Kolomeisky, E. B., 837
 Kondo effect, 819–828
 resistivity, 827
 scaling solution, 826
 scaling theory, **835**
 specific heat, 828
 Kondo temperature, 826
 Kondo, J., 819, 837
 Kontorova, T., 384, 386, 410
 Koopman's theorem, **258**
 Kortan, A. R., 135, 142, 150
 Kosevich, A. M., 480
 Koster, G. F., 193, 206, 271, 292
 Kosterlitz, J. M., 392, 410
 Kosterlitz–Thouless–Berezinskii transition, 392–399
 Kotliar, G., 831, 836
 Kouwenhoven, L. P., 608
 Kozlov, A. N., 657
 Kr
 band structure, 283
 Krakauer, H., 687
 Kramer, B., 566
 Kramers–Kronig relations, 618–623, **628**
 Krauth, W., 831, 836
 Kresse, G., *xvii*, 281, 282, 285, 291, 313, 318, 687
 Krieger, J. B., 480
 Krishnan, K. S., 523, 565
 Krishnan, R. S., 378
 Kronig, R., 189, 206
 Kronig–Penney model, 189, **204**
 Krueger, H. H. A., 686
 Krumhansl, J. A., 565
 Krusius, M., 837
 Kubo–Greenwood formula, 623–627
 direct optical absorption, 638
 lasers, 648
 Kubo–Greenwood formula, 706
 Kudo, E., 893
 Kugler, M., 891
 Kunz, C., 697, 719

 L214, *see* $La_{2-x}Sr_xCuO_4$ 882
 $La_{2-x}Ba_xCuO_4$, 881
 Ladell, J., 73
 Ladenburg, R., 657
 Lagally, M. G., 82, 95
 Lagrange multipliers, 248
 Lagrange's equations, 468
 Lagrangian
 for electron wave packets, 466–468, **478**
 for superconductivity, 857–858
 for superfluid helium, 439–442
 formalism, 905
 Lagrangian strain tensor, 321
 Lamb, S. H., 448
 Lamb–Mössbauer factor, 376
 Lamé constants, 328
 Landau damping, 696, 697, **718**
 Landau diamagnetism, 771–774, **793**
 Landau free energy, 745
 Landau levels, 772
 degeneracy, 772
 Landau parameters, 511
 Landau, L. D., 74, 94, 150, 173, 206, 232, 291, 318, 339, 410, 448, 521, 566, 657, 686, 758, 794, 795, 837, 892
 critical velocity in ^4He , 435
 Fermi liquid theory, 504
 free energy for phase transitions, 745
 impossibility of long range order in two dimensions, 389
 impossibility of long-range order in one dimension, **145**
 Landau damping, 696
 Landau diamagnetism, 769, 771
 magnetic domains, 737
 superconductivity, 844, 850
 superfluid hydrodynamics, 430
 Landau–Ginzburg equations, *see* superconductivity, Landau–Ginzburg equations
 Landauer, R., 601, 608
 Landé g factor, 765
 Landolt, H., 41, 291, 339, 480, 521, 608, 686, 719, 758, 795
 Lane, C. T., 448
 Lang, N. D., 574, 608
 Lang, W., 697, 719
 Langer, J. S., 150, 448
 pattern formation, 110
 superfluid vortices, 439
 Langevin equation, 112, **147**
 Langmuir, I., 264
 Lannin, J. S., 150
 lanthanides, *see* rare earths
 Laperiot, G., 893
 Lapeyre, G. J., 720
 Laplace's equation, 109, 394, 402
 LAPW, *see* linear augmented plane waves
 Larbalestier, D., 892
 Larkin, A. I., 890
 Larmor diamagnetism, 769
 lasers, 646–652
 four-state, 650
 Nd:YAG, 651

- ruby, 651
- semiconductor, 652
- solid-state, 649
- stimulated emission, 627, 646–649
- three-state, 650
- Lathrop, D. P., 449
- lattice, 6
 - two-dimensional, **376**
- lattice constant, 20
- lattice spacing, 20
- lattice sums for noble gases, **315**
 - table, 301
- lattice with basis, 9
 - examples, 24
 - phonons on, 348
 - scattering, 53
- lattices
 - base-centered orthorhombic, 32
 - body-centered cubic, 22, 30
 - body-centered orthogonal, 32
 - Bravais, 6
 - CaF₂, 26
 - CaTiO₃, 28
 - centered monoclinic, 32
 - centered rectangular, 7, 12
 - centered tetragonal, 32
 - CsCl, 26
 - CuO, 712
 - diamond, 24
 - face-centered cubic, 20, 30
 - face-centered orthorhombic, 32
 - hexagonal, 7, 23, 32
 - hexagonal close-packed, 23
 - honeycomb, 9, **14**
 - identity of, 13
 - monatomic, 20
 - NaCl, 25
 - oblique, 7
 - reciprocal, 49
 - rectangular, 7, 12
 - rhombohedral, 32
 - simple cubic, 20, 30
 - simple monoclinic, 32
 - simple orthorhombic, 32
 - simple tetragonal, 32
 - square, 7
 - three dimensional, 17
 - triangular, 7
 - triclinic, 32
 - trigonal, 32
 - two-dimensional, 6
 - ZnO, 28
 - ZnS, 27
- Laue method, 56, **72**
- Laughlin, R. B., 795
 - fractional quantum Hall effect, 787
 - integer Hall effect, 783
- law of mass action for semiconductors, 580
- Lax, B., 635, 656, 657
- LBCO, *see* La_{2-x}Ba_xCuO₄
- LCAO, *see* linear combination of atomic orbitals
- LDA, *see* local density approximation
- Leath, P. L., 565
- LED, *see* light-emitting diodes
- Lee, C. T., 263
- Lee, D. M., 443, 448, 449
- Lee, P. A., 74, 564, 892
- LEED, *see* low-energy electron diffraction
- Leggett, A. J., 443, 448, 449, 890
- Lennard-Jones potential, 299
- Levi, B. G., 608
- Levin, K., 891
- Levine, D., 134, 150
- Ley, L., 720
- Lhuillier, C., 836
- Li
 - martensitic transformation, 474
- Liang, S., 149
- Licciardello, D. C., 564
- Lieb, E. H., 263, 553, 837
 - Hubbard model solution, 829
 - Lieb–Mattis theorem, 800
 - stability of matter, 249, 250
- Lieb–Mattis theorem, 800–802
- Lieber, C. M., 892
- Liebmann, M., 94
- Liebowitz, H., 409
- Lifshitz, E. M., 74, 94, 150, 173, 206, 232, 291, 318, 339, 448, 521, 566, 657, 686, 758, 795, 837
 - magnetic domains, 737
- Lifshitz, I. M., 150, 473, 480
- Lifshitz, R., 36, 41
- light-emitting diodes, 652
- Likharev, K. K., 892
- Lin, J., 94
- Lindelof, P. E., 891
- Lindenfeld, P., 892
- Lindhard dielectric function, 244, 628, **630**
- linear augmented plane waves, 274–277, **286**
- linear combination of atomic orbitals, 219–222, **229**, 271
- linear elasticity, 325–336
 - table of constants for cubic crystals, 327
 - table of moduli for isotropic materials, 331
- linear expansion coefficient, 363

- linear response theory
 Maxwell's equations, 614
 thermoelectric phenomena, 491
- Lineberger, W. C., 302, 318
- Lines, M. E., 686
- lineshape, 626
- Liouville's theorem, 491
- Lipson, S. G., 4, 16
- liquid crystals, 120–123
 cholesterics, 121
 elasticity, 332–335
 Friedrichs transition, **338**
 hexatics, 393
 nematics, 120
 smectics, 121
- liquids, *see also* fluids
 structures, 113–116
- Litster, J. D., 149
- Littlejohn, R. G., 471, 480
- Littlewood, P. B., 263, 893
- Liu, A. J., 116, 150
- Liu, F., 66, 74, 318
- loadstone, 723, 732
- Lobb, C. J., 893
- local density approximation, 257
- local density of states, 537
- local energy, 261
- localization, 542–553
 exact results, 544–547
 experimental scaling curves, 552
 phonons and dielectric media, 553
 weak disorder, 547
- localization length, 544
- localized states, 540, 586, 781
- London equation, 840
- London penetration depth, *see*
 superconductivity, penetration depth
- London, F., 798, 800, 836, 892
- long-range order, 66, 67, 113, 372, 389, **409**
 quasi, 393
- Longinotti, L. D., 838
- longitudinal light waves, 616, 628, 667–669,
 671
- longitudinal phonon mode, 348, 353, 702, 862
- longitudinal sound waves, 331
- Lorentz force, 728
- Lorentz, H. A., 453, 480
- Lorenz number, 496
- loss modulus, 423
- Lothe, J., 410
- Loudon, R., 657
- Louie, S. G., 291, 709, 719
- Lounasmaa, O. V., 448, 758
- low-angle grain boundary, 81
- low-energy electron diffraction, 82
- Lowen, H., 686
- Lowenstein, J. H., 835
- lowering operator, 352
- LSCO, *see* $La_{2-x}Sr_xCuO_4$ 882
- Lu, J., 565
- Lubensky, T. C., 123, 149, 335, 339
- Lubliner, J., 426, 449
- Lüty, F., 680, 686
- Luther, A., 566
- Luttinger liquid, 553–559, **564**
- Luttinger, J. M., 480, 520, 553
- Lyddane–Teller–Sachs equation, 667
- Lynden-Bell, R. M., 410
- Lynn, J. W., 811, 837, 838
- Lyubarskii, G. Y., 193, 195, 206
- M center, 679
- MacDonald, A. H., 520
- Macfarlane, G. G., 657
- MacGillavry, C. H., 11, 16
- Mackenzie, J. K., 65, 74
- MacKinnon, A., 566, 608
- MacLaughlin, D. E., 892
- macroscopic wave function
 superconductivity, 844, 852
 superfluidity, 436
- Madelung constant
 ionic crystals, 304
 metals, 306
 table for ionic crystals, 304
 table for metals, 307
- Madison, K. W., 472
- Maggio-Aprile, I., 891
- magnetic breakdown, 476
- magnetic domains, 376, 736–739
- magnetic flux quantum, 486, 772
- magnetic groups, 36
- magnetic hysteresis, 739
- magnetic moments, 723, 727–729, **754**
 Anderson model, 820, **833**
 arising from impurities, 820–824
 interaction strength, 797
 table for rare earths, 768
 table for transition metals, 768
 table of density functional calculations,
 814
- magnetic permeability, 724
- magnetic susceptibility, 724
 ferrimagnets, 732
 near phase transition, 746
 table for diamagnetic insulators, 728
 table for metals, 775
 table for noble gases, 769

- versus temperature for EuO, 731
- magnetism, *see also* ferromagnetism *and* antiferromagnetism
 - atomic energy splitting in external field, 765
 - classical paradox, 759
 - Coulomb repulsion, 759, 760, 763
 - exchange forces, 737
 - free electron energy levels in magnetic field, 772
 - free electrons, 769–776
 - free electrons and boundaries, 774
 - free energy, 725
 - Heisenberg model, *see* Heisenberg model
 - hysteresis, **756**
 - important energies, 760–761
 - isolated atoms, 761–769
 - phenomenology, 724–739
 - spin Hamiltonian, 802
 - table of critical exponents, 750
 - thermodynamic ensembles, 726–727, **755**
 - tightly bound electrons, 777–779
- magnetite, 732
- magnetoresistance, 502
 - giant, 815
 - silver, 503
- magnons, *see* spin waves
- Mahan, G., 521
- Maiman, T. H., 646, 657
- Maki, K., 893
- Malozemoff, A. P., 894
- Manousakis, E., 831, 837
- Manson, S. T., 719
- many-body effects, 709
- many-body Green functions, 628
- Maple, M. B., 891, 892
- Maradudin, A. A., 378
- March, N. H., 262, 263, 527, 566
- Marcus, P. M., 837
- Marder, M., 410
- Maret, G., 566
- Margaritondo, G., 719
- Marion, J. B., 12, 16
- Martel, P., 449
- martensitic transformation, 311, 474
- Martin, J. H., 656
- Martin, R. M., 263
- Marzari, N., 232
- Maslen, V. W., 65, 74
- Maslov index, 471
- Massalski, T. B., 73, 150
- master equation, 99
- Masuda, Y., 880, 892
- Matsuda, T., 795, 893
- Matthias, B. T., 731, 758
- Matthiessen's rule, 528, 819
- Mattis, D. C., 553, 837
 - Lieb–Mattis theorem, 800
 - magnon bound states, 808
- Maugin abacus, 57, **72**
- maxon, 434
- Maxwell's equations, 613–616
- Maxwell, E., 858, 892
- Maxwell, J. C., *xxii*
- MBE, *see* molecular beam epitaxy
- McBride, C., 151
- McCaldin, J. O., 608
- McClintock, P. V. E., 447
- McEuen, P. L., 565
- McGill, T. C., 608
- McLean, T. P., 657
- McMillan, E. M., 74
- McMillan, W., 880, 892
- McMurry, S., 151
- McRae, E. G., 719
- mean field theory, **755, 756**
 - alloy superlattices, 741–743
 - Anderson model of magnetic impurities, **833**
 - Fermi liquids, 507
 - Hubbard model, 829
 - Ising model, 734–736
 - size of mean field, 736
 - superconductivity, 869
- mean free path, 175, 492, 526, 552, 693
 - table for liquid metals, 526
- mega-buck evaporator, *see* MBE
- Meier, F., 837
- Meilkhov, E. Z., 331, 339, 410, 448, 499, 520, 565, 728, 757, 846, 891
- Meinhardt, H., 150
- Meirav, U., 606, 608
- Meissner effect, *see* superconductivity, Meissner effect
- Meissner, W., 839, 843, 844, 892
- Mendez, E. E., 472, 480
- Meng, R. L., 893
- Menon, M., 118, 150
- Menon, R., 564, 566
- Mercereau, J. E., 854, 892
- Mermann, A., 292
- Mermin, N. D., 150, 151, 301, 318, 378, 410
 - Debye–Waller factor in single sentence, 371
 - Mermin–Wagner theorem, 391
 - orientational order, 391
 - quasicrystallography, 143
- Mermin–Wagner theorem, 391

- Meservey, R., 873, 892
 Messiah, A., 566
 metal–insulator transitions, 530–534
 summary of many systems, 534
 transition metal oxides, 712
 metal–oxide–silicon, 599–600
 metals
 cohesive energy, 305–311
 defined in single-electron theory, 277
 dielectric function, 617
 ductile, 423
 interband optical transitions, 698–701
 liquid, 524, 526–527
 optical absorption, 620
 optical properties, 689–718
 table of densities deduced from
 pseudopotentials, 308
 table of magnetic susceptibilities, 775
 table of mean free path in liquid, 526
 table of thermoelectric properties, 499
 metastable states, 624, 650
 method of successful approximations, xxi
 Métois, J. J., 4, 16
 metric tensor, 321
 Meyer, J. C., 16
 Mg
 Fermi surface, 281
 Michel, J., 657
 Michel, K. H., 410
 Micnas, R., 892
 microcrystalline, 106
 micromagnetics, 738
 Miedema, A. R., 758
 Mieghem, P., 657
 Miller index, 51
 in cubic crystals, 52
 in hexagonal lattices, 53
 Miller, A., 608
 Miller, T., 720
 Millikan, R. A., 156, 173
 Minnhagen, P., 410
 minority carriers, 593, 596, 645
 Mints, R. G., 891, 892
 Mises yielding condition, 425
 Mitrovic, B., 890
 MnF₂
 critical phenomena, 749
 MnO
 antiferromagnetism, 63
 mobility, 591, 600, 785
 mobility edge, 543, 550
 Mochiku, T., 887, 891
 mode counting for phonons and electrons, 348
 model problems, 155
 free Fermi gas, 155
 models
 nearly free electron, 207
 single electron, 157
 tight binding, 207
 tight-binding, 219
 modes
 optical, *see* phonons, optical
 modulus of elasticity, 330
 Mössbauer, R., 374, 378
 Mössbauer effect, 374–376, 730
 molecular beam epitaxy, 84
 molecular dynamics, 112, 115, 119, 313
 Mollwo, E., 675, 686
 momentum conservation
 inelastic light scattering, 701
 optical absorption, 640
 phonons, 364
 photoemission, 707
 Momono, N., 892
 MoNb
 resistance minimum, 820
 Moncton, D. E., 410
 Monin, A. S., 449
 Monte Carlo
 quantum, 252–255
 Monte Carlo method, 110, 144, 313
 Montroll, E. W., 378
 Mook, H. A., 838
 Morozov, S. V., 150
 Moruzzi, V. L., 814, 837
 MOS, *see* metal–oxide–silicon
 Moses, D., 566
 Mott insulator, 832
 Mott transition, 534
 Mott, N. F., 566, 675, 686, 719
 Mott insulators, 530, 711
 Mott–Bethe relation, 73
 Mott–Wannier excitons, 641
 Mott–Hubbard insulators, 832
 Mozer, B., 367, 378
 Müller, K. A., 881, 890
 muffin-tin potential, 275
 Mulay, L. N., 768, 794
 Muller, K. A., 890
 multiple scattering, 47, 83, 128
 Murakami, T., 893
 Murnaghan, F. D., 193, 199, 206
 Murray, C. A., 393, 410
 N₂, 241
 Na
 interband optical transitions, 698
 resistance versus temperature, 529

- specific heat, 359
- NaCl
 - atomic radii, 297
 - charge density, 296
 - coloration by sodium and X-rays, 674
 - structure, 25
 - X-ray scattering, 43
- Nadarzinski, K., 81, 94
- Nagaosa, N., 892
- Nagasaka, S., 305, 318
- Nagel, S. R., 116, 118, 149, 150, 339
- Nakano, T., 892
- nanotube, 12, 143
 - (*n*, *m*) indexing, **14**
 - band structure, **287**
 - indexing structures, **15**
 - multi-walled, 143
 - single-walled, **14**
- Narayanamurt, V., 891
- Näbauer, M., 850, 852, 891
- Navier–Stokes equation, 416
- Nb₃Ge
 - high superconducting temperature, 881
- NbSe₂
 - Abrikosov lattice, 850
- Nd
 - lasers, 650
- nearly free electron model, 207
- nearly free electrons, 208–217, **227**
- Néel state, 809
- Néel temperature, 732
- Néel, L., 732, 758
- Nelin, G., 367, 378
- Nelson, D. A., 263
- Nelson, D. R., 150, 410, 891
 - icosahedral symmetry, 142
 - two-dimensional melting, 392
- nematics, 120
- Nemirovskii, S. K., 449
- Nenciu, G., 226, 232, 480
- Nesbitt, L. B., 893
- Neumark, G. F., 657
- neutrons
 - creating and destroying phonons, 373
 - differential scattering cross section, 368
 - elastic scattering, 63
 - inelastic scattering, 363–376
 - scattering in ⁴He, 434, 442
 - thermal, 63
- Newman, J., 70
- Newton's laws, 112
- Ni
 - ferromagnetism, 731, 736, 814
 - neutron scattering, 367
- Nicklow, R. M., 73
- Nilsson, G., 367, 378
- NiO
 - insulator, 279, 711
 - magnetic structure, 733
- Niu, Q., 448, 466, 472, 480, 481, 520, 521
- Nix, F. C., 837
- NMR, *see* nuclear magnetic resonance
- Noakes, D. R., 757
- Nobel, J., 892
- noble gases
 - band structure, 282
 - cohesive energy, 299
 - table of cohesive energy parameters, 300
 - table of magnetic susceptibilities, 769
- noble metals
 - band structure, 280
 - Fermi surfaces, 475
 - interband optical absorption, 701
- Noguchi, T., 564
- noise
 - 1/*f*, 530
 - Johnson, 530
 - shot, 530
 - thermal, 529
- non-radiative decay, 650
- nondegenerate electron gas, 166
- nonsymmorphic, 36
- normal scattering, 527
- Norman, M. R., 887
- Norman, M. R., 891
- Norrby, L.-J., 719
- Novoselov, K. S., 16, 150
- Nozières, P., 449, 521, 837
- nuclear magnetic resonance, 730
- nucleation, 108, 442
- Nurmikko, A. V., 657, 795
- Nussbaumer, H. J., 900, 902
- Nyquist, H., 530, 566
- O'Keeffe, M., 319
- O'Quinn, B., 521
- oblique lattice, *see* lattices
- occupation number, 159, 507, 907
- Ochsenfeld, R., 839, 843, 844, 892
- Oda, M., 892, 893
- Ohm's law, 552
- ohmic contact, 584
- Ohmic junction, **606**
- Ohnishi, T., 564
- Ohtaka, K., 720
- Oja, A. S., 758
- Okaya, Y., 73
- one-electron model, *see* single-electron model

- Onsager relations, 491–492, 495, **517**
 Onsager, L., *481, 758*
 de Haas–van Alphen effect, 473
 superconductivity, 852
 two-dimensional Ising model, 734
 open orbits, 470, 471, 501, 502
 Oppenheimer, J. R., 86, 233, 262
 optical activity, 38
 optical branch, 344
 optical gap, *see* energy gap
 optical mass, 694
 optical phonons, *see* phonons, optical
 optical transitions, **206**
 direct, 638–639
 Franck–Condon effect, 679–683
 indirect, 639–641
 metals, 698–701
 OPW, *see* orthogonalized plane waves
 Orbach, R., 805, 837
 order parameters, 113
 liquid crystals, 122
 liquids, 113
 orientational order
 nematics, 120
 two dimensions, 391
 Oron, A., *449*
 Orowan, E., 381, *410*
 orthogonalized plane waves, 266
 Osakabe, N., *795, 893*
 Osheroff, D. D., *443, 449*
 osmotic pressure, 422
 Ostlund, N. S., *264*
 Otnes, K., *378*
 Ott, H. R., 829, *837*
 overlap integrals, 220

 P (phosphorus)
 in silicon, 531
 PAA, 120
 packing fraction, **39**
 Pais, A., *758*
 Pake, G. E., *758*
 Palevsky, H., *378*
 Palm, J., *657*
 Pan, S., 850
 Pancharatnam, S., 232
 Pandey, K. C., 710, *720*
 Pantelides, S. T., *566*
 Paoletti, M. S., *449*
 paraelectric, 660
 paramagnetism, 724, 729, 842
 Parisi, G., 743, *758*
 Park, R. M., *657*
 Parks, R. D., *892, 893*

 Parr, R. G., *258, 263*
 Parrinello, M., *272, 291*
 Parrot, J. E., *521*
 participation ratio, **561**
 Paskin, A., *757*
 pattern formation, 110
 Patterson function, 64
 Patterson, A. L., *64, 74*
 Patthey, F., *705, 720*
 Pauli exclusion principle, 156, 158, 235, 277,
 494
 Pauli paramagnetism, 770–771
 Pauli, W., *279, 291*
 Pauling, L., 133
 Pauthenet, R., *733, 757*
 Pb
 superconducting density of states, 881
 PBC, *see* periodic boundary conditions
 $\text{PbZr}_{1/2}\text{Ti}_{1/2}\text{O}_3$, 662
 PbZrTi , 88
 Peach, M., 386, *410*
 Peach–Köhler force, 386
 Pearson, W. B., *37, 41, 298, 304, 318*
 Pecora, R., *74*
 Peercy, P. S., *687*
 Peeters, F. M., *674, 686*
 Peierls distortion, 309–311
 Peierls substitution, 777, **792**
 Peierls, R. E., *232, 318, 410, 566*
 impossibility of long range order in two
 dimensions, 389
 nearly free electron approximation, 207
 Peierls distortion, 309
 Peierls substitution, 777
 Umklapp, 527
 Peik, E., *480*
 Peisl, J., *719*
 Peltier coefficient, 517
 Peltier effect, 498
 Penney, W. G., 189, *206*
 Penrose lattice, 139
 Penrose tiles, 139
 Penrose, R., 139
 Pepper, M., 780, *795*
 Pepy, G., *835*
 Perdew, J. P., 258, *263*
 Perepezko, J. H., 117, *151*
 periodic boundary conditions, 158
 non-cubic crystals, 184
 phonons, 342, 346
 with electric fields, 460
 periodic potential, 175
 periodic potentials
 weak, 208

- peritectic, **144**
 Permalloy, 740
 perovskite, *see* CaTiO₃, 882
 perovskites
 table of polarization values, 662
 perturbation theory
 $\vec{k} \cdot \vec{P}$ method, 458
 degenerate, 210
 Green's functions, 538
 localization theory, 545
 nearly free electrons, 208, 699
 optical response, 623
 polarons, 672
 polymeric solutions, 421
 superconductivity, 875
 Peschel, I., 566
 Pescia, D., 815, 837
 Peshkov, V. P., 433, 449
 Pethick, C., 520
 Petroff, F., 836
 Pettifor, D. G., 318
 phase diagrams, 102–108
 ferromagnets versus liquid–gas systems, 744
 geometrical construction, 107
 phase separation, 103–110, **144**
 criterion for, 105
 Philipsen, P. H. T., 318
 Phillips, A., 447
 Phillips, F. C., 17, 41
 Phillips, J. C., 151, 291, 720
 constraints in glasses, 119
 GaAs calculations, 710
 pseudopotentials, 266
 Phillips, R. A., 480
 Phillips, T. G., 656
 phonons, 341–376
 absorption, 366
 acoustic, 344–350, **376**, 862
 electrical resistivity, 527
 emission, 366
 excited by cracks, 405
 Hamiltonian for, 353
 in one dimension, 342–344
 optical, 344–350, **376**
 quantum mechanical, 351–363
 thermal conductivity, 363
 photoelectric effect, 611
 photoemission, 703–716
 high-resolution, 881
 superconductors, 881
 angle-resolved photoemission spectroscopy, 706
 core-level, 710–716, **718**
 inverse, 709
 raw data, 708
 sketch of experiment, 706
 ultraviolet photoemission spectroscopy, 708
 X-ray photoemission spectroscopy, 708, 710
 physisorption, 81
 Pichard, J. L., 563, 566
 Pick, H., 677, 686
 Pickett, W. E., 893
 Pierret, R. F., 608
 Pietronero, L., 94
 piezoelectricity, 37, 88
 Pilet, N., 94
 Pilgrim, W.-C., 151
 Pinczuk, A., 795
 Pindak, R., 393, 410
 Pine, D. J., 132, 151
 Pines, D., 242, 263, 449, 521, 893
 Pippard, A. B., 481, 521, 694, 720
 Plakida, N. M., 846, 893
 Planck, M., 354
 plane wave expanded in spherical harmonics, 276
 plane waves, 271–274, **287–290**
 plasma frequency, 618, 622, 636, 689–692
 plasmons, 695–698
 dispersion relation, 696
 experimental observation, 696–698
 plasticity, 423–426
 Platzman, P. M., 698, 719, 720
 Ploog, K. H., 94
 Plummer, E. W., 719
 Plummer, J. D., 607
 plunger, 603
 Pohl, R. W., 675
 point defects, 530, *see also* color centers
 point group, 12
 point-contact rectifier, 574, 583
 Poirier, D. M., 151
 Poisson's equation, 588
 Poisson's ratio, 330
 Polanyi, M., 381, 410
 polariton, 668
 polarizability of hydrogen-like atoms, 533
 polarization, 613, 659–664
 ambiguity, 659
 table, 662
 polarization catastrophe, 533
 polarons, 669–674, **685**
 effective mass, 673
 experimental observation, 674
 polycrystalline, 106

- polyethylene, 123
 polymers, 123–127
 basic integrals, **146**
 disordered conducting, 552
 mechanics of dilute solutions, 416–423
 rubber, 322
 stiffness of, **146**
 volume interactions, 126
 polystyrene, 423
 Pomeranchuk effect, 442
 Pond, R. C., 608
 Pople, J. A., 263
 population inversion, 649
 Posternak, M., 687
 potentials
 three-body, 314
 two-body, **15, 39**, 314
 powder method, 59, **73**
 Powell, R. J., 711, 720
 PPV, 552
 Prange, R. E., 794, 795
 Pratt, W. P., 565
 precession camera, 57
 Preisach model, **756**
 Press, W. H., 900, 902
 Preston, R. S., 375, 378, 730, 758
 Primakoff, H., 806, 836
 primary alloy, 102
 primitive unit cell, 9
 primitive vectors, 6
 Prost, J., 149, 339
 proteins
 determining structures, 65
 pseudogap, 884
 pseudopotentials, 266–271
 cohesive energy from, 307
 empirical, 267
 empty core, 267, **286**
 first-principles, 268
 from optical absorption, 700
 nonlocal, 267
 weak scattering conductivity, 523
 pumping, 650
 pyroelectricity, 37, 659
 PZT, *see* PbZrTi

 quadratic form, 577
 quantum dot, 603–605
 quantum Hall effect, 780–791
 electron density, 789
 fractional, 785–791
 integer, 780–785
 localized states, 781, 782
 resistance standard, 780
 wave function, 787
 quantum liquid, 786
 Quantum Monte Carlo, **261**, 252–261
 quantum Monte Carlo, 255
 quantum point contact, 600–602
 Quarrington, J. E., 657
 quasi-long-range order, 393
 quasi-neutral region, 592, 594, 645
 quasi-particles, 505
 quasi-static approximation, 109
 quasicrystals, 133–143
 generalized dual method, **148**
 one dimension, 134
 scattering from, 137
 scattering from two-dimensional, **148**
 three dimensions, 141
 two dimensions, 139
 Quate, C. F., 94
 Queisser, H. J., 565
 quenching, 104, 767, 768

 Rabson, D. A., 151
 radial correlation function, 114
 radius of gyration, 123
 radius parameter r_s , 162, 306
 table for selected metals, 167
 Rado, G. T., 837
 Radzihovsky, L., 339
 Raghavachari, K., 263
 raising operator, 352
 Raizen, M., 481
 Raizen, M. G., 472
 Rajagopal, A. K., 378
 Rakhmanov, A. L., 892
 Ralph, D. C., 837
 Ramakrishnan, T. V., 564
 Raman scattering, 702–703
 Raman shift, 702
 Raman, C. V., 701, 720
 Rammer, J., 608
 Randeria, M., 887, 891
 random forces, 112
 random packing, 115
 random walk, 100, 124
 Ranninger, J., 892
 Rapaport, D. C., 112, 151
 rare earths
 band structure, 286
 ferromagnetism, 731
 magnetic garnets, 733
 table of magnetic moments, 768
 Rasolt, M., 893
 Rassolov, V., 263
 Raveau, B., 893

- Rayleigh peak, 703
 Rayleigh waves, 337
 reciprocal lattice, 49, **71**, **228**
 cubic lattices, 51
 explicit construction, 51
 in Bloch's theorem, 177
 table, 52
 reciprocal space, 159
 recombination, 592
 rectangular lattice, *see* lattices, *see* lattices
 rectification, 567, 585, 590, 592–595
 Redfern, P. C., 263
 Redfield, A. G., 880, 892
 reduced temperature, 745
 reduced zone scheme, 188, 209, 213
 Reed, M., 608
 reflection, 621
 reflection high-energy electron diffraction, 84
 reflectivity, 621
 refrigeration, 498, **517**
 regeneration, 592
 Regnault, L. P., 893
 Reich, D. H., 263
 Reichardt, W., 835
 Reichel, J., 480
 Reid, W. H., 448
 relaxation time, 488, 524, 592, 600, 665
 relaxation time approximation, 487–489
 conditions for derivation, 524
 Renner, C., 891
 renormalization group, 398, 744
 renormalized perturbation expansion, 545
 repeated zone scheme, 189
 Reppy, J. D., 439, 448
 reservoirs, 601
 residual ray, 355, 668
 residual resistivity ratio, 529
 resistance minima, 819–820
 explained by scaling theory, 828
 resistance quantum, 548
 resistivity tensor, 502
 Resta, R., 661, 687
 Restrahl, *see* residual ray
 return-point memory, 756
 reverse bias, 596
 Reynolds, C. A., 858, 859, 893
 Reynolds, D. C., 657
 RHEED, *see* reflection high-energy electron diffraction
 Rice, T. M., 645, 656, 657, 893
 Rich, D. H., 710, 720
 Richardson, R. C., 443, 449
 Richardson–Dushman equation, 572, 703
 Richter, A., 831, 837
 Rigden, J. S., 758
 Rinzler, A. G., 565
 Ritchie, R. H., 263
 Robaszkiewicz, S., 892
 Roberts, V., 657
 Robinson, R. A., 838
 Roche, S., 291
 rocksalt, *see* NaCl
 rods, 83
 Röntgen, W. C., 674, 687
 Röpke, G., 837
 Roger, M., 837
 Rohrer, H., 86, 91, 94
 Roitburd, A. L., 311, 318
 Rokhsar, D. S., 151
 Rose, J. H., 318
 Rosenbaum, T. F., 263, 533, 534, 566
 Rosenblum, E. S., 657
 Rosi, F. D., 520
 Rossat-Mignod, J., 893
 Rossiter, B. W., 94
 rotating crystal method, 57
 Roth, S., 16
 Rothman, D. H., 151
 roton, 434
 Rottman, C., 92, 94
 Roukes, M. L., 838
 Rouse model, 419
 Rouse, P. E., 419, 420, 449
 Rowe, D. M., 520
 Rowell, J. M., 853, 890, 893
 Rozenberg, M. J., 831, 836
 RPE, *see* renormalized perturbation expansion
 RRR, *see* residual resistivity ratio
 RSJ, *see* superconductivity, resistively shunted junction model
 rubber elasticity, 322–325, **338**
 Ruckenstein, A. E., 893
 Rudigier, H., 837
 Rushbrooke relation, 752
 Russel–Saunders coupling, 763
 Ruthemann, G., 697, 720

 saddle point, 188, 439
 Sadovskii, M. V., 566
 Sági-Szabó, G., 687
 Saito, R., 232
 Sales, B., 521
 Salomaa, M. M., 449
 Salomon, C., 480, 481
 salt, *see* NaCl
 Samara, G. A., 687
 Saminadayar, L., 790, 791, 795
 sand, 116, 335

- Sander, L. M., 93, 95
 Sandercock, J. R., 703, 720
 Sanz, E., 151
 Sarachik, M., 820, 838
 Sarker, S., 831
 SARW, *see* self-avoiding random walk
 Saurenbach, F., 836
 Sawatzky, G. A., 719, 720
 sc, *see* lattices, simple cubic
 scaling theory, **562, 563**
 Bloch's theorem, 180
 critical phenomena, 744, 750–754, **756**
 Kondo problem, 824–828
 Kosterlitz–Thouless, 398
 localization, 547–553
 scanning tunneling microscopy, 86–90, 850
 scattering
 rotating crystal method, 57
 accuracy of structure determination, 66
 dynamic, 68
 elastic, 46
 form factor, 47
 from one-dimensional quasicrystal, 137
 inelastic, 47, 363–376, 698, 702, 703
 Laue method, 56, **72**
 particles used for, 60
 powder method, 59, **73**
 time in Fermi liquid, 506
 time measured in Fermi liquid, 515
 two-phonon, **377**
 scattering length, 367
 Schawlow, A. L., 646, 657
 Scheffler, M., *xxii*, 291, 319
 Schiff, L., 46, 64, 74, 86, 94, 182, 206, 521, 657, 687, 838
 Schiffer, P., 449
 Schlosser, H., 318
 Schluter, M., 263
 Schmitt, R. W., 743, 758
 Schmitt-Rink, S., 893
 Schnatterly, S. E., 698, 720
 Schneider, W. D., 720
 Schönflies notation, 36
 Schönflies, A., 17, 41, 341
 Schottky barrier, 570–572
 Schottky diode, 583–585
 Schottky effect, 572
 Schottky pair, 676
 Schottky, W., 572, 574, 608
 Schrieffer, J. R., 686, 839, 865, 890
 Schroeder, P. A., 565
 Schulte, F. K., 570, 608, 705, 719
 Schumacher, W., 831
 Schuster, A., 574, 608
 Schwartz, B. B., 873, 892
 Schwartz, L. M., 291
 Schwartz, U., 90
 Schwarz, K. W., 448
 Schwarz, U. D., 94
 Schweizer, J., 893
 Schwendmann, T. C., 94
 Schwinger representation, 805
 Schwinger, J., 805, 838
 screening, 244, **258, 630**
 screening length, **258, 286**
 screw axis, 12, 36, **39**
 Sears, V. F., 449
 second quantization, 907–912
 BCS Hamiltonian, 865
 excitons, **654**
 Hartree-Fock theory, 236
 Heisenberg model, 803
 Hubbard model, 829
 polarons, 672
 second sound, *see* ⁴He, second sound
 secondary alloys, 103
 Seebeck effect, 497–498
 Seidel, H., 678, 687
 Seitz, F., 265, 292
 self-avoiding random walk, 125
 Sellmyer, D. J., 291
 selvage, 77
 semiclassical dynamics, 455–459, **516**
 anomalous velocity, 469
 breakdown, 469
 cyclotron resonance, 634
 Hamiltonian, 470
 rules, 455
 wave packets, 465
 semiconductors, 574–583
 band structure, 283
 Boltzmann equation, 590–595
 defined in single-electron theory, 278
 degenerate, 583
 extrinsic, 581
 intrinsic, 580, **606**
 junctions, 587–590
 nondegenerate, 578
 optical absorption, 576, 620
 optical properties, 633–656
 Pauli's opinion, 279
 photoemission, 709
 pure, 575
 removing impurities, 102
 surface states, 586–587
 surfaces, 583
 table of impurity binding energies, 580
 table of properties, 577

- thermopower, **606**
- Zener tunneling, 465
- semimetals
 - defined in single-electron theory, 279
- Senatore, G., 263
- separation parameter, 303
- Serin, B., 893
- Shahar, D., 795
- Sham, L. J., 255, 263, 264
- Shankar, R., 838
- Shapiro, A. P., 720
- Sharp, J., 4, 521
- Sharvin, Y. V., 836
- Shaulov, A., 894
- Shaw, T. M., 890
- shear modulus, 330
 - complex, 423
- Shechtman, D., 133, 134, 151
- Sheel, K., 893
- Shen, Z., 891
- Sheng, P., 566
- Shi, J., 521
- Shina, S., 881, 894
- Shockley equation, 595
- Shockley, W., 608, 837
- Shoenberg, D., 473, 481
- short-range order, 113
- shot noise, 530, 790
- Shraiman, B. I., 149
- Shull, C. G., 63, 74, 378
- Si
 - band structure, 285
 - cyclotron resonance, 636
 - doped with phosphorus, 531
 - energy bands and photoemission, 710
 - form of effective mass, 577, 636
 - holes, 638
 - indirect gap, 576, 639, 652
 - irreducible representations, 200
 - perfection of, 530
 - phonon density of states, 357
 - phonon dispersion relation, 367
 - quantum Hall effect, 780
 - reconstruction of (111) surface, 89
 - theoretical strength, 381
- Si:P;metal-insulator transition, 532–534
- SiC
 - spiral growth on, 385
- Siedentop, H., 263
- Siegbahn, K., 74
- Siegel, R. W., 608
- Siegert relation, 69, 129
- Sienko, M. J., 534, 565
- SiGe
 - thermoelectric, 498
- Sigrist, M., 838, 893
- silicon
 - amorphous, 120
- Simon, R., 893
- simple cubic, *see* lattices
- Singh, J., 657
- single electron model, 157
- single mode approximation, 440
- single-electron model, 155–173, 266
- singlet, 798
- singular continuous spectrum, 137
- Singwi, K. S., 838
- SiO₂, 119
- Sivia, D. S., 838
- Sivola, E., 521
- skin depth, 693
- Skriver, H., xxii
- Slack, G. A., 363, 378
- Slater determinant, 236
- Slater type orbitals, *N* Gaussians, 240
- Slater, J. C., 235, 257, 264, 265, 271, 291, 292
- Slater–Koster parameters, 271
- Sleight, A. W., 893
- Slichter, C. P., 758
- Slick, P. I., 732, 758
- slip plane, 383, 424
- Slonczewski, J. C., 838
- Slonczewski, J. C., 816
- Smalley, R. E., 143, 151, 565
- smectics, 121
- Smit, J., 521
- Smith, E. N., 449
- Smith, H. I., 608
- Smith, J. L., 837
- Smith, J. R., 318
- Smith, N. V., 719, 720
- Smith, R. J., 720
- Smoluchowski, R., 201, 206
- Sn
 - flux quantization, 852
 - gray, 283
 - superconducting weak link, 854
 - white, 283
- soap cells, **145**
- sodium chloride, *see* NaCl
 - table of similar compounds, 25
- Sohncke, L., 17, 41
- Sokolnikoff, I. S., 339
- solar cells, 645
- Solovij, J. P., 263
- Sommerfeld expansion, 166–171, **172**
- Sommerfeld parameter, 170, 360
 - table for selected metals, 171

- Sommerfeld, A., 173, 893
 Bohr–Sommerfeld quantization, 471
 Sommerfeld expansion, 166
 superconductivity, 839
 X-ray scattering, 43
- Sondhi, S. L., 795
- Song, K., 94
- Sonin, E. B., 449
- Sood, A. K., 410
- Sordi, G., 831, 838
- sound waves, 331, **337**
 Bose gas, 447
 first sound, 432
 second sound, 431–434
 zero sound, 514–516, **520**
- Souza, I, 521
- space group, 12
- Spaepen, F., 150, 151
- spaghetti diagrams, 279
- sparks, 233
- specific heat
 critical behavior in ferromagnetic salts, 747
 effective mass, 170
 Fermi liquid theory, 510
 free electrons, 168
 magnetic phase transition, 731
 near phase transition, 746
 noninteracting electrons, 163
 paradox, 156
 phonons, 354
 relative contributions of electrons and phonons, 170, 360
 table for selected metals at low temperatures, 171
- Spence, J. C. H., 91, 94, 319
- sphere
 fluid flow around, 416
- spherical harmonics, 268
- Spicer, W. E., 711, 720
- spin glasses, 743
- spin valve, 815
- spin waves, 805–811, **833**
 antiferromagnets, 808–811
 bound states, 808
 dispersion relations, 808, 811
- spin–orbit coupling, 218, 281, 763
- spinodal decomposition, 108
- spintronics, 469
- spontaneous emission, 648
- spontaneous magnetization, 730, 733, 745
- spontaneous symmetry breaking, 736
- square lattice, *see* lattices
- SQUID, *see* superconductivity, superconducting quantum interference device
- Sr
 Fermi surface, 281
- Sreenivasan, K. R., 449
- Srinivasan, R., 378
- Störzer, M., 566
- stability of matter, 249–252
- stacking fault, 81
- stacking period, 79
- Stajic, J., 891
- Stampanomi, M., 837
- Starace, A. F., 719
- Starks, D. R., 448
- static structure factor, 67
- Stearns, M. B., 838
- steel, 424
- steepest descents, 361, 465, 906
- Steinfink, H., 58
- Steinhardt, P. J., 134, 150
- Steno, N., 3, 16
- Stephen, M. J., 151
- Stern, F., 794
- Stewart, G. R., 171, 173, 360, 378
- Stewart, K. H., 758
- Stiles, M. D., 837
- Stillinger, F. H., 319
- stimulated emission, 646
- STM, *see* scanning tunneling microscopy
- Störmer, H. L., 786, 795
- Stokes drag, 420
- Stokes flow, **444**
- Stokes scattering, 702
- Stokes shift, 677, 682
- Stokes, G. G., 449
- Stolovitzky, G., 449
- Stone, J. L., 657
- Stoner model, 811–813
 Fermi liquid theory, **833**
- Stoner, E. C., 812, 838
- Stoney, G. J., 567
- STONG, *see* Slater type orbitals, *N* Gaussians
- storage modulus, 423
- Stout, G. H., 75
- strain invariants, 324
- strain tensor, 37
- Straley, J. P., 151, 837
- Strandburg, K. J., 410
- Straub, D., 709, 710, 720
- Strauser, W. A., 74
- Streda, P., 781, 795
- Streetman, B. G., 608
- strength

- ideal, 402
 - practical, 380, 381
- stress intensity factor, 405, **406**
- stress invariants, 424
- stress tensor
 - for ideal fluid, 414
 - for polymeric solution, 418–419
 - for solids, 326
 - for viscous fluids, 415
 - physical interpretation in fluids, 414
 - physical interpretation in solids, 329
 - plastic flow, 424
- Stroud, D., 339, 565
- structure factors
 - for ^4He , 442
 - inelastic, 369, 525
 - liquid and amorphous nickel, 115
 - liquid and crystalline sulphur, 115
 - liquid and crystalline water, 115
 - static, 67
 - weak scattering conductivity, 527, 528
- Stuckes, A. D., 521
- Stumpf, R., *xxii*, 291, 319
- Sturge, M. D., 640, 657
- Su, W. P., 686
- sublattices, 742
- substitutional alloy, 102
- Suematsu, Y., 657
- Suhl, H., 837
- sum rules, 621–623
- sums
 - arising in scattering from lattices, 897–900
 - converting to integrals, 160
- Sundaram, G., 466, 481
- superconductivity, 839–888
 - Abrikosov lattice, 850
 - AC Josephson effect, 853
 - Bardeen–Cooper–Schrieffer model, 865–872, **889**
 - Bogoliubov equations, 873–879
 - Bogoliubov transformation, 870
 - boundary conditions, 841, 845
 - coherence length, 845, 847, 878, 883
 - Cooper pair, 863, 869
 - Cooper problem, 863–865
 - critical temperature, 881
 - d*-wave, 885–887
 - d*-wave experiment, 887
 - DC Josephson effect, 853
 - density of states, 881
 - diamagnetism, 840
 - dielectric function, 862
 - effective charge, 850–851
 - effective electron interaction, 862
 - electron–ion interaction, 859–862
 - entropy, 844
 - excitation energy sketch, 872
 - Fermi function sketch, 872
 - flux penetration, 848
 - flux quantization, 850–851
 - flux quantization experiment, 852
 - Fraunhofer diffraction experiment, 854, 887
 - gap equation, 868, 872
 - gap function, 867, 878
 - gauge invariance, 841, 843, 850, 853, 857, 876, 885, 886, **889**
 - gauge symmetry breaking, 857
 - high-temperature, 881–888
 - high-temperature superconductor phase diagram, 882–885
 - isotope effect, 858, 859
 - Josephson effect, 852–858, **889**
 - Josephson junction, 853, 854, **888**
 - Josephson junction circuits, 854–856
 - Lagrangian, 857–858
 - Landau–Ginzburg equations, 844–851
 - last word on high T_c , 887
 - latent heat, 844
 - London equation, 879
 - London gauge, 876, **889**
 - macroscopic wave function, 844, 852
 - McMillan theory, 881
 - mean field theory, 869
 - Meissner effect, 839, 841, 843, 876–879, **889**
 - occupation number sketch, 872
 - order parameter, 885–887
 - pairing instability, 865
 - penetration depth, 840, 848
 - persistent currents, 839
 - phenomenological free energy, 841–843
 - photoemission, 887
 - pseudogap, 885
 - resistively shunted junction model, 854
 - s*-wave, 885–887
 - specific heat experiment, 880
 - spin relaxation experiment, 880
 - superconducting quantum interference device, 855–856
 - surface energy, 848–850, **888**
 - table of critical temperatures and fields, 846
 - table of energy gaps and specific heats, 873
 - thermodynamics, 843–844, 869–872
 - type I, 848

- type II, 848, 883
- vortices, 850
- washboard potential, 855
- weak link, 852
- superexchange, 804
- superfluids, 427–443
- superlattices, 103–104
 - alloy phase transformations, 740–743
 - magnetic, 815
 - surfaces, 79, **91**
- surface energy, 80
- surface sound waves, **337**
- surface states
 - semiconductors, 586–587
- surfaces
 - Coulomb energy of, 303
 - experimental techniques, 82–91
 - geometrical description, 77–81
 - growth from spiral dislocation, 384
 - reconstruction, 77
- Sutton, A. P., 307, 319, 566
- Suzuki, M., 893
- Svensson, E. C., 442, 449
- Swinney, H. L., 70, 449
- symmetry
 - discrete rotational, 192
 - discrete translational, 175
 - icosahedral, 142
 - impossibility of five-fold, **15**, 36
 - phonons, 348
 - possibility of fivefold, 141
 - transport equations, 490–492
- symmorphic, 36
- synchrotron, 62, 704, 710
- Szabo, A., 264
- Sze, S. M., 481, 608, 656
- table
 - alkali halide cohesive energies, 305
 - alkali halide electron affinities and ionization potentials, 302
 - anomalous Hall effect, 504
 - bond dipole moments of selected molecules, 242
 - bond lengths of selected molecules, 242
 - calculated magnetic moments, 814
 - cesium chloride compounds, 26
 - cohesive energy parameterized for selected elements, 314
 - critical exponents, 750
 - critical temperatures and fields of superconducting materials, 846
 - crystal structure of elements, 19
 - Debye temperatures, 360
 - diamagnetic susceptibilities, 728
 - dielectric properties of ionic crystals, 670
 - effective radii of elements, 298
 - elastic constants of cubic crystals, 327
 - elastic moduli for isotropic materials, 331
 - energies of atoms, Hartree–Fock versus local density approximation, 257
 - F center absorption and emission peaks, 677
 - failure under tension, 381
 - Fermi liquid parameters of ^3He , 515
 - ferromagnets and antiferromagnets, magnetic ordering, 732
 - fluorite structures, 27
 - free-electron parameters for selected metals, 167
 - ionization potentials of selected molecules, 242
 - lattice sums for noble gases, 301
 - Lennard-Jones parameters, 300
 - low-temperature specific heats of metals, 171
 - Madelung constant for metals, 307
 - Madelung constants for ionic crystals, 304
 - magnetic susceptibilities of metals, 775
 - mean free path in liquid metals, 526
 - metallic densities from pseudopotentials, 308
 - noble gas magnetic susceptibilities, 769
 - perovskite structures, 29
 - plastic flow onset under shear, 380
 - polarization, 662
 - radiation scattering, 61
 - rare earth magnetic moments, 768
 - reciprocal lattices, 52
 - semiconductor impurity binding energies, 580
 - semiconductor properties, 577
 - sodium chloride structures, 25
 - superconducting energy gap and specific heat, 873
 - thermoelectric data, 499
 - transition metal magnetic moments, 768
 - vacancy energies, 676
 - viscosity of selected fluids, 416
 - work functions of selected compounds, 705
 - wurtzite structures, 28
 - zincblende structures, 28
- Takahashi, T., 887, 891
- Takhtajan, L. A., 836
- Tan, S., 891
- Tanabe, Y., 720
- Tanaka, M., 893

- Tasset, F., 893
 Tauer, K. J., 757
 Taylor, G. I., 381, 411
 Taylor, R. E., 378
 Teichmann, J., 41
 Tesanovic, Z., 893
 tessellation, 10
 Testardi, L. R., 893
 Teukolsky, S. A., 902
 thermal conductivity, 363, 496, **517**
 Drude model, 454
 thermal expansion, 361–363
 thermal fluctuations, 529
 thermal neutrons, 63
 thermionic emission, 571, 585
 thermoelectric figure of merit, 498, **517**
 thermoelectric phenomena, 492–504
 table, 499
 thermopower, 497–498, **606**
 Thèye, M. L., 701, 720
 Thole, B. T., 74
 Thomas, G. A., 656
 Thomas–Fermi theory, 247–249, **259, 260**
 Thomas–Fermi–Dirac theory, 248
 Thomson effect, 498, **518**
 Thomson, J. J., *xxiii*, 3, 16, 156, 168, 173, 453,
 481, 567, 611, 631
 Thomson, R., 400, 405, 409, 411
 Thorne, R. E., 311, 319
 Thornton, S. T., 12, 16
 Thouless, D. J., 392, 410
 three-body potentials, 314
 tight binding
 graphene band structure, **229**
 tight binding model, 207
 tight-binding method, **478**, 535–551
 Fermi surfaces, 476
 tight-binding model, 219, 226, **230**, 317, 420,
 456, **561**, 777, 810
 tightly bound electrons, 219–227
 tiling, 10
 Tilley, D. R., 449
 Tilley, J., 449
 tilt boundary, 81
 Timoshenko, S., 339
 Tinkham, M., 16, 193, 206, 893
 t - J model, **835**
 Tjeng, H., 719
 $Tl_2Ba_2CuO_{6+x}$, 884
 Tl2201, *see* $Tl_2Ba_2CuO_{6+x}$
 Tolstov, G. P., 206
 Tomonaga, S., 553, 566
 Tong, B. Y., 264
 Tonks, L., 264
 Tonomura, A., 776, 777, 795, 850, 893
 Torng, C. J., 893
 Tortonese, M., 90
 Tosi, M. P., 92, 95, 298, 319, 838
 Touloukian, Y. S., 355, 359, 363, 378
 Townes, C. H., 646, 657
 Toyozawa, Y., 657
 transfer matrix, **561, 563, 778**
 transistor, 595–598
 transition metals
 band structure, 284
 Fermi surfaces, 476
 ferromagnetism, 731, 736, 811–815
 Friedel model for cohesive energy, **317**
 magnetic structure in oxides, 733
 oxides, 711
 table of magnetic moments, 768
 translation group, 12
 translation operators, 182
 transverse light waves, 616, 667, 693
 transverse phonon mode, 348, 702
 transverse sound waves, 331
 Treger, D. M., 838
 Treloar, L. R. G., 324, 339
 Tremblay, A.-M. S., 831, 838
 trial wave function
 for fractional quantum Hall effect, 788
 for tightly bound electrons, 220
 triangular lattice, *see* lattices, **376**
 Triantafyllopoulos, 75, 151
 triaxial test, 335
 Trigg, G., 150
 triode, 568
 triplet, 798
 Tsong, T. T., 85, 95
 Tsuda, K., 893
 Tsui, D. C., 786, 795
 Tsunetsugu, H., 838
 tungsten anode, 56
 twin boundary, 81
 twinning, 312
 two-body potentials, 314
 two-dimensional electron gas, 599–605, 780,
 785
 two-fluid hydrodynamics, 430–434
 two-fluid model, 428
 two-particle correlation function, 66

 UBe_{13} , 828, 829
 Ueda, K., 838, 893
 Ueta, M., 644, 657
 Umklapp, 527
 unit cell, *see also* Wigner–Seitz cell
 conventional, 20

- nonprimitive, 11
- primitive, 9
- units
 - SI versus cgs, 724
- universality classes, 744, 750
- UPS, *see* photoemission, ultraviolet photoemission spectroscopy
- UPt₃, 828
- Urbach tails, 683, **685**
- Urbach, F., 687
- V (vanadium)
 - band structure, 285
 - superconducting specific heat, 880
- vacancies, 424, 530, 675
 - table of energies, 676
- vacuum tubes, 569
- Vainshtein, B. K., 36, 41, 75
- Valatin, J. G., 870, 893
- Vamanu, D., 757
- van Alphen, P. M., 473
- van Dam, H., 838
- Van Dau, F., 836
- van den Berg, G. J., 836
- van der Laan, G., 715, 720
- van der Marel, D., 608
- van der Waals interaction, 299, **316**, 427
- van der Waerden, B. L., 378, 657
- van Elp, J., 719
- van Harlingen, D. J., 893
- van Houten, H., 601, 608
- van Hove correlation function, 66
- van Hove singularities, 186–188, 281–285, 356, 638, 639
- Van Hove, L., 75
- van Kármán, T., 341
- van Leeuwen's theorem, 759
- van Leeuwen, H.-J., 759, 795
- van Vleck paramagnetism, 769
- van Vleck, J. H., 758, 759, 768, 795
- van Wees, B. J., 600, 608
- Vanderbilt, D., 686
- Vanderbilt, D., 74, 232, 318, 521
- Vanderkooy, J., 481
- variational Monte Carlo, 253
- variational principles, 210, 235, **260**, 866, 904–906
- Varma, C. M., 885, 893
- VASP, 281
- Vaterlaus, A., 837
- Vedernikov, M. V., 520
- Vega, C., 151
- Venkatasubramanian, R., 521
- Verlet algorithm, 112, **143**
- Verlet, L., 112, 151
- Vespignani, A., 94
- Vetterling, W. T., 902
- Vettier, C., 893
- Vicentini-Missoni, M., 750, 754, 758
- Vinen, W. F., 438, 449
- Vinokur, V. M., 890
- virial expansion, 126
- viscosity, **443**
 - due to polymers, 422
 - dynamic, 415
 - table for selected fluids, 416
- V_K center, 679
- VO
 - insulator, 711
- Vogel–Fulcher law, 117
- Vogtenhuber, D., 687
- Vollhardt, D., 521
- Volovik, G. E., 449
- volume expansion coefficient, 363
- von Klitzing constant, 780
- von Klitzing, K., 780, 795
- von Laue, M., 43, 74, 341
- von Meyenn, K., 292
- von Molnár, S., 838
- von Neumann's law, **145**
- von Neumann, J., 146
- vortices, **445**
 - classical, 438
 - in ⁴He, 437–439
 - in superconductors, 849, 850
 - quantized, 438, 850–851
- Vugmeister, B. E., 687
- vulcanized rubber, 322
- Vuorio, M., 837
- W (tungsten)
 - Fermi surface, 476
- Wachs, A. L., 709, 720
- Wagner, H., 391, 410
- Wahl, R., 687
- Walecka, J. D., 628, 631
- Wallis, R. F., 377, 378
- Wang, X., 521
- Wang, Y. Q., 893
- Wanklyn, B. M., 835
- Wannier functions, 222, **230**, **231**, **654**, 803
 - ambiguity, 223
 - Peierls substitution, **792**
 - polarization, 661
- Wannier, G. H., 232
 - Mott–Wannier excitons, 641
 - Wannier functions, 207
 - Wannier–Stark ladders, 472

- Wannier–Stark ladders, 472
 Want, J., 94
 Warren, J. L., 378
 Waseda, Y., 115, 151
 washboard potential, 855
 Washburn, S., 566
 water, 115
 wave function for correlated electrons
 ⁴He, 435
 fractional quantum Hall effect, 788
 superconductivity, 866
 wave number, 179
 wave packets, 185, 465–469, **479**
 sketch, 466
 wave vector, 182
 Weaire, D., 146, 151, 291, 318, 608
 weak disorder, 547
 weak localization, **563**
 Weart, S., 41
 Weaver, J. H., 151, 608
 Webb, M. B., 82, 95
 Webb, R. A., 566
 Weber, T. A., 319
 Wei, S., 367, 378
 Weinberg, S., 841, 893
 Weiss, G. H., 378
 Weiss, P., 734, 758
 Weiss, R. J., 757
 Weisskopf, V. F., 292
 Weissman, M. B., 758
 Weitering, H., 521
 Weitz, D. A., 132, 151
 Wen, X., 892
 Wentzel–Kramers–Brillouin approximation,
 86, 462
 Wertheim, N. R., 845, 893
 Westerink, J., 719
 Westra, C., 720
 wetting, 81
 Wheatley, J. C., 443, 449, 520
 Wick’s theorem, 69, 130, 370
 Widom, B., 750, 758
 Wiedemann, G., 455, 481, 496
 Wiedemann–Franz law, 455, 496
 Wiegmann, P. B., 820, 838
 Wigner crystal, 255
 Wigner, E., 206, 255, 264, 292, 411
 Breit–Wigner factor, 375
 first band structure calculation, 265
 group notation, 201
 key and glass, 379
 Wigner crystals, 255
 Wigner–Seitz cell, 10
 Wigner–Eckart theorem, 764
 Wigner–Seitz cell, 8, 11, 159
 fcc lattice, 21
 Wigner–Seitz radius, 312
 Wilczek, F., 850, 893
 Wilde, G., 117, 151
 Wilkinson, S. R., 472
 Wilks, J., 449
 Willardson, R. K., 657
 Williams, E. J., 104, 149, 742, 757
 Williams, G. P., 710, 720
 Williamson, J. G., 608
 Willis, R. F., 837
 Wilson, A. H., 277, 292, 521, 819, 838
 Wilson, K. G., 744, 758, 820, 838
 Winter, R., 151
 Witten, T. A., 93, 95, 151
 WKB approximation, *see*
 Wentzel–Kramers–Brillouin
 approximation
 Wohlfarth, E. P., 758
 Wolf, D., 95
 Wolf, E. L., 86, 95
 Wolf, H. C., 687
 Wolf, S. A., 838
 Wolfe, J. P., 657
 Wolff, P. A., 698, 720
 Wolkow, R., 89, 95
 Wollan, E. O., 74
 Wollman, D. A., 893
 Won, H., 893
 Wong, K. C., 480
 Wong, K. W., 719
 Woods, A. D. B., 449
 Wooten, F., 151
 work functions, 569–570
 optical measurements, 703–706
 scanning tunneling microscopy, 86
 table of values, 705
 versus chemical potential, 569
 work hardening, 425
 Wortis, M., 94, 838
 equilibrium crystals, 92
 magnon bound states, 808
 Wright, D. C., 151
 Wright, W. H., 893
 Wu, D. T., 108, 151
 Wu, F., 829, 837
 Wu, M. K., 893
 wurtzite, *see* ZnO
 Wyckoff, R. W. G., 19, 25–29, 37, 41, 66, 75,
 319
 X-rays
 coloration of NaCl, 674

- first scattering experiment, 44
- inelastic scattering, 702, 703
- interaction with matter, 60
- photoemission, 710
- production of, 56, 61
- scattering from superlattices, 104
- synchrotron, 62
- Xiao, D., 521
- Xing, X., 339
- XPS, *see* photoemission, X-ray photoemission spectroscopy
- Xu, Y., 719

- Y_2O_3
 - thermoelectric, 498
- YAG, yttrium aluminum garnet, 650
- Yaglom, A. M., 449
- Yamada, H., 795, 893
- Yamada, K., 893
- Yang, W., 263
- Yang, W. T., 263
- Yano, S., 795, 893
- Yao, Y., 521
- Yarnell, J. L., 365, 378
- Yates, J. R., 521
- YBCO, *see* $YBa_2Cu_3O_{6+x}$
- $YBa_2Cu_3O_{6+x}$, 882
- Yennie, D. R., 795
- Yeomans, J., 838
- Yeshurun, Y., 894
- Yethiraj, M., 811, 838
- yield stress, 424
- Yip, S., 95
- Yokoya, T., 881, 887, 891, 894
- Yonezawa, F., 117, 151
- Yoon, C. O., 566
- Young's modulus, 330, **337**
- Young, A. P., 392, 411, 757
- Young, R. A., 73
- Yu, C. C., 836
- Yu, E. T., 608
- Yu, P. Y., 580, 598, 608, 621, 631
- Yue, W., 263
- Yuval, G., 835

- Zachariasen, W. H., 119, 151
- Zak, J., 481
- Zaleski, S., 151
- Zalkin, A., 73
- Zallen, R., 152
- Zangwill, A., 81, 95, 574, 608
- Zeidler, E., 903, 906
- Zeiger, H. J., 656, 657
- Zener tunneling, 462–465
- Zener, C., 465, 481
- Zeng, C., 521
- zero point energy, 427
- zero sound, 514–516, **520**
 - attenuation, 516
 - measured in 3He , 516
- Zhang, Y., 150
- Zhao, Q., 258
- Zhao, Y., 224, 232
- Zhe, Z., 892
- Zheludev, I. S., 687
- Zhu, J. G., 757
- Ziman, J. M., *xxii*, 152, 292, 521, 526, 542, 566
- Zimm model, 419
- Zimm, B. H., 419, 420, 449
- Zimmerman, W., 448
- zinc oxide, *see* ZnO
- zinc sulfide, *see* ZnS
- zincblende, *see* ZnS
- Zinn, W., 836
- Zn
 - band structure energy, 311, **315**
 - Fermi surface, 281
- ZnO
 - insulator, 711
 - structure, 28
 - table of similar compounds, 28
- ZnS
 - structure, 27
 - table of similar compounds, 28
- Zok, F. W., 410
- zone refining, 102
- Zunger, A., 258, 263, 566
- Zuo, J. M., 319
- Žutić, 837

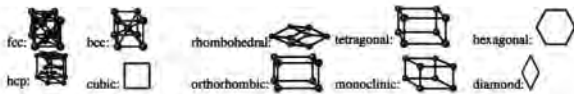
Atomic name
 Atomic number and symbol
 Ground state electron configuration
 Melting temperature in K
 Crystal structure, either at 293 K, or at melting if liquid at 293 K

SILICON
 14 Si $u=28.09$
 $n=4.99$
 $[\text{Ne}]3s^2 3p^3$
 $T=1683$ $\rho=1 \cdot 10^3$
 $a=5.43$

Atomic weight ($^{12}\text{C}=12$)
 Density in 10^{22} atoms cm^{-3} , at 293K or at melting
 Electrical resistivity in $\mu\Omega \cdot \text{cm}$ at 298 K
 Lattice parameters

Alkali Metals

Ia	IIa	Metal	Insulator	Semiconductor	Semi-metal				
LITHIUM 3 Li $u=6.94$ $1s^2 2s^1$ $n=4.63$ $T=454$ $\rho=8.55$ $a=4.38$	BERYLLIUM 4 Be $u=9.01$ $1s^2 2s^2$ $n=12.36$ $T=1551$ $\rho=4.0$ $a=2.29$ $c=3.58$								
SODIUM 11 Na $u=22.99$ $n=2.54$ $[\text{Ne}]3s^1$ $T=371$ $\rho=4.2$ $a=3.77$ $c=6.15$	MAGNESIUM 12 Mg $u=24.31$ $n=4.31$ $[\text{Ne}]3s^2$ $T=922$ $\rho=4.45$ $a=3.21$ $c=5.21$								
POTASSIUM 19 K $u=39.10$ $n=1.33$ $[\text{Ar}]4s^1$ $T=337$ $\rho=6.15$ $a=5.33$	CALCIUM 20 Ca $u=40.08$ $n=2.33$ $[\text{Ar}]4s^2$ $T=1112$ $\rho=3.43$ $a=5.59$								
RUBIDIUM 37 Rb $u=85.47$ $n=1.08$ $[\text{Kr}]5s^1$ $T=312$ $\rho=12.5$ $a=5.62$	STRONTIUM 38 Sr $u=87.62$ $n=1.75$ $[\text{Kr}]5s^2$ $T=1042$ $\rho=23.0$ $a=6.08$								
CESIUM 55 Cs $u=132.91$ $n=0.85$ $[\text{Xe}]6s^1$ $T=302$ $\rho=20.0$ $a=6.14$	BARIUM 56 Ba $u=137.33$ $n=1.57$ $[\text{Xe}]6s^2$ $T=1002$ $\rho=50$ $a=5.03$								
FRANCIUM 87 Fr $u\approx 223$ $n=?$ $[\text{Rn}]7s^1$ $T=300$ $\rho=?$	RADIUM 88 Ra $u=226.03$ $n=1.33$ $[\text{Rn}]7s^2$ $T=973$ $\rho=100$ $a=5.15$								
		Transition Metals							
		IIIb	IVb	Vb	VIb	VIIb	VIIIb		
		SCANDIUM 21 Sc $u=44.96$ $n=4.00$ $[\text{Ar}]3d^1 4s^2$ $T=1814$ $\rho=61.0$ $a=3.31$ $c=5.27$	TITANIUM 22 Ti $u=47.88$ $n=5.70$ $[\text{Ar}]3d^2 4s^2$ $T=1933$ $\rho=42.0$ $a=2.95$ $c=4.68$	VANADIUM 23 V $u=50.94$ $n=7.22$ $[\text{Ar}]3d^3 4s^2$ $T=2160$ $\rho=24.8$ $a=3.02$	CHROMIUM 24 Cr $u=52.00$ $n=8.32$ $[\text{Ar}]3d^5 4s^1$ $T=2130$ $\rho=12.7$ $a=2.88$	MANGANESE 25 Mn $u=54.94$ $n=8.15$ $[\text{Ar}]3d^5 4s^2$ $T=1517$ $\rho=185.0$ $a=8.91$	IRON 26 Fe $u=55.85$ $n=8.48$ $[\text{Ar}]3d^6 4s^2$ $T=1808$ $\rho=9.71$ $a=2.87$	COBALT 27 Co $u=58.93$ $n=9.09$ $[\text{Ar}]3d^7 4s^2$ $T=1768$ $\rho=6.24$ $a=3.54$	NICKEL 28 Ni $u=58.69$ $n=9.13$ $[\text{Ar}]3d^8 4s^2$ $T=1726$ $\rho=6.84$ $a=3.52$
		YTTORIUM 39 Y $u=88.91$ $n=3.03$ $[\text{Kr}]4d^1 5s^2$ $T=1795$ $\rho=57.0$ $a=3.65$ $c=5.73$	ZIRCONIUM 40 Zr $u=91.22$ $n=4.30$ $[\text{Kr}]4d^2 5s^2$ $T=2125$ $\rho=42.1$ $a=3.23$ $c=5.15$	NIObIUM 41 Nb $u=92.91$ $n=5.55$ $[\text{Kr}]4d^4 5s^1$ $T=2741$ $\rho=12.5$ $a=3.30$	MOLYBDENUM 42 Mo $u=95.94$ $n=6.41$ $[\text{Kr}]4d^5 5s^1$ $T=2890$ $\rho=5.2$ $a=3.15$	TECHNETIUM 43 Tc $u=98.91$ $n=7.00$ $[\text{Kr}]4d^5 5s^2$ $T=2445$ $\rho=22.6$ $a=2.74$ $c=4.40$	RUTHENIUM 44 Ru $u=101.07$ $n=7.37$ $[\text{Kr}]4d^7 5s^1$ $T=2583$ $\rho=7.6$ $a=2.71$ $c=4.28$	RHODIUM 45 Rh $u=102.91$ $n=7.26$ $[\text{Kr}]4d^8 5s^1$ $T=2239$ $\rho=4.51$ $a=3.80$	PALLADIUM 46 Pd $u=106.42$ $n=6.80$ $[\text{Kr}]4d^10 5s^0$ $T=1825$ $\rho=10.8$ $a=3.89$
		LUTETIUM 71 Lu $u=174.97$ $n=43.39$ $[\text{Xe}]4f^{14} 5d^1 6s^2$ $T=1936$ $\rho=79.0$ $a=3.50$ $c=5.55$	HAFNIUM 72 Hf $u=178.49$ $n=4.49$ $[\text{Xe}]4f^{14} 5d^2 6s^2$ $T=2503$ $\rho=35.1$ $a=3.19$ $c=5.05$	TANTALUM 73 Ta $u=180.95$ $n=5.54$ $[\text{Xe}]4f^{14} 5d^3 6s^2$ $T=3269$ $\rho=12.45$ $a=3.30$	TUNGSTEN (WOLFRAM) 74 W $u=183.85$ $n=6.32$ $[\text{Xe}]4f^{14} 5d^4 6s^2$ $T=3680$ $\rho=5.65$ $a=3.17$	RHENIUM 75 Re $u=186.20$ $n=6.80$ $[\text{Xe}]4f^{14} 5d^5 6s^2$ $T=3453$ $\rho=19.3$ $a=2.76$ $c=4.46$	OSMIUM 76 Os $u=190.2$ $n=7.15$ $[\text{Xe}]4f^{14} 5d^6 6s^2$ $T=3327$ $\rho=8.12$ $a=2.73$ $c=4.32$	IRIDIUM 77 Ir $u=192.22$ $n=7.07$ $[\text{Xe}]4f^{14} 5d^7 6s^2$ $T=2683$ $\rho=5.3$ $a=3.84$	PLATINUM 78 Pt $u=195.08$ $n=6.62$ $[\text{Xe}]4f^{14} 5d^9 6s^1$ $T=2045$ $\rho=10.6$ $a=3.92$
		LAWRENCIUM 103 Lr $u\approx 260$ $n=?$ $[\text{Rn}]5f^{14} 6d^1 7s^2$ $T=?$ $\rho=?$	RUTHERFORDIUM 104 Rf	DUBNIUM 105 Db	SEABORGIUM 106 Sg	BOHRNIUM 107 Bh	HASSIUM 108 Hs	MEITNERIUM 109 Mt	
		LANTHANIDES [Rare Earths]	CERIUM 58 Ce $u=140.12$ $n=3.54$ $[\text{Xe}]4f^1 5d^0 6s^2$ $T=1194$ $\rho=57$ $a=3.77$ $c=1.22$	PRASEODYMIUM 59 Pr $u=140.91$ $n=2.89$ $[\text{Xe}]4f^2 5d^0 6s^2$ $T=1204$ $\rho=68$ $a=3.67$ $c=1.83$	NEODYMIUM 60 Nd $u=144.24$ $n=2.93$ $[\text{Xe}]4f^3 5d^0 6s^2$ $T=1294$ $\rho=64.0$ $a=3.66$ $c=1.80$	PROMETHIUM 61 Pm $u\approx 145$ $n=3.00$ $[\text{Xe}]4f^4 5d^0 6s^2$ $T=1441$ $\rho\approx 50$ $a=?$	SAMARIUM 62 Sm $u=150.36$ $n=3.01$ $[\text{Xe}]4f^5 5d^0 6s^2$ $T=1350$ $\rho=94.0$ $a=9.00$ $c=23^\circ 13'$	EUROPIUM 63 Eu $u=151.97$ $n=2.08$ $[\text{Xe}]4f^6 5d^0 6s^2$ $T=1095$ $\rho=90.0$ $a=4.58$	
		ACTINIDES	ACTINIUM 89 Ac $u=227.03$ $n=2.67$ $[\text{Rn}]6d^1 7s^2$ $T=1320$ $\rho=?$ $a=5.31$	THORIUM 90 Th $u=232.04$ $n=3.04$ $[\text{Rn}]5f^0 6d^2 7s^2$ $T=2023$ $\rho=13.0$ $a=5.08$	PROTACTINIUM 91 Pa $u=231.04$ $n=4.34$ $[\text{Rn}]5f^2 6d^1 7s^2$ $T=2113$ $\rho=17.7$ $a=3.93$ $c=3.24$	URANIUM 92 U $u=238.03$ $n=4.79$ $[\text{Rn}]5f^3 6d^1 7s^2$ $T=1406$ $\rho=30.8$ $a=2.85$ $b=5.86$ $c=4.95$	NEPTUNIUM 93 Np $u=237.05$ $n=5.14$ $[\text{Rn}]5f^4 6d^1 7s^2$ $T=913$ $\rho=122$ $a=4.72$ $b=4.89$ $c=6.66$	PLUTONIUM 94 Pu $u\approx 244$ $n=4.89$ $[\text{Rn}]5f^6 6d^1 7s^2$ $T=914$ $\rho=146$ $a=4.82$ $b=10.96$ $c=101^\circ 48'$	AMERICIUM 95 Am $u\approx 243$ $n\approx 3.39$ $[\text{Rn}]5f^7 6d^0 7s^2$ $T=1267$ $\rho=68$ $a=3.47$ $c=11.24$



HYDROGEN 1 H $u=1.008$ $n=4.34$ l^1 $T=14.01$ $\rho=?$ $a=3.77$ $c=6.16$	HELIUM 2 He $u=4.003$ $n=3.11$ l^2 At 2 K, 26 atm $a=3.53$ $c=4.24$
--	---

Halogens
Noble Gases

Noble metals

1b 11b

IIIa		IVa		Va		VIa		VIIa		VIIIa	
BORON 5 B $u=10.81$ $n=13.03$ $l^2 2^2 2^2 p^1$ $T=2573$ $\rho=1.8 \cdot 10^{12}$ $a=8.74$ $c=5.06$	CARBON 6 C $u=12.01$ $n=17.59$ $l^2 2^2 2^2 p^2$ $T=3820$ $\rho=10^{18}$ $a=3.57$	NITROGEN 7 N $u=14.01$ $n=4.43$ $l^2 2^2 2^2 p^3$ $T=63.29$ $\rho=?$ $a=5.64$	OXYGEN 8 O $u=16.00$ $n=7.53$ $l^2 2^2 2^2 p^4$ $T=54.8$ $\rho=?$ $a=6.83$	FLUORINE 9 F $u=19.00$ $n=?$ $l^2 2^2 2^2 p^5$ $T=53.5$ $\rho=?$ $a=6.67$	NEON 10 Ne $u=20.18$ $n=4.30$ $l^2 2^2 2^2 p^6$ $T=24.5$ $\rho=?$ $a=4.45$						
ALUMINUM 13 Al $u=26.98$ $n=6.02$ $[Ne]3s^2 3p^1$ $T=934$ $\rho=2.65$ $a=4.05$	SILICON 14 Si $u=28.09$ $n=4.99$ $[Ne]3s^2 3p^2$ $T=1683$ $\rho=1 \cdot 10^5$ $a=5.43$	PHOSPHORUS 15 P $u=30.97$ $n=3.54$ $[Ne]3s^2 3p^3$ $T=317$ $\rho=1 \cdot 10^{17}$ $a=18.51$	SULFUR 16 S $u=32.07$ $n=3.89$ $[Ne]3s^2 3p^4$ $T=386$ $\rho=2 \cdot 10^{23}$ $a=10.46$ $b=12.87$ $c=24.42$	CHLORINE 17 Cl $u=35.45$ $n=3.45$ $[Ne]3s^2 3p^5$ $T=172$ $\rho=?$ $a=6.24$ $b=4.48$ $c=8.26$	ARGON 18 Ar $u=39.95$ $n=2.50$ $[Ne]3s^2 3p^6$ $T=83.8$ $\rho=?$ $a=5.31$						
COPPER 29 Cu $u=63.55$ $n=8.49$ $[Ar]3d^{10} 4s^1$ $T=1357$ $\rho=1.67$ $a=3.61$	ZINC 30 Zn $u=65.39$ $n=6.36$ $[Ar]3d^{10} 4s^2$ $T=693$ $\rho=5.92$ $a=2.66$ $c=4.95$	GALLIUM 31 Ga $u=69.72$ $n=5.10$ $[Ar]3d^{10} 4s^2 4p^1$ $T=303$ $\rho=27$ $a=4.52$ $b=7.66$ $c=4.53$	GERMANIUM 32 Ge $u=72.61$ $n=6.35$ $[Ar]3d^{10} 4s^2 4p^2$ $T=121$ $\rho=4 \cdot 6 \cdot 10^7$ $a=5.66$	ARSENIC 33 As $u=74.92$ $n=4.64$ $[Ar]3d^{10} 4s^2 4p^3$ $T=1090$ $\rho=26$ $a=4.13$ $b=54^{\circ} 10'$	SELENIUM 34 Se $u=78.96$ $n=3.65$ $[Ar]3d^{10} 4s^2 4p^4$ $T=490$ $\rho=1 \cdot 10^6$ $a=4.37$ $c=4.96$						
SILVER 47 Ag $u=107.87$ $n=5.86$ $[Kr]4d^{10} 5s^1$ $T=1235$ $\rho=1.59$ $a=4.09$	CADMIUM 48 Cd $u=112.41$ $n=4.63$ $[Kr]4d^{10} 5s^2$ $T=594$ $\rho=6.83$ $a=2.98$ $c=5.62$	INDIUM 49 In $u=114.82$ $n=3.83$ $[Kr]4d^{10} 5s^2 5p^1$ $T=429$ $\rho=8.37$ $a=3.23$ $c=4.94$	TIN 50 Sn $u=118.71$ $n=3.71$ $[Kr]4d^{10} 5s^2 5p^2$ $T=505$ $\rho=11.0$ $a=5.83$ $c=3.18$	ANTIMONY 51 Sb $u=121.75$ $n=3.31$ $[Kr]4d^{10} 5s^2 5p^3$ $T=904$ $\rho=39.0$ $a=4.51$ $b=57^{\circ} 7'$	TELEURIUM 52 Te $u=127.60$ $n=2.94$ $[Kr]4d^{10} 5s^2 5p^4$ $T=723$ $\rho=4.36 \cdot 10^3$ $a=4.46$ $c=5.93$						
GOLD 79 Au $u=196.97$ $n=5.90$ $[Xe]4f^{14} 5d^{10} 6s^1$ $T=1338$ $\rho=2.35$ $a=4.08$	MERCURY 80 Hg $u=200.59$ $n=4.07$ $[Xe]4f^{14} 5d^{10} 6s^2$ $T=234$ $\rho=94.1$ $a=2.99$ $\alpha=70^{\circ} 45'$	THALLIUM 81 Tl $u=204.38$ $n=3.49$ $[Xe]4f^{14} 5d^{10} 6s^2 6p^1$ $T=577$ $\rho=18.0$ $a=3.46$ $c=5.53$	LEAD 82 Pb $u=207.2$ $n=3.30$ $[Xe]4f^{14} 5d^{10} 6s^2 6p^2$ $T=601$ $\rho=20.65$ $a=4.95$	BISMUTH 83 Bi $u=208.98$ $n=2.81$ $[Xe]4f^{14} 5d^{10} 6s^2 6p^3$ $T=545$ $\rho=106.8$ $a=4.75$ $b=57^{\circ} 14'$	POLONIUM 84 Po $u=209$ $n=2.68$ $[Xe]4f^{14} 5d^{10} 6s^2 6p^4$ $T=527$ $\rho=140$ $a=3.35$						
IODINE 53 I $u=126.91$ $n=2.34$ $[Kr]4d^{10} 5s^2 5p^5$ $T=387$ $\rho=1.3 \cdot 10^{13}$ $a=7.26$ $b=4.79$ $c=9.78$	XENON 54 Xe $u=131.29$ $n=1.62$ $[Kr]4d^{10} 5s^2 5p^6$ $T=161$ $\rho=?$ $a=6.19$	ASTATINE 85 At $u=210$ $n=?$ $[Xe]4f^{14} 5d^{10} 6s^2 6p^5$ $T=575$ $\rho=?$	RADON 86 Rn $u=222$ $n=?$ $[Xe]4f^{14} 5d^{10} 6s^2 6p^6$ $T=202$ $\rho=?$ $a=?$								

GADOLINIUM 64 Gd $u=157.25$ $n=3.02$ $[Xe]4f^7 5d^1 6s^2$ $T=1586$ $\rho=134$ $a=3.64$	TERBIUM 65 Tb $u=158.93$ $n=3.12$ $[Xe]4f^7 5d^0 6s^2$ $T=1629$ $\rho=114$ $a=3.59$ $b=6.26$ $c=5.72$	DYSPROSIUM 66 Dy $u=162.50$ $n=3.17$ $[Xe]4f^9 5d^0 6s^2$ $T=1685$ $\rho=57.0$ $a=3.59$ $c=5.65$	HOLMIUM 67 Ho $u=164.93$ $n=3.21$ $[Xe]4f^{11} 5d^0 6s^2$ $T=1747$ $\rho=87.0$ $a=3.58$ $c=5.62$	ERBIUM 68 Er $u=167.27$ $n=3.26$ $[Xe]4f^{13} 5d^0 6s^2$ $T=1802$ $\rho=87$ $a=3.56$ $c=5.59$	THULIUM 69 Tm $u=168.93$ $n=3.32$ $[Xe]4f^{15} 5d^0 6s^2$ $T=1818$ $\rho=79.0$ $a=3.54$ $c=5.55$	YTERBIUM 70 Yb $u=173.04$ $n=3.24$ $[Xe]4f^{14} 5d^0 6s^2$ $T=1097$ $\rho=29.0$ $a=5.49$
CURIUM 96 Cm $u=247$ $n=3.24$ $[Rn]5f^7 6d^1 7s^2$ $T=1610$ $\rho=?$	BERKLIUM 97 Bk $u=247$ $n=3.60$ $[Rn]5f^7 6d^0 7s^2$ $T=?$ $\rho=?$	CALIFORNIUM 98 Cf $u=251$ $n=?$ $[Rn]5f^{10} 6d^0 7s^2$ $T=?$ $\rho=?$ $a=?$	EINSTEINIUM 99 Es $u=254$ $n=?$ $[Rn]5f^{11} 6d^0 7s^2$ $T=?$ $\rho=?$	FERMIUM 100 Fm $u=257$ $n=?$ $[Rn]5f^{12} 6d^0 7s^2$ $T=?$ $\rho=?$	MENDELEVIUM 101 Md $u=258$ $n=?$ $[Rn]5f^{13} 6d^0 7s^2$ $T=?$ $\rho=?$	NOBELIUM 102 No $u=259$ $n=?$ $[Rn]5f^{14} 6d^0 7s^2$ $T=?$ $\rho=?$

Fundamental physical constants

Quantity		CGS	SI
Electron charge	e	$4.803\,207 \cdot 10^{-10}$ esu	$1.602\,176 \cdot 10^{-19}$ C
Permittivity of vacuum	ϵ_0		$8.854\,187 \cdot 10^{-12}$ C ² J ⁻¹ m ⁻¹
Speed of light	c	$2.997\,925 \cdot 10^{10}$ cm s ⁻¹	$2.997\,925 \cdot 10^8$ m s ⁻¹
Planck's constant	\hbar	$1.054\,572 \cdot 10^{-27}$ erg s	$1.054\,572 \cdot 10^{-34}$ J s
		$6.582\,118 \cdot 10^{-16}$ eV s	$6.582\,118 \cdot 10^{-16}$ eV s
	h	$6.626\,069 \cdot 10^{-27}$ erg s	$6.626\,069 \cdot 10^{-34}$ J s
		$4.135\,667 \cdot 10^{-15}$ eV s	$4.135\,667 \cdot 10^{-15}$ eV s
Electron mass	m	$9.109\,382 \cdot 10^{-28}$ gm	$9.109\,382 \cdot 10^{-31}$ kg
Neutron mass	m_n	$1.674\,927 \cdot 10^{-24}$ gm	$1.674\,927 \cdot 10^{-27}$ kg
Boltzmann's constant	k_B	$1.380\,650 \cdot 10^{-16}$ erg K ⁻¹	$1.380\,650 \cdot 10^{-23}$ J K ⁻¹
		$8.617\,385 \cdot 10^{-5}$ eV K ⁻¹	$8.617\,385 \cdot 10^{-5}$ eV K ⁻¹
Avogadro's constant	N_A	$6.022\,141 \cdot 10^{23}$ mol ⁻¹	$6.022\,141 \cdot 10^{23}$ mol ⁻¹
Rydberg	R_∞	13.605 692 eV	13.605 692 eV
Bohr radius	a_0	\hbar^2/me^2	$4\pi\epsilon_0\hbar^2/me^2$
		$0.529\,177 \cdot 10^{-8}$ cm	$0.529\,177 \cdot 10^{-10}$ m
Bohr magneton	μ_B	$eh/2mc$	$e\hbar/2m$
		$9.274\,009 \cdot 10^{-21}$ erg G ⁻¹	$9.274\,009 \cdot 10^{-24}$ J T ⁻¹
Fine structure constant	α	$e^2/\hbar c$	$e^2/4\pi\epsilon_0\hbar c$
		$7.297\,353 \cdot 10^{-3}$	$7.297\,353 \cdot 10^{-3}$
Magnetic flux quantum	Φ_0	hc/e	h/e
		$4.135\,667 \cdot 10^{-7}$ G cm ²	$4.135\,667 \cdot 10^{-15}$ T m ²
von Klitzing constant	R_K	h/e^2	h/e^2
		$2.872\,062 \cdot 10^{-8}$ statohm	$2.581\,281 \cdot 10^4$ Ω
Josephson constant	K_J	$2e/h$	$2e/h$
		$1.449\,790 \cdot 10^{17}$ esu erg ⁻¹ s ⁻¹	$4.835\,979 \cdot 10^{14}$ Hz V ⁻¹

Source: P. J. Mohr, B. N. Taylor, and D. B. Newell (2008), CODATA recommended values of the fundamental physical constants: 2006, *Reviews of Modern Physics*, **80** 633–730; see also physics.nist.gov/constants

Various conversion factors

	1 s cm ⁻¹ /statohm		1 statohm/(s cm ⁻¹)
	1 cm erg/esu ²		1 esu ² /(cm erg)
	1 G/(erg cm ⁻¹ esu ⁻¹)		1 erg cm ⁻¹ esu ⁻¹ /G
$8.987\,554 \cdot 10^{11}$	Ω /statohm	$1.112\,650 \cdot 10^{-12}$	statohm/ Ω
$3.335\,640 \cdot 10^{-10}$	C/esu	$2.997\,925 \cdot 10^9$	esu/C
$1.602\,177 \cdot 10^{-12}$	erg/eV	$6.242\,197 \cdot 10^{11}$	eV/erg
$4.184 \cdot 10^7$	erg/cal	$2.390 \cdot 10^{-8}$	cal/erg
10^{-8}	cm/Å	10^8	Å/cm

All entries in the table equal unity.

